RIKEN Accelerator Progress Report

2006

vol. 40

BOOK & CD-ROM

独立行政法人理化学研究所 仁科加速器研究センター
RIKEN Nishina Center for Accelerator-Based Science

CONTENTS

III. RESEARCH ACTIVITIES II (Material Science and Biology)

1. Atomic and Solid State Physics (ions)

2. Atomic and Solid State Physics (muon)

Role of the tensor correlation on the halo formation in ^{11}Li

T. Myo,[*1] K. Katō,[*2] H. Toki,[*1] and K. Ikeda

[Nuclear structure, Unstable nuclei, Tensor force, Cluster model]

A pioneering secondary-beam experiment found that the size of ^{11}Li was surprisingly large, which was outside of the common sense of Nuclear Physics[1]. This large size was interpreted as the halo structure of two neutrons around ^{9}Li. Many experimental findings were shown later for ^{11}Li: a) The halo neutrons have almost equal amount of the s-wave component with respect to the p-wave one[2]. b) The $E1$ strength distribution has a large enhancement near the threshold[3]. c) The charge radius is larger than that of ^{9}Li[4].

The biggest puzzle from the theory side is the large s-wave component for the halo neutrons. If we interpret this fact in the shell model, the shell gap at $N = 8$ has to disappear. However, the mean field treatment of a central force is not able to provide the disappearance of the $N = 8$ shell gap. Essentially all the theoretical works of ^{11}Li had to accept that the $1s_{1/2}$ single particle state is brought down to the $0p_{1/2}$ state without knowing its reason. It is the real challenge for theoretician to understand this disappearance of the $N = 8$ shell gap, which is worked out in this report by developing a framework to treat the tensor force explicitly in the nucleon-nucleon interaction.

The tensor correlation was demonstrated important in the ^{4}He+n system[5]. We treated there the tensor force in the shell model basis with $2p2h$ excitations, and found that the $(0s_{1/2})^{-2}(0p_{1/2})^{2}$ of proton-neutron pair is important to describe the tensor correlation in ^{4}He[5]. This $2p2h$ excitation causes the Pauli-blocking in the ^{4}He+n system for the $p_{1/2}$-orbit, which contributes to the p-wave splitting[5]. Hence, it is important to study the effect of the tensor correlation on the $N = 8$ shell gap problem in ^{11}Li. This is the purpose of this study. We shall perform the configuration mixing with the shell model framework for ^{9}Li to describe the tensor correlation explicitly. For ^{11}Li, we solve the coupled ^{9}Li+n+n problem.

We base on the effective interaction GA′ for ^{9}Li, which has explicitly the tensor force applying the AV8′ potential from the G-matrix theory[5,6]. For ^{9}Li+n+n system, the ^{9}Li-n potential is given by folding potential [7], which strength is determined to reproduce the two-neutron-separation energy of ^{11}Li as 0.31 MeV. For the last two neutrons, we take an AV8′ potential.

For ^{9}Li, in addition to the $0p0h$ state, $(0s_{1/2})^{-2}(0p_{1/2})^{2}$ $2p2h$ excitation of proton-neutron pair caused by the tensor correlations are strongly mixed with 8.2%. Here, let us add two neutrons more to ^{9}Li. When two neutrons occupy the $0p_{1/2}$-orbit the $2p2h$ excitations of the tensor correlation in ^{9}Li are Pauli-blocked[5,7]. Accordingly, the correlation energy of ^{9}Li is lost inside ^{11}Li. For the $(1s)^{2}$ case of two neutrons, the Pauli-blocking does not occur and ^{9}Li gains its correlation energy fully with the $2p2h$ excitations. Hence, the energy distance between $(0p)^{2}$ and $(1s)^{2}$ configurations of ^{11}Li is expected to become small.

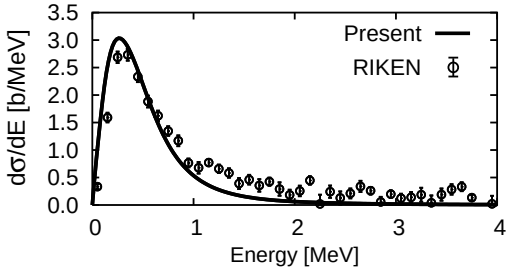

Fig. 1. Calculated Coulomb breakup cross section measured from the ^{9}Li+n+n threshold energy.

We perform the coupled three-body calculation of ^{11}Li with tensor correlations. Our solutions give a large $(1s)^{2}$ probability of 46.9% for the last two neutrons and a large matter radius, 3.41 fm for ^{11}Li, which are enough to explain the observations. This means that the blocking effect from the tensor correlation is essential to break the magicity and make the halo structure for ^{11}Li. The probabilities of $(p_{1/2})^{2}$, $(d_{5/2})^{2}$ and $(d_{3/2})^{2}$ for the last two neutrons are given as 42.7%, 4.1% and 1.9%, respectively.

We calculate the Coulomb breakup strength of ^{11}Li into ^{9}Li+n+n system in comparison with the new data[3]. In Fig. 1, it is found that the present model reproduces the experiment, in particular, for low energy enhancement and its magnitude. The charge radius of ^{11}Li was measured recently and its value is 2.467(37) fm, enhanced from the one of ^{9}Li, 2.217(35) fm[4]. The present model provide 2.44fm and 2.23fm, respectively, which are in good agreement with the experimental values. This enhancement is caused by the large distance between ^{9}Li and the paired $2n$ as 5.69 fm.

*1 Research Center for Nuclear Physics, Osaka University
*2 Graduate School of Science, Hokkaido University

References
1) I. Tanihata et al.: Phys. Rev. Lett. **55**, 2676 (1985).
2) H. Simon et al.: Phys. Rev. Lett. **83**, 496 (1999).
3) T. Nakamura et al.: Phys. Rev. Lett. **96**, 252502 (2006).
4) R. Sánchez et al.: Phys. Rev. Lett. **96** 033002 (2006).
5) T. Myo et al.: Prog. Theor. Phys. **113**, 763 (2005).
6) Y. Akaishi : Nucl. Phys. A **738**, 80 (2004).
7) T. Myo et al.: Prog. Theor. Phys. **108**, 133 (2002).

Proton inelastic scattering on neutron-rich nuclei ^{60}Cr and ^{62}Cr

E. Takeshita,[*1] N. Aoi, S. Ota,[*2] S. Takeuchi, H. Suzuki,[*3] H. Baba,[*4] S. Bishop, T. Fukui,[*2] Y. Hashimoto,[*5] E. Ideguchi,[*4] K. Ieki,[*1] N. Imai,[*6] H. Iwasaki,[*3] S. Kanno,[*1] Y. Kondo,[*5] T. Kubo, K. Kurita,[*1] K. Kusaka, T. Minemura,[*6] T. Motobayashi, T. Nakabayashi,[*5] T. Nakamura,[*5] T. Nakao,[*3] M. Niikura,[*4] T. Okumura,[*5] H. J. Ong,[*3] T. K. Onishi,[*3] H. Sakurai,[*3] S. Shimoura,[*4] R. Sugo,[*1] D. Suzuki,[*3] M. K. Suzuki,[*3] M. Tamaki,[*4] K. Tanaka, Y. Togano,[*1] and K. Yamada

[NUCLEAR STRUCTURE, ^{60,62}Cr(p,p′γ), Inelastic scattering, Unstable nuclei]

Neutron-rich nuclei $^{60}_{24}Cr_{36}$ and $^{62}_{24}Cr_{38}$ are suggested to have a large deformation, because their first 2^+ energies are significantly lower than those of the neighboring isotopes.[1)] In the present work, the nature of collectivity in ^{60}Cr and ^{62}Cr was further studied through their 2^+_1 and 4^+_1 states using proton inelastic scattering.

The experiment was performed using secondary ^{60}Cr and ^{62}Cr beams produced at RIPS.[2)] Proton inelastic scattering was observed in inverse kinematics by γ-spectroscopy. The experimental details are described in Ref.[3)]. Figure 1(a) shows a γ-ray spectrum measured in coincidence with inelastically scattered ^{60}Cr. Two peaks are seen at approximately 650 keV and 820 keV, which are consistent with the $2^+_1 \rightarrow 0^+_{\rm g.s.}$ and $4^+_1 \rightarrow 2^+_1$ transitions observed in a previous work.[4)] From the γ-ray yield, the angle-integrated cross section for the $0^+_{\rm g.s.} \rightarrow 2^+_1$ transition was obtained. The deformation parameter β_2 for ^{60}Cr was then deduced from DWBA analysis to be 0.37(5). A similar analysis was performed for ^{62}Cr and β_2 was obtained to be 0.38(3). These values are significantly larger than those of neighboring ^{56}Cr and ^{58}Cr obtained by Coulomb excitation (0.195(34), 0.254(36), respectively).[5)] The large β_2 values observed indicate that the collectivity in the neutron-rich Cr isotopes is enhanced as the neutron number increases toward $N \sim 40$, which is consistent with the rapid drop in the 2^+_1 energy systematics.

The cascade relation of γ rays at 820 keV and 650 keV was examined by γ-γ coincidence analysis. The γ-ray spectrum for ^{60}Cr obtained in coincidence with a 646-keV γ ray is shown in Fig. 1(b). The γ-ray peak at 820 keV is clearly seen showing that the 820-keV transition coincides with the 650-keV transition. A peak at approximately 650 keV is seen due to contamination of the compton scattering component of the 820-keV γ ray in the 650-keV γ-ray gate. The coincidence of two transitions indicates that the 820-keV transition populates the 2^+_1 state. This interpretation supports the $4^+_1 \rightarrow 2^+_1$ assignment to the 817-keV transition obtained in Ref.[4)]. The energy ratio $E_x(4^+_1)/E_x(2^+_1) = 2.3$ suggests that the surface vibration picture is more appropriate for the collectivity of ^{60}Cr rather than the rotation of a well-deformed nucleus.

The result exhibits the feasibility of the experimental study of the 4^+_1 state by proton inelastic scattering using fast secondary beams. The determination of the 4^+_1 energy in ^{62}Cr is in progress to explore the region of large collectivity.

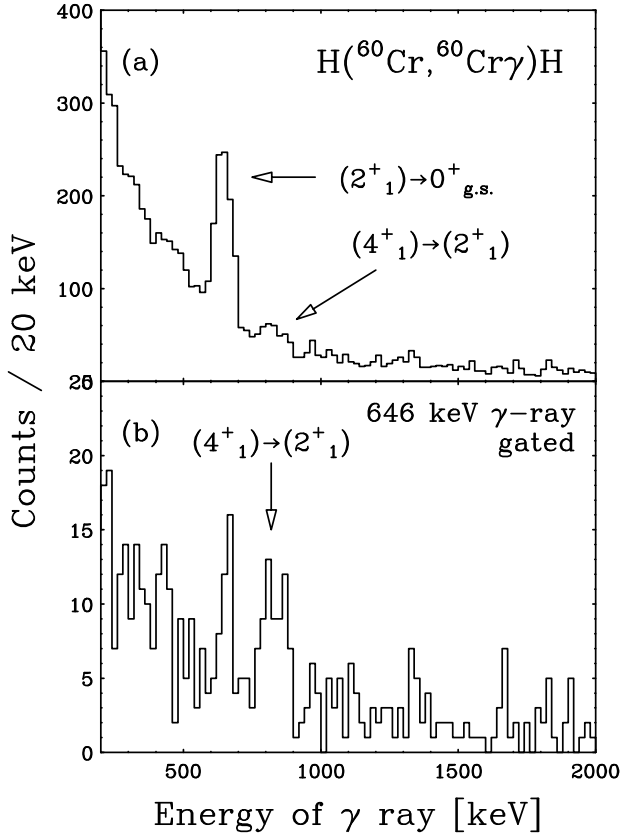

Fig. 1. (a) Gamma-ray energy spectrum obtained in coincidence with ^{60}Cr. (b) γ-γ spectrum in coincidence with $2^+_1 \rightarrow 0^+_{\rm g.s.}$ γ rays.

*1 Department of Physics, Rikkyo University
*2 Department of Physics, Kyoto University
*3 Department of Physics, University of Tokyo
*4 Center for Nuclear Study, University of Tokyo
*5 Department of Physics, Tokyo Institute of Technology
*6 KEK

References

1) O. Sorlin et al.: Eur. Phys. J. A **16**, 55 (2003).
2) T. Kubo et al.: Nucl. Inst. Meth. B **70**, 309 (1992).
3) E. Takeshita et al.: RIKEN Accel. Prog. Rep. **39**, 71 (2006).
4) N. Mărginean et al.: Phys. Lett. B **633**, 696 (2006).
5) A. Bürger et al.: Phys. Lett. B **622**, 29 (2005).

Small electric quadrupole moment of neutron-rich ^{32}Al

D. Kameda, H. Ueno, K. Asahi, M. Takemura,[*1] A. Yoshimi, T. Haseyama,[*1] M. Uchida,[*1] K. Shimada,[*1] D. Nagae,[*1] G. Kijima,[*1] T. Arai,[*1] K. Takase,[*1] S. Suda,[*1] T. Inoue,[*1] J. Murata,[*2] H. Kawamura,[*2] Y. Kobayashi, H. Watanabe,[*3] and M. Ishihara

[Nuclear structure, polarized RI beam, nuclear moments]

The electric quadrupole (Q) moment for the ground state of ^{32}Al($I^\pi = 1^+, T_{1/2} = 33$ ms) has been determined utilizing the β-NMR technique. ^{32}Al fragments were produced in RIPS using the fragmentation of 95 MeV/nucleon ^{40}Ar projectiles on a 0.37 g/cm^2-thick Nb target. In order to extract spin-polarized ^{32}Al, the off-center emission angles $\theta = 1.3^\circ - 5.7^\circ$ were selected[1)] and the momentum was selected in the maximum-yield region with an acceptance of 3 %. The ^{32}Al was implanted in a single-crystal α-Al_2O_3 stopper to which a static magnetic field, $B_0 \sim 0.5$ T, was applied. To detect the quadrupole resonance, oscillating magnetic fields were supplied to ^{32}Al by the adiabatic fast passage (AFP) method and the resulting β-ray asymmetry change was monitored using plastic scintillator telescopes located around the stopper[2)].

Figure 1 shows the obtained β-ray asymmetry changes as a function of the AFP-searched regions for the quadrupole coupling constant ν_Q. The sweep widths, Δ, were taken to be 137 kHz and 103 kHz in Figs. 1(a) and 1(b), respectively. The vertical bars denote the statistical uncertainties. Resonance was detected in the region of $\nu_Q \sim 400$ kHz. The solid curves indicate the fitting functions, which were determined by the least χ^2 method to reproduce the spectra (a) and (b) at the same time. The quadrupole coupling constant thus obtained was $\nu_Q = 407 \pm 32$ kHz. The error had two sources, the fitting error of 22 kHz and the error in the g-factor $|g| = 1.951(5)$, which was measured in this work using a single-crystal Si stopper. The Q moment was deduced from the relation $|Q(^{32}\mathrm{Al})| = |Q(^{27}\mathrm{Al}) \cdot \nu_Q(^{32}\mathrm{Al})/\nu_Q(^{27}\mathrm{Al})|$, where $Q(^{27}\mathrm{Al})$ and $\nu_Q(^{27}\mathrm{Al})$ denote the Q moment for ^{27}Al and the quadrupole coupling constant for ^{27}Al in α-Al_2O_3, respectively. Thus, by inserting $|Q(^{27}\mathrm{Al})| = 140.2(10)$ mb[3)] and $\nu_Q(^{27}\mathrm{Al}) = 2389(2)$ kHz[4)], the Q moment was determined to be $|Q(^{32}\mathrm{Al}_{\mathrm{g.s.}})| = 24(2)$ mb. The sign of the Q moment was not determined.

In Fig. 2, the known Q moments of the Al isotopes are plotted as a function of the neutron numbers. The Q moment of ^{32}Al was found to be markedly smaller than those of the other Al isotopes, but was well reproduced by the conventional *sd*-shell model calculation as shown by the open squares. This result clearly indicates the spherical *sd*-shell nature of the ground state of ^{32}Al. The small Q moment probably stemmed from a major part of the configurations of ^{32}Al, $|(\pi d_{5/2})^{-1} \otimes (\nu d_{3/2})^{-1}\rangle^{I^\pi=1^+}$, which possesses a small Q moment. The result is in sharp contrast to the large degree of deformation of ^{31}Mg due to the pf-intruder structure[5)], suggesting a sudden change in shell structures between the adjacent $N = 19$ isotones.

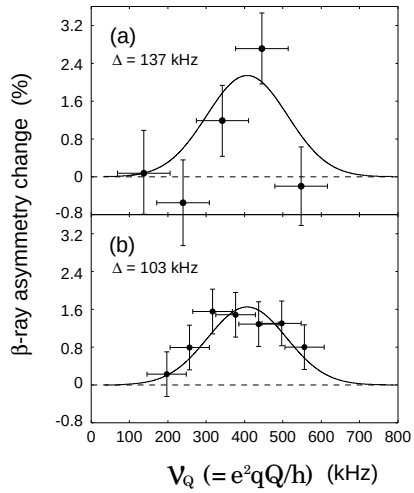

Fig. 1. β-Detected quadrupole resonance spectra obtained ^{32}Al implanted in an α-Al_2O_3 stopper with its c-axis parallel to an external field B_0. See text for more details.

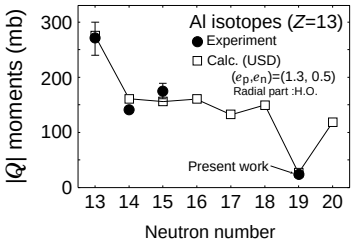

Fig. 2. Comparison of the known Q moments (solid circles) and the USD shell model calculations (open squares).

[*1] Department of Physics, Tokyo Institute of Technology
[*2] Department of Physics, Rikkyo University
[*3] Department of Nuclear Physics, The Australian National University

References

1) K. Asahi et al.,: Phys. Lett. B **251**, 488 (1990).
2) D. Kameda et al.,: Phys. Lett. B (2007) in press.
3) D. Sundholm et al.,: Phys. Rev. Lett. **68**, 927 (1992).
4) S. J. Gravina et al.,: J. Magn. Reson. **89**, 515 (1990).
5) G. Neyens et al.: Phys. Rev. Lett. **94**, 022501 (2005).

Medium modification for ρ, ω mesons in 12 GeV p+A reactions†

M. Naruki, H. En'yo, R. Muto, F. Sakuma,*2 and S. Yokkaichi for the KEK-PS E325 collaboration

[meson, mass modification, chiral symmetry]

It is well established that most of hadron masses are generated due to the spontaneous breaking of chiral symmetry, which is a crucial aspect of the strong interaction. The modification of hadron mass and decay width in hot and/or dense matter is theoretically predicted as a consequence of the restoration of the broken symmetry. Experimental observations of such phenomena have become one of the most interesting topics in hadron physics today.

The experiment E325 has been performed at the KEK 12-GeV Proton Synchrotron to measure the invariant mass spectra of $\rho, \omega, \phi \rightarrow e^+e^-$and $\phi \rightarrow K^+K^-$decay modes simultaneously. Our main goal is to detect the modification of the spectral shape of vector mesons in nuclear media.

Figure 1 shows the invariant mass spectra of e^+e^- pairs using all of the data taken in 2002. The invariant mass spectra were fitted with the combinatorial background and known hadronic sources: $\rho \rightarrow e^+e^-$, $\omega \rightarrow e^+e^-$, $\phi \rightarrow e^+e^-$, $\eta \rightarrow e^+e^-\gamma$, and $\omega \rightarrow e^+e^-\pi^0$. The combinatorial background was evaluated by the event-mixing method. The relativistic Breit-Wigner distributions, which were smeared by detector effects using Geant4[?)], were used to describe the spectral shapes of resonances. The relative abundances of these components were determined by the fitting, except for the ratio of $\omega \rightarrow e^+e^-\pi^0$ to $\omega \rightarrow e^+e^-$ decay which was fixed to their branching ratios, 59/6.95 given by PDG. The fit results are indicated by the solid lines shown in Fig.1. The region from 0.6 to 0.76 GeV/c^2 was excluded from the fit, because the fit including this region resulted in failure at C.L. 99.9%.

A significant excess can be seen on the low-mass side of the ω peak, whereas the high-mass tail of ω can be reproduced with the expected shapes. This procedure determines the ratio of ρ to ω, provided that ρ and ω follow the relativistic Breit-Wigner distribution without any mass modification. After the acceptance correction, the 95% C.L. allowed parameter regions are obtained as $\rho/\omega < 0.15$ and $\rho/\omega < 0.31$ for C and Cu targets, respectively. The systematic errors arises from the uncertainty of the background estimation, which amount to 0.09 and 0.21 for the C and Cu targets, respectively. The obtained ρ/ω ratios are much smaller than unity, as was previously measured in pp interactions at the same energy[?)]. A possible explanation is that most of the ρ are decaying inside the nuclei due to their short lifetime; their mass is modified in nuclear media and contribute to the excess.

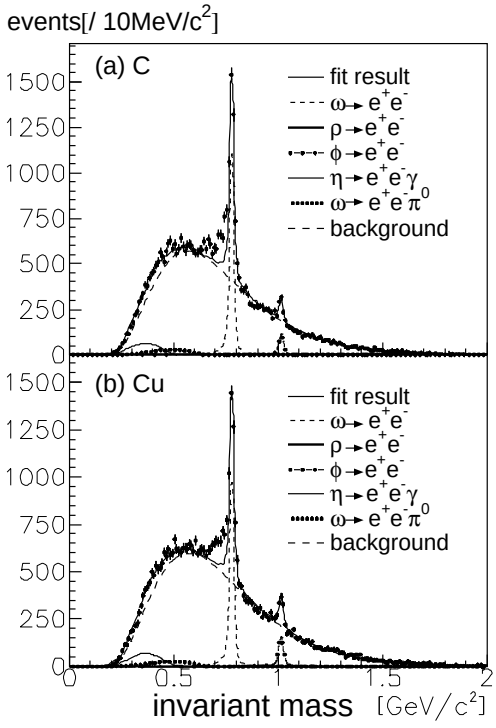

Fig. 1. Invariant mass spectra of e^+e^- for the (a) C and (b) Cu targets. The solid lines show the best-fit results, which is the sum of known hadronic decays, $\omega \rightarrow e^+e^-$ (dashed), $\phi \rightarrow e^+e^-$ (thick dash-dotted), $\eta \rightarrow e^+e^-\gamma$ (dash-dotted), and $\omega \rightarrow e^+e^-\pi^0$ (dotted) together with the combinatorial background (long-dashed). $\rho \rightarrow e^+e^-$ is not visible (see text).

The observed excess is understood by the model in which the mass of ρ/ω meson decreases by 9% at the normal nuclear density. This study experimentally verified the spectral-shape modification of ρ/ω mesons in nuclear matter.

This work was partly funded by the RIKEN Special Postdoctoral Researchers Program. We thank the staff members of the RIKEN Super Combined Cluster system and RIKEN-CCJ.

References

1) S. Agostinelli et al.: Nucl. Instr. and Meth. A **506**, 250-303 (2003).
2) V. Blobel et al.: Phys. Lett. B **48**, 73 (1974).

† Condensed from the article in Phys. Rev. Lett. **96**, 092301 (2006)

*2 Department of Physics, Kyoto University

Ferromagnetic and charge transfer phase transitions in $[Fe^{II}Fe^{III}(dto)_3]$ (dto = $C_2O_2S_2$) complexes examined by muon spectroscopy

N. Kojima*[1], M. Enomoto*[1], N. Kida*[1], I. Watanabe, and T. Suzuki

The iron mixed-valence complex $(n\text{-}C_3H_7)_4N[Fe^{II}Fe^{III}(dto)_3]$ shows a charge transfer phase transition (CTPT) with wide thermal hysteresis at around 120 K and a ferromagnetic transition at 7 K.[1, 2] ^{57}Fe Mössbauer spectroscopy measurement has shown that the Fe^{II} and Fe^{III} sites in $(n\text{-}C_3H_7)_4N[Fe^{II}Fe^{III}(dto)_3]$ are clearly distinguishable around the CTPT, which indicates that the time scale of the valence fluctuation due to the charge transfer between Fe^{II} and Fe^{III} is slower than that of ^{57}Fe Mössbauer spectroscopy measurement ($\sim$ 10^{-7} sec). Taking account of the wide characteristic time window (10^{-6} to 10^{-11} sec) of muon spectroscopy, we have investigated the dynamical property of the CTPT by muon spectroscopy.

Polycrystalline samples of $(n\text{-}C_nH_{2n+1})_4N[Fe^{II}Fe^{III}(dto)_3]$ (n = 3 and 5) were wrapped in aluminum foil and stuck to a silver plate with Scotch tape. We used a VARIOX cryostat and a mini-cryostat with temperature ranging from 1.9 to 30 K and from 40 to 200 K, respectively. The μSR time spectrum was measured in zero field (ZF) and longitudinal field (LF). The LF was applied along the direction of initial muon-spin polarization.

Figure 1 shows the ZF-μSR time spectra for n = 3. The ZF-μSR is analyzed using

$$A(t) = A_0\exp(-\lambda_0 t)\times G_Z(\Delta, H_{LF}, t) + A_1\exp(-\lambda_1 t), \qquad (1)$$

where A_0 and A_1 are the initial asymmetries of the slow and fast relaxation components, λ_0 and λ_1 are the respective muon-spin relaxation rates, respectively. The $G_Z(\Delta, H_{LF}, t)$ is the static Kubo-Toyabe function. The Δ/γ_μ is the distribution width of nuclear-dipole fields at the muon sites and γ_μ is the gyromagnetic ratio of the muon spin. The H_{LF} is LF. The first term was applied to spectra obtained above 30 K putting A_1 = 0. In this case, λ_0 describes effects of dynamically fluctuating internal fields at the muon site. Figure 2 shows the temperature dependences of λ_0 for n = 3 and 5. λ_0 shows the divergent peaks at 15 K and 22.5 K for n = 3 and 5, respectively, which are attributed to the critical slowing down due to the magnetic ordering. In the case of n = 3, λ_0 shows an anomalous enhancement with thermal hysteresis at around 80 K. Taking account of the fact that the CTPT is not observed in the case of n = 5,[3] the anomalous enhancement of λ_0 with thermal hysteresis at around 80 K observed for n = 3 is attributed to the dynamically fluctuating internal field due to the CTPT. In order to elucidate the origin of the relaxation, we measured LF-μSR. The tails of the time spectra for both n = 3 and 5 are almost quenched by the application of a LF of 100 G. There is substantial difference between each value of λ_0 in the vicinity of 80 K, so we can estimate the muon spin depolarization rate corresponding to the dynamically fluctuating internal field at the muon sites from the difference, i.e., $\lambda_{CT} \equiv \lambda_0(n = 3) - \lambda_0(n = 5)$. As a result, λ_{CT} shows a convex shape as a function of H_{LF} in a log-log plot and can be described by Redfield's equation.[4] Values of the correlation time of muon spins, τ_c, obtained from the fitting are 5.7 and 10.6 μs at 80 and 110 K, respectively.

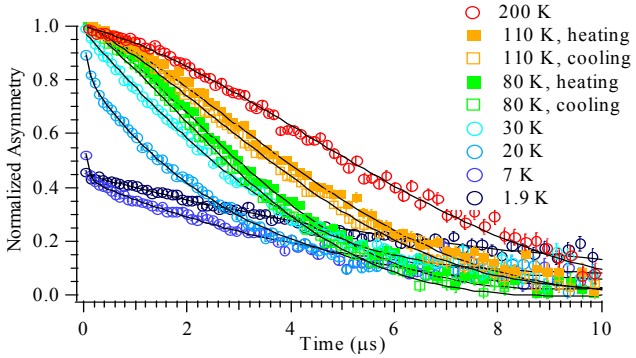

Fig. 1. ZF-μSR time spectra of $(n\text{-}C_3H_7)_4N[Fe^{II}Fe^{III}(dto)_3]$. Solid lines show the best fits of Equation (1).

In conclusion, the CTPT and the ferromagnetic phase transition were observed in the iron mixed-valence complex, $(n\text{-}C_3H_7)_4N[Fe^{II}Fe^{III}(dto)_3]$, by means of muon spectroscopy. The frequency of the valence fluctuation driven by the electron transfer between Fe^{II} and Fe^{III} sites in $(n\text{-}C_3H_7)_4N[Fe^{II}Fe^{III}(dto)_3]$ is on the order of 0.1 MHz.

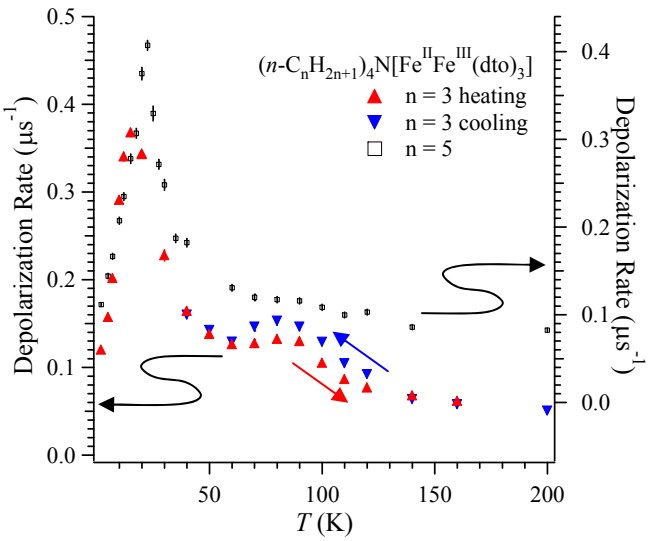

Fig. 2. Temperature dependences of the dynamic muon-spin depolarization rate, λ_0, for $(n\text{-}C_3H_7)_4N[Fe^{II}Fe^{III}(dto)_3]$ (left axis) and $(n\text{-}C_5H_{11})_4N[Fe^{II}Fe^{III}(dto)_3]$ (right axis).

*[1] Graduate School of Arts & Sciences, The University of Tokyo

References

1) N. Kojima et al.: Solid State Commun. **120**, 165 (2001).
2) M. Itoi et al.: Eur. J. Inorg. Chem. **6**, 1198 (2006).
3) N. Kojima et al.: Hyperfine Interact. **156/157**, 175 (2004).
4) C. P. Slichter: *Principles of Magnetic Resonance* (Springer-Verlag, Berlin, Heidelberg, 1978, 1990).

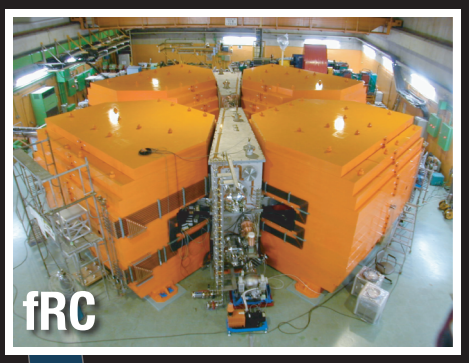

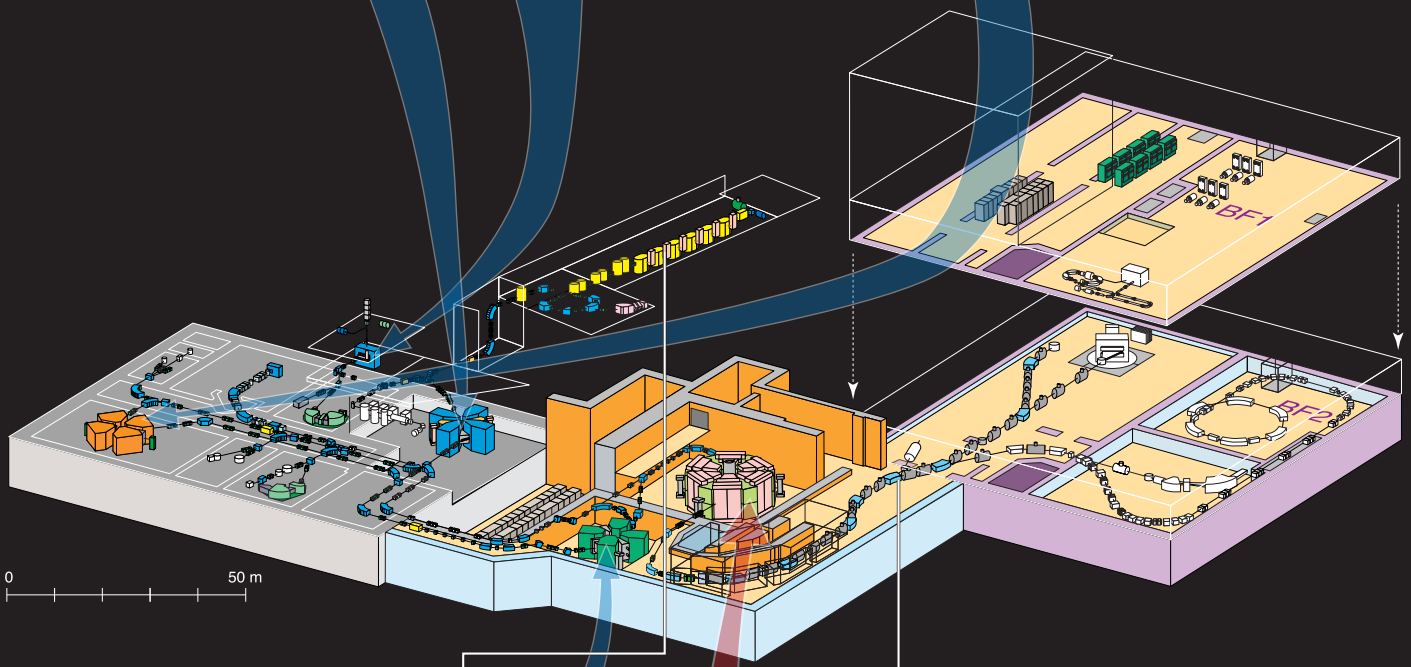

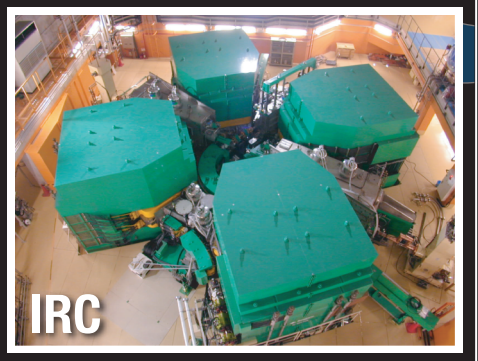

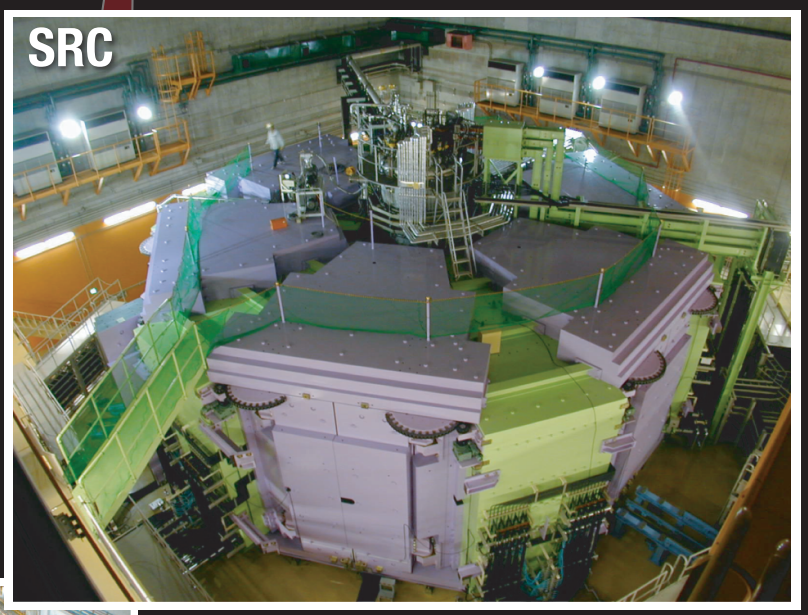

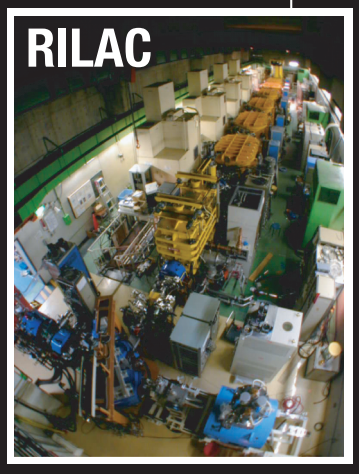

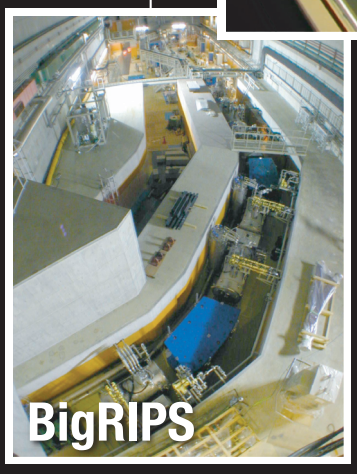

RI Beam Factory

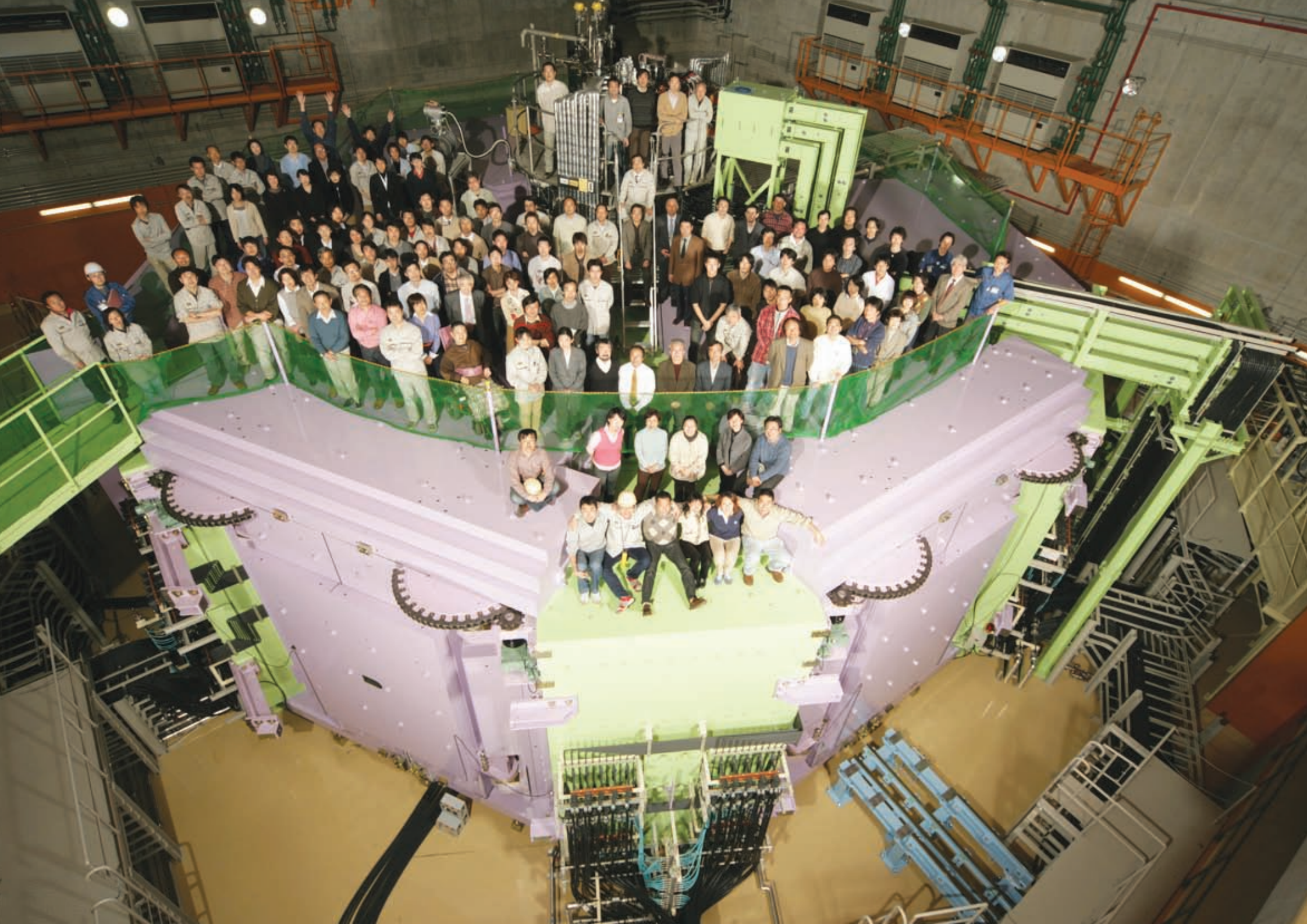

RIBF project passes a critical milestone: the successful extraction of the first beam from SRC

Akira Goto and the accelerator group

On December 28, 2006 at 4 pm, the first beam was extracted from the Superconducting Ring Cyclotron (SRC) of the RI Beam Factory (RIBF). The ion type and the energy of the beam were $^{27}Al^{10+}$ and 345 MeV/nucleon, respectively. This signifies that we have actually completed the world's first and most powerful cyclotron with K=2,500 MeV and have passed a critical milestone in the history of cyclotrons.

Figure 1 shows the history of construction of the three new ring cyclotrons: the fixed-frequency Ring Cyclotron (fRC), the Intermediate-stage Ring Cyclotron (IRC) and the SRC. The sector magnets of the SRC were completed in the autumn of 2005 after a construction period of more than ten years, and were successfully excited at the maximum field level for the first time on November 7 of that year. However, the following morning, a serious problem occurred; the liquid helium in the coil vessels and the control dewar instantly evaporated and was released into the atmosphere. This was because one of the feedthroughs of the superconducting trim coils on the liquid-helium vessel of the control dewar had cracked, allowing helium gas into the insulation vacuum. This trouble resulted in the construction falling about four months behind schedule. The field maps of the sector magnets were measured for about two months in April-June 2006, and the rf resonators and vacuum chambers were then installed. Compared with the SRC, the fRC and IRC, which are room-temperature ring cyclotrons, were constructed in a shorter period; the IRC was completed in September 2005 and the fRC was completed in June 2006. Photographs of the fRC, IRC and SRC are shown in Figs. 2, 3 and 4, respectively.

At the start of the commissioning, we set the ion type for the first beam to be uranium; the acceleration mode used is shown in Fig. 5. The commissioning of the fRC started in July 2006 with the acceleration of a uranium beam. The $^{238}U^{73+}$ ion beam passed through the electrostatic deflector of the fRC for the first time on July 21. From September to November, acceleration tests of the fRC using a uranium beam continued to be performed, in between which experiments using the existing facility were conducted. The commissioning of the IRC started after the rooms for the IRC and SRC were designated to be a radiation-controlled area on November 22. For the tuning of the IRC, it was decided that a krypton beam would be used, taking the low intensity of the uranium beam into account. The $^{84}Kr^{31+}$ ion beam, the charge-to-mass ratio of which is close to that of $^{238}U^{88+}$, was accelerated and extracted from the IRC for the first time on November 25; it took as little as about 2 hours for the tuning from the injection and extraction. The acceleration of the krypton beam was performed by bypassing the fRC. For the commissioning of the SRC, the beam was switched to an aluminum beam ($^{27}Al^{10+}$) on

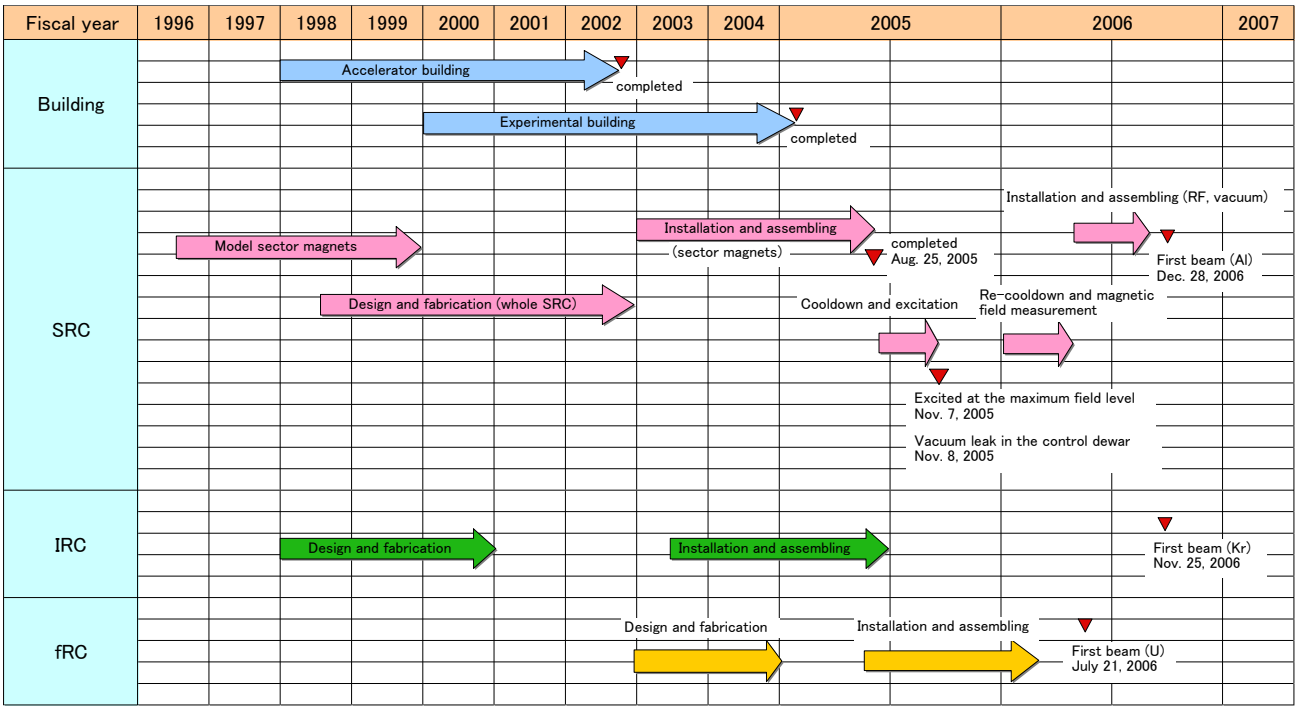

Fig. 1. History of construction of the three new ring cyclotrons: fRC, IRC and SRC.

December 13, which also has a charge-to-mass ratio close to that of the uranium beam and was expected to have higher intensity than the krypton beam. The acceleration of the aluminum beam was also performed by bypassing the fRC; the acceleration mode used is shown in Fig. 6. The beam injection into the SRC became possible on December 21 when the conditioning of two of the four rf resonators was complete. At this time, during the acceleration, an unexpected phenomenon occurred; a beam suddenly stopped at a position about 1,000 mm from the injection radius and did not proceed further. It was found that this was due to a quadrupole mass analyzer that had been placed by mistake at that position, obstructing the beam passage. On December 28 at 6 am, after its removal, the evacuation of the vacuum chamber and the necessary reconditioning of the rf resonators, the beam injection and acceleration were restarted. This time, the beam was accelerated up to the outermost radius immediately, but it took more time than expected for the extraction. However, by tuning the machine carefully, for instance using a radiation survey monitor temporarily set at the exit of the SRC, the extracted beam was finally detected at 4 pm using a beam profile monitor and a Faraday cup placed 5 m downstream of the SRC. The data obtained using these monitors are shown in Figs. 7 and 8, respectively. Some photographs of the scenes in the control room at the time the first beam was detected are shown in Figs. 9-14. A press conference was held from 8 pm in the 2F conference hall of the RIBF building.

We achieved our goal by the end of 2006 as scheduled. We plan to extract the first beam of uranium ions from the SRC by the end of March 2007.

Fig. 2. Photograph of the fRC.

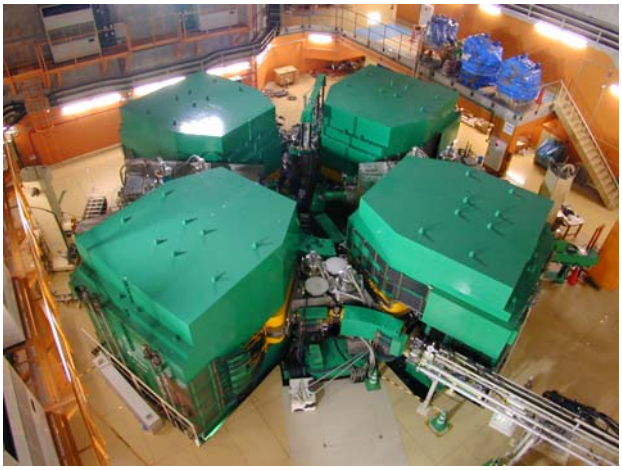

Fig. 3. Photograph of the IRC.

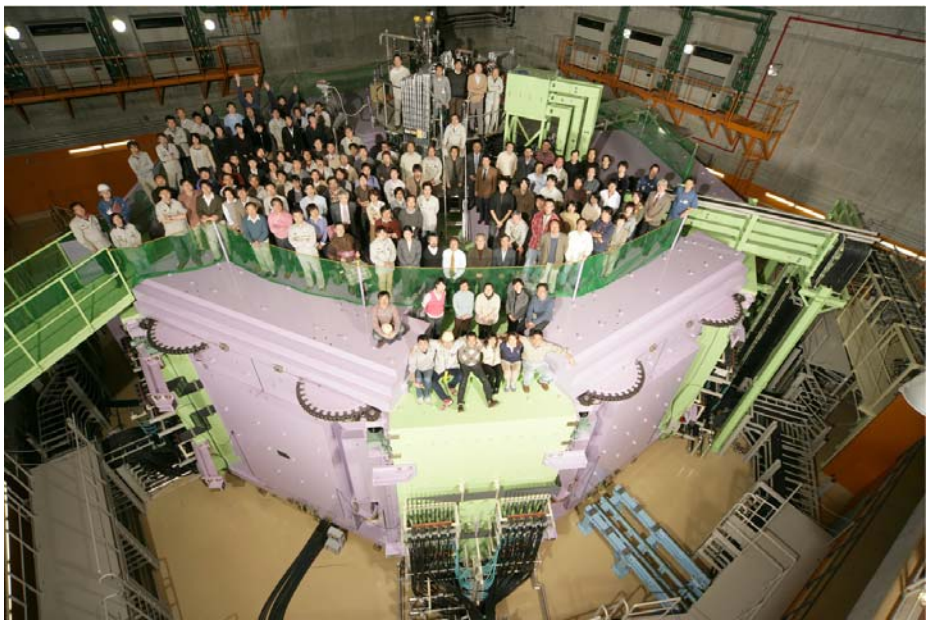

Fig. 4. Photograph of the SRC. People gathered on the top of the SRC just before the magnetic field measurement started in April 2006.

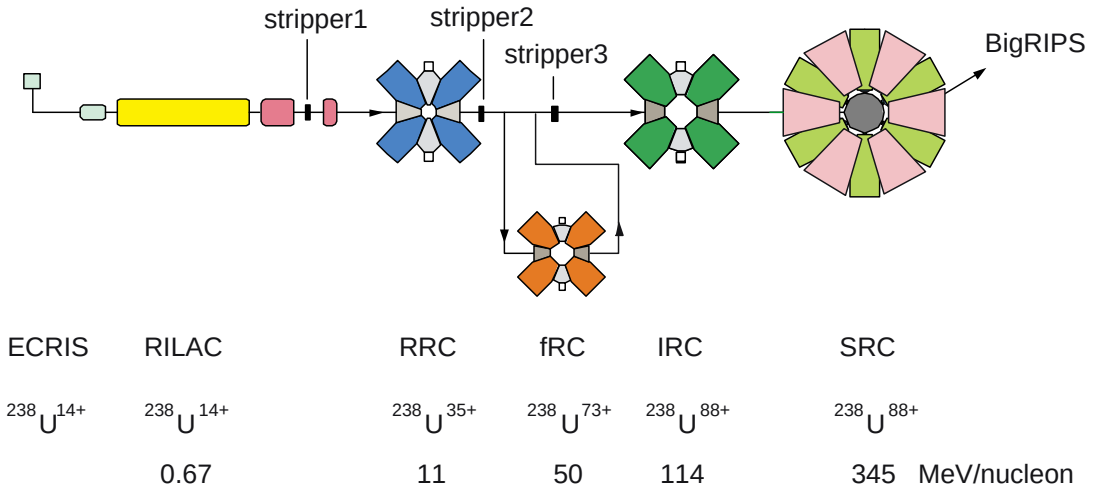

Fig. 5. Acceleration mode of the uranium beam planned in the initial commissioning. Note that we have decided from the acceleration tests performed so far that the uranium beam will be accelerated with 71+ ions instead of 73+ ions in the fRC, 86+ ions instead of 88+ ions in the IRC and SRC, and that 35+ ions instead of 14+ ions will be provided from the ECRIS.

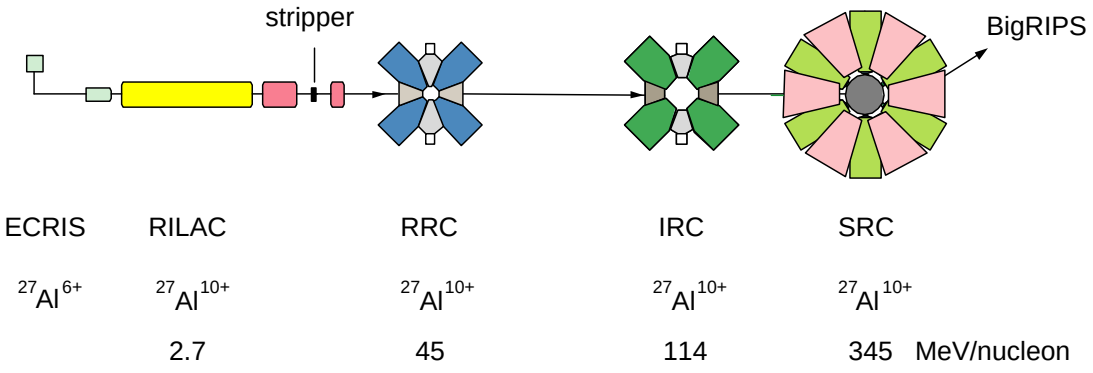

Fig. 6. Acceleration mode of the first aluminum beam used. The fRC is bypassed in this mode.

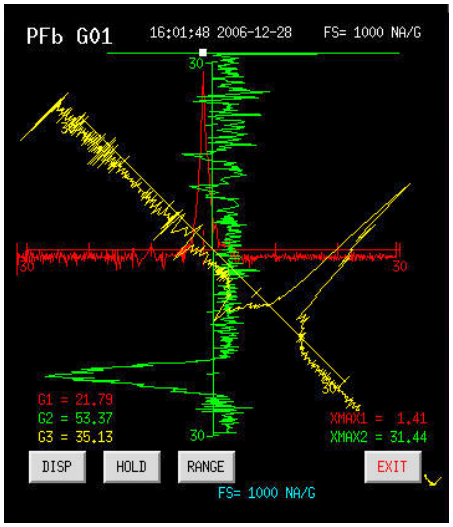

Fig. 7. Profile of the first beam.

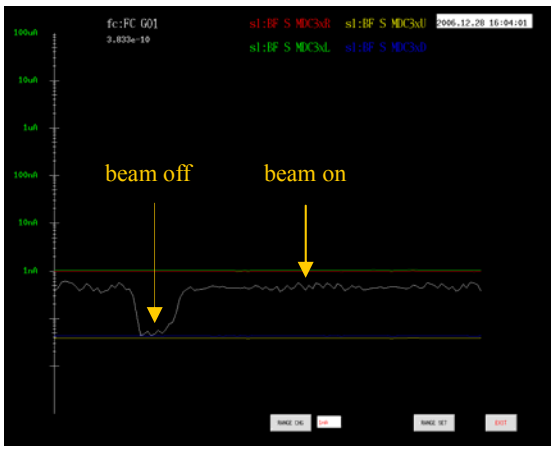

Fig. 8. Trend graph of beam current of the first beam.

Fig. 9. Photograph of the staff members operating the accelerators in the control room.

Fig. 10. Same as Fig. 9.

Fig. 11. Same as Fig. 9.

Fig. 12. Same as Fig. 9.

Fig. 13. Photograph of people cheering upon the detection of the first beam.

Fig. 14. Same as Fig. 13.

Status of BigRIPS separator project

T. Kubo, K. Kusaka, K. Yoshida, A. Yoshida, T. Ohnishi, N. Fukuda, M. Ohtake, Y. Yanagisawa, T. Haseyama, H. Sakurai, T. Motobayashi, and Y. Yano

The BigRIPS separator[1,2] and its RI-beam delivery line[3] are being constructed as a major experimental installation in the RI beam factory (RIBF). The construction is currently in the final stage of the 5-year construction period, which began in the fiscal year 2002.

Figure 1 shows a schematic layout of the BigRIPS separator and RI-beam delivery line along with RIBF cyclotrons. The BigRIPS separator is a superconducting in-flight separator, which is characterized by large acceptances and a two-stage separator scheme. The large acceptances were achieved by using large-aperture superconducting quadrupoles, enabling the efficient production of RI beams using the in-flight fission of uranium beams as well as the projectile fragmentation. The two-stage separator scheme makes it possible to deliver tagged RI beams as well as to realize two-stage isotopic separation. In the RI-beam tagging mode, the first stage of the BigRIPS separator serves to produce and separate RI beams, while the second stage is employed to identify RI-beam species in an event-by-event mode. The BigRIPS separator leads into the RI-beam delivery line, which was designed to serve as a zero-degree forward spectrometer, called ZeroDegree, as well as to transport RI beams to experimental setups placed downstream. When it is employed as a spectrometer, Zerodegree analyzes and identifies projectile reaction residues in secondary-reaction studies of the RI beams.

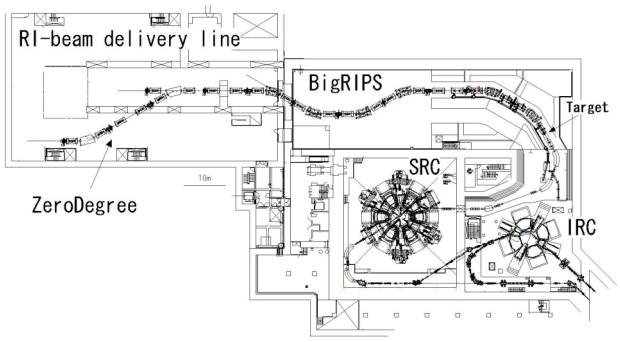

Fig. 1. Schematic layout of RI beam factory in 2007.

The BigRIPS magnets consist of fourteen superconducting triplet quadrupoles (STQs) and six room-temperature dipoles. Their installation in the beam line was completed in April 2006, and all the magnets have been successfully tested online. Coil quenching did not occur up to maximum operational currents for most of the STQs, even though they were once warmed up before the installation. Figure 2 shows photographs of the BigRIPS separator.

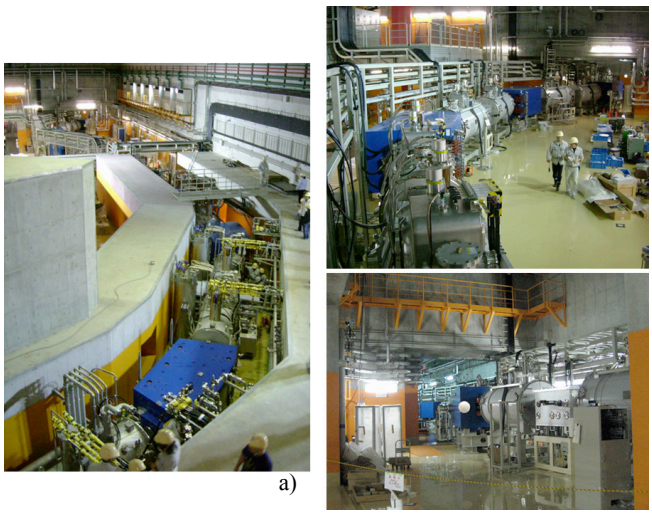

Fig. 2. Photographs of BigRIPS separator: a) the left photograph shows the first stage of the BigRIPS separator, and b and c) the right photographs show the second stage.

The five STQs on the BigRIPS first stage are cooled by a large liquid helium cryogenic plant using a 50-m-long transfer line. A cooling test was carried out several times to check the design and performance of the cryogenic plant, and the 4-K cooling capacity and total 4-K heat load were measured to be about 510 and 190 W, respectively. The excess cooling capacity of the plant amounts to about 320 W, which will be employed to cope with the head loads caused by the neutron radiation from the production target and beam dump (neutron heating). The gas-cooled current leads for the first-stage STQs have also been tested to ensure that they are cooled properly with design values of helium-gas flow rate. It took the plant about three weeks to cool the five STQs with a total cold-mass weight of about 42 tons down to the temperature of liquid helium (16 days) and then to fill the cryostats with liquid helium. Continuous operation of the cryogenic plant started in October 2006.

When a high level of neutron heating exists, the cryogenic plant has to supply much more liquid helium to the STQs by exploiting the excess cooling capacity. The heat load due to neutron heating often changes during the operation, causing instability of the liquid-helium level of the cryostat. We employ a heater installed in the helium vessel of the cryostat in order to compensate the change of neutron heating. This operation mode of the plant has

been tested, in which neutron heating was simulated using another heater. We were able to control the liquid-helium level, although further testing is needed to make the liquid-helium level more stable. By using the PHITS simulation code, the heat load due to neutron heating has been estimated to be about 200 W (mainly to the first STQ right after the production target) for the most serious case: uranium beams at 350 MeV/nucleon and 1 pμA. This is well within the measured excess cooling capacity of the cryogenic plant.

The rest of STQs on the BigRIPS second stage are cooled by a small stand-alone refrigeration system, which is mounted on the cryostat of each STQ and consists of a GM cryocooler and a GM/JT cryocooler. The GM crycooler has a cooling capacity of 100 W at 80 K, being employed to cool high-Tc current leads as well as 80-K thermal shields. The GM/JT cryocooler is used to recondense evaporating helium gas in the helium vessel of the STQs. The cooling capacity of the GM/JT cryocooler is as low as about 2.5 W at 4.3 K. Because the cryoccoler can only reliquefy evaporating helium, it is necessary to precool the cold mass using liquid nitrogen as well as liquid helium, in order to make the GM/JT cryocooler operational. About two weeks are needed to precool each STQ, which was carried out again at RIKEN since they were warmed up in a factory before shipping. All of the second-stage STQs have been kept at the temperature of liquid helium for more than one year by continuously operating the cryocoolers.

Field-map measurements have been carried out for some of the STQs and dipoles. The measured data are currently being analyzed. They will be employed for a ray-tracing calculation of the BigRIPS ion optics.

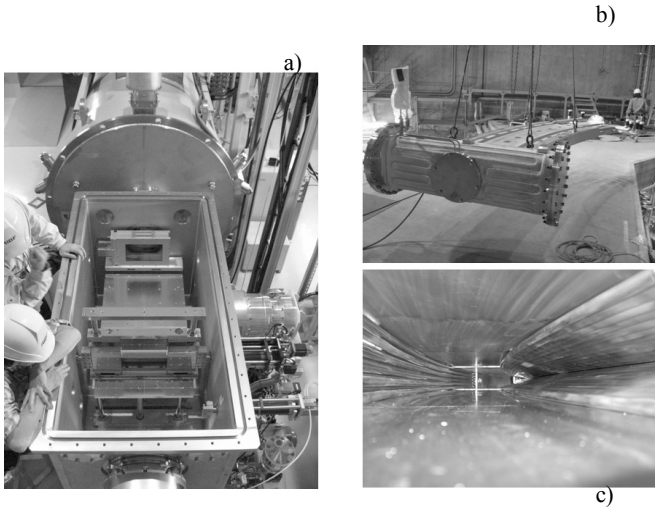

Fig. 3. a) Photograph of the focal-plane chamber at the final focus of BigRIPS separator, and b and c) photographs of high-power beam dump: beam-dump chamber to be installed at first dipole of BigRIPS separator (upper) and inside view of beam dump (lower).

Focal-plane chambers have been installed at the eight focuses of the BigRIPS beam line along with their vacuum pump system. The focal-plane chambers are equipped with focal-plane devices, such as the slit system, the energy-degrader system, the foil/target ladder system, and the detector stand system. They are employed for isotopic separation, RI-beam tagging and beam diagnoses, in combination with beam-line detectors mounted on the detector stands. Figure 3-a shows a photograph of one of the focal-plane chambers. The control systems for the focal-plane devices and the vacuum pump system have been successfully tested online.

Beam-line detectors, such as a delay-line parallel-plate avalanche counter (DL-PPAC) for position measurement and a multisampling ion chamber (MUSIC) for energy-loss measurement, have been fabricated and are presently being tested online. The data acquisition system for the beam-line detectors is also being assembled along with the arrangement of a data-acquisition room.

A high-power production target and a high-power beam dump have been fabricated and installed in the beam line. They have been designed to cope with beam powers as high as 83 kW, which corresponds to the case of a ^{238}U beam at 350 MeV/nucleon and 1 pμA. The production target is a water-cooled rotating-disk target system, and the beam dump is a water-cooled system for which a Cu screw tube and a Cu swirl tube are employed. Figures 3-b and 3-c show some photographs of the high-power beam dump.

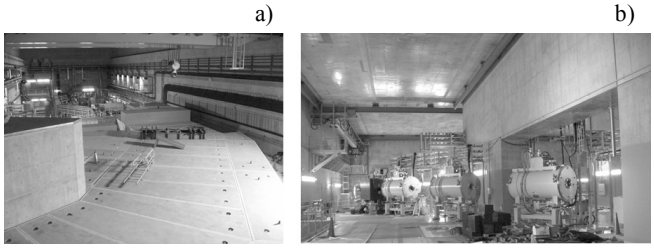

Fig. 4. a) Photograph of radiation shields being installed, and b) photograph of RI-beam delivery line being assembled.

The radiation shields for the BigRIPS first stage, which consist of approximately 200 concrete blocks and iron blocks and weigh approximately 4000 t in total, have been fabricated, and are currently being installed. Figure 4-a shows a photograph of the radiation shields after the first layer had been installed.

The RI-beam delivery line consists of ten STQs and two dipoles that have the same designs as the second-stage magnets of the BigRIPS separator. The fabrication and installation of these magnets along with the focal-plane chambers are almost complete. Figure 4-b shows a photograph of the delivery line.

The commissioning of the BigRIPS separator and the delivery line is scheduled in 2007.

References

1) T. Kubo: Nucl. Instr. and Meth., B 204, 97 (2003).
2) T. Kubo et al.: IEEE Trans. Appl., Supercond., in press.
3) Y. Mizoi et al.: RIKEN Accel. Prog. Rep., 38, 297 (2005).

Preface

On April 1, 2006, the RIKEN Nishina Center (RNC) for Accelerator Based Science was inaugurated as a completely new research center, integrating RIKEN's existing accelerator related laboratory and groups including RIKEN Brookhaven National Laboratory (BNL) Research Center (RBRC) in the USA and RIKEN Rutherford- Appleton Laboratory (RAL) Facility Office in the UK Presently, the RNC is organized into the following five divisions, one group and two affiliated research centers abroad: the Accelerator Division (comprising Accelerator Development Group and Accelerator Operation Group), Nuclear Physics Research Division (Heavy Ion Nuclear Physics Laboratory, Applied Nuclear Physics Laboratory , Radioactive Isotope Physics Laboratory, Superheavy Element Laboratory, Experimental Installations Development Group and Experimental Installations Operation Group), User Liaison and Support Division (User Liaison and Support Group), Sub Nuclear System Research Division (Radiation Laboratory , Advanced Meson Science Laboratory and Theoretical Physics Laboratory), Accelerator Applications Research Division (Accelerator Applications Research Group), Safety Management Group, RBRC (Theory Group and Experimental Group) and RAL Facility Office. The RNC oversees the extensive utilization of the RI Beam Factory (RIBF) and RAL muon facility by users worldwide, and promotes theoretical and experimental research in particle and nuclear physics. The promotion of accelerator applications research is another important mission.

Nishina center is RIKEN's first research center named after our pioneering scientist, Dr. Yoshio Nishina. He was a multi-faced scientist who exhibited expertise in the following fields: theoretical physics, experimental particle, nuclear and cosmic-ray physics, accelerator building, and accelerator applications such as radiation biology and nuclear chemistry. Nowadays it is quite rare to find out such multi-faced scientist. Thus, Nishina center, as a collective of experts, covers each and all of these fields.

In the context of the organizational change, starting this volume No. 40, RIKEN Accelerator Progress Report will be edited to report yearly progress of researches and projects conducted by RNC's laboratories and groups and by users of the RIBF and the RAL muon facility. It also records annually the RNC's administrative activities such as Scientific Policy Committee meetings and Program Advisory Committee meetings etc. as well as domestic and international collaborations and workshops.

Until now, we have called the existing accelerator facility as RIKEN Accelerator Research Facility (RARF), but hereafter we will address the existing and new heavy-ion accelerator system and their experimental installations in the Wako-city campus as RI Beam Factory or simply RIBF.

The existing facility commenced the regular operation for users in 1990. A K540-MeV ring cyclotron (RRC) properly uses a couple of pre-accelerators: a 16-MV variable-frequency linac (RILAC) following an 8-MV fixed-frequency booster linac (CSM), and a K70-MeV AVF cyclotron (AVF). The RILAC has an injector of a variable-frequency RFQ linac (FCRFQ) equipped with two 18 GHz ECR ion sources of normal conducting and superconducting (SCECR) types. The AVF is equipped with two ECR ion sources of 10 GHz and 14.5 GHz (installed by the University of Tokyo), and a polarized deuteron source of an atomic-beam type (DPOL). Various experimental apparatus are installed not only for the application to nuclear physics, but also to nuclear chemistry, bio and medical science, and materials science. Among them, a projectile-fragment separator (RIPS) is well known to produce very intense light-atomic-mass (less than nearly 60) RI beams.

The RIBF adds new dimensions to the existing facility's capabilities: a new high-power heavy-ion booster system consisting of three ring cyclotrons with K-values of 570 MeV (fixed frequency, fRC), 980 MeV (Intermediate stage, IRC) and 2500 MeV (superconducting, SRC), respectively, boosts energies of the output beams from the RRC up to 440 MeV/nucleon for light ions and 350 MeV/nucleon for very heavy ions. An 880 MeV polarized deuteron beam is also available. These primary heavy-ion beams is converted into intense RI beams via the projectile fragmentation of stable isotopes or the in-flight fission of uranium isotopes by a superconducting fragment separator, BigRIPS. The primary-beam intensity is targeted to be 1 particle micro ampere. The combination of the SRC and the BigRIPS will greatly expand our knowledge of nuclear world into presently inaccessible region on the nuclear chart.

RI beam transport lines downstream of the BigRIPS composing a zero-degree forward spectrometer (ZDS) which is one of major experimental installations is being assembled. Its regular operation for the users will commence in October, 2007.

Major other experimental installations planned to be constructed are: a large acceptance superconducting spectrometer (SAMURAI), a facility utilizing very slow RI beams (SLOWRI), a low-to-medium energy polarized RI beam facility at the RIPS (RI Spin Lab), a high-resolution RI beam spectrometer (SHARAQ) constructed by the University of Tokyo, a rare RI precision mass measurement apparatus (Rare RI mass ring), and an electron-RI scattering experimental apparatus (e-RI ring). A new additional injector

linac (New injector) to the RRC is also planned. An extensive R&D of each installation is under way as well.

I would like to summarize highlights of this year 2006 as follows:

Most remarkable achievement of accelerator research division is that they succeeded in the first beam extraction from the superconducting ring cyclotron, at 4 pm on December 28 in 2006, which was one hour and 20 minutes before the official end of RIKEN's working day in 2006. It was really amazing, because we had been declaring for many years to the international community that our first beam would be extracted in 2006, and actually we did it. The beam was aluminum $^{27}Al^{10+}$ with 345 MeV per nucleon. This means that the world's first ring cyclotron with superconducting sector magnets with K2500 MeV, strongest bending power ever in the cyclotron history, was born. On December 29, major Japanese newspapers and TV reported this event. *Science* magazine reported the completion of the new facility with the article entitled "Japan gets head start in race to build exotic isotope accelerators", while *Nature* magazine featured the article "Japan speeds up nuclear physics".

In nuclear physics research division, a problem with correlation of two halo-neutrons in ^{11}Li, which was unsolved for a few decades, has been experimentally resolved via a newly developed Coulomb break-up setup realized at RIPS. In this experiment, two-neutron detection efficiency at low excitation energy of ^{11}Li has been highly improved to observe low-lying E1 strength. The paper of this work was highlighted in *Physical Review Focus*. The other achievement was to examine the Einstein-Podolsky-Rosen paradox, the observation problem in quantum mechanics. In this work, a nuclear reaction of (d,^{2}He) was employed to realize a pure quantum state, and spin-correlation of two protons was measured at SMART. This result is in agreement with non-local quantum mechanical prediction. Concerning in-beam gamma-ray spectroscopy on light and neutron-rich nuclei at RIPS, a new method, "multi-channel direct reaction method", was developed to measure a proton-shell gap in the neutron-rich nucleus ^{23}F. Electric quadrupole moments of ^{31,} ^{32}Al, neutron-rich isotopes located on the borderline of the island of inversion, have been measured by taking advantage of spin-polarized radioactive beams. New program has been launched this year to develop low-energy spin-polarized radioactive beams using inversed-kinematics reactions, and a beam of polarized ^{17}N has been successfully produced. In-beam Moessbauer studies with radioactive beams have presented evidence for the synthesis of novel chemical species of Fe, (O2)-Fe-(O2), via a reaction between a solid oxygen and energetic ^{57}Mn nuclei.

In sub nuclear system research division, the paper entitled "Evidence for in Medium Modification of the Phi Meson at Normal Nuclear Density" was published in *Physical Review Letters*. This paper describes the final goal of KEK-PS E325 experiment which started in 1993, and the results experimentally verified in-medium vector meson mass modification as predicted as a signature of partially restored chiral symmetry in dense matter. The results were released to the press and the paper was highlighted in *Physical Review Focus*. In addition study of matrix models as the non-perturbative formulation of string theory is being pursued. In particular, a novel technique was introduced, by which one can incorporate space-time curvature into matrix models. A novel lattice Dirac operator of overlap type has been constructed which describes the propagation of a Dirac fermion in an external gravitational field. A new value for the fine structure constant was set with an uncertainty of 0.7 parts per billion. It was done by the high precision calculation of QED, together with the new high precision measurement of the electron's magnetic moment performed at Harvard University. The result was published in *Physical Review Letters*. Along with the other paper reporting the measurement, this development is praised as the physics story of the year 2006 by *Physics News Update*.

In accelerator applications research division, irradiation of heavy-ion beam has become a new method for mutation breeding of ornamental plants to produce new cultivars valuable in the market. The phenotypes related with sterility, variegation, and floral color were evaluated in the screening for new cultivars of garden flowers. This year, new mutants of the wheat, rice, *Chrysanthemum, Dianthus, begonia*, *Tricyrtis* and a red alga were established. The gas-jet transport system coupled with the gas-filled recoil ion separator GARIS was developed to start superheavy element chemistry in RIKEN in collaboration with Superheavy Element Laboratory. The performance of the system was appraised using ^{206}Fr and ^{245}Fm produced in the ^{169}Tm(^{40}Ar,3*n*)^{206}Fr and ^{208}Pb(^{40}Ar,3*n*)^{245}Fm reactions, respectively. The ^{206}Fr and ^{245}Fm separated with GARIS were transported to a rotating wheel system for a spectrometry under extremely low background condition. The gas-jet efficiency was almost 100% for the beam intensity up to 2 particle micro amperes.

As for safety management group, they applied for the permission of the IRC and the SRC operation to the Ministry of Education, Culture, Sports, Science and Technology in April, and obtained the authorization in May. Since the acceleration of the uranium beam has begun, they have been acquiring more knowledge on the safe handling of uranium. The construction of a new radiation interlock system, HIS was finished in November.

With regard to RBRC, due to the budgetary constraint of USA, there was concern that they may have to cancel the beam time. However the problem was cleared by a large sum of personal donation. Amongst many publications this year, followings are worth noting: 1) heavy quark production cross section and its flow in Au+Au collisions, 2) direct photon production in p+p and 3) J/psi production in Au+Au and p+p. They are essential measurements both in the proton spin-structure studies and in the QGP studies.

In RAL mon facility, the most intense pulsed muon beam in the world is produced, and a variety of muon experiments have been performed by applying unique characters of muon. Using positive muons, basic properties of various condensed matters, such as high temperature superconductors, quantum spin systems, molecular conductors and chemical complexes, were investigated by employing Muon Spin Relaxation (mSR) methods. One of interesting results is that muon detected the electron dynamics around charge-transfer phase transition associated with spin-state change in the iron mixed-valence complexes. In order to apply the mSR method to surface/interface science, an ultra low-energy muon beam has been developed, and the first application experiment with a thin foil of high temperature superconductor was performed. Negative muons generate spontaneously chain-reacting d-t fusions in D_2 + T_2 systems (muon catalyzed fusion). Experiments using ortho and para deuterium were conducted to observe a difference in the muon catalyzed fusion processes. By observing muonic X-rays produced in muonic atom formations of nuclei implanted in solid hydrogen, a fundamental experiment on nuclear charge density distribution was carried out to measure an isotope shift of muonic X-ray energies between ^{88}Sr and ^{86}Sr.

The Memorandum of Understanding on the Creation of the Council for China-Japan Research Collaboration on Nuclear Physics was signed by W. Shen, director of the Chinese Nuclear Physics Society and Y. Yano, director of the RNC on November 10 in Beijing. The council is created to promote and advance the collaborative activities between the Japanese and Chinese organizations in nuclear physics and related fields.

The Japan-US Theory Institute for Physics with Exotic Nuclei (JUSTIPEN) was established in July. The “institue” is located in the RNC Wako-city site, and collaborative activities are made in the area of low-energy nuclear structure, reactions, and nuclear astrophysics. JUSTIPEN is based on a program supported by the US Department of Energy, and operated jointly by the University of Tokyo and RIKEN under the comprehensive agreement among them. (The actual operatives are the Center for Nuclear Study (CNS), the University of Tokyo and the RNC.)

The Todai-RIKEN Joint International Program for Nuclear Physics research was established on June 30. The program is aimed at enhancing collaboration between the University of Tokyo and RNC on experimental studies, with equipments built by University of Tokyo in the RIBF and related theoretical studies on the international basis.

Supplementary Agreement for Implementation of Joint Research between RIKEN and National Innovation Center for Plant Biotechnology, South Africa was signed by S. G. Mundree, Chief Executive Officer of PlantBio Trust and Y. Yano, director of the RNC on June 21, at RIKEN. This is research cooperation for ion-beam mutagenesis on African crops.

On October 3, the Japanese Emperor and Empress visited RIKEN and toured RIKEN’s No.9 cyclotron, SRC. The Emperor first toured RIKEN’s No.5 cyclotron, RRC on March 12, 1992. In 2007, RIKEN will commemorate the 70th year since Dr. Nishina’s cyclotron, RIKEN’s No.1 cyclotron, began operation in1937.

Yasushige Yano
Director,
RIKEN Nishina Center for Accelerator-Based Science

Differential cross sections of the proton inelastic scattering on ^{32}Mg

S. Takeuchi, N. Aoi, H. Baba,[*1] T. Fukui,[*2] Y. Hashimoto,[*3] K. Ieki,[*4] N. Imai,[*5] H. Iwasaki,[*6] S. Kanno,[*4] Y. Kondo,[*3] T. Kubo, K. Kurita,[*4] T. Minemura,[*5] T. Motobayashi, T. Nakabayashi,[*3] T. Nakamura,[*3] T. Okumura,[*3] T. K. Onishi,[*6] S. Ota,[*2] H. Sakurai,[*6] S. Shimoura,[*1] R. Sugou,[*4] D. Suzuki,[*6] H. Suzuki,[*6] M. K. Suzuki,[*6] E. Takeshita,[*4] M. Tamaki,[*1] K. Tanaka, Y. Togano,[*4] and K. Yamada

[nuclear structure, in-beam γ-ray spectroscopy]

Large collectivity in ^{32}Mg has been found from a large B(E2) for the 2^+ state.[1)] For further understanding of the structure of ^{32}Mg, the location of the first 4^+ state is crucial. The 2321-keV state is suggested to have a spin and parity (J^π) of 3^- or 4^+,[1,2)] but no decisive evidence has been given. In the present experiment, proton inelastic scattering was applied to ^{32}Mg in inverse kinematics and the J^π of the 2321-keV state was studied by angular distribution of its differential cross sections.[3)]

Figure 1 shows the Doppler-corrected γ-ray spectrum associated with the ^{32}Mg(p,p') reaction. The two peaks at 885 keV and 1436 keV are clearly seen corresponding to the transitions from the 885-keV (2^+) state to the ground state and that from the 2321-keV state to the 885-keV state. Differential cross sections were obtained from the measured γ-ray yields in the 0.2° step for the laboratory scattering angle of ^{32}Mg.

Figure 2 shows the angular distributions for excitation to the 885-keV and 2321-keV states. The experimental data are compared with distorted-wave calculations assuming the possible angular momentum transfers ΔL of 3 and 4. The calculations were performed with CH89 optical potential parameters[4)] using the coupled channel calculation code ECIS97.[5)] For ΔL = 4, where the J^π of the 2321-keV state is assumed to be 4^+, the excitations to these two states were calculated by assuming a symmetric rotational model (solid curves). Multistep excitation processes are included in the calculation. For $\Delta L = 3$ or $J^\pi = 3^-$ for the 2321-keV state, the excitations to the 885-keV and 2321-keV states were calculated respectively using the symmetric rotational model and harmonic vibrational model (dashed curves). The angular distribution for the transition to the 2^+ state was well reproduced by the calculation for both cases. Comparisons between the data and the calculated distributions for the 2321-keV state indicate that the $\Delta L = 4$ transition is favored over the $\Delta L = 3$ transition.

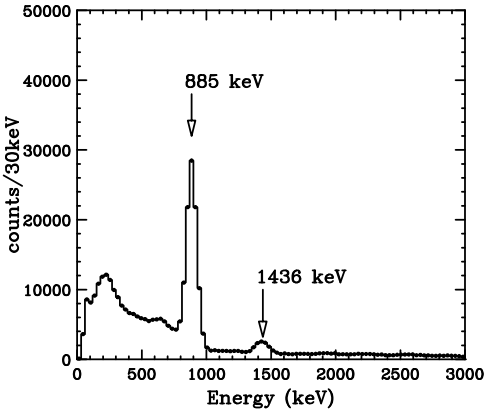

Fig. 1. Doppler-corrected γ-ray spectrum measured by ^{32}Mg(p,p') reaction.

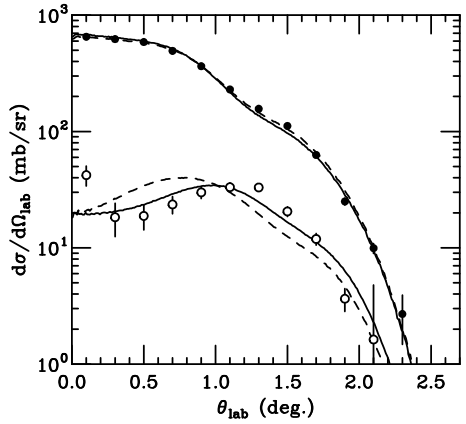

Fig. 2. Angular distributions of scattered ^{32}Mg particle for γ rays from the 885-keV(filled circles) and 2321-keV(open circles) states. Solid curves show the calculated distributions for the ΔL = 2 and 4 transitions. Dashed curves show the calculated distributions for the ΔL = 2 and ΔL = 3.

*1 Center for Nuclear Study, University of Tokyo
*2 Department of Physics, Kyoto University
*3 Department of Physics, Tokyo Institute of Technology
*4 Department of Physics, Rikkyo University
*5 Institute of Particle and Nuclear Studies, High Energy Accelerator Research Organization (KEK)
*6 Department of Physics, University of Tokyo

References

1) J. A. Church et al.: Phys. Rev. C **72** 054320 (2005) and references therein.
2) W. Mittig et al.: Eur. Phys. J. A **15**, 157 (2002).
3) S. Takeuchi et al.: RIKEN Accel. Prog. Rep. **39**, 63 (2006).
4) R. L. Varner et al.: Phys. Rep. **201** 57 (1991).
5) J. Raynal: unpublished *coupled-channel code ECIS97.*

Lifetime measurement of the first 2^+ state of ^{32}Mg

M. K. Suzuki,[*1] H. Iwasaki,[*1] H. Sakurai, A. Dewald,[*2] T. Fukuchi,[*3] T. Fukui,[*4] Y. Ichikawa,[*1] E. Ideguchi,[*5] M. Liu,[*5] T. Nakao,[*1] M. Niikura,[*5] H. J. Ong,[*1] T. K. Onishi,[*1] H. Otsu, T. Sumikama, D. Suzuki,[*1] H. Suzuki,[*1] Y. Zheng,[*5] and S. Shimoura,[*5]

[Nuclear reactions: ^{197}Au(^{32}Mg,^{32}Mg*)^{197}Au E=26MeV/u; RDM]

We applied the recoil distance method (RDM) at an intermediate energy to measure the mean lifetime of ^{32}Mg(2_1^+). ^{32}Mg is a typical nucleus of the 'island of inversion' where the experimental B(E2;$2_1^+ \rightarrow 0^+$) value implies the break of closed-shell structures. Unfortunately the measured B(E2) values of $454\pm78[e^2\mathrm{fm}^4]$[1)], $333\pm70[e^2\mathrm{fm}^4]$[2)], and $622\pm90[e^2\mathrm{fm}^4]$[3)] by the intermediate Coulomb scattering, $325^{+109}_{-65}[e^2\mathrm{fm}^4]$[4)] by the β-γ fast-electronic-timing technique reported so far are not consistent and have large experimental errors. Thus, high-precision measurement of B(E2) with an accuracy of 10% is desirable.

The RDM is an alternative technique to the ones used so far to extract the B(E2;$2_1^+ \rightarrow 0^+$) value in ^{32}Mg. Here, RI beams, excited by a reaction at the secondary target, fly to a degrader foil, which is mounted at a definite separation ($\sim$ 1 mm) downstream of the target. γ rays emitted before and after the degrader foil show different Doppler shifts according to the different ion velocities. As a consequence, in the γ ray spectra, two components of a γ transition are observed, from which the lifetime of the level can be determined.

The experiment was performed in the RIKEN accelerator facility. A radioactive beam of ^{32}Mg was produced via the fragmentation of a 95 MeV/nucleon ^{40}Ar beam using a 277-mg/cm^2-thick ^{9}Be target. The secondary beam was separated using the RIPS[5)] by the $B\rho$-ΔE-$B\rho$ method. Particle identification of the secondary beams was carried out using the energy deposited in a 0.1-mm thick Si detector placed in F2 and the TOF between a 0.1-mm-thick plastic scintillator placed in F2 and PPACs placed 5.3 m apart along the beam line. The ^{32}Mg beam had an intensity of 10^3 ions per second and a purity of about 21%. A reaction target system composed of a secondary target and degrader foil was placed at the final focal plane of RIPS. Two different systems were used, one with a 1353-mg/cm^2-thick Au target and the other with a 189.9-mg/cm^2-thick Au degrader separated by 1200 μm (target system 1) and a 1339-mg/cm^2-thick Au target with a 190.7-mg/cm^2-thick Au degrader separated by 5000 μm (target system 2). The mean energies of ^{32}Mg nuclei between the target and the degrader were calculated to be 26 MeV/nucleon for both systems.

Scattered particles were detected using two PPACs located 200 mm and 383 mm downstream from the target to measure the emission angle of the scattered particles. Moreover, the scattered particles were identified using a telescope comprised of three layers of Si detectors with thicknesses of 200 μm, 500 μm, and 500 μm. The telescope was located 458 mm downstream from the target and covered an area of 150 $\times$ 150 mm^2, corresponding to laboratory scattering angles of up to 12 degrees.

γ rays were detected using the position-sensitive Ge detector array GRAPE[6,7)], which is composed of 12 Ge crystals surrounding the target at an angle of 120 degrees with respect to the beam axis. Each crystal was placed at a distance of 135 mm from the target. To decrease the γ background, an active shield was installed upstream and downstream of the GRAPE consisting of seven BGO crystals with a size of 80 $\times$ 250 $\times$ 25 mm^3.

As shown in Fig. 1, we obtained γ-spectra using both target system 1 and 2, which were Doppler corrected to take account of the ion velocity between the target and the degrader under the condition of no BGO signals. As expected, the system 2 spectrum has a single-peak structure. On the basis of analysis of the system 2 spectrum, a double-peak structure is observed in the system 1 spectrum.

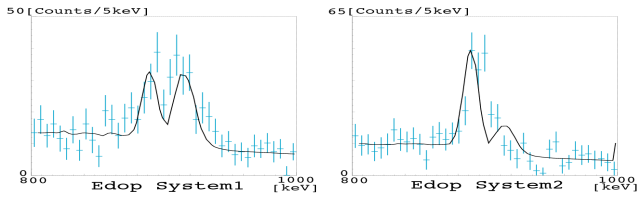

Fig. 1. Doppler-corrected γ-ray energy spectra using the target system 1 and the target system 2.

*1 Department of Physics, University of Tokyo
*2 Institut für Kernphysik Universität zu Köln
*3 Department of Physics, Osaka University
*4 Department of Physics, Kyoto University
*5 Center for Nuclear Study, Graduate School of Science, University of Tokyo

References
1) T. Motobayashi *et al.*; Phys. Lett. B **346** (1995) 9.
2) B. V. Pritychenko *et al.*; Phys. Lett. B **461** (1999) 322.
3) V. Chisté *et al.*; Phys. Lett. B **514** (2001) 233.
4) H. Mach *et al.*; J. Phys. G: Nucl. Part. Phys. **31** (2005) 1421.
5) T. Kubo *et al.*; Nucl. Instrum. Methods B **70** (1992) 309.
6) S. Shimoura; Nucl. Instrum. Methods A **470** (2004) 188.
7) M. Kurokawa *et al.*; IEEE Trans. Nucl. Sci. **50** (2003) 1309.

Proton inelastic scattering studies at the borders of the "island of inversion": The ^{30,31}Na and ^{33,34}Mg case

Z. Elekes,[*1] Zs. Dombrádi,[*1] A. Saito,[*2] N. Aoi, H. Baba,[*2] K. Demichi,[*2] Zs. Fülöp,[*1] J. Gibelin,[*3] T. Gomi,[*2] H. Hasegawa,[*2] N. Imai,[*4] M. Ishihara, H. Iwasaki,[*4] S. Kanno,[*2] S. Kawai,[*2] T. Kishida, T. Kubo, K. Kurita,[*2] Y. Matsuyama,[*2] S. Michimasa,[*4] T. Minemura, T. Motobayashi, M. Notani,[*4] T. Ohnishi,[*4] H.J. Ong,[*4] S. Ota,[*5] A. Ozawa,[*6] H.K. Sakai,[*2] H. Sakurai, S. Shimoura,[*4] E. Takeshita,[*2] S. Takeuchi, M. Tamaki,[*4] Y. Togano,[*2] K. Yamada,[*2] Y. Yanagisawa and K. Yoneda

[NUCLEAR STRUCTURE, Unstable nuclei, gamma-ray spectroscopy]

A ^{40}Ar primary beam of 94 MeV/nucleon energy with 60 pnA intensity was transported to a ^{181}Ta production target of 0.5 mm thickness. The RIPS fragment separator analyzed the momentum and mass of the reaction products. The ^{30,31}Na and ^{33,34}Mg beams were produced in two individual runs at different Bρ values. An aluminum wedged degrader of 221 mg/cm^2 was placed at the momentum dispersive focal plane (F1) to purify the constituents. In the first run of ^{30,31}Na, the secondary beam included neutron–rich O, F, Ne and Na nuclei with $A/Z \approx 3$ whereas mainly Mg and Al isotopes were mixed in the second run of ^{33,34}Mg. The fragment separator was set to its full 6% momentum acceptance to achieve as high beam intensities as possible. The total intensity was about 100 particle/s (pps) for both runs, while the ^{30,31}Na/^{33,34}Mg intensities reached 8, 6, 3 and 2 pps, respectively, on average. The incident beam species was identified on an event–by–event basis from energy loss, time–of–flight (TOF), and magnetic rigidity ($B\rho$).

The secondary beam hit a liquid hydrogen 30–mm–diameter target the thickness of which was 24 mm and its entrance and exit windows were made of 6.6 μm Aramid foil. The average areal density of hydrogen cooled to lower than 20 K was 210 mg/cm^2. The mean energy of the isotopes in the target was approximately 50 MeV/nucleon. Two PPACs at F3 upstream of the target monitored the position of incident particles. The reaction products and scattered particles were detected and identified by a PPAC and a silicon telescope of three layers with thicknesses of 0.5, 0.5, and 1 mm located about 80 cm downstream of the target. Z was identified by the TOF–energy loss method in which TOF was measured between the PPACs upstream and downstream of the secondary target. The isotopes was separated by the ΔE–E method. The de–exciting γ rays emitted by the inelastically scattered nuclei were detected by the DALI2 setup consisting of 146 NaI(Tl) scintillators surrounding the target. To determine the cross sections of the produced γ rays in proton inelastic scattering, the peak positions determined were fed into the detector simulation software GEANT4 and the resultant response curves plus smooth polynomial backgrounds were used to analyze the obtained experimental spectra. From a distorted wave analysis of the cross sections, we derived the "matter" deformation parameter (β_M) values, which are consistent with the charge deformations determined from Coulomb excitation experiments. On the basis of the "matter" and charge deformation parameter values, the neutron deformation parameter values were also extracted. The results (see Table 1) show that all of these nuclei are largely deformed; the deformations of the proton and neutron distributions are similar and cannot be distinguished at the present experimental uncertainties.

Isotope (peak)	Cross section	β_M	β_C	β_n
^{31}Na (370 keV)	24±4 mb	0.56±0.05 ($5/2^+_1 \rightarrow 3/2^+_{gs}$)	0.66±0.16	0.54±0.07
^{30}Na (403 keV)	18±4 mb	0.32±0.04 ($3^+_1 \rightarrow 2^+_{gs}$)	0.41±0.10	0.30±0.05
^{34}Mg (685 keV)	111±37 mb	0.68±0.16 ($2^+_1 \rightarrow 0^+_{gs}$)	0.58±0.06	0.70±0.13
^{33}Mg (483 keV)	33±10 mb	0.47±0.08 ($7/2^+_1 \rightarrow 5/2^+_{gs}$)	0.52±0.12	0.46±0.10

Table 1. Angle–integrated cross sections of the (p,p') process corrected for detection efficiency and deformations for ^{30,31}Na and ^{33,34}Mg nuclei.

† Condensed from article in Phys. Rev. **C73**, 044314 (2006)

*1 Insitute of Nuclear Research (ATOMKI)
*2 Rikkyo University
*3 Institut de Physique Nucléaire
*4 University of Tokyo
*5 Kyoto University
*6 University of Tsukuba

Proton inelastic scattering on very neutron-rich ^{36}Mg nucleus

S. Michimasa,[*1] Y. Yanagisawa, K. Inafuku,[*2] N. Aoi, Z. Elekes,[*3] Zs. Fülöp,[*3] Y. Ichikawa, N. Iwasa,[*2] K. Kurita,[*4] M. Kurokawa, T. Machida,[*4] T. Motobayashi, T. Nakamura,[*5] T. Nakabayashi,[*5] M. Notani,[*6] H. J. Ong,[*7] T. K. Onishi,[*7] H. Otsu, H. Sakurai, M. Shinohara,[*5] T. Sumikama, S. Takeuchi, K. Tanaka, Y. Togano,[*4] K. Yamada, M. Yamaguchi,[*8] and K. Yoneda

[Nuclear reactions: ^{1}H(^{36}Mg,^{36}Mgγ)]

We report here on the in-beam γ-ray spectroscopy of the very neutron-rich ^{36}Mg nucleus using proton inelastic scattering. The ^{36}Mg nucleus is located in the middle of the shell closures of $N = 20$ and 28, and is closer to the neutron drip line than nuclei belonging to the so-called 'island of inversion'. In previous experimental studies on neutron-rich magnesium isotopes, ^{32}Mg was reported to be a well-deformed nucleus[1] and the disappearance of the magicity at $N = 20$ was indicated. For ^{34}Mg, the deformation was reported to be larger than that of ^{32}Mg[2]. The present study is the first experiment to investigate the low-lying excited states in ^{36}Mg.

The experiment was performed at the unstable nuclear beam line RIPS at RIKEN. Ions of ^{48}Ca were accelerated up to 63 MeV/nucleon using the acceleration scheme of RFQ-RILAC-CSM-RRC. The average intensity of the primary beam was ∼80 particle nA. The primary target was a ^{181}Ta plate with a thickness of 150 μm. A radioactive ^{36}Mg beam was isotopically separated by RIPS. The momentum acceptance was set to be 6%. Particle identification of the secondary beam was performed by a standard method based on the energy deposit (ΔE), time of flight (TOF), and magnetic rigidity ($B\rho$). The magnetic rigidity of the fragments was deduced from the position on the first momentum-dispersive focal plane (F1) measured using a parallel-plate avalanche counter (PPAC). ΔE was obtained from the silicon detector arranged at the first achromatic focus (F2), and the TOF was measured between plastic scintillators arranged at F2 and the second achromatic focus (F3). The secondary beam bombarded a liquid hydrogen target[3] of 105 mg/cm^2 with havar foil windows, which was placed at F3. To obtain a sufficient mass resolution for the reaction products, the TOF spectrometer[4] was placed downstream of the secondary target. The scattered particles were detected using a telescope arranged at the end of the beam line, which consisted of a 100-μm silicon detector and two NaI(Tl) scintillators. The identification of the scattered particles was performed by the TOF-ΔE-E method. The scattering angle of the particle was measured using three PPACs placed before and after the secondary target. The de-excitation γ ray from the inelastically scattered particle was detected using 160 NaI(Tl) scintillators (DALI2)[5] surrounding the secondary target.

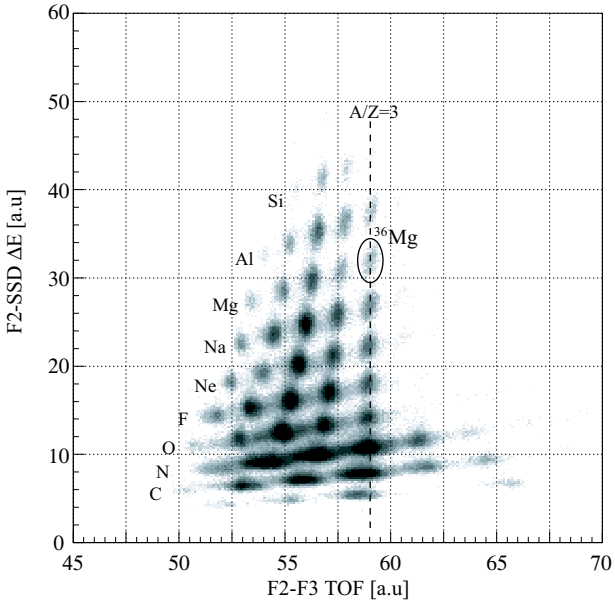

Fig. 1. Identification of the particles involved in the secondary beam. The horizontal and vertical axes correspond to the TOF between F2 and F3, and to the energy deposited in the F2 Si detector, respectively.

Figure 1 shows the identification of the particles involved in the secondary beam. The ^{36}Mg ion was clearly identified, and its intensity was approximately 0.3 counts per second. Data analysis is now in progress to deduce the excitation energy of the first 2^+ state and the deformation length of ^{36}Mg.

*1 Center for Nuclear Study, University of Tokyo
*2 Department of Physics, Tohoku University
*3 ATOMKI, Hungary
*4 Department of Physics, Rikkyo University
*5 Department of Physics, Tokyo Institute of Technology
*6 Argonne National Laboratory, USA
*7 Department of Physics, University of Tokyo
*8 National Institute of Advanced Industrial Science and Technology

References

1) T. Motobayashi et al.: Phys. Lett. B **346**, 9 (1995).
2) H. Iwasaki et al.: Phys. Lett. B **522**, 227 (2001).
3) H. Ryuto et al.: Nucl. Instrum. Methods Phys. Res. A **555**, 1 (2005).
4) N. Aoi et al.: RIKEN Accel. Prog. Rep. **38**, 176 (2005).
5) S. Takeuchi et al.: RIKEN Accel. Prog. Rep. **36**, 148 (2003).

Study of first excited state in ^{30}Ne by proton inelastic scattering in reverse kinematics

K. Inafuku,[*1] N. Iwasa,[*1] S. Michimasa,[*2] N. Aoi, Y. Ichikawa,[*3] K. Kurita,[*4] M. Kurokawa, T. Machida,[*4] T. Motobayashi, T. Nakabayashi,[*5] T. Nakamura,[*5] M. Notani,[*6] H.J. Ong,[*3] T.K. Onishi,[*3] H. Otsu, H. Sakurai, M. Shinohara,[*5] T. Sumikama, S. Takeuchi, K. Tanaka, Y. Togano,[*4] K. Yamada, M. Yamaguchi, Y. Yanagisawa, K. Yoneda, Z. Elekes,[*7] and Zs. Fülöp[*7]

[NUCLEAR REACTIONS: ^{1}H(^{30}Ne,^{30}Neγ)^{1}H]

The neutron-rich nucleus ^{30}Ne is an attractive nucleus because of its location in the region of the 'island of inversion'[1] where the $N = 20$ magicity disappears and enhanced quadrupole collectivity appears. The energy of the first excited state, most probably 2^+, in ^{30}Ne has been measured by proton inelastic scattering in reverse kinematics[2], suggesting the enhancement of deformation. In order to improve the accuracy of the excitation energy and transition strength, we have remeasured the proton inelastic scattering with higher statistics and better energy resolution using a higher-intensity beam and high-resolution detectors.

A radioactive ^{30}Ne beam was produced by the fragmentation of a ^{48}Ca beam at 63 MeV/nucleon with a typical intensity of 80 pnA on a ^{181}Ta target with a thickness of 250 mg/cm^2, and was isotopically separated by the RIKEN projectile fragment separator (RIPS). Particle identification of the secondary beam was performed by the $B\rho$-TOF-ΔE method using a parallel-plate avalanche counter (PPAC) placed at the dispersive focus (F1), two 100-μm-thick plastic scintillators placed at the first and last achromatic foci (F2 and F3) and a 100-μm-thick silicon detector at F2. A typical intensity of the ^{30}Ne beam was 1.4 cps, which was about seven times larger than that of the previous experiment[2].

A liquid-hydrogen target with a thickness of 105 mg/cm^2 at F3 was bombarded by the ^{30}Ne beam. The energy of the ^{30}Ne beam was 44 MeV/nucleon at the center of the target. The de-excitation γ-rays were detected by an array of 160 NaI(Tl) scintillators (DALI-II) that surrounded the target. The energy resolution of the Doppler-shift-corrected γ-rays at 1 MeV from a source moving with a velocity of $\beta \sim 0.3$ was 8%, which was better than the resolution of the previous experiment (12%). The reaction products were collected by the superconducting triplet quadrupole magnet (STQ)[3] and their charge (Z) and mass (A) were identified by the TOF-ΔE-E method. TOF was measured using two 100-μm-thick plastic scintillators placed 3.8 m apart. ΔE and E were measured using a 320-μm-thick silicon detector and two 120-mm-thick NaI(Tl) detectors placed at the focus of STQ. The resolution of the charge and mass were measured to be 0.16 and 0.37 in σ, respectively.

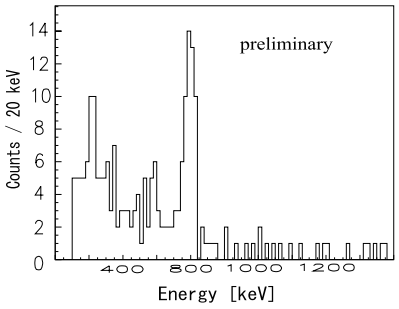

Fig. 1. Doppler-shift-corrected γ-ray spectra measured in coincidence with scattered ^{30}Ne particle.

Figure 1 shows the Doppler-shift-corrected γ-ray energy spectrum measured under the condition that both beam particles and reaction products were identified to be ^{30}Ne. Only the events with the γ detection multiplicity = 1 were employed in the spectrum. In the spectrum, a prominent γ peak was clearly observed. The energy was preliminarily deduced to be 799±12 keV, which is consistent with the result of the previous experiment (791±26 keV) but with much better accuracy. Further analysis is now in progress for accurate determination of the transition strength.

[*1] Department of Physics, Tohoku University
[*2] Center for Nuclear Study, University of Tokyo
[*3] Department of Physics, University of Tokyo
[*4] Department of Physics, Rikkyo University
[*5] Department of Physics, Tokyo Institute of Technology
[*6] Argonne National Laboratory
[*7] Institute of Nuclear Research of the Hungarian Academy of Science

References

1) E. K. Warburton et al.: Phys. Rev. C **41**, 1147 (1990).
2) Y. Yanagisawa et al.: Phys. Lett. B **566**, 84 (2003).
3) K. Kusaka et al.: IEEE Trans. Appl. Supercond. **14**, 310 (2004).

Proton single-particle states in neutron-rich ^{23}F nucleus

S. Michimasa,[*1] S. Shimoura,[*1] H. Iwasaki,[*2] M. Tamaki,[*1] S. Ota,[*1] N. Aoi, H. Baba, N. Iwasa,[*3] S. Kanno, S. Kubono,[*1] K. Kurita,[*4] M. Kurokawa, T. Minemura,[*5] T. Motobayashi, M. Notani,[*6] H. J. Ong,[*2] A. Saito,[*2] H. Sakurai, S. Takeuchi, E. Takeshita, Y. Yanagisawa, and A. Yoshida

[Nuclear reactions: ^{4}He(^{22}O,^{23}F*), ^{4}He(^{23}F,^{23}F*), ^{4}He(^{24}F,^{23}F*), ^{4}He(^{25}Ne,^{23}F*), Single-particle state, In-beam γ-ray spectroscopy]

We have reported in-beam γ-ray spectroscopy of ^{23}F using the proton transfer ^{4}He(^{22}O,^{23}F*), the α inelastic scattering ^{4}He(^{23}F,^{23}F*), the neutron-knockout ^{4}He(^{24}F,^{23}F*), and the two-nucleon knockout ^{4}He(^{25}Ne,^{23}F*) reactions[1]. In this paper, we discuss the proton shell structure in a neutron-rich ^{23}F nucleus on the basis of the cross sections of these reactions for each excited state. This study is the first application of the proton transfer reaction on an unstable nucleus to in-beam γ-ray spectroscopy.

The experiment was performed at the RIPS beam line in RIKEN. The ions of ^{40}Ar were accelerated up to 63 MeV/nucleon using the acceleration scheme of RFQ-RILAC-CSM-RRC. The average intensity of the primary beam was ∼500 particle nA. The primary target was a 1-mm-thick ^{9}Be plate. The secondary beam was a cocktail of ^{22}O, ^{23}F, ^{24}F and ^{25}Ne, and it bombarded a 100-mg/cm^2-thick liquid helium target[2] with havar foil windows. The reaction products were identified using a telescope consisting of 9 SSDs and 36 NaI(Tl) scintillators.[3] The scattering angles of the reaction products were measured using three PPACs. De-excitation γ rays from the reaction products were detected using 150 NaI(Tl) scintillators (DALI2)[4] surrounding the secondary target.

In the analysis, we examined the coincidences of multiple γ rays in these reactions and reconstructed the γ-decay scheme in ^{23}F, as shown in Fig. 1. The level energies with underlines show newly observed excited states in the present experiment. The bar graphs on the right side of the excitation energies show the relative cross sections for populating these excited states. In these relative cross sections, one can observe that the 2268- and 4059-keV states are strongly populated by the proton transfer reaction, but negligibly populated by the neutron knockout reaction. This strongly suggests that these states have a proton single-particle nature. Furthermore, the cross sections for these states in α inelastic scattering may indicate that the 2268 and 4059 keV states have the proton single-particle configurations of $s_{1/2}$ and $d_{3/2}$, respectively. These configurations are consistent with the angular momenta for these states deduced from angular distributions of scattered ^{23}F ions.

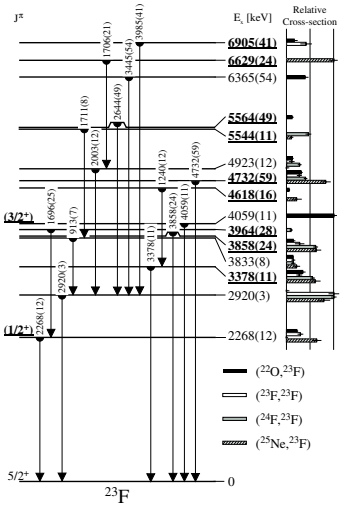

Fig. 1. Proposed level and γ-decay scheme in ^{23}F. The level energies with underlines show excited states newly observed in the present experiment. The spin-parities with underlines were assigned by the angular distributions from the proton transfer reaction. The bars on the right side of excitation energies show the relative cross sections to populate these states.

The excitation energies of these proton single-particle states are compared with the shell-model calculations on the basis of the USD[5] and SDPF-M[6] effective interactions. These states are located at higher energies than the predictions by ∼ 500 keV, although other states correspond to the predictions within 100 keV. This may indicate that the shell gaps of $d_{5/2}$-$d_{3/2}$ and $d_{5/2}$-$s_{1/2}$ in ^{23}F are wider than those in stable nuclei.

References
1) S. Michimasa et al.: Phys. Lett. B **638**, 146 (2006).
2) H. Ryuto et al.: Nucl. Instrum. Methods Phys. Res. A **555**, 1 (2005).
3) M. Tamaki et al.: CNS-REP-59, 76 (2003).
4) S. Takeuchi et al.: RIKEN Accel. Prog. Rep. **36**, 148 (2003).
5) B. H. Wildenthal et al.: Prog. Part. Nucl. Phys. **11**, 5 (1984).
6) Y. Utsuno et al.: Phys. Rev. C **60**, 054315 (1999).

† Condensed from the article in Phys. Lett. B **638**, 146 (2006)
*1 Center for Nuclear Study, University of Tokyo
*2 Department of Physics, University of Tokyo
*3 Department of Physics, Tohoku University
*4 Department of Physics, Rikkyo University
*5 National Cancer Center
*6 Argonne National Laboratory, USA

Vanishing N=20 shell gap: study of excited states in ^{27,28}Ne

Z. Elekes,[*1] Zs. Dombrádi,[*1] A. Saito,[*2] N. Aoi, H. Baba,[*2] K. Demichi,[*2] Zs. Fülöp,[*1] J. Gibelin,[*3] T. Gomi,[*2] H. Hasegawa,[*2] N. Imai,[*4] M. Ishihara, H. Iwasaki,[*4] S. Kanno,[*2] S. Kawai,[*2] T. Kishida, T. Kubo, K. Kurita,[*2] Y. Matsuyama,[*2] S. Michimasa,[*4] T. Minemura, T. Motobayashi, M. Notani,[*4] T. Ohnishi,[*4] H.J. Ong,[*4] S. Ota,[*5] A. Ozawa,[*6] H.K. Sakai,[*2] H. Sakurai, S. Shimoura,[*4] E. Takeshita,[*2] S. Takeuchi, M. Tamaki,[*4] Y. Togano,[*2] K. Yamada,[*2] Y. Yanagisawa, and K. Yoneda,

[NUCLEAR STRUCTURE, Unstable nuclei, γ-ray spectroscopy]

The aim of this work was to investigate the N=20 shell gap by studying the ^{27}Ne and ^{28}Ne nuclear structures. By detecting their low–lying bound excited states, we intended to answer whether N=20 is a magic number far from stability by comparing the experimental results with theoretical calculations. In this experiment, a 94 A·MeV energy primary beam of ^{40}Ar with an intensity of 60 pnA hit a ^{181}Ta production target of 0.5 cm thickness. Reaction products were momentum and mass analyzed using the RIPS fragment separator. The secondary beam included neutron-rich ^{24}O, ^{25,26,27}F, ^{27,28,29,30}Ne and ^{29,30,31,32}Na nuclei. The RIPS was operated at a momentum acceptance of 6% . The total intesity was approximately 100 cps. Incident beam species were identified on the basis of energy loss, time of flight and magnetic rigidity ($B\rho$). The secondary beam was transmitted to a liquid hydrogen target at the final focus of the RIPS. The average areal density of the hydrogen target was 210 mg/cm^2. The position of the incident particles was determined using two PPACs placed at F3 upstream of the target. The scattered particles were detected and identified using a PPAC and a silicon telescope. The telescope consisted of three layers with thicknesses of 0.5, 0.5 and 1 mm. Z identification was performed by a TOF-energy loss method. On the basis of ΔE-E information, isotope separation was carried out among the different neon isotopes. The DALI2 setup, including 146 NaI(Tl) scintillator detectors, was used to surround the target to detect de–exciting γ rays emitted by the inelastically scattered nuclei. In Fig. 1, the resulting γ–ray spectra can be observed. Determining the cross sections of γ-rays in ^{28}Ne, and using the previously measured B(E2), the neutron and proton transition matrix elements were deduced by DWBA analysis. The neutron transition probability was found to be more or less enhanced compared with pure *sd* shell model calculations depending on the effective charge. The number of bound excited states observed in ^{27}Ne by knocking out a neutron from ^{28}Ne was observed to be larger than that predicted using the *sd* shell model. The presence of a low-lying extra state intruding from the upper fp shell can be considered as an indication of a strongly reduced N=20 shell gap.

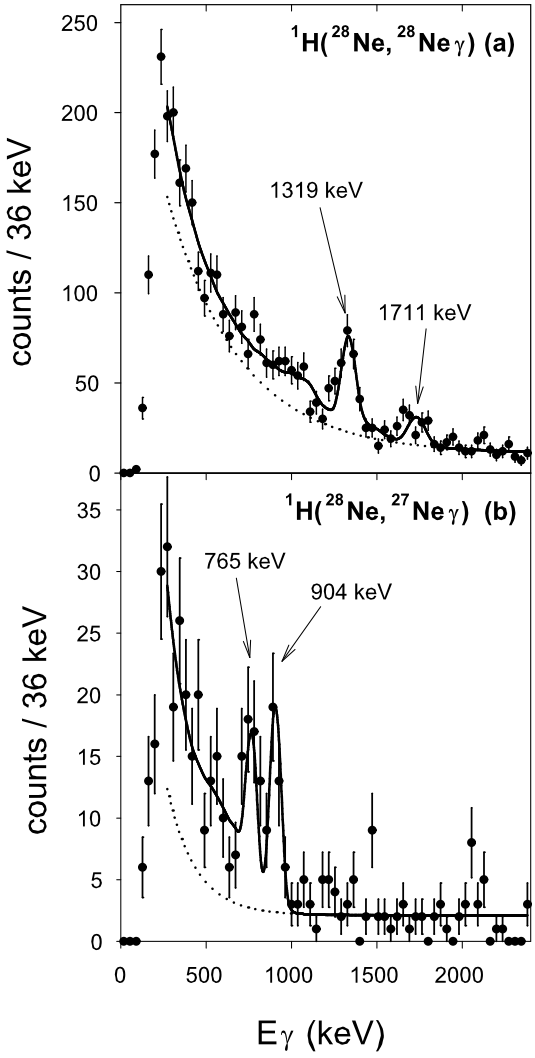

Fig. 1. Doppler-corrected spectra of γ rays emerging from ^{1}H(^{28}Ne,^{28}Ne) (a) and ^{1}H(^{28}Ne,^{27}Ne) (b) reactions. The solid line is the final fit including the spectrum curves from GEANT4 simulation and additional smooth polynomial backgrounds plotted as dotted lines for each nucleus.

† Condensed from article in Phys. Rev. Lett. **96**, 182501 (2006)

*1 Insitute of Nuclear Research (ATOMKI)
*2 Rikkyo University
*3 Institut de Physique Nucléaire
*4 University of Tokyo
*5 Kyoto University
*6 University of Tsukuba

Electric quadrupole moment of ^{31}Al

D. Nagae,[*1] H. Ueno, D. Kameda, M. Takemura,[*1] K. Asahi,[*1] K. Takase,[*1] A. Yoshimi, T. Sugimoto, T. Nagatomo, M. Uchida,[*1] K. Shimada,[*1] T. Arai,[*1] T. Inoue,[*1] S. Kagami,[*1] N. Hatakeyama,[*1] H. Kawamura,[*2] and K. Narita[*2]

[Nuclear structure, spin-polarized RI beam, electric quadrupole moment, β-NQR method]

In a region of island of inversion, nuclei are known to have a deformed shape. Neutron-rich Al isotopes, located near the borderline of the island of inversion, are important nuclei in investigating the mechanism of inversion. The electric quadrupole moment (Q moment) is sensitive to nuclear deformation. We have measured the Q moment of ^{31}Al by a β-detected nuclear-quadrupole resonance (β-NQR) method.

An ^{31}Al beam was obtained from the fragmentation of ^{40}Ar projectiles at an energy of E = 95 MeV/nucleon on a ^{93}Nb target of 0.37 g/cm^2 thickness. To obtain a spin-polarized ^{31}Al beam, the emission angle and outgoing momentum were selected[1]. Thus, fragments emitted at angles $\theta = 1.3^\circ - 5.7^\circ$ were accepted by RIPS using a beam swinger installed upstream of the target. A range of momentum $0.99p_0$ – $1.05p_0$, where $p_0 = 12.4$ GeV/c is a peak position in the momentum distribution, was selected by a slit at the momentum-dispersive focal plane. Spin-polarized fragments were introduced into the NQR apparatus located at the final focus. The experimental setup around a stopper was almost similar to that used in a μ-moment experiment[2]. ^{31}Al ions were implanted in an α-Al_2O_3 single-crystal stopper to which the static magnetic field $B_0 \sim 500$ mT was applied from bottom to top to maintain spin polarization. The angle $\theta_{c\text{-axis}}$ between the crystal c-axis and the B_0 direction was set at $\theta_{c\text{-axis}} = 0^\circ$.

In the β-NQR method, β-rays emitted from the implanted fragments were detected with plastic scintillator telescopes located above and below the stopper. The up/down ratio R of β-ray counting rates was expressed as $R \approx a(1 + 2A_\beta P)$ when $A_\beta P$ was small ($A_\beta P \ll 1$), where a is a constant factor representing asymmetries in counter solid angles and efficiencies. The spin reversal P to $-P$ was detected through a corresponding change, $R \approx a(1 + 2A_\beta P)$ to $R' \approx a(1 - 2A_\beta P)$. When the polarization was altered by a resonant spin change, a change appeared at the ratio $R'/R \approx 1 - 4A_\beta P$. Thus, the resonant frequency $\nu_Q = eqQ/h$ was derived from the observed peak or dip in a β-NQR spectrum, where eq, Q, and h denote the electric field gradient, the Q moment, and Planck's constant, respectively.

The Q moment was obtained using the electric field gradient $eq = 70.9(5) \times 10^{19}$ V/m^2 at an Al site in an α-Al_2O_3 sample[3]. Figure 1 shows the β-NQR spectra obtained for the ground states of ^{31}Al with the sweep width $\triangle\nu_Q$ = 411 kHz.The vertical and horizontal axes denote the R'/R ratio and ν_Q, respectively. Here, the horizontal bar indicates $\triangle\nu_Q$, whereas the vertical bar shows a statistical error in the R'/R ratio. The quadrupole coupling constant of ^{31}Al in α-Al_2O_3 was measured to be $\nu_Q = 1786(98)$ kHz. The Q moment of ^{31}Al was determined to be $|Q(^{31}\text{Al})| = 104(7)$ e·mb.

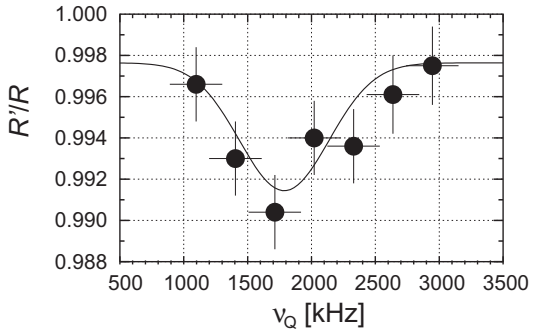

Fig. 1. NQR spectra obtained for ^{31}Al implanted in a α-Al_2O_3 stopper. The R'/R values are plotted as a function of the parameter ν_Q.

The obtained $|Q(^{31}\text{Al})|$ is smaller than that of obtained by shell model calculation performed using the code OXBASH[4] with USD interaction[5]. The proton and neutron effective charges $e_p = 1.3$ and $e_n = 0.5$ were used. The theoretical Q moment of ^{31}Al is 151 e·mb. A notable difference between the theoretical and experimental Q moments is observed. The *sd*-space shell model calculation is known to underestimate the Q moments of the nuclei in the region of island of inversion, since the $N = 20$ shell closure does not occur in these nuclei. The observed Q moment is even smaller than that obtained by *sd*-shell calculation. This finding indicates that ^{31}Al is located outside the island of inversion. Further analyses are now in progress.

[*1] Department of Physics, Tokyo Institute of Technology
[*2] Department of Physics, Rikkyo University

References
1) K. Asahi et al.: Phys. Lett. B **251**, 488 (1990).
2) H. Ueno et al.: Phys. Lett. B **615**, 186 (2005).
3) D. Sundholm et al.: Phys. Rev. Lett. **68**, 927 (1992).
4) B.A. Brown, A. Etchegoyen, and W.D.M. Rae : OXBASH, MSU Cyclotron Laboratory Report No. 524, 1986.
5) B.H. Wildenthal: Prog. Part. Nucl. Phys. **11**, 5 (1984).

Test experiment on ^{32m}Al isomeric moment

K. Takase,[*1] D. Kameda, H. Ueno, Y. Kobayashi, A. Yoshimi, T. Sugimoto, T. Nagatomo, K. Shimada,[*1] D. Nagae,[*1] M. Takemura,[*1] T. Inoue,[*1] T. Arai,[*1] M. Uchida,[*1] H. Watanabe[*2], and K. Asahi

[nuclear structure, TDPAD, isomer, ^{32}Al, neutron-rich nuclei]

In previous β-NMR studies, the magnetic[1] and electric quadrupole moments[2] of ^{32}Al were found to be well described by the normal *sd*-shell structure, in contrast to the neighbors, namely, ^{31}Mg and ^{32}Mg, which are reported to be strongly deformed nuclei[3,4]. However, the spacing and ordering of the low-lying excited levels of ^{32}Al including the 957 keV isomeric state of $T_{1/2} = 200(20)$ ns[5] were not reproduced well by the conventional *sd*-shell models, suggesting the presence of a pf-intruder structure with low excitation energies. To obtain further information on the wave functions of the low-lying excited levels of ^{32}Al, we introduce a measurement of the g-factor of the isomeric state using the time differential perturbed angular distribution (TDPAD) method[6]. We have thus constructed a prototype setup for this purpose, and obtained the γ-decay spectrum of ^{32m}Al.

The experiment was performed at the RIKEN Ring Cyclotron. ^{32}Al nuclei were produced through the projectile fragmentation reaction of a 95 MeV/nucleon ^{40}Ar primary beam with a 369 mg/cm^2-thick Nb target and were selected in RIPS. We restricted the emission angles of ^{32}Al fragments in the region = 1.0 +3.4 , and their momenta were apporoximately p_c =12.5 GeV/c with an acceptance of $\pm$3 %, in which p_c corresponded to the peak of the fragment yield. The ^{32}Al nuclei were implanted into a single-crystal-Si stopper placed between the poles of an electromagnet that provided a static magnetic field B_0 $\sim$0.5 T in the reaction normal. A schematic drawing of the setup is shown in Fig. 1. The two γ-ray lines, namely, 222 keV and 735 keV, cascading from the 957 keV isomeric state via the intermediate energy level of 735 keV were detected using four 5.5″ $\times$ 5.5″ NaI(Tl) scintillators located around the stopper as shown in Fig. 1. We also used two coaxial high-purity germanium detectors beside and behind the stopper to obtain γ-ray energies, in particular, for the background events. The thin plastic scintillator (F3PL in Fig. 1) located 20 cm upstream of the stopper was used in order to provide $t = 0$ signals, "^{32}Al coming", for the subsequent γ-decay. We collected only γ events in coincidence with a 1.5 μs time window of $t = 0$ signals. Each photomultiplier connected to the NaI scintillator was housed in a 2 mm-thick μ-metal magnetic shield, and its head was set about 100 cm from the center of the magnet pole to eliminate the influence of the magnetic field.

[*1] Department of Physics, Tokyo Institute of Technology
[*2] Department of Nuclear Physics, The Australian National University, Australia

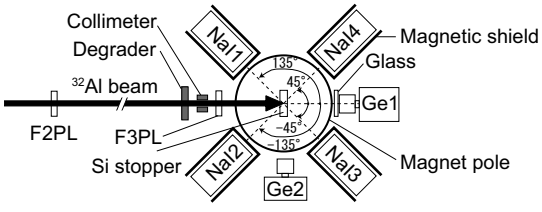

Fig. 1. Setup and geometry of detectors.

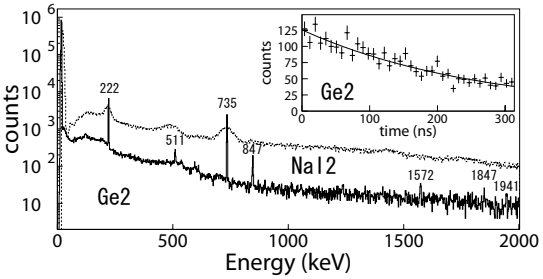

Fig. 2. Energy spectrum for Ge2 and NaI2, and 222 keV decay spectrum for Ge2.

Energy spectra for Ge2 and NaI2 are shown in Fig. 2. 222 keV and 735 keV γ-rays can clearly be seen. Also, several other peaks were assigned: 511 keV as the positron-electron annihilation, 846.8 keV as the prompt γ-ray from the ^{56}Fe 2_1^+ state, and 1572.3 keV, 1847.0 keV and 1941.4 keV for the β-delayed γ from the beam contaminations (^{35}P,^{33}Si and ^{32}Al), respectively. The decay spectrum of Ge2 obtained with a gate of 222 keV is also shown in Fig. 2. We derived $T_{1/2} = 196(16)$ ns, which is in good agreement with 200(20) ns[5]. The high background levels of the NaI scintillators prevented us from determining a precise half life. Background elimination and other analyses are now in progress.

References
1) H. Ueno et al.: Phys. Lett. B 615, 186 (2005).
2) K. Kameda et al.: Phys. Lett. B 647, 93 (2007).
3) G. Neyens. et al.: Phys. Rev. Lett. 94, 022501 (2005).
4) T. Motobayashi et al.: Phys. Lett. B 346, 9 (1995).
5) M. Robinson et al.: Phys. Rev. C 53, R1465 (1996).
6) G. Goldring et al.: in *Treatise in Heavy Ion Sciences*, edited by D. E. Bromley (Plenum Press, New York, 1985), Vol. 3, p. 539.

Direct capture component in ^{26}Si(p,γ)^{27}P reaction

Y. Togano,[*1] T. Gomi,[*2] T. Motobayashi, Y. Ando,[*1] N. Aoi, H. Baba, K. Demichi,[*1] Z. Elekes,[*3] N. Fukuda, Zs. Fülöp,[*3] U. Futakami,[*1] H. Hasegawa,[*1] Y. Higurashi, K. Ieki,[*1] N. Imai,[*4] M. Ishihara, K. Ishikawa,[*5] N. Iwasa,[*6] H. Iwasaki,[*7] S. Kanno, Y. Kondo,[*5] T. Kubo, S. Kubono,[*8] M. Kunibu,[*1] K. Kurita,[*1] Y. U. Matsuyama,[*1] S. Michimasa, [*8] T. Minemura, [*9] M. Miura,[*5] H. Murakami,[*1] T. Nakamura,[*5] M. Notani,[*10] S. Ota,[*8] A. Saito,[*8] H. Sakurai, M. Serata,[*1] S. Shimoura,[*8] T. Sugimoto, E. Takeshita, S. Takeuchi, K. Ue,[*7] K. Yamada, Y. Yanagisawa, K. Yoneda, and A. Yoshida

[^{208}Pb(^{27}P,p^{26}Si)^{208}Pb, Coulomb dissociation, Nuclear astrophysics]

The stellar ^{26}Si(p,γ)^{27}P reaction has been investigated by analyzing the Coulomb dissociation of ^{27}P. The galactic γ line at 1.8 MeV associated with ^{26}Al β decay is observed using satellite telescopes[1]. This reaction is suggested to affect the synthesis of ^{26}Al in novae and X-ray bursts. Direct proton capture is particularly important at stellar temperatures lower than 0.1 GK. The astrophysical S-factor was deduced by Guo et al. from the asymptotic normalization coefficients (ANCs) of the mirror nucleus ^{27}Mg[2]. Caggiano et al. estimated the S-factor using a shell model calculation[3]. In this report, these estimates are compared with the result experimentally obtained by the Coulomb dissociation of ^{27}P.

The experiment was performed using RIPS at the RIKEN Accelerator Research Facility. Details of the experimental setup are described in Ref. 4. The relative p-^{26}Si energy spectrum is shown in Fig. 1. The filled circles represent the experimental data. The solid curve shows the best fit with five components shown by the dotted and dashed curves. The detector responses were obtained using a Monte-Carlo simulation. Four resonant breakup components are represented by the dotted curves. The peak at 0.31 MeV corresponds to the known first excited state at 1.2 MeV in ^{27}P[3]. The bump at around 1 MeV is due to the known second excited state at 1.6 MeV and an unknown one at 2.0 MeV. The peak at 2.1 MeV is also due to an unknown one at around 3 MeV. The results of the resonant state are described in Ref. 4. The direct breakup component, which is shown by the dashed curve, corresponds to the direct proton capture process in the ^{26}Si(p,γ)^{27}P reaction.

An energy-independent E1 S-factor is assumed in the calculation of the direct breakup component. The dot-dashed curve shows the calculated results using the S-factors deduced by Guo et al.[2] (8.7 $\times 10^{-2}$ MeV b) and Caggiano et al.[3] (3.6 $\times 10^{-2}$ MeV b), respectively. Both calculated results are significantly larger than the present result of direct breakup component, suggesting a lower reaction rate at T $<$ 0.1 GK. The preliminarily extracted S-factor is 1.2 $\times 10^{-2}$ MeV b. In this analysis, we cannot resolve possible resonances in higher relative energies; thus, this result is regarded as an upper bound of the direct component. Therefore, the ambiguity in this result cannot explain the difference among the three results shown in Fig. 1, suggesting uncertainties in the shell model calculation or in the procedure used to extract the S factor from the ANC of the mirror nucleus.

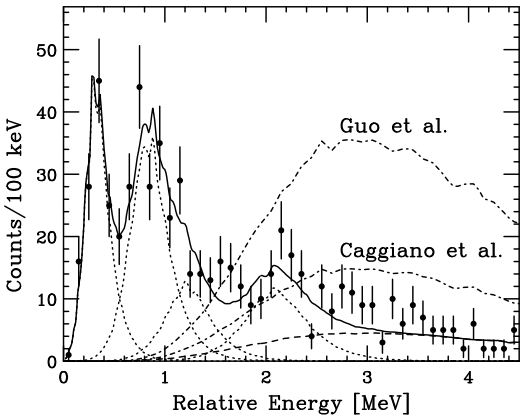

Fig. 1. Relative energy spectrum of ^{27}P breakup on Pb (filled circles). The data were fitted by taking into account the detector responses. The solid and dotted curves represent the best fit and individual components, respectively. The dashed curve denotes the direct breakup component. The dot-dashed curves show the calculated direct breakup component using the S-factors derived by Guo et al. and Caggiano et al.

*1 Department of Physics, Rikkyo University
*2 National Institute of Radiological Sciences
*3 Institute of Nuclear Research of the Hungarian Academy of Sciences (ATOMKI), Hungary
*4 Institute of Particle and Nuclear Studies, High Energy Accelerator Research Organization (KEK)
*5 Department of Physics, Tokyo Institute of Technology
*6 Department of Physics, Tohoku University
*7 Department of Physics, University of Tokyo
*8 Center for Nuclear Study, University of Tokyo
*9 National Cancer Center
*10 Argonne National Laboratory, USA

References

1) R. Diehl et al.: Astron. Astrophys. Suppl. 97, 181 (1993).
2) B. Guo et al.: Phys. Rev. C 73, 048801 (2006).
3) J. A. Caggiano et al.: Phys. Rev. C 64, 025802 (2001).
4) Y. Togano et al.: Eur. Phys. J. A 27, s01, 233 (2006).

Study of astrophysically important resonant states in ^{26}Si by ^{28}Si(^{4}He,^{6}He)^{26}Si reaction†

Y. K. Kwon,[*1] C. S. Lee,[*1] J. Y. Moon,[*1] J. H. Lee,[*1] J. Y. Lee,[*1] S. Kubono,[*2] N. Iwasa,[*3] K. Inafuku,[*3] H. Yamaguchi,[*2] J. J. He,[*2] A. Saito,[*2] Y. Wakabayashi,[*2] H. Fujikawa,[*2] G. Amadio,[*2] L. H. Khiem,[*4] M. Tanaka,[*5] A. Chen,[*6] S. Kato, [*7] Y. Fuchi, [*5] and N. Fukunishi [*8]

[Nuclear astrophysics, Two-nucleon transfer reaction, Magnetic spectrograph]

The emission of 1.809 MeV gamma ray from the first excited state of ^{26}Mg followed by the β decay of ^{26}Al in its ground state (denoted as ^{26}Al$_{g.s.}$) has been identified by gamma-ray telescopes such as those in the Compton Gamma-Ray Observatory (CGRO)[1]. To resolve the controversy over the possible sources of the observed 1.809 MeV gamma rays, one needs knowledge of the production rate of ^{26}Al. One possible source of the production of ^{26}Al$_{g.s.}$ is nova explosion[2]. Under the explosive hydrogen burning conditions in a nova site, production proceeds via the reaction sequence

$$^{25}Al(\beta^{+}\nu)^{25}Mg(p,\gamma)^{26}Al^{g.s.}(\beta^{+}\nu)^{26}Mg^{*}(\gamma)^{26}Mg^{g.s.}.$$

However, if the proton capture rate on ^{25}Al is faster than the β-decay rate of ^{25}Al, the above reaction sequence is bypassed by the

$$^{25}Al(p,\gamma)^{26}Si(\beta^{+}\nu)^{26}Al^{m}(\beta^{+}\nu)^{26}Mg^{g.s.}$$

reaction sequence. By shell model calculations and mirror nucleus consideration using past data, Illiadis et al.[3] suggested that the ^{25}Al$(p,\gamma)^{26}$Si reaction should be predominated by the 3^{+} unnatural parity state (E$_x$=5970(100) keV). Recent studies of ^{28}Si$(p,t)^{26}$Si[4], ^{24}Mg$(^{3}He,n\gamma)^{26}$Si[5], and ^{29}Si$(^{3}He,^{6}He)^{26}$Si[6] reduced the uncertainties in the ^{26}Si levels above the proton threshold and identified new states as candidates for the unnatural parity states. However, for such candidates, they[4–6] could not make any spin assignment directly using angular distribution measurement. In this work, we decided to study the astrophysically important resonant states in ^{26}Si via the ^{28}Si$(^{4}He,^{6}He)^{26}$Si reaction, which could excite an unnatural parity state directly, in contrast with the (p,t) reaction, which cannot excite an unnatural parity state.

The ^{28}Si$(^{4}He,^{6}He)^{26}$Si reaction was studied using a high-resolution QDD(quadrupole-dipole-dipole)-type magnetic spectrograph (PA) at the Center for Nuclear Study (CNS), University of Tokyo. A beam of ^{4}He at 120 MeV was extracted from RIKEN linear accelerator (RILAC) + RIKEN ring cyclotron (RRC). The beam intensity was typically 70 enA at the target position. A self-supporting natural silicon target (thickness $\sim$ 1 mg/cm^2) was used to populate states in ^{26}Si. The focal plane detection system consisted of a hybrid gas counter and plastic scintillators. Four proportional gas counters, namely, two position counters (X1 and X2) and two energy loss counters (ΔE1 and ΔE2) were installed in the hybrid drift chamber.

Table 1. Candidates for 3^{+} resonant state with previous results.

(p,t) [4]		$(^{3}He,n\gamma)$ [5]		$(^{3}He,^{6}He)$ [6]		This work
$E_x(keV)$	J^{π}	$E_x(keV)$	J^{π}	$E_x(keV)$	J^{π}	$E_x(keV)$
5916(2)	0^{+}	5912(4)	3^{+}			5918(8)
		5946(4)	0^{+}	5945(8)	3^{+}	

To obtain information on the level structure in ^{26}Si, we have measured the angular distribution at θ_{lab} = 8°, 11°, 15°, and 20°. The overall energy resolution was 100 keV (FWHM). The excitation energies below E$_x$ = 5.5 MeV are well in agreement with those from previous experimental results[4–6]. For the 3^{+} resonant state, the study of the $(^{3}He,^{6}He)$ reaction[6] suggested the spin-parity assignment of 3^{+} for the 5945 keV state by Coulomb shift calculation. The study of the $(^{3}He,n\gamma)$ reaction[5] suggested 5912 keV as a 3^{+} resonant state from the comparison of the measured differential cross section with the Hauser-Feshbach calculations. However, in the (p,t) reaction study[4], a 5916 keV was assigned directly as a 0^{+} state by the distorted-wave Born approximation (DWBA) analysis. We observed a 5918 keV state in our measurement. To clarify this level of information clearly, spin-parity assignment by DWBA calculation is in progress. We also observed several candidates for unnatural parity states at 5612 keV, 5825 keV, 6004 keV, and 6107(8) keV.

*1 Department of Physics, Chung-Ang University, Korea
*2 CNS, Graduate School of Science, University of Tokyo
*3 Department of Physics, Tohoku University
*4 Institute of Physics and Electronics, Vietnam
*5 KEK (The High Energy Accelerator Organization)
*6 Department of Physics and Astronomy, McMaster University, Canada
*7 Department of Physics, Yamagata University
*8 RIKEN

References
1) N. Prantzo and R. Diehl; Phys. Rep. **267**, 1 (1996).
2) R. D. Gerhz, J. W. Truran, R. E. Williams, and S. Starrfield; Publ. Astron. Soc. Pac. **110**, 3 (1998).
3) C. Illiadis et al.; Phys. Rev. C **53**, 475 (1996).
4) D. Bardayan et al.; Phys. Rev. C **65**, 032801(R)(2002).
5) Y. Parpottas et al.; Phys. Rev. C **70**, 065805 (2004).
6) J. A. Caggiano et al.; Phys. Rev. C **65**, 055801 (2002).

Cluster structures of even-even oxygen isotopes

N. Furutachi,[*1] M. Kimura,[*2] and S. Oryu [*1]

[Nuclear structure, cluster structure, unstable nuclei]

The importance of the cluster structure in unstable nuclei has been revealed through the studies of the 2 -clustering of neutron-rich Be isotopes. Oxygen isotopes are interesting targets for investigating the clustering systematics in unstable and N≠Z stable nuclei, because ^{16}O has the well-established ^{12}C+ structure in its excited state.

It has been known for a long time that the deformed 4p-2h configuration coexists with the ordinary $(sd)^2$ shell model space in the low-lying states of ^{18}O. There have been many investigations on the ^{14}C+ structure of ^{18}O both in theory[1] and in experiment[2], and the importance of the ^{14}C+ structure of ^{18}O has been revealed. The next question is whether or not the cluster correlation survives in ^{20}O. The cluster correlation may survive as in the case of ^{12}Be. However, there has been no investigation on the cluster structure of ^{20}O, although the coexistence of the 6p-2h configuration in the low-lying states of ^{20}O is suggested[3].

We have investigated the cluster structures of ^{18}O and ^{20}O, using the AMD+GCM framework. The AMD can describe the cluster structure together with the shell-like structure without any assumption on nuclear structure. Therefore, this framework is appropriate for investigating the cluster structure in unstable nuclei.

We have obtained excited rotational bands that have the cluster structures in ^{18}O and ^{20}O. The obtained rotational bands are shown in Fig. 1, and the density distributions of the intrinsic wave functions, which dominantly construct the bands, are also shown. We have found the ^{14}C+ cluster structure in ^{18}O. The $K^\pi=0^+$ band dominantly has the ^{14}C+ cluster structure, and the moment of inertia approximately agrees with that of the experimental candidates. Although the cluster state is fragmented into several states, the $K^\pi=0^-$ band also has the ^{14}C+ cluster structure. The $K^\pi=0^-$ band can be regarded as the parity doublet partner of the $K^\pi=0^+$ band. We have found more complicated structures in ^{20}O. The $K^\pi=0^+$ rotational band is obtained from the mixing of the ^{12}C+ +4n-like and ^{14}C+^{6}He-like cluster structures. The excitation energy of this state is much smaller than the ^{14}C+^{6}He threshold energy. The ^{14}C+^{6}He-like cluster structure also contributes to the $K^\pi=0^-$ band. Although mixing with the ^{12}C+ +4n-like structure is not seen in the $K^\pi=0^-$ band, this band can be regarded as the parity doublet partner of the $K^\pi=0^+$ band. Furthermore, the ^{16}C+ cluster structure has been obtained. The ^{16}C+ cluster structure also constructs the parity doublet $K^\pi=0^+$ and 0^- bands.

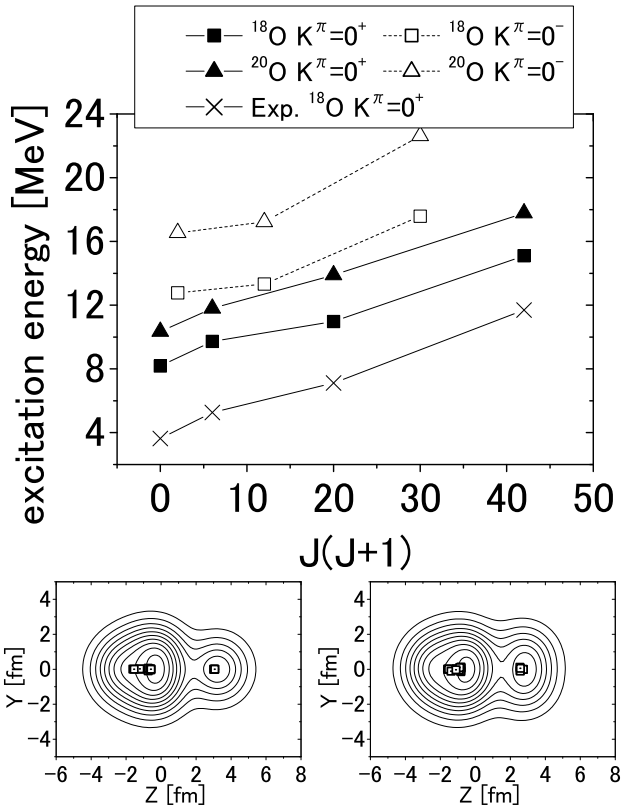

Fig. 1. Excited rotational bands of ^{18}O and ^{20}O. The matter density distributions of the intrinsic states that contribute to the $K^\pi=0^+$ band of ^{18}O (left side) and ^{20}O (right side) are also shown. The centers of the single-particle wave packet are plotted with density distributions using squares.

References

1) P. Descouvemont and D. Baye: Phys. Rev. C 31, 2274 (1985).
2) D. R. Tilley, H. R. Weller, C. M. Cheves, and R. M. Chasteler: Nucl. Phys. A 595, 1 (1995).
3) S. LaFrance, H. T. Fortune, S. Mordechai, M. E. Cobern, G. E. Moore, R. Middleton, W. Chung, and B. H. Wildenthal: Phys. Rev. C 20, 1673 (1979).

[*1] Department of Physics, Tokyo University of Science
[*2] Institute of Physics, Tsukuba University

Search for neutron decoupling in ^{22}O via (d,d'γ) reaction

Z. Elekes,[*1] Zs. Dombrádi,[*1] S. Bishop, Zs. Fülöp,[*1] J. Gibelin,[*2] T. Gomi, Y. Hashimoto,[*3] N. Imai, N. Iwasa,[*4] H. Iwasaki,[*5] G. Kalinka,[*1] Y. Kondo,[*3] A.A. Korsheninnikov,[*8] K. Kurita,[*6] M. Kurokawa, N. Matsui,[*3] T. Motobayashi, T. Nakamura,[*3] T. Nakao,[*5] E.Yu. Nikolskii,[*8] T.K. Ohnishi,[*5] T. Okumura,[*3] S. Ota,[*7] A. Perera, A. Saito,[*5] H. Sakurai,[*5] Y. Satou,[*3] D. Sohler,[*1] T. Sumikama, D. Suzuki,[*5] M. Suzuki,[*5] H. Takeda,[*7] S. Takeuchi, Y. Togano[*6] and Y. Yanagisawa

[NUCLEAR STRUCTURE, Unstable nuclei, gamma-ray spectroscopy]

The experiment was performed in RIKEN where a 94 A·MeV energy primary beam of ^{40}Ar with 60 pnA intensity hits a ^{9}Be production target of 0.3 cm thickness. The reaction products were momentum and mass analyzed by the RIPS fragment separator. The total intensity was approximately 1500 cps having an average ^{22}O intensity of 600 cps. The identification of incident beam species was performed by energy loss and time-of-flight. The secondary beam was transmitted to a secondary CD_2 target of 30 mg/cm^2 at the final focus of RIPS. The reaction occurred at an energy of 34 A·MeV. The position of the incident particles was determined by two PPACs placed at F3 upstream of the target. The scattered particles were detected and identified by a 2 x 2 matrix silicon telescope placed 96 cm downstream of the target. 80 NaI(Tl) scintillator detectors surrounded the target to detect de–exciting γ rays emitted by the inelastically scattered nuclei. In Fig. 1. the Doppler–corrected γ–ray spectra of ^{22}O nucleus is presented. The position of the single peak was determined at 3185(15) keV. The above energy for ^{22}O is in a good agreement with the 3199(8) keV determined earlier[1)]. After the peak position has been determined, we calculated the cross section for the ^{22}O+^{2}H reaction to be $\sigma(0_1^+ \rightarrow 2_1^+)$=19±3 mb. From a distorted wave analysis, we derived the "matter" deformation length to be δ_M=0.77±0.07 fm, which corresponds to a moderate mass deformation of β_M=0.23±0.02. We can compare this result with the data from the ^{22}O+^{197}Au reaction[2)] where the proton deformation β_p was derived to be between 0.2 and 0.24. This means that the neutron deformation of ^{22}O is very similar to the proton deformation taking into account the mass deformation determined in this study. This result is in contrast with the expectations that the increasing neutron number may lead to a stronger neutron decoupling. In reality, the $M_n/M_p \sim \beta_n/\beta_p$ ratios are 2, 3 and 1 for ^{18}O, ^{20}O and ^{22}O, respectively. The increasing trend is suppressed by the N=14 subshell closure, which makes both the proton and neutron distributions nearly spherical in ^{22}O.

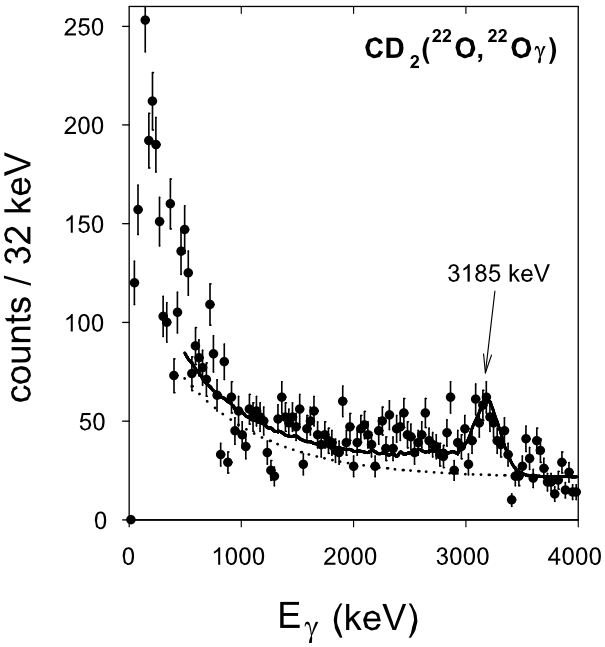

Fig. 1. Doppler-corrected spectra of γ rays emerging from ^{22}O+CD_2 reaction. The solid line is the final fit including the spectrum curve from GEANT4 simulation and an additional smooth polynomial background is plotted as a separate dotted line.

References

1) M. Stanoiu et al.: Phys. Rev. **C69**, 034312 (2004).
2) P. G. Thirolf et al.: Phys. Lett. **B485**, 16 (2000).

† Condensed from article in Phys. Rev. **C71**, 017306 (2006)

*1 Institute of Nuclear Research (ATOMKI)
*2 Institut de Physique Nucléaire
*3 Tokyo Institute of Technology
*4 Tohoku University
*5 University of Tokyo
*6 Rikkyo University
*7 Kyoto University
*8 Kurchatov Institute

Proton elastic scattering from light unstable nuclei at intermediate energies

S. Terashima, H. Takeda, H. Otsu, K. Yoneda, T. Ichihara, T. Suda, H. Sakaguchi,[*1] J. Zenihiro, [*2] Y. Iwao, [*2] A. Yoshida, [*2] T. Murakami, [*2] Y. Matsuda, [*3] T. Kobayashi,[*3] Y. Satou, [*4] and K. Ozeki[5]

[Nuclear structure, elastic scattering, unstable nuclei]

Proton elastic scattering at intermediate energies (200-400MeV) is a useful method of exploring matter density distributions in a nucleus. Due to the long mean free path in a nuclear medium, we can extract a more precise information of matter distribution. RIBF will provide a wide variety of unstable nucleus beams at intermediate energies. By measuring energies and scattering angles of recoil protons in inverse kinematics, we can distinguish between elastic and inelastic scattering. For this purpose, we have been developing a detector system including incident beam detectors.[1)]

This year, we performed two experiments at the Heavy-Ion Medical Accelerator in Chiba (HIMAC) facility in the National Institute of Radiological Science (NIRS). First, we performed a pilot experiment using a ^{20}O beam with a thin solid hydrogen target (SHT)[2)] to study matter distributions. The secondary beam of ^{20}O at 300 MeV/nucleon was produced by bombarding a 390MeV/nucleon ^{22}Ne beam on a ^{9}Be target. The intensity of ^{20}O was 10^5 particles/spill on the SHT. The momentum bite of the incident beam was $\pm$1%, which was determined event-by-event using a 2 mm segmented fiber scintillator on the dispersive focal plane (F1)[3)]. The beam was achromatically transported to the SHT. The thickness of the SHT was 1 mm, which was covered with 9 μm aramid windows on both sides. We have not yet established a method of fabricating a SHT that is uniformly a 1 mm thick, the thickness of the SHT we used was not uniform. The position and angle of the incident beam on the SHT were determined using a set of beam line multiwire drift chambers (BDCs). The distance between the BDCs was 1 m, the position resolution of each plane was estimated to be about 200 μm[σ]. The energies and angles of recoil protons from the SHT were measured using two sets of recoil detector arrays, which consisted of recoil multiwire drift chambers (RDCs), thin (2 mm) plastic scintillators, and NaI(Tl) scintillators. A recoil detector array covered a range between 67 and 84 degrees in the laboratory frame. Recoil protons were identified by the ΔE-E method using the plastic scintillator and the NaI(Tl) scintillators. Scattering angle was extracted from the angles of the incident beam and recoil protons.

*1 Department of Applied Physics, Miyazaki university
*2 Department of Physics, Kyoto university
*3 Department of Physics, Tohoku university
*4 Department of Physics, Tokyo Institute of Technology
*5 Cyclotron and Radioisotope Center, Tohoku university

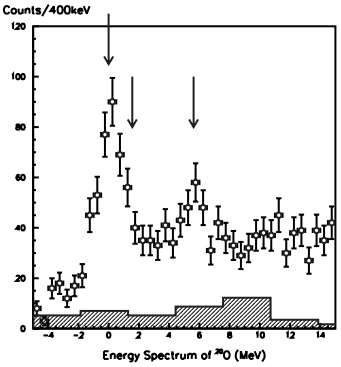

Fig. 1. Energy spectrum of scattered ^{20}O. The three arrows indicate 0^+(g.s.),2^+(1.64MeV), and 3^-(5.61MeV) [4)]. Hatched area is the background from mainly aramid window of the SHT estimated without SHT runs.

Figure 1 shows the preliminary energy spectrum of scattered ^{20}O. The energy resolution obtained in this study was 4-5 times worse than the design value. The resolution was mainly limited by the angular resolution of recoil protons. Further analysis including the improvement of tracking recoil protons and gain correction against position dependence of NaI(Tl) is now in progress. In the next run, we are going to improve angular resolution by adding anode planes to RDCs, and also to establish the method of fabricating a 1 mm-thick SHT to determine absolute cross sections.

Next, we developed low-energy recoil proton measurement. By measuring low-energy protons, we can cover an additional low-momentum transfer region. Because we need to use a thinner target, we used a $(CH_2)_n$ target instead of the SHT. Low-energy recoil protons were measured using three sets of silicon telescope arrays, which consisted of a 325 μm-thick Si strip detector and two 3 mm-thick Si(Li) detectors. Recoil protons were identified by the ΔE-E method using the Si strip and Si(Li). The determination of the angular distribution of differential cross sections is in progress

References

1) H. Takeda et al: RIKEN Accel. Prog. Rep. **39**, 146(2006).
2) T. Ohnishi et al: RIKEN Accel. Prog. Rep. **38**, 150(2005).
3) Y. Matsuda et al: RIKEN Accel. Prog. Rep. **40**(2007).
4) R.B. Firestone, Table of Isotopes, 8th edn., (1996).

β-decay study of C, N, O isotopes near neutron drip line

T. K. Onishi,[*1] H. Sakurai, H. Iwasaki,[*1] N. Aoi, T. Fukuchi,[*2] T. Fukui,[*3] A. Gelberg,[*4] Y. Ichikawa,[*1] E. Ideguchi,[*5] T. Kishida, M. Liu,[*5] T. Nakao,[*1] M. Niikura,[*5] S. Nishimura, H. J. Ong,[*1] H. Otsu, S. Shimoura,[*5] T. Sumikama, D. Suzuki,[*1] H. Suzuki,[*1] M. K. Suzuki,[*1] N. Yamada, and Y. Zheng[*5]

[Nuclear structure, unstable nuclei, β decay]

One of the most interesting phenomena in nuclei far from the stability line is a variation in magic number. The magic number $N = 20$ is broken in the region of "island of inversion"[?)] and the new magic number $N = 16$ is suggested in oxygen isotopes[?)]. In this region, the proton-neutron ratio becomes imbalance and residual interactions are modified from those in stable nuclei. This causes the modification of the shell structure.

The nuclei with $Z \approx 8$ provide an opportunity to investigate the effects of neutron excess on the *p*-*sd* shell gap of the proton side. In particular, the β decay of the neutron-rich C and N isotopes is an excellent probe. In these nuclei, valence neutrons occupy the *sd* shell, while valence protons occupy the *p* shell. Therefore, intruder states are populated selectively through an allowed transition because of the selectivity of the β decay.

The present study was performed using the RIKEN projectile fragment separator (RIPS) in the RIKEN accelerator research facility. Radioactive ions were produced by the projectile fragmentation of a 63 MeV/nucleon ^{40}Ar primary beam with an intensity of 500 pnA. The production target was Ta with a thickness of 333 mg/cm^2. Reaction fragments were collected and analyzed using RIPS and transported to the final focal plane (F3) of RIPS. Several RIPS settings were used depending on the nuclei of interest. The beam was pulsed for measuring the half-lives of the nuclei. The durations of the beam-on and beam-off periods were tuned to the nuclei of interest. However, if the secondary-beam intensity was lower than $1/\tau$, the beam was not pulsed. In this situation, a β-decay event can be related to a parent nucleus. Therefore, the half-lives were measured using the difference in time between the beam and β decay.

The radioactive ions were implanted into a plastic scintillator with a thickness of 5 mm at F3. This active stopper enables us to count the number of implanted ions.

The active stopper was also used as a β-ray detector. This stopper had two photomultiplier tubes at both ends for rejecting a single photon noise for the efficient detection of β rays.

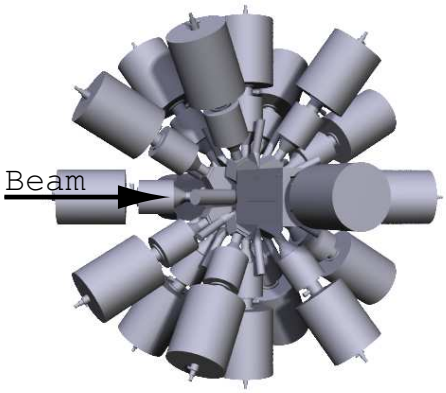

Fig. 1. Experimental setup for observation of β-delayed γ rays

The γ-ray detection system used consisted of two clover-type Ge detectors and a CNS Ge array (GRAPE [?)]). Figure **??** shows a schematic view of this system. The photopeak efficiency of this system was 4.3 % for 1 MeV γ rays. Each clover-type Ge detector was surrounded by an anti-Compton shield consisting of eight BGO scintillators. Each BGO scintillator was 80 $\times$ 250 $\times$ 25 mm^3. Rejecting β ray backgrounds of the Ge detectors, each Ge detector had a plastic scintillator at the front end. Plastic scintillators with a thickness of 1 mm were used for the clover-type Ge detectors and plastic scintillators with a thickness of 5 mm for GRAPE.

We have carried out an experiment involving β-γ measurements for C, N and O isotopes near a neutron-drip line. We observed β-delayed γ rays originating from these nuclei. The analysis of the obtained data is now in progress.

References

1) E. K. Warburton et al.: Phys. Rev. C **41** 1147 (1990).
2) B. A. Brown and W. A. Richier: Phys. Rev. C **72** 057301 (2005).
3) S. Shimoura: Nucl. Instr. and Meth. A **525** 188 (2004).

[*1] Department of Physics, University of Tokyo
[*2] Department of Physics, Osaka University
[*3] Department of Physics, Kyoto University
[*4] Institut für Kernphysik dei Universität zu Köln
[*5] Center for Nuclear Study, Graduate School of Science, University of Tokyo

Reaction cross sections for ^{19}C, ^{20}C and ^{22}C on proton target

K. Tanaka, T. Yamaguchi,[*1] T. Suzuki,[*1] A. Ozawa,[*2] T. Aiba,[*3] N. Aoi, H. Baba, M. Fukuda,[*4] Y. Hashizume,[*2] K. Inafuku,[*5] N. Iwasa,[*5] T. Izumikawa,[*6] K. Kobayashi,[*1] M. Komuro,[*1] Y. Kondo,[*7] M. Kurokawa, T. Matsuyama,[*3] S. Michimasa,[*8] T. Nakabayashi,[*7] S. Nakajima,[*1] T. Ohtsubo,[*3] R. Shinoda,[*1] M. Shinohara,[*7] H. Suzuki,[*9] M. Takechi,[*4] E. Takeshita, S. Takeuchi, Y. Togano,[*10] K. Yamada, T. Yasuno,[*2] M. Yoshitake,[*1] T. Kubo, T. Nakamura,[*7] Y. Sakurai, and T. Motobayashi

[Reaction cross section, unstable nuclei, ^{19}C, ^{20}C, ^{22}C]

Reaction cross sections (σ_R) for ^{19}C, ^{20}C and ^{22}C in the vicinity of the neutron drip line have been measured on a proton target at around 40 MeV /nucleon. ^{22}C has 16 neutrons, which has been found to be a new "magic number" for neutron-rich nuclei.[1] In that case, the energies of the $1d_{3/2}$ and $2s_{1/2}$ orbitals are well separated and the two-valence neutrons of ^{22}C are expected to mainly occupy the $2s_{1/2}$ orbital. The separation energy of the two-valence neutrons is predicted as 0.42 ± 0.94 MeV.[2] These conditions lead to the formation of a large neutron halo; thus a large σ_R would be observed. Because of low beam intensity, σ_R for ^{22}C has never previously been measured. σ_R for ^{19}C and ^{20}C were measured at around 1000 MeV/nucleon and their root-mean-square radii were deduced.[3] If σ_R for these nuclides are measured at lower energy, their density distributions can be deduced from their energy dependences.

The experiment was carried out at RIPS by the transmission method. Figure 1 shows the experimental setup. An ^{40}Ar primary beam of 100-particle nA was provided from the RIKEN ring cyclotron and bombarded a 333 mg/cm^2 Ta production target. The nuclides in the secondary beams were identified event by event using the time of flight (TOF) between two plastic scintillators located at F2 and F3 focal planes, and ΔE signal obtained from two silicon detectors (Si) of 100 μm thickness at F3. With all of the beam slits fully opened, the intensities were 5 cps for ^{19}C, 0.5 cps for ^{20}C and 0.003 cps for ^{22}C.

We modified the setup from the previous one[4] by taking into account the low-intensity beam. We applied liquid hydrogen[5] (liq. H_2) as a reaction target installed at F3 to obtain a higher reaction rate than that using a carbon target which has often been used in previous experiments. To achieve a high accuracy of around 1% for the target thickness over the whole area (40 mmϕ), we improved the liq. H_2 system.[5] We controlled the temperature to 15.9 ± 0.2 K which corresponds to 0.3% accuracy of the density, using a heater system[5] during the measurement. The target thickness was measured by using a laser displacement sensor to within 0.3 mm accuracy. The thickness of the target was estimated to be 205 mg/cm^2. The acceptance after the target was also improved by using a TOF spectrometer[6] of which the bore radius was twice of that of the previous setup.[4]

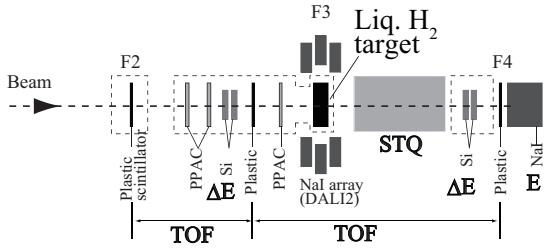

Fig. 1. Setup for this experiment.

Outgoing particles were identified by the TOF-ΔE-E method. The TOF between F3 and F4 was measured using two plastic scintillators, one immediately before F3 and another at F4. The ΔE signal was obtained by using two Si detectors of 320 μm thickness and 123 mmϕ diameter installed at F4. The E signal was obtained via a 5-inchϕ NaI(Tl) detector.

As a preliminary result, σ_R for ^{19}C and ^{20}C were obtained to be around 750 mb with a 10% error, and that of ^{22}C was around 1100 mb with a 20 % error. Although σ_R for ^{22}C has a large error, this result might indicate that ^{22}C has a large halo structure.

References

1) A. Ozawa et al.: Phys. Rev. Lett. **84**, 5493 (2000).
2) G. Audi et al.: Nucl. Phys. A **729**, 337 (2003).
3) A. Ozawa et al.: Nucl. Phys. A **693**, 32 (2001).
4) Y. Yamaguchi et al.: Phys. Rev. C **70**, 054320 (2004).
5) K. Tanaka et al.: RIKEN Accel. Prog. Rep. **39**, 151 (2006), and references therein.
6) N. Aoi et al.: RIKEN Accel. Prog. Rep. **38**, 176 (2005).

[*1] Department of Physics, Saitama University
[*2] Institute of Physics, University of Tsukuba
[*3] Department of Physics, Niigata University
[*4] Department of Physics, Osaka University
[*5] Department of Physics, Tohoku University
[*6] RI Center, Niigata University
[*7] Department of Physics, Tokyo Institute of Technology
[*8] Center of Nuclear Study, University of Tokyo
[*9] Department of Physics, University of Tokyo
[*10] Department of Physics, Rikkyo University

Search for extremely neutron-rich systems ^{7}H, ^{6}H and ^{4}n in the ^{2}H + ^{8}He collisions

E. Nikolskii,[*1] A. Korsheninnikov, H. Otsu, H. Suzuki,[*2] K. Yoneda, H. Baba, K. Yamada, Y. Kondo,[*3] N. Aoi, M. Golovkov,[*4] A. Fomichev,[*4] S. Krupko,[*4] M. Kurokawa, E. Kuzmin,[*5] I. Martel,[*6] W. Mittig,[*7] T. Motobayashi, T. Nakamura,[*3] M. Niikura,[*8] S. Nishimura, A. Ogloblin,[*5] P. Roussel-Chomaz,[*7] A. Sanchez-Benitez,[*6] Y. Satou,[*3] S. Sidorchuk,[*4] T. Suda, S. Takeuchi, K. Tanaka, G. Ter-Akopian,[*4] Y. Togano,[*9] M. Yamaguchi

[Nuclear reactions, d(^{8}He,^{3}He)^{7}H, d(^{8}He,t)^{7}He, unstable nuclei]

The existence of nuclear systems beyond the neutron drip-line is one of the most fascinating problems of nuclear physics. In our previous experiment we obtained experimental evidence for the formation of the ^{7}H state in the p(^{8}He,pp)^{7}H reaction.[1)] An announcement of the observation of stable tetra-neutron ^{4}n was made by the GANIL group.[2)] The first indication on possible existence of the ^{6}H resonance was obtained in the ^{7}Li(^{7}Li,^{8}B)^{6}H reaction about 20 years ago.[3)] We carried out a new experiment aimed to search for ^{7}H, ^{6}H and ^{4}n using ^{8}He secondary beam and deuteron target.

The experiment was performed at the fragment separator RIPS in RIKEN. The primary ^{18}O beam with an energy of 100 A MeV and intensity of ~ 500 particle nA bombarded a ^{9}Be target with a thickness of 12 mm. The secondary beam was a cocktail of ^{8}He and ^{12}Be with the average energies of 42 A MeV and 71 A MeV, and intensities of 1.4×10^{5} and 2.6×10^{5} pps, respectively. As a deuteron target, we used a gas cryogenic target filled with deuterium gas at a temperature of 30 K and a pressure of 0.5 atm resulting in a target thickness of 2.4×10^{20} deuterons/cm^{2}. The beam energy and parameters of the detection system were optimized in complete Monte-Carlo simulations preceding the experiment.

The experimental setup is shown in Fig.1. Two plastic scintillators (at F2 and F3) were used to identify each particle of the secondary beam and to measure its energy by time of flight. Trajectories of individual projectiles were measured by a pair of MWPCs. Recoiling particles like d, t, ^{3}He, ^{4}He and ^{6}Li were detected by the RIKEN telescope of solid-state position-sensitive (strip) Si-detectors with an additional dE-layer, which was an assembly of six thin (~ 40 μ) Si counters. The beam passes through the central hole in the telescope. This telescope allows to identify detected particles and to measure their energies and angles.

*1 On leave from Kurchatov Institute, Russia
*2 Department of Physics, University of Tokyo
*3 Department of Physics, Tokyo Institute of Technology
*4 Joint Institute for Nuclear Research, Russia
*5 Kurchatov Institute, Russia
*6 Departamento de Fsica Aplicada, Universidad de Huelva, Spain
*7 GANIL, Caen Cedex, France
*8 Center for Nuclear Study, University of Tokyo
*9 Department of Physics, Rikkyo University

Projectile-like particles from breakup channels (e.g. tritons and neutrons from the ^{7}H → t + 4n decay) were measured by a downstream detection system consisting of a dipole magnet, a ΔE(1 cm) – E(6 cm) hodoscope of plastic scintillators and a four-layer neutron hodoscope array. In front of the neutron array a thin layer of plastic scintillators was installed to reject events from charged particles.

Fig. 1. Setup of the experiment (the d(^{8}He,^{3}He)^{7}H channel is shown).

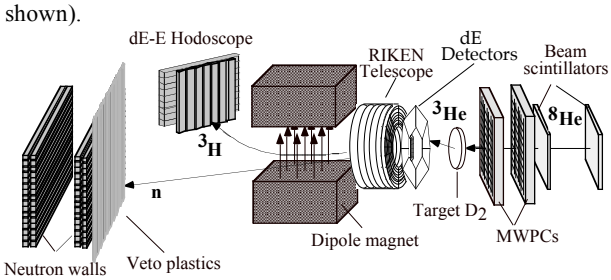

The following reaction channels are involved in the analysis:

- d(^{8}He,^{3}He)^{7}H; d(^{8}He,^{4}He)^{6}H;
- d(^{8}He,^{6}Li)4n; d(^{8}He,d^{4}He)4n;
- d(^{8}He,t)^{7}He
- d(^{12}Be,^{3}He)^{11}Li
- d(^{12}Be,^{6}Li)^{8}He; d(^{12}Be,d^{4}He)^{8}He;
- d(^{12}Be,t)^{11}Be

The first experimental results showed a pronounced peak in the ^{7}He excitation energy spectrum obtained in the d(^{8}He,t)^{7}He reaction. The peak is also clearly seen in coincidences with ^{6}He in hodoscope and represents the ^{7}He ground state. This reaction will be a good reference tool to control the experimental conditions. Detailed analysis of the experimental data is in progress.

References

1) A.A. Korsheninnikov et al.: Phys. Rev. Lett. **90**, 082501 (2003).
2) F.M. Marques et al.: Phys. Rev. C **65**, 044006 (2002).
3) D.V. Aleksandrov et al.: Yad. Fiz., **39**, 513 (1984).

Research on correlated two-nucleon system in ^{6}Li and ^{6}He nuclei

N.T. Khai *[1,2], T. Suda, A. Yoshida, T. Ohnishi, H. Takeda, A. Ozawa[*3], T. Suzuki[*4], T. Sugawara[*4], S. Nakajima[*4], K. Ogata[*4], K. Kobayashi[*4], S. Ishimoto, Y. Suzuki[*4], Y. Takahashi, L.H. Khiem[*1,2] and P.Q. Hung[*2]

[One-nucleon exchange reaction, strong di-neutron correlation, solid-H_2 target, backward scattering]

The ^{6}Li and ^{6}He nuclei are the typical six-nucleon systems consisting of α-core and two loosely bound nucleons. ^{6}He is the lightest halo nucleus showing Borromean binding mechanism, which suggests a strong di-neutron correlation for the formation of the two neutron halo (2n-halo) in this nucleus[1-3]. ^{6}Li is a stable nucleus whose cluster properties have been well investigated through the (e, e'd) experiment, in which the neutron-proton pair in the nucleus is found to have a similar wave function as that of a free deuteron[4].

For the ^{6}He nucleus, correlation between two neutrons is still an open problem. Recently, the experimental studies on 1n- and 2n-transfer reactions in the ^{6}He + p system, and 2n exchange in the ^{6}He + ^{4}He reaction have revealed the "di-neutron" and "cigar like" configurations for the ground state structure[2,3]. These predictions await further experimental verification.

The (d, p) elastic scattering experiment showed an increase in cross section at very backward scattering angles in the center of mass (CM) system[5]. This characteristic is mainly attributed to the nucleon exchange mechanism. This suggests that if a similar reaction can be observed for the 2n system in ^{6}He, the measurement will then provide a direct verification of the existence of the correlated two-neutron structure in this nucleus, because the exchange mechanism requires a rather high relative momentum between neutrons in the 2n system, typically 150 MeV/c.

We report on an experimental research in which we search for the 2n correlation in the ^{6}He nucleus via the one-nucleon exchange (ONE) reaction p(^{6}He, ^{4}He+n)d in inverse kinematics using an incident ^{6}He beam at an energy of 70 AMeV delivered by the RIKEN Accelerator Research Facility (RARF) and a newly developed solid-H_2 target (SHT)[6]. For reference, a similar reaction was also measured for the ^{6}Li + p system. The reaction products, which are an α-particle, a slow deuteron and a high-energy neutron for the ^{6}He + p system (and high-energy proton for the ^{6}Li + p system) have been measured in coincidence. The detector systems were designed to determine the kinematical characteristics of the particles at backward scattering angles in the CM system. The kinetic energy and scattering angle of the deuteron were measured by a two-strip-array system consisting of semi circular plastic strips. A thick plastic wall was used to measure the neutron (and proton). In addition, a thin plastic layer, called charge veto, was placed in front of the wall to identify charged particles. These detector systems were placed on two sides of the reaction plane and covered the same range of angles from 5° to 30° in the laboratory system. Located at the beam direction is the detector for α-particle measurement, which consists of three plastic layers covering ±4°. A multi wire proportional chamber (MWPC) is in front of this detector for position measurement.

As shown in Fig. 1, the ONE reaction was identified using energy correlation between α-particles and protons for the ^{6}Li + p system and between α-particles and neutrons for the ^{6}He + p system after particle identification in addition to slow-deuteron identification. This allowed us to confirm the appearance of another competitive reaction. Kinematically, it is consistent with the 1n-transfer process ("two-step"), although the beam energies are quite high.

At present, detailed data analysis is under way, and theoretical considerations are also being carried out to reach the conclusions from the physics viewpoint.

References

1) T. Kobayashi et al.: Phys. Rev. Lett. 60, 2599 (1988).
2) G. M. Ter-Akopian et al.: Physics Letters B 426, 251 (1998).
3) Yu Oganessian et al.: Phys. Rev. Lett., Vol. 82, No. 5, 4996 (1999).
4) R. Ent et al.: Nuclear Physics A 578, 93 (1994).
5) K. Sekiguchi et al.: Phys. Rev. C, Vol. 65, 034003, 1 (2002).
6) S. Ishimoto et al.: Nucl. Instr. and Meth. A 480, 304 (2002).

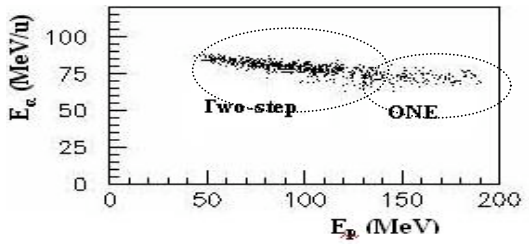

Fig. 1. Identification of the ONE reaction channel based on energy correlation between α-particles and protons for ^{6}Li + p system.

[*1] Hanoi Institute of Physics and Electronics
[*2] Hanoi University of Science
[*3] Tsukuba University
[*4] Saitama University

Coulomb dissociation of ^{6}He

M. Shinohara,[*1] T. Nakamura,[*1] Y. Satou,[*1] Y. Kondo,[*1] T. Nannichi,[*1] T. Shimamura,[*1] Y. Nakayama,[*1] K. Yoneda, N. Aoi, H. Baba, Y. Ichikawa,[*2] K. Ieki,[*3] H. Kimura,[*2] T. Kobayashi,[*4] T. Machida,[*3] T. Motobayashi, H. Otsu, H. Sakurai, S. Shimoura,[*5] A. Shiraki,[*2] T. Sugimoto, S. Takeuchi, Y. Togano,[*3] K. Yamada, M. Yamaguchi, Y. Yauchi,[*3] and M. Ishihara

[Nuclear Reaction: Pb(^{6}He,^{4}He2n), Coulomb dissociation, Invariant mass method]

We have studied the Coulomb dissociation of the two-neutron halo nucleus ^{6}He on a lead target at 69 MeV/nucleon. ^{6}He is a suitable nucleus for studying the two-neutron halo and Borromean properties since the interactions of the constituent subsystems, ^{4}He-n and n-n, are well known. In addition, the ground state of ^{6}He is rather well understood as having a hard core (α particle) surrounded by the two valence neutrons predominantly in the $p_{3/2}$ orbital.

Recently, the electric dipole ($E1$) excitation strength $B(E1)$ of the two-neutron halo nucleus ^{11}Li has been measured using the Coulomb dissociation.[1)] The observed $B(E1)$ strength was well reproduced by a three-body model with a strong two-neutron correlation. From this experiment, it was proved that the Coulomb dissociation is a useful tool for investigating a two-neutron correlation and a three-body property. In this experiment, we have studied ^{6}He to further clarify how the two-neutron correlation and three-body property can be observed in the $B(E1)$ distribution of this nucleus, whose structure and interactions between the constituent particles are established. The previous Coulomb dissociation data for ^{6}He reported from GSI[2)] and MSU[3)] are inconsistent with each other. Furthermore, there may be a similar loss of efficiency at low relative energies in these experiments as for ^{11}Li. Here, we used an identical experimental setup and technique to exclude the cross-talk events in the two-neutron detection, thereby enabling us to measure $B(E1)$ at low relative energies down to $E_{\rm rel}$=0 MeV. This study would also provide a good test of the three-body calculations, which have been intensively performed recently. The comparison between the $B(E1)$ distributions of ^{6}He and ^{11}Li would be useful to understand the property of ^{11}Li, which has a more complicated structure than ^{6}He.

The experiment was performed at the RIKEN projectile fragment separator RIPS at the RIKEN Accelerator Research Facility. A secondary ^{6}He beam was produced by the fragmentation reaction of a 100 MeV/nucleon primary ^{18}O beam incident on a Be target with a thickness of 1.48 g/cm^2. The secondary beam was identified event-by-event using the time-of-flight (TOF) between a cyclotron RF timing and a timing from a 1-mm-thick plastic scintillator placed at the second focal plane of RIPS. The ^{6}He particle bombarded a lead target with a thickness of 783 mg/cm^2 and was broken up into ^{4}He and two neutrons. The beam energy was 69 MeV/nucleon in the middle of the lead target. To measure the incident momentum vector of the small Z at a high ^{6}He beam rate (40 kcps), we used two multiwire drift chambers (MWDCs) placed upstream of the lead target. The efficiency and position resolution were 95% and 130 μm, respectively.

The outgoing neutrons were detected by a four-layered neutron hodoscope array (NEUT), which consists of 54 bars with a dimension of 6 cm $\times$ 6 cm $\times$ 2.1 m. Upstream of NEUT, a thin layer of plastic scintillators (VETO) was installed to reject the charged particle background. The momentum vectors of the two neutrons were reconstructed from the hit position and TOF information.

The ^{4}He fragment produced in the breakup reaction was bent by a large-gap dipole magnet and was traced by two MWDCs located at the entrance and exit of the magnet. The ^{4}He particles penetrated a hodoscope (HOD), which consists of seven plastic scintillator slats of 1 cm thickness. Particle identification of the charged fragment was performed using the information of ΔE and TOF obtained from HOD in combination with the magnetic rigidity information obtained by the tracking with MWDCs. The momentum vector of ^{4}He was deduced by the combination of TOF and tracking information.

Data analysis is now in progress. By using the momentum vectors of ^{4}He and two neutrons, the relative energy of ^{4}He+n+n will be reconstructed. By comparing the observed $B(E1)$ distribution with theoretical calculations, the behavior of the halo neutrons in ^{6}He, such as the two-neutron correlation, will be discussed.

References

1) T. Nakamura et al.: Phys. Rev. Lett. **96**, 252502 (2006).
2) T. Aumann et al.: Phys. Rev. C **59**, 1252 (1999).
3) J. Wang et al.: Phys. Rev. C **65**, 034306 (2002).

[*1] Department of Physics, Tokyo Institute of Technology
[*2] Department of Physics, University of Tokyo
[*3] Department of Physics, Rikkyo University
[*4] Department of Physics, Tohoku University
[*5] Center for Nuclear Study, University of Tokyo

Analyzing Power Measurement for the Proton Elastic Scattering on ^{6}He at 71 *A* MeV

S. Sakaguchi,[*1] T. Uesaka,[*1] T. Wakui,[*6] N. Aoi, Y. Hashimoto,[*5] M. Ichikawa,[*7] Y. Ichikawa,[*2] K. Itoh,[*3] M. Itoh,[*6] H. Iwasaki,[*2] T. Kawabata,[*1] T. Kawahara,[*4] H. Kuboki,[*2] Y. Maeda,[*1] R. Matsuo,[*7] T. Nakao,[*2] H. Okamura,[*6] H. Sakai,[*2] N. Sakamoto, Y. Sasamoto,[*1] M. Sasano,[*2] Y. Satou,[*5] K. Sekiguchi, M. Shinohara,[*5] K. Suda,[*1] D. Suzuki,[*2] Y. Takahashi,[*2] A. Tamii,[*8] K. Yako,[*2] and M. Yamaguchi

[nuclear structure, polarized target, unstable nuclei]

Spin-dependent interactions in unstable nuclei have recently attracted much interest. One of the most powerful tools to study these interactions is direct reactions induced by polarized light ions. To investigate the behavior of spin-orbit interaction in weakly bound systems, we have measured the vector analyzing power for the proton elastic scattering on ^{6}He at 71 *A* MeV. A solid polarized proton target, which was specially constructed for RI-beam experiments[1,2], was used.

The experiment was carried out at RIKEN Accelerator Research Facility with a 92 A MeV ^{12}C primary beam. A 71 A MeV ^{6}He beam was separated by the RIKEN projectile fragment separator (RIPS) with a purity of 95%. The typical beam intensity was 300 kcps. The ^{6}He beam bombarded a solid polarized proton target with a size of 14 mmϕ × 1 mm^t. The target material was a single crystal of naphthalene. the average polarization of the target was 13.5%. For the elimination of spurious asymmetry, polarization direction was reversed three times by the 180-degree NMR pulse method[3] during the beam irradiation. A schemetic view of the detecter setup is shown in Fig. 1. Leading particles were detected by a multiwire drift chamber (MWDC) and $\Delta E - E$ plastic scintillator hodoscopes with thicknesses of 5 and 100 mm. Recoiled particles were detected by single-wire drift chambers and CsI(Tl) scintillators placed on the left and right sides of the beam line.

^{6}He particles were identified by $\Delta E - E$ correlation measured by the plastic scintillator hodoscopes. Protons were identified by the correlation of the energy measured by CsI scintillators and the scattering angle determined by SWDCs. $\vec{p}$+^{6}He elastic scattering events were selected by requiring a kinematical consistency for protons and identified ^{6}He particles. Analyzing power was deduced from the spin-dependent asymmetry of scattering and target polarization.

Preliminary results are shown as closed circles in Fig. 2. Previously measured differential cross section data are also plotted as open circles[4] and open squares[5]. The solid and dashed lines show the results of the calculation by phenomenological optical model analysis and a prediction using a microscopic model[6], respectively. Further analysis is now in progress.

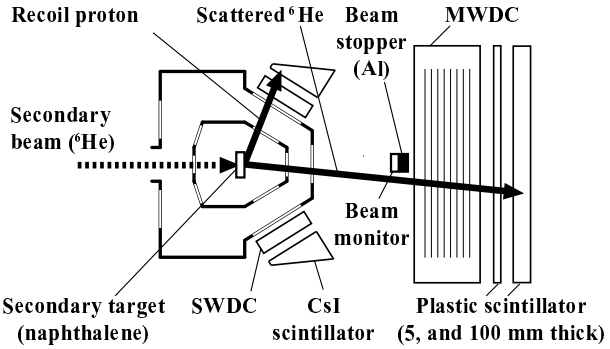

Fig. 1. Experimental setup. A secondary ^{6}He beam from RIPS bombarded the solid polarized proton target. Leading and recoil particles were detected.

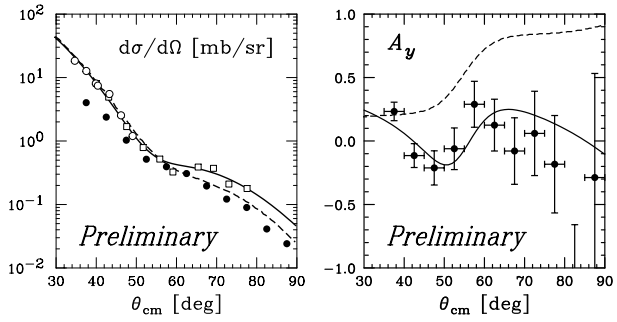

Fig. 2. Differential cross section and analyzing power are plotted. Details are in the text.

*1 Center for Nuclear Study, University of Tokyo
*2 Department of Physics, University of Tokyo
*3 Department of Physics, Saitama University
*4 Department of Physics, Toho University
*5 Department of Physics, Tokyo Institute of Technology
*6 Cyclotron and Radioisotope Center, Tohoku University
*7 Department of Physics, Tohoku University
*8 Research Center for Nuclear Physics, Osaka University

References
1) T. Wakui *et al.*, Nucl. Instrum. and Methods. A **550** (2005) 521.
2) T. Uesaka *et al.*, Nucl. Instrum. and Methods. A **526** (2004) 186.
3) T. Kawahara *et al.*, CNS Ann. Rep. 2005 (2006).
4) M. Hatano *et al.*, Eur. Phys. J. A **25** (2005) 255.
5) A. Korsheninnikov *et al.*, Nucl. Phys. A **617** (1997) 45.
6) K. Amos, private communication.

Elastic Scattering of ^{8}B on Pb, Liquid H_2 and Liquid He Targets

S. Bishop, T. Motobayashi, N. Aoi, H. Baba, T. Gomi, Y. Ichikawa, [*1] N. Imai, [*1] N. Iwasa, [*2] H. Iwasaki, [*1] S. Kawai, [*3] Y. Kondo, [*4] T. Nakamura, [*4] T. Nakao, [*1] S. Nishimura, T. Ohnishi, T. K. Onishi, [*1] H. J. Ong, [*1] S. Ota, [*4,5] A. Perera, S. Shimoura, [*4] T. Sumikama, D. Suzuki,[*1] H. Suzuki, [*1] M. K. Suzuki,[*1] S. Takeuchi, M. Tamaki, [*4] K. Tanaka, Y. Togano,[*3] and Y. Yanagisawa

The ^{7}Be(p,γ)^{8}B reaction, occurring in the solar PPIII reaction chain, has been under intense experimental and theoretical study for many years now. The subsequent β-decay of ^{8}B gives rise to the solar neutrino flux and the famous "solar neutrino problem", which has now been resolved[?)].

Studies of this reaction employing the Coulomb dissociation (CD) method have been performed in the past, but some questions still remain regarding the contribution of the target nuclear field to the ^{8}B dissociation cross section. Sophisticated continuum discretized coupled channel approaches are now used to analyze such ^{8}B CD reaction studies, but the validity of the nuclear models employed (folding models employing NN interactions, for example) have never been checked against ^{8}B elastic scattering data because such data has not existed until now.

In an effort to resolve this issue for ^{8}B CD, as well as future experiments employing the CD technique, we have performed a ^{8}B dissociation experiment utilizing targets comprising 57 mg/cm^2 Pb, 61.5 mg/cm^2 liquid H_2 and 116 mg/cm^2 liquid He. The experiment was performed using the RIKEN RIPS facility[?)]. Further experimental details can be found elsewhere[?)]. ^{8}B elastic scattering data were acquired concurrently, for all three targets. The resulting elastic angular distributions have been fit within the framework of a Woods-Saxon (WS) optical potential approach and these fits have been tested against the data by way of a GEANT simulation of the experiment. Figure **??** shows, in the form of laboratory frame $d\sigma/d\theta$ plots, our ^{8}B elastic data (black circles) for the three targets along with the resulting optical model predictions of the GEANT simulation (histograms). Table **??** summarizes the WS parameters obtained from our fits; note that the spin-orbit potential depth was held fixed at 6.2 MeV. These elastic data represent the first time ^{8}B elastic scattering has been measured and the first time WS optical model parameters have been obtained for ^{8}B elastic scattering. For the upcoming dissociation/breakup data analysis, these data will provide the basis for testing and constraining the nuclear models we will employ; any nuclear model constructed, in addition to reproducing the dissociation/breakup data, should also be able to reproduce these elastic distributions. Moreover, because the dissociation channel arises within the folding models from the imaginary component of the potential, successful reproduction of these elastic distributions will self-consistently constrain the dissociation channel within the nuclear model employed.

Table 1. Optical Parameter Results

	V_R	W_v	a_R	a_{so}	a_v	R_R	R_{so}	R_v
H_2	28.00	24.30	0.750	0.750	0.320	1.20	1.01	1.16
	24.95	13.32	0.750	0.750	0.335	1.17	1.01	1.32
He	65.80	30.32	0.801	–	0.545	1.345	–	1.56
	55.81	34.32	0.801	–	0.567	1.245	–	1.57
Pb	50.00	57.90	0.800	–	0.800	1.067	–	1.067

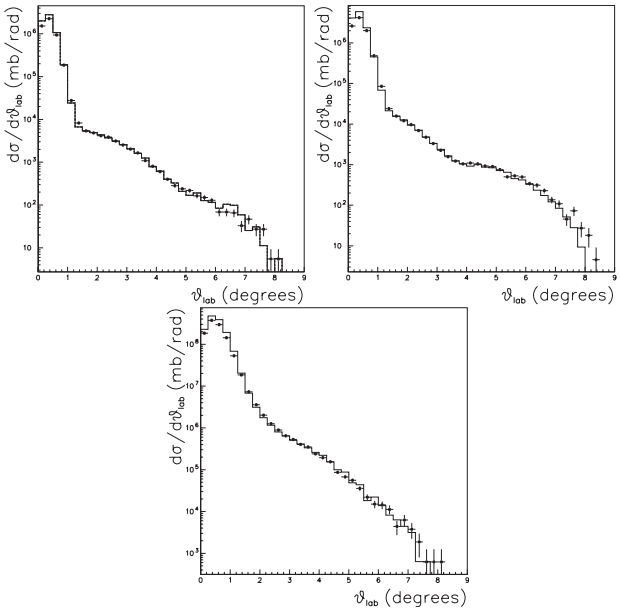

Fig. 1. Laboratory frame elastic angular distributions, $d\sigma/d\theta$, of ^{8}B. Top left: ^{8}B + p. Top right: ^{8}B + ^{4}He. Bottom: ^{8}B + Pb. Circles are the data, and the histograms are the GEANT simulation results.

References

1) Q. R. Ahmad et al.: Phys. Rev. Lett. 87, 071301, (2001).
2) T. Kubo et al.: Nucl. Inst. Meth. B 70, 309, (1992).
3) S. Bishop et al.: RIKEN Accel. Prog. Rep. 39, 44, (2006).

[*1] Department of Physics, University of Tokyo
[*2] Department of Physics, Tohoku University
[*3] Department of Physics, Rikkyo University
[*4] Department of Physics, Tokyo Institute of Technology
[*4] Center for Nuclear Study, University of Tokyo
[*5] Department of Physics, Kyoto University

^{14}Be$(p,n)^{14}$B$(1^+;1.28$ MeV$)$ reaction at 70 MeV/nucleon

Y. Satou,[*1] T. Nakamura,[*1] N. Fukuda, T. Sugimoto, Y. Kondo,[*1] N. Matsui,[*1] Y. Hashimoto,[*1] T. Nakabayashi,[*1] T. Okumura,[*1] M. Shinohara,[*1] T. Motobayashi, Y. Yanagisawa, N. Aoi, S. Takeuchi, T. Gomi, Y. Togano,[*2] S. Kawai,[*2] H. Sakurai, H. J. Ong,[*3] T. K. Onishi,[*3] S. Shimoura,[*4] M. Tamaki,[*4] T. Kobayashi,[*5] H. Otsu, Y. Matsuda,[*5] N. Endo,[*5] M. Kitayama,[*5] and M. Ishihara

$[(p,n)$ reaction, ^{14}Be$]$

The (p,n) reaction has been one of the major probes of a nuclear structure; it can provide essentially the same information as the nuclear beta decay without limitation due to an available energy window, and the phase space factor that scales as E_0^5 for allowed transitions with $E_0 \gg 1$ MeV (E_0 is the decay energy). In recent years, the (p,n) reaction has been successfully applied to the spectroscopic studies of unstable nuclei[1,2]. In this study, we have investigated the Gamow-Teller transition from ^{14}Be$_{\rm g.s.}$ leading to the 1^+ state at 1.28 MeV in ^{14}B. It is of interest to see if consistent interpretation of data can be made between the (p,n) and beta-decay studies[3,4]. Because the 1^+ state is located above the neutron decay threshold of 0.97 MeV in ^{14}B, we made use of the invariant mass method in inverse kinematics.

The experiment was performed at the RIKEN accelerator research facility. A ^{14}Be beam with an energy of 70 MeV/nucleon was produced using RIPS from a 100 MeV/nucleon ^{18}O primary beam with an intensity of 400 pnA. The production target was a 6-mm-thick Be plate; the aluminum energy degrader had a thickness of 4.63 mm. The typical beam intensity at F3 was 7 kcps for a momentum setting of $\Delta P/P = \pm 2\%$. The layout of the experimental setup is the same as that of the ^{19}C(p,p') measurement[5], except for the thickness of the secondary cryogenic hydrogen target (229 mg/cm^3).

Figure 1 shows a two-dimensional particle identification diagram of beamlike charged particles measured in coincidence with forward emitted neutrons. Among various beryllium isotopes with Z=4, we can clearly observe loci due to boron isotopes with Z=5. Such isotopes cannot be produced via ordinary fragmentation processes; instead charge exchange processes must be involved.

By selecting ^{13}B with a gate as shown in the figure, we can construct an invariant mass event-by-event for the decaying ^{13}B + n system. Figure 2 shows the invariant mass (relative energy) spectrum thus obtained. A prominent peak at $E_{\rm rel} \approx 0.3$ MeV corresponds to the known 1^+ state[4]. The forward peak nature in the angular distribution of ^{14}B (not shown) supports the 1^+ assignment for this state. Strength at $E_{\rm rel} \approx 1$ MeV may correspond to the known 2^- 1.86 MeV state. A comparison of the observed differential cross sections with DWBA calculations using shell model wave functions is in progress to clarify structures related to ^{14}Be and ^{14}B.

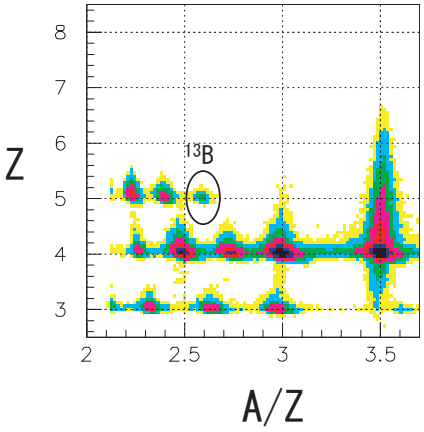

Fig. 1. Two-dimensional particle identification diagram of beamlike charged particles.

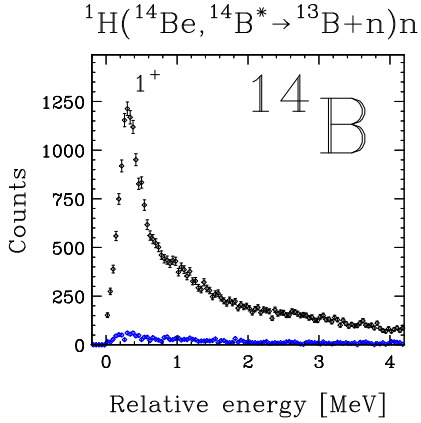

Fig. 2. Relative energy spectrum of ^{13}B + n system.

*1 Department of Physics, Tokyo Institute of Technology
*2 Department of Physics, Rikkyo University
*3 Department of Physics, University of Tokyo
*4 Center for Nuclear Study, University of Tokyo
*5 Department of Physics, Tohoku University

References

1) T. Teranishi et al.: Phys. Lett. B **407**, 110 (1997).
2) S. Takeuchi et al.: Phys. Lett. B **515**, 255 (2001).
3) M. D. Belbot et al.: Phys. Rev. C **56**, 3038 (1997).
4) N. Aoi et al.: Phys. Rev. C **66**, 014301 (2002).
5) Y. Satou et al.: RIKEN Accel. Prog. Rep. **39**, 51 (2006).

Invariant-mass spectroscopy of ^{13}Be and ^{14}Be

Y. Kondo,[*1] T. Nakamura,[*1] Y. Satou,[*1] T. Sugimoto, N. Matsui,[*1] Y. Hashimoto,[*1] T. Okumura,[*1] T. Nakabayashi,[*1] M. Shinohara,[*1] N. Aoi, N. Endo,[*2] N. Fukuda, T. Gomi, M. Ishihara, S. Kawai,[*3] M. Kitayama,[*2] T. Kobayashi,[*2] Y. Matsuda,[*2] T. Motobayashi, H. J. Ong,[*4] T. K. Onishi,[*4] H. Otsu, H. Sakurai, S. Shimoura,[*5] S. Takeuchi, M. Tamaki,[*5] Y. Togano,[*3] and Y. Yanagisawa

[NUCLEAR REACTIONS: ^{14}Be+p, Invariant mass method]

Unbound states in the neutron-rich nuclei ^{13}Be and ^{14}Be have been studied by applying the invariant mass method to the inelastic scattering and one-neutron knockout reaction of ^{14}Be on a proton target. Shell melting at the magic number $N = 8$ in the neutron-rich beryllium isotopes has been established by several experimental studies on ^{11}Be and ^{12}Be, while the shell evolution in the $N > 8$ region is still unknown. Recently, the first 2^+ state in ^{14}Be was observed in the unbound region by the inelastic scattering on a carbon target, and a lower excitation energy and smaller deformation than those for ^{12}Be were found.[1)] The mechanism of lowering of the 2^+ energy and the smaller deformation of ^{14}Be have not yet been well understood. For ^{13}Be, no decisive measurements for the ground state have been reported so far. In the present study, we aim at clarifying the shell evolution by studying the nuclear structure not only in the drip-line nucleus ^{14}Be but also in the unbound nucleus ^{13}Be. The structural information of ^{13}Be is also important in understanding the structure of ^{14}Be as a Borromean three-body system (^{12}Be+n+n).

In the present study, the inelastic scattering and one-neutron knockout reaction of ^{14}Be were measured by the same setup. For the inelastic scattering, the collectivity of ^{14}Be has been investigated. By comparing the deformation measured on the proton target with that on the carbon target, the collectivities of the neutrons and protons in ^{14}Be can be deduced independently. For the one-neutron knockout reaction, the low-lying resonant states in ^{13}Be are populated and its level structure was studied. The spectroscopic factor of ^{14}Be can also be deduced.

The experiment was performed using the RIPS beam line. A radioactive ^{14}Be beam was produced by projectile fragmentation of a primary ^{18}O beam at 100 MeV/nucleon and separated by RIPS. The secondary ^{14}Be beam at 69 MeV/nucleon bombarded a liquid hydrogen target, which then broke up into ^{12}Be and neutron(s). The outgoing ^{12}Be and neutron(s) were detected and analyzed in order to obtain their momentum vectors that are used to reconstruct the invariant mass of unbound states in ^{13}Be and ^{14}Be. Details of the detector setup are described in the previous report.[2)]

Figure 1(a) presents the decay energy spectrum for the ^{12}Be+n+n system in the inelastic channel obtained from the $M_n = 2$ (neutron multiplicity) events by removing the neutron crosstalk events. A narrow peak at around 0.3 MeV, corresponding to the first excited 2^+ state in ^{14}Be, has been observed. Figure 1(b) shows the spectrum for the ^{12}Be+n system in the one-neutron knockout channel obtained from the $M_n = 1$ events after subtracting the inelastic contribution. The peak observed at around 0.5 MeV may correspond to the ground state in ^{13}Be and the peak at 2 MeV corresponds to the d-wave resonance, as reported in previous experiments.[3–5)] Further analysis is now in progress.

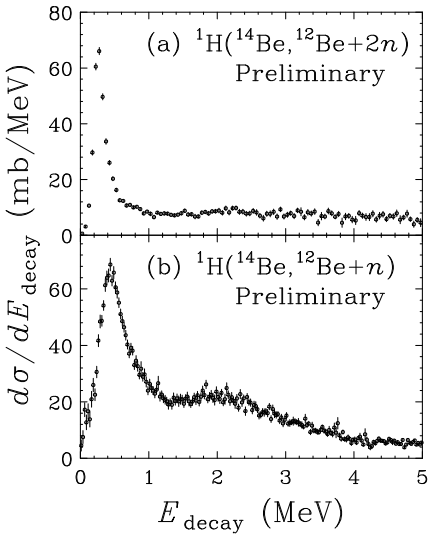

Fig. 1. Decay energy spectra for the ^{12}Be+2n (a) and ^{12}Be+n (b) systems obtained from the inelastic scattering and one-neutron knockout reaction of ^{14}Be, respectively.

*1 Department of Physics, Tokyo Tech
*2 Department of Physics, Tohoku University
*3 Department of Physics, Rikkyo University
*4 Department of Physics, University of Tokyo
*5 Center for Nuclear Study, University of Tokyo

References

1) T. Sugimoto: PhD thesis (2006).
2) Y. Kondo et al.: RIKEN Accel. Prog. Rep. **39**, 45 (2006).
3) A. A. Korsheninnikov et al.: Phys. Lett. B **343**, 53 (1995).
4) A. V. Belozyorov et al.: Nucl. Phys. A **636**, 419 (1998).
5) J. L. Lecouey: Few-Body Syst. **34**, 21 (2004).

Resonance levels in ^{14}O near the ^{13}N+p threshold

T. Teranishi,[*1] S. Kubono,[*2] H. Yamaguchi,[*2] J.J. He,[*2] A. Saito,[*2] H. Fujikawa,[*2] G. Amadio,[*2] M. Niikura,[*2] S. Shimoura,[*2] Y. Wakabayashi,[*2] S. Nishimura, M. Nishimura, J.Y. Moon,[*3] C.S. Lee,[*3] A. Odahara,[*4] D. Sohler,[*5] L.H. Khiem,[*6] Z.H. Li,[*7] G. Lian,[*7] and W.P. Liu[*7]

[Nuclear structure, unstable nuclei]

A set of $T = 1$ triplets in $A = 14$ nuclei (^{14}C, ^{14}N, and ^{14}O) is a good example of isobaric analog multiplets that has been studied for many years. However, knowledge of the ^{14}O levels is still poor compared with that of ^{14}C and ^{14}N.[1] The J^π value of the 6.8-MeV level is unknown. The 0^- level, which is supposed to be several hundreds of keV above the 1^- level at 5.2 MeV, is yet to be identified. The E_x, Γ, and J^π values for the low-lying ^{14}O levels should be further investigated to determine their correspondence to the analog levels and to study the wave functions. We have investigated resonance levels in ^{14}O populated in the ^{13}N+p elastic scattering, which was measured in inverse kinematics with a secondary beam of ^{13}N and a proton target. The secondary ^{13}N beam was produced by CRIB[2] of CNS in the RIKEN facility. We utilized the thick target method[3] to efficiently measure the excitation functions of ^{13}N+p elastic scattering without changing the ^{13}N beam energy. The proton target was a sheet of $(CH_2)_n$ with a thickness of 8.3 mg/cm^2 and a diameter of 3 cm. The secondary ^{13}N beam energy before the target was 48.6 MeV with a width of 1.6 MeV (FWHM). The ^{13}N intensity was approximately 2×10^5 particles/sec, which was 98% of the total secondary beam intensity. Recoil protons emitted from the proton target were detected using a silicon detector ΔE-E telescope at the laboratory angle of $_{\rm LAB} = 0$.

Figure 1 shows the ^{13}N+p excitation function measured using the silicon detector telescope. The spectrum covers $E_{\rm CM} = 0.4$–3.3 MeV ($E_x = 5.0$–7.9 MeV). Four resonance-like signatures are seen at $E_{\rm CM} \sim 0.5$, 1.6, 2.1, and 3.1 MeV in the spectrum. They may be attributed to the known ^{14}O levels at $E_x = 5.2$, 6.3, 6.8, and 7.7 MeV with $J^\pi = 1^-$, 3^-, (unknown), and 2^+, respectively. To determine J^π for the 6.8-MeV level, the experimental spectrum was fitted with an R-matrix-based calculation[4]. The result for the $J^\pi = 2^-$ case is shown by the solid line in Fig. 1 and is consistent with the experimental spectrum. Therefore, we assigned $J^\pi = 2^-$ to the 6.8-MeV level.

The 0^- level, which has never been observed in transfer reactions, is expected to be observed as an

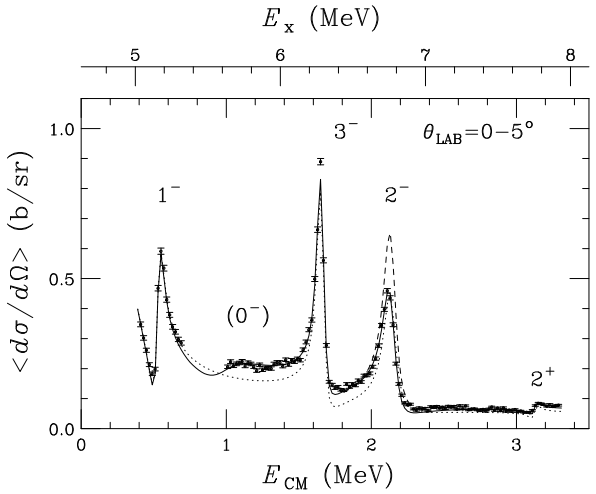

Fig. 1. Experimental excitation function for the ^{13}N+p scattering measured at around $\theta_{\rm LAB} = 0^\circ$. The solid line shows the result of the fitting calculation. The dashed line represents the result when J^π for the 6.8-MeV level is changed to 3^-. The dotted line shows the result without a contribution of the 0^- level at $E_x \sim 5.7$ MeV. The gap at $E_{\rm CM} \sim 0.8$ MeV is due to the dead layers of the ΔE-E telescope.

s-wave resonance in the ^{13}N+p spectrum. Therefore, we included the 0^- level in the fitting. The E_x and Γ values for the 0^- level were preliminarily determined to be 5.72 MeV and 0.4 MeV, respectively. This result is roughly consistent with the calculated E_x and Γ values using the s-wave resonance phase shift in a proton scattering model with a Woods-Saxon potential[5].

The widths of the 1^-, 3^-, and 2^- levels were preliminarily determined to be 42, 42, and 90 keV, respectively, by the fitting. These widths are comparable to the single-particle widths estimated by the Woods-Saxon potential model, where the resonance proton orbital was assumed to be $2s_{1/2}$ for the 1^- level and $1d_{5/2}$ for the 3^- and 2^- levels.

*1 Department of Physics, Kyushu University
*2 Center for Nuclear Study, the University of Tokyo
*3 Chung-Ang University, Republic of Korea
*4 Department of Physics, Osaka University
*5 ATOMKI, Hungary
*6 Institute of Physics and Electronics, Vietnam
*7 China Institute of Atomic Energy, P.R. China

References

1) F. Ajzenberg-Selove: Nucl. Phys. A523, 1 (1991).
2) Y. Yanagisawa et al.: Nucl. Instrum. and Methods A539, 74 (2005).
3) K.P. Artemov et al.: Sov. J. Nucl. Phys. 52, 408 (1990).
4) T. Teranishi et al.: Phys. Lett. B556, 27 (2003).
5) R. Sherr: Phys. Rev. C73, 037310 (2006), and references therein.

Proton resonance scattering of ^{7}Be

H. Yamaguchi,[*1] Y. Wakabayashi,[*1] G. Amadio,[*1] H. Fujikawa,[*1] S. Kubono,[*1] A. Saito[*2] J.J. He[*3] T. Terahishi[*4] Y.K. Kwon[*5] S. Nishimura Y. Togano[*6] N. Iwasa[*7] K. Inafuku[*7] M. Niikura[*1] and L.H. Khiem[*8]

[Nuclear structure, nuclear astrophysics]

$S_{17}(E)$ is regarded as an important factor for the solar neutrino problem in the standard solar model. Although great efforts were spent by many experimental groups[1)], the experimental precision remains still around 10 %, because of the small reaction cross section. It is claimed that the determination of the S_{17} below 300 keV with a precision better than 5 % may make a major contribution to our knowledge for the solar model[2)].

Besides the small cross section of the reaction, the existence of excited levels of ^{8}B can also be a problem on the determination of S_{17}. However, we do not have sufficient knowledge of the nuclear structure of ^{8}B. Only the lowest two excited states at 0.77 MeV and 2.32 MeV were clearly observed in past experiments. Another excited state around 3.5 MeV was observed as an unexpectedly wide resonance, and this was explained as a low-lying 2s state[3,4)]. This kind of wide states may affect the measurement of ^{7}Be(p,γ)^{8}B cross section even at very low energies (much less than 1 MeV). Thus we intended to measure the resonances of ^{8}B, to evidently observe the 3.5 MeV resonance reported in the past measurements, and also to explore the totally unknown region E >3.5 MeV, where we may find new resonances.

The measurement was performed at CRIB[8,9)]. The primary beam used in this measurement was ^{7}Li^{3+} of 8.76 MeV/nucleon, with the beam current of about 100 particle nA. The RI-beam production target was pure hydrogen gas, which was enclosed in an 8 cm-long cell, at 760 Torr and room temperature ($\sim$ 300 K). The ^{7}Be beam energy used in this measurement was 53.8 MeV, of which the corresponding center-of-mass energy is 6.7 MeV. The intensity of the produced ^{7}Be^{4+} beam was 3×10^5 particles per second at the resonance scattering target. We used a standard experimental method for the proton elastic resonance scattering (thick target method), well-established at CRIB[10)].

Excitation functions were obtained by calculating the cross section from the numbers of the proton events, Figure 1 shows an excitation function at zero degree. The analysis is still going on, and this specturm should be regarded as a preliminary one. The cross section agree well with the past measurements[3,4)] in the energy region around the known 2.2 MeV resonance. The 3.5 MeV resonance, which was reported as a wide resonance, is not clearly seen in this spectrum, possibly due to its large width. Some part of the continuum in the spectrum is considered as contributions from inelastic scatterings and three-body decays of ^{8}B. In a near future, we will make a more detailed analysis including these effects.

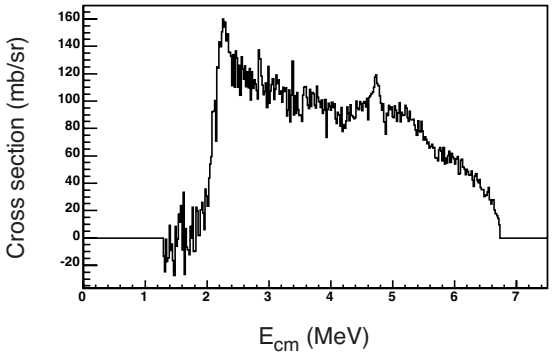

Fig. 1. Preliminary analysis result on the proton excitation function of ^{7}Be measured at 0 degrees. The excitation energy of ^{8}B, E_{ex} equals to E_{cm}+0.1375 MeV.

We are grateful to the accelerator staff in RIKEN and CNS for their help. This work was supported by the Grant-in-Aid for Young Scientists (B) (Grant No. 17740135) of JSPS.

References

1) C. Angulo, *et al.*: Nucl. Phys. A **656** (1999) 3.
2) E. Adelberger, *et al.*: Rev. of Mod. Phys. **70** (1998) 1265.
3) V. Gol'dberg *et al.*: *JETP Lett.* **67**, (1998) 1013.
4) G. Rogachev *et al.*: Phys. Rev. C **64** (2001) 061601(R).
5) A. van Hees and P. Glaudemans: Z. Phys. A **314** (1983) 323.
6) A. van Hees and P. Glaudemans: Z. Phys. A **315** (1984) 223.
7) F. Barker, and A. Mukhamedzhanov: Nucl. Phys. A **673** (2000) 526.
8) S. Kubono *et al.*: Eur. Phys. J. A **13** 217 (2002).
9) Y. Yanagisawa *et al.*: Nucl. Instrum. Methods Phys. Res., Sect. A **539** 74 (2005).
10) T. Teranishi *et al.*: Phys. Lett. B **556** 27 (2003).

*1 Center for Nuclear Study, Graduate School of Science, University of Tokyo
*2 Department of Physics, Graduate School of Science, University of Tokyo
*3 School of Physics, The University of Edinburgh
*4 Department of Physics, Kyushu University
*5 Department of Physics, Chung-Ang University
*6 Department of Physics, Rikkyo University
*7 Department of Physics, Tohoku University
*8 Institute of Physics and Electronics, Vietnam Academy of Science and Technology

In-beam γ-ray measurement using ^{20}Ne + ^{96}Zr reaction

Y. Zheng,[*1] E. Ideguchi,[*1] S. Ota,[*1] M. Niikura,[*1] M. Liu,[*1] H. Baba,[*2] D. Suzuki,[*3] S. Shimoura,[*1] and H. Yamaguchi[*1]

[NUCLEAR REACTION: ^{20}Ne + ^{96}Zr at E_{lab}=130 MeV; in-beam γ-ray measurement]

Nuclei in the A∼110, Z∼50 mass region are of great interest for providing clear images of a nuclear structure. Single-particle motions are expected to predominate the excitation scheme in these nuclei due to the Z = 50 shell closure. However, other excitation mechanisms such as collective rotations exhibiting smooth band terminations, where terminating configurations involve proton particle-hole excitations across the Z = 50 gap[1], and magnetic rotations (M1 bands)[2] are also presented to generate angular momentum in this mass region. Recent theoretical calculations have been used to predict that a region of shape minima at deformations with 2:1 axis ratios (or larger) exists at a high angular momentum in A∼110 nuclei[3]. A superdeformed (SD) band was observed in ^{108}Cd[4] and it was suggested to be among the most deformed structures ever observed. Its deformation corresponds to an axis ratio larger than 2:1 as predicted by the calculations. In this region, ^{109}In is also expected to have M1 band, SD band, and smooth band terminations at high-spin states. To find such a nuclear structure, we have investigated high-spin states in ^{109}In. In this report, in-beam γ-ray measurement of A ∼ 110 nuclei using the ^{20}Ne + ^{96}Zr reaction is presented.

The experiment was performed at RIKEN accelerator research facility. High-spin states of A∼110 nuclei were populated using the ^{20}Ne + ^{96}Zr reaction at 6.5 MeV/A beam energy, which was chosen so that the cross section to produce ^{109}In becomes predominant. The ^{20}Ne beam was provided by AVF cyclotron. The ^{96}Zr target had a thickness of 1 mg/cm^2. To check the production cross sections of evaporation residues, the beam current was measured using a Faraday cup during the measurement. γ rays from fusion-evaporation residues were detected by a coaxial Ge detector placed at an angle of 90° relative to the beam direction.

The production cross sections of evaporation residues as a function of beam energies for the ^{20}Ne + ^{96}Zr reaction were estimated using the statistical model code CASCADE[5]. In the measured energy region, nuclei in the evaporation channels of 1p5n-1p7n ($^{108-110}$In) and 1α4n-1α6n ($^{106-108}$Cd) will be mainly produced. Figure 1 shows the γ-ray energy spectrum obtained in this work. γ-Ray assignments were performed using previously reported peak energies. In the spectrum, the most intense γ peaks originate from

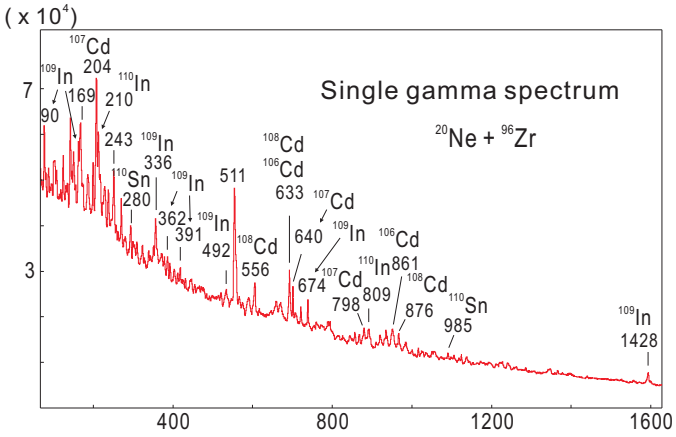

Fig. 1. γ-ray energy spectrum at 6.5 MeV/A.

$^{108-110}$In and $^{106-108}$Cd as predicted by CASCADE calculation.

The production cross sections of these nuclei have been extracted in the 6.5 MeV/A data from the γ-ray peak intensities, beam current and the detection efficiency of the Ge detector. The results are shown in Table 1. Although there is a discrepancy in the production cross sections between the experimental result and the CASCADE calculation, the relative yields of the nuclei are consistent with those of the calculation (see Table 1) and ^{109}In has the largest production cross section (∼129 mb) among the residual nuclei obtained with the measured energy.

Further analysis of the experimental data is in progress.

Table 1. Production cross sections

Nuclei (channel)	Production cross section (mb) theoretical	experimental
^{109}In (1p6n)	215.3	129(3)
^{107}Cd (2p7n)	192.7	111(3)
^{106}Cd (2p8n)	152.3	90(8)
^{110}In (1p5n)	107.8	73(3)
^{108}Cd (2p6n)	72.9	69(3)
^{108}In (1p7n)	63.9	37(2)

*1 Center for Nuclear Study, Graduate School of Science, University of Tokyo
*2 RIKEN (The Institute of Physical and Chemical Research)
*3 Department of Physics, University of Tokyo

References
1) I. Ragnarsson et al.: Phys. Rev. Lett. **74**, 3935 (1995).
2) A. Gadea et al.: Phys. Rev. C **55**, R1 (1997).
3) R. R. Chasman: Phys. Rev. C **64**, 024311 (2001).
4) R. M. Clark et al.: Phys. Rev. Lett. **87**, 202502 (2001).
5) F. Fühlhofer: Nucl. Phys. A **280**, 267 (1977).

Study of high-spin states in $^{49-51}$Ti by secondary fusion reaction

M. Niikura,[*1] E. Ideguchi,[*1] N. Aoi, H. Baba, T. Fukuchi,[*2] Y. Ichikawa,[*3] H. Iwasaki,[*3] T. Kubo, M. Kurokawa, M. Liu,[*1] S. Michimasa,[*1] T. Ohnishi, T. K. Onishi,[*3] S. Ota,[*1] S. Shimoura,[*1] H. Suzuki,[*3] D. Suzuki,[*3] Y. Wakabayashi,[*1] K. Yoshida, and Y. Zheng,[*1]

[NUCLEAR REACTION, ^{9}Be(^{46}Ar, xn)$^{55-x}$Ti, unstable nuclei, fusion reaction]

In-beam γ-ray spectroscopy by fusion-evaporation reactions is one of the most efficient methods of studying nuclear structure at high spin, because large amounts of angular momentum can be brought into the system. However, nuclei produced via fusion-evaporation reactions using stable isotope beams are limited, in many cases, to the proton-rich side relative to the β-stability line. To investigate the high-spin states of neutron-rich nuclei by the fusion-evaporation reaction, it is necessary to use neutron-rich secondary beams. In the doubly magic nuclei ^{48}Ca, the onset of deformed collective states due to the presence of deformed shell gaps in $Z = 20, 22$ and $N = 28$ is expected at high spin. In this report, the in-beam γ-ray measurements in $^{49-51}$Ti by secondary fusion reaction, i.e., ^{46}Ar $+^{9}$ Be, are described.

The experiment was performed at the RIPS beam line in RIKEN[1]. A low-energy secondary ^{46}Ar beam was produced by projectile fragmentation and its energy was lowered using aluminum degraders placed at the first and second focal planes of RIPS. The secondary beam bombarded a 10-μm-thick ^{9}Be target placed at the third focal plane to induce secondary fusion reactions, i.e., $^{9}\mathrm{Be}\left(^{46}\mathrm{Ar}, xn\right)^{55-x}\mathrm{Ti}$. Details on the production of a secondary beam are reported in ref.[2].

Gamma rays emitted from the high-spin states of evaporation residues were detected by the CNS Gamma-Ray detector Array with Position and Energy sensitivity (GRAPE)[3] together with two clover and one coaxial germanium detectors. These γ-ray detectors were placed around the secondary target to cover the angular range between 30° and 120° relative to the beam direction.

We have obtained the γ-ray spectra of ^{49}Ti, ^{50}Ti and ^{51}Ti, wherein we reconfirmed known cascade γ transitions from the spin $(19/2)^{-}$, (11^{+}) and (13/2,17/2) states in ^{49}Ti, ^{49}Ti and ^{49}Ti[4–6], respectively.

To identify cascade γ transitions, we performed a γ-γ coincidence analysis. Figure 1 shows the total projected γ-γ spectrum gated by known γ rays of ^{51}Ti. We reconfirmed coincidence relations between known γ rays and found new γ transitions at 761 and 678 keV.

The left panel of Fig. 2 shows the relative γ-ray yield as a function of detected γ-ray multiplicities.

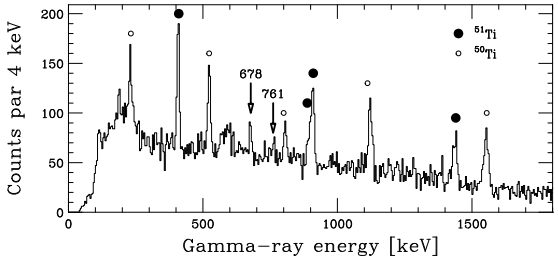

Fig. 1. Total projected γ-γ coincidence spectrum gated by known γ rays of ^{51}Ti.

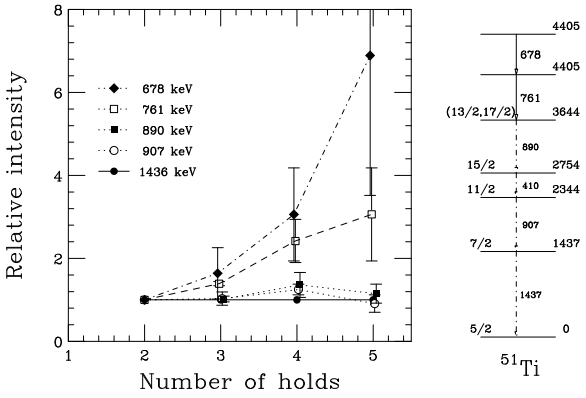

Fig. 2. Relative γ ray intensity normalized to that of lowest transition at 1437 keV as function of detected γ-ray multiplicity (left) and proposed level scheme of ^{51}Ti (right).

The γ-ray yields are normalized to the intensity of the lowest transition at 1437 keV. Because the newly observed γ rays at 761 and 678 keV are enhanced in the high-multiplicity spectrum, these γ-rays are placed above the known 3644 keV state (see the right panel of Fig. 2).

Further analysis to assign spins for the newly observed states using angular distribution is now in progress.

*1 Center for Nuclear Study, University of Tokyo
*2 Department of Physics, Osaka University
*3 Department of Physics, University of Tokyo

References

1) T. Kubo et al.: Nucl. Instrum. and Methods B **461**, 309 (1992).
2) E. Ideguchi. et al.: in this report.
3) S. Shimoura: Nucl. Instrum. and Methods A **525**, 188 (2004).
4) M. Behar et al.: Nucl. Phys. **A366**, 61 (1981).
5) B. Gass et al.: Phys. Rev. Lett. **40**, 1313 (1978).
6) S. E. Arnell et al.: Phys. Scr. **6**, 222 (1972).

Low-energy ^{46}Ar beam for secondary reaction

E. Ideguchi,[*1] M. Niikura,[*1] N. Aoi, H. Baba, T. Fukuchi,[*2] Y. Ichikawa,[*3] H. Iwasaki,[*3] T. Kubo, M. Kurokawa, M. Liu,[*1] S. Michimasa,[*1] T. Ohnishi, T.K. Onishi,[*3] S. Ota,[*1] S. Shimoura,[*1] H. Suzuki,[*3] D. Suzuki,[*3] Y. Wakabayashi,[*1] K. Yoshida, and Y. Zheng[*1]

[NUCLEAR REACTION, ^{46}Ar+^{9}Be, unstable nuclei, fusion-evaporation reaction]

In ^{48}Ca and ^{50}Ti, a highly deformed band structure is expected to be present at high-spin states as in the case of ^{40}Ca[1] due to the deformed shell gaps of Z=20, 22 and N=28. To investigate high-spin states in these nuclei, we employ a fusion-evaporation reaction with an RI beam, ^{46}Ar+^{9}Be. In order to realize such a low-energy nuclear reaction, we have developed a low-energy ^{46}Ar beam.

An experiment was performed at the RIPS[2] facility in RIKEN. A secondary ^{46}Ar beam was produced by the fragmentation reaction of a ^{48}Ca beam impinging on a ^{9}Be target of 1.625 mm thickness. The primary ^{48}Ca beam of 63 MeV/nucleon with a typical intensity of 100 pnA was provided by the RIKEN Ring Cyclotron. The energy of the ^{46}Ar beam right after the primary target was ∼40 MeV/nucleon. An aluminum curved degrader with a mean thickness of 0.6 mm placed at the momentum-dispersive focal plane (F1) was used to achieve a clear isotope separation and to lower the energy of the fragment to ∼23 MeV/nucleon. The energy of the ^{46}Ar beam was further lowered by a plastic scintillator of 0.1 mm thickness and an Al rotatable degrader of 0.3 mm thickness at the achromatic focal plane (F2). It was adjusted to be ∼4 MeV/nucleon at the center of the secondary ^{9}Be target of 0.01 mm thickness (Fig. 1). After passing through the rotatable degrader, the ^{46}Ar beam had a broad charge state distribution and the dominant charge state was estimated to be 16^{+}. The typical intensity of the ^{46}Ar beam at F2 was 1.5×10^{6} pps.

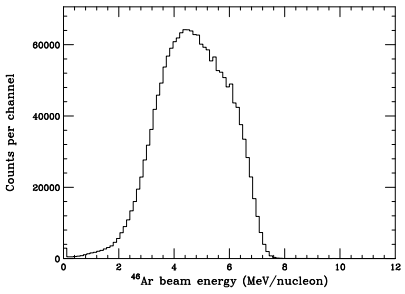

Fig. 1. Energy spectrum of the ^{46}Ar beam at secondary target.

Particle identification of the beam was carried out by the TOF-ΔE method. TOF and ΔE data were obtained from the timing of the plastic scintillator relative to the RF signal of the cyclotron and Si detector at F2, respectively. The purity of the beam was measured to be 98%, and the main contaminant was ^{44}Cl.

The ^{46}Ar beam was transported to the third focal plane (F3) and irradiated on the secondary target to make a fusion-evaporation reaction, ^{46}Ar + ^{9}Be. The typical intensity of the ^{46}Ar beam at F3 was 1.2×10^{6} pps. Two PPAC counters[3] were placed upstream of the secondary target in order to profile the image and the incident angle of the beam on the target. The beam spot sizes (σ) at the target were found to be 13.1 mm and 11.8 mm, respectively, in horizontal and vertical directions as shown in Fig. 2. The energy of the beam was determined from the TOF between the timing of plastic at F2 and that of PPAC at F3, event by event.

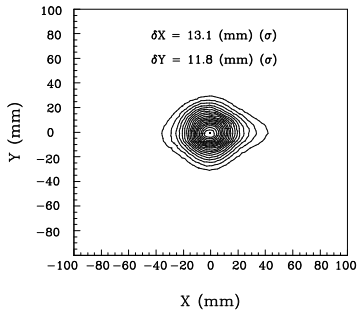

Fig. 2. Beam spot at secondary target.

After the target, another PPAC counter was placed to detect reaction products so as to deduce their energy and angle. A TOF spectrometer[4] was also placed after the third PPAC, and reaction product and the ^{46}Ar beam passing through the target was transported to the final focal plane (F4). At F4, another PPAC counter was placed to measure the position and timing of the transported particles. The TOF between F3 and F4 was used to purify the event associated with the fusion-evaporation reaction.

Data analysis is still in progress.

*1 Center for Nuclear Study, the University of Tokyo
*2 Department of Physics, Osaka University
*3 Department of Physics, University of Tokyo

References

1) E. Ideguchi et al.: Phys. Rev. Lett. **87**, 222501 (2001).
2) T. Kubo et al.: Nucl. Instrum. and Methods B **461**, 309 (1992).
3) H. Kumagai et al.: Nucl. Instrum. and Methods A **470**, 562 (2001).
4) N. Aoi et al.: RIKEN Accel. Prog. Rep. **38**, 176 (2005).

Development of secondary beams produced by fusion reactions for β-decay measurement

Y. Wakabayashi,[*1] H. Yamaguchi,[*1] S. Hayakawa,[*1] G. Amadio,[*1] S. Nishimura, A. Kim,[*2] D. N. Binh,[*3] Y. Gono,[*1] and S. Kubono[*1]

[β-decay, unstable nuclei beam]

For the rapid proton capture process (*rp*-process) in X-ray burst and the core-collapse stage of supernova, proton-rich *pf*-shell nuclei far from stability play important roles[1]. Studies of the β and electron capture decays of these proton-rich *pf*-shell nuclei are of great astrophysical interest. These decays involved in the charged-current processes are predominated by the Fermi and Gamow-Teller (GT) transitions. Information on the GT transitions can be derived directly from β-decay measurements. However, the GT transition strengths (B(GT)'s) of these proton-rich nuclei far from stability were measured for only a few low-lying states with large uncertainties due to the small production cross sections and short half lives. To determine the accurate B(GT), it is important to know the feeding ratio and half-life of the β-decay accurately.

In this study, the final purpose of the experiment is to measure i) the total half-life of the β-decay with an accuracy better than 10 %, ii) the decay branching ratios to the ground state (Fermi transition) and GT states accurately.

Test experiments of different primary beam conditions were performed using CRIB[2,3]. A self-supporting ^{12}C primary target of 0.4 mg/cm^2 was installed at F0. This ^{12}C target was bombarded by primary beams of ^{40}Ar^{11+} of 4.5 MeV/u and ^{40}Ca^{11+} of 5.6 MeV/u to produce secondary beams. A parallel-plate avalanche counter (PPAC) was set at a dispersive focal plane (F1) for beam monitoring. Another PPAC and a Si detector of 1.5 mm thickness were installed for particle identification (PI) at an achromatic focal plane (F2). For PI, a monolithic Si detector[4] was placed behind the PPAC at F1. This Si detector consists of 1.5-μm-thick and 500-μm-thick layers that are used as ΔE and E counters, respectively. A Ge detector was set at 260 mm from the ^{12}C primary target for measuring γ rays emitted from the fusion reaction products. A 2.2-μm-thick Havar foil was installed at the entrance of the F0 chamber to enclose helium gas and used as a gas-filled recoil isotope separator (GARIS). Helium gas was supplied from the entrance of the F0 chamber to the exit of the F2 chamber.

Figure 1 shows the single spectrum measured by the Ge detector placed at F0. In the measurement using the ^{12}C + ^{40}Ar reaction, the primary beam intensity was 10 enA considering the limit of the count rate of the Ge detector. The bombarding energy was 4.1 MeV/u after installing the Havar foil. Gamma rays emitted from $^{45-48}$Ti, $^{47-49}$V and ^{49}Cr could be identified as shown Fig. 1. Sharp peaks such as 1333 keV were derived from the background γ-rays.

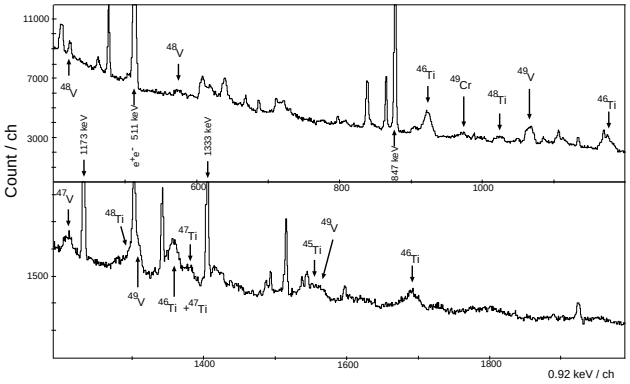

Fig. 1. Single spectrum of Ge detector placed at F0.

The proper gas pressure for the GARIS condition was searched using a primary beam with a beam energy of around 4 MeV and a $Z \approx 20$ region. The half widths of the momentum distribution become narrower from 2.7 to 1.6 % when the helium gas pressure was increased from 6 to 20 Torr. However, PPAC could not be operated over 20 Torr and the proper He gas pressure was not found.

PI using the ΔE-E counter of the monolithic Si detector was performed with a helium gas pressure of 8 Torr. To confirm that the fusion products reached the ΔE-E counter, the coincidence of the ΔE counter and Ge detector was measured.

Further analysis is now in progress.

References

1) K. Langanke and G. Martinez-Pinedo: Rev. Mod. Phys. **75**, 819 (2003).
2) S. Kubono et al.: Eur. Phys. J. A **13**, 217 (2002).
3) Y. Yanagisawa et al.: Nucl. Instrum. Methods Phys. Res. A **539**, 73 (2005).
4) A. Musumarra et al.: Nucl. Instrum. Methods Phys. Res. B **409**, 414 (1998).

*1 Center for Nuclear Study, University of Tokyo
*2 Department of Physics, Ewha Woman University
*3 Institute of Physics and Electronic, Vietnam Academy of Science and Technology

Production of low-energy polarized radioactive beams using CRIB

K. Shimada,[*1] D. Nagae,[*1] K. Asahi, T. Arai,[*1] M. Takemura,[*1] T. Inoue,[*1] K. Takase,[*1] S. Kagami,[*1] N. Hatakeyama,[*1] Y. Kobayashi, H. Ueno, A. Yoshimi, D. Kameda, T. Nagatomo, T. Sugimoto, S. Kubono,[*2] H. Yamaguchi,[*2] Y. Wakabayashi,[*2] G. Amadio,[*2] S. Hayakawa,[*2] J. Murata,[*3] and H. Kawamura[*3]

A beam of radioactive nuclei (RNB) with their spins polarized has been applied to various fields. Studies of RNBs are performed not only in nuclear physics such as nuclear moments and β decays[1], but also in condensed matter physics including magnetism in metals and insulators, impurities and electronic dynamics in semiconductors[2], and superconductivity[3]. RNBs may even be an exclusive tool for investigating surfaces, layers and nanosized structures, if the energy and spatial distribution (spot size) of spin-polarized RNBs are controlled with sufficient precision.

One of the most appropriate methods of obtaining such RNBs may be RNB production via inverse-kinematics reactions. The spin polarization of a recoil product in the low-energy nucleon-transfer reaction depends on both the recoil angle and kinetic energy of the product nuclei[2,4]. In inverse-kinematics, the distribution in the recoil angle in normal kinematics is forward focusing, thus facilitating a very efficient collection of RNB particles. However, the small but finite widths of the angular and energy distributions of RNB preserve the memory of the recoil angle and energy. Thus, by selecting a certain region of angles and energies of RNB emission, the RNB may be spin-polarized. In addition, in inverse-kinematics, we could use an in-flight separator that provides the separation of the RNB particles from other species and facilitates the formation of a well-focused RNB.

We are developing a method of producing a spin-polarized ^{17}N or ^{18}N beam via inverse-kinematics reactions using a low-energy in-flight separator for RNBs, called CRIB[5]. CRIB consists of a double achromatic system and Wien filter, and its configuration is shown in Fig. 1. A primary beam of $^{18}O^{7+}$ at 7.0 MeV/u and with an intensity of 240 pnA bombarded a thin Be target of 2.8 mg/cm^2 , which was installed in a target chamber at F0. The ^{17}N (^{18}N) beam was produced by nucleon transfer (exchange), and its momentum was 1.83 GeV/c (1.86 GeV/c). By limiting the emission angle to $-(0.6°$–$2.8°)$ and the momentum dispersion to 1.83 GeV/c –1.85 GeV/c, the yield of the ^{17}N (^{18}N) beam was typically 10^5 cps (10^4 cps). In this scheme, however, it is hard to exclude other impurities mixed in the beam. In order to check the ratio of impurities and the possibilities of excluding them in the off-line analysis, we stopped the beam particles and observed the time spectrum of β emitted in their β decay. The

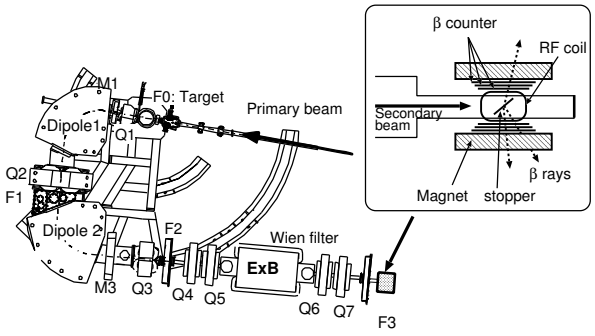

Fig. 1. Schematic view of CRIB and β-NMR apparatus.

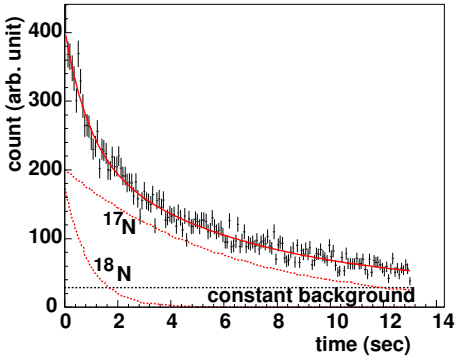

Fig. 2. Time spectrum of detected β rays. The solid curve represents the best fit to the data with the theoretical function consisting of two exponentials plus a constant background. The dashed curves show the decay curves of ^{17}N ($T_{1/2} = 4.173$ s) and ^{18}N ($T_{1/2} = 624$ ms), and constant background fitting, respectively.

time spectrum for the ^{17}N beam is shown in Fig. 2. The ratios of the β rays emitted from ^{17}N and ^{18}N are 67 % and 10 %, respectively.

The measurement of spin polarization by β-NMR is being prepared. After the production of spin-polarized ^{17}N or ^{18}N beams is established, we plan to use them for the study of structures formed by N impurities in a diamond crystal[6].

*1 Department of Physics, Tokyo Institute of Technology
*2 Center for Nuclear Study, Tokyo University
*3 Department of Physics, Rikkyo University

References

1) H. Ueno et al.: Phys. Lett. B **615**, 186–192 (2005).
2) T. Izumikawa et al.: Hyp. Int. **136/137**, 599 (2001).
3) J. P. Araújo et al.: Nucl. Instrum. Methods Phys. Res. B **148**, 807 (1999).
4) M. Tanaka et al.: Nucl. Phys. A **263**, 1 (1976).
5) Y. Yanagisawa et al.: Nucl. Instrum. Methods Phys. Res. A **539**, 74–83 (2005)
6) T. Arai et al.: RIKEN Accel. Prog. Rep. **39**, 90 (2006).

Electron scattering from unstable nuclei by the SCRIT method (III)†

T. Suda, T. Emoto, Y. Furukawa[1], K. Ishii[2], S. Ito, K. Kurita[2], A. Kuwajima[1], T. Tamae[1], M. Wakasugi, S. Wang and Y. Yano

[electron scattering, RI, SCRIT]

Electron scattering is one of the most precise probes for studying the internal structure of atomic nuclei, and will surely play an essential role in the structure studies of radioactive isotopes (RI) when an electron-RI (eRI) scattering experiment becomes possible.

We have proposed a novel scheme for an eRI scattering experiment, SCRIT (Self-Confining RI Target). On the basis of numerical simulations, a sufficiently high luminosity for elastic electron scattering, $10^{27}/\mathrm{cm}^2/\mathrm{s}$, is expected for 10^7/s ion injection with a 500-mA electron beam current[1)]. Since 2004, we have started feasibility studies by installing a SCRIT prototype at an existing electron storage ring, KSR, in Kyoto University.

This year, we have installed a set of pure CsI calorimeters for the scattered electron detection. The detector consists of seven optically isolated pure CsI crystals, and each crystal has a hexagonal cross section with a diameter of 80 mm and a length of 200 mm. The detector was placed at a scattering angle of 30 deg. and the SCRIT region was viewed through a drift chamber.

The response of each crystal was measured using cosmic rays. In addition, we installed a W wire in the SCRIT chamber, whose thickness was 50 μm. The wire position is remotely controllable, and it can be placed very close to the circulating electron beam. The elastically scattered electrons from the wire were clearly observed, and the response function of the CsI detector for a 100-MeV electron was determined.

Figure 1 shows the electron energy spectrum measured with continuous injection of Cs ion from an external ion source. The storaged electron beam current was kept at about 50 mA.

In the figure, a bump at about 100 MeV is observed. A GEANT simulation, in which the prototype geometry is completely taken into account, shows that the low-energy region of the spectrum is due to background, which originates from halo electrons that produce the electro-magnetic showers in the materials in the SCRIT region. The energy dependence is well reproduced by this background simulation. The energy spectrum obtained after background subtraction is shown together in Fig.1, in which a broad peak at about $E = 90$ MeV is clearly observed. The position and width of the peak shown in the upper figure of Fig.1 are both consistent with the response to the 100-MeV scattered electrons from the W-wire. Since the peak was not observed before starting the Cs ion injection, one can conclude that the elastically scattered electrons are from the injected Cs ions. The achieved luminosity is estimated to be 2 x $10^{25}/\mathrm{cm}^2/\mathrm{s}$.

Measurements with and without Cs ion injection, which is periodically repeated at a frequency of 10 Hz, however, do not show any difference in the number of elastic events. This observation suggests that the elastic events may not come from the externally injected Cs ions but from Cs ions probably evaporated from the surface of materials such as electrodes. Since we injected so many Cs ions in our previous measurement, many Cs ions may have adhered on the surface of such materials. We will soon start further measurements to confirm this with efforts to reduce the contribution from evaporated Cs ions.

References

1) M. Wakasugi, T. Suda and Y. Yano: Nucl. Instrum. Methods **A532**, 216 (2004).

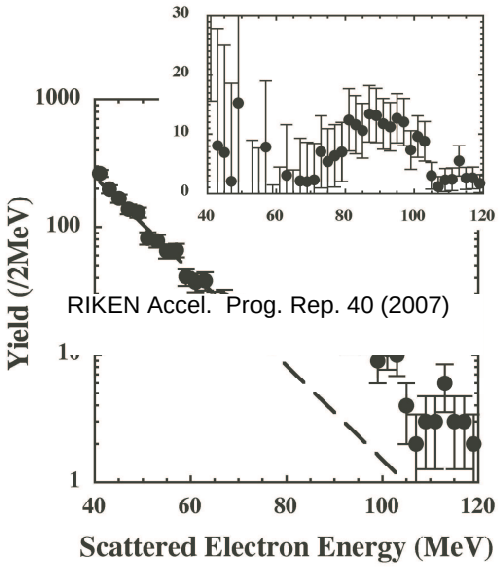

Fig. 1. Electron energy spectrum. The overlaid figure shows the energy spectrum after background subtraction. The dashed line in the figure is an extrapolation from the low energy spectrum, which is consistent with the GEANT simulation. A peak centering at about 90 MeV corresponds to elastic scattering events from Cs ions.

*1 Tohoku University
*2 Rikkyo University

Electron scattering off wire targets in SCRIT

Y. Furukawa,[*1] A. Kuwajima,[*1] T. Tamae,[*1] T. Emoto, K. Ishii,[*2] S. Ito, K. Kurita,[*2] A. Noda,[*3] T. Shirai,[*3] T. Suda, H. Tongu,[*3] M. Wakasugi, S. Wang, and Y. Yano

[electron scattering, wire targets, SCRIT]

We are testing a prototype of the SCRIT (Self-Confining RI Target) at KSR (Kaken Storage Ring) of Kyoto University. In the SCRIT, targets ions are confined transversely by a negative potential produced an electron beam, and longitudinally using an electrostatic mirror potential generated by electrodes. The longitudinal length of the trapped ions is 12 cm, and their density is very low. As the number of scattered electrons from the SCRIT is very few, it is hard to calibrate electron detection counters and a luminosity monitor using those electrons. We installed a wire target system for such calibrations. It is also used for improvement of the spacial resolution of a drift chamber.

Two 105 mm-long wires of thick tungsten with 50 μm in diameter, and of thin carbon with about 10 μm in diameter, have been stretched on the holder as shown in Fig. 1. The lower wire is of tungsten and the upper one is of carbon. The distance of the two wires is 12 mm. The wires can be inserted by remote control onto the storaged electron beam through the space between two electrodes at 6.6 cm upstream from the center of the SCRIT.

An energy spectrum of scattered electrons off the tungsten wire measured using a pure CsI calorimeter is shown in Fig. 2 by a solid line. The calorimeter consists of seven optically-separated crystals of pure CsI with a hexagon cross section of 80 mmϕ and 200 mm long. It was set at a scattering angle of 30°. The incident electron energy is 121 MeV. The energy was calibrated by comparing the cosmic-ray spectrum with a GEANT simulation. There is a large energy loss of scattered electrons in the material between the wire and the CsI calorimeter, such as plastic scintillators for trigger and plastic covers for protection of the drift chamber. The material also broadens the peak of elastically-scattered electrons. The energy spectrum calculated using the GEANT simulation is also shown in Fig.2 by a broken line. Overall agreement between the calculation and measurement is seen except the highest energy part of the spectrum; the source of this discrepancy is under investigation. The material between the target and the CsI calorimeters should be removed as much as for obtaining a more accurate spectrum.

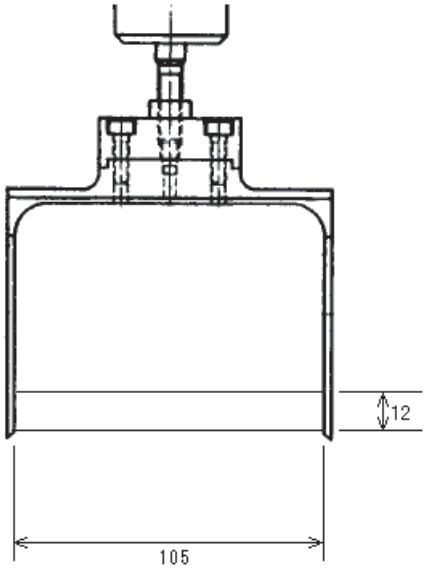

Fig. 1. Wire targets. The lower is 50 μm tungsten, and the upper is 10 μm carbon.

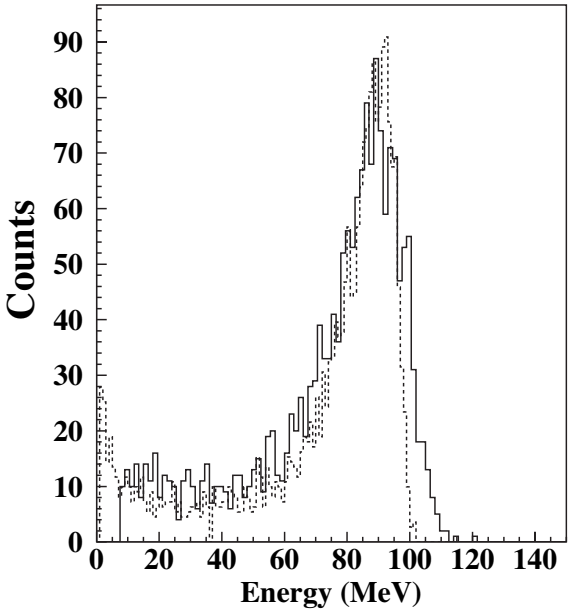

Fig. 2. Energy spectrum of the scattered electrons off the tungsten wire measured with a CsI calorimeter. A solid line shows the measured spectrum, and a broken line represents a GEANT simulation.

*1 Tohoku University
*2 Rikkyo University
*3 Kyoto University

Laser spectroscopy of $^{7,10}Be^{+}$ in an online ion trap at SLOWRI

T. Nakamura, M. Wada, K. Okada,[*1] A. Takamine,[*2] Y. Ishida, Y. Yamazaki, T. Kambara, Y. Kanai, T. M. Kojima, Y. Nakai, N. Oshima, [*3] A. Yoshida, T. Kubo, S. Ohtani,[*4] K. Noda,[*5] I. Katayama,[*6] V. Lioubimov,[*7] H. Wollnik,[*8] V. Varentsov[*9] and H. A. Schuessler[*7]

[online ion trap, laser spectroscopy, $^{10}Be^{+}$, $^{7}Be^{+}$, isotope shift]

An online ion trap for precision laser spectroscopy has been developed at the prototype slow radioactive ion beam facility (SLOWRI) of RIKEN. Energetic radioactive beryllium isotope ions ($^{7}Be^{+}$ and $^{10}Be^{+}$) provided by the projectile fragment separator RIPS are decelerated and cooled in a gas catcher cell, and the thermal ions are extracted and collected in a linear rf trap by an rf carpet ion guide.[1)]

Laser spectroscopy of the $2s\ ^2S_{1/2} \rightarrow 2p\ ^2P_{3/2}$ transition for trapped $^{7,9,10}Be^{+}$ ions had been performed and their absolute transition frequencies were measured with accuracies of $\sim 10^{-8}$. From these frequencies, we determined the absolute isotope shifts of beryllium isotopes for the first time.[2)]

Neglecting, for the time being, the small effect from the nuclear charge radii, the isotope shift is given by the observable transition frequency $_{\rm obs}$ between the two energy levels ϵ_a and ϵ_b as,

$$h\ _{\rm obs} = \epsilon_a \quad \epsilon_b = h\ ^{\infty} \quad \frac{\mu}{M_{\rm n}} h\ ^{\infty} + \frac{\mu}{M_{\rm n}}\kappa, \qquad (1)$$

where μ is the reduced electron mass, $M_{\rm n}$ is the nuclear mass, $^{\infty}$ is the transition frequency of the infinite heavy nucleus, $\kappa = K_a \quad K_b$ is the differential mass polarization parameter, $K = \left\langle \sum_{i<j}^{N} \mathbf{p}_i \quad \mathbf{p}_j \right\rangle / m_e$ is the mass polarization parameter of an N-electron atomic system, $\mathbf{p}_k$ is the momentum of the k-th electron, and m_e is the electron mass. In Eq. (1), the second term is the normal mass shift (NMS) and the third term is the specific mass shift (SMS).

The absolute transition frequencies of the $2s\ ^2S_{1/2} \rightarrow 2p\ ^2P_{3/2}$ transition of $^{7}Be^{+}$, $^{9}Be^{+}$ and $^{10}Be^{+}$ ions were determined to be 957 347.37(12) GHz, 957 396.515(14) GHz and 957 414.839(35) GHz, respectively. By fitting with Eq. (1), we determined the transition energy of infinitely heavy Be, $^{\infty} = 957\,569.55(28)$ GHz, and the differential mass polarization parameter $\kappa/h =$ 1 884.5(46) THz. Figure 1 illustrates these results. Details of these experiments are described in Ref.[2)].

We plan to proceed to isotope shift measurements of even higher accuracies, such as 10^{-10}, by utilizing the laser-laser double-resonance spectroscopy method [3)] and the frequency comb[4)] clockwork frequency calibration. Such measurements will enable us to determine the charge radii of the beryllium isotopes when more accurate theoretical atomic structure calculations are also available.

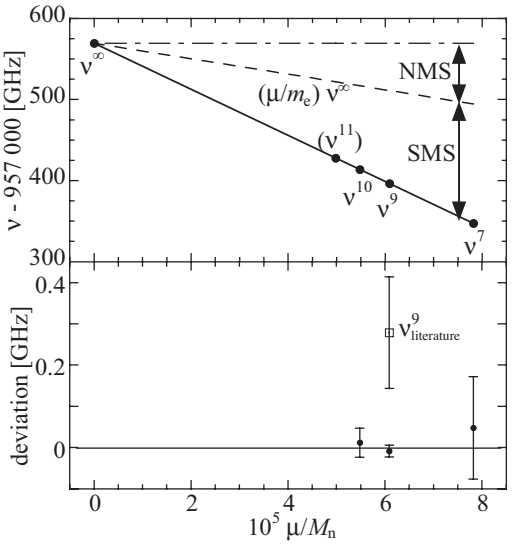

Fig. 1. Transition frequencies ^{A} are plotted as a function of $/M_{\rm n}$ to indicate the two contributions — the NMS and the SMS — to the isotope shifts. The deviations from the fits are also indicated at the bottom. The old value for stable $^{9}Be^{+}$[3)] which is an extrapolated value from the measurement at high magnetic field is indicated as $^{9}_{\rm literature}$.

A combination of the charge radii values with the isotope shift measurements and the magnetization distribution with the hyperfine anomaly measurements would allow us to perform complete measurements of the different distributions of neutrons and protons in a nucleus of the beryllium isotopes obtainable with a purely electromagnetic probe.

*1 Department of Physics, Sophia University
*2 Graduate School of Art and Science, University of Tokyo
*3 National Institute of Advanced Industrial Science and Technology (AIST)
*4 Institute for Laser Science, University of Electro-Comm.
*5 National Institute for Radiological Science
*6 High Energy Accelerator Research Organization (KEK)
*7 Department of Physics, Texas A&M University, USA
*8 II. Physikalisches Institute, Giessen University, Germany
*9 Kholopin Radium Institute, Russia

References
1) A. Takamine et al.: Rev. Sci. Instrum. **76**, 103503 (2004).
2) T. Nakamura et al.: Phys. Rev. A **74**, 052503 (2006).
3) J. J. Bollinger et al.: Rhys. Rev. A **31**, 2711 (1985).
4) T. Udem et al.: Nature (London) **416**, 233 (2002).

Pumping ^{229m}Th by hollow-cathode discharge [IV]

Hiromitsu Haba, Mitsuo Hara,[*1] Takashi T. Inamura, Yoshitaka Kasamatsu,[*2] Hidetoshi Kikunaga, Toshiaki Mitsugashira,[*1] Takashi Nakanishi,[*3] Tsutomu Ohtsuki,[*4] Atsushi Shinohara,[*5] Yoshimitsu Suzuki,[*1] Koichi Takamiya,[*6] Shin Watanabe,[*1] Akihiko Yokoyama,[*3] and Hideyuki Yuki [*4]

[Nuclear structure, NEET by electric discharge, alpha decay]

This is the 4th report of our series of endeavors to search for evidence of an extremely low-lying isomer in ^{229}Th, the energy of which is believed to be 3.5 ± 1.0 eV.[1)] Since it was first postulated by Kroger and Reich in 1976,[2)] this exotic isomer has long been sought but has yet not been confirmed. Here, we summarize what we have learned for the last three years and what we are going to do.

In 2002, Inamura and his international collaborators proposed a novel method of populating the "3.5-eV isomer" ^{229m}Th by hollow-cathode electric discharge as follows:[3)] The atomic states are excited as is the case of optical spectroscopy and then NEET (nuclear excitation by electron transition or inverse internal conversion)[4)] through a certain excited atomic state is expected to populate ^{229m}Th, although its exact excitation energy is not known. This method was coupled with α measurement to detect the population of ^{229m}Th after switching off the electric discharge by fully making use of the high S/N ratio in α measurement.[5,6)] Schematic excitation and deexcitation processes of ^{229m}Th are shown in Fig. 1. First, assuming its half-life to be 14 ± 3 hours according to a preliminary measurement by means of the ^{230}Th (γ,n) reaction,[7)] we started measuring α decay from ^{229m}Th after the electric discharge. Our first measurement did not confirm the preliminary half-life and instead suggested that it is definitely shorter than 20 minutes.[8)] Recently, we conducted rapid chemistry of the ^{229}Th sample,[9)] which was subjected to the discharge in the hollow-cathode tube for about 20 minutes, to have high-resolution α spectra (17-keV fwhm for ^{241}Am 5486-keV alphas) as a function of time. The whole process was repeated four times and each measurement was started about 5 minutes after the discharge. However, no trace of delayed α components was found. Not only did that confirm our previous measurements,[8,10)] but it also indicated that the half-life should be less than 2 minutes; otherwise, we would have detected delayed α components.

Now, we have to deal with a small α branching from the isomer that would be some five hundred times smaller than the branching expected at the beginning. [5, 6)] (See Fig. 1.) To start the measurement in the hollow-cathode tube immediately after switching off the discharge with a better energy resolution we have removed an Al-coated Mylar window (see Ref. 10) and set a shutter to shield the intense light coming from the hollow cathode during the discharge. We have tested the whole setup and confirmed that we can start the measurement within 30 seconds after the discharge. The next and probably last measurement with this setup will be carried out shortly.

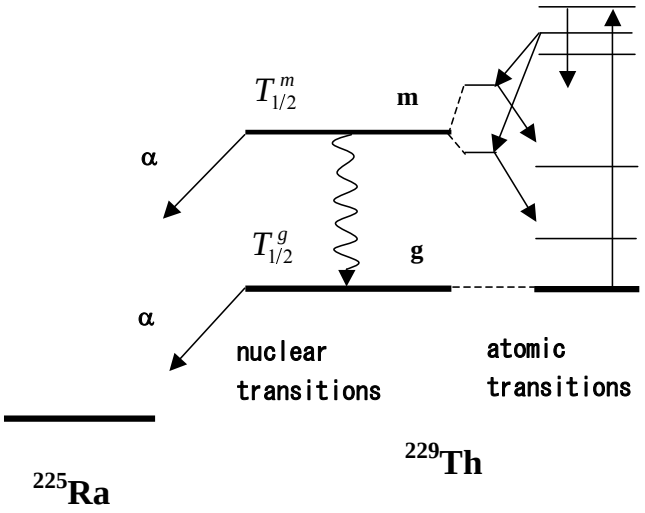

Fig. 1. Schematic excitation and deexcitation processes of ^{229m}Th during hollow-cathode electric discharge. Nuclear ground and isomeric states are denoted by g and m, respectively; probable intermediate states produced by coupling atomic and nuclear states are denoted by two short lines.

References

1) R. G. Helmer and C. W. Reich: Phys. Rev. C **49**, 1845 (1994).
2) L. A. Kroger and C. W. Reich: Nucl. Phys. **A259**, 29 (1976).
3) T. T. Inamura et al.: Annual Report 2002, Heavy Ion Laboratory, Warsaw University, p. 42; Czech. J. Phys. **53**, B349 (2003).
4) M. Morita: Prog. Theor. Phys. **49**, 1574 (1973).
5) H. Haba et al.: RIKEN Accel. Prog. Rep. **37**, 263 (2004).
6) T. T. Inamura, T. Mitsugashira, and the Oarai Collaboration: Hyp. Interact. **162**, 115 (2005).
7) T. Mitsugashira et al.: J. Radioanal. and Nucl. Chem. **255**, 63 (2003).
8) S. Enomoto et al.: RIKEN Accel. Prog. Rep. **38**, 249 (2005).
9) H. Kikunaga et al.: Radiochim. Acta **93**, 507 (2005).
10) H. Haba et al.: RIKEN Accel. Prog. Rep. **39**, 227 (2006).

[*1] Oarai Branch, Institute for Materials Research, Tohoku University
[*2] Advanced Science Research Center, JAEA, Tokai
[*3] Graduate School of Natural Science and Technology, Kanazawa University
[*4] Laboratory of Nuclear Science, Tohoku University
[*5] Graduate School of Science, Osaka University
[*6] Research Reactor Institute, Kyoto University

Dependence on ortho-para D_2 ratio of $dd\mu$ formation rate in muon-catalyzed fusion

K. Ishida, H. Imao,[*1] T. Matsuzaki, Y. Matsuda, N. Kawamura,[*2] A. Toyoda,[*2] and K. Nagamine[*2,*3,*4]

[muon, nuclear fusion, deuterium]

In the muon-catalyzed fusion cycle, the formation of a muonic molecule is usually the slowest of all the processes; thus, increasing its rate is the key to improving μCF efficiency. In a previous report[1)], we showed the result of a preliminary measurement of $dt\mu$ molecular formation rate at the RIKEN-RAL Muon Facility, in which we compared the rate in an ortho-D_2/T_2 mixture with that in normal-D_2/T_2. The result was not conclusive because of the possibility of fast ortho-para equilibration in the presence of radioactive tritium. Thus, we are studying a simpler system, namely, $dd\mu$ formation in ortho D_2 and normal D_2. The information on $dd\mu$ formation will be useful for elucidating $dt\mu$ formation since both processes occur as a result of a resonant molecular formation mechanism.

The experiment was performed[2)] at the TRIUMF M9B muon channel in Canada. The timing spectrum of fusion neutron emissions relative to muon injection has two exponentially decaying components. The faster and larger one is due to resonant $dd\mu$ formation from $d\mu$ in the upper hyperfine state ($F = 3/2$) and the slower one is due to nonresonant formation from $d\mu$ in $F = 1/2$. The resonant $dd\mu$ formation rate is defined as the rate that a $d\mu$ ($F = 3/2$) reacts with a surrounding D_2 to form a $dd\mu$ molecule and can be determined from the amplitude of the faster decaying component. The measured rates in solid and liquid D_2 are shown in Fig. 1. We observed a clear decrease in the rate for ortho D_2 compared with that for normal D_2, which was opposite of the theoretical predictions based on the isolated gas model.

For the gas case, the timing spectrum showed a small deviation from the two-exponential structure. Thus, instead of fitting the spectrum with two components, the total yields of fusion neutrons were compared in Fig. 2. The ortho-para dependence for gas D_2 was found to be the opposite of that in liquid and solid D_2. According to a recent theory[5)], the resonance condition could be modified by surrounding molecules (density effect). Thus far, the measurement with gas had been carried out only up to 0.17-fold the liquid hydrogen density. We are planning an experiment to fill the density gap between liquid and gas using D_2 near the critical point.

*1 JSPS Fellowship
*2 High Energy Accelerator Research Organization
*3 Department of Physics, University of California, Riverside, USA
*4 RIKEN

References
1) K. Ishida et al.: RIKEN Accel. Prog. Rep. 39, 82 (2006).
2) H. Imao et al.: Phys. Lett. B 632, 192 (2006).
3) M.P. Faifman et al.: Muon Catalyzed Fusion 4, 1 (1989).
4) M.P. Faifman: private communication.
5) A. Adamczak et al.: Phys. Rev. A 64, 052705 (2001).

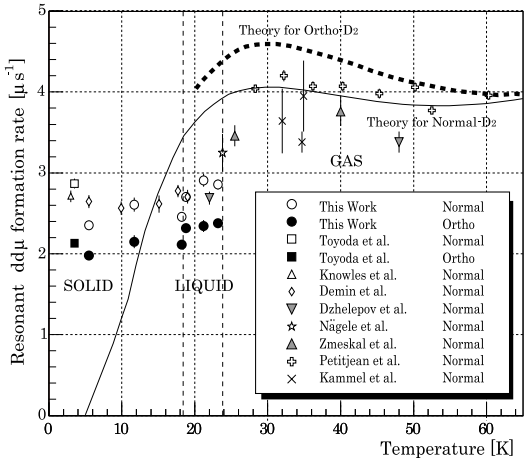

Fig. 1. Temperature dependence of resonant $dd\mu$ formation rate. The solid line represents a theory fit[3)] to the gaseous normal-D_2 data and the dotted line represents the increase for ortho-D_2 predicted by the isolated gas model[4)].

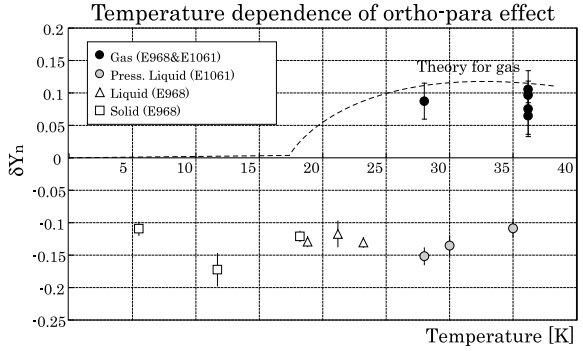

Fig. 2. Relative increase in fusion neutron yield in ortho D_2 ($Y_n^{\rm ortho}$) compared with that in normal D_2 ($Y_n^{\rm norm}$) obtained in our two runs, E968 and E1061. Here, $\delta Y_n = (Y_n^{\rm ortho} - Y_n^{\rm norm})/(Y_n^{\rm ortho} + Y_n^{\rm norm})/0.33$. The factor 0.33 takes account of the difference of the ortho D_2 fraction in two targets. The dashed line shows a prediction for gas[4)].

Temperature dependence of muon transfer reaction†

N. Kawamura, K. Nagamine, T. Matsuzaki, K. Ishida, H. Imao, Y. Matsuda, S. N. Nakamura,[*1] M. Tanase,[*2] M. Kato,[*2] H. Sugai,[*2] K. Kudo,[*3] N. Takeda,[*3] and G. H. Eaton[*4]

[Muon catalyzed fusion, muon transfer reaction]

The muon transfer reaction from muonic hydrogen to helium is an important problem in muon catalyzed fusion (μCF) study as well as in mesic-atom study, since this reaction occurs through the formation of muonic molecules: $h\mu + (\mathrm{He}\,2e^-) \rightarrow [(h\mathrm{He}\mu)e^-] + e^-$, where h stands for a hydrogen isotope nucleus and He for a helium one. An intermediate state, such as $t\mathrm{He}\mu$, is formed in an unstable excited state and then deexcites to the dissociated ground state, *i.e.*, triton and muonic helium, through a radiative process with 6.8-keV photon emission or nonradiative process. The transition rate from muonic hydrogen to helium is predominately determined by the formation rate of the intermediate muonic molecule. The formation rate was expected to show an isotope dependence and also strong temperature dependence. In particular, in the case of $t\mu$ and helium, the strongest temperature dependence was predicted[1]. However, few experiments have been conducted because of technical difficulties.

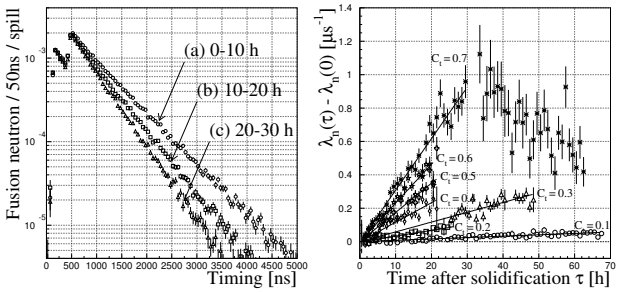

Fig. 1. Typical time spectra of fusion neutrons at (a) $\tau = 0-10$ h, (b) $10-20$ h and (c) $20-30$ h after solidification. (left) Plot of the increase of λ_n, $\lambda_n(\tau) - \lambda_n(0)$. (right)

On the other hand, in the study of μCF in a solid deuterium and tritium (D-T) mixture, we found that ^{3}He from tritium β-decay accumulated in solid D-T[2]. Namely, ^{3}He increases with time after solidification, and thus the probability for muon loss from the μCF cycle (W) increases, and consequently the neutron disappearance rate (λ_n) also increases, as shown in Fig. 1. From the tritium concentration dependence of the increase rate in W, the muon transfer rate from $t\mu$ to ^{3}He was determined to be about $(4.3 \pm 0.1) \times 10^9$ s^{-1} at 16 K.

Applying this helium accumulation effect, we can observe the temperature dependence of the muon transfer rate. In order to determine the helium transfer rate, it is required for all helium from tritium β-decay to accumulate in the solid. However, because of sublimation due to β-ray heating[3], in some cases of former μCF experiments, the D-T target was deformed and some helium escaped from the solid. In a recent study, this problem was solved using a specially prepared D-T solid. Thus, at present, we are ready to take data. The present study can be realized only at the RIKEN-RAL Muon Facility, where a pure (^{3}He free) solid D-T target and an *in-situ* tritium gas-handling system are available.

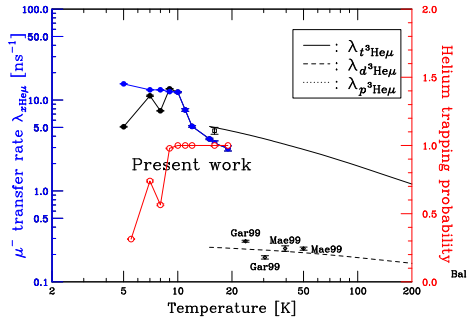

Fig. 2. Temperature dependence of muon transfer rate from muonic hydrogen to helium.

The present study was conducted at the RIKEN-RAL Muon Facility. An advanced tritium gas-handling system, which had an *in-situ* ^{3}He-removal capability with a palladium filter, was applied to prepare a D-T mixture gas with the intended tritium concentration. By controlling the cryogenic system, the target cell was adjusted to a temperature from 5 to 16 K.

Figure 2 shows a preliminary result of the muon transfer rate that was determined by detecting fusion neutrons. Through the present study, we found an evidence of helium escape from solid hydrogen below 10 K. In order to gain further knowledge of the muon transfer reaction, this helium escape phenomenon must be understood.

References

1) A. V. Kravtsov and A. I. Mikhailov; J. Exp. Theor. Phys. 90 (2000) 45.
2) N. Kawamura *et al.*; Phys. Lett. B 465 (1999) 74.
3) J. K. Hoffer and L. R. Foreman; Phys. Rev. Lett. 60 (1988) 1310.

*1 Department of Physics, Tohoku University
*2 Japan Atomic Energy Agency
*3 Advanced Industrial Science and Technology
*4 Rutherford Appleton Laboratory

Muon Transfer Reaction Studies in Solid Deuterium Films with Implanted Ions

P. Strasser, [*1] K. Nagamine, [*2] T. Matsuzaki, K. Ishida, Y. Matsuda, and M. Iwasaki

[Muonic atom spectroscopy, Solid hydrogen film, Ion implantation]

We proposed the cold hydrogen film method[1)] to expand muonic atom spectroscopy by utilizing nuclear beams, including, in the future, radioactive isotope (RI) beams, to produce radioactive muonic atoms. This method will enable the study of unstable nuclei using the muonic X-ray method at facilities in which both intense μ^- and RI beams will be available. The basic concept is to stop both μ^- and nuclear beams simultaneously in a solid hydrogen film, followed by the application of the direct muon transfer reaction to higher Z nuclei to form radioactive muonic atoms.

An experimental program to implant stable ions in a solid hydrogen (H_2/D_2) film has been initiated at the RIKEN-RAL muon facility to experimentally establish the feasibility of this method. The first test experiments were performed with a relatively large number of implanted argon ions, because of the relatively low μ^- beam intensity at 27 MeV/c. Future intense muon beams will require fewer implanted ions. New measurements were performed with lower ^{40}Ar concentrations to investigate the muon transfer reaction and the diffusion process of dμ atoms in pure solid D_2 films with argon ions implanted non-uniformly. The advantage of using a pure D_2 film for the formation of μZ atoms, compared with a pure H_2 film, is that after ddμ muonic molecule formation, the μ^- is mostly released, while it is lost after ppμ is formed. Since the range of 33-keV Ar ions in solid D_2 is only about 0.25 μm, with a range straggling of 0.1 μm, it is very difficult to perform a uniform implantation in a thick D_2 layer. Consequently, each Ar implantation was separated from the next by depositing a fixed amount of D_2 to yield a total D_2 layer thickness of 1 mm. Every implantation region was identical, with a local concentration of nearly 1000 ppm, and the distance between each implantation was changed for each target. Figure 1 shows the total energy spectra measured by the Ge detector with 1-mm pure D_2 and (a) 20 implantations separated by 50 μm, (b) 10 implantations separated by 100 μm, and (c) 5 implantations separated by 200 μm, corresponding to average Ar concentrations throughout the D_2 layer of about 2, 1, and 0.5 ppm. Even with an inhomogeneous target and only 5 implantations spaced 200 μm apart, or a total concentration of 0.5 ppm, very strong muon transfer μAr(2-1) X-rays at 644 keV can still be detected. Unfortunately, owing to a trouble with the compressor of the muon decay channel solenoid, only

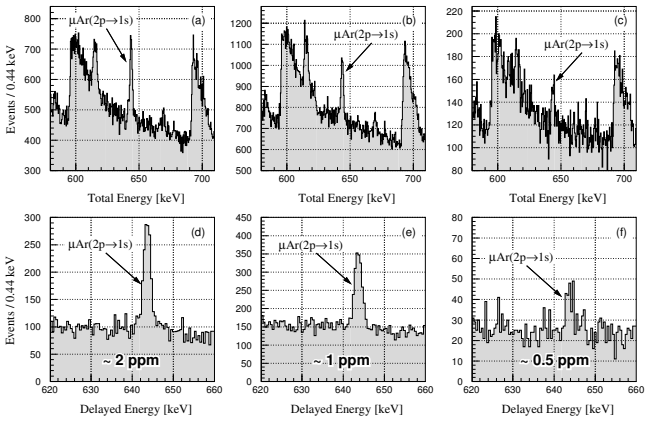

Fig. 1. Energy spectra with 1-mm pure D_2 and about 2, 1 and 0.5 ppm of ^{40}Ar ions implanted non-uniformly. Total energy spectra (top) and delayed events (bottom) from 250 ns to 32 μ after the second muon pulse.

12 hours of data was accumulated. Because of the marked decrease in the Bragg cross section at a low dμ collision energy in solid D_2[2)], the dμ atom mean-free-path is significantly increased to nearly 10–20 μm below ~1 meV, resulting in a high dμ atom mobility and a very long diffusion length (similar effects are predicted for pμ in solid H_2 and tμ in solid T_2). With 1 ppm, the number of argon ions implanted was 6×10^{16} in an ~4-cm-diameter and 1-mm-thick D_2 film, or 6×10^{15}/cm^2. At a ppm level Ar concentration, most of the muon transfer occurs delayed, and the S/N ratio can be greatly improved by selecting only delayed events as shown in Figs. 1d, 1e and 1f, demonstrating the advantage of using a pulsed muon beam.

Preliminarily, we can conclude that uniform implantation is not critical to observe a muon transfer reaction. A diffusion length of dμ atoms in solid deuterium of approximately 20 μm can be extracted by fitting the different X-ray yields as a function of the implantation distance, which is consistent with the predicted value based on calculated cross sections[2)]. This solid state effect seriously limits the minimum layer thickness, and makes the use of a very thin layer impossible because of the significant dμ loss.

References

1) P. Strasser et al.: Hyp. Int. 119, 317 (1999); Nucl. Instr. and Meth. A 460, 451 (2001); AIP Conf. Proc. 793, 242 (2005).
2) A. Adamczak: Hyp. Int. 119, 23 (1999).

*1 Muon Science Laboratory, IMSS, KEK
*2 Univ. of California Riverside, CA, USA

Coulomb breakup effects on elastic cross section of ^{6}He+^{209}Bi scattering near Coulomb barrier energy

T. Matsumoto, T. Egami,[*1] K. Ogata,[*1] Y. Iseri,[*2] M. Kamimura, and M. Yahiro[*1]

[Nuclear reaction, unstable nuclei]

Recently, Keeley *et al.*[1] have analyzed ^{6}He+^{209}Bi scattering at 19 and 22.5 MeV near the Coulomb barrier energy[2,3] by a continuum-discretized coupled-channel method (CDCC)[4] that is a fully quantum-mechanical method for describing the scattering of a three-body system. In the analysis, a ^{6}He+^{209}Bi system was assumed to be a ^2n+^{4}He+^{209}Bi three-body system, that is, the neutron pair in ^{6}He was treated as a single particle, dineutron (^2n). However, their calculation did not reproduce the experimental data of the elastic and total reaction cross sections. This indicates that ^{6}He+^{209}Bi scattering cannot be described by the three-body system. Since ^{6}He is well known as a two-neutron halo nucleus, its structure should be described by an n+n+^{4}He three-body system rather than the ^2n+^{4}He two-body system. Thus, it is necessary to analyze ^{6}He+^{209}Bi scattering using an n+n+^{4}He+^{209}Bi four-body model.

In this work, we analyze ^{6}He+^{209}Bi scattering at 19 and 22.5 MeV using an n+n+^{4}He+^{209}Bi four-body model that is an extension of the CDCC and is called a four-body CDCC. This is the first application of the four-body CDCC to low-energy scattering in which both nuclear and Coulomb breakup processes are significant. In the four-body CDCC, the three-body breakup continuum of 6He is discretized by diagonalizing the internal Hamiltonian in a space spanned by a Gaussian basis function. Thus far, the Gaussian basis function has been successfully used for solving the bound-state problems of few-body systems. This approach is called a Gaussian expansion method (GEM)[5].

In our previous work[6], we showed that the four-body CDCC is successfully applied to ^{6}He+^{12}C scattering at 18 and 229.8 MeV in which only nuclear breakup is significant. Furthermore, the applicability of the four-body CDCC with the GEM to Coulomb breakup processes was also shown in Ref. 7. Thus, it is expected that the four-body CDCC with the GEM will accurately describe four-body breakup reactions near the Coulomb barrier energy.

Figure 1 shows the angular distributions of the measured elastic cross sections for ^{6}He+^{209}Bi scattering at 19 and 22.5 MeV. We found that the solid lines analyzed by the four-body CDCC reproduce the experimental data, whereas the dushed lines analyzed by the CDCC based on the dineutron model of ^{6}He underestimate the data at middle angles of 50°–100°. Also, the total reaction cross sections calculated by the four-body CDCC are in good agreement with the experimental data. We thus conclude that the n+n+^{4}He+^{209}Bi four-body reaction model is necessary for accurately describing ^{6}He+^{209}Bi scattering, and that the four-body CDCC is indispensable for analyzing low-energy ^{6}He scattering in which both nuclear and Coulomb breakup processes are significant.

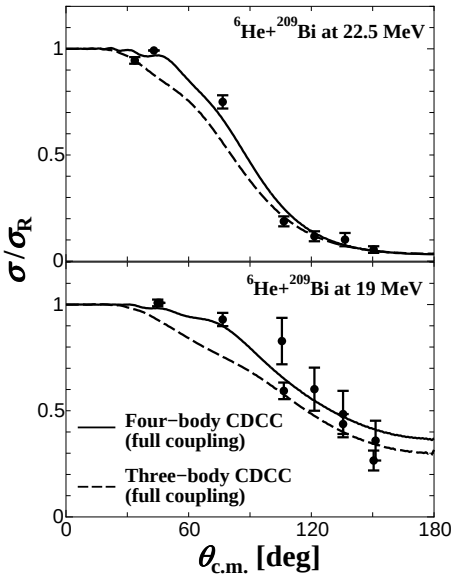

Fig. 1. Angular distributions of elastic differential cross section as a ratio to the Rutherford cross section for ^{6}He+^{209}Bi scattering at 19 and 22.5 MeV.

References

1) N. Keeley *et al.*: Phys. Rev. C **68**, 054601 (2003).
2) E. F. Aguilera *et al.*: Phys. Rev. Lett. **84**, 5058 (2000).
3) E. F. Aguilera *et al.*: Phys. Rev. C **63**, 061603(R) (2001).
4) M. Kamimura *et al.*: Prog. Theor. Phys. Suppl. **89**, 1 (1986).
5) E. Hiyama *et al.*: Prog. Part. Nucl. Phys. **51**, 223 (2003).
6) T. Matsumoto *et al.*: Phys. Rev. C **70**, 061601 (2004).
7) T. Egami *et al.*: Phys. Rev. C **70**, 047604 (2004).

† Condensed from the article in Phys. Rev. C **73**, 051602 (2006)

*1 Department of Physics, Kyushu University
*2 Department of Physics, Chiba-Keizai College

Nonadiabatic dynamics in ^{10}Be with α+α+N+N model†

M. Ito

[NUCLEAR STRUCTURE, cluster model, unstable nuclei]

In the last two decades, developments of experiments with a secondary RI beam have extensively proceeded in terms of studies on light neutron-rich nuclei. In particular, much effort has been devoted to the investigation of the molecular structure of Be isotopes. Theoretically, molecular models with π and σ orbitals along the axis have been successful in making us understand the low-lying states of this isotopes[1].

In recent experiments, the reaction cross-sections induced by the low-energy ^{6}He beam have been accumulated. In future experiments, it will also be possible to investigate the molecular states of Be isotopes through reactions by ^{6}He beams. Therefore, it is very interesting to study theoretically the low-energy scattering of ^{6}He by an target.

In studying the reaction processes exciting the molecular states, it is very important to construct a unified model that is capable of describing both structure and reaction on the same footing. For this purpose, we proposed a microscopic model, the generalized two-center cluster model (GTCM)[2,3]. In this study, we apply GTCM for ^{10}Be with the $+$ $+N+N$ structure.

In GTCM, the total wave function is expressed by a linear combination of the "atomic-orbitals" (AOs) around two cores. The particle is described by the $(0s)^4$ configuration and the valence neutrons are specified by the atomic orbitals in which the neutrons are localized at one of the cores with $0p$ orbitals. In the calculation, the – distance S and the mixing weights among the AOs are treated as variational parameters. In the region where two -cores are near, the total system is expected to form the molecular orbital structure (π^-, σ^+,...), whereas in the region where two core nuclei are far apart, the molecular orbitals smoothly change into product wave functions consisting of atomic orbitals.

We can obtain adiabatic energy surfaces (AESs) by diagonalizing the Hamiltonian at a fixed S, whereas the energy spectra are calculated by solving the eigenvalue problem with the variation in both the S and the AO weights. In Fig. 1, the AES and energy spectra for J^π=1$^-$ are shown. We have identified two 1$^-$ states having the $(\pi^-\sigma^+)$ configuration. The lower state is generated from the AES around the lowest local minimum, whereas the higher state originates from the higher AES, as indicated by the arrow in Fig. 1. Around S=6 fm, we can clearly observe the avoided crossing between the lowest AESs. In the asymptotic region, the lowest AES and the first excited AES correspond to the $[\ +^6\mathrm{He}(0_1^+)]_{L=1}$ and $[\ +^6\mathrm{He}(2_1^+)]_{L=1}$ channels, respectively.

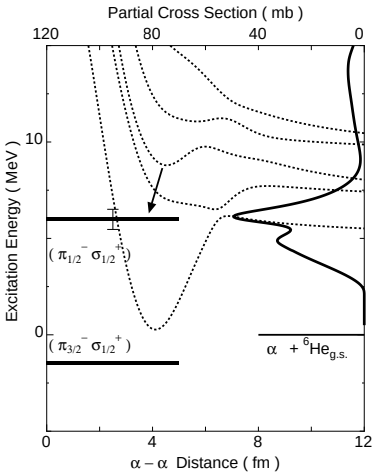

Fig. 1. Energy spectra (horizontal bars) and adiabatic energy surfaces (dotted curves) for J^π=1$^-$. The error bar means the decay width of the resonance state. The solid curve shown in the right part is the partial cross section for the inelastic scattering $[\ +^6\mathrm{He}_{g.s.}]_{L=1} \rightarrow [\ +^6\mathrm{He}(2_1^+)]_{L=1}$ with a respective scale at the up-most axis.

We next discuss how the AES profile appears in the low energy reactions. We show the partial cross section for the inelastic scattering to ^{6}He(2_1^+) excitation. A strong enhancement can be observed at $E_{c.m.}\sim$ 6 MeV. The energy of the enhancement is quite similar to that of the avoided crossing at S=6 fm. We have solved the coupled-channel problem between the lowest AESs and confirmed that this peak is generated by the coupling between the lowest two AESs. Therefore, we can conclude that this inelastic peak is due to the Landau Zener transition at the avoided crossing.

The present calculation predicts the enhancement in the cross section for the inelastic scattering $+^6\mathrm{He}_{g.s.} \rightarrow +^6\mathrm{He}(2_1^+)$. Therefore, an experiment on the $+^6$He low energy scattering is strongly desired.

† Condensed from the article in Phys. Lett. **B636**, 293 (2006)

References

1) N. Itagaki, S. Okabe and K. Ikeda : Phys. Rev. C **62**, 034301 (2000), and references therein.
2) M. Ito, K. Kato and K. Ikeda : Phys. Lett. B**588**, 43 (2004).
3) M. Ito and K. Yabana : Prog. Theor. Phys. **113**, 1047 (2005)

α+^{12}C inelastic angular distribution and nuclear size of ^{12}C(0_2^+)†

M. Takashina*1 and Y. Sakuragi*2

[Nuclear reaction, condensate state]

Recently, it was proposed[1,2] that the 0_2^+ state in ^{12}C could be interpreted as an -particle condensate state. One of the remarkable features of the condensed state is a dilute density distribution, resulting in a large nuclear radius of the state. Therefore, if the large nuclear radius of the candidate state is experimentally confirmed, it will be strong evidence indicating the formation of the condensed state. However, the direct measurement of the nuclear radius or nucleon density distribution of excited states is not possible at the moment. Therefore, an indirect procedure is necessary to prove the dilute density distribution of excited states. In the present study, we investigate how the spatial extension of the 0_2^+ state is reflected in the details of the angular distribution of inelastic scattering.

We perform the microscopic coupled-channel (MCC) calculation based on the double-folding model using the DDM3Y interaction for the effective nucleon-nucleon interaction. The density distribution of ^{12}C is given by condensate model (ACM) calculations[2,3]. We refer to the ACM wave function originally obtained[2] as the , and those for which the spatial extension of the 0_2^+ state is artificially modified[3] as the . We use four types of modified ACM wave functions (i) $\sim$ (iv), the root-mean-square (rms) radii $\langle r^2\rangle^{1/2}$ of which are (i) 2.97 fm, (ii) 3.55 fm, (iii) 4.38 fm and (iv) 5.65 fm, while that of the original ACM wave function is 3.81 fm[3]. Note that the orthogonality of the 0_2^+ state and the 0_1^+ ground-state wave functions is also satisfied in the modified ACM calculation. The transition density between the ground and the 0_2^+ states is calculated from the ground-state wave function and each of these wave functions for the 0_2^+ state. The ground-state wave function is not modified throughout the present analysis. The normalization factor N_R of the real folded potential and the parameters for the Woods-Saxon-type imaginary potential are taken to be the same as those used in Ref.4.

The result of the MCC calculation for the $+^{12}$C(0_2^+) channel at the incident energy of E_α=240 MeV is shown in Fig. 1. The solid curve represents the result using the original ACM wave function. The other curves are the results of the MCC calculations in which the modified ACM wave functions (i) - (iv) are used, where we use the same Woods-Saxon-type imaginary potential as that used in the calculations for the solid curves. It is found that the oscillation pattern of the angular distribution is hardly changed even when the density distribution of the 0_2^+ state is artificially shrunk or extended, although the absolute value changes. This is because the change in the nuclear radius of the excited 0_2^+ state does not significantly affect the shape of the transition density between the ground state and the 0_2^+ state, but it only changes the magnitude of the transition density, as shown in Ref.3.

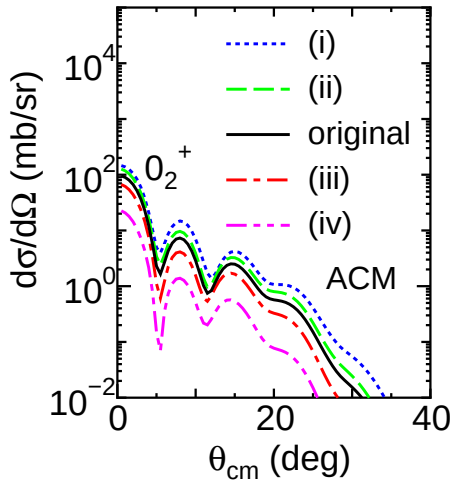

Fig. 1. The inelastic angular distribution of $+^{12}$C(0_2^+) channel at the incident energy of E_α=240 MeV. The solid curve represents the result using the original ACM, while the other curves represent the results using the modified ACM.

In the present study, it is found that the number of minima and their positions in the inelastic angular distribution are almost unchanged by the modification of the nuclear radius of the 0_2^+ state. However, the nuclear radius of the excited state can be deduced from the absolute value of the inelastic differential cross sections, as shown in Fig. 1, through the amplitude of the transition density calculated in a microscopic nuclear structure model such as ACM.

References

1) A. Tohsaki et al.: Phys. Rev. Lett. **87**, 192501 (2001).
2) Y. Funaki et al.: Phys. Rev. C **67**, 051306 (R) (2003).
3) Y. Funaki et al.: Eur. Phys. J. A **28**, 259 (2006).
4) S. Ohkubo and Y. Hirabayashi: Phys. Rev. C **70**, 041602 (R) (2004).

† Condensed from the article in Phys. Rev. C **74**, 054606 (2006).

*1 Yukawa Institute for Theoretical Physics, Kyoto University
*2 Department of Physics, Osaka City University

Cluster states in ^{13}C($1/2^-_3$)

Y. Kanada-En'yo,[*1]

[NUCLEAR STRUCTURE, Unstable nuclei, Cluster]

The present study has been motivated by the recent works on three-center cluster states in excited states of ^{12}C and ^{11}C. In ^{12}C, it is known that 3 -cluster states develop in such the excited states as the 0^+_2(7.65 MeV) state. Recently, Tohsaki [1,2] proposed that the 0^+_2 is a dilute state which is considered to be a weakly interacting gas of 3 particles. Similar states of the cluster gas have been suggested in the excited states of ^{11}C, ^{11}B[3] and ^{16}O[1,4]. It leads to a question whether such loosely bound multicluster states may appear in other nuclear systems.

In the present paper, we focus on the excited states of ^{13}C. As we mentioned, the 0^+_2 state of ^{12}C is regarded as a 3 -cluster gas with a dilute density. Considering the 3 $+n$ system, it is natural to expect a possible cluster gas state with an additional neutron in ^{13}C. Our aim here is to theoretically study the structure of the $1/2^-_2$ and $1/2^-_3$ states, which are the candidates of cluster gas states, and clarify their cluster aspect.

We apply the method of antisymmetrized molecular dynamics (AMD). We perform energy variation after spin parity projection (VAP) within the AMD model space, as was done in the previous studies[5,6]. The adopted interaction consists of the central force of MV1 ($m = 0.62$, $b = h = 0.20$), the spin-orbit force of GSRS ($u_I =$ $u_{II} = 3000$ MeV), and Coulomb force.

In Table 1, we show the calculated excitation energies and root mean square radii(r.m.s.r.). The experimental data of the $M1$ transition strengths are well reproduced by the present calculations. Therefore, the theoretical $1/2^-_2$ and $1/2^-_3$ should be assigned to the observed $1/2^-_2$ at 8.86 MeV and the $1/2^-_3$ at 11.08 MeV, though the excitation energies are overestimated by the theory. By analyzing the obtained wave function, we find that the ground and the $1/2^-_2$ states have no cluster structure, while the $1/2^-_3$ has a cluster state with the 3 $+n$ structure. One of the interesting points is that the spatial development of the cluster state is not remarkable. As a result the radius of the $1/2^-_3$ is not large as shown in table 1. This results indicate that the $1/2^-_3$ is not a cluster gas with a dilute density but a compact state with the 3 core. Comparing the dilute cluster structure in the ^{12}C(0^+_2) and ^{11}B($3/2^-_3$), the cluster aspect in the ^{13}C($1/2^-_3$) differs from those of the cluster-gas states. In Fig.1, the single particle energies of protons and neutrons in the $1/2^-_3$ are displayed. It clearly indicates 3 $+n$ structure. Namely, the lowest 12 orbits form the 3 core and the final neutron has a nature of valence nucleon. It is expected that the valence neutron plays an important role to form the compact cluster structure in the ^{13}C($1/2^-_3$).

In conclusion, the cluster state with the 3 $+n$ structure appears in the $1/2^-_3$ state of ^{13}C. It is found that the state is not a cluster gas with a dilute density but a compact state with the 3 core and the valence neutron.

Table 1. Excitation energies and root mean square radii of the 1/2− states of ^{13}C.

	exp.	theor.	
J^π_k	E_x (MeV)	E_x (MeV)	r.m.s.r.(fm)
$1/2^-_1$	0.0	0.0	2.5
$1/2^-_2$	8.86	11.3	2.6
$1/2^-_3$	11.08	13.8	2.7

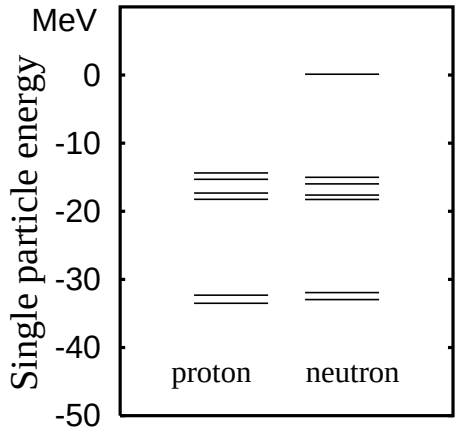

Fig. 1. Single particle energies of the calculated $1/2^-_3$ state of ^{13}C.

References

1) A. Tohsaki et al., Phys. Rev. Lett. **87**, 192501 (2001).
2) Y. Funaki et al., Phys. Rev. C **67**, 051306 (2003).
3) T. Kawabata *et al.*, Phys. Lett. **B646**, 6 (2007).
4) T. Yamada and P. Schuck, Phys. Rev. C **69**, 024309 (2004).
5) Y. Kanada-En'yo, Phys. Rev. Lett. **81**, 5291 (1998).
6) Y. Kanada-En'yo, H. Horiuchi and A. Doté, Phys. Rev. C **60**, 064304 (1999).

[*1] Yukawa Institute for Theoretical Physics, Kyoto University, Japan

Fusion reaction of ^{15}C+^{144}Sm

M. Ito, K. Yabana,[*1] and T. Nakatsukasa[*1]

[NUCLEAR REACTION, unstable nuclei]

Nuclear reactions involving halo nuclei have been attracting the attention of many researchers since the discovery of halo structures in a secondary beam experiment. For reactions at medium and high incident energies, the Glauber and eikonal approximations have been successful. In a low-energy collision, however, the reaction mechanism of halo nuclei remains an open question in spite of the many experimental and theoretical studies that have been performed in the last decades.

To elucidate the reaction mechanism of a halo nuclei at low incident energies, we have been developing a time-dependent wave-packet approach using the three-body reaction model[1–4]. In our previous studies, we have applied this method to the sub-barrier fusions of the ^{11}Be+^{209}Bi and ^{6}He+^{238}U systems and have shown that fusion cross sections are suppressed by the presence of a neutron halo[4]. In this paper, we present our extended analyses of the ^{15}C+^{144}Sm system that will be measured in a future experiment[5]. ^{15}C is a weak binding system (S_n=1.2MeV) and its spectroscopic factor is close to unity for the s-wave ^{14}C+n configuration[5] in contrast to that for another typical one-neutron halo system, ^{11}Be, that has about 20% d-wave components with a deformed ^{10}Be core. Therefore, ^{15}C is a model case for maximizing the effect of a dilute system in solving a multidimensional tunneling problem.

We adopt a three-body model of a halo nucleon (n) and a core nucleus (C) constituting the projectile ($P = C+n$) colliding with a target nucleus (T). The method is based on the time-dependent Schrödinger equation for the three-body model given as

$$i\hbar\frac{\partial}{\partial t}\Psi(\mathbf{R},\mathbf{r},t) = \left\{ \frac{\hbar^2}{2\mu}\nabla^2_{\mathbf{R}} \quad \frac{\hbar^2}{2m}\nabla^2_{\mathbf{r}} \right.$$

$$\left. +V_{nC}(r) + V_{CT}(R_{CT}) + V_{nT}(r_{nT})\right\}\Psi(\mathbf{R},\mathbf{r},t), \quad (1)$$

where the relative n-C coordinate is $\mathbf{r}$ and the relative P-T coordinate is $\mathbf{R}$. The reduced masses of the n-C and P-T motions are m and μ, respectively. We prepare an initial wave packet boosted toward collision, then calculate the time evolution in real coordinate space. Fusion is identified as the flux loss due to the imaginary part of the core-target potential, $V_{CT}(R_{CT})$. The energy projection before and after the time evolution gives fusion probability as a function of energy. In Fig. 1, we show the calculated fusion cross section of ^{15}C+^{144}Sm. The result of the three-body calculation clearly predicts a slight hindrance compared with that in the case of the fusion cross section for the system without a neutron halo, ^{14}C+^{144}Sm.

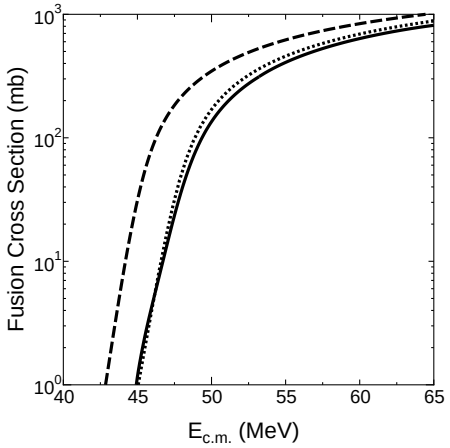

Fig. 1. Fusion cross section as function of incident energy. The solid curve shows the result of the three-body calculation, whereas the dotted one shows the cross section of the ^{14}C+^{144}Sm system. The dashed curve indicates the fusion cross section obtained by solving the single-channel problem of ^{15}C+^{144}Sm. See text for details.

In the same figure, we also show the result of the single-channel calculation for ^{15}C+^{144}Sm. In this calculation, ^{15}C is frozen to its ground state with a halo structure and the scattering problem is solved by employing the static potential between ^{15}C$_{g.s.}$ and ^{144}Sm. The fusion cross section of the single-channel calculation becomes much larger than that of ^{14}C+^{144}Sm. This is due to the extended nuclear interaction generated by the halo effect in ^{15}C$_{g.s.}$. This behavior can be seen in many previous studies on fusion reaction using neutron-halo systems, but such enhancement completely disappears when we explicitly solve three-body dynamics. According to our studies, we expect a slight hindrance of the fusion cross section in future experiments on ^{15}C+^{144}Sm.

References

1) K. Yabana : Prog. Theor. Phys. **97**, 437 (1997).
2) K. Yabana, M. Ito, M. Kobayashi, M. Ueda, T. Nakatsukasa : Nucl. Phys. **A738**, 303 (2004).
3) T. Nakatsukasa, K. Yabana, M. Ito, M. Kobayashi, M. Ueda : Prog. Theor. Phys. Suppl. **154**, 85 (2004).
4) M. Ito, K. Yabana, T. Nakatsukasa, M. Ueda : Phys. Lett. **B637**, 53 (2006), and references therein.
5) A. Navin, private communications.

[*1] Institute of Physics, University of Tsukuba

An *s*-wave halo structure of ^{22}C†

W. Horiuchi*1 and Y. Suzuki*2

[Nuclear structure, unstable nuclei]

The subshell closure of N=14 and N=16 is one of the intensively discussed topics in the study of neutron-rich nuclei, and the N=14 closure has been confirmed experimentally around ^{22}O[1–5]. This issue is closely related to the competition of $0d_{5/2}$ and $1s_{1/2}$ neutron orbits. In fact, they play a vital role in determining the ground state structure of A=15–20 carbon isotopes. For example, the ground state of ^{16}C is found to contain the $(1s_{1/2})^2$ and $(0d_{5/2})^2$ configurations almost equally[6,7], whereas the last neutron in ^{19}C is in the $1s_{1/2}$ orbit, forming one-neutron halo structure[8,9].

No information is available to determine whether the N=14 subshell closure occurs in ^{20}C. The systematics of the interaction cross section suggests, however, that the radius of ^{20}C is smaller than that of ^{19}C[10], so it is natural to assume that the ground state of ^{20}C predominantly consists of a $(0d_{5/2})^6$ configuration. If its dominant component were $(0d_{5/2})^4(1s_{1/2})^2$, one more neutron could be added to the $0d_{5/2}$ orbit to form a particle-stable ^{21}C, which is in contradiction to obserbed results.

In this study, we will demonstrate that ^{22}C is an s-wave two-neutron halo nucleus on the basis of the analysis of its structure including the neutron and proton densities. For $Z \leq 8$, ^{22}C is the only dripline nucleus for which the interaction or reaction cross section measurement on a ^{12}C target has not reached yet[10], so it is of interest for future measurement to predict the reaction cross section of ^{22}C. The neutron and proton densities obtained here will be useful for estimating the reaction cross section of ^{22}C on a proton target, which is being investigated experimentally[11].

Our model is that ^{22}C is a three-body system of ^{20}C+n+n, and that ^{20}C has the $(0d_{5/2})^6$ configuration. The valence neutrons, interacting via a realistic potential, are constrained to be orthogonal to the occupied orbits in ^{20}C. We obtain ample results supporting the fact that ^{22}C is an ideal s-wave two-neutron halo nucleus: The ground state is bound by 390-570 keV, the root mean square neutron and proton radii are 4.0 and 2.4 fm, respectively. The matter radius is 3.6 fm, which corresponds to that of a stable nucleus with $A \approx 60$. These densities are displayed in Fig. 1. The contribution of the halo density to ρ^n exceeds that of the core density beyond $r = 6.1$ fm. Note that $\rho_h/2$ is, roughly speaking, the square of the single halo-neutron wave function. The two neutrons are predominantly in $(s_{1/2})^2$ orbits more than 90 percent, and that the non-central forces play no active role in binding this fragile system. In a separate study, we use the density obtained this work to calculate the reaction cross section of ^{22}C.

To conclude, we studied the ground state structure of ^{22}C in the ^{20}C+n+n three-body model with the orthogonality constraint. The N=14 subshell closure was assumed for ^{20}C. We showed that ^{22}C is an almost pure s-wave two-neutron halo nucleus. A measurement of the reaction cross section of ^{22}C is desired to establish the halo structure experimentally.

The authors thank A. Kohama for his interest and valuable discussions.

References

1) A. Ozawa *et al.*, Phys. Rev. Lett. **84**, 5493 (2000).
2) P. G. Thirolf *et al.*, Phys. Lett. **B485**, 16 (2000).
3) D. Cortina-Gil *et al.*, Phys. Rev. Lett. **93**, 062501 (2004).
4) M. Stanoiu *et al.*, Phys. Rev. C **69**, 034312 (2004).
5) E. Becheva *et al.*, Phys. Rev. Lett. **96**, 012501 (2006).
6) T. Yamaguchi *et al.*, Nucl. Phys. **A724**, 3 (2003).
7) W. Horiuchi and Y. Suzuki, Phys. Rev. C **73**, 037304 (2006).
8) T. Nakamura *et al.*, Phys. Rev. Lett. **83**, 1112 (1999).
9) V. Maddalena *et al.*, Phys. Rev. C **63**, 024613 (2001).
10) A. Ozawa, T. Suzuki and I. Tanihata, Nucl. Phys. **A693**, 32 (2001).
11) K. Tanaka *et al.*, private communication.

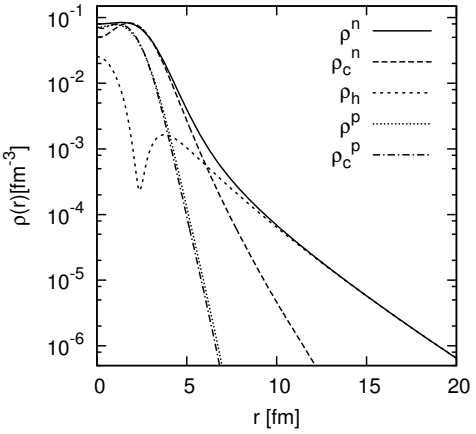

Fig. 1. The neutron and proton densities of ^{22}C and ^{20}C. ρ_h is the halo-neutron density.

† Condensed from the article in Phys. Rev. C **74**, 034311 (2006).

*1 Graduate School of Science and Technology, Niigata University
*2 Department of Physics and Graduate School of Science and Technology, Niigata University

Systematic analysis of reaction cross sections of carbon isotopes

B. Abu-Ibrahim,[*1] W. Horiuchi,[*2] A. Kohama, and Y. Suzuki,[*3]

[Nuclear reaction, total reaction cross sections, unstable nuclei]

The structure of carbon isotopes has recently attracted considerable attention as experimental information accumulated toward its neutron dripline. The topics discussed include, for example, the subshell closure of N=14 and N=16, and the anomalously small $E2$ transition strength observed in ^{16}C.[1,2] These topicss are closely related to the competition of $0d_{5/2}$ and $1s_{1/2}$ neutron orbits. In fact, they play a predominant role in determining the ground state structure of a carbon isotope with $N > 8$.

In this study, we systematically analyzed the total reaction cross sections of carbon isotopes with $N = 6$–16 on a proton target as well as on a ^{12}C target for a wide incident energy range of 40 to 1000 A MeV. The papers regarding this study are in preparation and will be submitted soon.

The intrinsic structure of the carbon isotopes is firstly described by a Slater determinant generated from a phenomenological mean-field potential. Woods-Saxon-type potential depth is determined separately for neutrons and protons to reproduce nucleon separation energies. The intrinsic density of each carbon isotope is constructed from the single-particle states by separating, in a good approximation, the center of mass motion from the Slater determinant.

Our model reasonably well describes the ground states of even N isotopes, but the mean-field potential depth of odd N isotope tends to be too small, yielding too large neutron and matter radii. This unrealistic feature has been largely improved by performing separate studies which take into account the specific structure of core+n. We also utilized the core+n+n three-body model for ^{16}C and ^{22}C,[3] in order to consider the mixing of the *sd* orbits in ^{16}C and the Borromean character of ^{22}C, respectively.

For the calculations of the cross sections of the carbon target, we sed two schemes: the Glauber approximation[4,5], and the eikonal model using a global optical potential. By setting the parameters of nucleon-nucleon scattering amplitude, we calculated the cross sections of the proton target. Empirical data exist only for a proton-^{12}C reaction, and the agreement of our numerical results with the data is fairly well. The numerical results for the other carbon isotopes are obtained as predictions. The experimental results for some isotopes including ^{22}C are reported in this volume by another RIKEN research group.

There exist some data for the reactions of the carbon target, and we observed that both of our two schemes successfully reproduce low and high incident energy data on the cross sections of ^{12}C, ^{13}C and ^{16}C on ^{12}C. The calculated reaction cross sections of ^{15}C are found to be considerably smaller than the empirical values observed at a low energy. We find a consistent parameterization of nucleon-nucleon scattering amplitude, which is different from that previously reported. Finally, we predicted the total reaction cross section of ^{22}C on ^{12}C (Fig. 1).

Our framework offers a prescription for the simple, consistent analyses of a broad range of reaction cross section data for neutron-rich unstable nuclei. Such data are expected to be provided by radioactive ion beam facilities, such as GSI and Radioactive Ion Beam Factory at RIKEN.

References

1) N. Imai *et al.*: Phys. Rev. Lett. **92**, 062501 (2004).
2) Z. Elekes *et al.*: Phys. Lett. B **586**, 34 (2004).
3) W. Horiuchi and Y. Suzuki: Phys. Rev. C **74**, 034311 (2006).
4) R. J. Glauber: *Lectures in Theoretical Physics* (Interscience, New York, 1959) Vol. 1, p.315.
5) B. Abu-Ibrahim and Y. Suzuki: Phys. Rev. C **61**, 051601(R) (2000).

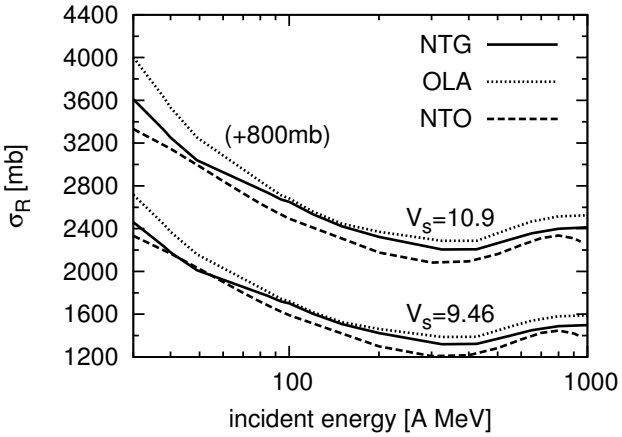

Fig. 1. Prediction of total reaction cross section for collision of ^{22}C on ^{12}C target as a function of incident energy. V_s is parameter for controling the s wave strength of the n-^{20}C relative motion.

*1 Department of Physics, Cairo University, Egypt
*2 Graduate School of Science and Technology, Niigata University
*3 Department of Physics and Graduate School of Science and Technology, Niigata University

Study of the tensor correlation in ^{17}O using the shell model

S. Sugimoto,[*1] K. Ikeda,[*2] and H. Toki[*3]

[Nuclear structure, tensor correlation, shell model]

The tensor force plays important roles in a nuclear structure. The study of nuclear matter with the Brueckner theory showed that the tensor force has a large effect on the binding mechanism and is related to the saturation property of nuclear matter. Variational calculations with very large model spaces exhibit a large attractive energy from the tensor force. The tensor force seems to be responsible for about one-half of the single-particle ls splitting in light nuclei[1].

Recently, we have developed a mean field framework (a charge- and parity-projected Hartree-Fock (CPPHF) method) that can treat the two-particle–two-hole (2p-2h) correlations induced by the tensor force. To treat the tensor correlation, we introduce single-particle states with parity and charge mixing, inspired by the pseudoscalar and isovector character of a pion, which mediates the tensor force. We applied the CPPHF method to the alpha particle[3], ^{8}Be[4], and oxygen isotopes[5], and obtained sizable potential energies from the tensor force for these nuclei.

Because the CPPHF method is based on a mean field model, the correlations that can be treated by the CPPHF method are limited. Shell model calculations with 2p-2h configurations were performed by Myo and his collaborators[1,6]. They found that a large correlation energy from the tensor force is obtained by introducing single-particle wave functions for particle states with small range-parameters compared with the ones of typical harmonic oscillator wave functions. The importance of the single-particle wave functions with small range-parameters for the tensor correlation was also observed in our mean field calculations[3,5]. Furthermore, the shell model calculations indicate that the configurations that cannot be considered by the CPPHF method are important for the tensor correlation[1,6]. The shell model calculations also reveal that the tensor correlation is responsible for the ls-splitting in a ^{4}He-n system[1]. Therefore, it is interesting and important to study the tensor correlation in large-mass nuclei, such as oxygen, using the shell model.

Here, we show the result of the shell model calculation for ^{17}O. On the basis of the paper by Myo and his collaborators[1,6] we introduce single-particle wave functions with the Gaussian form for particle states in addition to typical harmonic oscillator single-particle wave functions. The range parameters for the Gaussian wave functions are about one-half of those of the harmonic oscillator wave functions ($b_{\rm HO}$=1.8fm). As for the orbital angular momenta l of single-particle states, we consider l values up to l=3 (f-orbit). In Table 1, the results for the spin-orbit partners in ^{17}O are shown. We consider the Volkov force No. 1[7] for the central part, the G3RS force[8] for the LS part, and the Furutani force[9] for the tensor part. The central force is reduced by 10%. In this case, the total energy of ^{16}O is $-$132.5MeV. The large potential energy from the tensor force is about $-$60MeV. The ls splitting results in an energy of 4.5MeV, which is comparable to the experimental data. The ls splitting mainly comes from the LS force. The contribution from the tensor force is small. The contributions for the ls splitting from the kinetic energy, central force and tensor force almost cancel out each other. The small effect on the ls splitting of the tensor force compared with the ^{5}He case is probably attributed to the multiplicities of the d-orbits lager than those of the p-orbits.

Table 1. Results for ^{17}O. E, T, $V_{\rm C}$, $V_{\rm T}$, and $V_{\rm LS}$ are the total energy, the kinetic energy, and the potential energies from the central, tensor, and LS forces, respectively. These are given in MeV. In the last row, the differences between the values of the $J^\pi = 5/2^+$ and $J^\pi = 3/2^+$ cases are shown.

	E	T	$V_{\rm C}$	$V_{\rm T}$	$V_{\rm LS}$
$5/2^+$	-132.2	289.5	-357.4	-57.0	-7.3
$3/2^+$	-127.7	288.6	-356.7	-56.7	-2.8
diff	-4.5	0.8	-0.6	-0.2	-4.5

References
1) T. Myo, K. Katō, and K. Ikeda, Prog. Theor. Phys. **113**, 763 (2005).
2) T. Otsuka, T. Suzuki, R. Fujimoto, H. Grawe, and Y. Akaishi, Phys. Rev. Lett. **95**, 232502 (2005).
3) S. Sugimoto, K. Ikeda, and H. Toki, Nucl. Phys. A **740**, 77 (2004).
4) S. Sugimoto, K. Ikeda, and H. Toki, nucl-th/0511087.
5) S. Sugimoto, K. Ikeda, and H. Toki, nucl-th/0607045.
6) T. Myo, S. Sugimoto, K. Katō, H. Toki, and K. Ikeda, nucl-th/0607059.
7) A. B. Volkov, Nucl. Phys. **74**, 33 (1965).
8) R. Tamagaki, Prog. Theor. Phys. **39**, 91 (1968).
9) H. Furutani, Prog. Theor. Phys. Suppl. **68** 193 (1980).

*1 Department of Physics, Graduate School of Science, Kyoto University
*2 The Institute of Physical and Chemical Research (RIKEN)
*3 Research Center for Nuclear Physics (RCNP), Osaka University

Exotic structure of unstable nuclei around N=28 due to tensor force

Y. Utsuno,[*1] T. Otsuka,[*2,*3] T. Mizusaki,[*3,*4] and M. Honma,[*5]

[NUCLEAR STRUCTURE, shell model, unstable nuclei]

The evolution of the shell structure in exotic nuclei is an intriguing issue and should be clarified by RIBF at RIKEN in the near future. The disappearance of the $N = 20$ magic number is most likely related to a narrowing $N = 20$ shell gap toward smaller proton number, which has been investigated by a large-scale shell-model calculation with the Monte Carlo shell model (MCSM)[1]. It has been recently pointed out[2] that the change of the shell structure, often called shell evolution, is caused by the tensor force. It is very successful in accounting for similar phenomena for spherical nuclei in other regions.

In the present study, we examine whether or not this leads to an exotic nuclear structure such as an unexpected deformation using the shell model. We focus especially on persistence or disappearance of the magic structure around $N = 28$ in the very neutron-rich region, where the *sd-pf* cross shell interaction plays a key role. The shell model can treat the deformation and the correlation in a proper way. This study is conducted as a RIKEN-CNS collaboration project on large-scale nuclear structure calculations.

To investigate the proper strength of the tensor force as the shell-model effective interaction, we extract the tensor part from the GXPF1 interaction[3] for pf-shell nuclei. Since GXPF1 is an interaction that excellently reproduces and predicts many nuclear properties over the region, it should have a reasonable spin/isospin structure. As a result, the monopole centroid of the $T = 0$ tensor force in GXPF1 is very similar to that of the $\pi+\rho$ exchange force and the GT2 interaction[4] that has been newly constructed for the mean-field calculation. Thus, the tensor force in the shell-model interaction seems similar to that of mean-field calculation and almost independent of region.

Based on the above discussion, we construct a new *sd-pf* shell Hamiltonian whose tensor force of the cross-shell part is identical to GT2 (hereafter simply denoted by GT2). As a reference, a Hamiltonian with this part replaced by Millener-Kurath (MK) tensor force[5] is also constructed, and we compare results between them. Note that the tensor force of MK is about one third as weak as that of GT2.

The shell-model calculation shows that GT2 well reproduces the reduction of the $Z = 16$ shell gap moving from $N = 20$ to 28 such as the inversion of the ordering between $1/2_1^+$ and $3/2_1^+$ states in ^{47}K, whereas MK does not sufficiently. The tensor force affects the $Z = 14$ shell structure and relevant nuclear structure, too. Figure 1 shows the low-lying structure of neutron-rich Si isotopes. The present calculation predicts that the $N = 28$ isotope ^{42}Si is not a typical magic nucleus due to a narrower the $Z = 14$ shell gap by the tensor force, which will be accessible by RIBF.

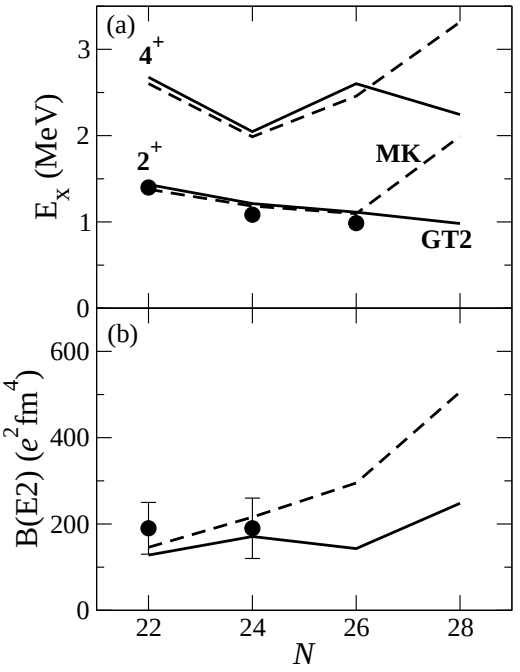

Fig. 1. (a) 2_1^+ and 4_1^+ energy levels and (b) $B(E2; 0_1^+ \rightarrow 2_1^+)$ values of Si isotopes from $N = 22$ to 28 compared between experiment (circles) and shell-model calculations with different cross-shell interactions MK and GT2.

*1 Advanced Science Research Center, Japan Atomic Energy Agency
*2 Department of Physics, University of Tokyo
*3 Center for Nuclear Study, University of Tokyo
*4 Institute of Natural Sciences, Senshu University
*5 Center for Mathematical Sciences, University of Aizu

References
1) Y. Utsuno, T. Otsuka, T. Glasmacher, T. Mizusaki and M. Honma: Phys. Rev. C **70**, 044307 (2004).
2) T. Otsuka, T. Suzuki, R. Fujimoto, H. Grawe and Y. Akaishi: Phys. Rev. Lett. **95**, 232502 (2005).
3) M. Honma, T Otsuka, B.A. Brown and T. Mizusaki: Phys. Rev. C **69**, 034335 (2004).
4) T. Otsuka, T. Matsuo and D. Abe: Phys. Rev. Lett. **97**, 162501 (2006).
5) D.J. Millener and D. Kurath: Nucl. Phys. A **255**, 315 (1975).

Effective interaction for f5pg9-shell nuclei and two-neutrino double-beta-decay matrix elements†

M. Honma,[*1] T. Otsuka,[*2] T. Mizusaki,[*3] and M. Hjorth-Jensen[*4]

[shell model, effective interaction, double beta decay]

Effective interaction is a key ingredient for successful shell-model calculations. Owing to recent developments in computers as well as novel numerical techniques such as the Monte Carlo shell model[1], the applicability of the shell model is rapidly expanding. On the other hand, our knowledge of the effective interaction is still insufficient, particularly for cases where more than one major shell should be taken as the active valence space. Such a treatment is essential for describing neutron-rich nuclei.

We have developed a new effective interaction for shell-model calculations in the model space consisting of valence orbits $1p_{3/2}$, $0f_{5/2}$, $1p_{1/2}$ and $0g_{9/2}$, assuming an inert ^{56}Ni core (f5pg9 shell). It can be regarded as a first step for future extensions to the pf+sdg model space. We have carried out the similar iterative fitting calculations as in the case of the the pf shell[2]. Starting from a microscopic interaction (renormalized G matrix)[3] based on a realistic nucleon-nucleon potential, we varied 45 linear combinations of Hamiltonian parameters (133 two-body matrix elements and four single-particle energies) by a least-squares fit to 400 experimental binding and excitation energy data out of 87 nuclei with masses A=63-96. In the latest iteration, we attained an rms error of 185 keV.

As an application of this interaction, we have evaluated the nuclear matrix element of double β decay for ^{76}Ge and ^{82}Se, focusing on the two-neutrino mode. Shell-model calculations were carried out in the conventional way using the code MSHELL.[4] For these nuclei, the double-β-decay lifetime was measured experimentally, which is related to the nuclear matrix elements $M_{GT}^{(2\nu)}$. We can compare the experimental values with our shell-model results, which are calculated according to the following expression:

$$M_{GT}^{(2\nu)} = \sum_m \frac{\langle 0_f^+ \parallel T_{\mathrm{GT}-} \parallel 1_m^+ \rangle \langle 1_m^+ \parallel T_{\mathrm{GT}-} \parallel 0_i^+ \rangle}{\frac{1}{2}Q_{\beta\beta} + E_x(1_m^+) - E_0},$$

where E_0 stands for the mass difference between the parent and intermediate nuclei. Since this matrix element depends on both the initial- and the final-state wave functions as well as the Gamow-Teller strength distribution in the intermediate 1^+ states, it provides us with a stringent test of the theoretical model.

In usual shell-model calculations, the Gamow-Teller operator $T_{\mathrm{GT}-} = \sum_k \sigma_k \tau_k^-$ is multiplied by a "quenching" factor q to obtain a reasonable agreement with the experimental data. This factor depends on the adopted model space, and one can find standard values in the literature: q=0.82 for the p shell[5], 0.77 for the sd shell[6] and 0.74 for the pf shell.[7] Thus, we first estimated a suitable quenching factor in the present f5pg9 shell by carrying out a fitting calculation to the available experimental data for the Gamow-Teller β decay among low-lying states. As a result, we obtained the value $q = 0.6$, which is much smaller than that for other model spaces mentioned above.

For the evaluation of $M_{GT}^{(2\nu)}$, we need the excitation energies of the intermediate 1^+ states. Experimentally, the excitation energy of the lowest 1^+ state is 0.044 MeV (0.075 MeV) in ^{76}As (^{82}Br), while our shell model gives 0.286 MeV (0.470 MeV) for this energy. We consider two cases: (1) the shell-model excitation energies are used as they are, and (2) the shell-model energies of all the intermediate states are shifted commonly so as to reproduce the experimental value of $E_x(1_1^+)$. The results are summarized in Table 1. It can be seen that the shell model with the quenching factor $q = 0.6$ reasonably accurately reproduces the experimental values for both ^{76}Ge and ^{82}Se.

Table 1. Comparison of the nuclear matrix element $M_{GT}^{(2\nu)}$ (MeV^{-1}) between the experimental data and the shell-model calculations.

	^{76}Ge	^{82}Se
Exp.[8]	$0.127^{+0.006}_{-0.004}$	$0.090^{+0.002}_{-0.010}$
Cal. q=0.6, $E_x(1_1^+)_{\mathrm{cal.}}$	0.111	0.106
Cal. q=0.6, $E_x(1_1^+)_{\mathrm{exp.}}$	0.120	0.124
Cal. q=1, $E_x(1_1^+)_{\mathrm{cal.}}$	0.308	0.295
Cal. q=1, $E_x(1_1^+)_{\mathrm{exp.}}$	0.333	0.345

References
1) T. Otsuka et al.: Phys. Rev. Lett. **81**, 1588 (1998).
2) M. Honma et al.: Phys. Rev. C **65**, 061301(R) (2002); Phys. Rev. C **69**, 034335 (2004).
3) M. Hjorth-Jensen et al.: Phys. Rep. **261**, 125 (1995).
4) T. Mizusaki: RIKEN Accel. Prog. Rep. **33**, 14 (2000).
5) W. T. Chou et al.: Phys. Rev. C **47**, 163 (1993).
6) B. H. Wildenthal et al.: Phys. Rev. C **28**, 1343 (1983).
7) G. Martinez-Pinedo et al.: Phys. Rev. C **53**, R2602 (1996).
8) H. Ejiri : Phys. Rep. **338**, 265 (2000).

† Condensed from the article in J. Physics: Conf. Series **49**, 45 (2006).

*1 Center for Mathematical Sciences, University of Aizu
*2 Department of Physics and Center for Nuclear Studies, University of Tokyo
*3 Institute of Natural Sciences, Senshu University
*4 Department of Physics and Center of Mathematics for Applications, University of Oslo

Rotational motion in weakly bound superfluid nuclei

M. Yamagami and Y. R. Shimizu[*1]

[Neutron-rich nuclei, nuclear structure, collective motion]

We studied rotational excitation in neutron-rich Mg isotopes. Because the rotational moment of inertia strongly reflects the properties of many-body correlations, particularly the pairing correlation, it is expected to be a good measure of the unique correlations in weakly bound nuclei. The moment of inertia $\Im_{\rm B}$ is calculated by the Belyaev formula[1],

$$\Im_{\rm B} = 2 \sum_{k<k'} \frac{|\langle kk' | J_x | HFB \rangle|^2}{E_k + E_{k'}}. \quad (1)$$

The quasi-particle (QP) energies E_k, the Hartree-Fock-Bogoliubov (HFB) ground state $|HFB\rangle$ and the two-QP states $|kk'\rangle$ are obtained by the HFB calculation in two dimensional polar lattice space. This study is the first attempt to evaluate the moment of inertia that fully takes into account the pairing correlation involving weakly bound and continuum states. As is well known for stable nuclei, strong pairing correlation reduces the value of $\Im_{\rm B}$[1]. On the other hand, the matrix elements in the numerator of Eq. 1 can be large when spatially extended weakly bound and continuum states are involved. This effect can enhance the moment of inertia[2].

In Fig. 1, the neutron pairing gaps in $^{24-40}$Mg obtained by HFB calculations are shown. The Woods-Saxon potential with the standard parameterization[1] and the quadrupole deformation parameter $\beta_{WS} = 0.3$ is utilized for the Hartree-Fock mean field. On the other hand, the pairing potential is self-consistently derived from the surface-type contact interaction. In the HFB calculations, not only bound and resonant states but also non-resonant continuum states are taken into account. For comparison, the neutron pairing gaps obtained by the BCS approximation are also shown. In the BCS approach, non-resonant continuum states are omitted from the model space. Within the HFB calculations, the pairing gaps in $^{30-40}$Mg are almost constant at around 2 MeV. On the other hand, the BCS pairing gaps start to deviate from the HFB values at ^{32}Mg with the neutron chemical potential $\lambda_n = -3.7$ MeV, and they decrease while approaching the neutron drip-line nucleus ^{40}Mg. The role of non-resonant continuum states is obvious. Moreover, we found that non-resonant continuum states with unexpectedly high angular momenta of $j_z \geq 13/2$ must be included in the calculations. This strong angular correlation of neutron pairs implies dineutron correlation.

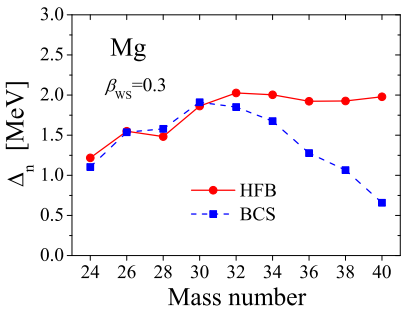

Fig. 1. Neutron pairing gaps in neutron rich Mg isotopes. Results obtained by the HFB and BCS calculations are shown.

The excitation energies of the rotational 2^+ states in $^{30-40}$Mg are shown in Fig. 2. The energies are calculated as $E(I) = \hbar^2 I(I+1)/2\Im_{\rm B}$. Results obtained by HFB and BCS calculations as well as by the rigid-body estimation are shown. For the HFB approach, the 2^+ energies change smoothly approaching ^{40}Mg, whereas the BCS energies decrease and approach the rigid-body values. This is due to the collapse of the pairing correlation around ^{40}Mg in the BCS approximation. Therefore, the systematic studies of the excitation energies and the $B(E2)$ values of the first 2^+ states can be a good indicator in the investigation of the pairing correlation in weakly bound nuclei. Namely, if the 2^+ states have high excitation energies in spite of large $B(E2)$ values, it may imply dineutron pairing.

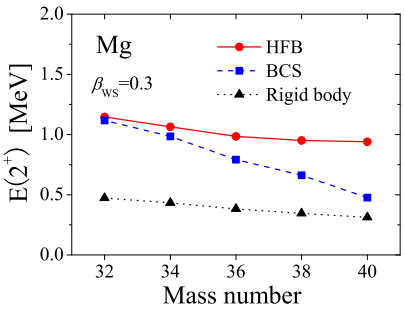

Fig. 2. Excitation energies of the rotational 2^+ states in neutron rich Mg isotopes. Results obtained by HFB and BCS calculations as well as by the rigid-body estimation are shown.

*1 Department of Physics, Kyushu University

References

1) A. Bohr and B. R. Mottelson: *Nuclear Structure, Vol. 1* (Benjamin, New York, 1969).
2) M. Yamagami and Y. R. Shimizu: in preparation.

Configuration mixing calculation for complete low-lying spectra with the mean-field Hamiltonian†

S. Shinohara,[*1] H. Ohta,[*2] T. Nakatsukasa,[*1,*3] K. Yabana[*1,*3]

[NUCLEAR STRUCTURE]

One of the goals in the microscopic nuclear many-body theory is the ab-initio nuclear structure calculation starting with a fixed Hamiltonian[1]. However, the ab-initio calculations are still limited to nuclei with mass number less than around twelve and to the lowest energy state for each parity and angular momentum. Systematic description of ground and excited states in nuclei in a wide mass region requires development of a new computational approach.

One of difficulties of the nuclear many-body problem is due to the strong short-range correlation. This forbids a naive mean-field approach using the bare NN interaction. In order to overcome this difficulty, effective NN interactions have been extensively developed in history of the nuclear theory. Namely, the short-range behavior of two-body correlation is effectively renormalized in the interaction. Then, nuclear many-body wave functions should take account of long-range correlations only. Most of microscopic nuclear structure models adopt the effective interactions; e.g., nuclear mean-field models, shell models, cluster models, etc. The success of these models indicates that a variety of low-lying modes of excitation are governed by nothing but the long-range correlations. In the present study, we aim for developing a new method to treat the whole correlation of long range beyond the mean field, utilizing the effective interaction for the mean-field models. Our method consists of three steps;

(1) Generation and selection of Slater determinants (SD's) important for ground and low-lying excited states.
(2) Parity and angular-momentum projection.
(3) Configuration mixing (diagonalization of the Hamiltonian).

First, many SD's are stochastically generated, then they are evolved in imaginary time to remove all the high-energy components [Step (1)]. The imaginary-time evolution eventually leads to a Hartree-Fock (HF) state, but we store several (or a few) SD's before reaching the HF minimum. This process is repeated until we obtain N linearly independet SD's ($N \sim 50$).

The selected SD's form a basis set, $\{|\Phi_n\rangle; n = 1, \quad , N\}$. We then make parity and angular-momentum projection for each SD [Step (2)]. The Hamiltonian and the norm kernels for the fixed parity ($\pi = \pm$) and angular-momentum (J, K), where K indicates its body-fixed component, are given by

$$\left\{ \begin{array}{c} H^{J(\pm)}_{nK,n'K'} \\ N^{J(\pm)}_{nK,n'K'} \end{array} \right\} = \langle \Phi_n | \left\{ \begin{array}{c} H \\ 1 \end{array} \right\} \hat{P}^{\pm} \hat{P}^{J}_{KK'} | \Phi_{n'} \rangle. \quad (1)$$

Here, $\hat{H}$ is the many-body Hamiltonian with effective interaction, $\hat{P}^{\pm}$ is the parity projection operator, and $\hat{P}^{J}_{KK'}$ is the angular-momentum projection operator. Finally, we solve the following generalized eigenvalue problem [Step (3)].

$$\sum_{n'K'} (H^{J(\pm)}_{nK,n'K'} \quad E^{J(\pm)} N^{J(\pm)}_{nK,n'K'}) g_{n'K'} = 0. \quad (2)$$

Single-particle wave functions in each SD are represented in the three-dimensional (3D) Cartesian coordinate space without any symmetry restriction.

To test our theory, we apply the method to light $N = Z$ even-even nuclei, using the simplified mean-field Hamiltonian, the so-called BKN force[2]. Results for ^{12}C are shown in Fig. 1. The calculation produces the ground state rotational band, but its moment of inertia is larger than the observed values. This is due to simplicity of the BKN interaction that does not include the LS interaction. In the negative parity, our calculation produces 3^- state in the lowest energy, also 1^- and 2^- states at low excitation energies. These are qualitatively in agreement with experiments. In the positive parity excited states, the calculation indicates two 0^+ states around 10 and 12 MeV. These may correspond to the measured states around 8 and 10 MeV.

Studies adopting a more realistic Skyrme interaction are currently under progress.

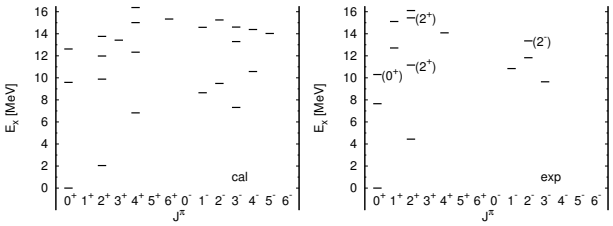

Fig. 1. Calculated and experimental spectra for ^{12}C.

† Condensed from the article submitted to Phys. Rev. C (preprint: nucl-th/0607004)

*1 Institute of Physics, University of Tsukuba
*2 Sumitomo Chemical Co. Ltd.
*3 Center for Computational Sciences, University of Tsukuba

References

1) B. S. Pudliner, et al, Phys. Rev. Lett. **74**, 4396 (1995).
2) P. Bonche, S. Koonin, and J. W. Negele, Phys. Rev. C **13**, 1226 (1976).

Quadrupole-coupling model for doublet bands in doubly odd nuclei†

N. Yoshinaga*1 and K. Higashiyama*2

[Nuclear structure, quadrupole coupling model, chopsticks configurations]

The yrast and yrare states based on the $h_{11/2} \otimes \pi h_{11/2}$ configuration in doubly odd nuclei with mass number $A \sim 130$ have been studied using the pair-truncated shell model (PTSM)[1–3]. The model accurately reproduces the experimental energy levels and ratios $B(M1; I \rightarrow I \quad 1)/B(E2; I \rightarrow I \quad 2)$ for the yrast states. Through the analysis of PTSM wave functions, it is found that the main structure of the yrast and yrare states is described in terms of the weak coupling of the chopsticks configurations, which represent two angular momenta of the unpaired neutron and unpaired proton, to the multiphonon excitations of the even-even part of the nucleus.

To confirm the structure, we have recently proposed a quadrupole-coupling model (QCM). In the model, a system of one-neutron hole in the orbital j_ν and one-proton particle in the orbital j_π is specified as the state $|j_\nu j_\pi; L\rangle$, where L is the angular momentum of the particle-hole state. The collective-core state is denoted as $|R\rangle$, where R indicates the angular momentum of the core state. Then, the total wave function of any doubly odd nucleus is written as a product of the collective-core state and the particle-hole state,

$$|\Phi(RL; I)\rangle = [|R\rangle \otimes |j_\nu j_\pi; L\rangle]^{(I)} , \qquad (1)$$

where I is the total spin. The model Hamiltonian employed in the present calculation consists of the Hamiltonian of the collective core and the quadrupole-quadrupole interactions between the collective core, neutron hole, and proton particle.

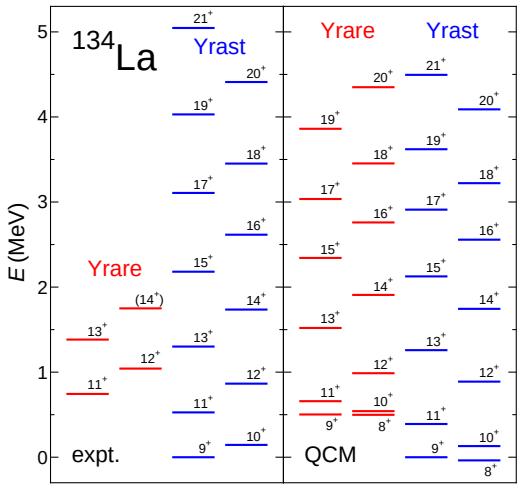

Fig. 1. Experimental energy levels of ^{134}La (expt.) compared with those of QCM calculation.

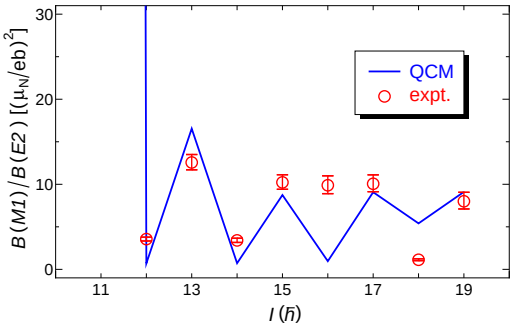

Fig. 2. Comparison of ratios $B(M1; I \rightarrow I-1)/B(E2; I \rightarrow I-2)$ in QCM with experimental data (expt.).

Figure 1 shows the comparison of the theoretical energy levels of the QCM with the experimental data for ^{134}La. Concerning the yrast states, the calculated energy levels are in good agreement with the experimental levels. There is no experimental evidence for the 8^+_1 state, but the QCM calculation predicts the 8^+_1 state near the 9^+_1 state. For the yrare band, our theoretical result provides a clear description of the energy levels, although only four levels are observed experimentally.

Figure 2 shows the comparison of the theoretical ratios $B(M1; I \rightarrow I \quad 1)/B(E2; I \rightarrow I \quad 2)$ for the yrast states with the experimental values. The large-amplitude staggering of the $B(M1)/B(E2)$ ratios obtained in theory is in good agreement with experimental data, except for the 16^+_1 state.

By analyzing the QCM wave functions, it turns out that the even-odd staggering of the $B(M1)/B(E2)$ ratios occurs only when the coupling of the collective core and particles is weak, and that the staggering is caused by a chopsticks motion of two angular momenta of the neutron hole and proton particle. This result is consistent with the previous PTSM calculations[1–3].

References

1) K. Higashiyama and N. Yoshinaga: Prog. Theor. Phys. **113**, 1139 (2005).
2) K. Higashiyama, N. Yoshinaga, and K. Tanabe: Phys. Rev. C **72**, 024315 (2005).
3) N. Yoshinaga and K. Higashiyama: J. Phys. G **31**, S1455 (2005).

† Condensed from the article in Eur. Phys. J. A **30**, 343 (2006)
*1 Department of Physics, Saitama University
*2 Department of Physics, Chiba Institute of Technology

Tilted-axis rotation and wobbling motion on 3D-CHFB states

Y. Hashimoto,[*1] T. Horibata[*2]

[3D-CHFB, tilted-axis rotation, generator coordinate method]

The rotational motion of a nucleus is due to the collective motion of the nucleons and is regarded as a macroscopic manifestation of the microscopic quantum effects that prevail in the nucleus. When the axial symmetry is lost in the shape of the nuclear mean field, a general type of rotational motion occurs, in which the rotational axis is not parallel with the principal axis (PA) with the largest moment of inertia but fluctuates around the PA[1,2]. This type of rotational motion is called wobbling motion. From a theoretical point of view, a much more general type of rotation is expected, where the rotational axis is located away from any of the principal axes[3,4]. This is called tilted-axis rotation (TAR)[5]. The three-dimensional cranking model plays a central role in the study of wobbling motion and TAR. To clarify the relations among the PA rotations, the wobbling motion and the TAR, we carried out three-dimensional cranked Hartree-Fock-Bogoliubov (3D-CHFB) calculations. Making use of the 3D-CHFB solutions, we performed calculations by the generator coordinate method (GCM) to include the quantum mechanical fluctuations around the mean-field solutions.

The model Hamiltonian used in the present calculation is the pairing plus quadrupole (P+QQ), as is used in Ref. [5]. The parameters in the model Hamiltonian are the interaction strengths for the quadrupole-quadrupole and the pairing interactions, whose values are the same as those used in the previous calculations in Ref. [6].

The wave function $|\Phi(\psi)\rangle$ for the tilt angle ψ is obtained by solving the 3D-CHFB equation,

$$\delta\langle\Phi(\psi)|\Big[\hat{H} \quad \sum_{k=1}^{3}\Big(\mu_k\hat{J}_k+\xi_k\hat{B}_k\Big) \quad \sum_{\tau=p,n}\lambda_\tau\hat{N}_\tau\Big]|\Phi(\psi)\rangle=0, \qquad (1)$$

where the quantities μ_k, ξ_k and λ_τ are Lagrange multipliers used to satisfy the constraints with respect to the angular momentum and number constraints. $\hat{B}_k$ are the three off-diagonal components of the mass-quadrupole tensor in the Cartesian coordinate representation.[5]

In Ref. [5], it was suggested that there is an extremum point along the tilt angle, which is measured from the x-axis to the z-axis (symmetry axis). We take the tilt angle ψ as the generator coordinate in the GCM calculation. As the space of states, we take into account the states on the g-branch and s-branch in the 3D-CHFB calculations.

In Fig. 1, we show the GCM amplitude of the solution of the GCM equation with the lowest eigenenergy for angular momentum J = 18 in the case of osmium ^{182}Os. The diagonal elements (DEs) of the Hamiltonian kernel are also shown in the figure. There is a wide dip along the DE of the s-branch. There is also a "well" with almost the same depth as the s-branch dip along the DE of the g-branch[7]. The strength of the amplitude is separated roughly into two parts. We expect a coupling effect between the wobbling motion on the g-branch around the point $\psi = 0$ and the TAR motion in the dip on the s-branch around $\psi = 40$. Analyses of the coupling mechanism are in progress.

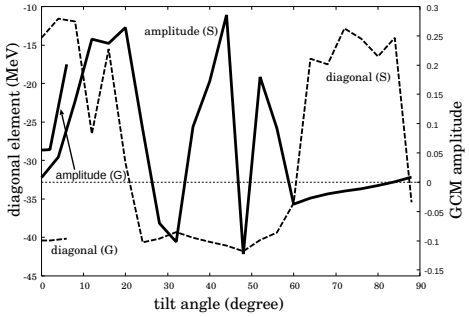

Fig. 1. Amplitude of the GCM solution with the lowest eigenvalue (solid curve). Broken curves denote the diagonal elements of the Hamiltonian kernel.

References

1) A. Bohr and B. R. Mottelson: *Nuclear Structure*, Vol.II (Benjamin, Reading, MA, 1975).
2) S. Frauendorf: Rev. Mod. Phys. 73, 463 (2001).
3) A. K. Kerman and N. Onishi: Nucl. Phys. A361, 179 (1981).
4) N. Onishi: Nucl. Phys. A456, 279 (1986).
5) T. Horibata and N. Onishi: Nucl. Phys. A596, 251 (1996).
6) T. Horibata, M. Oi, N. Onishi, and A. Ansari: Nucl. Phys. A646, 277 (1999); A651, 435 (1999).
7) Y. Hashimoto and T. Horibata: Phys. Rev. C74, 017301 (2006).

*1 Graduate School of Pure and Applied Sciences, University of Tsukuba, Tsukuba, Ibaraki 305-8571, Japan
*2 Department of Software and Information Technology, Aomori University, Aomori, Aomori 030-0943, Japan

Thermal pairing in Richardson model*

N. Dinh Dang

[NUCLEAR STRUCTURE, thermal fluctuations, pairing, superfluid-normal phase transition, BCS theory, Richardson model]

Infinite systems undergo a sharp phase transition from the superfluid phase to the normal- fluid one at finite temperature. This phase transition is a second-order one as it is marked by a collapse of the pairing correlations (pairing gap), and a near divergence of the heat capacity at a critical temperature T_c.

The application of the BCS theory and its generalization, the Hartree-Fock-Bogoliubov theory , to finite Fermi systems paved the way to study the superfluid-normal (SN) phase transition in nuclei at finite temperature T. Soon it has been realized, however, that the BCS and HFB theories ignore a number of quantal and thermodynamic fluctuations, which become large in small systems due to their finiteness. Although it has been shown that thermal fluctuations in the pairing field wash out the second-order SN phase transition, it was unclear about the origin of these fluctuations. In the recently proposed modified-BCS (MBCS) theory, and its generalization, the modified-HFB (MHFB) theory[1)], it has been shown for the first time that it is the fluctuations of quasiparticle number that smooth out the sharp SN phase transition and lead to the non-vanishing thermal pairing in finite systems.

The present work tests the validity of the MBCS theory by applying it to the Richardson model for pairing with a level distance of 1 MeV at various values for the number of levels Ω and particles N. It is shown that the limitation of the configuration space sets a limiting temperature T_M up to which the MBCS can be applied. Enlarging the space in the half-filled case ($\Omega = N$) by one valence level ($\Omega = N + 1$) extends T_M to a much higher temperature so that the predictions by the MBCS can be compared directly with the exact results up to $T \leq 4$ - 5 MeV even for small N. The MBCS gap does not collapse, but decreases monotonously with increasing T [Fig. 1]. The total energy and heat capacity predicted by the MBCS are closer to the exact results than those predicted by the BCS, especially in the region of the SN phase transition. The discontinuity in the BCS heat capacity at the BCS phase-transition temperature T_c is smoothed out within the MBCS, especially for small N, showing the disappearance of superfluid-normal phase transition in very light systems. With increasing N the peak at T_c in the heat capacity becomes more pronounced, showing a phase-transition-like behavior in heavy systems.

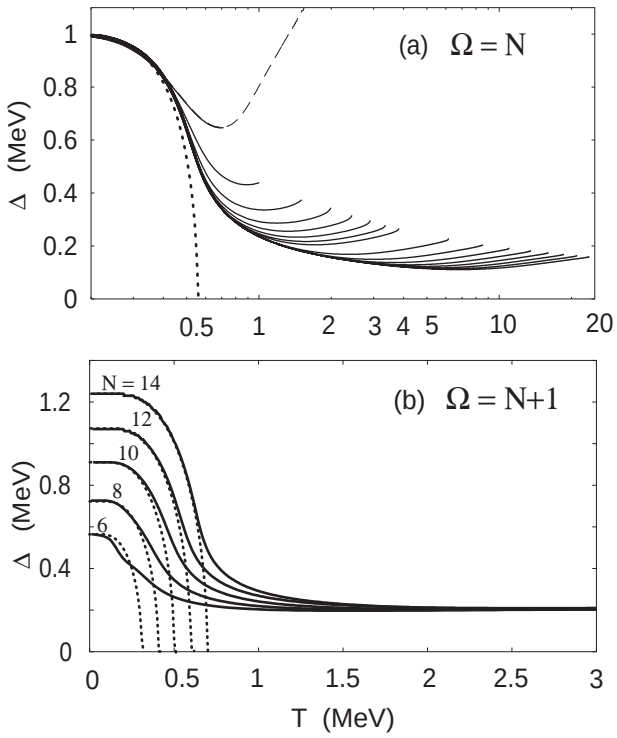

Fig. 1. (a): Pairing gaps for $\Omega = N$ as functions of temperature. The dotted line denotes the BCS gap obtained at $N = 100$. The solid lines represent the MBCS gaps obtained at N = 6, 8, 10, 12, 14, 16, 18, 20, 30, 40, 50, 60, 70, 80, 90 and 100, where a solid line, which is extended to a larger T_M, corresponds to a larger a large value of N. The dashed line at $N = 6$ shows the part of the MBCS gap, which increases with T due to the limitation of the configuration space. (b): Pairing gaps within BCS (dotted lines) and MBCS (solid lines) for $\Omega = N + 1$ as functions of temperature at $N \leq 14$, as shown atop the lines (G = 0.4 MeV).

References

1) N. Dinh Dang and V. Zelevinsky, Phys. Rev. C 64, 064319 (2001); N. Dinh Dang and A. Arima, Phys. Rev. C 67, 014304 (2003); N. Dinh Dang and A. Arima, Phys. Rev. C 68, 014318 (2003).

* Condensed from Nucl. Phys. A **784**, 147 (2007).

Consistency of particle-particle random-phase approximation and renormalization*

N. Dinh Dang

[NUCLEAR STRUCTURE, particle-particle RPA, self-consistent RPA, two-particle separation energy.]

The random-phase approximation (RPA) has been widely used in the theoretical study of nuclei within the valley of β-stability. Its success is mainly based on the use of the quasiboson approximation (QBA), which considers fermion pairs as boson operators, just neglecting the Pauli principle between them. As a result, the linear equations (RPA equations), were derived, which reveal the physics of collective excitations generated by the RPA boson-like modes. The simplicity of the RPA equations allows a feasible treatment of a number of many-body problems. However, this approach breaks down at a certain critical value of the interaction's parameter, where the RPA yields imaginary solutions. The reason of this well-known RPA instability is the violation of Pauli principle within the QBA.

In β-stable medium and heavy nuclei, the QBA is a good approximation, and the RPA is a very powerful tool for the description of several important quantities such as the ground-state and excited-state energies, electro-magnetic transition probabilities and their distribution, transition densities, etc. However, with reducing the particle number, the concept of collective excitations, which are described by the RPA modes, becomes less and less firm. The ground-state correlations (GSC) which are left beyond the RPA become stronger in light systems. This feature makes the validity of the QBA, and therefore of the RPA itself, questionable in the systems with small particle numbers.

Several approaches were developed to take into account the GSC beyond RPA in a simple way such as to restore the Pauli principle among the fermion pairs, from which the RPA operators are constructed. The popular one, known as the renormalized RPA (RRPA)[1] includes the expectation value over the ground state of the diagonal elements of the commutator between two fermion-pair operators, neglected in the QBA. In this way the Pauli principle is approximately taken care of. The inclusion of GSC beyond RPA within the RRPA eventually renormalizes the interaction in such a way that the collapse of RPA is avoided, and the RRPA has solutions at any value of the interaction's parameter. This scheme has been tested in several exactly solvable schematic models such as the Lipkin model for *ph* RRPA, the SO(8) model for the renormalized quasiparticle RPA, and the Richardson model for the *pp* RRPA and self-consistent RPA (SCRPA)[2]. The results of these studies showed that the difference between the energies of the first excited state given by the *pp* RPA, *pp* RRPA, and SCRPA increases noticeably with increasing the interaction parameter and/or decreasing the particle number. The SCRPA solutions are the closest ones to the exact solutions. These results raise a serious question of the applicability of the RPA to the calculations for realistic light-neutron rich nuclei. As a matter of fact, a close agreement between the RPA results and the experimental data for light neutron-rich nuclei can be considered really reasonable if the corrections due to GSC beyond RPA are negligible, which justify the validity of the QBA. In the opposite case such agreement may be even illusory.

This concern is the motivation of the present work, whose goal is to test the consistency of the *pp* RPA and its renormalizations, the *pp* RRPA and SCRPA, at different particle numbers as the interaction strength varies. The consistency condition is tested making use of the Richardson model of pairing. The two-particle separation energy is calculated in two ways, namely as the energy of the first addition mode, which adds two particles to a core with N particles, and as the energy of the first removal mode, which removes two particles from the $N+2$ particle system to get back to the same N-particle core. The consistency condition is satisfied when the two ways of calculations give the same result. It is found that the results obtained in these two ways of calculations are close to each other only at large values of particle number N and/or small interaction strength. At $N \leq 10$ for a given value of the interaction strength, the discrepancy between the results obtained in two ways of calculations within the SCRPA is much smaller than those given by the RPA and RRPA. Therefore, it is quite important to include the effects of GSC beyond RPA in light systems. Among the approaches considered here, the most consistent one turns out to be the SCRPA.

References

1) K. Hara, Prog. Theor. Phys. **32**, 88 (1964), K. Ikeda, T. Udagawa, and H. Yamamura, Prof. Theor. Phys. **33**, 22 (1965); D.J. Rowe, Phys. Rev. **175**, 1283 (1968); F. Catara, N.D. Dang, and M. Sambataro, Nucl. Phys. A **579**, 1 (1994).
2) J. Dukelsky and P. Schuck, Phys. Let. B**464**, 164 (1999); N. Dinh Dang, Phys. Rev. C **71**, 024302 (2005).

* Condensed from Phys. Rev. C **74**, 024318 (2006).

Self-Consistent Quasiparticle RPA for Multi-Level Pairing Model

N. Quang Hung and N. Dinh Dang

[Nuclear structure, random phase approximation, multi-level pairing model]

The random-phase approximation (RPA), which includes correlations in the ground state, provides a simple theory of excited states of the nucleus. However, the RPA equation breaks down at a certain value of interaction strength where it yields imaginary eigenvalues because it neglects the Pauli principle between fermion pairs in the quasi-boson approximation (QBA). The RPA theory therefore needs to be extended to correct this deficiency.

The self-consistent RPA (SCRPA)[1] is one of the extensions of RPA. It has been applied to the exactly solvable multi-level pairing model in the critical region and gives a good agreement with exact results for ground-state energy and the low-lying part of the spectrum.

Recently, the SCRPA was developed for the superfluid region by a theory called the self-consistent quasiparticle RPA (SCQRPA). The SCQRPA was applied for the first time for the description of superfluid Fermi systems[2] where a set of SCQRPA equations was solved analytically within a two-level pairing model.

In this work, the SCQRPA theory is applied for multi-level pairing model, the so-called picket-fence model, which is an exactly solvable model extensively employed in nuclear physics to test many-body approximations. This model consists of Ω doubly-fold equidistant levels interacting via a pairing force with parameter G. The model Hamiltonian is given as:

$$H = \sum_{j=1}^{\Omega}(\epsilon_j - \lambda)N_j - G\sum_{j,j'=1}^{\Omega} P_j^+ P_{j'} \ , \tag{1}$$

where $N_j = a_j^+ a_j + a_{-j}^+ a_{-j}$ is the particle-number operator, and $P_i^+ = a_j^+ a_{-j}^+, P_j = (P_j^+)^+$ are pairing operators. In the SCQRPA, by using the Bogolyubov transformation from particle operators a_j^+ and a_j to quasi-particle ones α_j^+ and α_j, the Hamiltonian (1) is transformed into:

$$\begin{aligned} H \ &= \ a + \sum_j b_j \mathcal{N}_j + \sum_j c_j \mathcal{A}_j^+ \mathcal{A}_j + \sum_{jj'} d_{jj'} \mathcal{A}_j^+ \mathcal{A}_{j'} \\ &+ \ \sum_{jj'} g_j(j')(\mathcal{A}_{j'}^+ \mathcal{N}_j + \mathcal{N}_j \mathcal{A}_{j'}) \\ &+ \ \sum_{jj'} h_{jj'}(\mathcal{A}_j^+ \mathcal{A}_{j'}^+ + \mathcal{A}_{j'} \mathcal{A}_j) + \sum_{jj'} q_{jj'} \mathcal{N}_j \mathcal{N}_{j'}, \end{aligned} \tag{2}$$

with the quasiparticle number operator $\mathcal{N}_j = \alpha_j^+ \alpha_j + \alpha_{-j}^+ \alpha_{-j}$ and the quasiparticle pairing operators $\mathcal{A}_j^+ = \alpha_j^+ \alpha_{-j}^+$ and $\mathcal{A}_j = (\mathcal{A}_j^+)^+$. The coefficients $a, b_j, c_j, d_{jj'}, g_j(j'), h_{jj'}, q_{jj'}$ are given in terms of the coefficients of the Bogolyubov transformation u_j and v_j and the single particle energies ϵ_j.

The SCQRPA equations are given in the matrix form as:

$$\begin{pmatrix} A & B \\ B & A \end{pmatrix} \begin{pmatrix} X \\ Y \end{pmatrix} = \omega \begin{pmatrix} X \\ -Y \end{pmatrix}, \tag{3}$$

where the SCQRPA sub-matrices are given as:

$$\begin{aligned} A_{jj'} \ &= \ 2 \Bigg[b_j + 2q_{jj'} + 2\sum_{j''} q_{jj''} < (1 - D_{j''}) > \\ &- \ \frac{1}{< D_j >} \Bigg(\sum_{j''} d_{jj''} < \mathcal{A}_{j''}^+ \mathcal{A}_j > \\ &- \ 2\sum_{j''} h_{jj''} < \mathcal{A}_{j''} \mathcal{A}_j > \Bigg) \Bigg] \delta_{jj'} \\ &+ \ d_{jj'} \sqrt{< D_j >< D_{j'} >} \\ &+ \ 8q_{jj'} \frac{< \mathcal{A}_j^+ \mathcal{A}_{j'} >}{\sqrt{< D_j >< D_{j'} >}}, \end{aligned} \tag{4}$$

$$\begin{aligned} B_{jj'} \ &= \ -2 \Bigg[h_{jj'} + \frac{1}{< D_j >} \Bigg(\sum_{j''} d_{jj''} < \mathcal{A}_{j''} \mathcal{A}_j > \\ &+ \ 2\sum_{j''} h_{jj''} < \mathcal{A}_{j''}^+ \mathcal{A}_j > \Bigg) \Bigg] \delta_{jj'} \\ &+ \ 2h_{jj'} \frac{< D_j >< D_{j'} >}{\sqrt{< D_j >< D_{j'} >}} \\ &+ \ 8q_{jj'} \frac{< \mathcal{A}_j \mathcal{A}_{j'} >}{\sqrt{< D_j >< D_{j'} >}}, \end{aligned} \tag{5}$$

where $< D_j >= 1 - < \mathcal{N}_j >$ is the ground-state correlation factor. The expectation values $< \mathcal{A}_j^+ \mathcal{A}_{j'} >$ and $< \mathcal{A}_j \mathcal{A}_{j'} >$ are given in terms of amplitudes X_j^ν and Y_j^ν.

The SCQRPA equations are solved numerically using the FORTRAN IMSL Library by Visual Numerics on the RIKEN Super Combined Cluster (RSCC) System. We hope to improve the description of superfluid Fermi systems using this SCQRPA for multi-level pairing model.

References

1) P. Schuck, Z. Phys. **241**, 395 (1971); P. Schuck and S. Ethofer, Nucl. Phys. A**212**, 269 (1973); J.Dukelsky and P. Schuck, Phys. Lett. B **464**, 164 (1999)
2) A. Rabhi, R. Bennaceur, G. Chanfray, and P. Schuck, Phys. Rev. C**66**, 064315(2002)

Formula for proton-nucleus reaction cross section at intermediate energies and its application†

K. Iida,[*1] A. Kohama, and K. Oyamatsu[*2]

[Nuclear reaction, reaction cross section, nuclear radius, unstable nuclei]

Nuclear size and mass are fundamental quantities characterizing the bulk properties of nuclei. In fact, the saturation of the binding energy and density deduced from systematic data for the masses and charge radii of stable nuclei reflects the behavior of the equation of state (EoS) of nearly symmetric nuclear matter near the saturation density. The extension of such data to a more neutron-rich regime opens up an opportunity of probing the EoS of asymmetric nuclear matter.[1)]

Recently, we have systematically analyzed the proton elastic scattering and reaction cross section data for stable nuclei at a proton incident energy of $T_p \sim$ 800–1000 MeV on the basis of a "black-sphere picture" of nuclei.[2,3)] This picture is originally expected to give a decent description of the reaction cross section of any kind of incident particle that tends to be attenuated in nuclear interiors. We showed that for proton beams incident on stable nuclei, the cross section of the black sphere of radius a ($= \pi a^2$), which was determined by fitting the angle of the first elastic diffraction peak calculated for proton diffraction by a circular black disk of radius, a, to the measured value, is consistent with the measured reaction cross section.[3)] This consistency suggests that the black sphere radius corresponds to a reaction radius inside which the reaction with incident protons occurs. For real nuclei, this radius must be a radius at which the mean free path of incident protons becomes of the order of penetration length.

In this work, we construct a formula for a proton-nucleus total reaction cross section, $\sigma_{\rm R}$, as a function of the mass and neutron excess of the target nucleus and T_p in a way free from any adjustable T_p-dependent parameter. We deduce the dependence of $\sigma_{\rm R}$ on T_p from a simple argument involving the proton "optical" depth within the framework of a black sphere approximation of nuclei, while we describe the neutron excess dependence by introducing the density derivative of the symmetry energy, L, on the basis of a radius formula constructed from macroscopic nuclear models. This parameter is still uncertain, but mainly controls the saturation density of nuclear matter at nonzero neutron excess.

We find that, for stable nuclei, this formula remarkably well reproduces the empirical T_p dependence of $\sigma_{\rm R}$ at T_p = 100–1000 MeV without introducing any adjustable energy-dependent parameter. This prescription is easily extended to nucleus-nucleus reactions, and an illustrative example is shown in Fig. 1. In addition, we consider the effects of a large neutron excess typical of unstable nuclei and nuclear deformation on the reaction cross section.

We thus find out a possible way of examining the effect of the density dependence of the symmetry energy.

References

1) K. Oyamatsu and K. Iida: Prog. Theor. Phys. **109**, 631 (2003).
2) A. Kohama, K. Iida, and K. Oyamatsu: Phys. Rev. C **69**, 064316 (2004).
3) A. Kohama, K. Iida, and K. Oyamatsu: Phys. Rev. C **72**, 024602 (2005).

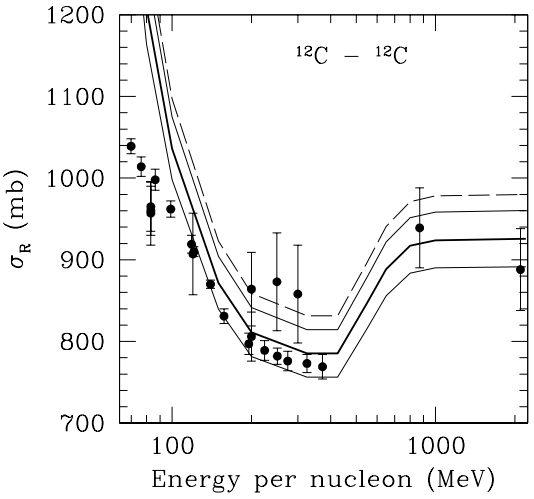

Fig. 1. ^{12}C-^{12}C reaction cross section as function of energy per nucleon. Filled circles indicate empirical data. Lines indicate the results obtained using our formula in which a_0 is set to be 2.7 fm (bold), 2.65 fm (lower, thin), 2.75 fm (upper, thin), and $1.214A^{1/3}$ fm (dashed).The choice of 2.65–2.75 fm is based on the measured diffraction peak angle in proton elastic scattering.

† Condensed from the article in nucl-th/0601039 (J. Phys. Soc. Japan in press).

*1 Department of Materials Science, Kochi University
*2 Department of Media Theories and Production, Aichi Shukutoku University

More Accurate Estimation of Ground-State Energy and Spin-Zero Dominance

N. Yoshinaga [*1] and A. Arima [*2]

[Nuclear shell model, Spin-zero dominance]

The ground states of all even-even nuclei have a zero spin, $I = 0$, and a positive parity, $\pi = +$. The predominance of $I^\pi = 0^+$ ground states was discovered by Johnson et al. using the two-body random ensemble (TBRE)[1]. Since then, many studies have been devoted to understanding and solving this problem from various viewpoints (see Ref. 2 for a recent review). In our previous studies[3], we obtained a semiempirical formula for evaluating the ground-state energy in terms of average energy (centroid), standard deviation (width), and the number of spin I states. On the basis of this formula, we studied the problem of the spin-zero ground state (0 g.s.) dominance in the presence of the TBRE. In this paper, we report a method for a more accurate evaluation of ground-state energy.

To simplify our argument, we take a single j^n configuration for fermions. The Hamiltonian used is

$$\hat{H} = \sum_{J=0,\mathrm{even}}^{2j-1} \sqrt{2J+1}\, G_J \left[A^{\dagger(J)} \tilde{A}^{(J)}\right]^{(0)}, \qquad (1)$$

where G_J's are two-body interactions between fermions and are assumed to follow the TBRE

$$\rho(G_J) = \frac{1}{\sqrt{2\pi}} \exp\left(-G_J^2/2\right). \qquad (2)$$

Then the variance of eigenenergies around the average energy (the width squared) is denoted as

$$\left(\sigma_I\left\{G_J\right\}\right)^2 \equiv \frac{1}{d_I} \mathrm{Tr}\left[\left(\hat{H} - \bar{E}_I\right)^2\right], \qquad (3)$$

where d_I indicates the dimension of the Hamiltonian matrix.

Let us estimate the ground-state energy of the Hamiltonian $\hat{H}$ by assuming that it can be expressed in terms of average energy ($\bar{E}_I$), width ($\sigma_I\left\{G_J\right\}$) and the number of states (d_I) as

$$E_I^{(2)} = \bar{E}_I - \Phi(d_I)\, \sigma_I\left\{G_J\right\}, \qquad (4)$$

where $\Phi(d_I)$ is assumed to depend only on the dimension of the Hamiltonian matrix and to take the form

$$\Phi(d_I) = \sqrt{a \ln d_I + b}. \qquad (5)$$

Here, the parameters $a = 0.99$ and $b = 0.36$ are determined phenomenologically.

We further make an approximation of ground-state energy. Now, ground-state energy is approximated as

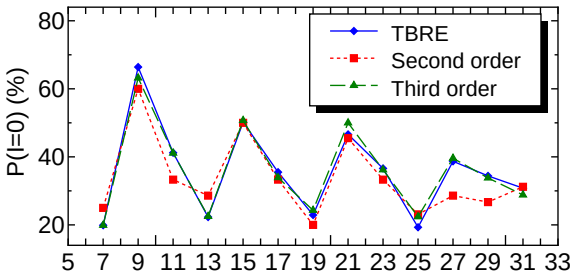

Fig. 1. $P(0)$'s of four fermions in single-j shell. The diamonds are obtained by performing 1000 runs of the TBRE Hamiltonian. The squares are obtained using the energies obtained by second-order approximation and the triangles, using those obtained by third-order approximation.

$$E_I^{(3)} = \bar{E}_I - \sqrt{a \ln d_I + b}\, \sigma_I - c\, \gamma_I \qquad (6)$$

where

$$(\gamma_I)^3 \equiv \frac{1}{d_I} \mathrm{Tr}\left[\left(\hat{H} - \bar{E}_I\right)^3\right]. \qquad (7)$$

In Fig. 1, we show the $P(0)$'s of four fermions in single-j shells. The diamonds are obtained by performing 1000 runs of the TBRE Hamiltonian. The squares are the results of the present method in terms of second-order approximation (second order). The triangles are the results of third-order approximation (third order). It is seen that both predictions perfectly describe the staggering behavior of $P(0)$'s. A small refinement is obtained using third-order approximation for ground-state energy.

To summarize, we proposed a new analytical expression for evaluating the ground-state energy of spin I states. With this simple formula, a remarkably successful description of the spin I ground-state probabilities was obtained in the presence of the TBRE.

[*1] Department of Physics, Saitama University
[*2] Science Museum, Japan Science Foundation

References

1) C. W. Johnson, G. F. Bertsch and D. J. Dean: Phys. Rev. Lett. **80**, 2749 (1998).
2) Y. M. Zhao, A. Arima and N. Yoshinaga: Phys. Rept. **400**, 1 (2004).
3) N. Yoshinaga, A. Arima and Y. M. Zhao: Phys. Rev. C **73**, 017303 (2006), N. Yoshinaga, A. Arima and Y. M. Zhao: RIKEN accel. Prog. Rep. **39**, 24 (2005).

Fusion Hindrance Due to One-Body Penetration at Deep Sub-Barrier Energies for ^{64}Ni+^{64}Ni

T. Ichikawa, K. Hagino,[*1] and A. Iwamoto,[*2]

[Fusion reactions, coupled-channel model, medium-mass nuclei]

In fusion reactions in the medium-mass region such as ^{64}Ni+^{64}Ni, ^{58}Ni+^{58}Ni and ^{64}Ni+^{89}Y, it has been found that experimental fusion cross sections at extremely low incident energies become much lower than ones calculated using the coupled-channel (CC) model using the Wood-Saxon potential[1]. This steep fall-off of experimental fusion cross sections is known as fusion hindrance. The physical origin of the fusion hindrance is not yet understood well.

To explain this fusion hindrance, we propose a two-step model based on an adiabatic scheme, in which the neck formation in a one-body system is taken into account. This model is used to consider the fission like adiabatic potential-energy surface with the neck shape after the colliding nuclei come into contact. This one-body potential acts as an inner barrier that has to be overcome to reach the compound state. This mechanism only works when the incident energies are below the potential energy at the configuration when the nuclei come into contact.

Our two-step model consists of the capture process in a two-body potential pocket, which is followed by the penetration of the adiabatic one-body potential to reach a compound state after the nuclei come into contact. We describe the former process using the coupled-channel framework, while the latter is described using the WKB approximation by taking into account the coordinate-dependent inertia mass. The fusion cross section in this two-step model is

$$\sigma(E) = \frac{\pi\hbar^2}{2\mu E}\sum_{\ell}(2\ell+1)T_{\ell}(E)P_{\rm 1bd}(E,\ell), \qquad (1)$$

where μ and E denote the reduced mass and the incident energy in the center-of-mass system, respectively. T_ℓ denotes the sticking probability in the two-body system, which is calculated with the CC model using the computer code `CCFULL`[2] from the infinite separation of the nuclei to the configuration when they come into contact. $P_{\rm 1bd}$ is the penetrability of the composite system for penetrating the adiabatic one-body barrier to reach the compound nucleus, which is calculated using the WKB approximation taking account of the coordinate-dependent inertia mass. The inertia mass is calculated as the irrotational-flow mass using the Werner-Wheeler approximation.

We apply this two-step model to the fusion reaction of the ^{64}Ni+^{64}Ni system. In this work, we employ the potential energy calculated using the Krappe-Nix-Sierk (KNS) model[3], as shown in Fig. 1. The radius parameter is adjusted to $r_0 = 1.204$ fm to fit the experimental fusion cross section at high incident energies. In the KNS model, the saturation property is phenomenologically taken into account. In the one-body system after the two nuclei come into contact, we assume that the shape configuration is described by lemniscatoid parametrization[4].

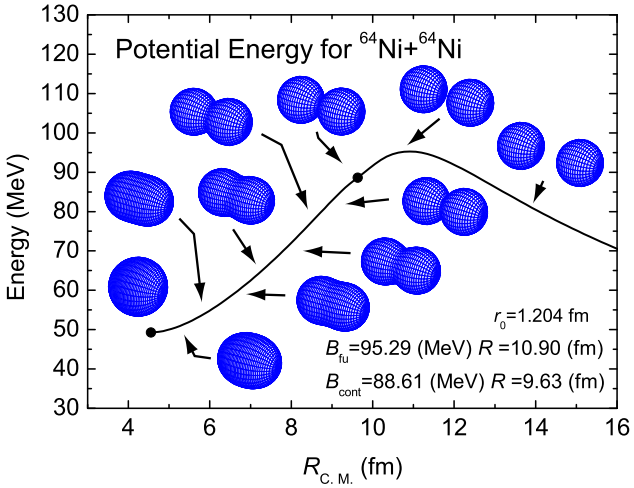

Fig. 1. One- and two-body potential energy for ^{64}Ni+^{64}Ni calculated using the KNS model. We assume that the shape configuration in the one-body system is described by a lemniscatoid parametrization.

By taking into account the penetration of the adiabatic one-body potential with the neck formation after the nuclei come into contact, we find that the fusion cross section calculated using this model accounts well for the experimental data. This result shows that the fusion hindrance can be explained in terms of the extra barrier in the one-body system. The detailed calculation is now in progress.

References

1) C. L. Jiang et al.: Phys. Rev. C **73**, 014613 (2006).
2) K. Hagino et al.: Phys. Commun. **123**, 143 (1999).
3) H. J. Krappe et al.: Phys. Rev. C **20**, 992 (1979).
4) G. Royer et al.: J. Phys. **G8**, L159 (1982).

[*1] Department of Physics, Tohoku University
[*2] Japan Atomic Energy Agency

Late-time supernova evolution induced by anisotropic neutrino radiation and r-process environment†

H. Madokoro and Y. Motizuki

[shock waves—hydrodynamics—stars:neutron—supernovae:general—nucleosynthesis]

It has been found that multidimensional simulations are necessary to understand the mechanism underlying core-collapse supernova explosions. We performed two-dimensional (2-D) simulations with particular attention paid to the role of globally anisotropic neutrino radiation. Our previous studies[1–3] showed that a few percent of anisotropy markedly increases explosion energy.

We now extend our calculations to the later phase of explosions ($t > 1$ sec after bounce) to investigate the r-process environment. In our previous studies, we made several assumptions that are valid only under the conditions of high temperature and high density, following a common description of core-collapse supernovae. To extend our simulation to the later phase, we have updated a number of points in our numerical code. The most important one is that we used exact expressions of the neutrino-matter interactions, which can be applied to low-temperature and low-density regions. We have also included the important effect of internal shock heating, which is caused by the accretion of matter onto the surface of a protoneutron star.

Our calculations start when a supernova shock wave is stalled at 150 km from the center of a protoneutron star. The radius of the proto-neutron star was taken to be 15 km. We assumed that the neutrino temperature is 7.8 MeV at the beginning of our simulation, and decays with time. The anisotropy of neutrino radiation, l_z/l_x, is set to be 3 for the 2-D model.

Figure 1 shows a contour plot of entropy distribution with velocity fields at 2150 ms after the shock stall. We obtain very high values of entropy (more than 200 in units of Boltzmann constant per nucleon). This enhancement of entropy is mainly caused by an improved neutrino heating rate and the effect of internal shock heating. The improved neutrino heating rate affects the evolution of entropy distribution to a large extent for late-time evolution. The internal shock heating forms new shock waves, which propagate outwards and merge into the original shock wave. This increases matter temperature, and subsequently the value of entropy. We estimated that entropy is enhanced more than 50 % when the internal shock heating is included.

Figure 2 shows the evolution of the electron-baryon fraction (Y_e). The evolution is strongly suppressed ($\sim 0.02 - 0.03$) just above the surface of the protoneutron star. This is because very strong electron captures onto free protons occur in the vicinity of the surface. Accreting matter onto the surface of the proto-neutron star goes through such a low-Y_e region, and moves upward along the polar axis due to global convection. Note that the expansion velocity of our 2-D model is much larger than that of the spherical model. Thus, we obtained a promising environment as an r-process site in our 2-D simulation, that is, high entropy and low Y_e values, and a rapid expansion. The r-process network calculations based on the present supernova simulations are now in progress.

References

1) T. M. Shimizu et al.: Astrophys. J. **552**, 756 (2001).
2) H. Madokoro, T. Shimizu and Y. Motizuki: Astrophys. J. **592**, 1035 (2003).
3) H. Madokoro, T. Shimizu and Y. Motizuki: Publication of Astronomical Society of Japan **56**, 663 (2004).

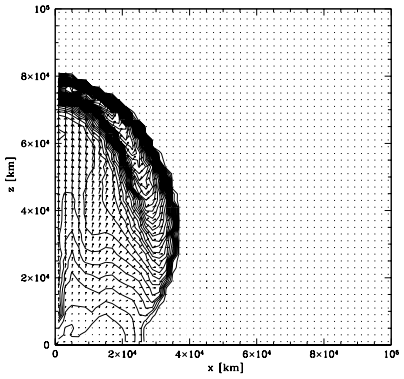

Fig. 1. Contour plot of entropy distribution with velocity fields at 2150 ms after shock stall. The maximum value of entropy reached more than 200 in units of Boltzmann constant per nucleon.

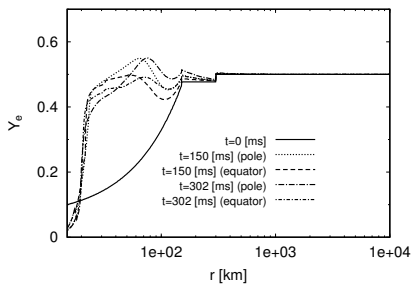

Fig. 2. Evolution of electron-baryon fraction.

Estimation of the in-medium modification parameters for ϕ meson†

R. Muto, H. En'yo, M. Naruki, F. Sakuma,*1 and S. Yokkaichi for the KEK-PS E325 Collaboration

[QCD, chiral symmetry, normal nuclear density, mass modification, vector meson]

The KEK-PS E325 experiment was conducted at the KEK Proton Synchrotron to detect possible in-medium modification of vector mesons. Invariant mass spectra of $\phi \to e^+e^-$ decays were measured in 12-GeV $p + A$ interactions. Copper and carbon targets were used to study the nuclear-size dependence. We fitted the mass spectrum with a resonance shape of $\phi \to e^+e^-$ and a quadratic background curve. A significant excess on the low-mass side of the ϕ meson peak was observed in the lowest $\beta\gamma$ region of ϕ mesons ($\beta\gamma < 1.25$) with copper targets[1].

We attempted to reproduce the obtained mass spectra with a Monte-Carlo-type model calculation that includes the in-medium mass modification of the ϕ mesons. We introduced the in-medium modification parameters, k_1, $k_2^{\rm tot}$ and k_2^{ee} as follows. We assumed the density dependence of the ϕ meson mass as $m_\phi(\rho)/m_\phi(0) = 1 - k_1(\rho/\rho_0)$, where ρ_0 is the normal nuclear density[2]. For the density dependence of the total width broadening, we assumed $\Gamma_\phi^{\rm tot}(\rho)/\Gamma_\phi^{\rm tot}(0) = 1 + k_2^{\rm tot}(\rho/\rho_0)$; $k_2^{\rm tot} \geq 0$. For Γ_ϕ^{ee} (the partial width for the $\phi \to e^+e^-$ decay), we assumed $\Gamma_\phi^{ee}(\rho)/\Gamma_\phi^{ee}(0) = 1 + k_2^{ee}(\rho/\rho_0)$, and examined the following two cases: (i) the branching ratio $\Gamma_\phi^{ee}/\Gamma_\phi^{\rm tot}$ remains unchanged in the medium ($k_2^{ee} = k_2^{\rm tot}$), and (ii) Γ_ϕ^{ee} does not increase in the medium ($k_2^{ee} = 0$).

We modified the resonance shape of the ϕ meson with the modification parameters k_1, $k_2^{\rm tot}$ and k_2^{ee}, then fitted again the observed mass spectra with the same procedure as before. The best-fit results in both cases are shown in Fig. 1. The modification parameters are common to the six spectra. Figure 2 shows the confidence ellipsoids for the variation of χ^2 with k_1 and $k_2^{\rm tot}$ in cases (i) and (ii). In case (i), the obtained best-fit parameters are $k_1 = 0.034^{+0.006}_{-0.007}$, $k_2^{\rm tot} = 2.6^{+1.8}_{-1.2}$, and the minimum χ^2 ($\chi^2_{\rm min}$) is 316.4. In case (ii), the best-fit parameters are $k_1 = 0.033^{+0.011}_{-0.008}$, $k_2^{\rm tot} = 0^{+5.6}$, and $\chi^2_{\rm min}$ is 320.8. In both cases, $\chi^2_{\rm min}$ was obtained with parameter $k_1 \simeq 0.034$, meaning the pole mass of the ϕ meson decreases by 3.4 % at normal nuclear density. The $\chi^2_{\rm min}$ in case (ii) (=320.8) is larger than that in case (i) (=316.4) by 4.4. When we fitted only the Cu data in the lowest $\beta\gamma$ region, where the major discrepancy occurs, case (ii) was rejected at 99% C.L. and the best-fit parameters of k_1 and $k_2^{\rm tot}$ do not change, while case (i) was not rejected. The data thus favor an increase in Γ_ϕ^{ee} by a factor of 3.6 at normal nuclear density.

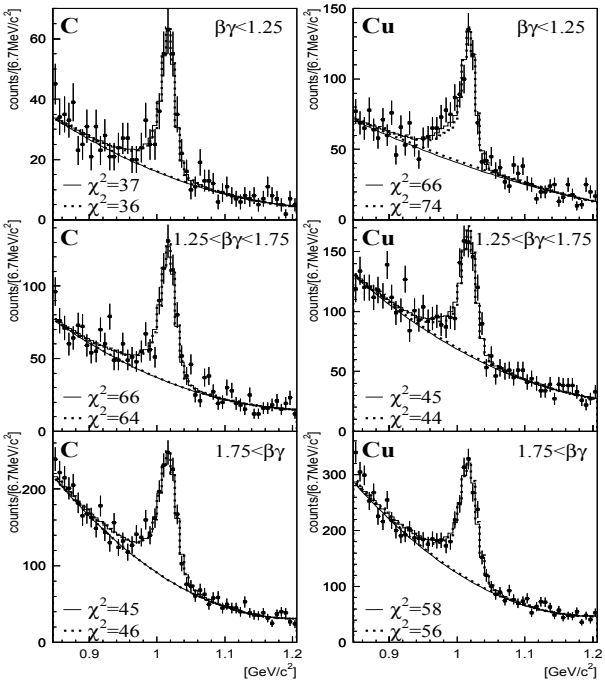

Fig. 1. Best-fit results in cases (i) (solid line) and (ii) (dotted line). The shift parameter k_1 and the broadening parameters $k_2^{\rm tot}$ and k_2^{ee} are common for the six spectra. The values of χ^2 are the sum of the squares of the deviations over 54 data points in each panel.

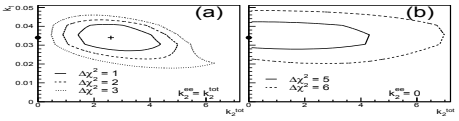

Fig. 2. Confidence ellipsoids for the modification parameters k_1 and $k_2^{\rm tot}$ (a) in case (i) and (b) in case (ii). The values of $\Delta\chi^2$ in both panels are the differences from the $\chi^2_{\rm min}(= 316.4)$ at the best-fit point in case (i), which is shown by the cross in panel (a). The best-fit point in case (ii) is shown by the closed circle in panel (b), and also in panel (a) since the ordinates are common to both cases in the parameter space.

In these analyses, we used the excellent cpu power of CC-J and RSCC at RIKEN. We are grateful for support from these computing facilities.

References

1) R. Muto *et al.*: RIKEN Accel. Prog. Rep. **39**, 80 (2006).
2) T. Hatsuda and S. H. Lee: Phys. Rev. C **45**, R34 (1992).

† Condensed from the article in Phys. Rev. Lett. 98(2007), 042501

*1 Department of Physics, Kyoto University

Nuclear mass number dependence of ϕ-meson production in the e^+e^- and K^+K^- decay channels studied in 12 GeV $p + A$ reactions†

F. Sakuma,*1 H. En'yo, M. Naruki, R. Muto, and S. Yokkaichi for KEK-PS E325 collaboration

[ϕ meson, mass number dependence, e^+e^-, K^+K^-]

In the experiment, KEK-PS E325, we measured e^+e^- and K^+K^- pairs produced in the 12 GeV $p+A$ reaction, in order to search for in-medium modification of vector mesons. In the present study, the nuclear mass number dependence of ϕ-meson production is compared between the e^+e^- and K^+K^- decay channels to determine whether the ratio of the partial decay width $\Gamma_{\phi\to K^+K^-}/\Gamma_{\phi\to e^+e^-}$ depends on the nuclear size.

The nuclear mass number dependence of the cross section for particle production is parameterized as $\sigma(A) = \sigma_0 \times A^\alpha$ for a target nucleus with mass number A. When the spectral function of the ϕ meson and/or kaon is modified in a medium and $\Gamma_{\phi\to K^+K^-}/\Gamma_{\phi\to e^+e^-}$ changes[1], the ratio of the ϕ-meson yield measured in the e^+e^- and K^+K^- decay channels, $R = N_{\phi\to K^+K^-}/N_{\phi\to e^+e^-}$, becomes dependent on the mass number since a larger number of ϕ mesons are to be modified in a larger nucleus. Consequently, by using two different nuclear targets A_1 and A_2, the difference in the α parameter between $\phi \to e^+e^-$ ($\alpha_{\phi\to e^+e^-}$) and $\phi \to K^+K^-$ ($\alpha_{\phi\to K^+K^-}$) can be related to R as follows:

$$\Delta\alpha = \alpha_{\phi\to K^+K^-} - \alpha_{\phi\to e^+e^-} = \ln[R(A_1)/R(A_2)]/\ln(A_1/A_2).$$

It is important that most of the experimental effects, which include large systematic errors arising from tracking efficiency and beam intensity, are canceled in obtaining α.

In the present article, we report the results of the analysis of all the data obtained in 2001/2002. In order to observe the nuclear size dependence, we accumulated data using two types of targets: carbon and copper. A detailed description of the E325 spectrometer can be found elsewhere[2].

The observed α parameters are plotted as functions of $\beta\gamma$ ($= p/m$) in Fig. 1(a) and as functions of the rapidity (y) and transverse momentum (p_T) in (b) and (c), respectively. Since the e^+e^- and K^+K^- decay channels cannot be compared directly because of the difference in the detector acceptance between the e^+e^- and K^+K^- decay channels, we determined $\alpha_{\phi\to e^+e^-}$ two-dimensionally on the y-p_T plane, under the assumption that $\alpha_{\phi\to e^+e^-}$ is linearly dependent on y and p_T, and estimated the values of $\alpha_{\phi\to e^+e^-}$ corresponding to the kaon acceptance windows. In Fig. 1(a), we show the estimated values of $\alpha_{\phi\to e^+e^-}(\beta\gamma)$ in the kaon acceptance window as a hatched band; this can be compared with the measured value of $\alpha_{\phi\to K^+K^-}$. The difference $\Delta\alpha$ in the kaon acceptance is plotted in Fig. 1(d). We expect $\Delta\alpha$ to be zero when $\Gamma_{\phi\to K^+K^-}/\Gamma_{\phi\to e^+e^-}$ does not change in the nuclear medium. Although it is interesting to observe that $\Delta\alpha$ increases when $\beta\gamma$ decreases, $\Delta\alpha$ at the lowest $\beta\gamma$ bin is only 0.33 ± 0.17; the average value is 0.14 ± 0.12. Therefore, $\alpha_{\phi\to e^+e^-}$ and $\alpha_{\phi\to K^+K^-}$ are statistically the same in the measured kinematic region.

To expedite the analysis, we have used CC-J and RSCC at RIKEN. We would like to thank the staff members of CC-J and RSCC for their support.

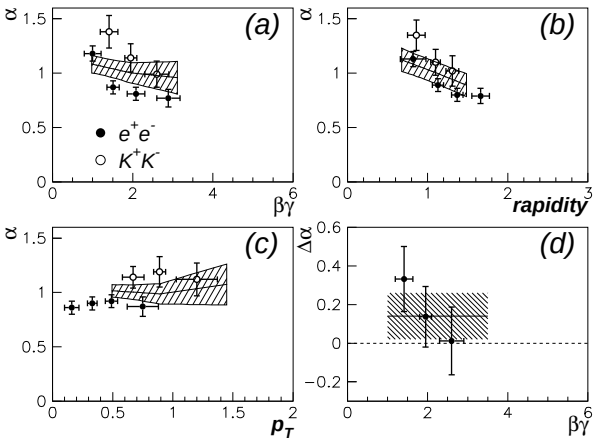

Fig. 1. α parameters of $\phi \to e^+e^-$ (closed circles) and $\phi \to K^+K^-$ (open circles) as functions of (a) $\beta\gamma$, (b) rapidity, and (c) p_T. The horizontal error bars are the RMS values of the horizontal bins. The hatched bands show corrected $\alpha_{\phi\to e^+e^-}$ to be compared with $\alpha_{\phi\to K^+K^-}$ (see text). (d) The differences between $\alpha_{\phi\to K^+K^-}$ and $\alpha_{\phi\to e^+e^-}$ in the kaon acceptance window. The average value and error are also plotted as a hatched band.

References

1) D. Lissauer and E. V. Shuryak: Phys. Lett. **B253**, 15 (1991); P.-Z. Bi and J. Rafelski: Phys. Lett. **B262**, 485 (1991); J. P. Blaizot and R. Mendez Galain: Phys. Lett. **B271**, 32 (1991).
2) M. Sekimoto et al.: Nucl. Instrum. and Meth. **A516**, 390 (2004).

† Condensed from the article in Phys.Rev.Lett.**9**8,152302(2007).

*1 Department of Physics, Kyoto University

Proposed spectrometer for electron pair measurement at J-PARC 50-GeV PS

S. Yokkaichi and K. Ozawa [1]

We proposed to perform a next-generation experiment to explore the chiral symmetry restoration in nuclear matter. The experiment is the successor of the KEK-PS E325 experiment[1], which has been successfully completed recently. We intend to measure electron pairs from the decay of low-mass vector mesons (/ω/) in nuclear matter at the J-PARC[2] 50-GeV proton synchrotron (PS) in use of a newly constructed spectrometer. Our proposal[3] was granted a physics approval in March 2007.

The goal of the proposed experiment is to collect 1∼2 ×10^5 mesons in 30 days of operation with comparable (or improved) mass resolution to that achieved by the E325 (∼ 11 MeV/c^2). The statistics is ∼100 times as high as that of E325. Such data enable us to discuss whether the origin of the observed spectral modification is the chiral symmetry restoration or not, by quantitative comparison with many theoretical predictions.

To improve the statistics by a factor of 100, we use a larger production cross section of for a factor of two, which is brought by the higher incident energy, a larger acceptance spectrometer for a factor of five, and a beam intensity ten times as high as E325, i.e., 1 × 10^{10} pps, for a remained factor of ten.

To cover a larger acceptance and to cope with the higher interaction rate (10^7 Hz on target), we must use new technologies such as a tracker with a Gas Electron Multiplier (GEM) and a Hadron Blind Detector (HBD)[4] for electron identification. The schematic figure of the proposed spectrometer is shown in Fig. 1.

To achieve a 10 MeV/c^2 mass resolution, 200 m position resolution is required, thus a 0.7 mm pitch of strip readout is used for the GEM Tracker. The trackers are placed at radii of 200, 400, and 600 mm from the center of the spectrometer magnet.

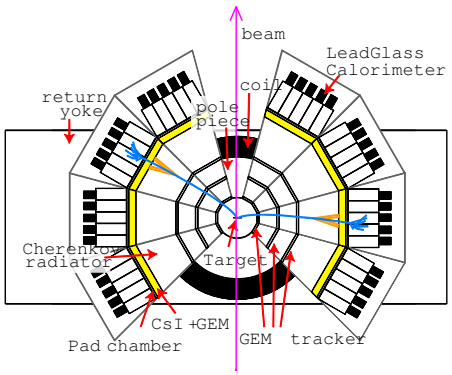

Fig. 1. Schematic plan view of proposed spectrometer.

The typical expected particle rate is 5 KHz/mm^2 for the forwardmost region in the innermost layer of the tracker, in other words, a point 12° apart from the beam horizontally and 200 mm apart from the center of the magnet where the target is located. Further, 1 KHz/mm^2 is expected even at a point of 60°/200 mm. These values are based on our E325 experience and the factor of ten is multiplied due to the proposed beam intensity. For the 4mm(W)×100mm(H) cell of a drift chamber, the operation is marginal at 60° (400 KHz) and impossible at 12° (2 MHz). For the GEM Tracker, the effective cell size is 0.7 mm(W)×100 mm(H) and the expected counting rate is 350 KHz at a point of 12°/200 mm; thus the tracker is operational.

HBD is a threshold type gas Čerenkov counter, which uses the CsI photocathode to convert Čerenkov photons to electrons and the stacked GEM foils for gas-amplification of electrons. The radiator gas, CF_4 (index=1.00062), is also used as the amplification gas, thus UV-transparent window to separate an amplification zone from the radiator is not required. The readout pads are hexagonal with a "diameter" of 32 mm, which corresponds to the size of the photon distribution area from the radiator 500 mm in length. Hit information is also readout from the last GEM foil of the stack and used to trigger electron pairs. The electrode of the last foil is divided in 100 × 100 mm^2 areas, corresponding to the size of the lead glass EM calorimeter located just behind the HBD. A coincidence of the HBD, EM calorimeter and the last layer of the GEM Tracker composes an electron candidate. Such fine segmentation of a trigger unit is essential for dropping accidental coincidences, which is expected as a main trigger background. Covering such a large acceptance with a small dead region and such fine segmentation cannot be achieved with the conventional segmented gas Čerenkov counter using a PMT readout.

For detector simulation for designing the new spectrometer, RIKEN-CCJ [5] is used.

References

1) M. Naruki *et al* , Phys. Rev. Lett. **96**, 092301 (2006), and in this report
R. Muto *et al* , Phys. Rev. Lett. **98**, 042501 (2007), and in this report
2) `http://j-parc.jp/`
3) `http://j-parc.jp/NuclPart/Proposal_0606_e.html`
4) A. Frankel *et al* , Nucl. Instr. Meth. **A546**, 466 (2005).
5) S. Kametani *et al* , in this report.

[1] University of Tokyo

Search for Θ^+ via $K^+p \to \pi^+X$ reaction at KEK-PS E559†

K. Miwa*1 from the E559 collaboration

Since the first report giving evidence on the existence of an exotic baryon Θ^+ by the LEPS collaboration[1], many studies from both theoretical and experimental aspects have been conduced. Recently, however, null results have been reported from several high-energy experiments, and some of the initial positive evidence was denied by the same collaboration with higher statistics[2]. Therefore, the situation for the existence of Θ^+ is controversial. On the other hand, the LEPS and DIANA collaborations have shown new evidence supporting its existence[3][4]. Therefore, confirmation of the existence (or nonexistence) of Θ^+ is urgent and important.

We have performed an experiment to search for Θ^+ via the $K^+p \to \pi^+X$ reaction at the K6 beam line with high missing-mass resolution using the SKS spectrometer at the KEK 12 GeV proton synchrotron. The experimental periods were about one month from June 2005 (1st run) and two weeks from December 2005 (2nd run). A 125-mm-long liquid hydrogen target was used. We used a K^+ beam of 1.2 GeV/c. The typical intensity was 14k counts during the 2 seconds of spill. The momentum of each beam particle was analyzed using the K6 beam line spectrometer, of which the resolution is expected to be $\Delta p/p = 0.047\%$ (FWHM). Scattered particles were detected using the SKS spectrometer, which covered a forward angle between 0 to 20 degrees, and the acceptance in the laboratory frame was 0.11 sr. The analysis was performed using RIKEN-CCJ. Since the missing-mass peak of Σ^+ is clearly reconstructed with the expected resolution using the $\pi^+p \to K^+\Sigma^+$ reaction taken for the calibration, a missing-mass resolution of 2.4 MeV/c^2 (FWHM) is expected for Θ^+.

The main background of the measurement is the 3-body decay of K^+, such as $K^+ \to \pi^+\pi^+\pi^-$ or $K^+ \to \pi^+\pi^0\pi^0$. The rejection of the decay background is essential for Θ^+ search. To separate hadronic reactions such as Δ production from these decay events, we installed a large acceptance chamber and a range counter behind the target. The suppression factor for the decay events by analysis using these detectors is obtained to be about 98% from a Monte Carlo simulation. The efficiency of this analysis for signal events is obtained to be about 70%, when we assume that Θ^+ is produced isotropically in the center of mass system. The vertex distribution after the rejection of decay events is shown in Fig. 1 with the distribution of the empty-target data (hatched histogram) for the 1st run. The 125 mm liquid hydrogen image is clearly observed. We selected a vertex region of the LH_2 target in order to select $K^+p \to \pi^+X$ events and obtained approximately 17,000 and 12,000 reaction events in the 1st and 2nd runs, respectively.

Figure 2 shows the missing-mass spectrum of the $K^+p \to \pi^+X$ reaction, which is the sum of data in the 1st and 2nd runs. The hatched peak is the expected spectrum assuming that Θ^+ is produced isotropically in the center of mass system and the total cross section of the $K^+p \to \pi^+\Theta^+$ reaction is 50 μb. We could not observe any significant peak structure in the spectrum. Therefore, we derived the upper limit of the cross section (averaged over 0 to 20 degrees in the laboratory frame) to be a very preliminary value of 1.9 μb/sr. This limit is much smaller than the theoretical calculation, which predicts more than 30 μb/sr for this production channel by taking the K^{0*} exchange into account[5].

References

1) T. Nakano *et al.*, Phys. Rev. Lett. **91**, 012002 (2003).
2) K. H. Hicks, Prog. Part. Nucl. Phys. **55**, 647 (2005).
3) N. Muramatu *et al.*, presentation at JPS meeting (2006).
4) V. V. Barmin *et al.*, hep-ex/0603017.
5) Y. Oh *et al.*, Phys. Rev. D **69**, 074016 (2004).

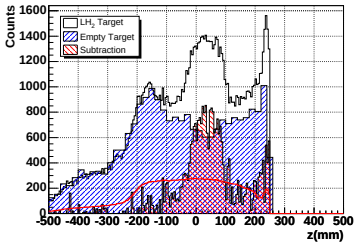

Fig. 1. Vertex distribution of $K^+p \to \pi^+X$ reaction.

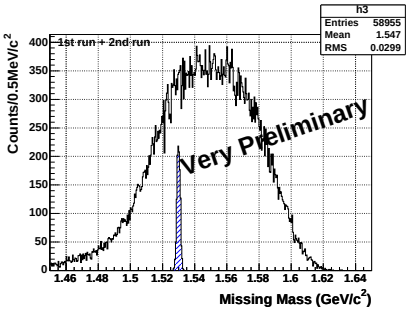

Fig. 2. Missing-mass spectrum of $K^+p \to \pi^+X$ reaction. The hatched spectrum shows the expected spectrum for Θ^+ (see text).

*1 Department of Physics, Tohoku University

Measurement of high-p_{T} Single Electrons from Heavy-Flavor Decays in $p+p$ Collisions at $\sqrt{s} = 200$ GeV

Y. Akiba, R. Averbeck,[*1] A. Dion,[*1] F. Kajihara,[*2] H. Themann[*1] for the PHENIX collaboration

Heavy-flavor (charm and bottom) production serves as a testing ground of QCD. Because of the large quark mass, it is expected that next-to-leading order perturbative QCD (NLO pQCD) can describe the production cross section of charm and bottom at high energy, particularly at high p_{T}. Since heavy-flavor production at RHIC energies is dominated by gluon-gluon fusion, its production in polarized p+p collisions probes the gluon distribution $G(x)$ and the gluon polarization $\Delta G(x)$. Furthermore measurements of heavy-flavor production in $p+p$ collisions provide a baseline for studying hot and dense matter effects in heavy ion reactions.

We have measured the momentum distribution of electrons from decays of heavy flavor (charm and bottom) for midrapidity $|y| < 0.35$ in $p+p$ collisions at $\sqrt{s} = 200$ GeV over the transverse momentum range $0.3 < p_{\mathrm{T}} < 9$ GeV/c[1]. The data were collected by the PHENIX detector during the 2005 RHIC run using the two central arm spectrometers. Each spectrometer covers $|\eta| < 0.35$ in pseudo-rapidity and $\Delta\phi = \pi/2$ in azimuth. It includes a drift chamber (DC) and pad chambers (PC1) for charged particle tracking, a Ring Imaging Čerenkov detector (RICH) for electron identification, and an electromagnetic calorimeter (EMCal) for electron identification and trigger. Two independent methods, the cocktail method and the converter subtraction method, have been used to determine the heavy flavor yields.

In Fig. 1, filled circles (squares) show the ratio of non-photonic electrons relative to photonic background determined by the converter (cocktail) method. The non-photonic electrons are dominantly heavy-flavor decay signals. The two methods are consistent with each other.

Figure 2 (a) shows the invariant differential cross section of electrons from heavy-flavor decays. The data from the two analysis methods are combined. The data are compared with a fixed-order-plus-next-to-leading-log (FONLL) pQCD calculation[2]. The top curve in Fig. 2 (a) shows the central values of the FONLL calculation. The contributions of charm and bottom are also shown. In Fig. 2 (b), the ratio of the data to the FONLL calculation is shown. The ratio is nearly p_{T} independent over the entire p_{T} range. Fitting to a constant for $0.3 < p_{\mathrm{T}} < 9.0$ GeV/c yields a ratio of $1.71 \pm 0.02^{\mathrm{stat}} \pm 0.18^{\mathrm{sys}}$. The total charm production cross section at this energy has also been deduced to be $\sigma_{c\bar{c}} = 567 \pm 57^{\mathrm{stat}} \pm 193^{\mathrm{sys}}$ μb.

*1 StonyBrook University, USA
*2 University of Tokyo

References

1) A. Adare et al.: Phys. Rev. Lett. 97, 252002 (2006).
2) M. Cacciari et al.: Phys. Rev. Lett. 95, 122001 (2005).

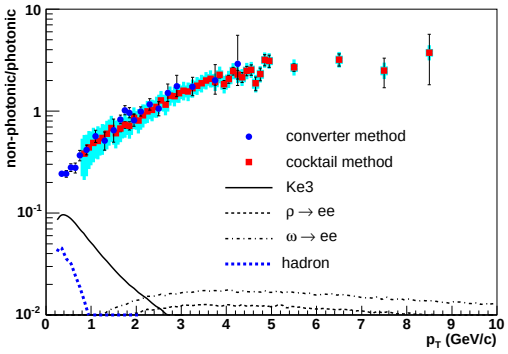

Fig. 1. Ratio of non-photonic electrons to photonic background. Error bars are statistical errors and the error bands show the cocktail systematic errors. The curves in the plot show the remaining non-photonic background.

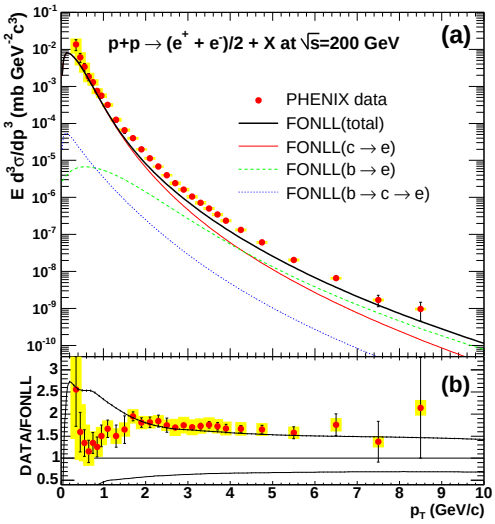

Fig. 2. (a) Invariant differential cross sections of electrons from heavy-flavor decays. The error bars (bands) represent the statistical (systematic) errors. The curves are the FONLL calculations (see text). (b) Ratio of the data and the FONLL calculation. The upper (lower) curve shows the theoretical upper (lower) limit of the FONLL calculation. In both panels a 10% normalization uncertainty is not shown.

Heavy Quark Measurement by Single Electrons in Au+Au Collisions†

F. Kajihara,[*1] Y. Akiba, R. Averbeck,[*2] A. Dion,[*2] H. Hamagaki,[*1] K. Ozawa,[*1] and S. Sakai,[*3]
for the PHENIX Collaboration

[PHENIX, RHIC, QGP, QCD, Heavy quark, Single electron, Jet quenching]

Strong suppressions of π^0 and other light hadrons at high transverse momentum ($p_{\rm T}$) have been observed in high energy heavy ion collisions at RHIC.[1–3] The suppressions are due to significant energy loss of partons through an extremely dense matter, not conventional hadronic matter. Further insight into properties of the produced medium can be gained from the production and propagation of particles carrying heavy quarks (charm and bottom). A fixed-order-plus-next-to-leading-log (FONLL) pQCD calculation describes the cross sections of heavy-flavor decay electrons in p + p collisions at $\sqrt{s}$ = 200 GeV within theoretical uncertainties.[4,5] In heavy ion collisions, the total yield of heavy-flavor decay electrons was found to scale with the number of nucleon-nucleon collisions.[6] Energy loss via gluon radiation is expected to be reduced for quarks with larger mass due to suppression of forward radiation, thus increasing the expected thermalization time.[7] Consequently, a decrease of high $p_{\rm T}$ suppression is expected from light to charm to bottom quarks, with the absolute values and their $p_{\rm T}$ dependence being sensitive to the properties of the medium.

The PHENIX experiment took high statistic data at $\sqrt{s_{\rm NN}}$ = 200 GeV in Run-4 Au + Au collisions (2004). Electrons (e^+/e^-) in $0.3 < p_{\rm T}^e < 9.0$ GeV/c were detected by two PHENIX central arms, each covering azimuthal angle $\Delta\phi = \pi/2$ and pseudo-rapidity $|\Delta\eta| < 0.35$.[8] All measured electrons can be categorized into two groups: *photonic* or *non-photonic*. Photonic electrons mainly come from Dalitz decays of mesons (π^0, η, etc.) and photon conversions, while signal electrons from open charm/bottom decays are dominant sources of non-photonic electrons. Two methods, *cocktail* and *converter* methods were applied to extract non-photonic electrons.[5,6]. The both methods give the consistent result. Backgrounds in the non-photonic electrons come from mainly weak decays of Kaon (K_{e3}), vector meson decays and Drell-Yan processes. Kaon contributes < 10 % at $p_{\rm T}^e$ = 0.5 GeV/c compared to photonic electron yields, while vector mesons are very small, and Drell-Yan process is negligible in our measurable $p_{\rm T}^e$ range. Since Kaon and vector mesons have been already measured by the PHENIX, backgrounds from those sources can be evaluated with simulations and subtracted from non-photonic electrons.

Invariant differential yields of heavy-flavor decay electrons have been calculated in Au + Au collisions.† To quantify the suppression, the nuclear modification factor, $R_{\rm AA}(p_{\rm T}^e)$ is shown in Fig. 1.

$$R_{\rm AA}(p_{\rm T}^e) = \frac{dN_e^{\rm AA}/dp_{\rm T}^e}{T_{\rm AA}\cdot d\sigma_e^{pp}/dp_{\rm T}^e} = \frac{dN_e^{\rm AA}/p_{\rm T}^e}{N_{\rm col}\cdot dN_e^{pp}/dp_{\rm T}^e}. \quad (1)$$

Here, $T_{\rm AA}$ is the nuclear thickness function for Au + Au . $N_{\rm col} = T_{\rm AA}\cdot\sigma_{\rm in}^{pp}$. $\sigma_{\rm in}^{pp}$ is the inelastic scattering cross section of p + p . Very strong suppression is clearly seen at high-$p_{\rm T}$ in central collisions, comparable to the suppression observed for π^0 and η[1,3].

In conclusion, we have measured electrons from semileptonic decays of heavy quarks in RHIC Run-4 Au + Au at $\sqrt{s_{NN}}$ = 200 GeV. $R_{\rm AA}$ shows a very strong suppressive effect. The result suggests that even heavy quarks lose their energy in high dense medium. To understand it systematically, we need to separate the contributions from charm or bottom in the future experiment. The mass difference will provide us the more information of the energy-loss mechanism in the high dense matter.

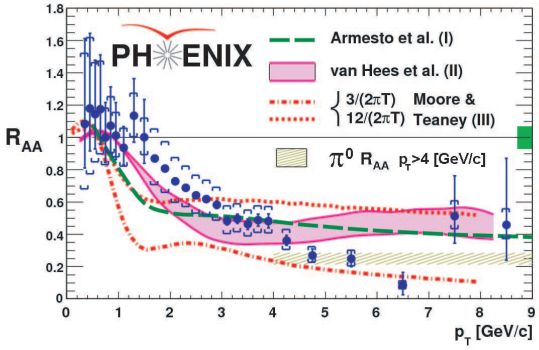

Fig. 1. $R_{AA}(p_{\rm T}^e)$ of heavy-flavor electrons in 0-10 % central collisions compared with π^0 data and model calculations (curve I[9], II[10], and III[11]). The box at $R_{AA} = 1$ shows the uncertainty in T_{AA}.

References
1) S. S. Adler *et al.*, Phys. Rev. Lett. **91**, 072301, (2003).
2) J. Adams *et al.*, Phys. Rev. Lett. **91**, 172302, (2003).
3) S. S. Adler *et al.*, Phys. Rev. Lett. **96**, 202301, (2006).
4) M. Cacciari *et al.*, Phys. Rev. Lett. **95**, 122001, (2005).
5) A. Adare *et al.*, Phys. Rev. Lett. **97**, 252002, (2006).
6) S. S. Adler *et al.*, Phys. Rev. Lett. **95**, 082301, (2005).
7) Y. L. Dokshitzer, D. E. Kharzeev, Phys. Lett. **B519**, 199, (2001).
8) K. Adcox *et al.*, Nucl. Instrum. Methods. A **499**, 460, (2003).
9) N. Armesto *et al.*, Phys. Lett. **B637**, 362 (2006)
10) H. van Hees, V. Greco, R. Rapp, Phys. Rev. **C73**, 034913 (2006)
11) G. D. Moore, D. Teaney, Phys. Rev. **C71**, 064904 (2005).

† Condensed from Phys. Rev. Lett. 98, 172301 (2007).

*1 The University of Tokyo
*2 Stony Brook University, NY, USA
*3 University of Tsukuba

$J/\psi \to e^+e^-$ Measurements in Au+Au Collisions at $\sqrt{s_{NN}} = 200$ GeV by RHIC-PHENIX†

T. Gunji,[*1] H. Hamagaki,[*1] K. Ozawa,[*2] C. D. Silva,[*3] Y. Akiba, and X. Wei[*4]

[J/ψ, Heavy Ion Collisions, Quark-Gluon-Plasma]

Heavy quarknoia (J/ψ, ψ', χ_c and Υ) has been long considered as one of the most promising probes for studying the formation of Quark-Gluon-Plasma (QGP), where the quarks and gluons are deconfined, and its properties. In deconfined matter, the yield of heavy quarkonia is predicted to be suppressed due to the dymanical color screening effect[1]. The dissociation temperature depends on the binding energy of quarkonia and is extracted to be $\sim 2\ T_c$ for J/ψ and $\sim 1.1\ T_c$ for $\psi\prime$ and χ_c by quenched lattice QCD calculations[2]. Although the primordial J/ψ is expected to be dissolved in QGP due to the dynamical color screening effect, J/ψ yield is expected to be enhanced due to the recombination of uncorrelated $c\bar{c}$ pairs at the later stage of collisions at the RHIC energy, where the abundant $c\bar{c}$ quarks are created[3]. Initial state effects (Cold Nuclear Matter effects, CNM) such as gluon shadowing, absorption of J/ψ in a nuclear environment or Color Glass Condensate (CGC) formation would modify the J/ψ yield. Therefore, it is very important to study J/ψ production as a function of colision centralities, rapidity, transverse momentum p_T and collision species. PHENIX[4] measured J/ψ yield in $p+p$, d+Au, Au+Au and Cu+Cu collisions to extract the CNM and medium effects on J/ψ production. The nuclear modification factor R_{AA} is a variable widely used for quantifying the medium effects in A+A collisions. The R_{AA} of J/ψ is the ratio of the J/ψ yield in Au+Au collisions to that in $p+p$ collisions scaled by the average number of binary nucleon-nucleon collisions N_{col}. The R_{AA} of J/ψ is expected to be 1 in the absence of medium effects and the production of J/ψ is suppressed due to the medium effects in A+A collisions if R_{AA} is less than 1.

Au+Au collisions at $\sqrt{s_{NN}} = 200$ GeV were performed at RHIC in 2004. During the period, PHENIX recorded an integrated luminosity of $\sim 240\ \mu\text{b}^{-1}$. After the quality assurance of the data, an integrated luminosity of $\sim 160\ \mu\text{b}^{-1}$ was used in the analysis. J/ψ is reconstructed via the e^+e^- decay mode and the number of J/ψ reconstructed is ~ 1000.
The formula of the J/ψ invariant yield is

$$B\frac{dN}{dy} = \frac{N_{J/\psi}}{N_{evt}}\frac{1}{\Delta y \epsilon_{acc}\epsilon_{embed}}, \quad (1)$$

where B is the branching ratio of the e^+e^- decay mode (5.93% from PDG[5]), $N_{J/\psi}$ and N_{evt} stand for the number of J/ψ counts and the number of analyzed event, respectively. Δy in Eq. (1) is the rapidity coverage. The correction factor ϵ_{acc} is the acceptance for e^-e^+ pairs from J/ψ, where the detection efficiency of e^+e^- pairs and the run-by-run fluctuation of the detector acceptance are taken into account. The correction factor ϵ_{embed} is the embedding efficiency, which has a centrality dependence.

Figure 1 shows the R_{AA} of J/ψ as a function of the number of participants in Au+Au at $\sqrt{s_{NN}} = 200$ GeV. The bar and bracket correspond to the uncorrelated error and correlated error, respectively. The box is the systematic error of N_{col}. The band represents the global systematic errors due to the uncertainty of the J/ψ yield in $p+p$ collisions. From Fig. 1, the suppression of J/ψ by a factor of 3 was observed for most central collisions. This result will be

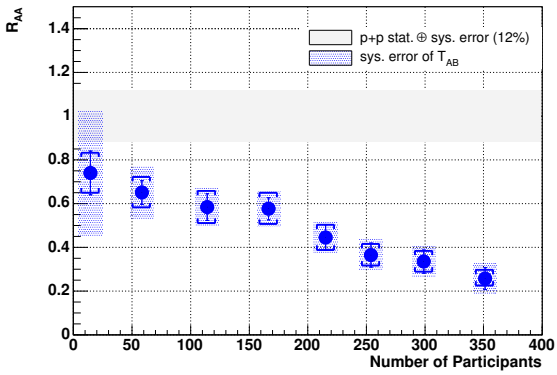

Fig. 1. R_{AA} as function of number of participants in Au+Au collisions

useful for discriminating the theoretical predictions of J/ψ production in A+A collisions and comparison to the theoretical models is on going.

References

1) T. Matsui and H. Satz; Phys. Lett. **B 178**, 416, (1986).
2) M. Asakawa and T. Hatsuda; Phys. Rev. Lett. **92**, 012001, (2004).
3) L. Grandchamp *et al.*; Phys. Rev. Lett. **92** 212301, (2004).
4) K. Adcox, *et al.*; (PHENIX Collaboration), Nucl. Instr. and Meth. **A 499** 469, (2003).
5) K. Hagiwara *et al.*; Phys. Rev. **D 66**, 010001, (2002).

† Condensed from the article in nucl-th/0611020, submitted to Phys. Rev. Lett.

*1 Center for Nuclear Study, University of Tokyo
*2 Department of Physics, University of Tokyo
*3 Universidade de São Paulo, Instituto de Física, Brazil
*4 RBRC, Brookhaven National Labratory

PHENIX measurements on J/ψ production in $\sqrt{s} = 200$ GeV p+p collisions†

W. Xie* for the PHENIX collaboration

Keywords: J/ψ, rapidity, QCD, proton.

PACS: 25.75.Dw

The J/ψ production involves the production of ccbar pairs that can be well described by perturbative QCD (pQCD) due to its large mass and the formation of J/ψ from ccbar pairs that belong to the non-perturbative QCD regime and therefore provides crucial information to understand QCD. Experimental data including the results from lower energy fixed target experiment and especially those from the high energy collider experiments [1] have stimulated intensive theoretical interests. However, many unsolved discrepancies between data and theoretical predictions require high quality experimental results at different collision energies. The results from RHIC with high luminosity would provide crucial constraints to different models.

A detailed description of the PHENIX experiment is provided in [2]. The central arm detectors are used to detect J/ψ–>e^+e^- decays at midrapidity (|y|<0.35). The muon detectors are used to measure J/ψ ->$\mu^+\mu^-$ at forward (1.2 < y < 2.2) and backward rapidity (-2.2 < y < -1.2). The data in the year 2005 p+p run corresponds to 2.6 pb^{-1} at midrapidity, 2.7 pb^{-1} and 3.5 pb^{-1} in the forward and backward rapidity, respectively. Totally ~1500 J/ψ–>e^+e^- and ~8000 J/ψ–> $\mu^+\mu^-$were reconstructed.

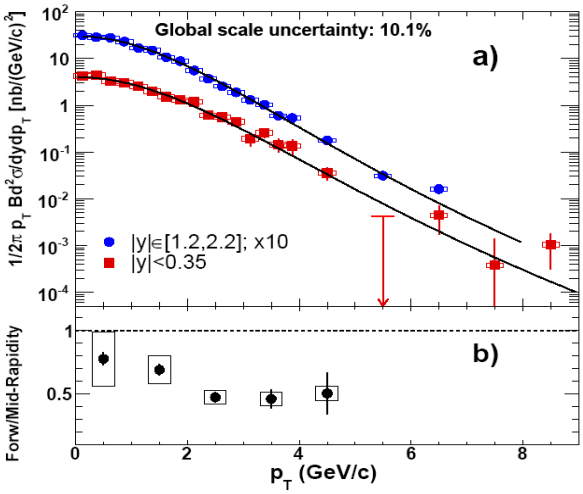

Fig.1. (a) The mid and forward rapidity J/ψ differential cross section times di-lepton branching ratio versus p_T and (b) the ratio of the mid and forward p_T spectra.

Fig1.a shows the transverse momentum spectra at both mid and forward rapidity. $\langle p_T^2 \rangle$ are extracted via fitting the data with the function, $A\,(1 + (p_T/B)^2)^6$. At mid-rapidity $\langle p_T^2 \rangle = 4.14 \pm 0.18(stat)^{+0.30}_{-0.20}(sys)$ $(\mathrm{GeV/c})^2$. At forward rapidity $\langle p_T^2 \rangle$ = 3.59±0.06(stat)±0.16(sys) $(\mathrm{GeV/c})^2$. The ratio of the invariant cross section at forward and mid-rapidity is shown in Fig. 1b. The data indicates that the forward rapidity pT distribution is substantially softer than mid-rapidity.

Fig.2 shows the J/ψ differential cross section vs. rapidity. The total cross section is determined to be $B_{ll} \cdot \sigma_{pp}^{J/\psi} = 178 \pm 3 \pm 53 \pm 18$ nb via fitting the rapidity

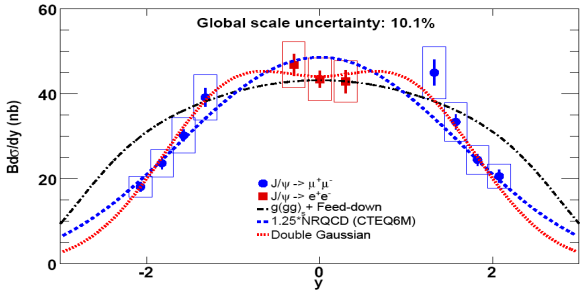

Fig.2. J/ψ rapidity distribution

distribution with many theoretical shapes. An empirical double Gaussian fit (dot-dot curve) that can reproduce the data best is used as the central value of the total cross section. The first error is statistical, the second systematic and the third is from the uncertainty in the minimum-bias trigger cross section. The systematic error is estimated from the maximum variation observed when shifting the mid-rapidity and forward rapidity measurements independently by their point-to-point correlated systematic errors. Theoretical calculations including a NRQCD calculation (dashed curve) [3] and a pQCD calculation (dot-dashed curve) [4] failed to describe the data

In summary, new J/ψ results for p + p collisions at $\sqrt{s} = 200$ GeV are presented that extend the reach in transverse momentum to 9 GeV/c. The rapidity distribution can not be reproduced by the pQCD and NRQCD calculations in [3,4]. These data not only constrain production models for heavy quarkonia, but also provide a critical baseline for similar studies in deuteron-nucleus and heavy-ion collisions.

References

1) F. Abe et al., Phys. Rev. Lett. 79, 572 (1997);
S. S. Adler et al., Phys.Rev.Lett. 92 (2004) 051802
2) K. Adcox et al., Nucl. Instr. Meth. A499, 469 (2003).
3) F. Cooper et al., Phys. Rev. Lett. 93, 171801 (2004);
and private communication.
4). V. A. Khoze et al. , Eur. Phys. J. C39, 163-171 (2005)

† Condensed from the article at hep-ex/0611020.

* Riken-BNL research center, Brookhaven National Lab

Measurement of High-p_{T} Direct Photons in $\sqrt{s_{\mathrm{NN}}} = 200$ GeV Au+Au Collisions at RHIC-PHENIX

T. Isobe,[*1] H. Hamagaki,[*1] T. Sakaguchi,[*2] G. David,[*2] and B. Sahlmueller[*3] in collaboration with PHENIX

[Relativistic Heavy-Ion Collision, Quark-Gluon Plasma, Direct Photon]

The PHENIX experiment[1] has been carried out at RHIC to search for evidence of the phase transition from normal nuclear matter to quark-gluon plasma (QGP). QGP is a new phase of matter consisting of deconfined quarks and gluons.

Since photons do not interact strongly, direct photons are a powerful probe for studying the initial state of matter produced at RHIC. Direct photons in this report mean photons not originating from hadronic decays. They are emitted from all the states such as the initial state, the QGP, and the final hadron-gas state. In addition, it is predicted that the contribution of photons from jet-photon conversion in the dense medium to direct photon can be as large as the photon yield from hard scattering[2].

In the 2004 run, PHENIX recorded a high-quality Au+Au data set. The data set allows us to measure direct photons at up to 20 GeV/c as shown in Fig. 1. The amount of nuclear effect in Au+Au collisions is quantified by a nuclear modification factor (R_{AA}). R_{AA} is the ratio of the measured yield to the expected yield from the p+p result[3], and is defined as

$$R_{\mathrm{AA}}(p_{\mathrm{T}}) = \frac{d^2N_{\mathrm{AA}}/dp_{\mathrm{T}}d\eta}{T_{\mathrm{AA}}(b)d^2\sigma_{\mathrm{NN}}/dp_{\mathrm{T}}d\eta}, \qquad (1)$$

where the numerator is the invariant direct-photon yield in unit rapidity and the denominator is the expected yield from p+p collisions binary scaled by the number of underlying nucleon-nucleon collisions ($T_{\mathrm{AA}}(b)$) in Au+Au. $T_{\mathrm{AA}}(b)$ is defined as $T_{\mathrm{AA}}(b) = N_{\mathrm{coll}}(b)/\sigma_{\mathrm{NN}}$, where $N_{\mathrm{coll}}(b)$ is the average number of nucleon-nucleon collisions determined by the distance (b) between the two nucleons with an inelastic cross section σ_{NN}. Figure 2 shows the R_{AA} of the direct photon in $\sqrt{s_{\mathrm{NN}}} = 200$ GeV Au+Au central (0-10%) collisions. The R_{AA} is in good agreement with unity within the error. This suggests that the initial hard-scattering probability is not reduced by nuclear effect. The direct-photon R_{AA} seems to be below unity above 14 GeV/c. This tendency may indicate that the compensation of jet-quenching and additional photons by a nuclear effect breaks up above 14 GeV/c. Since the direct photons measured in a p+p system consist of the photons promptly produced directly from the hard scattering and the jet fragmentation photons from hard-scattered partons, the direct-photon yield measured in Au+Au collisions is expected to be suppressed by the jet-quenching effect. The agreement with scaled p+p direct-photon data might simply be a coincidence caused by mutually counterbalancing effects such as energy loss and jet-photon conversion.

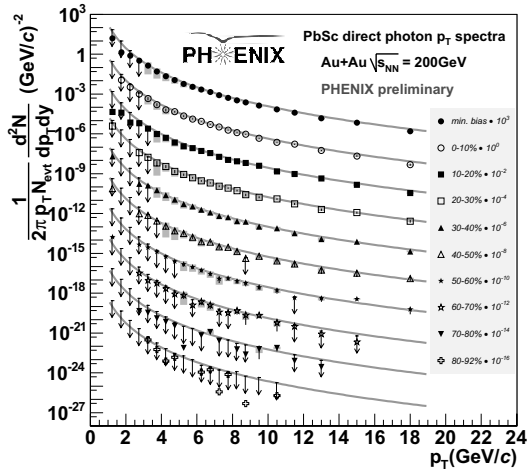

Fig. 1. p_{T} spectra of direct photons in $\sqrt{s_{\mathrm{NN}}} = 200$ GeV Au+Au central collisions. In addition to the statistical and p_{T}-uncorrelated errors, point-to-point varying systematic errors are shown on the data points as boxes. T_{AA}-scaled p+p direct-photon data are overlaid.

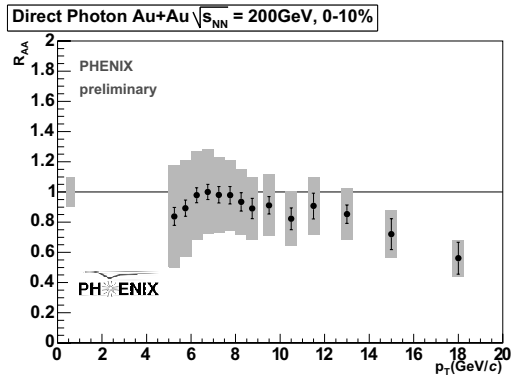

Fig. 2. Nuclear modification factor of direct photons in $\sqrt{s_{\mathrm{NN}}} = 200$ GeV Au+Au central (0-10%) collisions. The overall systematic error of T_{AA} normalization is shown at 1.

References

1) K. Adcox et al.: Nucl. Instrum. Methods Phys. Res. **A499**, 469 (2003).
2) S. Turbide et al.: Phys. Rev. **C72**, 014906 (2005).
3) K. Adcox et al.: hep-ex/0609031 (2006).

*1 Center for Nuclear Study, Graduate School of Science, University of Tokyo
*2 Brookhaven National Laboratory, USA
*3 University of Muenster, Germany

Elliptic flow of electrons from heavy flavor decay in $\sqrt{s_{NN}} = 200$ GeV Au+Au collisions at RHIC-PHENIX

S. Sakai,[*1] Y.Akiba, R. Averbeck,[*2] A. Dion,[*2], F. Kajihara,[*3] for the PHENIX collaboration

Charm quarks are believed to be produced in the initial stage of heavy ion collisions by gluon fusion and to propagate through the hot and dense medium created in the collisions. Therefore, charm quarks can be a good probe for studying the medium created in Au+Au collisions at RHIC. For the medium study, charm quark energy loss and flow measurements are useful analysis tools. A recent study of charm by electron measurement suggests the large energy loss of charm quarks in the medium created in the Au+Au collisions at $\sqrt{s_{NN}} = 200$ GeV[1].

The azimuthal anisotropy of particle emissions is a powerful tool for studying flow in ultra relativistic nuclear collisions. The azimuthal anisotropy is defined by

$$\frac{dN}{d\phi} = N_0 \left\{ 1 + \sum_n 2v_n \cos(n(\phi \quad \Psi_{R.P.})) \right\}, \qquad (1)$$

where N_0 is a normalization constant, ϕ is a azimuthal angle of the particle, and $\Psi_{R.P.}$ is the direction of the nuclear impact parameter ("reaction plane") in a given collision. One of the most significant discoveries at RHIC is that the v_2 of hadrons made of u, d, s quarks is large and consistent with a hydrodynamical model[2]. Furthermore, it was found that v_2 scales with the number of constituent quarks. This result suggests that the v_2 of hadrons made of u, d and s quarks develops in the partonic phase. If charm quarks flow similaery to light quarks, an unexpectedly strong interaction of charm with the medium is expected.

In the PHENIX experiment at RHIC, a charm quark has been studied by measuring electrons from their semileptonic decays[1]. An inclusive electron sample has two components: (1)"nonphotonic" - primarily semileptonic decays of mesons containing heavy (charm and bottom) quarks and (2)"photonic" - Dalitz decays of light neutral mesons (π_0, η, η', ω and ϕ) and photon conversions in a detector material. The azimuthal distribution of the inclusive electron ($dN^e/d\phi$) is given as the sum of the azimuthal distributions of photonic electrons ($dN^\gamma/d\phi$) and nonphotonic electrons ($dN^{non-\gamma}/d\phi$):

$$\frac{dN_e}{d\phi} = \frac{dN_e^\gamma}{d\phi} + \frac{dN_e^{non-\gamma}}{d\phi}. \qquad (2)$$

From Eq. 2, the nonphotonic electron v_2 ($v_2^{non-\gamma}$) is expressed as

$$v_{2_e}^{non-\gamma} = \frac{(1+R_{NP})v_{2_e} \quad v_{2_e}^\gamma}{R_{NP}}, \qquad (3)$$

where v_{2_e} is the inclusive electron v_2, $v_{2_e}^\gamma$ is the photonic electron v_2 and R_{NP} is the ratio of the number of nonphotonic electrons to that of photonic electrons ($N_e^{non-\gamma}/N_e^\gamma$). The photonic electron v_2 (v_2^γ) is calculated using a Monte Carlo generator that includes π^0, η, and direct photons. The measured $v_2(p_T)$ of $\pi^\pm$,π^0 and $K^\pm$ is used as input, assuming $v_2^{\pi^\pm} = v_2^{\pi^0}$, $v_2^\eta = v_2^{K^\pm}$, and $v_2(\text{direct}\gamma) = 0$.

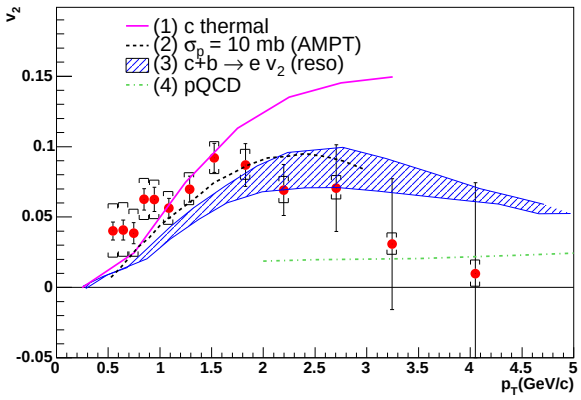

Fig. 1. Transverse momentum dependence of heavy-flavor electron v_2. The lines in the figure represent model calculations.

Figure 1 shows the transverse momentum dependence of the heavy-flavor electron v_2. A small background due to Ke3 decays is subtracted. The lines in the figure represent model calculations. The model (1) assumes charm quark thermalization and flow[3]. The model (2) is for AMPT model calculation assuming a large cross section (10 mb)[4] and (3) resonant D and B meson correlations in the sQGP[5]. The model (4) involves pQCD calculation (no interaction)[6]. The models (1), (2) and (3) well represent the measured v_2. Therefore, the result indicates that charm quarks are strongly coupled to the matter and flow.

*1 Univ. of Tsukuba
*2 Univ. of Stony Brook
*3 Univ. of Tokyo

References
1) PHENIX Collaboration, S. S. Adler *et al.*, Phys. Rev. Lett. *96*, 032301 (2006).
2) PHENIX Collaboration, S. S. Adler *et al.*, Phys. Rev. Lett. **91**, 182301 (2003).
3) V. Greco *et al.*, Phys. Lett. B **595** 202-208 (2004).
4) Bin Zhang *et al.*, Phys. Rev. C **72**, 024906 (2005).
5) H. van Hendric *et al.*, Phys. Rev. C **73**, 034913 (2006).
6) N. Armesto *et al.*, Phys. Lett. B **637**, 362 (2006).

Measurement of Double-Helicity Asymmetry in Multiparticle Production from Polarized Proton-Proton Collision at PHENIX

K. Nakano [1], Y. Akiba and Y. Goto

One of the goals of the PHENIX experiment is to obtain the polarized gluon distribution function in the proton, $\Delta g(x)$. $\Delta g(x)$ is evaluated by measuring the double-helicity asymmetry, $_{LL}$, of reactions in longitudinally polarized proton-proton collisions, for example, jet, ^{0} or direct photon production. A jet is measured as a cluster of multiple particles. The particle cluster measurement gives higher statistics at high transverse momentum (p_T) than single-particle measurements such as ^{0}. $_{LL}$ is defined as

$$_{LL} = \frac{1}{|P_B||P_Y|}\frac{N_{++} - RN_{+}}{N_{++} + RN_{+}}. \quad (1)$$

Here, N_{++} and N_{+} are the number of measured particle clusters with the same and opposite beam helicities, respectively; $R \equiv L_{++}/L_{+}$ is the relative luminosity; and P_B and P_Y are the beam polarizations of the colliding beams.

We used proton-proton collision data obtained in 2005 at $\sqrt{s} = 200$ GeV with an average beam polarization of ~46%. The integrated luminosity of the analyzed data is 2.2 pb ^{1}. The PHENIX Central Arm detector was used. Two arms are positioned almost back-to-back, and each arm covers a pseudorapidity region | | 0.35 and a 90 degree azimuthal angle. Photons with $p_T > 0.4$ GeV/c were measured using electromagnetic calorimeters, and charged particles with 0.4 p_T 4 GeV/c were measured using drift chambers and pad chambers. For each event, a high-p_T (> 2 GeV/c) photon was required to exist.

Particles that satisfied the experimental criteria were clustered by a cone method with a cone radius R of 0.3[1)]. The transverse momentum of the cone, $p_T^{\rm cone}$, was defined as the vector sum of p_T of particles the in cone; $p_T^{\rm cone} \equiv \left|\sum_{i\in{\rm cone}} \vec{p}_{Ti}\right|$. The relation between the measured $p_T^{\rm cone}$ and the original $p_T^{\rm jet}$ was evaluated using PYTHIA and GEANT simulations[1)].

The largest systematic uncertainty in this measurement results from the p_T scale difference between measurement and theory. This originates from the fact that a jet is defined with a cone at the hadron level in the measurement and at the parton level in the theory. In $_{LL}$ measurement, we assigned 10% to the p_T scale uncertainty, by which the p_T scale in the theory varies when a theoretical cone size is changed in a typical range. We can check the p_T scale uncertainty by measuring cross sections because the difference in the p_T scale appears as a shift of cross-section curve. Figure 1 shows the yield per luminosity of the particle cluster as a function of $p_T^{\rm cone}$. The experimental data is drawn as red points with systematic errors as a gray band. The predicted values are drawn as three solid or dashed lines, which are based on the NLO jet cross section and the $p_T^{\rm jet}$-$p_T^{\rm cone}$ relation. The band around the solid line shows the deviation range of the solid line caused by a ±10% p_T scale variation. The experimental data and the predicted value are within the range.

Figure 2 shows the $_{LL}$ of particle cluster production as a function of $p_T^{\rm cone}$. The predicted $_{LL}$'s are drawn as solid lines, which are based on the NLO jet $_{LL}$, the three $\Delta g(x)$ models[3)] and the ratio of $p_T^{\rm cone}$ to $p_T^{\rm jet}$. The bands around the solid lines show the 10% p_T scale uncertainty. This result excluded the "GRSV-max" case. A stronger constraint on $\Delta g(x)$ will be imposed by further statistics.

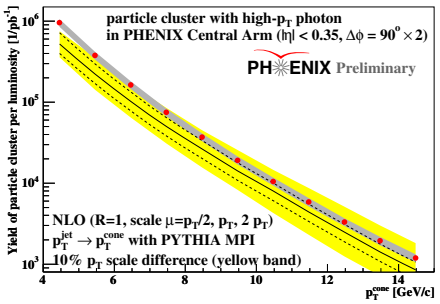

Fig. 1. Yield per luminosity of particle clusters.

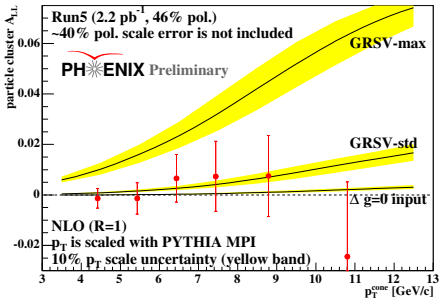

Fig. 2. Particle cluster A_{LL}.

[1] Department of Physics, Tokyo Institute of Technology

References

1) K. Nakano *et al.*; RIKEN Accel. Prog. Rep. **39**, 183 (2006).
2) R. Field [CDF Collaboration], Acta Phys. Pol. B **36**, 167 (2005).
3) M. Gluck, E. Reya, M. Stratmann, and W. Vogelsang, Phys. Rev. D **63**, 094005 (2001).

Direct photon production in $p+p$ at $\sqrt{s}=200$ GeV, and its double spin asymmetry measurement

K. Okada, R. Bennett,[*1] and T. Horaguchi,[*2]

As regards the RHIC-PHENIX spin program, direct photon production is believed to be a golden channel for accessing the gluon polarization in proton. Using Run3(2003) data set ($\mathcal{L}=0.24\text{pb}^{-1}$), we improved the precision of measurement of direct photon cross section [1]. The analysis starts from the inclusive photon in the PHENIX detector[2], and backgrounds, mainly π^0 decay photons, are subtracted statistically. Figure 1 shows the spectra overlaied with a Next-to-Leading-Order (NLO) calculation. The result is described well by the theoretical calculation.

The double spin asymmetry, defined by the difference in production ratio between parallel and antiparallel helicities of the colliding bunches of protons divided by the sum of them, is sensitive to gluon spin polarization. The statistical background subtraction for each helicity state does not provide the highest precision. Instead, we subtract the background asymmetry afterward[3]. The asymmetry of the signal (A^{sig}) is calculated from the asymmetry of all photons (A^{raw}) and the asymmetry of background (A^{BG}) by $A^{sig}=\frac{A^{raw}-rA^{BG}}{1-r}, \sigma_{A^{sig}}=\frac{\sqrt{\sigma^2_{A^{raw}}+r^2\sigma^2_{A^{BG}}}}{1-r}$, where r is related to the purity defined by the ratio of BG to raw, and $\sigma_{A^{sig}}$ is the statistical uncertainty.

To obtain a purer sample (=lower r), we applied an isolation cut on a photon sample, because direct photons are expected not to come with other jet activities. We also determined that 80 $\sim$ 90% of direct photons satisfy the isolation cut for the region of p_T higher than 7 GeV/c[1].

It should be reasonable to measure the asymmetry of background (A^{BG}) using photons associated with π^0's decay partner. On the basis of real Run5(2005) data ($\mathcal{L}=2.5\text{pb}^{-1}$), assuming the statistical uncertainty to be the root mean square of the yield, the size of $\sigma_{A^{sig}}$ was obtained and shown in Fig. 2. The bin size is large at p_T higher than 10GeV/c. An advantage of the isolation cut can be noted in the figure. In the case without the isolation cut, $\sigma_{A^{sig}}$ is underestimated, because the combinatorial background contamination in the π^0 tagging process is not taken into account.

In summary, we proved that the theoretical baseline is applicable to direct photon production at $\sqrt{s}=200$ GeV $p+p$ collisions by the cross section measurement. For spin asymmetry measurement, the precision was evaluated. The isolation cut improves the measurement. The values shown in Fig. 2 are scaled by luminosity ($1/\sqrt{\mathcal{L}}$) and beam polarization ($1/P^2$).

The machine performance is improving each year in both luminosity and polarization. We have collected $\mathcal{L}=7.5\text{pb}^{-1}$ with longitudinal polarization at $P=62\%$ in Run6(2006). In the next 3 years, we plan to accumulate $\mathcal{L}=65\text{pb}^{-1}$. By then, the experimental uncertainty of this channel will be comparable to our current knowledge of gluon polarization.

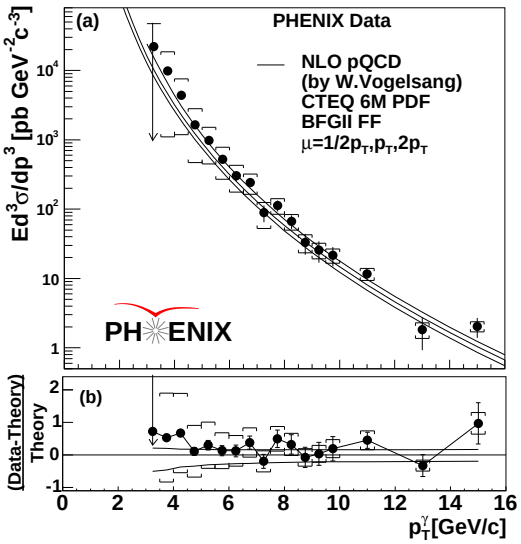

Fig. 1. Direct photon spectra overlaied with NLO pQCD calculation

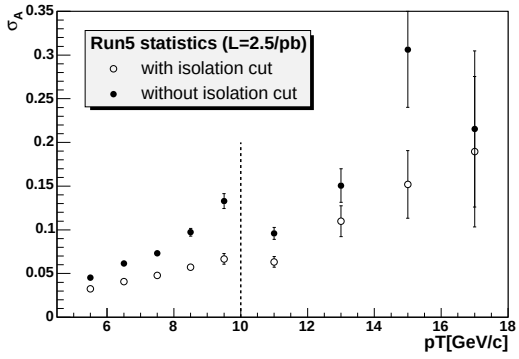

Fig. 2. σ_A estimation using Run5pp statistics.

*1 SUNY, USA
*2 Hiroshima University, Japan

References

1) S. S. Adler et al.: Phys. Rev. Lett. **98**, 012002 (2007)
2) K.Adcox et al.: Nucl. Inst. Meth. A**499**, 469 (2003).
3) S. S. Adler et al.: Phys. Rev. Lett. **93**, 202002 (2004)

Measurement of the mid-rapidity double helicity asymmetry of η mesons in p+p collisions at $\sqrt{s} = 200$GeV

F. Ellinghaus*1 and J. Seele*1 for the PHENIX Collaboration

Measurements of double helicity asymmetries for inclusive hadron production in polarized proton-proton collisions are sensitive to spin–dependent parton distribution functions (PDFs), in particular to the gluon distribution, Δg. First results from the PHENIX collaboration at the Relativistic Heavy Ion Collider (RHIC) are available for inclusive π^0 production[1]. The double helicity asymmetry A_{LL} is given as

$$A_{LL} = \frac{\sigma^{++} - \sigma^{+-}}{\sigma^{++} + \sigma^{+-}} = \frac{\Delta\sigma}{\sigma}$$

where the cross section σ^{++} (σ^{+-}) describes the reaction where both protons have the same (opposite) helicity. The spin–dependent term $\Delta\sigma$ is a convolution of the spin–dependent PDFs for quarks (u,d,s) and gluons, of the spin–dependent hard scattering cross sections calculable in perturbative QCD, and of the fragmentation functions (FFs). It is apparent that the extraction of the spin–dependent PDFs from data on inclusive hadron production critically depends on the knowledge of the FFs. Therefore it is desirable to extract the spin–dependent PDFs using different channels, not only because of possibly different systematic uncertainties involved in the A_{LL} measurement, but also because of the different FFs involved. An effort is under way to extract the presently unknown η FFs, mainly based on cross–section measurements from e^+/e^- collider data.

This study focuses on A_{LL} in η production ($\vec{p}+\vec{p} \rightarrow \eta + X$), where the η subsequently decays into two photons with a branching ratio of about 40%. The data was taken with the PHENIX spectrometer in 2005. The position and energy of the photons are reconstucted using the electromagnetic calorimeter. The invariant mass is then calculated from all possible photon pairs and is shown in Fig. 1. Besides the prominent π^0 peak between about 0.1 and 0.2 GeV/c^2, the η peak (grey region) can also be clearly seen.

Experimentally, the double helicity asymmetry is defined as

$$A_{LL} = \frac{1}{|P_B||P_Y|}\frac{N_{++} - RN_{+-}}{N_{++} + RN_{+-}}, \quad \text{with} \quad R \equiv \frac{L_{++}}{L_{+-}},$$

where N_{++} (N_{+-}) is the experimental yield for the case where the beams have the same (opposite) helicitiy. The achieved uncertainty on the relative luminosity R is on the order of 10^{-4}. The polarizations of the two colliding beams at RHIC are denoted by P_B and P_Y. The preliminary average polarization value

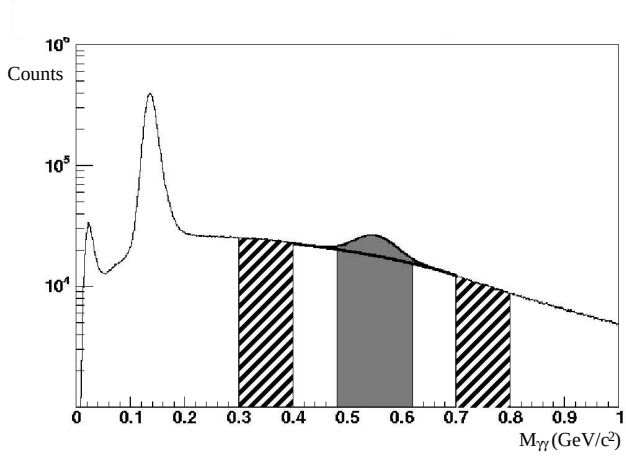

Fig. 1. Two photon invariant mass for $p_T > 2$ GeV/c.

for the data from 2005 is 47% with an uncertainty of 20% per beam, leading to a 40% scale uncertainty in the preliminary A_{LL} result.

Calculating the asymmetry $A_{LL}^{\eta+BG}$ in the grey region (see Fig. 1), consisting of signal and background, and the asymmetry A_{LL}^{BG} in regions with only background (the hatched regions), the background corrected η asymmetry can be extracted by

$$A_{LL}^{\eta} = \frac{A_{LL}^{\eta+BG} - rA_{LL}^{BG}}{1-r}, \quad \text{with} \quad r \equiv \frac{N^{BG}}{N^{\eta} + N^{BG}}.$$

The resulting background corrected asymmetry A_{LL}^{η} as a function of p_T is shown in Fig. 2.

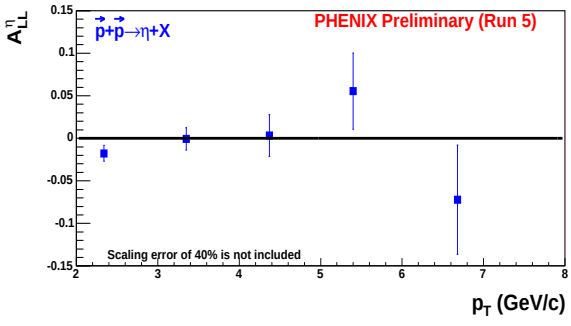

Fig. 2. Double helicity asymmetry for the inclusive η production as a function of p_T.

References

1) [PHENIX Collaboration], S.S. Adler et al., Phys. Rev. Lett. 93 (2004) 202002. S.S. Adler et al., Phys. Rev. D 73 (2006) 091102.

*1 University of Colorado, Boulder, Colorado, USA

Accessing the Gluon Polarization through $\pi^{\pm} A_{LL}$ at PHENIX

A. Morreale,[*1] C. Aidala,[*2] K. Boyle,[*3]

[Proton Spin, Pi Mesons, Charged Pions]

The double longitudinal asymmetries (A_{LL})of pion production in polarized proton proton collisions, is one of the various probes that will form part of Δg global analysis that aims to disentangle all of the partonic contributions to the proton spin[1)]. In proton-proton collisions at PHENIX central rapidities, π production proceed from quark-gluon and gluon-gluon initiated sub processes in the measured p_T range of 5-10GeV/c. This, along with other π meson properties such as zero spin and pseudo scalar under parity transformation, makes the π an accessible channel whose importance may elucidate information on the gluon's contribution to the proton's spin. Preferential fragmentation of up quarks to π^+ and down quarks to π^- leads to dominance of up-gluon and down-gluon contributions in the sum over flavors in a factorized pQCD calculation of π production. In addition, the polarized parton distribution functions(pdf's) are well known to be Δu >0 and Δd < 0 from polarized DIS experiments. This dominance of u or d combined with the different signs on their polarized distributions translates into potentially measurable differences in the asymmetries for the different π species that depend on the sign of Δg.

The PHENIX detector at RHIC has fine-grained calorimetry 100 times finer than previous collider detectors, making particle identification excellent, the resolution of the electromagnetic calorimeter (EMCal) is $\delta\eta * \delta\phi = 0.01 * 0.01$.[2)]. We select the $\pi^{\pm}$ signal by requiring a deposition of an energy cluster in the EMCal associated with a charged track in coincidence with the collision trigger. Due to the hadronic response in the EMCal, less than $\frac{2}{3}$ of the $\pi^{\pm}$ signal triggers an event. We furthermore identify $\pi^{\pm}$ by selecting particles that produced Čerenkov light in our ring imaging Čerenkov detector (RICH) but did not pass an electromagnetic shower-shape cut in the EMCal cluster.

The measurement presented consists of 0.89 billion events analyzed within p_T range of of 5-10 GeV/c, corresponding to an analyzed sample of approximately 2.3 pb^{-1} with an average polarization of 47%. The primary source of potential background in this analysis comes low energy electrons with misreconstructed momentum and charged hadron tracks firing the RICH. We performed a series of detector cuts which include: EMCal shower-shape cut designed to eliminate 80% of all electrons, a p_T-dependent energy cut to remove tracks with mis-reconstructed momentum and a cut of energy/momentum < 0.9 to remove the remaining electrons with nearly the correct reconstructed momentum. To estimate the remaining background fraction, the p_T region below 4 GeV/c was fit to a power law. Above 4GeV/c an extrapolation of the fit under the signal region was performed. The background using this method was estimated to be < 5%.

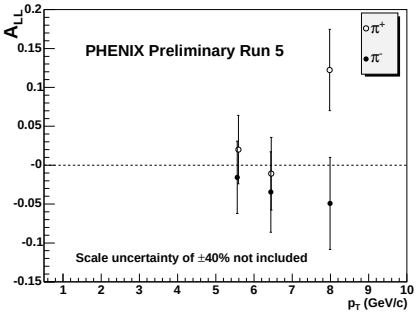

Fig. 1. Measurement of negative(solid circles) and positive(open circles)$\pi^{\pm}$ A_{LL}. A scale uncertainty of 40% due to the polarization uncertainty of the beams is not included.

The A_{LL} formula used in this analysis is as follows:

$$A_{LL} = \frac{\sigma_{++} - \sigma_{+-}}{\sigma_{++} + \sigma_{+-}} = \frac{1}{|P_Y||P_B|} \frac{N_{++} - RN_{+-}}{N_{++} + RN+-} \quad (1)$$

$$R = \frac{L_{++}}{L_{+-}} \quad (2)$$

Where ++(+-)are the beams in same(opposite) helicity configuration.

The first measurement of Run-05 $\pi^{\pm}$ A_{LL} at the p_T range 5-10GeV/c and the associated statistical errors are shown in Fig. 1. A scale uncertainty of 40% due to the polarization uncertainty on the beams is not included. The statistical uncertainty in A_{LL} using Run-06 data currently in production is expected to be aproximately 2.7 times smaller. While the background in this measurement is significantely lower than π^0[3)], current statistical uncertanties do not constrain Δg significantly. We expect that this analysis with the higher statistics and the cross-section measurement will be forthcoming and essential in pQCD interpretations and the constrain of Δg.

*1 Department of Physics, University of California at Riverside
*2 Department of Physics, University of Massachusetts Amherst
*3 Department of Physics, Stony Brook University

References

1) B. Jäger et al: Phys. Rev. D **67**, 054005 (2003).
2) K. Adcox et al.: Nucl. Inst. Meth. A **499**, 469 (2003)
3) S.S. Adler et al.: Phys. Rev. Lett. **93**,202002 (2004).

Double Helicity Asymmetry of Inclusive π^0 Production in Polarized pp Collisions at $\sqrt{s} = 62.4$ GeV

K. Aoki,[*1] A. Bazilevsky,[*2] K. Boyle,[*3] A. Deshpande,[*3] Y. Goto for the PHENIX Collaboration

Despite various efforts towards the understanding of proton spin, there remains a large uncertainty on ΔG, the gluon spin contribution to the proton. RHIC, the world's first polarized pp collider, provides us with an opportunity to directly probe gluons in the proton and investigate ΔG. The double helicity asymmetry (A_{LL}) of inclusive π^0 production in polarized pp collisions is sensitive to ΔG because π^0 production is dominated by quark-gluon and gluon-gluon interactions.

The PHENIX experiment at RHIC has the ability to clearly identify π^0 through its gamma decay using EMCal (electromagnetic calorimeter), which covers the central rapidity region ($|\eta| < 0.35$) and half the azimuthal angle.[1)] PHENIX also has an excellent gamma-triggering capability (the threshold is 0.8 GeV or 1.4 GeV), which makeshigh-statistics π^0 measurement feasible.[2)] PHENIX has previously reported $\pi^0 A_{LL}$ in pp collisions at $\sqrt{s} = 200$ GeV, [3)] which indicates that ΔG is not large.[4)] However, a large uncertainty remains for large Bjorken x (> 0.1) and more statistics are needed. During the run in 2006 (Run 6), data were collected over one week at $\sqrt{s} = 62.4$ GeV. Spin-rotator commissioning was successful and we had longitudinally polarized collisions.[5)] Even in this short period of data collection with a small integrated luminosity of 60 nb^{-1} and an average polarization of 48%, the lower-energy collision is advantageous for covering a larger x region. At a fixed x_T, the cross section is ~ 300 times larger than that at $\sqrt{s} = 200$ GeV. Ten-times-higher statistics are expected compared with the previosly reported $\pi^0 A_{LL}$ at $\sqrt{s} = 200$ GeV, which is based on an integrated luminosity of 1.8 pb^{-1} with an average polarization of 47%. In this report, the preliminary results of $\pi^0 A_{LL}$ at $\sqrt{s} = 62.4$ GeV are presented.

A_{LL} is calculated as

$$A_{LL} = \frac{1}{|P_B||P_Y|}\frac{N_{++} - RN_{+-}}{N_{++} + RN_{+-}}, \quad R = \frac{L_{++}}{L_{+-}}, \qquad (1)$$

where $P_{B(Y)}$ denotes the beam polarization in the Blue (Yellow) RHIC ring, N is the π^0 yield, L is the luminosity and ++ (+-) represents the helicity state of the beams. We used Beam-Beam Counter[1)] to measure R. Its uncertainty is estimated by comparing the count to Zero-Degree Calorimeter[1)] counts, and it is found to be $\delta R = 1.3 \times 10^{-3}$. This corresponds to $\delta A_{LL} = 2.8 \times 10^{-3}$, which is less than the statistical uncertainty.

*1 Kyoto University, Kyoto, Japan.
*2 Brookhaven National Laboratory (BNL), USA.
*3 Department of Physics, Stony Brook University, USA.

The systematic uncertainty is evaluated by the bunch-shuffling technique,[3)] and it is found to be negligible. Figure 1 shows the Run 6 results of $\pi^0 A_{LL}$ as a function of p_T. Theoretical curves based on perturbative QCD (pQCD) using the four models for polarized parton distribution functions are also shown.[6)] Figure 2 shows the Run 6 results of $\pi^0 A_{LL}$ as a function of x_T together with Run 5 results at $\sqrt{s} = 200$ GeV. A clear statistical improvement is in the large-x_T region.

To test the pQCD applicability at $\sqrt{s} = 62.4$ GeV, analysis on the π^0 production cross section is ongoing. With our cross section result, we will be able to discuss our A_{LL} result further with pQCD calculations.

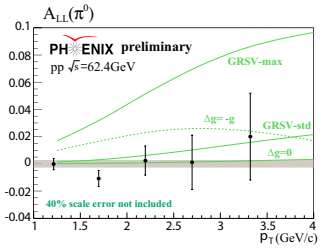

Fig. 1. $\pi^0 A_{LL}$ as a function of p_T. The error bar denotes statistical uncertainty. The gray band denotes the systematic error from relative luminosity.

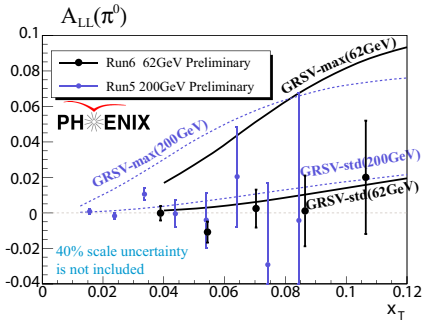

Fig. 2. $\pi^0 A_{LL}$ as a function of x_T.

References

1) K. Adcox et al.: Nucl. Instrum. Methods Phys. Res. A **499**, 469 (2003).
2) K. Okada et al.: RIKEN Accel. Prog. Rep. **36**, 248 (2003).
3) Y. Fukao et al.: RIKEN Accel. Prog. Rep. **39**, 175 (2006).
4) M. Hirai et al.: Phys. Rev. D **74**, 014015 (2006).
5) M. Togawa et al.: RIKEN Accel. Prog. Rep. **40**, 84 (2007).
6) B. Jäger et al.: Phys. Rev. D **67**, 054005 (2003).

Measurement of Double Helicity Asymmetry in π^0 Production in Polarized Proton Collisions at PHENIX

K. Boyle,[*1] A. Bazilevsky,[*2] A. Despande,[*1,*3] and Y. Fukao[*4] for the PHENIX Collaboration

[Proton spin, Proton structure]

The quark spin contribution to the proton spin has been found using fixed target polarized DIS measurement to be only about 25%. The other possible sources, gluon spin and orbital angular momentum of quarks and gluons, must contribute the remaining spin.

At PHENIX, we can constrain the gluon spin contribution to the proton spin through measurements of a double helicity asymmetry, A_{LL}, in longitudinally polarized proton collisions. In this report we focus on A_{LL} for π^0 production at $\sqrt{s}$=200 GeV. A_{LL} is defined as

$$A_{LL} = \frac{\sigma_{++} - \sigma_{+-}}{\sigma_{++} + \sigma_{+-}} \quad (1)$$

where σ_{++} (σ_{+-}) is the cross section with same (opposite) helicity. Experimentally, we measure

$$A_{LL} = \frac{1}{|P_1||P_2|}\frac{N_{++} - RN_{+-}}{N_{++} + RN_{+-}}, \quad R = \frac{L_{++}}{L_{+-}}. \quad (2)$$

where L is the integrated luminosity, R is the relative luminosity, P_1 and P_2 are beam polarizations and N is the particle yield.

The relative luminosity measurement has been described[1]. In 2005 (2006), the systematic uncertainty in A_{LL} due to relative luminosity was $\delta A_{LL}|_R = 2.3 \times 10^{-4}$ ($\delta A_{LL}|_R = 1.5 \times 10^{-4}$).

Average beam polarization for 2005 (2006) was 47% (62%). The remaining transverse components in 2005 were 10.3±2.1% and 14.5±2.2% for the two beams[2]. The asymmetry we actually measure is

$$A_{meas} = (1-\epsilon)A_{LL} + \epsilon A_{TT}, \quad A_{TT} = \frac{\sigma_{\uparrow\uparrow} - \sigma_{\uparrow\downarrow}}{\sigma_{\uparrow\uparrow} + \sigma_{\uparrow\downarrow}} \quad (3)$$

where ϵ is the product of the remaining transverse components, and A_{TT} is an azimuthally independent double transverse spin asymmetry. This was measured in PHENIX[3] and found to be consistent with zero. Therefore, a systematic uncertainty due to the remaining transverse polarization in the proton beams for $A_{LL}^{\pi^0}$ of $0.075 \times \delta A_{LL}|_{stat}$ is assumed.

The measurement technique has been described[4]. Figure 1 shows $A_{LL}^{\pi^0}$ from the 2005 RHIC run (blue circles) and the 2006 RHIC run (red triangles). The 2005 (2006) result was based on 1.8 (7.5) pb^{-1} and 47% (62%) polarization. Final 2005 results will include ∼30% more data. Full production for the 2006 data set was not completed at the time of this report, but a filtered data set requiring a high p_T photon was available. Due to this high p_T photon requirement, 2006 data with p_T<5 is not yet available.

In Fig. 1, four NLO pQCD theory calculations[5] are plotted with the data, assuming, at Q^2=0.4 GeV^2, an input value for Δg of $+g$ (GRSV-max), $-g$, 0, and the best fit to world data for Δg as of[5] (GRSV-std). By calculating the χ^2/NDF for each curve with respect to both the 2005 and 2006 results, we can estimate how well these values agree with the data. Theoretical uncertainties are not considered in these calculations. Both $\Delta g = +g$ and $\Delta g = -g$ are strongly disfavored by the data, with a likelihood of less than 0.1%. GRSV-std and $\Delta g = 0$ are consistent with our data, with likelihoods of 2-9% and 11-12%, respectively. The range in likelihoods come from including a 40% scaling uncertainty due to beam polarization measurement uncertainty. The addition of low p_T data may allow us to differentiate between GRSV-std and Δg=0.

References

1) K. Boyle et al.: RIKEN Accel. Prog. Rep. 39, 197 (2005).
2) M. Togawa et al.: RIKEN Accel. Prog. Rep. 39, 198 (2005).
3) K. Boyle et al.: RIKEN Accel. Prog. Rep. 40, (2006).
4) S. S. Adler et al.: Phys. Rev. Lett. **91**, 241803 (2001).
5) M. Glück et al.: Phys. Rev. D **63**, 094005 (2001).

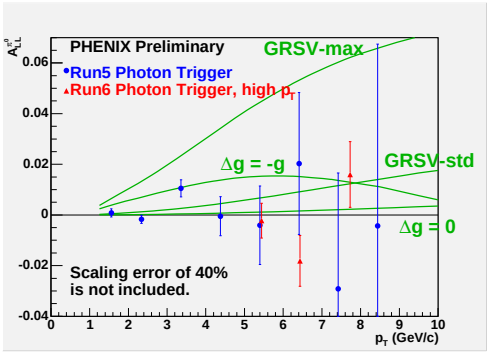

Fig. 1. $A_{LL}^{\pi^0}$ from 2005 RHIC run (blue circles) and 2006 RHIC run (red triangles) plotted with four theory curves calculated with NLO pQCD[5]. Curves are calculated with results from polarized DIS, assuming four values for gluon polarization described in the text. Run6 result currently only includes high p_T photon filtered data, with more data at lower p_T expected soon.

*1 Department of Physics, Stony Brook University
*2 Brookhaven National Laboratory
*3 RIKEN BNL Research Center
*4 Department of Physics, Kyoto University

Measurement of Double Transverse Spin Asymmetry in π^0 Production in Transversely Polarized Proton Collisions at PHENIX

K. Boyle,[*1] A. Bazilevsky,[*2] A. Despande,[*1,*3] and Y. Fukao[*4] for the PHENIX Collaboration

[Proton spin, Proton structure, transversity]

One of the primary goals of the RHIC spin program is to measure Δg, the gluon contribution to the spin of the proton, by measuring a double longitudinal spin asymmetry, A_{LL}, in the production of different probes in polarized proton collisions. Due to large statistics in pion production, and the high resolution electromagnetic calorimetry at PHENIX, the asymmetry in π^0 production has offered a significant constraint on Δg[1)].

At RHIC, the stable beam polarization direction is vertical, and so the polarization must be rotated onto the beam momentum axis at PHENIX. Small transverse polarization components remain, and have been measured[2)]. This remaining transverse component is a background in our measured A_{LL}:

$$A_{meas} = (1-\epsilon)A_{LL} + \epsilon A_{TT}, \quad (1)$$

where ϵ is the product of the remaining transverse components in the two beams, and A_{TT} is the double transverse spin asymmetry defined as

$$A_{TT} = \frac{\sigma_{\uparrow\uparrow} - \sigma_{\uparrow\downarrow}}{\sigma_{\uparrow\uparrow} + \sigma_{\uparrow\downarrow}}. \quad (2)$$

Here, $\sigma_{\uparrow\uparrow}$ ($\sigma_{\uparrow\downarrow}$) is the cross section for protons collisions with the parallel (antiparallel) transverse polarization. A_{LT} terms have been ignored as they are parity violating.

Non-zero A_{TT} theoretically arises from parton transversity distributions, $\delta f(x, Q^2)$, which describe the difference in the number density of partons with the same and different polarization in a transversely polarized proton. As the gluon is a massless spin 1 particle, $\delta g(x, Q^2) = 0$. Therefore, the numerator in Eq. 2 depends only on quark transversity. As both quarks and gluons contribute to π^0 production, the denominator includes both quark and gluon interactions. Thus, A_{TT} is expected to be quite small.

In 2005, a short running period was taken with transversely polarized beams specifically to constrain the systematic uncertainty from $A_{TT}^{\pi^0}$ in the measurement of $A_{LL}^{\pi^0}$. Experimentally, we actually measure

$$A_{TT} = \frac{1}{|P_1||P_2|}\frac{N_{\uparrow\uparrow} - RN_{\uparrow\downarrow}}{N_{\uparrow\uparrow} + RN_{\uparrow\downarrow}}, \quad R = \frac{L_{\uparrow\uparrow}}{L_{\uparrow\downarrow}}. \quad (3)$$

where L is the integrated luminosity, R is the relative luminosity, P_1 and P_2 are beam polarizations and N is the particle yield. The measurement of $A_{TT}^{\pi^0}$ is similar to that of $A_{LL}^{\pi^0}$, which is described in[1)].

The results for $A_{TT}^{\pi^0}$ are plotted in Fig. 1. The data sample corresponds to a luminosity of 0.15 pb^{-1} and average polarization of 47%. A scaling uncertainty of 40%, resulting from a 20% per beam polarization uncertainty, has not been included in the data in Fig. 1. As $A_{TT}^{\pi^0}$ is consistent with zero for the entire p_T range measured, we assume a systematic uncertainty in $A_{LL}^{\pi^0}$ of $0.075\times\delta A_{LL}^{\pi^0}$, where 0.075 is the ratio of longitudinal to transverse luminosity times ϵ.

The theoretical expectation for A_{TT} for $p + p \rightarrow \pi^0 + X$ has been calculated[3)] for the measured p_T range. Assuming maximal transversity, as defined by the Soffer bound,[3)] find $A_{TT}^{\pi^0}$<0.001 in the rapidity range covered by PHENIX. Such a precise measurement would require a transversely polarized luminosity of 320 pb^{-1}, which is not currently expected.

References

1) S. S. Adler et al.: Phys. Rev. Lett. **91**, 241803 (2001).
2) M. Togawa et al.: RIKEN Accel. Prog. Rep. 39, 198 (2005).
3) A. Mukherjee et al.: hep-ph/0507023 (2005).

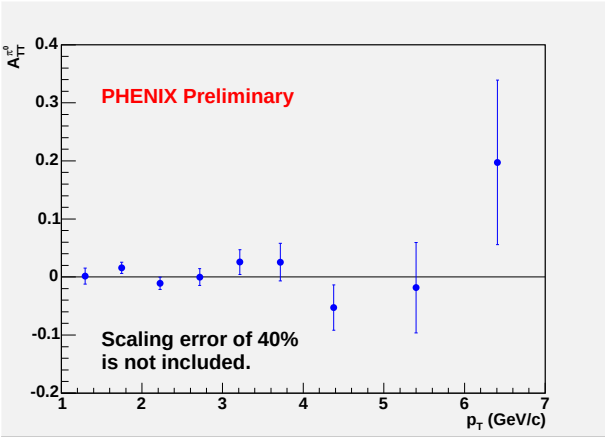

Fig. 1. Azimuthally independent double transverse spin asymmetry, A_{TT}, in π^0 production during 2005 RHIC running period with transversely polarized protons. Due to small remaining transverse beam polarizations in longitudinally polarized beams, A_{TT} is a contamination in our measured asymmetry. A systematic uncertainty of $0.075\times\delta A_{LL}$ is applied to the measured $A_{LL}^{\pi^0}$.

*1 Department of Physics, Stony Brook University
*2 Brookhaven National Laboratory
*3 RIKEN BNL Research Center
*4 Department of Physics, Kyoto University

k_T Asymmetry in Longitudinally Polarized pp Collisions at PHENIX

D. E. Fields,[*1,*2] I. Younus,[*1]

The history of theoretical interest in orbital angular momentum in hadrons can be traced to a paper by Chou and Yang[1] describing hadronic matter current inside a polarized hadron. Later, Meng Ta-chung et al.,[2] proposed two experiments to access hadronic matter currents, one in semi-inclusive deep inelastic scattering of unpolarized leptons on transversely polarized protons, and the second in the measurement of the net pair transverse momentum of Drell-Yan pairs in collisions of longitudinally polarized protons. The latter lays the theoretical basis for this analysis.

We propose here a method to probe the spin-correlated transverse momentum of partons involved in hard collisions of longitudinally polarized protons leading to jet events at PHENIX. The basic picture is that if some part of the transverse momentum of partons is correlated to the (longitudinal) spin direction, as it would be in the case of orbital angular momentum, then hard collisions involving these rotating partons may lead to jets with more or less average transverse momentum k_T, depending upon the relative orientation of the spin directions and the centrality of the collision. Since, at present, there is no good experimental tool to determine the collision centrality in $p+p$ collisions, one must determine if the effect remains when the impact parameter is undetermined. In[2], with a simple picture of the transverse spatial and momentum distributions, a net overall effect is still found.

PHENIX cannot measure the true jet axis as a direct way to measure the pair transverse momentum. An alternative method has been developed[3] that examines the π^0-hadron azimuthal angle correlation to extract the average pair transverse momentum on a statistical basis for two subsets of the data - like helicity collisions and unlike helicity collisions. The extracted average transverse momentum k_T for the two sets are compared as a measure of the helicity dependence of the interacting parton transverse motion.

The correlation function is obtained by measuring the distribution of the azimuthal angle difference, $\Delta\phi = \phi_t - \phi_a$, between π° (triggered particle) and charged hadron (associated particle). Whenever a π^0 is found in the event, the *real* ($dN_{real}/d\Delta\phi$) and *mixed* ($dN_{mix}/d\Delta\phi$) distributions are accumulated. Mixed events are obtained by pairing a π^0 in an event with $h^\pm$ from another randomly selected event. The jet fragmentation transverse momentum j_T and the partonic transverse momentum k_T can be extracted from the widths of the peaks in the correlation function.

To check systematic errors, bunch shuffling method was used. In bunch shuffling, we randomly flip the beam polarization signs for each event with a 50% probability, and then obtain the $\Delta\phi$ distributions for the two helicity combinitaions. The mixed event background is obtained from the whole data disregarding the helicity, and is kept the same for both helicity combinations. Since the mixed event background is used to correct the correlation function for effects of limited PHENIX azimuthal acceptance and for the detection efficiencies, we don't expect it to change with helicity. The results of the bunch shuffling indicate that the quoted errors on the fit parameters are correct.

Since any spin dependent effect should scale with the polarization of each beam, all helicity differences are scaled by the run-averaged beam polarization in the blue and yellow beams, both taken to be 0.47. A scale uncertainty of 40% is not shown on the figure. We look at the k_T helicity combination differences and find $\Delta\sqrt{\langle k_T\rangle} = 670 \pm 390$ MeV/c to be large, but with limited statistical significance.

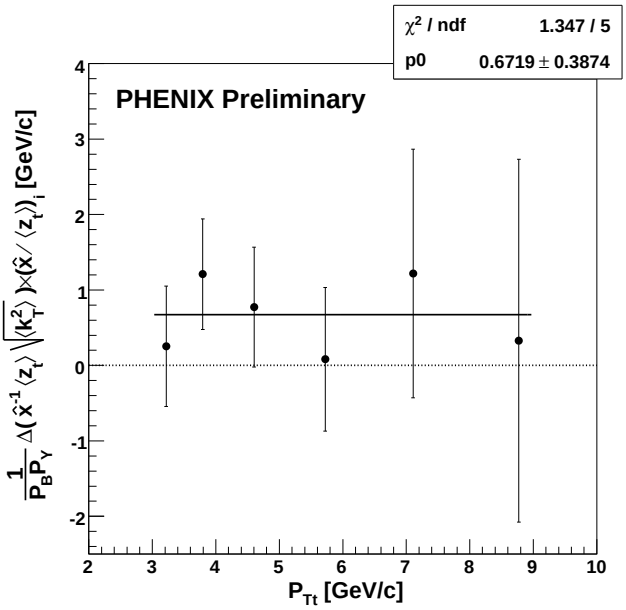

Fig. 1. $\Delta\sqrt{\langle k_T^2\rangle}$ (like- minus unlike-helicity combinations).

References

1) Chou, T. T. and Yang, Chen Ning, Nucl. Phys. B 107 1 (1976).
2) Meng, Ta-chung and Pan, Ji-cai and Xie, Qu-bing and Zhu, Wei, Phys. Rev. D 40 769 (1989).
3) Adler, S. S. et al., Phys. Rev. D 74 072002 (2006).

*1 University of New Mexico
*2 RIKEN-BNL Research Center

Measurement of Transverse Single-spin Asymmetries with J/Ψ in Polarized p+p Collisions at $\sqrt{s}$=200GeV

H. Liu*1 and M. Liu*2 for the PHENIX Collaboration

[Spin, J/Ψ, Asymmetry]

The measurement of transverse single-spin asymmetries (A_N) enables us to probe the quark and gluon structures of transversely polarized nucleons. Large transverse single-spin asymmetries of up to 20% - 40% were found for pions produced at a large x_F and $\sqrt{s}$ = 20 GeV[1] and have been found to persist at $\sqrt{s}$ = 200 GeV during the STAR[2]and BRAHMS experiments, although they were expected to vanish according to pQCD calculations at the leading order. A number of pQCD based models have been developed to explain this phenomenon. Among them are the Sivers effect[3], the Collins effect[4], and the interference between quark and gluon fields in the initial or final state[5].

At RHIC energy, heavy flavor production is dominated by gluon-gluon interactions. Thus, Collins effect has minimum impact on A_N because the gluon's transversity is zero. Therefore, the production of heavy flavor particles in transversely polarized p+p collisions in the PHENIX experiment offers a good opportunity to gain information on gluon's Sivers effect.

In this report, we present the first measurement of the transverse single-spin asymmetry of J/Ψ in polarized p+p collisions at RHIC. The PHENIX muon spectrometers have measured J/Ψ production through the J/Ψ → $\mu^+\mu^-$ channel at forward rapidities ($1.2 < |\eta| < 2.4$).

The transverse single-spin asymmetry A_N can be determined by:

$$A_N = \frac{1}{P_b}\frac{\sigma^\uparrow - \sigma^\downarrow}{\sigma^\uparrow + \sigma^\downarrow} = \frac{1}{P_b}\frac{N^\uparrow - RN^\downarrow}{N^\uparrow + RN^\downarrow}, \quad (1)$$

where P_b is the beam polarization, $\sigma^\uparrow(\sigma^\downarrow)$ is the production cross section, $N^\uparrow(N^\downarrow)$ is the J/Ψ yield from up(down)-polarized bunches, and $R = L^\uparrow/L^\downarrow$ is the relative luminosity measured with BBC(ZDC).

The inclusive J/Ψ sample is contaminated by other background (mainly come from Drell-Yan process, open charm and light hadrons decay). The measured A_N^{incl} is related to $A_N^{J/\Psi}$ by

$$A_N^{J/\Psi} = \frac{A_N^{incl} - r \cdot A_N^{BG}}{1 - r}, \quad (2)$$

$$\delta A_N^{J/\Psi} = \frac{\sqrt{(\delta A_N^{incl})^2 + r^2 \cdot (\delta A_N^{BG})^2}}{1 - r}, \quad (3)$$

where r is the background fraction, and A_N^{BG} is the averaged background asymmetry. A_N^{BG} is obtained using the like (unlike) sign dimuon pairs within 2.0 GeV< $M_{\mu\mu}$ < 2.5 GeV, and the like sign dimuon pairs within 2.8 GeV< $M_{\mu\mu}$ < 3.5 GeV.

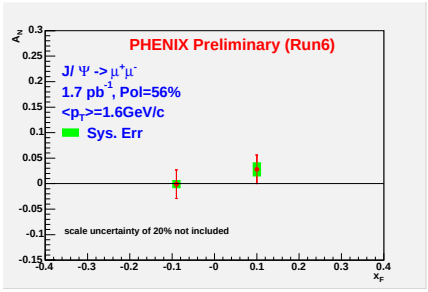

Fig. 1. A_N of J/Ψ vs x_F at $\sqrt{s}$ = 200 GeV.

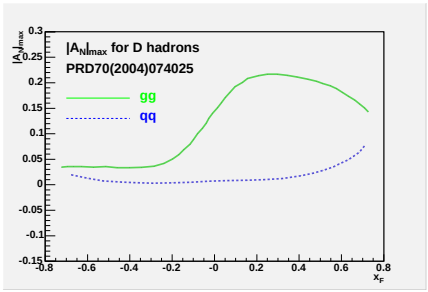

Fig. 2. A_N vs x_F in D meson production at p_T = 1.5GeV/c and $\sqrt{s}$ = 200GeV.

Preliminary result of J/Ψ A_N vs x_F from the 2006 RHIC run is shown in fig.1. Currently, there is no theoretical calculation of J/Ψ A_N. However, there is a prediction of A_N in D meson production at RHIC energy, as shown in fig.2[6]. The solid line shows $|A_N|_{max}$ when the gluon Sivers function is set to its maximum and the quark Sivers function is set to zero, and the dashed line corresponds to the opposite situation. If the asymmetry came from the initial state, then we would expect A_N in J/Ψ and D meson production to be very similar. The fact that there is no sizable asymmetry observed in fig.1 indicates that our results disfavor the maximum contribution of gluon's Sivers function.

*1 New Mexico State University, Las Cruces, NM, USA
*2 Los Alamos National Laboratory, Los Alamos, NM, USA

References

1) D.L. Adams *et al.*: Phys. Lett. B 264, 462-466 (1991); A. Bravar *et al.*: Phys. Rev. Lett. 77, 2626-2629 (1996).
2) J. Adams *et al.*: Phys. Rev. Lett. 92, 171801 (2004).
3) D. Sivers: Phys. Rev. D 41, 83-90 (1990).
4) J.C. Collins: Nucl. Phys. B 396, 161-182 (1993).
5) J. Qiu *et al.*: Phys. Rev. D 59, 014004 (1999); Y. Kanazawa *et al.*: Phys. Lett. B 478, 121-126 (2000).
6) M. Anselmino *et al.*: Phys. Rev. D 70, 074025 (2004).

Measurement of cross section and single transverse spin asymmetry of forward neutrons from *pp* collisions at RHIC-PHENIX

M. Togawa[*1], K. Aoki[*1], K. Boyle[*2], S. Dairaku[*1], A. Deshpande[*2], Y. Goto, K. Imai[*1], N. Saito[*3], J. Seele[*4] and K. Tanida[*1] for the PHENIX collaboration

Forward neutron production in *pp* collision has been studied and provide intriguing results. In the ISR experiment at $\sqrt{s}$=30.6 to 62.7 GeV in *pp* collisions, the neutron cross section in the very forward region ($p_T \sim$ 0 GeV) has a peak structure at high Feynman-x (x_F) and their cross sections scaled well with x_F[1]. One possible explanation for these interesting results is given by the one pion exchange model[2,3].

The Relativistic Heavy Ion Collider (RHIC) at the Brookhaven National Laboratory (BNL) has been operated with polarized proton beams colliding at $\sqrt{s}$=200 GeV for the spin program. In RUN2 (2001-2002), an unexpected large single transverse spin asymmetry (A_N) of the forward neutrons was discovered in the 12 o'clock interaction point experiment[4]. The measured asymmetry may also be explained by the pion exchange which is a spin flip interaction. The forward neutron asymmetry can be a new tool for understanding the production mechanism.

Through 2003-2006, in the PHENIX experiment has measured the forward neutrons using Zero-Degree Calorimeter (ZDC) with a position-sensitive Shower-Max Detector (SMD)[5]. They cover ±2.8 mrad of the forward and backward directions with 20% energy resolution for 100 GeV neutrons. Detector performances and signal identifications have been studied by Monte-Carlo simulations based on GEANT3 with PYTHIA and single-particle event generators to obtain the cross sections and A_N of neutrons.

The preliminary result of the neutron cross section at $\sqrt{s}$=200 GeV is plotted with the ISR results in Fig. 1. The PHENIX result is consistent with the ISR data and no evidence for violation of x_F scaling at this high energy. In Fig. 2, the neutron A_N is shown as a function of x_F. A significant asymmetry can be seen in the forward ($0<x_F$) and the curve is flat. The physics implications of this result are currently being discussed.

In the running period, forward neutron asymmetry is a very useful observable quantity for evaluating the spin direction of the proton beam at the collision point. It has been successful through the 2003-2006 RUN period[6]. In RUN 2006, $\sqrt{s}$=62.4 GeV polarized *pp* collision was performed for the first time[7]. A significant finite value, similar to $\sqrt{s}$=200 GeV, was obtained for the forward neutron asymmetry and the evaluation of spin direction was successfully accomplished. Longitudinal components were 98∼100% for both beams in the longitudinal polarized *pp* period at 62.4 GeV.

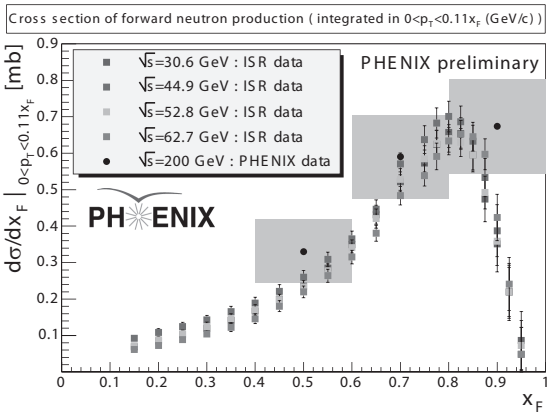

Fig. 1. Cross section of the forward neutron production from *pp* collisions at $\sqrt{s}$=200 GeV (Circles. Systematic errors are plotted as gray boxes). Squares show the results from ISR with various center of mass energies. No evidence for violation of x_F scaling at this high energy.

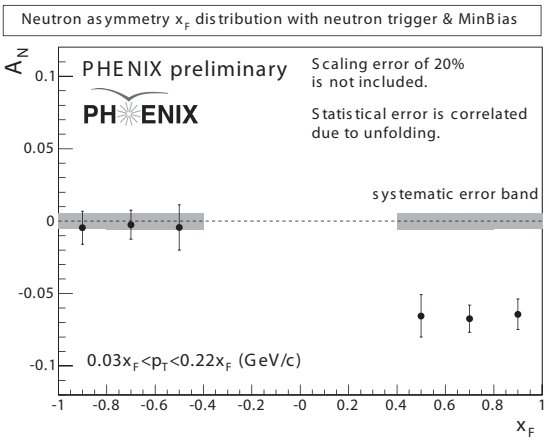

Fig. 2. Single spin asymmetry of neutron production from *pp* collisions at $\sqrt{s}$=200 GeV. A significant asymmetry can be seen in the forward region ($0<x_F$), and is flat as a function of x_F.

*1 Department of Physics, Kyoto University
*2 Department of Physics, Stony Brook University, SUNY
*3 J-PARC Office, High Energy Accelerator Research Organization (KEK)
*4 Department of Physics, University of Colorado

References

1) W. Flasher et al., Nucl. Phys. **B109** (1976) 347.
2) B. Kopeliovich et al., Z. Phys. **C73** (1996) 125.
3) U. D'Alesio and H.J. Pier, Eur. Phys. J. **A7** (2000) 109.
4) A. Bazilevsky et al., hep-ex/0610030 (to be in Phys. Lett. **B**).
5) C. Adler et al., Nucl. Instr. And Meth. **A470** (01) 488.
6) A. Deshpande et al., RIKEN Accel. Prog. Rep. **37** (04) 246. ; M. Togawa et al., RIKEN Accel. Prog. Rep. **39** (06) 198.
7) K. Aoki et al., RIKEN Accel. Prog. Rep. **40** (07).

Spin-dependent fragmentation function measurements at Belle experiment

R. Seidl,[*1] M. Grosse-Perdekamp,[*1] K. Hasuko and A. Ogawa,[*2]

[QCD, e^+e^- annihilation, fragmentation, transversity]

The Belle experiment[1] at the asymmetric e^+e^- collider KEKB[2] at Tsukuba, Japan, is mainly dedicated for studying CP violation in B meson decays. It is tuned to the $\Upsilon(4S)$ resonance at 10.58 GeV, whereas background studies are performed at 10.52 GeV. The first results on the fragmentation of polarized light quarks into pions obtained on a data set of 29.1 fb $^{-1}$ have been published[6]. The inclusion of the full data set of 547 fb $^{-1}$ will be presented.

The Collins effect[3] occurs in the fragmentation of a transversely polarized quark with polarization $\mathbf{S_q}$ transverse to its 3-momentum $\mathbf{k}$ into an unpolarized hadron of transverse momentum $\mathbf{P}_{h\perp}$ with respect to the original quark direction. The Collins function $H_1^{\perp q}(z, P_{h\perp}^2)$, where $z \overset{CMS}{=} \frac{2E_h}{Q}$ is the fractional energy the hadron carries in the center of mass system, causes a $\sin(\phi)$ modulation in the azimuthal distribution of the hadron yields around the original quark momentum axis. ϕ is the azimuthal angle between the transverse momentum of the hadron and the plane defined by the quark spin and its momentum. In e^+e^- hadron production, the Collins effect can be observed by correlating the fragmentations of quark and anti-quark in opposing hemispheres. The combination of two hadrons from different hemispheres in two-jetlike events, with azimuthal angles ϕ_1 and ϕ_2, results in a $\cos(\phi_1 + \phi_2)$ modulation of the observed di-hadron yield. In the CMS, these azimuthal angles are defined between the transverse component of the hadron momenta with regard to the jet axis $\hat{n}$ and the plane spanned by the lepton momenta and $\hat{n}$. Following Ref.[4] one either computes the azimuthal angle of each pion relative to the jet axis which results in a $\cos(\phi_1 + \phi_2)$ modulation or one calculates the azimuthal angle (ϕ_0) relative to the axis defined by the 2^{nd} pion which results in a $\cos(2\phi_0)$ modulation. We measure the normalized yields $N(\beta_\alpha)/\langle N_0\rangle$, where $N(\beta_\alpha)$ denotes the number of hadron pairs in the bins of either $\beta_0 = 2\phi_0$ or $\beta_{12} = \phi_1 + \phi_2$ and $\langle N_0\rangle$ is the average number of hadron pairs in the whole angle interval. The main background, producing similar azimuthal asymmetries as the Collins effect, is the radiation of soft gluons. This gluonic contribution is proportional to the unpolarized FF and is independent of the charge of the hadrons. Consequently, taking the ratio of the normalized distributions for unlike-sign over like-sign pairs the gluonic distributions drop out in leading order:

$$R_\alpha := \frac{N(\beta_\alpha)}{\langle N_0\rangle}\Big|_{\text{unlikesign}} \Big/ \frac{N(\beta_\alpha)}{\langle N_0\rangle}\Big|_{\text{likesign}} \quad , \qquad (1)$$

A similar expression for the ratio of unlike-sign over all charged pion pairs[7] also exists. These double ratios are then fit by the sum of a constant term and a cosine modulation $R_\alpha = B_\alpha + A_\alpha \cos(\beta_\alpha)$. The reconstruction of azimuthal asymmetries was tested by a Monte Carlo simulation. The results for the A_0 results are shown as a function of the fractional energies in Fig. 1. A significant rising asymmetry can be observed.

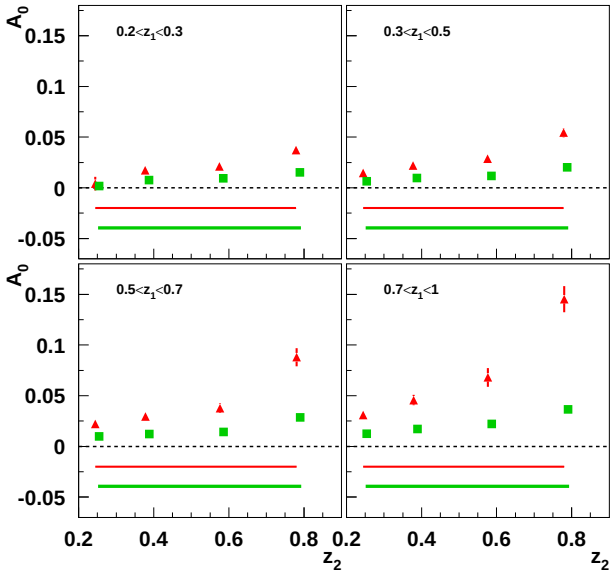

Fig. 1. Light quark (uds) A_0 asymmetries as a function of z_2 for the 4 z_1 bins. The UL data is described by the triangles, its systematic error being the top error band while the UC data is described by the squares and its systematics by the lower error band.

*1 University of Illinois
*2 Brookhaven National Laboratory

References
1) A. Abashian et al.(Belle): Nucl. Instrum. Meth. **A479** (2002) 117.
2) S. Kurokawa, E. Kikutani: Nucl. Instrum. Meth. **A499** (2003) 1.
3) J. C. Collins: Nucl. Phys. **B396** (1993) 161.
4) D. Boer, R. Jakob, P. J. Mulders: Phys. Lett. **B424** (1998) 143.
5) A. Airapetian et al.(Hermes) Phys. Rev. Lett.**94**(2005)012002.
6) R. Seidl, et al.(Belle): Phys. Rev. Lett. **96**(2006):232002.
7) A. Efremov, K. Goeke and P. Schweitzer: [arXiv:hep-ph/0603054].

Measurement of A_N and A_{NN} in pp Elastic Scattering in the CNI Region with a Polarized Atomic Hydrogen Gas Jet Target

H. Okada,[*1,*2] G. Bunce,[*2,*3] K.O. Eyser,[*4] and I. Nakagawa.[*1]

[Elastic scattering, spin, coulomb nuclear interference]

Precise measurements of the single and double spin asymmetries, A_N and A_{NN}, in proton-proton elastic scattering in the region of four-momentum transfer squared $0.001 < -t < 0.032$ (GeV/c)^2 have been performed using a polarized atomic hydrogen gas jet target and the RHIC proton beam in 2004 [a)]. We took data for two beam momenta at 24 GeV/c ($\sqrt{s}$ = 6.7 GeV) and 100 GeV/c ($\sqrt{s}$ = 13.7 GeV).

This $-t$ region is known as the Coulomb Nuclear Interference (CNI) region. The interference of the electro-magnetic spin-flip amplitude with a hadronic non spin-flip amplitude is predicted to generate A_N of few %, peaking at $-t \simeq 0.003$ (GeV/c)^2[1)], and the presence of a hadronic spin-flip amplitude (ϕ_5^{had}) would modify this calculable prediction. A_{NN} is thought to be sensitive to the hadronic double spin-flip amplitude (ϕ_2^{had})[2)] but there is no solid theoretical prediction for its energy dependence nor magnitude.

Fig. 1 and Fig. 2 display the results of A_N and A_{NN} in the the CNI region as a function of $-t$. The filled and empty circles are results at $\sqrt{s}$ = 6.7 GeV and 13.7 GeV[3)], respectively. The errors on the data points are statistical. The lower bands represent the total systematic errors. The solid and dashed lines in Fig. 1 are the function without allowing for ϕ_5^{had} contribution to A_N for these $\sqrt{s}$, respectively. A_N at $\sqrt{s}$ = 13.7 GeV are consistent with the dashed line (χ^2/ndf=13.4/14). On the other hand, although the accuracy is statistically limited, A_N at $\sqrt{s}$ = 6.7 GeV are *not* consistent with the solid line (χ^2/ndf=35.5/9). This discrepancy implies the presence of ϕ_5^{had}. A_{NN} for these $\sqrt{s}$ have no clear $-t$ dependence and the average values are consistent with zero within the uncertainty of 1.5 σ.

In summary, A_N and A_{NN} results provide experimental knowledge of poorly known ϕ_2^{had} and ϕ_5^{had} at these energy. The $\sqrt{s}$ dependence of ϕ_5^{had} is provided by A_N results. The theoretical interpretation is under way in order to have a comprehensive understanding of ϕ_2^{had} and ϕ_5^{had}. In addition, the analysis of A_N at $\sqrt{s}$ = 7.6 GeV which were measured in 2005 is under way and will give us the third $\sqrt{s}$ point data.

References

1) N.H. Buttimore *et al.*, Phys. Rev. D **59**, 114010 (1999).
2) T.L. Trueman, RHIC Spin Note, September 27, (2005), hep-ph/0604153.
3) H. Okada *et al.*, Phys. Lett. B **638**, 450 (2006); H. Okada, Doctororal Thesis, July (2006).
4) A. Zelenski *et al.*, Nucl. Inst. and Meth. A **536**, 248 (2005); T. Wise *et al.*, Nucl. Inst. and Meth. A **559**, 1 (2006).

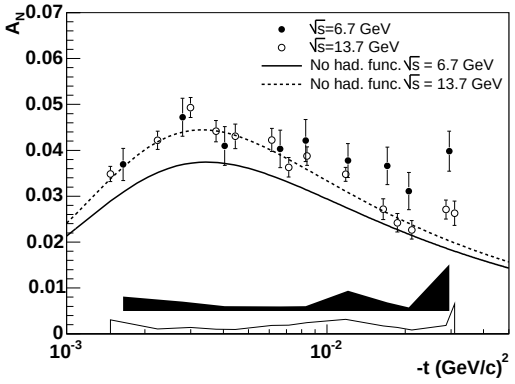

Fig. 1. The filled and open circles are measured at $\sqrt{s}$ = 6.7 GeV and 13.7 GeV, respectively. The errors on the data points are statistical. The lower bands represents the total systematic errors. The solid and dashed lines are the function without allowing for ϕ_5^{had} contribution to A_N for these $\sqrt{s}$, respectively.

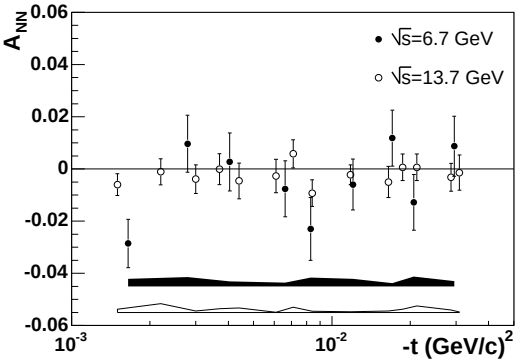

Fig. 2. The filled and empty circles are measured at $\sqrt{s}$ = 6.7 and 13.7 GeV. The errors on the data points are statistical. The lower bands represents the total systematic errors.

[*1] RIKEN, Wako, JAPAN
[*2] Brookhaven National Lab., Upton NY, USA
[*3] RIKEN BNL Research Center, Upton NY, USA
[*4] University of California, Riverside CA, USA

[a)] The details of experimental setup are described in[3,4)]. These references contain a complete list of authors of the collaboration.

Absolute beam polarization measurements at RHIC in 2005

K.O. Eyser,[*1] I. Alekseev,[*2] A. Bravar,[*3] G. Bunce,[*4,*5] S. Dhawan,[*6] R. Gill,[*4] W. Haeberli,[*7] H. Huang,[*4] O. Jinnouchi,[*8] Y. Makdisi,[*4] I. Nakagawa,[*9,*5] A. Nass,[*10] H. Okada,[*11,*9] E. Stephenson,[*12] D. Svirida,[*2] T. Wise,[*7] J. Wood,[*4] A. Zelenski,[*4]

Accurate knowledge of the beam polarization is essential in the spin program at the Relativistic Heavy Ion Collider (RHIC). Measurements of beam polarizations utilize scattering processes. Fast measurements are based on proton-carbon scattering off carbon fiber targets[1)], for which the necessary normalization is provided from elastic proton-proton scattering with a polarized hydrogen gas jet target.

The jet polarimeter is located at one of the collision points in the RHIC accelerator. It consists of a polarized hydrogen atomic jet target with a Breit-Rabi polarimeter[2)] and a set of six separate detectors each of 16 silicon strips. The hydrogen molecular content has been determined and is removed from the effective polarization $P_{target} = (92.4 \pm 1.8)\%$.

The detectors are centered with respect to the interaction point of the proton beam with the target. In this geometry, eight downstream strips on each detector can detect elastically scattered recoil protons when one RHIC beam hits the target. In routine operation, one of the two RHIC beams is displaced, so the respective eight non-signal strips can be used to estimate the background fraction below the elastic signal peak.

The silicon detectors are read out with waveform digitizers, running at 420 MHz. Two α-sources are used for energy calibration of the ADC signal. Additional time of flight offsets are individually adjusted for each strip using the pronounced proton signal. Particle identification is based on time of flight and energy.

The determination of the RHIC beam polarization is based on a set of four vertical polarization combinations of target and beam. Yields are combined to separate beam and target asymmetries. The beam polarization P_{beam} is then derived from the ratio of the asymmetries ϵ_{beam} and ϵ_{target} and a known P_{target}:

$$P_{beam} = -\frac{\epsilon_{beam}(T_R)}{\epsilon_{target}(T_R)} \cdot P_{target}. \quad (1)$$

While the kinematic correlation of the detector strip position and the recoil energy T_R suppresses the background outside of the considered energy range, P_{beam} has been determined for different T_R before averaging. Figure 1 shows the typical peak of the asymmetries at $T_R \approx 1.5$ MeV from a subset of the data. The ratio between 1.0 and 4.0 MeV is used to determine the beam polarization, lower and higher recoil energies are discarded due to asymmetric acceptance and background. Figure 1 compares the data with the expected shape of the analyzing power A_N from a formal description in terms of helicity amplitudes scaled with target and beam polarizations.

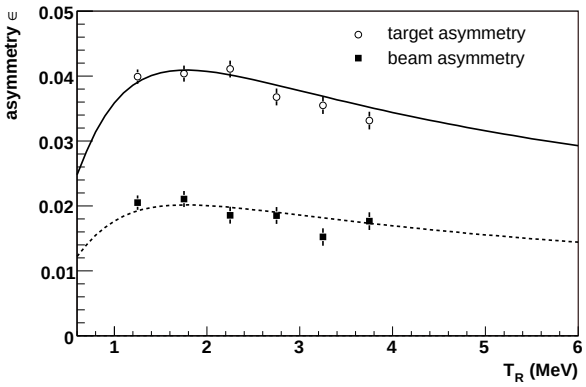

Fig. 1. Target and beam asymmetries as functions of T_R.

In 2005, beam polarizations of nearly 50% have been measured in RHIC with good statistical accuracy. Systematic errors were estimated from background yields of empty target runs and subdivision with respect to separate bunches in the accelerator. No significant polarization dependence has been observed in the background. Other checks included many thousand repetitions of random assignments to the polarization directions of bunches and calculating the resulting asymmetries. The effect on the determination of the beam polarization has been estimated by purposefully widening the signal region on the detectors, this way increasing the background by factors of up to four and consecutively lowering the beam and target asymmetries. The ratio of asymmetries, on the other hand, is largely unaffected by the growing background and an upper limit of $\Delta P/P = 1.1\%$ has been assigned to the beam related background. This does not include the molecular content in the jet target.

*1 University of California, Riverside, USA
*2 ITEP, Moscow, Russia
*3 University of Geneva, Switzerland
*4 Brookhaven National Laboratory, USA
*5 RIKEN BNL Research Center, USA
*6 Yale University, USA
*7 University of Wisconsin, USA
*8 KEK, Japan
*9 RIKEN, Japan
*10 University of Erlangen, Germany
*11 Kyoto University, Japan
*12 Indiana University, USA

References

1) I. Nakagawa, this publication (2006).
2) H.G. Gaul and E. Steffens, NIM A316, 297 (1992).

Stability for Run05 Operation of pC-Polarimeter

I. Nakagawa, I. Alekseev,[*1] A. Bravar,[*2] G. Bunce,[*3*4] S. Dhawan,[*5] K.O. Eyser,[*6] R. Gill,[*3] W. Haeberli,[*7] H. Huang,[*3] O. Jinnouchi,[*8] Y. Makdisi,[*3] A. Nass,[*3] H. Okada,[*9] E. Stephenson[*10] D.N. Svirida,[*1] T. Wise,[*7] J. Wood,[*3] and A. Zelenski[*3]

The Relativistic Heavy Ion Collider (RHIC) at BNL provides a unique opportunity to collide polarized protons. The decompsition of nucleon spin in terms of the contributions from its constituents has been studied using various observed asymmetries. The 2005 run (RUN05) was the first extended operation of the polarized RHIC-pp program. During the running period, continuous studies were performed to improve the performance characteristics of an accelerator, for example, intensity, emittance, and backgrounds, whereas polarization measurements were regularly executed every 2 to 3 hours for both beams using RHIC pC-polarimeters [1]. The stability and reliability of the polarization measurements under various beam/detector conditions are the major concern in evaluating the average polarization, which provides normalization for experiments. One of the dominant sources of uncertainties in pC-polarimetry has been the absolute energy determination for low-energy recoiling carbon ions[2].

We detect elastically recoiling carbon ions at a scattering angle of 90° in the kinetic energy E range of 400 keV $< E <$ 900 keV using six silicon detectors mounted at azimuth angles of 45°, 90° and 135° on both sides of the beam axis. Each detector is segmented into 12 strips (72 strips in total). These low-energy carbon ions stop at very shallow depths (< 1.3 μm) in a silicon sensor and the response of the detector is sensitive to the surface structure of the silicon. A 400 keV carbon ion loses about 1/3 of its energy in a typical dead region followed by a partially inefficient charge collection region before it reaches a fully active region. There are two main difficulties in correcting for the unobserved energy loss. First, we have been unable to separate the energy-dependent energy loss in the dead-layer from charge collection inefficiency near the surface region. Secondly, it is nontrivial to model the inefficiency as a function of depth. The charge collection efficiency is initially characterized by the Landau distribution of the implanted Boron atoms in the doping process. In reality, the efficiency depends on many other conditions, such as the magnitude of radiation damage, and event rate. These dependencies make the efficiency function complex.

To avoid such a complexity that cannot be sufficiently controlled, here we consider net energy correction by introducing *"effective dead-layer thickness"*, which can be determined from a fit to the measured timings and pulse height using the kinematic correlation between time-of-flight and carbon energy. A time offset with respect to a beam clock and the effective thickness of the dead-layer are treated as free parameters.

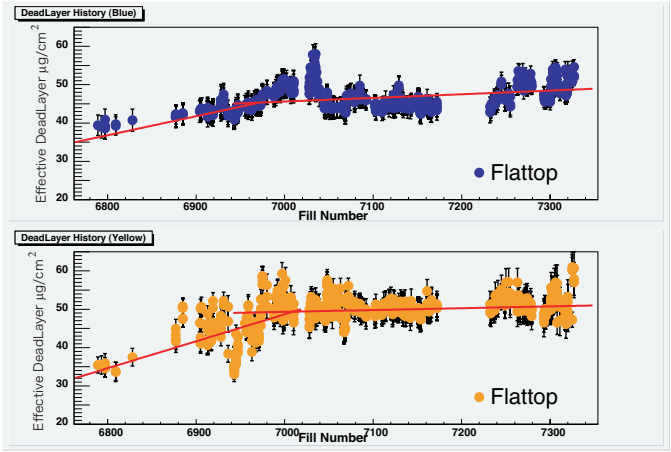

Fig. 1. Stability of *effective dead-layer thickness* averaged over 72 strips plotted as function of fill number for blue (top) and yellow (bottom) polarimeters.

The estimated *effective dead-layer thicknesses* in μg/cm^2 units averaged over 72 strips are shown in Fig. 1. Data points represent individual measurements performed at a beam energy of 100 GeV. As illustrated by the solid line in the figure, the effective thickness of the dead-layer increases with time. The increase in of the inefficiency can be interpreted as the deteriorated charge collection efficiency due to the accumulated radiation damage in the surface region. Besides the fitting error, the cause of varying *effective dead-layer thickness* is unknown, except for a minor average rate dependence (data points in the figure are already corrected for this). These fluctuations are thus accounted for by uncertainties in absolute energy determination. Considering 1σ of the fluctuations in effective dead-layer thickness, (~ 3 μg/cm^2), corresponds to a few percent uncertainty in beam polarization.

*1 Institute for Theoretical and Experimental Physics, Russia
*2 University of Geneva, 1205 Geneva, Switzerland
*3 Brookhaven National Laboratory, USA
*4 RIKEN-BNL Research Center, BNL, USA
*5 Yale University, USA
*6 University of California, Riverside, USA
*7 University of Wisconsin, USA
*8 KEK
*9 Kyoto University
*10 Indiana University Cyclotron Facility, USA

References

1) I. Nakagawa *et al.*: RIKEN Accel. Prog. Rep. **39**, 186 2005, and references therein.
2) I. Nakagawa *et al.*: RHIC/CAD Accelerator Physics Note, Vol.275 (2007).

Absolute luminosity determination using vernier scan technique at PHENIX

Y. Goto and R. Bennett*1 for the PHENIX Collaboration

For any absolute cross-section measurement at PHENIX[1], we require an absolute integrated luminosity determination. Absolute luminosity ($\mathcal{L}$) is determined from the number of events triggered by the beam-beam counter (BBC) of the PHENIX detector (N_{BBC}) using an absolute calibration of the BBC trigger cross section (σ_{BBC}): $\mathcal{L} = N_{BBC}/\sigma_{BBC}$. The BBC trigger is a minimum-bias trigger of the PHENIX trigger system and requires that the collision vertex is within 30 cm of the center of the interaction region. The BBC consists of two detectors located on either side of the colliding beam along the beam line at ±1.44 m from the nominal interaction point and covers the pseudorapidity range ±(3.0–3.9) and the full azimuthal angle. The vertex is reconstructed from the difference in the arrival times of particles at two BBC detectors.

The absolute calibration of the BBC trigger cross section is obtained via the vernier scan (or van der Meer scan) technique.[2] In a scan, the transverse profile of the beam overlap is measured by sweeping one beam across the other in steps while monitoring BBC trigger rate. This information, the bunch intensities of the two beams as provided by the wall current monitors of the RHIC accelerator (N_b and N_y), and the revolution frequency for one bunch in the beam ($f_{\rm beam}$) are used to compute machine luminosity:

$$\mathcal{L}_{\rm machine} = \frac{f_{\rm beam}}{2\pi\sigma_x^v\sigma_y^v} \cdot \sum_{\rm crossings} (N_b \cdot N_y)_i. \qquad (1)$$

Here σ_x^v and σ_y^v are the transverse widths of beam overlap as measured by vernier scans in the horizontal and vertical directions respectively, and "crossings" means pairs of colliding bunches in the PHENIX interaction region. The BBC trigger cross section is the ratio of BBC trigger rate when the beams are overlapping maximally ($R_{\rm max}$) to the effective machine luminosity observable using the BBC trigger with the collision vertex selection:

$$\sigma_{BBC} = \frac{R_{\rm max}}{\mathcal{L}_{\rm machine} \cdot \epsilon_{\rm vertex}}, \qquad (2)$$

where $\epsilon_{\rm vertex}$ is the vertex selection efficiency obtained by the vertex reconstruction analysis of the BBC detector.

In the 2001 – 2002 run of RHIC, the BBC trigger cross section was determined to be 21.8 ± 0.9 (2.8) mb at a 68.5% (95%) confidence level with an absolute error of 0.7 mb on the basis of three scans. Because this result was obtained from only three scans, the remaining issue is a better systematic understanding to achieve smaller systematic uncertainties.

Since the 2003 run, we have recorded the number of BBC-trigger events in each bunch crossing using a special crossing-sorted scaler, the so-called GL1P scaler (Global Level-1 physics scaler), at PHENIX during vernier scans. The live time of the BBC trigger in each crossing is normalized by the live-time clock also recorded in the GL1P scaler. With this crossing-sorted data, we can use each bunch crossing as one piece of vernier scan data, and calculate the machine luminosity with eq.(1) without the summation of crossings and the BBC trigger cross section with eq.(2) in each bunch crossing. Figure 1 shows measured transverse profiles of the beam overlap in each crossing obtained by horizontal and vertical scans. The distances between two beams (abscissa of the figure) are provided by the beam position monitors of the RHIC accelerator. The widths of these profiles determined by the horizontal and vertical scans are σ_x^v and σ_y^v, respectively. In the 2005 run and the 2006 run, more than ten vernier scans were performed. Using the crossing-sorted data, we can study the effects of varying each bunch crossing. Using multiple vernier-scan data, we can study other effects from the accelerator conditions fluctuating in each RHIC store, e.g., nonzero crossing angle, transverse and longitudinal bunch shapes, intensity, and the blow-up of the beam. The final analysis is underway.

References

1) S. S. Adler *et al.*: Phys. Rev. Lett. 91, 241803 (2003): Phys. Rev. Lett. 92, 051802 (2004): arXiv:hep-ex/0609031: A. Adare, arXiv:hep-ex/0611020.
2) A. Drees and Z. Xu: PAC-2001-RPAH116 *Presented at IEEE Particle Accelerator Conference (PAC2001), Chicago, Illinois, 18-22 Jun 2001.*

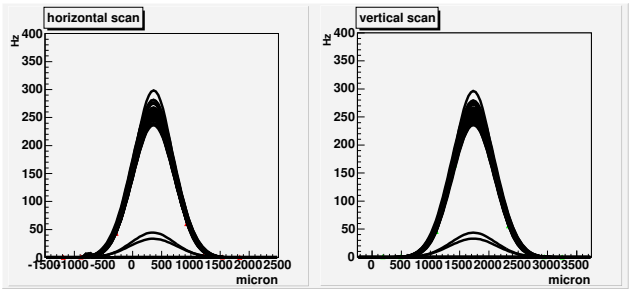

Fig. 1. Transverse profiles of beam overlap in each bunch crossing by horizontal (left) and vertical (right) scans.

*1 Department of Physics, Stony Brook University

Data production for RHIC-PHENIX experiment

Z. You*1, J. Seele*2, H. Torii*3, Y. Mao*1, S. Yokkaichi, S. Kametani, Y. Watanabe, Y. Goto for the PHENIX collaboration

1 Overview

The data production for the PHENIX experiment at RHIC (Relativistic Heavy Ion Collider) has been performed at CCJ[1-4] (RIKEN Computing Center in Japan for RHIC[5] physics) since 2002. In 2005-2006, the PHENIX run5 p+p data production was performed at CCJ and run6 p+p data production began in late 2006.

2 Run5 data production

In run5, RHIC provided PHENIX with polarized p+p collisions at √s=200GeV from April to July 2005. During this period, the raw data was transferred from BNL (Brookhaven National Laboratory) to CCJ concurrently as it was taken. The transfer was completed on June 26th, 2005. Over 260 TB raw data was transferred in 80 days using GridFTP[7], with an average speed of 40MB/sec. HPSS[8] at CCJ is used to store the raw data and also the DSTs (Data Summary Tape) which contain the reconstructed data made during production.

The first version of run5 p+p production was performed from June to September in 2005 by H.Torii et al[9]. 16TB of nDSTs (nano Data Summary Tape) were produced and stored in HPSS at RSCC (RIKEN Super Combined Cluster). They were also transferred to dCache at RCF[10] (RHIC Computing Facility), a mass data storage system.

The second version of run5 p+p production began in April 2006 and ended in September 2006, as is shown in Fig.1, with Linux system and the PHENIX libraries upgraded. 128 PC nodes (dual Xeon 3.06 GHz/2GB memory/100 GB local disk) at RSCC that are specifically assigned to CCJ were used for this production. 904 longitudinally polarized runs with good calibrations were successfully produced. The nDST files from 10 PRDFs (PHENIX Raw Data Format) are aggregated into fewer files for analysis and are then stored at HPSS. The production rate was maintained at approximately 50MB/s.

The second version of production is a full and final production for run5. All 28 flavors of nDSTs with different triggers were produced. The total size of the final nDST files is 38TB; the data is stored in HPSS at CCJ. Like the first version of production, they are transferred to dCache at RCF at BNL using bbftp[11]. The average transfer speed obtained was 6MB/s. Details of production are shown on the web page: http://ccjsun.riken.go.jp/~phnxreco

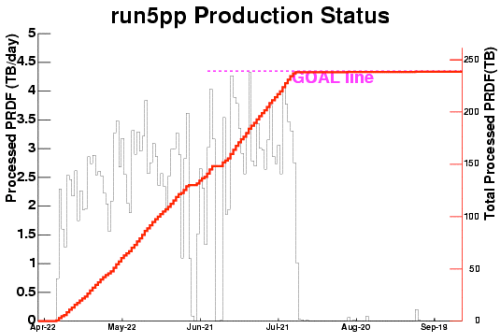

Fig. 1. The PHENIX run5 p+p daily data processing speed and data accumulation.

3 Run6 data production

During the run6 running period (March 2006 through June 2006), RHIC provided polarized p+p collisions at √s=200GeV to the PHENIX experiment. Two modes of collisions were used: one where the polarizations of the bunches were transverse to the beam momentum and one where the polarizations were longitudinal to the beam momentum. A total luminosity of 2.7pb^{-1} was taken in the transverse mode and 7.5pb^{-1} in the longitudinal mode. This compares with 3.78pb^{-1} taken in the longitudinal running in run5. The size of the raw data set is approximately 320TB. The raw data was transferred from PHENIX to CCJ using GridFTP. The data was transferred to CCJ in near simultaneity to the data being taken by PHENIX.

The longitudinal data set will be produced at CCJ and the transverse data set will be produced at RCF. The data will be processed at CCJ in a similar manner to the run5 production though with upgraded software for both the HPSS system and the PHENIX libraries.

The production began in late 2006 and proceeded into 2007. The data will then be transferred back to RCF using GridFTP.

*1 School of Physics, Peking University, China
*2 Department of Physics, University of Colorado
*3 Hiroshima University

References

1) http://ccjsun.riken.go.jp/ccj/
2) S. Yokkaichi et al.: RIKEN Accel. Prog. Rep. 37, 257 (2004).
3) Y. Watanabe et al.: RIKEN Accel. Prog. Rep. 36, 262 (2003), T. Ichihara et al.: RIKEN Accel. Prog. Rep. 35, 236 (2002).
4) S. Yokkaichi et al.: RIKEN Accel. Prog. Rep. 38, 247 (2005).
5) http://www.bnl.gov/rhic
6) http://www.phenix.bnl.gov
7) http://www.globus.org/datagrid/gridftp.html
8) http://www.hpss-collaboration.org/
9) H. Torii et al.: RIKEN Accel. Prog. Rep. 39, 220 (2006).
10) http://www.phenix.bnl.gov/RCF
11) http://doc.in2p3.fr/bbftp/

Development of Nose Cone Calorimeter in PHENIX Forward Region

I. Nakagawa, E. O'Brien,[*1] V. Dzhordzhadze,[*2] D. Karmanov,[*3] E. Kistenev,[*1] Z. Li,[*1] A. Litvinenko,[*4] M. Merkin,[*3] V. Peresedov,[*4] R. Seto,[*2] A. Taketani, A. Sukhanov,[*1] V. Volkov,[*3] A. Voronin,[*3] V. Vrba,[*5] and L. Zolin[*3]

The present baseline detector of PHENIX measures muons in two muon spectrometers located forward of mid-rapidity and measures hadrons, electrons, and photons in two central spectrometer arms, each of which covers 90° in azimuth and 0.35 units of rapidity. The nose cone calorimeter[1)] (NCC) will extend the rapidity coverage for hadronic and electromagnetic signatures by upgrading the functionality of PHENIX muon spectrometers to include photon and jet measurement capabilities. The forward production of inclusive jets, direct photons or Drell-Yan pairs at a large x_F in nucleon-ion collisions at RHIC will provide a new window for the observation phenomena expected at high parton number densities. Also, in conjunction with the muon spectrometer, the NCC will enable isolation cuts for the study of W bosons to measure antiquark spin structure functions.

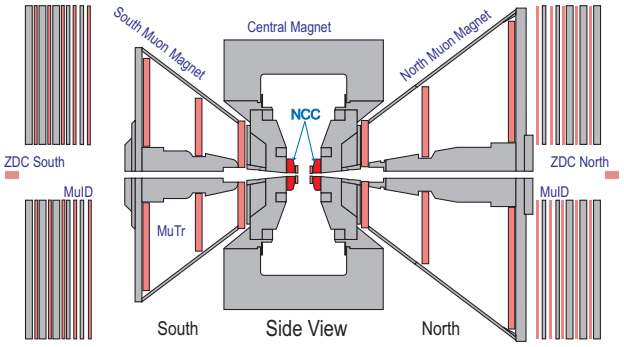

Fig. 1. Side view of PHENIX detector with nose cone brasses, which will be replaced by NCC pairs.

The NCCs are located 40 cm from the nominal collision point on both the north and south poles of the PHENIX central magnet as shown in Fig. 1 The NCCs are limited to a depth of about 20 cm, which is the depth of the present brass nose cones (hadron absorber), that will be replaced by this device. The NCCs are a combination of highly segemented electromagnetic and hadronic compartments supplemented with high-resolution position detector located downstream of the active converter (at $2X_0$, preshower detector) to count photons, and at a shower max position to measure decay asymmetries. The NCC distinguishes between electromagnetic and hadronic showers, measuring shower development over a total calorimeter depth of $\sim 40X_0$. To that effect, it is longitudinally segmented into a relatively shallow electromagnetic compartment (16 X_0, two depth segments) and a near 1-absorption-length-deep leakage segment (hadronic compartment), as shown in Fig. 2. The energy resolution is limited by the sampling fluctuations in silicon readout layers, which are interleaved between the Tungsten/Lead absorber plates.

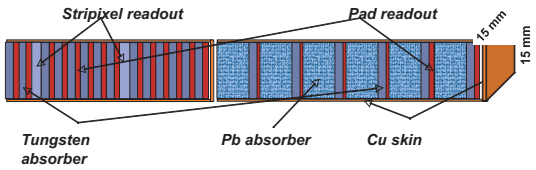

Fig. 2. Longitudinal structure of NCC.

As shown in Fig. 3, the NCC has a circular geometrical coverage within a 50 cm radius corresponding to a forwad rapidity range from 0.9 to 3.5. The calorimeter is built of 20 pad-structured silicon layers organized into towers in readout and two strip-structured silicon layers (pixelated strips[2)]) used to track individual charged particles and resolve close showers. The pad size chosen for NCC is 1.5 × 1.5 cm^2, and the strip size is 0.5 × 0.5 mm^2.

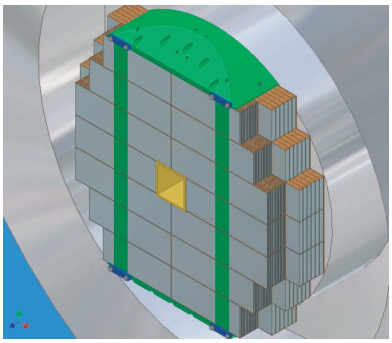

Fig. 3. 3-dimentional mechanical rendering of NCC.

The optimization of the deatiled design and the construction of the prototype tower with a full longitudinal structure are underway. The first NCC unit is scheduled to be installed and comissioned in 2010.

References

1) PHENIX proposal for a Nose Cone Calorimeter (2006).
2) Z. Li, Nucl. Inst. Meth. A518, 738 (2004).

*1 Brookhaven National Laboratory, U.S.A.
*2 University of California at Riverside, U.S.A.
*3 D.V. Skobeltyn Institute of Nuclear Physics, Russia
*4 Joint Institute for Nuclear Research, Russia
*5 Institute of Physics, Academy of Sciences of the Czech Republic, Czech

Development of a Trigger for High-p_T Charged Pions for the PHENIX Detector at RHIC

D. Kawall,[1,2]

The determination of the polarized gluon distribution function, $\Delta g(x)$, of the proton is a major objective of the PHENIX collaboration at the Relativistic Heavy Ion Collider (RHIC)[1]. Currently Δg is so poorly known that even its sign has not been determined conclusively.

Measurements of the beam helicity dependence in the production of various final states from collisions of like- and unlike-helicity protons at $\sqrt{s} = 200$ GeV can be analyzed to shed light on $\Delta g(x)$. Charged pions are an interesting final state to consider since it is expected that if $\Delta g(x) > 0$ then the double helicity asymmetry in longitudinally polarized proton collisions $_{LL}^{pp\to\pi^+X} > {}_{LL}^{pp\to\pi^0X} > {}_{LL}^{pp\to\pi^-X}$ for pions whose p_T are above several GeV/c.

Charged pions above a few GeV can fire some of the level-1 triggers in the PHENIX central arms, but with low efficiency. Examining these triggers has led to a promising, but poor statistics measurement of $_{LL}^{pp\to\pi^\pm X}$[2]. The reason for this is that all level-1 triggers currently require a hit in the Pb-glass or Pb-scintillating fiber electromagnetic calorimeters with a minimum energy deposit of 800 MeV. This is more than double what a minimum ionizing particle would leave. The calorimeters are ≈ 1 nuclear interaction length, so the probability that a charged pion will pass through without interacting is of the order of 40%, and the probably it leaves less than 800 MeV is even greater. The combination of low efficiency and high susceptibility to background suggests that other approaches to triggering be considered.

One such approach is to incorporate information from the new Hadron Blind Detector (HBD)[3] recently installed in the PHENIX interaction region. The HBD, which is now the first detector outside of the beam pipe, is essentially a windowless Cherenkov detector with a 50 cm long radiator of CF_4 at atmospheric pressure ($n \approx 1.00046$), a CsI photocathode and three stages of Gas Electron Multipliers (GEMs). The incorporation of a mesh at high voltage above the photocathode prevents the amplification of electrons produced by ionizing particles, rendering the detector blind to charged pions below the Cherenkov threshold of about 4.6 GeV/c. However, the detector is sensitive to $^\pm$ above the threshold.

The $_{LL}$ measurement of $^\pm$[2] detected $^\pm$ by looking for a hit in the calorimeter linked by a charged particle track to a hit in the the Ring Imaging Cherenkov (RICH)[4]. The latter has a threshold for charged pions of just under 5 GeV/c, so the $_{LL}$ measurement could be made for charged pions with a $p_T > 5$ GeV/c. This technique suffers because the RICH is susceptible to electrons coming from photons converted elsewhere in the detector. Also, charged hadron tracks can be wrongly associated with the RICH ring, leading to backgrounds in the $_{LL}$ measurement.

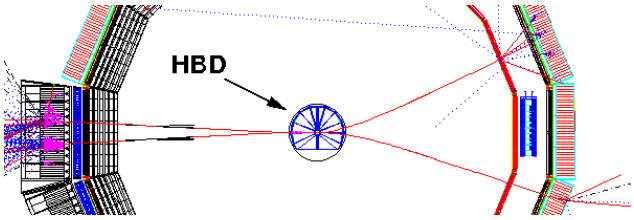

Fig. 1. Beam's eye view of the PHENIX, showing in red the tracks from 6 GeV/c $\pi^\pm$ on the left, and 1 GeV/c $\pi^\pm$ on the right. The HBD is shown in blue in the center.

The proposed new trigger involves a coincidence between hits in the HBD and RICH. This trigger should fire on $^\pm$ with $p_T > 5$ GeV/c with high efficiency, and should be clean (*i.e.* have a large rejection factor of unwanted events). Such high p_T charged pions bend very little in the magnetic field of PHENIX (see simulation in Fig. 1) so a hit in the HBD at a particular azimuthal angle can only be associated with hits in a small range in azimuth in the RICH. Low energy electrons and other backgrounds bend much more in the field and can be rejected by incorporating a lookup table in an FPGA which links hits in the HBD with an allowed range of hits in the RICH.

Currently this triggering scheme is being analyzed for its efficiency and rejection power. A large scale simulation of 5 million high p_T $^+$ and events in the PHENIX detector is underway. From this, we hope to develop the lookup table to be incorporated at level-1. If the trigger is too noisy, we can always form a triple coincidence with the calorimeter, with at least a 50% loss in efficiency but a substantial gain in rejection.

[1] RIKEN-BNL Research Center, Brookhaven National Laboratory, USA
[2] Department of Physics, University of Massachusetts, USA

References

1) G. Bunce *et al.*, Ann. Rev. Nucl. Part. Sci. **50**, 525 (2000).
2) See "Accessing the Gluon Polarization through $\pi^\pm$ A_{LL} at PHENIX", A. Morreale, C. Aidala, and K. Boyle in this volume.
3) I. Ravinovich*et al.*, Nucl. Phys. A **774**, 903 (2006).
4) Y. Akiba *et al.*, Nucl. Instrum. Meth. A **433** 143 (1999).

Spin dependent structure functions of finite nuclei†

W. Bentz,*1 I. C. Cloet,*2 and A. W. Thomas*3

[NUCLEAR STRUCTURE FUNCTIONS, Spin dependence, Effective Quark Theories]

The most famous effect which shows how the nucleon structure responds to the environment inside a nucleus is the EMC effect, which is expressed by the following ratio:

$$R_A = \frac{F_{2A}}{ZF_{2p} + NF_{2n}}\,, \tag{1}$$

where F_{2A} is the spin independent nuclear structure function, and F_{2p}, F_{2n} are the spin independent free nucleon structure functions. In this paper, we will use a mean field model for the nucleus, which incorporates the quark substructure of the nucleons, to calculate the ratio (1), and also to make predictions for the corresponding polarized EMC ratio:

$$R_{As}^{JH} = \frac{g_{1A}^{JH}}{P_p^{JH} g_{1p} + P_n^{JH} g_{1n}}\,. \tag{2}$$

Here g_{1A}^{JH} is the spin dependent structure function of a nucleus with spin J and helicity H (along the direction of the incoming electron momentum), g_{1p} and g_{1n} are the spin dependent free nucleon structure functions, and the polarization factors are defined as the expectation values of the proton and neutron spin operators in the polarized nucleus: $P_\alpha^{JH} =< J, H|2S_z^\alpha|J, H >$ $(\alpha = p, n)$. The ratios (1) and (2) are defined so that they reduce to unity in the absence of medium (including Fermi motion) effects. One important difference between the ratios (1) and (2) is that, for the latter case, in order to pin down the medium effects we need the polarization factors, which incorporate the nuclear structure effects and are not known a priori. From the experimental standpoint, if g_{1A} can be measured, one should use the most realistic polarization factors to form the ratio (2). From the theoretical standpoint, one should calculate both the numerator and denominator of (2) in the same framework.

In our calculations, we describe the single nucleon as a bound state of a quark and a scalar or axial vector diquark, following the Faddeev approach to the Nambu-Jona-Lasinio (NJL) model. This allows us to compute the single nucleon structure functions[1]. The nucleus is treated in the mean field approximation where the sources of the mean scalar and vector fields are the quarks inside the nucleons, similar in spirit to the successful quark-meson coupling model. This allows us to compute the momentum distributions of the nucleons in the nucleus. The nuclear structure function is then obtained by the convolution formalism[2].

In Figs. 1 and 2 we show the EMC ratios for the proton-hole nuclei ^{7}Li and ^{27}Al. The line which tends to have a dip for large Bjorken x refers to the ratio (2) for $H = 3/2$, while the other spin dependent ratio refers to the leading multipole ($K = 1$) combination[2] of $H = 3/2$ and $H = 1/2$. Our calculations predict that the polarized EMC effect is stronger than the unpolarized one, with the possible exception of ^{7}Li at large x. This is related to a quenching of the spin sum in the nucleus: Our calculated spin sums for a free nucleon, ^{7}Li, ^{27}Al and infinite nuclear matter are 0.67, 0.62, 0.59 and 0.49.

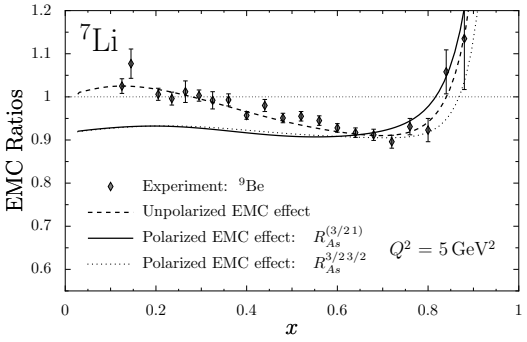

Fig. 1. Polarized (solid and dotted lines) and unpolarized (dashed line) EMC ratios for ^{7}Li.

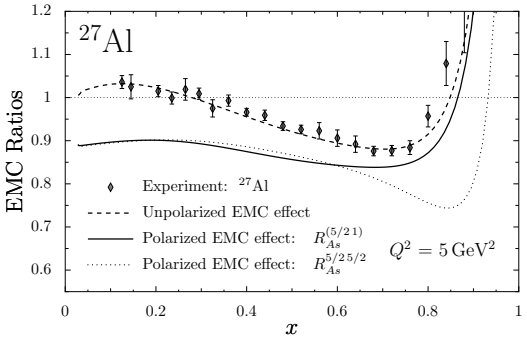

Fig. 2. Same as Fig. 1 for ^{27}Al.

References

1) I.C. Cloet, W. Bentz and A.W. Thomas, Phys. Lett. **B 621** (2005) 246.
2) R.L. Jaffe and A. Manohar, Nucl. Phys. **B 321** (1989) 343.

† Condensed from an article by I.C. Cloet, W. Bentz, and A.W. Thomas, Phys. Lett. **B 642** (2006) 210.

*1 Department of Physics, Tokai University, Kanagawa, Japan
*2 Department of Physics, University of Adelaide, Australia
*3 Jefferson Laboratories, Newport News, VA, U.S.A.

Color superconductivity and neutron star structure†

W. Bentz,[*1] S. Lawley, [*2] and A. W. Thomas,[*3]

[MATTER AT HIGH DENSITY, Compact stars]

Effective quark theories enable us to incorporate the quark structure of hadrons into the description of nuclear matter (NM) at normal densities, and at the same time to investigate the structure of compact stars, where a phase transition to quark matter (QM) may take place at high baryon densities. In this paper, we report on our recent calculations on the equation of state (EOS) of 2-flavor matter and compact star structure in the Nambu-Jona-Lasinio (NJL) model.

The single nucleon is constructed as a quark-diquark bound state, where both the scalar and the axial vector diquark channels are included. We also include the pion cloud effect on the nucleon mass, which typically leads to mass shifts (Σ_π) of 200 - 400 MeV. In this work we will consider the following cases: (A): $\Sigma_\pi = 0$ (no pion cloud); (B): $\Sigma_\pi = -200$ MeV; (C): $\Sigma_\pi = -300$ MeV; (D): $\Sigma_\pi = -400$ MeV. For each case, the strengths of the scalar and axial vector diquark interactions are adjusted so as to reproduce the experimental nucleon and delta masses.

The EOS of charge neutral NM in beta-equilibrium is then described in the mean field approximation, where the mean scalar-isoscalar, vector-isoscalar and vector-isovector fields couple to the quarks inside the nucleons, rather than to point nucleons. The most important effect of the quark substructure at normal densities is summarized in the scalar polarizability of the nucleon, which is very important for saturation[1)].

By using the same effective quark theory, we also calculate the EOS of QM, including the possibility of quark pairing (color superconductivity) in the scalar diquark channel. The Gibbs conditions (equality of pressure and chemical potentials for baryon number and isospin) are then used to investigate the transition from NM to QM[2)]. The key point in our present work is to equate the pairing strength for the color superconducting pairs in QM with the scalar diquark interactions inside the nucleons in NM. From our above discussion, it is clear that the scalar pairing strength will decrease as we go (A) → (B) → (C) → (D). Since for case (A) (no pion cloud) the scalar diquark pairing is so strong that QM would become the ground state even at normal densities, we consider this case only for the pure NM EOS.

In Fig.1 we show the pressure as a function of the baryon density for the 4 cases, and in Fig.2 we show the corresponding star masses vs. central baryon density. We see that decreasing the pairing strength has 2 effects: The phase transition moves to higher densities, and the EOS on the NM side becomes softer. The phase transition to QM leads to plateaus in the star masses, which correspond to hybrid stars with a small region of QM in the center. For the cases (B) and (C) we also get "twin" solutions at high central densities, which correspond to quark stars with radii of about 8 km.

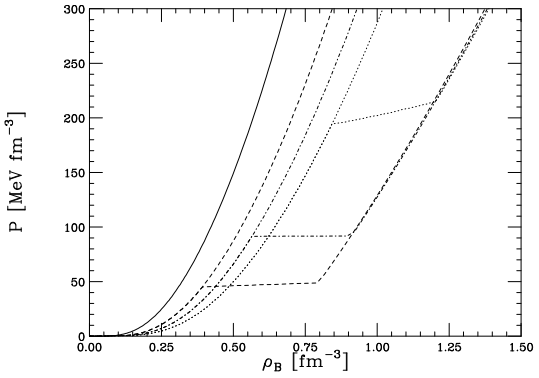

Fig. 1. Pressure vs. baryon density for the cases (A) (solid line), (B) (dashed line), (C) (dash-dotted line) and (D) (dotted line) discussed in the text.

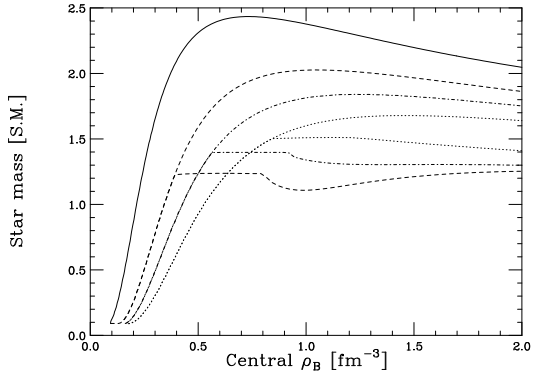

Fig. 2. Star masses vs. central density for the same cases as in Fig.1.

References

1) W. Bentz and A.W. Thomas, Nucl. Phys. **A 696**, 138 (2001).
2) S. Lawley, W. Bentz and A.W. Thomas, Phys. Lett. **B 632**, 495 (2006).

† Condensed from an article by S. Lawley, W. Bentz, and A.W. Thomas, J. Phys. **G 32**, 667 (2006).

*1 Department of Physics, Tokai University, Japan
*2 Department of Physics, University of Adelaide, Australia
*3 Jefferson Lab, Newport News, VA, U.S.A.

Isospin breaking on baryons with N_f=2 domain wall fermions†

T. Doi,[*1] T. Blum,[*1,*2] M. Hayakawa,[*3] T. Izubuchi,[*1,*4] and N. Yamada[*5,*6] (for the RBC collaboration)

In this work, we study the isospin breaking effect on baryons, such as the proton-neutron (p-n) mass difference, which is one of the most fundamental quantities in nuclear physics. In fact, this quantity governs the β-decay of the neutron, i.e., the lifetime of the neutron, and correspondingly, the nucleosynthesis and the history of the universe. In the experiment, the isospin breaking effect is observed as splitting between isomultiplets in octet/decuplet members, and also as charge symmetry breaking in the N-N interaction.

The study of isospin breaking corresponds to the determination of both the u, d quark mass difference in QCD and the electromagnetic (EM) effect in QED. The former is interesting from the viewpoint of the strong CP problem, i.e., we can examine whether massless quark(s) really exist or not. The latter also becomes an urgent task in the search for new physics beyond the standard model. For example, in the muon $g-2$ calculation, hadronic light-by-light scattering causes large uncertainty, and the QCD + QED simulation has been proposed to resolve this problem[1].

We study the EM effect on the mass difference between baryon isomultiplets as $m_p - m_n$, $m_{\Sigma^+} - m_{\Sigma^0}$, $m_{\Sigma^-} - m_{\Sigma^0}$, $m_{\Sigma^+} - m_{\Sigma^-}$, $m_{\Sigma^+} + m_{\Sigma^-} - 2m_{\Sigma^0}$, $m_{\Xi^-} - m_{\Xi^0}$ using the QCD + QED simulation. Our study for the meson sector is given in Ref.[2] In the QCD sector, we use the N_f=2 unquenched QCD configurations[3] generated by the domain-wall fermion and the DBW2 gauge action with the parameters of $V = 16^3 \times 32$, $L_s = 12$, $M_5 = 1.8, \beta = 0.8$ and $m_{\rm sea} = 0.02, 0.03, 0.04$. We pick up about 200 configurations at each sea quark mass. In the QED sector, we employ a noncompact formulation at the quenched level[4]. The advantage of this formulation is that there is no autocorrelation between the configuration even for an arbitrary small coupling and that there is no need for the renormalization of QED coupling $\alpha_{\rm em} \equiv e^2/4\pi$, because the photon dynamics becomes a free theory. In order to study the QED charge dependence, we use not only the physical QED charge but also the charges of $e = (0), 0.6, 0.85, 1.0$. The baryon mass is measured using the two-point correlator. In the $Q = 0, S = -1$ channel, the variational method is used to extract Σ^0 as the first excited state in this channel.

Because the isospin breaking has a rather small effect on the mass (δm(breaking) $\sim$ 1MeV vs $m \sim$ 1GeV), it is necessary to explore an effective way of improving S/N. For this purpose, we analyze the ratio between the correlators of the isomultiplets. Considering the p-n for instance, we can express $R_{p/n}(t) \equiv \Pi_{pp}(t)/\Pi_{nn}(t) = 1 + 2(\lambda_p - \lambda_n)/(\lambda_p + \lambda_n) - (m_p - m_n) \cdot t + \mathcal{O}(e^4)$, where λ_p (λ_n) is the proton (neutron) overlap constant between the state and the operator. The plot of $R_{p/n}(t)$ is given on the left-hand side of Fig. 1. Unfortunately, S/N is not so good as to allow us to make a conclusive statement.

In order to overcome the above difficulty, we examine the origin of the fluctuation in the lattice result. In particular, we focus on the $\mathcal{O}(e)$ contamination in the correlator, which is nothing but statistical noise because the EM effect on observables appears only from $\mathcal{O}(e^2)$. In order to eliminate $\mathcal{O}(e)$ contamination, we evaluate the correlator for not only $e = +|e|$ but also $e = -|e|$, and take the average between them. This corresponds to the use of the QED configuration of $\{A_\mu^{\rm QED}\} \to \{A_\mu^{\rm QED}, -A_\mu^{\rm QED}\}$ with binning. The result is shown on the right-hand side of Fig. 1. We observe a clear negative linear slope for each QED charge, which indicates $m_p > m_n$ from the EM effect. It is found that $\mathcal{O}(e)$ contamination is the dominant source of the fluctuation, and that $e = \pm|e|$ average is the essential procedure. We also observe that this procedure is effective for studying isospin breaking in the meson sector as well. As a result of the marked success of S/N improvement, we can determine the EM effect precisely. The determination of the EM effect, as well as the u, d quark mass difference effect, is in progress.

References

1) M. Hayakawa, T. Blum, T. Izubuchi and N. Yamada, PoS LAT2005, 353 (2006), hep-lat/0509016.
2) N. Yamada, T. Blum, M. Hayakawa and T. Izubuchi (RBC), PoS LAT2005, 092 (2006), hep-lat/0509024.
3) Y. Aoki *et al.*, (RBC), Phys. Rev. **D72**, 114505 (2005).
4) A. Duncan, E. Eichten and H. Thacker, Phys. Rev. Lett. **76**, 3894 (1996); *ibid.* Phys. Lett. **B409**, 387 (1997).

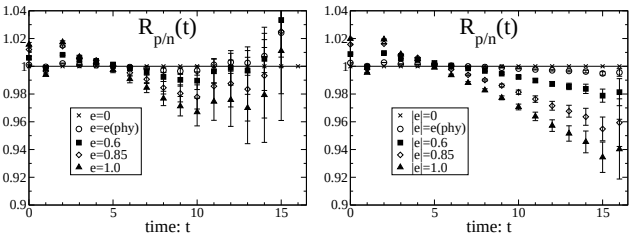

Fig. 1. Ratio of correlators of proton and neutron $R_{p/n}$ at $m_{\rm sea}$=0.03 against t for each QED charge e. The left (right) figure is obtained with $e = |e|$ ($e = \pm|e|$).

† Condensed from the article in PoS LAT2006, 174 (2007)

*1 RIKEN BNL Research Center, Brookhaven National Lab.
*2 Physics Department, University of Connecticut
*3 Department of Physics, Nagoya University
*4 Institute for Theoretical Physics, Kanazawa University
*5 High Energy Accelerator Research Organization (KEK)
*6 The Graduate University for Advanced Studies (Sokendai)

Initial Singularity in the Little Bang

K. Fukushima, F. Gelis[*1] and L. McLerran[*2]

[Color Glass Condensate, heavy-ion collision, instability, quantum fluctuation]

The Color Glass Condensate (CGC) provides a description of the wave function of a hadron at very small values of x. The CGC is a high-density state of gluons that is controlled by a weak coupling because of the high gluon density. Its properties are computable from first principles in Quantum Chromodynamics (QCD), at least in the limit of extremely high density.

The CGC has also been applied to heavy-ion collisions to generate the initial conditions for the evolution of matter in the forward light cone[1)]. There are boost-invariant solutions of the equations of motion supposedly appropriate for the high-energy limit. It has recently been discovered[2)], however, that the boost-invariant solution of the equations of motion are unstable with respect to rapidity-dependent perturbations. This instability has, in fact, close connections with the Weibel instabilities encountered in the physics of anisotropic plasmas, and it is speculated that such an instability may help the system created after heavy-ion collisions reach a state of local equilibrium.

The evolution from the initial collision to the final state is shown in Fig. 1. Because of the similarities between the expansion of the universe in cosmology and the expansion of matter in heavy-ion collisions, we call the latter the "little bang". The initial singularity in cosmology is replaced by the singularity in the classical equations of motion associated with the collision. It is in the forward light cone that instabilities develop, and there could be a Kolmogorov spectrum of density fluctuations generated. This spectrum is similar to the spectrum of density fluctuations generated during inflationary cosmology. After inflation, the system reheats and thermalizes, forming an electroweak plasma. In the little bang, thermalization might also be achieved after the expansion in the forward light cone.

In this work, we discuss a generic approximation scheme for calculating the quantum expectation value of an observable that depends on field configurations at late times. In the WKB approximation, we obtained a formula giving this expectation value from the classical equations of motion, with an initial condition that includes fluctuations. The spectrum of these initial fluctuations is described by the Wigner transform of the wave function, the latter being obtained as a ground-state solution of the Schrödinger equation.

An application of particular interest to heavy-ion collisions is to calculate the Wigner function of these

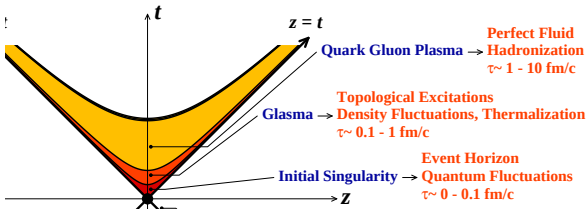

Fig. 1. A light-cone diagram illustrating the evolution of matter produced in heavy-ion collisions.

fluctuations immediately after the initial impact of the two nuclei in the weak-coupling regime. These initial quantum fluctuations provide the seeds that trigger the instability of the rapidity-dependent modes. The precise determination of initial fluctuations or seeds is of crucial importance for the estimate of the growth rate of the unstable modes.

By identifying the physically relevant gauge fluctuations and the singularity in the Hamiltonian density, we derived the discontinuity between the wave functions in the backward and forward light cones. It turns out that the initial singularity results only in a shift in the transverse gauge fields by the classical background field.

This wave function and the resultant Wigner function describe the spectrum of initial fluctuations. There are two noteworthy features in our results.

Firstly, both the transverse gauge fields and their canonical momenta fluctuate with 2-point correlations that are inversely related to one another. This means that if the boost invariance is significantly violated by momentum fluctuations, then gauge-field fluctuations are suppressed, and vice versa. Thus, the prescription, in which only momentum fluctuations are taken into account[2)], needs to be extended to include gauge-field fluctuations also.

Secondly, the off-diagonal correlation between different transverse components does not vanish. Again, this feature was not apparent in the preceding study[2)].

References

1) T. Lappi and L. McLerran: Nucl. Phys. A**772**, 200 (2006).
2) P. Romatschke and R. Venugopalan: Phys. Rev. Lett. **96**, 062302 (2006).

† Condensed from the article in hep-ph/0610416.

*1 Service de Physique Théorique, Saclay, France
*2 Department of Physics, Brookhaven National Lab., USA

Heavy Quarkonium States in a Gluon Plasma

Ágnes Mócsy and Péter Petreczky*1

"Melting" of heavy quarkonium has been long been thought of as an unambiguous signature of a transition to deconfined matter in finite temperature QCD[1]. This in turn would translate into the suppression of the J/ψ peak in the dilepton spectrum, providing an experimentally detectable signal for deconfinement. This signature has been looked for in relativistic heavy ion collisions at SPS-CERN and RHIC-BNL[2].

Recently available quarkonia studies performed in lattice QCD suggest however that the J/ψ not only survives to temperatures much higher than the deconfinement transition temperature, but also that its properties (mass, amplitude) are unchanged up to at least $1.5T_c$[3].

We investigated the source of this unexpected discrepancy by determining the spectral functions and current-current correlators in the different quarkonia channels - these being the quantities obtained on the lattice. We assumed that the interaction between the heavy quark and antiquark is described by a temperature-dependent potential - as customarily used in the potential model studies also yielding the original predictions.

In our initial studies[4,5] we design a spectral function that includes bound states, as well as the perturbative continuum above some threshold. The temperature-dependence of the quarkonium properties is obtained by solving the two-body Schrodinger equation with a temperature-dependent potential. While a description in terms of the Schrodinger equation is in order, since the heavy quark mass allows for a nonrelativistic treatment of the quarkonium, the use of a potential description of the interaction between the quark and the antiquark is highly questionable at finite temperature. The validity of potential models is restricted to the case when the interaction between the heavy quark and antiquark is instantaneous, i.e. the gluon-exchange between the quarks is much faster than the internal time-scale of the bound state. At zero temperature this condition is given by the hierarchy of energy scales which also allows for the derivation of the Cornell-potential directly from QCD[6]. Whether such condition is fulfilled at finite temperature is not at all clear, and requires further QCD-based studies, that are not yet available. Due to a lack of knowledge different assumed potentials are used in the literature, such as a screened Cornell potential, the free- and the internal-energy of a heavy quark-antiquark pair as determined on the lattice, and also a combination of these energies. In view of these uncertainties our results are not surprising: we found that the correlators and spectral functions in the vector and pseudoscalar quarkonium channels as determined in our calculations show a behavior not seen in the lattice QCD results.

In a refined analysis we further investigated the behavior of the quarkonium states at finite temperature by replacing the two-body Schrodinger calculation with a full Green's function analysis. This is necessary in order to take into account multi-particle effects and have a consistent description of bound- and scattering states, as well as threshold effects. The spectral functions obtained from the nonrelativistic Green's function calculation together with the nonrelativistic perturbative continuum at high energies, and the correlators calculated from these, again, show disagreement with the lattice data. We identify as the source for disagreement the strong modification of the ground state properties. This is an intrinsic outcome of all the screened potentials. If however, the ground state would stay unchanged, as suggested by the lattice spectral function data, then the behavior of lattice correlators can be recovered from the model calculations. In this case the melting of the higher excited states is compensated for by the decrease of the continuum threshold with increasing temperature. This result is consistent with our study based on a simple toy model[10].

*1 Physics Department and RIKEN-BNL Research Center, Brookhaven National Laboratory, Upton, NY, USA

References

1) T. Matsui and H. Satz, Phys. Lett. B **178**, 416 (1986).
2) P. Cortese *et al.* [NA50 Collaboration], J. Phys. G **31** (2005) S809; R. Arnaldi *et al.* [NA60 Collaboration], Eur. Phys. J. C **43** (2005) 167; M. Calderon de la Barca Sanchez, arXiv:nucl-ex/0606009; R. G. de Cassagnac [the PHENIX Collaboration], arXiv:nucl-ex/0608041.
3) Most recent results: A. Jakovac, P. Petreczky, K. Petrov and A. Velytsky, Phys. Rev. D **75**, 014506 (2007) [arXiv:hep-lat/0611017].
4) Á.Mócsy and P.Petreczky, Eur. Phys. J. C **43**, 77 (2005) [arXiv:hep-ph/0411262].
5) Á. Mócsy and P. Petreczky, Phys. Rev. D **73**, 074007 (2006) [arXiv:hep-ph/0512156].
6) N. Brambilla *et al.*, arXiv:hep-ph/0412158, and references therein.
7) E. V. Shuryak and I. Zahed, Phys. Rev. C **70**, 021901 (2004); Phys. Rev. D **70**, 054507 (2004); C. Y. Wong, Phys. Rev. C **72**, 034906 (2005); W.M.Alberico et al, Phys. Rev. D **72**, 114011 (2005); M.Mannarelli and R.Rapp, arXiv:hep-ph/0509310.
8) Á. Mócsy and P. Petreczky, arXiv:hep-ph/0606053.
9) Á. Mócsy, P. Petreczky and J. Casalderrey-Solana, arXiv:hep-ph/0609205.
10) Á. Mócsy, arXiv:hep-ph/0606124.

Nucleon structure in lattice QCD with dynamical domain-wall fermions

S. Ohta,[*1*2*3]

[Hadron structure, Quantum Chromodynamics]

I summarize lattice quantum chromodynamics numerical calculations of nucleon structure done in the past year using parallel supercomputers at RIKEN-BNL Research Center. The calculations are parts of the RIKEN-BNL-Columbia (RBC) Collaboration and RBC-UKQCD Intercollaboration.

The RBC collaboration have been calculating various form factors and moments of structure functions of nucleon in numerical lattice QCD with domain-wall fermion (DWF) quarks. In contrast to more conventional lattice fermions such as Wilson or staggered, the DWF preserves the important chiral and flavor symmetries. With quenched calculations we demonstrated the importance of these symmetries near the chiral limit[1)], in reproducing the mass of nucleon and its parity partner[2)], and in calculating meson decay constants[3)] and nucleon form factors[4)] and structure functions[5)].

Here we report two sets of calculations[6)]: one with RBC ensembles with two degenerate dynamical DWF flavors corresponding to up and down, and another with RBC-UKQCD ensembles with one strange and two degenerate (up and down) dynamical DWF flavors. The former was completed using the QCDSP computer and has about 200 gauge configurations at each of the three up/down mass values[7)]. The latter is still on-going on the QCDOC computer and has 20-30 gauge configurations at each of the three up/down mass values while the strange mass is fixed at about the physical value[8,9)].

In Figure 1 we present the ratio of the isovector axial and vector charges, g_A/g_V, for both sets of calculations plotted against the calculated pion mass squared. This ratio is naturally renormailized when calculated with DWF, and so is directly comparable with experiment. The results show mild dependence on the pion mass squared which is linear in up/down quark mass near the chiral limit. If fitted with a linear behavior, we obtain a value of g_A/g_V consistent with the experiment.

Also in Figure 1 we present the ratio of the first moments of two structure functions, $\langle x\rangle_{u-d}/\langle x\rangle_{\Delta u-\Delta d}$ or the ratio of the momentum and helicity fractions of quarks, again for both sets of calculations plotted against the calculated pion mass squared. Again the ratio is naturally renormailized when calculated with DWF, and so is directly comparable with experiment.

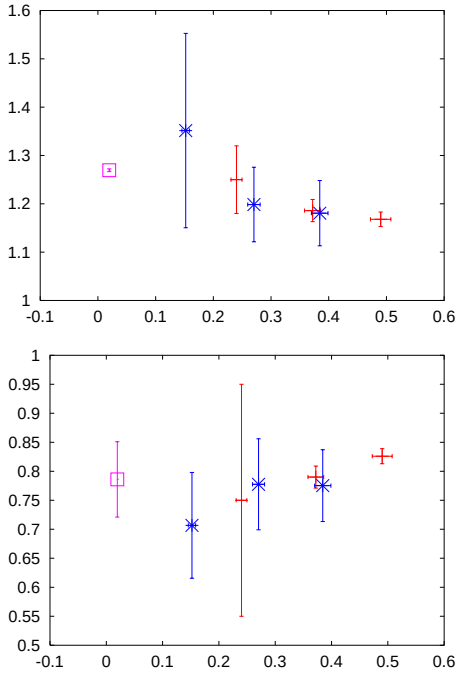

Fig. 1. Above: ratio of the isovector axial and vector charges of nucleon, g_A/g_V. Below: ratio of the momentum and helicity fractions of quarks within nucleon. Both plotted against the calculated pion mass squared in $(\mathrm{GeV})^2$. The RBC 2-flavor results are denoted by red + symbols while the RBC-UKQCD (2+1)-flavor results are by blue ×. The experiments are in purple □.

The results show mild dependence on the pion mass squared, and is in broad agreement with experiments.

I thank the members of the RBC, UKQCD and QCDOC collaborations.

References

1) Blum, T. et al. *Phys. Rev.* **D69**, 074502 (2004).
2) Sasaki, S., Blum, T., and Ohta, S. *Phys. Rev.* **D65**, 074503 (2002).
3) Blum, T. et al. *Phys. Rev.* **D68**, 114506 (2003).
4) Sasaki, S., Orginos, K., Ohta, S., and Blum, T. *Phys. Rev.* **D68**, 054509 (2003).
5) Orginos, K., Blum, T., and Ohta, S. *Phys. Rev.* **D73**, 094503 (2006).
6) Lin, H.-W. and Ohta, S. *PoS* **LAT2006**, 118 (to be published).
7) Aoki, Y. et al. *Phys. Rev.* **D72**, 114505 (2005).
8) Lin, M. *PoS* **LAT2006**, 185 (to be published).
9) Tweedie, R. *PoS* **LAT2006**, 096 (to be published).

*1 Institute of Particle and Nuclear Studies, KEK
*2 RIKEN-BNL Research Center, BNL, USA
*3 Department of Physics, SOKENDAI

Finite temperature transition in three flavor QCD

P. Petreczky,[*1]

Lattice QCD has established the existence of a transition from hadron gas to a new state of strongly interacting matter where quarks and gluons are no longer confined inside hadrons and which is usually called the Quark Gluon Plasma[1,2]. The nature of this transition depends on the quark content and quark masses. For infinite or very large quark masses the transition is a 1st order deconfining transition. In the opposite case of zero quark masses one may have a 2nd order chiral phase transition for 2 flavors or a 1st order chiral phase transition for 3 flavors. For arbitrary masses the transition is just a rapid crossover, meaning that thermodynamic quantities change very rapidly in a narrow temperature interval. The boundary of the 1st order transition region of 3-flavor QCD as a function of mass has been studied using improved (p4)[3] and standard staggered actions[4,6]. There is a significant discrepancy regarding the value of the quark masses, or equivalently the value of the pseudo-scalar meson masses where the transition changes from crossover to 1st order. With an improved action it was found that the 1st order transition ends for pseudo-scalar meson masses of about 70 MeV, while with the standard action it ends for pseudo-scalar meson masses of about 190 MeV[4,5] or larger[6].

We investigate the finite temperature transition in 3 flavor QCD using the improved staggered p4 action and the standard R algorithm. Numerical calculations have been done on lattices with temporal extent $N_\tau = 4$ and 6 and at several values of the quark mass. We use the Polyakov susceptibility and the disconnected part of the chiral susceptibility to locate the pseudo-critical gauge coupling β_c. To set the lattice spacing we use the Sommer scale defined from the static potential as $r^2 dV/dr|_r = r_0 = 1.65$. Thus we determined the transition temperature in units of the Sommer scale, i.e. $r_0 T_c$. The quark masses used in our study correspond for pseudo-scalar meson masses $m_{ps} r_0 = 0.4 - 1.45$ for $N_\tau = 4$ lattices and $m_{ps} r_0 = 0.8$ and 1.25 for $N_\tau = 6$ lattices. We find no evidence for a 1st order phase transition for these quark masses. Since we have the value of the transition temperature for two different lattice spacings and quark masses we attempted a combined extrapolation to the continuum and chiral limit. We expect that the finite lattice spacing errors should scale as $\mathcal{O}(a^2)$ and thus the lattice errors in $T_c r_0$ should scale as $1/N_\tau^2$. If there is a critical point in the (T, m)-plane, then universality dictates that $T_c(m) - T_c(m^e) \sim (m - m^e)^{1/(\delta\beta)}$ with β and δ being critical exponents. In the case of three degenerate flavors the line of the 1st order transition in the $T-m$ plane ends in a critical end-point $T_c(m^e)$ belonging to the Z(2) universality class. For this universality class we have $\delta\beta = 1.5654$. Therefore we attempted a combined continuum and chiral extrapolation using the following extrapolation ansatz

$$r_0 T_c(m_{ps}, N_\tau) = r_0 T_c|_{cont}(m^e_{ps}) + A r_0^2 \left(m^2_{ps} - m^2_{ps,c}\right)^{1/(\delta\beta)} + B/N_\tau^2. \quad (1)$$

The value of the quark mass where the transition changes from 1st order to crossover, i.e. the mass corresponding to the end-point, has been estimated using $N_\tau = 4$ lattices to be $m^e = 0.0007(4)$[3]. This translates into the value of the pseudo-scalar mass $r_0 m^e_{ps} = 0.16^{+3}_{-5}$. The cutoff dependence of m^e_{ps} is expected to be smaller than the statistical error. It turns out that this large uncertainty in the value of m^e_{ps} produces an uncertainty in the extrapolated value of $T_c(m^2_{ps})$ which is much smaller than the statistical errors. The extrapolation according to Eq. (1) yields $r_0 T_c(m^e_{ps}) = 0.429(8)$ with $\chi^2/dof = 0.7$.

The value of T_c could be compared with the corresponding $2+1$ flavor value $T_c r_0 = 0.444(6)[+12][-6]$ in the chiral limit[7]. Thus the flavor dependence of T_c is about or smaller than 5%. One should also note that the difference between the transition temperature calculated on $N_\tau = 4$ and $N_\tau = 6$ lattices is very similar to that found in 2+1 flavor case[7]. The results presented in this report are based on work done with RBC-Bielefeld Collaboration. The majority of the calculations reported here were carried out using the QCDOC supercomputers of the RIKEN-BNL Research Center and the U.S. DOE. In addition some of the work was done using the APE1000 supercomputer at Bielefeld University.

[*1] Physics Department and RIKEN-BNL Research Center, Brookhaven National Laboratory, Upton, NY, USA

References

1) F. Karsch, Lect. Notes Phys. **583**, 209 (2002)
2) E. Laermann and O. Philipsen, Ann. Rev. Nucl. Part. Sci. **53**, 163 (2003)
3) F. Karsch, et al., Nucl. Phys. Proc. Suppl. **129**, 614 (2004)
4) C. Schmidt, C. R. Allton, S. Ejiri, S. J. Hands, O. Kaczmarek, F. Karsch and E. Laermann, Nucl. Phys. Proc. Suppl. **119**, 517 (2003) [arXiv:hep-lat/0209009]. F. Karsch, E. Laermann and C. Schmidt, Phys. Lett. B **520**, 41 (2001)
5) P. de Forcrand and O. Philipsen, Nucl. Phys. Proc. Suppl. **129**, 521 (2004) P. de Forcrand and O. Philipsen, Nucl. Phys. Proc. Suppl. **129**, 521 (2004)
6) N.H. Christ and X. Liao, Nucl. Phys. B (Proc. Suppl.) **119**, 514 (2003)
7) M. Cheng *et al.*, Phys. Rev. D **74**, 054507 (2006)

Automatic O(a) improvement for twisted-mass QCD†

S. Aoki*1,*2 and O. Bär*3

[Lattice QCD, twisted-mass, improvement]

It becomes more and more apparent that twisted mass Lattice QCD (tmLQCD)[1,2] is a promising formulation to approach the chiral limit of QCD. A twisted mass protects the Wilson-Dirac operator against small eigenvalues and therefore solves the problem of exceptional configurations,thus making numerical simulations with small quark masses feasible.This numerical advantage of tmLQCD is supplemented by the property of automatic O(a) improvement[3]. The so-called "maximal twist" condition, required for the proof of automatic O(a) improvement[3], however, causes some confusions[4]. Therefore, in this report, we reconsider the proof of the automatic O(a) improvement of tmLQCD[5], by clarifying an exact condition for the maximal twist.

We give a main idea of the proof. The lattice theory can be described by an effective continuum theory, whose effective action is restricted by locality and symmetries of the underlying lattice theory. Taking into account the symmetries such as U(1)⊗U(1) vector symmetry, the extended parity symmetry and the standard charge conjugation symmetry, one finds $S_{\rm eff} = S_0 + aS_1 + a^2S_2 + \cdots$ for the quark part, where

$$S_0 = \int d^4x\, \bar\psi(x) \left[\gamma_\mu D_\mu + M_R e^{i\theta\gamma_5\tau^3}\right] \psi(x), \qquad (1)$$

$$S_1 = C_1 \int d^4x\, \bar\psi(x)\sigma_{\mu\nu}F_{\mu\nu}(x)\psi(x). \qquad (2)$$

In addition to the effective action we have to specify the direction of the chiral condensate, since chiral symmetry is spontaneously broken. From the fact that the direction of the chiral condensate is completely controlled by the direction of the symmetry breaking external field in the continuum theory, we can take

$$\langle \bar\psi^i_\alpha \psi^j_\beta \rangle_{S_0} = \frac{v(M_R)}{8} \left[e^{-i\theta\gamma_5\tau^3}\right]^{ji}_{\beta\alpha}, \qquad (3)$$

where $\lim_{M_R\to 0}\lim_{V\to\infty} v(M_R) \neq 0$. Here the vacuum expectation value (VEV) is defined with respect to the continuum action S_0.

We now want to argue that the choice $\theta = \pi/2$ (or $-\pi/2$) corresponds to "maximal twist". In terms of the mass parameters this is equivalent to $\mu_R = M_R$ and $m_R = 0$, where $m_R = M_R\cos\theta$ and $\mu_R = M_R\sin\theta$. In this case the action and the VEVs become

$$S_0 = \int d^4x\, \bar\psi(x) \left[\gamma_\mu D_\mu + iM_R\gamma_5\tau^3\right] \psi(x), \qquad (4)$$

$\langle\bar\psi\psi\rangle_{S_0} = 0$, $\langle\bar\psi i\gamma_5\tau^3\psi\rangle_{S_0} = v(M_R)$. It is easy to check that S_0, the continuum part of the effective action is invariant under $\psi \to e^{iw\gamma_5\tau^{1,2}}\psi$, $\bar\psi \to \bar\psi e^{iw\gamma_5\tau^{1,2}}$, and therefore also under the Z_2 subgroup T_1 of this continuous transformation, defined by $T_1\psi = i\gamma_5\tau^1\psi$, $T_1\bar\psi = \bar\psi i\gamma_5\tau^1$. Since $T_1^2 = 1$ in the space of fermion number conserving operators, which contain equal numbers of ψ and $\bar\psi$, the eigenvalues of T_1 are 1 (T_1-even) or -1 (T_1-odd). The crucial observation is that the VEVs $\langle\bar\psi\psi\rangle$ and $\langle\bar\psi i\gamma_5\tau^3\psi\rangle$ are also invariant under this transformation. The T_1 symmetry is *not* spontaneously broken, hence it is an exact symmetry of the continuum theory. The O(a) term $aS_1 = aC_1\int d^4x\ \bar\psi(x)\sigma_{\mu\nu}F_{\mu\nu}(x)\psi(x)$, on the other hand, is odd under T_1. Therefore, non-vanishing physical observables, which must be even under T_1, can not have an O(a) contribution, since the O(a) term is odd under T_1 and therefore must vanish identically. This is automatic O(a) improvement at "maximal twist". Note that non-invariant, i.e. T_1-odd quantities, which vanish in the continuum limit, can have O(a) contributions.

The above argument gives just the main idea of our proof for automatic O(a) improvement, and we have already given a detailed proof in Ref.[5]. However, one of the most important points of our analysis is that the condition for automatic O(a) improvement is the invariance of theory under T_1 transformation, or more generally its continuous version, which corresponds to a part of the exact vector symmetry in continuum QCD at "maximal twist". One might even say that the T_1 invariance is more fundamental for automatic $O(a)$ improvement than the notion of "maximal twist", which is one of the consequences of T_1 invariance.

This work is supported in part by the Grants-in-Aid for Scientific Research from the Ministry of Education, Culture, Sports, Science and Technology. (Nos. 13135204, 15204015, 15540251, 16028201), O. B. is supported in part by the University of Tsukuba Research Project.

References

1) R. Frezzotti, S. Sint and P. Weisz, JHEP **07** (2001) 048.
2) R. Frezzotti, P. A. Grassi, S. Sint and P. Weisz, JHEP **08** (2001) 058.
3) R. Frezzotti and G. C. Rossi, JHEP **10** (2004) 070.
4) S. Aoki and O. Bär, Phys. Rev. **D70** (2004) 116011.
5) S. Aoki and O. Bär, Phys. Rev. **D74** (2006) 034511.

† Condensed from the article in Phys. Rev. D74, 034511 (2006)

*1 Graduate School of Pure and Applied Sciences, University of Tsukuba, Tsukuba, Ibaraki 305-8571, Japan
*2 Riken BNL Research Center, Brookhaven National Laboratory, Upton, NY 11973, USA
*3 Institute of Physics, Humboldt University Berlin, Newtonstrasse 15, 12489 Berlin, Germany

Proton decay matrix elements with $N_f = 0$ and 2 domain-wall QCD†

Y. Aoki, C. Dawson, J. Noaki,*1 A. Soni,*2

[Lattice QCD, grand unified theories]

Proton decay, once observed, is a smoking gun evidence of the physics beyond the standard model. It naturally happens under (SUSY) GUT. On-going deep mine experiments, though yet to observe an event, are pushing up the lower bound of of the proton lifetime, excluding GUT models which allow protons decay more frequently. Hadronic matrix elements of the proton decay are essential ingredients in estimating lifetime of proton. Lattice QCD provides the most reliable estimate for such low energy hadronic quantities.

There are two ways to calculate the matrix elements on the lattice: the direct calculation using three point functions and the indirect calculation which uses chiral perturbation theory with two low energy parameters (α and β) to be calculated on the lattice. The indirect calculation is nothing but an approximation at the lowest order in the final state pion energy, which is order of the nucleon mass in CM frame, thus quite large. As such, it is expected to have limited applicability on the matrix elements in the physical kinematics, though historically this approach dominates over the direct calculation, which requires typically a factor of 10 more computation than the indirect calculation.

Until quite recent, even for the easier indirect calculation, lattice results of the low energy parameters from different groups have not converged to the common values. The failure could be ascribed to lattice-intrinsic systematic errors.

This study aims to remove many of the systematic errors, and it has been quite successful. We have developed a method of non-perturbative renormalization (NPR) of the proton-decay operators by the Rome-Southampton RI/MOM scheme. Using the NPR, ambiguity of the lattice perturbation has been completely removed. The usage of domain-wall fermion reduced the discretization error which is demonstrated in Fig. 1 for the low energy parameter. Fig. 2 summarizes our result of the relevant form factors for each decay process in quenched approximation. Both results with the direct and indirect calculations are shown. Any matrix element of nucleon decaying to pseudoscalar meson via four-fermion operator can be calculated from those shown in the figure. It is noted that the indirect method poorly approximates the values by the direct method. Especially for the final-pion matrix elements the indirect method overestimates by an approximate

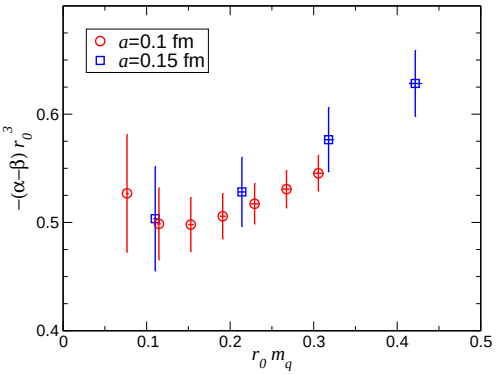

Fig. 1. The low energy parameter of proton decay as a function of the quark mass in quenched approximation with DWF. Both axes have been normalized by r_0 ($r_0 \simeq 0.5$ fm) to be dimension-less. Results from two different lattice spacings are consistent.

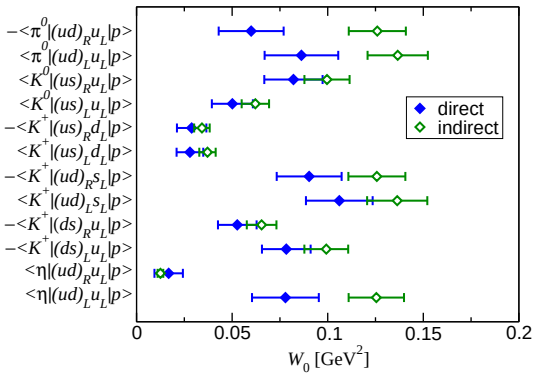

Fig. 2. Relevant form factors W_0 of the proton decay matrix elements in the quenched approximation. Operators have been matched to $\overline{\text{MS}}$, NDR at $\mu = 2$ GeV to NLO, using NPR.

factor of 2, which shortens the proton lifetime by a factor of 4.

There could still be a systematic error due to quenched approximation. To remove it, we need to perform the direct calculation with the three-flavor dynamical fermions. As a first step toward this ultimate goal, we have investigated the dynamical fermion effects on the low energy parameters using the two-flavor dynamical DWF configurations. So far, the values are consistent with those with the quenched approximation,[1] although the statistical errors are still large.

† Condensed from the article[1].

*1 High Energy Accelerator Research Organization (KEK)
*2 Brookhaven National Laboratory

References

1) Y. Aoki et al., Phys. Rev. D75 (2007) 014507.

Lattice QCD with dynamical overlap fermions

JLQCD Collaboration: S. Aoki,[*1] H. Fukaya,[*2] S. Hashimoto,[*3,*4] K.-I. Ishikawa,[*5] K. Kanaya,[1] T. Kaneko,[*3,*4] H. Matsufuru,[*3] K. Ogawa,[*6] M. Okamoto,[*3] M. Okawa,[*5] T. Onogi,[*7] A. Ukawa,[*1,*8] N. Yamada,[*3,*4] and T. Yoshie,[*1,*8]

[Lattice gauge theory, chiral symmetry]

The lattice gauge theory has become one of the standard methods to evaluate the non-perturbative phenomena of QCD. In the previous works, many low-energy quantities, such as hadron spectrum, matrix elements etc. have been calculated by the numerical simulations. Their results, however, have sizable uncertainties due to the use of Dirac operator which breaks chiral symmetry and the difficulty in reaching the chiral limit.

Although it is known that the overlap Dirac operator (the overlap fermion) can realize an exact chiral symmetry on the lattice, no numerical study with $N_f \neq 0$ dynamical quarks could employ it so far except for very small size lattices, because of the large numerical cost of the overlap Dirac operator itself, and another theoretical problem that the fermion determinant is not continuous, which requires an extra numerical cost proportional to the volume squared.

The latter problem is due to the fact that the QCD vacuum is a mixture of di erent topological sectors. In 1), we studied several gauge actions that automatically satisfy Lüscher's admissibility condition which require the lattice gauge elds to be smooth and the topological charge to be conserved. We found the additional 2- avor Wilson fermion and ghost with a cut-o scale mass can completely prevent the discontinuity of the fermion determinant and their e ect on the low-energy is small.

At KEK, the supercomputer was replaced by a multiple system of Hitachi SR11000 and IBM Blue Gene/L with a total peak speed of around 60TFLOPS. Now, we can perform the dynamical overlap fermion simulations with our topology preserving method. We have carried out the large-scale simulations with 2- avor overlap quarks with sea quark masses down to quarter of the strange quark mass or smaller[2]. The lattice size is $16^3 \times 32$ and the lattice spacing is around 0.125fm. As one of preliminary results, the pion mass is plotted in Fig.1, which shows the chiral behavior is really good and consistent with the well-known prediction of the chiral perturbation theory at tree level;

$$m_{\rm PS}^2 \propto m_{\rm sea}\Sigma/F_\pi^2, \tag{1}$$

where $m_{\rm PS}^2$ is the pion mass, $m_{\rm sea}$ is the quark mass, Σ denotes the chiral condensate and F_π is the pion decay constant.

The exact and quantum-level chiral symmetry has been achieved by the overlap Dirac operator and the topology preserving determinant in the numerical simulations. Many dramatic results are expected to appear soon[3–6] .

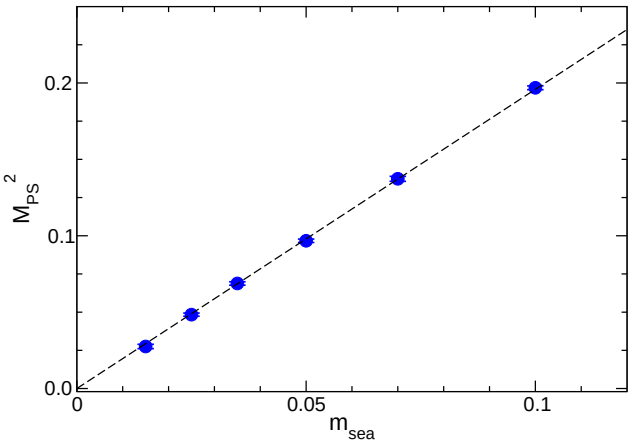

Fig. 1. Chiral extrapolation of the pseudo-scalar (pion) mass.

*1 Graduate School of Pure and Applied Sciences, University of Tsukuba
*2 Theoretical Physics Laboratory, RIKEN
*3 High Energy Accelerator Research Organization (KEK)
*4 School of High Energy Accelerator Science, The Graduate University for Advanced Studies(Sokendai)
*5 Department of Physics, Hiroshima University
*6 Department of Physics, National Taiwan University
*7 Yukawa Institute for Theoretical Physics, Kyoto University
*8 Center of Computational Science, University of Tsukuba

References

1) H. Fukaya, S. Hashimoto, K. I. Ishikawa, T. Kaneko, H. Matsufuru, T. Onogi and N. Yamada [JLQCD Collaboration], Phys. Rev. D **74**, 094505 (2006) [arXiv:hep-lat/0607020].
2) T. Kaneko *et al.* [JLQCD Collaboration], arXiv:hep-lat/0610036.
3) N. Yamada *et al.* [JLQCD Collaboration], "Mobility edge and locality of the overlap-Dirac operator with and without arXiv:hep-lat/0609073.
4) S. Hashimoto *et al.* [JLQCD Collaboration], arXiv:hep-lat/0610011.
5) H. Fukaya *et al.* [JLQCD Collaboration], arXiv:hep-lat/0610024.
6) H. Matsufuru *et al.* [JLQCD Collaboration], arXiv:hep-lat/0610026.

Overlap lattice fermion in a gravitational field†

M. Hayakawa,*1 H. So,*2 and H. Suzuki

[Lattice gauge field theories, anomalies in field and string theories, lattice models of gravity]

In any sensible constructive definition of quantum gravity by discretized space-time, the quantum effects of matter fields should correctly be incorporated. In the context of lattice gauge theory, it is known that lattice Dirac operators that satisfy the Ginsparg-Wilson (GW) relation[1] can naturally incorporate the nontrivial quantum effects of fermions such as the axial anomaly and the Dirac operator index, even with finite lattice spacings.[2–4]

In the present work, as a generalization of that of the lattice gauge theory, we constructed a lattice Dirac operator of the overlap type[3] that describes the propagation of a Dirac fermion in an external gravitational field. The local Lorentz symmetry can be manifestly realized on the lattice as

$$\begin{aligned}
&\psi(x) \to g(x)\psi(x), \quad \overline{\psi}(x) \to \overline{\psi}(x)g(x)^{-1}, \\
&U(x,\mu) \to g(x)U(x,\mu)g(x+\hat{\mu})^{-1}, \\
&\gamma^\mu(x) \equiv \sum_a e_a^\mu(x)\gamma^a \to g(x)\gamma^\mu(x)g(x)^{-1}, \\
&e_a^\mu(x) \to \frac{1}{2^n}\sum_b \mathrm{tr}\{\gamma_a g(x)\gamma^b g(x)^{-1}\}e_b^\mu(x),
\end{aligned} \tag{1}$$

where the link variables $U(x,\mu)$ and the gauge transformations $g(x)$ take the values in $G = \mathrm{spin}(2n)$, while it is believed that the general coordinate invariance is restored only in the continuum limit. Our doubler-free lattice Dirac operator is given by

$$D = 1 - A(A^\dagger A)^{-1/2}, \quad A \equiv 1 - D_\mathrm{w}, \tag{2}$$

where D_w is a Wilson-type lattice Dirac operator

$$D_\mathrm{w} = \frac{1}{2}\{\not{\nabla} + \not{\nabla}^* - \frac{1}{2}(\not{\nabla}^*\not{\nabla} + \not{\nabla}\not{\nabla}^*)\}, \tag{3}$$

with covariant differences ($e(x) \equiv \det_{\mu,a}\{e_\mu^a(x)\}$)

$$\begin{aligned}
\not{\nabla}\psi(x) &\equiv \sum_\mu \gamma^\mu(x)\{U(x,\mu)\psi(x+\hat{\mu}) - \psi(x)\}, \\
\not{\nabla}^*\psi(x) &\equiv \sum_\mu e(x)^{-1}e(x-\hat{\mu}) \\
&\quad \times U(x-\hat{\mu},\mu)^{-1}\gamma^\mu(x-\hat{\mu})U(x-\hat{\mu},\mu) \\
&\quad \times \{\psi(x) - U(x-\hat{\mu},\mu)^{-1}\psi(x-\hat{\mu})\}.
\end{aligned} \tag{4}$$

The lattice Dirac operator D satisfies the conventional GW relation

$$\gamma_5 D + D\gamma_5 = D\gamma_5 D. \tag{5}$$

It also possesses γ_5-hermiticity $D^\dagger = \gamma_5 D \gamma_5$ with respect to the inner product,

$$(f,g) \equiv \sum_x e(x)f(x)^{T*}g(x), \tag{6}$$

which is suggested by the general coordinate invariance, provided that the external vielbein and link variables satisfy the constraint

$$\sum_\mu \nabla_\mu^*\{e(x)\gamma^\mu(x)\} = 0, \quad \text{for all } x, \tag{7}$$

a lattice analogue of the metric condition in the continuum.

Because of the above properties of D, the lattice index theorem in the presence of a gravitational field

$$\sum_x \mathrm{tr}\,\Gamma_5(x,x) = n_+ - n_-, \quad \Gamma_5 \equiv \gamma_5\left\{1 - \frac{1}{2}D\right\}, \tag{8}$$

where $n_\pm$ denote the numbers of zero eigenmodes with positive and negative chiralities, respectively, holds. Moreover, the classical continuum limit of the index reproduces the Dirac genus[5] as

$$\begin{aligned}
&\lim_{a\to 0} a^{2n}\sum_x \mathrm{tr}\,\Gamma_5(x,x) \\
&= \int_{M_{2n}} \det\left\{\frac{i\hat{R}/4\pi}{\sinh(i\hat{R}/4\pi)}\right\}^{1/2},
\end{aligned} \tag{9}$$

where $\hat{R}$ denotes the curvature 2-form.

Similar results are obtained for other Lorentz representations, such as the spinor-vector and the bispinor representations. In the paper, reduction to a single Majorana fermion is also considered and it was observed that the reduction is possible for $8k+2$ and $8k+4$ dimensions, but not for $8k$ dimensions, as is consistent with the existence of Witten's global gravitational/gauge anomalies in $8k$ dimensions. Matter fields with a definite chirality are also briefly considered along the lines of ref. 6).

† Condensed from the article in Prog. Theor. Phys. **116**, 197 (2006).

*1 Department of Physics, Nagoya University
*2 Department of Physics, Ehime University

References
1) P. H. Ginsparg and K. G. Wilson: Phys. Rev. D **25**, 2649 (1982).
2) P. Hasenfratz, V. Laliena and F. Niedermayer: Phys. Lett. B **427**, 125 (1998).
3) H. Neuberger: Phys. Lett. B **417**, 141 (1998); Phys. Lett. B **427**, 353 (1998).
4) M. Lüscher: Phys. Lett. B **428**, 342 (1998).
5) See for example, K. Fujikawa and H. Suzuki: *Path Integrals and Quantum Anomalies* (Oxford Univ. Press, Oxford, 2004).
6) M. Lüscher: Nucl. Phys. B **549**, 295 (1999); Nucl. Phys. B **568**, 162 (2000).

Gauge anomaly associated with the Majorana fermion in $8k+1$ dimensions†

M. Hayakawa*1 and H. Suzuki

[Gauge field theories, symmetry and conservation laws, field theories in dimensions other than four]

The Majorana fermion in $8k+1$-dimensional Minkowski space-time is very peculiar. The charge conjugation matrix is symmetric, $C^T = +C$, in $8k+1$ dimensions and only a possible Lorentz invariant mass term for a single Majorana fermion, $m\psi^T C^{-1}\psi$, identically vanishes. This implies that one cannot apply the gauge invariant Pauli-Villars regularization to a single Majorana fermion. This situation generally persists for an odd number of Majorana fermions. A similar phenomenon is also found with the lattice regularization.[1] The most impressive example is given by the 1-dimensional ($k=0$) case, i.e., quantum mechanics, for which a lattice action of a free Majorana fermion $\widetilde{\psi}$ in the momentum space would be

$$\int_{-\pi/a}^{\pi/a} \mathrm{d}p\, \widetilde{\psi}^T(-p)\widetilde{D}(p)\widetilde{\psi}(p), \tag{1}$$

where a denotes the lattice spacing. Since $\widetilde{\psi}$ is Grassmann-odd, the kernel $\widetilde{D}(p)$ must be odd under $p \leftrightarrow -p$. Also, $\widetilde{D}(p)$ must be periodic in the Brillouin zone $\widetilde{D}(p+2\pi/a) = \widetilde{D}(p)$ for locality. These two requirements, however, imply that the kernel inevitably possesses a zero at $p = \pi/a$, that corresponds to the species doubler. Thus, one cannot write down a lattice action of a free single Majorana fermion which is consistent with locality, at least in the form of the ansatz Eq. (1).

These "phenomenological" observations strongly suggest the existence of some sort of anomaly associated with the Majorana fermion in $8k+1$ dimensions. Since there is no perturbative (or local) gauge anomaly in these *odd* dimensions, one expects that something similar to the global gauge anomaly in even-dimensional spaces[2,3] occurs. This possibility has been suggested in ref. 4) and the global *gravitational* anomaly for the Majorana fermion in these dimensions has been demonstrated.[5] Also, the global *gauge* anomaly associated to the Majorana fermion in 1 dimension ($k=0$) has been known[6]. To our knowledge, however, no examples of the global gauge anomaly associated with the Majorana fermion in higher ($k \geq 1$) dimensions have thus far been given.

In this work, using an elementary argument, we give an example of the gauge anomaly for the Majorana fermion in $8k+1$ dimensions. Our construction works for the Majorana fermion in the $(\mathbf{N}, \mathbf{8_v}, \ldots, \mathbf{8_v})$ representation of the gauge group $\mathrm{SO}(N) \times \mathrm{SO}(8)^k$ ($N \geq 3$). The topology of the base space is taken to be $S^1 \times S^8 \times \cdots \times S^8$. Basically the construction takes the following steps.

First, we explicitly solve the eigenvalue problem of a one-dimensional Dirac operator D_1 on S^1 (i.e., the $k=0$ case) and show that the Majorana pfaffian $\mathrm{Pf}\{iD_1\}$ changes the sign under a certain $\mathrm{SO}(N)$ gauge transformation. This global gauge anomaly in one dimension implies that the two-dimensional Dirac operator $\not{D}_2 = \sigma^2 \frac{\partial}{\partial x_0} + \sigma^1 D_1$ with an appropriate gauge field possesses an odd number of right-handed zero modes. Second, we consider an $8k+2$-dimensional Dirac operator $\not{D}_{8k+2}$ whose odd number of right-handed zero modes implies the global gauge anomaly in $8k+1$ dimensions. We then assume an appropriate gauge-field configuration which allows a separation of variables such as $\not{D}^\dagger_{8k+2}\not{D}_{8k+2} = \not{D}^\dagger_2\not{D}_2 \otimes 1 + 1 \otimes \not{D}^\dagger_{8k}\not{D}_{8k}$. Then the number of right-handed zero modes of $\not{D}_{8k+2}$ is odd if and only if the index of the $8k$-dimensional Dirac operator $\not{D}_{8k}$ is odd. Finally, through the index theorem

$$\mathrm{index}\{i\not{D}_{8k}\} = \frac{1}{(2\pi)^{4k}(4k)!}\int \mathrm{tr}\{F^{4k}\}, \tag{2}$$

we show that $\mathrm{index}\{i\not{D}_{8k}\}$ is odd for a collection of k SO(8) instantons[7] on $S^8 \times \cdots \times S^8$. For all the technicalities, the interested readers are referred to the original paper. We are expecting interesting applications of our observation in quantum mechanics ($k=0$) and in string theory ($k=1$).

References

1) T. Inagaki and H. Suzuki: J. High Energy Phys. **0407**, 038 (2004). H. Suzuki: Prog. Theor. Phys. **112**, 855 (2004).
2) E. Witten: Phys. Lett. B **117**, 324 (1982).
3) S. Elitzur and V. P. Nair: Nucl. Phys. B **243**, 205 (1984).
4) L. Alvarez-Gaumé and E. Witten: Nucl. Phys. B **234**, 269 (1984).
5) E. Witten: Commun. Math. Phys. **100**, 197 (1985).
6) D. Friedan and P. Windey: Nucl. Phys. B **235**, 395 (1984). E. Witten: "Global anomalies in string theory," Proc. Argonne Symp. on Geometry, Anomalies and Topology, Argonne, IL, Mar 28-30, 1985.
7) B. Grossman, T. W. Kephart and J. D. Stasheff: Commun. Math. Phys. **96**, 431 (1984) [Errata, **100**, 311 (1985)]. D. H. Tchrakian: Phys. Lett. B **150**, 360 (1985).

† Condensed from the article in Prog. Theor. Phys. **115**, 1129 (2006).

*1 Department of Physics, Nagoya University

Note on massless bosonic states in two-dimensional field theories†

H. Fukaya, M. Hayakawa,*1 I. Kanamori, H. Suzuki and T. Takimi*2

[Symmetry and conservation laws, chiral symmetries, currents and their properties]

Obtaining a constructive de nition of supersymmetric eld theory, which allows nonperturbative study, has been a long-standing problem in theoretical particle physics. Our group[1] is now undertaking lattice Monte-Carlo simulations of the two-dimensional (2d) $\mathcal{N} = (2, 2)$ supersymmetric Yang-Mills (SUSY YM) theory, on the basis of the recent proposal in ref. 2). For such a numerical study, any theoretical information on the property of the target theory is highly welcome. The present work is a by-product, obtained in the process of seeking some exact statement on the 2d $\mathcal{N} = (2, 2)$ SUSY YM theory.

In this work, we consider 2d super-renormalizable eld theories (not necessarily supersymmetric)

$$\mathcal{L} = \frac{1}{4}F^A_{\mu\nu}F^{A\mu\nu} + \overline{\psi}i\gamma^\mu D_\mu\psi + \frac{1}{2}D_\mu\sigma D^\mu\sigma + \frac{1}{2}D_\mu\pi D^\mu\pi \quad Y(\psi,\overline{\psi},\sigma,\pi) \quad V(\sigma,\pi), \quad (1)$$

where Y is the Yukawa interaction and V is the scalar potential. We assume that $\mathcal{L}$ is parity-invariant with the assignment that σ is a scalar and π is a pseudoscalar. We also assume that $\mathcal{L}$ possesses $G_L \times G_R$ global symmetry, namely, with suitable transformations on scalar elds σ and π, and that $\mathcal{L}$ is invariant under (writing $\psi_{R,L} = \{(1 \pm \gamma_5)/2\}\psi$)

$$\psi_L(x) \to \exp\{i\ {}^a_L T^a\}\psi_L(x),$$
$$\psi_R(x) \to \exp\{i\ {}^a_R T^a\}\psi_R(x), \quad (2)$$

where T^a are hermitian generators of a compact Lie group G in the representation R. Then we showed that, irrespective of the details of the system, the odd-parity part of the two-point function of Noether currents associated with the $G_L \times G_R$ symmetry, $J^a_{L,\mu}(x)$ and $J^a_{R\mu}(x)$, can be determined up to all orders of perturbation theory as

$$\text{F.T.}\langle 0|T^* J^a_{5\mu}(x)J^b_\nu(y)|0\rangle = \frac{i}{2\pi}(\dim r)T(R)\delta_{ab} \times \left\{\frac{1}{p^2}(p_\mu\epsilon_{\nu\rho}p^\rho + p_\nu\epsilon_{\mu\rho}p^\rho) + L(p^2)\epsilon_{\mu\nu}\right\}, \quad (3)$$

where $J^a_\mu \equiv J^a_{R,\mu} + J^a_{L,\mu}$ and $J^a_{5\mu} \equiv J^a_{R,\mu}$ $J^a_{L,\mu}$. In the above expression, $\dim r$ is the dimension of the gauge-group representation r of the fermion and $T(R)$ is the second Casimir of the representation R of the avor group G. $L(p^2)$ is an undetermined scalar function. The proof of the statement is based on the (anomalous) Ward-Takahashi identities and power counting.

The two-point function exhibits a massless pole, that corresponds to massless bosonic physical states. Thus, there is no mass gap in the above system. We note that the massless pole in the two-point function of conserved currents does not contradict with Coleman's theorem that prohibits a massless pole between a scalar eld and the conserved current in two dimensions.

The above statement covers all known super-renormalizable examples, such as the multi avor Schwinger model, the 2d massless QCD, and the Kogut-Sinclair model, in which the existence of massless bosonic states has been shown by other methods. The statement applies, in particular, to the 2d $\mathcal{N} = (2, 2)$ SUSY YM theory (our original target) in which

$$Y = g\,\mathrm{tr}\left\{\overline{\psi}\,[\sigma + i\gamma_5\pi, \psi]\right\}, \quad V = g^2\,\mathrm{tr}\{[\sigma,\pi]^2\}, \quad (4)$$

and which possesses $\mathrm{U}(1)_L \times \mathrm{U}(1)_R$ symmetry. The same is true even with matter multiplets, as long as there is no superpotential. Similarly, the $\mathcal{N} = (4, 4)$ SUSY YM theory possesses $\mathrm{SU}(2)_L \times \mathrm{SU}(2)_R$ symmetry and our statement applies. The fact that $\mathcal{N} = (2, 2)$ and $\mathcal{N} = (4, 4)$ SUSY YM theories have no massgap has been noted[3] on the basis of the 't Hooft anomaly matching argument.

For the 2d $\mathcal{N} = (2, 2)$ SUSY YM theory with the gauge group $\mathrm{SU}(N_c)$, the two-point function in the (euclidean) position space is given by

$$\langle J_{5\mu}(x)J_\nu(y)\rangle = \frac{i}{2\pi^2}(N_c^2 \quad 1)\frac{1}{(r^2)^2}(r_\mu\epsilon_{\nu\rho}r_\rho + r_\nu\epsilon_{\mu\rho}r_\rho), \quad (5)$$

for $x \neq y$, where $r_\mu = x_\mu \quad y_\mu$. Moreover, a supersymmetric Ward-Takahashi identity shows that (if supersymmetry is not spontaneously broken) a two-point function of certain fermionic operators also exhibits a power-law behavior, corresponding to a massless fermionic state. At present, we are measuring this two-point function in Monte-Carlo simulations to examine the restoration of supersymmetry in the continuum limit, which was suggested in ref. 2).

† Condensed from the article in Prog. Theor. Phys. **116**, 1117 (2007).

*1 Department of Physics, Nagoya University
*2 Yukawa Institute for Theoretical Physics, Kyoto University

References
1) H. Fukaya, I. Kanamori, H. Suzuki, T. Takimi and Y. Taniguchi: work in progress.
2) H. Suzuki and Y. Taniguchi: J. High Energy Phys. **0510**, 082 (2005).
3) E. Witten: Nucl. Phys. B **460**, 335 (1996).

RIKEN Accel. Prog. Rep. **40** (2007)

Hermiticity and Majorana condition for two-dimensional super Yang-Mills model on a lattice with Dirac-Kähler twist

A. D'Adda,[*1] I. Kanamori, N. Kawamoto,[*2] K. Nagata,[*3] and J. Saito[*2]

[supersymmetry, lattice, Hermiticity]

Supersymmetry (SUSY) provides a unified description of bosons and fermions but it lacks a regularization that maintains the SUSY in general. One of the most powerful regularizations is a lattice regularization that treats space-time as a discrete space. Among the many attempts to provides a lattice formulation for SUSY, we previously proposed a lattice formulation for a super Yang-Mills model with a Dirac-Kähler twist and with a kind of noncommutativity[1)]. We report our recent development of the Hermiticity and Majorana condition of our model[2)].

We used supercharges on lattice links and discretized the algebra in the previous model. The essential difficulty in formulating SUSY on the lattice comes from the fact that the supertransformation is the square root of an infinitesimal translation, whereas on the lattice we have only finite translations. Geometrically, the finite translations correspond to links on the lattice, so that it is very natural to place the supercharges on links. With the help of the kind of noncommutativity, which is closely related to the link structure, we succeeded in discretizing the algebra. Our algebra is two-dimensional $N = 2$ algebra with a Dirac-Kähler (or topological) twist.

In conventional lattice gauge theory, the gauge field exists on a link as an exponentiated field (link variable). On the oppositely oriented link, its Hermitian conjugate exists. The fact that the gauge field is real shows that the link variable is unitary. In this report, we discuss a similar relation for the supercharges on a link.

We have four supercharges in the model, which is generated by $\nabla, \tilde{\nabla}, \nabla_1$ and ∇_2. We can locate a pair $(\nabla, \tilde{\nabla})$ on the same link but with opposite orientation to each other (Fig. 1). The situation is the same for the (∇_1, ∇_2) pair as well as for the bosonic pair of link fields $(\mathcal{U}_{+\mu}, \mathcal{U}_{-\mu})$, where $\mathcal{U}_{\pm\mu}$ gives the forward and backward differences. Therefore, we identify $\nabla^\dagger = \tilde{\nabla}$ and $\nabla_1^\dagger = \nabla_2$. These relations are exactly those of the Majorana condition for twisted charges. This simple identification, however, does not work easily because it contradicts the algebra. We need to make a (counter-)Wick rotation from a Euclidean to a Lorentzian signature. Eventually, we obtain the following algebra:

$$\{\nabla, \nabla_1\} = i\mathcal{U}_{+1}, \quad \{\tilde{\nabla}, \nabla_1\} = i\mathcal{U}^{-1} = i\mathcal{U}_{-1}, \qquad (1)$$

$$\{\nabla, \nabla_2\} = i\mathcal{U}_{+2}, \quad \{\tilde{\nabla}, \nabla_1\} = -i\mathcal{U}^{-2} = i\mathcal{U}_{-2}. \qquad (2)$$

The twisted charges can be untwisted to normal spinor charges through

$$\nabla_{i\alpha} = \left(\nabla C^{-1} + i\nabla_\mu \gamma^\mu C^{-1} + \tilde{\nabla}\gamma^5 C^{-1}\right)_{i\alpha}, \qquad (3)$$

where α is a SO(1,1) spinor suffix of space-time, i is a SO(1,1) spinor suffix of R-symmetry (internal symmetry) and C is a charge conjugation matrix. Since the spinor charges are given as a linear combination of charges on different links, they cannot be kept exact on the lattice. Note that because the twist operation mixes the space-time and internal space of the R-symmetry, Wick rotation in the twisted space-time leads to that of the untwisted space-time and the internal space. Using the Dirac conjugation

$$\overline{\nabla}^{j\beta} = (\nabla_{i\alpha})^* (\gamma^0)_i{}^j (\gamma^0)_\alpha{}^\beta, \qquad (4)$$

we obtain the Majorana condition for the spinor charges

$$\nabla_{i\alpha} = (\gamma^5 C^{-1})_{ij} C^{-1}_{\alpha\beta} \overline{\nabla}^{j\beta} \qquad (5)$$

and the algebra

$$\{\nabla_{i\alpha}, \overline{\nabla}^{j\beta}\} = -2(\gamma^5)_i{}^j (\gamma^\mu)_\alpha{}^\beta \nabla_{\underline{\mu}} + 2(\gamma^5\gamma^a)_i{}^j \delta_\alpha{}^\beta \phi_a, \qquad (6)$$

where $\nabla_{\underline{\mu}}$ is a space-time covariant derivative and ϕ_a is a scalar field in the SUSY multiplet.

Finally, a different treatment of the Hermiticity requires that the number of charges should be doubled in general. That kind of treatment may be related to $N = 4$ multiplet.

References

1) A. D'Adda, I. Kanamori, N. Kawamoto and K. Nagata: Phys. Lett. B **633**, 645 (2006).
2) A talk given by I.K in Joint Meeting Pacific Region Particle Physics Communities, Honolulu, USA, 2006-10. A related paper is in preparation.

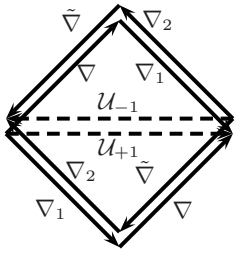

Fig. 1. Link structure for $\{\nabla, \nabla_1\} = i\mathcal{U}_{+1}$ and $\{\tilde{\nabla}, \nabla_2\} = i\mathcal{U}_{-1}$. $(\nabla, \tilde{\nabla})$, (∇_1, ∇_2) and $(\mathcal{U}_{+1}, \mathcal{U}_{-1})$ are located on the same but oppositely oriented links.

*1 INFN Torino and Torino University, Italy
*2 Department of Physics, Hokkaido University
*3 Department of Physics, Indiana University, USA

Nonlocal Matching Condition and Scale-invariant Spectrum in Bouncing Cosmology†

C. S. Chu,*1 K. Furuta and F. L. Lin,*2

[Models in early universe, General relativity, Noncommutative geometry]

In cosmological scenarios such as the pre-big bang or ekpyrotic scenario[1,2], a matching condition between the metric perturbations in the pre-big bang phase and those in the post-big bang phase is often assumed. Nevertheless, obtaining a scale invariant cosmic microwave background (CMB) spectrum via a concrete mechanism remains impossible. We examine this problem from the point of view of local causality. We prove the following no-go theorem: independent of the details of the matching condition, a scale-invariant spectrum is impossible as long as the local causality condition is satisfied. By considering nonlocal effects of noncommutative field theory, we consider the possibility of obtaining a scale-invariant spectrum.

We consider a scalar field φ coupled to gravity. Consider spacelike hypersurfaces S_- and S_+ separated by the bounce where the former is before the bounce and the latter is after it. Local causality requires that there exists a finite region Ω_- on S_- such that the metric and the scalar field data $\{g_{ij}, g'_{ij}, \varphi, \varphi'\}$ at P' on S_+ is determined only by data $\{g_{ij}, g'_{ij}, \varphi, \varphi'\}$ on Ω_-, modulo local spatial coordinate transformation (Fig. 1).

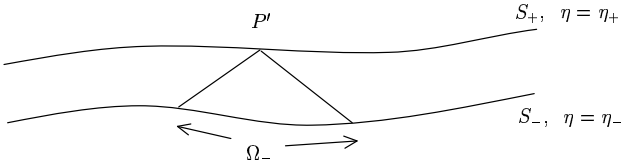

Fig. 1. Local causality

The matching condition takes the form

$$g_{ij}\big|_{\eta=\eta_+,P'} = H_{ij}(g_{ij}, g'_{ij}, \varphi, \varphi', \nabla_k)\big|_{\eta=\eta_-,P} \ . \quad (1)$$

The function H_{ij} is a rank 2 symmetric tensor. We can eliminate extra coordinate dependence by choosing a map from S_- to S_+ appropriately. We expand (1) in the wave number k. This is in the same principle used in the method of spatial gradient expansion[3]. However, the validity of a four-dimensional effective theory during the bounce is not assumed in our approach.

The gauge-invariant metric fluctuation is given by

$$\Phi = S(k)\left(l^2\frac{\mathcal{H}}{a^2} + O(k^2)\right) + D(k)\left(\frac{1}{a}\left(\frac{1}{a}\int d\eta a^2\right)' + O(k^2)\right). \quad (2)$$

Here, a is the scale factor and $\mathcal{H} \equiv a'/a$ is the Habble parameter. l stands for the Planck scale. The coefficients $S(k)$ and $D(k)$ are time-independent.

Using the explicit form of the metric fluctuation and the matching condition (1), the coefficients $S^{(+)}$ and $D^{(+)}$ after the bounce is given by

$$\begin{pmatrix} S^{(+)} \\ D^{(+)} \end{pmatrix} = \begin{pmatrix} C_S & C_D \\ Ak^2 & 1 \end{pmatrix} \begin{pmatrix} S^{(-)} \\ D^{(-)} \end{pmatrix} \quad (3)$$

with undetermined coefficients C_S and C_D. Thus, we have obtained the matching condition. To obtain the scale-invariant CMB spectrum, the constant mode $D^{(+)}$ must behave as $D^{(+)} \sim k^{-3/2}$. For the ekpyrotic and cyclic scenario, it is known that

$$S^{(-)} \sim k^{-3/2} \text{ and } D^{(-)} \sim k^{-1/2}. \quad (4)$$

We conclude that nonlocal causality is necessary to obtain a scale-invariant spectrum. A similar analysis can be carried out for the pre-big bang scenario.

In string theory, nonlocal effects such as noncommutativity of the space-time are known. For example, in the noncommutative φ^4 theory, the low-energy effective action provides a nonlocal term[4]

$$\mathcal{L}_{\text{eff}} \sim \frac{1}{2}\frac{g^2}{96\pi^2(|k_i(\theta^2)^{ij}k_j|/a^2 + \frac{1}{\Lambda^2})}\varphi(k)\varphi(-k), \quad (5)$$

where θ^{ij} is the noncommutative parameter. The time evolution of φ has nonlocal effects if the ultraviolet cutoff scale Λ is taken to infinity.

By modifying the time evolution of the metric fluctuation to include the $1/k$ term, it is possible to obtain the scale-invariant power spectrum with the magnitude

$$P(k) \sim \left(\frac{l}{l_b}\right)^2. \quad (6)$$

Here, l_b is the noncommutative scale. Thus, the Hubble scale around which the bounce occurs should be at around 10^{-5} of the Planckian energy scale.

† Condensed from the article in Phys. Rev. D. **73**, 103505 (2006)

*1 Centre for Particle Theory and Department of Mathematics, University of Durham, UK
*2 Department of Physics, National Taiwan Normal University, Taiwan

References

1) M. Gasperini and G. Veneziano: Astropart. Phys. **1**, 317 (1993).
2) J. Khoury, B. A. Ovrut, P. J. Steinhardt, and N. Turok: Phys. Rev. D **64** (2001) 123522.
3) J. Parry, D. S. Salopek, and J. M. Stewart: Phys. Rev. D **49**, 2872 (1994).
4) S. Minwalla, M. Van Raamsdonk, and N. Seiberg: JHEP **0002**, 020 (2000).

Field Equations of Massless Fields Based on the New Interpretation of Matrix Models †

M. Hanada,[*1] K. Furuta, H. Kawai, and Y. Kimura,[*2]

[String theory, Matrix model, General relativity]

Recently, some of the authors have introduced a new interpretation of matrix models in which covariant derivatives can be expressed by large-N matrices[1]. In this interpretation, the Einstein equation is derived at the classical level. We generalize this argument to covariant derivatives with torsion. Some components of the torsion field can be identified with the dilaton and the B-field in string theory. However, the other components do not seem to have string theory counterparts. We also consider the matrix model with a mass term or a cubic term, in which the equation of motion in string theory is exactly satisfied.

We consider the large-N reduced model

$$S = -\frac{1}{4g^2} Tr\Big([A_a, A_b] \left[A^a, A^b\right] \Big), \tag{1}$$

which is the bosonic part of the IIB matrix model[2]. A_a are $N \times N$ Hermitian matrices and a and b run from 1 to d. The gauge transformation is given by $\delta A_a = i[\Lambda, A_a]$, where Λ is an $N \times N$ Hermitian matrix.

We consider that the matrices A_a act on the space of functions on the principal $Spin(d)$ bundle over the space-time manifold[1]. The covariant derivative ∇_a is shown to be mapped to a set of matrices $\nabla_{(a)}$ by

$$\begin{aligned} \nabla_{(a)} &= R_{(a)}{}^{b}(g^{-1})\nabla_b \\ &= R_{(a)}{}^{b}(g^{-1}) e_b{}^{\mu}(x) \left(\partial_\mu + \omega_\mu{}^{cd}(x)\mathcal{O}_{cd}\right), \end{aligned} \tag{2}$$

where g is the coordinate of the fiber $Spin(d)$, $R_{(a)}{}^{b}(g^{-1})$ is the vector representation of $Spin(d)$ and $\mathcal{O}_{ab}$ is the Lorentz generator of the $Spin(d)$ group.

A_a can be expanded as a series in powers of $\nabla_{(a)}$ and $\mathcal{O}_{ab}$. By introducing contorsion $S_a{}^{bc}(x)$, we consider the general form of the first-order differential operator

$$\begin{aligned} A_a &= iR_{(a)}{}^{b}(g^{-1})D_b \\ &= iR_{(a)}{}^{b}(e_b{}^{\mu}(x)\nabla_\mu + S_b{}^{cd}(x)\mathcal{O}_{cd}). \end{aligned} \tag{3}$$

The gauge parameter at the first-order in the differential operator $\Lambda = i\lambda^\mu(x)\nabla_\mu + i\lambda^{ab}(x)\mathcal{O}_{ab}$ generates the diffeomorphism and the local Lorentz transformation and fixes the unphysical modes of $e_a{}^{\mu}(x)$. However, no components of the contorsion $S_a{}^{bc}(x)$ can be gauged away. The equation of motion reduces to the following two equations:

$$-\mathcal{R}_{bc} + D^a T_{abc} + T_{ab}{}^{d} T^{a}{}_{dc} = 0, \tag{4}$$

$$D^a \mathcal{R}_{ab}{}^{cd} + T^{a}{}_{b}{}^{e} \mathcal{R}_{ae}{}^{cd} = 0. \tag{5}$$

where $T_{abc} = S_{abc} - S_{bac}$ is the torsion and $\mathcal{R}_{ab}{}^{cd}$ is the Riemann tensor with the contribution from the torsion.

We solve the equations of motion Eqs. (4) and (5) at the linearized level. The contorsion $S_a{}^{bc}$ can be decomposed to irreducible tensors as

$$S_{abc} = V_b\delta_{ac} - V_c\delta_{ab} + L_{abc} + H_{abc}, \tag{6}$$

where H_{abc} is antisymmetric and L_{abc} satisfies the relations $L_{[abc]} = 0$ and $L^{a}{}_{ac} = 0$. Since no component of the contorsion $S_a{}^{bc}(x)$ can be gauged away, negative norm modes appear in $S_a{}^{bc}(x)$. For this reason, we regard $S_a{}^{bc}(x)$ as the field strength and consider the following form of solutions:

$$V_a = \partial_a \phi, \tag{7}$$

$$H_{abc} = \partial_{[a} B_{bc]}, \tag{8}$$

$$L_{abc} = 0. \tag{9}$$

Then, the equations of motion reduce to

$$R_{ab} = (3-d)\partial_a\partial_b\phi, \tag{10}$$

$$\partial^2\phi = 0, \tag{11}$$

$$\partial^a H_{abc} = 0. \tag{12}$$

These equations are the same as the linearized equations of motion for the system of the dilaton and the antisymmetric B-field coupled to gravity, which arise naturally from the string theory.

Although we have considered solutions that satisfy the conditions Eqs. (7)-(9), there are many solutions that do not satisfy these conditions. Any solution of the linearized equations can be shown to be extended to solutions to higher orders. None of the solutions in the linear order can be discarded. It seems that the space of the matrix needs to be restricted in some way to enable a physical interpretation of the result.

We can generalize the analysis to a model with a mass term and a cubic term. In those cases, the equation of motion is satisfied by the covariant derivative on a group manifold which satisfy

$$[D_a, D_b] = \alpha f_{abc} D_c. \tag{13}$$

The structure constants are identified with the field strength of the B-field.

† Condensed from the article hep-th/0611093

*1 Department of Physics, Kyoto University
*2 Department of Physics, Queen Mary, University of London, UK

References

1) M. Hanada, H. Kawai, and Y. Kimura: Prog. Theor. Phys. **114** (2006) 1295.
2) N. Ishibashi, H. Kawai, Y. Kitazawa, and A. Tsuchiya: Nucl. Phys. **B498** (1997) 467.

RIKEN Accel. Prog. Rep. **40** (2007)

Improved perturbation method and its application to matrix models

T. Aoyama, H. Kawai, T. Kuroki, and Y. Shibusa

[String theory, Matrix model, Nonperturbative analysis]

String theory is the unique theory that contains massless spin-two particles, i.e. gravitons, and is thus considered to provide unified microscopic description of the universe including gravity. However, it has been recognized that perturbative string theory fails to single out our universe as the unique vacuum of the theory. Therefore, we are forced to pursue nonperturbative formulations. The IIB matrix model (also called the IKKT matrix model)[1] has been proposed as a constructive formulation of the superstring theory, and it has been subjected to intensive studies.

A significant feature of the IIB matrix model is that the space-time itself is expressed by the eigenvalue distribution of ten bosonic matrices, and thus it is treated as a dynamical variable of the model. The origin of our four-dimensional space-time can be argued in this framework by a spontaneous breakdown of the Lorentz symmetry. It is also of great importance to clarify whether the non-Abelian gauge group of the standard model type emerges dynamically in the context of matrix models. It is natural that this gauge group is embedded in the original $U(N)$ gauge group of the matrix model. We are thus motivated to investigate the dynamical aspects of matrix models in a nonperturbative manner.

It is generally believed that the perturbative series expansion is asymptotic and diverges beyond some finite order. Nevertheless, for most theories, we can only evaluate such series expansions, from which we have to deduce as much information as possible on the theory. Therefore, we need a method for estimating the *exact* values of observables at the parameter values (coupling constants and other parameters) outside the original radius of convergence. We employ here an optimization technique, which we refer to as the improved perturbation method.[2]

The concrete procedure of the improved perturbation method is as follows. Assuming that we have a perturbative series $F(\lambda, m)$, where λ is a coupling constant and m denotes a parameter of the model, we perform a shift of parameters that involves an artificial parameter m_0,

$$\begin{aligned} \lambda &\longrightarrow g\,\lambda, \\ m &\longrightarrow m_0 + g(m - m_0). \end{aligned} \tag{1}$$

Then we reorganize the series in terms of g, truncate it at a finite order of g, and set g to 1. Although $g = 1$ means that this manipulation is nominal, the series turns to be dependent on m_0 by the truncation at some finite order of g. To determine the optimal value of m_0, we adopt here the principle of *minimal sensitivity*. It means that the *exact* value of F would be reproduced when the dependence on the artificial parameter m_0 of the improved series becomes weakest. Thus far, the improved perturbation method is considered as a sort of resummation of the series by a variational approach. We have investigated this method in detail.[3] In particular, we developed an efficient prescription to extract the approximate values of observables when the model contains many parameters.

We applied the improved perturbation method to the IIB matrix model and examined the spontaneous breakdown of the ten-dimensional rotational symmetry.[3–5] We considered configurations in which the $SO(d)$ subgroup of $SO(10)$ stays intact as the ansatz. By comparing the estimated values of the free energy based on the perturbative series expansion up to the 8th order, we found that the $SO(4)$-symmetric configuration, in which the extended four-dimensional space-time is realized, is preferred.[3,4] We also examined the extended ansatz to confirm the above result.[5] Thus, we conclude that the IIB matrix model has a solution with four-dimensional rotational symmetry, which corresponds to our universe as a nonperturbative vacuum.

To study whether a spontaneous breakdown of $U(N)$ gauge symmetry occurs in the matrix models in the large-N limit, we examined the massive Yang-Mills Chern-Simons matrix model as a simplified bosonic model by the improved perturbation method.[6] It has been claimed that this model has several phases with respect to the coupling constant of the Chern-Simons term α and the mass parameter m^2. We studied the phase structure and confirmed in a nonperturbative manner that a phase called the 5-brane phase, in which the configuration consists of $O(N)$ coincident small fuzzy spheres, is realized. This implies that the non-Abelian gauge group of rank N is generated dynamically.

References

1) N. Ishibashi, H. Kawai, Y. Kitazawa, and A. Tsuchiya: Nucl. Phys. B **498**, 467 (1997).
2) J. Nishimura and F. Sugino: JHEP **0205**, 001 (2002); H. Kawai, S. Kawamoto, T. Kuroki, T. Matsuo, and S. Shinohara, Nucl. Phys. B **647**, 153 (2002).
3) T. Aoyama and Y. Shibusa: Nucl. Phys. B **754**, 48 (2006).
4) T. Aoyama and H. Kawai: Prog. Theor. Phys. **116**, 405 (2006).
5) T. Aoyama, H. Kawai, and Y. Shibusa: Prog. Theor. Phys. **115**, 1179 (2006).
6) T. Aoyama, T. Kuroki, and Y. Shibusa: Phys. Rev. D **74**, 106004 (2006).

Non-Abelian duality from vortex moduli

M. Eto,[*1] L. Ferretti,[*2] K. Konishi,[*3,*4] G. Marmorini,[*5,*4] M. Nitta,[*6] K. Ohashi,[*7] W. Vinci,[*3,*4] and N. Yokoi

[Non-Abelian duality, magnetic monopole and vortex, supersymmetric gauge theory]

The mechanism of quark confinement and chiral symmetry breaking in quantum chromodynamics (QCD) still remains mysterious. Supersymmetric gauge theories provide a promising clue to understanding the problem. Actually, a non-Abelian version of the dual Meissner effect in supersymmetric gauge theories has been proposed as a good model for quark confinement occuring in QCD[1].

An example of a non-Abelian extension of the electric-magnetic duality is the GNOW duality conjectured by Goddard-Nuyts-Olive and Weinberg[2]. In a system where the gauge symmetry is spontaneously broken $G \to H$ (H is a non-Abelian subgroup of G), degenerate magnetic monopole solutions can be constructed as regular solitonic solutions. The GNOW duality states that these monopoles form a multiplet of the dual group H^* of unbroken H, which is generated by the dual roots, $\alpha^* \equiv \frac{\alpha}{\alpha\cdot\alpha}$, where α are the roots of H. However, problems with such an interpretation are known for the simple monopole configuration, where the globally conserved charges of H cannot be defined and the semiclassical quantization breaks down because of non-normalizable zero modes.

In our article[3], we discuss the transformation properties of the monopole solutions in the breaking $G \to H$ by placing a low-energy system with gauge symmetry H into the Higgs phase. As a model for our idea, we consider the softly broken $\mathcal{N} = 2$ supersymmetric gauge theory, which realizes hierarchical symmetry breaking, $G \overset{v_1}{\to} H \overset{v_2}{\to} \emptyset$ ($v_1 \gg v_2$).

As a simplest example, we consider the softly broken $\mathcal{N} = 2$ supersymmetric $SU(N+1)$ gauge theory with N_f matter multiplets in the fundamental representation. The vacuum expectation value (VEV) of an adjoint Higgs field, v_1 breaks $SU(N+1) \to SU(N)\times U(1)$ in a higher-energy scale and this breaking produces the solitonic monopole solutions. At low energy, the effective theory becomes softly broken $\mathcal{N} = 2$ $SU(N) \times U(1) \sim U(N)$ gauge theory with N_f fundamental matter multiplets of $U(N)$. Then, the VEV of the fundamental Higgs field, v_2 breaks the gauge symmetry $U(N)$ completely. This second-stage symmetry breaking produces the non-Abelian vortex solutions with non-Abelian flux[4]. A topological argument for the high-energy $SU(N+1)$ theory and the low-energy $U(N)$ theory demonstrates the correspondence between the topological charges of monopoles in $\pi_2\left(SU(N+1)/U(N)\right)$ and vortices in $\pi_1\left(U(N)\right)$. As the consequence, we are led to the monopole-vortex coupled configuration in our full theory (see below).

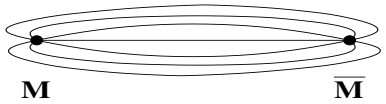

It is important that our full theory has an exact unbroken symmetry $SU(N)_{C+F}$, which is the diagonal subgroup of $SU(N)$ gauge symmetry with $SU(N_f)$ global symmetry for flavors. On the basis of the above configuration, we can discuss the transformation law of GNOW monopoles under $SU(N)_{C+F}$ symmetry in terms of the transformation properties of non-Abelian vortices. Utilizing the moduli matrix formalism for the vortex solutions[5], the transformation properties of non-Abelian vortices under $SU(N)_{C+F}$ can be obtained. We showed that the vortices with minimum flux transform to become the fundamental (**N**) representation under $SU(N)_{C+F}$[6], and determined that GNOW monopoles with minimum magnetic charge also transform to become the fundamental representation of $SU(N)_{C+F}$. We also discussed the interpretation of $SU(N)_{C+F}$ symmetry as GNOW dual symmetry $H^* \sim U(N)^*$. Note that our analysis does not depend on the semiclassical form of monopole solutions. Our idea $SU(N)_{C+F} \Leftrightarrow H^*$ is tested against the quantum behavior of non-Abelian monopoles in the exact low-energy effective theory à la Seiberg-Witten[7]. Generalizations to $SO(N)$ and $USp(2N)$ gauge theories are also discussed.

*1 Institute of Physics, University of Tokyo
*2 SISSA and INFN, Sezione di Trieste
*3 Department of Physics, University of Pisa
*4 INFN, Sezione di Pisa
*5 Scuola Normale Superiore di Pisa
*6 Department of Physics, Keio University
*7 Department of Physics, Tokyo Institute of Technology

References

1) K. Konishi, G. Marmorini, and N. Yokoi: Nucl. Phys. **B741**, 180 (2006).
2) P. Goddard, J. Nuyts, and D. Olive: Nucl. Phys. **B125**, 1 (1977); E. J. Weinberg: Nucl. Phys. **B167**, 500 (1980); Nucl. Phys. **B203**, 445 (1982).
3) M. Eto, L. Ferretti, K. Konishi, G. Marmorini, M. Nitta, K. Ohashi, W. Vinci, and N. Yokoi: hep-th/0611313.
4) A. Hanany and D. Tong: J. High Energy Phys. **07**, 037 (2003); R. Auzzi, S. Bolognesi, J. Evslin, K. Konishi, and A. Yung: Nucl. Phys. **B673**, 187 (2003).
5) For a review see, M. Eto, Y. Isozumi, M. Nitta, K. Ohashi, and N. Sakai: J. Phys. **A39**, R315 (2006).
6) M. Eto, K. Konishi, G. Marmorini, M. Nitta, K. Ohashi, W. Vinci,and N. Yokoi: Phys. Rev. **D74**, 065021 (2006).
7) N. Seiberg and E. Witten: Nucl. Phys. **B426**, 19 (1994); Nucl. Phys. **B431**, 484 (1994).

QCD Effects in the Decays of TeV Black Holes†

C. Alig,*1 M. Drees,*1 and K. Oda*2

[Black hole, TeV scale gravity, Large Hadron Collider, Quark-gluon plasma]

The Planck scale can be as low as TeV if we live in a four-dimensional subspace in the $4 + n$ dimensional spacetime and the extra n dimensions are compacti ed with a "large" radius, e.g., of the order of sub-mm for $n = 2$. The Randall-Sundrum scenario also predicts that the e ective Planck scale is $O(\mathrm{TeV})$ if we live in the infrared (IR) brane.

In such a scenario, the CENR Large Hadron Collider (LHC), which will start taking data from the summer of 2008, will become a black hole factory—the LHC can produce a black hole every few seconds.

The black hole is one of the most profoundly mysterious objects in theoretical physics. The black hole itself is described by the classical Einstein's law of gravity, yet it sits in the high-energy ultraviolet (UV) limit to be matched with the low-energy IR stringy description according to the correspondence principle for black holes and strings. We try to describe the production and evaporation of the black hole as precisely as possible[1] because the quantum gravitational e ects, the thing which we really want to explore, will then appear as a deviation from the black hole picture.

The black holes will decay via the Hawking radiation mainly into the "visible" standard model elds that are localized on our brane. The decay rate and its energy spectrum can be computed from the greybody factors that are calculated using the eld equations for the brane-localized elds.[1] The resulting spectrum is peaked around the black hole temperature which is approximately $T \gtrsim 100\,\mathrm{GeV}$.

The Hawking radiation is proportional to the number of degrees of freedom and therefore roughly 75% of the decay products are quarks and gluons. Anchordoqui and Goldberg claimed that these quarks and gluons will form a "chromosphere," a quark-gluon plasma, rather than forming distinct jets.[2] The argument was that the number of the bremsstrahlung reactions, which increases the total number of partons, makes each parton scatter $O(10)$ times.

However, these interactions are rather soft and will not change the energies and momenta of the participating partons very much. Such interactions would *not* impede the formation of well-de ned hadronic jets. Given the complexity of QCD processes, a quantitative investigation of their e ect can only be performed with the help of a QCD simulation program. For that purpose, we wrote such a simulation code, based on the VNI program[3]. We modi ed it by forcing scattering reactions to take a nite amount of time, which we estimate using the uncertainty principle.

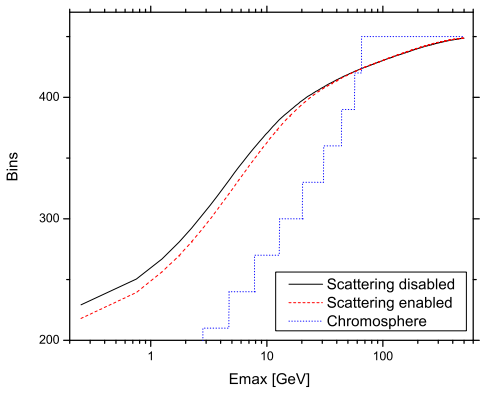

Fig. 1. Number of phase space cells where the deposited energy satis es $E < E_{\max}$ as a function of $E_{\max}$, for black hole mass $M = 10$ TeV. The blue, steplike curves show the prediction from an ideal chromosphere.

One of our main results is shown in Fig. 1. We set the higher dimensional Planck scale to 0.65 TeV because this maximizes the number of initial partons, and hence, the number of parton-parton interactions within a given black hole's decay. We also consider relatively heavy black holes with $M = 10\,\mathrm{TeV}$ to minimize the temperature in favor of the chromosphere formation. We see that the number of cells with $E < E_{\max}$ indeed shows nontrivial dependence on $E_{\max}$ over a wide range. Even for $M = 10\,\mathrm{TeV}$, in about 50% of the cells, almost no energy is deposited; on the other hand, about twenty cells contain more than 100 GeV. These results are consistent with the existence of well–de ned jets. Parton-parton scattering has practically no e ect on the number of cells containing at least 30 GeV, again indicating that it does not a ect the jet structure at all.

References

1) D. Ida, K. Oda and S. C. Park: Phys. Rev. D 67, 064025 (2003) [Erratum-ibid. D 69, 049901 (2004)] [arXiv:hep-th/0212108].
2) L. Anchordoqui and H. Goldberg: Phys. Rev. D 67, 064010 (2003) [arXiv:hep-ph/0209337].
3) S. A. Bass *et al.*: Phys. Rev. C 60, 021901 (1999), [arXiv:nucl-th/9902055].

† Condensed from the article in arXiv:hep-ph/0610269, accepted for publication in JHEP (Journal of High Energy Physics).

*1 Physikalisches Institut, Universität Bonn, Germany
*2 Theoretical Physics Laboratory, RIKEN

Towards Full Automation of the Lepton $g-2$ Calculation in QED

T. Aoyama, M. Hayakawa,[*1] T. Kinoshita,[*2] and M. Nio

[QED, anomalous magnetic moment, muon, electron, automation]

The anomalous magnetic moments of leptons, called $g-2$, have been playing a central role in testing the validity of Quantum Electrodynamics (QED) and the standard model. The electron $g-2$ was precisely measured by Harvard's group in 2006. Their anomaly value $a_e = (g-2)/2$ is[1)]

$$a_e = 1\ 159\ 652\ 180.85(0.76) \times 10^{-12}\ (0.66\text{ppb}). \quad (1)$$

This value has a 5.5 times smaller uncertainty than University of Washington's measurement in 1987.[2)] The muon $g-2$ was measured at Brookhaven National Laboratory and the final results were announced in 2004.[3)] The average of the positive and negative muons is

$$a_\mu = 11\ 659\ 208(6) \times 10^{-10} \quad (0.5\text{ppm}). \quad (2)$$

Theoretical calculations of $g-2$ have achieved the matching precision of the measured anomaly values. By now, the QED contributions up to the eighth order of perturbation theory are known.[4,5)] Using the measured electron $g-2$ value in Eq. (1) and QED prediction,[5)] a new value of the fine structure constant α was determined:[6)]

$$\alpha^{-1} = 137.035\ 999\ 710\ (96) \quad (0.70\text{ppb}), \quad (3)$$

which is an order of magnitude better than other α's.

Both Harvard and BNL plan to improve their measurements by a factor three and more. Considering such a situation, we started evaluating the tenth-order contributions a few years ago. There are 12672 Feynman diagrams contributing to electron $g-2$ and 9080 to muon $g-2$. These numbers of diagrams are so huge and very discouraging.

It turns out, however, that a good estimate for the tenth-order contribution to muon $g-2$ can be obtained without performing gigantic calculations. The diagrams that give the leading contribution can be computed with the slightly modified computer programs for lower-order ones. We directly calculated 2958 diagrams and obtained a new estimation of the coefficient of $(\alpha/\pi)^5$ muon $g-2$:[7)]

$$A_2(m_\mu/m_e) = 663\ (20), \quad (4)$$

which is a factor-of-8 improvement over the previous estimation 930(170).[8)]

In contrast to muon g–2, none of the 12672 diagrams dominates the electron $g-2$. The most difficult to evaluate are 6354 diagrams belonging to Set V, which contain no closed fermion loop. To carry out this huge calculation without error, it is inevitable to automate the whole process of computation.

The first version of the automation code was completed in 2005.[9)] Given a one-line information of a diagram, this automatic code creates the following:

(1) building blocks for the diagram,
(2) $g-2$ amplitude,
(3) ultraviolet renormalization terms,
(4) outputs ready to go to numerical integration.

Among those in Set V, 2232 diagrams were generated with this version and were numerically evaluated. The remaining 4122 diagrams suffer from infrared (IR) divergence. In the first attempt, we treated IR divergence by giving a small fictitious mass to the photon. This IR cut-off method surely works for the lower-order cases, but it seems difficult to improve the numerical precision of integration, particularly for the tenth order.

Therefore, we have further developed our automation code, which has just been completed. The new version analyzes the IR structure of a given diagram and automatically creates the IR subtraction terms. So far, we have tested the new automation code for the sixth- and eighth-order cases. Both results are in good agreement with known ones. We are now investigating and evaluating the tenth-order diagrams on RIKEN's supercomputer system (RSCC). We expect to get the final result from Set V within several months.

*1 Present Address: Department of Physics, Nagoya University
*2 Permanent Address: Laboratory for Elementary-Particle Physics, Cornell University

References

1) B. Odom, D. Hanneke, B. D'Urso, and G. Gabrielse: Phys. Rev. Lett. **97**, 030801 (2006).
2) R. S. Van Dyck, Jr., P. B. Schwinberg, and H. G. Dehmelt: Phys. Rev. Lett. **59**, 26 (1987).
3) G.W. Bennett, et. al. (muon $g-2$ collaboration): Phys. Rev. Lett. **92**, 161802 (2004).
4) T. Kinoshita and M. Nio: Phys. Rev. D **70**, 113001 (2004).
5) T. Kinoshita and M. Nio: Phys. Rev. D **73**, 013003 (2006).
6) G. Gabrielse, D. Hanneke, T. Kinoshita, M. Nio, and B. Odom: Phys. Rev. Lett. **97**, 030802 (2006).
7) T. Kinoshita and M. Nio: Phys. Rev. D **73**, 053007 (2006).
8) S. G. Karshenboim: Phys. Atom. Nucl. **56**, 857 (1993).
9) T. Aoyama, M. Hayakawa, T. Kinoshita, and M. Nio: Nucl. Phys. B **740**, 138 (2006); Nucl. Phys. Proc. Suppl. **157**, 106 (2006); T. Kinoshita, T. Aoyama, M. Hayakawa, and M. Nio: Nucl. Phys. Proc. Suppl. **160**, 235 (2006).

Transverse double spin asymmetries in dimuon production at small Q_T in pp and $p\bar{p}$ collision

H. Kawamura, J. Kodaira,[*1] and K. Tanaka[*2]

[Transversity, Drell-Yan process, Soft gluon resummation]

The transversity $\delta q(x)$, the distribution of transversly polarized quarks inside transversly polarized nucleon, is one of the fundamental quantities which describe the spin structure of nucleon. Tranversly polarized Drell-Yan (tDY) process: $p^\uparrow p^{\uparrow\downarrow}, p^\uparrow \bar{p}^{\uparrow\downarrow} \to l + \bar{l} + X$ is one of the processes where we can measure the transversity. In fact, tDY is the simplest process to access $\delta q(x)$ since it is inclusive for the final state, but whether it is actually useful to measure $\delta q(x)$ or not depends on the magnitude of the asymmetry: $A_{TT} \equiv \frac{\Delta_T d\sigma}{d\sigma} \equiv \frac{d\sigma^{\uparrow\uparrow} - d\sigma^{\uparrow\downarrow}}{d\sigma^{\uparrow\uparrow} + d\sigma^{\uparrow\downarrow}}$. Unfortunately, A_{TT} are likely to be rather small at RHIC[1)], because (i) pp collider probes antiquark's distributions which is likely to be small and (ii) the rapid growth of unpolarized sea distributions suppresses A_{TT} at low-x where tDY at RHIC typically probes. On the other hand, much larger asymmetries are expected at the proposed spin experiments at GSI, where polarized $p\bar{p}$ collisions are performed at lower energies[2,3)]. In this work, we study the asymmetries in Q_T distribution of dimuon, especially at small Q_T where the bulk of dimuon is produced. Here we calculate the asymmetries in the cross section which is differential in invariant mass Q, transverse momentum Q_T and rapidity y of dimuon, and in the azimuthal angle ϕ of one of the outgoing leptons:

$$A_{TT} = \frac{[\Delta_T d\sigma / dQ^2 dQ_T^2 dy d\phi]}{[d\sigma / dQ^2 dQ_T^2 dy d\phi]}. \qquad (1)$$

The Q_T distribution of dimuon in tDY is calculated in Ref.[4)]. At small Q_T, the resummation of large logarithmic corrections is crucial to make a reliable predictions. In Ref.[4)], the resummation at the next-to leading logarithmic (NLL) accuracy is carried out and combined with the fixed order result at the leading order (LO) in a consistent way. Using this "NLL+LO" cross section of tDY and the corresponding one for unpolarized DY process, we calculate A_{TT} in (1). As the nonperturbative input, we use a model of $\delta q(x)$ which saturates the Soffer bound as $\delta q_i(x, \mu_0^2) = [q_i(x, \mu_0^2) + \Delta q_i(x, \mu_0^2)]/2$ at the low input scale $\mu_0 \sim 0.6$GeV and is evolved to the higher μ^2 with NLO DGLAP kernel[5)]. A_{TT} in pp collision at RHIC kinematics are shown in Fig.1. In this case, A_{TT} is about 4-8% and rather flat in small Q_T region. We have smaller A_{TT} for smaller Q due to the suppression at small x. Comparing $y = 0$ and $y = 2$ cases, we obtain slightly larger

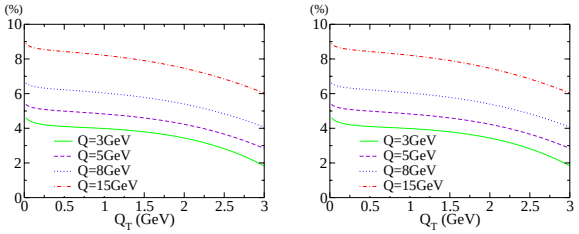

Fig. 1. A_{TT} in pp collision at RHIC kinematics: $\sqrt{S} = 200$GeV, $Q = 3, 5, 8, 15$GeV and $\phi = 0$ with $y = 0$ (left panel) and $y = 2$ (right panel).

A_{TT} for $y = 2$, but y dependence of A_{TT} is small. On the other hand, Fig.2 shows A_{TT} in $p\bar{p}$ collision at GSI kinematics. Here the valence distributions of both incoming hadrons contribute, and large A_{TT} of 15-30% are obtained. Again the asymmetries become larger as Q increases, and y dependence is very small. The flat shape of Q_T distribution at small Q_T is a common feature of A_{TT}, which shows the dominance of the soft gluon efects, whichi is universal at NLL level in both polarized and unpolarized channels.

References

1) O. Martin, A. Schäfer, M. Stratmann and W. Vogelsang, *Phys. Rev.* **D57**, 3084 (1998); *ibid.* **D60**, 117502 (1999).
2) H. Shimizu, G. Sterman, W. Vogelsang and H. Yokoya, *Phys. Rev.* **D71** 114007 (2005);
3) V. Barone et al., *Phys. Lett* **B639** 483 (2006).
4) H. Kawamura, J. Kodaira, H. Shimizu and K. Tanaka, *Prog. Theor. Phys.* **115**, 667 (2006).
5) A. Hayashigaki, Y. Kanazawa and Y. Koike, *Phys. Rev.* **D56** 7350 (1997); S. Kumano and M. Miyama, *Phys. Rev.* **D56** 2504 (1997); W. Vogelsang, *Phys. Rev.* **D57** 1886 (1998).

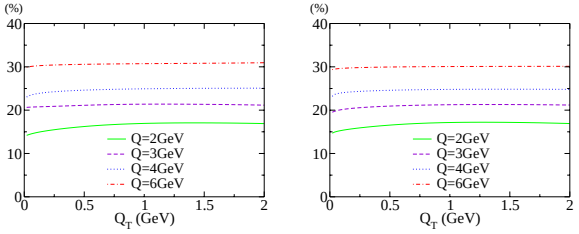

Fig. 2. A_{TT} in pp collision at GSI kinematics: $\sqrt{S} = 14.5$GeV, $Q = 2, 3, 4, 6$GeV and $\phi = 0$ with $y = 0$ (left panel) and $y = 0.5$ (right panel).

*1 Theory Division, High Energy Accelerator Organization (KEK)
*2 Department of Physics, Juntendo University

Towards a global analysis of polarized parton densities

M. Stratmann

[Perturbative QCD, spin structure of nucleons, theoretical uncertainties]

Extracting information about parton densities from hadronic cross sections is an intricate problem, even more so if one is investigating the spin structure of nucleons. If applicable, the factorization theorem allows us to study the non-perturbative hadronic spin structure, as parametrized by the polarized parton densities Δf, with the help of perturbatively calculable partonic hard-scattering cross sections $d\Delta\hat{\sigma}$. To quantify theoretical uncertainties, knowledge of the next-to-leading order (NLO) QCD corrections is essential.

The relevant numerical expressions are often too time-consuming to be of direct use in a "global analysis", which usually requires thousands of evaluations of the cross section for any given data point to determine the set of parameters used to describe the parton distributions $\Delta f(x,\mu_0)$ at some initial momentum scale μ_0. Therefore the prospects of learning from data depend on our ability to efficiently *and* reliably evaluate, e.g., the cross section for $pp \to \pi X$

$$d\Delta\sigma = \sum_{abc} \Delta f_a \otimes \Delta f_b \otimes d\Delta\hat{\sigma}_{ab\to cX} \otimes D_c^{\pi} \qquad (1)$$

at NLO with $\otimes$ denoting a convolution. Simple approximations of (1), e.g., the assumption that NLO corrections drop out in experimentally relevant spin asymmetries, $A_{\rm LL} \equiv d\Delta\sigma/d\sigma$, or the use of some average momentum fraction $\langle x\rangle$ to get rid of the convolutions in (1), have been shown to be notoriously unreliable for most processes in polarized pp and lp collisions, see, e.g.,[1,2]. In general, without knowing the polarized parton densities, in particular the elusive Δg, it is virtually impossible to assess theoretical uncertainties and the relevance of NLO corrections.

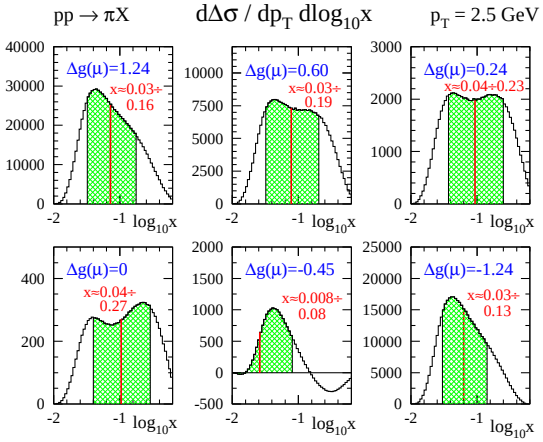

Fig. 1. The shaded areas denote the x-range dominantly contributing to $d\Delta\sigma$ for different values of $\Delta g(\mu_0)$.

The complications in pinning down Δg from pp data are exemplified further in Fig. 1.[1)] Here we study the range of momentum fractions x predominantly probed in $pp \to \pi X$ at RHIC energies for different assumptions about the first moment of $\Delta g(\mu_0)$. While gluon-gluon initiated subprocesses give a positive contribution to $d\Delta\sigma$, the sign of quark-gluon channels is correlated with the unknown sign and size of Δg. Since both contributions peak at significantly different values of x, the non-local x-distributions are readily explained.

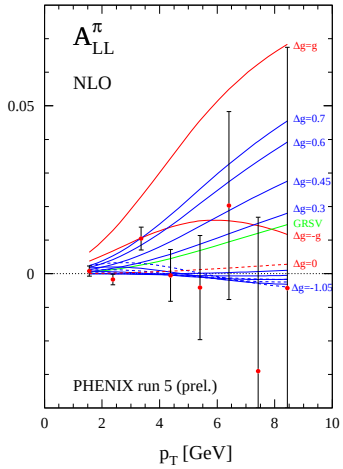

Fig. 2. PHENIX data for $A_{\rm LL}$ compared to NLO analyses.

Since these complications are most relevant for realistic, moderate gluon polarizations the goal must be to circumvent all approximations. This can be accomplished by transforming (1) into complex Mellin moment space.[3)] This allows to store all time-consuming integrations in (1) in large grids *prior* to the global analysis. The growing amount of data from RHIC has put this technique to the test.[4)] Figure 2 compares NLO calculations based on different constraints on the first moment of Δg with recent PHENIX data on $A_{\rm LL}$. Δg's with a large and positive first moment are clearly disfavored. Upcoming data will further close in on Δg and will eventually clarify its role in the spin sum rule.

References

1) M. Stratmann, contribution to the proceedings of "DIS 2006", Tsukuba, Japan, World Scientific (to appear).
2) B. Jäger, M. Stratmann, W. Vogelsang, Phys. Rev. D **67**, 054005 (2003); ibid. D **68**, 114018 (2003); ibid. D **70**, 034010 (2004); Eur. Phys. J. C **44**, 533 (2005).
3) M. Stratmann and W. Vogelsang, Phys. Rev. **D64**, 114007 (2001).
4) M. Stratmann and W. Vogelsang, work in progress.

Production of U beam from RIKEN 18GHz ECRIS

Y. Higurashi, T. Nakagawa, M. Kidera, H. Haba, T. Aihara*, M. Kase, A. Goto and Y. Yano

One of the requirements of the RIKEN RI beam factory (RIBF) project is production of U ion beams[1]. We, therefore, study how to produce the U ion beams. Here, we report the detailed experimental procedure and results of experiments using UF_6 and sputtering method.

We used UF_6 for the production of U ion beams from the ECR ion source. When using UF_6, it does not require an oven nor an insertion system for solid rods to be vaporized under plasma sputtering. It is possible to produce U ions in the same manner as in the case of gaseous elements. Figure 1 show a cross-sectional view of the RIKEN 18GHz ECRIS and a schematic drawing of a UF_6 bottle. Details of the description of the RIKEN 18GHz ECRIS and its performance are described in ref. 2. The UF_6 bottle (50 cm^3 in volume) was connected to a gas-feeding tube via a variable slow-leak valve to control the flow rate of UF_6 vapor. About 10 g of UF_6 was filled in the UF_6 bottle. No gas-mixing method was applied in these present experiments. To minimize contamination, the plasma chamber wall was covered with a thin aluminum tube (of 1 mm thickness), which is easily replaceable. Furthermore, the aluminum surface emits several secondary electrons per primary electron impact, which increases the plasma density.[3]

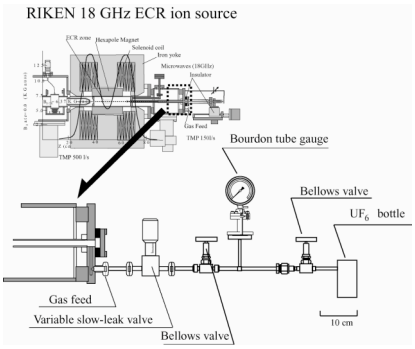

Fig. 1. Cross-sectional view of RIKEN 18 GHz ECRIS and schematic drawing of UF_6 bottle..

Figure 2 shows the charge state distribution of U ions. The ion source was tuned for production of the U^{14+} ions. The injected microwave power was 60 W. The gas pressures of the plasma chamber and extraction stages were 4.3×10^{-7} and 4.0×10^{-8} Torr, respectively. The extraction voltage was 14.1 kV. Using this method, we successfully produced an intense beam of U^{14+} ions (~1.5 pμA) continuously for 6 days for RIBF commissioning.

A U^{35+} ion beam is required from an ion source, unless we use the first charge stripper. To produce U^{35+} ions, we used the sputtering method. First, we measured the

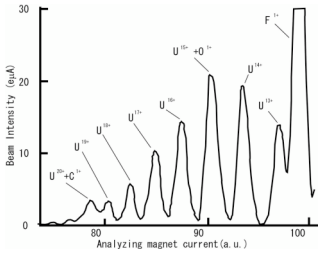

Fig. 2. Charge state distribution of U ions. The ion source was tuned for the production of U^{14+} ions.

beam intensity of U ions from a metal uranium rod. The size of the rod was 6×3×25 mm. To check the effect of ionized gas (base gas for production of plasma) on beam stability and intensity, we chose N_2, O_2, and Ne gases as ionized gases. In this experiment, the beam intensity of U ions using O_2 gas is more stable than that using N_2, or Ne gas. However, the beam intensity of U ions produced using Ne gas is higher than that using N_2 or O_2 gas, because the sputtering effect of Ne ions is much better than that of N or O ions. Figure 3 shows the charge state distribution of U ions. The ion source was tuned for the production of U^{35+} ions. The ionized gas was O_2, the injected microwave power was 500 W, the sputtering voltage was 1.9 kV, the gas pressure was $1.0*10^{-6}$ Torr, and the extraction voltage was 12.7 kV. Using this method, we successfully produced a beam of U^{35+} ions (~0.06 pμA) for 24 hours.

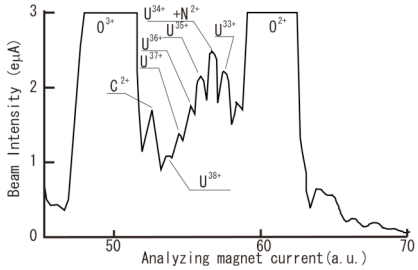

Fig. 3. Charge state distribution of U ions. The ion source was tuned for the production of U^{35+} ions.

References

1) Y. Yano: Proc. 17th Int. Conf. on Cyclotrons and Their Applications. (Tokyo, JAPAN, 2004), p. 169.
2) T. Nakagawa, Y. Higurashi, M. Kidera, T. Aihara, M. Kase and Y. Yano: Nucl. Instrum. Methods Phys. Res. Sect. **B 226** (2004) 392.
3) Nakagawa, T. Kurita, M. Kidera, M. Imanaka, Y. Higurashi, M.Tsukada, S. M. Lee, M. Kase and Y. Yano: Rev. Sci. Instrum. **73**(2002) 513.

* SHI Accelerator Service, Ltd

Design of superconducting magnet system for RIKEN 28 GHz SC-ECR ion source

T. Nakagawa, J. Ohnishi, M. Kidera, Y. Higurashi, H. Saito and A. Goto

To meet the required beam intensity of heavy ions (1 particle μA on target) for the RIKEN RI beam factory project[1], we constructed several high performance 18 GHz ECR ion sources[2,3]. However, to achieve a 1 particle μA U ion beam at 350 MeV/u, U^{35+} ion beam with the intensity higher than 15 particle μA is required from an ion source, unless we use a first charge stripper.[1] To produce such an intense beam of U^{35+} ions, we have to use a high magnetic mirror ratio and a high microwave frequency (> 18 GHz) to increase plasma density and ion confinement time. For this reason, we plan to construct a new RIKEN Superconducting ECR ion source that has an operational frequency of 28 GHz.[4]

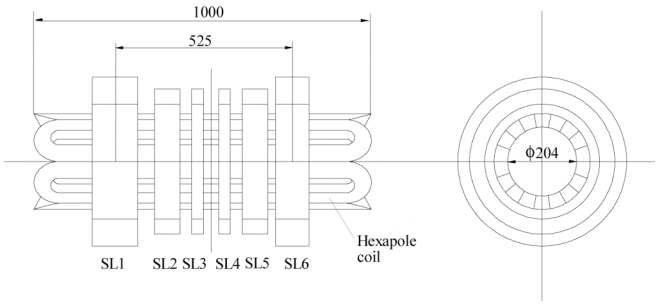

Fig.1. Arrangement of superconducting coil assembly.

Figure 1 shows the arrangement of the superconducting coil assembly developed. The coils are composed of six solenoid coils (SL1 ~ SL6) and one hexapole coil (HX).

Figure 2 shows the mirror magnetic field strength on axis. Magnetic fields strength was calculated using 3d-code "TOSCA". The peak fields at the RF injection and the beam extraction sides are 4 T and 2 T, respectively. The minimum magnetic field can be changed from 0 T to 1 T. Four solenoid coils (SL2~ SL5) work to produce a flat magnetic field in the central region for increasing the size of ECR surface.

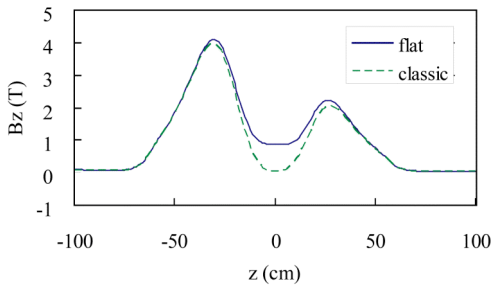

Fig.2. Mirror magnetic field strength on axis.

Figure 3 shows the magnetic field distributions on the surface of the plasma chamber with an inside radius of 75 mm. The curve 'By' indicates the magnetic field produced by the hexapole coil and the curve 'B' indicates the magnetic field strength including the axial field. The hexpole coils have iron poles with a length of 300 mm to incresae the magnetic field at the central region. The hexapole field of 2.1 T at maximum can be produced.

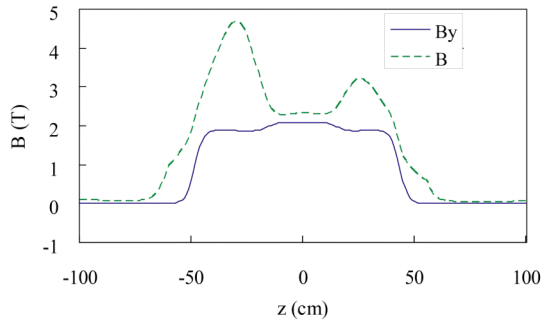

Fig.3. Magnetic field strength on inner wall of plasma chamber (radius of 75 mm).

The coil dimensions and parameters are shown in Table 1. The inside radii of the hexapole and solenoid coils are 102 mm and 170 mm, respectively. The maximum field strengths in the coils for the solenoids and hexapole coils are 7.5 T and 6.9 T, respectively. The magnetic stored energy is 830 kJ with all coils at the design current.

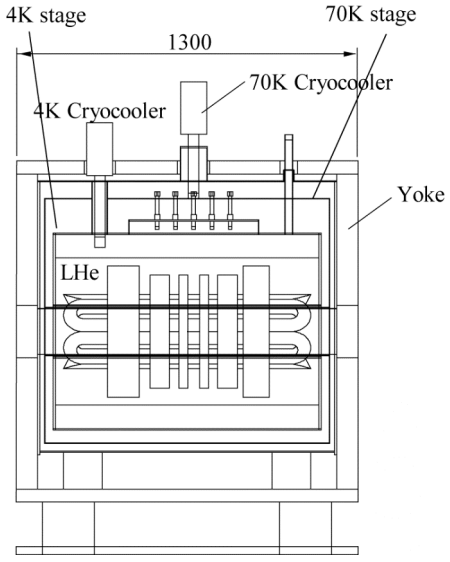

Fig.4. Cross-sectional view of cryostat.

Figure 4 shows a cross-sectional view of a cryostat. The superconducting solenoid and hexapole coils are located in a liquid-He vessel. The amount of liquid He in the vessel is assumed to be ~500 L. The cryostat is equipped with two small refrigerators for 4 K and 70 K stages and operated

without adding liquid-He after the initial pour. The heat load to 4 K stage is estimated to be 6 W, which includes 3 W due to the estimated X-ray irradiation from the plasma. Nine current leads made of high temperature superconducting material are used to reduce the heat load at 4 K stage. The estimated heat load at 70 K stage is 160 W owing to copper current leads, supports of a cold mass and radiation through out the multi-layer insulation. A magnetic shield with a 50 mm thick iron yoke surrounds the cryostat.

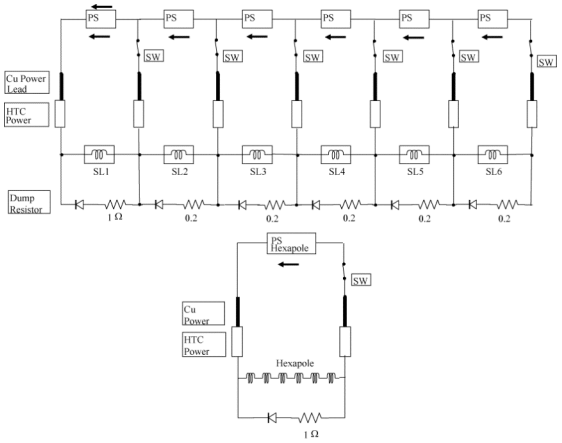

Fig.5. Diagram of electric circuit of superconducting coils.

The maximum electromagnetic force between the magnetic shields and the cold mass is estimated to be 8 tons in the axial direction. The cold mass is supported with GFRP belts from an outer tank at room temperature.
Figure 5 shows a connection diagram of the electric circuit of the superconducting coils. The six solenoids and the hexapole coils are excited individually with seven power supplies. The solenoid coils are excited with seven high temperature superconducting current leads. The current leads between two adjacent solenoids is used to reduce the heat load. When a quench happens to any coil, all power supplies are disconnected from the coils and the stored energy is discharged to the dump resistors. The resistances are 1 ohm for SL1, SL6 and HX, and 0.2 ohm for the others. The dump resistors and diodes are placed in the liquid-He vessel to protect the coils when any of the high-T_c current lead breaks.

References

1) Y. Yano: Proc. of 17th Int. Conf. on Cyclotrons and their applications p. 169.
2)T. Nakagawa et al. : Nucl. Instrum. Methods B226,392(2004).
3)T. Nakagawa et al. : Rev. Sci. Instrum. 75, 1394 (2004).
4)T. Nakagawa and Y. Yano: Nucl. Instrum. Methods B241, 935 (2005).

Table 1. Coil dimension and parameters

	SL1	SL2	SL3	SL4	SL5	SL6	HX
Inner radius (mm)	170	170	170	170	170	170	102
Outer radius (mm)	250	215	215	215	215	250	142
Length (mm)	135	75	35	35	75	100	961
Conductor size (mm)	2.0 x 1.0	2.0 x 1.0	2.0 x 1.0	2.0 x 1.0	2.0 x 1.0	2.0 x 1.0	2.0 x 1.0
Conductor size inc. insulation (mm)	2.1 x 1.1	2.1 x 1.1	2.1 x 1.1	2.1 x 1.1	2.1 x 1.1	2.1 x 1.1	2.1 x 1.1
Cu/SC	1.5	4	4	4	4	4	1.5
No. turns	4464	1360	640	640	1360	3312	684
Occupation factor	83%	81%	81%	81%	81%	83%	80%
Current density (A/mm^2)	135	145	90	90	115	115	180
Current (A)	327	360	221	221	285	278	448
Bmax(max) (T)	7.5	5.0	4.0	4.0	4.7	5.5	6.9
Ic (A)	1072	988	1168	1168	1042	898	1292
Ic/Iop	3.3	2.7	5.3	5.3	3.7	3.2	2.9
Inductance (H)	5.71	0.89	0.24	0.24	0.89	5.13	1.87
Dump resistor (Ω)	1.0	0.2	0.2	0.2	0.2	1.0	1.0

Control System for RIKEN Accelerator Research Facility and RIKEN RI-Beam Factory

Misaki Kobayashi-Komiyama, Masaki Fujimaki, Akito Uchiyama [*1], Makoto Nagase and Masayuki Kase

The control system of the RIKEN RI-Beam Factory (RIBF) is based on the control system of the RIKEN Accelerator Research Facility (RARF), which is constructed using EPICS[1]. We expanded a console at the control room in the Nishina building for RIBF control and have started the beam commissioning of RIBF since July. The latest improvements of the system are indicated in this paper.

Figure 1 shows groups of accelerators and their interface devices in the RARF and RIBF control system. Except stand-alone systems, such as a system for an ion source or rf, most parts are controlled using EPICS. We control GP-IB devices using EPICS device support programs supported by EPICS collaboration. On the other hand, NIO, CC/NET, DIM, N-DIM and PLC are controlled using device support programs developed by ourselves originally. In particular, device support programs for CC/NET, N-DIM and PLC were developed with the control group of KEK; thus, we use the same programs among RIKEN, KEK and J-PARC control systems[2].

Table 1 shows the current number of interface devices used in the RARF and RIBF control system. It includes the number of devices from RILAC to SRC, excluding an injection beamline for Big-RIPS.

Table 1. Current number of interface devices

DIM (PS)	80
DIM (BD)	100
GP-IB (GMACS)	4
GP-IB (IDX)	5
NIO-S	420
N-DIM (PF)	90
N-DIM (RP)	12
N-DIM (FC)	60
N-DIM (VAC)	70
PLC (Omron)	2
PLC (Melsec)	2
PLC (FA-M3)	3

Figure 2 shows the structure of RARF and RIBF control system. A file server based on an HP-UX system and Force VME computers placed in the Nishina building are the oldest devices in our system. We introduced the file server in 2001 and the VME computers in 1999. Except RILAC, most power supplies and beam diagnostic devices composing RARF are still controlled using these computers. Furthermore, many application programs, including GUI, graphic formulas and data taking also run on the file server.

	RARF			RIBF						
	RILAC	AVF/RRC	BT	fRC	BT (in Nishina)	BT (in RIBF)	IRC	SRC	Injection Line for Big-RIPS	Big-RIPS
Ion Source	Hard wire /WE 7000	WE 7000								
RF	PLC (CVM1)	PLC(Melsec) /DIM		PLC (CS1)			PLC (CS1)	PLC (CS1)		
Magnet Power Supply	GP-IB/NIO/DIM	DIM	DIM/NIO	DIM/NIO	NIO/DIM	NIO	NIO	NIO	NIO	NIO
Beam Diagnostics	DIM/N-DIM	DIM	DIM/N-DIM	N-DIM/DIM	N-DIM	N-DIM	N-DIM	N-DIM	N-DIM	PLC(FA-M3)
Driving Controller	DIM	DIM	DIM	PLC (FA-M3) /N-DIM/DIM		N-DIM	PLC (CS1) /N-DIM	PLC (Melsec) /N-DIM		PLC(FA-M3)
Vacuum	N-DIM	PLC (CS1)	DIM/N-DIM	PLC(FA-M3)	N-DIM	N-DIM	PLC (CS1)	PLC (Melsec)	N-DIM	PLC(FA-M3)
Beam Interlock	Hard wire /PLC (Melsec)	DIM	DIM	PLC (Melsec)						
Cooling	Local Control	Local Control	Local Control	Local Control	Local Control	PLC (Melsec)				

: controlled by existing EPICS system
: monitored by existing EPICS system
: will be controlled by expanded existing EPICS system
: will be monitored by existing EPICS system

* NIO: Network-I/O (NDS)

Fig.1. Interface devices used in RARF and RIBF control system

*1 SHI Accelerator Service, Ltd.

The file server had functioned very stably; however, a very serious accident on two disks after the summer maintenance of RARF occurred. We changed the two disks and recovered the programs hardly. Now, we are attempting at replacing the system with another system because of its age and high-cost maintenance. There are seven CAMAC crates in the RARF control system, and we have already replaced two of these crates with a network crate controller, CC/NET, which is manufactured by TOYO Corporation. We have a plan to replace the remaining five crates next year. Furthermore, we are attempting at implementing the application programs on the HP-UX server to the Linux server. After successfully implementing the programs, we will remove the HP-UX server and the Force VME computers from the control system.

For replacing the system of the HP-UX server and the Force VME computers, we introduced two types of system, namely, a system consisting of the Linux server and Motorola VME computers, and a Linux PC system, which functions as both an operator interface and an I/O controller (IOC). The former controls magnet power supplies (NIO). Although we mounted an upgraded EPICS base on the former, almost all current and device support programs can be used in the new system with a small change. The later mainly controls beam diagnostic devices and vacuum systems. Following the rearrangement of the EPICS control network system last summer, we set up one Linux PC to each subnet and each building. Although we introduced them step by step and there are some versions of Linux kernel, EPICS base and device support program, the entire system ran smoothly. However, it will be difficult to support many independent IOCs in the future; thus, we are now rearranging the Linux IOC system. To achieve a high performance, a high stability and a high security, we are going to introduce new file servers and small single board computers for IOCs. To share common programs with all IOCs, each board computer requires to obtain necessary files from the file server by NFS to run as an IOC, for example, EPICS base, device supports and runtime database. We have already constructed a test system using a PC as a file server and a wireless router application platform (WRAP) [3] as an IOC. To date, it has functioned well without any serious troubles. We will replace a PC for a server machine with a RAID system as soon as possible.

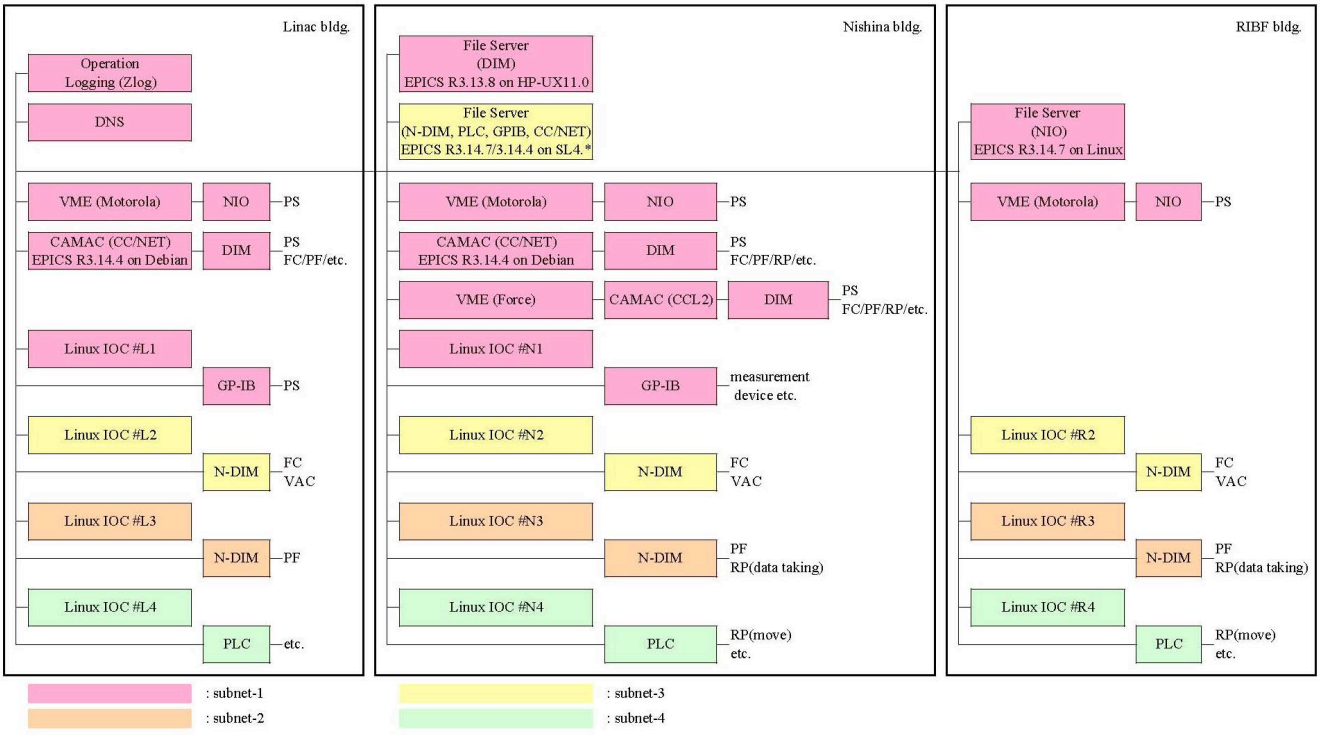

Fig.2. Structure of RARF and RIBF control system

References

1) http://www.aps.anl.gov/epics/

2) J. Odagiri et al.: Proc. 3 Annu. Meet. Particle Accelerator Society of Japan and 31 Linear Accelerator Meet. in Japan, Sendai, 2006-8 (2006).

3) http://www.pcengines.ch/

Development of Beam Phase Measurement System using Lock-In Amplifier for RARF/RIBF

R. Koyama,[*1] M. Kase, T. Watanabe, M. Fujimaki, Y. Kotaka,[*1] N. Fukunishi, and Y. Yano

In conventional tuning for an isochronous magnetic field of cyclotrons, we have used an oscilloscope to observe the beam bunch signal from the phase probe (PP). However, when the beam current is small, it is difficult to observe the beam bunch signal with an oscilloscope because rf and its higher harmonics from cyclotron cavities are superimposed on the signal. There is also a disadvantage in that we cannot obtain tuning results for an isochronous field as quantitative data in this method. Hence, we have developed a new measuring system using a lock-in amplifier (LIA) for beam phase measurement. Our final goal is to apply this system to a tuning procedure for an isochronous magnetic field of the cyclotrons of RARF/RIBF.

LIAs are used to detect and measure very small AC signals — as small as a few nanovolts. LIAs are used with a technique called phase-sensitive detection to single out the specific frequency component. Noise signals such as an rf signal and its higher harmonics from cavities at frequencies other than the reference frequency of LIAs are neglected and do not affect the measurement. We have adopted the SR844 RF lock-in amplifier[1)] manufactured by Stanford Research Systems. Its main specifications are listed in Table 1. The functional block diagram of the SR844 is shown in Fig. 1.

The block diagram for signal capturing using the SR844 is shown in Fig. 2. In our system, the accelerating rf signal from a signal generator (SG) and the beam bunch signal from PP is used as the reference and the input signals of the SR844 system, respectively. The higher harmonics of the SG was also used as the reference signal of the SR844 depending on the S/N ratio. Using these signals, we can obtain in-phase (I) and quadrature (Q) components of the beam phase with reference to SG.

We have built a LabVIEW[2)] program to control the SR844 system and to obtain data continuously via the GPIB interface (GPIB-USB-HS). The program also provides the phase and amplitude of the beam bunch signal from the measured IQ components, and plots them on the LabVIEW front panel (Fig. 3).

Thus far, we have carried out several test measurements using the SR844 system (Fig. 2) for RILAC, AVF, and RRC. The tuning results for the isochronous field are compared with those obtained by the conventional method using an oscilloscope for AVF and RRC. A good agreement of results were obtained.

Recently, we have commissioned the use of the fRC[3)] with 10.75 MeV/u $^{238}U^{73+}$ beam preaccelerated by RILAC and RRC. The injection beam current was about 100 enA. In the commissioning, we had no choice but to use the SR844 system for the tuning of the isochronous field, because currently, the $^{238}U^{73+}$ injection beam current of fRC is too small to observe the beam bunch

Table 1. Main specifications of the SR844 system.

Signal Channel:	
Input impedance	50 Ω or 1 MΩ + 30 pF
Damage threshold	±5 V (DC + AC)
Bandwidth	25 kHz to 200 MHz
Dynamic reserve	up to 80 dB
External Reference:	
Input impedance	50 Ω or 10 kΩ + 40 pF
Input level	0.7 Vpp pulse or 0 dBm sine
Demodulator:	
Time constants	100 μs to 30 ks with 6, 12, 18 or 24 dB/octave rolloff
"No-Filter" mode	10 to 20 μs update rate
Displays:	
Channel 1	I, R, I-noise, or AUX In 1
Channel 2	Q, θ, Q-noise, or AUX In 2
Reference	Freq., phase, offsets, AUX out, IF freq., or elapsed time
Channel 1 and 2 Outputs:	
Voltage range	± 10 V full scale proportional to I, Q or Ch.1, 2 displayed quantity
Update rate	
I, Q	48 to 96 kHz
R, θ, AUX inputs	12 to 24 kHz
I-noise, Q-noise	512 Hz
General:	
Interfaces	IEEE-488.2 and RS-232 interfaces

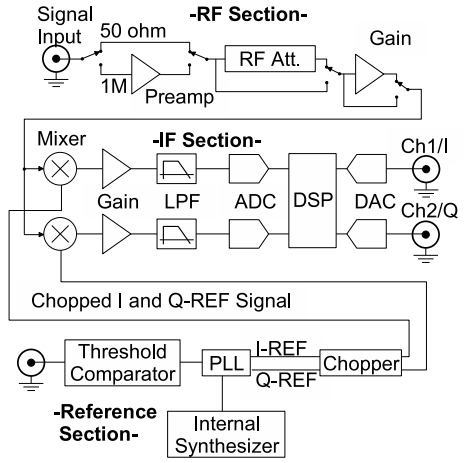

Fig. 1. Functional block diagram of the SR844 system.

[*1] SHI Accelerator Service, Ltd.

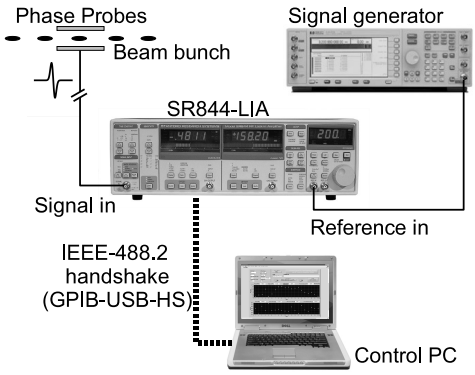

Fig. 2. Block diagram for signal capturing using the SR844 system.

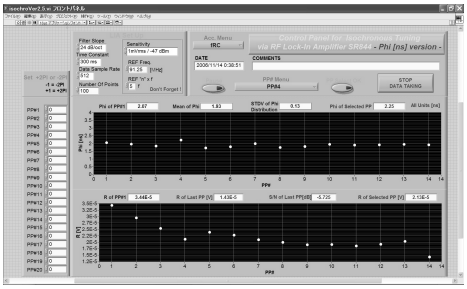

Fig. 3. Screen capture of the front panel of the built LabVIEW program.

signal by the conventional method using an oscilloscope.

The fRC sector magnet has one main coil and 10 trim coils for the tuning of the isochronous magnetic field. The electric current of these coils are variable individually. The 14 PPs are installed in the valley box of fRC. Each PP consists of a pair of parallel plate pick-ups with a gap of 30 mm. The PP measures the beam phase by timing the beam bunch passing through the pick-ups. The time required to pass through the beam bunch at each PP changes when the electric current of each trim coil is slightly changed and can be evaluated by the orbital calculation within a first-order approximation. On the basis of this calculation, a χ^2 fitting is performed as the fluctuation of the phase distribution at all PPs measured by SR844 system becomes minimum. From the fitting, the electric current of each trim coil that makes the isochronous magnetic field closer to the ideal one is evaluated. The appearance in which the isochronous field is iteratively made by this method is shown in Fig. 4. As the result of five iterations, the obtained standard deviation of the phase distribution for all 14 PPs was 0.13 nsec. This value is comparable to the tuning results for RRC obtained by the conventional method using an oscilloscope. From these results, our SR844 system was found feasible for

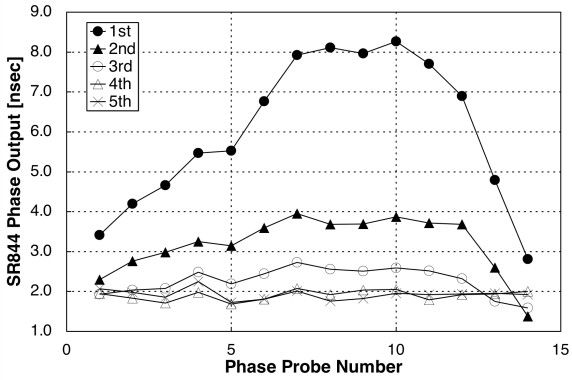

Fig. 4. SR844 phase output for each PP of fRC. The injection beam was 10.75 MeV/u $^{238}U^{73+}$ and its beam current was about 100 enA. The appearance in which the isochronous magnetic field is iteratively made is shown.

the tuning of the isochronous magnetic field with a small beam current.

The commissioning of the IRC is currently in progress and the SR844 system works basically well. However, because large fluctuations of the noise level has been observed, we are presently modifying the LabVIEW program to solve this problem. We will also soon have the commissioning of the SRC following the IRC and use the SR844 system for the tuning of the isochronous magnetic field.

We have to address the following issues to make our system applicable to the tuning of the isochronous magnetic field of RARF/RIBF cyclotrons:

(1) Search reference frequencies, harmonics of the beam frequency, which is nearly undisturbed by accelerating rf and its higher harmonics for each cyclotron of RARF/RIBF.
(2) Make efforts to reduce noise level on the beam bunch signal such as rf and its higher harmonics from cavities of cyclotrons.
(3) Evaluate systematic errors of the measurement.
(4) Modify further the LabVIEW program (e.g. responds to noise fluctuation and communication with N-DIM[4].).

Finally, the authors are grateful to the operation crews of SHI Accelerator Service Ltd. for their cooperation with the measurements using the SR844 system.

References

1) " Users Manual; Model SR844 RF Lock-In Amplifier ", Revision 2.6, Stanford Research Systems Inc., (2003).
2) <http://www.ni.com/labview/>, National Instruments Corp., (6th November 2006, Last accessed).
3) N. Inabe et al.: Proc. 17th Int. Conf. on Cyclotrons and Their Applications, Tokyo, 2004-10 (Japan Particle Accelerator Physics Society, 2005), p. 200.
4) M. Fujimaki et al.: RIKEN Accel. Prog. Rep. **38**, 258 (2004).

Study of New Flat-Top Resonator for RRC

L. Stingelin, A. Goto, O. Kamigaito, N. Sakamoto, and Y. Yano

Our study of the flat-top resonator[1,2] for the RIKEN Ring Cyclotron (RRC) has been advanced in three points:

(1) The thermomechanical design was discussed with the industry partner Sumitomo Heavy Industries.
(2) The rf-model was refined using ANSYS'[3] three-dimensional electromagnetic eigenmode solver. Coupling and fine-tuning methods were investigated.
(3) Beam dynamics simulations were performed to analyze the effect of the flat-top resonator on beam quality.

It is expected that the flat-top resonator will minimize the energy spread of particle bunches and hence the extraction losses of the RRC. Therefore, it might help in the future to increase the beam intensity of the RIKEN RI Beam Factory (RIBF).

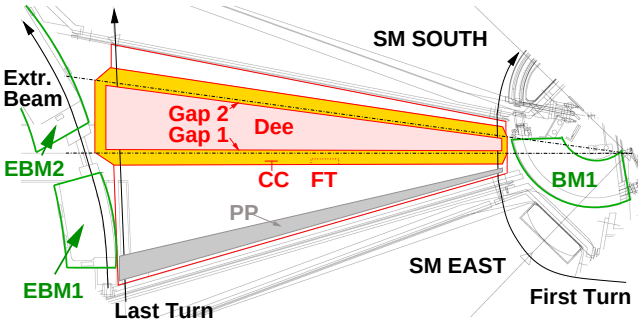

Fig. 1. Top view of proposed valley box with flat-top resonator: phase probe (PP), capacitive coupler (CC), fine tuner (FT), injection- and extraction-bending magnets (BM1, EBM1, EBM2) and sector magnet (SM).

The flat-top will be achieved by a third-harmonic resonator with a frequency range of 54-120 MHz and a total peak gap voltage of approximately 135 kV. It was possible to find an rf-geometry for the flat-top resonator that might fit into the RRC and allows reliable operation. Figure 2 and 3 show the power density and current density of the proposed flat-top resonator. The highest current density in the shorting plate of 23 A/cm was found at an operation frequency of 113 MHz and the maximum electric field in the resonator of 3.7 MV/m at a frequency of 90 MHz. The maximum power requirement is about 15 kW[1].

As indicated in Fig. 1, the injection- and extraction-bending magnets (BM1 and EBM2) prevent the use of the standard capacitive coupling and tuning methods at the shorter resonator walls. However, simulations with ANSYS' eigenmode solver[4] predicted that

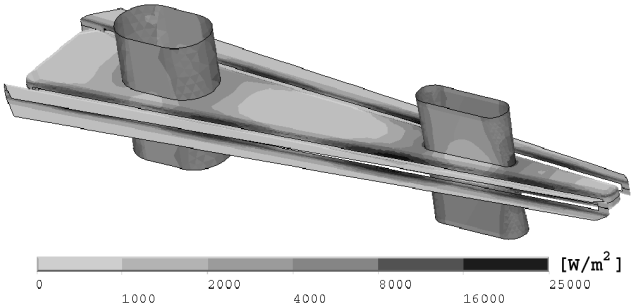

Fig. 2. Side view of Dee, electrodes and stems. The power density is shown for operation at maximum frequency.

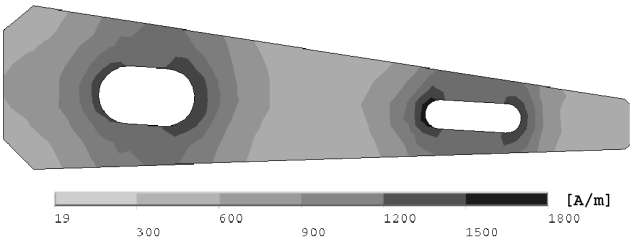

Fig. 3. The current density of the shorting plate is shown for operation at maximum frequency.

capacitive power coupling could be achieved even if the coupler is located at the larger sidewall of the resonator (see Fig. 1). Compared with an inductive coupling loop located near one of the shorting plates, this design has the advantage of easier manufacturing and maintenance because less movable parts are used.

For the analysis of the effect of the flat-top resonator on the ion beam quality, the focusing properties of the sector magnets had to be known. Because the measured field map data were no longer available, the magnetic field had to be calculated from scratch. ANSYS' magnetostatic solver with hexahedral mesh (ANSYS element types *SOLID96, SOURC36* and *INFIN111*) was used for this simulation. For the accurate representation of the sector magnet geometry, fine stairs (B-constant profile) and steps (Purcell gap and shims) had to be taken into account. This made the mesh generation very challenging; however, it was possible to create a mesh with a total of about 717,000 elements and 679,000 nodes. A comparison with the measured field on the center line showed a difference of less than 0.5%.

The beam dynamics program[5] was written in *C/C++*. A fourth-order Runge-Kutta algorithm with third-order interpolation of the magnetic fields was chosen for particle tracking and *MayaVi*[6] and *PyLab*[7]

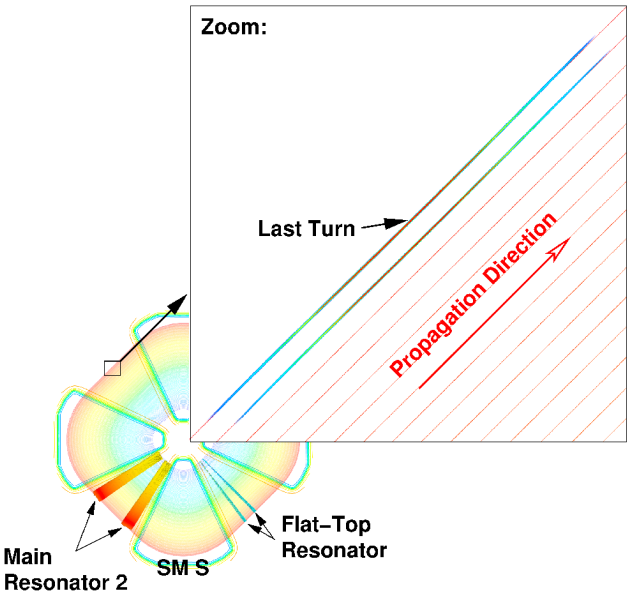

Fig. 4. Graphical output of beam dynamics program for $10.7MeV/u$ $^{238}U^{35+}$ acceleration with flat-top resonator. Schematic top view of RRC in small picture. The charge distributions for the last two turns are shown in the magnified rectangle.

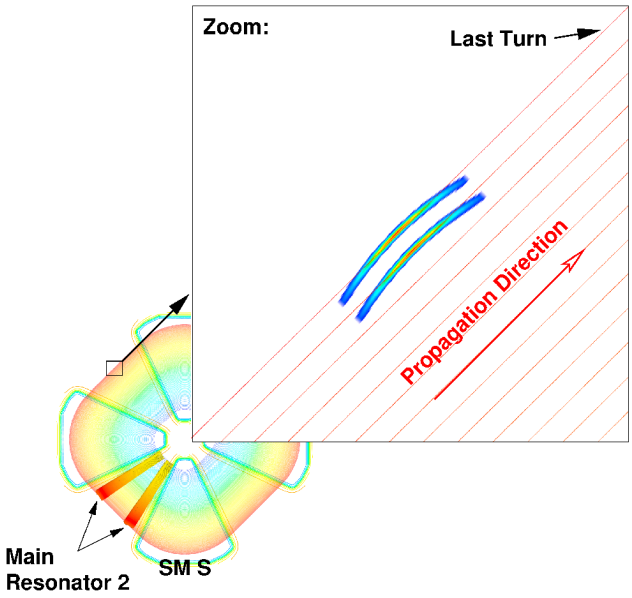

Fig. 5. Case of $10.7MeV/u$ $^{238}U^{35+}$ acceleration without flat-top resonator.

were used for the visualization of the simulation data.

Figure 4 shows the charge distributions at the last two turns for flat-top acceleration. The injected beam had a phase width of about ±8.58° and the energy spread was about ±0.187%. These parameters are actually expected to be near the injection conditions currently used. The rf-frequency is 18.25 MHz in the main resonators and 54.75 MHz in the flat-top resonator. Since the gap-voltage distributions are almost constant at these frequencies, only a small phase compression can be observed. At extraction, the beam reached a phase width of about ±7.29° and an energy spread of ±0.017%. It can be observed that the bunches are clearly separated at extraction.

The extraction losses of the RRC could also be reduced for conventional acceleration, if the injection beamline between RILAC and RRC is improved. A stronger bunching of the beam could then lead to a reduction of the energy spread at the extraction location. For example, a shorter phase width of about ±2.87° at the RRC injection location could first lead to an increased initial energy spread of about ±0.560%, if the longitudinal emittance is conserved. However, the shorter phase width would finally result in a reduced growth of the absolute energy spread during the acceleration in the RRC. Figure 5 shows the calculated charge distributions at the last two turns for this case. At extraction, the beam reached a phase width of about ±2.40° and an energy spread of ±0.080%. Compared with the case of flat-top acceleration shown in Fig. 4, the bunches are slighly bent to a banana shape and the trajectories of the ions are almost overlapping at the extraction location.

It can be concluded that extraction efficiency will be higher for flat-top acceleration. The installation of a flat-top resonator therefore seems promising for the acceleration of higher intensity beams in the RRC. As discussed above, the injected bunches must have a smaller energy spread (at larger phase width) than that for conventional acceleration for optimal extraction conditions.

On the other hand, it should also be considered that the extracted beam must satisfy the matching condition for injection into the fRC[8] and IRC.

This work was supported by the Japanese Society for the Promotion of Science in the form of a postdoctoral fellowship. The RIKEN Computing Center is also gratefully acknowledged for providing the necessary simulation resources.

References

1) L. Stingelin et al.: RIKEN Accel. Prog. Rep. **39**, 237 (2006).
2) L. Stingelin et al.: Proc. 3rd Annu. Meet. Particle Accelerator Soc. Jpn. and 31st Linear Accelerator Meet. Jpn., Sendai, 2006-8 (2006).
3) http://www.ANSYS.com
4) P. Balleyguier: Part. Accelerators **34**, 113 (1997).
5) L. Stingelin: Thesis No. 3169, Swiss Federal Institute of Technology Lausanne (2005).
6) http://mayavi.sourceforge.net
7) http://matplotlib.sourceforge.net
8) T. Aoki et al.: RIKEN Accel. Prog. Rep. **39**, 246 (2006).

Construction of Rebuncher for fRC

T. Aoki,[*1] L. Stingelin, O. Kamigaito, N. Sakamoto, N. Fukunishi, S. Yokouchi, T. Maie, M. Kase, and A. Goto

A rebuncher between the RIKEN Ring Cyclotron (RRC) and the Fixed-frequency Ring Cyclotron (fRC) has been constructed. It is now used for the commissioning of fRC. In the future, it will be used for reducing the phase width of the beam injected to fRC. In this report, design studies of the resonator and test results are described.

The rebuncher resonator is based on a new type of H-mode structure[1], as illustrated in Fig. 1. An advantage of this structure is that the intergap voltages are almost equal to each other, which is difficult to realize in conventional Interdigital-H (IH) and Crossed-bar-H (CH) structures. In addition, we can make a large pumping port in the lower part of the resonator without increasing the rf-power losses, because the rf-magnetic field is very weak in that part.[2]

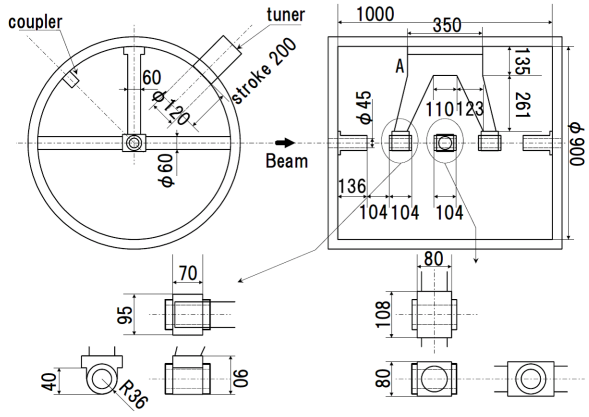

Fig. 1. Schematic drawing of rebuncher resonator and detailed structure of drift tubes.

The detailed study of the rf-field was started using the MAFIA code.[3] The cell length was set to be 208 mm, which is 1/12 of the beam-bunch separation, with a gap length of 104 mm. A cylindrical tuner of 120 mm diameter is placed in the upper half of the resonator for tuning the frequency in the range of ±390 kHz. The rf-power is fed through an inductive coupler that could be rotated for matching the input impedance. The edges of the drift tubes have been rounded as shown in Fig. 2, to keep the surface electric field less than 8.0 MV/m at maximum gap voltage of 150 kV. The maximum surface current was simulated to be 29 A/cm at the roots of the horizontal stem.

It is known that the MAFIA code sometimes gives lower resonant frequencies particularly when the number of mesh points is not sufficient in the simulations. We observed that the frequency was increased by 0.2 % when we changed the number mesh points from 1.4×10^6 to 4.0×10^6. Therefore, we made the upper stem (indicated by "A" in Fig. 1) slightly wider than that giving the desired frequency of 109.5 MHz. This width has been adjusted to give the desired frequency after the fabrication, as mentioned below. The simulated frequency and unloaded Q-value are listed in Table 1.

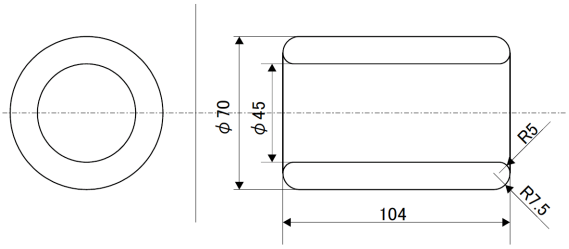

Fig. 2. Detailed geometry of drift tube.

Table 1. MAFIA simulations and measured results for initial shape of stem shown in Fig. 1.

	f[MHz]	Q_0
MAFIA	109.65	2.4×10^4
Measurement	110.01	1.9×10^4

The resonator was fabricated by Sumitomo Heavy Industries, Niihama Works. The inner electrodes such as the drift tubes and stems were made of oxygen-free copper (C1020), whereas the outer wall was made of steel (SS400) plated with 30-75 μm copper. The resonator is equipped with a turbomolecular pump of 1100 l/s for normal operation and a rotary pump of 20 m^3/h for initial evacuation. The designed vacuum level is 2.7×10^{-5} Pa. The required water flow is 35 l/min at a pressure loss of 0.38 MPa.

After the fabrication, the resonant frequency and Q-value were first measured. As shown in Table 1, the measured frequency was slightly higher than the calculated value. We have decided to cut both sides of the stem by 17 mm, as shown in Fig. 3, because the MAFIA code predicted that the frequency would decrease by 965 kHz by this modification. The computer code ANSYS[4], which is known to give a better prediction, also supported this decision.

After this modification, the desired frequency of 109.5 MHz has been achieved. The measured frequencies of the fundamental and higher modes are listed in Table 2, as well as the ANSYS results for the final configuration. As shown in Table 2, the measured frequencies are in very good agreement with the ANSYS

*1 Department of Physics, School of Science, The Graduate University of Tokyo, Japan

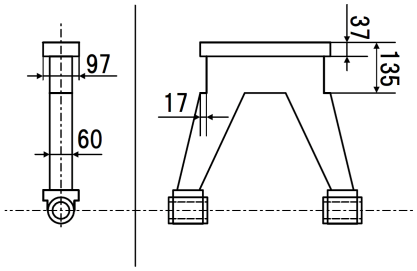

Fig. 3. Final shape of stem. Both sides have been cut by 17 mm.

Table 2. Measured results and simulations by ANSYS for final shape of stem shown in Fig. 3.

	Measurement		ANSYS	
Mode	f[MHz]	Q_0	f[MHz]	Q_0
(1)	109.50	1.8×10^4	109.52	2.3×10^4
(2)	149.49	2.0×10^4	150.21	2.7×10^4
(3)	172.88	2.1×10^4	172.76	2.2×10^4
(4)	244.86	4.4×10^4	245.37	5.2×10^4
(5)	264.28	4.5×10^4	264.69	5.2×10^4
(6)	298.86	3.2×10^4	299.71	3.6×10^4
(7)	358.26	6.8×10^4	358.62	6.8×10^4

results with deviations less than 0.5 %.

As for the second step of the low power test, the distribution of the electric field strength was measured on the beam axis by the perturbation method[5] using Teflon balls with radii of 8 and 5 mm. The measured results are shown in Fig. 4, along with the calculations by MAFIA and ANSYS. The calculated results given are scaled so that the integral of the field strength ($|E|$) might become equal to that of the results of measurement. As shown in Fig. 4, the ANSYS code gives a better prediction for the measured data; the maximum deviation is less than 5 %.

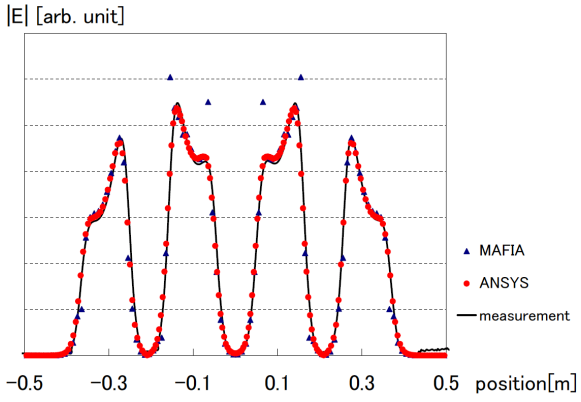

Fig. 4. Electric field on beam path.

From the perturbation measurements, we deduced the voltage ratio V_1/V_2 to be 1.26, where V_1 and V_2 denote the voltage at the two outer gaps and the voltage of two center gaps, respectively. This value is in good agreement with the simulation result.

We also deduced the shunt impedance R_s of the resonator, which is defined by

$$R_s = \frac{[2\,(V_1 + V_2)]^2}{2P}.$$

The measured shunt impedance reached 26.1 MΩ. The ratio of the measured R_s to the calculated R_s and that of the measured Q_0 to the calculated Q_0 are very similar.

The high-power test was started just after installation in the beamline in June 2006 (see Fig. 5). The rf-power was fed with a solid-state amplifier of 5 kW maximum output power. Although multipactoring effects were observed at the total voltage ($2\,[V_1 + V_2]$) range of 200-300 kV, we could achieve the maximum voltage of 470 kV at 5 kW in 3 hours. The vacuum stays at approximately 9.0×10^{-5} Pa during the normal operation.

The rebuncher has been used for the commissioning of the acceleration of uranium ions. The first operation has shown that the beam intensity in fRC has been increased twice when the rebuncher was used. Further investigation of the optimal operation conditions such as phase and voltage is under way.

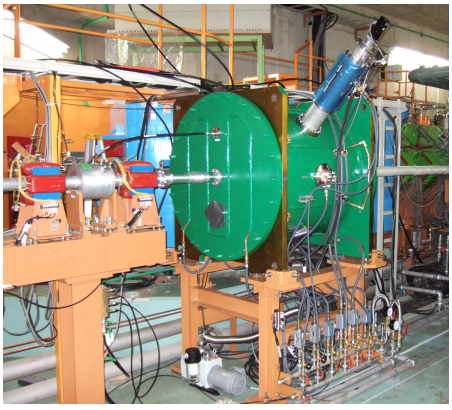

Fig. 5. Rebuncher installed in beamline.

References

1) T. Aoki et al.: RIKEN Accel. Prog. Rep. **39**, 246 (2006).
2) T. Aoki et al.: "Rebuncher resonator between RRC and fRC in RIKEN" Proc. 3rd Annual Meet. of Particle Accel. Soc. of Jpn. and 31th Linear Accel. Meet. in Jpn. (2006).
3) http://www.cst.com
4) http://www.ansys.com
5) L. C. Maier. Jr. and J. C. Slater: J. Appl. Phys. **23**(1), 68 (1952).

Preparation of polymer coating carbon stripper foils

H. Hasebe, H. Ryuto, N. Fukunishi, A. Goto, M. Kase, and Y. Yano

Thin carbon foils (C-foils) have a common problem on handling; they are easy to break when separated from a substrate, mounted on a holder, or placed at a stripper changer. There is a method of strengthening the C-foil mechanically by coating it with a polymer. Although such polymer-coated C-foils, whose thickness range is 3 – 20 μg/cm^2, were commercially available before, thicker carbon foils are required for the acceleration of heavy ions at the RIKEN RI Beam Factory [1]. We thus searched for the optimum polymer and found that poly-monochloro-para-xylylene (PPX-C) could be used for this purpose. PPX-C also has an advantage in that it is removed by evaporation during irradiation with a beam.

The deposition of PPX-C consists of three steps, as shown in Fig. 1. PPX-C is produced from the same monomer by replacing one of the aromatic hydrogens with a chlorine atom. The first step is to vaporize a solid dimer at approximately 175°C. The second step is to cleave the vapor dimer (pyrolysis) at the two methylene-methylene bonds at approximately 690°C to yield a stable monomeric diradical, monochloro-para-xylylene. The final step is to transport the monomers to a room-temperature deposition chamber where they simultaneously adhere and polymerize on a substrate.

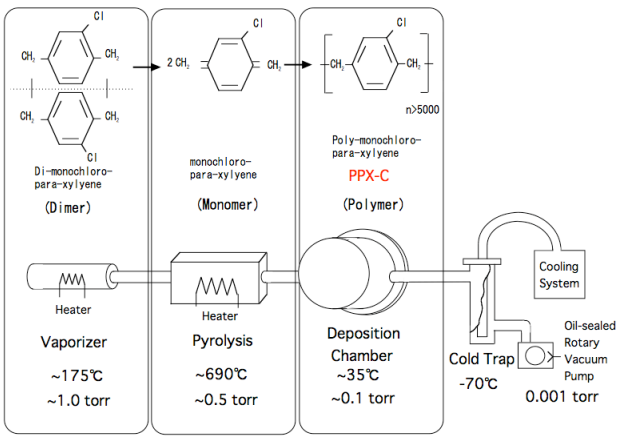

Fig. 1. Deposition of PPX-C.

The vapor deposition system LABCOTER (PDS 2010 by Specialty Coating Systems) [2] was introduced in August, 2005; a photograph of the system is shown in Fig. 2. On top of the device, a deposition chamber is placed, in which three or four substrates of 5 inches diameter are set. Carbon is deposited on the substrates beforehand. An appropriate amount of dimer is set in the vaporizer, and PPX-C of 20 – 30 μg/cm^2 thickness is coated on the C-foils. We chose these thicknesses because thinner PPX-C became weak due to a low molecular weight, and because thicker PPX- C shrank due to heat stress and resulted in a shorter lifetime for beam irradiation than the C-foil without coating. The thickness of PPX-C is determined by measuring the difference in the weight of the test sample placed near the substrate before and after the deposition. It takes approximately an hour for one cycle of coating.

Fig. 2. Photograph of LABCOTER (PDS 2010).

Either the arc discharge method or magnetron sputtering can be applied to the first carbon layer. The atomic force microscope (AFM) images of ACF-40 (Arizona Carbon Foil Co.) [3] with and without the deposition of 20 - 30 μg/cm^2 PPX-C are shown in Fig. 3. It can be seen that the surface of carbon is smoothed. We found that PPX-C of this thickness range can make the film sufficiently strong.

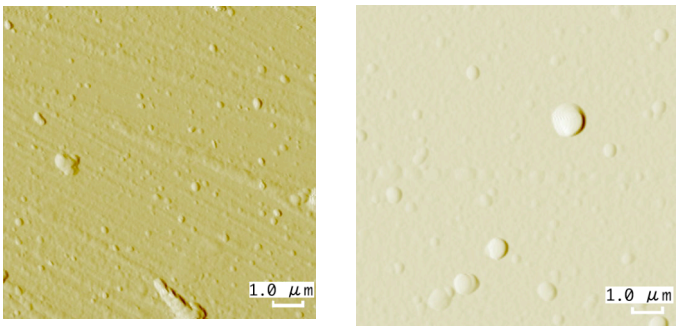

(a) (b)

Fig. 3. AFM images of ACF-40: (a) without and (b) with deposition of 20 - 30 μg/cm2 PPX-C.

We found that the second carbon layer coated on the PPX-C layer was hard to peel off and that multilayer films could be fabricated using this method. Magnetron sputtering was more suitable for the second layer onward, although either the arc discharge method or magnetron sputtering

could be applied to the first layer. When the arc discharge method was applied to the second and other layers, pin holes were easily made in the film. The most desirable thickness of one layer of carbon was approximately 50 μg/cm^2; a thicker carbon lager also caused pin holes. Figure 4 shows a photograph of the film consisting of 11 layers of carbon and PPX-C attached on a 5-inch-diameter glass substrate. For this film, chloride was used as a releasing agent. The thickness of carbon is 500 μg/cm^2 in total. PPX-C becomes blue depending on its thickness, although it is originally colorless.

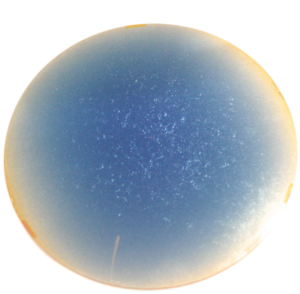

Fig. 4. Multilayer of carbon and PPX-C on substrate.

A carbon foil of 10 cm diameter and 500 μg/cm^2 thickness was produced by this method, separated from the substrate and mounted on a foil holder (see Fig. 5). The holder with this large film will be mounted on a " rotating cylinder stripper" with which the holder rotates at 1,000 rpm [4] (see Fig. 6).

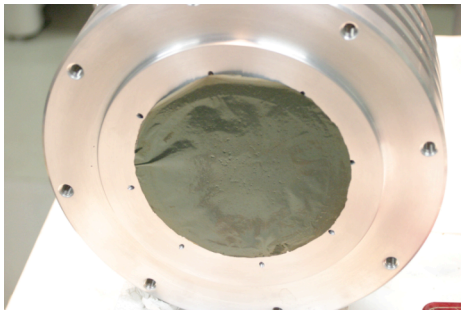

Fig. 5. Film mounted on holder.

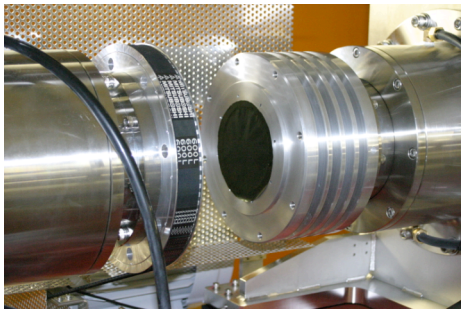

Fig. 6. Holder installed on " rotating cylinder stripper".

To investigate the effect of PPX-C on the lifetime of the film against beam irradiation, we measured the lifetime of singly coated C-foils. The C-foils used were ACF-10, 20, 40 and 80 whose thicknesses were 10, 20, 40 and 80 μg/cm^2, respectively. The measurement was carried out by irradiating the C-foils with a 32 keV/u $^{136}Xe^{9+}$ beam at an intensity of 420 pnA that was delivered from a 500 kV Cockcroft-Walton terminal. The beam was focused on the C-foil of 5 mm diameter. The lifetime was determined by monitoring both the beam intensity of the stripped ions and the C-foil image on a TV display. The results of the measurement are shown in Fig. 7, in which the lifetimes with and without PPX-C coating are compared for the four types of C-foil. It was found that the coating caused no marked degradation in lifetime. We also measured the lifetime of a long-lived C-foil [5] that we had developed and observed no degradation of lifetime due to coating.

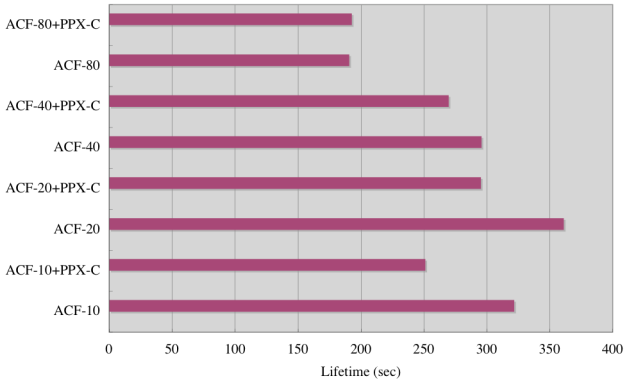

Fig. 7. Measured lifetimes of C-foils with and without PPX-C coating. No marked degradation due to coating is observed.

References

1) H. Ryuto, N. Fukunishi, H. Hasebe, N. Inabe, S. Yokouchi, O. Kamigaito, A. Goto, M. Kase, and Y. Yano, Proceedings of 2005 Particle Accelerator Conference, Knoxville, Tennessee, 2005, p. 3751.
2) Specialty Coating Systems (SCS).
URL: http://www.scscoatings.com/
3) ACF-Metals Arizona Carbon Foil Co., Inc.,
URL: http://www.techexpo.com/firms/acf-metl.html.
4) H. Ryuto, H. Hasebe, N. Fukunishi, S. Yokouchi, A. Goto, M. Kase, and Y. Yano: "Rotating charge strippers for acceleration of intense heavy-ion beams at RIKEN ", Nucl. Instrum. Methods Phys. Res. A **569**, 697 (2006).
5) H. hasebe, M. Kase, H. Ryuto, and Y. Yano: "Long-lived carbon stripper foils for intense heavy-ion beams", 17th International Conference on Cyclotrons and Their Applications (Cyclotrons 2004), Tokyo, Oct. (2004).

Rotating cylinder charge stripper†

H. Ryuto, H. Hasebe, N. Fukunishi, S. Yokouchi, A. Goto, M. Kase, and Y. Yano

Four charge stripper sections have been prepared for the RIKEN RI-beam factory[1]. Among these sections, an approximately 0.5-mg/cm^2-thick carbon foil is planned to be used as a charge stripper placed between the RIKEN ring cyclotron (RRC) and the fixed-frequency ring cyclotron (fRC). The foil is expected to receive a 1 kW power when a 15 pμA uranium beam passes through the foil. A conventional method of dealing with the heat problem is to rotate the foil. The method increases the area from which thermal radiation is emitted. To solve the heat problem of the charge stripper between the RRC and the fRC, a rotating-cylinder charge stripper was constructed. The rotating-cylinder charge stripper rotates a relatively thin carbon foil that cannot be rotated by the previously constructed rotating-shaft charge stripper[2].

Figure 1 shows a schematic view of the rotating-cylinder charge stripper. A carbon foil is attached to one of the two ends of an Al cylinder. The length and inner diameter of the cylinder are 120 mm and 100 mm, respectively. The outer surface of the cylinder shapes air-cooling fins. Both ends of the cylinder are connected to hollow-shaft ferrofluid-sealed rotary-motion feedthroughs. A timing pulley is placed between the cylinder and one of the feedthroughs. The cylinder and feedthroughs form a vacuum duct for beams. The feedthroughs are attached to the side walls of rectangular vacuum chambers. The distance between the beam spot and the rotation axis is 30 mm. The rectangular vacuum chambers are connected with a 165-mm-diameter duct to avoid a pressure difference while evacuating the chambers. The timing pulley and a motor placed outside the vacuum chambers are connected with a timing belt. The maximum rotation frequency is 1000 rpm. The thermal radiation emitted by the foil is absorbed by water-cooled Al disks whose surfaces facing the rotating foil are coated with thermally sprayed alumina to increase emissivity. The Al disks are stable and have holes for beams. The operation of the rotating-cylinder charge stripper was examined by rotating a 0.5-mg/cm^2-thick carbon foil at 500 rpm. The foil was rotated stably without breakage.

References

1) H. Ryuto et al.: Proc. 2005 Particle Accelerator Conference, Knoxville, USA, 2005, p. 3751.
2) H. Ryuto et al.: RIKEN Accel. Prog. Rep. **38**, 264 (2005).

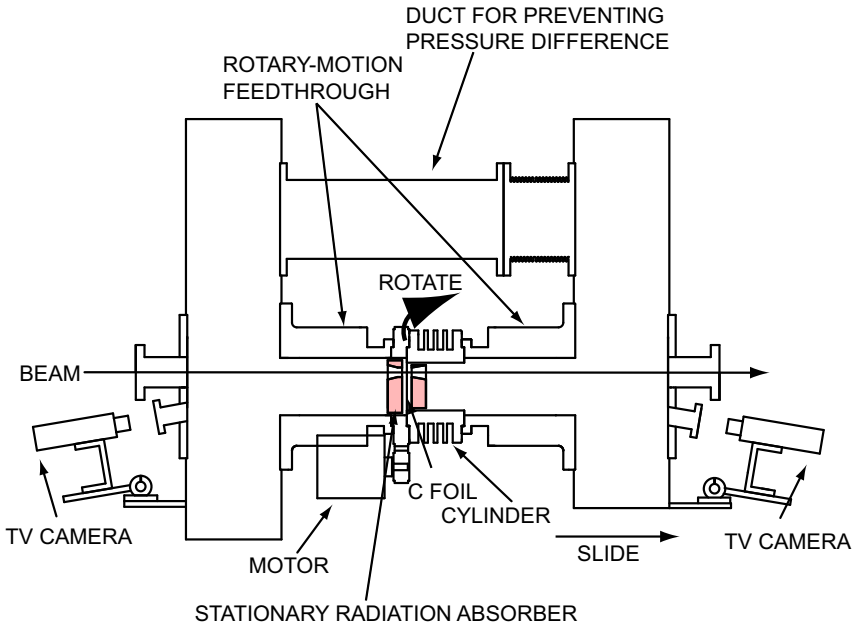

Fig. 1 Schematic view of rotating-cylinder charge stripper.

† Condensed from the article in Nucl. Instrum. Methods A 569, 697 (2006).

Measurements of beam energy and longitudinal beam profile using plastic scintillation monitors for RIBF

T. Watanabe, M. Fujimaki, M. Wakasugi, M. Kase, N. Fukunishi, K. Yamada, Y. Kotaka, R. Koyama, A. Goto, and Y. Yano

New plastic scintillation profile monitors (scintillation monitors) have been fabricated to evaluate the energy and longitudinal profiles of heavy-ion beams for the RIKEN RI beam factory (RIBF)[1]. Four sets of scintillation monitors (8 monitors) were installed into the transport lines of the RIKEN heavy-ion linac (RILAC), the RIKEN ring cyclotron (RRC), the fixed-frequency ring cyclotron (fRC) and the intermediate-stage ring cyclotron (IRC) to measure the accelerated energy of heavy-ion beams. Furthermore, two scintillation monitors were also installed into the transport line upstream of the injection point of the RRC and the fRC to optimize the phases of the rebunchers. Preliminary experimental results obtained during the commissioning of the RIBF using the heavy-ion beams are described in this article.

When a scintillation material is struck by a charged particle, fluorescence photons are produced. Then, these photons are amplified by a photomultiplier that has extremely high sensitivity. Longitudinal beam profiles are obtained using a time-to-digital converter (TDC), which digitizes the time lag between the start pulse (deteced signal) and the stop pulse (bunch clock). The energy of the beam can be obtained from the measured time of flight (TOF) of the beam using a longitudinal profile monitor set. A photograph of the longitudinal profile monitor installed into the transport line between the RRC and the IRC are shown in Fig. 1. The plastic scintillator is pneumatically inserted into the beam transport chamber by the pneumatic rotary feeder when the measurement is started.

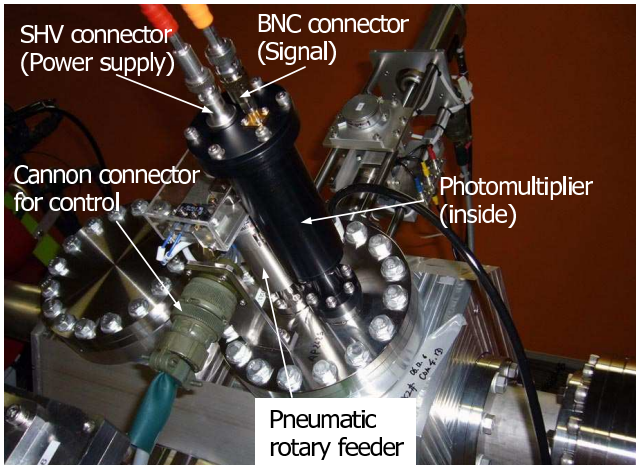

Fig. 1. Photograph of longitudinal profile monitor using plastic scintillator installed into transport line between RRC and fRC.

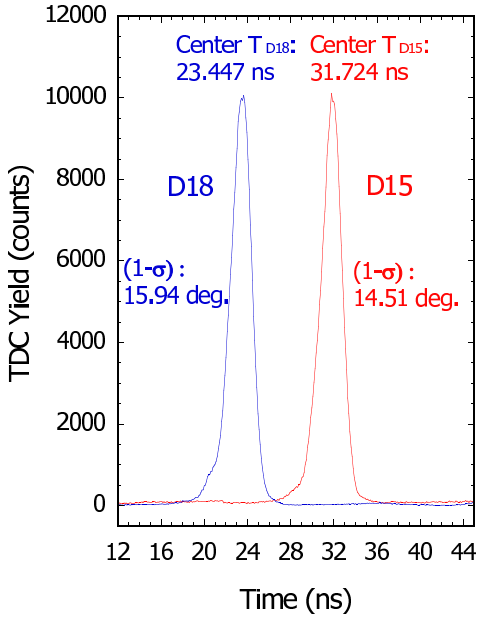

Fig. 2. Time spectra (D15, D18) measured using $^{84}Kr^{26+}$ (45.4 MeV/u) beam, which represent longitudinal beam profile.

The energy measurements of a $^{84}Kr^{26+}$ (45.4 MeV/u) beam accelerated by the RRC were carried out using the TOF method. To maintain the minimal background, the Kr beam was attenuated to between 200 s^{-1} and 300 s^{-1}, and the stop pulse was

Table 1. By fitting time spectra in Fig. 2 using Gaussian curves, center times (T_{D15}, T_{D18}) of spectra and the longitudinal phase widths (1-σ) were obtained and results were tabulated.

Location	Center (ns)	1-σ (ns)	1-σ (deg.)
D15	31.724 (T_{D15})	1.104	14.51
D18	23.447 (T_{D18})	1.213	15.94

Table 2. Nominal and measured values of TOF, β (ratio of beam velocity to light velocity) and energy of $^{84}Kr^{26+}$ beam.

	TOF (ns)	β	Energy (MeV/u)
Nominal values	228.08	0.301462	45.4
Measured values	227.56	0.302153	45.62
			$\Delta E/E$=+0.48%

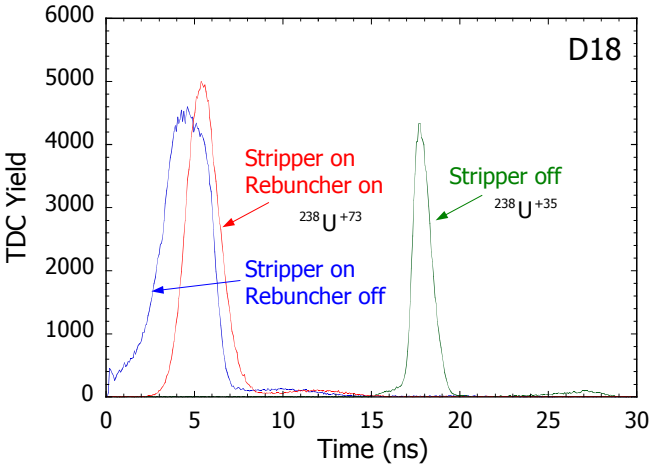

Fig. 3. Measured time spectra of a $^{238}U^{35+}$ and a $^{238}U^{73+}$ (10.75 MeV/u) beam.

operated at an RF frequency of 36.5 MHz (a period (τ_{RF}) of 27.3973 ns) in the measurements. The time spectra measured at D15 and D18 using the $^{84}Kr^{26+}$ beam, which represent the longitudinal beam profile, are shown in Fig. 2. By fitting the time spectra in Fig. 2 using Gaussian curves, the center times (T_{D15}, T_{D18}) of the spectra and the longitudinal phase widths (1-σ) were obtained and the results are shown in Table 3. The time of flight (τ_{tof}) between D15 and D16 is given by

$$\tau_{tof} = k \times \tau_{RF} + (T_{D15} - T_{D18}), \quad (1)$$

where k is a wave number. The length L between the scintillation monitor of D15 and a scintillation monitor of D18 was measured to be 20.611 m using a laser distance meter, which has a measuring accuracy of ±1.5 mm. The kinematic energy of the beam T is given by

$$\beta = L/(\tau_{tof} \times c),$$
$$T = E_0(1/\sqrt{1-\beta^2} - 1), \quad (2)$$

where β is the ratio of beam velocity (v) to light velocity (c) and E_0 is the rest mass of the heavy ion. By using these equations, the energy of the $^{84}Kr^{26+}$ beam was obtained and the nominal and measured values are shown in Table 2. Finally, it was found that the energy difference (ΔE/E) between the nominal value and the measured value was +0.48%. Hence, the beam was operated under appropriate conditions.

To optimize phases of the rebuncher[2], preliminary measurements of the longitudinal profiles of a $^{238}U^{35+}$ beam and a $^{238}U^{73+}$ (10.75 MeV/u) beam were carried out. For the experimental measurements, the scintillation profile monitor of D18, located relatively close to the injector of the fRC and far from the rebuncher (11.096 m), was used. The time spectra were taken

Table 3. Measured FWHM of the longitudinal phase width under several conditions.

Condition	Center (ns)	1-σ (ns)	1-σ (deg.)
Rebuncher off	4.60	2.054	17.99
Stripper off	17.83	0.611	5.35
Rebuncher on	5.45	1.25	10.97

under the same conditions used for the TOF measurement, and the results are shown in Fig. 3. The results show that the longitudinal phase width were 5.35 deg. in FWHM (carbon stripper off) and 17.99 deg. in FWHM (carbon stripper on). However, it has been found that the rebuncher, which was operated at a frequency of 109.5 MHz (a period of 9.1324 ns), compressed the longitudinal phase width from 17.99 deg. to 10.97 deg. according to these measurements.

The CAMAC system used for data acquisition is controlled by a Linux-based PC, and the PC is linked to a laptop in the main control room located 200 m from the RRC hall using Ethernet. The measured results are displayed by the PAW++ based on several components of the CERN Program Library. The driving control and status monitoring of the plastic scintillator are controlled by the EPICS system[3].

The authors thank the operation crews for their great help.

References

1) T. Watanabe et al.: RIKEN Accel. Rep. **39**, 241 (2006).
2) T. Aoki et al.: RIKEN Accel. Rep. **39**, 246 (2006).
3) M. Kobayashi-Komiyama et al.: RIKEN Accel. Rep. **37**, 277 (2004).

Development of new HTS current sensor and HTS magnetic shields for HTS-SQUID monitor

T. Watanabe, Y. Sasaki,[*1] M. Kase, S. Watanabe,[*2] T. Ikeda, T. Kawaguchi[*3] and Y. Yano

Last year, a prototype of a highly sensitive beam current monitor with a high-temperature superconducting (HTS) SQUID and an HTS magnetic shield[1–8], that is, the HTS-SQUID monitor, was installed in the beam transport line of the RIKEN Ring Cyclotron (RRC). As a result, a 10 μA $^{40}Ar^{15+}$ beam intensity (63 MeV/u) was successfully measured with a 500 nA resolution[9,10]. Although the intensity of a submicroampere beam can be measured, a minimum current resolution lower than two orders of magnitude (1nA) is required for the measurements of fainter heavy ion beams. Therefore, we have developed a new HTS-SQUID and high-permeability cores introduced into two input coils of the HTS-SQUID to improve sensitivity. These are very important parts for a new current sensor of the HTS-SQUID monitor. A test using a current wire for simulating beam current shows a 50-fold improvement in gain, because the newly installed high-permeability cores and SQUID improved the transfer coupling efficiency of the magnetic field induced by the beam current[9,10].

This year, both the new HTS current sensor and the new HTS magnetic shields were developed. Their schematic drawing is shown in Fig. 1 and a picture of Ag substrates are shown in Fig. 2. The substrates made of MgO ceramic tubes used for the prototype HTS SQUID monitor were changed to substrates made of 99.9% silver (Ag), because the new substrates must be fabricated precisely. Then, the surfaces of the substrates are coated by a thin layer (70 μm) of Bi_2-Sr_2-Ca_1-Cu_2-O_x (Bi-2212), which is a high-temperature superconducting material[11]. Although silver has a high conductivity and is used as the material of the substrates, there are no problems encountered in its use. Because the superconducting material has a completely zero resistance, then the current should flow only in the superconducting material. In addition,

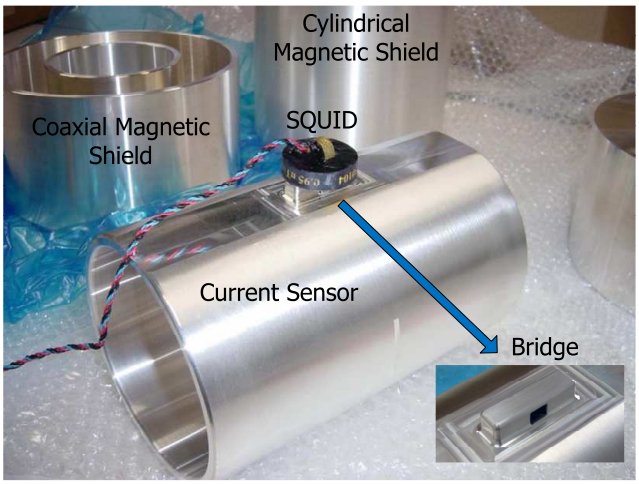

Fig. 2. Picture of Ag substrates of new HTS current sensor, HTS cylindrical magnetic shield and coaxial magnetic shields.

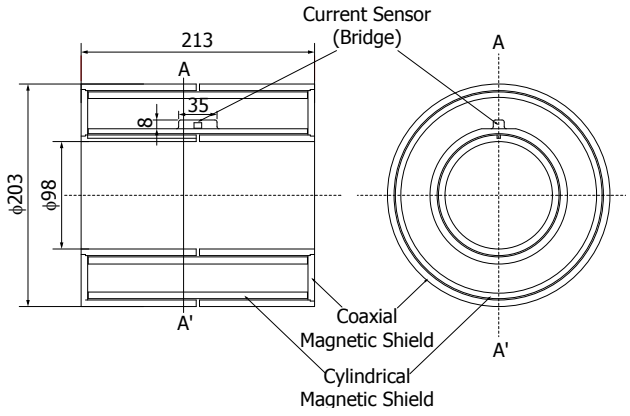

Fig. 1. Schematic drawing of new HTS current sensor and HTS magnetic shields for HTS-SQUID monitor.

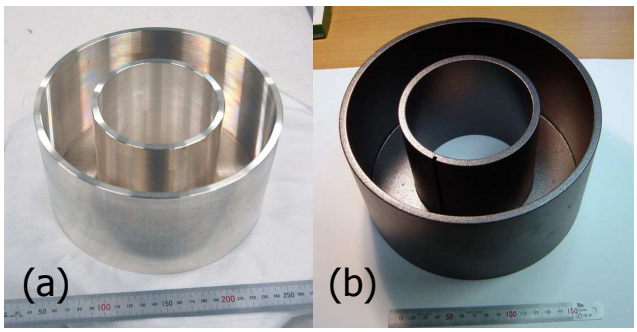

Fig. 3. (a) Ag substrate of the coaxial magnetic shield. (b) HTS coaxial magnetic shield coated by the thin layer of Bi2212.

*1 Matsushita Electric Industrial
*2 Center for Nuclear Study (CNS), Graduate School of Science, University of Tokyo
*3 KT Science Ltd.

it was observed using an Electron Probe (X-ray) Micro Analyzer (EPMA) in RIKEN that the surface of the HTS material Bi2212 was clearly smooth and that Bi2212 adhered strongly to the Ag substrate compared with Bi2223[8]. The Ag tube used as the current sensor is coated by a thin layer of Bi2212 on both the inner and outer walls of the tube. While a beam is passing through the tube, a shielding current produced by the Meissner effect flows in the opposite direction along the wall, so as to screen the magnetic field generated by the beam. The surface of the outer wall has a narrow slit without coating Bi2212 to form a bridge circuit. Then, the induced current concentrates in the bridge circuit and forms an azimuthal field. The HTS SQUID is located near the bridge circuit and can detect the azimuthal magnetic field. The HTS magnetic shields that are used on the basis of the Meissner effect consist of coaxial magnetic shields, a cylindrical magnetic shield and also the current sensor. The current sensor plays an important role for not only the current detector but also the magnetic shielding. Then, the SQUID is almost surrounded by the HTS magnetic shields to shield environmental magnetic noise strongly. Regarding the processing, we fabricated several parts: (1) two cylinders and one disk with a hole for the substrates of each coaxial magnetic shield, and (2) one cylinder and the bridge for the substrate of the current sensor. After the fabrication, we welded each part by electron beam welding. The measured processing accuracy after the electron beam welding was within ± 100 μm.

Now, we have coated the thin layer of Bi2212 on all the substrates. Figure 3(a) shows the Ag substrate of the coaxial magnetic shield and (b) shows the one coated by the thin layer of Bi2212. The current sensor and cylindrical magnetic shield could be fabricated with no problems. However, some pinholes were formed after coating the HTS material on the substrates of the coaxial magnetic shields. We are now in the process of completing the coaxial magnetic shields as well as preventing the formation of pinholes by grinding the surface of the Ag substrates, and changing the baking temperature and thickness of Bi2212.

The authors are grateful to S. Ono, B. Mizuno, H. Kanada, N. Murakami, S. Kojima and N. Amazaki for their fruitful collaboration.

References

1) T. Watanabe et al.: RIKEN Accel. Rep. **35**, 314 (2002).
2) T. Watanabe et al.: Proc. 8th European Particle Acc. Conf., Paris, France, 2002-6, (EPS-IGA, 2002) p. 1995.
3) T. Watanabe et al.: RIKEN Accel. Rep. **36**, 331 (2003).
4) T. Watanabe et al.: CNS Annual Rep. **59**, 71 (2003).
5) T. Watanabe et al.: Proc. 14th Symp. on Acc. Sci. and Technology, Tsukuba, 2003-11, (KEK 2003), p. 99.
6) T. Watanabe et al.: RIKEN Accel. Rep. **37**, 310 (2004).
7) T. Watanabe et al.: Supercond. Sci. and Technol. **17**, S450 (2004).
8) T. Watanabe et al.: RIKEN Accel. Rep. **38**, 273 (2005).
9) T. Watanabe et al.: Proc. 7th Symp. on European Conf. on Appl. Supercond., Vienna, 2005-9, (IOP publishing, 2006), **43**, p. 1215.
10) T. Watanabe et al.: RIKEN Accel. Rep. **39**, 243 (2006).
11) Y. Ishikawa et al.: Advances in Supercond. (ISS'91) **4** 1992 p. 1076.

Construction of vacuum pumping system for RIBF beam transport line

S. Yokouchi, M. Fujimaki, N. Fukunishi, M. Nishida,* and M. Kase

The vacuum pumping system for the injection and extraction beam transport (BT) lines of the fRC were constructed from June to October 2006. A part of the existing BT line from the RRC was modified to be applied to the fRC injection line. The vacuum pumping system for the BT line from the IRC to the SRC, which was nearly completed in 2005, was connected with the SRC in November 2006, and the vacuum pumping system for all the BT lines to the SRC was completed. Figure 1 shows a schematic layout of the vacuum pumping system for the BT lines from the RRC to the SRC in the RIBF.

The vacuum pumping system for the BT lines is divided into some sections by gate valves (GVs). Each section has one or two vacuum pumping units (VPUs). A VPU is composed of a turbomolecular pump, GVs, vacuum gauges, a local controller, and other vacuum components.[1] Figure 2 shows a photograph of the VPU installed in the BT line, and Fig. 3 shows that of the local controllers mounted on a rack. The attainable average pressure along the BT line was designed to be below 2×10^{-5} Pa. The VPUs and GVs can be operated both locally using their controllers and remotely from the control console.

After the installation of magnets, first, the beam diagnostic chambers made of aluminum alloy were installed precisely on robust frames at their fixed positions. Vacuum ducts, bellows, and GVs, all of which were made of aluminum alloy, were constructed between those chambers. VPUs were mounted on their fixed chambers, whereas their local controllers were installed at some places free from radiation. Electric wiring and pneumatic piping works were carried out last.

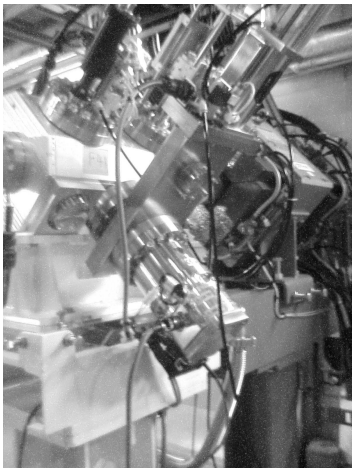

Fig. 2. VPU.

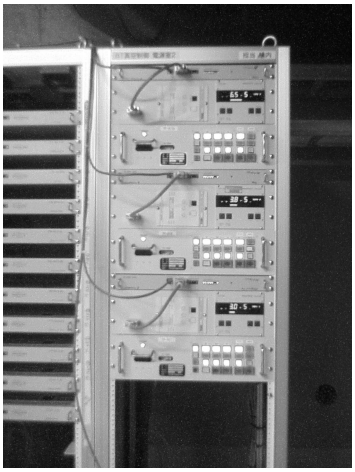

Fig. 3. Local controller of VPU.

The up-to-date pressures measured at each VPU are listed in Table 1. From these data, the actual average pressure along the BT lines seems to be higher than the expected pressure. The cause of this disagreement will be investigated later.

Table 1. Measured pressures at VPU. Measured on 30 Nov. 2006.

Unit	Pressure(Pa)	Unit	Pressure(Pa)
TP-A01	1.9×10^{-5}	TP-A03	1.3×10^{-4}
TP-A11	1.3×10^{-5}	TP-M04	1.2×10^{-5}
TP-D11	5.5×10^{-5}	TP-Str	6.4×10^{-5}
TP-D13	1.6×10^{-4}	TP-M11	1.2×10^{-4}
TP-D61	9.0×10^{-6}	TP-H12b	6.5×10^{-5}
TP-D14	8.4×10^{-6}	TP-H18	3.8×10^{-5}
TP-D16	2.6×10^{-6}	TP-H31	3.0×10^{-5}
TP-D17	1.1×10^{-4}	TP-K51	3.1×10^{-5}
TP-D1A	1.3×10^{-5}	TP-K01	5.9×10^{-5}
TP-F41	1.5×10^{-5}	TP-K02	1.7×10^{-5}
TP-F01b	1.9×10^{-5}	TP-G10	3.4×10^{-5}
TP-DA1a	8.9×10^{-6}	TP-G12	3.1×10^{-5}
TP-DA2	1.0×10^{-5}	TP-G21	1.4×10^{-5}
TP-DA4a	4.1×10^{-6}	TP-G26	1.4×10^{-4}
TP-AA6	1.1×10^{-4}	TP-K40	6.2×10^{-5}

References

1) S. Yokouch et al.: RIKEN Accel. Prog. Rep. **37**, 275(2004).

* SHI Accelerator Service, Ltd.

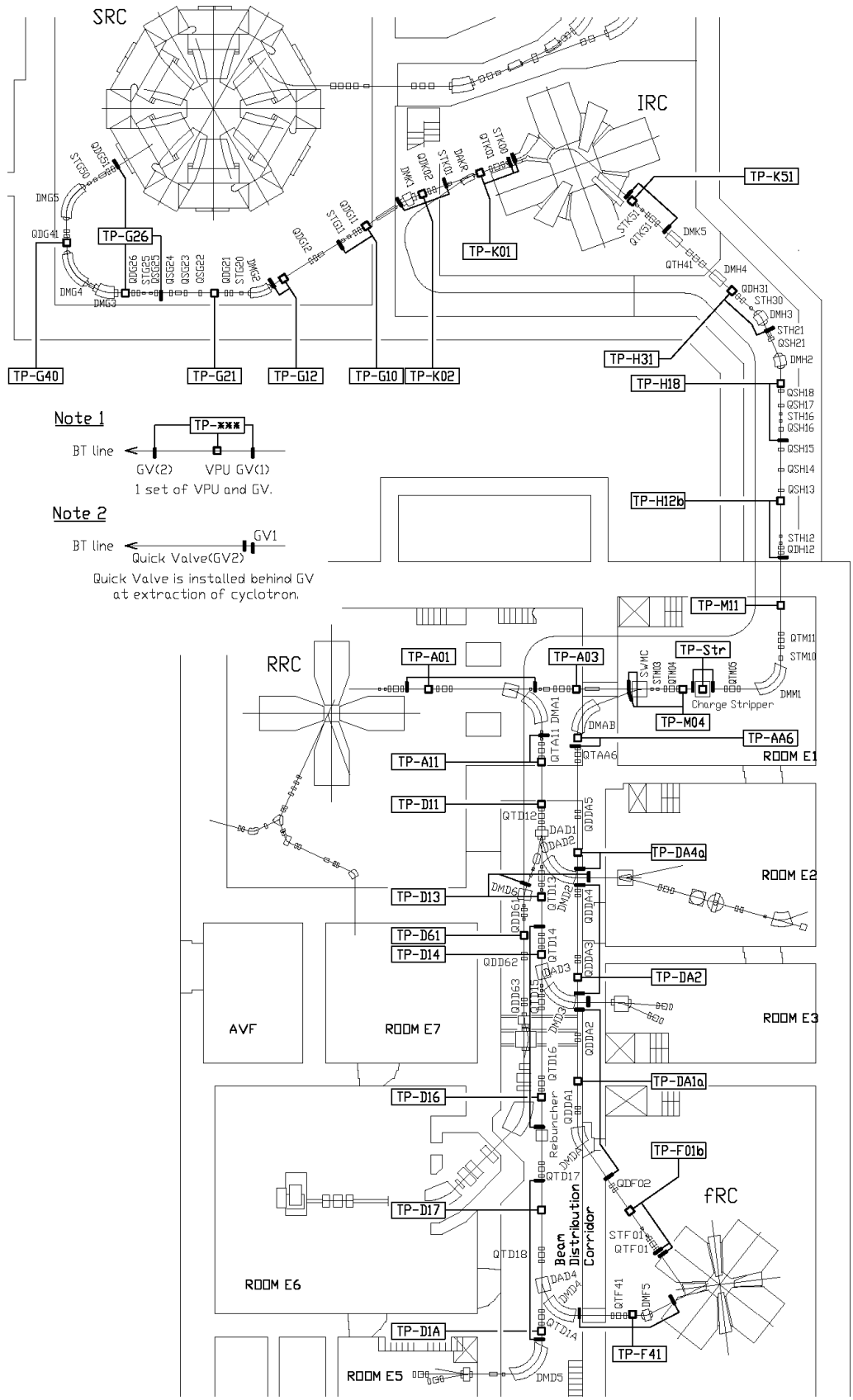

Fig. 1. Schematic layout of vacuum pumping system for BT line

Status of the SRC

H. Okuno, J. Ohnishi, K. Yamada, N. Fukunishi, T. Maie, K. Ikegami, M. Hamanaka*[1], A. Goto, M. Kase and Y. Yano

In this paper, we report the progress of the SRC for the first beam scheduled in 2006. The second cool-down of the SRC started on March 16th and the superconducting magnet was fully excited on April 15th again. Magnetic field measurements were carried out for two months to evaluate the qualities of the generated fields and to develop a database for various acceleration conditions. The details of the measurements are described in reference [1]. We performed a fast-shutdown test when all the superconducting coils were at full excitation on June 14th. This test is very important to check the coil protection system. After the fast-shutdown test, the construction of the parts other than the superconducting magnet system was started. On June 25th, four acceleration resonators and one flattop resonator were installed as shown in Fig. 1. After the resonators were aligned carefully, they were connected with the sector magnets to make a vacuum chamber for ion beams. Parts used for the connections are shown in Fig. 2. Evacuation pumps and beam diagonics were also installed. Figure 3 shows the main radial probe (MDP) installed in the vacuum chamber. On September 29th a rough pumping of the beam chamber was started for a leak test, which found several leaks at flanges. On October 24th, the cryopump was switched on and the vacuum reached 5.0 x 10^{-6} Pa, which is the designed value. The superconducting coils were fully excited several times to check that the AC servo motors, flow switches and electromagnetic valves inside or near the SRC work properly under stray fields from the sector magnets. Local magnetic shields made of iron were applied to the parts that did not work properly under the stray fields. We started acceleration tests on the SRC after aging the resonators in various magnetic field levels induced by the sector magnets. Finally the first beam was extracted from the SRC on December 28th.

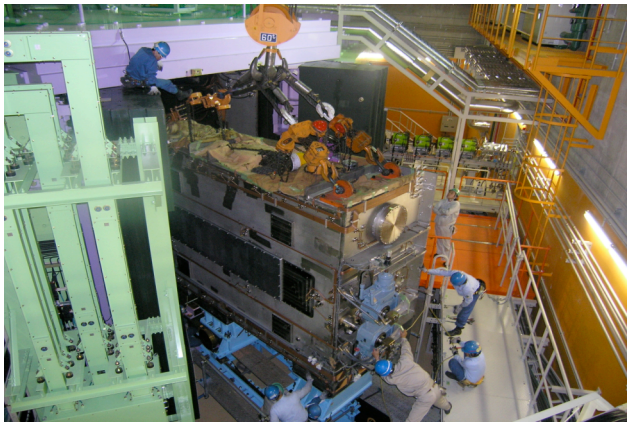

Fig. 1. Installation of acceleration resonator.

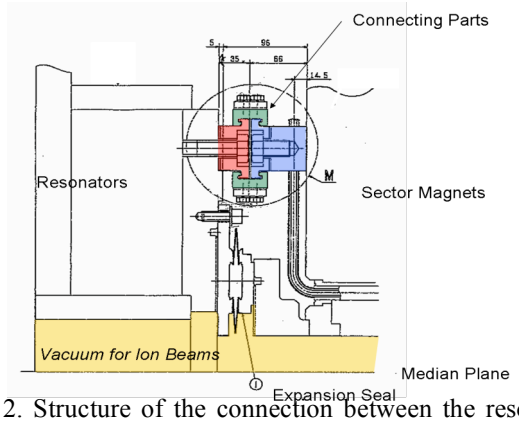

Fig. 2. Structure of the connection between the resonators and the sector magnets.

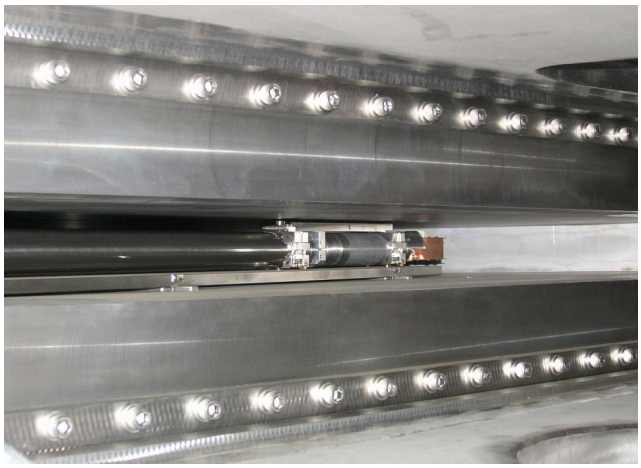

Fig. 3. A head of the MDP (main differential probe) for the SRC.

References

[1] J. Ohnishi, et. al.: in this progress report.

* [1] SHI Acceleration Service Ltd.

Present Status of Liquid-Helium Supply and Recovery System

K. Ikegami, H. Okuno, T. Yoshida, K. Nakano, T. Maie, H. Hasebe, M. Nakamura, and M. Kase

The liquid-helium supply and recovery system, which can generate liquid helium at a rate of 200 L/h from pure helium gas, has been stably operated since the beginning of April 2001. The volumes of liquid helium supplied per year are listed in Table 1. The volume supplied has gradually increased over the years since 2001. The volume supplied to the low-temperature physics laboratory from 2004 to 2005 markedly increased more than threefold. The reason is the extensive implemention of the nanoscience project.

A recovery helium gas observation system[1)] for measuring helium of the recovered helium gas was completed at the beginning of May. The system consists of eight data recorders (Daqstation DX1000) made by Yokogawa Co., and 13 helium purity sensors distributed in the Wako campus. The purity of the helium gas recovered from laboratories is improved gradually after the completion of the system. At the end of August, the control system of the liquid-helium supply and recovery system, which is called MPICS (multiperformance integrate control system) developed by Taiyo Nissan Co., was replaced.

The measuring and tally system for liquid helium supplied to the researchers was completed at the end of October. The system measures the weight of liquid helium and stores the measured weight to a database installed in a computer. Figure 1 shows a photograph of the liquid helium measuring and tally system.

Fig. 1. Liquid helium measuring and tally system.

Reference

K. Ikegami et al.: RIKEN Accel. Prog. Rep. **39**, 254 (2005).

Year	2001	2002	2003	2004	2005
Laboratory and institute	Amount of supplied liquid helium (ℓ)				
Magnetic materials laboratory	3392	7024	7713	11829	15672
Low-temperature physics laboratory	1270	3090	6966	9515	34713
Advanced device laboratory	9977	10849	9726	7401	11264
Condensed molecular materials laboratory	1939	1615	3079	5353	5912
Surface chemistry laboratory	1146	1676	4533	5007	5370
Brain science institute	6277	8144	5055	6292	7285
Etc. (others laboratories)	3535	7730	14476	9487	15717
Total	27536	40182	51530	54884	95933

Table 1. Volumes of liquid helium supplied to laboratories per year from 2001 to 2005.

New Energy Establishment Committee of Wako City District and RIBF

T. Fujinawa, M. Kitano[*1], M. Watanabe[*2]and Y. Yano

Wako city is within commuting distance of Tokyo and features easy living. This area also experiences no gale force winds (yearly average 1m /s) or dry spells. The area also receives 1600 hours of sunlight per year.

The population was approximately 72,000 in 2004 and which increases by 1400 people every year on average. The city covers an area of 11.04 km^2, is 40.71 m above sea level, and has a yearly average ambient temperature of 15.2℃.

The new energy establishment committee of Wako city district[1)] was established on 26 August 2005. This committee is in line with the basic policy of the Rationalization of Energy Use Law and Kyoto Protocol. This committee is also supported by the New Energy and Industrial Technology Development Organization (NEDO).

The committee researched potential new energy sources available to this district. The results are as follows.

1. Solar energy, wind force power generation, and mini-hydropower among others are the supply side (natural) potential power sources. Environmentally friendly cars and vehicles, natural gas cogeneration and fuel cells are the demand side (energy saving/efficient) aspects related to energy users.

2. The regarding situations installations of new energy equipment are as follows.

The ratio of solar cell power generation for 10,000 people of Wako city is 37 kW. However, this is less than the national average of 49 kW. RIKEN has a solar cell capacity of 10 kW. The sunlight received by the Wako city district is only 1600 h/year, which is low compared with other districts around the country. For example Ota city in Gunma prefecture has 2000 h of 8760 h (a year) sunshine time.

The percentage of clean cars and vehicles in the Wako city with respect to the total number of cars is 0.4%, which is the same as the national average.

・ Wako city's power generation through Natural Gas Cogeneration (CGS) is 1 MW for 10,000 people, which is five times larger than the national average of 185 kW. The generator of the CGS of RIKEN's RIBF produces more power than any other single CGS within Tokyo Gas's supply district for general consumer use. Due to the success of RIBF's CGS, several other businesses and organizations in Wako city are also using this system for their power and hot water requirements. Currently, there are nine systems in use within Wako city, which is well above the national average for use of this system (See table 1).

3.Temperature difference energy will be the main characteristic energy of the Wako region.

The RI Beam Factory (RIBF) is under construction as scheduled. The completion of the RIBF will be a great achievement for RIKEN enabling further advances in nuclear physics and other fields. However, the accelerators require a huge amount of electricity (25 MW) and generate large amounts of heat. The accelerator will run 24h/day, totaling more than 6500 hrs/year, but this will also produce a constant supply of warm (40°C) water.

Our plan is as follows. In the first stage, cross-linked poly ethylene (XLPE) hot insulation piping, (known as "onsen piping") which is mainly used for spas, will be laid down between the RIBF and the 4th elementary school, which is situated next to RIKEN's RIBF.

A pair of 95 mm-diameter pipes will transport 51 m^3/h of warm water to and from the school. At this rate of flow, the energy at 5°C temperature difference is equal to 255 Mcal, which is equivalent to 297 kW/h = 1,067.6 MJ.

In terms of petroleum oil, this is equivalent to 275 KL/h (1 MJ=258 L) which means that more than a drum of petroleum oil can be saved each hour. This is referred to as Monergy. In winter, this water will be used for heating class rooms and other rooms at the school with "base board heaters". It will also supply heat to the swimming pool in early summer and autumn.

In the second stage, heat will be supplied to the National Saitama Medical Center via the 4th elementary school's piping. The hospital requires steam for sterilization, humidification, and heat. The hospital also uses large amounts of hot water. For this reason the Wako Medical Center is using the CGS. RIBF can also supply hot water to the hospital boilers.

The cooling water from the CGS absorption chiller is recommended for this application because of its nonstop year round supply and the absence of radio activity.

At the completion of this project, Wako city will have a new energy source for parts of the local community and RIBF will supply this energy.

	Name	Capacity	Unit
1	RIKEN RIBF	6500kW	1
2	Tax practice Academy	300kW	1
3	Legal Research and Training Institute	200kW	1
4	Wako medical center	90kW	1
5	Sports club	28kW	1
6	Chinese restaurant	6kW	1
7	Wakocity elder care facility	9.9kW	3
	Total	7154KW	9

Table-1 CGS List

References

1) M. Kitano et al.: Wako city district new energy vision. 2006 Feb.

2) T.Fujinawa et al.: RIKEN Accel. Prog. Rep. 36,310(2003)

*1 Department of Applied Chemistry School of Science and Technology Meiji University.

*2 Wako City office.

Spin mismatch of the AGS

J. Takano*1, *2, *3

To preserve the polarization of protons in the Alternating Gradient Synchrotron (AGS), partial Siberian snakes have been installed. The first partial Siberian snake is the Solenoidal Snake (SSNK)[1], which was used to overcome all imperfection resonance. The AGS has another strong depolarizing resonance, which is called intrinsic resonance. Four strong intrinsic resonances can be avoided by using the RF dipole[2]. With these components, 40% polarization was achieved at the AGS extraction energy in 2003. However, the Solenoidal Snake produces transverse coupling resonance, which is caused by the coupling of the horizontal-vertical betatron oscillation of the beam. To reduce the coupling resonance and overcome all imperfection resonance, a normal conducting helical dipole Siberian snake (Warm Snake, WSNK)[3] was developed. With the WSNK and the RF dipole, 50% polarization was achieved in 2004 and 55% in 2005.

To overcome all intrinsic resonance and imperfection resonance with a component, a superconducting helical dipole partial Siberian snake (Cold Snake, CSNK)[4] has been installed. However, with only the Cold Snake, the spin mismatch should be larger at AGS injection and extraction, since the spin stable direction (SSD) in the synchrotron has large precession when using the strong partial Siberian snake. To reduce the spin mismatch, the double-snake scheme[5] was proposed and realized in 2006. As the result, 65% polarization was achieved with the Cold Snake and the Warm Snake without using the RF dipole. In this case, the spin mismatch was reduced, but it still had small spin mismatches. To make the mismatch be zero, the triple-snake scheme is a good solution. If the snakes are located along 1/3 of the ring, they will work effectively for the spin tune gap and spin mismatch. On the basis of this idea, the Cold Snake and the Warm Snake were placed along 1/3 of the ring. However, the Solenoidal Snake was not positioned at the ideal point. If the Solenoidal Snake is relocated to a symmetrical point relative to the Warm Snake and the Cold Snake, the Solenoidal Snake will be effective in reducing the spin mismatch.

The strengths of the Cold Snake and Solenoidal Snake are variable. Table 1 shows several patterns of snake strength combinations and spin matching at AGS injection. The percentages represent the degrees of spin direction tilted by the snake. For example, the 10% snake can tilt the direction by 18 degrees.

TABLE1. Spin matching with partial snakes

Case	CSNK	WSNK	SSNK	Spin matching
A	15%			97.2%
B	10%			98.8%
C	10%	6%		99.8%
D	6%	6%		100%
E	10%	6%	4%	100%

On comparing cases A, B and C, the double-snake scheme is found to reduce the spin mismatch. If the strength of the Cold Snake is reduced, as in case D, the spin mismatch will be cancelled completely. In this case, the spin tune gap may not be sufficient to overcome the intrinsic resonance. In the 2006 run, case D was operated briefly and 60% polarization was achieved at the AGS extraction energy. The experimental result indicated that the intrinsic resonance could be overcome with a weak Cold Snake and the Warm Snake. If the closed orbit of the AGS beam is optimized, the polarization will be increased.

We have another choice for reducing the spin mismatch with the combination of the three snakes: case E. If the Solenoidal Snake is relocated to the ideal point, the spin mismatch can be cancelled completely by adjusting the strength of the Solenoidal Snake. With this combination, the spin tune gap is larger than that in case D. Therefore it will be easy to overcome the depolarizing resonance. However, the coupling resonance should be considered in using case E. To overcome the horizontal intrinsic resonance as well, the horizontal betatron tune is going to be optimized in the next polarized proton run in the AGS. The operation with no spin mismatch, such as cases D and E, will increase the polarization at AGS extraction.

References

1) H. Huang *et al.*: Phys. Rev. Lett. **73**, 2982 (1994); Ph. D. thesis Indiana University (1995)
2) M. Bai: Ph. D. thesis, Univ. of Indiana (1999)
3) J. Takano *et al.*: Proc. of 2005 Particle Accelerator Conference, Knoxville, TN, 1003 (2005)
4) H. Huang *et al.*: Proc. of 2005 Particle Accelerator Conference, Knoxville, TN, 1404 (2005)
5) T. Roser *et al.*: Proc. of SPIN2004, Trieste, 687 (2004)

*1 RIKEN, Saitama, Japan
*2 Brookhaven National Laboratory, Upton, NY 11973, USA
*3 RLNR, Tokyo Institute of Technology, Tokyo, Japan

Laser based heavy ion production†

M. Okamura,*1 J. Tamura,*2 T. Kanesue,*3 R. A. Jameson,*4 and S. Kondrashev*5

Generally, laser ion source (LIS) is advantageous for providing intense pulsed heavy ion beams with a highly charged state. To meet a particular purpose, some parameters of the LIS must be selected carefully.

A typical LIS consists of a laser system, a target and an extraction electrode, as shown in Fig.1. Here, we assume that the laser pulse duration is in the range from 1 ns to 100 ns. During 1 ns of laser irradiation, the plasma expands up to 4.5 mm, which is much longer than the focusing laser spot size, assuming an expansion speed of 100 eV/u, which is a typical speed of the ion energy included by a laser plasma.

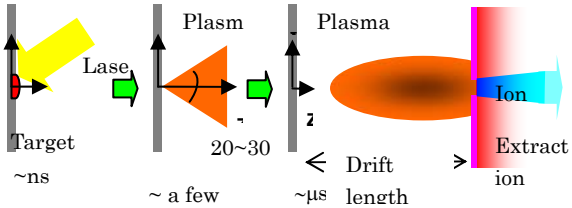

Fig. 1 LIS scheme

This condition causes the laser power to first be mainly absorbed by electrons in the plasma, and then, stepwise ionization occurs. The plasma travels to an extraction region with a very high momentum spread and becomes thinner. Then, ions can be extracted to form the initial ion beam.

In generally solid material is used as a target. The purity of the target material is very important. It was proved that a pure graphite target with less than 5 ppm of impurity did not show even a hydrogen peak in our plasma analysis experiment using a secondary electron multiplier detector. The ratio of isotopes and the oxidized surface condition should be also taken care of. For instance, it is difficult to obtain a pure beam from a Ti target without any special treatment. Also the stability of a beam of heavier species is more difficult to maintain.

Higher laser power generates more ions. Higher laser power density on the target produces higher charge states and higher velocity of the plasma expansion. We found that each laser has its own limitation in the heaviness of the target element. We tested two laser systems, a Nd-Glass laser and a Nd-YAG laser. The glass laser could ionize iron with reasonable charge states, but could not produce highly charged ions from materials heavier than iron. For example, Ge and Nb were ionized up to 8+ and 9+, respectively. The YAG laser, which has a shorter pulse duration, could ionize up to silver ions. If we require highly charged ions from Ta or Au, a higher power density laser beam will be needed. On the other hand, 200 ~ 300 mJ 10 ns laser is sufficient to provide C^{6+}. It is commonly said a shorter wavelength of the laser is better for energy absorption. However the wavelength depends on the laser medium. Usually, there are stronger constraints due to laser availability on the market.

Table 1: Limitation in heaviness of species.

Laser	Power	Width	Ions
Nd Glass-1062 nm	3.45 J	37 ns	Up to Fe^{17+}
Nd-YAG-1064 nm	2.3 J	6 ns	Up to Ag^{15+}

The emittance of the laser beam affects the achievable focusing spot size, similarly to ion beam optics. Also, the effect of the wavelength should be considered.

A shorter focal length of the final focusing element can provide higher power density, and its value is determined by the geometrical configuration in the ion source chamber.

The distance between the target and ion extraction point determines the ion pulse duration. The laser pulse is only 1 ~ 100 ns and it takes the plasma 2 ~ 3 μs to travel within this distance. If a 10 μs of ion pulse is needed, the plasma drift length must typically be 2 ~ 4 m. In this case, a higher power laser is needed to compensate the low ion density at the extraction point. The ion pulse width is proportional to the plasma drift length and the peak current amplitude is inversely proportional to the cube of this value. These relations were verified in our experiments. Also, the solid angle for capturing the expanding plasma is important, since the plasma starts from a pinpoint on the target.

As a result, a short plasma drift length dramatically improves the ion capturing efficiency. However, in this case, a strong electric field is required for ion extraction, and space-charge repulsion force becomes serious after the extraction. The direct plasma injection scheme (DPIS) can overcome these issues. A target can be placed approximately 30 cm upstream of the entrance of a first-stage linear accelerator, typically an RFQ. The induced plasma is guided through a pipe to the inside of the RFQ tank and then the contained ions are extracted in the tank. All the high voltage parts can be inside the compact vacuum box.

To obtain a beam matched with the RFQ input acceptance, the incoming beam must be focused, in general. On the contrary, in the DPIS scheme, the diverging beam is injected into the RFQ. The extracted beam emittance from the guide pipe changes due to the density variation of the plasma in a single pulse and it is almost impossible to achieve a perfect matching condition. However, using DPIS, the ion density is very high and only the overlapped area of the beam emittance and the RFQ acceptance contains a sufficient number of ions. As a result, we can accelerate an intense beam easily without the need for an LEBT that includes a complex focusing magnet. This scheme is well suited for providing an intense pulsed beam.

References

1) M. Okamura et al,: Radiation Effects & Defects in Solids, 160, 10-12 (2005) 445-449.

† Condensed from the proceedings of LINAC 2006.

*1 Brookhaven National Laboratory, USA
*2 Tokyo Institute of Technology
*3 Kyusyu University
*4 Frankfurt University, Germany
*5 Institute for Theoretical and Physical Experiment, Russia

Aluminum beam acceleration with DPIS†

J. Tamura,*1 M. Okamura, *2 T. Kanesue,*3 R. A. Jameson,*4 and S. Kondrashev*5

*1 Tokyo Institute of Technology
*2 Brookhaven National Laboratory, USA
*3 Kyusyu University
*4 Frankfurt University, Germany
*5 Institute for Theoretical and Physical Experiment, Russia

Since end of the last year, we have studied acceleration of Aluminum ions with direct plasma injection scheme (DPIS). In this experiment, the 4 rod RFQ fabricated in IAP (Institute of Applied Physics, Frankfurt University) and the 2.3 J 6 ns Nd-YAG laser, thales SAGA230, were used. The basic parameters of the RFQ are summarized in Table 1.

Table 1 : Basic design parameters of the RFQ

Frequency	100 MHz
Total length	2.0 m
Modulated vane length	1.42m
Intervane voltage	120 kV (q/A = 4/12)
I_{out} at 100 mA C^{4+} in	76 mA (pteq-H)
Injection energy	20 keV/u
Extraction energy	100 keV/u
Acceptance	0.14 cm.rad
Aperture	0.655 cm

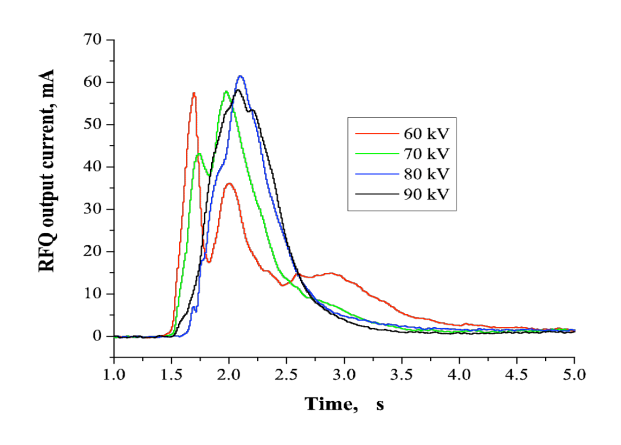

Fig. 1 Accelerated beam shape.

Figure 1 shows accelerated currents varying the extraction voltage. Although the laser is capable of producing Al^{12+}, the laser power density was optimized to get Al^{9+}. The extraction voltage of 60 kV matches q/A = 9/27 condition. Due to the changing extraction condition, a dip caused by too high plasma density was observed at lower extraction voltages. The longer plasma drift length will reduce the density at the peak position and longer ion beam pulse might give more total number of ions. Maximum current and pulse duration are 60 mA and 0.65 μs for extraction potentials in the range of 70-90 kV.

† Condensed from the proceeding of High Intensity High Brightness Hadron Beams, Tsukuba, May 2006, THBY01.

The charge state distribution was measured using an electro static analyzer situated after the RFQ. Figure 2 indicated analyzed result. The fraction of Al^{9+} was about 65 % of the total current.

Shot-to-shot reproducibility of output RFQ current amplitude over 150 shots was investigated. The fluctuation was ±6% for total current. In the experiment, RF frequency has been tuned manually. Automatic phase tuning is expected to improve the statistics. The result is shown in Fig. 3.

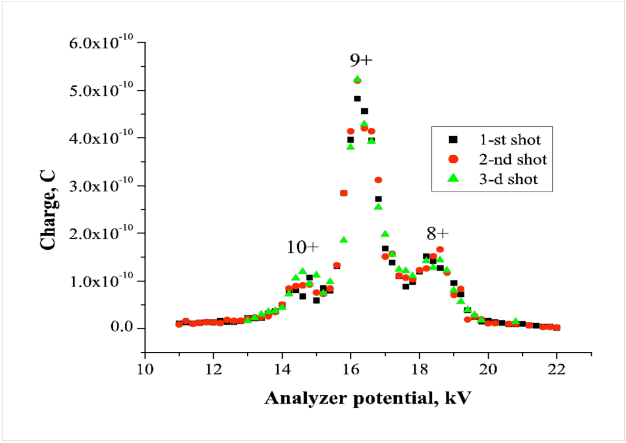

Fig. 2 Analyzed accelerated Al beam.

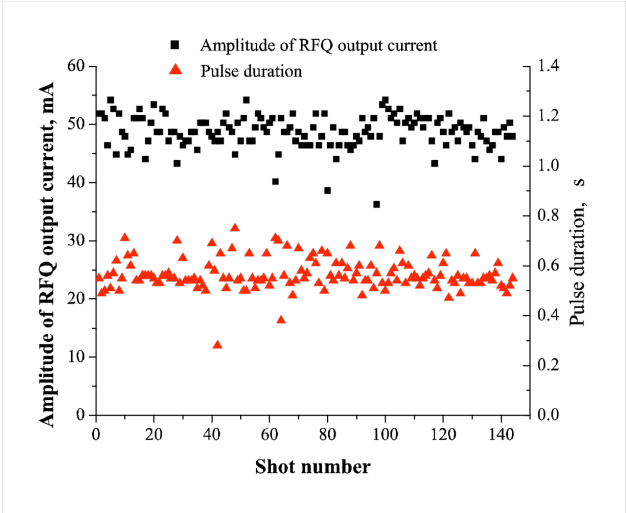

Figure 3: Shot-to-shot fluctuations of output RFQ current amplitude and pulse duration (extraction potential – 60 kV, RF voltage amplitude – 120 kV).

We also trying to use gas at room temperature as a LIS target. Except He, almost all the gas can be condensed on cooled substrate. We confirmed that a surface of a cryo-cooled 5 K Cu block can capture rare gases and the frozen rare gas can provide a plasma by a laser irradiation. In the experiment, we could obtain Ne plasma which expected to provide mA class ion beam from the RFQ. Analysis of the experimental result is in progress.

Reference

[1] Masahiro Okamura, Hirotsugu Kashiwagi, Kazuhiko Sakakibara, Jumpei Takano, Toshiyuki Hattori, Noriyosu Hayashizaki, Robert A. Jameson, and Kazuo Yamamoto, “High current carbon beam production with direct plasma injection scheme”, Rev. Sci. Instrum. 77, 03B303 (2006)

[2] M. Kojima, K. Nishigori, M. Yoshida, A. Sakumi, J. Hasegawa, U. Funk, U. Neuner, Y. Oguri and M. Ogawa, “laser plasma induced from solid hydrogen for beam–plasma interaction”, Nuclear Instruments and Methods in Physics Research A 464 (2001) 262-266

Development of ion-guiding system for RIABR experiments

T. Sugimoto, A. Yoshimi, H. Ueno, J. Murata,[*1] H. Kawamura,[*1] D. Nagae,[*2] K. Shimada,[*2] and K. Asahi

The atomic-beam resonance (ABR) method is an effective tool for determining nuclear moments.[1] We have worked on developing a new technique for applying the ABR method to the measurement of the nuclear moments of radioisotopes (RIs). In this paper, we report the present status of the development of an ion-guiding system. This ion-guiding system will be used to produce a low-energy RI atomic beam in the ABR system.

The test experiments were performed at the Cyclotron and Radioisotope Center of Tohoku University. A primary $^{15}N^{5+}$ beam was accelerated by the 930 cyclotron at 150 MeV and transported to the experimental area. Figure 1 shows the experimental setup of the reaction target and gas degrader. The 17.6-mg/cm^2-thick CD_2 target was bombarded with the ^{15}N beam, and ^{16}N was produced from the $d(^{15}\mathrm{N}, ^{16}\mathrm{N})p$ reaction. A Faraday cup and a sheet of aluminum oxide (Al_2O_3) were installed in the gas degrader to monitor the beam current and its spot image, respectively. The Faraday cup was also used to prevent the gas buffer cell from irradiation by the unreacted ^{15}N beam. The geometrical configuration of the collimators was chosen to give an angular range of 2.5°–3.0°. This angle was chosen by taking into account the following three factors. 1) The ratio of the production yield of ^{16}N to the amount of the unreacted ^{15}N beam. 2) The measured production rate of ^{16}N as a function of the emission angle normalized by the current of the primary ^{15}N beam, as shown in Fig. 2. 3) The typical current of the primary ^{15}N beam was 10 nA; thus, the yield of secondary ^{16}N was expected to be about 10^4 counts per second in the gas buffer cell. The gas degrader was filled with argon gas, and the pressure was regulated using a mass-flow controller.[2] The degraded and collimated ^{16}N particles entered the gas buffer cell.

Figure 3 shows a schematic view of the gas buffer cell. The gas cell was filled with neon gas at a pressure of 170 Torr and was equipped with a DC electrode assembly, which consisted of 33 thin aluminum discs with a 5 cm bore. The gap between the discs was 1 cm and the discs were connected by a 300 kΩ resister. The end electrode was connected to the chamber by a 33 MΩ resister. By applying a high voltage between the entrance of the electrode element and the chamber, a DC electric field was generated to transport the ions in the downstream direction. The applied voltage of the electrodes was 450 V, which corresponds to a DC electric field of 5 V/cm. By utilizing the β decay of ^{16}N, the positions of ions in the cell were measured

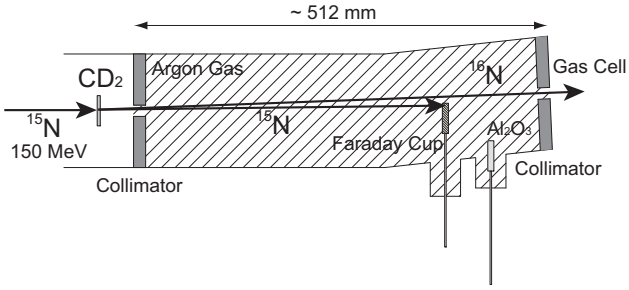

Fig. 1. Experimental setup of the reaction target and gas degrader. The secondary ^{16}N beam, which is produced from the $d(^{15}\mathrm{N}, ^{16}\mathrm{N})p$ reaction, were degraded in the argon gas. The geometrical configuration of the two collimators was chosen to give an angular range of 2.5°–3.0°. The unreacted ^{15}N particles were stopped by the Faraday cup. The effective length of the gas degrader was about 512 mm. The typical pressure of the gas was about 130 Torr.

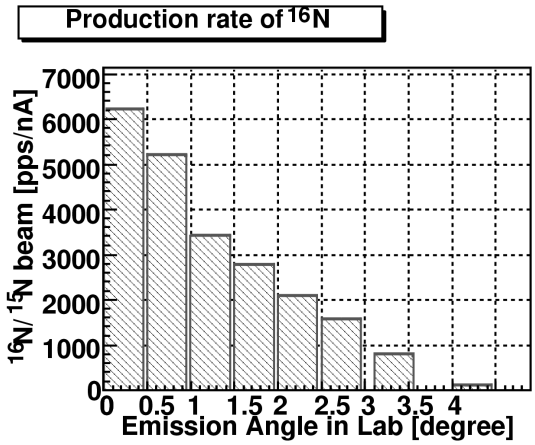

Fig. 2. Production rate of ^{16}N normalized by the current of the ^{15}N beam as a function of the emission angle.

using a two-layered plastic-scintillator beta telescope, which was located beside the cell.[3] The typical resolution of the telescope was 8 cm (FWHM). From the decay-time spectrum, the purity of ^{16}N was about 40%.

By comparing the measurements with and without the DC electric field, difference of about 1% in the ^{16}N distribution was observed. However this result is insufficiently accurate to enable quantitative comparison with calculated results; thus, further development is required such as by improving statistics, purity, position resolution, applied voltage and moving efficiency.

References

*1 Department of Physics, Rikkyo University
*2 Department of Physics, Tokyo Institute of Technology

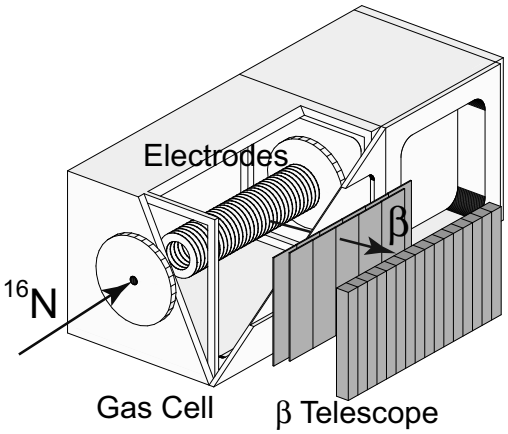

Fig. 3. Schematic view of the gas buffer cell. The incident ^{16}N ions are stopped by the neon gas and then transferred by the DC electric field toward the downstream of the cell. β rays from ^{16}N were detected to obtain the position distribution of ^{16}N.

1) I. I. Rabi et al.: Phys. Rev. **55**, 526 (1939).
2) K. Shimada et al.: RIKEN Accel. Prog. Rep. **39**, 156 (2006).
3) H. Miyoshi et al.: RIKEN Accel. Prog. Rep. **37**, 171 (2004).

Improvement of slow RI beam transport using carbon-OPIG

A. Takamine*1, M. Wada, Y. Ishida, T. Nakamura, K. Okada*2, Y. Yamazaki, Y. Kanai, T. M. Kojima, A. Yoshida, T. Kubo, S. Ohtani*3, K. Noda*4, I. Katayama*5, V. Lioubimov*6, H. A. Schuessler*6, V. Varentsov*7, and H. Wollnik*8

[slow RI beams, rf-carpet ion guide, carbon-OPIG]

A universal facility for slow radioactive ion beams (SLOWRI) is being developed[1] as part of the RI Beam Factory. SLOWRI aims at providing universal slow RI beams of high purity and small emittance by slowing down and cooling energetic RI ions using an rf ion guide. We achieved a high overall efficiency of ∼5% and a maximum intensity of ∼24 kcps in slow beams (∼eV)[2] for ∼100A MeV ^{8}Li ions from the projectile fragment separator RIPS.

Although we succeeded in trapping several hundreds of $^{7,10}Be^{+}$ ions in the linear trap and measured the isotope shift of $^{7,10}Be^{+}$ for the $2s\ ^2S_{1/2}$-$2p\ ^2P_{3/2}$ transition[3], the intensity of the slow $^{10}Be^{+}$ ions was only a few tens cps due to a problem in the SPIG[4]. When we used the two-segmented SPIG made of metallic rods, slow $^{8}Li^{+}$ ions was transported only at a low He buffer gas pressure of 13 mbar, although a higher pressure of about 133 mbar was the best condition to extract slow $^{8}Li^{+}$ ions up to the short, about 10 cm long, SPIG. Even at such a low pressure, a relatively high dc voltage of 100 V between the 10-cm-long upstream section and the 50-cm-long downstream section was required to transport slow RI ions. These problems are considered to be due to the finding that the presence of residual He gas ($1{\sim}10^{-4}$ mbar) in the upstream region of the SPIG blocks the stream of slow ions in the SPIG.

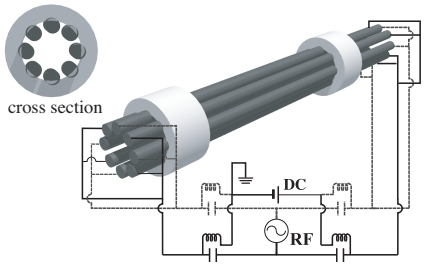

Fig. 1. Schematic drawing of OPIG. The OPIG consists of eight 1-mm-dimeter rods made of CFRP with an inner diameter of 2.5 mm.

*1 Graduate School of Arts and Sciences, University of Tokyo
*2 Department of Physics, Sophia University
*3 Institute for Laser Science, University of Electro-Communications
*4 National Institute for Radiological Science
*5 Institute of Particle and Nuclear Studies, High Energy Accelerator Research Association, KEK
*6 Department of Physics, Texas A&M University
*7 Kholopin Radium Institute
*8 II. Physikalisches Institute, Justus-Liebig-Universitaet

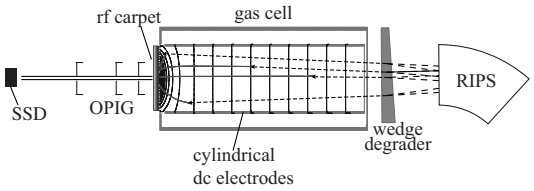

Fig. 2. Schematic of experimental setup. Ions thermalized in the gas cell filled with 26 or 133 mbar of He are transported by dc fields and rf fields to the exit nozzle and transported under carbon-OPIG. The intensity of slow $^{8}Li^{+}$ beams was measured by counting delayed alpha particles by SSD behind the OPIG.

A solution to provide continuous force to the ion stream in such a buffer gas environment is to provide a continuous dc electric field in the axial direction. For this purpose, we searched for a resistive material to be used as the rods of the SPIG. We originally constructed a new beam guide, carbon-OPIG (Fig. 1), which is made of carbon-fiber-reinforced plastic (CFRP), and now has an octopole configuration due to a practical reason. The rod has about 60 Ω resistance when the diameter is 1 mm and the length is 60 cm, and therefore, it is quite easy to provide an axial dc potential gradient of 2 V for a 60 cm length with a reasonably low electric current of 0.2 A.

In a preliminary test experiment using 100A MeV ^{8}Li beams from RIPS, we confirmed that intensities of 2.2 kcps and 2.7 kcps of slow $^{8}Li^{+}$ ions that were transported up to the end of the carbon-OPIG at He pressures of 26 mbar and 133 mbar in the gas cell, respectively, were obtained. Although the operation parameters were not optimized, and thus far it has been difficult to evaluate the absolute efficiency of the new carbon-OPIG, this performance should be sufficient for precise measurements of the hyperfine structure and isotope shifts of stored $^{7,11}Be^{+}$ ions in a trap, which is our next goal.

References

1) M. Wada et al.: Nucl. Instrum. Methods Phys. Res. B 204, 570 (2003).
2) A. Takamine et al.: Rev. Sci. Instrum. 76, 103503 (2005).
3) T. Nakamura et al.: Phys. Rev. A 74, 052503 (2006).
4) A. Takamine et al.: RIKEN Accel. Prog. Rep. 39, 157(2006).

Status of Rare RI–Ring project

Y. Yamaguchi, A. Ozawa,[*1] I. Arai,[*1] T. Fujinawa, N. Fukunishi, A. Goto, T. Kikuchi,[*2] T. Ohnishi, T. Ohtsubo,[*4] H. Sakurai, T. Suzuki,[*3] M. Wakasugi, T. Yamaguchi,[*3] Y. Yasuda,[*1] and Y. Yano

To measure precisely the mass of radioisotopes (RIs) including the r–process region, we are considering a device similar to a storage ring. Arbitrary RIs are generated in RIBF by projectile fragmentation and/or uranium fission, and they are identified using the BigRIPS[1)] fragment separator. After their identification at the BigRIPS, they are injected into the storage ring individually. Then their flight time (revolution time) is measured at the storage ring.[a)]

The measurement is based on the following principles. According to the cyclotron principle, revolution time is the inverse of cyclotron frequency. In addition, when an isochronous magnetic field is formed, the revolution time (T_0) is expressed as

$$T_0 = 2\pi \frac{m_0}{q}\frac{1}{B}\gamma_0 = 2\pi \frac{m_0}{q}\frac{1}{B_0}, \qquad (1)$$

where B_0 is a uniform magnetic field, γ_0 is the relativistic factor defined as $\gamma_0 = 1/\sqrt{(1-\beta_0^2)}$ and $\beta_0 = v/c$. The isochronous magnetic field at specific momentum spaces inside the storage ring are calibrated with 10^{-6} or less accuracy using an already known stable nucleus. In such an isochronous ring, we measure the revolution time of an unknown mass nucleus, which has the almost same m/q value as that of the stable nucleus. In such nuclei with slightly different mass–to–charge ratios (*i.e.*, m_1/q=m_0/q+ $\Delta(m_0/q)$), isochronism is no longer fulfilled. In this case, m_1/q can be expressed as

$$\frac{m_1}{q} = \frac{m_0}{q}\frac{T_1}{T_0}\frac{\gamma_0}{\gamma_1} = \frac{m_0}{q}\frac{T_1}{T_0}\sqrt{\frac{1-\beta_1^2}{1-(\frac{T_1}{T_0}\beta_1)^2}}, \qquad (2)$$

where T_1 is the revolution time for nuclei with m_1/q and $\gamma_1 = 1/\sqrt{1-\beta_1^2}$. To evaluate the mass of nuclei with non–isochronism, correction for the velocity β_1 is required. The relative differential value of m_1/q is expressed as

$$\frac{\delta(m_1/q)}{m_1/q} = \frac{\delta(m_0/q)}{m_0/q} + \frac{\delta(T_1/T_0)}{T_1/T_0} + k\frac{\delta\beta_1}{\beta_1}, \qquad (3)$$

where

$$k = -\frac{\beta_1^2}{1-\beta_1^2} + (\frac{T_1}{T_0})^2\frac{\beta_1^2}{1-(T_1/T_0)^2\beta_1^2}. \qquad (4)$$

When we require an accuracy on the order of 10^{-6} for 1% difference in mass, we must measure T_1 with 10^{-6} accuracy and β_1 with 10^{-4} accuracy independently.

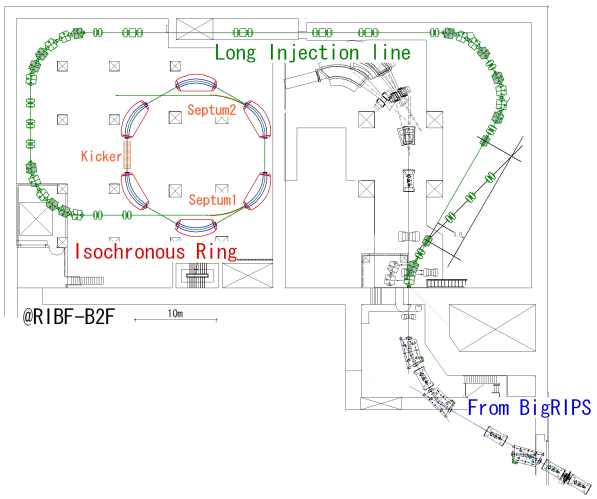

Fig. 1. Floor arrangement of isochronous ring and long injection line according to the design.

Figure 1 shows the floor arrangement of the isochronous ring and a long injection line according to the design. The long injection line of 200 m is necessary to measure β with the required accuracy. It is extended from the BigRIPS to the isochronous ring and gives more than 1 μs flight time for nuclei of 200 MeV/nucleon. Because the time resolution of a typical plastic scintillator is better than an order of 100 ps, the long injection line enables the measurement of the velocity of nuclei with 10^{-4} accuracy. To determine the arrangement of the magnets of the long injection line, we are presently examining using GIOS[3)] and/or COSY INFINITY[4)]. Incidentally, we have already kept those magnets and power supplies, and began to check their status.

Concerning the injection method, we adopt the individual injection method[5)], which is highly efficient for the stacking of rare nuclei. A certain nucleus is identified using BigRIPS, and the trigger signal must be transmitted to a kicker system faster than the nucleus itself. The long injection line enables this relation. Under the present conditions, it takes about 1350 ns at a distance of 230 m (from the trigger point to the kicker magnet) in the case of a nucleus of 200 MeV/nucleon. On the other hand, the transmission time of the trigger signal is about 1300 ns from the signal start to a state ready for injection at the kicker system. That is, the above conditions satisfy the individual injection

*1 Institute of Physics, University of Tsukuba
*2 Department of Electrical and Electronic Engineering, Utsunomiya University
*3 Department of Physics, Niigata University
*4 Department of Physics, Saitama University
a) For details please refer to ref. 2.

method.

The nucleus is brought onto the closed orbit of the isochronous ring using the combination of the septum magnet and kicker system. After it turns about 3000 times in high–precision magnetic field regions at the isochronous ring of about 56 m in circumference, it is ejected from the isochronous ring, then we can measure its revolution time with 10^{-6} accuracy. After that the ejected particle is identified again using some detectors. The ejection scheme is simply inverse of the injection scheme (see Fig. 1).

To decide the rough specifications of the septum magnet, the kicker system and the isochronous ring itself, we performed calculation using a transfer matrix method in hard-edge approximation. In the following estimations, the beam Bρ is assumed to be 6.43 Tm. This Bρ value corresponds to A/Z=3 in 200 MeV/nucleon.

Table 1. Specifications of isochronous ring

——RING——	
Sector number	6
Circumference	56.13 m
——SECTOR MAGNET——	
Bending angle	1.047 rad
Rotation angle	0.155 rad
Magnetic pole length	4.5 m
Straight section length	4.855 m
Radius of curvature	4.297 m
Magnetic strength	1.5 T

The isochronous ring specifications are summarized in Table 1. We calculated the rotation angle for forming an isochronous magnetic field in the first order. More higher–order isochronous magnetic fields will be adjusted with trim coils.

Under this condition, we calculated TUNE values and TWISS parameters using the MAD program[6]. The horizontal TUNE value is 1.26 and the vertical TUNE value is 0.79. The phase advance between the septum magnet and the kicker system is about $3\pi/2$ (see Fig. 1). Regarding device spaces, each septum for injection and ejection does not interfere with each orbit of injection and ejection.

The septum magnet specifications are shown in Table 2. The septum magnet will be operated as a DC magnet. The magnetomotive force is about 30000 AT.

Table 2. Specifications of septum magnet

Bending angle	30 deg.
Radius of curvature	8.573 m
Magnetic strength	0.75 T

The kicker system specifications are summarized in Table 3. A traveling wave type will be used for this kicker system. In relation to the transmission time of the trigger signal, the response time of power supply for the kicker system is a crucial issue. Because the response time of power supply accounts for about half of the transmission time of the trigger signal. A technical improvement that decreases the response time of power supply as much as possible is needed. The kicker system must generate a high magnetic field with rapid rise and fall times, and a uniform flattop for efficient injection and ejection must be made. Because the injected nucleus passes the kicker system 330 ns after injection, the magnetic field strength should be completely adjusted to 0 T at that time. Furthermore, the injected nucleus should be ejected from the isochronous ring using the same kicker system about 1 ms (330 ns/turn x 3000 turns) later. Although the specifications for the kicker system can be technically viable, we should empirically confirm them using a new model of the kicker system as soon as possible.

Table 3. Specifications of kicker system

Kick angle	29.24 mrad
Total core length	2.4 m
Aperture	hight; 0.05 m, width; 0.2 m
Rise time	130 ns
Magnetic strength	0.079 T
Characteristic impedance	12.5 Ω
Current	3120 A
PFN voltage	78 kV
Total number of unit kicker	12
Kick angle per unit kicker	2.437 mrad
Cell number per unit kicker	8
Inductance per unit cell	126 μH
Capacitance per unit cell	800 pF

We continuing our calculations of the beam optics for the long injection line and the isochronous ring, and we are going to determine the specifications of the injection and the ejection scheme devices in detail. Moreover, to realize a magnetic field of the isochronous ring with 10^{-6} or less accuracy, we must concentrate on the design of its magnets using TOSCA.

References

1) T. Kubo: Nucl. Instrum. Methods Phys. Res. B **204**, 97 (2003).
2) T. Yamaguchi et al.: Proc. of 6th International Conf. on Nucl. Phys. at Storage Rings, (STORI'05).
3) H. Wollnik et al.: Nucl. Instrum. Methods Phys. Res. A **258**, 408 (1987).
4) M. Benz: Nucl. Instrum. Methods Phys. Res. A **298**, 473 (1990).
5) I. Meshkov et al.: Nucl. Instrum. Methods Phys. Res. A **523**, 262 (2004).
6) H. Grote et al.: CERN SL 90-13 (AP), (1996).

A multireflection time-of-flight mass spectrometer using cryogenic linear ion trap for injection

Yoshihisa Ishida, Michiharu Wada, Yasunori Yamazaki, and Hermann Wollnik*1

We have developed a multireflection time-of-flight mass spectrometer (MRTOF)[1] and a linear ion trap for the precise mass measurement of short-lived nuclei, which will be provided at the slow RI-beam facility (SLOWRI) of RIKEN-RIBF.[2] Bunched slow ions from SLOWRI will be transferred to the trap to be compressed in phase space. Subsequently, they will be injected into the MRTOF, which consists of two coaxially arranged ion mirrors. Ions inside the MRTOF will move back and forth repeatedly between the ion mirrors in an energy-isochronous manner.

In a previous report,[3] a mass resolving power, $m/\Delta m$, of more than 100,000 was reported. This resolving power is sufficient for studying the global properties of the nuclear structure and for probing theoretical models. However, further system improvements are desirable because the small yield in the region far from β stability limits the number of events. Furthermore, it would be useful to separate the ions of nuclei in the ground state from those in the isomeric state using the mass spectrometer for nuclear decay studies.

To improve the resolving power of the system, the ion trap was cooled using a cryogenic refrigerator. This reduces not only the spacial distribution of the ion but also the average ion velocity in the trap. It is expected that short ion pulses will be extracted from the trap. The ion trap was connected to the cryogenic head by silver-coated copper wires to reduce the transmission of acoustic noise from the cryogenic head to the trap. A heat shield of multilayer aluminum-coated Mylar films was placed inside a vacuum chamber. He buffer gas was introduced into the trap to cool the trapped ions by the buffer gas cooling. The temperature of the trap measured using a silicon diode thermometer was about 80 K.

Figure 1 shows a mass spectrum of the CO-N_2 mass doublet after a flight time of $\approx$7 ms. A mass resolving power of 200,000 has been achieved in this spectrum. The time width of the extracted ion pulse from the ion trap is 4 ns, which is 20% less than that from the ion trap at room temperature. It is expected that one of the components for the width will be reduced by the cooling effect, which is the so-called turn-around time $\Delta t = 2m\Delta v_0/qE$, where m, Δv_0, q, and E are mass, initial velocity difference in the direction of extraction, charge of the ion, and strength of the extracting electric field in the trap, respectively. This time width depends on the kinetic energies of the ions in the trap. The present results indicate that other components for the width contribute as much as the turn-around time.

To investigate the impurity ions in the trap, we measured a wide range of masses in the single-path TOF mode. A comparison of the mass spectra with and without cooling the trap is shown in Fig. 2. In both measurements, the sample gas pressure in the ion source and the electron current of the source of $\sim$500 pA were held constant. The sample gas pressure in the source was estimated to be $\sim 10^{-3}$ Torr. The most remarkable difference between the spectra with and without cooling the trap is the 10 times more intense ion beam at mass 28. Also, the disappearance of the peaks at masses 18 and 19, which are derived from water molecules was observed. There are also unchanged results such peaks at mass 29. It is thought that the components of this peak are the isotopes of the sample, such as $^{14}N^{15}N^+$ and $^{13}C^{16}O^+$, and protonated molecules, such as COH^+ and N_2H^+. The natural abundances of $^{13}C^{16}O^+$ and $^{14}N^{15}N^+$ are 1% and 0.7%, respectively. In the case of cooling the trap, the ratio of mass 28 to 29 is 2.3%, which is comparable to the natural abundance. Therefore, it is found that the production of unwanted molecules was suppressed by cooling the trap.

The relative intensity of the ions as a function of time of flight is shown in Fig. 3. Even after 10 ms of ion flight, a transmission efficiency of about 50% has been achieved by cooling the trap. Although the pressure in the chamber of the trap became lower due to the adsorption of water molecules on the cryogenic head, the pressure of the chamber of the MRTOF remained almost constant. This suggests that the improvement in transmission efficiency is attributed to the small transverse emittance of the ion beam extracted from the trap.

*1 University Giessen

References

1) Y. Ishida, M. Wada, and H. Wollnik: Nucl. Instrum. Methods Phys. Res. B **241**, 983 (2005).
2) M. Wada et al.: Nucl. Instrum. Methods Phys. Res. B **204**, 570 (2003).
3) Y. Ishida, M. Wada, Y. Yamazaki, and H. Wollnik: RIKEN Accel. Prog. Rep. **39**, 148 (2006).

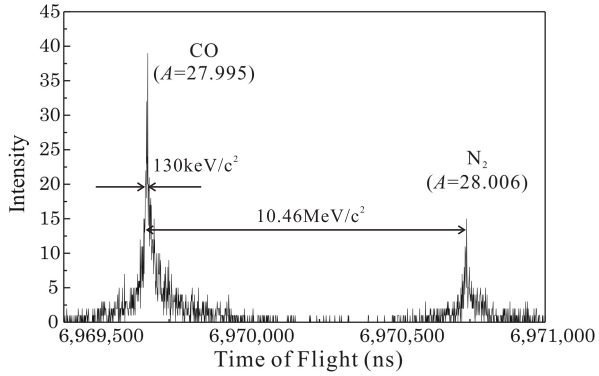

Fig. 1. Mass spectrum of CO-N_2 mass doublet after flight time of ≈7 ms.

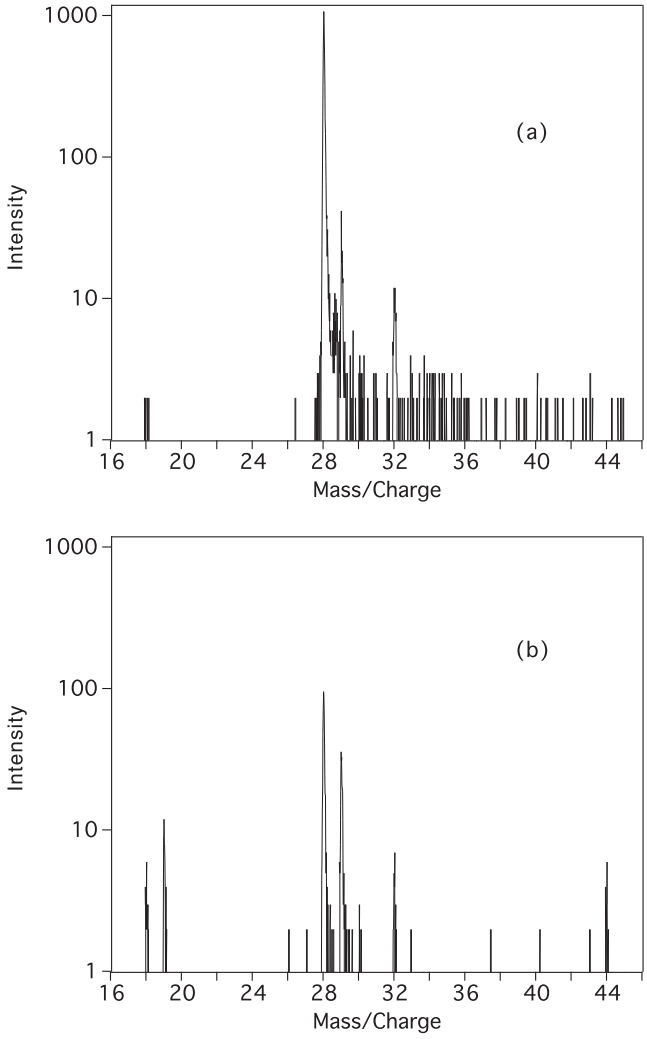

Fig. 2. Comparison of mass spectra (a) with and (b) without cooling of trap.

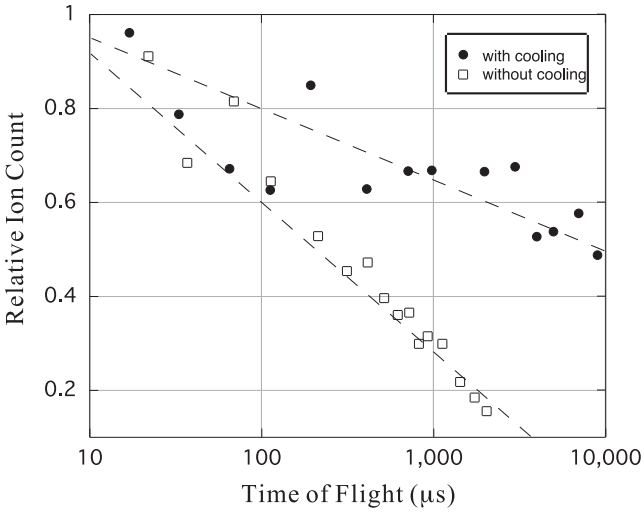

Fig. 3. Recorded ion intensity as function of ion flight time relative to intensity after one pass. The dashed lines are guides for the eyes.

Calibration Test of Space Radiation Measurement Instruments

T. Komiyama,[*1] H. Matsumoto,[*1] Y. Sasaki, [*1] H. Kato, and T. Goka[*1]

1. Introduction

Some accidents involving satellites have happened with irreversible damage since a few years ago. For example, an electrostatic discharge in a solar panel system and an upset of an advanced microprocessor have occurred. Because the space radiation environment is a major source of these accidents, a space radiation environment monitoring system should be implemented on a satellite. In addition, an estimation of the space radiation environment has become increasingly important in the satellite design phase. Our group has accumulated data on the space radiation environment since 1987. On the basis of these data, a radiation model has been developed, which will be proposed as an ISO standard.

Now, we are developing a space radiation measurement instrument for the JASON-2 satellite, which is being developed by the Centere National D'etudes Spatiales (CNES), the French space agency, and will be launched in 2008. The monitoring instrument called the "Light Particle Telescope" (LPT) was calibrated for the Proto-Flight Model (PFM) using RIKEN Ring Cyclotron in 2006.

2. Description of LPT [1) 2)]

LPT is composed of two units, which are the electric unit LPT-E and the sensor unit LPT-S. LPT-E provides an electrical interface to the Jason-2 satellite system. LPT-S consists of four sensors, ELS-A, ELS-B, APS-A, and APS-B. The expected measurement range of each sensor is shown in Table 1.

ELS-A, APS-A, and APS-B consist of a stack of three or four silicon semiconductor detectors (SSDs), and ELS-B consists of one SSD and a crystal of Ce-added Gd_2SiO_5 (GSO) scintillator. Each sensor can identify particle species (e.g.; electron, proton, and ^{4}He) using energy deposited in the first SSD, assuming that there are more electrons than protons or other particles on the orbit of the JASON-2 satellite. In addition, each sensor can measure the energy of particles by combining energies deposited in the first SSD and in the other SSDs.

Table 1 Measurement Range of LPT sensors

Sensors	Measurement Range
ELS-A	Electron 0.03 – 1.3MeV
ELS-B	Electron 0.28 – 20MeV
APS-A	Proton 0.4 – 37MeV ^{4}He 0.75 – 40MeV/n
APS-B	Proton 1.5-250MeV ^{4}He 2.5-100MeV/n

3. Calibration Test

We have conducted energy calibration tests on deposited energy for APS-B using 210MeV protons. Moreover, we have confirmed APS-B can identify incident particle species using fragmented particles derived from the collision of 95MeV/n ^{40}Ar particles with an aluminum target, such as protons, deuterons, tritons, ^{3}He, and ^{4}He with energies in the range of 0-90MeV/n.

Figure 1 shows typical scatter plots of energies deposited in the first SSD and the second and third SSDs we obtained in the test for APS-B using fragmented particle irradiation. The sensor was confirmed to be able to identify protons, deuterons, tritons, ^{3}He and ^{4}He.

4. Future Plans

We will analyze the data we obtained in these calibration tests and perform several environment tests for LPT to be integrated to the JASON-2 satellite.

In addition, we are developing space radiation measurement instruments for GOSAT, a Japanese satellite. We plan to perform calibration tests of those instruments using RIKEN Ring Cyclotron in 2007.

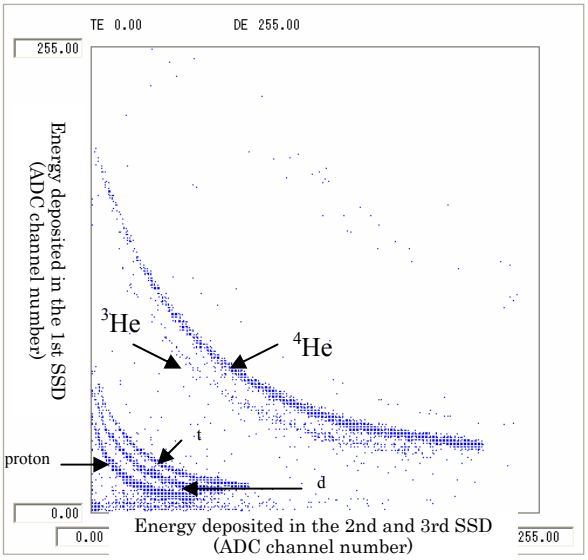

Figure 1 Typical scatter plots of APS-B using fragmentation particles derived from the collision of 95MeV/n ^{40}Ar particles with an aluminum target (18mm thick)

References

1) H. Matsumoto and T. Goka: Technical Report of the Institute of Electronics, Information and Communication Engineers, Vol.101 No.157, 83-87 (2001)
2) T. Komiyama, H. Matsumoto and T. Goka: Proceedings of the 2006 IEICE General Conference, BS-6-21 (2006

*1 Japan Aerospace Exploration Agency (JAXA)
Space Environment Measurement Group

High-Resolution Beam Line for SHARAQ Spectrometer

T. Kawabata,[*1] T. Kubo, H. Sakai,[*2] S. Shimoura,[*1] and T. Uesaka[*1]

The construction of the SHARAQ spectrometer was started in 2005 by the Center for Nuclear Study[1]. The SHARAQ spectrometer is designed to achieve a high momentum resolution of $\Delta p/p \sim 1/15000$ for charged particles with a magnetic rigidity of $B\rho = 6.8$ Tm. The SHARAQ spectrometer will be used for nuclear spectroscopic studies using radioactive-isotope (RI) beams produced by the RI beam factory (RIBF) at RIKEN. Since the RI beams have a variety of isospins, spins, and internal energies, RI-beam-induced reactions are expected to be useful tools for probing nuclear many-body systems.

Since the RI beams generally have a large emittance, the dispersion matching technique[2,3] must be introduced to perform high-resolution measurements. If the dispersions of the SHARAQ spectrometer and its beam line are properly "matched", the missing-mass resolution can be significantly improved better than the momentum spread of the RI beam.

Following the notation of the computer code TRANSPORT[4], the horizontal position x and angle at the focal plane of the spectrometer are related to those at the starting point of the beam line using the transfer matrix elements of the spectrometer (s_{ij}) and beam line (b_{ij}).

$$\begin{aligned} x =&(s_{11}b_{11} + s_{12}b_{21})x_0 \\ &+ (s_{11}b_{12} + s_{12}b_{22})\ _0 \\ &+ (s_{11}b_{16} + s_{12}b_{26} + s_{16})\delta_0, \qquad (1) \\ =&(s_{21}b_{11} + s_{22}b_{21})x_0 \\ &+ (s_{21}b_{12} + s_{22}b_{22})\ _0 \\ &+ (s_{21}b_{16} + s_{22}b_{26} + s_{26})\delta_0. \qquad (2) \end{aligned}$$

The x_0, $_0$, and δ_0 are the horizontal position, angle, and fractional momentum deviation from the central trajectory ($\delta \equiv \Delta p/p$) at the starting point of the beam line. When the coefficients of the momentum-dependent terms in Eqs. 1 and 2 are zero as

$$s_{11}b_{16} + s_{12}b_{26} + s_{16} = 0, \qquad (3)$$
$$s_{21}b_{16} + s_{22}b_{26} + s_{26} = 0, \qquad (4)$$

the horizontal position and angle at the focal plane are independent of the momentum spread of the beam. Equations 3 and 4 are commonly called as the lateral- and angular-dispersion matching conditions, respectively. It is necessary for high-resolution spectroscopy with a secondary RI beam to construct a beam line satisfying these matching conditions. From Eqs. 3 and 4, and the SHARAQ design values of s_{ij}, the dispersion matching conditions for the beam-line transfer matrix elements are determined to be $b_{16} =$ 14.76 m and $b_{26} = 4.79$ rad.

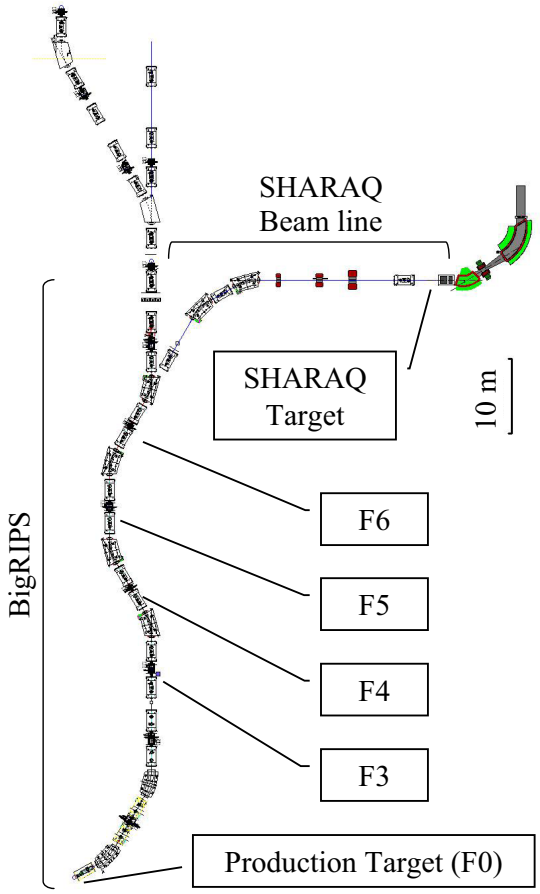

Fig. 1. Layout of SHARAQ spectrometer and high-resolution beam line at RIBF.

The SHARAQ spectrometer will be installed in the E20 experimental room at RIBF, as shown in Fig. 1. Since the RI beam emitted from the production target at F0 is achromatically focused at F3 in the normal beam transport procedure for the BigRIPS fragment separator[5], we determined F3 to be the starting point of the SHARAQ beam line.

The SHARAQ beam line shares magnetic elements with the BigRIPS fragment separator up to F6. After F6, the SHARAQ beam line branches from BigRIPS and bends 60 toward the SHARAQ target. Since the layout of the magnetic elements of the BigRIPS fragment separator has already been determined, the layout between the branching point and the target can be optimized to satisfy the dispersion matching conditions

*1 Center for Nuclear Study, Graduate School of Science, University of Tokyo
*2 Department of Physics, Graduate School of Science, University of Tokyo

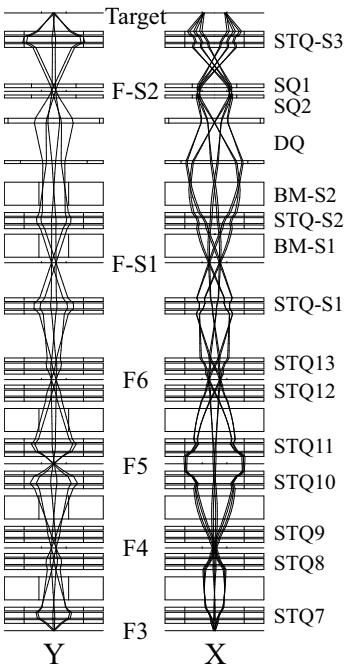

Fig. 2. Envelopes of dispersive beam transport from F3 to SHARAQ target in horizontal (right) and vertical (left) planes. Trajectories are drawn for particles with $x_0 = \pm 3$ mm, $_0 = \pm 3$ mm, $\theta_0 = \pm 10$ and 0 mr, $_0 = \pm 30$ and 0 mr, and $\delta_0 = \pm 0.3\%$.

using the computer code GIOS[6].

One realistic solution for the dispersive beam transport is shown in Fig. 2. Two 30 bending magnets (BM) are used with several quadrupole magnets for the beam transport from F6 to the SHARAQ target. Although most of the quadrupole magnets are superconducting triplet quadrupole magnets (STQ) with a warm bore radius of 12 cm[7], the doublet (DQ) and singlet (SQ) quadrupole magnets are normal conducting magnets. To save construction cost, PQ2 and PQ3 magnets that were used for the SMART spectrograph will be utilized for the DQ magnets. Additionally, the existing 400-mm and 500-mm quadrupole magnets will be employed for the SQ1 and SQ2 magnets. The DQ and SQ magnets are located between BM-S2 and STQ-S3. The maximum magnetic rigidity of the beam line is 8.5 Tm, which is limited by the maximum field gradient of the DQ magnets.

The magnetic-field gradients for the several couples of STQs are constrained to be symmetric. Namely, the field gradients of the three quadrupole magnets of STQ9 are equal to those of STQ12. Similarly, the field gradients of STQ10 and STQ13 are equal to those of STQ11 and STQ-S1, respectively. This symmetric constraint for the field gradients is helpful to simplify beam-line tuning and to minimize higher order aberration.

The beam is focused both horizontally and vertically at SF-2 between SQ1 and SQ2 in the last straight section after BM-S2. At this point, the horizontal size of the beam envelope is large, whereas the vertical size is relatively small. The horizontal beam size is predominated by the momentum spread of the beam due to a large dispersion of 21 m. Thus, SQs can change the correlation between the momentum and the horizontal angle of the beam trajectory, which is presented by the b_{26} term in the transfer matrix, whereas the other ion optical properties such as dispersion are nearly unchanged. The b_{16} term is easily changed by tuning STQ-S3. Thus, the double focusing point between SQ1 and SQ2 in the last straight section is useful for realizing the dispersion matching conditions.

$(x\|x)$ $(= b_{11})$	-1.00	$(x\|\theta)$ $(= b_{12})$	0.00
$(\theta\|x)$ $(= b_{21})$	0.21	$(\theta\|\theta)$ $(= b_{22})$	-1.00
$(x\|\delta)$ $(= b_{16})$	-14.76	$(\theta\|\delta)$ $(= b_{26})$	4.79
$(\ \|\ )$ $(= b_{33})$	1.13	$(\ \|\ )$ $(= b_{34})$	0.00
$(\ \|\ )$ $(= b_{43})$	0.89	$(\ \|\ )$ $(= b_{44})$	0.89

Table 1. Beam transfer matrix of SHARAQ beam line obtained by first-order ion optical calculation by GIOS. The units for the lengths and angles are m and radian, respectively.

The transfer matrix of the SHARAQ beam line obtained by the first-order ion optical calculation is tabulated in Table 1. The dispersion matching conditions are successfully satisfied, whereas the horizontal and vertical magnifications are almost unity. The off diagonal terms of b_{21} and b_{43} are maintained small to reduce the angular spread caused by x_0 and y_0.

In this calculation, only the first-order effects are taken into account, however, the higher-order aberration is not negligible since the secondary RI beams have a large emittance. The hexapole and octupole magnets are useful for correcting such higher-order effects. To optimize the layout of these multipole magnets and their field strengths, it is necessary to perform higher-order ion optical calculation. This higher-order calculation is still in progress, and the calculation results will be reported elsewhere soon.

References

1) T. Uesaka *et al.*: in this report.
2) B. L. Cohen: Rev. Sci. Instr. **30**, 415 (1959).
3) T. Wakasa *et al.*: Nucl. Instrum. Methods A **482**, 79 (2002), and references therein.
4) K. L. Brown *et al.*: SLAC Report No. 91 Rev. 1, 1974 (unpublished).
5) T. Kubo: Nucl. Instrum. Methods B **204**, 97 (2003).
6) H. Wollnik *et al.*: Ion-optics code GIOS, University of Giessen, Germany.
7) K. Kusaka *et al.*: IEEE Trans. Appl. Supercond. **14**, 310 (2004).

High-resolution SHARAQ spectrometer

T. Uesaka,[*1] S. Shimoura,[*1] H. Sakai,[*2] T. Kawabata,[*1] A. Saito,[*2] K. Nakanishi,[*1] Y. Sasamoto,[*1] T. Kubo,[*3] G. P. A. Berg,[*4] S. Kubono,[*1] E. Ideguchi,[*1] and H. Yamaguchi[*1]

1 Overview

The SHARAQ spectrometer is a high-resolution magnetic spectrometer designed for radioactive isotope (RI) beam experiments at the RI Beam Factory (RIBF). It can be used to analyze particles with a magnetic rigidity of 1.8–6.8 Tm, corresponding to an energy of 40–440 MeV/A for $A/Z = 2$ particles. The spectrometer is designed for momentum and angular resolutions of $\delta p/p$ ∼1/15000 and $\delta\theta \sim 1$ mrad, respectively. The magnet system can rotate around its target position in the range from $-2°$ to $15°$ to allow $0°$ and forward angle measurements. Figure 1 gives an overview of the SHARAQ spectrometer.

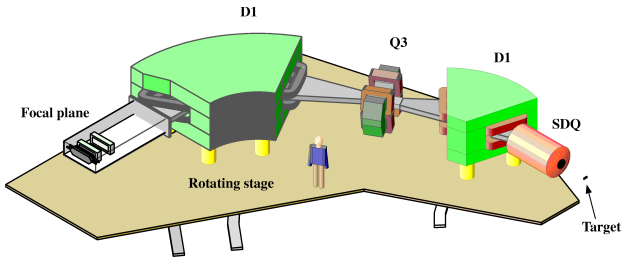

Fig. 1. SHARAQ spectrometer.

RI beams, produced at the primary target position of BigRIPS, are transported to the SHARAQ target position through the BigRIPS beamline[1)] and a newly constructed SHARAQ beamline[2)]. The beamline and the spectrometer are fully dispersion-matched. Simultaneous lateral and angular dispersion matchings are crucial to achieving the high spacial and angular resolving powers of the spectrometer in view of the large intrinsic momentum spread of RI beams. The beamline can also operate in an achromatic mode to provide a small beam spot at the target position for diagnostic and experimental purposes. The beamline will be equipped with tracking detectors[3)] both for beam tuning and for beam monitoring.

2 Configuration

The SHARAQ spectrometer consists of three quadrupole and two dipole magnets.

The first quadrupole doublet (SDQ) consists of two superconducting quadrupoles (Q1 and Q2) with a design adopted from the superconducting triplet quadrupoles of BigRIPS[4)]. The modification is mainly made to the 240-mm-diameter of warm bore in the original triplet quadrupoles: The warm bore of SDQ is diamond shaped with a 340 mm (horizontal) × 230 mm (vertical) opening to accept the horizontally extended envelope of the reaction products. The following normal-conducting dipole (D1) and quadrupole (Q3) magnets are recycled from the decommissioned spectrograph SMART. The D1 magnet, which was used as a $60°$ bending magnet with a bending radius of $\rho = 2.4$ m in SMART, is used as a $32.7°$ bending magnet with a bending radius of $\rho = 4.4$ m in SHARAQ. Both entrance and exit axes to the magnet are titled by $13.7°$ in a horizontally focusing direction.

The second dipole magnet, D2, is a new magnet specially designed to achieve the spectrometer specifications. The D2 magnet is a $60°$ bending magnet with a pole gap of 200 mm. At the exit, an edge angle of $30°$ is provided for horizontal focusing. This reduces the distance from the D2 magnet to the focal plane. Details of its design are described in Section 4.

The specifications of Q1, Q2, and Q3 and of D1 and D2 are listed in Tables 1 and 2, respectively. It should be noted that the effective lengths of the quadrupoles are dependent on the magnetic field strength and thus the values in the table represent typical ones.

Table 1. Specifications of magnets Q1–3.

	Q1	Q2	Q3
Bore [mm]	$340^W \times 230^H$		$\phi 270$
Max. gradient [T/m]	14.1	14.1	7.4
Effective length [mm]	530	1020	840

Table 2. Specifications of magnets D1 and D2.

	D1	D2
Bending radius [m]	4.4	4.4
Bending angle [deg]	32.7	60
Gap [mm]	230	200
Max. field strength [T]	1.55	1.55
Weight [t]	102	∼280

3 Ion-optical calculation

First-order ion-optical calculations using GIOS[7)] were performed to achieve the design specifications of the spectrometer and to accommodate the existing magnets and other constraints. Q1 and Q2 field strengths were optimized to match the beam envelops to the acceptances of Q2 and Q3. At the same time, the strength of Q3 was adjusted to achieve zero vertical magnification ($y|y$). The vanishing vertical magnification is essential in obtaining the required vertical angular resolution. Results of the first-order ion-optical cal-

*1 Center for Nuclear Study, University of Tokyo
*2 Department of Physics, University of Tokyo
*3 RIKEN (the Institute for Physical and Chemical Research)
*4 Department of Physics and Joint Institute for Nuclear Astrophysics, University of Notre Dame

culations are shown in Fig. 2. In the upper and lower parts, particle trajectories in the vertical and horizontal planes are shown for $\Delta x = \pm 30$ mm, $\Delta y = \pm 5$ mm, $\Delta a = \pm 1°$, $\Delta b = \pm 3°$, and $\Delta p/p = \pm 1\%$.

The ratio of the dispersion $[(x|\delta) = 5.86$ m] and the magnification in the dispersive plane $[(x|x) = 0.397]$ is 14.8 m, resulting in a resolving power of $p/\delta p$ =14800 for a target spot of 1 mm in diameter. A large value of $|(y|b)| = 2.3$ m/rad and a vanishing vertical magnification of $(y|y) = 0.0$ leads to a high angular resolution of Δb <1 mrad in the vertical direction. The horizontal angular resolution Δa is also as small as 1 mrad. Other first-order matrix elements can be found in Ref. 5. The designed parameters of the SHARAQ spectrometer are presented in Table 3.

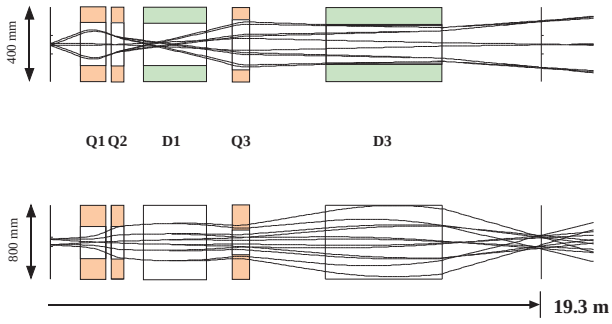

Fig. 2. Results of the first-order ion-optical calculation. Upper and lower panels represent particle trajectories in the vertical and horizontal planes, respectively.

Table 3. Design parameters of the SHARAQ spectrometer.

Dispersion (D) [m]	5.86
Horizontal magnification (M_x)	0.40
D/M_x [m]	14.8 m
Resolving power (for image size of 1 mm)	14800
Vertical magnification	0.0
Angular resolution	<1 mrad
Vertical acceptance [mrad]	±50
Horizontal acceptance [mrad]	
in dispersion matching mode	±17
in achromatic beam line mode	±30
Solid angle [msr]	
in dispersion matching mode	2.7
in achromatic beam line mode	4.8

Ion optical calculations using COSY INFINITY[8] are also carried out to evaluate the effects of higher-order aberrations. It was found that major aberrations $(x|aa)$ and $(x|aaa)$ originate from the inhomogeneous field distribution of Q1 and Q2 in the region of radii $r > 12$ cm. The entrance pole of D2 will have the shape of a 3rd-order polynomial to minimize these aberrations. In this way, the higher-order aberrations can be kept small enough to not effect the first order design.

4 Design of magnet D2

Since D2 is the largest magnet in SHARAQ providing 60° bending, its design is the most critical part in the design of the spectrometer.

A pole width of 1400 mm is needed to provide a good field region of ±400 mm from the central orbit. In addition, round fillets are introduced to both sides of the pole pieces to achieve field homogeneity in the wide field range of 0.4–1.55 T. The radii of the fillets are 180 mm at the low-momentum side and 200 mm at the high-momentum side. Actual arcs of the fillets are approximated by step functions with nine steps. Rose shims with a thickness of 1 mm are added on both sides of the pole. Their lengths are 49 mm at the low-momentum side and 44 mm at the high-momentum side. Results of magnetic field calculations show that the field produced with the pole is as homogeneous as $\Delta B/B \sim 1$–4×10^{-4} in the region of ±400 mm from the central orbit[5,6].

Excitation of the magnet up to $B = 1.55$ T requires a magnetomotive force of $\sim 2.6\times10^5$ A·turns. Coils are wound using a hollow conductor with a square cross section of 20×20 mm^2 area and a water cooling channel of 14 mm diameter. The circumference of the coil winding is about 14 m. The coil consists of five pancakes with 20 windings for each. The temperature increase is expected to be ∼20°C for pressure a drop of 5 atm.

5 Schedule

The SHARAQ spectrometer is scheduled to be operational in 2008. The construction of dipole magnet D2 is expected to be finished in FY2006. During the first half of FY2007, all magnets including the rotating stage will be installed in the experimental area E20 of RIBF. After completing the installation, field mapping measurements of the magnets will be made in the second half of FY2007. Design and construction of the beamline elements and the focal plane detector system will be carried out in simultaneously in FY2007. Testing will be conducted at the end of FY2007.

References

1) T. Kubo: Nucl. Instrum. Methods Phys. Res. B **204** (2003) 97.
2) T. Kawabata et al:, RIKEN Accel. Prog. Rep. **39** (2006).
3) A. Saito et al:, RIKEN Accel. Prog. Rep. **39** (2006).
4) K. Kusaka et al.: IEEE Trans. Appl. Supercond. **14** (2004) 310.
5) T. Uesaka et al.: CNS Annual Report 2005.
6) G. P. Berg: "Design Study of a New Dipole Magnet D2 for the SHARAQ Spectrometer", *unpublished*.
7) H. Wollnik et al:, AIP Conf. Proc. **177** (1998) 74.
8) M. Berz et al: Phys. Rev. C **47** (1993) 537.

Developments of multiwire drift chambers for SHARAQ beamline

A. Saito,[*1] S. Shimoura,[*2] T. Kawabata,[*2] Y. Sasamoto,[*2] T. Uesaka,[*2] and H. Sakai[*1]

We are developing beamline detectors that will be used at the high-resolution beamline for the SHARAQ spectrometer, which are now under construction at RI Beam Factory (RIBF)[1,2]. The spectrometer is designed to achieve a resolving power of $p/\delta p \sim 1.5 \times 10^4$ and an angular resolution better than 1 mrad for charged particles with magnetic rigidity of 6.8 Tm at the maximum. The beamline for the SHARAQ spectrometer is designed to fulfill dispersion-matching conditions when combined with the SHARAQ spectrometer[3]. The simultaneous achievement of lateral dispersion matching and angular dispersion matching conditions are crucially important in the use of the SHARAQ spectrometer for RI beams, which necessarily accompany a large momentum spread. Details of the dispersion-matched beamline is described in other reports[3]. A dispersion matching technique and/or the event-by-event tagging of the beam momentum will be introduced to compensate for the energy spread of the RI beam. Figure 1 shows the calculated optics of dispersive beam transport. The event-by-event tagging and tracking are needed at F3 for monitoring image size and at the target position to measure the momentum vector of the RI beam. There are some requirements for the tracking detectors. The thickness of the detectors should be as small as $\sim 10^{-4}$ of radiation length to reduce the effects of multiple scattering in the detectors to $\sim$0.1 mrad. The efficiency should be as large as possible even for light RI beams such as ^{8}He at 300 A MeV. The position resolution is required to be less than 300 μm at FWHM. The maximum counting rate should be 1 MHz for the dispersive beam transport.

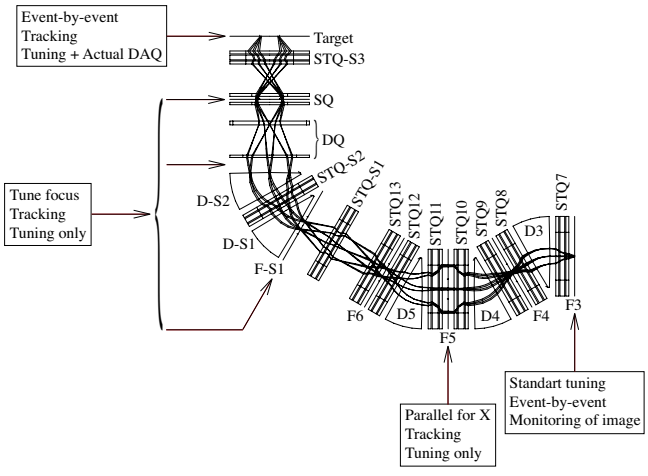

Fig. 1. Calculated optics of the dispersive beam transport.

In order to realize the performance described above, low-pressure multiwire drift chambers (LP-MWDC's) are being developed. A low-pressure operation at around 10–20 kPa is needed to reduce multiple scattering in the detector to as small as 0.1 mrad. The anode and potential wires are 12.5-μmϕ Au-W and 75-μmϕ Au-Cu, respectively. The size of one cell is 5×5 mm^2. The maximum counting rate of each cell is 10^4–10^5 Hz for dispersive beam transport. The specifications are summarized in Table 1. The signals from the anode wires are amplified and discriminated by the REPIC RPA-130 64-ch. preamplifier and discriminator card. The timing signals from RPA-130 are digitized by CAEN V1190A/B multi-hit TDC.

Table 1. Specifications of beamline detectors.

	LP-MWDC	LP-MWDC with stripped cathodes
position resolution	<300 μm†	
efficiency	>95%†	
multiple scattering	$\sim$0.1 mrad†	$\sim$0.1 mrad†
counting rate	$\sim$1 MHz†	
anode wire	12.5 μmϕ	20 μmϕ
potential wire	75 μmϕ	75 μmϕ
cell size	5×5 mm^2	6×6 mm^2
anode-cathode pitch	2.4 mm	2.5 mm
cathode	2 μm^t	1.5 μm^t
gas	i-C_4H_{10}	i-C_4H_{10}
gas pressure	10–20 kPa†	10–20 kPa†

† designed value.

In addition, we are developing LP-MWDC with stripped cathodes. The structure of the detector is shown in Fig. 2. The anode and potential wires and the electronics are the same as those for LP-MWDC described above. The cathodes are stripped with 2.5 mm pitch and the signals are read out using the delay lines that were developed for the PPAC[4]. Since the latter readout system has only four channels, the number of channels can be reduced. Their prototypes are now being tested.

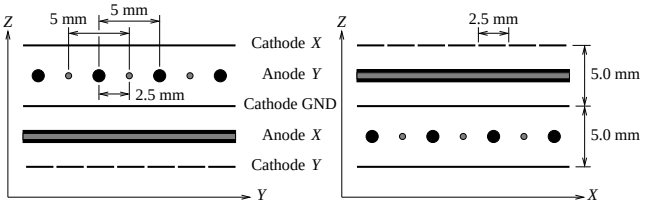

Fig. 2. Schematic view of LP-MWDC with stripped cathodes.

[*1] Department of Physics, University of Tokyo
[*2] Center for Nuclear Study, University of Tokyo

Fig. 3. Low-pressure multiwire drift chamber.

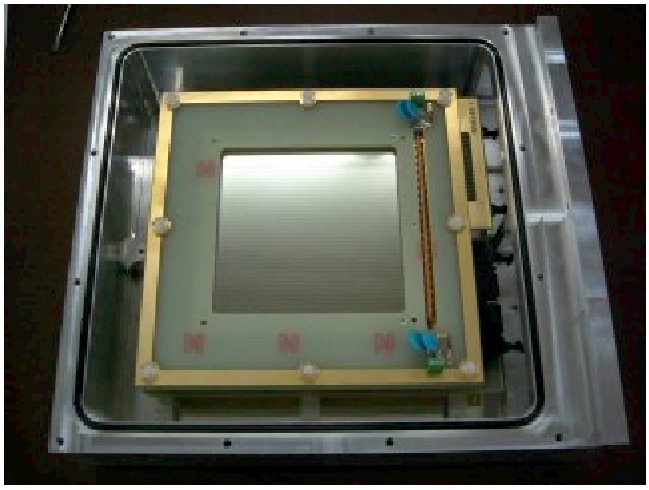

Fig. 4. Low-pressure multiwire drift chamber with stripped cathodes.

References

1) T. Uesaka et al.: Eur. Phys. J. **A** (RNB7 Conf. Proc.) in press.
2) T. Uesaka et al.: CNS Ann. Rep. 2005 (2006) 61.
3) T. Kawabata et al.: CNS Ann. Rep. 2005 (2006) 63.
4) H. Kumagai et al.: Nucl. Instrum. Meth. in Phys. Res. **A470** (2004) 562.

Preparation of self-supporting boron target

Y. Sasamoto,[*1] T. Kawabata,[*1] M. Hamagaki, I. Sugai,[*2] and Y. Takeda[*2]

The ^{11}B nucleus attracts a broad interest from the viewpoint of nuclear cluster physics since a dilute-gas-like cluster state has been recently observed in ^{11}B[1]. For further clarification of the cluster structure of ^{11}B, a precise measurement of the alpha inelastic scattering has been planned. For the precise measurements, a self-supporting and high-quality ^{11}B target with a thickness of about 500 μg/cm^2 is needed. Although vapor deposition is widely used to prepare a thin boron target, it is difficult to prepare a sufficiently thick enough self-supporting target by this method. The pressing method is also useful for the preparation of boron targets; however, the boron target prepared by this method is thicker than 10 mg/cm^2. In the present work, a ^{11}B target was prepared by sputtering with the electron-beam-excited plasma (EBEP).

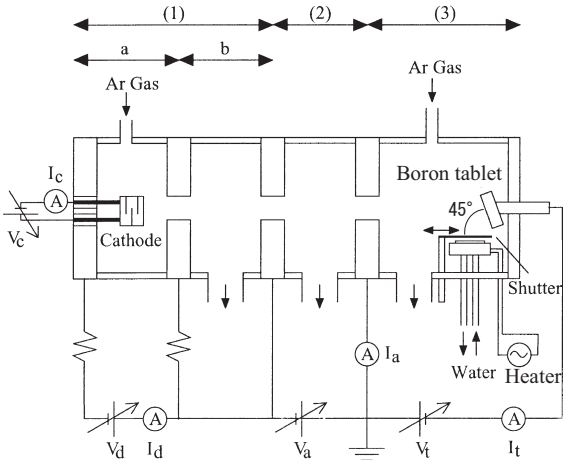

Fig. 1. Schematic view of experimental setup. Electrons are emitted from the cathode and accelerated by applying the acceleration voltage V_a. Then, the electron beam produces the argon plasma in region (3) and heats an isotopically enriched boron tablet. The argon ions extracted from the EBEP sputter the boron tablet. The size of the target is 40 mm × 5 mm.

A schematic view of the experimental setup for the preparation of the boron films is shown in Fig. 1. Electrons are emitted from the cathode and accelerated by applying the acceleration voltage V_a. Then, the electron beam produces a high-density argon plasma in region (3) and bombards an isotopically enriched boron tablet. Heating of the boron tablet by the bombardment of the electron beam is necessary to apply a negative bias voltage to the boron tablet. Although boron is an electrical insulator at room temperature, it becomes a conductor around 1000 C. After the boron tablet is heated sufficiently, a negative bias voltage is applied to the boron tablet. Then, the argon ions extracted from the EBEP sputter the boron tablet. In the sputtering using the EBEP method, the electron beam produces the argon plasma and heats the boron tablet. Finally, the sputtered boron particles are deposited on a substrate.

Table 1. Optimal deposition conditions in present work.

Discharge voltage (V_d)	45 V
Discharge current (I_d)	10 A
Acceleration voltage (V_a)	100 V
Electron beam current (I_a)	4 A
Target bias voltage (V_t)	−200 V
Ion current (I_t)	0.4 A
Deposition rate	0.07 nm/s
Substrate	glass plate with $NiCl_2$
Temperature of substrate	200 °C
Distance between tablet and substrate	4 cm

To obtain a self-supporting target, a water-soluble compound is deposited on the substrate before the tablet is sputtered. After boron is deposited on the substrate, the substrate is placed in water. Since the water-soluble compound dissolves in water, the boron film deposited on the substrate floats on water. The floating boron films are scooped up and self-supporting boron films are obtained. In the present study, $NiCl_2$ is used as the water-soluble compound. Since large boron films do not have sufficient strength to support their own weight, the films are scooped up on a polyethylene film with a hole of 10 mm diameter. The details of the procedure for the preparation of the boron target using the EBEP method are described in Ref. 2.

For the preparation of self-supporting boron films, internal stress is an important matter. When a large internal stress exists in the films, the films become breakable. Since internal stress depends on the deposition conditions, the deposition condition should be optimized. To find the optimal deposition conditions, boron was deposited under various conditions. The deposition rate was changed depending on the argon ion currents. The temperature of the substrate was controlled by a heater. The distance between the target and the substrate was also changed. The optimal deposition conditions in the present work are summarized Table 1.

The thickness of the obtained films was determined by measuring the energy loss of the alpha particles in the films. The energy of the alpha particles was

*1 Center for Nuclear Study, University of Tokyo
*2 High Energy Accelerator Research Organization (KEK)

measured by a Si detector. The thickest film obtained in the present work is 100 μg/cm^2 thick. The thickness is smaller than our initial expectation. However, the planed experiment for ^{11}B can be performed when an other experimental condition is improved, i.e., beam intensity is increased or lower statistics is accepted.

The uniformity of the film thickness is also examined. Figure 2 shows the position dependence of the thickness of the obtained boron film in the horizontal and vertical directions. The large variation in the vertical direction is caused by the variation in the distance between the boron tablet and the substrate. Since the substrate is placed with an angle of about 45 against the sputtering tablet (see Fig. 1), the distance between the boron tablet and the substrate is gradually changed in the vertical direction. The difference in the distance between the tablet and the substrate leads to the difference in the deposition rate. Therefore, the variation in the film thickness with inclination was observed in the vertical direction. This variation is not a serious problem for the experiment because the beam spot size is very small compared with the thickness variation.

The purity of the boron films was analyzed by the

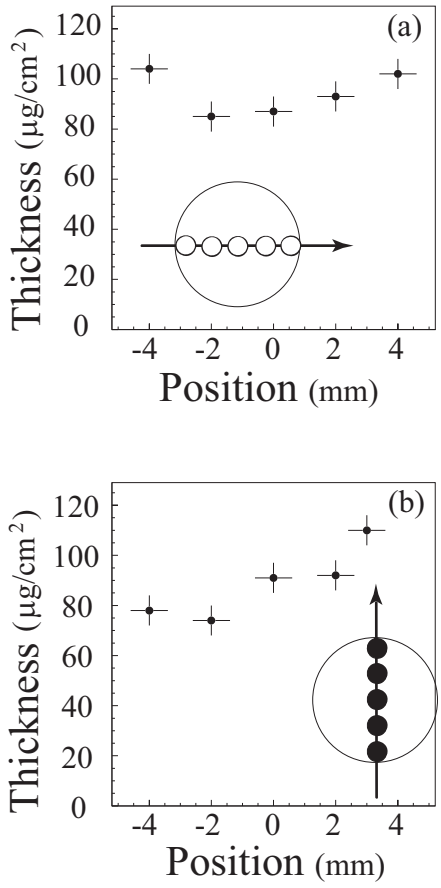

Fig. 2. Position dependence of thickness of obtained film in horizontal direction (upper figure) and vertical direction (lower figure).

Table 2. Contaminating impurities in boron films. The boron films contain about 10 % contaminants.

carbon	6.5 %
nitrogen	1.2 %
oxygen	1.9 %
argon	less than 1 %

electron probe microanalyzer (EPMA) method. In the EPMA measurement, an electron beam was irradiated to a sample and the characteristic X-rays emitted from the sample were detected. The EPMA measurement shows an unsatisfactory result in that the boron films are contaminated with carbon, nitrogen, oxygen, and argon. The contaminating impurities in the films are summarized in Table 2. The boron films contain about 10 % contaminants, which is not acceptable for the experiment. In a previous work using the EBEP method[2], no impurities were detected in the EPMA measurement. The possible origins of these impurities are the carbon parts in the surrounding material, the residual gases in the vacuum chamber, and the impurities in the boron tablet. It is expected that the surrounding material is not sputtered because the carbon parts are surrounded by the insulator. The amount of impurities originating from the residual gases is expected to decrease when the film is baked. A baked film was analyzed with the expectation of a decrease in the oxygen contamination originating from water; however, the same amount of oxygen was found in the baked film. These impurities were not detected from the boron tablet in the EPMA measurement. The origins of these impurities are still unclear; therefore, further investigation is necessary.

References

1) T. Kawabata et al.: Phys. Rev. C **70**, 034318 (2004).
2) S. Ozawa and M. Hamagaki: Vacuum **74**, 417-421 (2004).

Development of solid hydrogen target for ESPRI

H. Takeda, Y. Matsuda,[*1] S. Ishimoto,[*2] T. Ohnishi, K. Ozeki,[*3] T. Suda, S. Suzuki[*2] and J. Zenihiro[*4]

Proton elastic scattering at intermediate energies (200 – 400MeV) is one of the best probes for investigating the internal information of nuclei because of the large mean free path in the nuclear medium. With the aim of extracting the density distributions of short-lived radioactive isotopes (RI), we have carried out an ESPRI (Elastic Scattering of Protons with RI beam) project. The elastic scattering of RIs is measured by an inverse kinematics method. A solid hydrogen target (SHT) system has been developed for this purpose. We have already succeeded in forming a windowless 3-mm-thick SHT[1].

This year, we have developed 1-mm- and 5-mm-thick SHTs with thin window films to perform proton-elastic-scattering experiments on ^{20}O and ^{9}C at HIMAC[2]. The 1-mm-thick SHT was developed for the ^{20}O experiment. A thin SHT was indispensable for the ^{20}O measurements since the multiple scattering, energy loss and energy straggling inside the SHT made it difficult to distinguish the ground state from the first excited state of ^{20}O. On the other hand, a thick target could be used for the ^{9}C measurement, since ^{9}C has no bound excited states. The thick target enabled us to obtain sufficient statistics even with a low-intensity ^{9}C beam. Since it was difficult to form a 1-mm-thick windowless SHT, we used thin 9μm aramid films glued onto both sides of the cell. The flatness of the SHT is important in determining the cross sections of elastic scattering accurately. To prevent the thin window films from swelling due to hydrogen gas, we used an assembly developed to fabricate a windowless SHT (Fig. 1). Instead of using Teflon-coated stainless-steel plates, we installed thermally isolated copper plates to cover the cell. The plates were pressed onto the cell using stainless-steel bellows with 0.5 atm helium gas inside. Pt-Co resistance thermometers were inserted in the cell and the plate. The starting temperatures of the cell and the plates were ∼5.4K and ∼60K, respectively. Hydrogen gas was stored in a 20L buffer tank at 50∼250 Torr and was introduced into the cell. At first, a constant flow was maintained using a mass flow controller, then the flow was gradually decreased according to the decrease in the buffer tank pressure. It took about 10 minutes until the flow completely stopped. We waited for several minutes until the cell temperature became stable. Then the plates were removed by evacuating the helium gas in the bellows.

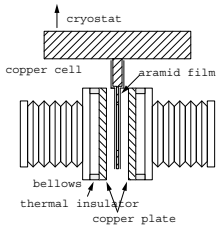

Fig. 1. Schematic view of the assembly to avoid the swelling of window films.

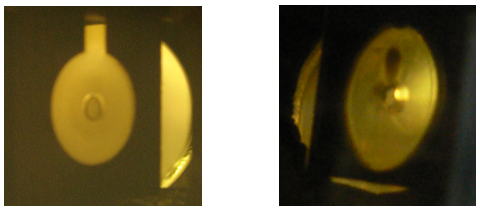

Fig. 2. 1-mm- and 5-mm-thick SHTs covered with 9μm aramid films are shown on the left and right sides, respectively. Some structures can be seen. See the text for detail.

Figure 2 shows photographs of the SHTs used in the HIMAC experiments. The left figure shows the 1-mm-thick SHT used for the ^{20}O measurement, while the right one shows the 5-mm-thick SHT used for ^{9}C measurement. The SHTs were almost free of holes when the copper plates were retracted. However, holes formed within a few minutes at the center for both cases, as can be seen in Fig. 2. The formation of the holes is not due to heat from the beam, since it occurred before the beam hit the SHTs. This was the first time that we observed such a phenomenon, and we have no clear explanation for it at this moment.

We can also see a dark region above the hole of the 5-mm-thick SHT. On the basis of our experiences, this seems to be a group of voids formed after the confinement of the liquid hydrogen surrounded by the solid, since the volume of the hydrogen shrank during the solidification. To avoid this phenomenon, it is desirable to form the crystal directly from hydrogen gas without passing through the liquid phase. Careful choices of the initial conditions such as pressure and the hydrogen gas flow from the inlet are necessary. It is also important to achieve as low cell temperature as possible since the acceptable range of conditions becomes broader. The shape of the cell should also be considered carefully.

*1 Department of Physics, Tohoku University
*2 High Energy Accelerator Research Organization (KEK)
*3 Cyclotron and Radioisotope Center, Tohoku University
*4 Department of Physics, Kyoto University

References

1) T. Ohnishi *et al.*: RIKEN Acc. Prog. Rep. **38**, 150 (2005).
2) S. Terashima *et al.*: in this RIKEN Acc. Prog. Rep.

Development of the recoil ion detector for SCRIT experiment†

K. Ishii[1], T. Emoto, Y. Furukawa[2], S. Ito, K. Kurita*1, A. Kuwajima[2], T. Suda, T. Tamae[2], M. Wakasugi, S. Wang, and Y. Yano

[electron scattering, RI, SCRIT]

We are developing a recoil ion detector for SCRIT (the Self-Confining RI Target). SCRIT is used in an electron scattering experiment method we are establishing. SCRIT is used to determine the behavior of the charge density of RI. The method using SCRIT involves the trapping of ions in electron beam potential and letting beam electrons to scatter the trapped ions. Presently we are investigating ion trapping in the electron beam passage using ions of a stable nucleus (i.e. Cs ions) at Kyoto University. Cs ions are injected externally.

The trapping efficiency of ions is low. Thus, it is necessary to confirm that the electrons are scattered by the target ions but not by other residual gas ions. To this end, it is necessary to measure the coincidence between recoiled ions and scattered electrons.

The problem in detect recoil ions is that the detector should be placed in a high-vacuum environment and the energy of recoil ion is as low as 50keV. Therefore the choice of detectors is limited. We determine a technical choice on the basis of the environment and detector efficiency. Additionally, we should determine the background level at which the recoil ion detector should be placed.

We calculate ion transport as the first step toward recoil ion detector development. For an easy recoiled ion detection, we change ion transport slightly. We chose a microchannel plate(MCP) and Channeltron for detection. The purpose of using the two types of detector is to examine the difference in efficiency of detecting background particles.

The transportation of recoiled ions was calculated and a prototype device was fabricated. The device is shown in figure 1. We install a deflector and an einzel

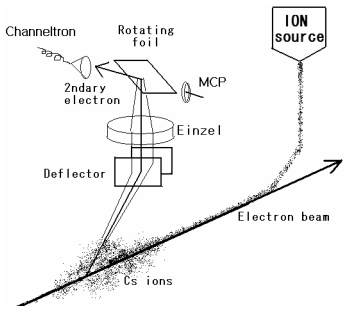

Fig. 1. Schematic view of experimental setup

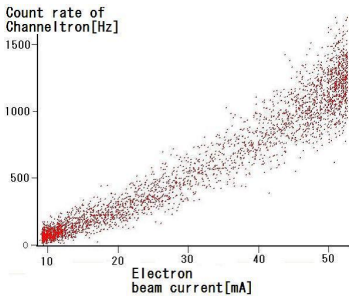

Fig. 2. Channeltron count[Hz] vs electron beam[mA]

separately to change ion transport and improve acceptance. Furthermore, instead of placing detectors such that they face the recoil ion direction, we decided to utilize a secondary electron emitter foil, so that background particles do not hit the sensitive volume. The two detectors were placed symmetrically with respect to the secondary electron emitter foil to determine detection efficiency.

A large number of signals that originate from residual gas are detected. Some externally injected ions are diffused into the recoil port directly. However, we obtain interesting information on other background particles originates from synchrotron radiation. We found that intensity of this background is proportional to electron beam current, as shown in figure 2. The counting rate is about 1kHz at 50mA electron beam current.

The next step is to develop a method of decreasing the counting rate from background of residual gas and improve the acceptance of recoiled ions. The main existing problem is residual gas. It is necessary to remove influence of residual gas to establish the SCRIT method. Our goal is to decrease the background level to less than a few kHz to be able to measure the coincidence between recoiled ions with scattered electrons. We decrease the number of background by deflecting ions away from photons with a deflector, and installing more slits. We need to optimize ion transport to improve the acceptance of recoiled ions.

References

1) T. Suda et al.: RIKEN Accel. Prog. Rep. **37**, 81 (2004).
2) T. Suda et al.: RIKEN Accel. Prog. Rep. **38**, 71 (2005).

*1 Rikkyo University
*2 Tohoku University

New method of polarization reversal using 180-deg pulse nuclear magnetic resonance

T. Kawahara,[*1] T. Wakui,[*2] T. Uesaka,[*3] and S. Sakaguchi[*3]

1 Introduction

The polarized proton target for a RI beam experiment should be operated in a low magnetic field (0.01–0.3 T) and at a high temperature (77–300 K) to detect a low–energy recoil proton. One possible method to achieve the polarization is to make use of a population difference of electrons in Zeeman sublevels in the photoexcited triplet state of aromatic molecules[1)]. Because this population difference is independent of temperature or magnetic field,a proton can be polarized in a low magnetic field of 0.3 T and at a high temperature of 100 K, by transferring the population difference of electrons. The polarized proton target using the method has been successfully constructed and applied to RI beam experiments[2,3)].

In the measurement of polarization observables, it is indispensable to reverse the direction of polarization to reduce systematic uncertainties. In the previous measurement[3)], no efficient polarization reversal method was available and polarization was built up in the opposite direction, which costs a time loss of more than a numerical value is suggested if possible. Surely, a new method to flip the polarization axis is needed for more efficient use of machine time. We have applied a pulse NMR method for the purpose.

2 Pulse NMR method

In the pulse NMR method, the spin is flipped by applying the transverse magnetic field B_1 that is perpendicular to the static magnetic field B_0. Here, the flip angle of the spin can be written as

$$= \gamma_I B_1 \Delta t, \quad (1)$$

where $\gamma_1 = 2.68 \times 10^8 s^{-1} T^{-1}$ is the gyromagnetic ratio of a proton, and Δt is the pulse width. After turning off the B_1 pulse, the spin processes around the static magnetic field B_0, which causes an induced current in the NMR coil. The induced signal is called the "free induction decay" (FID) signal. Its amplitude, i.e., FID amplitude, is proportional to the degree of polarization. For the reversal of the spin, the flip angle must be 180-deg. It can be easily understood that a flip angle of 180-deg can be achieved by the long pulse duration Δt and /or the strong perpendicular magnetic field B_1. Long pulse duration, however, leads to a decrease in polarization due to the spin–lattice relaxation during the reversal.

To avoid the loss of polarization, we tried to make a stronger B_1 field keeping the pulse duration as short as a few a numerical value is suggested if possible. An NMR coil was modified for this part .

3 Improvement to carry out method of 180-deg pulse NMR

We improved the NMR coil as a first step.The spin flip angle is directly related to the FID signal amplitude V_{FID}, as $V_{\mathrm{FID}} \propto \sin$. V_{FID} for the original NMR coil, which is 10-turn of a 0.35-mmϕ copper wire, is shown in the left panel of Fig. 1 as a function of the RF pulse lebel of the transverse magnetic field B1. It is clearly observed that the spin is rotated by only 90-deg($\sin \sim 1$) even for the strongest B_1 that is limited by a maximum output of a RF amplifier. Various combinations of wire diameter and turn number were tried to produce a stronger B_1. Note that, not only turn number but also wire diameter affects the B_1 strength. This is because the wire diameter changes the impedance of the coil and thus is related to matching between the coil and the RF circuit. Whenever a new NMR coil was made, its impedance matching to the circuit was adjusted using a tuner, which is made of variable capacitances, at an appropriate frequency that is determined by the magnetic field strength. Finally, a coil of 35-turns of a 0.35 mmϕ copper wire was found to be the best coil in the current conditions. Using this NMR coil, we succeeded in rotating the polarization of a water sample by 180-deg. The result is shown in the right panel of Fig. 1.

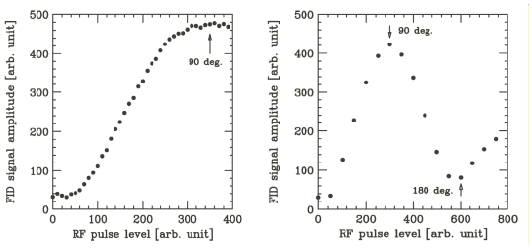

Fig. 1. FID signal amplitude. The left panel shows the FID signal measured using an orignal NMR coil. The right panel shows the FID signal measured using the upgrade NMR coil

In the next step, we optimized the RF pulse width. Since spin relaxation is fast during the rotation procedure, a shorter pulse width is preferable. On the other hand, the rotation angle can be smaller than 180-deg when the pulse width is too short. The efficiency of

*1 Department of Physics, Toho University
*2 Cyclotron and Radioisotope Center, Tohoku University
*3 Center for Nuclear Study, Graduate School of Science, University of Tokyo

the polarization reversal was evaluated by measuring the polarization loss in repeated reversals. The results for the pulse widths between 1.0 μsec and 4.0 μsec are shown in Fig 2. From the results, the pulse width was optimized to 2.2 μsec.

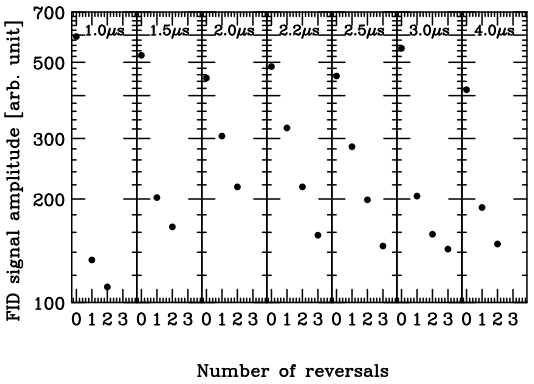

Fig. 2. The efficiency of polarization reversal is shown. The polarization was reversed three times during the experiment. The RF pulse width was changed between 1.0 sec and 4.0 sec. An optimum pulse width was found at $\Delta t = 2.2$ *sec.*

4 Results

We applied this polarization reversal technique to the actual polarized proton target made of naphthalene doped with a small amount of pentacene. Since the efficiency of the reversal depends on the line width of the NMR spectrum, it then depends on different materials. The result of the polarization measurement during the $\vec{p} + {}^6$He scattering experiment[2] is shown in Fig. 3. Closed circles denote the results taken in 2005, where in our new technique was applied, where as open circles represent data for the 2003 measurement. At $t = 0$ hour, the polarization was reversed in both cases. It is found that the efficiency of the polarization reversal by the new technique is about 70% using naphthalene.

5 Summary

Using the 180-deg pulse NMR method, we have succeeded in the reversal of the polarization direction. The NMR coil was upgraded by inereasing the turn number 10 to 35 times. In addition, we optimized the RF pulse width to achieve high efficiency of the polarization reversal. The RF pulse width was determined at 2.2 μsec. The new proton reversal methods was actually applied during the $\vec{p} + {}^6$He scattering experiment. The efficiency of the polarization retversal was about 70% using naphthalene, and the polarized time was 2.2 μsec, which was dramatically shortened from 10 hours in the 2003 experiment[3].

- - - - -

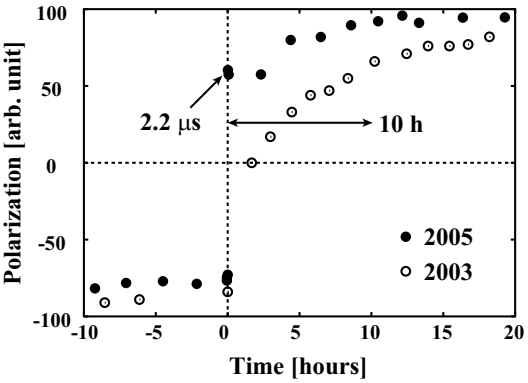

Fig. 3. Time development of proton polarization. Closed and open circles indicate data in 2005 and 2003, respectively. The polarization is reversed at T=0.

References

1) T. Wakui *et al.*; Nuclear Instruments and Methods in Physics Research A **550** (2005) 521,
2) S. Sakaguchi *et al.*; RIKEN Accelerator Progress Report vol. 40 (2006).
3) M. Hatano *et al.*; European Physical Journal A **25** (2005) 255.

Scintillation fiber detector for momentum analysis

Y. Matsuda,[*1] T. Kobayashi,[*1] M. Itoh,[*2] K. Ozeki,[*2] T. Murakami,[*3] J. Zenihiro,[*3] Y. Iwao,[*3] T. Ichihara, T. Suda, H. Otsu, H. Takeda, S. Terashima, Y. Watanabe, T. Ohnishi, K. Yoneda, and H. Sakaguchi[*4]

In most RI beam experiments, the momentum of the incident RI beam must be measured. At the momentum-dispersive focal plane of the beam line, position-sensitive gas detectors such as PPACs or MWPCs are often used. However, the efficiency of such gas detectors tends to decrease at high beam rates. There is also a risk of gas handling in a high vacuum, which sometimes causes a fatal problem. To overcome these difficulties, we have developed a simple one-dimensional scintillation fiber detector (SFD). We have studied the performance using beams from two accelerators.

Figure 1 shows a schematic view of the SFD. The SFD consists of sixty rows of scintillation fibers, each with a cross section of 2 mm square. The effective area is 120 mm×50 mm. Scintillation light from each fiber is collected by a 64-channel PMT (Hamamatsu H8500). The anode outputs are converted into LVDS signals by four ASDs (GNomes Design GNA-180) and fed to TDCs. On the other hand, the dynode output is amplified using a preamplifier, which uses the same ASD chip,[1)] it is further amplified using a PM amplifier, then fed to a charge ADC.

At first, the efficiency of the SFD and its dependence on the HV and beam intensity were studied at the HIMAC facility in the NIRS. The SFD was set perpendicular to the beam axis in the achromatic focal plane and irradiated using a 390 MeV/nucleon ^{22}Ne primary beam (a 300 MeV/nucleon ^{20}O secondary beam) with intensities of 2×10^6 (1×10^6) particles/pulse (ppp, one pulse=1.2 sec) and 5×10^3 (4×10^3) ppp, respectively. The efficiency turned out to be independent of beam intensity, and the maximum efficiency obtained for a single-cluster event (C1) was 90% at the HV plateau. The efficiency does not reach 100%, because the surface of each fiber is covered with PMMA cladding with a finite thickness, which gives rise to an insensitive area. With higher HV, the total efficiency reaches 100%, while the efficiency for C1 starts to decrease because of crosstalk. Most crosstalk can be eliminated by correlating the dynode output with the anode outputs.

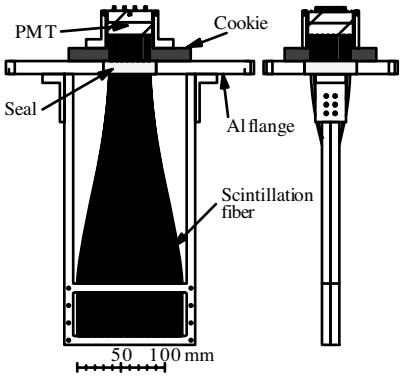

Fig. 1. Schematic view of SFD.

The loss of efficiency due to the insensitive areas could be recovered by injecting ions obliquely. This effect was examined at CYRIC at Tohoku University. Elastically scattered protons obtained by bombarding a 92.5 mg/cm^2 carbon target with a 45 MeV proton beam were used to irradiate the SFD. By tilting the SFD, the efficiency for C1 was able to reach nearly 100% without complex analysis. For actual use at a momentum-dispersive focal plane, beams would be mostly injected obliquely when the SFD is placed along the focal plane, because momentum-dispersive focal planes are often tilted.

Finally, the SFD was installed along the tilted momentum-dispersive focal plane of the SB course at the HIMAC facility for testing. Figure 2 shows the efficiency of the SFD for ^{20}O beams at 300 MeV/nucleon as a function of HV. The intensities of cocktail beams were $> 10^6$ ppp during the experiment; nevertheless, the detection efficiency for $Z = 8$ was maintained at nearly 100%.

From these measurements, it was confirmed that the SFD is useful as a beam-momentum tagging counter. Such a detector would be useful at the Big RIPS in the RIBF.

References

1) O. Sasaki et al.: IEEE Trans. Nucl. Sci. **46**, 1871 (1999).

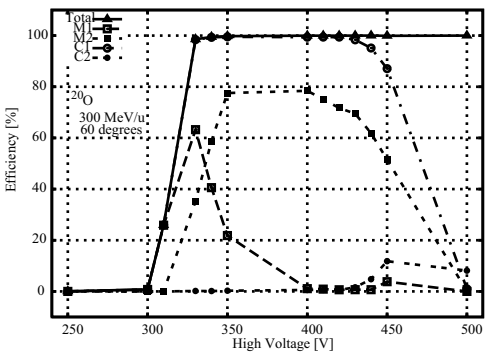

Fig. 2. HV dependence of efficiency for ^{20}O beams.

*1 Department of Physics, Tohoku University
*2 Cyclotron and Radioisotope Center , Tohoku University
*3 Department of Physics, Kyoto University
*4 Department of Applied Physics, Miyazaki University

A collinear fast beam laser spectroscopy apparatus for Ni isotopes

V. Lioubimov,[*2] M. Wada,[*1] A. Takamine,[*1,*3] T. Nakamura,[*4] Y. Ishida,[*1] H. Iimura,[*5] K. Okada,[*6] H. A. Schuessler,[*2] and Y. Yamazaki,[*1,*3]

Collinear fast laser spectroscopy is a powerful method to obtain nuclear data from optical measurements. We have chosen to study the Ni isotopes as the first candidates to be investigated at SLOWRI since they belong to an unexplored region of nuclear structure and due to their refractory properties have not been available at other accelerator facilities. We plan to determine the nuclear charge radii via isotope shift (IS) measurements and the nuclear moments via hfs measurements.[1)]

An off-line collinear fast beam apparatus is being constructed as shown in Fig. 1. An electro-magnetic mass separator which consists of a hollow-cathode ion source, an electrostatic quadrupole quartet and a 90° magnetic deflector having the mean beam radius of 30 cm and the maximum magnetic field of 1 T was build and being tested. The guiding principle of the ion optics design is to have wide beam in horizontal direction inside the dipole magnet to achieve high mass dispersion with a limited size of the magnet. The mass separated ion beam is guided to the collinear fast beam apparatus via an electrostatic qudrupole triplet with some steering devices. All the power supplies and monitor devices are controlled by a network-based system with Labview software.

The interaction region with a laser beam has two modes: one is for ionic beams whose velocity at the fluorescence detection point can be varied by an electrostatic acceleration / deceleration for ±3 kV. Other is for neutral beams. A charge exchange cell can be located at just upstream of the fluorescence detection point and the velocity of the neutralized atom can be varied by changing the potential of the cell. The fluorescence photons from the ions or atoms at the interaction region are accumulated by a spherical mirror and two condenser lenses and focused on to a photomultiplier. The total detection efficiency for a 320 nm photon is evaluated to be 5%.

We had tested the setup with $^{36,40}Ar^{+}$ ion beam for the transitions at 611.6616 nm from the metastable state.The laser induced fluorescence spectrum for $^{40}Ar^{+}$ is shown in Fig. 2. Our next plan is to proceed to Ni isotopes with the charge exchange and fluorescence detection scheme. The collinear resonance ionization scheme for Ni is also planned in the next step to improve the sensitivity drastically.

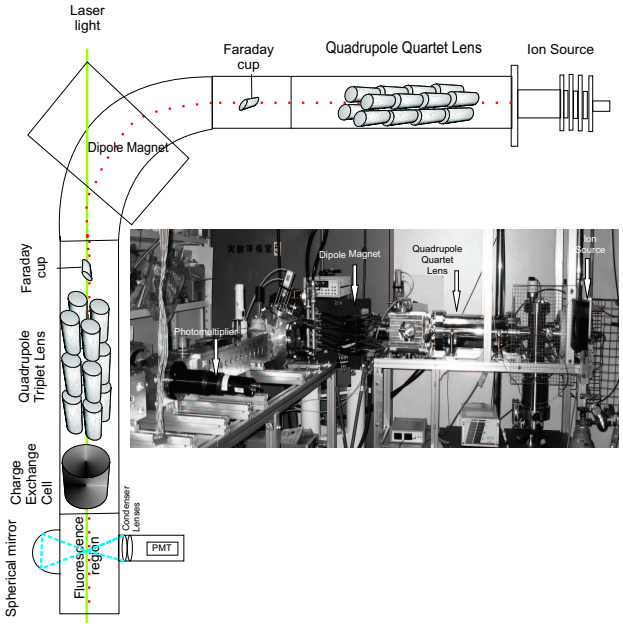

Fig. 1. The photo and the scheme of the off-line collinear fast beam apparatus.

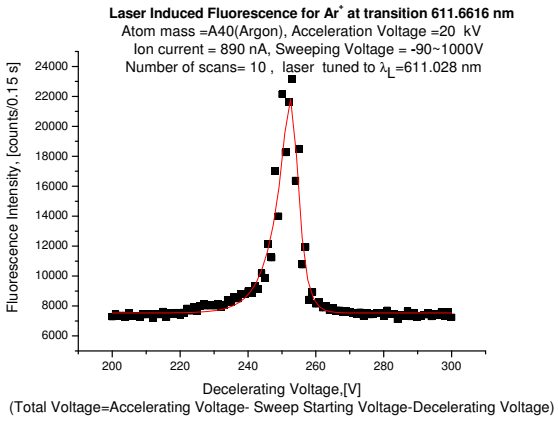

Fig. 2. Laser induced fluorescence intensity of $^{40}Ar^{+}$ as a function of the decelerating voltage. Laser wavelength was fixed at 611.028 nm .

*1 Atomic Physics Laboratory, RIKEN
*2 Department of Physics, Texas A&M University
*3 Graduate School of Arts and Science, University of Tokyo
*4 Institute of Particle and Nuclear Studies, High Energy Accelerator Research Organization (KEK)
*5 Japan Atomic Energy Research Institute
*6 Department of Physics, Sophia University

References

1) M. Wada et al.: RIKEN Accel. Prog. Rep. **38**, 168 (2005).

Development of a Mott polarimeter for T-violation experiment

H. Kawamura[*1], T. Arai[*2], K. Asahi[*2], T. Inoue[*2], D. Kameda, J. Murata[*1], D. Nagae[*2], T. Nagatomo, K. Narita[*1], K. Shimada[*2], T. Sugimoto, M. Takemura[*2], K. Takase[*2], T. Toyoda[*1], R. Tsutsui[*1], M. Uchida[*2], H. Ueno, and A. Yoshimi

A new Mott polarimeter for a time-reversal violation experiment has been developed. A test experiment using plastic scintillation counters was performed at RARF E6 beamline in order to evaluate the detector performance as a polarimeter.

According to the CPT theorem, any violation of the combined particle-anti particle and space inversion symmetries is equal to a violation of time-reversal symmetry. Any observation of a time-reversal symmetry violation would be a signal of new physics beyond the standard model. The terms appear in the allowed β-decay rate function W; the usual parity violating β asymmetry parameter A and the parity and time-reversal violating triple correlation coefficient R[1)].

$$W \propto 1 + A\frac{\vec{p}_e}{E_e}\cdot\frac{\langle\vec{J}\rangle}{J} + R\vec{\sigma}_e\cdot\frac{\langle\vec{J}\rangle}{J}\times\frac{\vec{p}_e}{E_e} + \dots \quad .$$

Here $\vec{J}$ denotes the spin of the parent nucleus, whereas $\vec{p}_e$, E_e, and $\vec{\sigma}_e$ correspond to the momentum, energy, and spin of the electron, respectively.

In this experiment, ^{31}Al or ^{32}Al were used as a parent nucleus. Spin-polarized Al nuclei were produced from the projectile fragmentation reaction from 95MeV/nucleon ^{40}Ar beam on a Nb target. The Al fragments were separated using RIPS. The polarized fragments were implanted in a single crystal stopper to which the external static magnetic field was applied. The polarization of the Al nucleus was deduced from the β-decay asymmetry detected by the plastic scintillator telescopes placed $\theta = 0°$ and 180° with respect to the Al polarization axis.

The transverse polarization of the electrons emitted in the β-decay is deduced from the up-down asymmetry in the Mott scattering at backward angles. At backward scattering angles the cross-section is small but the analyzing power is large, and the figure of merit reaches the maximum value at ∼120°. A 9μm-thick gold foil is used as the analyzer foil. The Mott polarimeter was placed at 90cm from the stopper.

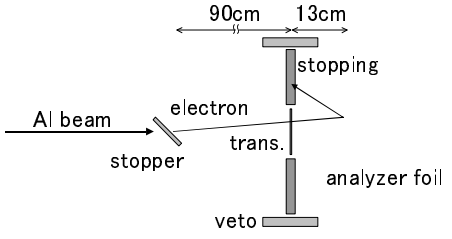

Fig. 1. Setup of the experiments.

*1 Department of Physics, Rikkyo University
*2 Department of Physics, Tokyo Institute of Technology

Our detection system is based on plastic scintillators; 2mm thick transmission counter (center) and 1cm thick stopping counters (up or down) (Fig.1). Figure 2 shows the obtained TDC spectrum between the center and up counters. No accidental events are observed in the experimental results, guaranteeing the performance of our polarimeter. However the electrons scattered at the inactive parts of the setup, such as frames or supports, were not rejected at all. Therefore, the effect of analyzing power was small and couldn't be confirmed in this test.

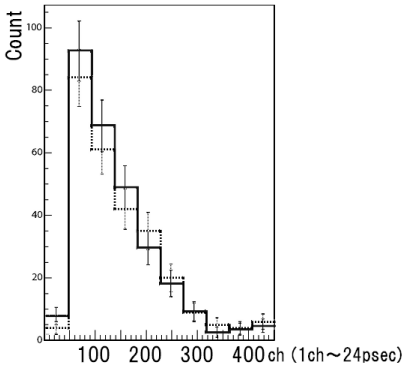

Fig. 2. TDC spectrum of the β-decay measurement with up counter. The counts "with foil (solid line)" exceed "without foil (dotted line)".

As a result, it is concluded that the polarimeter using plastic scintillators is susceptible to backgrounds and have a small solid angle. A tracking detector-based polarimeter can provide the high efficiency and reduces dominant backgrounds. In addition, the Mott polarimeter can detect the β-decay asymmetry. By using a tracking detector between an electron source and a scattering foil, both tracks before and after scattering can effectively be detected in a test measurement using a radiation source. From this motivation, therefore, we would apply a 3-dimensional tracking detector to overcome the problems.

We have tested the plastic scintillation counter array as a Mott polarimeter. In order to obtain a sufficient rejection power for the background events, multi-wire drift chamber has been employed. We are testing the performance of a polarimeter in more detail. In the future, an experiment to study a time reversal symmetry violation will be performed with a multi-wire drift chamber at KEK-TRIAC.

References

1) J.D. Jackson, S.B. Treiman, and H.W. Wyld: Phys. Rev. **106**, 517 (1957); Nucl. Phys. **4**, 206 (1957).

PHENIX silicon vertex tracker project

Y. Akiba, J. Asai, E.T Atomssa,[*1] K. Boyle,[*2] S. Chollet,[*1] V. Cianciolo,[*3] A. Deshpande,[*2,*4] A. Dion,[2] O. Drapier,[*1] A. Drees,[*2] H. En'yo, K. Fujiwara,[*5] F. Gastaldi,[*1] Y. Goto, R. Granier de Cassagnac,[*1] R. Ichimiya, H. Kano, M. Kawashima,[*6] K. Kurita,[*6] M. Kurosawa, Z. Li,[*7] A. Lebedev,[*8] E.J. Mannel,[*9] R. Muto, R. Nouicer[*7] M. Nguyen,[*2] C. Ogilvie[*8] H. Ohnishi, Y. Onuki, R. Pak,[*7] C. Pancake,[*2] K. Sakashita,[*10] M. Sekimoto,[*11] E. Shafto,[*2] W. Sondheim,[*12] A. Taketani, H. Themann,[*2] J. Tojo, T. Yamamoto[*13], and PHENIX VTX collaboration.

We have proposed a silicon vertex tracker (VTX) for the PHENIX experiment at RHIC. The VTX will substantially enhance the physics capabilities of the PHENIX central arm spectrometers. Our primary aim is to carry out precise measurements of heavy-quark production (charm and beauty) in $A + A$, $p(d) + A$, and polarized $p + p$ collisions. These are key measurements that are required for future RHIC programs, both for studies of the dense partonic matter produced in heavy-ion collisions and for the measurements of the nucleon spin-structure functions.

The main physics topics addressed by the VTX are as follows.

- Probing high-density partonic matter
  - Energy loss of heavy quarks (charm and bottom) in dense matter
  - Elliptic flow of heavy quarks in dense matter
  - Precise measurement of open heavy-quark production
  - Modification of jets by medium effects
  - Thermal dileptons from dense matter
- Measurements of gluon spin structure of nucleon
  - $\Delta G/G$ with heavy-quark production
  - $\Delta G/G$ with γ-jet measurement
- Nucleon structure in nuclei
  - Gluon shadowing over broad x-range

PHENIX has studied heavy quark production in p+p and Au+Au collisions from heavy-flavor decay electrons[1,2]. The VTX detector will improve the measurements by separating charm and bottom decay components. Figure 1 shows expected distributions of distance to the closest approach (DCA) of electrons from heavy flavor decay measured by the VTX detector. The bottom and charm decay components can be statistically separated from the DCA distribution. This will enable us to measure the nuclear modification factor, R_{AA}, and the elliptic flow strength, v_2, of charm and bottom. Figure 2 shows expected statistical accuracy of charm and bottom v_2 measurements in the first year of operation of the VTX detector in Au+Au collisions. The VTX also provides charged particle tracking in a large solid angle, which enable us to measure direct photon plus jet in p+p as well as di-hadron correlation from di-jets and γ + jet in Au+Au collisions.

The VTX detector consists of two inner layers of silicon pixel detectors and two outer layers of silicon strip detectors. The detector covers $|\eta| < 1.2$ in pseudo-

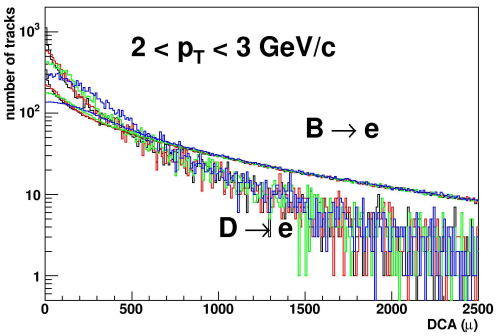

Fig. 1. Expected DCA distributions of electrons from heavy flavor decay (charm and bottom) for $2 < p_T^e < 3$ GeV/c measured by the VTX detector.

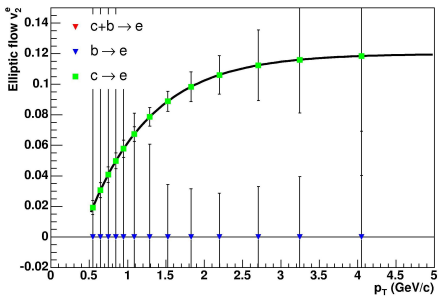

Fig. 2. The inclusive $v_2(p_T)$ of heavy flavor decay electrons is separated into charm (green squares) and bottom (blue triangles) component based on the DCA distribution. The error bars are expected statistical errors. The v_2 of bottom is assumed to be zero.

*1 LLR, Ecole Polytechnique, CNRS-IN2P3, France
*2 StonyBrook University, USA
*3 Oak Ride National Laboratory, USA
*4 RIKEN BNL Research Center, USA
*5 Niigata University, Japan
*6 Rikkyo University, Japan
*7 Brookhaven National Laboratory, USA
*8 Iowa State University, USA
*9 Columbia University, USA
*10 Tokyo Institute of Technology, Japan
*11 High Energy Accelerator Research Organization, Japan
*12 Los Alamos National Laboratory, USA
*13 University of Electron-Communications, Japan

rapidity and $\Delta\phi \approx 2\pi$ in azimuth. The pixel detector[3] has been developed in collaboration with the ALICE group at CERN (RIKEN–ALICE collaboration). The pixel chips were used and worked very well in the NA60 experiment. The silicon strip detector[4] uses a novel "stripixel" sensor developed at BNL. The sensor is read out using the SVX4 chips developed at FNAL. Figure 3 and figure 4 show 3D mechanical drawings of the VTX detector, rendered by a mechanical engineering firm HYTEC.

The main points of progress this year are as follows.

- The US side of the project have been included in the US FY07 budget. The total budget is 4.6 M US dollars over three years (FY07-FY09).
- We have a successful review of the project by DOE in May 2006, and a subsequent meeting at DOE in October 2006. The project received approval for starting the construction of the detector.
- First round prototypes of all components of the pixel system were completed[3,5]. The prototypes includes the pixel half-ladders, the SPIRO read-out modules[6], and a pixel Front End Module (FEM). A prototype pixel half-ladder consisted of two pixel sensor modules, a 3 cm wide prototype read-out bus[7], and a bus extender.
- A cosmic ray test of a pixel system prototype was performed[8]. The test system included three sets of the half-ladder prototypes, three prototype SPIRO modules, and a prototype FEM. Clear cosmic ray tracks were observed in the test.
- Fabrication of the final prototype (1.5 cm) bus is under way[7].
- Development of a pixel detector assembly system is under way[9].
- The first Read Out Card (ROC) prototype of the strip detector is tested at ORNL. A clear MIP peak of cosmic rays has been observed. The second round prototype ROCs are fabricated and they will be tested soon.
- Production of the strip sensor is under way.
- Extensive Quality Assuarance (Q/A) tests of the pre-production strip sensor were carried out at BNL. Q/A procedure for the sensor has been established.
- Extensive radiation damage tests of the stripixel sensors have been performed. Prototype sensors were exposed to neutrons and proton beams[10,11]. Sensors were also placed in PHENIX IR to measure the radiation damage in the actual environment[12]. A paper describing these test experiments is in preparation.
- The mechanical and thermal engineering work of the VTX system is under way by HYTEC.

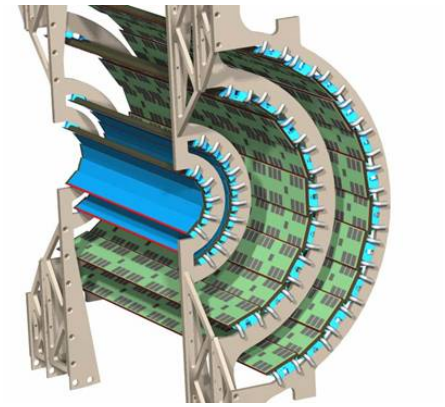

Fig. 3. A 3D mechanical drawing of one half of the PHENIX VTX detector. Two inner pixel layers, two outer strip layers, and the support structure are shown.

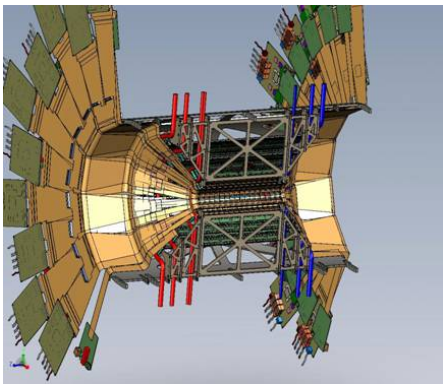

Fig. 4. A 3D mechanical drawing of the PHENIX VTX detector. The drawing includes the suppor structures, the 4 layers of detectors, the signal cables, the read-out modules, and cooling tubes.

References

1) A. Adare et al.: Phys. Rev. Lett. 97, 252002 (2006).
2) A. Adare et al.: Phys. Rev. Lett. 98, 172301 (2007).
3) A. Taketani et al.: RIKEN Accel. Prog. Rep. **40**, 170 (2007).
4) A. Deshpande et al.: RIKEN Accel. Prog. Rep. **40**, 173 (2007).
5) E. J. Mannel et al.: RIKEN Accel. Prog. Rep. **40**, 182 (2007).
6) R. Ichimiya et al.: RIKEN Accel. Prog. Rep. **40**, 176 (2007).
7) K. Fujiwara et al.: RIKEN Accel. Prog. Rep. **40**, 186 (2007).
8) M. Kurosawa et al.: RIKEN Accel. Prog. Rep. **40**, 180 (2007).
9) Y. Onuki et al.: RIKEN Accel. Prog. Rep. **40**, 171 (2007).
10) M. Kawashima et al.: RIKEN Accel. Prog. Rep. **40**, 188 (2007).
11) K. Sakashita et al.: RIKEN Accel. Prog. Rep. **40**, 190 (2007).
12) J. Asai et al.: RIKEN Accel. Prog. Rep. **40**, 174 (2007).

Status overview status of Silicon Pixel detector for PHENIX

A. Taketani, Y. Akiba, J. Asai, E. T. Atomssa,[*1] S. Chollet,[*1] O. Drapier,[*1] A. Dress, [*2] H. En'yo, M. Finger,[*3] K. Fujiwara, [*4] F. Gastaldi, [*1] R. Granier de Cassagnac,[*1] Y. Goto, R. Ichimiya, H. Kano, T. Kawasaki,[*4] M. Kawashima,[*5] K. Kurita,[*5] M. Kurosawa, E. J. Mannel,[*6] Y. Miyamoto,[*7] R. Muto, H. Ohnishi, Y. Onuki, C. Pancake,[*2] P. Riedler,[*8] E. Shafto,[*2] K. Sakashita,[*9] M. Sekimoto,[*10] T-A. Shibata[*9] W. Sondheim,[*11] J. Tojo,[*9] L. Tomasek,[*12] V. Vrba,[*11] T. Wakabayashi[*7] S. Watanabe[*17], and Y. Yamamoto[*13]

The PHENIX experiment at the Brookhaven National Laboratory will be upgraded with the introduction of a silicon vertex tracker (VTX)[1] in 2009 to enhance the physics capability of the PHENIX in both spin and heavy ion programs in the Relativistic Heavy Ion Collider. It is important to identify charm and bottom quark productions in large solid-angle coverage in both programs. The VTX is composed of two inner layers of pixel detector and two outer layers of stripixel detector. In this article we describe development and construction of the pixel detector part.

The pixel detector is composed of a pixel sensor, a dedicated readout chip, a readout flexible bus, their control/readout board (SPIRO), and a support structure. A signal from each sensor pixel is fed into a preamplifier on the readout chip, by bump bonding. The signal is digitized in the chip and then transferred to the SPIRO board through the bus. The SPIRO sends all data to the PHENIX data acquisition system (DAQ) via a 1.6 GBps optical link[2]. The support structure, which is made up of a carbon-epoxy composite, holds a mechanical sensor-readout chip assembly (sensor hybrid) and the flexible bus precisely within $10\mu m$. Also, the stucture includes a cooling pipe with a chlorofluorocarbon-based liquid to remove heat from the readout chip.

The sensor hybrid has been delivered to RIKEN by VTT Inc. A probe station for ensuring the performance of the sensor hybrid was set up at RIKEN Wako last year.[3] The readout chip performance was checked in terms of functionality electronically and then beta rays from a checking source were irradiated on the sensor and pixel hit data was readout.[4] Only the sensor hybrid with good performance[3] was assembled with the bus and support structure. Evaluated information is stored in a database and referred to the detailed selection of sensor hybrids.

A trial flexible bus of 3 cm width[5] was fabricated and assembled with the sensor hybrid and a 45 cm long bus extender. The bus was fabricated with a design rule of 70 μm line and 50 μm space. This assembled stave was connected to the SPIRO board.[6]. Three sets of stave and SPIROs were made. Individual combinations of a stave and a SPIRO board combination were tested using a VME-based control/data acquisition system. Then these were stacked vertically as a telescope array. Forty eight cosmic ray events were read out and reconstructed as straight line of pixel hits.[7]

Owing to the small space around the beam pipe region, the width of the bus should be 1.5 cm, the same as the width of the sensor hybrid with 188 signal lines. A 3 μm-thick Cu foil is used as a bus signal conductor for 60 μm-pitch signal lines. The design and performance the simulation of electorical performance were performed, and a 1.5 cm-wide bus is under fabrication at the time of this report submission.[8]

The required accuracy of assembly is less than 10 μm. A dedicated assemble machine was designed and fabricated. An assembly procedure is developed[9].

For what production in 2007, a test bench for readout electronics is developed. It has many test pins on the board for the observing real signal shape.[6]

A pixel readout system was developed and tested. The prototype system successfully read out cosmic-ray events. A mechanical assembly procedure was developed with actual jigs. The production of such mechanical staves and electronics will start in 2007 in RIKEN, Ecole Polytechnique, and Stony Brook University. The entire VTX detector will be ready at the PHENIX experimental hall in 2009.

*1 Ecole Polytechnique, CNRS-IN2P3, France
*2 Stony Brook University, USA
*3 Charles University, Czech Republic
*4 Niigata University, Japan
*5 Rikkyo University, Japan
*6 Columbia University, USA
*7 Tokyo Metropolitan College of Industiral Technology, Japan
*8 European Organization for Nuclea Research, Switzerland
*9 Tokyo Institute of Technology, Japan
*10 High Energy Accelerator Research Organization, Japan
*11 Los Alamos National Laboratory, USA
*12 Institute of Physics, Academy of Sciences, Czech Republic
*13 University of Electro-Communications

References

1) N. Baker et.al:Proposal for Silicon Vertex Tracker(VTX) for the PHENIX Experiment. (2005)
2) E. J. Eric et. al.: RIKEN Accel. Prog. Rep. **40**(2007)182
3) K. Fujiwara et al.: RIKEN Accel. Prog. Rep.**39**(2006)207
4) K. Kurosawa et.al.: RIKEN Accel Prog. Rep. **40**(2007)178
5) A. Taketani et.al.: RIKEN Accel Prog. Rep. **39**(2006)209
6) R. Ichimiya et.al.: RIKEN Accel Prog. Rep. **40**(2007)176
7) K. Kurosawa et.al.: RIKEN Accel Prog. Rep. **40**(2007)180
8) K. Fujiwara et.al.: RIKEN Accel Prog. Rep. **40**(2007)186
9) Y. Onuki et.al.: RIKEN Accel Prog. Rep. **40**(2007)171

Silicon pixel detector assembly procedure for PHENIX upgrade

Y. Onuki, Y. Akiba, J. Asai, H. En'yo, K. Fujiwara,[*1] R. Ichimiya, H. Kano, M. Kurosawa, R. Muto, H. Ohnishi, A. Taketani, Y. Yamamoto[*2] and PHENIX VTX Collaboration

The relativistic heavy-ion collider (RHIC) has been operated at Brookhaven National Laboratory (BNL) to provide collisions of polarized proton-proton $\sqrt{s}$ up to 500 GeV and heavy ion $\sqrt{s_{NN}}$ up to 200 GeV. The pioneering high energy nuclear interaction experiment (PHENIX) detector has been installed at one of the 6 intersection regions of RHIC.

The silicon vertex tracker (VTX) for the PHENIX detector will be installed in summer 2009 to enhance the physics capabilities. The upgrade will enable the precise measurement of heavy quarks, which carry direct signals from quark gluon plasma in heavy-ion collisions and fundamental information on gluon polarization in polarized proton-proton collisions. VTX consists of two major parts: the inner two layers are pixel-type sensors and the outer two layers are strip-type sensors. The inner two pixel layers have 10, 20-pixel staves in the ϕ direction. RIKEN is responsible for fabricating all the staves. A stave is formed by 4 sensor hybrids[3,4]. A stave can be separated into 4 components, two buses[1)] which are flexible circuit boards made with Al/Cu and kapton, 4 sensor hybrids, a support plate[2)] which is made with Carbon/Carbon(C/C) composite and a cooling structure. These components have to be assembled to maintain high alignment precision such as $10\mu m$.

In December 2005, we achieved a milestone: the first prototype stave had been assembled. The prototype was assembled manually at Hayashi-Seimitsu Co. It takes about 1 week to assemble without the wire bonding procedure. However this manufacturing method for stave is too expensive and time consuming for the production phase. Next, what we should establish is on assembly procedure for the production phase.

In this report, we describe the assembly procedure for the production phase. In particular, we focused on the alignment procedure.

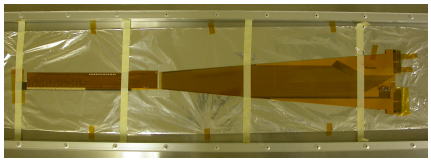

Fig. 1. Prototype half stave.

Several special jigs for assembly were fabricated last year by Daiya Seiki Co. The alignment procedure was established using these jigs.

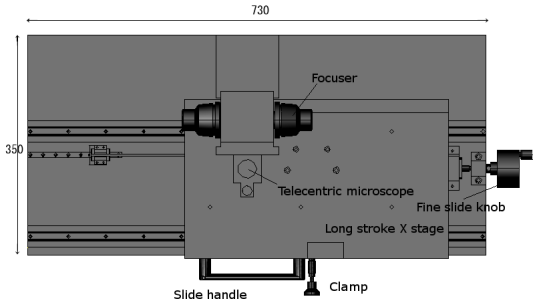

Fig. 2. *Microscope jig.*
The microscope has sufficient magnification to visualize the alinment mark on the sensor hybrid. We can see the mark on the monitor. The long-stroke X-stage has good precision for parallelism maintaining with less than 10 μm in the running range. Also, the stage has a magnemeter, which is used for precise position measurement with sub-μm accuracy.

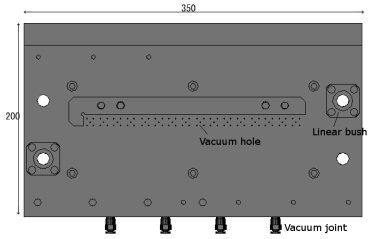

Fig. 3. *Alingment jig*
An alingment jig is used by putting it on the microscope jig. sensor hybrids are placed on the jig and fixed one by one independently by vacuum holes.

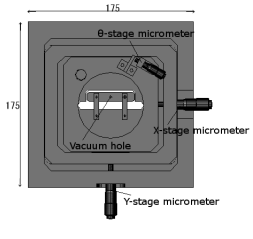

Fig. 4. *XYθ stage jig*
The jig has X-Y-translation and rotation θ stages with micrometers for aligning a sensor hybrid. Top of a sensor hybrid is chucked by the vacuum holes of the jig and aligned for proper position monitoring using the microscope jig. The alignment of the sensor hybrid can be performed one by one with the jig.

*1 Science and Technology, Niigata University, Japan
*2 Uvniversity of Electro-Communications, Tokyo, Japan

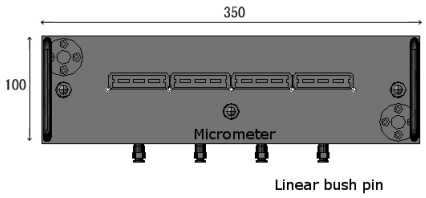

Fig. 5. *Turn jig*
The jig is used for upside-down aligned sensor hybrids and gluing between the sensor hybrids and the support plate. The micrometer is used to prevent from weight on the sensor hybrids and to set the gap between the sensor hybrids and the support plate for gluing. Vacuum hole equipped on the bottom.

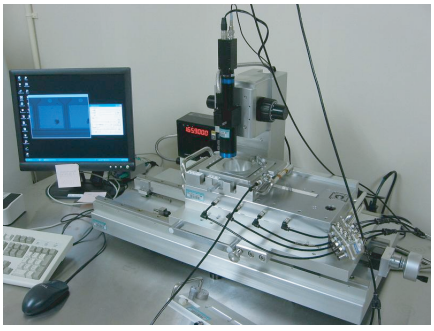

Fig. 6. *Procedures 2 and 3.*

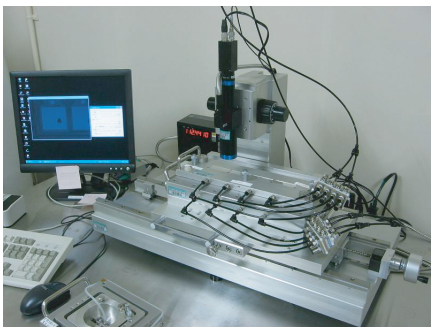

Fig. 7. *Procedure 4.*

Fig. 8. *Procedure 7.*

In particular, we considered aligning 4 sensor hybrids in a line and glue aligned ladders and a support.

Procedure 1: Set the sensor hybrids one by one in a line at the same interval with the magnescale and microscope on the alignment jig. Vacuum chucking ON to fix.

Procedure 2: Place the XYθ stage jig on the alignment jig. Release the vacuum chucking of the alinment jig for the first sensor hybrid. When the vacuum chucking of the XYθ jig is turn ON, the sensor hybrid can be moved each direction with micrometers of the XYθ jig. When the alignment is complete, turn ON the vacuum chucking of the alignment jig, and release the vacuum chucking of the XYθ jig.

Procedure 3: Take off the XYθ stage, and attach second sensor hybrid. The second, third and fourth sensor hybrids are aligned one by one using the same procedure.

Procedure 4: Set the turn jig on the 4 aligned sensor hybrids. Move the turn jig as close as possible to the ladder with the micrometer. Chuck the up side of the ladder with the vacuum hole of the turn jig. Release the vacuum of the alignment jig. Confirm whether the alignment is maintained with the through hole window of the turn jig. If the ladder moved and does not satisfy the $10\mu m$ alignment, repeat the previous procedure.

Procedure 5: Take off the turn jig from the alignment jig. The ladders are picked up on the turn jig to maintain the alignment.

Procedure 6: Place the support plate on the alignment jig and chucking to fix. Glue on the support plate with a dispenser machine.

Procedure 7: Place the turn jig on the support plate. Move down the turn jig as close as possible to the support with the micrometer. The thickness of the glue layer can be controlled with the micrometer. Leave glue until it is cured maintaining chucking.

These procedures can reduce the assembly time from 1 week to 1 day. In particular, alignment can be completed in just twenty minutes. We think the same procedures can be applied for the assembly of the bus.

In summary, the assembly of PHENIX/VTX detector has been discussed and is currently progressing with cooperation from researchers and companies. The first round of manufacturing using the production phase method will start in beginning of 2007.

References

1) A. Taketani: RIKEN Accel. Prog. Rep. **38**, 233 (2005).
2) J. Asai: RIKEN Accel. Prog. Rep. **38**, 235 (2005).
3) K. Fujiwara: RIKEN Accel. Prog. Rep. **38**, 228 (2005).
4) H. Ohnishi: RIKEN Accel. Prog. Rep. **38**, 230 (2005).
5) Y. Onuki: RIKEN Accel. Prog. Rep. **39**, 205 (2006).

Phenix VTX Tracker Upgrade: Stripixel Layers

A. Deshpande*[1] for the PHENIX VTX Collaboration

The PHENIX silicon vertex tracker (VTX)[1,2] has four layers: the inner two layers consist of silicon pixel detectors and the outer two of silicon strips of a novel design. The pixel detectors are funded by RIKEN[3], while the outer two "stripixel layers" were recently approved for funding by the US-DOE at the cost of $4.6M in US FY07, and will be the main focus of this contribution.

The PHENIX VTX has been primarily motivated by the study of heavy quark (charm and beauty) production in high energy $A-A, d-A$ and $p-p$ collisions at RHIC. The interaction of heavy quarks with the dense partonic matter produced in heavy ion collisions will allow us an unprecedented study of the properties of that matter. We will study energy loss of the heavy quarks as they traverse through this medium, study their flow properties in this medium using the VTX detector[1,2]. The heavy quark production in polarized $p-p$ collisions also allows us to explore the nucleon spin structure. Another advantage the VTX will afford us is the wide acceptance range $-1 < \eta < 1$ and $0 < \phi < 2\pi$, which will allow us to determine the direction of a jet produced in a $pp \rightarrow \gamma jet$ event using the track multiplicity in the jet production. Knowing the jet direction is crucial for determining the event kinematics with precision, leading to better understanding of the gluon's role in proton structure.

The silicon "stripixel" sensor is a novel design for a detector of this kind, developed at BNL.[4]. The silicon sensor is a single ended, DC-coupled, two dimensional sensitive detector. The design has distinct advantages for the fabrication and the signal processing. The reader is referred to[1] for detailed design diagrams and dimensions. The stripixel silicon sensor technology developed for the PHENIX upgrade, including the mask design and the processing technology were transferred to Hammamatsu Photonics (HPK) in Japan for mass production. In 2005/6 HPK delivered the first pre-production wafers of 625, 500 μm. The dicing of the pre-production wafers was done at BNL as well as HPK. A preproduction stripixel sensor is shown in Fig.1.

Initial sensor testing to learn and to develop the QA criteria was performed at the RBRC laboratory at BNL (BNL). Some specialized tests on mechanical dimensions were also performed at University of New Mexico (UNM). Each sensor went through a detailed mechanical and electrical check. The 500 μm sensors were rejected early as they showed significantly higher leakage currents at comparable bias voltages,

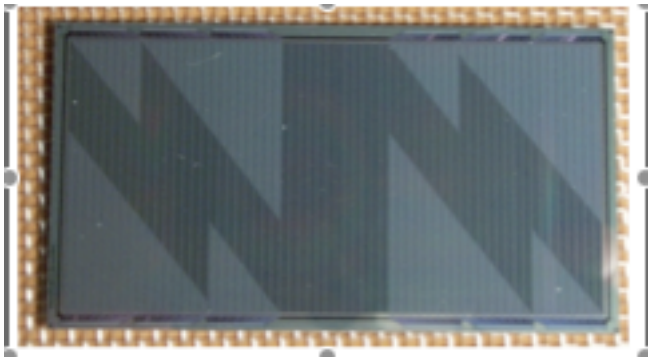

Fig. 1. Photograph of the silicon stripixel sensor from the pre-production batch produced by HPK.

compared to their 625 μm counterparts (6 μA compared to 300 nA at V_{FD} = 120V). After significant testing and discussions a general criteria for acceptance of a wafer was defined and delivered to HPK: That includes

(1) passing of visual inspection: no scratches etc.
(2) sensor thikness 625 ± 15 μ.
(3) Si resistivity 5-19 kOhms
(4) depletion voltage 50-250 V
(5) junction breakdown > 350 V
(6) passivated top of the active area except for bonding pads and ground ring
(7) maximum of 1% bad stripixels in the whole sensor and maximum 3 bad sensors in one section

A number of graduate students and post doctoral fellows in the group were trained to do sensor testing and QA. The QA of the production sensors will be performed in the three QA stations planned in the project: The RBRC Laboratory at BNL (BNL facility), the silicon QA laboratory at Stony Brook University (SBU) , and a laboratory for specialized tests (especially of mechanical properties) at the University of New Mexico (UNM). The first batch of the silicon wafers is expected to arrive at BNL around January'07., at which detailed QA operations will begin. As this article goes to print, the first efforts to design and build a prototype ladder are being initiated.

*[1] Department of Physics & Astronomy, Stony Brook University

References

1) PHENIX Silicon vertex tracker upgrade, http://www.-phenix.bnl.gov/phenix/WWW/public/docs/proposals/-VTX-PROPOSAL_jul2004.pdf
2) Y. Akiba et al., RIKEN Accel. Prog. Rep. **40**, xxx, 2007
3) A. Taketani et al., RIKEN Accel. Prog. Rep. **40**, xxx, 2007
4) Z. Li, Nucl. Inst. and Meth. A518 (2004) 738

Radiation Damage Study of Silicon Stripixel Sensor at the PHENIX Interaction Region

J. Asai, R. Ichimiya, M. Kawashima,[*1] K. Kurita,[*1] K. Sakashita,[*2] and A. Taketani.

We are studying the characteristics of quark gluon plasma (QGP) and the spin structure of protons using the Relativistic Heavy Ion Collider (RHIC) at Brookhaven National Laboratory (BNL). The PHENIX is a detector for measuring particles in A + A, p(d) + A, and polarized p + p collisions. A silicon vertex tracker (VTX) will be installed to upgrade PHENIX in 2009 for succeeding a running period of 10 years.[1] The VTX can identify the decay of heavy quarks by the precise measurement of the decay vertex and works as a large-solid-angle detector. It consists of a barrel detector and a forward detector. In the barrel detector, the inner two cylindrical layers use a silicon pixel detector[2] and the outer two cylindrical layers use a silicon strip detector. In this article, we report the radiation damage study of the silicon stripixel sensor[3,4] at the PHENIX Interaction Region (IR) in 2006. We estimated the radiation damage from the increase of leakage current and extrapolate it for a running period of 10 years.

The stripixel sensor will be placed at 10 cm and 14 cm away from the beam line. The expected integrated luminosity is 4000 pb^{-1}. Radiation damage is mainly caused by point defects in Si. The main damage effect is the increase of leakage current. We will use the SVX4 readout chip produced by FERMILAB.[5] The preamplifier has a 200 fC dynamic range, and the change accumulated in the preamp needs to be discharged periodically. This preamp reset is done every 13 μsec, which is the beam bunch circulation cycle around the RHIC ring. Therefore, it allows a 15 nA/strip maximum to avoid preamp saturation within the reset interval. The leakage current of the non-irradiated stripixel sensor is about 0.1 nA/strip. The biggest concern is the increase of leakage current caused by radiation damage. The increase of leakage current (ΔI) in the volume (V) can be written as;

$$\Delta I/V = \alpha \Phi_{eq}, \qquad (1)$$

where α is the radiation damage parameter constant. It depends on the thermal history from the start of the irradiation. The typical value of α is 4×10^{-17} A/cm after annealing. Φ_{eq} is the fluence per cm^{-2} of 1 MeV neutrons which causes the equivalent radiation damage to the detector.

We determined the increase of leakage current of the irradiated stripixel sensor in a 14.1 MeV neutron beam experiment at the Rikkyo Univ. and a 16 MeV proton beam experiment at the Univ. of Tsukuba[6,7]. In addition, the stripixel sensor was also irradiated at the PHENIX IR in 2006. It was placed at r = 10 cm from the beam line. The setup of the stripixel sensor is shown in Fig. 1. It is exactly the same in therms of its location on the real VTX detector, which will be installed. Two kinds of diodes were placed for the radiation reference monitor of the stripixel sensor on the same fixture. The diode sizes were 0.1 cm^2 and 0.25 cm^2. The thicknesses were both 400 μm. The stripixel sensor and the reference diodes were held in place in the PHENIX IR for 44 days. The integrated luminosity during the irradiation period was 12 pb^{-1}. Then the stripixel sensor and diodes were shipped to RIKEN for the measurement of their characteristic change. The bias voltage dependences of measured distributions of capacitance (C) and leakage current (I) are shown in Fig. 2. The full depletion voltage (V_{FD}) was determined graphically utilizing of the flat positions of the C-V curve. The increase of leakage current was determined before and after irradiation at V_{FD}. The radiation damage parameter constant α was calculated to be 3.21×10^{-17} A/cm by the temperature history from the start of the irradiation. The fluences of both the stripixel sensor and diodes estimated using Eq. 1. are shown in Fig. 3. The fluence of the stripixel sensor was 9.2×10^9 N_{eq}/cm^2. The average fluence of the diodes was 10×10^9 N_{eq}/cm^2. The expected fluence of the stripixel sensor for a 10-year running period is 3.1×10^{12} N_{eq}/cm^2.

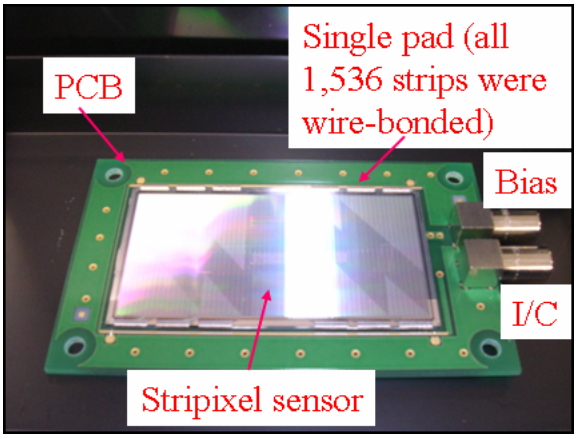

Fig. 1. Stripixel sensor setup

We combine the three experimental results to draw a conclusion on the effect of radiation on the stripixel sensor. Results measured at 20 °C are found to lie on

*1 Department of Physics, Rikkyo University
*2 Department of Physics, Tokyo Institute of Technology

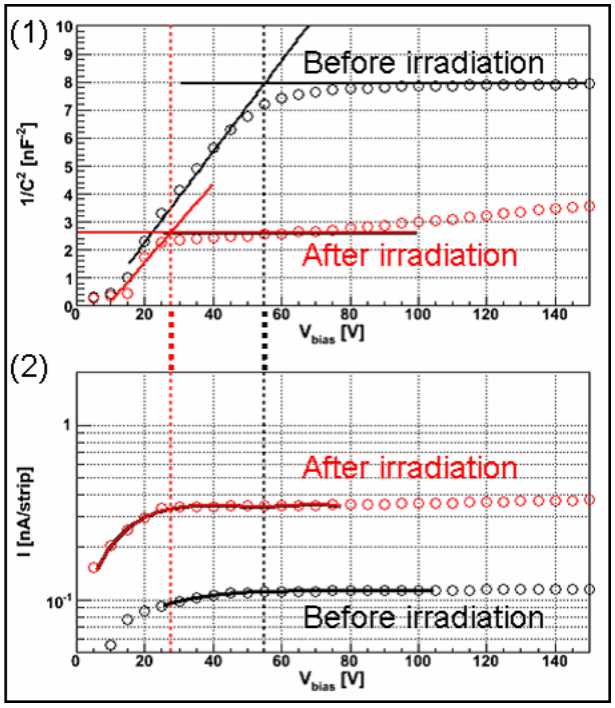

Fig. 2. (1): Bias voltage dependences of capacitance before and after irradiation. (2) Bias voltage dependences of leakage current before and after irradiation

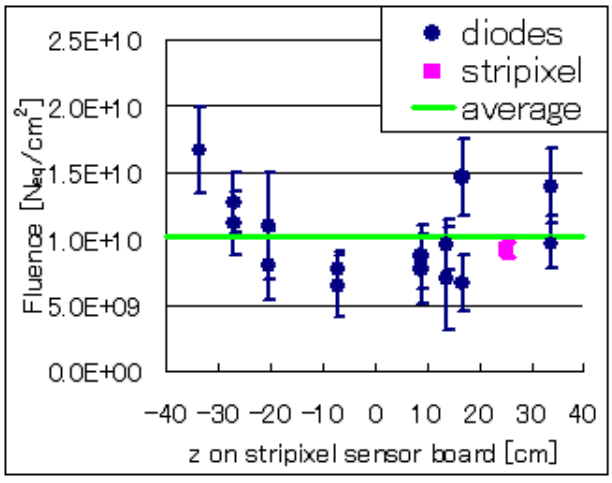

Fig. 3. Fluences of irradiated stripixel sensor and diodes on the stripixel sensor board at the PHENIX IR

a line expressed by Eq. 1 as shown in Fig. 4. Leakage current I depends on the temperature T [K] as;

$$I = AT^2 exp(-E_g/2k_BT), \quad (2)$$

Here, A is the sensor constant, E_g is the energy gap of silicon ($E_g = 1.2$ eV), and k_B is the Boltzmann constant ($k_B = 8.6 \times 10^{-5}$ eV/K), respectively, the leakage currents for various temperatures are also plotted together in Fig. 4. The saturation level of the circuit at 15 nA/strip crosses the expected fluence $\Phi_{eq} = 3.1 \times 10^{12}\,N_{eq}/\mathrm{cm}^2$ for the 10-year running period at around the 0 °C line. Therefore, the required operating temperature of the stripixel sensor is about 0 °C to avoid preamp saturation due to the constant leakage current caused by radiation damage.

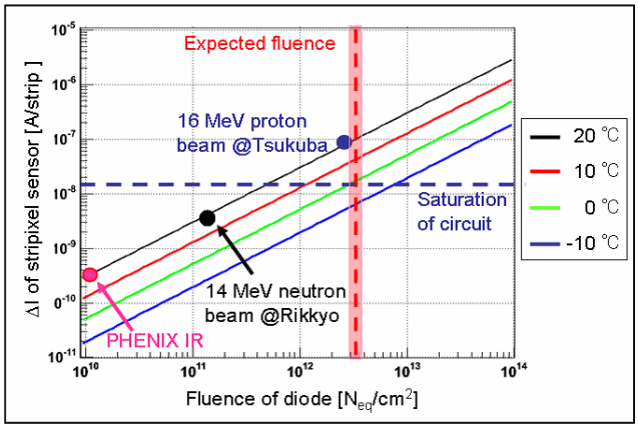

Fig. 4. Three experimental results of increase of leakage current as a function of fluence of reference diode. The temperature dependence is obtained follows Eq. 1. The vertical dashed line is the expected fluence for the 10-year running period: 3.1×10^{12} N_{eq}/cm^2. The horizontal dashed line is indicates the saturation level of the circuit: 15 nA/strip.

References

1) Y. Akiba et al.: Proposal for a Silicon Vertex Tracker (VTX) for the PHENIX Experiment (Brookhaven National Laboratory, Upton, NY, 2005); RIKEN Accel. Prog. Rep. **40**, 168 (2007).
2) A. Taketani et al.: RIKEN Accel. Prog. Rep. **40**, 170 (2007).
3) Z. Li et al.: Nucl. Instrum. Methods Phys. Res. **518**, 300 (2004).
4) J. Tojo et al.: RIKEN Accel. Prog. Rep. **38**, 231 (2005).
5) B. Krieger et al.: IEEE Trans. Nucl. Sci. **51**, 1968 (2004).
6) M. Kawashima et al.: RIKEN Accel. Prog. Rep. **40**, 188 (2007).
7) K. Sakashita et al.: RIKEN Accel. Prog. Rep. **40**, 190 (2007).

Development of PHENIX Silicon Pixel Interface ReadOut (SPIRO) Module

R. Ichimiya, F. Gastaldi, *2 Y. Akiba, J. Asai, E. T. Atomssa, *2 R. Granier de Cassagnac, *2 S. Chollet, *2 O. Drapier, *2 H. E'nyo, K. Fujiwara,*1 H. Kano, M. Kurosawa, E. J. Mannel, *4 H. Ohnishi, Y. Onuki, C. Pancake, *3 E. Shafto, *3 A. Taketani
and PHENIX VTX Collaboration

As part of the upgrade program of the PHENIX detector at RHIC, a silicon **Ver**tex **Te**racker (VTX) [1,2] is being developed for installation in 2009. This VTX provides $\sim 2\pi$ coverage in azimuth over a rapidity range of $|\eta| < 1.3$ and will have a 50 μm resolution in **D**istance of **C**losest **A**pproach (DCA). It consists of two inner pixel barrels followed by two outer strip barrels. Each pixel barrel is formed by 10 (first barrel at 2.5 cm) and 20 (second barrel at 5 cm) ladders. Each pixel ladder consists of two half-ladders with an active length of 11 cm for covering the $\eta > 0$ and $\eta < 0$ regions. The readout system for the pixel detector is divided into 60 subsystems; each subsystem contains one half-ladder, as shown in Fig. 1.

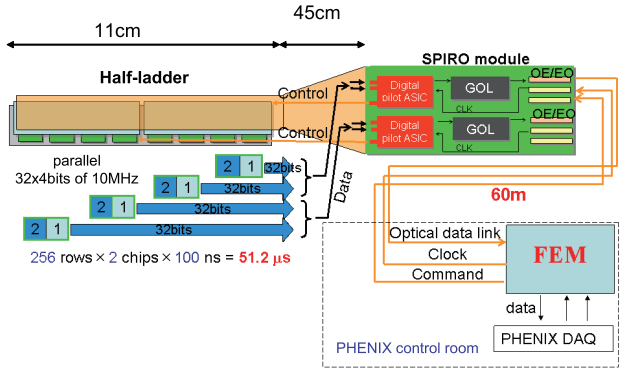

Fig. 1. Pixel detector readout scheme.

The half-ladder consists of two pixel sensors with four bump-bonded ALICE1LHCb readout chips[3]. Each readout chip measures 13.6 mm × 12.8 mm sensitive area and is divided into 8192 pixel cells (256 rows × 32 columns) of 50μm × 425μm. The sensors and readout chips used in the pixel detector were originally developed for the ALICE experiment[4] and LHCb experiment[5] at CERN.

Data are readout through four 32-bit buses on the half-ladder by a SPIRO board. The SPIRO board receives data from pixel bus and sends it to a **F**ront-**E**nd **M**odule (FEM) via optical links. The FEM receives data from the SPIRO board, reformats it into the standard PHENIX data format and transmits it to the PHENIX DAQ system. In addition, it provides clock, trigger and slow control to the SPIRO boards.

1 SPIRO board

The SPIRO board has the following functions:

- Sending control signals to the half-ladder.
- Multiplexing data from the half-ladder and sending it to the FEM via optical links.
- Providing a slow control to the pixel readout chips and SPIRO board itself.
- Data format conversion to match the PHENIX requirement.

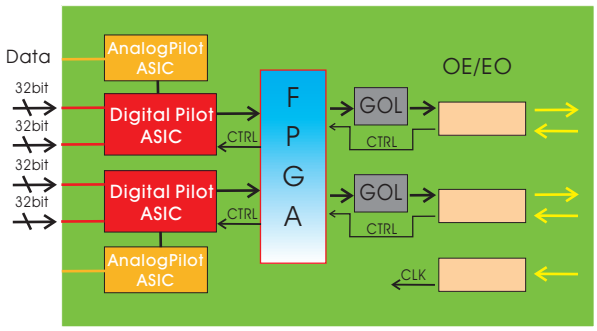

Fig. 2. Block diagram of SPIRO.

The core component of the SPIRO board is the Digital Pilot ASIC.[6] On the pixel readout chip being initialized, each of the two pixel chip pairs presents 256×2 sequential words of data on a 32-bit bus synchronously at a beam collision clock frequency of 10 MHz as shown in Fig. 1. In order to meet the readout timing requirements of PHENIX, four readout chips need to be readout in parallel. Due to the limited space for the SPIRO boards, a new Digital Pilot ASIC with twice the number of input channels was developed using same design rules and radiation tolerant technology as the ALICE Digital Pilot ASIC. The PHENIX Digital Pilot ASIC with 2 × 32 inputs can simultaneously read a 32-bit word from two pixel readout chip. Each 32-bit input handles on output from a pair of chips, which represent 512 sequential words of pixel data. Thus, two Digital Pilot ASICs are required to fully readout a pixel half-ladder, meeting the PHENIX DAQ readout timing re-

*1 Graduate School of Science and Technology, Niigata University, Japan
*2 Laboratoire Leprince-Ringuet, École Polytechnique, CNRS-IN2P3, France
*3 Department of Physics and Astronomy, Stony Brook University, USA
*4 Columbia University, Nevis Laboratories, USA

quirements.

Each SPIRO board has two Analog Pilot ASICs that supply reference voltages and currents for the pixel readout chips and monitor voltages, currents and temperature on the pixel half-ladder.

The data transmission from a readout chip to a pilot chip is performed as follows. A bus carries 2 × 32-bit data at a frequency of 10 MHz to a Digital Pilot chip. The Digital Pilot chip is designed to produce an output at 40 MHz. This allows four 25 ns transmission cycles to be available before the next data word from the readout chips arrives. The first two clock cycles are referred to as "cycle-0" and the last two clock cycles as "cycle-1". If no pixel data readout is performed, only status data (slot-0) is transmitted in cycle-0. In this case, cycle-1 contains (empty) data. During pixel data readout, after transmission of status data (slot-0) in cycle-0, event header information (slot-1a) is transmitted in cycle-1. This initial transmission is followed by the repeated transmissions of (slot-0) and (slot-1b) containing the pixel hit information. The principle of data transmission is illustrated in Fig. 3.

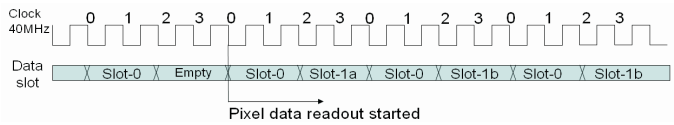

Fig. 3. Data transmission from pixel detector.

2 First Prototype

The first SPIRO prototype was designed by the École Polytechnique group. In this prototype, a data format conversion which replaced redundant "fast-or" fields by parity fields and a protocol change from CIMT (G-Link) to 8B/10B encoding was implemented in a Xilinx FPGA[7]. During the testing of the prototype, it was discovered that a FIFO between the PHENIX Digital Pilot ASIC and GOL serializer was required. The FIFO implemented in this FPGA, forms the clock domain interface between a PHENIX global clock (≈ 38 MHz) and a low-jitter local clock (40 MHz) for high-speed links. More specifically, the data serialization is performed by a GOL chip, which is a CERN solution capable of serializing up to a 32-bit data input at 40 MHz and driving high-speed serial links at a frequency of 1.6 Gbps. The GOL chip requires a 40 MHz input clock with a peak-to-peak jitter less than 100 ps. A quartz crystal located on the SPIRO board generates the 40 MHz clock to feed the GOL chip with the required jitter specifications, whereas the Digital Pilot chip works on the PHENIX global clock.

3 Final Design

Using Xilinx FPGAs has technical difficulties in overcoming in the PHENIX high radiation environments and may expense radiation induced effects such as **S**ingle **E**vent **E**ffect (SEE) in its configuration memory (e.g. bit flips) and **T**otal **I**onizing **D**amage (TID) for the flash memory used by PROM (e.g. malfunction of write feature).[8,9] Therefore, an antifuse FPGA (Axcelerator family by Actel)[10], which has no configuration memory but is a one-time programmable device, was chosen for the final design. This FPGA (commercial grade, which is much inexpensive than the special rad-hard grades) has already been tested by the ATLAS group[8]. A **T**riple **M**odule **R**edundancy (TMR) library for immunization against SEE for user registers and a FIFO library are also provided by Actel.

The final prototype was designed by the École Polytechnique group to satisfy the following criteria:

- Feedback of all knowledge from the first prototype testing.
- Use only radiation-tolerant qualified devices.
- Minimize its board size.

4 summary

The first prototype board was designed, built and tested in the 2006. The prototype was used to readout three half-ladders in a cosmic ray test[11] done in the summer of 2006. The pre-production design (should be a final design) work has been completed, and its prototype boards will be delivered in February 2007.

References

1) Y. Akiba et al.: Proposal for a Silicon Vertex Tracker (VTX) for the PHENIX Experiment, BNL-72204-2004, Physics Dept. BNL (2004).
2) Y. Akiba et al.: RIKEN Accel. Prog. Rep. **40** (2007).
3) K. Wyllie: ALICE1LHCB Preliminary Users Manual Version 3/7/01, http://kwyllie.home.cern.ch/kwyllie/ALICE1LHCB.htm
4) ALICE Experiment: http://aliceinfo.cern.ch/
5) LHCb Experiment: http://lhcb.web.cern.ch/lhcb/
6) A. Kluge: ALICE Silicon Pixel On Detector Pilot System OPS2003-The missing manual, ALICE-INT-2004-030, CERN (2005).
7) Xilinx Inc.: http://www.xilinx.com/
8) R. Ichimiya et al.: IEEE Trans. Nucl. Sci., **Vol.52**, Issue 4, 1061-1066 (2005). http://cdsweb.cern.ch/search.py?recid=812814&ln=en
9) T. Miyahira and G. Swift: Proc. MAPLD Conf. (1998). http://klabs.org/richcontent/MAPLDCon98/Abstracts/c4.htm
10) Actel Corp.: http://www.actel.com/
11) M. Kurosawa et al.: RIKEN Accel. Prog. Rep. **40** (2007).

Quality assurance test of readout chips and pixel sensor hybrids for PHENIX

M. Kurosawa, Y. Akiba, J. Asai, H. En'yo, R. Ichimiya, K. Fujiwara,[*1] R. Muto, Y. Onuki, K. Sakashita,[*2] A. Taketani and Y. Yamamoto[*3]

PHENIX at RHIC-BNL has been upgraded with a silicon vertex tracker (VTX)[1], which consists of four layers of barrel detectors, namely, two inner silicon pixel detectors (SPD) and two outer silicon strip detectors (SSD). In the plan of upgrading PHENIX VTX, we are developing inner SPD. SPD is made up of 30 ladders, each of which consists of four sensor hybrids[2]. A sensor hybrid is an assembly of a silicon pixel sensor and four readout chips[3] (ALICE1LHCb) bump-bonded with 20-μm-diameter bumps to the sensor (bonded by VTT[a]). The readout chip has 8192 pixel cells arranged in 32 columns and 256 rows. The size of pixel is 50 μm × 425 μm. Before installation in the experiment, quality assurance (QA) is required for the readout chips and the pixel sensor hybrids. In this report, we describe a recent results of the QA test.

The QA test system mainly consists of a probe station (SUSS MacroTec), a DAQ adapter board, VME equipment for a DAQ system, and a Windows machine. Figure 1 shows the QA test system in a clean room at RIKEN. A readout chip wafer, which has 86 readout chips, and the sensor hybrid are tested with the probe station. Probe data are taken and analyzed using a LabVIEW-based program running on the Windows machine.

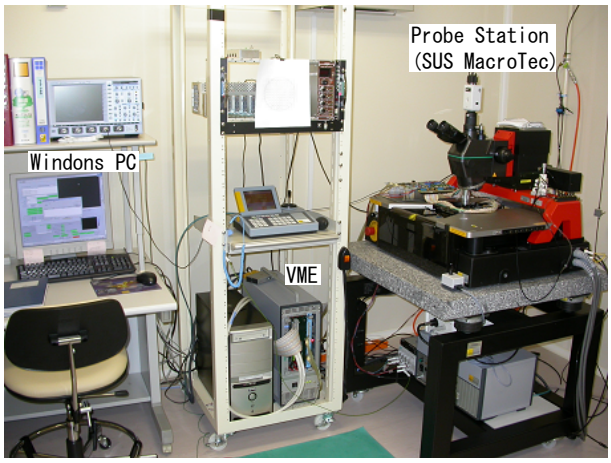

Fig. 1. QA test system in a clean room at RIKEN.

A check list items for the QA test of the readout chips and sensor hybrids is as follows.

Items to be Checked for Readout Chips

(1) Measurement of current consumption.
- The current consumptions of analog and digital circuits of the readout chips are measured.

(2) Test of JTAG and DAC functionality.
- It is confirmed whether configuration settings in the chip are readable and writable by means of a JTAG protocol.
- The digital-to-analog converter (DAC) linearity is calibrated.

(3) Measurement of minimum threshold and noise level.
- Minimum threshold in all pixel matrix is determined.

(4) Measurements of mean threshold and mean noise for the complete pixel matrix.
- The test pulse from the pulsar inside the chip is sent to each pixel cell and the mean threshold and noise levels are determined.

Items to be Checked for Sensor Hybrids

(1) The same tests as those in items 1, 3 and 4 and part of JTAG functionality test in item2.
- The sensor is biased at 50 V during the measurements.

(2) Performance test of SPD with the β source (^{90}Sr).
- Faulty bump bonds and maximum efficiency are checked by β source measurement.

At the end of the QA test, the measured and analyzed data are sent to a PostgreSQL database server located at a secure area accessible only from the internal RIKEN network. The secure shell (SSH) connection is used to transfer the data from the Windows machine to the database server. The data in the database can be accessed from the web interface in the secure area.

The tested readout chips and the sensor hybrids are categorized into three classes, Class I, II, and III. The chips and sensor hybrids classified into Class I are used for the experiment. The readout chips (sensor hybrids) categorized into Class I satisfy the following criteria.

- Current consumptions lower than 350 mA and 270 mA for analog and digital circuits, respectively.
- A complete JTAG and DAC functionality for readout chips and a complete JTAG functionality for sensor hybrids.
- Mean threshold lower than 1800 electrons (3000

*1 Science and Technology, Niigata University, Japan
*2 Tokyo Institute of Technology, Japan
*3 University of Electro-Communications, Tokyo, Japan
a) VTT Electronics, Tekniikantie 17, Epsoo, P.O. Box 1101, FIN-02044 Epsoo, Finland

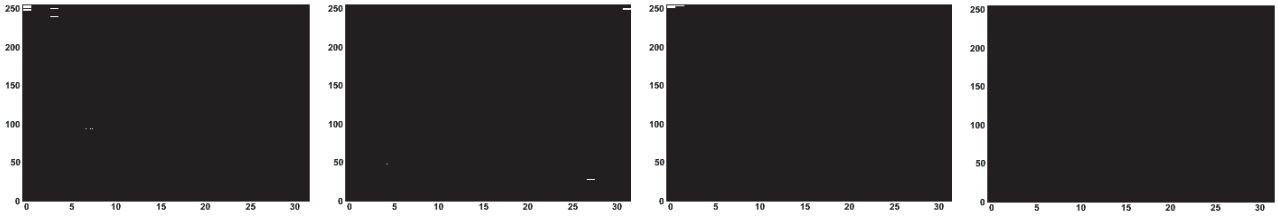

Fig. 2. Typical response of a sensor hybrid, categorized into Class I, to β rays. Good and faulty bump bonds are shown in black and white, respectively.

electrons).
- Less than 1% defect pixels in mean threshold scan (and source test).

The readout chips or sensor hybrids with a percentage of dead pixels higher than 1% are categorized into Class II. The others are classified into Class III.

In the 22 readout chip wafers, 1892 readout chips have been tested. Figure 3 shows typical results. In accordance with the criteria described above, the results of the QA test are summarized in Table 1. The average of the mean threshold and the mean noise for the Class I readout chips are about 1400 electrons and 120 electrons, respectively.

Table 1. Summary of QA test results for readout chips.

Classification	Number of Chips
Class I	692
Class II	174
Class III	1026

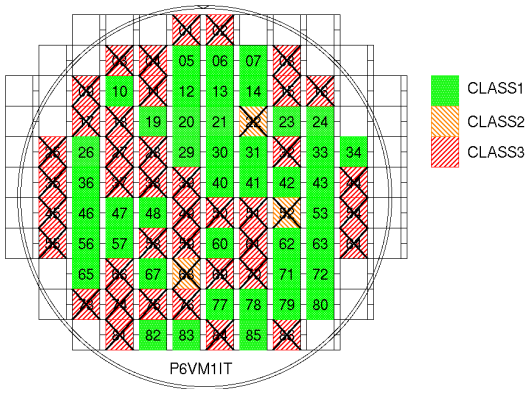

Fig. 3. Typical classification map of a chip wafer. Readout chips with a cross mark are not used for the experiment.

Eighteen sensor hybrids have been tested. Table 2 shows the summary of QA test results. We obtained the mean threshold and mean noise of 2600 electrons and 140 electrons for Class I sensor hybrids, respectively. The average maximum efficiency of Class I sensor hybrids is about 98%. A typical response to β rays from ^{90}Sr is shown in Fig. 2.

Table 2. Summary of QA test results for sensor hybrids.

Classification	Number of Hybrids
Class I	8
Class II	2
Class III	8

We have obtained 8 sensor hybrids and 692 readout chips classified into Class I. A total of 120 sensor hybrids and 680 readout chips are required for the experiment. The required number of tested readout chips for the experiment was satisfied. We intend to focus on the QA test of the sensor hybrids.

References

1) Y. Akiba et al.: RIKEN Accel. Prog. Rep. **40**, 168 (2007).
2) Y. Onuki et al.: RIKEN Accel. Prog. Rep. **40**, 171 (2007).
3) K. Fujiwara et al.: RIKEN Accel. Prog. Rep. **38**, 228 (2005).

Cosmic-ray experiment with PHENIX silicon pixel sensor hybrids

M. Kurosawa, R. Ichimiya, Y. Akiba, J. Asai, H. En'yo, K. Fujiwara,[*1] Y. Onuki, C. Pancake,[*2] E. Shafto,[*2] A. Taketani and PHENIX VTX Collaboration

The PHENIX is an experiment aiming to study hot and dense matter and the spin structure of nucleons at Brookhaven National Laboratory's Relativistic Heavy Ion Collider (RHIC). The PHENIX is being upgraded with the introduction of a silicon vertex tracker (VTX) to extend it's physics capability[1]. The VTX is composed of a four-layer barrel detector, two outer silicon strip detectors (SSD) and two inner silicon pixel detectors (SPD). The basic component of the SPD is a ladder assembled using four sensor hybrids[2]. One sensor hybrid has four readout chips bump-bonded to a silicon pixel sensor, with pixel sizes of 50 μm in the z (row)-direction and 425 μm in the ϕ (column)-direction[3]. To test the data taking system (DAQ) and the performance of the silicon pixel detector, a cosmic-ray experiment was performed at Stony Brook University (NY, USA) in June 2006. In this report, we show the first tracking results of the cosmic-ray experiment with silicon pixel sensors.

The setup of the cosmic-ray experiment is shown in Fig. 1. Three sensor hybrids with SPIRO boards, one FEM module and two plastic scintillators as an event trigger were used in the experiment. The SPIRO board is an on-detector electronic that controls the sensor hybrid components, collects data from the sensor hybrid and sends them to the FEM module via optical links. The FEM (Front End Module) is the off-detector electronic that sends clock and command signals to the SPIRO boards and collects data. The data will be sent to the PHENIX DAQ system. The FEM has a USB interface for connecting a PC. In this experiment, a stand-alone DAQ system was constructed using the FEM module and a Windows PC. When the FEM module receives a trigger signal from a scintillator trigger, it generates a sequence of Trigger&DAQ commands to take the data. The taken data are stored in the FEM module and then read out by the Windows PC. This data taking system has been operated successfully.

Forty-eight cosmic-ray events with hits in three sensor hybrids were collected. An event display of a cosmic-ray event is shown in Fig. 2. The top three images show the hit positions of cosmic rays on each sensor hybrid. The bottom image represents a reconstructed track in 3D with three hit positions (cross points) on each layer. The track was reconstructed by the least-squares fit method after the position alignment described below.

Three sensor hybrids were aligned manually with a

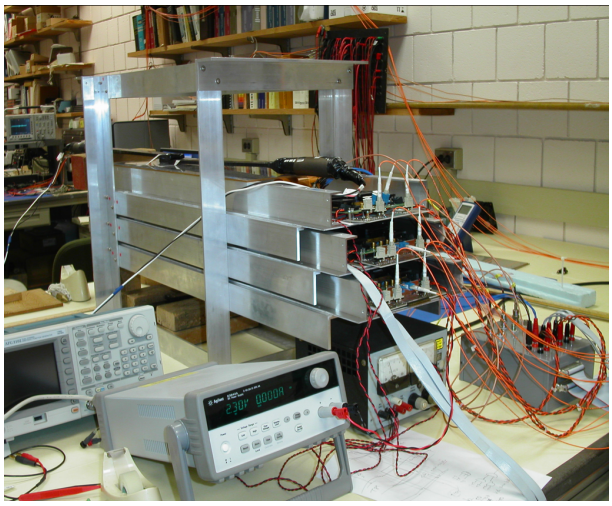

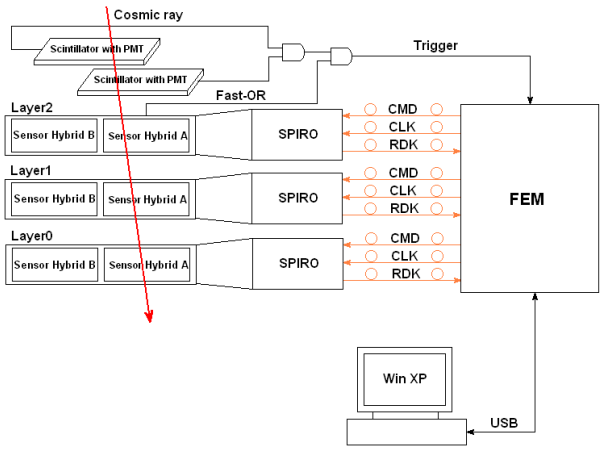

Fig. 1. Setup of cosmic-ray experiment. The vertical distance between the sensor hybrids was 60 mm. Sensor hybrid B was not used in the experiment.

precision on the order of 1 mm. A much more precise alignment was performed by offline analysis. The alignment of sensor hybrids were made for only translation not for rotation using a residual value. The residual was defined as the distance between an intersection position of a reconstructed track and a hit position on the sensor. The mean residual was taken as the correction horizontal plane position. The correction and fitting of what were iterated until the mean residual for three layers was minimum. Figure 3 shows the residual distributions of Layer 1 after the alignment. The standard deviations of these residual distributions were calculated to be 184 $\pm$ 27 μm and 140 $\pm$ 24 μm in the column and row directions, respectively. These standard deviations were used to obtain an intrinsic

*1 Science and Technology, Niigata University, Japan
*2 Stony Brook University, USA

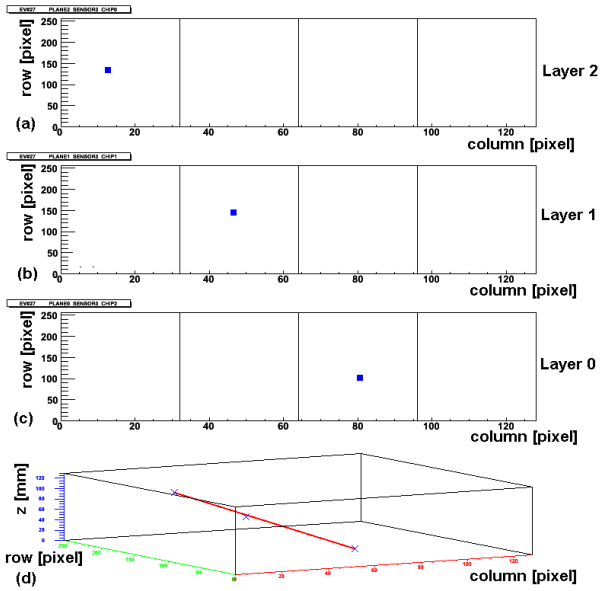

Fig. 2. Event display of typical cosmic ray event. (a)-(c) The square point represents the hit position on each layer. (d) The cross points and straight line are the hit position and reconstructed track, respectively.

position resolution of a sensor hybrid.

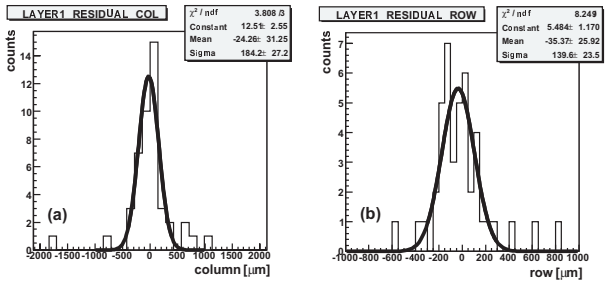

Fig. 3. (a) and (b) are the residual distributions in the column and row directions on Layer 1.

The position resolution of the sensor hybrid is due to two components. One is the intrinsic position resolution and the other one is the effect of multiple scattering in the support of the sensor hybrids. We obtained the intrinsic position resolution by estimating the effect of multiple scattering.

The multiple scattering angle is given by the following equation[4].

$$< \theta_0 >^2 = \frac{13.6\mathrm{MeV}}{\beta p}\sqrt{\frac{x}{X_0}}\left[1 + 0.038 ln\left(\frac{x}{X_0}\right)\right] \quad (1)$$

Here, x/X_0 represents the thickness of the scattering medium. The following conditions were used to evaluate the resolution due to multiple scattering.

- The average energy of cosmic rays at ground level is 4 GeV.
- The energy loss of the 4 GeV cosmic rays passing through concrete with an average thickness of 6 m is 2.5 GeV (The experiment was performed in an underground area of a six-story building.).
- The thickness of the scattering material is estimated to be the average thickness of the material through which the particle passed.

From the calculation under the above conditions, the multiple scattering angle on each layer was estimated to be $\theta_0 = 2.5$ mrad. Then, the resolution of each layer due to the multiple scattering was calculated to be $\sigma_0 = 150$ μm. Thus, we obtained the intrinsic position resolution in the column and row directions to be $\sigma_{col} = 160 \pm 33$ μm and $\sigma_{row} = 65 \pm 30$ μm, respectively.

The intrinsic position resolution depends on pixel pitch sizes of 50 μm in the row direction and of 425 μm in the column direction. Then the expected resolutions of the pixel sensor are 123 μm ($425/\sqrt{12}$ μm) and 14 μm ($50/\sqrt{12}$ μm) in the column and row directions, respectively. The difference between the measured and expected intrinsic position resolutions is due to a poor statistic of the cosmic-ray data and the ambiguity of the estimation of the effect of multiple scattering. In the future, we intend to carry out a more precise estimation of multiple scattering resolution.

The first measurement of cosmic rays has been performed with silicon pixel sensor hybrids at Stony Brook University. The data taking system was successfully operated. Forty-eight clear tracks of cosmic rays were measured. It was found that the sensor hybrid had sufficient performance for the PHENIX experiment.

References

1) Y. Akiba et al.: RIKEN Accel. Prog. Rep. **40**, 168 (2007).
2) Y. Onuki et al.: RIKEN Accel. Prog. Rep. **40**, 171 (2007).
3) K. Fujiwara et al.: RIKEN Accel. Prog. Rep. **38**, 228 (2005).
4) Particle Data Group: Phys. Lett. B592, 245 (2004).

Overview of the Readout Electronics for the Silicon Vertex Tracker for the PHENIX Experiment

E.J. Mannel,[*1] Y. Akiba, E.T. Atomssa,[*2] M. Bobrek,[*3] C.L. Britton,[*3] S. Chollet,[*2] V. Cianciolo,[*3] L.G. Clonts,[*3] A. Deshpande,[*4] O. Drapier,[*2] K. Fujiwara,[*5] R. Granier de Cassagnac,[*2] F. Gastaldi,[*3] R. Ichimiya, H. Kano, R. Nouicer,[*6] C. Pancake,[*4] H.Pei,[*7], A. Semenov,[*6] E. Shafto,[*4] A. Taketani, L. Tomasek,[*8] J. Tojo, T. Yamamoto, and PHENIX VTX Collaboration

[RHIC, PHENIX, Silicon Detectors, Electronics]

The PHENIX experiment at the Relativistic Heavy Ion Collider (RHIC) at Brookhaven National Laboratory has approved the silicon vertex tracker (VTX) upgrade to be installed in 2009. The goal of the VTX upgrade is to provide precise measurements of heavy-quark production (charm and beauty) in $A+A$, $p(d)+A$ and polarized $p+p$ interactions at RHIC. These are essential measurements for future heavy-ion and spin-physics programs at RHIC. In addition, the precise tracking capabilities of the VTX will provide significant improvements to other PHENIX physics measurements.

The VTX consists of two detector sub-systems, the pixel detector and the stripixel detector. The VTX provides nearly full coverage in azimuth over the rapidity range of $|\eta| < 1.2$, with 50μm resolution in the distance to closest approach. A preliminary design of the detector is shown in Fig. 1.

The pixel detector consists of two inner barrels approximately 22cm long. The first barrel with a radius of 2.5cm is built from 10 pixel ladders, while the second barrel is built from 20 pixel ladders.[1,2)] Each ladder is constructed from two half-ladders which are mounted on a carbon composite stave which provides mechanical support and cooling for the ladder. Each half-ladder consists of two sensor modules wire-bonded to a multi-layer readout bus (pixel bus) and bus-extender and is connected to a Silicon PIxel Read-Out (SPIRO) module. The SPIRO module provides all voltages, control and timing signals and reads out the pixel data for a half ladder. The SPIRO module is connected via optical fiber to the pixel Front End Module (FEM) which is the interface to the PHENIX data acquisition system (DAQ).

The pixel detector uses the ALICE1LHCb readout chip designed by the CERN EP-MIC group for the ALICE and LHCb experiments.[3)] Four readout chips

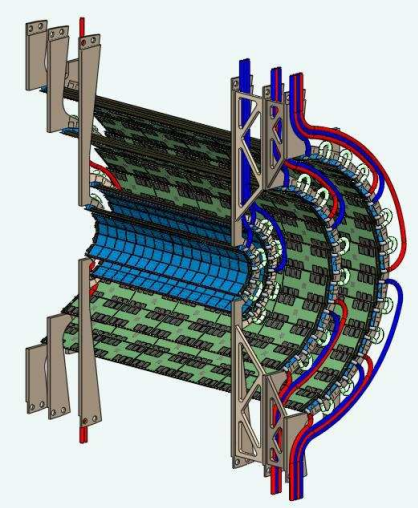

Fig. 1. A cut-away view of the proposed VTX detector showing the two inner pixel barrels, two outer stripixel barrels, and cooling and support structure.

are bump-bonded to a sensor module. The sensor modules are mounted on the pixel bus, which is a kapton/copper/aluminum printed circuit board (PCB) providing power and control signals to the readout chips and bring data out to the SPIRO module on a 128 bit bus. Connections between the readout chip and bus are made by wire-bonds. The bus-extender, a flexible multi-layer copper/kapton PCB, is used to the extend the bus to the SPIRO board, allowing the SPIRO board to be located outside the acceptance of the PHENIX detector and in a lower radiation environment. The pixel bus and bus-extender are being designed, prototyped and built at RIKEN.

The SPIRO module is used to control and readout the the ALICE1LHCb chips. In order to meet the readout timing requirements for PHENIX, four ALICE1LHCb chips must be readout in parallel. Two PHENIX Digital Pilot ASIC's on the SPIRO board each readout two ALICE1LHCb chips in parallel at a rate of 10MHz, allowing a half ladder to be completely read out in 51.2μs, achieving a maximum data rate of 25kHz. The PHENIX Digital Pilot ASIC was developed by the RIKEN group using the same design rules and radiation tolerant technology as used for the

*1 Columbia University, Nevis Laboritories, USA
*2 Laboratoire Leprince-Ringuet, Ecole Polytechnique, CNRS-IN2P3, France
*3 Oak Ridge National Laboratory, USA
*4 Department of Physics and Astronomy, Stony Brook University, USA
*5 Graduate School of Science and Technology, Niigata Univeristy, Japan
*6 Brookhaven National Laboratory, USA
*7 Iowa State Univeristy, USA
*8 Institute of Physics, Academy of Sciences, Czech Republic

ALICE pixel pilot ASIC.[4] Data from the PHENIX Digital Pilot chip is serialized with the Gigabit Optical Link (GOL) chip which is radiation tolerant and capable of transmitting data at 1.6 Gbits/sec.[5] The SPIRO module also has two Analog Pilot chips used for voltage control and monitoring on the half-ladder.[6] The SPIRO modules are being designed, prototyped and built at LLR-Ecole Polytechnique in France.

The Pixel FEM is the interface between two SPIRO modules and the PHENIX DAQ and slow control systems. Commands, initialization parameters and clock timing information is transmitted to the SPIRO modules and pixel data is received from the SPIRO modules, requiring three optical fibers per SPIRO module. In addition, the FEM formats the pixel data into standard PHENIX data packages, prior to inclusion of the data into a PHENIX data stream. The pixel FEM is being designed and prototyped at Stony Brook University.

Prototype pixel buses, bus-extenders, SPIRO boards and pixel FEM's were used to build three pixel half ladders for a cosmic ray test stand which was successfully tested at Stony Brook University in the summer of 2006.[7]

The stripixel detector consists of the two outer barrels located at a radius of 10cm and 14cm and is composed of 18 and 26 ladders respectively. Each ladder contains 5 or 6 stripixel sensor modules for the inner and outer barrels respectively. Each sensor module consists of a sensor with x and y strips providing stereo readout of the sensor, and a ReadOut Card (ROC) and are mounted on a carbon fiber stave providing the mechanical support and cooling for the ladder. Each ladder is readout from one end to a stripixel FEM located near the detector which provides the interface to the PHENIX data acquisition system.

Readout of the stripixel sensors is controlled by the ROC which has 12 SVX4 chips developed at Fermi National Laboratory and Lawrence Berkeley National Laboratory.[8] Each SVX4 chip reads out 128 strips with 8 bit ADC's, allows for on-board zero suppression, has a 46 deep pipeline buffer and is radiation hard. Control of the readout is done by the ROC Control Chip (RCC), a custom radiation tolerant ASIC designed at Oak Ridge National Laboratory. The RCC serves as a de-multiplexer, directing the serial, clock and control inputs, and the data outputs minimizing the effects of single-point failures and reducing the number of readout cables required for each ladder. All RCC's on a ladder share a common bus which is also connected to the Pilot Module (PM). The PM passes all data between the stripixel FEM and the ladder and provides voltage regulation, filtering and distribution to the ladders.

The stripixel FEM serves as the interface between the ROC's and the PHENIX DAQ and slow control systems. The FEM consists of a Controls Interface Board (CIB) and 11 Data Interface Boards (DIB) housed in a single crate. The CIB receives control and timing information from the PHENIX DAQ and slow control system and distributes the information to the DIB's. The DIB's send the control and clock information to the stripixel ladders and receive and format accepted event data from the stripixel ladders and transmit it to the PHENIX DAQ via fiber optical cables. The ROC's, PM's and FEM's are being designed, prototyped, and built at Oak Ridge National Laboratory.

A prototype stripixel ROC and FEM was successfully tested with cosmic-rays at Oak Ridge National Laboratory in the summer of 2006. The energy distribution in ADC counts for minimum ionizing particles and noise from this test is shown in Fig. 2. A clear separation of minimum ionizing particles from the noise is seen with a signal-to-noise ratio of ~ 10.

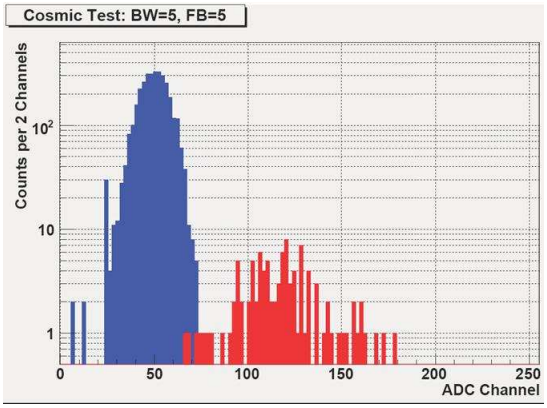

Fig. 2. The Energy distribution in ADC counts from the stripixel cosmic ray test.

The design and prototyping of the electronics for the VTX detector for PHENIX has started. Prototypes of the pixel and stripixel detectors have been successfully tested using cosmic rays in 2006. Fabrication of the electronics will begin in 2007 and be completed in time for testing and installation in the summer of 2009. Data taking by the VTX detector at PHENIX is scheduled to start in the fall of 2009, with the first physics results expected in 2010.

References

1) H. Kano, et al. : RIKEN Accel Prog. Rep. 39(2006)211
2) K. Fujiwara, et al.: RIKEN Accel Prog. Rep. 40(2007)
3) K. Wyllie: ALICE1LHCB Documentation**40** (2001)
4) A. Kluge: ALICE Silicon Pixel On Detector Pilot System OPS2003-The missing manual **40** (2005)
5) P. Moreira et al.: GOL Reference Manual **40** (2005)
6) G. Anelli, R. Dinapoli, A. Kluge: Specification of the digital control part of the ANAPIL2 **40** (2004)
7) R. Ichimiyma et al.: RIKEN Accel Prog Rep. **40** (2007)
8) L. Christofek et al.: SVX4 User's Manual (2003)

Development of amplifier-discriminator readout system of cathode strip chamber for muon trigger upgrade at RHIC PHENIX

K. Shoji,* for the PHENIX Collaboration

One of the major goals of the PHENIX experiment[1] at the Relativistic Heavy Ion Collider (RHIC) is the understanding of the spin structure of a proton. W boson production in proton-proton collisions is a good probe for investigating the sea quark spin contribution because the production depends on both quark flavor and helicity.[2] Experimentally, W boson production can be measured by detecting high-momentum muon decayed from W. The trigger upgrade for the high-momentum muon is proposed for studying the W physics in the PHENIX experiment.

PHENIX can detect W via the muon decay channel with the forward Muon Arm,[3] which consists of the Muon Tracker (MuTr) and Muon IDentifier (MuID). The MuTr is a set of cathode strip chambers that are used for momentum measurement with a magnetic field. The MuID is a set of five chamber layers with alternating layers of steel walls that can distinguish muons from hadrons. The MuID also serves as a first-level muon trigger for each beam crossing.

Most of the muons that decayed from a W boson have a momentum above 40 GeV/c. However, with the MuID trigger whose momentum threshold is ∼2 GeV/c, low-momentum muons dominate, and trigger rate will become a problem in the near future. When the RHIC design luminosity of $2 \times 10^{32}\mathrm{cm}^{-2}\mathrm{s}^{-1}$ at $\sqrt{s} = 500$ GeV is achieved, the expected reaction rate is 12 MHz. With the existing MuID trigger whose rejection factor (RF) is about 250, the trigger rate is as high as 48 kHz. However, 2 kHz is the allowed bandwidth in the PHENIX data acquisition system. Therefore we need a new trigger system with an RF of 6000 to record all the W signals. By selecting high-momentum muons at the trigger level, the desired RF can be achieved. We propose a new trigger using MuTr cathode strip hit information. Figure 1 shows the schematic of the new trigger. We can obtain the rough track of a particle from the strip hit pattern at the trigger level and select high-momentum muons by determining sagitta, which is the distance between the passage point at Station 2 and the interpolation point from Station 1 and Station 3. The simulation results show that this new trigger can provide a maximum RF of 24000.

The current front end electronics (FEE) of the MuTr chamber is designed to measure the amount of charge induced on strips. This information is used to measure the passage point of a particle by offline analysis. The position resolution with a standard deviation of 100 μm is the value desired for the design and we need to achieve 1% noise level for a typical charge on FEE.

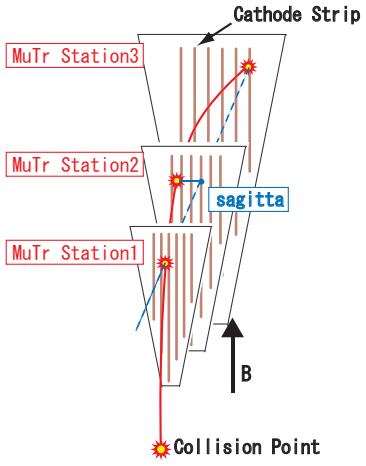

Fig. 1. New trigger schematic

To realize a new trigger system, we need not only information about the amount of charge induced on strips but also strip hit information for trigger decision. Therefore, we propose to split the raw signal line from the chamber as shown in Fig. 2. One signal line goes to the cathode preamplifier (CPA) on current FEE as in the old system and the other signal line connects to the amplifier-discriminator board (AD-board) to provide strip hit information. This configuration has the advantages in that we need not change the entire readout system and it is cost-effective.

The split ratio can be controlled by adding the capacitor Csplit as shown in Fig. 2. The ratio of the charge flowing into FEE and the AD-board equals the ratio of the CPA's effective capacitance (∼900pF) and the Csplit value. Very low noise level should be achieved on FEE for the required position resolution so that stealing too much raw signal is not allowed. Moreover, seeing from FEE, to add the Csplit means increasing load capacitance, which results in high noise level. However, we need a sufficient charge for the AD-board to obtain an efficiency as that is as good that of the trigger. We should determine the Csplit value with extreme caution considering these factors.

The split signal is amplified and discriminated to send out strip hit information. The time jitter of this output is preferred to be within 100 nsec because RHIC beam bunch crossing occurs at 9.4 MHz. We

*1 Department of Physics, Kyoto University

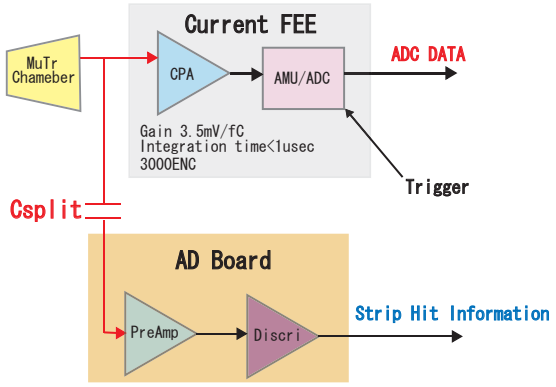

Fig. 2. New configuration of chamber readout

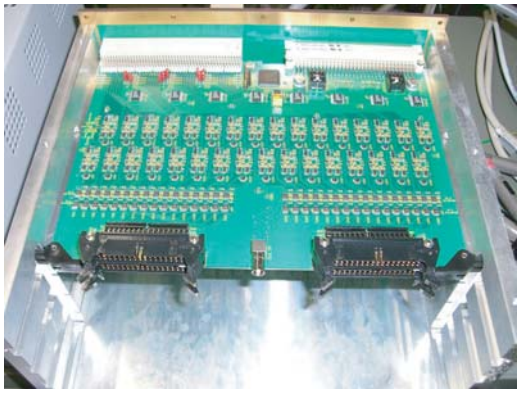

Fig. 3. Picture of prototype amplifier-discriminator board

use a cable-less constant fraction discriminator (CFD), which is modeled after the MuID readout system and called pseudo-CFD, to minimize the time jitter due to pulse height variations. The fact that the pseudo-CFD technique requires no delay cable, which saves space and we can obtain high channel density.

On the basis of these concepts, we produced an AD-board prototype (Fig. 3) that has 64 channels on a 6U size card. To estimate its performance, we performed an experiment using the duplicate of the MuTr chamber exposed to electron beam at the Laboratory of Nuclear Science, Tohoku University in November 2006.

Figure 4 shows the most probable values (MPVs) of ADC counts from FEE as the function of a high voltage applied to the MuTr chamber. In PHENIX, the current operating voltages are usually in the range of 1850-1900V. The plot shows MPVs when the MuTr chamber is read out with FEE alone or both FEE and AD-board whose Csplit is 100pF. When the AD-board is added to the readout system, we can obtain about 10% of signals from FEE. The RMS noise is also shown in Fig. 5 with ADC value and it increases by a factor of 1.25 on average. These observations indicate that

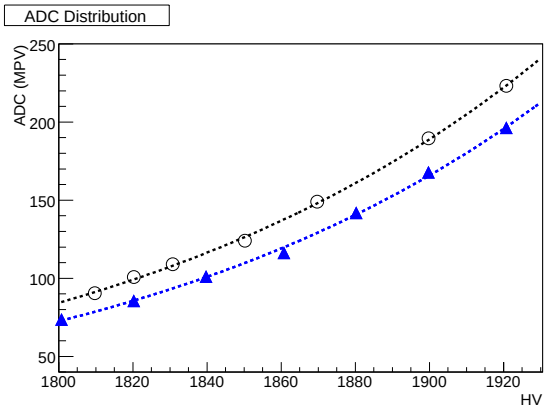

Fig. 4. The Most Probable Value (MPV) of ADC counts vs High Voltage (HV) of MuTr chamber. Results from readout with FEE alone is shown as open circle. Triangles come from the readout with combined system of FEE and AD-board. Csplit is 100pF.

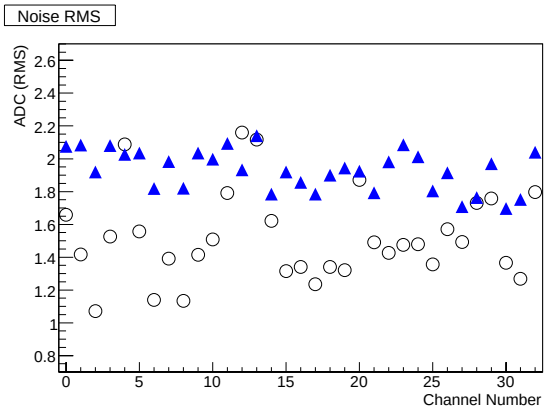

Fig. 5. The RMS noise measurement for typical channels in units of ADC counts. Symbols are the same as Fig. 4.

when the Csplit is 100pF, we need a signal gain of ∼1.4 to recover the noise level before the split.

The analysis of the position resolution of the MuTr chamber and the performance study of the AD-board as the trigger system, for example, efficiency, will be finished soon. We obtained data with several Csplit values and tested some patterns of the pseudo-CFD circuit. Therefore, we will be able to finalize our studies of the parameters. We hope to finish the AD-board development soon.

References

1) K. Adcox et al.: Nucl. Instrum. Methods Phys. Res. A **499**, 469 (2003).
2) G. Bunce et al.: Annu. Rev. Nucl. Part. Sci. **50**, 525 (2001).
3) K. Adcox et al.: Nucl. Instrum. Methods Phys. Res. A **499**, 537 (2003).

Development of pixel readout bus for PHENIX upgrade

K. Fujiwara[*1], Y. Akiba, J. Asai, H. En'yo,
R. Ichimiya, H. Kano, T. Kawasaki[*1], H. Ohnishi, Y. Onuki, K. Takano[*2], A. Taketani and S. Watanabe[*2]

The PHENIX experiment at the relativistic heavy ion collider (RHIC) at Brookhaven National Laboratory will be upgraded by installing a four-layer silicon vertex tracker (VTX) by summer 2009. The VTX will enhance the physics capabilities of the laboratory to enable the investigation of new hot and dense nuclear matter in heavy-ion collisions and the structure of proton spin in polarized proton-proton collisions at the RHIC. The VTX will directly identify heavy-quark production by measuring displaced decay vertices, and will reconstruct jets with the acceptance of almost full azimuthal coverage over the rapidity of $|\eta| < 1.2$. It has a high spatial resolution of 30 $\sim$ 50 μm for the distance to the closest approach[1]. We report the status of the development of the pixel readout bus of the PHENIX silicon pixel detector.

The inner two layers are built from 30 hybrid sensor staves with pixel sensors placed cylindrically covering approximately 22 cm along the beam direction. The first layer has a 2.5 cm radius consisting of 10 staves and the second layer has a 5 cm radius consisting of 20 staves. One ladder is electrically divided into two independent half-ladders[2]. Four readout chips are bump-bonded on a single sensor chip using microscopic solder balls of 20 μm diameter. The device is called sensor hybrid. One half-ladder has two sensor hybrids. The sensor hybrids of one half-ladder are wire-bonded to a readout bus of a copper-aluminum-polyimide flexible printed circuit board (FPC), which is supported by a carbon-composite beam.[3] The bus is connected to a SPIRO board[2], which controls the readout chips, reads out the data and transfers the binary pixel data to the PHENIX DAQ system via 1.6 Gbit/sec optical links.

The size of the sensor hybrid is 15.6 mm $\times$ 57 mm and the total thickness is $\sim$ 350 μm. The sensor chip is based on $P^+/N/N^+$ silicon with a thickness of 200 μm and is fabricated by CANBERA[4]. It is partitioned into four active areas, each of which has 32 columns (z) $\times$ 256 rows (ϕ) with pixels of 425 μm (z) $\times$ 50 μm (ϕ). For the readout chips, ALICE1LHCb readout chips are used, which are fabricated using the IBM 0.25 μm CMOS process of incorporating radiation-hardened technology. A radiation tolerance of up to 30 MRad was demonstrated by CERN EP Division, MIC group[5]. The size of the chip is 15.6 mm $\times$ 13.7 mm with 150 μm thickness. One chip has 8,192 (32 $\times$ 256) input channels, each of which processes an input signal individually. A raw signal from each pixel is preamplified and discriminated using a configurable threshold level. The discriminated binary signal is delayed for a programmable duration and then stored to be read out by a downstream data acquisition system. The chip has 42 internal 8-bit digital-to-analog converters (DACs) for controlling the threshold of discriminators and various timings. All configurations are set via a JTAG serial interface (IEEE Std. 1149.1-1990). The chip is operated using a 10 MHz clock; therefore, the maximum readout speed is 25.6 μsec/chip with a 32-bit line[5].

The SPIRO board includes a digital PILOT chip[6], which multiplexes and controls the readout chips. The multiplexed data is passed to a serializer chip (GOL). The serialized data is transmitted via optical links at 1.6 Gbit/sec. The analog PILOT provides regulated voltages, current and reference bias to the chips.

The silicon pixel detector has to be operated within the constraint of the PHENIX DAQ speed of 40 μsec. We have chosen to expand the number of parallel 32-bit data width in the original design of ALICE[6] to 128 bits. At first, we modified the digital PILOT chip, which has 2 $\times$ 32-bit data width. Using two digital PILOT chips for each half-ladder, the bus becomes 128 bits wide. Thus, four readout chips can be read in parallel. However, this expansion requires a circuit with a four-times-denser layout on the bus. The development of such a fine-pitch FPC is necessary.

Finally, by expanding the data width and adopting a copper-aluminum-polyimide FPC, the silicon pixel detector is expected to achieve a readout speed of 51.2 μsec with a total material budget as 1.44 % X_0.

We have been developing a new copper-aluminum-polyimide FPC that has 128-bit data bus width. The advantage of the FPC is not only its ability to increase the data bus width fourfold but also it has a reduced material budget. Although the choice of copper for signal layers and aluminum for the power and ground layers is a challenge using existing technology, an aluminum conductor can have less radiation length than a copper one. For our FPC, we are aiming at less than 0.28 % X_0. The pixel readout FPC has six layers that consist of copper, aluminum and polyimide layers. It contains three signal layers, a through-halls layer, a power layer and a ground layer. Additionally, the FPC has 188 longitudinal lines. The size of the FPC is 13.9 $\times$ 250 mm^2. [7] Therefore, one signal and control line is 60 μm pitch, the line width is 30 μm and the space is 30 μm and the thickness is 3 μm.

To develop this fine-pitch FPC, we adopted the following procedure. 1) We used a HSPICE[9] simulation code for the test bus to estimate signal propagation

*1 Graduate School of Science and Technology, Niigata University, Japan
*2 Tokyo Metropolitan College of Industrial Technology

behavior, crosstalk and the characteristic impedance of lines. 2) Both a wider test bus (the width is 3 cm) and a Cu extender for checking the electrical functionality are fabricated. The test bus has a line of 80 μm, spaces between lines are 60 μm. The Cu extender is connected with the test bus by wire bonding for for electrical connection to the SPIRO board. 3) The simulation result is compared with measurement using a scope. 4) The simulation model of the FPC is fabricated. Then, the performance is verified as in step 1. 5) The FPC is fabricated, then it is tested by the same procedure as that used for the test bus.
Concerning the functionality of the test bus, it is evaluated as follows. The half-ladder, which contains two wire-bonded sensor hybrids, is built. Then, the controllability of the readout chips is verified by sending a control signal in JTAG protocol. The supply of the reference voltage and current for the DACs, and thresholds for all the chips are confirmed. Next, the number of and the location of hits on a hybrid sensor induced by a β-ray source of ^{90}Sr is obtained. The result is shown in Fig. 1. The source is placed on chip 3 and chip 2, and number of triggers is 50,000. At the same time, a telescope composed of three half-ladders was able to detect cosmic ray tracks[8].

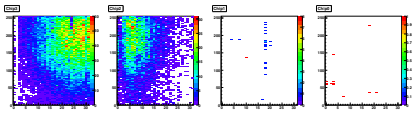

Fig. 1. Hitmap on one hybrid sensor.

The characteristic impedance, the behavior of the propagation signal and the crosstalk on the test bus are estimated using the HSPICE simulator[9]. The HSPICE model includes the GTL transmitter in the ALICE1LHCb readout chip, the FPC, the Cu extender and the GTL receiver in the digital PILOT chip. The resistance of pull-up registers used for the test bus is 100 Ω. The calculated characteristic impedance is 104 Ω $\sim$ 151 Ω. The simulation result is shown in Fig. 2 (left) and the measured signal is shown in Fig. 2 (right). Line A shows an input pulse in the readout chip. Line B in the simulation result shows the data signal at the input pin on a digital PILOT. The amplitude of the pulse is 2.5 V. The rise time is $\sim$ 30 nsec. The fall time is $\sim$ 15 nsec. Line C shows the logic in a digital PILOT. The duty cycle is 1:1. The signal for data #29 in Fig. 2 is measured using a scope with 300 MHz analog bandwidth. The amplitude is 2.5 V. The rise time is $\sim$ 20 nsec. The fall time is $\sim$ 15 nsec.
The induced signal of line D is calculated. The amplitude is 0.6 V_{pp}, and the measured crosstalk is 0.8 V_{pp}. As a result, the HSPICE simulation result is consistent with the measured result. Consequently, this simulation is shown to be reliable.
Also, a simulation model of a 1.5 cm FPC is simulated. The model is similar to the model of the test bus. Because of the small crosssection of signal lines on the FPC, its resistance is higher than that of the test bus. The resistance of the FPC is $\sim$ 43 Ω/line. The higher resistance inhibits the pulse from decreasing to the 0 V. Therefore, we choose a 220 Ω pull-up register instead of 100 Ω. The pull-up voltage is 1.8 V because the next version of SPIRO will employ a pull-up voltage of 1.8 V. The calculated characteristic impedance is 178 Ω $\sim$ 190 Ω. The simulation result is shown in Fig. 3. Line B in Fig. 3 shows the data signal at the input pin on a digital PILOT. The rise time is $\sim$ 70 nsec. The fall time is $\sim$ 10 nsec. The threshold voltage is 0.8 V and the low level of line B is 0.3 V. Hence, the margin for noise is 0.5 V. Line C shows the logic level in the digital PILOT. The duty cycle is 1:1. By selecting the value of the pull-up register, it is expected that the FPC can send correct data from a readout chip to the SPIRO.

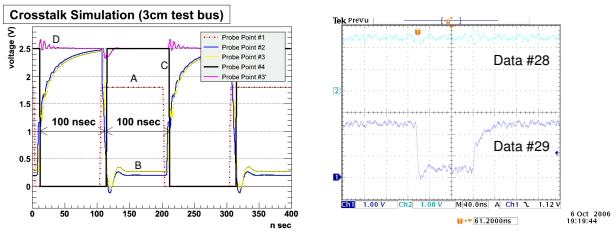

Fig. 2. Simulated signal for the test bus (left), measured signal (right)

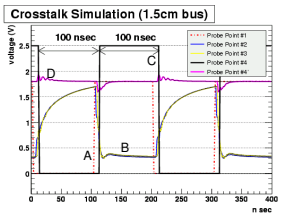

Fig. 3. Simulated signal for 1.5 cm FPC.

In summary, we have established a simulation model for a test bus. Then, we showed that the comparison of the simulation result of the test bus and the measured result using a scope is reliable. By using the established simulation model for the 1.5 cm FPC, it is confirmed that the functionality of the FPC can work with the HSPICE simulator successfully. Currently the FPC is under fabrication. We will fabricate a prototype ladder using the FPC and its functionality will be evaluated.

References

1) Y. Akiba: RIKEN Accel. Prog. Rep. **40**, xxx (2006).
2) R. Ichimiya: RIKEN Accel. Prog. Rep. **40**, xxx (2006).
3) Y. Onuki: RIKEN Accel. Prog. Rep. **39**, xxx (2005).
4) V. Manzari et al.: J. Phys. G**30**, S1091-S1095, (2004).
5) W. Snoeys et al.: Nucl. Instr Meth. A**466**, 366, (2001).
6) A. Kluge et al.: Proc PIXEL 2002 Workshop (Monterey, CA) eConfC020909.
7) K. Fujiwara, et al.: Czech. J. Phys. **55** (2005), No. 12
8) M. Kurosawa: RIKEN Accel. Prog. Rep. **40**, xxx (2006)
9) Synopsys Inc: HSPICE Manual (2006).

Beam Test of Stripixel Si Sensor for Radiation Damage Study

M. Kawashima,[*1] J. Asai, K. Kurita,[*1] K. Sakasita,[*2] R. Ichimiya and T. Komatsubara[*3]

In the PHENIX experiment at the Relativistic Heavy Ion Collider (RHIC) in Brookhaven National Laboratory (BNL), research utilizing high-energy heavy-ion collision and polarized proton collision is being advanced. We plan to install a silicon vertex detector to improve the vertex tracking performance with higher resolution of the PHENIX detector system.

We are going to install the newly developed stripixel[1)] silicon sensor at the PHENIX interaction region (IR). It is important to confirm that the detector can be operated in the PHENIX environment. RHIC will deliver polarized proton and heavy-ion beams in the next ten years, which is the foreseeable duration of detector usage. The expected integrated luminosity during the run period is 4 fb^{-1} when the beams are converted to proton-proton collision.

Our goal of the beam test is to confirm the radiation hardness of the silicon sensor. We irradiated the stripixel sensor with particle beams (proton and neutron) and estimated the degradation in 10 years of RHIC operation.

The increase in leakage current is the biggest concern for us among the known radiation damage effects, because the maximum leakage current allowed by our readout electronics is 15 nA/strip. The main concept of the stripixel sensor is the two-dimensional position sensitivity realized by charge sharing while allowing single-sided readout. The sensitive area of the sensor is 30.7 mm $\times$ 60.0 mm and the thickness is 625 μm. The entire area is segmented into 80 μm $\times$ 1000 μm rectangular pixels and there are 30 columns and 384 rows. Every pixel consists of two independent spiral electrodes wound around each other as shown in Fig. 1. In addition to the charge collection pixel, two large electrically isolated interconnection layers are implemented. One layer is used to interconnect 15 clockwise spirals in the x-direction and other layer is used to interconnect 15 counterclockwise spirals in another directions called the u-direction. Interconnected pixels are considered to be strips, hence, the name "stripixel", results the two-dimensional sensitivity is realized by the combination of x and u hit information while readout electronics are mounted on one side of the sensor. The electronic components we chose are FNAL SVX4 chips[2)] and they are all directly coupled to each of the individual x and u strips on the pixel side of the sensor. The total number of channels is 1536 (384×2 x-strips and 384×2 u-strips).

We aimed at the irradiation test with equivalent

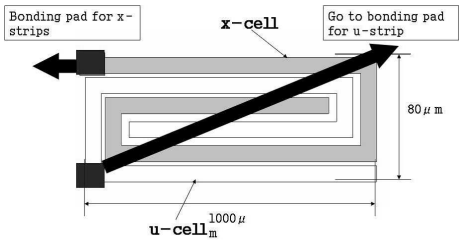

Fig. 1. Stripixel sensor

fluence $\phi_{\mathrm{eq}}(\mathrm{particles/cm}^2) < 10^{13}\mathrm{cm}^{-2}$, where ϕ_{eq} is defined as the fluence of 1 MeV neutrons, which causes equivalent radiation damage to the silicon sensors. The Tandem Accelerator Center at the University of Tsukuba was used for the irradiation test. The test was performed effectively with a 20 MeV proton beam and ϕ_{eq} of more than $10^{12}/\mathrm{cm}^2$ was achieved.

The setup of the irradiation experiment at Tsukuba is shown in Fig. 2.

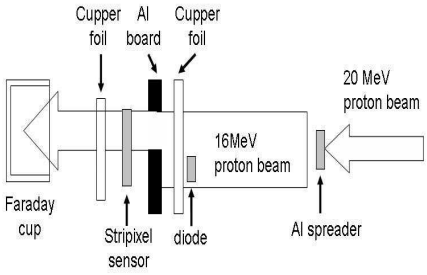

Fig. 2. Setup

To simulate the uniform irradiation of the stripixel sensor in the PHENIX environment, we chose to spread the proton beam using Coulomb multiple scattering. An Al plate of 5 mm thickness was inserted 139 cm upstream of the sensor in the 20 MeV proton beams. The beam intensity had a Gaussian sharp but we were able to limit the variation of the fluence over the irradiated stripixel area (3 $cm \times 3$ cm) to be less than 10 percent. The energy loss of the proton beam in the Al plate was considered and the hardness factor was used for 16 MeV protons. A Faraday cup was placed at 19.5 cm downstream of the sensor. Blank and spare sensor setups were also installed on the rotation table in the irradiation chamber.

The penetrating proton beam was monitored by a Faraday cup, while the sensors were irradiated. The rotation table in the chamber was used to locate each

*1 Rikkyo University
*2 Tokyo Institute of Technology
*3 University of Tsukuba

sensor. The sensors were irradiated in turn without breaking the vacuum.

As a result, the fluence measured by the Faraday cup and the monitoring diode readings agree with each other. We found the proportionality between the fluence and the leakage current. We were able to obtain consistent values for the amount of irradiation with the reference diode reading. We also confirmed the proton fluence by activating the Cu foil.

The data are plotted in Fig. 3. They include the results of experiments that have been carried out previously (experiments at Rikkyo and Kyoto).

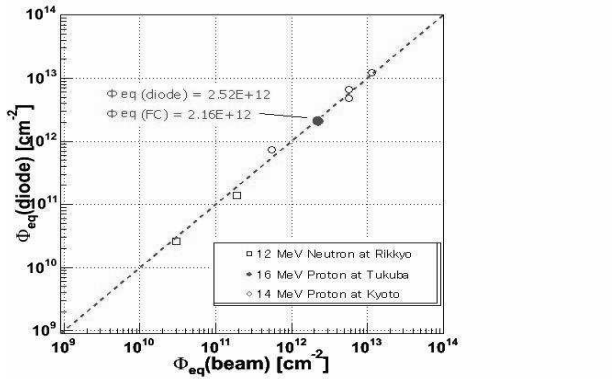

Fig. 3. Distribution of comparison of fluence between diode and beam information.

When experimental results of different irradiation conditions (i.e. species of the beam particle and its energy) are compared, it is conventional to convert what to ϕ_{eq} using the already known conversion factor κ called the hardness factor. The particle fluence is obtained from the increase in leakage current ΔI per sensor volume according to the following equation.

$\Delta \mathrm{I}/\mathrm{V} = \alpha \times \phi_{\mathrm{eq}}$,

where α is the proportionality constant called the current-related damage rate and has a typical value of $4.0 \times 10^{-17}\mathrm{A} \cdot \mathrm{cm}^{-1}$ after the annealing process is completed. The newly obtained Tsukuba result lies on the same straight line as that of the data obtain from Rikkyo and Kyoto Universities.

As a result, we confirmed that the diodes and the stripixel sensor have similar respons to radiation.

References

1) Z. Li,et.al.,"Novel stripixel detector for PHENIX Upgrade", NIMA 518 300-304 (2004).
2) B. Krieger et al.: IEEE Trans. Nucl. Sci. 51 1968-1973 (2004).

Fluence Measurement for Radiation Damage Study of Silicon Stripixel Sensor

K. Sakashita,[*1] Y. Akiba, J. Asai, R. Ichimiya, M. Kawashima,[*2] K. Kurita,[*2] M. Sekimoto,[*3] A. Taketani, and PHENIX VTX Collaboration

A silicon vertex detector (VTX) will be installed in the PHENIX central arm detector in 2009 and will be worked for 10 years[1]. The VTX is composed of four layers. The inner two layers are silicon pixel sensors[2,3] and the outer two layers are silicon stripixel sensors[4], which are single-sided two-dimensional readout sensors. The silicon stripixel sensors will be placed at 10cm and 14cm away from the beam line. The expected integrated luminosity irradiating the silicon stripixel sensors for 10 years is approximately 4fb^{-1}, and thus, the total fluence is estimated to be 3×10^{12}([1MeV neutron equivalent]/cm^2)[5]. Such strong radiation would cause significant damage to the silicon stripixel sensor resulting to an increase in the leakage current. The leakage current of more than 15nA/strip will saturate the front-end electronics. Therefore, the leakage current of the silicon stripixel sensor has been studied.

We irradiated the stripixel sensor with a 16MeV proton beam, which is equivalent to 3×10^{12}cm^{-2}, using the tandem accelerator at the University of Tsukuba[6]. It is important to accurately measure the fluence to study radiation damage. The fluence that irradiated the silicon stripixel sensor was measured by two methods. One is by use of a silicon diode, whose irradiation damage characteristics are well known. The other is by the activation method using a copper (Cu) foil, which was irradiated simultaneously with the silicon stripixel sensor. The measurements of the fluence during this radiation damage test will be described in this report.

The experimental setup is shown in Fig. 1. The energy of the proton beam was 20MeV. The beam size was much smaller than the size of the silicon stripixel sensor. Therefore the proton beam was spread by a Coulomb multiple scattering through a 5mm-thick aluminum plate placed upstream of the beam. The beam energy is degraded to about 16MeV in this process. The spread proton beam was irradiated with the silicon stripixel sensor to measure the radiation damage using setup A, in which the silicon stripixel sensor was mounted with a collimator to define the irradiated area.

The fluence was first measured using the Cu foil A, which was placed behind the silicon stripixel sensor, and was thus irradiated with the same amount of fluence as the silicon stripixel sensor. When the Cu foil was irradiated with the 16 MeV proton beam, ^{63}Zn is produced in the Cu foil (eq. 1).

$$p + {}^{63}\mathrm{Cu} \rightarrow n + {}^{63}\mathrm{Zn} \quad (1)$$

Then the ^{63}Zn decays into ^{63}Cu* with β^+-decay followed by γ-ray emissions with energies of 662keV, 962keV and 1412keV. Then the fluence was obtained from the activity of the Cu foil by counting γ-rays using a germanium (Ge) detector through the following relations.

$$\Phi = \frac{N_\gamma \lambda T_r}{\epsilon Br \sigma N_{Cu} d\Omega A} \times F \quad (2)$$

$$A = (1 \quad \exp^{-\lambda T_r})\{\exp^{-\lambda t_1} \quad \exp^{-\lambda(t_1+t_2)}\} \quad (3)$$

Here, N_γ is the number of γ-rays emitted from the produced ^{63}Zn, λ is the decay constant of ^{63}Zn, T_r is irradiation time, ϵ is γ-ray detection efficiency, Br is the branching ratio of the relevant γ-ray, N_{Cu} is the number of ^{63}Cu atoms, $d\Omega$ is the solid angle between the activated Cu foil and the Ge detector, t_1 is start time for measurement of γ-rays, t_2 is measurement time and F is a conversion factor for 16MeV proton to 1MeV neutron. The energy calibration and the detection efficiency measurement of the Ge detector were carried out using ^{60}Co and ^{137}Cs standard sources. The measured fluence with statistical error is shown in Fig. 2. The fluence values obtained from three γ-ray lines were averaged by weighting their error. It is 2.4×10^{12} cm^{-2}.

The fluence was measured by an independent method using the silicon diode to use the proportionality relation between the fluence and the leakage current of the silicon diode placed by the silicon stripixel sensor. The coefficient is known from our previous experiment[7]. Knowladge of the spatial intensity distribution of the spread beam to transfer the fluence value at the silicon diode to the one at the position of the silicon stripixel sensor is necessary.

The spatial distribution and the fluence were measured with a foil activation method using setup B. The Cu foil B was placed at the same position where the silicon stripixel sensor had been located by revolving the turntable on which all the setups were mounted. The spatial intensity distribution of the beam is obtained through the ^{63}Zn distribution by measuring β^+-rays and X-rays emitted in the β^+-decay of ^{63}Zn with an imaging plate (IP).

The IP includes fluorescent material. The $\beta^{(+)}$-rays

*1 Tokyo Institute of Technology
*2 Rikkyo University
*3 High Energy Accelerator Research Organization

and X-rays from ^{63}Zn generate hole-electron pairs in the IP. Then the pairs are trapped by the fluorescent material. The IP is then stimulated by the Ne-He laser to release the trapped electrons and holes. When the released electrons and holes are annihilated, ultraviolet (UV) photons are generated.

From the intensity of the UV photons, the spatial distribution of the spread beam was obtained, as shown in Fig. 3. The ratio of the intensity averaged over the silicon stripixel sensor to that at the beam center is 93%. The ratio of the intensity at the silicon diode to that at the beam center is 73%. It agrees with our estimation, which is based on the Coulomb multiple scattering calculation. The fluence that irradiated the silicon stripixel sensor obtained using the silicon diode is 2.5×10^{12} cm^{-2}. The fluence values obtained by the two methods agree with each other and are close to our goal fluence value, which is 3×10^{12} cm^{-2}.

The leakage current of the silicon stripixel sensor is close to 15nA/strip at 0 degree operation temperature.

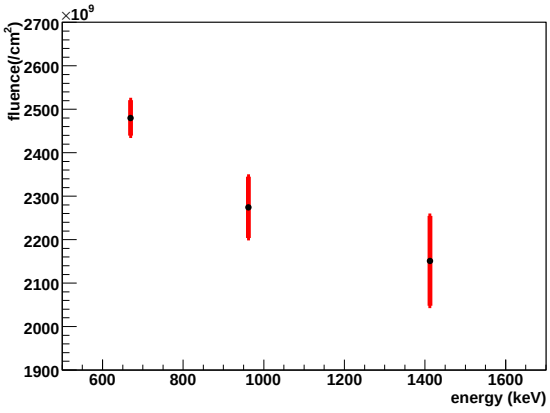

Fig. 2. Fluece obtained from three γ-rays counts. Error bar shows statistical error.

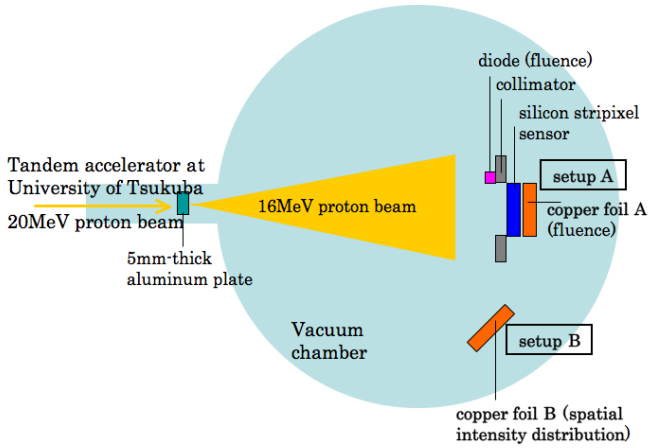

Fig. 1. Schematic of the irradiation setup. Setups A and B are setup for the measurement of the spatial intensity distribution and the radiation damage study of the silicon stripixel sensor and the fluence, respectively.

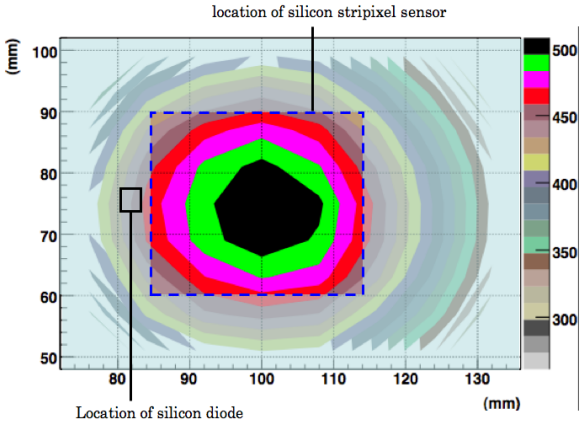

Fig. 3. Spatial intensity distribution of the proton beam.

References

1) Y. Akiba et al.: Proposal for a Silicon Vertex Tracker (VTX) for the PHENIX Experiment.
2) A. Taketani et al.: RIKEN Accel. Prog. Rep. 40 (2007) xxx.
3) Z. Li et al.: Nucl. Instrum. Methods Phys. Res. 518 (2005) 300.
4) J. Tojyo et al.: RIKEN Accel. Prog. Rep. 38 (2005) 231.
5) J. Asai: RIKEN Accel. Prog. Rep. 40 (2007) xxx.
6) M. Kawashima: RIKEN Accel. Prog. Rep. 40 (2007) xxx.
7) Y. Inoue: Study on radiation damage of the PHENIX Silicon Vertex Tracker (2005)

PHENIX reaction plane detector

W. Xie for the PHENIX collaboration

Keywords: reaction plan, heavy-ion collisions, RHIC, photo-multipliers, scintillator.

PACS: 29.40.Mc

Event anisotropy is one of the most important observables in nucleus-nucleus collisions at RHIC. The large anisotropy amplitude, v_2, provides key evidence of the formation of a hot and dense partonic matter in Au+Au collisions at RHIC. Measurements of v_2 in rare observables such as electrons, photons, and high p_T particles can provide even richer information on the properties of partonic matter.

The measurements of the v_2 of these rare probes are not only limited by luminosities but also rely on accurate reaction plane measurements. In PHENIX, we use the BBC to determine the reaction plane. The statistical power of the v_2 measurement is reduced by a factor of 6 to 100 compared with the ideal case in Au+Au collisions due to the poor reaction plane resolution. The situation is even worse for light ions such as Cu+Cu or at lower energy. This relatively poor reaction plane resolution of the present PHENIX detector is a major limiting factor of our v_2 measurement of rare signals. Reaction plane determination by other methods, such as central arm tracks or v_1 measurement by ZDC/SMD do not provide better reaction plane resolution

We propose a new detector for reaction plane measurement in PHENIX. Comparing to the existing BBC detector, the new detector will improve the statistical power of v_2 measurements in PHENIX by about a factor of three.

The reaction plane detector will be a paddle type detector situated in front of the nosecone as shown in Fig.1. The active area will be composed of plastic scintillating material with a lead converter in front to increase the detector performance. The scintillator will have a thickness of 2 cm and will be positioned at $38<|z|<40$ cm. The inner edge of the scintillator will begin at r = 5 cm and extend to r = 33 cm. This allows the detector to cover a pseudorapidity range of $1.0<|\eta|<2.8$. This coverage was chosen to balance the competing effects of maximum acceptance and jet induced autocorrelations with the central arm. The detector will be segmented into 12 sectors in phi to minimize the impact from dead channels. Each phi sector will be further divided into two radial sections. The inner eta segment will extend from a radius of 5cm to 18cm and the outer eta segment will continue from 18cm to a radius of 33cm. This effectively divides the detector into two rapidity regions, $1.0<\eta<1.5$ and $1.5<\eta<2.8$, which will allow the possibility to study the effect of jet induced autocorrelations on the reaction plane determination.

Embedded fiber light guides made of BCF92 will connect the plastic scintillator to the photomultiplier tubes. An adapter in which the fibers can be embedded will be used to join the fibers to the photomultiplier tube. The use of fiber light guides has several advantages for this detector design. Most significantly, the light collection along the radial length of the scintillator is more uniform using embedded fibers than solid light guides. Additionally, the fibers allow for flexibility in the final positioning the photomultiplier tubes. This is important due to the sensitivity of the tube response to the magnetic field and will allow the tubes to be repositioned if necessary after installation.

Mesh dynode photomultiplier tubes, Hamamatsu H6155, will be used due to the strength of the magnetic field in the region where the reaction plane detector will be positioned.

A 2 cm thick lead-antimony composite converter is installed directly in front of the scintillator. The addition of 2-3% of antimony hardens the converter material and will improve the mechanical stability of converter when it is mounted. An LED calibration system will be used online to monitor the stability of the detector.

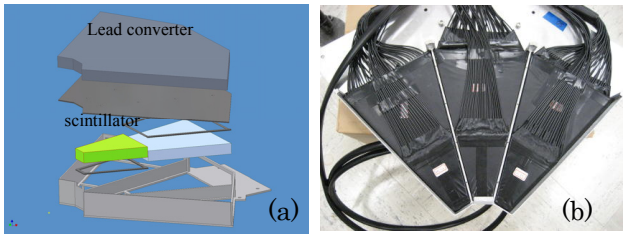

Fig.1. (a). One sector of the detector assembly; (b). One sector of real detector in the process of assembly. Converter is not installed yet.

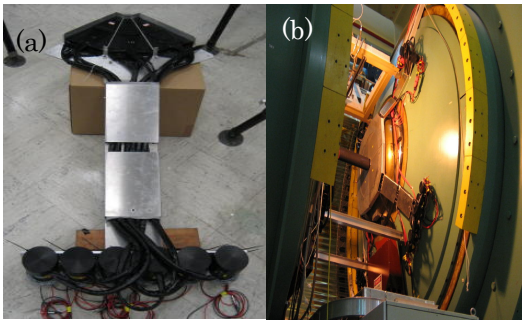

Fig.2. (a). One fully assembled sector before installation of converter.; (b) One arm of the detector in PHENIX inner center area.

The installation of the detector has been successfully finished and we are in the process of commissioning the detector. The plan is to make it fully functional before the start of RHIC year 2007 Au+Au run and provide the improved reaction plane measurements. Beside that, the detector has the potential of serving as the PHENIX minimum-bias trigger during the low energy Au+Au run and p+p run. We are currently setting up the trigger and will also commission the trigger simultaneously.

Ubiquitous detector system

Y. Watanabe, Y. Kawasaki, Y. Takizawa, T. Hamada, K. Hirota, H. Sato, H.M. Shimizu, T. Ebisuzaki, H. Baba, M. Kurokawa, T. Fukuchi,[*1] S. Shimoura,[*2] S. Ota,[*2] and T. Motobayashi

We are developing a next-generation DAQ system that consists of autonomic data-acquisition modules distributed over a DAQ network. Each module is attached to its partner detector and can memorize the detector's characteristic and history.

In these 30 years, DAQ systems for nuclear physics experiments have been based on a modular structure, because of their universality and flexibility. Advanced studies require more precise measurement and more detector channels, which cause, for example, complicated cabling and more noise. On the other hand, the information technology (IT) field is growing rapidly, and fast CPUs, large memories, and network technology, among others, have become available at very low costs. Under such circumstances, we are now developing autonomic data-acquisition modules distributed over a DAQ network for a more universal and flexible DAQ system. The system is analogous to "ubiquitous computing", which has widely been recognized recently. Thus, we call our project "ubiquitous detector system".

1 Introduction

The word ubiquitous means "being or seeming to be everywhere at the same time" (American Heritage Dictionary). It is used in terms such as "ubiquitous computing" or "ubiquitous networks". In both cases, many tiny computers hidden away from people work autonomously by communicating with each other, as shown in Figure 1. To satisfy a person in a house, a decision must be made on the basis of information from indoor and outdoor temperatures. Two typical methods are used the decision: centralized management and distributed management. The ubiquitous system is the latter. Each device has a computer and communicates with other devices to make a decision. If there were more devices (e.g. sensors: illuminometers or hygrometers; actuators: light switches or motors for curtains), they can make the person more comfortable. It is obvious that distributed management is easier to realize in terms of, for example, expansion because each device is independent and only connected to the network. The memory of each device is also important. It stores not only the characteristics of the device but also its history, such as temperature trends or operation logs.

With the ubiquitous concept, we are trying to develop a new DAQ system for nuclear physics experiments, whose style has not changed for more than 30 years now. The ubiquitous computing/network will normally be applied to organize discrete objects. On the other hand, our ubiquitous detector will be applied to a system that is already set up with numerous physical cables to make it simple for us to, for example, unravel tangled threads.

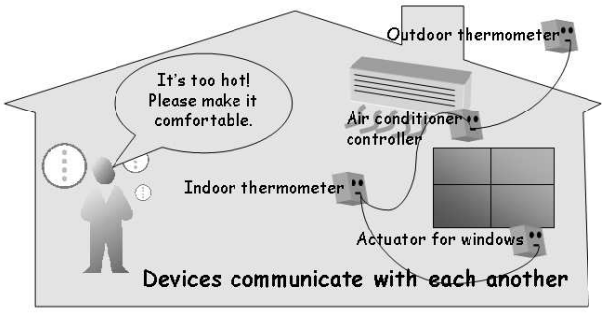

Fig. 1. Each device communicates with others and makes decisions to satisfy the person.

2 Ubiquitous detector

"Plug & Play" is a key concept in the ubiquitous detector system. Figure 2 shows a simple image of a ubiquitous detector's usage. Just plugging electric-power and network cables is enough to gather data.

To realize the "plug & play" concept, the ubiquitous detector has autonomic functions; i.e., record, process, judge, and communicate. In other words, a bare detector must to be connected to the autonomic unit, which consists of a digitizer, a signal processor, a network interface, and a controller, as shown in Figure 3.

In fact, the autonomic unit is divided into two units: an autonomic digital signal processing unit (ADSP unit) and a digitizer subunit. We are now develop-

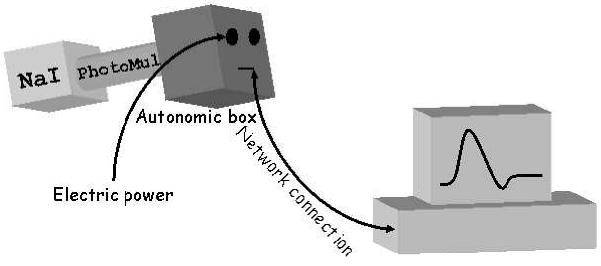

Fig. 2. A ubiquitous detector can be used by simply plugging cables.

*1 Research Center for Nuclear Physics, Osaka University
*2 Center for Nuclear Study, University of Tokyo

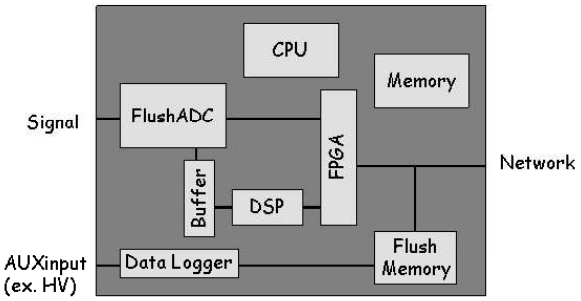

Fig. 3. Basic idea of the autonomic unit. This block diagram is similar to that of a digital oscilloscope.

ing a FADC unit[1] and multichannel photon counting unit for the digitizer subunit as well as the ADSP unit.

3 Autonomic digital signal processing unit (ADSP unit)

The ADSP unit is the most important unit on the ubiquitous detector, because it functions as the brain of each detector. Figure 4 and Table 1 show a photo and the specifications of the ADSP unit (model: EP101). The DAPDNA chip[2] has a unique architecture of a two-dimensional array of 376 32-bit processing elements, which is good for digital signal processing operations, e.g., waveform analysis or making a histogram. The 512 MB of memory can hold more than 2 sec of 100 MHz 16-bit FADC waveform data. It gives a good margin to wait for delayed trigger signals. The 2 MB of Flash-ROM is used to store the detector's characteristics and history, e.g., calibration data.

Now, we are testing the ADSP unit as a stand-alone component. The following is a list of items that have been already confirmed:

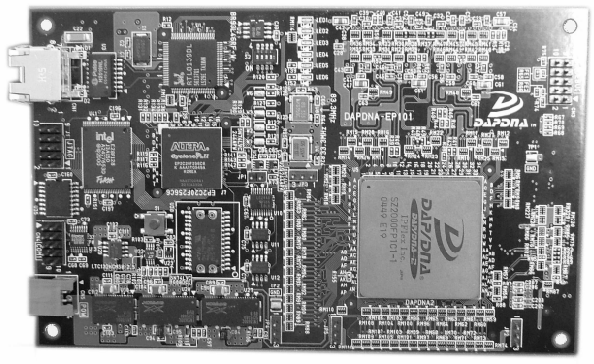

Fig. 4. A photo of ADSP unit: EP101. The largest chip is a DAPDNA, that is the heart of a ADSP unit. 128-bit digital I/O and 512 MB DDR-SDRAM are placed at the back.

Table 1. Specifications of the ADSP unit: EP101.

CPU	DAPDNA-2
Clock	166 MHz
Memory	512 MB DDR-SDRAM
Nonvolatile memory	2 MB for user (FlashROM)
Network interface	100BaseT
Digital I/O to subunit	128 bits : 166 MHz SSTL_2
OS	AxLINUX
Power	5 V, 1 A
Size	100 mm x 150 mm

- Booting of AxLINUX
- Use of Ethernet
- Use of TCP/IP communication (remote login, http, NFS)
- Running applications on AxLINUX
- Reading/Writing data in SDRAM from DNA processor elements

We will start testing the ADSP unit and FADC subunit as a connected module soon.

References

1) H. Baba et al.: In this report.
2) DAPDNA chip, IPFlex Inc. http://www.ipflex.com/

Development of FADC unit for UBIQUITOUS detector system

H. Baba, M. Kurokawa, Y. Watanabe, T. Fukuchi,[*1] S. Shimoura,[*2] S. Ota,[*2] T. Ebisuzaki, T. Hamada, K. Hirota, Y. Kawasaki, H. Sato, H. M. Shimizu, Y. Takizawa, and T. Motobayashi

A FADC unit for the UBIQUITOUS detector system[1] has been developed. The FADC unit is a subunit of an autonomic digital signal processing (ADSP) unit. FADC, which stands for flash analog-to-digital converter, can acquire the waveforms of analog signals because its conversion time is sufficiently short. In this work, a 100-MHz-sampling-rate FADC with 14-bit resolution was employed. It can digitize an analog signal every 10 ns with 14-bit resolution. The digitized waveform signal is sent to the ADSP unit for further analysis to extract physical values, e.g., energy, timing, position, and particle identification. The detector system will be applied to the output signals from a NaI(Tl) detector[2], a Ge detector[3], a CdTe detector [4] and a Si detector[5]. The FADC unit works without a break and continuously sends waveform data to the ADSP unit, which also works continuously with pipeline processing. Therefore, by combining these units, the resulting detector system will have the capability of dead-time-free analog to physical value conversion.

The specifications of the FADC unit are listed below.

- Inputs
  - 2 × LEMO connectors
  - 1 k / 50 Ω impedance (with the gain amplifier)
  - 50 Ω impedance (with the ramp circuit)
- Analog signal processing
  - 2 × Gain amplifiers
    - Programmable gain
    - Course gain: ×1 – ×128 (8 steps)
    - Fine gain: ×0.4 – ×1 (8 steps)
  - 1 × Ramp circuit
    - Input: NIM negative logic signal
    - Output: 5 mV/ns triangular signal
- Digitizer
  - 2 × FADCs
    - 100 MHz sampling rate
    - 14 bit resolution
    - ±1 V input range
  - 2 × Clock counters
    - 16 bit resolution
    - Debugging purpose only
- Outputs
  - 120 pin, 1/4 inch pitch, SMT plug
  - Total 60 bits/sample
    - FADC: 14 bits/sample × 2
    - Clock counter: 16 bits/sample × 2
  - SSTL_2 Class II logic signal
- Power consumption
  - 5 W (+5 V, 1 A)
- Size and weight
  - 100 × 150 mm
  - 150 g

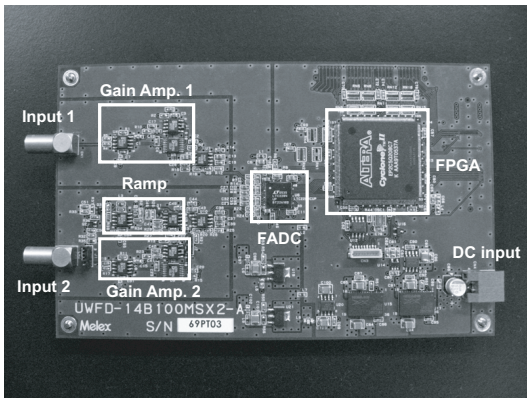

Fig. 1. Photograph of FADC unit. The details of this FADC unit are described in a text.

Figure 1 shows a photograph of the FADC unit. The FADC unit has two input connectors. One of them is connected to the gain amplifier. The other is connected to the gain amplifier or ramp circuit, which are selected by a jumper switch. The input range of the FADC chip is ±1 V. To adjust the full-scale range, input signals are amplified by the gain amplifier. Their amplitude is controlled by the ADSP unit. If we try to obtain timing information from NIM logic signals with the 100-MHz FADC, the extracted timing will have the same ambiguity as the sampling interval of 10 ns. In order to achieve a good timing resolution on less than the nanosecond order from logic signals, the ramp circuit is implemented. This ramp circuit generates triangular signals whose width and pulse height are proportional to the width of input NIM logic signals. Timing information will be derived by a linear extrapolation of the digitized triangular signals. In order to implement the clock counter, field programmable gate array (FPGA) is mounted. The clock counter counts clock at 100 MHz. It will be used for debugging purposes only.

*1 Research Center for Nuclear Physics, Osaka University
*2 Center for Nuclear Study, University of Tokyo

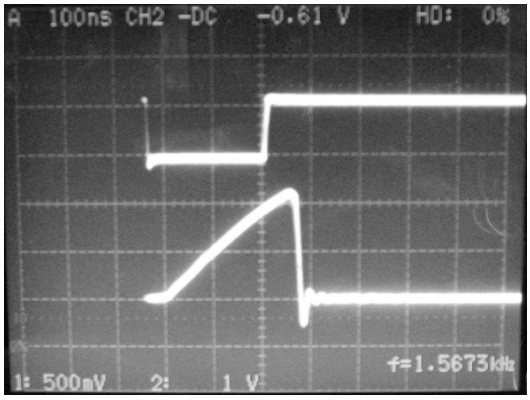

Fig. 2. The operation of the ramp circuit. Ramp signal (lower triangular signal) is generated according to input NIM logic signal (upper rectangular signal).

The power consumption of the FADC unit is about 5 W (5 V, 1 A). The FADC unit can provide power to the ADSP unit that power consumption is also about 5 W (5 V, 1 A).

We are going to connect the FADC unit with an ADSP unit and implement digital signal processing for detector signals.

References

1) Y. Watanabe et al.: This report.
2) H. Baba et al.: CNS Annual Report 2004 (2005) 87.
3) T. Fukuchi et al.: CNS Annual Report 2004 (2005) 73.
4) T. Moriguchi et al.: CNS Annual Report 2005 (2006) 75.
5) M. Kurokawa et al.: This report.

CCJ operation in 2005-2006

S. Kametani, H. En'yo, Y. Goto, H. Hamagaki,[*1] T. Ichihara, Y. Watanabe and S. Yokkaichi

RIKEN PHENIX Computing Center in Japan (RIKEN CCJ) is a large-scale computing system mainly dedicated to the analysis of RHIC-BNL[1] physics: the study of the spin structure of a nucleon and the investigation of QGP. The production of Data Summary Tape (DST) from raw data in the PHENIX[2] experiment, one of two major experiments being performed at RHIC, and the subsequent analysis are performed at CCJ. In this article, we report on the following three activities: the operation, upgrade and maintenance of CCJ.

CCJ is composed of calculation nodes, a mass-storage system, a medium-scale storage system using RAID and a networking system that connects these components to each other. CCJ owns 150 calculation nodes. In addition, 128 nodes of the RIKEN Super Combined Cluster (RSCC) of the Advanced Center for Computing and Communication[3] are dedicated to CCJ. These CPU resources are allocated to jobs by LSF[4], the batch-job system of Platform Inc.

The mass-storage system is composed of a tape robotic system and disks, and is managed by the High Performance Storage System (HPSS)[5]. CCJ and RSCC share the mass-storage system. As of Dec. 2005, the mass-storage system had a total volume of 0.8 PByte using 4000 tape cartridges, each with a 200 GByte capacity, and the total capacity of the medium-scale storage system was 47 TByte. The detailed specifications can be found in the previous report[6].

During 2005-2006, CCJ experienced two major programs. The first one was the transfer of PHENIX raw data in the PHENIX year-6 experiment. In the experiment, the recorded data are stored in buffer disks and then transferred to a mass-storage system at BNL. In parallel with this, data in the buffer disks are also transferred to RIKEN. The transferred data are not only archived as a backup, but are also used to produce the PHENIX official DST.

In the beginning of the year-6 experiment, 700 TByte of data space was used to store the data of the previous (year-2/3/4/5) experiments, i.e., only 100 TByte of space was left on the mass-storage system. We purchased 1000 tapes (200 TByte). We also returned 300 tapes located at BNL back to RIKEN, which were reserved for airplane data transfer. The data transfer between BNL and RIKEN was carried out using GridFTP[7], the same method at last year[8]. Figure 1 shows the amount of data transferred from BNL to CCJ. The amount of transferred data was 4-7 TByte each day. This amount corresponds to 30-70 MByte/sec in transfer speed. A total of 310 TByte of data were transferred over about 2 months during the experiment.

The second major program was the reproduction of DST for the year-5 experiment. DST is the first calibrated data set on which all the PHENIX collaborators perform physics analysis. A detailed description of this program can be found in this volume[9]. The production began at Apr. 2006 and ended at Sep. 2006. To support the DST production, change of the operating system of calculation nodes was performed to follow up the PHENIX analysis framework. Scientific Linux 3.0.5 was installed to 152 hosts of CCJ computing servers including RSCC.

Figure 2 shows the amount of data stored in HPSS over time. As a result of the raw data transfer and DST production, the total amount of data stored in HPSS reached 1.1 PByte.

Other analytical activities can be found on the web page: http://ccjsun.riken.go.jp/ccj/proposals/. Achievements of these activities are reported in this volume.

Our activity in the system upgrade was mainly focused on the establishment of new storage spaces. In the mass-storage system, a new tape drive was installed in Aug. 2006 because the physical space used to store the tape cartridges of the robotic system was almost full. Therefore, the tape cartridges needed to be replaced by larger ones. We introduced a T10000 tape drive of Sun Microsystems. T10000 can handle 500 GByte tape cartridges, whereas the previous tape drives (T9940B) could handle only 200 GByte tape cartridges. For the operation of T10000, a version upgrade of the HPSS system from 4.2 to 6.2 was also performed. We purchased 160 of the 500 GByte tape cartridges and obtained an extra storage space of 80 TByte as a result. The installation of T10000 was executed during Aug. 2006. The data repacking from 200 GByte tapes to 500 GByte tapes is now ongoing. We are planning to purchase an additional drive and tape cartridges.

We decided to establish a contract with San Diego Supercomputer Center for the maintenance of HSI and HTAR, the advanced tools of HPSS. The standard tool of HPSS, called "pftp", performs random access when multiple files are specified. The poor random access is well-known weak point of tape media. HSI and HTAR have an optimizing function for accessing tape media, to mitigate this weak point.

The medium-scale storage system was also upgraded. First, an additional RAID system was installed in May 2006. The capacity of the additional

*1 Center for Nuclear Study, Graduate School of Science, the University of Tokyo

RAID is 10 TByte. A Sun Fire V40 machine was installed as the corresponding server. Since Solaris10 for x86 does not support pftp, the server is operated by Scientific Linux 4.2.

Moreover, a new storage system is being tested as the successor of the RAID system. We installed a 300 GByte HDD in each of 36 CCJ calculation nodes. The total disk space reached 10.8 TByte. There are two merits of this system compared with the existing network server-client systems. The first merit is the cost reduction. The second merit is the improvement of the data supply speed to the CPU. In the existing systems, data to be analyzed on the client computer is transferred from servers via the network. The load on the data server increases as the number of the clients increases. This phenomenon results in a bottleneck in our current system. In the new system, a job is allocated to the computer, which stores the data to be analyzed. As a result, the accumulation of the load on disk servers never occurs and the total computing speed improves. We plan to apply the system to RSCC nodes, which are dedicated to CCJ.

The maintenance issues during 2005-2006 are listed below. A version upgrade was performed for LSF (5.1 to 6.0) in Dec. 2005. The RAID system had trouble on HDD and FC HUB. The replacement of broken parts already has been carried out. Five computing servers crashed and four of them recovered with the replacement of the HDD. One CPU of a NFS server broke and was replaced. Two exhausted Sun servers that served several system services are retired. The services served by these hosts were integrated into the main NFS server. Two air conditioners in the CCJ server room broke and were repaired. At the same time, the air conditioners stopped because of the dirt in the outdoor unit.

Here, we report on the security of the network. The security policy of BNL was tightened during 2006. First, since Oct. 2006., we can only have SSH access to the RHIC Computing Facility (RCF)[10] when using a public key for authentication. RCF accepts only one public key per user. Therefore, for the connection between CCJ and RCF, a user needs to put their private key into the CCJ machine or to use agent-forwarding method from CCJ. In each case, the responsibility of CCJ for the management of security has become heavier.

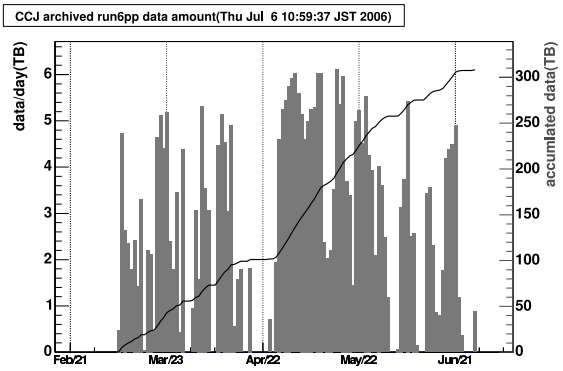

Fig. 1. The amount of data transferred each day to CCJ are shown by gray bars. The cumulative amount is shown by the solid line.

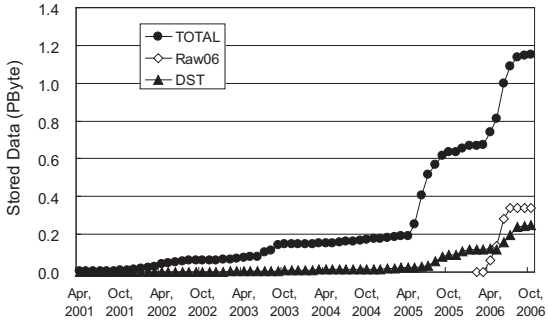

Fig. 2. The amount of data stored in HPSS over time. Closed circles show the total amount used. Open diamonds show the amount of raw data transferred during the year-6 experiment. Closed triangles show the cumulative amount of DST data produced from the data in the year-2/3/4/5 experiments. The total amount of data stored in HPSS reached 1.1 PByte.

References

1) M. Harrison, T. Ludlam and S. Ozaki: Nucl. Instrum. Meth. A **499**, 235 (2003).
2) D. P. Morrison et al.: Nucl. Phys. A **638**, 565c (1998).
3) http://accc.riken.jp
4) http://www.platform.com/products/LSF/
5) http://www.hpss-collaboration.org/hpss/index.jsp
6) S. Kametani et al.: RIKEN Accel. Prog. Rep. **39**, 224 (2006).
7) http://www.globus.org/grid_software/data/gridftp.php
8) Y. Watanabe et al.: RIKEN Accel. Prog. Rep. **39**, 222 (2006).
9) Z. You et al.: RIKEN Accel. Prog. Rep. **40** (2007).
10) http://www.rhic.bnl.gov/RCF/

Network and Computing Environment for RIKEN Nishina Center

T. Ichihara, Y. Watanabe, K. Yoshida, and A. Yoshida

We have been operating Unix/Linux NIS/NFS cluster systems at Nishina Center so far. The central server used for general computing and the mail service was *RARFAXP*. Four sets of 64 bit Alpha EV6 CPUs with 2 GB memory are used for *RARFAXP* and the operating system is Tru 64 UNIX (OSF/1). However, the development of Alpha CPU was discontinued and support of the Tru 64 operating system is scheduled to be discontinued soon. In addition, several new software packages cannot be installed on Tru 64 UNIX because they can no longer run on the operation system.

Therefore, we have replaced the *RARFAXP* server by two servers, *RIBF* and *RIBF00* this year [1]. Both new servers are HP ProLiant 585 high-reliability servers, equipped with AMD dual-core Opteron 885 CPUs of 2.6 GHz. *RIBF* consists of four CPUs (8 cores) and 16 GB memory, while *RIBF00* consists of two CPUs (4 cores) and 8 GB memory. Power supplies and fans are duplicated for high availability. System disks are striped and mirrored (RAID0+1) by the hardware.

RIBF is used for the mail server and the NFS server for the user home directory. *RIBF00* is a ssh login server and a general-purpose computational server. Scientific Linux 4.4 (X86_64)[2] operating system has been adopted for these new servers. Scientific Linux is freely available and widely used in the nuclear physics and high-energy physics communities.

At *RIBF*, Postfix[3] is used for mail transport software and Dovecot[4] is used for imap and pop services. These software packages enable secure and reliable mail delivery.

A new 3.3 TB fiber-channel Raid was connected to *RIBF* for the user home directory. Half of the RAID is used as backup area. This RAID controller is duplicated for high availability.

Figure 1 shows the current configuration of the Linux/Unix servers of Nishina Center. *RARFLX1, RARFLX2*, and *RARFLX3*, which have also been replaced in this year, are located in the 1F counting room of Nishina Memorial Buildings, and they are used as user terminals for experiments at the Ring cyclotron. Dual-core AMD Athlon 64X2 CPUs are used for these nodes.

RARFSMTP and *RARFSMTP2* are mail front-end servers used to tag spam mails and isolate virus-infected mails. Spamassassin[5] software is used to identify spam mails.

An anonymous ftp server *ftp.riken.jp* is managed and operated at RIKEN Nishina Center. Recently, many research laboratories in Nishina Center have adopted Linux as their computer operating system. To conduct

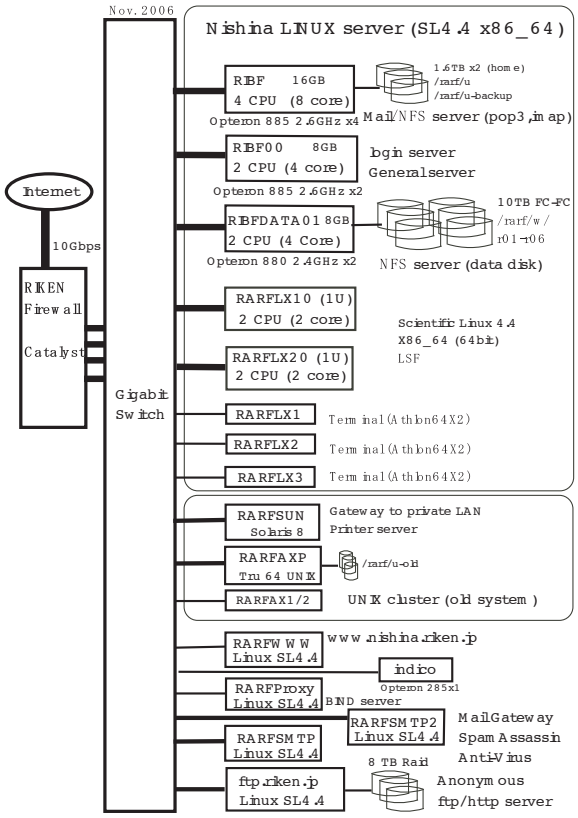

Fig. 1. Configuration of the Linux/Unix server.

the installation and daily management of Linux easily and efficiently, major Linux distributions are mirrored at the ftp servers.

Most of the users of Nishina Center have e-mail addresses of the following forms:

username@ribf.riken.jp or *username@riken.jp.*

The former one represents an e-mail address of the Nishina Center mail server (*RIBF*) and the latter represents an e-mail address of the RIKEN mail server (*postman*). Mail to the previous E-mail addresses of *username@rarf.riken.jp* and *username@rarfaxp.riken.jp* are forwarded to the new mail address *username@ribf.riken.jp* automatically.

Two sets of a Dual-core Opteron 1U server and a 6TB SATA Raid system have been installed as a prototype DAQ event builder and analyzer for RIBF experiments.

References

1) *http://ribf.riken.jp/*
2) *https://www.scientificlinux.org/*
3) *http://www.postfix.org/*
4) *http://www.dovecot.org/*
5) *http://spamassassin.apache.org/*

Comparison of Single-Event Burnout tolerance of space-use power MOSFETs

N. Ikeda, S. Kuboyama, Y. Sato,[*1] H. Ohira, H. Otomo, O. Shimada, H. Ozono,[*2] N. Inabe, and M. Kase

A power metal-oxide-semiconductor field-effect transistor (MOSFET) is a key device in a power circuit that has a low ON-resistance and a fast switching. A MOSFET for use in space is required to have radiation hardness. Protons, heavy ions and other particles in space may have single-event effects that may lead to semiconductor device malfunction or failure. Single-event burnout (SEB) is the main concern for power MOSFETs. SEB is triggered by a heavy ion passing through a device when it is off. A transient current induced by such an ion turns on a parasitic bipolar transistor, which results in the burning out of a device and its possible destruction[1]. Because commercial power MOSFETs are not SEB-tolerant and SEB occurs at voltages far below rated voltages, MOSFETs particularly developed for space application must be used.

Japan Aerospace Exploration Agency (JAXA) started developing radiation-tolerant power MOSFETs several years ago and successfully completed the development of several types of SEB-free power MOSFET with low ON-resistance. MOSFETs with drain-source voltage (V_{DS}) values between 100 V and 250 V were developed and proven to be SEB-tolerant at rated voltages up to a linear energy transfer (LET) of 48 MeV/(mg/cm^2). Because there is another organization developing space-use power MOSFETs, an irradiation test was conducted to compare the radiation tolerance of MOSFETs from JAXA and the organization using RIKEN Ring Cyclotron. MOSFETs with V_{DS}=100V were irradiated with 373 MeV $^{58}Ni^{19+}$ ions whose LET and projected range in the devices were 25 MeV/(mg/cm^2) and 61.3 μm, respectively. The Energetic Particle Induced Charge Spectroscopy (EPICS) system developed by JAXA was used to observe SEB[2], and the spectra of collected charges were examined in the same manner as in a previous study[3]. Typically, two peaks were observed in the spectra, which are designated here as the first peak and the second peak. A large charge collection in the second peak implies a low SEB tolerance.

Figure 1 shows the spectra of collected charges of the MOSFETs. Although no SEB was observed for both devices, a difference in EPICS spectra was observed. Whereas small second peaks with small collected charges were observed for MOSFETs from JAXA, apparent second peaks with large collected charges were observed for the MOSFET from the other organization. This result suggests that MOSFETs from JAXA have better radiation tolerance. Moreover 200 V and 250 V devices were irradiated under the same conditions and the experiment showed that MOSFETs from the other organization have a thicker active layer, which provides a higher ON-resistance.

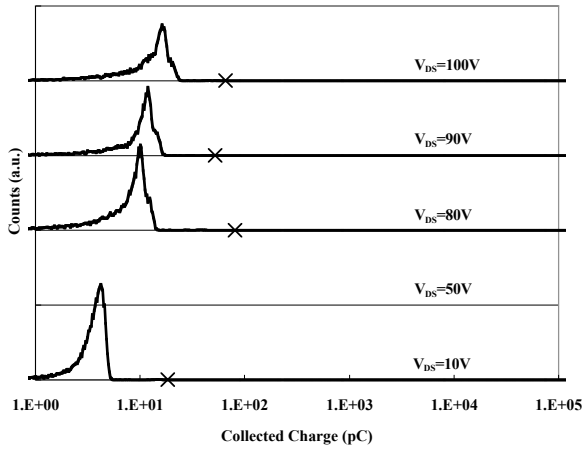

(a) MOSFET from JAXA

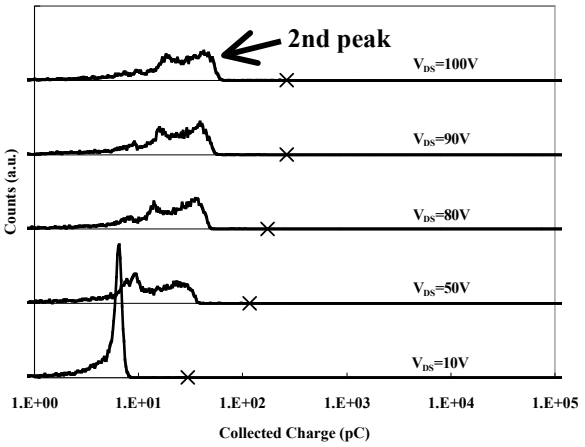

(b) MOSFET from another organization

Fig. 1. EPICS spectra of MOSFETs. "x"is the maximum collected charges.

References

1) JAERI and NASDA Joint Research Report, **2** (1999), p. II-9
2) S. Kuboyama et al.: IEEE Trans. Nucl. Sci., **39** (1992), pp 1698
3) N. Ikeda et al.: RIKEN Acce. Prog. Rep., **37** (2003), pp 98

[*1] Japan Aerospace Exploration Agency
[*2] Ryoei Technica Company

Synthesis of Pd-Au nanoparticles by GeV ion irradiation

N. Maeda*[1], F. Hori*[1], T. Kambara, T. Abe、H. Ryuto and A. Iwase*[1]

In a previous paper, we showed that GeV heavy ion irradiation reduces Au ions in aqueous solutions and synthesizes Au nanoparticles, the diameter of which was about 10-50 nm[1, 2]. In this report, we show the result of 1.6 GeV carbon ion irradiation to the solutions containing Au and Pd ions.

Samples were dilute aqueous solutions with 0.5 mM $NaAuCl_4/2H_2O$ as a precursor of Au^{3+} ions, 0.5 mM $PdCl/2NaCl/3H_2O$ as a precursor of Pd^{2+} ions, and 8 mM sodium dodecyl sulfate (SDS) as a surfactant. The samples were sealed in polystyrene vessels and irradiated with 1.6 GeV full-stripped carbon ions at the E5B beam line of the RIKEN ring cyclotron accelerator. The irradiation doses used were 300, 1500, 5000 and 10000 Gys. After the irradiation, the optical absorption spectra of each solution were measured using an ultraviolet-visible spectrophotometer (UV-vis).

The solution remained yellow, indicating the existence of Au and Pd ions at irradiation doses below 300 Gy. When the dose reached 1500 Gy, the solution turned reddish violet. For doses higher than 1500 Gy, the solution showed a dark brown color. Figure 1 shows the change in UV-vis spectra with the dose of carbon ion irradiation. The UV-vis absorption peak around 300 nm originates from Au and Pd ions in an unreduced solution. After the irradiation of 1500Gy, an absorption peak around 530 nm, which corresponds to the surface plasmon peak of Au nanoparticles, appears, and the absorption yield of Au and Pd ions decreases.

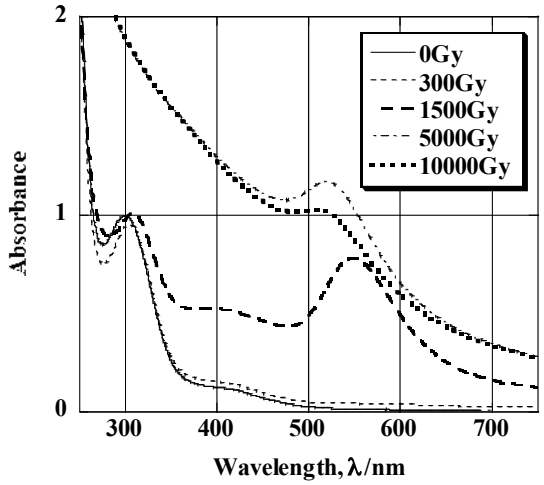

Fig. 1. Change in UV-vis spectra with dose of 1.6 GeV carbon ion irradiation.

With increasing carbon irradiation dose, the background of the absorption yield increases and the yield around 530 nm decreases. The dependence of the absorption yield around 530 nm on the dose of carbon irradiation can be observed more clearly in Fig. 2. As the increase in the background of the absorption yield is considered to be due to the surface plasmon of Pd, the present result can be explained as follows: 1.6 GeV carbon ion irradiation reduces Au ions first and Au nanoparticles are produced. After the production of the Au nanoparticles, Pd ions are reduced on the surfaces of the Au nanoparticles. Since the surfaces of the Au nanoparticles are coated with Pd atoms, the Au surface plasmon peak intensity (around 530 nm) decreases with increasing carbon irradiation dose. The present experiment suggests the possibility of synthesizing nanoparticles with Au cores and Pd shells by GeV ion irradiation. To confirm the structure and the size of Pd-Au nanoparticles synthesized by GeV carbon ion irradiation, transmission electron microscopy observation is now in progress.

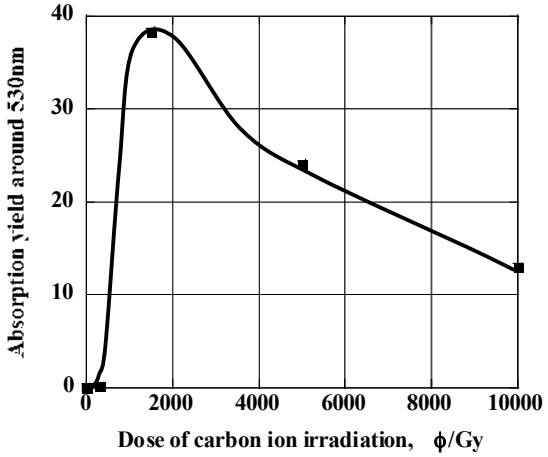

Fig. 2 Dependence of UV-vis absorption yield around 530 nm on dose of 1.6 GeV carbon ion irradiation.

References

1) N. Maeda, T. Hiroki, F. Hori, S. Okuda, R. Taniguchi, T. Kojima, T. Kambara, T. Abe, and A. Iwase: Mater. Res. Soc. Symp. Proc. Vol. 900E, 0900-O06-16. 1-6.
2) N. Maeda, F. Hori, T. Kambara, T. Abe, and A. Iwase: RIKEN Accelerator Progress Report 2005.

*1 Osaka Prefecture University

^{57}Fe diffusion in Si after GeV- implantation of ^{57}Mn

Y. Yoshida*1, Y. Kobayashi, K. Yukihira*1, K. Hayakawa*1, K. Suzuki*1,
A. Yoshida, H. Ueno, A. Yoshimi, K. Shimada*2, D. Nagae*2, K. Asahi, and G. Langouche,*3

Iron impurities are known to degrade seriously the electronic properties of silicon-based devices and solar cells. Dilute systems of FeSi, therefore, have been intensively investigated for more than 50 years by different experimental techniques including ^{57}Fe Mössbauer spectroscopy. Generally, iron atoms are thought to occupy only the interstitial sites in silicon leading to a fast diffusion.[1] On the other hand, substitutional iron atoms were not found experimentally by standard evaluation techniques, although Mössbauer spectroscopy provided clear lines of evidence for substitutional iron atoms not only after the implantation of ^{57}Fe into Si matrix,[2-4] but also after the deposition and subsequent thermal diffusion of ^{57}Fe into Si.[3,5,6] The present investigation is carried out to clarify the impurity diffusion of Fe atoms and the formation processes of "substitutional Fe atoms" in Si at high temperatures.

^{57}Mn nuclei were produced by the nuclear projectile fragmentation of $^{58}Fe^{21+}$ primary beam (E = 63 MeV/nucleon) with a Be target, and subsequently separated by an on-line isotope separator, RIPS. Mössbauer spectra of ^{57}Mn/^{57}Fe in n-type CZ-Si were measured between 300 and 1200 K immediately after the implantation of the radioactive isotope of ^{57}Mn ($\tau_{1/2}$=1.45m). The implantation was performed through an aluminum foil with a thickness of 200 μm, so that the ^{57}Mn probes stopped at approximately 200 μm from the surface of the Si sample. The total fluence of ^{57}Mn was 2×10^{12} ^{57}Mn/cm^2 typically for one spectrum.

The spectra from 300 K to 700 K can be fitted by two Lorentzians corresponding to Fe atoms at interstitial and substitutional sites. The interstitial fraction decreases markedly at about 600 K. The results are in good agreement with those of previous experiments.[3,4] On the other hand, the spectra from 800 K to 1200 K (Fig. 1), which are successfully obtained for the first time, can be analyzed only by a broad singlet. The total area decreases up to 800 K with increasing temperature, as expected from a Debye model. The area, however, suddenly decreases at 900 K and 1000 K, but increases again at 1100 K. The center shift of the substitutional component shows a strong deviation from the second-order Doppler shift in the temperature region between 600 K and 1000 K.

The relaxation behaviors observed in the present experiment can be interpreted in terms of a diffusion-reaction process of interstitial Fe atoms with vacancies within the time scale of 100 ns, leading to the formation of substitutional Fe atoms in the Si matrix. The process must be related to the recovery processes from the nonequilibrium state to the equilibrium state of the Si lattice around the ^{57}Fe nuclear probes.

*1 Shizuoka Institute of Science and Technology, Japan
*2 Department of Physics, Tokyo Institute of Technology
*3 Institute for Nuclear and Radiation Physics, Physics Department, Leuven, Belgium

References

1) A. Istratov, H. Hieslmair and E. R. Weber; Appl. Phys. **A69**, 13 (1999).
2) H. P. Gunnlaugsson, G. Weyer et al.; Appl. Phys. Lett. **80,** 2657 (2002).
3) Y. Yoshida; in ALTECH 2003 Analytical and Diagonistic Techniques for Semiconductor Materials, Devices, and Processes, **479** (2003); Y. Kobayashi, Y. Yoshida et al.; Hyperfine Interactions, **126**, 417（2000）; Y. Yoshida, K. Kobayashi et al.; Defect and Diffusion Forum **194-199**, 611 (2001).
4) Y. Yoshida, Y. Kobayashi, K. Hayakawa, K. Yukihira, A. Yoshida, H. Ueno, F. Shimura and F. Ambe; Physica B, **376-377**, 69 (2006).
5) Y. Yoshida, S. Ogawa and K. Arikawa; Physica B, **340-342**, 605 (2003).
6) Y. Yoshida, S. Horie, K. Niira, K. Fukui and K. Shirasawa; Physica B, **376-377**, 227 (2006).

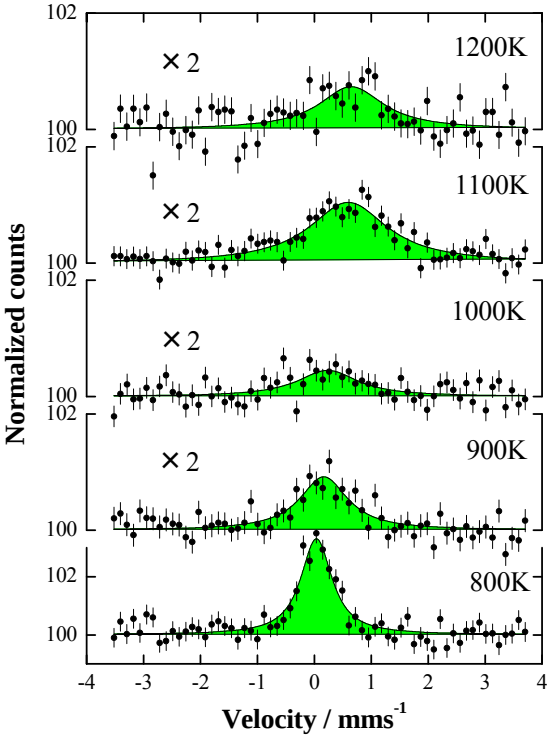

Fig. 1. Mössbauer spectra of ^{57}Mn/^{57}Fe in n-type Si measured from 800 K to 1200 K. Notice that the vertical scale for the spectrum at 800 K is different from those for the others.

^{99}Ru Mössbauer spectroscopic studies of $SmRu_4P_{12}$ †

S. Tsutsui,[*1] Y. Kobayashi, T. Okada, H. Haba, H. Onodera,[*2] Y. Yoda,[*1] C. Sekine,[*3] I. Shirotani,[*3] D. Kikuchi,[*4] H. Sugawara,[*5] and H. Sato[*4]

$SmRu_4P_{12}$ is one of the attractive compounds among filled skutterudites. Its electric resistivity shows a metal-insulator transition at T_{MI} = 16 K similar to that of the isomorphous $PrRu_4P_{12}$. The specific heat measurement with an applied magnetic field suggests that successive transitions occur around T_{MI}. The magnetic susceptibility of $SmRu_4P_{12}$ shows a cusp around 14 K, suggesting an antiferromagnetic ordering. The successive transitions were initially ascribed to antiferroquadrupole and antiferromagnetic orderings, since the entropy at T_{MI} reached R*log* 4 and the magnetic phase diagram was similar to that of $Ce_{1-x}La_xB_6$. However, the recent results obtained by macroscopic methods, such as those used in ultrasound experiments, have suggested the possibility of the transition being due to magnetic octupole ordering instead of the quadrupole ordering. The clear jumps of the specific heat and antiferromagnetic-like temperature dependences of the magnetic susceptibility in $SmRu_4P_{12}$ resemble those in NpO_2, which is a typical system showing the octupole ordering.

We have carried out the X-ray absorption spectroscopy, ^{149}Sm nuclear resonant forward scattering, and ^{99}Ru Mössbauer spectroscopy of $SmRu_4P_{12}$. X-ray absorption spectra indicate that Sm ions are trivalent up to 14 K. Quantum beats due to magnetic dipolar ordering are observed at 4.5 K in the ^{149}Sm nuclear resonant forward scattering. The temperature dependence of time-integrated intensity in the ^{149}Sm nuclear resonant forward scattering suggests that the magnetic dipolar ordering occurs immediately below the metal-insulator transition temperature. We have also carried out ^{99}Ru Mössbauer spectroscopy. The source nuclide ^{99}Rh ($T_{1/2}$ = 15.0 d) was prepared by the ^{99}Ru(p,n)^{99}Rh reaction with 12 MeV protons accelerated by the AVF Cyclotron.

The ^{99}Ru Mössbauer spectra of $SmRu_4P_{12}$ obtained at 5 and 77 K are shown in Fig. 1. The spectra could be analyzed satisfactorily with typical doublets in the absence of a magnetic field. This implies the absence of transferred hyperfine interactions or the accidental cancellation of transferred hyperfine interactions at the ^{99}Ru nuclei. The present result suggests a magnetic ordering accompanied by a magnetic dipole moment at the metal-insulator transition temperature in $SmRu_4P_{12}$ in spite of the proposal of the magnetic ordering accompanied by a T^{β}-type octupole.

.

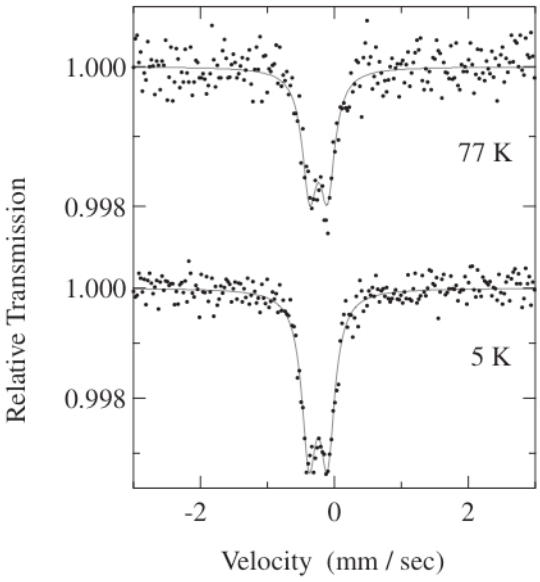

Fig. 1. ^{99}Ru Mössbauer spectra of $SmRu_4P_{12}$ at 77 and 5 K.

† Condensed from the article in *J. Phys. Soc. Jpn.*, **75** (2006) 093703.

*1 Japan Synchrotron Radiation Research Institute (SPring-8)
*2 Graduate School of Science, Tohoku University
*3 Department of Electric and Electronic Engineering, Muroran Institute of Technology
*4 Department of Physics, Tokyo Metropolitan University
*5 Faculty of Integrated Arts and Sciences, University of Tokushima

Continuum luminescence of α-alumina under heavy-ion irradiation

M. Koshimizu*, K. Kimura, H. Ryuto, K. Asai*, and M. Kase

Fast processes occurring along an ion trajectory are known to be characterized by high-density electronic excitation. Permanent irradiation effects, particularly, the formation of an ion track, should be profoundly related to these processes, e.g., interaction among excited states at a high density or that between excited electrons and a lattice system. We have been concerned mainly on the involvement of the self-trapping of charge carriers or excitons in track formation. This involvement has already been reported[1]; however, there have been few experimental reports regarding this. In this report, we present a study of α-alumina luminescence under heavy-ion irradiation, for which there have been many experimental reports on luminescence properties in a VUV-UV-VIS region under X-ray or electron irradiation[2,3].

One of the authors (K. K.) has already reported the time-resolved luminescence spectra of α-alumina under heavy ion irradiation[4] and found an ultrafast luminescence band in a UV region. Also, we have reported that the decay rate of the luminescence band in the VUV region increases with increasing excitation density[5]. In both cases, the ultrafast decay of the luminescence band under high-density excitation has been ascribed to the large oscillator strength of the collective excited states analogous to the electron-hole plasma in semiconductors[6]. In this report, we focus on the luminescence between the two luminescence bands in the UV and VUV regions indicated above.

The measured sample was a single crystal of α-alumina. The sample was irradiated with Xe ions at an energy of 2.0 MeV/nucleon at 3.3 K. Time-resolved luminescence spectra were obtained by a single-photon counting method. The time resolution of the entire measuring system was smaller than 100 ps.

The time-resolved luminescence spectrum of the α-alumina irradiated with Xe ions is shown in Fig.#1 In addition to the prominent luminescence band at about 170 nm, luminescence continuum exists at a longer wavelength into the UV region, where no fast luminescence band is observed for low-density excitation. The decay curve of the luminescence intensity at 219.4 nm is also shown in Fig.#2. It is clearly seen that the decay curve of the luminescence continuum can be described with a single exponential decaying function convolved with the resolution function and that its lifetime is as short as about 100 ps. This continuum prevails over the UV region toward the luminescence peak in the UV region reported previously[4].

The possible origin of the continuum is described as follows. Because the lifetime of the continuum is similar to the fast component of the UV and VUV bands, it is natural to consider that the origin of the continuum is the same as that of the bands, i.e., the high-density electron-hole pair analogous to the electron-hole plasma in semiconductors. In addition, no intrinsic luminescence band has been observed in this wavelength region. Here, we propose the hot luminescence of the collective excitation state as a possible origin. In the case of low-density excitation under X-ray or electron irradiation, luminescence occurs at the energy minima in the configuration coordinate, which leads to the discrete luminescence bands in the UV and VUV regions. In contrast, in the case of high-density excitation under heavy-ion irradiation, because of the short luminescence lifetime, luminescence occurs even at states other than the energy minima in the configuration coordinate before relaxation to the minima, which leads to the luminescence continuum.

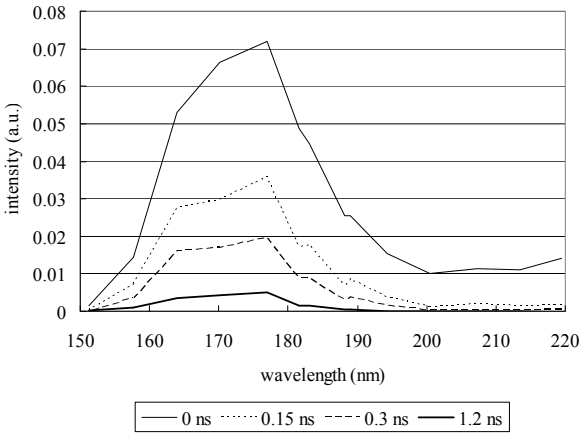

Fig.1 Time-resolved luminescence spectrum of α–alumina irradiated with Xe ions at 3.3 K.

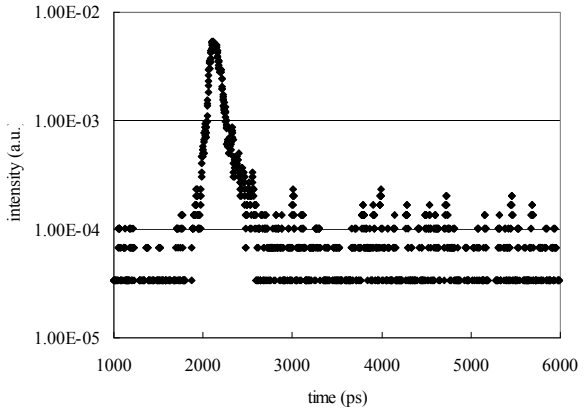

Fig.2 Decay curve of luminescence intensity at 219.4 nm.

* Department of Applied Chemistry, Graduate School of Engineering, Tohoku University

References

1) N. Itoh and A.M. Stoneham, Nucl. Instrum. Methods Phys. Res. B **146**, 362 (1998).
2) J. Valbis and N. Itoh, Radiat. Eff. Defects in Solids **116**, 171 (1991).
3) M. Kirm, G. Zimmerer, E. Feldbach, A. Lushchik, Ch. Lushchik, and F. Savikhin, Phys. Rev. B **60**, 502 (1999).
4) K. Kimura, J. Kaneko, S. Sharma, W. Hong, and N. Itoh, *Phys. Rev. B* **60**, 12626 (1999).
5) M. Koshimizu, K. Kimura, H. Ryuto, K. Asai, and M. Kase, RIKEN Accel. Prog. Rep. **39**, 94 (2005).
6) C. Klingshirn and H. Haug, Phys. Rep. **70**, 315 (1980).

Ultra-short-pulse continuum of ion track: Release of spectral missing in alkali halides

Kazuie Kimura, Masanori Koshimizu[*1], Hiromichi Ryuto, Keisuke Asai[*1], and Masayuki Kase

Heavy-ion irradiation can deposit extremely vast and dense energy in solids. However, time integrated luminescence spectra has not revealed so different luminescence from those obtained by electron (or photo-) irradiation. Otherwise, measurement of fast time-resolved luminescence (<100ps) could observe quite new luminescence. Namely, almost all insulator crystals irradiated by heavy ions present broad and ultra-fast (<100ps) pulsed luminescence continuum (UFLC) which has not observed so far. Succeeding studies have characterized the new luminescence as follows. Since the first observation for alumina[1], studies have been extended to number of crystals: Almost all alkali halides except for NaI, metal oxides as TiO_2, SiO_2, MgO, Al_2O_3, a semiconductor like CdS, and a few kind of diamonds. UFLC was observed universally in all the heavy-ion irradiated insulator crystals except for diamonds. UFLC is very broad but structured continuum from vacuum ultraviolet region to a visible end. Its efficiency increases largely with increasing atomic number of a projectile ion, i.e. excitation density, moreover super linearly in many cases. This means that. the luminescence process is due to multi orders. It is, nevertheless, significant that decay curves are close to exponential. Also, luminescence efficiency shows large material dependence. For examples, the luminescence efficiency for KI is about 100 times larger than that for KCl, furthermore diamonds does not emit UFLC. Also, it is worth noting that the continuum has structures. The band peaks position near the luminescence peaks of the known luminescence bands. The structure may be explained because the continuum feels the similar potentials to those in case of known luminescence derived at self-trapped holes, defect-, and impurity- centers. Recent studies shows that hole formation takes only few ps while systems comprised of electrons like the self-trapped exciton take as long as 100 ps. On balance, the UFLC may be owing to electrons at higher levels of states quantized under potential by holes. Such electrons are considered to be those released densely by ionization and returned to the cylindrical hole of the track core[1]. Such electrons may exist adjacently because of extremely high-density by heavy ion irradiation. The UFLC is, we propose, a kind of induced radiation which originates from the interactions among the electrons near continuum levels. Then, UFLC would be better to be renamed as ion track luminescence continuum (ITLC).

In this report, we show that so-called spectral missing[2] known in alkali halides can be released in case of ITLC. Recently, self-trapped excitons (STE) in alkali halides were found to have three morphologies, type I, II and III[2] by means of systematic experiments. An alkali halide however does not have three STE luminescence bands although it has three morphologies, but has usually two bands. One band of the three types I, II, and III is used to be missing in luminescence. Figure 1 shows the missing for 9 alkali halides by combinations of 3 alkalis x 3 halogens. The slightly inclined lines show positions of the type I, II, and III with change in alkali metals from Na to Rb, where solid lines show actual STE luminescence and dotted lines show missing in luminescence. The triplet bands are shaded and the singlet band not shaded. These data belongs to electron or photo-irradiation at 4.2 K. Results of ITLC for Xe-ion irradiation are shown by broken lines. One may see that ITLC exists at every missing position. This may be interpreted because the potential due to dotted lines are too shallow for electrons to stay in enough period to make STE luminescence, but ITLC need not long stay because of strong radiative interaction by extremely dense electron-hole pairs.

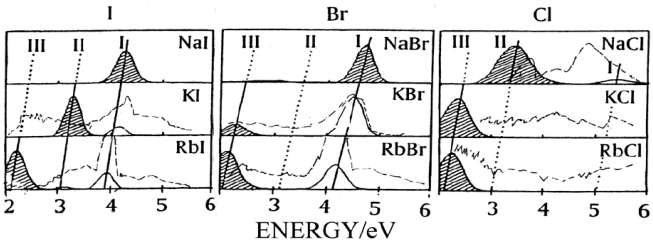

Fig. 1. STE luminescence spectra of nine alkali halides, with predominantly triplet bands shaded and predominantly singlet bands not shaded. STEs are categorized into three types I, II, and III. A dotted line means that anticipated luminescence bands are missing. TLC, time resolved luminescence at time 0 with Xe-ion irradiation, are shown by broken lines.

References

1) K. Kimura, J. Kaneko, S. Sharma, W. Hong, and N. Itoh: Phys. Rev. B **60**, 12626 (1999); K. Kimura: Nucl. Instr. Meth. Phys. Res., B **212**, 123 (2003).
2) K. S. Song and R. T. Williams: in *Self-trapped excitons*, (Springer, Berlin, 1993) p.168

*1 Department of Applied Chemistry, Graduate School of Engineering Tohoku University

Displaced-*T* site occupancy of hydrogen in Nb alloyed with a high concentration of Mo†

E. Yagi,*1 S. Koike,*2 T. Sugawara,*3 T. Shishido,*3 T. Urai, and K. Ogiwara

An interaction of hydrogen with solute atoms in metals is one of the fundamental problems on the behaviour of hydrogen in metals. In order to elucidate the mechanism for the effect of solute atoms on various properties of hydrogen, knowledge of the state of hydrogen, especially its lattice location is highly required. However, such information has been extremely limited, because of experimental difficulties. To locate deuterium D, both neutron diffraction method and channelling method with a ^{3}He beam are useful, and a number of experiments have been carried out, but for hydrogen H there had been only a few neutron experiments because of its experimental difficulties and no channelling experiments despite their usefulness. As the behaviour of H is not necessarily the same as that of D as recognized, e.g., in a phase diagram between metal-H and metal-D systems, experiments on H are indispensable. Hence, to study the lattice location of H the channelling method utilizing a nuclear reaction ^{1}H(^{11}B, α)$\alpha\alpha$ with a ^{11}B beam of about 2 MeV has been developed.[1,2] In this method hydrogen can be detected by measuring emitted α-particles. Yields of both ^{11}B ions backscattered by host metal atoms and α-particles are measured as a function of the incident angle of a ^{11}B beam by tilting the crystal around a channel in question. From such channelling angular profiles the lattice location of hydrogen is determined.

We have been investigating the atomic state of H in Nb-based Nb-Mo alloys on the basis of its lattice location determined by the channelling method described above. Nb is one of the group V_a metals in the periodic table and it is alloyed here with an element smaller than itself, Mo. Regarding the terminal solubility of hydrogen (TSH) in the group V_a metals, it has been reported that undersized metal solutes increase the TSH rapidly with solute concentration up to a certain solute concentration. One of the objectives of the study for the Nb-Mo alloys is to obtain information helpful to understand the effect of undersized solutes on the TSH. In addition, the Nb-Mo system forms a solid solution over the entire Mo concentration (C_{Mo}) range, keeping a bcc crystal structure with decreasing lattice parameter from that of Nb to that of Mo. The TSH in Nb at room temperature is about 3 % in the hydrogen-metal atom ratio (C_H=[H]/[M]), whereas it is very low in Mo. It is considered, therefore, that this alloy system provides the stage suitable for H to show various states in a bcc lattice. The systematic study on the C_{Mo} dependence of the location of H is expected to give information on the fundamental properties of H in a bcc crystal.

The location of H has hitherto been studied up to C_{Mo}=26 at.%. In Nb hydrogen is located at a terahedral (T) site. At low C_{Mo}, hydrogen is trapped by a Mo atom at room temperature to be displaced from a T site by about 0.6 Å towards its nearest neighbour lattice point, i.e., a Mo atom (trapped site; T_{tr}).[3] At high C_{Mo}, 20 at.%Mo, hydrogen is not observed at such T_{tr} sites, but 70-80 % of H atoms are located at T sites and 20-30 % of them are at octahedral (O) sites for low C_H.[4] At 26 at.%Mo, most of H atoms are located at T sites.[5] The site occupancy of hydrogen changes sensitively with C_{Mo}. In the present study the location of H in a more concentrated 52 at.%Nb-48 at%Mo alloy has been investigated at room temperature for C_H=2.8 and 5.5 %. Figure 1 shows the channelling angular profiles obtained for C_H=5.5 %, indicating that hydrogen occupies a site different from T and T_{tr}. From an analysis it is concluded that 75-85% of H atoms are located at sites displaced from T sites by about 0.3 Å towards their nearest neighbour O sites. These sites are similar to the displaced-T sites which were observed in V under applied stress (stress-induced site change).[2] The site change of H observed on alloying with 48 at.%Mo is considered to be due to lattice distortion introduced by alloying with high concentration of Mo.

---

† Condensed from the article in J. Phys. Soc. Jpn. **75,** 034802 (2006)

1 RIKEN and The School of Sci. and Eng., Waseda University

2 Department of Physics, Tokyo University of Science

3 Institute for Materials Research, Tohoku University

References
1) E. Yagi, T. Kobayashi, S. Nakamura, Y. Fukai, and K. Watanabe: J. Phys. Soc. Jpn. **52**, 3441 (1983).
2) E. Yagi, T. Kobayashi, S. Nakamura, F. Kano, K. Watanabe, Y. Fukai, and S. Koike: Phys. Rev. B **33**, 5121 (1986).
3) E. Yagi, S. Nakamura, F. Kano, T. Kobayashi, K. Watanabe, Y. Fukai, and T. Matsumoto: Phys. Rev. B **39**, 57 (1989).
4) E. Yagi and S. Koike: J. Phys. Soc. Jpn. **67**, 340 (1998).
5) E. Yagi, S. Koike, T. Matsumoto, T. Urai, and K. Ogiwara: Phys. Rev. B **66**, 024206 (2002).

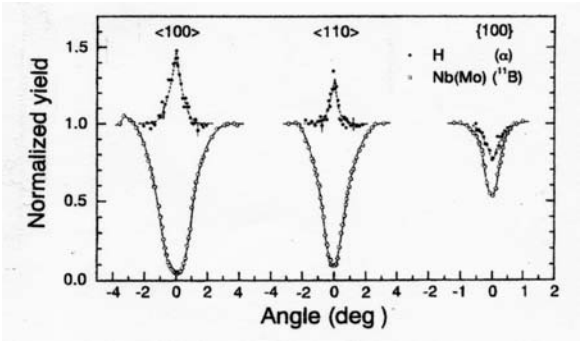

Fig. 1. Channelling angular profiles obtained for the 52 at.%Nb-48 at.%Mo alloy with hydrogen of C_H=5.5

Production of microbeam of slow highly charged ions with tapered glass capillary†

T. Ikeda, Y. Kanai, T. M. Kojima, Y. Iwai, T. Kambara, M. Hoshino*1, T. Nebiki*2, T. Narusawa*2, and Y. Yamazaki*3

We have developed a method of collimating a slow highly charged ion (HCI) beam with a single tapered glass capillary. Even if the initial beam has a relatively poor emittance, the glass capillary can realize a beam size down to the micrometer range, maintaining the initial charge state and kinetic energy. By considering the high reactivity of slow HCIs with the wall surface, one can conclude that the ions never touch the inner wall of the glass capillary during transmission. A self-organized charge-up of the glass capillary inner wall is expected to play a vital role in these interesting phenomena. [1–3] A similar glass capillary was used to transport a proton or He ion beam in the MeV range[4]. In this case, however, the beam touches the inner wall and suffers from a small angle scattering with the wall surface during the transport.

Slow HCIs have a high capability of modifying surfaces and cause efficient sputtering without markedly damaging the substrate. For example, a single HCI induces a nanometer dot on graphite[5–7] and Al_2O_3 surfaces.[5] It was also found that the F-Si bond direction of a Si(001)-F surface can be reconstructed from the three-dimensional momentum distribution of F^+ ions desorbed by slow HCIs; i.e., a stereochemical analysis can be performed with slow HCIs.[8] Once a microbeam is available, these functions specifically for slowing HCIs can be used to realize, e.g., the micropatterning of nanodots and element-sensitive microimaging. Note that a microbeam of slow HCIs was not practically available because the HCI beam is relatively weak and its emittance is poor.

An ion beam of 8 keV Ar^{8+} was extracted from a 14.5 GHz Caprice electron cyclotron resonance ion source at RIKEN, and then transported to an experimental chamber via an analyzing magnet. The ion beam was then collimated by a 2 mmϕ aperture (Fig. 1(a)), injected in a tapered glass capillary, and finally detected by a position-sensitive detector (PSD) via a deflector. The divergence of the incoming beam after the aperture was at most $\pm$3.3 mrad. The deflector was used for the charge-state analysis of the transmitted ions. The outer and inner diameters of the glass capillary at the inlet were 2 and 0.8 mm, and 55 and 24 μm, respectively at the outlet. The typical length of the glass capillary was 50 mm (Fig. 1(b)). To

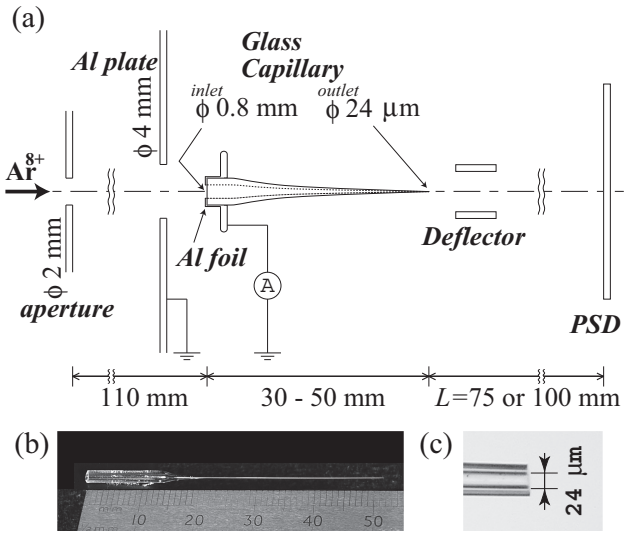

Fig. 1. (a) Schematic view of the experimental setup, (b) image of the tapered glass capillary, and (c) microscopic image of capillary outlet.

avoid macroscopic charge-up of the entrance surface of the glass capillary, it was covered by an Al foil with a 0.8 mm hole. The foil was used to monitor incoming ion currents of 0.1 - 5 pA. The secondary electron yield for several keV Ar^{8+} ions from the Al foil is expected to be $\sim$7; [9] the real current should be reduced 0.47-fold. The ion current injected in the 0.8 mm hole of the glass capillary was evaluated from the beam diameter on the Al foil and the hole diameter. The incident currents hereafter correspond to the corrected current mentioned above. The PSD consisted of a stack of multichannel plates and a wedge-and-strip-type anode and its detection efficiency was $\sim$50 %.

The glass capillary was made of borosilicate, which has a volume resistivity of $10^{15}\Omega$cm at 25 C and a softening temperature of 821 C. Tapered glass capillary was prepared by heating a straight glass tube, and then stretched by pulling both ends with a constant force. The taper angle can be controlled by tuning the temperature and force. Figure 1(c) shows a microscope image of such a capillary used for the present experiment.

We observed the transmission of an ion beam as a function of time for the tapered glass capillary injected with an 8 keV Ar^{8+} ion beam of 0.2 pA ($\sim 1.5\times10^5 Ar^{8+}$ions/s) with a stability of $\sim$10 %. It

† Condensed from article in Appl. Phys. Lett. **89**, 163502 (2006)

*1 Department of Physics, Sophia University
*2 Kochi University of Technology
*3 Also at the Institute of Physics, University of Tokyo

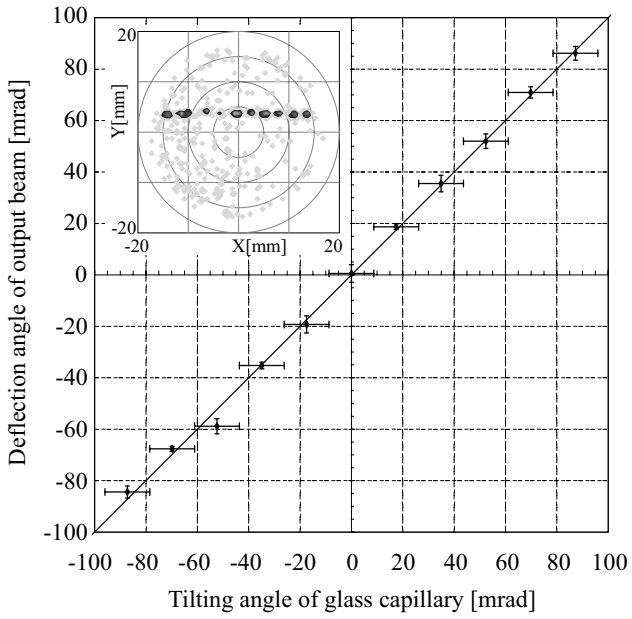

Fig. 2. Tilting angle dependence of peak position for incident current of ∼0.01 pA: The horizontal axis is the tilting angle. The vertical axis corresponds to the reconstructed deflection angle of the beam from the peak positions at the PSD. The horizontal and vertical error bars show the accuracy of the tilting dial reading and the spot size (FWHM), respectively.

was observed that the transmission current increased slowly with a time constant of several tens of seconds, and then became stable for more than 1200 s. The peak count was about 1600 cps. The focusing factor, defined by the ratio of N_t/S_o to N_i/S_i, is estimated to be ∼10, where N_t is the number of transmitted ions, N_i is the number of injected ions into the glass capillary, and S_o and S_i are the geometrical outlet and inlet cross sections of the glass capillary, respectively. This factor depends on the taper angle, outlet size, and input current.

The upper left inset of Fig. 2 shows the position of the transmitted beam on the PSD (L=100 mm) when the glass capillary was tilted relative to the axis of the incident current of ∼0.01 pA. The relationship between the tilting angle of the glass capillary and the deflected angle of the beam is shown in Fig. 2, which proves that the beam was well guided to the direction of the glass capillary tilted by as large as 100 mrad. Note that the deflection angle is an order of magnitude larger than the half opening angle (∼8 mrad) of the tapered glass capillary when the cross section of the glass capillary along its axis is assumed to be trapezoid.

The charge-state distribution of the transmitted HCIs for an incident current of 0.3 pA was measured by biasing the deflector downstream of the glass capillary without tilting. The transmitted beam profile at the PSD (L=75 mm) showed a single spot, which corresponds to the initial charge, i.e., the transmitted ions were properly guided along the glass capillary without changing the incident charge state. The angular divergence of the transmitted beam was evaluated from the spot sizes and was found to be ∼ ±5 mrad.

Conventionally, magnetic and/or electrostatic lenses have been employed to produce microbeams. By using such lenses, a submicron ion beam of a few tens of keV range was reported,[10] wherein lenses with small aberration and an ion source with good emittance were employed. Our method presented here is not very sensitive to the initial beam with broad energy spread and divergence, and was realized just by a tiny tapered glass tube of ∼50 mm in length. In irradiation experiments, the beam position can be determined easily.

References

1) N. Stolterfoht, J.-H. Bremer, V. Hoffmann, R. Hellhammer, D. Fink, A. Petrov, and B. Sulik: Phys. Rev. Lett. **88**, 133201 (2002).
2) Y. Kanai, M. Hoshino, T. Kambara, Y. Yamazaki, R. Hellhammer, and N. Stolterfoht: 24th International Conference on Photonic Electronic and Atomic Collisions Abstract, Fr131 (2005).
3) Y. Kanai, M. Hoshino, T. Kambara, T. Ikeda, R. Hellhammer, N. Stolterfoht, and Y. Yamazaki: Nucl. Instrum. Methods Phys. Res., Sect. B **258**, 155 (2007).
4) T. Nebiki, T. Yamamoto, T. Narusawa, M. B. H. Breese, E. J. Teo, and F. Watt: J. Vac. Sci. Technol. A **21**, No.5, 1671 (2003).
5) I. C. Gebeshuber, S. Cernusca, F. Aumayr, and H. Winter: Int. J. Mass Spectrometry **229**, 27 (2003).
6) N. Nakamura, M. Terada, Y. Nakai, Y. Kanai, S. Ohtani, K. Komaki, and Y. Yamazaki: Nucl. Instrum. Methods Phys. Res., Sect. B **232**, 261 (2005).
7) M. Terada, N. Nakamura, Y. Nakai, Y. Kanai, S. Ohtani, K. Komaki, and Y. Yamazaki: Nucl. Instrum. Methods Phys. Res., Sect. B **235**, 452 (2005).
8) N. Okabayashi, K. Komaki, and Y. Yamazaki: Nucl. Instrum. Methods Phys. Res., Sect. B **205**, 725 (2003).
9) A. Arnau, F. Aumayr, P. M. Echenique, M. Grether, W. Heiland, J. Limburg, R. Morgenstern, P. Roncin, S. Schippers, R. Schuch, N. Stolterfoht, P. Varga, T. J. M. Zouros, and H. P. Winter: Surface Science Reports **27**, 113 (1997).
10) Y. Ishii, A. Isoya, and T. Kojima: Nucl. Instrum. Methods Phys. Res., Sect. B **210**, 70 (2003).

Auger electrons from excited N ions after passing through Ni microcapillaries

Y. Kanai, Y. Nakai, Y. Iwai, K. Nishio,[*1] H. Masuda,[*1] and Y. Yamazaki

When highly charged ions(HCIs) approach a metallic surface, multiple electrons from the surface transfer to the excited states of ions and hollow atoms/ions are produced. Previously, we measured X-rays[1–3] and visible lights[4] emitted from such excited ions in order to study hollow atom formation and its decay processes. We used a metallic microcapillary foil as a target to produce such excited ions, which permits us to study the final stage of the decay of excited ions[5]. Recently, we have started the measurements of Auger electrons emitted from excited ions produced by the interaction between HCIs and an inner wall of a microcapillary, which gives us information complementary to our previous X-ray measurements.

Experiments were performed at the Slow Highly Charged Ion facility in RIKEN. N^{6+}(25-60keV) ions from a 14.5GHz electron cyclotorn resonance ion source were used. Auger electrons, which were emitted from excited ions, were measured using an electrostatic analyzer at an observation angle of 0 with respect to the beam direction. A typical spectrum is shown in Fig. 1. Taking into account previous studies[6–8] using a flat metal target and theoretical calculations[9,10], the higher-energy region of the spectrum may be attributed to the K-LL Auger electrons emitted from hollow atoms, which have one K vacancy and many electrons in the L- and M-orbitals, and the lower-energy region to the K-LL Auger electrons from Li- and Be-like excited states.

To identify Auger transitions, we measured an electron spectrum at approximately 310-340eV and higher-energy resolution (1.5eV). The spectrum is shown in Fig. 2. Arrows indicate the K-LL Auger electron energies for Li- and Be-like N ions[9,10]. We observed a clear, single peak at 316eV, which can be attributed to the Auger electron from the ($1s2s2p\ ^4P$) states within our experimental error (1.5eV). These states were predicted by previous X-ray measurements[1].

References

1) S. Ninomiya et al.: Phys. Rev. Lett. **78**, 4557 (1997).
2) Y. Kanai et al.: Nucl. Instrum. Methods Phys. Res. B **233**, 103 (2005).
3) Y. Iwai et al.: Nucl. Instrum. Methods Phys. Res. B **235**, 468 (2005).
4) Y. Morishita et al.: Phys. Rev. A **70**, 012902 (2004).
5) Y. Yamazaki: Int. J. Mass Spectro. **192**, 437 (1999).
6) F. W. Meyer et al.: Phys. Rev. Lett. **67**, 723 (1991).
7) J. Limburg et al.: Phys. Rev. Lett. **73**, 786 (1994).
8) J. Ducrée et al.: Phys. Rev. A **58**, R1649 (1998).
9) R. Mann et al.: J. Phys. B **14**, 1161 (1981).
10) M. H. Chen: Phys. Rev. A **31**, 1449 (1985).

*1 Department of Applied Chemistry, Tokyo Metropolitan University

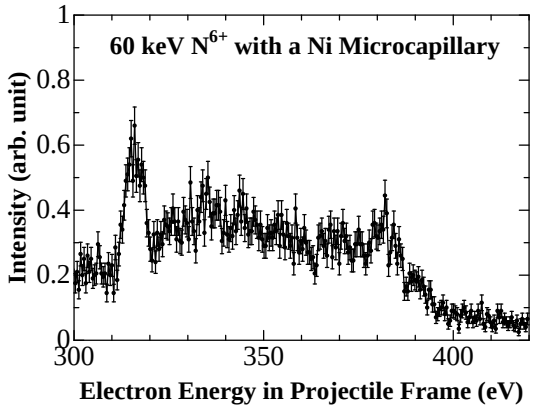

Fig. 1. Typical Auger electron spectrum for 60keV N^{6+} with an energy resolution of about 6eV. The higher-energy region (340-400eV) of the spectrum may be attributed to the K-LL Auger electrons from hollow atoms. K-LM Auger electron signals from excited states of Li-like ions may also exist at about 380eV. The lower-energy region (310-340eV) of the spectrum can be attributed to K-LL Auger electrons from excited states of Li- and Be-Like ions.

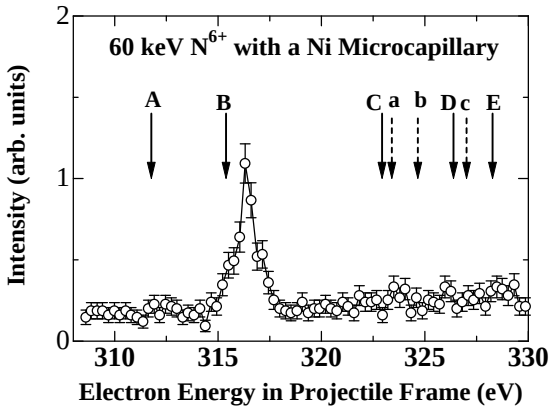

Fig. 2. High-energy-resolution spectrum for 60keV N^{6+}. Reported energy positions for K-LL Auger electrons are indicated by arrows. Corresponding excited states are A: ($1s2s^2\ ^2S$), B: ($1s2s2p\ ^4P$), C: ($1s2s2p\ ^2P$), D: ($1s2p^2\ ^4P$), E: ($1s2s2p\ ^2P$)[9], a: ($1s2s^22p\ ^3P$), b: ($1s2s2p^2\ ^5P$), and c: ($1s2s^22p\ ^1P$)[10]. A clear single peak at about 316eV can be attributed to the K-LL Auger electrons from ($1s2s2p\ ^4P$) excited states. The energy resolution was about 1.5eV.

Hyperfine structure of Rb and Cs atoms in superfluid helium

T. Furukawa, Y. Matsuo, A. Hatakeyama,[*1] T. Ito,[*2] Y. Ota,[*2] K. Fujikake,[*2] T. Kobayashi, and T. Shimoda[*3]

We have been studying the spin properties of impurity atoms in superfluid helium (He II) with the aim of establishing a versatile method for determining the nuclear moments of unstable nuclei[1]. Recently, we have measured the hyperfine resonances of alkali Cs atoms precisely using the sweep of microwave frequencies[2]. With the same system, we have also successfully measured the hyperfine resonances of alkali Rb atoms for the first time. In this report, we describe the experimental results of a measurement of the hyperfine structures of alkali Rb and Cs atoms immersed in superfluid helium (He II).

The experimental setup used is described in Ref. 2. In measuring the Rb hyperfine resonances, we used a RbCl crystal as a sample. The wavelengths of the pumping laser (cw Ti:Sapphire) and the monochromator are also tuned to the absorption (780nm) and emission (793nm) lines of Rb D1 transition in He II[3]. The other conditions are same as those described in Ref. 2.

Figure 1 shows LIF intensity as a function of microwave frequency. Considering the Zeeman effect[4], the hyperfine coupling constant A is determined from the peak frequencies. The preliminary values of the measured hyperfine coupling constants are listed in Table 1. The values are slightly different (0.5-0.6% larger) from those in vacuum, owing to the effects of He II pressure[5]. The differences in values of the constants of ^{85,87}Rb atoms are smaller than that of ^{133}Cs. This is probably due to the fact that Cs atoms are affected more strongly by the interaction from surrounding He atoms. The difference in the magnitude of interaction is attributed to the differences in factors such as atomic radius and the combined strength of valence electrons.

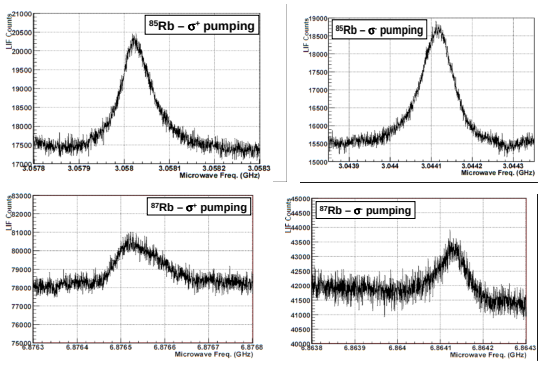

Fig. 1. Measured hyperfine transitions of ^{85}Rb (above) and ^{87}Rb with σ^+ (left) and σ^- (right) pumping.

*1 Dept. of Basic Sci., University of Tokyo
*2 Inst. of Phys., Meiji University
*3 Dept. of Phys., Meiji University

	He II (GHz)	vacuum (GHz)	ratio
^{133}Cs	2.31276(1)	2.29815794	1.006353(4)
^{85}Rb	1.01702(2)	1.01191092	1.00505(2)
^{87}Rb	3.43517(3)	3.41734131	1.005217(9)

Table 1. Hyperfine coupling constants of Rb and Cs atoms in He II (preliminary).

From the measured constants A of ^{85,87}Rb atoms in He II, we determined the nuclear magnetic moment of ^{87}Rb with repspect to the nuclear moment of ^{85}Rb. The hyperfine coupling constant A, nuclear spin I, and nuclear magnetic moment μ between the isotopes ^{a}X and ^{b}X are related as

$$\frac{A_a I_a}{\mu_I^a} = \frac{A_b I_b}{\mu_I^b} \times (1 + {}^a\Delta^b), \tag{1}$$

where $^a\Delta^b$ is a magnetic hyperfine anomaly[6]. From Eq. (1), neglecting hyperfine anomaly, the nuclear moment of ^{85}Rb is deduced as

$$\mu_I^{85Rb} = \mu_I^{87Rb} \times \frac{A^{85Rb}\ I^{85Rb}}{A^{87Rb}\ I^{87Rb}}, \tag{2}$$

where the nuclear moment $\mu_{I,HeII}^{85Rb} = 1.35784(1)\mu_N$ with the measured constants A in He II, and $\mu_{I,vacuum}^{85Rb} = 1.357782(1)\mu_N$ with the measured constants A in vacuum[7]. The actual nuclear moment of ^{85}Rb is $\mu_{I,true}^{85Rb} = 1.3533515(8)\mu_N$[8]. The deduced nuclear moment from the measured constants A in He II is slightly (<1%) different from the actual nuclear moment. This difference is attributed to the effect of hyperfine anomaly. From Eq. (1), the hyperfine anomaly for ^{85}Rb and ^{87}Rb in He II is deduced as ${}^{85Rb}\Delta_{HeII}^{87Rb} = -0.003307$ and that in vacuum is deduced as ${}^{85Rb}\Delta_{vacuum}^{87Rb} = -0.003474$.

The two hyperfine anomaly values are slightly (∼5%) different. The difference is probably due to the deformed (compressed) wave function of a valence electron in a Rb atom. The detailed mechanism of such a shift is still under investigation. We will calculate the atomic status in He II theoretically in the future.

References

1) T. Furukawa *et al.*: Phys. Rev. Lett. 96, 095301 (2006).
2) T. Ito *et al.*: RIKEN Accel. Prog. Rep. 40, to be published.
3) Y. Takahashi *et al.*: Phys. Rev. Lett. 71, 1035 (1993)
4) T. Furukawa *et al.*: RIKEN Accel. Prog. Rep. 39, 104 (2006)
5) Y. Takahashi *et al.*: Z. Phys. 98, 391 (1995).
6) S. Büttgenbach: Hyperfine Int. 20, 1 (1984).
7) E. Arimondo *et al.*: Rev. of Mod. Phys. 49, 31 (1977).
8) N.J. Stone *et al.*: Atomic Data and Nuclear Data Tables 90, 76 (2005).

Precise measurement of the hyperfine splitting of Cs atoms in superfluid helium

T. Itou,[*1] T. Furukawa, Y. Matsuo, A. Hatakeyama,[*3] T. Kobayashi, Y. Ota,[*1] K. Fujikake,[*1] H. Odashima,[*1] and T. Shimoda[*2]

Laser spectroscopy in superfluid He (He II) is an effective method of determining the nuclear moments of unstable nuclei from their hyperfine structure[1]. Atoms in He II show a shift and broadening of their atomic excitation spectra that are large, whereas the shift and broadening are relatively small in the emission stage, because implanted atoms reside in bubble-like cavities (He bubble)[2]. In contrast, the widths and frequencies of hyperfine resonant lines of the atoms in He II are very close to those in free space. Moreover, the electronic spin relaxation time of Cs atoms in He II is particularly long because of the spinless property of He atoms[3]. These findings suggest that the hyperfine and Zeeman sublevel structures are not strongly perturbed by surrounding He atoms. Therefore, the precise measurement of atomic hyperfine splitting is feasible in He II.

In this study, we measured the hyperfine transition of Cs atoms in the ground state obtained by observing laser-induced fluorescence (LIF)[2]. The experimental setup is shown in Fig. 1. The apparatus consisted of a cryostat chamber (Oxford) with quartz windows, a detection system, a microwave sweeping system, and three lasers. The bottom part of the cryostat contained liquid He. An open-top quartz cell ($70 \times 70 \times 70$ mm^3) was placed above the liquid surface and was filled with He II by transferring liquid He utilizing the fountain effect of He II. A CsI sample held about 1 cm above the quartz cell was ablated with an output of the third harmonic generation of a Nd:YAG laser (wavelength, 355nm; pulse energy, 3mJ; repetition rate, 10Hz; pulse width, 10ns) through one of the windows. Cs clusters produced by laser ablation and introduced into He II were dissociated to disperse Cs atoms in the observation region of He II by a femtosecond pulsed Ti:Sapphire laser (wavelength, 790nm; pulse energy, 150μJ; repetition rate, 500Hz; pulse width, 200fs). The densities of implanted Cs atoms were about 10^8-10^{10} cm^{-3} in He II. The other cw Ti:Sapphire laser (wavelength, 876nm; power, 150mW) for the optical pumping of Cs atoms were irradiated continuously into the observation region where a magnetic field of $\sim$ 5G was applied in the direction of the pumping laser. Then the implanted Cs atoms were optically pumped and polarized immediately. The optically pumped atoms were subjected to microwave radiation with frequency sweeping. The emitted photons were detected using a photomultiplier tube (PMT) through a monochromator set at a Cs emission wavelength of 892 nm, and the obtained signals were sent to a multi-channel scaler.

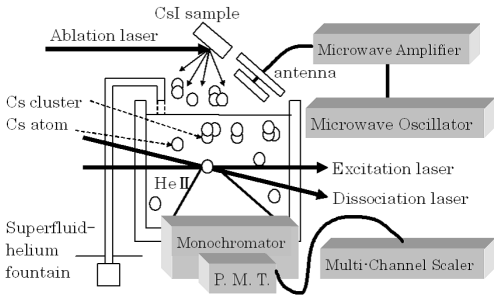

Fig. 1. Experimental setup.

Figure 2 shows the hyperfine transition spectrum of Cs atoms in He II. The peak position and width of the hyperfine resonant spectrum are 9.2580915(4) GHz and about 100 kHz, respectively. This narrow and clearly Lorentz-formed spectrum suggests the feasibility of a precise laser spectroscopic study of atoms in He II. A detailed discussion about the hyperfine structure in He II is described in Ref. 4

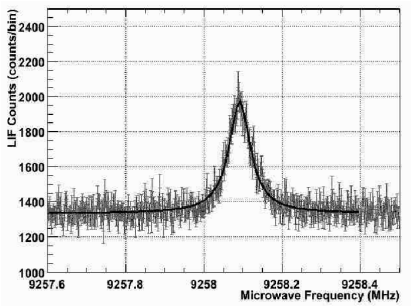

Fig. 2. Hyperfine transition spectrum of Cs atoms in He II.

References

1) T. Furukawa et al.: RIKEN Accel. Prog. Rep. **38**, 99 (2005).
2) B. Tabbert, H. Günther, and G. zu Putlitz: J. Low Temp. Phys. **109**, 653 (1997).
3) T. Furukawa et al.: Phys. Rev. Lett. **96**, 095301 (2006).
4) T. Furukawa et al.: RIKEN Accel. Prog. Rep. in press.

[*1] Department of Physics, Graduate School of Science and Technology, Meiji University
[*2] Department of Physics, Graduate School of Science, Osaka University
[*3] Institute of Physics, Graduate School of Arts and Sciences, The University of Tokyo

Properties of laser ablation plasma generated by high power Nd:YAG laser

T. Kanesue,[*1] S. Kondrashev,[*2] and M. Okamura

We have developed the Direct Plasma Injection Scheme (DPIS) that consists of the Laser Ion Source (LIS) and RFQ linac for extracting and accelerating highly charged intense ion beams from the laser ablation plasma. We succeeded in accelerating a 60 mA Carbon beam using DPIS[1)].

The performance of LIS strongly depends on the laser performance and it is nessesary to investigate the properties of the laser produced from plasma before performing acceleration experiments.

We used a 2.3 J / 6 ns Nd:YAG laser (1064 nm wavelength), Thales SAGA230. The estimated laser power density focused onto the solid state target with the convex lens (100 mm focal length) is $3.2 \times 10^{12}\ W/cm^2$. We investigated the laser ablation plasmas of C, Al, Fe, Ag and Ta, respectively. Charge state distribution, current density and the number of ions in the plasma were measured at a distance of 3.7 m from the target. The current density at an arbitrary position can be calculated with the relationship showing that the plasma current is proportional to L^{-3} (L : drift distance)[2)]. The details of the experimental procedure are shown in ref.[3)].

Table 1 shows the number of ions per shot under the RFQ injection condition (30 cm away from the target and ϕ 6 mm) and the current densities at 30 cm and 60 cm away from the target for the highest charge state. The data for the highest yield charge state are shown in Table 2. Here, current density represents the peak value of one pulse.

According to these tables, ions lighter than Fe should be acclerated with some mA-order using our scheme with the RFQ designed to accelerate charge to mass ratio (Q / M) = 1 / 3 ions, even considering the losses through injection. In contrast, Ag and Ta might not be accelerated with high intensity because we did not observe Q / M > 1 / 3 ions.

From these data, we succeeded in achieving 60 mA Al beam formation at the exit RFQ[4)]. We are preparing for Ag^{+15} acceleration using the new RFQ dedicated for Q / M = 1 / 8 (0.125).

- - - - -

References

1) M. Okamura, et al.: Rev. Sci. Instrum. 77, 03B303 (2006)
2) B. Yu. Sharkov, S. A. Kondrashev: Proc. EPAC96, Sitges, Spain, 1996, p. 1550
3) T. Kanesue, et al.: Proc. EPAC 2006, Edinburgh, Scotland, p. 1720
4) in this progress report

Table 1. Summary of plasma properties for highest charge state at 30 cm away from target.

Element	Highest charge state	Q / M	Number of particles	Current density $[mA/cm^2]$ at 30 cm	Current density $[mA/cm^2]$ at 60 cm
^{12}C	6	0.50	1.27×10^{11}	1458	182
^{27}Al	11	0.41	2.50×10^{10}	183	23
^{56}Fe	20	0.36	1.23×10^{9}	29	3.7
^{107}Ag	20	0.19	1.49×10^{8}	6.1	0.8
^{181}Ta	9	0.05	1.62×10^{9}	1.4	0.2

Table 2. Summary of plasma properties for highest yield charge state.

Element	Highest yield charge state	Q / M	Number of particles	Current density $[mA/cm^2]$ at 30 cm	Current density $[mA/cm^2]$ at 60 cm
^{12}C	6	0.50	1.27×10^{11}	1458	182
^{27}Al	10	0.37	4.72×10^{10}	746	93
^{56}Fe	16	0.29	1.70×10^{10}	520	65
^{107}Ag	15	0.14	2.19×10^{9}	119	15
^{181}Ta	4	0.02	1.06×10^{10}	28	3.5

*1 Department of Applied Quantum Physics and Nuclear Engineering, Kyushu University
*2 Institute of Theoretical and Experimental Physics, Moscow, Russia

Time-delay matrix analysis of several overlapping resonances

K. Aiba,[*1] A. Igarashi,[*1] and I. Shimamura

[Overlapping resonances, time delay, atomic scattering, photoionization, nuclear reactions]

Resonance structures often occur in the cross sections $\sigma(E)$ for multichannel scattering and photoionization. Such structures may be analyzed to extract resonance parameters, i.e., the position E_r, width Γ, and the shape parameter. However, the eigenphase sum $\delta(E)$ for the continuum wave function, which increases abruptly in a narrow resonance energy region, is more useful for resonance analysis than $\sigma(E)$; $\delta(E)$ satisfies the same Breit-Wigner formula as for the single-channel scattering phase shift.[1)] An even better technique is to detect sudden changes in $d\delta(E)/dE$.

The time-delay matrix $Q(E)$ $(=i\hbar S[dS^\dagger/dE])$ introduces another perspective,[2,3)] S being the S matrix and $S^\dagger$ its Hermitian conjugate. For $S(E)$ or $\delta(E)$ of *any* E-dependence, the trace $\mathrm{Tr}\,Q$ is related to δ by

$$2\hbar d\delta/dE = \mathrm{Tr}\,Q(E) \equiv \textstyle\sum_i Q_{ii}(E) = \sum_i q_i(E),$$

where $\{q_i(E)\}$ are the eigenvalues of the Q matrix.[3)]

When N resonances overlap each other, the analysis of $S(E)$ or $\sigma(E)$ is very complex, while $\delta(E)$ increases rapidly by $\sim N\pi$. Also, $\mathrm{Tr}\,Q(E)$ is expressible as a superposition of N Lorentzian profiles $L_\nu(E)$

$$\mathrm{Tr}\,Q(E) = \sum_\nu L_\nu(E) + 2\hbar d\delta_\mathrm{b}(E)/dE, \qquad (1)$$

δ_b being the background part of δ. We proved analytically for double resonances that two eigenvalues $\{q_i(E)\}$ take such Lorentzian shapes avoided from each other only near their crossing point.[4)] The $\{q_i(E)\}$ look almost like crossing Lorentzians if the avoidance is weak, but need careful examination for recognizing the avoided crossing if the avoidance is strong.

We examine the eigenvalues $\{q_i(E)\}$ for He(^{1}P^o) obtained by the hyperspherical coupled-channel method; see Fig. 1 for E below the energy of $He^+(n{=}5)$. Actually, most $\{q_i(E)\}$ are too small to distinguish from the base line, but many overlapping resonances are seen. The highest energy region of Fig. 1 is enlarged in Fig. 2. Rapid increase in $\delta(E)$ occurs twice in Fig. 2(a), suggesting two resonances. Another one emerges in $\mathrm{Tr}\,Q(E)$ in Fig. 2(b), showing that $d\delta/dE$ is a better probe of resonances than $\delta(E)$. An even more sensitive probe turns out to be $\{q_i(E)\}$ in Fig. 2(b). Obvious avoided crossings are observed, which, if diabatically connected, reveal as many as five Lorentzians. At least two of them would have been missed by the conventional means of analysing $\delta(E)$ or $d\delta(E)/dE$. The detailed structure in $\{q_i(E)\}$ having been uncovered, Eq. (1) with five Lorentzians is now fitted to the calculated $\mathrm{Tr}\,Q(E)$ of Fig. 2(b). Figure 2(c) includes all the obtained Lorentzians, which are effectively the diabatization of $\{q_i(E)\}$ and may be called *diabatic resonances*. This procedure affords a transparent visual understanding of the overlapping resonances.

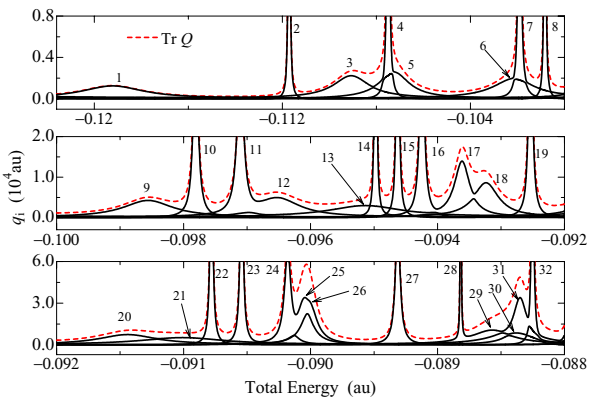

Fig. 1. The eigenvalues $\{q_i(E)\}$ of the time-delay matrix (E) for He(^{1}P^o) and their sum, Tr (E).

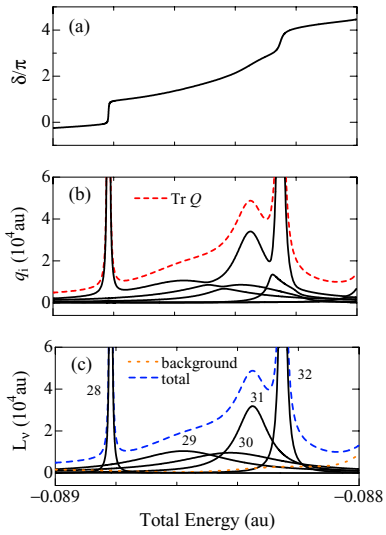

Fig. 2. (a) Eigenphase sum $\delta(E)$. (b) Eigenvalues $\{q_i(E)\}$ and their sum, Tr . (c) Lorentzians $L_\nu(E)$ representing diabatic resonances, the background, and their sum.

*1 Department of Applied Physics, University of Miyazaki

References

1) A. U. Hazi: Phys. Rev. A **19**, 920 (1979).
2) F. T. Smith: Phys. Rev. **118**, 349 (1960).
3) A. Igarashi and I. Shimamura: Phys. Rev. A **70**, 012706 (2004); J. Phys. B **37**, 4221 (2004).
4) I. Shimamura, J. F. McCann, and A. Igarashi: J. Phys. B **39**, 1847 (2006).

μSR study of the impurity e ects on the Cu-spin fluctuations in the overdoped $La_{2-x}Sr_xCu_{1-y}Zn_yO_4$

T. Adachi,[*1] Risdiana,[*1] N. Oki,[*1] S. Yairi,[*1] Y. Tanabe,[*1] K. Omori,[*1] T. Suzuki[*2] I. Watanabe[*2] A. Koda[*3] W. Higemoto[*4] and Y. Koike,[*1]

In the La-214 high-T_c system, the dynamical stripe correlations of spins and holes tend to be pinned and statically stabilized not only by the characteristic structure of the tetragonal low-temperature structure[1] but also by nonmagnetic Zn impurities.[2] So far, impurity effects on Cu-spin dynamics and superconductivity in the underdoped regime of $La_{2-x}Sr_xCu_{1-y}Zn_yO_4$ with $x \leq 0.15$ have been investigated by zero-field (ZF) muon-spin-relaxation (μSR) measurements.[2,3] It has been found that the Cu-spin fluctuations around Zn exhibit a slowing down due to the pinning of the dynamical stripe correlations by Zn, leading to the formation of a static stripe order and the destruction of superconductivity around Zn. It is clear that the static stripe order competes with superconductivity, but the dynamical stripe correlations may play an important role in the appearance of superconductivity. If this is the case, similar impurity effects must be observed not only in the underdoped regime but also in a wide hole concentration range.

Therefore, we have investigated Zn-impurity effects on Cu-spin fluctuations by μSR measurements in the overdoped regime of $La_{2-x}Sr_xCu_{1-y}Zn_yO_4$ with $x =$ 0.18 0.30 and $y = 0$ 0.10 to elucidate whether or not the stripe-pinning model holds well even in the overdoped regime of $La_{2-x}Sr_xCuO_4$. Polycrystalline samples prepared by the ordinary solid-state reaction method were used in ZF-μSR measurements at the RIKEN-RAL Muon Facility in the UK and at the KEK-MSL in Japan.

The ZF-μSR time spectra of $La_{2-x}Sr_xCu_{1-y}Zn_yO_4$ with $x = 0.18$ 0.30 and $y = 0.03$ at 0.3 K are shown in Fig. 1. In samples with $x = 0.18$ 0.27, an exponential-like depolarization of muon spins is observed, indicating the Zn-induced slowing down of Cu-spin fluctuations. The rate of such depolarization systematically decreases with increasing x and almost no fast depolarization of muon spins is observed for $x = 0.30$, at which superconductivity disappears. The present results suggest that dynamical stripe correlations exist in a wide range of x's where superconductivity appears and that the stripe-pinning model holds well in the overdoped regime as well as in the underdoped regime. These results are consistent with those of the inelastic neutron-scattering experiment on $La_{2-x}Sr_xCuO_4$ with $x = 0.25$ 0.30,[4] in which the maximum dynamic spin susceptibility of the incommensurate magnetic peaks, $\chi''(\omega)$, decreases linearly with increasing x and disappears at $x = 0.30$. The present results also indicate that there is no quantum critical point at $x \sim 0.19$, as proposed by Panagopoulos et al.[5] In addition, the phase-separation model in the overdoped regime[6] is also consistent with the present results, because the maximum depolarization rate of muon spins decreases with increasing x in agreement with the decrease in superconducting volume fraction. That is, superconducting and normal-state regions may be phase-separated in an overdoped sample of $La_{2-x}Sr_xCuO_4$.

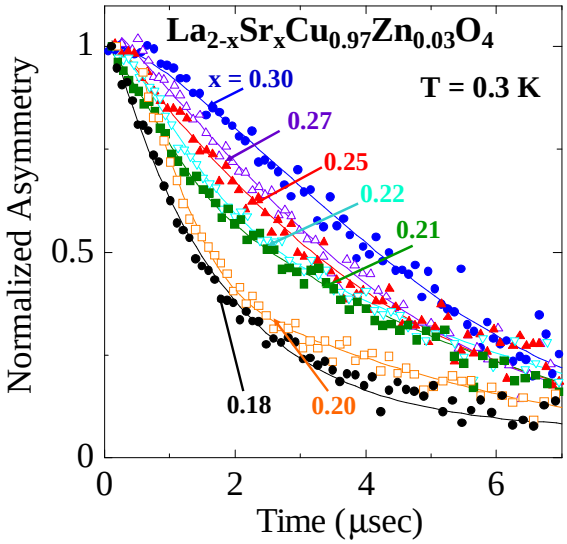

Fig. 1. Zero-field SR time spectra of $La_{2-x}Sr_xCu_{0.97}Zn_{0.03}O_4$ with $x = 0.18 - 0.30$ at 0.3 K

References
1) J. M. Tranquada et al.: Nature **375**, 561 (1995).
2) T. Adachi et al.: Phys. Rev. B **69**, 184507 (2004).
3) Y. Koike et al.: Physica C **426-431**, 189 (2005).
4) S. Wakimoto et al.: Phys. Rev. Lett. **92**, 217004 (2004).
5) C. Panagopoulos et al.: Phys. Rev. B **69**, 144510 (2004).
6) Y. Tanabe et al.: J. Phys. Soc. Jpn. **74**, 2893 (2005).

[*1] Department of Applied Physics, Tohoku University
[*2] The Institute of Physical and Chemical Research (RIKEN)
[*3] Muon Science Laboratory, Institute of Materials Structure Science, High Energy Accelerator Research Organization (KEK-IMSS)
[*4] Advanced Science Research Center, Japan Atomic Energy Agency (JAEA)

μSR study of the impurity e ects on the Cu-spin fluctuations in electron-doped high-T_c superconductor $Pr_{0.86}LaCe_{0.14}Cu_{1-y}Zn_yO_{4+\alpha-\delta}$

Risdiana,[*1] T. Adachi,[*1] T. Suzuki,[*2] I. Watanabe,[*2] and Y. Koike[*1]

Although the mechanism of the superconductivity in high-T_c superconducting cuprates has not yet been clarified, a mechanism based upon the dynamical stripe correlations of spins and charges is a probable one[1]. So far, the effects of impurities on the Cu-spin dynamics and superconductivity have been investigated by zero-field (ZF) muon-spin-relaxation (μSR) measurements in the underdoped regime of $La_{2-x}Sr_xCu_{1-y}Zn_yO_4$ with $x < 0.15$[2]. It has been found that the fluctuations of Cu spins around Zn exhibit slowing due to the pinning of the dynamical stripes by Zn, leading to the formation of a static stripe order and the destruction of superconductivity around Zn. This is an interpretation called the stripe-pinning model. It is of great interest whether or not the stripe-pinning model holds even for the electron-doped high-T_c cuprates and whether or not the mechanism in the electron-doped high-T_c cuprates is different from that in the hole-doped ones. The study in the electron-doped high-T_c cuprates and the following comparison with the results of the hole-doped ones will lead to a general understanding of the mechanism of superconductivity. Therefore, we have investigated the effects of Zn substitution on the Cu-spin dynamics in electron-doped $Pr_{0.86}LaCe_{0.14}Cu_{1-y}Zn_yO_{4+\alpha-\delta}$ (PLCCZO) by ZF-μSR measurements at low temperatures down to 0.3 K, and increasing y to up to 0.05 and the oxygen-reduced value δ to up to 0.09.

Figure 1 shows the ZF-μSR time spectra of the suitably oxygen-reduced PLCCZO for various y values. For $y = 0$, Gaussian behavior is observed at high temperatures above $\sim$ 100 K due to randomly oriented nuclear spins, and an exponential depolarization of muon spins is observed at low temperatures below $\sim$ 50 K. The temperature-dependent change in the spectra above 20 K is regarded as being due to the static random magnetism of small Pr^{3+} moments[3]. It is found that the asymmetry A(t), namely, the μSR time spectrum in the long-time region above 5 μsec increases with decreasing temperature at low temperatures, suggesting the possible slowing of the Cu-spin fluctuations. It is interesting that the slowing of the Cu-spin fluctuations is observed even in the impurity-free sample. This may be due to the possible enhancement of the Cu-spin correlation assisted by the Pr^{3+} moments. The increase in A(t) in the long-time region at low temperatures is still observed for Zn-substituted samples with y up to 0.05. However, the temperature dependences of the spectra are similar regardless of the y value. That is, no Zn-induced slowing of the Cu-spin fluctuations is observed, which is very different from the case for hole-doped $La_{2-x}Sr_xCu_{1-y}Zn_yO_4$[2]. Possible reasons are as follows: (i) There may be no dynamical stripe correlations of spins and electrons in the electron-doped system. (ii) The effect of Pr^{3+} moments on the μSR spectra may be stronger than that of a small amount of Zn impurity.

To obtain conclusive results, another electron-doped cuprates without rare-earth moments should be used for the μSR measurements.

References

1) J. M. Trangquada et al.: Nature **375**, 561 (1995).
2) T. Adachi et al.: Phys. Rev. B **69**, 184507 (2004).
3) R. Kadono et al.: J. Phys. Soc. Jpn. **72**, 2955 (2003).

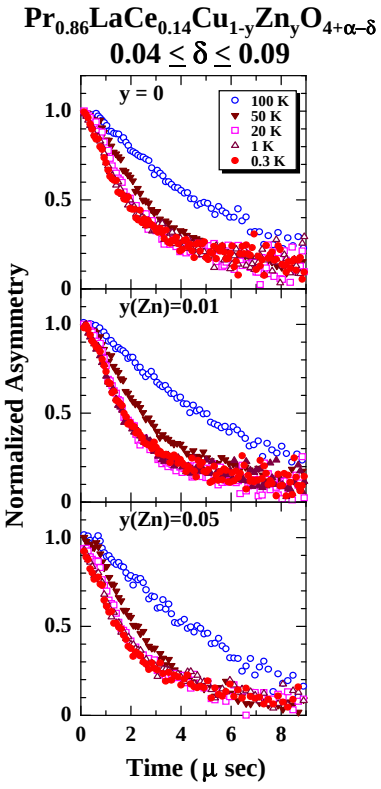

Fig. 1. ZF- SR time spectra of the suitably oxygen-reduced $Pr_{0.86}LaCe_{0.14}Cu_{1-y}Zn_yO_{4+\alpha-\delta}$ with = 0, 0.01, and 0.05 and $0.04 \leq \delta \leq 0.09$ at temperatures down to 0.3 K.

[*1] Department of Applied Physics, Tohoku University
[*2] The Institute of Physical and Chemical Research (RIKEN)

μSR study of impurity e ects on Cu-spin dynamics and superconductivity in $La_{2-x}Sr_xCu_{1-y}(Zn,Ni)_yO_4$ with $x = 0.15$

T. Adachi,[*1] N. Oki,[*1] Risdiana,[*1] S. Yairi,[*1] Y. Koike,[*1] and I. Watanabe[*2]

In recent years, the effects of nonmagnetic and magnetic impurities on the dynamical stripe correlations of spins and holes[1] have attracted attention. It has been proposed that the dynamical stripe correlations are pinned and stabilized by nonmagnetic Zn, leading to the strong suppression of superconductivity around the hole concentration per Cu, $p \sim 1/8$.[2] To clarify the relationship between Cu-spin dynamics and superconductivity, we have performed the zero-field muon-spin-relaxation (ZF-μSR) and magnetic-susceptibility, χ, measurements in Zn- or Ni-substituted $La_{2-x}Sr_xCu_{1-y}(Zn,Ni)_yO_4$ with $x = 0.13$, finely changing y up to 0.10, and have found a close relation between them.[3–5] Therefore, we have carried out ZF-μSR and χ measurements in optimally doped $La_{2-x}Sr_xCu_{1-y}(Zn,Ni)_yO_4$ with $x = 0.15$ and $y = 0$ 0.10, using sintered polycrystals, to clarify the relationship between Cu-spin dynamics and superconductivity.[6,7] The ZF-μSR measurements were performed at the RIKEN-RAL Muon Facility in the UK at temperatures down to 0.3 K.

The ZF-μSR time spectra of $La_{2-x}Sr_xCu_{1-y}(Zn,Ni)_yO_4$ with $x = 0.15$ and typical y values are shown in Fig. 1. At high temperatures above 15 K, all the spectra show Gaussian-like depolarization due to randomly oriented nuclear spins. For $y = 0$, the spectra are Gaussian-like down to 0.3 K, indicating that Cu spins fluctuate fast beyond the μSR time window (10^{-11} 10^{-6} s). At low temperatures, a fast depolarization of muon spins is observed for y(Zn)= 0.01, indicating the development of a magnetic correlation between Cu spins. Moreover, a fast depolarization and an almost flat spectrum with a normalized asymmetry of $\sim 1/3$ are observed for y(Zn)= 0.02 0.03, indicating the formation of an incoherent magnetic order.

In the case of Ni substitution, on the other hand, the spectra are Gaussian-like for y(Ni)= 0.01 and a fast depolarization is observed for y(Ni)$\geq$ 0.02. These results indicate that the formation of a magnetic order requires a larger amount of Ni than that of Zn, which is consistent with our previous result for $x = 0.13$.[5]

We have estimated the volume fractions of Cu-spin states with different fluctuation frequencies by fitting the time spectrum[4,5] and the superconducting (SC) state from the χ measurements on field cooling (Meissner volume fraction). It has been found that the volume fractions of both the SC region and the region in which Cu spins fluctuate fast beyond the μSR time window decrease strongly in the presence of a small amount of Zn and the decrease observed is stronger than that observed for Ni. Moreover, both fractions correspond to each other. These results can be interpreted as follows: both Zn and Ni tend to pin the dynamical stripe correlations so that superconductivity is destroyed around Zn and Ni. The area of non-SC and slowly fluctuating or static region of Cu spins around Zn is larger than that around Ni, suggesting that the pinning by Zn is stronger than that by Ni.

References

1) J. M. Tranquada et al.: Nature **375**, 561 (1995).
2) T. Adachi et al.: J. Low Temp. Phys. **117**, 1151 (1999).
3) I. Watanabe et al.: Phys. Rev. B **65**, 180516(R) (2002).
4) T. Adachi et al.: Phys. Rev. B **69**, 184507 (2004).
5) T. Adachi et al.: Phys. Rev. B **70**, 060504(R) (2004).
6) Y. Koike et al.: Physica C **426-431**, 189 (2005).
7) T. Adachi et al.: Physica C (2007), in press.

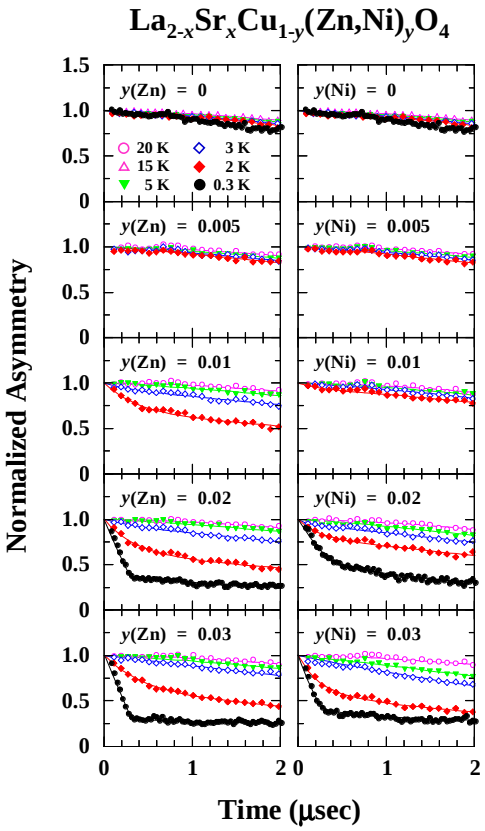

Fig. 1. Zero-field SR time spectra of $La_{2-x}Sr_xCu_{1-y}(Zn,Ni)_yO_4$ with $x = 0.15$ and $= 0 - 0.03$ at various temperatures down to 0.3 K.

[*1] Department of Applied Physics, Tohoku University
[*2] The Institute of Physical and Chemical Research (RIKEN)

Cu-Spin Dynamics Studied by μSR in $La_{2-x}Sr_xCuO_4$ at about 100 K

I. Watanabe, T. Adachi*1 and Y. Koike*1

[μSR, High-T_c, Cu-Spin Dynamics]

One of the fascinating models for describing the mechanism of high-T_c superconductivity is the stripe model[1]. This model assumes the microscopic segregation of spins and holes in the CuO_2 plane forming stripes, which has theoretically been discussed to be possibly important for the occurrence of high-T_c superconductivity[2]. To clarify the correlation between the dynamical properties of spins and holes, precise zero-field muon-spin-relaxation (ZF-μSR) measurements of $La_{2-x}Sr_xCuO_4$ (LSCO) have been carried out at the RIKEN-RAL Muon Facility over a wide range of hole concentrations from x=0.024 to 0.15, probing a change in the Cu-spin dynamics at a high temperature of about 100 K at which hole domains are expected to be formed.

Figure 1 shows ZF-μSR time spectra of LSCO with x=0.024, 0.04, 0.115 and 0.15 at various temperatures. The inset shows the entire time spectrum of x=0.115 at 100 K. All time spectra show more or less a similar Gaussian-type depolarization behavior. Therefore, the analysis function $A_0e^{-\lambda t}G_z(\Delta,t)$ was used. A_0 and λ are the initial asymmetry at t=0 and the dynamic depolarization rate, respectively. $G_z(\Delta,t)$ is the static Kubo-Toyabe function with a half-width of Δ describing the distribution of the nuclear-dipole field at the muon site.

An overall analysis has shown that changes of the time spectrum can be parametized in terms of changes of λ. For instance, λ of LSCO with x=0.115 starts to increase monotonically with decreasing temperature at about 100 K, showing a change in the dynamics of the internal field at the muon site For convenience, the temperature at which λ starts to increase with decreasing temperature is named T_μ and plotted in Fig. 2 as open circles. The superconducting transition temperature determined from the resistivity measurements is also shown and indicated by open triangles.

The temperature $T\rho_{min}$ at which resistivity is the minimum is taken from the literature[3–5] and plotted in Fig. 2 as closed triangles and squares. It is found that the x dependence of T_μ is in good agreement with that of $T\rho_{min}$. This means that the origin of T_μ is related to the localization of holes in the normal state. Therefore, the present study proves the coupling between the localization of holes and the change in the dynamics of Cu-spin fluctuations, which is an important feature of the stripe model.

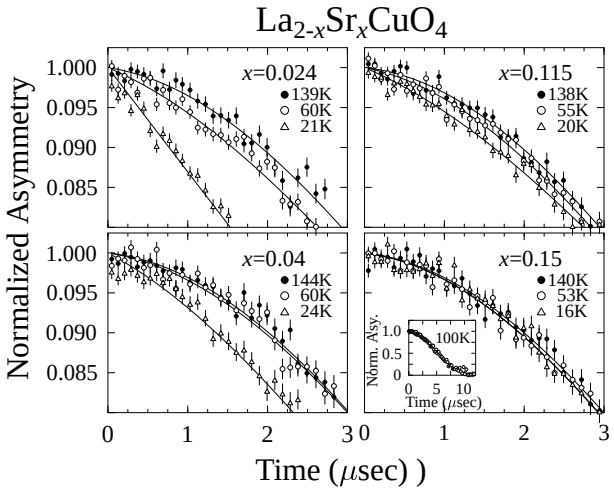

Fig. 1. Zero-field SR time spectra of $La_{2-x}Sr_xCuO_4$ with x=0.024, 0.04, 0.115 and 0.15 at various temperatures.

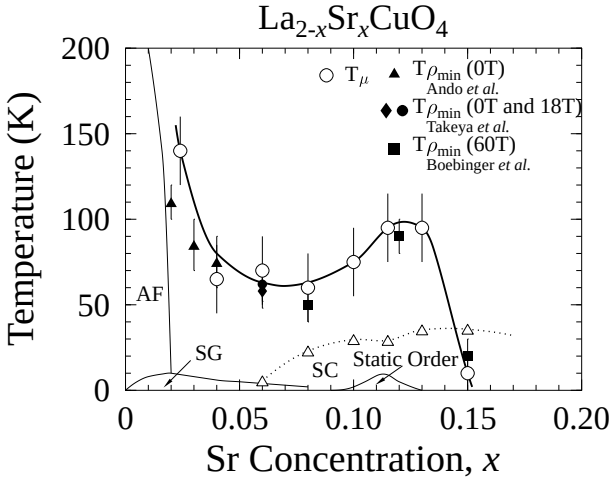

Fig. 2. Phase diagram of $La_{2-x}Sr_xCuO_4$. Lines are guides for the eyes.

References

1) J. M. Tranquada *et al.*, *Nature* (London) **375**, 561 (1995).
2) V. J. Emery and S. A. Kivelson, Physica C **235-240**, 189 (1994).
3) G. S. Boebinger *et al.*, Phys. Rev. Lett. **77**, 5417 (1996).
4) J. Takeya *et al.*, Phys. Rev. Lett. **88**, 077001 (2002).
5) Y. Ando *et al.*, Phys. Rev. Lett. **88**, 137005 (2002).

*1 Department of Applied Physics, Graduate School of Engineering, Tohoku University

Magnetism of lightly doped $Ca_{2-x}Na_xCuO_2Br_2$ probed by μSR†

S. Kuroiwa,*1 Y. Zenitani,*1 Y. Tomita,*1 J. Akimitsu,*1 R. Kadono*2,*3, I. Watanabe, S. Ohira*

A class of hole-doped cuprates, $Ca_{2-x}Na_xCuO_2$ $_2$ (=Cl, Br), which has the La_2CuO_4-type crystal structure with apical halogen atoms, has been attracting much interest as a stage for elucidating the role of apical atoms over the CuO_2 planes.[1,2] A peculiar doping dependence of superconductivity has been observed in oxybromide cuprate (=Br, Na-CCOB), where T_c = 19 K develops over an optimally hole-doped region of $x \sim 0.25$, which is substantially shifted from that of typical cuprates.[2] Therefore, to investigate the magnetic properties in the low-doping region, we conducted μSR experiments on Na-CCOB with intermediate sodium concentrations ($0.03 < x < 0.15$).

μSR measurements were performed at the RIKEN-RAL Muon Facility, UK. ZF- and LF-μSR spectra were obtained between 2 K and ambient temperature.

Figure 1 shows ZF-μSR time spectra at several temperatures (inset: $x = 0.04$ at 2 K) in Na-CCOB with x = 0.05. The ZF-μSR time spectra exhibit no clear precession signal over a region of $0.03 < x < 0.15$, which is situated between antiferromagnetic (AF) and superconducting phases. This suggests a strongly disordered magnetic ground state dominating over the AF long-range order. These spectra were analyzed using the equation $P_z(t) = \sum_{i=1}^{2} A_i G_{KT}(\Delta_{dip}, t)$ exp($\lambda_i t$) + A_B, where A_i is the decay asymmetry for signals from the sample, A_B is that from the sample holder, λ_i is the relaxation rates and Δ_{dip} is the nuclear dipolar width. The second component ($i = 2$) is needed to fit the data only below 10 K to the strongly damped oscillation seen in the spectra at 2 K. This suggests that a disordered magnetic ground state similar to a spin-glass (SG) (or spin density wave) state is present, which is either static or dynamically fluctuating. Therefore, we have performed LF-μSR measurements in order to distinguish these two possibilities (see Fig. 1 (b)).

As shown in Fig. 2, the longitudinal relaxation rate increases at low temperatures for all Na-doped samples. This is attributed to the slowing down of the thermal fluctuation of Cu moments. Since the enhancement of the longitudinal relaxation rate occurs over a temperature region that is wider than that associated with the AF transition, such behavior in these samples ($0.03 < x < 0.15$) is attributed to the SG-like magnetic state.

Consequently, these results indicate that the phase diagram is qualitatively similar to that of an ordinary cuprates. However, these characteristic doping levels are higher than those found in typical 2-1-4 cuprates, suggesting a positive shift of the entire phase diagram for carrier concentration x. This may be due to the trapping of hole carriers on the energy band of apical Br rather than the O-2p orbital, because the energy band of Br is located slightly closer to the Fermi level.

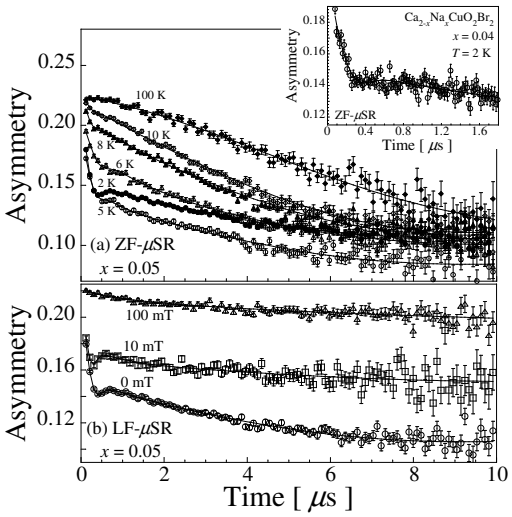

Fig. 1. (a) ZF- and (b) LF- SR time spectra in Na-CCOB with $x = 0.05$ (Inset : $x = 0.04$).

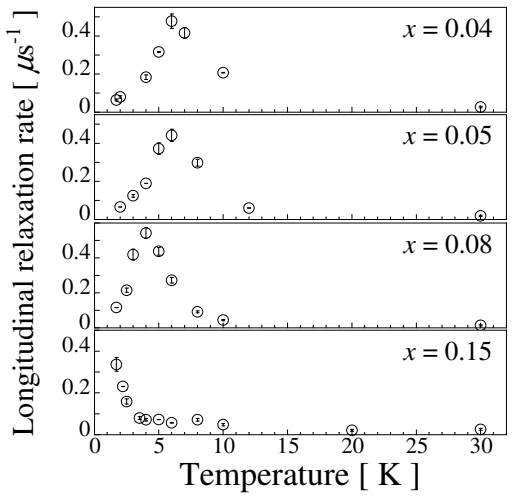

Fig. 2. Temperature dependence of longitudinal relaxation rate under LF = 100 mT for several values of x.

References

1) Z. Hiroi et al.: Nature **371**, 139 (1994).
2) Y. Zenitani et al.: Physica C **419**, 32 (2005).

† Condensed from the article in Physica B **374**, 75 (2006)

*1 Department of Physics and Mathematics, Aoyama-Gakuin University, Japan
*2 Muon Science Laboratory, IMSS-KEK, Japan
*3 Department of Materials Structure Science, The Graduate University for Advanced Studies (SOKENDAI)
* Present address: Department of Physics, Ochanomizu University, Japan

μSR study of localized spin triplets in $Tl_{1-x}K_xCuCl_3$[†]

T. Suzuki, I. Watanabe, A. Oosawa,[*1] T. Goto,[*1] F. Yamada,[*2] and H. Tanaka[*2]

[Bose-Einstein condensation, Bose glass phase, μSR]

Field-induced magnetic ordering has been investigated extensively $TlCuCl_3$ and $KCuCl_3$, and the obtained results are qualitatively well described by the magnon Bose-Einstein condensation theory[1–4]. Recently, the bond randomness effect on the singlet ground state was reported in the mixed system $Tl_{1-x}K_xCuCl_3$[5,6]. In zero field (ZF), the ground state has no gap (magnetic) in the mixed system, although both the parent materials have finite excitation gaps (nonmagnetic). Magnetization measurement results indicate that this system is in a paramagnetic state down to 1.8 K[5]. Shindo *et al.* carried out specific heat measurements in magnetic fields, and observed field-induced phase transitions that are described by the Bose-Einstein condensation of triplets of Cu-3d spins[5,6]. They discussed the obtained phase diagram in connection with the appearance of a new phase, the Bose glass phase, in lower magnetic fields at $T = 0$ as argued by Fisher *et al.*[7] In the mixed system, as mentioned above, a gapped phase accompanied by zero magnetization is absent. Thus, in zero field, the Bose glass phase at $T = 0$ is possible although the Bose glass phase generally appears between the gapped and ordered phases. However, whether or not the Bose glass phase exists in the zero-field on the mixed system $Tl_{1-x}K_xCuCl_3$ is not yet known. The purpose of this study is to investigate the magnetic properties of $Tl_{1-x}K_xCuCl_3$ at low temperatures by the muon-spin-relaxation (μSR) technique, and to probe a glimpse of the evidence of the existence of the Bose glass phase. μSR measurements were carried out at the RIKEN-RAL Muon Facility in the U.K. using a spin-polarized pulsed positive surface-muon beam. Single crystals used in this study were grown from a melt by the Bridgman method.

Figure 1 shows ZF-μSR time spectra of $Tl_{1-x}K_xCuCl_3$ with $x = 0.20$ in the earlier time region from 0 to 10 μsec at each temperature. The shape of the time spectrum tends to change with decreasing temperature. The μSR time spectra are analyzed using the simple function $A_0e^{-\lambda t}G_Z(\Delta, t)$, where A_0 is the initial asymmetry and λ is the relaxation rate of the muon-spin polarization. $G_Z(\Delta, t)$ is the static Kubo-Toyabe function with a half width Δ describing the distribution of the nuclear-dipole field at the muon site. All the time spectra are well fitted by the above function, as shown by solid lines in Fig. 1.

Figure 2 shows the temperature dependence of the obtained relaxation rate λ of muon spins in zero field. The solid line is a guide for the eye. With decreasing temperature down to about 3 K, λ shows a rapid increase. This proves that the slowing down of spin fluctuations with high frequency in a paramagnetic state occurs, and that the frequency of the spin fluctuations comes into the μSR time window below about 3 K. This slowing down of the spin fluctuations is possibly a precursor of the Bose glass phase at $T = 0$.

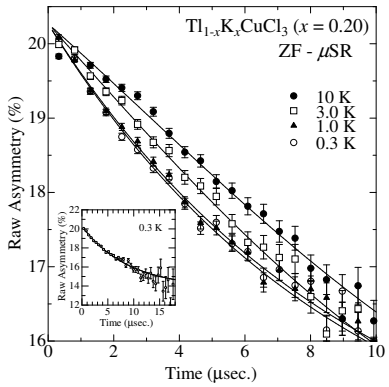

Fig. 1. Time spectrum of the zero-field muon-spin-relaxation (ZF-μSR) of $Tl_{1-x}K_xCuCl_3$ with $x = 0.2$ at each temperature. Solid lines are fitted results. The inset shows the time spectrum in the entire time region at 0.3 K.

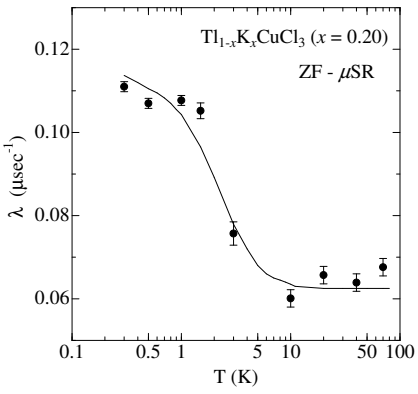

Fig. 2. Temperature dependence of the relaxation rate λ of muon spins. The solid line is a guide for the eye.

References

1) T. Nikuni *et al.*: Phys. Rev. Lett. **84**, 5868 (2000).
2) H. Tanaka *et al.*: J. Phys. Soc. Jpn. **70**, 939 (2001).
3) Ch. Rüegg *et al.*: Nature (London) **423**, 62 (2003).
4) M. Matsumoto *et al.*: Phys. Rev. B **40**, 054423 (2004).
5) A. Oosawa *et al.*: Phys. Rev. B **65**, 184437 (2002).
6) Y. Shindo *et al.*: J. Phys. Soc. Jpn. **73**, 2642 (2004).
7) M. P. A. Fisher *et al.*: Phys. Rev. B **40**, 546 (1989).

[†] Condensed from the article in J. Phys. Soc. Jpn. **75**, 025001 (2006) .

[*1] Department of Physics, Sophia University
[*2] Department of Physics, Tokyo Institute of Technology

μSR study of the randomness-induced new magnetic phase in $Tl(Cu_{1-x}Mg_x)Cl_3$

T. Suzuki, I. Watanabe, A. Oosawa,[*1] T. Goto,[*1] F. Yamada,[*2] and H. Tanaka[*2]

[Bose-Einstein condensation, the impurity effect, μSR]

In $TlCuCl_3$ and $KCuCl_3$, the neighboring spin dimers couple antifferomagnetically, and the magnetic ground states are spin singlets with excitation gaps of 7.5 K and 31 K [1, 2]. In low magnetic fields, the magnetization goes to zero because of the singlet ground state. In high magnetic fields, however, the magnetization begins to increase below the temperature T_N. Neutron elastic scattering experiments have revealed that the field-induced Néel ordering occurs and that the vertical component of spins orders antiferromagnetically[3]. This field-induced magnetic order can be represented as a Bose-Einstein condensation (BEC) of excited triplets (magnons) theoretically[4]. Recently, $Tl(Cu_{1-x}Mg_x)Cl_3$ single crystals into which the randomness (impurity) was introduced were grown, and new intriguing phenomena observed by magnetization measurements were reported [5]. The magnetic phase transition to an ordered state was observed by magnetization measurements in the zero-field limit, although the no-impurity $TlCuCl_3$ was nonmagnetic. Neutron scattering measurements identified that the ordered state is an antifferomagnetically ordered state. The purpose of this study is to investigate the magnetic properties of the randomness-induced ordered state in $Tl(Cu_{1-x}Mg_x)Cl_3$ at low temperatures using the μSR technique. μSR measurements were carried out at the RIKEN-RAL Muon Facility in the U.K. using a spin-polarized pulsed positive surface-muon beam. The single crystals used in this study were grown from a melt by the Bridgman method.

Figure 1 shows the longitudinal-field muon-spin-relaxation (LF - μSR) time spectrum in $Tl(Cu_{1-x}Mg_x)Cl_3$ with $x = 0.0026$ at 80 mK. Time spectra are well fitted using the the three-component function $A(t) = A_1 \exp(-\lambda_1 t) G_{KT}(\Delta, t) + A_2 \exp(-\lambda_2 t) + A_3 \exp(-\lambda_3 t)$. λ is the relaxation rate of the muon-spin polarization, and the $G_Z(\Delta, t)$ is the static Kubo-Toyabe function. From the fitting results, we obtained the ratio of asymmetry as $A_1 : A_2 : A_3 = 18 : 56 : 26$. Figure 2 shows the magnetic field dependences of the relaxation rates λ_1 and λ_2. Both data are well fitted using the Redfield formula of $\lambda(H) = \gamma_\mu^2 H_{loc}^2 \tau / (1 + \gamma_\mu^2 H^2 \tau^2)$. Local magnetic fields H_{loc} at the muon site and their frequencies of fluctuation, f, are deduced from the fitting (shown in Fig. 2). These results indicate that 74% of the Cu-3d spins in the crystal are in the "static" state; however, they are not freezing. These spins are slowly fluctuating at a frequency of ~ 1 MHz at lower temperatures, although the neutron measurement results have suggested the magnetically ordered state.

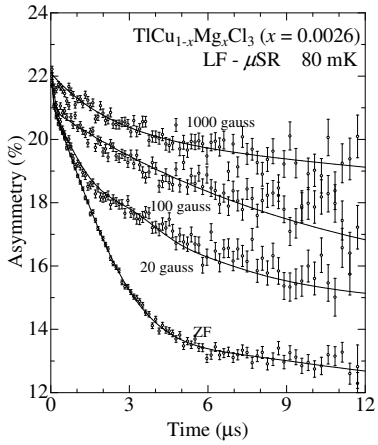

Fig. 1. Time spectrum of the longitudinal-field muon-spin-relaxation (LF - μSR) of $TlCu_{1-x}Mg_xCl_3$ with $x = 0.0026$ at 80 mK. Solid lines are fitted results.

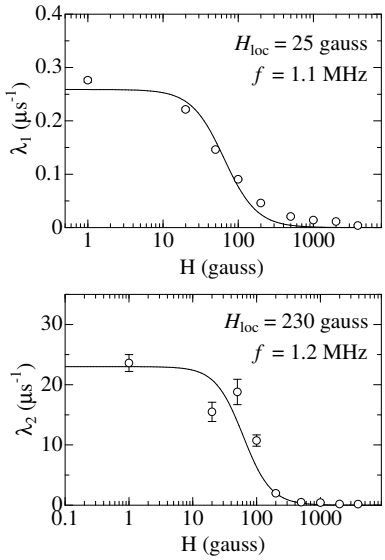

Fig. 2. Longitudinal magnetic field dependence of the muon spin relaxation rates λ_1 and λ_2. Solid lines are fitted results.

[*1] Department of Physics, Sophia University
[*2] Department of Physics, Tokyo Institute of Technology

References

1) H. Tanaka *et al.*: J. Phys. Soc. Jpn. **70**, 939 (2001).
2) A. Oosawa *et al.*: Phys. Rev. B **66**, 104405 (2002).
3) A. Oosawa *et al.*: Phys. Rev. B **65**, 184437 (2002).
4) T. Nikuni *et al.*: Phys. Rev. Lett. **84**, 5868 (2000).
5) A. Oosawa *et al.*: Phys. Rev. B **66**, 020405(R) (2002).

Magnetic ordering in solid solution of two spin gap systems $(CH_3)_2CHNH_3CuCl_3$ and $(CH_3)_2CHNH_3CuBr_3$†

T. Goto*, T. Saito*, A. Oosawa*, T. Suzuki, I. Watanabe

Quantum spin fluctuation destabilizes the magnetic order even at absolute zero, and often brings a new ground state completely different from what is expected in a classical picture. In fact, many low-dimensional spin systems with antiferromagnetic interaction have the gapped singlet state. Title compounds $(CH_3)_2CHNH_3$-$CuCl_3$ and $(CH_3)_2CHNH_3$-$CuBr_3$ abbreviated as IPA-CuX_3 are typical one dimensional spin systems, which have the non magnetic ground state with an energy gap at zero field[1]. The origin of the energy gap is quite different in the two systems of X=Br and Cl. In the X=Br system, neighboring two spins interact antiferromagnetically to form a singlet dimer, while in the X=Cl system, there are a ferromagnetic (strong) and antiferromagnetic (weak) bond alternations along the one-dimensional chain, so that each two neighboring spins form effective S=1 spins, which realize the Haldane state with a spin gap. The purpose of this study[2] is to investigate the ground state of the solid solution of these two nonmagnetic compounds.

Single crystals of IPA-$Cu(Cl_xBr_{1-x})_3$ with x=0.85 and 0.95 were grown by an evaporation method. The mixing ratio x in the crystals was determined by the inductively coupled plasma (ICP) method. The outer shape of the crystals was a rectangular solid. Measurements of μSR were carried out at the Riken-RAL Muon Facility in the U.K. using a spin-polarized pulsed surface-muon (μ^+) with a momentum of 27 MeV/c.

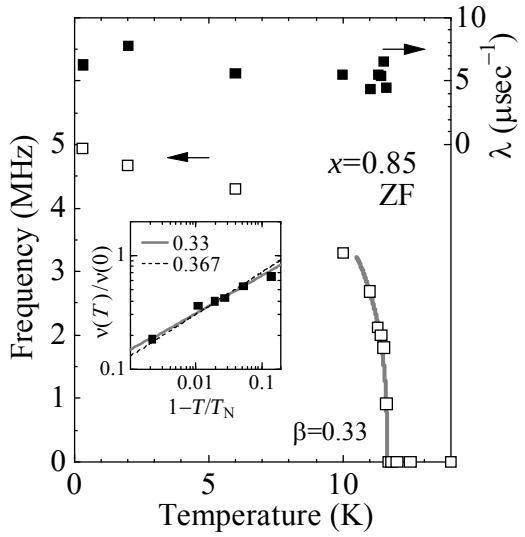

FIG. 1. Temperature dependence of the rotation frequency ν and the relaxation rate λ.

The two single crystals with x=0.85 and one with x=0.95 were used for muon measurements. They were attached by using Apiezon N grease on the silver plate with a purity of four nines, connected at the bottom of the cryostat.

The sample with x=0.85 showed a clear muon spin rotation at low temperatures, demonstrating the existence of a static long-range magnetic order. Relaxation curves are fit to the function $\exp(-\lambda t)\cos(2\pi\nu t+\phi)$, where λ, ν, and ϕ are fitting parameters, corresponding to the inhomogeneity of the local field, the mean value of the local field, and the phase constant. Figure 1 shows the temperature dependences of ν and λ. The inset shows a scaling function $(1-T/T_N)^{\beta}$ fitted to the data to obtain the transition temperature T_N=11.65(±0.05) K and the critical exponent β=0.33(±0.02), which agrees with the 3D-Ising model. The local field of the muon site at 0.33 K is estimated to be H_{loc}=360 Oe.

The sample with x=0.95 showed no rotation at low temperatures down to 0.3 K. However, λ showed a significant increase, indicating the existence of a critical instability toward the quantum critical point and hence the magnetic ground state of x=0.95. The characteristic frequency and amplitude of the fluctuating local field were estimated from the LF experiments to be 2.3 MHz and 55 Oe respectively. These results make a clear contrast with results of macroscopic measurements[1], which determine that x=0.95 is in a gapped state.

References

1) H. Manaka *et al.*: Phys. Rev. B**63**, 104408 (2001).
2) T. Saito *et al.*: Phys. Rev. B**74**, 134423 (2006).

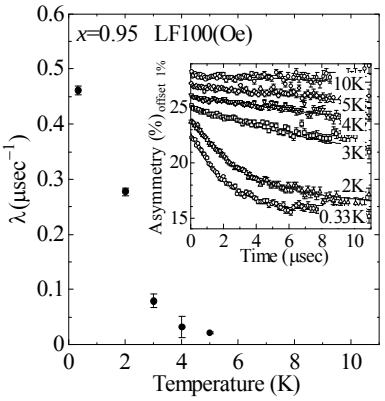

FIG. 2. Temperature dependence of λ in the sample x=0.95.

† Condensed from the article in Phys. Rev. B**74**, 134423 (2006)

* Faculty of Science and Technology, Sophia University

μSR studies of sulfospinel $CuCrZrS_4$

H.S. Suzuki,[*1] T. Furubayashi,[*1] Y. Kawashima,[*2] S. Nagata,[*2] T. Suzuki,[*3] I. Watanabe,[*3] and T. Matsuzaki[*3]

A novel spinel compound, $CuCrZrS_4$, is suggested to show the ferromagnetically ordered state with a Curie temperature of 54 K[1]. An interesting feature of this compound is the very large negative magnetoresistance (MR)[2] with the ratio reaching 80 at 16 K in a magnetic field of 90 kOe. The spin alignment of the suggested ferromagnetically ordered state has not been clarified yet, so that the mechanism of the negative MR is still unknown. Since the magnetization of this system in the ferromagnetic state is rather small, a novel unconventional magnetically ordered state may be expected to appear at lower temperatures below about 60 K. In addition, a spin glass behavior has been reported below 10 K suggesting the existence of a re-entrant magnetic behavior from an unconventional magnetically ordered state.

The purpose of this work is to confirm the appearance of an unconventional magnetically ordered state in the expected ferromagnetic phase and the re-entrant to a spin-glass state by μSR measurements under a zero-field condition, obtaining information of the magnetic property from the microscopic viewpoint to argue the mechanism of the large negative MR.

A powder sample of $CuCrZrS_4$ was prepared by direct solid-state reaction[1]. μSR measurements were carried out using AUGUS spectrometer at RIKEN-RAL Muon Facility.

We have observed characteristic changes in the time spectrum of the zero-field muon-spin relaxation at each magnetic phase boundary. Above 30 K, the time spectrum was analyzed using the simple function as $A_0 exp(-\lambda t) G_Z(\Delta,t)$, where A_0 is the initial asymmetry, λ is the relaxation ratio and $G_Z(\Delta,t)$ is the static Kubo-Toyobe function. Below 60 K, the relaxation rate λ was increased rapidly with the decrease of the temperature, as shown in Fig.1. In this first magnetic phase (FM1) between 10 K and 60 K, no oscillations were shown in the time spectrum. The enhancement of λ at approximately 60 K without oscillation in the time spectrum indicates a partial ferromagnetic ordering at approximately 60 K. Below 30 K, the time spectrum of the relaxation was well reproduced by 2 components of the relaxation rate, *i.e.*, fast depolarization behavior started to appear. In the second magnetic phase below 10 K (FM2), the relaxation rate of the fast depolarization component was increased rapidly with the decrease of the temperature, as shown in Fig.1, indicating that the internal exchange field is enhanced. The ferromagnetic ordering with a long range is a candidate of the origin of the enhancement of the exchange field. We could not, however, confirm oscillation in the time spectrum because the relaxation of the fast component is too fast for the pulse μSR measurement.

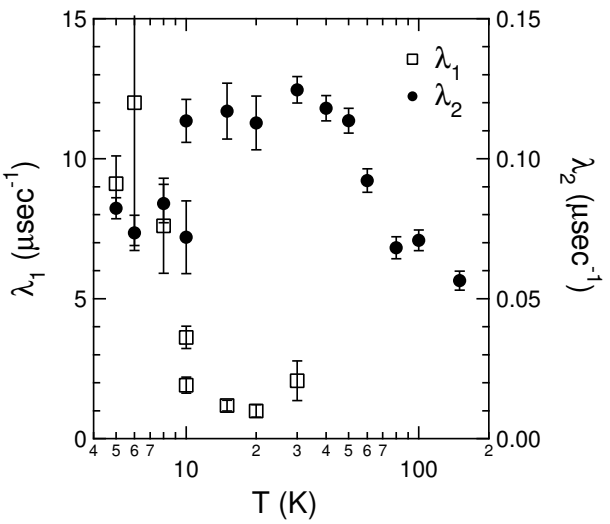

Fig. 1. Temperature dependence of zero-field muon-spin-relaxation rate λ of muon spins.

The longitudinal magnetic field dependence of the time spectrum in the FM1 phase has shown interesting behavior. In the FM1 phase, the time spectrum of the relaxation had 2 components of the relaxation rate under the magnetic field, which were similar to those in the FM2 phase as mentioned above. Moreover, the relaxation rate of the fast depolarization component below about 100 Oe was enhanced by the magnetic field. This unusual response by the magnetic field implies that the magnetic field introduces the development of a ferromagnetic correlation in each partial ferromagnetic area, *i.e.*, ferromagnetic domain, which seems to be coupled antiferromagnetically to each other. This competition between the ferromagnetic coupling in the domain and the antiferromagnetic coupling among the domains can be a candidate for the origin of the large negative MR in this system.

References

1) Y. Iijima et al.: Phil. Mag. **83**, 2521 (2003).
2) T. Furubayashi et al.: Solid State Commun. **131**, 505 (2004).

*1 National Institute for Materials Science, NIMS
*2 Department of Materials Science and Engineering, Muroran Institute of Technology
*3 Advanced Meson Science Laboratory, Nishina Center for Accelerator-based Science, RIKEN

Magnetic properties of S=1/2 quantum spin system on kagomé lattice Cu-titmb

S. Ohira-Kawamura,[*1] R. Kaji,[*2] T. Itou,[*2] and S. Maegawa[*2]

[Quantum spin system, Kagomé lattice antiferromagnet, muon spin relaxation]

The geometrical frustration of magnetic interactions gives rise to the cooperative behavior of spin systems. Heisenberg antiferromagnets on a kagomé lattice are known as strongly frustrated spin systems. In particular, an S=1/2 kagomé lattice system is even attractive, because quantum effects play important roles in such a system. $[Cu_3(titmb)_2(CH_3CO_2)_6]\cdot H_2O$ (Cu-titmb) is an S=1/2 quantum spin system on a kagomé lattice. A theoretical study has indicated that the system has a singlet ground state and a triplet excited state separated by an energy gap, which is filled with many nonmagnetic states.[1)] However, in a static field magnetization measurement, a magnetization plateau, which indicates the existence of the energy gap, is not observed.[2)] Neither a ^{1}H NMR measurement nor the magnetization measurement indicates the realization of a singlet ground state. Moreover, a magnetization plateau appears in a pulsed field magnetization measurement depending on the sweeping rate of the magnetic field.[3)] Namely, the M-H curve shows a hysteresis loop. These results suggest that the complex cooperation of the ferromagnetic (FM) and antiferromagnetic (AFM) interactions exists in this system. We performed a μSR measurement on Cu-titmb to investigate its magnetic properties.

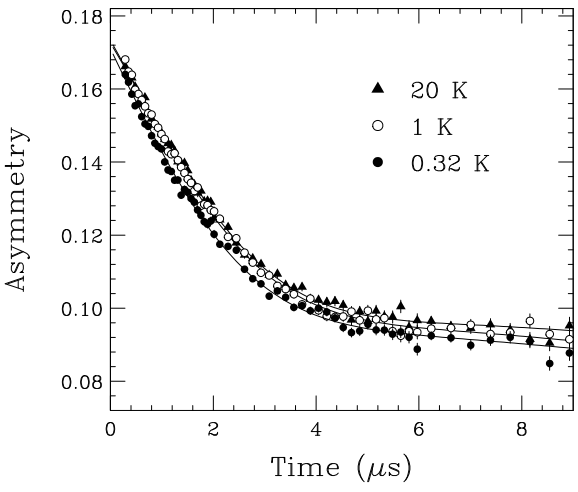

Fig. 1. ZF-μSR time spectra of Cu-titmb. Solid lines are the best fits to the relaxation function mentioned in the text.

Figure 1 shows the ZF-μSR time spectra of Cu-titmb. No clear change was observed at temperatures from 80 K to 0.32 K. The dynamical fluctuations of Cu spins can be extracted by fitting the spectra to the relaxation function, $A(t) = AG_{\rm KT}(\Delta, t)e^{-\lambda t}$, where $G_{\rm KT}(\Delta, t)$ is the Kubo-Toyabe function for describing a random static field due to nuclear dipoles and λ is the muon spin relaxation rate. The temperature dependence of the relaxation rate λ is shown in Fig. 2. The

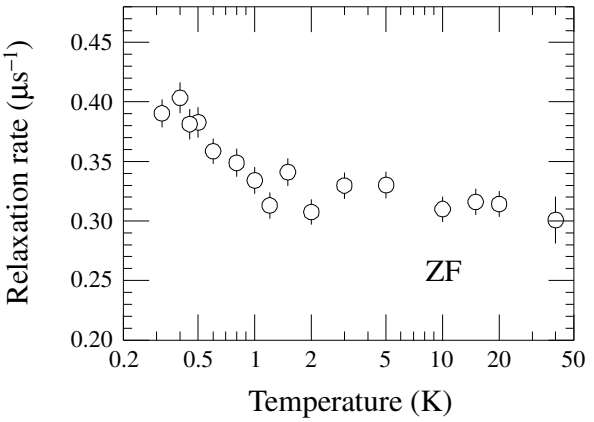

Fig. 2. Temperature dependence of muon spin relaxation rate λ.

λ value is nearly constant independently of temperature down to 1 K, and then it starts to increase as the temperature decreases. The enhancement of the muon spin relaxation is expected to be attributable to the dynamical fluctuations of Cu spins. Because it is unclear whether this enhancement indicates a quantum fluctuation or the onset of a particular critical slow-down effect, we cannot conclusively determine the ground state of this system at present. Recently, a specific heat measurement has indicated an FM transition at 59 mK. Our result might reveal the critical slow-down effect associated with the FM transition.

References

1) Ch. Waldtmann et al.: Eur. Phys. J. **B 2**, 501 (1998).
2) S. Kawahara et al.: J. Mag. Mag. Mat. **272**, e999 (2004).
3) Y. Narumi et al.: Europhys. Lett. **65**, 705 (2004).

*1 Present address: Academic & Information Board, Ochanomizu University
*2 Graduate School of Human and Environmental Studies, Kyoto University

μSR study on spin dynamics of Mn_2^{III}-Ni^{II} Single-Chain Magnet

H. Miyasaka,[*1] A. Saitoh,[*2] and S. Ohira-Kawamura[*3]

[Single chain magnet, one-dimensional ferromagnetic chain, muon spin relaxation]

Single-chain magnets (SCMs) are the current focus of many research groups, as well as single-molecule magnets (SMMs), in the field of molecule-based magnetism. SCM is a one-dimensional (1D) spin system consisting of high-spin units with a uniaxial anisotropy. The Mn_2^{III}-Ni^{II} SCM forms the $S = 3$ trimer units of Mn^{III}-Ni^{II}-Mn^{III} with antiferromagnetic (AFM) couplings, and a weak ferromagnetic (FM) interaction exists between the units, as shown in Fig. 1. We have performed μSR measurements on the SCM system $[Mn_2(saltmen)_2Ni(pao)_2(py)_2](PF_6)_2$[1,2] to understand its characteristic spin dynamics. The SMM system $[Mn_2(5\text{-}Clsaltmen)_2Ni(pao)_2(phen)](ClO_4)_2$,[3] where only the intraunit AFM interaction exists, was also measured for comparison.

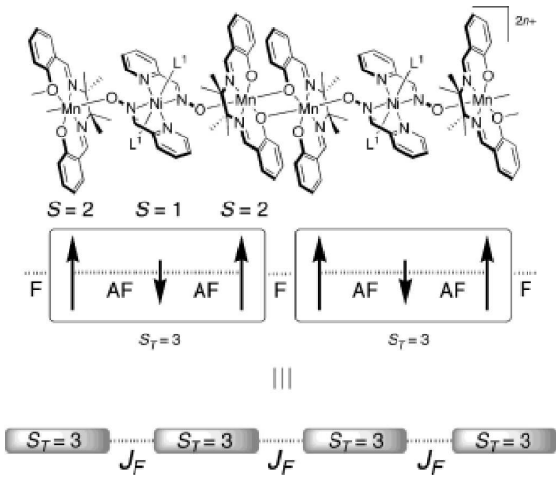

Fig. 1. Structure of Mn_2^{III}-Ni^{II} single-chain magnet.

The ZF-μSR time spectra (not shown) are well fitted with the stretched exponential function, $A(t) = A_0 e^{-(\lambda t)^\beta}$, where A_0 is the initial asymmetry, λ is the muon spin relaxation rate, and β is the index for describing the shape of the time spectra. The temperature dependences of λ and β are shown in Figs. 2(a) and (b), respectively, The closed and open circles indicate the results as in Fig. 2 legend. In both the SCM and SMM systems, an enhancement of the muon spin relaxation is observed. λ diverges at approximately 10 K, indicating that the spin fluctuation of the $S = 3$ units of Mn^{III}-Ni^{II}-Mn^{III} is suppressed across the frequency range of μSR (on the order of MHz). It is interesting that the slope of the temperature-dependent β for the SCM changes at ~20 K. Because the SCM system then behaves as a 1D FM system with $S = 3$ below ~20 K, the fluctuation will be even more suppressed.

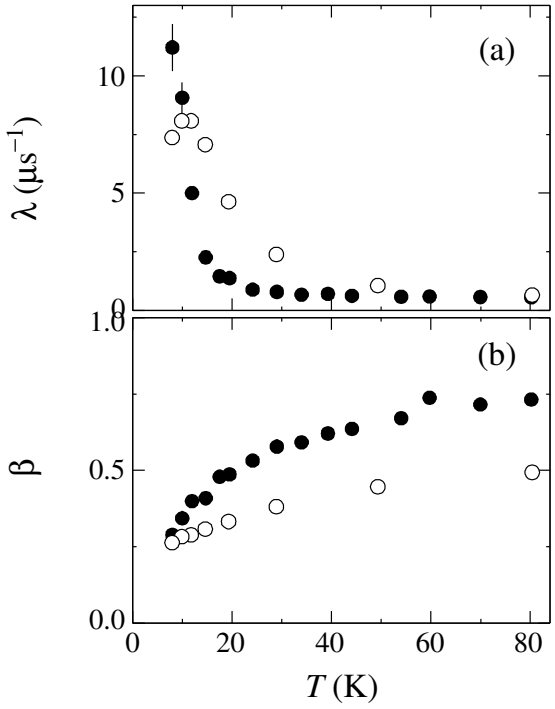

Fig. 2. Temperature dependences of (a) muon spin relaxation rate λ and (b) index β. The closed and open circles indicate the results of the SCM and SMM systems, respectively.

The magnetic correlation within the chain grows to achieve a finite chain length because of the strong uniaxial anisotropy, and the system exhibits a slow magnetic relaxation at low temperatures. The "spin-flip-type" relaxation is suggested for the model of this relaxation.[4] We currently expect a certain complicated relaxation due to both the spin flip and the spin wave, based on the longitudinal-field decoupling result.

References

1) R. Clérac et al.: J. Am. Chem. Soc. **124**, 12837 (2002).
2) H. Miyasaka et al.: Inorg. Chem. **42**, 8203 (2003).
3) H. Miyasaka et al.: Chem. Eur. J. **11**, 1592 (2005).
4) R. J. Glauber: J. Math. Phys. **4**, 294 (1963).

*1 Department of Chemistry, Tohoku University
*2 Department of Chemistry, Tokyo Metropolitan University
*3 Present address: Academic & Information Board, Ochanomizu University

μSR studies of the ground state of a new spin-ladder material

A. Kikkawa,[*1] K. Katsumata,[*1] Z. Honda,[*2] I. Watanabe,[*3] T. Suzuki,[*3] and T. Matsuzaki,[*3]

[μSR, spin ladder, quantum phase transition]

A spin-ladder material, in which linear-chain antiferromagnets are coupled with an inter-chain exchange interaction, has attracted much attention in recent years. The ground state of a two-leg antiferromagnetic spin-ladder is a singlet with an energy gap (spin gap) to the lowest excited state. In a real material, because of the presence of an inter-ladder exchange interaction, J', magnetic long-range order is observed [1,2]. The effect of an inter-ladder interaction on the phase transition in a spin, $S = \frac{1}{2}$ two-leg Heisenberg antiferromagnetic ladder has been studied theoretically[3,4]. Troyer *et al.*[4] have shown that a quantum phase transition (QPT) from a disordered to Néel states occurs at a critical value of $J'/J \simeq 0.11$, where, J is the exchange interaction within the ladder. In a previous paper[5], we showed that a spin ladder compound, $Na_2Co_2(C_2O_4)_3(H_2O)_2$ (abbreviated to SCO, hereafter) is a candidate material exhibiting this QPT. In order to obtain direct microscopic evidence for the QPT, we have made positive muon spin-relaxation (μ^+SR) measurements on SCO.

Muon spin-relaxation measurements were conducted at the RIKEN-RAL Muon Facility at the Rutherford Appleton Laboratory. More than 400 single crystals were glued on a silver plate, with their a axis parallel with each other, using Apiezon N grease. The plate was mounted in a ^{3}He cryostat.

Figure 1 shows the time spectra obtained at a longitudinal field (LF) of 3950 Oe and at the designated temperatures. At high temperatures, above about 80 K (not shown), the muon decay is completely suppressed by this field. At 40 K, we see a considerable amount of muon spin relaxation and the relaxation becomes faster at 20 K. On lowering temperature further, the relaxation becomes slow and at the lowest temperature (0.3 K) the time spectrum shows the relaxation is extremely slow. The μ^+ spin relaxation at such a high field must come from electron spins and the data show the fluctuation of the electron spins depends strongly on temperature. We fitted the data to $G_z(t) = B\cdot\exp[-(\lambda t)^\beta]$, which reduces to the one obtained by Hayano *et al.*[6] for $\beta = 1$ and to the one given by McHenry *et al.*[7] and by Uemura *et al.*[8] for $\beta = \frac{1}{2}$. Here, B is a constant.

From the analysis of the experimental data we draw the following conclusions. We have successfully extracted information on the fluctuation of electron spins by application of a strong longitudinal field. We find

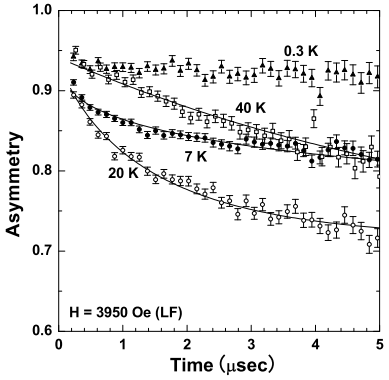

Fig. 1. Temperature dependence of the μ^+ spin decay of an assembly of single crystal samples of $Na_2Co_2(C_2O_4)_3(H_2O)_2$ measured at an LF of 3950 Oe. The solid lines are the fit with the equation discussed in the text.

that the μ^+ spin relaxation rate, λ increases with decreasing temperature and shows a peak at $T_{\rm peak} \simeq 18$ K. Below $T_{\rm peak}$, λ decreases with decreasing temperature. This indicates the observation of a spin gap formation by μ^+SR technique. The approach of the exponent β in the longitudinal relaxation function to 0.5 with decreasing temperature indicates a freezing of dilute Co moments. We suggest that these dilute Co moments arise from a many-body quantum effect with a help of the uniaxial anisotropy. The Co moments are distributed uniformly at lattice sites and fluctuate in time. Below about 5 K, we observe a sinusoidal oscillation in the time spectrum, which indicates an onset of a long-range magnetic order. All these experimental results give a microscopic evidence that the material SCO is Néel ordered at low temperatures and is close to the quantum critical point separating a spin liquid and Néel ordered phases.

References

1) S. Matsumoto *et al.*: Phys. Rev. B **53**, R11942 (1996).
2) R. Kadono *et al.*: Phys. Rev. B **54**, R9628 (1996).
3) B. Normand and T. M. Rice: Phys. Rev. B **54**, 7180 (1996).
4) M. Troyer *et al.*: Phys. Rev. B **55**, R6117 (1997).
5) Z. Honda *et al.*: Phys. Rev. Lett. **95**, 087204 (2005).
6) R. S. Hayano *et al.*: Phys. Rev. B **20**, 850 (1979).
7) M. R. McHenry *et al.*: Phys. Rev. B **5**, 2958 (1972).
8) Y. J. Uemura *et al.*: Phys. Rev. B **31**, 546 (1985).

*1 RIKEN SPring-8 Center, Harima Institute
*2 Faculty of Engineering, Saitama University
*3 Advanced Meson Science Laboratory, RIKEN

μSR study of ferromagnetic filled skutterudite compound $SmFe_4P_{12}$ †

Y. Kohori,[*1] K. Hachitani,[*1,*2] H. Fukazawa,[*1] I. Watanabe,[*2] C. Sekine,[*3] and I. Shirotani,[*3]

[$SmFe_4P_{12}$, μSR, ferromagnetic order]

Filled skutterudite compound $RT_4{}_{12}$ (R: rare earth, actinide, T: Fe, Ru, and Os, : P, As and Sb) crystallizes in the body-centered cubic (BCC) structure of the space group $Im\ \bar{3}$ (No. 204). These compounds have recently attracted much attention as the improved thermoelectric materials and for their wide variety of the electrical and magnetic properties, such as the magnetic ordering (ferro-/antiferro-magnetism), the superconductivity, the metal-insulator transition, the heavy fermion and the non-Fermi-liquid behaviors.

Among them, $SmFe_4P_{12}$ was reported to exhibit the heavy fermion behavior with the ferromagnetic ground state.[1,2] The susceptibility and specific heat measurements show that Sm ions are in trivalent state and the system has the magnetic ground state below 1.6 K. Here, we report microscopic magnetic properties of $SmFe_4P_{12}$ obtained by muon spin resonance (μSR) measurements. The μSR technique is crucial for the study of the magnetic property of the system in zero external field.

Figure 1 shows the temperature T dependence of the ZF-μSR spectra between 0.31 and 10 K. With decreasing T, the depolarization of muon spins becomes very rapid untill 1.6 K, which reflects the critical slowing down phenomenon at the Curie temperature. With further decreasing T, the spontaneous precession of muon spins was observed as shown in Fig.2. The corresponding internal field is 650 Oe. The μSR measurment clearly shows apearence of the spontaneous magnetic order at 1.6 K in $SmFe_4P_{12}$.

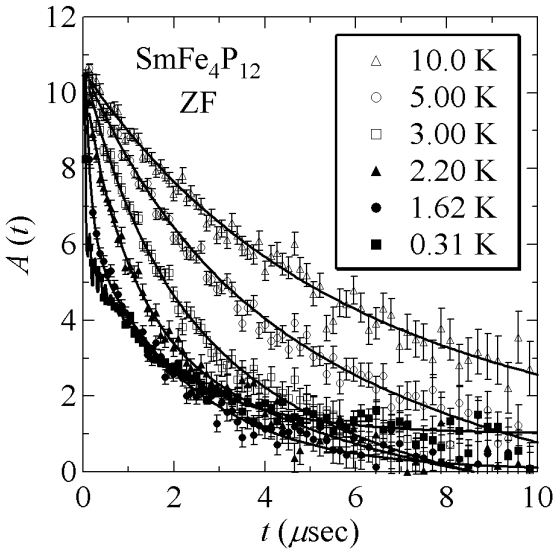

Fig. 1. ZF- SR spectra at several temperature.

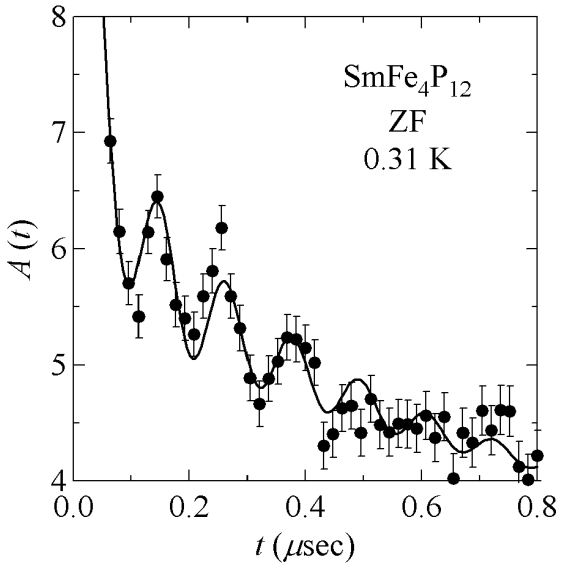

Fig. 2. ZF– SR spectra at 0.31K.

References
1) N. Takeda and M. Ishikawa: J. Phys.: Condens. Matter **15** (2003) 229.
2) K. Matsuhira, Y. Hinatsu, C. Sekine, T. Togashi, H. Maki, I. Shirotani, H. Kitazawa, T. Takamasu and G. Kido: J. Phys. Soc. Jpn., **71** (2002) Supple. 237.

† Condensed from the article in J. Phy. Soc. Jpn. **75** (2006) 124717.

*1 Graduate School of Science and Technology, Chiba University
*2 Advanced Meson Science Laboratory, RIKEN
*3 Department of Electrical and Engineering, Muroran Institute of Technology

Possible octupolar order in filled skutterudite $SmRu_4P_{12}$ probed by muon spin relaxation†

K. Hachitani,[*1*2] H. Fukazawa,[*1*3] Y. Kohori,[*1*3] I. Watanabe,[*2] C. Sekine[*4] and I. Shirotani[*1,*2]

$SmRu_4P_{12}$ is one of the most interesting systems in the filled skutterudites RT_4 $_{12}$ (R: rare earth, actinoid; T: Fe, Ru, Os; : P, As, Sb), which have attracted considerable attention because of their various remarkable phenomena.[1)] This system was reported to exhibit a metal-insulator (M-I) transition at a T_{MI} of 16.5 K.[2)] It has been considered that the antiferroquadrupolar (AFQ) order and the following antiferromagnetic (AFM) one successively occur below T_{MI} and a T_N of 15 K in the zero field (ZF), respectively.[3,4)] The transition temperatures show characteristic magnetic field dependence.[4)]

In order to explain the phase diagram, the octupolar order is recently suggested as a probable candidate for the order parameter below T_{MI} from elastic constant measurements and group-theoretical considerations.[5)] In this case, the time reversal symmetry (TRS) should be spontaneously broken below T_{MI}, on the contrary, TRS is not broken in the case of the AFQ order. The ^{31}P-NMR measurements in low magnetic fields suggest that the order is "magnetic" but not "nonmagnetic" AFQ.[6)] Note that a measurement in the absolutely zero field is necessary to confirm whether TRS is spontaneously broken. However, ^{31}P-NMR cannot be performed in ZF.

Thus, μSRs in ZF and in longitudinal fields (LFs) have been carried out in order to clarify the transition at T_{MI}. In this paper, we report the results of measurements on $SmRu_4P_{12}$.

A single-phase polycrystalline $SmRu_4P_{12}$ sample was synthesized at high temperatures and high pressures.[2)] The sample was crushed to a powder for the experiments. The experiments were performed by implanting pulsed surface positive muons into the sample. In the ZF-μSR experiment, the residual field at the sample position was suppressed to less than 0.03 Oe using correction coils, which is sufficiently small for our measurement. The LF-μSR experiment was performed by applying fields along the initial muon-spin.

In the ZF-μSR time spectra obtained, the muon-spin precession was observed at low temperatures below about 5 K, which indicates that the ground state is a magnetically ordered state. The spectra above T_{MI} gradually decreases with time, and the decrease becomes rapid at temperatures below about T_{MI}. Both the initial asymmetry and the muon-spin relaxation rate obtained by analyzing the spectra exhibit an anomaly around T_{MI}. Since the precession was not clearly observed just below T_{MI}, LF-μSR was also performed in order to confirm whether the anomaly is due to the appearance of a static internal field. The LF-spectra below T_{MI} show the decoupling pattern observed in the case of a static internal field. The magnitudes of the internal fields (H_{int}) at several temperatures (T) were estimated by analyzing the spectra. As shown in Fig. 1, the static internal field appears below T_{MI}.

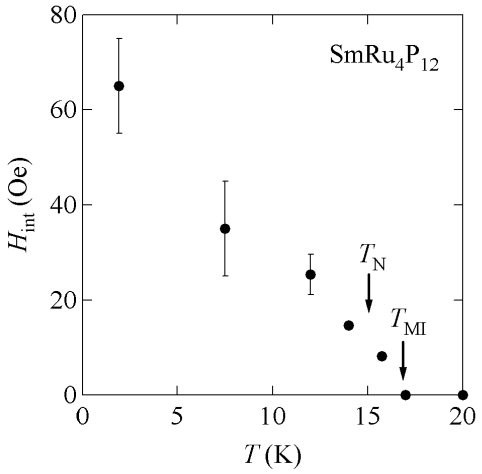

Fig. 1. Temperature dependence of H_{int} in $SmRu_4P_{12}$ estimated from LF- SR.

These results indicate that the order below T_{MI} is not AFQ but magnetic. This means the spontaneous TRS breakdown below T_{MI}, which supports a scenario in which the octupolar order occurs below the temperature in $SmRu_4P_{12}$.[7)]

References

1) W. Jeitschko and D. Braun: Acta Crystallogr. Sect. B 33, 3401 (1977).
2) C. Sekine *et al.*: *Science and Technology of High Pressure*, ed. M. H. Manghnant *et al.* (Universities Press, Hyderabad, 2000) p. 826.
3) K. Matsuhira *et al.*: J. Phys. Soc. Jpn. 71 Suppl., 237 (2002).
4) C. Sekine *et al.*: Acta Phys. Pol. B 34, 983 (2003).
5) M. Yoshizawa *et al.*: J. Phys. Soc. Jpn. 74, 2141 (2005).
6) K. Hachitani *et al.*: J. Phys. Soc. Jpn. 75, 124712 (2006).
7) K. Hachitani *et al.*: Phys. Rev. B 73, 052408 (2006).

† Summarized from the article in Phys. Rev. B **73**, 052408 (2006)

*1 Graduate School of Science and Technology, Chiba University
*2 Advanced Meson Science Laboratory, RIKEN
*3 Department of Physics, Faculty of Science, Chiba University
*4 Department of Electrical and Electronic Engineering, Muroran Institute of Technology

μSR study of ferrimagnetism on K clusters in low-silica X zeolite†

T. Nakano,*1 K. Goto,*1 J. Matsumoto,*1 I. Watanabe, T. Suzuki, F. L. Pratt,*2 and Y. Nozue*1

Alkali metal clusters can be generated in the periodically arrayed nanospace of zeolite crystals. Ferromagnetism and antiferromagnetism have been found in K clusters in zeolite A[1] and Na clusters in sodalite[2], respectively. They are novel magnetic materials because the magnetically ordered states are realized by the mutual interaction of s-electrons confined in the clusters. In the present work, ferrimagnetism is newly found in K clusters in low-silica X (LSX) zeolite. The observed magnetization is rather weak, but μSR study confirms the magnetic phase transition occurs in almost the full volume of the sample.

LSX is one of the aluminosilicate zeolites with the FAU-type structure. The framework is constructed of β cages with the inside diameter of $\sim$ 7 Å, and supercages with the diameter of $\sim$ 13 Å are formed among β cages, as shown in Fig. 1. Both types of cages are arrayed in a diamond structure.

In this work, we used LSX with the chemical formula of $Na_4K_8Al_{12}Si_{12}O_{48}$ in the structural unit of the supercage, where Na^+ and K^+ ions are distributed in the space of the $Al_{12}Si_{12}O_{48}$ framework (see Fig. 1). K clusters are formed by the loading of guest K atoms into dehydrated zeolites via the sharing of the 4s-electrons among several K^+ ions in the cage. The number of guest K atoms per supercage (namely, 4s-electrons per cluster), n, was changed from 0 to the saturation value of $\sim$ 9.0. For the samples with $6.5 < n < 9.0$, the temperature dependence of magnetization is found to show a typical behavior of N-type ferrimagnetism. The Curie temperature, T_C, varies depending on n, and shows a maximum value of $\sim$ 20 K at $n \sim 7.8$. The observed spontaneous magnetization is as weak as $\sim$ 0.1 μ_B per cluster. We performed μSR measurements on the sample with $n \sim 6.8$ and $T_C = 5$ K at the RIKEN-RAL Muon Facility. The zero-field (ZF-) μSR spectra show a Gaussian-like relaxation above T_C due to the static random field from nuclear magnetic moments. With decreasing temperature, the spectral shape changes to an exponential-like one. Throughout the whole temperature range, the spectra can be fitted by the product of the Kubo-Toyabe relaxation function, $G_{KT}(t)$, and two exponential functions:

$$G(t) = [A_1 \exp(\ \ \lambda_1 t) + A_2 \exp(\ \ \lambda_2 t)] G_{KT}(t) + B, \quad (1)$$

where B indicates the background. The exponential terms can be assigned to the contribution of the electronic magnetic moment of K clusters. Figure 2 shows the temperature dependence of relaxation rates, λ_1 and λ_2, which rise suddenly below T_C of 5 K, indicating the appearance of an internal field due to the magnetic phase transition. The longitudinal-field μSR spectra confirmed that the internal field is almost static at 2 K. The ratio of the relaxation terms to the total asymmetry, $(A_1 + A_2)/(A_1 + A_2 + B)$, is estimated to be $\sim$ 0.7. This value is high enough to conclude that the internal field under the magnetic phase transition arises in almost the full volume of the sample.

For ferrimagnetism, we must consider nonequivalent magnetic sublattices. We propose a model assuming that two sublattices are formed by clusters in the β cages and supercages. We found that the internal-field distribution obtained from the ZF-μSR spectra is consistent with this model[3].

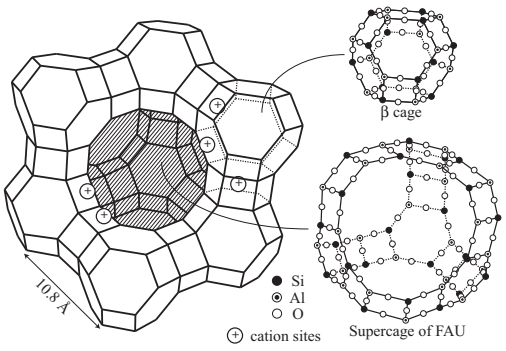

Fig. 1. Schematic illustration of the crystal structure of low-silica X zeolite.

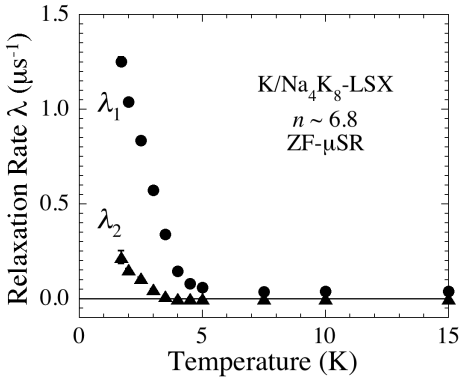

Fig. 2. Temperature dependence of muon spin relaxation rate obtained from ZF- SR spectra for K clusters in LSX zeolite with $n \sim 6.8$.

† Condensed from the article in Physica B **374-375**, 21 (2006)

*1 Department of Physics, Osaka University
*2 Rutherford Appleton Laboratory, UK

References

1) Y. Nozue et al.: Phys. Rev. Lett. **68**, 3789 (1992).
2) V. I. Srdanov et al.: Phys. Rev. Lett. **80**, 2449 (1998).
3) T. Nakano et al.: to be submitted.

μSR study on nano sized cage material, $12CaO{\cdot}7Al_2O_3$

Y. Miyake,[*1] Y. Ikedo,[*1] K. Hayashi,[*2] S. Matsuishi,[*2] M. Hirano,[*2] H. Hosono,[*2] K. Shimomura,[*1] K. Nishiyama,[*1] Y. Matsuda,[*3] and I. Watanabe[*3]

We have been studying a mechanism of the insulator-to-semiconductor transition of a novel material, 12CaO $7Al_2O_3$(C12A7) using the μSR technique. Crystalline C12A7 is a transparent insulating material that has twelve subnanometer-sized cages in the unit cell. Each cage has a mean effective charge of +1/3 (+4 charge/12 cages), leading to the expectation that such a positively charged cage behaves like an F^+ center upon capturing an electron. Hydrogen-treated C12A7(C12A7:H^-), which encages a negative hydrogen ion in the cage, can be converted into an electrical conductor by irradiation with the ultraviolet light.[1)] A possible mechanism for the photo induced conversion is based on the idea that the ultraviolet irradiation induces an electron emission from the encaged H^- ion, ($H^- \rightarrow H^0 + e^-$), and then an empty cage electrostatically captures the photo ionized electron and forms an F^+-like center. As the electron is weakly bound in the cage, the wave function could spread spatially. Consequently, the electron may migrate throughout the crystal by variable-range hopping.

To clarify the mechanism of the insulator-to-conductor transition, we performed μSR experiments to investigate muonium (Mu) and negative muonium ion (Mu^-) states in C12A7. We focus on the dynamics of Mu because we can regard Mu as light isotope of hydrogen. The experiments were carried out both at Port 2 in RIKEN-RAL and at PiA port in KEK using the pulsed positive surface muon beam. We prepared two samples: insulator (C12A7:H^-) and semiconductor (C12A7:H^0); C12A7:H^0 is the same crystal as C12A7:H^- but has already been irradiated with UV light. To measure the Mu fraction for both samples, TF-μSR experiments at 50 G have been carried out for the temperature range of 4-300 K. We found that the asymmetry of the diamagnetic component of "insulator" was gradually decreased with decreasing temperature, while that of "semiconductor" was almost independent of T (see Fig. 1), and the missing fractions of the asymmetries at 290 K of both samples were estimated to be 0.09 and 0.13, respectively.

We also performed LF decoupling experiments for both samples in the range of 10 G to 4 kG at 5 K. We observed almost identical decoupling curves for both samples (see Fig. 2), and their hyperfine constants are almost the same as that of Mu in vacuum, indicating that Mu exists in the same site in both samples. We are trying to identify the sites of Mu and diamagnetic muon in both samples by further analysis of LF- and ZF-μSR spectra for C12A7 samples.

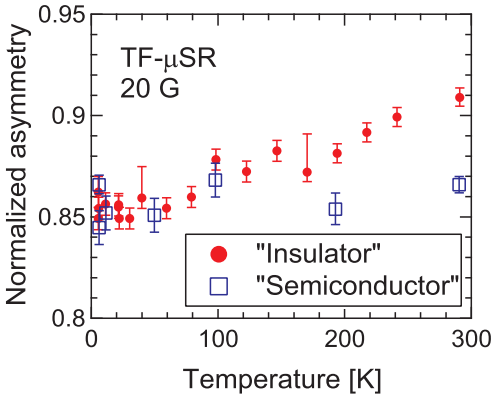

Fig. 1. Temperature dependences of initial asymmetries obtained from TF- SR spectra. Solid circles represent the fit results for the spectra of "insulator" and open squares show those of "semiconductor".

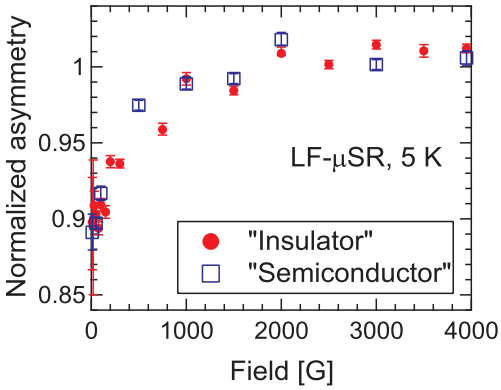

Fig. 2. Longitudinal magnetic field dependence of the initial asymmetries for both "insulator" (solid circle) and "semiconductor" (open square) samples.

References

1) K. Hayashi, S. Matsuishi, T. Kamiya, M. Hirano and H. Hosono: Nature 419, 462 (2003).

[*1] Muon Science Laboratory, IMSS, KEK
[*2] Frontier Collaborative Research Center, Tokyo Institute of Technology
[*3] Advanced Meson Science Laboratory, RIKEN

Effects of molecular adsorption on magnetism of edge state spins in nanographite

K. Takahara,[*1] K. Takai,[*1] T. Enoki,[*1] F. L. Pratt,[*2] T. Suzuki,[*3] and I. Watanabe[*3]

Nanosized systems, whose size is between that of a molecule and that of a bulk solid, give a new aspect in materials science. In particular, π-electron-based nanosized systems are of special interest. Nanographite is composed of a few sheets of nanographene, which is defined as a nanosized flat π-electron system. In spite of the diamagnetic features of bulk graphite, nonbonding π-electron states (edge states) due to the presence of open edges give localized spin magnetism to nanographite. Activated carbon fibers (ACFs), which consist of a disordered network of nanographite domains, accommodate a large amount of guest species in nanopores between nanographite domains. The molecular-adsorption-induced switching effect of nanomagnetism is the most interesting phenomenon among the various unconventional electronic and magnetic properties of ACFs in connection with the edge states. To investigate the detailed mechanism of the magnetic switching effect microscopically, we carried out μSR measurement using a specially designed vacuum-tight sample cell, in which ACFs can be handled in vacuum at temperatures up to 473 K and in a controlled atmosphere throughout a muon experiment. Here, we report the effect of molecule adsorption on the local magnetism of the nanographite network of ACFs using argon, which is chemically inert and has no nuclear dipole moment. These μSR measurements were carried out at the RIKEN-RAL Muon Facility in the Rutherford Appleton Laboratory.

To remove the adsorbed ambient gas species in the nanopores, ACFs were evacuated at a pressure of ca. 1×10^{-6} mbar at a temperature of 473 K for more than 48 h in advance. Subsequently, the nonadsorbed sample was kept in vacuum throughout the experiment. For the argon-adsorbed sample, a sufficient amount of argon gas was introduced into the sample cell by gradually decreasing the temperature to the boiling point of argon (87 K), and then the sample was valve-sealed. Measurements were carried out in the temperature range from 3 K to 300 K at the magnetic fields up to 3900 G.

For the nonadsorbed sample, ZF-μSR shows a Lorentz-type depolarization behavior in the entire temperature range investigated. LF-μSR shows the complete decoupling of muon spins due to a local internal field of 20 G with the remaining depolarization component, which cannot be decoupled by applying a magnetic field of 3900 G. For the argon-adsorbed sample, ZF-μSR also shows the Lorentz-type depolarization behavior above at the boiling temperature of 87 K. On the other hand, a precession component clearly appears below 80 K, as shown in Fig.1. The rotational field of the precession corresponds to 20 to 30 G depending on conditions. By applying even 1 G, the precession component disappears and re-appears by setting the field to 0 G. The behavior of LF-μSR for the argon-adsorbed sample at a field higher than 1 G is the same as that for the nonadsorbed sample.

By considering the absence of the nuclear dipole moment in argon atom, the depolarization of muons injected into ACFs must have been caused by the local internal field of edge-state spins. The clear emergence of the rotational component suggests that argon adsorption induces a magnetic ordering with a static internal field in a nanographite domain. A reduction in the inter-nanographene-sheet distance in the nanographite domain, which is induced by argon adsorption, is responsible for the enhancement of the exchange interaction between the edge-state spins on nanographenes. This results in the development of the novel magnetic order in the disordered nanographite network. This remains an open question in comprehending the mechanism behind the disappearance of the internal field by applying an extremely weak magnetic field.

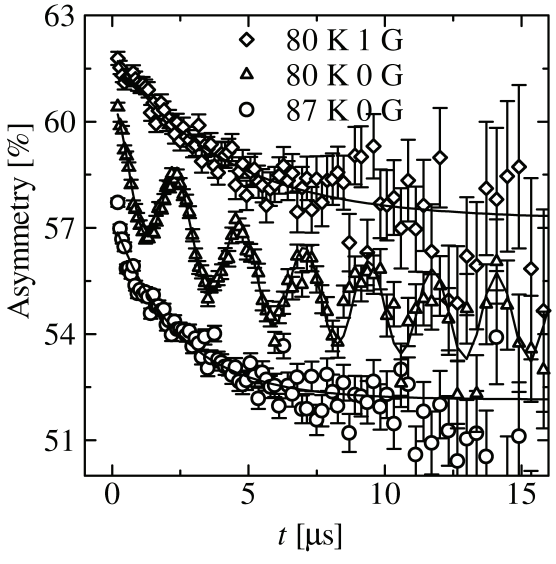

Fig. 1. ZF- and LF-μSR time spectra of argon-adsorbed sample. For clarity, the data at 80 K, 0 G and 80 K, 1 G are shifted up by 1.5 and 3, respectively.

*1 Department of Chemistry, Tokyo Institute of Technology
*2 ISIS, RAL
*3 Advanced Meson Science Laboratory, Nishina Center for Accelerator-based Science, RIKEN

μSR Study of CDW in Potassium

Haruhiko Suzuki*[1], Yun Xue*[1], Yoshifumi Nagasaki,*[1] and Isao Watanabe

Since the prediction of a CDW state in alkali metals by Overhauser in 1962[1], many groups have searched for this state in these metals. However, no clear evidence has been reported. Overhauser and coworkers claimed in many papers that they had observed CDW and electron-phason scattering effects[2]. However, these experimental results involved only observing a deviation from the isotropic Fermi sphere in experiments. We attempted to observe the phase transition in potassium at low temperatures. We have already published our experimental results on magnetic susceptibility in potassium[2]. We also performed specific heat and X-ray diffraction analyses. All of these experimental results show an anomalous behavior at around 20 K. The temperature dependence of the lattice constant of potassium shows the anomalous behavior, suggesting the crystal distortion from a bcc crystal at around 20 K. To confirm the phase transition at 20 K, a muon spin rotation (μ^+SR) experiment was performed between 15 and 300 K.

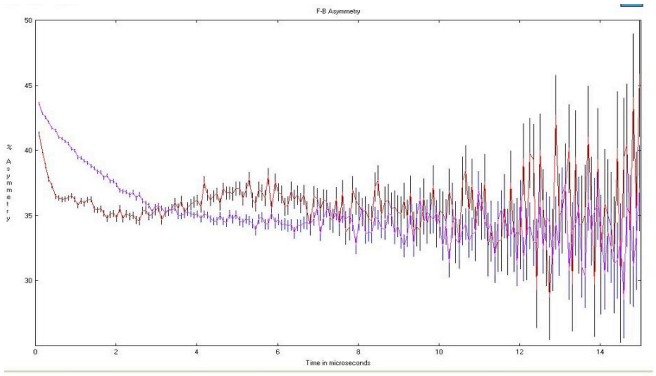

The time spectra of asymmetry A_0 were measured in the temperature range between 300 and 15 K, the lowest temperature in our experiment. Unfortunately, the lowest temperature of the specimen had a high, value probably owing to the large heat capacity of the sample holder.

To determine the resonance between the muon spin and nuclear quadrupole splitting of potassium due to the CDW crystal distortion in a longitudinal field, the time spectra A_0 were measured in various longitudinal magnetic fields. In this resonance experiment, we observed a certain anomaly, but it was not so clear. This should be due to the lowest temperature being not low enough compared to the transition temperature. When we improve the cryogenic system and obtain lower temperatures, we expect to observe clearer results.

In zero field (ZF), μSR spectra did not show any marked change in our measured temperature range. The time spectrum of asymmetry A_0 was well fitted to the exponential damping function. However, after applying a large magnetic field, such as 3000 Oe, a very rapid relaxation was observed at temperatures below 19 K, as shown in the figure. This result suggests the occurrence of a phase transition at about 19 K, which is consistent with our previous experimental results.

References

1) A. W. Overhauser: Phys. Rev. **128**, 1437 (19621)., Review article: A. W. Overhauser: Electron Correlation in Solids, Molecules, and Atoms, edited by J. T. Devreese and F. Brosens (Plenum Publishing Corp., 1983) , p. 41.
2) M. Sekine, S. Abe, Y. Tanaka, S. Nakagawa, H. Suzuki, H. Abe, K. Ohshima, and T. Nakajima: J. Low Temp. Phys. **101**, 651 (1995).

* [1] Department of Physics, Kanazawa University

Muon spin resonance study of shallow muonium in ZnO†

K. Shimomura,*1 I. Watanabe, and T. Suzuki

Hydrogen is a ubiquitous impurity in most semiconductors, including elemental (e.g., Si), and compound (e.g., GaAs) semiconductors. In these systems, hydrogen is amphoteric, acting as an acceptor in *n*-type and a donor in *p*-type materials. In contrast, hydrogen can lead to electron conduction in some wide-gap semiconductors such as zinc oxide (ZnO) semiconductors [1,2]. The muonium spin rotation method is now considered to be one of the most powerful techniques to experimentally investigate these theoretical predictions. The muonium center (Mu; an analog of isolated hydrogen whose proton is substituted with a positive muon) is readily observed in a wide variety of semiconductors after positive muon implantation, and has been serving as a unique source of information on the electronic structure of isolated hydrogen centers. Although the dynamical aspect (e.g., diffusion property) may differ considerably between Mu and H owing to the light mass of Mu (~1/9 that of H), the local electronic structure of Mu is virtually equivalent to that of H after a small correction due to the difference in the reduced mass (~0.4%). In this report, we describe our recent studies of the isolated hydrogen center in ZnO semiconductors using the muon spin resonance method in the RIKEN-RAL Muon Facility.

The ZnO semiconductor is one of the most promising semiconductors for the next generation of electronic and optoelectronic devices. It has already been applied in transducers, phosphors, and varistors, because of its unique piezoelectric, optical, and electrical properties. In these applications, polycrystalline material has mainly been used. Moreover, recent progress in single-crystal growth has opened up new possibilities, such as bright blue-light and uv-light emitters. Optical uv lasing has already been observed even at room temperature.

In a previous paper [3], we reported that two species of Mu centers with extremely small hyperfine (HF) parameters were observed below 40 K. Both Mu centers have an axial-symmetric HF structure along the *c* axis, indicating that they are located at the antibonding and bonding-center sites. It is inferred from their small ionization energies (~6 and 50 meV) and HF parameters (~10^{-4}-fold the vacuum value) that these centers behave as shallow donors, strongly suggesting that hydrogen is one of the primary origins of *n*-type conductivity in as-grown ZnO semiconductors, which was predicted in theoretical studies. However, another group reported only a single species of muonium existing in ZnO semiconductors [4, 5]. To further studiy of the existence of the second species, we performed muon spin resonance experiments, which are similar to typical NMR methods.

The better frequency resolution, obtained by the weak radio frequency (RF) field (~1 G), allowing us to distinguish the signals from these muoniums. Figure 1 shows our preliminary results of RF measurements in ZnO, where 50.000 MHz RF a and longitudinal magnetic field were applied perpendicular and parallel to the [11$\bar{2}$0] axis, respectively. Unfortunately, the preliminary analysis did not distinguish two species of muonium, which might have been due to the inhomogenity of the applied static field. Further improvements in what are required.

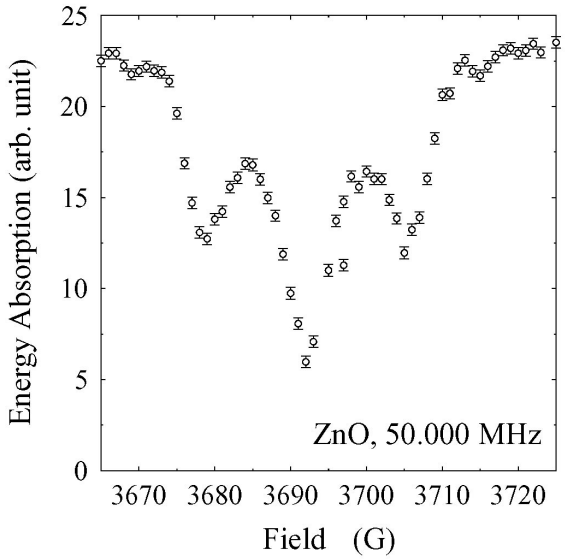

Fig. 1. Diamagnetic muon and muonium resonance spectra in ZnO at 2.0 K with 50 MHz RF field and 0.35 T static field parallel to [11$\bar{2}$0] axis.

References

1) C. G. Van de Walle, Phys. Rev.: Lett. 85, 1012 (2000).
2) C. G. Van de Walle *et al.*: Nature 423, 626 (2003).
3) K. Shimomura *et al.*: Phys Rev. Lett. 89, 255505 (2002).
4) S. F. J. Cox *et al.*: Phys Rev.Lett. 86, 2601 (2001).
5) J. M. Gil *et al.*: Phys Rev. B 64, 075205 (2001).

† Condensed from the article in Physisca. B 376-377, 444 (2006).

*1 Institute of Material Structure Science, KEK

Positive muons in calcium phosphate

T. Kakuyama, [*1] M. K. Kubo, [*1] I. Watanabe, T. Suzuki, Y. Kobayashi, A. Koda, [*2] and K. Nishiyama [*2]

A stable hydrogen atom was observed at room temperature by an ESR study in X-ray-irradiated tricalcium phosphate (β-$Ca_3(PO_4)_2$, TCP).[1)] The authors suggested that the hydrogen atom occupied only one site and survived for months. The purpose of this study is to investigate the formation and sites of muoniums and the behavior of diamagnetic muons in TCP as analogues of neutral hydrogen atom and hydrogen ion, respectively. The μSR method with its extremely high sensitivity is suitable for obtaining detailed information on the chemical and physical behaviors of trace amount of hydrogen in TCP.

The experiment was performed at port 2 of the RIKEN-RAL Muon facility. The sample was prepared by pressing polycrystalline TCP (30 mm in diameter, 0.3 gcm^{-2}) into a pellet and placing it in a He cryostat. A positive muon beam was irradiated onto the sample, and decay positrons were detected with a plastic scintillator array. External magnetic fields perpendicular (transverse, 0.6 and 6.0 mT) or parallel (longitudinal, 0.1 to 380 mT) to the initial muon spin direction were applied. Before applying these fields, the geomagnetism in the sample space was reduced to less than 1 μT. μSR measurements were carried out at 290 K down to 8.8 K.

Precession spectra in a 6.0 mT transverse field were fitted assuming a Gaussian spin relaxation due to the local magnetic field originating from ^{31}P nuclei. The yield of diamagnetic muon was about 60% at 290 K, which decreased to 50 % at 8.8 K. The relaxation rate of the spin polarization of diamagnetic muon increased with decreasing temperature from 0.06 ± 0.01 μs^{-1} at 290 K to 0.12 ± 0.01 μs^{-1} at 8.8 K (Fig. 1). This temperature dependence was interpreted to be a result of an increase in the correlation time of the muon and ^{31}P in TCP due to the decrease in the hopping rate of diamagnetic muon.

Muoniums were detected by transverse field spin precession in 0.6 mT transverse field at 290K. No clear precession signals were observed at RIKEN-RAL; however, at KEK-MSL, muonium spin precession spectra were obtained at 8 MHz under similar conditions. The muon pulse width (70 ns) at RAL being larger than that (50 ns) at KEK could obscure the fast precession signal.

Figure 2 shows μSR spectra with applied longitudinal fields at 290 K. The initial asymmetry at t=0 increased as the applied field increased. This increase was explained by the decoupling of the muonium spin from the ^{31}P dipole moment, and the suppression of the fast spin relaxation of paramagnetic muons.

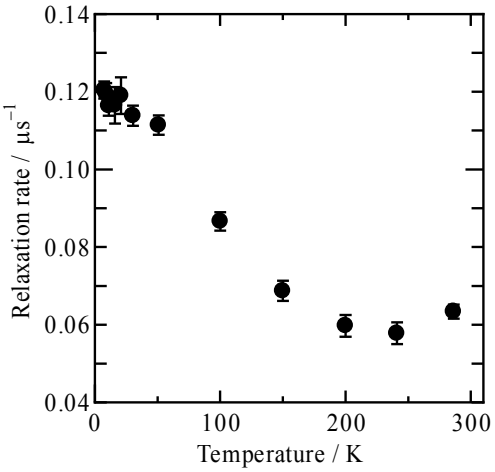

Energy Accelerator Research Organization (KEK)

Fig. 1. Temperature dependence of relaxation rate of diamagnetic muon in TCP.

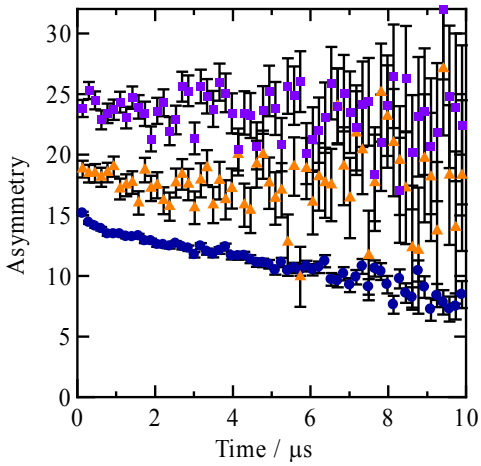

Fig. 2. μSR spectra of TCP during application of longitudinal fields at 290 K (●) 0 mT, (▲) 50 mT, and (■) 380 mT.

In summary, good-quality μSR spectra of TCP can be obtained using positive muons. The formation of muoniums in TCP was confirmed by the increase in the initial asymmetry in the longitudinal decoupling experiment. The changes in spin relaxation rate and asymmetry of diamagnetic muons were understood from the temperature-dependent muon hopping rate observed in TCP.

References

1) K. Nakashima and J. Yamauchi: J. Am. Chem. Soc. 127, 1606-1607 (2005).

[*1] International Christian University

[*2] Meson Science Laboratory, Institute of Materials Structure Science, High

RF-μ^-SR on Si

I. Watanabe, K. Shimomura,[*1] and R. Scheuermann[*2]

[μSR, Hyperfine Interaction, RF]

The investigation of hyperfine interactions at impurity centers in a semiconductor such as Si is interesting for the fundamental science and technical applications of semiconductors. Accordingly, the importance of a good understanding of hyperfine interactions at acceptor centers is rapidly growing. However, the electron paramagnetic resonance signal associated with acceptor centers is hardly observed because of fast electron relaxation, and detailed investigations of hyperfine interactions at acceptor centers reamins one an importantance of study in the field of semiconductors.

μSR measurement using negative muons (μ^-SR) is a powerful tool for studing hyperfine interactions at nuclear sites in a material from a microscopic viewpoint. When μ^- is implanted into a material, μ^- sits at a much deeper orbital than 1s because of its mass being heavier than that of the electron ($\sim$200 m_e). Because of this deep orbital of μ^-, the nuclear charge Z is shielded to be Z-1 by the negative charge of μ^-. Therefore, the implanted spin-polarized μ^- in Si is regarded as the acceptor center of Al (μAl) enabling us to investigate hyperfine interactions at acceptor centers in Si. Some μ^-SR measurements determine the hyperfine field at the μAl site have been performed in a transverse field (TF)[1–3]. However, no agreements in the value of the hyperfine field at the μAl site and also in the mechanism of hyperfine interactions at accepter centers have been obtained yet. Thus, to resolve this, we carried out μ^--resonance measurement using radio frequency (RF-μ^-SR) at the RIKEN-RAL Muon Facility using an intense pulsed muon beam. RF-μSR is a consderlably useful technique for determining directly hyperfine fields at the muon sites. Beucause a negative muon has a half-integer spin, the resonance of the muon spin, which is the absorption of RF energy induced by the spin flip of a muon, can be observed in external fields with RF. The hyperfine field at the μAl site can be calculated from this resonance frequency. The gyromagnetic ration of a muon spin is 135.5 MHz/10kOe. This value is about four times larger than that of a proton spin, so that the RF-μ^-SR technique has a higher resolution rather than a normal NMR technique.

Figure shows a resonance curve of RF-μ^-SR on Si at 45 MHz at 300 K. The external field was applied parallel to the muon-spin direction, and RF was applied perpendicular to the muon spin. The "sum of the asymmetry" means the degree of muon-spin polarization in an external field around the resonance point. The depth of the field dependence of muon-spin polarization was observed at approxmately 3,330 G. The solid line in the figure is the best-fit result of the resonance curve using the Gaussian function. The resonance field obtained from the minimum of the resonance curve was 3,334±0.1 G. The resolution obtained is about 10-fold higher than that obtained by TF-μ^-SR measurement[1–3]. The hyperfine field obtained was less than 0.1 G. Thus, it is concluded that hyperfine interactions at Si-nuclear sites are almost zero at 300 K within experimental errors. Low-temperature measurements are under way. We aim to determine a change in hyperfine fields at Si-nuclear sites below approximately 50 K, at which the unresolved fast electron relaxation starts.

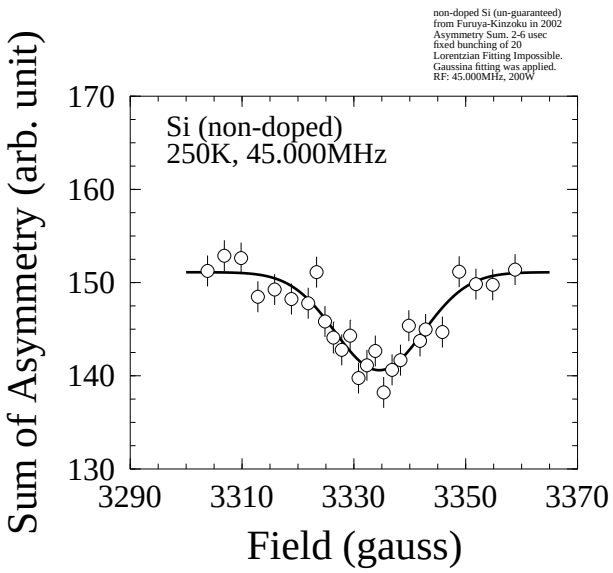

Fig. 1. Resonance curve of RF- $^-$SR on pure Si at 45 MHz at 300 K.

References

1) M. Kock *et al.*, Hyperfine Interact. **65**, 1039 (1990).
2) T. N. Mamedov *et al.*, Hyperfine Interact. **86**, 717 (1994).
3) T. N. Mamedov *et al.*, J. Phys. Cond. Matt. **11**, 2849 (1999).

*1 Institute of Materials Structure Science, KEK, Japan
*2 Muon Group, PSI, Switzerland

μSR studies on a thin $Nd_{0.5}Sr_{0.5}MnO_3$ film

Y. Matsuda, P. Bakule, I. Watanabe, Y. Miyake,[*1] Y. Murakami,[*2] M. Izumi,[*3] and K. Miyano,[*3]

[thin film, magnetism, perovskite]

$Nd_{0.5}Sr_{0.5}MnO_3$ (NSMO) is one of the manganese oxides with a perovskite-like structure, which has been attracting interest in the last few years. The bulk crystals of NSMO are paramagnetic at room temperature, and show a ferromagnetic transition at 250K and a successive antiferromagnetic transition at 170K with a very sharp metal-insulator transition. The ground state of NSMO is the charge and orbital order (COO) state, with CE-type antiferromagnetic spin texture. It is known that when a small external field (magnetic field, electric field, or light) is applied at the boundary between the COO state and the ferromagnetic-metallic state, the resistivity changes markedly, which has great promise for device applications.

One of the obstacles preventing device application was that it had been difficult to realize the COO state in thin films. Several attempts had been made to grow NSMO thin films on substrates, but the properties of the obtained NSMO films appeared to be different from those of the bulk crystal, and there had been no report of a clear metal-insulator transition until recently. Nakamura et al. succeeded in realizing the COO state in NSMO film grown on (110)-oriented $SrTiO_3$ and observed a clear metal-insulator transition for the first time[1]. The transition temperature of 170K coincides with the COO transition temperature in bulk crystal. Following this, Wakabayashi et al. conducted synchrotron x-ray diffraction measurement on NSMO/$SiTiO_3$(110) and reported that there is an additional transition at 140K, below which a novel type of COO structure is realized[2].

Notably, Watanabe et al. presumes that the magnetic structure of the new COO state should be different from that of the ground state of the bulk crystal. To investigate the magnetic property of NSMO thin film on $SrTiO_3$(110), particularly that of this novel orbital order structure, we carried out μSR measurement using a newly constructed μSR spectrometer with a low-energy muon beam line at the RIKEN-RAL muon facility[3]. In contrast to conventional μSR experiments, which use polarized muons with a fixed kinetic energy of 4MeV, our low-energy muon beam line can provide variable implantation energy of 1-30 keV to polarized muons so that we can stop all of polarized muons in a thin film sample, without any penetration into the substrates. This is a unique advantage of low-energy muons, and this experiment is the first demonstration of this technique at the RIKEN-RAL muon facility.

In the experiment, we used four NSMO films on (110)-oriented $SrTiO_3$. Each film was epitaxially grown by pulsed-laser deposition. The thickness of the films was about 100nm, and the size was 10mm by 10mm. Unfortunately, the available yield of low-energy muons was only $5 \sim 10$/sec, because of the reduced intensity of the initial muon beam due to a failure in a beam transport magnet in the ISIS proton beam line. This severely limited the amount of data we were able to accumulate in the given beam time. In spite of these circumstances, our preliminary result shows a clear paramagnetic to ferromagnetic transition at around 220K. This transition temperature is below that of bulk crystal, but is consistent with a previous resistivity measurement of NSMO film on $SrTiO_3$(110)[1]. We also observed a change in the initial asymmetry (and relaxation time) between 100K and 155K, which may correspond to the newly discovered phase transition at 140K, but we need more data points to form a definite conclusion. We hope to measure in detail the temperature variation of μSR time spectra to reveal the magnetic properties in various phases below 170K during the allocated beam time in December 2006.

References

1) M. Nakamura, Y. Ogimoto, H. Tamaru, M. Izumi, and K. Miyano: Appl. Phys. Lett. **86**, 182504 (2005).
2) Y. Wakabayashi, D. Bizen, H. Nakano, Y. Murakami, M. Nakamura, Y. Ogimoto, K. Miyano, and H. Sawa: Phys. Rev. Lett. **96**, 017202 (2006).
3) P. Bakule, Y. Matsuda, M. Iwasaki, Y. Miyake, K. Nagamine, Y. Ikedo, K. Shimomura, and P. Patrick: Physica B **374-375**, 456 (2006).

*1 High Energy Accelerator Research Organization
*2 Faculty of Science, Tohoku University
*3 Research Center for Advanced Science and Technology, the University of Tokyo

Development of Gas-Pressurized Cell for High-Pressure μSR Experiments at the RIKEN-RAL Muon Facility

I. Watanabe, and F.L. Pratt[*1]

[μSR, pressure]

The RIKEN-RAL Muon Facility can provide higher-momentum muons of up to 120 MeV/c. One important application of this higher-momentum muon beam is in high-pressure experiments. High-momentum muons can be injected into a high-pressure cell to probe the magnetic properties of samples under pressure. Worldwide, only a few groups are working on high-pressure μSR experiments. However, because μSR can sense magnetic properties of materials in the ideal zero-field condition, the demand for high-pressure μSR experiments has been growing recently to investigate the magnetic properties of organic materials, strongly correlated systems etc. Therefore, establishing high-pressure experiments is very important and urgent to allow the further progress of scientific work at RIKEN-RAL and attract many users from Europe.

We have collaborated with the high-pressure group of RAL since 2005 and have started to develop a high-pressure cell that is pressurized using a gas. Such a system has been developed for neutron-scattering experiments at RAL. The RAL high-pressure group therefore has a lot of experience using high-pressure systems. The gas-pressurized system has an advantage in being able to change the pressure continuously without any change in sample conditions. Also, the designed system can be used with existing equipment at the RIKEN-RAL Muon Facility.

¿From the upper limitation of the muon momentum available at the RIKEN-RAL Muon Facility, we have determined the maximum pressure to be 7 kbar. After much discussion with the RAL high-pressure group, we have produced the first test cell, as shown in Fig. 1. The gas is pressurized at the top of the cell and the sample is mounted at the rear of the cell. The inside pressure is held by a normal Bridgman clamp and piston, which are located at the rear of the cell. The material of the cell is CuBe. The diameter of the sample space is 18 mm and the depth is about 8 mm. The sample volume is about 2 cc. The thickness of the window that muons pass through is 9 mm and the wall can withstand pressures up to 10 kbar. The cell itself can be cooled using an existing cryostat to about 2 K. Any gas can be used to pressurize the samples, but we are planning to use helium.

Figure 2 shows the high-pressure compressor and intensifier set. The gas is compressed to up to 3 kbar using the high-pressure compressor. When we need more than 3 kbar, we use an additional intensifier. In this case, the gas is compressed to up to 3 kbar using the high-pressure compressor and the compressed gas is finally pressurized by the intensifier to up to 7 kbar. The pressure can easily be controlled by the number of turns of the handle of the intensifier.

All the systems are now ready to be tested. We are planning to carry out cooling and pressurization tests in Feb. 2007. After the long shut down of RAL, we will use this high-pressure system for experiments at the RIKEN-RAL Muon Facility.

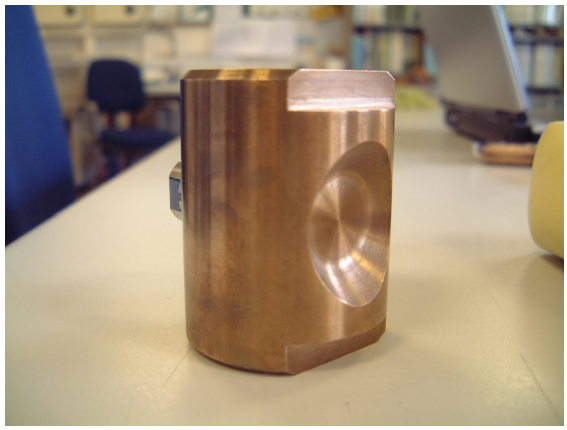

Fig. 1. Developed gas-pressurized high-pressure cell.

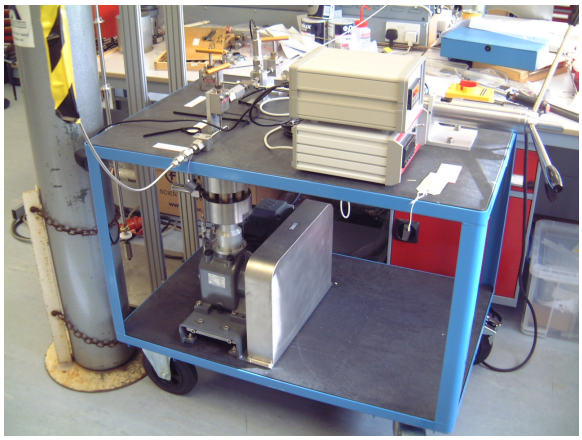

Fig. 2. High-pressure compressor and intensifier set used to pressurize the cell.

*1 Muon Group, ISIS, Rutherford Appleton Laboratory, UK

Performance of Gas-Jet Transport System Coupled to GARIS

H. Haba, D. Kaji, H. Kikunaga, N. Sato, T. Akiyama, K. Morimoto, A. Yoneda, K. Morita, T. Takabe,[*1] and A. Shinohara[*1]

We are developing a gas-jet transport system coupled to the RIKEN gas-filled recoil ion separator GARIS to perform superheavy element (SHE) chemistry in RIKEN.[1] In this work, the performance of the system was evaluated using ^{206}Fr and ^{245}Fm produced in the ^{169}Tm(^{40}Ar,3n)^{206}Fr and ^{208}Pb(^{40}Ar,3n)^{245}Fm reactions, respectively.

The metallic ^{169}Tm and ^{208}Pb targets of 120 and 420 μg cm^{-2} thicknesses, respectively, were prepared by vacuum evaporation on 30 μg cm^{-2} carbon backing foils. The ^{40}Ar beam was supplied from the RIKEN linear accelerator. The beam energies were 170 MeV for ^{169}Tm and 199 MeV for ^{208}Pb at the middle of the target. The typical beam intensity was 2 particle μA (pμA). The reaction products of interest were separated in-flight from the beam and the majority of the nuclear transfer products by GARIS and were guided into the gas-jet chamber of 70 mm i.d. × 60 mm length through a Mylar vacuum window of 3.5 μm thickness. The separator was filled with helium gas at a pressure of 88 Pa. The magnetic rigidities of GARIS were set at 1.64 for ^{206}Fr and at 2.01 Tm for ^{245}Fm.

In the gas-jet chamber, the reaction products were stopped in helium gas, attached to KCl aerosols generated by the sublimation of KCl powder at 620 °C, and continuously transported through a Teflon capillary (1.59 mm i.d. × 4 m length) to a rotating wheel system for α spectrometry (RIKEN MANON).[1] The helium flow rate was 5 L min^{-1}, and the inner pressure of the chamber was 90 kPa. In MANON, the reaction products were deposited onto Mylar foils of 0.68 μm thickness and 20 mm diameter placed at the periphery of a 40-position stainless steel wheel of 420 mm diameter. After the aerosol collection, the wheel was stepped at 30-s and 2-s intervals for ^{206}Fr and ^{245}Fm, respectively, to position the foils between seven pairs of Si PIN photodiodes (Hamamatsu S3204-09). To evaluate the number of ^{206}Fr and ^{245}Fm atoms that passed through the Mylar window, the gas-jet chamber was replaced with a detector chamber equipped with a 12-strip Si detector of 60 × 60 mm^2 (Hamamatsu 12CH SD).

In the α-particle spectra obtained using MANON and SD, α peaks of ^{206}Fr ($T_{1/2}$ = 15.9 s) and ^{205}Fr (3.85 s) and of their daughter nuclides, ^{202}At (182 s; 184 s) and ^{201}At (89 s), were identified. In Fig. 1, the gas-jet efficiencies of ^{206}Fr are shown by closed circles as a function of ^{40}Ar beam intensity. High gas-jet efficiencies of over 90% are obtained. For a comparison, the open squares shown in Fig. 1 are the data of ^{173}W produced in the ^{nat}Gd(^{22}Ne,xn) reaction with a conventional gas-jet system. Owing to the plasma condition induced by the beam in the chamber, the gas-jet efficiency of ^{173}W decreases from 40% at 6.6 pnA to 25% at 0.5 pμA with a ^{22}Ne beam intensity. Since the primary beam is separated using GARIS, such a decrease in gas-jet efficiency is not seen for ^{206}Fr up to 2 pμA.

The α-particle spectrum of ^{245}Fm (4.2 s) separated using GARIS and transported by the gas-jet is shown in Fig. 2. A beam dose of 9.76×10^{16} was accumulated. The 8.15-MeV peak of ^{245}Fm is clearly identified under the desired low background condition, although a large number of background events are measured in SD even after the GARIS separation. The background activities, such as those from ^{211}Bi and ^{211m,212m}Po, which are produced in the transfer reactions on ^{208}Pb, are completely removed by the present system. The gas-jet efficiency of ^{245}Fm is determined to be 83±9%.

The present results suggest that the GARIS/gas-jet system is a promising tool for future SHE chemistry: the identification of SHE nuclides under extremely low background conditions, and high efficiencies of the gas-jet transport. In the future, productions of SHE nuclides with long half-lives for chemical experiments involving elements such as ^{261}Rf, ^{262}Db, ^{265}Sg, ^{269}Hs, and ^{283}112 will be investigated using ^{238}U and ^{248}Cm targets.

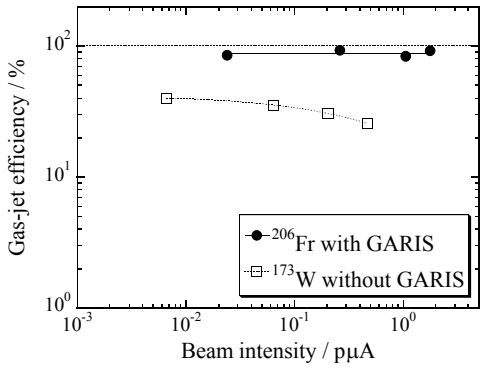

Fig. 1. Variation of gas-jet efficiency of ^{206}Fr and ^{173}W as function of beam intensity.

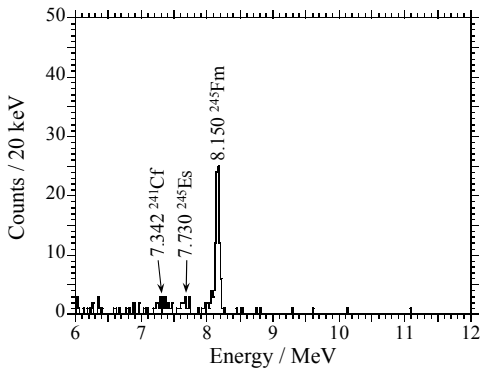

Fig. 2. Sum of α-particle spectrum measured with MANON in the ^{208}Pb(^{40}Ar,3n)^{245}Fm experiment (seven top detectors).

Reference

1) H. Haba et al.: RIKEN Accel. Prog. Rep. 39, 109 (2006).

*1 Graduate School of Science, Osaka University

Heavy element production for chemical characterization of seaborgium

T. Takabe,[*1] H. Haba, D. Kaji, H. Kikunaga, D. Saika,[*1] K. Matsuo,[*1] Y. Tashiro,[*1] K. Ooe,[*1] T. Kuribayashi,[*1] T. Yoshimura,[*1] A. Toyoshima,[*2] H. Kudo,[*3] T. Mitsugashira,[*4] K. Morita and A. Shinohara[*1]

In recent years, we have been constructing a heavy-element production system on the beam line of the RIKEN K70 AVF Cyclotron to investigate chemical properties of seaborgium (Sg, Z=106).[1] Prior to the production of the isotope ^{265}Sg via the ^{248}Cm(^{22}Ne,5n)^{265}Sg reaction, the performance of the system we developed was evaluated using ^{255}No and ^{261}Rf produced via the ^{238}U(^{22}Ne,5n)^{255}No and ^{248}Cm(^{18}O,5n)^{261}Rf reactions, respectively, in this study.

A ^{238}U target of 630 μg/cm^2 thickness and a ^{248}Cm target of 480 μg/cm^2 thickness were prepared by electrodeposition onto a beryllium backing foil of 2.0 mg/cm^2 thickness. The beams first passed through a beryllium vacuum window (1.9–3.2 mg/cm^2), the helium cooling gas (0.09 mg/cm^2), the beryllium target backing, and finally entered the target material. The beam energies on target were 105.9, 107.3, 109.0, 113.4, 116.6, and 120.9 MeV for ^{22}Ne and 94.4 MeV for ^{18}O. The beam intensity was approximately 350 pnA. Reaction products recoiling out of the target were stopped in helium gas at 130 kPa (98 kPa)[2], attached to KCl aerosols generated at 640°C (620°C)[2], and transported through a Teflon capillary of 2.0 mm i.d. and 45 m long (11 m long)[2] to the rotating wheel system MANON for α spectrometry. The transported products were deposited onto thin Myler foils of 0.68 μm thickness. The foils were periodically rotated to position the products between seven pairs of Si PIN-photodiodes for α-particle detection. The flow rate of helium gas was 2.0 L/min (5.0 L/min)[2].

In the α spectrum, the α particles of ^{255}No ($T_{1/2}$ = 3.1 min, E_α = 7.620–8.312 MeV)[3] were identified and the radioactivity of ^{255}No was evaluated by the two-component decay curve analysis of ^{255}No and ^{254}No (55 s, 8.093 MeV)[3]. The gas-jet efficiency was determined to be 50% from radioactivities of the daughter nuclide ^{255}Fm by the catcher foil method with chemical separation. It was found that the maximum cross section of the ^{238}U(^{22}Ne,5n)^{255}No reaction is 90 nb at 113 MeV, although the excitation function measured by Donets et al.[4] shows the peak of 200 nb at 118 MeV. It is noted here that the measurements by Donets et al.[4] were carried out on the basis of the α decay of the daughter nuclide ^{251}Fm only in ~1%. The peak cross section corrected for the latest α-decay branch of 1.80%[3] (~100 nb) is in good agreement with the present result.

In the ^{261}Rf experiment, a beam dose of 3.49×10^{16} was accumulated. Figure 1 shows the sum of the α-particle spectra measured in the seven top detectors of MANON for 5 to 210 s after the 30-s aerosol collection. A total of 155 time-correlated α pairs of ^{261}Rf (68 s, 8.28 MeV)[3] and its daughter ^{257}No (25 s, 8.222 and 8.323 MeV)[5] were registered in the α-energy range of interest. The gas-jet efficiency of ^{261}Rf in the present system was evaluated to be 74%, by referring to the cross section of 13 nb[6] at 94 MeV.

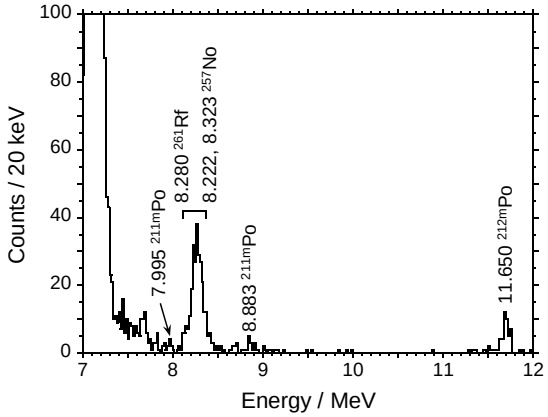

Fig. 1. Sum of α-particle spectra measured in the seven top detectors of the rotating wheel system MANON for 5 to 210 s after the 30-s aerosol collection.

Reference

1) T. Takabe et al.: RIKEN Accel. Prog. Rep. **39**, 113 (2006).
2) The values given in parentheses refer to the condition for the ^{248}Cm(^{18}O,5n)^{261}Rf experiment.
3) R. B. Firestone and V. S. Shirley: *Table of Isotopes*, 8th edn. (John Wiley and Sons, New York, 1996).
4) E. D. Donets et al.: Sov. J. Nucl. Phys. **2**, 723 (1966).
5) M. Asai et al.: Phys. Rev. Lett. **95**, 102502 (2005).
6) Y. Nagame et al.: J. Nucl. Radiochem. Sci. **3**, 85 (2002).

[*1] Graduate School of Science, Osaka University
[*2] Advanced Science Research Center, Japan Atomic Energy Agency
[*3] Faculty of Science, Niigata University
[*4] Institute for Materials Research, Tohoku University

Preparation of ^{83}Rb for ^{83}Kr Mössbauer Spectroscopy

M. K. Kubo,[*1] Y. Kobayashi, G. G. Pedoussaut[*1] Y. Yamada,[*2] and H. Haba

Krypton is one of the rare-gas (RG) elements. After xenon was found to form fluorides and be not truly inert to chemical reactions, the first krypton compound KrF_2 was synthesized in 1963.[1)] Since then, there have been numerous studies on the synthesis of RG compounds and on the clarification of the nature of their chemical bonds. On the basis of *ab initio* molecular orbital calculations, the nonfluorinated compound HKrCl was prepared in 1995.[2)] There have been a few attempts to prepare novel RG compounds containing RG-C bonds using the matrix-isolation-laser-excitation (MILE) technique.[3)] A reactant compound, *e.g.*, hydrogen chloride is condensed onto a CsI substrate with a RG to form a reaction matrix. After condensation, the matrix is irradiated with a laser beam to excite the reactant to form a RG compound. RG compounds formed are confirmed by IR spectroscopy. In such MILE experiments, there is a limitation that one RG atom can form a chemical bond to only one reactant molecule, since the reactant concentration is kept low (molar ratio of RG / reactant $\geq$ 1000) in order to observe clear IR spectra. Compounds with xenon and acetylene were prepared in 2003.[4)] Krypton compounds with a similar structure are believed to exist on the basis of calculations, but have not been experimentally confirmed.

Fortunately, krypton has the Mössbauer active nuclide ^{83}Kr. Mössbauer spectroscopy provides information on the valence state and electric field gradient at the Kr nucleus, complementary to IR spectroscopy, which provides atom-atom bond parameters. With the aim of producing compounds consisting of one krypton and two or more reactant molecules beyond the scope of the dilute MILE condition, we have started a new project on ^{83}Kr Mössbauer spectroscopy using the RIKEN cyclotron. As the first step, we are setting up a Mössbauer spectrometer for ^{83}Kr using a radioisotope source, ^{83}Rb ($T_{1/2}$ = 86.2 d).

The Mössbauer level of ^{83}Kr is the first excited state at 9.396 keV. Above this level there is a metastable state, ^{83m}Kr, with a half-life of 1.83 h. There have been ^{83}Kr Mössbauer studies since the 1960s. Most of the previous studies used ^{83}Rb as the radiation source embedded in solid matrices. We chose a ^{83m}Kr source separated from ^{83}Rb to reduce the radiation background from ^{83}Rb. Carrier-free ^{83m}Kr deposited on a cold plate will enable us to obtain Mössbauer spectra of good quality.

A $CaBr_2$ target was irradiated with an α particle beam of 25 MeV energy. After the irradiation, the target was dissolved in water. Ammonium carbonate solution was added to precipitate and separate most of the $CaCO_3$. Unfortunately, some of the aluminum cover foil merged into the target $CaBr_2$ during the beam irradiation. For the separation of aluminum and ^{83}Rb, we applied the ion exchange chromatography technique using a cation exchange resin Amberlite IR-120B. By gradually changing the concentration of eluent HCl, 83Rb was successfully separated from aluminum. A low-energy gamma-ray spectrum measured with a CdZnTe detector is shown in Fig. 1. A 9.4 keV peak from the first excited state of ^{83}Kr can be observed with Kr KX-ray peaks. An absorber Kr-quinone

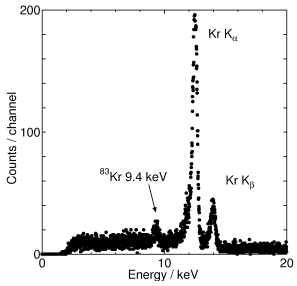

Fig. 1. Gamma-ray spectrum of ^{83}Rb prepared.

clathrate was synthesized. Solid krypton was collected in a vacuum trap cooled by liquid nitrogen. The solid krypton was transferred to a stainless pressure vessel with an inner teflon capsule containing concentrated hydroquinone aqueous solution and a spinner, and the cap of the vessel was tightly closed. The vessel was slowly heated to 360 K. The increase in inner pressure caused by the evaporation of krypton led to the formation of Kr-quinone clathrate. A small hexagonally cylindrical crystal was formed and collected by filtration.

For the next step, we will construct a gas handling system for the extraction of ^{83m}Kr and its condensation onto a cryohead, and measure ^{83}Kr Mössbauer spectra.

*1 Department of Chemistry, International Christian University
*2 Department of Chemistry, Tokyo University of Science

References

1) J. J. Turner and G. C. Pimentel: Science **140**, 974 (1963).
2) M. Pettersson, J. Lundell, and M. Räsänen: J. Chem. Phys. **102**, 6423 (1995).
3) For example, M. Pettersson, J. Lundell, L. Khriachtchev, and M. Räsänen: J. Chem. Phys. **109**, 618 (1998).
4) L. Khriachtchev et al.: J. Amer. Chem. Soc. **125**, 4695 (2003), V. I. Feldman et al.: J. Amer. Chem. Soc. **125**, 4698 (2003).

Reactions of ^{57}Mn Implanted into Solid Oxygen at γ-Phase

Y. Kobayashi, H. Kato[*1], J. Miyazaki[*1], M. K. Kubo[*2], H. Ueno, A. Yoshimi, K. Shimada[*3], D. Nagae[*3], K. Asahi, and Y. Yamada[*1]

The novel chemical reactions of ^{57}Mn atoms with oxygen have been studied by in-beam Mössbauer spectroscopy using a short-lived radioactive beam, ^{57}Mn ($T_{1/2}$=1.45 min). The direct implantation of particles into an appropriate substance produces various novel chemical species and exotic valence states unavailable under normal conditions. In our previous study, a high valence state of Fe(VIII) was obtained from the in-beam Mössbauer spectra of ^{57}Fe/^{57}Mn implanted into $KMnO_4$ at low temperatures.[1] We have also studied the *in situ* characterization of the reaction products between Fe and oxygen by ^{57}Fe/^{57}Mn implantation Mössbauer spectroscopy, and succeeded in measuring the Mössbauer spectra at 18 and 32 K. The spectra were fitted to a combination of four doublets, assuming that the species obtained by the reaction of Fe and O_2 were simple iron oxide species.[2] It is reported that solid O_2 appears in α- (0 ≤ T ≤ 24 K), β- (24 ≤ T ≤ 44 K), and γ-phases (44 ≤ T ≤ 54 K), and that α-O_2 and β-O_2 are antiferromagnetic, and γ-O_2 is paramagnetic. A sextet might be observed in the spectra if the magnetic hyperfine is produced by the antiferromagnetism of solid α-O_2 and β-O_2, and it is also possible to fit the spectra, assuming a combination of two sextets. To confirm our previous assignments of the observed spectra, the spectrum of ^{57}Mn in paramagnetic γ-O_2 was measured. In this study, we measured the spectra at a high temperature (45 K). The measured spectrum showed similar doublet peaks and the absence of a sextet.

^{57}Mn particles were produced as a secondary RI beam following the nuclear projectile fragmentation of ^{58}Fe^{21+} beams (E = 63 MeV/nucleon, I = 40 pnA) accelerated by a linac and a ring cyclotron with a Be production target. ^{57}Mn was separated and focused by an in-flight isotope separator using RIPS. Subsequently, ^{57}Mn was implanted into a solid O_2 sample after passing through an Al plate with an appropriate thickness to reduce the beam energy to about 26 MeV/nucleon. The stopping range of ^{57}Mn in the solid O_2 sample was calculated to be 180 μm from the surface with the straggling range of ±100 μm. The beam intensity of ^{57}Mn was typically 5 × 10^6 particles/s.

The solid O_2 sample was prepared on an Al plate (18 K). The thickness of the sample was estimated to be approximately 1 mm. To maintain the solid O_2 sample at a high temperature without subliming, O_2 gas was introduced into a cryostat to compensate the loss of O_2 solid at its vapor pressure. The 14.4 keV γ-rays emitted from ^{57}Mn were detected by a parallel-plate avalanche counter (PPAC) with an ^{57}Fe-enriched stainless-steel foil.

The ^{57}Fe/^{57}Mn in-beam Mössbauer spectra were measured at 45 K (paramagnetic γ-O_2) during the implantation of ^{57}Mn. The counting time was 18 h. The total implantation dose of ^{57}Mn was typically 5×10^{11} ^{57}Mn/cm^2 for one spectrum. The spectra obtained at 45 K (Fig.1) showed intense doublet peaks, which have the same Mössbauer parameters as those observed at temperatures lower than 45 K (18 and 35 K). Therefore, it was proved that the Mössbauer spectra obtained in this study do not show magnetic components. In our previous measurements, the spectra obtained at 32 and 40 K had the components of Fe in the Al substance, namely, a substitutional Fe atom and an interstitial Fe atom; some ^{57}Mn particles reached the Al substance when the thickness of solid O_2 decreased as O_2 molecules evaporated owing to a high vapor pressure at a high temperature. However, in this study, the components of Fe in the Al substance were not observed because the thickness of solid O_2 was kept constant by introducing O_2 gas to the cryostat.

Our results for in-beam Mössbauer spectra indicated a combination of Lorentzian doublets: FeO (S = 2), Fe(O_2) (S = 1), (O_2)FeO_2 (S = 0), and Fe$(O_2)_2$ (S = 0).[2] Although an energetic ^{57}Mn atom certainly creates defects and decomposes O_2 molecules until it stops at a suitable final position in solid O_2, the ^{57}Fe atom at the final position is neatly surrounded by O_2 molecules, and Fe$(O_2)_2$ is obtained as the primary ^{57}Fe product.

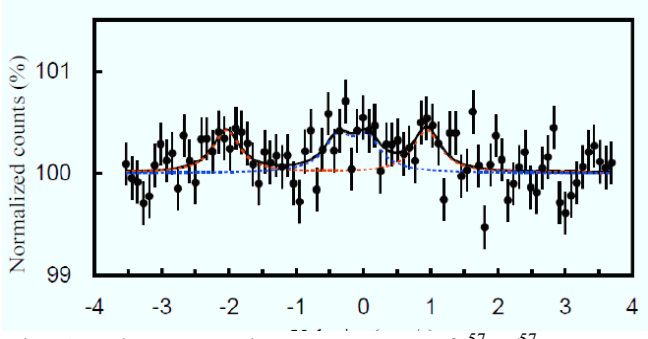

Fig. 1 In-beam Mössbauer spectrum of ^{57}Fe/^{57}Mn atoms implanted into solid O_2 at 45 K.

References

1) Y. Kobayashi et al.: J. Radiochem. Nucl. Chem. **255,** 403 (2003).
2) Y. Yamada et al.: Appl. Radiat. Isot. **52,** 157 (2000).

*1 Department of Chemistry, Tokyo University of Science
*2 College of Liberal Arts, International Christian University
*3 Department of Physics, Tokyo Institute of Technology

The Distribution and Metabolism of ^{14}C –labelled Carnosine in Mice

T. Ando,[*1] Y. Nakanishi,[*1] M. Suzuki,[*1] M. Ozaki,[*1] Y. Kanayama, S. Enomoto, and S. Kimura, [*1]

Carnosine(β-alanyl-L-histidine) is a histidine-containing peptide particulaly abundant in exitable tissues such as brain and skeletal muscle of humans and other mammal animals at relatively high concentrations (up to 20 mM). It has the potential to suppress many of the biochemical changes (e.g., protein oxidation, glycation, AGE formation, and cross-linking) that accompany aging and associated pathologies. Through its distinctive combination of antioxidant and antiglycating properties, carnosine is able to attenuate cellular oxidative stress and can inhibit the intracellular formation of reactive oxygen species and reactive nitrogen species. Boldyrev et al. showed that carnosine attenuated the development of senile features when used as a supplement to a standard diet of senescence accelerated mice (SAM). Its effect was apparent on physical and behavioral parameters and on average life span. In the present study, we show biodistribution and metabolism of orally administered radio-labelled carnosine in mice.

Carnosine, [β-alanine-3-^{14}C, 2.4μCi/0.5ml] was orally adminiministered to fasted ddy mice (4 weeks-old, male). After oral administration, mice were sacrificed by cutting the cervix part at differenet time (1,3,6,12 or 24 h), and whole blood were collected; liver, kidney, brain, gastrocneminal muscle, and muscles soleus were removed and weighed. Each organ and blood put in vials (Packard Co.) was solubilized by mixing with 6 ml of tissue solubilizer (NCS-II, Amersham Pharmacia Biotech, Inc.) with shaking whole day. Subsequently, each solubilized sample was added 10 mL of liquid scintillation cocktail (OCS, Packard) and its radioactivity was counted in a liquid scintillation counter (Packard Co.). The coloring liquid had been bleached with CH_3COO_3 of the proper quantity before OCS was added.

Biodistribution in organs and uptake of the radioactivity that administered the oral into blood and each organ were shown in Figure1.The radioactivities in organs showed similar transition during 24 hours.

After administering carnosine, its radioactivity reached the highest value at 1 h in kidney and musculus soleus, while in liver, brain, Hifc muscle, and whole blood the highest values were observed at 3 h. Then the elevated levels of radioactivity present in the circulation at 1 h and 3 h post-administration in musculus soleus, Hifc muscle, and whole blood were reduced to near-background levels by 24 h post-administration. Relatively higher radioactivity was observed in liver and kidney, while it was lower in brain.

Uptake of its radioactivity in liver and kidney were 18% at 3 h and 16% at 1 h, respectively, although it in brain was only 1.6% at 3 h.

Anserine(β-alanyl-L-methylhistidine) is a histidine containing dipeptides like carnosine, and carnosine and carnosine which did methylation, and also present in high concentrations in the muscle and brain of many animals and humans. It has been shown that the amount of The taking % of the radioactivity that oral administered to blood and each organization was compared. After it had administered it, the kidney and the musculus soleus reached the highest value in one hour, and the liver, the brain, the gastroceminal muscle, and all bloods reached the highest value in three hours. Afterwards, it decreased gradually and the same transition was seen.

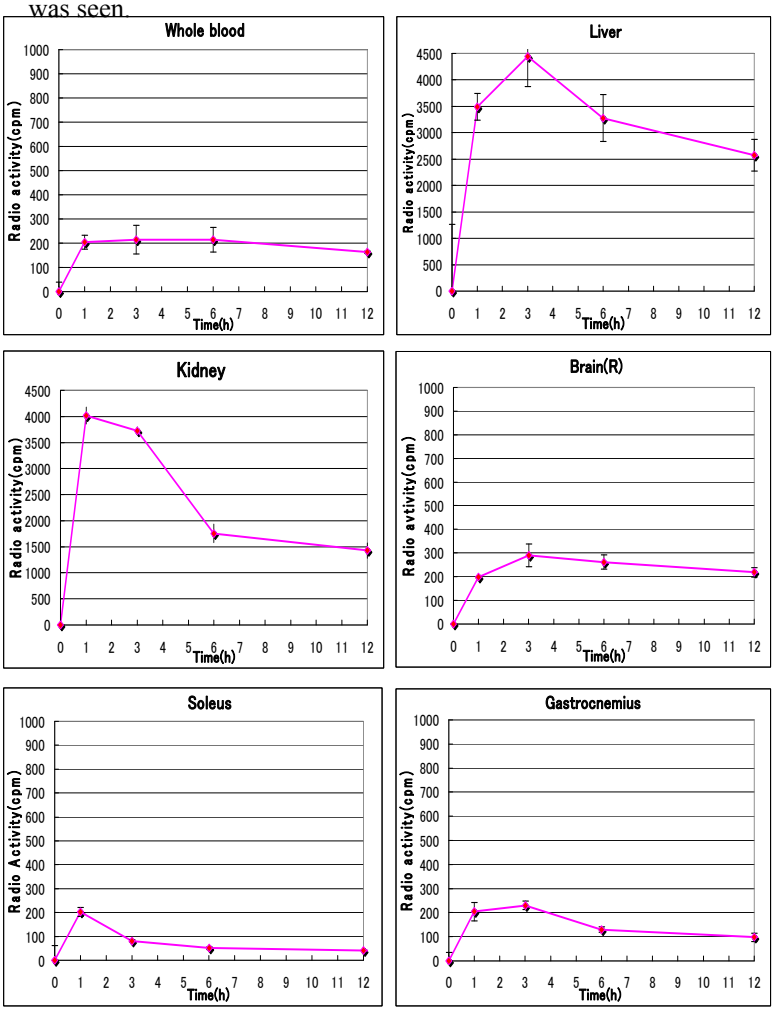

Fig.1. Tissue concentration of Carnosine, [β-alanine-3-^{14}C] in ddy mice at various time after injection.

References

1) K. Horisaka and A. Musashi et al.: Pharmacometrics **11**(4) 475-485(1976).
2) S. Furuta and S. Toyama et al.: Medical Pharmacy .vol8.No5.1057-1063(1993)
3) J. N. A. van Balgooy and E. Roberts, Biochem.Pharmac.**24** 1421-1425(1975)
4) H. Joshima and M. Kashima et al.:Health Physics Instruction. **11**. 97-103(1976)

[*1] Graduate School of Human Life Science, Showa Women's University

Effect of carnosine on gastric secretion in rats

K. Igarashi*[1], Y. Kanayama, S. Kimura*[2] and S. Enomoto

Iron deficiency is the most frequently occurring nutritional disorder in the world. One of the main causative factors of iron deficiency is the poor absorption of dietary iron. Dietary iron is classified into two types, heme iron and non-heme iron. Heme iron contained in red meat, poultry and fish has a high intestinal absorption efficiency, because it directly enters mucosal cells. Non-heme iron, the main form of dietary iron, should be released from conjugation for absorption. Gastric secretion is necessary for the optimal absorption of iron by rats, and the administration of HCl can increase iron absorption in achlorhydrics[1]. However, the absorption of released iron is affected by the composition of other foods in the gut. The absorption rate of vegetable iron is only about 1-2 %[2]. Therefore, the enhancement of non-heme iron absorption is important for improving iron status.

It is well established that the bioavailability of non-heme iron from foods is enhanced by vitamin C, citric acid and the meat factor[3]. Vitamin C and citric acid maintain iron in a more soluble form and prevent it from binding to inhibitors by their chelating properties[3]. On the other hand, red meat, poultry and fish also enhance non-heme iron absorption. However, the factor associated with improving iron absorption in these foods has yet to be clarified.

Carnosine is a well-known neuropeptide consisting of alanine and histidine (β-alanyl-L-histidine), and is found in millimolar concentrations in the skeletal muscle. Carnosine acts as a natural antioxidant with hydroxyl-radical-scavenging and lipid-peroxidase activities[4]. Furthermore, the pharmacological activity of the carnosine-metal complex has been clarified recently [5].

Thus, to investigate the effect of carnosine on the solubility of iron, we investigated gastric secretion in pylorus-ligated rats administered carnosine.

Eight-week-old male Wistar rats were purchased from Japan SLC, Inc. and housed in stainless-steel cages. The rats were restricted food intake but they had free access to drinking water for 18 h. The abdomen of each rat was opened and the pylorus was ligated under ether anesthesia. After closure, 50, 100 or 200 mg of carnosine or saline was immediately administered into the gut through a tube. The rats were sacrificed 6 h after the carnosine administration, and the gastric juice of each rat was collected and analyzed for volume, acidity and pepsin activity. Acidity was determined by titrating the gastric juice against 0.1 mol/L NaOH to pH 7.0[6]. Pepsin activity was determined by the Anson-Mirsky revised method using bovine hemoglobin as a substrate[5]. Pepsin activity was calculated using

$$\text{Pepsin activity}=(\text{A-B})\times 50\times\frac{7.5}{0.5}\times\frac{1}{10}=(\text{A-B})\times 75,$$

where A is the concentration of tyrosine in the sample, and B is the concentration of tyrosine in the blank.

Pepsin output was calculated using pepsin activity × volume[6]. The statistical significance of group differences was determined using Student's *t*-test.

The pepsin activities, pepsin outputs and volumes in the control and carnosine-administered rats are shown in Table 1. The rats administered 50 and 200 mg of carnosine had increased pepsin activities compared with the control rats. The pepsin activity in the 50-mg-carnosine-administered rats was significantly higher than that in the control rats. However, no significant differences were observed between the 100- and 200-mg-carnosine-administered rats and the control rats, indicating that 50 mg of carnosine increases pepsin activity.

*[1] Department of Health and Nutrition, University of Human Arts and Sciences

*[2] Graduate School of Human Life Sciences, Showa Women's University

Table 1 Pepsin activities, pepsin outputs and volumes in control and carnosine-administered rats.

	Pepsine activity (μg/ml/min)	Pepsine output (trypsine μg)	Volume (ml)
control	1085±149	4079±1531	3.4±0.9
50 mg of carnosine	1913±251*	11717±1814*	5.8±1.0*
100 mg of carnosine	1000±90	3289±514	3.3±0.3
200 mg of carnosine	1344±243	3589±363	2.8±0.3

All values represent the mean±S.E. for four or five rats. * Significant differences were observed between the control and carnosine-administered rats ($P<0.05$).

The pepsin output in the 50-mg-carnosine-administered rats was significantly higher than that in the control rats. Although there were no significant differences in pepsin output between the control rats and the 100- and 200-mg-carnosine-administered rats, the pepsin outputs in the 100- and 200-mg-carnosine-administered rats were lower than that in the control rats. This indicates that 50 mg of carnosine increases pepsin output.

The gastric juice volume in the 50-mg-carnosine-administered rats was significantly higher than that in the control rats. The 100-mg-carnosine-administered rats exhibited a gastric juice volume similar to that of the control rats. On the other hand, the volume in the 200-mg-canosine-administered rats was lower than that in the control rats, indicating that the rats administered 50 mg of carnosine have an increased gastric juice secretion.

These results indicate that 50 mg of carnosine increases gastric juice volume, pepsin activity and pepsin output, although this effect does not depend on carnosine dose. It is considered that carnosine enhances iron absorption by increasing iron solubility.

References

1) E. R. Morris: *Trace Elements in Human and Animal Nutrition*, edited by W. Mertz (Academic Press, California, 1987), p. 91.

2) L. Hallberg: Ann. Rev. Nutr. **1**, 123 (1981).

3) I.M. Zijp, O. Korver, and L.B. Tijburg: Crit. Rev. Food Sci. Nutr. **40**(5), 371 (2000).

4) M.A. Babizhayev, M. Seguin, J. Gueyne, R.P. Evstigneeva, E.A. Ageyeva and G.A. Zheltukhina: Biochem. J. **304**, 509 (1994).

5) M. Seiki, S. Ueki, Y. Tanaka, M. Soeda, Y. Hori, H. Aita, T. Yoneta, H. Morita, E. Tagashira and S. Okabe: Nippon Yakurigaku Zasshi **95**(5), 257 (1990).

6) I. Kanai: *Kanai's Manual of Clinical Laboratory*, edited by M. Kanai (Kanahara & Co., Ltd., Tokyo, 1993), p. 1320.

Rapid solvent extraction of No^{2+} with multitrack microchips

Y. Tashiro,[*1] D. Saika,[*1] Y. Kitamoto,[*1] K. Matsuo,[*1] T. Takabe,[*1] T. Kuribayashi,[*1] K. Ooe,[*1] T. Yoshimura,[*1] W. Sato,[*1] N. Takahashi,[*1] A. Toyoshima,[*2] H. Haba, S. Enomoto, and A. Shinohara[*1]

A relativistic effect markedly affects the chemical properties of the elements at the uppermost end of the periodic table. We have been studying the solvent extraction behavior of actinides because the distribution ratios of heavy actinides are related with the chemical properties. For heavy actinide chemistry, rapid chemical operations are required because the half-lives of heavy actinides are very short. In previous experiments, we developed a rapid solvent extraction system using a microchip to overcome the problem, and performed the online solvent extraction of lanthanides using this system.[1] The large specific interfacial area of the microchip makes it possible to achieve extraction equilibrium very rapidly, but processing rate per unit time is very low. We therefore developed multitrack microchips comprised of two microchips in order to increase processing rate. Here, we show the result of the rapid solvent extraction of ^{255}No using the multitrack microchips.

The solvent extraction was performed for diluted ammonia water as an aqueous phase and 0.01 M HDEHP(di(2-ethylhexyl)phosphoric acid)-toluene solution as an organic phase. Before the experiments, the ammonia water and HDEHP-toluene solution were mixed and shaken until the equilibrium was achieved. An online chemical experiment was performed at the hot laboratory of the RIKEN Accelerator Research Facility. A ^{238}U target was irradiated with ^{22}Ne ions at an energy of 112.4 MeV/nucleon in E3b course to produce ^{255}No by the ^{238}U(^{22}Ne,5n)^{255}No reaction. During the irradiation performed for 5 min per run, the product nuclei were continuously transported to the hot laboratory by a gas jet method. The transported products were dissolved in diluted ammonia water and subsequently fed into a multitrack microchip through a Teflon capillary. Simultaneously the HDEHP-toluene solution was fed from the other inlet to extract ^{255}No from the aqueous phase. The aqueous and organic effluents from the microchip were separately recovered on respective tantalum plates. The effluents of the aqueous and organic phases collected on each plate were evaporated to dryness, and the samples were subjected to α spectrometry. The extraction ratio D was derived from the equation $D = V_{aq} \cdot A_{org}/V_{org} \cdot A_{aq}$, where V is the volume of the solution and A is the radioactivity of each phase. The total chemical processing time was about 3 min.

We observed, in 34 runs, 28 events of α particle emission from ^{255}No, namely, 12 from the aqueous phase and 16 from the organic phase, as shown in Figs. 1 and 2. This result agrees with the amount of ^{255}No (31±6 counts) estimated from the integrated beam currents and cross section. The extraction ratio D was determined to be 0.8± 0.3 under the present condition. Compared with Ca^{2+} and Sr^{2+}, which have electronic states for the outer shell analogous to No^{2+}, D increases in the order $Sr^{2+} < No^{2+} < Ca^{2+}$.[2] This result is consistent with the ionic radii of these elements,[3] in the same manner as the result of the previous solvent extraction of No^{2+} using HDEHP-octane solution.[4]

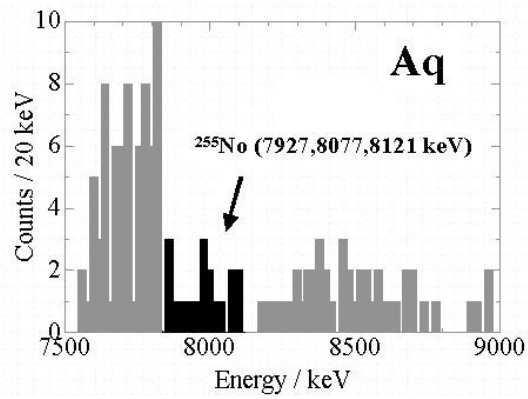

Fig. 1. Alpha spectrum of ^{255}No in aqueous phase.

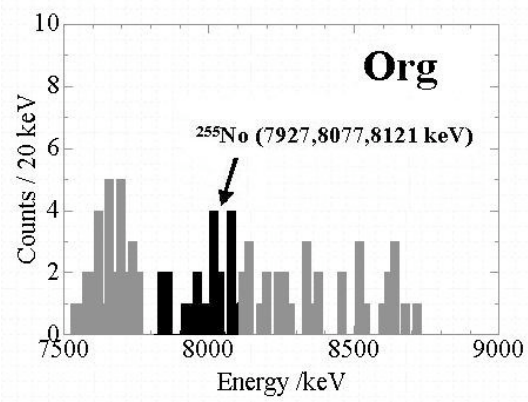

Fig. 2. Alpha spectrum of ^{255}No in organic phase.

References

1) D. Saika et al.: RIKEN Accel. Prog. Rep. **39**, 111 (2005).
2) P. M. Shanbhag et al.: J. Inorg. Nucl. Chem. **41**, 1033 (1979).
3) R. D. Shannon: Acta Cryst. **A32**, 751 (1976).
4) R.J.Silva et al.: Inorg. Chem. **13**, 2235 (1974).

*1 Graduate School of Science, Osaka University
*2 Advanced Science Research Center, Japan Atomic Energy Agency

Lack of phosphorylated histone H2AX in the pericentric heterochromatin

M. Izumi

In eukaryotes, DNA is packaged into nucleosomes, which are in turn arranged in various higher-order structures to form chromatin. The nucleosome is composed of 145 bp of DNA and histone octamers, two from each of the four histone protein families, H2A, H2B, H3, and H4. The histone H2A family includes three subfamilies, H2A1-H2A2, H2AZ, and H2AX. In mammalian cells, H2AX constitutes approximately 10% of the total H2A. Histone H2AX becomes phosphorylated on the residue serine 139 in cells when double-stranded breaks are introduced into the DNA by ionizing radiation (1). Phosphorylated H2AX directly interacts with many components involved in DNA repair, including the Mre11/Rad50/Nbs1 complex, Brca1, NFBD1, and 53BP1, and stimulates the accumulation of these proteins around DNA double-strand breaks. Furthermore, phosphorylated histone H2AX recruits cohesin and several chromatin remodeling factors, which facilitate the homologous recombination repair.

The chromatin structures are regulated by chromatin-associated factors and thereby contribute to the formation of domains within the genome, referred to as euchromatin and heterochromatin. Our previous experiments showed that DNA double strand breaks decreased the rate of DNA synthesis more efficiently in the heterochromatic region than in the euchromatic region (2). However, it is unknown how repair reactions and checkpoint responses are regulated by the chromatin structures. It is also unknown whether H2AX proteins are distributed on the entire genome homogeneously.

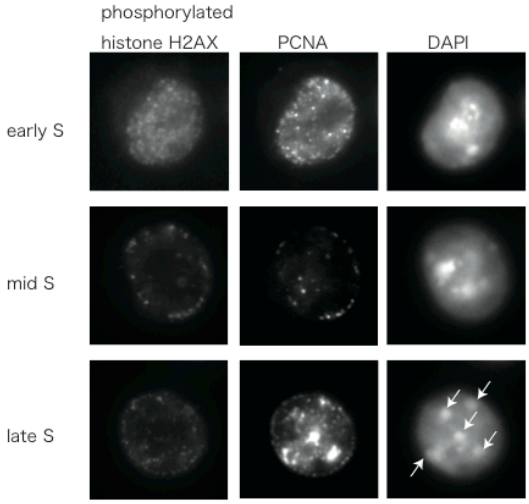

Fig. 1 Localization of phosphorylated H2AX and PCNA in mouse FM3A cells. Cells were treated with 4 mM hydroxyurea for 1 h. The cells were then immunostained with a rabbit anti-phosphorylated histone H2AX antibody and a mouse anti-PCNA monoclonal antibody and counterstained with DAPI. Arrows indicate pericentric heterochromatin.

To address these questions, I focused on pericentric heterochromatin regions, which are transcriptionally inactive and contain generally hypoacetylated histones in combination with histone H3 methylated on lysine 9. Because pericentric heterochromatin can be easily identified by dense DAPI staining in rodent cells, I investigated whether the phosphorylation of histone H2AX occurs in the heterochromatic region as well as in the euchromatic region.

In the presence of DNA replication inhibitors, a histone H2AX molecule that is adjacent to the DNA replication fork is phosphorylated by ATR (ataxia telangiectasia and Rad3-related) kinase. Because transcriptionally active and inactive chromatin domains generally replicate at different times during the S-phase (3), the phosphorylation of histone H2AX is induced in the specific chromatin regions in the presence of DNA replication inhibitors.

The sites of DNA replication were detected by an anti-PCNA antibody as shown in figure 1. In the early S phase, genetically active chromatin is replicated. In this stage, several hundred PCNA foci were distributed throughout the nucleus, except for in the nucleolus. In the mid-S phase, PCNA was localized in the periphery of the nucleus. From the early S phase to the mid-S phase, the distribution of phosphorylated histone H2AX was similar to that of PCNA, and some of the foci were colocalized. In contrast, genetically inactive chromatin is replicated in the late S phase. In this stage, PCNA foci were observed on the periphery of the nucleus or in the pericentric heterochromatin (indicated by arrows). Although the foci of phosphorylated histone H2AX were observed on the periphery of the nucleus, they were not detected in the heterochromatin. These results suggest that histone H2AX is absent from pericentric heterochromatin or that histone H2AX is not phosphorylated in pericentric heterochromatin efficiently.

Because homologous recombination depends on phorphorylated histone H2AX, it is assumed that DNA double strand breaks in pericentric heterochromatin are repaired by non-homologous end joining. The repair process in pericentric heterochromatin is now under investigation using mammalian cells irradiated with heavy ions.

References

1) C. Thiriet and J. J. Hayes: Mol. Cell 18, 617 (2005).
2) M. Izumi et al.: RIKEN Accel. Prog. Rep. 37, 144 (2004)
3) J. Quivy et al.: EMBO J. 23, 3516 (2004).
4) A. J. McNairn and D. M. Gilbert: BioEssays 25, 647 (2003).

Effect of DNA-PK inhibitors on the cellular sensitivity to heavy ions

M. Tomita,*1 T. Tsukada, N. Fukunishi, H. Ryuto, and M. Izumi

Accelerated heavy ions with high linear energy transfer (LET) can induce complex clustered DNA damage involving two or more DNA double-strand breaks (DSBs). The complexity of clustered DNA damage shows a strong LET dependence, which makes it a good candidate for the prime determinant of the higher biological effectiveness of high-LET heavy ions than low-LET X-rays.[1)]

In vertebrate cells, there are two major DSB repair pathways: non-homologous end-joining (NHEJ) and homologous recombination (HR).[2)] DNA-dependent protein kinase (DNA-PK), which is composed of a catalytic subunit (DNA-PKcs) and DNA-binding Ku70 and Ku86 heterodimer, is required for the repair of DSBs by NHEJ.[3,4)] We previously reported that DNA-PKcs phosphorylated on Thr2638 is recruited in the vicinity of clustered DNA damage induced by heavy ions.[5)] In addition, the relative biological effectiveness (RBE) for cell killing in DNA-PKcs-defective cells is significantly lower than that in normal cells.[6,7)] In this study, we investigate the sensitivity to heavy ions of human cervical cancer HeLa cells pretreated with DNA-PK inhibitors, wortmannin and NU7026.[8–10)]

Figure 1 shows the clonogenic surviving fractions of HeLa cells pretreated with 20 μM of wortmannin or 50μM of NU7026 irradiated with 250 kV X-rays (A), 135 MeV/u C ions at 80 keV/μm (B), or 95 MeV/u Ar ions at 310 keV/μm (C). The surviving fractions were determined by a colony formation assay. The pretreatment of wortmannin or NU7026 for 1 h significantly decreased the clonogenic survival of HeLa cells irradiated with X-rays (Fig. 1A) as previously reported[8–10)]. On the other hand, the sensitizing effect of inhibitors to C ions (Fig. 1B) or Ar ions (Fig. 1C) was lower than that to X-rays. Table 1 shows the dose required for 10% cell survival (D_{10}) calculated from the cell survival curve, and the RBE relative to that of X-rays. The RBE values in the cells pretreated with inhibitors were lower than those in the cells without inhibitors (control). Our present and previous results[5–7)] suggest that DNA-PK cannot efficiently react with the complex DSBs induced by high-LET heavy ions in the higher-vertebrate cells.

Table 1. D_{10} and RBE values

Inhibitor	D_{10}[a] (Gy)			RBE	
	X-rays	C	Ar	C	Ar
Control	5.7	2.4	1.8	2.3	3.2
50 μM NU7026	1.7	0.90	0.98	1.9	1.7
20 μM wortmannin	1.3	1.2	1.2	1.1	1.1

[a]The dose leading to 10% cell survival

*1 Central Research Institute of Electric Power Industry

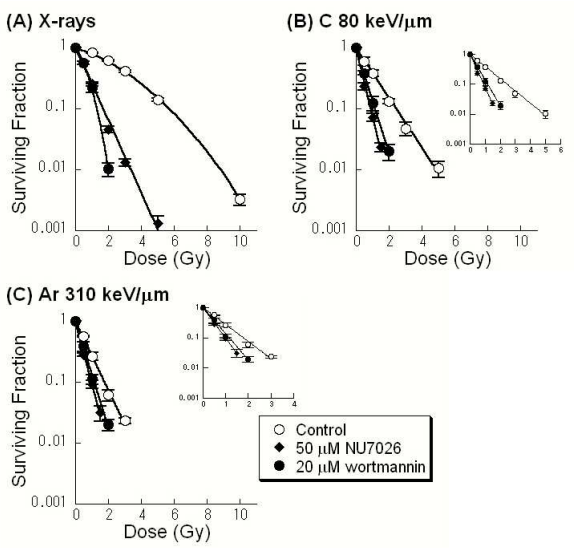

Fig. 1. Cell survival curves for HeLa cells pretreated with or without 50 μM of NU7026 or 20 μM of wortmannin for 1 h. Cells were irradiated with 250 kV X-rays (A), 135 MeV/u C ions (80 keV/μm) (B), or 95 MeV/u Ar ions (310 keV/μm)(C). Error bars represent standard errors of the means (SEM), which were obtained from two to three independent experiments.

References

1) D. T. Goodhead: J. Radiat. Res. **40**, Suppl. 1 (1998).
2) K. K. Khanna and S. P. Jackson: Nat. Genet. **27**, 247 (2001).
3) G. C. M. Smith and S. P. Jackson: Genes Dev. **13**, 916 (1999).
4) Y. Matsumoto et al.: FEBS Lett. **478**, 67 (2000).
5) M. Tomita et al.: RIKEN Accel. Prog. Rep. **38**, 129 (2005).
6) M. Tomita et al.: RIKEN Accel. Prog. Rep. **37**, 145 (2004).
7) M. Tomita et al.: RIKEN Accel. Prog. Rep. **39**, 131 (2006).
8) M. Tomita et al.: J. Radiat. Res. **41**, 93 (2000).
9) M. Tomita et al.: Radiat. Res. **160**, 467 (2003).
10) S. J. Veuger et al.: Caner Res. **63**, 6008 (2003).

Heavy ion irradiation of human cultured cells: The irradiated medium can reduce the rate of spontaneously induced mutations

F. Yatagai, Y. Umebayashi, M. Honma[*1], T. Abe, and M. Iwaki

It is important to elucidate the indirect effects of ionizing radiation at the cellular level. Here, the indirect effects means the cellular responses induced not in the cells directly hit by the ionizing radiation but in their neighboring cells, generally called as "bystander effect". The accelerated heavy-ions are very convenient for elucidating the above effects, because a hit or not-hit can be easily judged by the ion traversal through the cell. As a beginning stage of this line of studies, the preliminary experiments were performed by using the 135MeV/u carbon beam, as schematically illustrated in Fig.1.

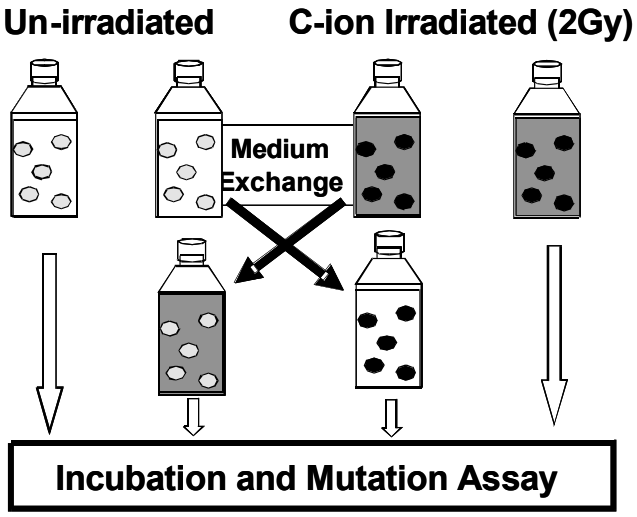

Fig. 1. A schematic illustration for the irradiation of cells and medium exchange

Human lymphoblastoid cell TK6 cells were incubated in RPMI1640 medium supplemented with HAT to eliminate pre-existing TK^- (thymidine kinase) mutants[1,2]. The cells were resuspended in fresh medium at 8×10^5 cells/ml, and 25 ml of cell suspension was dispensed into the culture flasks (Nunc, 25 cm^2). Unirradiated cells were suspended in the same flasks at 5×10^4 cells/ml. After the C-ion irradiation, both un-irradiated and irradiated cells were centrifuged and resuspended in the original medium or the exchanged medium as shown in Fig. 1. The suspensions of un-irradiated and C-ion irradiated cells were transferred to new T75 flasks (Falcon, non-treated tissue culture) and incubated for about 60 hrs (4 doubling-time) to reach 8×10^5 cells/ml at the end.

*1 National Institute of Health Sciences

In the mutation assay[1,2], the plating efficiency was measured by limiting dilution methodology to determine the fraction of viable cells. The TK^- mutant clones were judged by seeding cells into 96-well micro-well plates at 4×10^4 cells per well, in RPMI medium containing 4 μg/ml trifluorothymidine (TFT). Early TK^- mutant clones (EMs) and late mutant clones (LMs) were separately selected after two and four weeks of incubation with this selection medium, respectively, because the radiation exposure effects can be easily estimated by EM collection. The results are summarized in Table1. The exchange of medium for 2 Gy irradiated cells did not make any significant influences on both fractions of EM and LM in TK mutation frequency. Although the data is not shown in Table 1, this 2Gy irradiation reduced the cell surviving-fraction to about 10% or less. On the other hand, the EM for the un-irradiated cells were decreased from $(1.0 \pm 0.5) \times 10^{-6}$ to $(0.38 \pm 0.21) \times 10^{-6}$ by the medium change. However, the LM was not changed by this procedure. In other wards, the irradiated medium used for the cell irradiation could reduce the rate of spontaneous mutations induced at relatively early period.

Table 1 Measurements of TK^- mutation frequencies ($X10^{-6}$).

Un-irradiated Sample				Irradiated Sample (C-ion 2 Gy)			
Un-irradiated medium		Irradiated medium		Un-irradiated medium		Irradiated medium	
EM	1.0 ±0.5	EM	0.38 ±0.21	EM	13.8 ±2.4	EM	11.4 ±4.0
LM	1.2 ±0.2	LM	1.4 ±0.5	LM	23.5 ±1.8	LM	22.9 ±4.2
To-tal	2.3 ±0.6	To-tal	1.8 ±0.6	To-tal	37.3 ±1.4	To-tal	34.3 ±7.0

Data from 3 independent experiments are shown as mean ± SD.

The bystander effect is generally believed to provide the additional damage to the neighboring cells, for example mutation induction. From this kind of aspect, the present phenomenon might be classified as an adaptive response, which is defined to reduce the toxic and mutagenic effects of a particular stress by pre-treatment of the cells, for example, a pre-exposure with low-dose of ionizing radiation. We are now planning to elucidate the molecular mechanisms underlining the new phenomenon of indirect radiation effects.

References

1) F. Yatagai et al.: Mutat. Res. **560**: 133-145 (2004).
2) Y. Umevbayashi et al.: Biol. Sci. Space **19**: 237-241 (2005).

Mutation induction by heavy-ion irradiation in *Cyanidioschyzon merolae* 10D

M. Ohnuma[*1], T. Yokoyama[*2], T. Inoue[*2], H. Ichida, Y. Hayashi, N. Fukunishi, H. Ryuto, T. Abe, Y. Sekine[*2], K. Tanaka[*1]

Cyanidioschyzon merolae 10D is a unicellular red alga that lives in acidic hot springs. The *C. merolae* cell contains one nucleus, one mitochondrion and one plastid, assumed to be a primitive feature of this eukaryotic cell. The genome sequence of the nucleus and organelles of *C. merolae* have been completely determined. Bioinformatic analyses of the genome revealed that the alga has the simplest genome in photosynthetic eukaryotes and that many plastid genes, which have been lost or migrated to nucleus during evolution in higher plants, are found in the plastid genome in *C. merolae*. These features suggest that *C. merolae* preserves characteristics of ancient origin in the plant lineage.[1)] To utilize genome information of *C. merolae*, we are developing a transformation system for this alga.

Because few antibiotics are effective for what selection under cultivation conditions (pH 2.5, 42°C), the UMP synthase (*URA5.3*, the fusion gene of orotate phosphoribosyltransferase and orotidine-5'-phosphate decarboxylase) gene was considered the selection marker. Previously, we isolated a 5-fluoroorotic acid (5-FOA)-resistant mutant strain, M4.[2)] As expected, this strain showed uracil auxotrophy, and one base insertion mutation was found in the *URA5.3* gene. Thus, this strain was used as the host for the transformation experiments, in which wild-type *URA5.3* was used as the selection marker.[2)] However, the high frequency of reversion mutations made it difficult to discriminate true transformants from reverted mutants. Thus, the development of a host strain devoid of background reversion mutation is expected. In this study, we tried to isolate a mutant with a deletion mutation in *URA5.3* induced by irradiation with heavy ions.

For the irradiation of liquid culture, *C. merolae* cells were grown to about OD_{750}=1 in MA2 medium (40 mM $(NH_4)_2SO_4$, 4 mM $MgSO_4 \cdot 7H_2O$, 8 mM KH_2PO_4, 1 mM $CaCl_2 \cdot 2H_2O$, 0.1 mM $FeCl_3$ (EDTA·2Na), twofold concentration of trace elements described in Minoda et al. (2004), pH 2.5) containing 0.5 mg/ml uracil at 40°C under illumination. They were cultured in thin tubes (outside diameter: 5.57 mm, inside diameter: 4.29 mm) and irradiated with C (LET 23, 30, 42, 61 keV/μm), N (LET 30, 60 keV/μm) and Ne (LET 63 keV/μm) ions at a dose range of 0-200 Gy. The irradiated cells were incubated at 37°C in the dark for more than 10 hours. The cells were diluted and plated onto MA2 plates containing 2 mg/ml uracil and 0.8 mg/ml 5-FOA or spotted on a filter paper laid on the culture medium. The plates were incubated at 40°C under continuous illumination. Because of the poor colony formation efficiency of *C. merolae*, survival rate was calculated as follows: After incubation at 37°C in the dark for more than 10 hours, the irradiated cells were diluted to OD_{750}=0.05 and incubated at 40°C under illumination. After seven days, survival rate was calculated as OD_{750} relative to the OD_{750} of the nonirradiated cells set at 100%. The results are shown in Fig. 1. When an identical dose of C ions was used for irradiation, survival rate decreased with an increase in LET from 23 to 42 keV/μm. However, an increase in survival rate was observed at LET 61 keV/μm. The survival rate of the N-ion-irradiated cells at LET 60 keV/μm was higher than at LET 30 keV/μm. In these cases, the cells were irradiated around the stopping point and the beams would not have had sufficient energy to penetrate tubes. When Ne ions were used for irradiation at LET 63 keV/μm, they had sufficient energy to penetrate tubes. The LD_{50} values of C (LET 23 keV/μm), N (LET 30 keV/μm) and Ne (LET 63 keV/μm) ions were estimated to be 50, 60 and 40 Gy, respectively.

Eight 5-FOA-resistant strains were obtained and isolated from the plates on which cells in liquid culture were irradiated with C ions at LET 23 keV/μm and 25 Gy, and spotted onto filter papers (total approximately 10^7 cells). No 5-FOA-resistant cells arose with irradiation at 50, 75, 100 and 200 Gy. Because the spontaneous reversion mutation rate from M4 to the wild type was approxymately 2×10^{-7} (unpublished data), the eight 5-FOA resistant strains obtained are expected to have been derived from heavy-ion mutagenesis. However, sequence analyses of these 5-FOA resistant strains revealed that the strains harbor base change or insertion mutations in *URA 5.3* (Table 1).

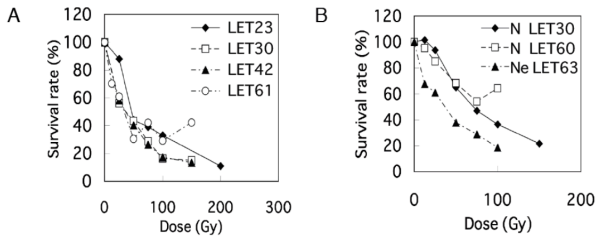

Fig. 1. Survival rate of *C. merolae* irradiated onto liquid culture. (A) C ion, (B) N or Ne ion.

Table 1. Mutation sites of *URA5.3* of 5-FOA-resistant mutants of *C. merolae* obtained by C ion irradiation.

	Mutation site	Mutation	No. of amino acid residues
WT	-	-	463
M4	ins-698A	Frameshift	248
25 Gy-1	C1069A	Nonsense	366
25 Gy-2	G962A	Nonsense	320
25 Gy-3	G962A	Nonsense	320
25 Gy-4	A271T	Nonsense	90
25 Gy-5	ins-1034T, C1039G	Frameshift	366
25 Gy-6	T437C	Miss-sense	463
25 Gy-7	T437G	Miss-sense	463
25 Gy-8	ins-698A	Frameshift	248

ins-indicates a base was inserted at the position.

References

1) M. Matsuzaki et al.: Nature 428, 653-657 (2004).
2) A. Minoda et al.: Plant Cell Physiol. 45, 667-671 (2004).

[*1] IMCB Univ. Tokyo
[*2] College of Science, Rikkyo (St. Paul's) Univ.

Isolation of salt-tolerant mutants of rice induced by heavy-ion irradiation

Y. Hayashi, H. Takehisa,[*1] Y. Kazama, C. Kanba,[*1] H. Saito, S. Ohbu, A. Tabayashi,[*2] H. Ryuto, N. Fukunishi, H. Tokairin, T. Sato,[*1] and T. Abe

Heavy-ion beam irradiation is an effective mutagen for various plants. In our previous paper, we reported the isolation of a lesion-mimic mutant and a tall mutant of rice by C or Ne ion irradiation[1]. In this report, we describe the isolation of salt-tolerant mutants of rice grown in a saline paddy field from M_2 progenies.

Rice (*Oryza sativa* L. cv. Nipponbare) seeds were presoaked for 3 days in water at 28℃ without light. The seeds that have imbibed water were then exposed to C or Ne ions accelerated to 135MeV/nucleon by the RRC within a dose range from 10 to 160Gy. After irradiation, the seedlings were transplanted to a paddy field. M_2 seeds were harvested separately from each M_1 plant approximately 6 months after irradiation. The seeds of 371 M_2 lines were presoaked as described above, sown on seedbeds in April, and grown in a greenhouse for 4 weeks. The plants were transplanted to the field at the end of May, and the paddy field was flooded with salt water two weeks after transplanting. The salt concentration of floodwater was maintained from 50 to 100mM Na+ during the experimental period by flooding with salt water (Na+ 120mM) or fresh water every week. Salt-tolerant mutants were observed in late October.

We isolated four lines of salt-tolerant mutants from 371 M_2 progenies examined (Table 1). All of these mutants were obtained from populations irradiated with C ions. Plant length was used for the evaluation of salt sensitivity. The mutant lines 6-99, 19-59 and 19-74 grown in the saline paddy field showed large plants height (Fig. 1). The mutant 19-55 line did not grow so tall but was still green when other plants were already withered up. The M_2 progenies of the 6-99 line as well as the 19-74 line were segregated into salt-tolerant and salt-sensitive plants, and salt-tolerance was fixed in M_3 generation. The M_2 plants of the 19-55 line were all salt-tolerant. However the M_3 plants of the 19-59 line were still showed segregation (Table 3).

Table 1. Effect of ion-beam irradiation on the induction of salt-tolerant mutation in rice

Ion	Dose (Gy)	LET (KeV/μm)	No. of M_2 lines with salt treatment	No. of salt-tolerant lines
C	20	23	82	3
C	20	37.4	77	0
C	40	23	91	1
Ne	10	60	121	0

*1 Graduate School of Life Sciences, Tohoku University
*2 Mitui Nourin Co.,Ltd.

Table 2. Height of salt-tolerant mutant plants

	Control paddy field (cm)	Saline paddy field (cm)	Rate* (%)
Control	94.34 ± 9.11	87.50 ± 4.94	92.7
6-99	106.96 ± 4.73	96.84 ± 9.15	102.6
19-55	88.60 ± 2.35	82.68 ± 2.61	87.6
19-59	−	94.50 ± 3.94	100.2

*Rate: height of plant grown in saline paddy field / control (94.34cm)

Table 3. Frequency of salt-tolerant mutants generated by C-ion irradiation

	Survival rate	Sensitive	Tolerant
6-99 (M_2)	38/50	29	9
(M_3)	49/50	0	49
19-55 (M_2)	46/50	0	46
19-59 (M_3)	46/50	22	24
19-74 (M_3)	49/50	0	49

Fig. 1. Segregated plants from salt-tolerant mutants grown in saline paddy field

Tolerant Sensitive
Control 6-99 (M_2)

Salinity is a serious problem in rice-growing countries. Breeding for salt tolerance involving multiple genes in rice is difficult, although the achievement of this breeding has been highly desired. It is suggested that these mutants have monogenic mutation in nuclear genes because of the rapid fixation of mutant lines. They are highly expected to be new cultivars for the fields on soil salination by parental use of these mutants. Furthermore, these mutants could be important resources for studies of the mechanisms controlling the salt tolerance of rice plants. Morphological and physiological analyses of these salt-tolerant mutants are in progress.

Reference

1) T. Abe et al.: RIKEN Accel. Prog. Rep. 39, 137(2006)

Isolation of inflorescence mutants induced by heavy-ion radiation in barley (*Hordeum vulgare* L.)

Eiko Hanzawa[*1], Hiroyuki Ichida[*2], Yoriko Hayashi, Hiromichi Ryuto, Nobuhisa Fukunishi, Tomoko Abe, Tadashi Sato[*1] and Atsushi Higashitani[*1†]

To isolate reproductive mutants in barley (*Hordeum vulgare* L.), dry seeds of two-rowed cultivar "Haruna Nijo" were irradiated with 30, 40 or 50 Gy of $^{12}C^{6+}$-ion beams (135MeV/u) by Riken Ring Cyclotron. Survival frequencies in both M_1 seeds and M_2 progenies did not decrease by the irradiation with less than 50 Gy of the ion beams (Table 1,2). On the other hand, the frequencies of appearance of chlorophyll-deficient mutants (Albino) in M_2 progenies increased as 0.2% at 30 Gy, 0.5% at 40 Gy and 0.6% at 50 Gy, respectively (Table 2). However, these frequencies are much lower than that of rice seeds irradiated with 40 Gy of the $^{12}C^{6+}$-ion beams (M_2: 7.3%)[1]. It may be due to larger size of chromosomes in barley plants.

We also isolated two mutant lines with six-rowed spikes among 1,436 M_2 seeds irradiated with 30 Gy. Six-rowed mutant phenotype in both lines was stably inherited into next generation (M_3). It has been reported that three six-rowed mutants were selected among 5,000 M_2 progenies after irradiation with 30kR of γ-ray[2]. The results from genetic analyses indicate that one of them is symbolized as *vrs1* on chromosome 2H, and the rest are the same mutant allele but different from *vrs1* locus. Lundqvist and Franckowiak have reported that at least four recessive alleles *vrs1*, *vrs2*[3], *vrs3*[4], and *vrs4*[5] are related to six-rowed spikes in barley plant. We are now attempting to determine the locus of the two mutant lines isolated in this study and to isolate other reproductive mutants from the M_2 pool.

Table 1. Survival and mutational frequencies in M_1 seeds.

Dose (Gy)	No. of seeds sowed	No. of survival plants (%)	Albino (%)	Six-rowed spikes (%)
0	24	24 (100)	0	0
30	675	667 (98.8)	0 (<0.1)	0 (<0.1)
40	669	621 (92.8)	1 (0.16)	0 (<0.1)
50	679	664 (97.8)	1 (0.15)	0 (<0.1)

Table 2. Survival and mutational frequencies in M_2 progenies.

Dose (Gy)	No. of seeds sowed	No. of survival plants (%)	Albino (%)	Six-rowed spikes (%)
0	110	100 (90.9)	0	0
30	1436	1268 (88.3)	3 (0.24)	2 (0.16)
40	1291	1155 (89.5)	6 (0.52)	0 (<0.1)
50	1339	1246 (93.1)	7 (0.56)	0 (<0.1)

[*1]Graduate School of Life Sciences, Tohoku University
[*2]Faculty of Horticulture, Chiba University
[†]Corresponding author:
Phone: +88-22-217-5715
FAX: +88-22-217-5745
E-mail: ahigashi@ige.tohoku.ac.jp

References
1) T. Abe, T. Matsuyama, S. Sekido, I. Yamaguchi, S. Yoshida and T. Kameya: J. Radiat. Res. 43, S157-S161 (2002)
2) T. Makino, M. Furusho and T. Fukuoka: BGN. 24, 122 (1995)
3) U. Lundqvist and J.D. Franckowiak: BGN. 26, 263 (1997)
4) U. Lundqvist and J.D. Franckowiak: BGN. 26, 264-265 (1997)
5) U. Lundqvist and J.D. Franckowiak: BGN. 26, 159-160 (1997)

Mutation induction by heavy-ion beam irradiation in tartary buckwheat

T. Morishita*[1], Y. Miyazawa*[2], H. Saito, Y. Hayashi, H. Ryuto, N. Fukunishi and T. Abe

Recently, heavy-ion beams have been regarded as a new mutagen for plant breeding because of their high LET (linear energy transfer) and high RBE (relative biological effectiveness). We previously reported the biological effects of ion beams on buckwheat[1]. In this report, we describe the mutation inducing effect of ion beams on tartary buckwheat.

Dry tartary buckwheat (var: Rotundatum) seeds were irradiated with $^{12}C^{6+}$ (135 MeV/u), $^{20}Ne^{10+}$ (135 MeV/u), ^{13}N (135 MeV/u, 26.4 keV/μm), $^{40}Ar^{17+}$ (95 MeV/u, 305 keV/μm), and $^{56}Fe^{24+}$ (90 MeV/u, 630 keV/μm) ions. To adjust the LET of $^{12}C^{6+}$ and $^{20}Ne^{10+}$-ions at the surface of the seeds, an absorber was placed in front of the samples. The irradiated seeds (M_1) were sown and M_2 seeds were harvested from the M_1 plants. M_2 seeds were sown in the upland field in plant-to-row lines. Visible mutant traits, such as leaf color and morphological mutations were investigated.

Table 1 shows the mutation frequencies and types of mutants in the M_2 generation. Mutation frequency increased with an increase in dose. In particular, when irradiation dose was 100 Gy, a high mutation frequency (more than 10%) was observed. Various mutants were obtained by irradiation treatments. Among the morphological mutations observed, dwarfism was the mutation most frequently observed. Leaf color mutants were also observed frequently. However albino mutants were only observed for 100 Gy carbon ions with 39 keV/μm irradiation treatment. Because some of these mutants were fertile, we collected M_3 seeds and will research the agronomic characteristics of the mutants in the future.

Reference

1) T. Morishita et al.: RIKEN Accel. Prog. Rep. 36, 137 (2003)

Table 1. Mutation frequencies and types of mutants in M_2 generation

Radiation	LET (keV/μm)	Dose (Gy)	No. of lines	Mutation No.	Mutation Frequency (%)	No. of mutants: Leaf Color: Albino	Yellow	Yellowish green	Dark green	Other	Morphological character: Dwarf	Wrinkle leaf	Dense leaf	Small leaf	Other
Carbon	23	10	16	1	6.2	0	0	0	0	0	1	0	0	0	0
		20	64	5	7.8	0	0	0	0	0	5	0	0	0	0
		30	42	2	4.8	0	0	0	0	0	1	0	0	0	1
		40	94	3	3.2	0	0	0	0	0	3	0	0	0	0
		50	90	2	2.2	0	0	0	0	1	1	0	0	0	0
		100	33	5	15.2	0	0	0	0	0	3	1	0	0	1
		200	38	7	18.4	0	0	1	0	1	2	1	1	0	1
		300	24	3	12.5	0	1	0	1	0	0	0	0	0	1
Carbon	39	100	101	11	10.9	1	2	0	3	0	3	1	1	0	0
		200	38	5	13.2	0	0	0	1	1	1	1	0	1	0
		300	4	0	0.0	0	0	0	0	0	0	0	0	0	0
Carbon	62	10	41	4	9.8	0	0	0	0	0	2	1	1	0	0
		30	32	3	9.4	0	0	0	1	0	1	0	0	0	1
		50	14	3	21.4	0	0	0	1	0	2	0	0	0	0
		100	10	0	0.0	0	0	0	0	0	0	0	0	0	0
Carbon	98	10	86	7	8.1	0	0	0	0	0	6	1	0	0	0
Nitrogen	26	10	229	1	0.4	0	0	0	0	0	0	0	0	0	1
Neon	63	100	41	0	0.0	0	0	0	0	0	0	0	0	0	0
		200	20	3	15.0	0	0	0	0	0	1	0	1	1	0
Argon	305	10	111	4	3.7	0	0	0	0	0	3	0	0	0	1
		20	89	4	4.5	0	0	0	0	0	4	0	0	0	0
		10	45	2	4.4	0	0	1	0	0	0	0	0	0	1
		20	8	2	25.0	0	0	1	0	1	0	0	0	0	0
Iron	630	10	180	12	6.7	0	1	0	1	0	7	0	0	0	1
		20	156	11	7.1	0	0	0	3	0	3	3	1	1	0
		10	89	11	12.4	0	0	1	2	1	4	0	2	0	1
		20	33	1	3.0	0	0	0	0	0	0	1	0	0	0
		30	25	2	8.0	0	0	0	0	0	2	0	0	0	0

*1 National Institute of Agrobiological Sciences

*2 Grad. Sch. Life Sci., Tohoku Univ.

Effects of carbon-ion beam irradiation on plant growth and mutation induction in *Nicotiana tabacum*

H. Saito, H. Ryuto, N. Fukunishi and T. Abe

In our previous study, we successfully induced frequent mutations in tobacco by irradiating developing embryos with a heavy-ion beam[1]. However, it is difficult to apply this method at specific stages of plant development. In this study, therefore, we examined the effects of heavy-ion beams on plant growth and mutation induction in seeds and *in vitro* leaf cultures of tobacco.

Dry seeds, imbibition seeds and *in vitro* leaf culturs of tobacco (*Nicotiana tabacum* cv. Xanthi) were irradiated with ^{12}C-ion beams (135 MeV/nucleon) at a dose ranges of 0 - 300, 10 - 20 and 0 - 20 Gy, respectively. The LET of ions corresponded to 23keV/μm. To prepare imbibition seeds, dry seeds were incubated on 1/2MS agar medium plates for 1 to 2 days before irradiation. For leaf cultures, intact true leaves (5-10mm in diameter) were prepared from two-week-old seedlings incubated *in vitro* and cultured in MS medium containing 1mg/l BA, 3% sucrose and 0.2% gellan gum under continuous illumination for one or 14 days before irradiation. After irradiation, dry and imbibition seeds were incubated in 1/2MS agar medium for two weeks. On the other hand, leaf explants were transferred to the same fresh medium to regenerate adventitious shoots. Regenerated shoots were cut from explants and transferred to 1/2MS agar medium for rooting. All plantlets were grown in a green house at 25°C under a 16h/8h (light/dark) illumination cycle. The frequency of albino plants in 20 M_2 seeds of each line was measured two weeks after sowing in 1/2MS agar medium.

Seed germination was not affected by any of the irradiation treatments tested (**Table 1**). However, a decrease in the number of plants surviving after germination was observed only in the plants from 300 Gy-irradiated dry seeds. Although there was little difference in the growth rates of all the plants cultivated to the seed harvest, high-dose irradiation for each imbibition treatment decreased the yield of M_2 seeds. In the irradiation treatments of leaf cultures, decreases in the number of adventitious shoots regenerated and the frequency of the rooting of adventitious shoots were observed with an increase in dose (**Table 2**). Additionally, differences in sensitivity to the C-ion beams between the one- and 14-day precultures were observed. Although most transplanted plants flowered, high-dose irradiation decreased the number of plants producing seeds and the yield of seeds. In this study, few M_1 plants with solid morphological abnormalities were produced in any of the treatments. Additionally, most M_2 seeds germinated and most seedlings developed normal true leaves. Thus, no albino plants in any of the lines (367 M_2 lines) were obtained in this study. Five M_2 seedlings obtained from each irradiation treatment were cultivated in pots, and the isolation of mutants and characterization of the M_2 generation are in progress.

Acknowledgement

This work was supported by a grant from the Research project for utilizing advanced technologies in agriculture, forestry and fisheries from the Ministry of Agriculture, Forestry and Fisheries of Japan.

References

1) T. Abe et al.: in *Modification of Gene Expression and Non-Mendelian Inheritance*, edited by K. Ono and F. Takaiwa, (NIAR, 1995), p. 469.

Table 1.
Effects of C-ion beam irradiation on germination, growth and mutation induction in dry and imbibition seeds of *Nicotiana tabacum* cv. Xanthi [a].

Days of imbibition	Irradiation dose (Gy)	No. of seeds irradiated	No. of seeds germinated (%)	No. of plants surviving (%)	No. of plants flowering (%)	Plant height at flowering (cm)	No. of plants producing seeds (%)	No. of seed pods produced in the first inflorescence	Yield of seeds per pod (mg)	% of M_2 seeds germinated	No. of albino plants in M_2 seedlings
0 [b]	0	60	60 (100)	60 (100)	60 (100)	150.6±1.8	59 (98.3)	8.8±0.7	38.8±3.8	95.8±1.2	0
	200	40	39 (97.5)	39 (97.5)	39 (97.5)	152.1±3.4	37 (92.5)	11.8±0.8	35.5±3.6	97.3±0.6	0
	250	40	39 (97.5)	39 (97.5)	39 (97.5)	143.8±4.2	31 (77.5)	10.1±1.0	26.2±3.7	98.4±0.5	0
	300	40	38 (95.0)	24 (60.0)	-	-	-		-		
1	10	40	40 (100)	40 (100)	-	-	-		-		
	15	40	40 (100)	40 (100)	-	-	-		-		
	20	40	39 (97.5)	39 (97.5)	39 (97.5)	136.7±2.6	36 (90.0)	10.8±1.1	27.8±3.8	97.9±1.0	0
2	10	40	40 (100)	40 (100)		-	-		-		
	15	40	40 (100)	40 (100)	-						
	20	40	40 (100)	40 (100)	40 (100)	148.6±1.7	38 (95.0)	7.9±0.8	31.6±4.3	84.1±5.5	0

a: Irradiation-derived plants were grown in a greenhouse during summer.
b: Irradiation of dry seeds.

Table 2.
Effects of C-ion beam irradiation on adventitious shoot regeneration, shoot growth and mutation induction in *in vitro* leaf cultures of *Nicotiana tabacum* cv. Xanthi [a].

Days of culture before irradiation	Irradiation dose (Gy)	No. of leaf explants irradiated	No. of shoots regenerated per explant (%)	% of shoots rooted	No. of shoots planted	No. of plants flowering (%)	Plant height at flowering (cm)	No. of plants producing seeds (%)	No. of seed pods produced in first inflorescence	Yield of seeds per pod (mg)	% of M_2 seeds germinated	No. of albino plants in M_2 seedlings
1	0	50	22.2±1.3	82.9	21	18 (85.7)	141.1±4.6	18 (85.7)	6.5±0.7	50.5±5.6	98.9±0.6	0
	5	50	15.1±1.0	42.6	80	80 (100)	126.5±3.3	60 (75.0)	12.2±1.2	15.0±1.9	86.8±3.9	0
	10	50	6.9±0.7	45.2	50	50 (100)	104.3±3.3	17 (34.0)	6.7±1.6	5.3±1.5	92.0±4.1	0
	15	50	1.8±0.4	39.1		-						
	20	50	0	-		-						
14	0	50	15.8±1.5	91.9	14	14 (100)	146.8±5.2	14 (100)	7.9±0.7	65.6±7.3	99.6±0.4	0
	5	50	11.6±1.3	68.4	86	82 (95.3)	129.6±1.9	77 (89.5)	11.6±0.8	33.8±2.5	97.0±1.3	0
	10	50	10.5±0.1	47.1	41	40 (97.6)	132.0±3.3	31 (75.6)	9.7±1.2	21.9±3.5	94.1±3.3	0
	15	50	8.0±0.7	34.8	44	44 (100)	111.8±4.0	26 (59.1)	11.6±1.8	10.3±2.3	97.7±0.7	0
	20	50	4.7±2.0	25.7	-	-						

a: Irradiation-derived plants were grown in a greenhouse during winter.

Establishment of sex identification method and effect of N-ion beam irradiation in dioecious plant *Carica papaya*

Y. Kazama, H. Ichida, Y. Hayashi, H. Ryuto, N. Fukunishi, N. Wakita[*1], K. Yamamoto[*1], S. Ijichi[*2] and T. Abe

Papaya (*Carica papaya* L.) is a widely cultivated fruit crop in tropical and subtropical regions worldwide. It is one of the special products of Wadomari. Wadomari is located in the Okinoerabu Island, which is struck by typhoons during the harvest time of papaya every year. A papaya tree is so tall that it is frequently blown down by typhoons. It is therefore desired to produce a dwarf papaya, which is resistant to a strong wind. The aim of this study is to induce dwarfism in papaya by heavy-ion irradiation. Papaya is a polygamous species with three basic sex types: female, male, and hermaphrodite. The sex in papaya is determined by XY-type sex chromosomes[1),2)]. The male genotype is XY, the female genotype, XX, and the hermaphrodite genotype, XY^h, where Y^h is the modified Y chromosome. Because papaya is a fruit crop, females (XX) and hermaphrodites (XY^h), which bear fruit, are profitable. In particular, hermaphrodites (XY^h) are a desirable material for mutation breeding, because they are capable of self-pollination. However, the sex of papaya cannot be morphologically distinguished before the flowering stage (6-9 months after the seedling satage). The establishment of a sex-identification method in the seedling stage is required to increase the efficiency of mutation breeding. We report here the sex-identification method in the seedling stage and the effect of N-ion beam irradiation on the survival rate of native papaya in Wadomari.

To establish the sex-identification method in the seedling stage, we examined the optimum conditions of polymerase chain reaction (PCR) with sex-specific primers. Two hermaphrodite- or male-specific primer sets, Nafp[3)] and PSDM[4)], and a sex-neutral primer set, GN[3)], were tested. Seeds were harvested from a hermaphrodite fruit and grown in flower pots at 26°C until the seedling stage. Seedlings include females and hermaphrodites. Genomic DNAs were isolated from the seedlings and subjected to 30 cycles of PCR amplification (94°C for 1 min, annealing temperatures for 1 min, and 70°C for 1 min) with each primer set. The annealing temperatures ranged from 45 to 55°C. Amplification products were analyzed on a 1.5% agarose gel and visualized by SYBR-Green I staining. Nafp and GN primer sets successfully amplified their specific products at the annealing temperature of 45°C (Fig. 1). The Nafp primer set of produced a single badn corresponding to an 831-bp sex-specific fragment only in hermaphrodites, whereas the GN primer set produced a single 600-bp band in both hermaphrodites and females. The PSDM primer set did not produce any bands. We conclude that the Nafp primer set is suitable for sex identification in native papaya in Wadomari.

To ditermine the survival rate, dry papaya seeds were exposed to N-ion beams accelerated to 135 MeV/nucleon by the RRC within 100 to 175 Gy. The seeds were incubated at 70 degree of water for 15 min. One month after sowing on flower pots with peat moss, viable plants were counted. The survival rate decreased with increasing irradiation dose (Fig. 2). The LD_{50} of the seeds was 175 Gy. From this result, we conclude that the appropriate irradiation dose for papaya mutagenesis is 100-125 Gy. The mutagenesis and screening of dwarf mutants are in progress.

This work was partly supported by a grant from Wadomari.

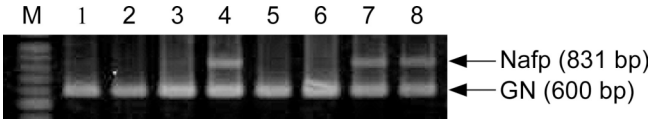

Fig. 1 Sex identification by PCR using sex-specific markers. Nafp and GN indicate hermaphrodite-specific and sex-neutral products, respectively. M: molecular marker, 1, 2, 3, 5, and 6: females, and 4, 7, and 8: hermaphrodites.

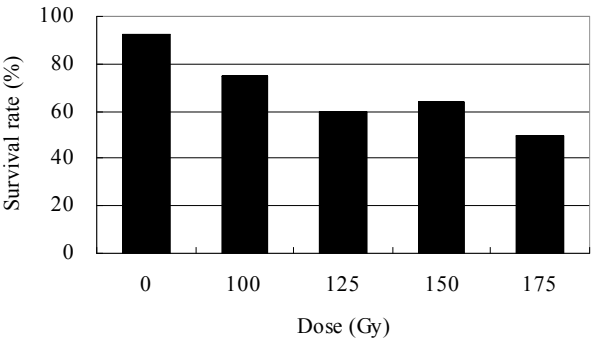

Fig. 2 Effect of N-ion beam irradiation on survival rate of papaya.

References

1) S. Horovitz and H. Jimenez: Agron. Trop. **17**, 323 (1967).
2) Z. Liu et al.: Nature **427**, 348 (2004).
3) A.S. Parasnis et al.: Mol. Breed. **6**, 337 (2000).
4) N. Urasaki et al.: Theor. Appl. Genet. **104**, 281 (2002).

[*1] Wadomari-Cho Agricultural Experimental Station
[*2] Mayor of Wadomari

Floral and sexual mutants yielded by C-ion beam irradiation on the dioecious plant *Silene latifolia*

K. Nishihara,* Y. Kazama, A. Koizumi,* H. Ichida, Y. Hayashi, H. Ryuto, N. Fukunishi, S. Kawano,* and T. Abe

The caryophyllaceous perennial herb *Silene latifolia* is a dioecious plant whose sex is determined genetically by the sex chromosomes. A plant with an X chromosome and a Y chromosome has male flowers, whereas a plant with two X chromosomes has female flowers. It is presumed that the Y chromosome has some regions involved in the suppression of gynoecium development, the promotion of early stamen development, and the promotion of anther maturation[1]. However, the genes responsible for sex determination have not been identified in *S. latifolia*. To identify them, we planned to produce chromosome deletion mutants, investigate the relationship between the deletions and phenotypes, and corroborate the transmission of the mutations to their progenies.

Since C-ion beam irradiation induces the local deletion of chromosomes, this treatment can be used to develop new cultivars in various plants. In this study, dry seeds of *S. latifolia* were exposed to C-ion beams (135MeV/nucleon) to produce floral and sexual mutants by chromosome cleavage and fusion. To determine an appropriate absorption dose for differential induction, the dry seeds were irradiated with C-ion beams within a dose range of 20 - 200 Gy. We counted the number of individuals that sprouted true leaves 20 days after sowing the irradiated seeds to plot a survival rate to dosage curve (Fig. 1). The survival rate was 90% at 75 Gy or less but decreased with an increase in dosage from 75 Gy. Growth inhibition was observed in the irradiated and surviving plants. Growth inhibition rate correlated to dosage in similarly to with survival rate.

By cultivating M_1 generations and screening their morphology, we obtained six mutants that showed morphological aberrations from the 170 individuals irradiated at 100 and 120 Gy. Two albino mutants were obtained. One mutant had entirely white leaves and another had variegated leaves that were partially white. Of the three numeric-aberration mutants, two had six petals (Fig. 2, a and b) and the other mutant had six or seven carpels with normal 5-petaled flowers, respectively (Fig. 2, c and d). A wild-type flower has five petals and five carpels (Fig. 2, e and f). The last mutant was a bisexual-flower mutant that had both stamens and gynoecium.

Blooming distribution showed that 10 of 54 flowers were males and the others were the bisexual flower shown in the bisexual-flower mutant. This bisexual-flower mutant originated from a male plant because it does not have female flowers except for the male and bisexual flowers. Bisexual flowers of this mutant self-pollinate between their own stamens and stigmas to produce seeds. The germination percentage of these self-pollinated seeds was 25%.

We plan to screen for hermaphrodite progeny from the segregated M_2 progenies and examine the mutated regions on the Y chromosome. We have started to irradiate C-ion beams on 1,000 fresh dry seeds at 100 Gy and perform a broad-scale screening for more sexual mutants.

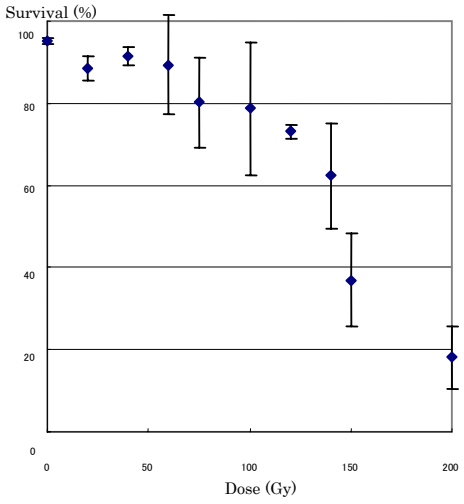

Fig. 1. Survival curve of dry seeds irradiated with C-ion beams in *S. latifolia*.

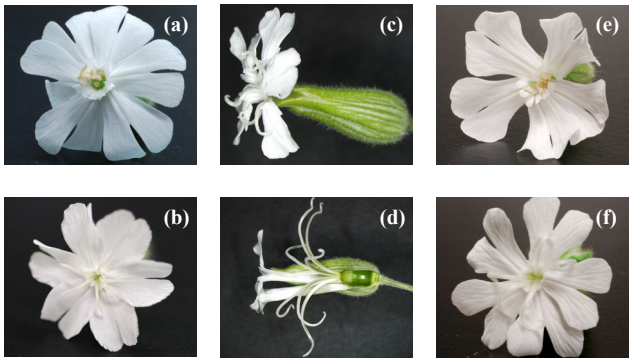

Fig. 2. Numeric-aberration mutants produced by C-ion beam irradiation. (a) male flower with six petals. (b) female flower with six petals. (c) female flower with seven carpels. (d) longitudinal section of female flower with seven carpels. (e) wild-type male flower. (f) wild-type female flower.

* Department of Integrated Biosciences, Graduate School of Frontier Sciences, The University of Tokyo

References

1) Westergaard: Hereditas 32, 419 (1946).

Effect of ion beam irradiation in Chinese chive (*Allium ramosum* L.)

M. Takahashi*, Y. Matsuda*, Y. Kazama, Y. Hayashi, H. Saito, H. Ryuto, N. Fukunishi, T. Abe and T. Murata*

It is difficult to improve the agronomic traits of Chinese chive (*Allium ramosum* L.), by the the traditional method of crossing, because of its apomict nature by diprospory (parthenogenesis and chromosome doubling). We report here the effects of subjecting Chinese chive seeds to ion beam irradiation in order to induce mutants.

Mature seeds of two Chinese chive cultivars, 'Wide Green' (for leaf use: W.G.) and 'Flower Pole' (for flower stem use: F.P.) were irradiated by $^{12}C^{6+}$ ions (135 MeV/nucleon, LET 22.6 keV/μm) within a dose range of 2.5 to 50 Gy. The irradiated seeds were sowed in the pots containing commercial soil (N=2.5 g, P=11 g, K=3 g /10 kg) on April 4, 2003, and cultivated under the natural conditions. Plants were transplanted into the pots containing new soil, in early of April of every year.

Leaf length and leaf width were measured in August, 2005. Both length and width were varied in irradiated W.G.. In particular, both parameters were larger in the plants that grow from seeds subjected to 25 Gy irradiation than in the control (Fig. 1).

Such variation may have been induced by chromosome doubling; thus, the ploidy of the plants was estimated using a flow cytometer (EPICS XL / XL-MCL System II). From the results of flow cytometory, ploidy was found to have not changed (data not shown). These results suggest that morphological variation is induced by ion beam irradiation. Further estimation of the mutations will be achieved in the next progeny derived from the irradiated generation.

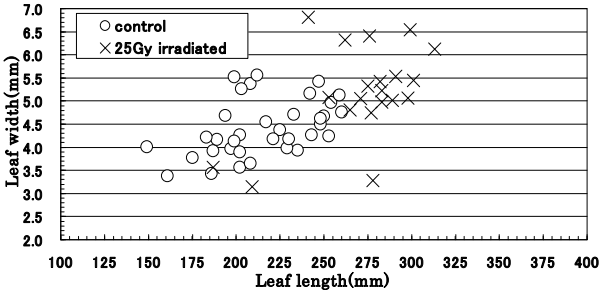

Fig.1 Morphological variation of leaves in ion-beam-irradiated *A.ramosum* L.cv.'Wide Green'.

Variations in morphological and the number of floral organs were observed in florets of the irradiated plants (Fig. 2).

The frequency of parthenogenesis was estimated by embryo sac analysis (Kojima and Nagato 1992a) in the period of August to September in 2005, for the florets 4 days after flowering. Abnormal ovules (swollen integument and depauperated embryo sac: Fig. 3A and B) were observed in florets of irradiated plants, and the frequency of abnormal ovule formation increased with increasing dosage (Fig. 3C). However, nonparthenogenetic plants were detected in 4 plants. One plant each for 10Gy and 50Gy irradiation, and two plants for 25Gy irradiation (Table 1) were obtained. We will examine the utility of this character, further.

In this study, the effect of ion beam irradiation on Chinese chive seeds showed mutation induction in both vegetative and sexual organs, Ion beam irradiation will be useful for genetic magnification in this species. We will try to cross between 4 nonparthenogenetic plants and apomict plants to produce a hybrid seed by sexual reproduction, and discuss its useful as a new breeding material.

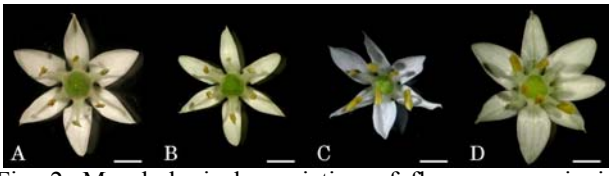

Fig. 2. Morphological variation of flower organ in ion-beam-irradiated *A.ramosum* L. cv.'Wide Green'. A: Floret in control plant. B,C,D: Florets in irradiated plants. The scale bar represents 3mm

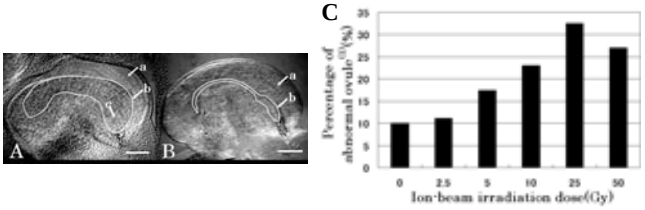

Fig.3 Aberration of ovule in ion-beam-irradiated *A.ramosum* L. cv. 'Flower Pole'. A:Normal ovule in non-irradiated specium. B: Abnormal ovule in irradiated specium. a: Integument cell. b: Embryo sac. c: Parthenogenetic embryo. The scale bar represents 200 μm. C: Effect of ion beam does on frequency of abnormal ovule formation in *A.ramosum* L. cv. 'Flower Pole'. (1) Number of ovules which has atrophy embryo sac and hypertrophic integument cell / total number of observed ovules × 100.

Table 1 Frequency of parthenogenesis in ion beam irradiated *A.ramosum* L. cv. 'Flower Pole'

Irradiation dose(Gy)	No. of observed plants	No. of non parthenogenetic plants(1)	No. of parthenogenetic plants	Percentage of parthenogenesis(%)
0	34	0	34	0
2.5	22	0	22	0
5	29	0	29	0
10	27	1	26	3.7
25	27	2	25	7.4
50	25	1	24	4.0
total	164	4	160	2.5

(1) : Plant ovule did not develop parthenogenic embryo

Sch. Agr. Kyushu Tokai U.

Floral Color Mutations Derived from Heavy-Ion Beam irradiation in a *Torenia* Cultivar

Takeshi Kanaya[*1], Kiyoshi Miyazaki[*1], Kenichi Suzuki[*1], Kazunari Iwaki[*1], Hiroyuki Saito, Yoriko Hayashi, Hiromichi Ryuto, Nobuhisa Fukunishi, Tomoko Abe
[*1]Suntory Flowers, Ltd.

The heavy-ion beam is known as an effective mutagen for various plants. Riken and Suntory Flowers, Ltd., have jointly developed some new ornamental varieties of *Verbena* and *Petunia* using heavy-ion beam irradiation[1]. We report here a new mutant of *Torenia* obtained by heavy –ion beam irradiation.

Horticultural varieties of *Torenia* are one of the most important worldwide summer bedding plants. However, the flower color range of these varieties is limited.

Meanwhile, Miyazaki et al. (2006) reported the heavy-ion beam irradiation of *Torenia*[2]. The *Torenia* hybrid 'Summer Wave Blue' (Suntory Flowers, Ltd.) was used as the starting material. Tissue culture materials of leaf tissue and stem internodes without lateral meristems were irradiated with N ions and Ne ions. As a result, some floral color mutants including pale blue, blue without blotches, pale pink, and pink were obtained. The maximum frequencies per acclimatized plant obtained by N-ion and Ne-ion irradiation were 1.89% for N 50Gy and 1.64% for Ne 20Gy. These mutants were maintained by cuttings. However, some back mutations were observed on several shoots.

In the present study, tissue culture materials of the leaf tissue of 'Summer Wave Blue' were used and irradiated with C ions. Irradiation treatment was conducted at dosages of 5, 10, and 20 Gy; 40 leaves were treated at each dosage.

The number of developed shoots from the leaves is shown in Fig.1. There was no significant difference in the number of developed shoots for different dosages. However, some floral color mutants including light blue, and white with pink blotches were obtained from the irradiated materials. Cuttings were made of all the mutants and they were maintained. Some back mutations were observed on several shoots as well as N ions and Ne ions. However, a mutation that was white with pink blotches was obtained (Fig.2). This mutant showed a high level of floral color stability. There are no differences in other characteristics, such as flowers size, plant form, and, vigorous growth habit, from the parent plant.

As a conclusion, it is difficult to obtain highly stable floral color mutants of *Torenia* using heavy-ion beams. However, as indicated by the present study, it is possible that *Torenia* mutants with high stability can be obtained.

For this reason, heavy-ion beams demonstrate high potential for obtaining artificial mutants of *Torenia*.

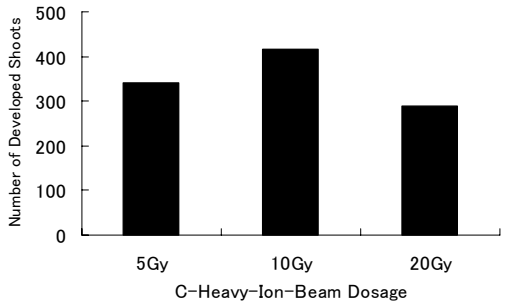

Fig.1. Number of shoots developed from 40 pieces of leaves irradiated with C-ion beam.

Fig.2. Flowers of *Torenia* mutant.

References

1) K. Suzuki et al.: Radiation & Industries 99, P40 (2003).
2) K. Miyazaki et al.: Plant Biotechnology 23, P163-167 (2006).

Induction of flower mutant by heavy-ion beam irradiation of cyclamen

M. Sugiyama,* T. Terakawa,* H. Saito, H. Ichida, Y. Hayashi, N. Fukunishi, H. Ryuto, and T. Abe

Recently, we have investigated the effect of heavy-ion beam irradiation on the cyclamen, an ornamental plant displayed in winter, with the aim of establishing a protocol for efficiently producing a novel mutant.[1] In this study, the effect of a heavy-ion beam on the cyclamen was examined using the tuber of this plant as a target for irradiation.

Tubers of the cyclamen (8-15 mm in diameter, cv. Hokko mini no. 3) produced by tissue culture were placed on hormone-free 1/3 MS medium after their leaves and roots had been removed. Then, the tubers were irradiated with a ^{12}C ion beam (135 MeV/nucleon, LET 23 KeV/μm) at doses of 4, 8, 12 and 16 Gy (30 specimens/dose). The irradiated samples were transplanted onto the aforementioned medium for plant elongation and rooting. Three months after the irradiation, the plants were transplanted to flowerpots and were grown in a greenhouse. Ten months after the planting, the surviving rate of the plants relative to the total number of irradiated tubers and the mutations in flower morphology were examined.

The effects of the irradiation on the plants are shown in Table 1. The survival rate ranged from 50 to 90%. Sterile male mutants whose anthers were atrophic or deficient were obtained at a range from 8 to 16 Gy (Figs. 1 (b), (c)). Two petal color mutants were obtained at 12 Gy. The petals of one mutant was reddish purple, whereas the petals of the original was bluish purple. The petals of the other mutant exhibited a striped pattern of white over the underlying original color (Fig. 2 (b)). All the mutated plants showed not only mutated flowers but also normal ones, which suggests the chimeric nature of these mutants.

Traditionally, a new variety of cyclamen has been developed mainly by crossbreeding, which requires many crossings and considerable time. Results of this report suggest that mutation induction by heavy-ion beam irradiation is useful for changing flower characteristics and can shorten the breeding process of cyclamen. The sterile male mutant did not produce pollen. Thus, the genes of such mutant never spread to the offspring through the pollen. Male-sterilizing a transgenic crop lowers the risk of undesirable gene flow from the transgenic plant to the wild type plants via pollination. The development of a sterile male mutant of a transgenic cyclamen by heavy-ion beam irradiation is in progress.

This work was supported by a grant from the Research project for utilizing advanced technologies in agriculture, forestry and fisheries.

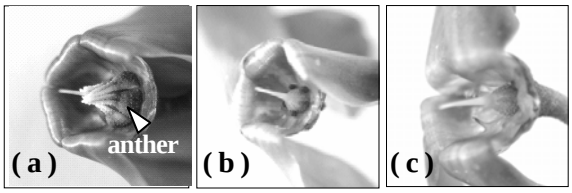

Fig. 1. Sterile male mutant obtained by heavy-ion beam irradiation. (a) Wild type, (b) mutant whose anther is atrophic, and (c) mutant whose anther is deficient.

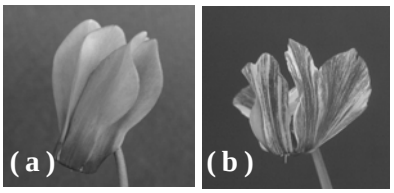

Fig. 2. Petal color mutant obtained by heavy-ion beam irradiation. (a) Wild type (bluish purple) and (b) petal color mutant (striped pattern).

References

1) M. Sugiyama et al.: RIKEN Accel. Prog. Rep. 39, 142 (2006)

Table1. Number of plants surviving irradiation with heavy-ion beam and number of mutants obtained.

Dose (Gy)	Number of plants surviving §1	Survival rate (%)	Number of mutants	
			Sterile male mutants	Petal color mutants
Control	27	90	0	0
4	20	67	0	0
8	26	87	1 (3.8) §2	0
12	15	50	2 (13)	2 (13)
16	19	63	1 (5.3)	0

§1 : 30 specimens were submitted for each dose
§2 : Frequency of mutants (%)

*Hokko Chemical Industry Co., Ltd.

Proton conducting polymer

J. Sugiyama,[*1] H. Nozaki,[*1] Y. Ikedo,[*1] K. Mukai,[*1] A. Kamiya,[*1] M. Kawasumi[*1], T. Suzuki[*2], and I. Watanabe[*2]

[Polymer, muon, diffusion]

1 Introduction

Among several electrolytes for fuel cells (FC), only Nafion[1], perfluorinated sulfonic acid copolymer, is commercially available to make an FC working at ambient temperature. Nafion is however ionically conductive only when it contains water, meaning a very limited performance above 373 K, although we need an electrolyte with high proton conductivity up to ∼ 423 K. In order to know information on proton conductivity without water, we have performed a μ^+SR experiment on Nafion for detecting proton hopping via muon diffusion.

2 Experimental

After immersing in H_2O, Nafion films with ∼180 μm thickness were dried in vacuum at 100^{o}C for 12 hours, then six films with 26 mm diameter were stacked in a sealed sample cell in an Ar-filled globe-box in Toyota CRDL, and then the cell was transferred to the UK and was set onto the oven sample holder. The μ^+SR experiment was carried out on the ARGUS surface muon beamline at RIKEN Muon Facility at ISIS in the temperature range between 300 and 450 K.

3 Results

The ZF- and LF-μ^+SR spectra for dry Nafion are well fitted by a combination of a dynamic Kubo-Toyabe signal and an exponential relaxation signal (see Fig. 1); the former is caused by randomly oriented ^{1}H and ^{19}F nuclear magnetic moments, while the latter due to the formation of F-μ^+ and/or F-μ^+-F state[2].

$$A_0 P_{\rm ZF}(t) = A_{\rm KT} G^{\rm DGKT}(t, \Delta, \ ) \exp(\ \ \lambda_{\rm KT} t) + A_{\rm fast} \exp(\ \ \lambda_{\rm fast} t), \quad (1)$$

where A_0 is the empirical maximum muon decay asymmetry, $A_{\rm KT}$ and $A_{\rm fast}$ are the asymmetries associated with the two signals. $\lambda_{\rm KT}$, and $\lambda_{\rm fast}$ are their relaxation rates, Δ is the static width of the local frequencies at the disordered sites, and is the field fluctuation rates due to muon hopping.

The T dependence of Δ for dry Nafion indicates the existence of a thermally activated process for , as expected (see Fig. 2). Since $\gg \Delta$ at high T, it is reasonable to fit the ZF-spectra by an exponential relaxation function[3]. The (T^{-1}) curve for the related material CF650, in which the density of sulfonic acid is roughly twice as large as that in Nafion, however exhibits a very different behavior with that for Nafion and the past result[3], for reasons currently unknown. In order to further elucidate muon diffusion in polymer electrolytes, we need to continue the μ^+SR experiments systematically.

*1 Toyota Central R&D Labs., Inc.
*2 Advanced Meson Science Laboratory, Nishina Center for Accelerator-based Science, Riken

References

1) http://www.fuelcells.dupont.com/
2) K. Nishiyama et al., Physica B **326** (2003) 41.
3) J. Sugiyama et al., KEK-MSL Report 2004 (2004) 20.

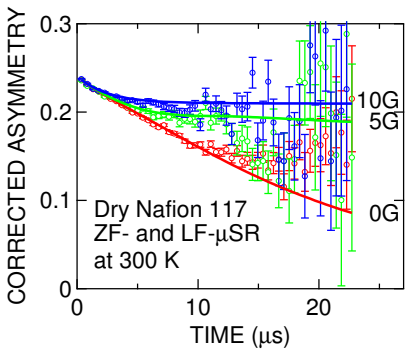

Fig. 1. ZF- and LF- $^+$SR spectra for dry Nafion at 300 K. The solid lines represent the fitting result using Eq. (1).

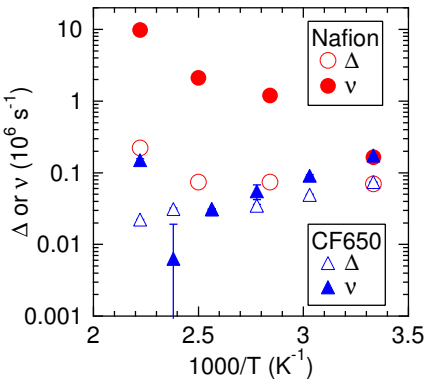

Fig. 2. The relationship between Δ ( ) and T^{-1} for dry Nafion and the related material CF650. The data were obtained by fitting of ZF- and LF-spectra using Eq. (1).

Muon diffusion in lithium battery materials

K. Mukai,[*1] Y. Ikedo,[*1] J. Sugiyama,[*1] T. Suzuki,[*2] I. Watanabe,[*2] K. Ariyoshi,[*3] and T. Ohuzku[*3]

[muon, lithium battery materials, Jahn-Teller effect]

The $(Li)_{8a}[Li_xMn_{2-x}]_{16d}(O_4)_{32e}$ (LMO:Fd$\bar{3}$m) spinel is extensively investigated as a positive electrode material for rechargeable lithium batteries[1]. In the cubic LMO lattice, Li^+ ions are located at the both tetrahedral 8*a* and octahedral 16*d* sites, Mn ions at the 16*d* sites, and O^{2-} ions at the 32*e* sites to form a cubic-closed packed array. Based on the recent μSR experiments in LMO with $x \sim 0$[2,3], the Li^+ diffusion is proposed to be very fast particularly above 250 K compared with the result of ^{7}Li-NMR[4]. Since the Li^+ ions at the 16*d* site alter the magnetic and electrochemical properties of LMO[5], we have carried out a μSR experiment on LMO with x=0-0.15 to clarify the interrelationship between microscopic magnetic and structural nature and x.

Powder samples of LMO with x=0, 0.05, 0.1, and 0.15 were prepared from LiOH$*$H$_2$O and MnOOH (manganite) by a conventional solid-state reaction technique. According to an ICP-AES analysis, the Li/Mn ratios of the samples were 1.00/2.00, 1.04/1.96, 1.09/1.91, and 1.15/1.85. For the μ^+SR experiments, powder was pressed into a disk of $\sim$20 mm diameter and 1 mm thickness, and subsequently placed on a silver sample holder. The μ^+SR spectra were measured in the surface muon beam line of the RIKEN-RAL Muon Facility at the ISIS.

The μSR spectra above 50 K of each LMO are well fitted by a dynamic Kubo-Toyabe function G^{DGKT};

$$A_0\, P_{\mathrm{ZF}}(t) = A_{\mathrm{KT}} G^{\mathrm{DGKT}}(t, \Delta, \nu) \exp(-\lambda_{\mathrm{KT}} t), \quad (1)$$

where A_0 is the empirical maximum muon decay asymmetry, A_{KT} and λ_{KT} are the asymmetry and relaxation rate of the Kubo-Toyabe signal, Δ is the static width of the local frequencies at the disordered sites, and ν is the field fluctuation rates.

Figure 1 shows the T dependences of ν, Δ, and χ^{-1} for the four LMO samples. For the sample with x=0, as T increases from 50 K, ν decreases monotonically up to 100 K, then increases with an increasing slope, finally reaching a maximum at $\sim$270 K, and then decreases with further increase in T. The $\Delta(T)$ curve exhibits a sudden decrease at $\sim$270 K accompanying the maximum in ν. Since the $\chi(T)$ curve shows a small cusp at 275 K due to the orbital ordering of Mn^{3+} at the Jahn-Teller transition[6], the peak of the $\nu(T)$ curve and the sudden decrease in Δ are assigned to be caused by the JT transition, not by the diffusion of Li^+ ions.

For the samples with x=0.05-0.15, although there are no anomalies in the $\chi^{-1}(T)$ curve, the $\nu(T)$ curve still exhibits a maximum at $\sim$ 270 K, and Δ decreases with increasing T above $\sim$ 270 K, while both changes are suppressed with increasing x. The weak transverse field (wTF-) μ^+SR measurements clearly confirm the absence of any inclusions of a phase with x=0 in the samples with $x \geq 0.05$. Therefore, the anomalies in the $\nu(T)$ and $\Delta(T)$ curves are due to the intrinsic behavior of the LMO samples. In other words, μ^+SR detects a short-range cooperative JT distortion even in the samples with x=0.15, whereas no anomalies are detected by χ and other macroscopic measurements for LMO with $x \geq 0.05$.

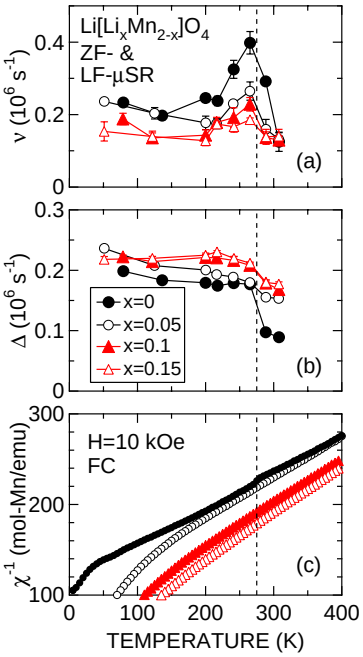

Fig. 1. Temperature dependences of (a) field fluctuation rate (ν), (b) field distribution width (Δ), and (c) inverse susceptibility for powder samples of $Li[Li_xMn_{2-x}]O_4$ with x=0, 0.05, 0.1, and 0.15.

*1 Toyota Central Research and Development Labs., Inc.
*2 Muon Science Laboratory, RIKEN
*3 Department of Applied Chemistry, Osaka City University

References
1) G. Amatucchi and J.-M. Tarascon; J. Electrochem. Soc. **149**, K31 (2002), and references cited therein.
2) C. T. Kaiser *et al.*; Phys. Rev. B **62**, R9236 (2000).
3) M. J. Ariza *et al.*; J. Phys. Chem. B **107**, 6003 (2003).
4) V. M. J. Verhoeven *et al.*; Phys. Rev. Lett. **86**, 4314 (2001).
5) T. Ohzuku *et al.*; J. Power Sources, **68**, 646 (1997).
6) J. R.-Carvajal *et al.*; Phys. Rev. Lett. **81**, 4660 (1998).

RILAC operation

Eiji Ikezawa, Masayuki Kase, Osamu Kamigaito, Takahide Nakagawa, Naruhiko Sakamoto, Hiroki Okuno, Naohito Inabe, Masanori Wakasugi, Nobuhisa Fukunishi, Misaki Kobayashi-Komiyama, Masanori Kidera, Yoshihide Higurashi, Hiromichi Ryuto, Tamaki Watanabe, Shigeo Kohara, Masaki Fujimaki, Makoto Nagase, Tadashi Kageyama, Shigeru Yokouchi, Akira Yoneda, Toshimitsu Aihara,* Tomonori Ohki,* Hiromoto Yamauchi,* Akito Uchiyama,* Kazuyuki Oyamada,* Ryo Koyama,* Akira Goto, and Yasushige Yano

Throughout this reporting period, RILAC has been in steady operation and has supplied various ion beams in various experiments. Table 1 shows statistics for the RILAC operation from January 1 through December 31, 2006. In preparation for the beam commissioning of the RI Beam Factory (RIBF), acceleration tests with RILAC and the RIKEN Ring Cyclotron (RRC) using a ^{238}U ion beam were carried out in February and from May through June, 2006. The beam commissioning of RIBF started in July 2006. To achieve such purposes, 0.669 MeV/nucleon ^{238}U, 2.675 MeV/nucleon ^{84}Kr, and 2.653 MeV/ nucleon ^{27}Al ion beams accelerated by RILAC were injected intensively into RRC. Therefore, the percentage of the beam service time injected into RRC was approximately 43% of the total RILAC beam service time, and increased by approximately 23% compared with that one year ago. ^{4}He, ^{22}Ne, ^{40}Ar, ^{48}Ca, ^{58}Fe, ^{70}Zn, and ^{136}Xe ion beams accelerated by RILAC were injected into RRC for the experiments. The machine troubles encountered hardly affected the operation time schedule throughout this reporting period.

Table 1. Statistics for RILAC operation from January 1 through December 31, 2006.

Operation time of RILAC	5886	hr
Beam service time of RILAC	4527	hr
Machine trouble	0	hr
Beam service time of RILAC standalone	2566	hr
Beam transport to RRC	1961	hr

Table 2. Beam service time of RILAC standalone allocated to each beam course in No. 1 target room of RILAC in 2006.

Beam course	Total time (hr)	%
e2	416	16.2
e3	2150	83.8
e4	0	0.0
Total	2566	100.0

Table 2 shows a summary of the beam service time of the RILAC standalone allotted to each beam course (e2, e3, and e4) in the No. 1 target room of RILAC in 2006. The e2 beam course has been mainly used for the study of radiation chemistry and accelerator mass spectrometry. The e3 and e4 beam courses have been exclusively used for research experiments on the heaviest elements and for various studies in the Center for Nuclear Study (CNS), the University of Tokyo, respectively. Compared with that one year ago, the beam service time of the RILAC standalone decreased by approximately 14% because of the beam commissioning of RIBF.

Table 3. Operation statistics for two ion sources (18G-ECRIS and SC-ECRIS) in 2006. The operation times using SC-ECRIS are indicated in parentheses.

Ion	Mass	Charge state	Total time (hr)
He	4	1	0 (62)
Ne	22	6	0 (108)
Al	27	6	314 (0)
Ar	40	9, 11	50 (123)
Ca	48	11	404 (0)
Fe	58	13	234 (0)
Zn	70	16	1753 (0)
Kr	84	18	363 (0)
Xe	136	8, 27	0 (240)
U	238	14, 35	949 (0)
	Total		4067 (533)

* Sumiju Accelerator Service Ltd.

This year, research experiments on the heaviest elements were carried out using a gas-filled recoil isotope separator (GARIS) at the e3 beam course of RILAC for 61 days from March through May and 17 days in June. A 5 MeV/nucleon ^{70}Zn ion beam was supplied in the experiments. The percentage of the beam service time for the experiments was approximately 39% of the total RILAC beam service time, and decreased by approximately 34% compared with that one year ago.

Table 3 shows statistics for the operation times of an 18 GHz ECR ion source (18G-ECRIS) and a superconducting ECR ion source (SC-ECRIS) in 2006. The percentages of the operation time used by 18G-ECRIS and SC-ECRIS were approximately 88% and 12% of the total ion source operation time, respectively. The ion beams of 10 elements were used in various experiments, beam acceleration tests, and beam commissioning.

We carried out the following machine improvements and overhauls during this reporting period.

(1) The vacuum control systems for the No. 5 and No. 6 RILAC cavities were replaced with new systems using a Network Device Interface Module (N-DIM). The interface circuits are connected to the Ethernet and are remote-controlled by the experimental physics and industrial control system (EPICS).

(2) A turbomolecular pump of 2400 l/s for the No. 5 RILAC cavity was replaced with a cryogenic pump of 13000 l/s. The other vacuum pumps were subjected to annual inspection.

(3) In the water cooling system, three cooling water pumps, three air cooling fans of cooling towers, and three heat exchangers were overhauled. The other cooling water pumps were subjected to annual inspection.

(4) Plate power supplies as the final stages of rf systems were subjected to annual inspection.

RRC operation and beam line construction for RIBF

Masayuki Kase, Eiji Ikezawa, Tadashi Kageyama, Nobuhisa Fukunishi,
Takahide Nakagawa, Osamu Kamigaito, Hiromichi Ryuto, Hiroki Okuno, Naruhiko Sakamoto,
Masanori Kidera, Masanori Wakasugi, Misaki Kobayashi-Komiyama, Yoshihide Higurashi,
Makoto Nagase, Shigeo Kohara, Masaki Fujimaki, Shigeru Yokouchi, Yukimitsu Ohshiro*[1],
Noritoshi Tsukiori*[2], Ryuichi Ohta*[2], Yasuteru Kotaka*[2], Kiyoshi Kobayashi*[2], Minoru Nishida*[2],
Kunikazu Masuda*[2], Seiji Fukuzawa*[2], Takeshi Nakamura*[2],
Akira Goto, and Yasushige Yano
*[1] The Center of Nuclear Science, the University of Tokyo.
*[2] Sumiju Accelerator Service Ltd.

Table 1 shows the statistical data of the RIKEN Ring Cyclotron (RRC) operation from Jan. to Dec. 2006. The total operation time for the year was about half of that in 2005 and the beam service time was 40% of 2005. This reduction was due to the following two reasons. A three-month shutdown of RRC operation was made to modify the beam lines of the RRC for beam delivery to new injection lines to the RIBF. In the second half of the year, most of the available beam time was devoted to the commissioning of the RIBF. Thus, the regular beam service was made only for three months from January to March in 2006. Even for these periods, the beam time was limited owing to a lack of electric power budget in the fiscal year of 2005.

The installation of the fixed-frequency Ring Cyclotron (fRC) in the E4 room was completed at the end of June 2006, together with the beam lines connecting RRC and fRC. That was the last construction work in the Nishin-Memorial Building. The acceleration test of fRC started in July using a uranium beam, with a frequency of 18.25 MHz, supplied from RRC. Developments for improving the beam quality of RRC were performed in order to increase the efficiency of fRC acceleration.

At the end of November 2006, the acceleration test of Intermediate Ring Cycltoron (IRC) started after the completion the of the injection beam line. RRC supplied a krypton beam, with a frequency of 36.5MHz, directy to IRC.

During the shutdown in spring, the vacuum leakage of the valley chamber of RRC was repaired. Long-term irradiation of fast neutrons from the septum of electrostatic deflection channel (EDC) in the RRC probably had caused the hardening of the viton o-ring seal in a vacuum chamber, triggering the crack. This leakage occurred for the first time in the 20-year-term of the RRC operation.

The beam transport line from RRC to fRC uses a major part of the existing one in the D room. The entrance of the E4 room was shifted downstream by 10m. The series of triplet quadrupole magnets were rearranged to make a space for the new sixth-harmonic rebuncher. The extraction beam line from fRC to the E1 room was newly constructed in the D room along the south wall of the D room, crossing twice the existing beam lines. To create make for a dipole magnet to be installed, a large hole was made in the four-meter-thick concrete wall separating the RRC vault and the E1 room. The two transport lines, one from fRC and another directly from RRC, were merged immediately just before the stripper foil system in the E1 room.

Table 1. Operation Statistical data of RRC in 2006.

Operation time of RRC	2853	(5730) hr
Beam service time	1628	(4201) hr
RIBF commissioning	496	(0) hr
Machine troubles	75	(1394) hr
Nuclear physics experiments	65	(78) %
Non-nuclear physics experiments	35	(22) %
RILAC-RRC operation	36	(33) %
AVF-RRC operation	64	(67) %

Figures in parentheses are data obtained in 2005.

AVF operation

Masayuki Kase, Tadashi Kageyama, Yukimitsu Ohshiro[*1], Nobuhisa Fukunishi, Takahide Nakagawa, Osamu Kamigaito, Hiromichi Ryuto, Hiroki Okuno, Naruhiko Sakamoto, Masanori Kidera, Masanori Wakasugi, Misaki Kobayashi-Komiyama, Yoshihide Higurashi, Makoto Nagase, Shigeo Kohara, Shigeru Yokouchi, Noritoshi Tsukiori[*2], Ryuichi Ohta[*2], Yasuteru Kotaka[*2], Kiyoshi Kobayashi[*2], Minoru Nishida[*2], Kunikazu Msuda[*2], Seiji Fukuzawa[*2], Takeshi Nakamura[*2], Akira Goto, and Yasushige Yano

[*1] Center of Nuclear Science, the University of Tokyo.
[*2] Sumiju Accelerator Service Ltd.

Table 1 shows the statistical data of the AVF cyclotron (AVF) operation during the period from January to December 2006 together with the data obtained during the same period of the previous year. The operation time, in which the AVF was used as an injector of the RRC, decreased markedly in 2006, because the RRC operation was suspended in spring owing to the construction of its beam lines and because, after the construction was completed, the RRC was frequently operated with the RILAC for RIBF commissioning in the second half of the year. More than 2000 hours of AVF operation was spent for stand-alone use in 2006. This was threefold longer than the operation time of the previous year.

In terms of a beam course, the beam time was largest in E7a (CRIB) at 60%, followed by C03 at 24%. In 2006, the low-energy secondary beam experiments in CRIB were carried out very frequently, which have been managed by CNS, the University of Tokyo.

The three types of ion source have been producing a various ion beams since 2003. In the case of ions heavier than Ar, the 10 GHz ECR ion source is mainly used. For lighter ions, both the 10 GHz ECR and the Hyper-ECR are used alternately. The development of production methods for a new beam such as $^{7}Li^{3+}$ was always carried out in the Hyper-ECR. The polarized ion source (PIS) was not used at all after the shutdown of the SMART.

The upgrading of the AVF is in progress in cooperation with CNS. The flattop acceleration system was added to the AVF cavities in 2002. A ceramic part in the rf amplifier is now improved so that high-power operation will be possible. The power supplies for the sector magnets were improved to increase the maximum energy of the light ion beam at the beginning of 2005. The maximum current of the main coil was raised from 1100 A to 1200 A. The two sets of power supplies for the trim coils were also improved. As a result, the K-value of the AVF increased from 70 to 78MeV. The maximum energy of $^{15}N^{5+}$ beam became higher than 9 MeV/nucleon, extending the availability of RI beams by the CRIB in E7. Acceleration tests have not been performed yet, because of the lacks of both input electric power and the capacity of the water cooling system.

A magnetic channel in the extraction system of the AVF was damaged in September during a tuning of a high-intensity beam. A serious vacuum leakage occurred in the casing of the magnetic channel. A thin stainless steel metal melted partially owing to irradiation of a stray beam.

The second half of the Glazer lens of the injection system of the AVF was replaced with a new one in the summer of 2006, which had been out-of-order for many years.

Table 1. Statistical data of AVF operation in 2005 - 2006.

Year	2006	2005
Total operation time	**3963hr**	**4858 hr**
Beam tuning	**853hr (22%)**	**1262 hr (26%)**
Injection to RRC	**1051 hr (27%)**	**2799 hr (58%)**
AVF stand-alone	**2059hr (52%)**	**715 hr (15%)**
Beam course (AVF stand-alone)		
E7a (CRIB)	**1275 hr (62%)**	**535 hr (74%)**
E7b	**257 hr (12%)**	**36 hr (5%)**
C03	**527 hr (26%)**	**143 hr (20%)**

Routine Work for Radiation Safety in Ring Cyclotron Facility

Y. Uwamino, S. Fujita, H. Sakamoto, R. Hirunuma, H. Mukai[*1], A. Horigome, T. Yamaki and N. Yukawa

We report the measurement of residual radioactivity and radiation leakage at the RIKEN ring cyclotron (RRC) facility.

Residual radioactivity in the facility was measured at various locations using AE133V ionization-chamber gamma-ray survey meters from Applied Engineering, Inc. The scheduled overhaul of the cyclotrons started 9 days after their operation using an ^{40}Ar beam of 63 MeV/nucleon at RRC and a ^{19}F beam of 6 MeV/nucleon at AVF. The dose rates at the AVF cyclotron and RRC deflectors were found to be 1 mSv/h and 20 mSv/h on January 6, 2006, respectively. Figure 1 shows the variations of the dose rates at these deflectors since 1986. The rates for 2002 and 2004 at RRC were not measured. The variations of these dose rates have not been large since 2000.

In addition to the above measurement, the dose rate inside the injector AVF cyclotron was measured on May 22, 2006 when air leakage near the magnetic channel was repaired. The dose rate was 90 mSv/h at the magnetic channel.

During the period from October 1, 2005 to September 30, 2006, the dose rates were measured along the beam lines after almost every experiment. Points **a**–**z** in Fig. 2 show the places where the dose rates exceeded 18 μSv/h. Table 1 summarizes the observed dose rates and gives the dates on which the measurements were performed. The maximum dose rate was found to be 2000 μSv/h at the RIKEN projectile-fragment separator (RIPS) target in the beam distribution corridor, denoted by **p** in Fig. 2. Whenever we observed a high dose rate, we roped-off the area and posted a warning sign indicating that it was dangerous to remain for a long time at that place.

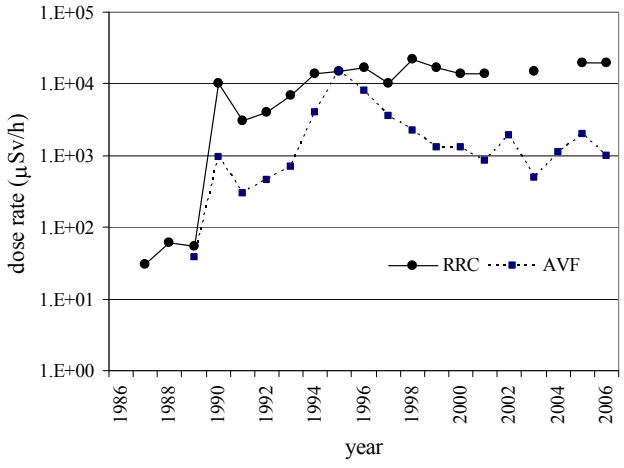

Fig. 1. Variation of the dose rates at the RRC and AVF deflectors since 1986.

We continuously monitored the radiation leakage from the RRC facility using neutron and gamma-ray active area monitors and passive monitors with a thermoluminescence dosimeter (TLD). The passive monitor for neutrons was developed by us, and it measures the effective neutron dose. The radiation leakages were below the detection limit of the area monitors placed near the site boundary. We evaluated the radiation level at the boundary of the radiation-controlled area using an area monitor installed in the computer room on the ground floor immediately above a bending magnet that guides the beams from the RRC vault to the distribution corridor, and it was approximately 6.4 μSv/y, which was much lower than the allowable dose limit (5000 μSv/y). The variation of the annual radiation leakage measured using this area monitor for the last 8 years is shown in Fig. 3. The value increased until 2005, and decreased in 2006 due to the shorter operation time of RRC, which was stopped during the construction of the new fRC beam line.

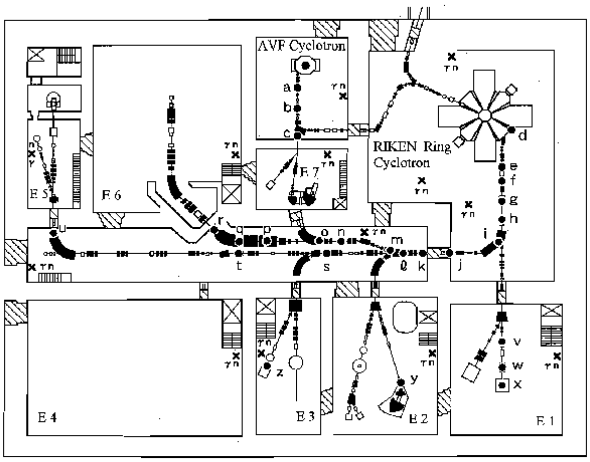

Fig. 2. Layout of RIKEN ring cyclotron facility as of 2006. The measurement locations of residual radioactivity along the beam lines are indicated by points **a**-**z**.

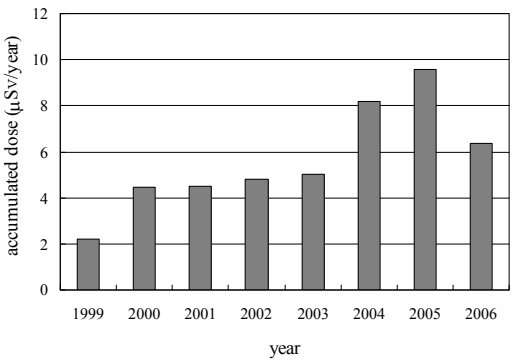

Fig. 3. Variation of the accumulated radiation leakages at the boundary of the radiation controlled area since 1999.

*1 Japan Environment Research Corp.

The results obtained using the passive dosimeters placed around the radiation-controlled area were below the detection limit, which was approximately 0.2 mSv/y, and the results obtained using them placed in the RRC facility at points near the entrances of E6 and E7 experimental rooms were 4.8 mSv/y and 1.6 mSv/y, respectively. These points are in the corridor of the 2nd basement floor, and below the RIPS target. The legal dose limit for these positions is 50 mSv/y.

Table 1. Summary of dose rates measured along the beam lines using ionization-chamber survey meters. Detection points **a-z** indicate measurement locations shown in Fig. 2.

Detection point	Measured dose rate (μSv/h)	Date	Particle	Energy (MeV/u)	Intensity (enA)	Period (days)
a	90	Mar 3, '06	p	14	5800	1
b	200	Mar 3, '06	p	14	5800	1
c	130	Mar 3, '06	p	14	5800	1
d	35	Jan 4, '06	Ar-40	63	5000	11
e	45	Jan 4, '06	Ar-40	63	5000	11
f	400	Jan 4, '06	Ar-40	63	5000	11
g	500	Mar 3, '06	O-18	100	3300	9
h	200	Mar 3, '06	O-18	100	3300	9
i	300	Mar 3, '06	O-18	100	3300	9
j	350	Jan 4, '06	Ar-40	63	5000	11
k	50	Mar 9, '06	O-18	100	3300	9
l	90	Mar 9, '06	O-18	100	3300	9
m	120	Mar 9, '06	O-18	100	3300	9
n	80	Mar 9, '06	O-18	100	3300	9
o	500	Mar 9, '06	O-18	100	3300	9
p	2000	Mar 9, '06	O-18	100	3300	9
q	150	Mar 9, '06	O-18	100	3300	9
r	130	Mar 9, '06	O-18	100	3300	9
s	50	Jan 4, '06	Ar-40	63	5000	11
t	50	Jan 4, '06	Ar-40	63	5000	11
u	18	Jan 4, '06	Ar-40	63	5000	11
v	20	Nov 4,'05	Ar-40	63.1	10000	0.5
w	150	Nov 4,'05	Ar-40	63.1	10000	0.5
x	200	Nov 4,'05	Ar-40	63.1	10000	0.5
y	60	Nov 24,'05	He-4	120	100	4.5
z	100	Nov 4,'05	N-14	135	2900	1

Operation of the tandem accelerator

T. Kobayashi and K. Ogiwara

The tandem accelerator (Pelletron, 1.7MV) was operated for a total of 113 days for experiments during the annual reporting period from Oct.1, 2005 to Sep.30, 2006. A total of 16 days was spent for machine inspection, beam test and recovery for electric power failure. The period for troubleshooting was only 4 days for the control system and vacuum pumps which remarkably decreased from that of previous year (18 days required for repairing SF_6 leakage, wear of carbon sheaves, damage of a charge transfer chain and contamination of quartz tube in ion source).

The accelerated ion species in this period are H^+, He^+ and B^+ with energies from 1.6 to 2.5 MeV summarized in table 1.

Experimental studies on the following subjects were performed, and are still in progress except for (3)-(b).

(1) Nuclear reaction analysis (NRA) using $^1H(^{11}B,a)2a$ reaction (57days)

(a) The state of hydrogen in Nb-based and Ta-based alloys, and V as investigated by the channeling method

(b) Effect of irradiation on the state of hydrogen in metals

(2) Particle-induced X-ray emission (PIXE) (16days)

(a) Development and application of a highly sensitive high-resolution in-air PIXE system for chemical state analysis

(b) Trace element analysis of biological and environmental samples using energy dispersive X-ray spectrometry

(3) The analysis using elastic scattering (40days)

(a) Rutherford backscattering spectrometry (RBS) analysis of polymers, carbon materials.

(b) Ion channeling RBS analysis of GaN, AlGaN and ZnO epitaxial thin films grown on Si and MgO substrates.

(c) Elastic recoil detection (ERD) analysis of diamond-like carbon (DLC) thin films and ion-implanted polymers for determining hydrogen distribution.

Table 1 The beam conditions and the analysis techniques of the tandem accelerator

Ion	Energy [MeV]	Beam current [nA]	Analysis	Operation time [days]
$^1H^+$	1.6 – 2.5	30 – 50	PIXE	16
$^4He^+$	1.5 – 2.3	3 – 30	RBS, ERDA	40
$^{11}B^+$	2.0	1.0 – 1.5	NRA	57

V. Records (Including the contents of annual report)

Events of in Nishina Center fiscal 2006

2006

1, Apr.	Inauguration of RIKEN Nishina Center (RNC) for Accelerator-Based Science
1∼2, June	The 21st RIKEN-RAL Muon Facility Program Advisory Committee
7∼9, June	RIKEN Advisory Council (RAC)
21, June	The Signing Ceremony for 'Supplementary Agreement for Implementation of Joint Res. between RIKEN and National Innovation Center for Plant Biotechnology, South Africa'
30, June	The 12th Meeting of the Management Steering Committee of RIKEN BNL Collaboration
30, June	Signing Ceremony for 'The Todai-RIKEN Joint International Program for Nuclear Physics Research'
3∼4, Aug.	The 1st RIBF International Users Meeting
10∼11, July	Establishment of JUSTIPEN (The Japan US Theory Institute for Physics with Exotic Nuclei)
25∼27 Oct.	Collaboration Meeting on Experiments with the RIBF Facility
27, Sept.	The 1st Scientific Policy Committee
3, Oct.	The Emperor and Empress's visit to RIKEN
10, Nov.	The signing ceremony for the Memorandum of Understanding on the Creation of the Council for China-Japan Research Collaboration on Nuclear Physics, in Beijing
18, Nov.	The signing of The Agreement on Academic Exchange with Asia Pacific Center for Theoretical Physics in Pohang, Korea
22, Dec.	RIBF Nuclear Physics Collaboration Committee
28, Dec.	First successful extraction of Aluminum beam from the SRC

2007

16, Jan.	Commemorative lecture by Prof. T. D. Lee "Symmetry and Dynamical Symmetry, Commemorate the Decoration of the Order of the Rising Sun, Gold and Silver Star (Koshiba Hall, Univ. of Tokyo)"
16, Jan.	A Signing Ceremony for Memorandum of Understanding for RIKEN-BNL collaboration
16, Jan.	The 14th Meeting of The Management Steering Committee of RIKEN BNL Collaboration
1, Feb.	The 1st Program Advisory Committee Meeting for Materials and Life Science
5, Feb.	The film shoot of the Hollywood movie "Jumper"
9∼10, Feb.	The 1st Program Advisory Committee Meeting for Nuclear Physics experiments
12, March	First successful extraction of Kr beam from the SRC
15, March	First successful extraction of RI beam from BigRIPS
23, March	First successful extraction of U beam from the SRC
25, March	THE RIBF Users Informal Meeting

Accelerator Team

1. Abstract

Our aim is to commission and develop the accelerator-complex system, mainly the rf systems, of the RI Beam Factory. We focus on further efficient use of the RI Beam Factory through R&D associated with a new injector for parallel operation of both RI beam factory experiments and the super-heavy elements experiment. Another objective of our team is to carry out an upgrading project of the AVF cyclotron on the expansion of region of its acceleration beam energies.

2. Major Research Subjects

(1) Commissioning and development of the accelerator-complex system
(2) R&D of a new injector for the RRC
(3) Upgrading project of the AVF cyclotron

3. Summary of Research Activity

(1) Commissioning and development of the accelerator system

O. Kamigaito, N. Sakamoto, S. Kohara, J. Ohnishi and A. Goto

We perform operation, maintenance and development of the RIBF accelerator system: mainly radio-frequency acceleration system. We also perform beam commissioning of the accelerators.

(2) Development of a new injector for the RRC

O. Kamigaito, N. Sakamoto and A. Goto

We are performing design and fabrication of a new injector for the RRC in order to make the efficient use of the accelerator beam time by making it possible to simultaneously conduct both experiments using RI's and the super-heavy-element search experiment. We are in charge mainly of design and development of linacs.

(3) Upgrading of the AVF cyclotron

A. Goto

We are advancing the project of modification of the center region of the AVF cyclotron in collaboration with CNS, Univ. of Tokyo, in order to expand the region of its available acceleration energies. We are performing orbit simulations in detail for that purpose. We have already completed upgrade of the performance of the coil power supplies, improvement of the radio-frequency acceleration system, etc.

Team Leader
Akira GOTO

Members
Osamu KAMIGAITO
Shigeo KOHARA
Kiyoshi OGIWARA
Jun-ichi OHNISHI
Naruhiko SAKAMOTO

Visiting Researcher
Lukas STINGELIN (JSPS Postdoctoral Fellow)

Visiting Scientists
Mitsuhiro FUKUDA (RCNP, Osaka Univ.)
Masatoshi ITO (CYRIC, Tohoku Univ.)
Yoshitaka IWASAKI (SAGA Light Source)
Satoshi KURASHIMA (JAEA, Takasaki)
Nobumasa MIYAWAKI (JAEA, Takasaki)
Hajime SAITO (SHI Accel. Serv. Ltd.)

Research Consultants
Yoshiaki CHIBA
Shoushichi MOTONAGA

Students

Junior Research Associate
Hironori KUBOKI (Grad. Sch. of Sci., Univ. of Tokyo)

Student trainees
Takamichi AOKI (Grad. Sch. of Sci., Univ. of Tokyo)
Keisuke ITOH (Grad. Sch. Sci. Eng., Saitama Univ.)
Hiroaki MATSUBARA (Grad. Sch. Sci., Osaka Univ.)
Ryo MATSUO (Grad. Sch. of Sci., Tohoku Univ.)
Yuji TAMESHIGE (Grad. Sch. Sci., Osaka Univ.)
Tomohiro TERAZONO (Grad. Sch. of Sci., Tohoku Univ.)

Ion Source Team

1. Abstract

Our aim is to commission and develop the ECR ion sources for the accelerator-complex system of the RI Beam Factory. We focus on further upgrading the performance of the RI Beam Factory through R&D associated with a superconducting ECR heavy-ion source for high-intensity uranium ions.

2. Major Research Subjects

(1) Commissioning and development of the ECR ion sources
(2) R&D of a superconducting ECR heavy-ion source for high-intensity uranium ions

3. Summary of Research Activity

(1) Operation and development of ECR ion sources

T. Nakagawa, M. Kidera, Y. Higurashi, H. Haba, T. Kageyama and A. Goto

We routinely produce and supply various kinds of heavy ions such as zinc ions for the 113th-element experiment as well as uranium ions for RIBF experiments. We also perform R&D's to meet the requirements for stable supply of high-intensity heavy ion beams.

(2) Development of a superconducting ECR ion source for use in production of a high-intensity uranium beam

T. Nakagawa, J. Ohnishi, M. Kidera, Y. Higurashi and A. Goto

The RIBF is required to supply uranium beams with very high intensity so as to produce RI's. We are developing an ECR ion source with high magnetic field and high microwave-frequency, since the existing ECR ion sources have their limits in beam intensity. The coils of this ion source are designed to be superconducting for the production of high magnetic field.

Team Leader
Akira GOTO

Members
Hiromitsu HABA
Tadashi KAGEYAMA
Takahide NAKAGAWA

Special Postdoctoral Researcher
Yoshihide HIGURASHI

Contract Researcher
Masanori KIDERA

Visiting Scientists
Takehiro MATSUSE (Fac. Text. Sci. Technol., Shinshu Univ.)
Ryouichi WADA (Texas A&M Univ., USA)

Student Trainee
Hiroyuki HIGASHIJIMA (Grad. Sch. Sci., Rikkyo Univ.)

RILAC Team

1. Abstract

The operation and maintenace of the RIKEN Heavy-ion Linac (RILAC) have been cariied out. The maintenace of these devices is important to keep the log-term stablitiy of RILAC beams.

2. Major Research Subjects

(1) The long term stability of the RILAC operation.
(2) Improvement of efficiency of the RILAC operation.

3. Summary of Research Activity

RIKEN Heavy-ion Linac (RILAC) is a frequency-tunable linac. The RILAC is composed of a Heavy-ion ECR ion source, RFQ linac, six main cavities, and six energy booster cavities. Thousands hours are spent in a year for delivering many kinds of heavy-ion beams to various experiments.

The RILAC has two operation modes: the stand-alone operation delivering low-energy beams directly to experiments and the injection mode operation supplying beams into the RIKEN Ring Cyclotron (RRC). In the first mode, the RILAC supplyies very important beam to the nuclear physics experiment of "the research of super heavy elements". In the second mode, RILAC plays very important role as upstream end of the RIBF accelerators.

The maintenance is very important in order to keep the high quality performance of the RILAC. Improvements are always carried out for the purpose of more efficient operation.

Team Leader
Masayuki KASE

Member
Eiji IKEZAWA

Research Consultants
Toshiya CHIBA
Masatake HEMMI
Yoshitoshi MIYAZAWA

Cyclotron Team

1. Abstract

We are carryng out the operation and maintenance of five cyclotorons in RIKEN (AVF cyclotron, Riken Ring cyclotoron: RRC, fRC, IRC, and super-conducting cyclotron: SRC). We are trying to deliver stably a high-energy and high intensity beam to experiments.

2. Major Research Subjects

(1) Operation technology of cyclotrons.
(2) Maintenance of cyclotrons.
(3) Maintenance of super-conducting cyclotron.

3. Summary of Research Activity

We are carryng out the operation and maintenance of five cyclotorons in RIKEN (AVF cyclotron, Riken Ring cyclotoron: RRC, fRC, IRC, and super-conducting cyclotron: SRC). We are trying to deliver stably a high-energy and high intensity beam to experiments. Detailed research subjects are the following,

Operation technology of cyclotrons.

Maintenance of cyclotrons.

Maintenance of superconducting ring cyclotron..

Team Leader
Masayuki KASE

Members
Naohito INABE
Keiko KUMAGAI
Makoto NAGASE
Hiroki OKUNO

Contract Technical Scientists
Tadashi FUJINAWA
Shigeru YOKOUCHI

Visiting Scientists
Masahiko HAYASHI (JAXA)
Naomi IKEDA (JAXA)
Chihiro KAMEZAWA (JAXA)
Satoshi KUBOYAMA (JAXA)
Masahiko MIDORIKAWA (JAXA)
Hideharu OHIRA (JAXA)
Hiromitsu OOTOMO (JAXA)
Yohei SATOH (JAXA)
Osamu SHIMADA (JAXA)
Hiroyuki SHINDO (JAXA)

Beam Technology Team

1. Abstract

In order to realize the efficient acceleration in RIBF accelerators, the operation is being improved by doing varioous computer symulations. For this purpose, related technology (beam diagnosys, computer control, and charge stripper) was developed.

2. Major Research Subjects

(1) Improvement on the beam transmission along the multi-stage accelerator system.
(2) Development of beam diagnosis.
(3) Development of computer control.
(4) Development of charge stripper for high intensity heavy ion beam.

3. Summary of Research Activity

(1) Development of the beam diagnostic technology.
(2) Development of the charge-stripping foil.
(3) Development of the computer control system of accelerator.
(4) Investigation of beam behavior in accelerators.

Team Leader
Masayuki KASE

Members
Masaki FUJIMAKI
Nobuhisa FUKUNISHI
Sachiko ITO
Tamaki WATANABE

Contract Researcher
Hiromichi RYUTO

Contract Technical Scientist
Misaki KOBAYASHI-KOMIYAMA

Visiting Scientists
Masanori KOSHIMIZU (Grad. Sch. Eng., Tohoku Univ.)
Hideo MIKAMI (SHI Accel. Serv. Ltd.)
Dung NGUYEN (INST, Vietnam)

Research Consultants
Kazuie KIMURA
Mutsuko SASAKI

Cryogenic Technology Team

1. Abstract

We are operating the helium cryogenic system in the south area of RIKEN Wako campus and delivering the liquid helium to users in RIKEN.

2. Major Research Subjects

(1) The high efficiency of the liquid herium production cycle.
(2) Optimization of the large-scaled superconductinf cyclotron.

3. Summary of Research Activity

We are operating the herium cryogenic system located in the south area of Wako campass of RIKEN. We are producing liquid helium and supplying them to RIKEN inside users. For the purpose of efficient operation, we are trying to collect the gas after the use of liquid helium.

Team Leader
Masayuki KASE

Members
Kumio IKEGAMI
Masato NAKAMURA

Technical Staff-I
Hiroo HASEBE
Takeshi MAIE

Part-time Staff
Kazushiro NAKANO

Research Consultant
Ken-ici KATO

Heavy Ion Nuclear Physics Laboratory

1. Abstract

With fast RI beams provided by the RIBF cyclotron complex, we study exotic behavior of nuclei far from the stability valley, explosive nuclear burning in high-temperature and high-density environment in stars and early universe, and nuclear reactions related to solar neutrino production. For that purpose, we develop various experimental methods based on intermediate-energy inelastic scattering including Coulomb excitation, Coulomb dissociation, transfer- and fragmentation-reactions coupled with gamma-ray and particle-decay measurements. We perform also study of the three-nucleon forces by precise measurements of elastic scattering and breakup reactions of few-nucleon systems, and development of new technics including new laser-spectroscopy for exotic nuclei. Developments of radiation detectors such as semiconductor detectors and scintillation detectors, data processing methods, and construction of experimental equipment, together with theoretical studies on nuclear structure and nuclear reaction, are also made.

2. Major Reserch Subjects

(1) Spectroscopy of unstable nuclei with direct reactions
(2) Development of radiation detector systems with high precision and high efficiency
(3) Study of astrophysical nuclear reactions with fast beams of unstable nuclei
(4) Development of laser spectroscopy for unstable nuclei
(5) Theoretical studies on nuclear structure and nuclear reactions

3. Summary of Research Activity

(1) Spectroscopy of unstable nuclei by direct reactions associated with γ-ray measurements

(i) Spectroscopy of neutron-rich C isotopes

Proton inelastic scattering on ^{17,19}C was studied. Two transitions were observed in both nuclei indicating existing of two bound excited states in ^{17,19}C nuclei in agreement with certain shell-model predictions. Spin assignments to these excited states were tentatively made. From the analysis of the excitation cross sections, ^{17}C was found to be strongly deformed.

(ii) Proton and neutron collectivity in neutron-rich light nuclei

Studies of proton (or deuteron) inelastic scattering on ^{17}B, ^{16}C, ^{22}O, ^{28,30}Ne, ^{32,34,36}Mg, and ^{34}Si were performed with γ-ray spectroscopy technique. Matter deformation parameters β_2 for the lowest excited states were determined from the inelastic scattering cross sections. Together with their B(E2) values, neutron and proton multipole matrix elements (M_n, M_p) were deduced separately. The M_n value for the 2^+ excitation of ^{16}C is much larger than the M_p value, supporting the picture of neutron-proton decoupling for the 2^+ excitation of ^{16}C drawn by earlier results of the lifetime measurement and ^{208}Pb+^{16}C inelastic scattering experiment. On the other hand, the M_n values for ^{17}B and ^{28}Ne are much smaller than the corresponding M_p values, while M_n and M_p take similar values for ^{22}O, ^{32,34}Mg and ^{34}Si.

(iii) Spectroscopy of neutron-rich medium-mass nuclei

Proton inelastic scattering experiments were performed for ^{60,62}Cr and ^{58}Ti. Measurements of coincident γ-rays deduced the locations of their first 2^+ states and the matter deformation parameters.

(2) Spectroscopy of unbound states of unstable nuclei by breakup and transfer reactions

(i) Invariant mass spectroscopy of nuclei in the vicinity of the neutron drip line.

(a) Strong E1 transitions at low excitation energies (soft E1 excitation) were observed for ^{11}Li by the new Coulomb breakup experiment. The good statistics allow for precise analysis for the two-neutron correlation in the "Borrmean" nucleus ^{11}Li.

(b) Inelastic scattering, one-neutron knockout, and charge exchange reactions of ^{14}Be were measured for proton and ^{12}C targets. The transition to the first 2^+ state of ^{14}Be at $E_\mathrm{x} = 1.55\,\mathrm{MeV}$ was measured, which showed smaller deformation lengths compared to ^{12}Be. The invariant mass spectrum of ^{13}Be in the one-neutron knockout channel showed two peaks. The higher energy peak around $E_\mathrm{x} = 2\,\mathrm{MeV}$ was found to have a d-wave property.

(c) Two resonant states were found in the invariant mass spectrum for ^{23}O produced by the (d,p) reaction in inverse kinematics. Their locations imply disappearance of the $N = 20$ shell gap.

(d) Invariant mass spectra were obtained for ^{6}He, ^{17}C, and ^{19}C by the breakup and proton inelastic scattering in inverse kinematics. New peaks were found for the neutron-rich carbon isotopes.

(e) Precise measurements of E1 transitions were performed for ^{6}He and ^{8}He by the Coulomb breakup.

(ii) Invariant mass spectroscopy of proton-rich nuclei

Coulomb dissociation of the proton-rich nuclei ^{23}Al, ^{27}P on ^{208}Pb was measured. Relative energy spectra for

^{22}Mg+p, ^{26}Si+p were obtained. The extracted cross sections provide information useful for the astrophysical network calculation on the nucleosynthesis in novae.

(iii) Missing mass spectroscopy of very neutron-rich light nuclei

Search for extremely neutron-rich systems was performed by using the missing mass method in the ^{2}H+^{8}He collision. The reaction channels d(^{8}He,^{3}He)^{7}H, d(^{8}He,^{4}He)^{6}H, and d(^{8}He,^{6}Li)4n were of major interest. The reference peak in the d(^{8}He,t)^{7}He$_{\mathrm{g.s.}}$ channel was clearly observed.

(3) Nuclear reaction study using the high-resolution spectrograph SMART.

(i) Clear signatures of three-nucleon-force (3NF) effects are observed in the cross section minima of deuteron-proton elastic scattering at an intermediate energy ($E/A = 135\,\mathrm{MeV}$). To assess further three-nucleon-force effects, we have extended the measurement to the deuteron-proton breakup reactions. The measurements were focused on the polarization transfer coefficients and all deuteron analyzing powers for the specific coplanar configurations, where large 3NF effects are theoretically predicated. We have found a model dependence of 3NFs in a polarization transfer coefficient.

(ii) Many experiments have been performed to test experimentally the Bell's inequality. However, tests using hadron systems are limited. We tested Bell's inequality in the proton-neutron system by measuring the spin correlation between the proton-neutron pair in ^{1}S$_{0}$ state produced by the ^{2}H(d,pn)pn reaction. The proton polarization was measured by EPOL located at the second focal plane of the magnetic spectrograph SMART. The neutron polarization was analyzed by a newly constructed neutron polarimeter SMARTNPOL.

(4) Laser spectroscopy of RI atoms in super fluid helium

We are developing a new laser spectroscopy technique for RI atoms trapped in super fluid helium. We have successfully measured hyper fine coupling constants of ^{133}Cs and ^{85,87}Rb atoms in super fluid helium with laser-microwave double resonance method for the first time. The accuracy of the measurement is sufficient to reveal anomalous feature of helium as a host matrix as well as to determine nuclear moments of isotopes whose moments are unknown

(5) SCRIT (Self-Confining RI Target)

We have been performing feasibility studies of the SCRIT concept using a prototype installed at an existing electron ring, KSR, of Kyoto, since 2004. We have observed elastically scattered electrons from Cs ions trapped by circulating electron beam. The luminosity was determined to be $2 \times 10^{25}/\mathrm{cm}^2/\mathrm{s}$ at the electron beam current of 50 mA. The number of trapped Cs ions was estimated to be an order of 10^6.

(6) Development of experimental devices for RIBF

(i) DALI2

DALI2, a NaI(Tl) array, for in-beam γ-ray spectroscopy has been constructed. Several experiments with fast RI beams ($\beta = v/c = 0.3$) were performed at RIPS. For the use of DALI2 with faster RI beams ($\beta = 0.6$) at RIBF, upgraded detector configuration is being considered.

(ii) SAMURAI

SAMURAI (Superconducting Analyzer for Multiparticle from Radio Isotope Beams) is a large acceptance multi-particle spectrometer we proposed to construct at RIBF. The main part of SAMURAI is a large-gap superconducting magnet with 7 Tm of bending power. SAMURAI enables momentum analysis of heavy projectile fragments and projectile-rapidity protons with large angular and momentum acceptance. SAMURAI also affords projectile-rapidity neutron measurements with large angular acceptance in coincidence with heavy projectile fragments. In this fiscal year, the detailed designing of the SAMURAI magnet was started. Through the informal information exchange with major magnet companies in Japan, the specification documents with as good performance as possible are being prepared.

(iii) Data acquisition system for RIBF

We have been developing a data acquisition system in a network-distributed structure with event-builders.

(iv) Autonomic detector system with UBIQUITOUS concept

We have developed the UBIQUITOUS detector system consisting of a unit for the autonomic digital signal processing and its sub-unit implementing a flush analog-to-digital converters.

(7) Nuclear theory

Theoretical works are also promoted for the following subjects in strong cooperation with experimental approaches: Cluster Aspects of Nuclear Physics/ Nuclear matter density distributions and nuclear radii/ Nuclear structure studies using nuclear reactions / Collective excitation modes in unstable nuclei/ Astronuclear Physics/ Effects of the tensor force to nuclear structure/ Self-consistent studies of quantal and thermal correlations in finite nuclei.

Head

Tohru MOTOBAYASHI

Members

Nori AOI
Akihisa KOHAMA
Yukari MATSUO
Toshimi SUDA
Ken-ichiro YONEDA

Special Postdoctoral Researchers

Hidetada BABA
Yasuro FUNAKI
Takeshi FURUKAWA
Shoko KANNO
Takuma MATSUMOTO
Satoshi TAKEUCHI
Kazunari YAMADA

Contract Researchers

Shawn BISHOP
Nguyen Dinh DANG
Kimiko SEKIGUCHI
Meiko UESAKA
Mitsutaka YAMAGUCHI

Asia Program Associates

Nguyen Quang HUNG
T. Khai NGUYEN
Shuo WANG

Senior Visiting Scientists

Hisashi HORIUCHI (Grad. Sch. of Sci., Kyoto Univ.)
Takaharu OTSUKA (Grad. Sch. of Sci., Univ. of Tokyo,)
Hideyuki SAKAI (Grad. Sch. of Sci., Univ. of Tokyo)
Hiroyuki SAKURAGI (Grad. Sch. of Sci., Osaka City Univ.,)

Visiting Scientists

Yasuhisa ABE (RCNP, Osaka Univ.)
Yasuo AOKI (Grad. Sch. of Pure and Applied Sci., Univ. of Tsukuba,)
Shigeyoshi AOYAMA (Niigata Univ. Integrated Information Processing Center)
Ichiro ARAI (Grad. Sch. of Pure and Applied Sci., Univ. of Tsukuba,)
Yoshihiro ARITOMO (Flerov Lab. Nucl. Reactions, JINR, Russia)
Daniel BAMMERER (Tech. Univ. Berlin Inst., Germany)
Daniel BAZIN (MSU, NSCL, USA)
Didier BEAUMEL (Paris-XI Univ., France)
Fa BECK (Strasbourg Nucl. Inst., France)
Carlos BERTULANI (Univ. Arizona, USA)
Yorick BLOMENFELD (Paris-XI Univ., France)
Richard BOYD (Dept. of Phys., Ohio State Univ., USA)
BO CEDERWALL (Royal Insti. Tech., Sweden)
Alan CHEN (McMaster Univ., Canada)
Silvio CHERUBINI (Catania Univ., Italy)
Tien Khoa DAO (Inst. Nucl. Sci. Tech., Center for Basic Res. Computation)
Mahananda DASGUPTA (Bompay Univ., India)
Zsolt DOMBRADI (ATOMKI, Hungary)
Zoltan ELEKES (ATOMKI, Hungary)
Henning ESBENSE (Argonne Nat. Lab., USA)
Michael FAMIANO (MSU, NSCL, USA)
Hubert FLOCARD (Orsay Nucl. Inst., France)
Yoshihide FUCHI (KEK)

Shinichiro FUJII (CNS, Grad. Sch. Sci., Univ. of Tokyo)
Yoshitaka FUJITA (Grad. Sch. of Sci., Osaka Univ.)
Tomonori FUKUCHI (Fac. of Sci., Rikkyo Univ.)
Mitsunori FUKUDA (Sch. of Sci., Osaka Univ.)
Zsolt FULOP (ATOMKI, Hungary)
Ken-Ichi FUSHIMI (Fac. of Integrated Arts and Sci., Univ. of Tokushima)
Tomoko GOMI (Natl. Inst. Radiol. Sci.)
Valdir GUIMRAES (Sao Paulo Univ. Brazil)
Kevin Insik HAHN (Ewaha Womans Univ., Korea)
Hideki HAMAGAKI (CNS, Grad. Sch. Sci., Univ. of Tokyo)
Ikuko HAMAMOTO (Lund Univ., Sweden)
Jun HASEGAWA (Tokyo Inst. of Tech., Res. Lab. for Nucl. Reactors)
Jianjun HE (Edinberg Univ.)
David HINDE (Australia Nat. Univ., Australia)
Satoru HIRENZAKI (Fac. of Sci., Nara Women's Univ.)
Michio HONMA (Univ. Aizu)
Takatoshi HORIBATA (Fac. of Software and Information Tech., Aomori Univ.)
Akos HORVATH (Eotvos Lorand Univ., Hungary)
Munetake ICHIMURA (Fac. of Computer and Information Sci., Hosei Univ.)
Eiji IDEGUCHI (CNS, Grad. Sch. Sci., Univ. of Tokyo)
Kazuo IEKI (Fac. of Sci., Rikkyo Univ.,)
Kei IIDA (Kochi Univ. of Tech., Physical Sci.)
Nobuaki IMAI (Inst. of Particle and Nucl. Studies, KEK)
Astrid IMIG (Univ. of North Carolina, USA)
Tetsuro ISHII (JAEA)
Shigeru ISHIMOTO (Inst. of Particle and Nucl. Studies, KEK)
Naoyuki ITAGAKI (CNS, Grad. Sch. Sci., Univ. of Tokyo)
Akira IWAMOTO (JAEA)
Naohito IWASA (Dept. of Phys., Tohoku Univ.)
Hironori IWASAKI (CNS, Grad. Sch. Sci., Univ. of Tokyo)
Takuji IZUMIKAWA (Niigata Univ. RI Center)
Gai JANOS (Hungarian Academy Sci., Inst. Nucl. Res., Hungary)
Toshitaka KAJINO (National Astronomical Observatory of Japan)
Nasser KALANTAR (Univ. Groningen, The Netherlands)
Gabor KALINKA (Hungarian Academy Sci., Inst. Nucl. Res., Hungary)
Yoshiko KANADA-EN'YO (Kyoto Univ., Yukawa Inst. for Theoretical Phys.)
Seigo KATO (Fac. of Sci., Yamagata Univ.)
Kiyoshi KATO (Fac. of Sci., Dept. of Phys., Nonlinear Phys., Hokkaido Univ.,)
Takahiro KAWABATA (CNS, Grad. Sch. Sci., Univ. of Tokyo)
Takeshi KIKUCHI (Fac. of Eng., Utsunomiya Univ.)
Jongchan KIM (Seoul National Univ., Korea)
Masaaki KIMURA (Grad. Sch. of Pure and Applied Sci., Univ. of Tsukuba,)
Kikuo KIMURA (Nagasaki Inst. of Applied Sci.)
Adam KISS (Eotvos Lorand Univ., Hungary)
Takeshi KOIKE (Dept. of Phys., Tohoku Univ.)
Tetsuro KOMATSUBARA (Grad. Sch. of Pure and Applied Sci., Univ. of Tsukuba,)
Alexe KORSHENINNIKOV (Inst. Generall & Nucl. Phys., Kurchatov Inst., Russia)
Evgueni KOUZMINE (Russian Res. Center, Kurchatov Inst., Russia)
Shigeru KUBONO (CNS, Grad. Sch. Sci., Univ. of Tokyo)
Kazuyoshi KURITA (Fac. of Sci., Rikkyo Univ.,)
Chie KUROKAWA (Meme Media Lab., Hokkaido Univ.,)
Marco LA COGRATA (Catania Univ., Italy)
Karin LAGERGREN (Royal Insti. Tech., Sweden)
Khiem LE (CNS, Grad. Sch. Sci., Univ. of Tokyo)
Chen LI (Peking Univ., China)
Weiping LIU (China Inst. Atomic Energy, China)
Minliang LIU (CNS, Grad. Sch. Sci., Univ. of Tokyo)
Jingbin LU (Fac. of Sci., Kyusyu Univ.,)
William LYNCH (MSU, NSCL, USA)
Yukie MAEDA (CNS, Grad. Sch. Sci., Univ. of Tokyo)

Kazushige MAEDA (Dept. of Phys., Tohoku Univ.)
Kensaku MATSUTA (Sch. of Sci., Osaka Univ.)
Kenichi MATSUYANAGI (Fac. of Sci., Kyoto Univ.,)
Jie MENG (Sch. of Phys., Peking Univ., China)
Alberto MENGONI (Univ. of Tokyo)
Johannes MESSCHENDOR (Univ. of Groningen, Netherlands)
Yasuo MIAKE (Grad. Sch. of Pure and Applied Sci., Univ. of Tsukuba)
Shin'ichiro MICHIMASA (CNS, Grad. Sch. Sci., Univ. of Tokyo)
Mototsugu MIHARA (Grad. Sch. of Sci., Osaka Univ.)
Toshiyuki MINEMURA (Inst. of Particle and Nucl. Studies, KEK)
Shiro MITARAI (Fac. of Sci., Kyusyu Univ.,)
Wolfgang MITTIG (GANIL, France)
Takashi MIYACHI (Adv. Res. Inst. Sci. Eng., Waseda Univ.)
Hiroari MIYATAKE (Inst. of Particle and Nucl. Studies, KEK)
Yutaka MIZOI (Osaka Elec.-Commun. Univ.)
Takahiro MIZUSAKI (Sensyu Univ.)
Peter MOLLER (Los Alamos Nat. Lab., USA)
Sadao MOMOTA (Kochi Univ. of Tech., Intelligent Mechanical Systems Eng.)
Tsuneyasu MORIKAWA (Fac. of Sci., Kyusyu Univ.,)
Ben MOTTELSON (Copenhagen NORDITA, Denmark)
Hiroyuki MURAKAMI (Fac. of Sci., Rikkyo Univ.,)
Takayuki MYO (Theoretical Nucl. Phys., RCNP, Osaka Univ.)
Yasuki NAGAI (RCNP, Osaka Univ.)
Takeshi NAGATA (CNS, Grad. Sch. Sci., Univ. of Tokyo)
Takashi NAKAMURA (Tokyo Inst. of Tech., Particle-, Nucl.-, and Astro-Phys.)
Kosuke NAKANISHI (CNS, Grad. Sch. Sci., Univ. of Tokyo)
Takashi NAKATSUKASA (Univ. of Tsukuba)
Shintaro NAKAYAMA (Fac. of Integrated Arts and Sci., Univ. of Tokushima)
Evgueni NIKOLSKI (Russian Res. Center, Kurchatov Inst., Russia)
Masahiro NOTANI (Argonne Nat. Lab., USA)
Atsuko ODAHARA (Grad. Sch. of Sci., Osaka Univ.)
Kazuyuki OGATA (Fac. of Sci., Kyusyu Univ.,)
Alexey OGLOBLIN (Russian Res. Center, Kurchatov Inst., Russia)
Yukimitsu OHSHIRO (CNS, Grad. Sch. Sci., Univ. of Tokyo)
Takashi OHTSUBO (Dept. of Phys., Niigata Univ.)
Kazutaka OHZEKI (Tohoku Univ. CYRIC, Detector Group)
Hiroyuki OKAMURA (CYRIC, Tohoku Univ.)
Shinsuke OTA (CNS, Grad. Sch. Sci., Univ. of Tokyo)
Masahisa OTA (Dept. of Phys., Konan Univ.)
Kazuhiro OYAMATSU (Fac. of Studies on Contemporary Society, Aichi Shukutoku Univ.,)
Kyoichiro OZAWA (CNS, Grad. Sch. Sci., Univ. of Tokyo)
Jonathan PEARSON (McMaster Univ., Canada)
P. A. Atoy PERERA (Univ. Kelaniya, Sri Lanka)
Gianluca PIZZONE (Catania Univ., Italy)
Chilakamarri RANGACHARYULU (Univ. Saskatchewan, Canada)
Stefano ROMANO (Catania Univ., Italy)
Hiroyuki SAGAWA (The Univ. of Aizu, Center for Mathematical Sci.)
Akito SAITO (Dept. Phys., Grad. Sch. Sci., Univ. of Tokyo)
Takao SAKAGUCHI (BNL, USA)
Harutaka SAKAGUCHI (Dept. of Applied Phys., Fac. of Eng., Univ. of Miyazaki)
Mitsuo SAKAI (CNS, Grad. Sch. Sci., Univ. of Tokyo)
Badawy SARHAN (Cairo Univ., Egypt)
Kimikazu SASA (Univ. of Tsukuba)
Yoshiteru SATOU (Grad. Sch. of Sci., Tokyo Inst. of Tech.)
Ryoichi SEKI (California State Univ., Northridge, USA)
Noritaka SHIMIZU (Grad. Sch. of Sci., Univ. of Tokyo)
Youhei SHIMIZU (Theoretical Nucl. Phys., RCNP, Osaka Univ.)
Yoshifumi SHIMIZU (Fac. of Sci., Kyusyu Univ.,)
Cosimo SIGNORINI (Univ. of Padova, INFN, Italy)
Dorottya SOHLER (ATOMKI, Hungary)

Andreas STOLZ (MSU, NSCL, USA)
Kenji SUDA (CNS, Grad. Sch. Sci., Univ. of Tokyo)
Kazuko SUGAWARA-TANABE (Otuma Women's Univ.)
Satoru SUGIMOTO (Grad. Sch. of Sci., Kyoto Univ.)
Kohsuke SUMIYOSHI (Div. of Liberal Arts, Phys. Group, Numazu College of Tech.)
Yang SUN (Univ. of Notre Dame, USA)
Toshio SUZUKI (Univ. of Fukui, Fac. of Enginerring)
Takeshi SUZUKI (Faculity of Eng., Saitama Univ.)
Shoji SUZUKI (Inst. of Particle and Nucl. Studies, KEK)
Akihiro SUZUKI (Suzuki Corp.)
Nobuyuki SUZUKI (Dept. of Phys., Niigata Univ.)
Yoshihiro TAGISHI (Univ. of Tsukuba, Inst. of Phys.,)
Naoki TAJIMA (Univ. of Fukui, Fac. of Enginerring)
Tadayuki TAKAHASHI (JAXA)
Yutaka TAKAHASHI (Sch. of Sci., Osaka Univ.)
Masatoshi TAKANO (Waseda Univ. RISE)
Masaaki TAKASHINA (Kyoto Univ., Yukawa Inst. for Theoretical Phys.)
Noboru TAKIGAWA (Fac. of Sci., Tohoku Univ.,)
Tadaaki TAMAE (Lab. of Nucl. Sci., Dept. of Phys., Tohoku Univ.)
Atsushi TAMII (RCNP, Osaka Univ.)
Masahiko TANAKA (KEK)
Gurgen TER-AKOPYAN (JINR. Flerov Lab. of Nucl. Reaction, Russia)
Takashi TERANISHI (Kyusyu Univ.)
Jun TERASAKI (Peking Univ., Dept. of Phys., China)
Mariko TERASAWA (Hogh Sch. of NHK GAKUEN)
Renju THOMAS (Australia Nat. Univ., Australia)
Wendong TIAN (Shanghai Inst. Applied Phys., China)
Manyee TSANG (MSU, NSCL, USA)
Tomohiro UESAKA (CNS, Grad. Sch. Sci., Univ. of Tokyo)
Yutaka UTSUNO (JAEA)
Peter VON BRENTANO (Koln Univ., Germany)
Takahiro WADA (Fac. of Sci. and Eng., Konan Univ.)
Yasuo WAKABAYASHI (CNS, Grad. Sch. Sci., Univ. of Tokyo)
Tomotsugu WAKASA (Fac. of Sci., Kyusyu Univ.,)
Takashi WAKUI (Tohoku Univ. CYRIC)
Shin-ichi WATANABE (CNS, Grad. Sch. Sci., Univ. of Tokyo)
Yutaka WATANABE (Inst. of Particle and Nucl. Studies, KEK)
Shuwei XU (Chinese Academy of Sci., China)
Kazuhiro YABANA (Univ. of Tsukuba, Inst. of Phys., Nucl. Theory Group)
Kentaro YAKO (Grad. Sch. of Sci., Univ. of Tokyo)
Takayuki YAMAGUCHI (Saitama Univ.)
Hidetoshi YAMAGUCHI (CNS, Grad. Sch. Sci., Univ. of Tokyo)
Shoichi YAMAKA (CNS, Grad. Sch. Sci., Univ. of Tokyo)
Norio YAMAZAKI (CNS, Grad. Sch. Sci., Univ. of Tokyo)
Yanlin YE (Peking Univ., China)
Naotaka YOSHINAGA (Faculity of Sci., Saitama Univ.)
Akira YOSHINO (CNS, Grad. Sch. Sci., Univ. of Tokyo)
Chongcheoul YUN (Chung-Ang Univ., Korea)
Tao ZHENG (Peking Univ., China)
Yong ZHENG (CNS, Grad. Sch. Sci., Univ. of Tokyo)
Shan-Gui ZHOU (Peking Univ., China)

Research Consultants
Kiyomi IKEDA
Shuhei YAMAJI
Toshimitsu YAMAZAKI

Students

Junior Research Associates
Hironori KUBOKI (Dept. Phys., Grad. Sch. Sci., Univ. of Tokyo)

Takeo ONISHI (Grad. Sch. of Sci., Univ. of Tokyo)
Masaru SUZUKI (Grad. Sch. of Sci., Univ. of Tokyo,)

Student Trainees

Takeshi AIBA (Grad. Sch. of Sci. & Tech. Niigata Univ.)
Guilherme AMADIO (Grad. Sch. of Sci., Univ. of Tokyo)
Yoki ARAMAKI (Grad. Sch. of Sci., Univ. of Tokyo)
Tae-Eun CHOI (Ewaha Womans Univ., Korea)
Vincenzo CRUCILLA (Univ. of Catania, Italy)
Binh DAM (Inst. Theoretical Phys., Vietnam)
Koutaro FUJIKAKE (Sch. of Sci. and Tech., Meiji Univ.)
Yukihiro FURUKAWA (Dept. of Phys., Tohoku Univ.)
Taku GUNJI (Grad. Sch. of Sci., Univ. of Tokyo)
Seiya HAYAKAWA (CNS, Grad. Sch. Sci., Univ. of Tokyo)
Toshikazu HORI (Grad. Sch. of Sci., Osaka Univ.)
Wataru HORIUCHI (Grad. Sch. of Sci. & Tech. Niigata Univ.)
Takeshi HOYA (Grad. Sch. of Pure and Applied Sci., Univ. of Tsukuba,)
Kiyohiko INAFUKU (Dept. of Phys., Tohoku Univ.)
Kenichi ISHII (Fac. of Sci., Rikkyo Univ.,)
Tatsuhiro ITO (Dept. of Sci. and Tech., Meiji Univ.)
Chen JUN (McMaster Univ., Canada)
Hyo-Soon JUNG (Chung-Ang Univ., Korea)
David KAHL (McMaster Univ., Canada)
Tomomi KAWAHARA (Grad. Sch. of Sci., Toho Univ.)
Jung-Lan KIM (Ewaha Womans Univ., Korea)
Jang Youl KIM (Chung Ang Univ., Korea)
Aram KIM (Ewaha Womans Univ., Korea)
Mituhisa KITAYAMA (Dept. of Phys., Tohoku Univ.)
Kei KOBAYASHI (Grad. Sch. of Sci. & Eng., Saitama Univ.)
Yosuke KONDO (Grad. Sch. of Sci. and Eng., Tokyo Inst. of Tech.)
Takamasa KUBOKI (Grad. Sch. of Sci. & Eng., Saitama Univ.)
Kenichiro KURA (Sch. of Sci., Osaka Univ.)
Yuzo KURIHARA (Grad. Sch. of Sci. and Eng., Tokyo Metropolitan Univ.)
Young Kwan KWON (Chung Ang Univ., Korea)
Livio LAMIA (Univ. of Catania, Italy)
Ki-Woo LEE (Chung-Ang Univ., Korea)
Juhahn LEE (Chung Ang Univ., Korea)
Tomohiro MACHIDA (Fac. of Sci., Rikkyo Univ.,)
Tetsuya MASUDA (Fac. of Sci., Rikkyo Univ.,)
Toshiyuki MASUE (Grad. Sch. of Sci., Osaka Univ.)
Yohei MATSUDA (Dept. of Phys., Tohoku Univ.)
Ryohei MATSUMIYA (Grad. Sch. of Sci., Osaka Univ.)
Yuuichi MATSUYAMA (Fac. of Sci., Rikkyo Univ.,)
Kenjiro MIKI (Grad. Sch. of Sci., Univ. of Tokyo)
Kazutaka MIYAKAWA (Grad. Sch. of Pure and Applied Sci., Univ. of Tsukuba,)
JunYoung MOON (Chung Ang Univ., Korea)
Tetsuaki MORIGUCHI (Grad. Sch. of Pure and Applied Sci., Univ. of Tsukuba)
Yuhei MORINO (Grad. Sch. of Sci., Univ. of Tokyo)
Takumi NAKABAYASHI (Grad. Sch. of Sci.,Tokyo Inst. of Tech.)
Shinpei NAKAJIMA (Grad. Sch. of Sci. & Eng., Saitama Univ.)
Takashi NANNICHI (Sch. of Sci., Tokyo Inst. of Tech.)
Shumpei NOJI (Sch. of Sci., Univ. of Tokyo,)
Susumu ODA (Grad. Sch. of Sci., Univ. of Tokyo)
Naoto OKAICHI (Sch. of Sci., Tokyo Inst. of Tech.)
Hooi Jin ONG (Grad. Sch. Sci., Univ of Tokyo)
Shota SAITO (Grad. Sch. of Sci., Univ. of Tokyo)
Satoshi SAKAGUCHI (Grad. Sch. of Sci., Univ. of Tokyo)
Satoshi SANO (CNS, Grad. Sch. Sci., Univ. of Tokyo)
Yoshiko SASAMOTO (Grad. Sch. of Sci., Univ. of Tokyo)
Masaki SASANO (Grad. Sch. of Sci., Univ. of Tokyo)
Maria SERGI (Univ. of Catania, Italy)

KIANA SETOODEHNIA (McMaster Univ., Canada)
Tomoyuki SHIMAMURA (Sch. of Sci., Tokyo Inst. of Tech.)
Mayuko SHINOHARA (Grad. Sch. of Sci. and Eng., Tokyo Inst. of Tech.)
Susumu SHIMOURA (CNS, Grad. Sch. Sci., Univ. of Tokyo)
Syota SUGAWARA (Sch. Sci. Eng., Waseda Univ.)
Tomokazu SUZUKI (Tohoku Univ. RI senter)
Hiroshi SUZUKI (Grad. Sch. of Sci., Univ. of Tokyo)
Kunihiko TAJIRI (Sch. of Sci., Osaka Univ.)
Maya TAKECHI (Grad. Sch. of Sci., Osaka Univ.)
Hidemitsu TAKEDA (Fac. of Sci., Kyusyu Univ.,)
Tasutaka TANIGUCHI (Grad. Sch. of Sci., Kyoto Univ.)
Yasuhiro TOGANO (Fac. of Sci., Rikkyo Univ.,)
Yorito YAMAGUCHI (Grad. Sch. of Sci., Univ. of Tokyo)
Yuji YAUCHI (Fac. of Sci., Dept. of Phys., Rikkyo Univ.,)
Jung-Sook YOO (Ewaha Womans Univ., Korea)
Akira YOSHIDA (Grad. Sch. of Sci., Kyoto Univ.)
Michiori YOSHITAKE (Grad. Sch. of Sci. & Eng., Saitama Univ.)

Secretaries
Tomoko IWANAMI
Shinko ODAI
Kayoko WADA

Applied Nuclear Physics Laboratory

1. Abstract

The Laboratory conducts the microscopic investigation of physical and chemical processes by nuclear techniques which take advantage of the intrinsic nuclear properties and phenomena (spins, electromagnetic moments, decay modes etc.). In particular, the precession/resonance of a polarized/aligned nuclear spin under an external field is observed through change in the angular distribution of radiation, for the study of nuclear structures via nuclear moments. The same method, as well as the Moessbauer technique, are used for the investigation of condensed matter such as ferromagnets, fullerenes, systems with dilute magnetic impurities etc. by capitalizing radioactive nuclei as microscopic probes into them. Also, the laser-polarization of stable/unstable nuclei and the spin maser technique are being developed for application to fundamental interaction studies through high-precision measurement of the spin precession frequency. All these research activities are to be extended to wide variety of unstable nuclei which the forth-coming facility, RI Beam Factory (RIBF), will provide. A method to produce beams of highly polarized radioactive nuclei, taking full advantage of RIBF, is being developed.

2. Major Research Subjects

(1) Nuclear structure study of unstable nuclei through electromagnetic moments and γ-ray spectroscopy
(2) Condensed matter studies with radioactive nuclear probes
(3) Test of the standard model through β-decay and laser-nuclear spin interaction
(4) Development of highly polarized slow RI beams

3. Summary of Research Activity

The Laboratory conducts studies covering nuclear physics, solid state physics/chemistry, and fundamental interactions, through the observation of nuclear spin, electromagnetic moments, and β and γ decays. Specifically, structures and interactions in nuclei in the regions far from the β stability line are studied through the observation of ground- and excited-state properties such as the magnetic moments, electric quadrupole moments and decay characteristics. For the determination of magnetic moments and electric quadrupole moments, the asymmetric/anisotropic emission of β or γ rays from spin-polarized/aligned nuclei are utilized to detect nuclear magnetic resonance or spin precession. The same methods, as well as the Mössbauer technique, are also used for the investigation of condensed matter such as ferromagnets, semiconductors, systems with dilute magnetic impurities etc. by capitalizing radioactive nuclei as microscopic probes into them. Also, the laser-polarized stable/unstable nuclei are used for fundamental interaction studies through high-precision measurement of spin precession frequency. All these research activities are to be extended to wide variety of unstable nuclei which the forth-coming facility, RI Beam Factory (RIBF), will provide. A method to produce ultra-low energy beams of highly polarized radioactive nuclei, taking full advantage of RIBF, is being developed.

(1) Nuclear structure studies with radioactive nuclear beams

Taking advantage of the β-NMR method with the spin-polarized radioactive-isotope beams (RIBs) produced from the projectile fragmentation reaction, the ground-state electric-quadrupole moments for ^{32}Al was measured. The μ-moment results presented above have provided scope for the neutron-rich aluminum isotopes viewed mainly from nucleon occupancy in the different single-particle orbits. The structural change would be investigated in a more straightforward way through the measurement of their Q moments because of its high sensitivity to nuclear deformation. From the obtained nuclear quadrupole resonance spectrum, we have determined experimental Q moment $|Q_{\rm exp}[^{32}{\rm Al}]| = 24(2)$ $e$mb. We found that the obtained $|Q_{\rm exp}|$ takes a very small value of 24(2) $e$mb, whereas near the stability line value of $|Q_{\rm exp}|$ stays almost constant at $|Q| \sim 150$ $e$mb. This observation indicates that the ground-states shape of the neutron-rich aluminum isotopes stays spherical when $N = 19$ is approached, and the ground state of ^{32}Al is the normal state described by valence particles in the *sd* orbits. It is interesting to note that the observed *normal* character of ^{32}Al is in contrast to that of ^{31}Mg, for which anomalous nuclear structure has been reported despite that these two nuclei differ only in the proton number. The $|Q_{\rm exp}|$ values are compared with shell-model calculations.

(2) Applications of Unstable RI Beams to Condensed Matter Studies

(K. Asahi, Y. Kobayashi, H. Ueno, A. Yoshimi, H. Watanabe[1*], T. Okada[2*], M. K. Kubo[2*], Y. Yamada[2*], M. Murata[2*], Y. Einaga[2*], Y. Nagata[2*], T. Taniguchi[2*], T. Kurahashi[2*], E. Yagi[2*], Y. Yoshida[2*], H. Ogawa[2*], W. Sato[2*], K. Asai[2*], J. Nakamura[2*], S. Nasu[2*], J. Miyazaki[2*], T. Fujita[3*], Y. Nemoto[3*], H. Nonaka[3*], K. Kawaguchi[3*], K. Taguchi[3*], Y. Ono[3*], Ohkubo[3*], Nakamoto[3*], H. Miyoshi[3*], D. Kameda[3*], K. Shimada[3*], T. Kato[3*], Emori[3*] ; H. Haba, A. Yoshida, M. Kase, A. Goto, Y. Yano (Cyclotron Center))

[1*] Contract Researcher, [2*] Visiting Researcher, [3*] Trainee

In-beam Mössbauer spectroscopic studies using an unstable short-lived nuclei ^{57}Mn ($T_{1/2}$ = 1.45 min) beam have been performed to investigate the "exotic" chemical states and the fast atomic-jump processes in solid. In this period, we have carried out a ^{57}Mn in-beam Mössbauer experiment to study the electronic structures, especially "exotic" chemical species, of ^{57}Fe atoms decaying from ^{57}Mn implanted into a silicon wafer and solid oxygen. In more reactive matrices, Fe species with extraordinarily higher oxidation states and "exotic" chemical structures are expected to be produced. Reactions between localized Fe atoms and reactant O_2 molecules provide important information on chemistry under non-equilibrium conditions and on the production of novel species. We succeed to obtain the well-defined in-beam ^{57}Fe ($\leftarrow^{57}$Mn) Mössbauer spectra of solid O_2 at 18 and 30 K. The spectrum obtained at 18 K can be analyzed by four components of doublets. They are preliminarily assigned to be Fe(O_2), FeO, (O_2)Fe(O_2), and an exotic high oxidation state of Fe species, respectively. The ^{57}Mn implantation Mössbauer experiment has been applied to the diffusion study of Fe impurity in Si, too. From the temperature dependence of the area intensities and the isomer shifts in the in-beam Mössbauer spectra, it is found that a fast diffusion of interstitial Fe atoms occurs over 500 K, and that there are a motional averaging between substitutional and interstitial Fe atoms in Si.

Another type of in-beam Mössbauer study using neutron beam has been continued. The advantage of this technique is that it is possible to investigate non-destructively the chemical effects and the dynamics of a hot atom produced just after the nuclearreaction. The Mössbauer spectrometer using the prompt γ-rays was installed at a neutron beam line at JRR-3M, Japan Atomic Research Institute. We succeeded to obtained the in-beam Mössbauer spectra of FeS_2 (pyrite- and marcasite-type) at room temperature. The spectra obtained at room temperatures can be fitted two doublets. Ones of doublets are originated from host matrix of pyrite and marcasite, the others are suggested to be novel Fe species produced by neutron capture reaction.

We studied the magnetic stable state and the antiferromagnetic ordering mechanism of (Ca, Sr)RuO_3 system and the characterizations of a filled-skutterudite, $SmRu_4P_{12}$, by ^{99}Ru Mössbauer spectroscopy and magnetization measurement. The ^{83}Rb source for ^{83}Kr Mössbauer spectroscopy was produced by a chemical separation after the a-irradiation of $CaBr_2$.

^{57}Fe Mössbauer spectroscopy was applied to investigate the structural conversion and spin separation triggered by proton-coupled electron transfer in p-conjugated ferrocene-quinone and ferrocene-naphthoquinone system, and the exotic valence states of Fe atoms in salen complex as a model for active sites of mononuclear non-heme iron enzymes.

(3) Fundamental symmetry studies with spin-polarized nuclei

The development of a low-frequency nuclear spin maser with ^{129}Xe for application to the search for a permanent electric dipole moment (EDM) is in progress. Key point of this project is to measure a small frequency shift of the spin precession by using the continuously precessing nuclear spin.

The performance of the good homogeneous solenoid coil for a low static field and high-stability current source for the solenoid coil was investigated. In the previous investigation the major source of the frequency fluctuation in a spin maser was traced to be a fluctuation in the solenoid field, which turned out to be originated from a current source in the previous setup with a nominal current stability of 10^{-4}. The newly developed current source includes a low noise circuit as the voltage reference, and a stability of 10^{-6} has been confirmed with a precision ammeter. This corresponds to a field fluctuation of a 10 nG order. The spin precession of ^{129}Xe nucleus was observed in thus stabilized magnetic field. The χ^2-fitting with a single frequency sine wave times exponential decay function can be performed for the measured free precession signal which continued 500-600 seconds after the 90 degree NMR pulse. The frequency error was found to be 1 μHz. In the previous setup, such a χ^2-fitting could not be performed. The measurement of the maser oscillation in this new setup is now in progress and the improvement of the frequency stability in the long-term. We have also launched the construction of the electrode system to produce the electric field for the EDM experiment. The mesh-type electrodes were made in order to path the probe laser light for magnetometry through the glass cell and the electrodes. We are now trying to reduce the leak current in this electrode system.

Head
Koichiro ASAHI

Members
Yoshio KOBAYASHI
Akihisa SHIRAHAMAYOSHIMI
Hideki UENO

Special Postdoctoral Researchers

Daisuke KAMEDA
Takashi NAGATOMO

Contract Researcher

Takashi SUGIMOTO

Visiting Scientists

Hisazumi AKAI (Grad. Sch. Sci. Eng., Osaka Univ.)
Yasuaki EINAGA (Fac. Sci. Eng., Keio Univ.)
Kazuo HAYAKAWA (Shizuoka Inst. of Sci. and Tech.)
Koji HIGASHIYAMA (Grad. Sch. of Sci., Univ. of Tokyo)
Norimichi KOJIMA (Grad. Sch., College of Arts and Sci., Univ. of Tokyo)
Kenya KUBO (Div. Natl. Sci., Int. Chr. Univ.)
Takuya KURAHASHI (Inst. Mol. Sci.)
Jun MIYAZAKI (Fac. Sci., Tokyo Univ. of Sci.)
Jiro MURATA (Fac. Sci., Rikkyo Univ.)
Masaki MURATA (Grad. Sch. of Sci., Univ. of Tokyo)
Kazuo MUTO (Grad. Sch. Sci. Eng., Tokyo Inst. Technol.)
Yujiro NAGATA (Coll. Sci. Technol., Aoyama Gakuin Univ.)
Hiromichi NAKAHARA (Tokyo Metropolitan Univ.)
Jin NAKAMURA (Dep. Appl. Phys. and Chem., Univ. Electro-Commun.)
Saburou NASU (Grad. Sch. Eng. Sci., Osaka Univ.)
Hiroshi OGAWA (Natl. Inst. Adv. Ind. Sci. Tech.)
Hiroyuki SAGAWA (The Univ. of Aizu, Center for Mathematical Sci.)
Wataru SATO (Grad. Sch. Sci. Eng., Osaka Univ.)
Tadashi SHIMODA (Grad. Sch. Sci. Eng., Osaka Univ.)
Satoshi TSUTSUI (JASRI)
Makoto UCHIDA (Grad. Sch. Sci. Eng., Tokyo Inst. Technol.)
Masahiko UTSURO (Kyoto Univ. Res. Reactor Inst.)
Hiroshi WATANABE (Dept. of Nucl. Phys., The Australian National Univ., Australia)
Schmidt-Ott WORF-DIETER (The Univ. of Goettingen, Germany)
Eiichi YAGI (Sch. Sci. Eng., Waseda Univ.)
Yasuhiro YAMADA (Fac. Sci., Tokyo Univ. of Sci.)
Yutaka YOSHIDA (Fac. Sci. Technol., Shizuoka Inst. Sci. Technol.)

Research Consultant

Takuya OKADA

Visiting Researcher

Langouche GUIDO (Dept. of Phys. and Astronomy, Katholieke Universiteit Leuven, Belgium)

Students

Junior Research Associates

Daisuke NAGAE (JAEA)
Kenji SHIMADA (Grad. Sch. Sci. Eng., Tokyo Inst. Technol.)

Student Trainees

Masahiko ADACHI (Fac. Sci. Technol., Shizuoka Inst. Sci. Technol.)
Takamasa ARAI (Grad. Sch. Sci. Eng., Tokyo Inst. Technol.)
Hideki FUKASAWA (Grad. Sch. of Sci., Tokyo Univ. of Sci.)
Yuka FUNAYAMA (Div. Natl. Sci., Int. Chr. Univ.)
Yuta HASEGAWA (Grad. Sch. of Sci., Univ. of Tokyo)
Naoto HATAKEYAMA (Fac. Sci., Tokyo Inst. Technol.)
Takeshi INOUE (Grad. Sch. Sci. Eng., Tokyo Inst. Technol.)
Sota KAGAMI (Fac. Sci., Tokyo Inst. Technol.)
Tomoko KAKUYAMA (Div. Natl. Sci., Int. Chr. Univ.)
Tomohiro KAMIMURA (Fac. Sci. Technol., Shizuoka Inst. Sci. Technol.)
Hirokazu KATO (Fac. Sci., Tokyo Univ. of Sci.)
Hirokazu KAWAMURA (Grad. Sch. Sci., Rikkyo Univ.)
Mio KONDO (Grad. Sch. of Sci., Univ. of Tokyo)

Katsuhiro KOUNO (Grad. Sch. of Sci., Tokyo Univ. of Sci.)
Namiko MIURA (Fac. Sci. Technol., Shizuoka Inst. Sci. Technol.)
Keigo NARITA (Grad. Sch. Sci., Rikkyo Univ.)
GUILLAUME PEDOUSSAUT (Div. Natl. Sci., Int. Chr. Univ.)
Kazumasa SAKATA (Fac. Sci. Technol., Grad. Sch. of Shizuoka Inst. Sci. Technol.)
Yutaka SUZUKI (Fac. Sci. Technol., Shizuoka Inst. Sci. Technol.)
Kunifumi SUZUKI (Fac. Sci. Technol., Grad. Sch. of Shizuoka Inst. Sci. Technol.)
Kaori TAGUCHI (Grad. Sch. of Sci. and Eng., Tokyo Metropolitan Univ.)
Kenichi TAKASE (Grad. Sch. Sci. Eng., Tokyo Inst. Technol.)
Makoto TAKEMURA (Grad. Sch. Sci. Eng., Tokyo Inst. Technol.)
Takeshi TOYODA (Fac. of Sci., Rikkyo Univ.)
Yoji TSURUOKA (Div. Natl. Sci., Int. Chr. Univ.)
Ryousuke TSUTSUI (Grad. Sch. Sci., Rikkyo Univ.)
Maai UCHIKAWA (Grad. Sch. of Sci., Univ. of Tokyo)

Secretaries
Shizue UMEBAYASHI
Kayoko WADA

Radioactive Isotope Laboratory

1. Abstract

This laboratory explores exotic nuclear structures and dynamics in unstable nuclei that have never been investigated before, such as those with largely imbalanced proton and neutron numbers. Our aim is to develop new experimental techniques utilizing fast RI beams to discover new phenomena and properties in unstable nuclei. Another important subject is the equation-of-state of asymmetric nuclear matter, and its association with the origin of elements and with neutron stars. For instance, we are making attempts to the better understand underlyning mechanism for exotic stability-enhancements of very neutron-rich fluorine isotopes, the large deformation of the nucleus 34Mg with N=22 in spite of its vicinity to the N=20 magic neutron number and anomalous collectivity in 16C. We are further extending these studies to medium- and heavy-mass regions by developing facilities, detectors and unique methods at RIBF, thereby leading on the challenging task to find new exotic phenomena. We also perform numerical simulations of nucleosynthesis under the environment of core-collapse supernovae, and moreover quest for footprints of supernovae and solar activities in the past, embedded in Antarctic ice core, in collaboration with Cosmic radiation laboratory and National Institute of Polar Research.

2. Major Research Subjects

(1) Study of structure and dynamics of unstable nuclei through development of new methods utilizing fast RI beamsI beams
(2) Stability of exotic nuclei and exploration into limit of nuclear existence
(3) Research on equation-of-state in asymmetric nuclear matter via heavy-ion induced reaction
(4) Promotion of nuclear astrophysics in an interdisciplinary organization

3. Summary of Research Activity

(1) Program based on missing mass method

Missing mass method is an essential tool to identify and observe both bound and unbound states. Especially for highly excited states beyond particle threshold, any models of particle and gamma decay processes are not necessary in reconstructing excitation energy. Difficulties stemming from inverse kinematics are low energy of recoiled out particles from targets and high accurate measurement necessary for emission angles. To overcome the difficulties, we are developing new detection systems for proton (in)elastic scattering; ESPRI(Elastic Scattering of Proton with RI beam), and a magnetic spectrometer for particles emitted at zero degree. The two systems have been employed for light mass nuclei for matter distributions as well as spectroscopic studies.

(2) Program based on in-beam gamma spectroscopy

In the medium and heavy mass region explored at RIBF, collective natures of nuclei are one of important subjects, which are obtained through production and observation of high excited and high spin states. To populate such states, heavy-ion induced reactions such as fragmentation, fission are useful and development of in-beam gamma methods fit for the reactions is necessary. So far, we have developed two-step fragmentation method as an efficient method to identify and populate excited states, and lifetime measurements to deduce transition strength.

(3) beta spectroscopy

Beta-spectroscopy is a traditional and efficient method for nuclear spectroscopy, especially out non-yrast levels. In the light mass region, several light-mass nuclei in both neutron-rich and proton-rich region have been investigated at RIPS through beta-gamma and beta-p coincidence technique. Concerning the medium and heavy mass region available at RIBF, we are developing two position-sensitive active-stoppers to achieve low-background via position correlation; strip-silicon detectors and a cylindrical active stopper called CAITEN.

(4) Equation-of-state via heavy-ion central collisions

Eos in asymmetric nuclear matter is essentially important to understand mechanism of supernovae explosion as well as crust structure of neutron stars. We are designing an experimental setup to detect pions and multiplicity in central collisions with RIBs at the intermediate energy at RIBF.

(5) Interdisciplinary study for nuclear astrophysics

To understand the origin of elements beyond ion, interdisciplinary works are important in linking data from nuclear physics program. We are promoting simulation of nucleosynthesis in the r- process path, and investigation of Antarctic ice core to search for footprints of supernovae as well as solar activity in the past via mass spectrometer, to link data obtained from nuclear physics program.

Head

Hiroyoshi SAKURAI

Members

Takashi ICHIHARA
Takashi KISHIDA
Yoichi NAKAI
Shunji NISHIMURA
Hideaki OTSU
Heiko SCHEIT

Special Postdoctoral Researcher

Toshiyuki SUMIKAMA
Hiroyuki TAKEDA
Eri TAKESHITA
Kanenobu TANAKA
Satoru TERASHIMA
Masayuki YAMAGAMI

Contract Researcher

Makoto ITO
Yuko MOCHIZUKI
Hideki MADOKORO

Senior Visiting Scientist

Wolfgang MITTIG (GANIL, France)

Visiting Scientists

Sachiko AMARI (Washington Univ.,USA)
Xiangzhou CAI (Shanghai Inst. Applied Phys., China)
Alfred DEWALD (Univ. Cologna Insti. Nucl. Phys.)
DEQING FANG (Shanghai Inst. Applied Phys., China)
Adrian GELBERG (Univ. zu KoelnInst. Fur Kern Physik, Germany)
Wei GUO (Shanghai Inst. Applied Phys., China)
Hiroyuki KOURA (JAEA)
YUGANG MA (Shanghai Inst. Applied Phys., China)
Masayuki MATSUO (Grad. Sch. of Sci. and Tech., Niigata Univ,)
Tetsuo NORO (Kyusyu Univ. Fac. of Sci.)
YURI PENIONZHKEVICH (Flerov Lab. Nucl. Reactions, JINR, Russia)
Ryoichi SEKI (California State Univ., Northridge, USA)
Takahiro TACHIBANA (Waseda High Sch., Waseda Univ.)
Kohji TAKAHASHI (Universite Libre de Bruxelles, Belgium)
Noboru TAKIGAWA (Fac. of Sci., Tohoku Univ.,)
OLEG TARASOV (MSU, NSCL, USA)
Ryouichi WADA (Texas A&M Univ., USA)
Juzo ZENIHIRO (Grad. Sch. of Sci., Kyoto Univ.)

Research Fellow

Lisheng GENG (Beijin Univ., CHINA)

Students

Junior Research Associates

Yuichi ICHIKAWA (Grad. Sch. of Sci., Univ. of Tokyo)
Taro NAKAO (Grad. Sch. of Sci., Univ. of Tokyo)
Megumi NIIKURA (Grad. Sch. of Sci., Univ. of Tokyo)
Takeo ONISHI (Grad. Sch.. of Sci., Univ. of Tokyo)
Masaru SUZUKI (Grad. Sch. of Sci., Univ. of Tokyo,)

Student Trainees

Yuhei HASHIZUME (Grd. Sch. of Pure and Applied Sci.,Univ. of Tsukuba)
Yoshihiko IWAO (Grad. Sch. of Sci., Kyoto Univ.)
Hitomi KIMURA (Grad. Sch. of Sci., Univ. of Tokyo)

Hiroaki MATSUMOTO (Grad. Sch. of Sci., Kyoto Univ.)
Hooi Jin ONG (Grad. Sch. Sci., Univ of Tokyo)
Akio SHIRAKI (Grad. Sch. of Sci., Univ. of Tokyo)
Daisuke SUZUKI (Grad. Sch. of Sci., Univ. of Tokyo)

Secretary

Shizuka KATO

Superheavy Element Laboratory

1. Abstract

The elements with their atomic number Z>103 are called as trans-actinide or superheavy elements. The chemical properties of those elements have not yet been studied in detail. Those elements do not exist in nature therefore, they must be produced by artificially for the scientific study of those elements. In our laboratory, we have been studying the physical and chemical properties of the superheavy elements utilizing the accelerators in RIKEN and various methods of efficient production of the superheavy elements.

2. Major Research Subjects

(1) Search for new supreheavy elements
(2) Decay spectroscopy of the heaviest nuclei
(3) Study of the chemical properties of the heaviest elements
(4) Study of the reaction mechanism of the fusion process (theory)

3. Summary of Research Activity

(1) Searching for new elements

To expand the periodic table of elements and the nuclear chart, we will search for new elements.

(2) Spectroscopic study of the nucleus of heavy elements

Using the high sensitivity system for detecting the heaviest element, we plan to perform a spectroscopic study of nuclei of the heavy elements.

(3) Chemistry of superheavy elements

Study of chemistry of the trans-actinide (superheavy element) has just started world-wide, making it a new frontier in the field of chemistry. Relativistic effects in chemical property are predicted by many theoretical studies. We will try to develop this new field.

(4) Study of a reaction mechanism for fusion process

Superheavy elements have been produced by complete fusion reaction of two heavy nuclei. However, the reaction mechanism of the fusion process is still not well understood theoretically. When we design an experiment to synthesize nuclei of the superheavy elements, we need to determine a beam-target combination and the most appropriate reaction energy. This is when the theory becomes important. We will try to develop a reaction theory useful in designing an experiment by collaborating with the theorists.

Head
Kosuke MORITA

Members
Hiromitsu HABA
Kouji MORIMOTO

Special Postdoctoral Researcher
Takatoshi ICHIKAWA
Daiya KAJI

Contract Technical Scientist
Akira YONEDA

Research Associate
Hidetoshi KIKUNAGA

Visiting Scientists
Masato ASAI (Japan Atomic Energy Agency)
Shin-ichi GOTO (Niigata Univ.)
Kouichi HAGINO (Tohoku Univ.)
Hisaaki KUDO (Fac. Sci., Niigata Univ.)
Tetsuya MURAKAMI (Grad. Sch. Sci., Kyoto Univ.)
Keisuke SUEKI (Grad. Sch. Pure Appl. Sci., Univ. Tsukuba)
Fuyuki TOKANAI (Dept. Phys., Yamagata Univ.)

Research Consultants
Takashi INAMURA
Kenji KATORI
Toru NOMURA

Students

Junior Research Associate
Takahiro AKIYAMA (Saitama Univ.)

Part-time Staff I(*Research Support*)
Nozomi SATO (Grad. Sch. Sci. Eng., Tohoku Univ.)

Student Trainees
Tomohiro NANRI (Dept. Chem., Kanazawa Univ.)
Itsuro YAMAZAKI (Dept. Chem., Kanazawa Univ.)

SLOWRI Team

1. Abstract

A next-generation slow radioactive nuclear ion beam facility (SLOWRI) which provides slow, high-purity and small emittance ion beams of all elements is being build as one of the principal facilities at the RIKEN RI-beam factory (RIBF). High energy radioactive ion beams from the projectile fragment separator BigRIPS are thermalized in a large gas catcher cell. The thermalized ions in the gas cell are guided and extracted to a vacuum environment by a combination of dc electric fields and inhomogeneous rf fields (rf carpet ion guide). From there the slow ion beam is delivered via a mass separator and a switchyard to various devices: such as an ion trap, a collinear fast beam apparatus, and a multi-reflection time of flight mass spectrometer. In the R&D works at the present RIKEN facility, an overall efficiency of 5% for a 100 A MeV ^{8}Li ion beam from the present projectile fragment separator RIPS was achieved and the dependence of the efficiency on the ion beam intensity was investigated.

First spectroscopy experiment at the prototype SLOWI was performed on Be isotopes. Energetic ions of ^{10}Be and ^{7}Be from the RIPS were trapped and laser cooled in a linear rf trap and the specific mass shifts of these isotopes were measured for the first time. The evaluated ion temperature of about 1 K demonstrates that a reduction of more than 13 orders of magnitude for the kinetic energy of radioactive Be was achieved online. Precise investigation of the hyperfine structure will confirm the anomalous mean radius of the valence neutron of the so called neutron halo nucleus.

Other spectroscopy experiments using the slow RI-beams are also under progress in off-line setups. A collinear fast beam apparatus for nuclear charge radii measurements was build and tested with stable Ar+ ion beams. A multi-reflection time-of-flight mass spectrograph was build for precise and fast measurements of short-lived radioactive nuclei. A high mass resolving power of 100,000 has been achieved with a 3 ms measurement period.

2. Major Research Subjects

(1) Development and constraction of the next-generation slow RI-beam facility
(2) Precision hyperfine spectroscopy of trapped ions for magnetization distribution in a halo nuclues
(3) Nuclear charge radii measurements using ion trap and collinear fast beam apparatus
(4) Precision mass measurements of short-lived nucei using a multi-reflection TOF mass spectrograph
(5) Development of deceleration and cooling devices for energetic beams using gas cell and rf fields.
(6) Atomic physics and fundamental symmetry research investigating nuclear decay of an isolated atom

3. Summary of Research Activity

(1) Development of universal slow RI-beam facility

WADA, Michiharu, NAKAMURA, Takashi, TAKAMINE, Aiko, ISHIDA, Yoshihisa, OKADA, Kunihiro, LIOUBIMOV Vladimir, KANAI, Yasuyuki, YOSHIDA, Atsushi, KUBO, Toshiyuki, YAMAZAKI, Yasunri, WOLLNIK, Hermann, SCHUESSLER, Hans, NODA, Koji, OHTANI, Shunsuke, KATAYAMA Ichiro

A next-generation slow radioactive nuclear ion beam facility (SLOWRI) which provides slow, high-purity and small emittance ion beams of all elements is being build as one of the principal facilities at the RIKEN RI-beam factory (RIBF). High energy radioactive ion beams from the projectile fragment separator BigRIPS are thermalized in a large gas catcher cell. The thermalized ions in the gas cell are guided and extracted to a vacuum environment by a combination of dc electric fields and inhomogeneous rf fields (rf carpet ion guide). From there the slow ion beam is delivered via a mass separator and a switchyard to various devices: such as an ion trap, a collinear fast beam apparatus, and a multi-reflection time of flight mass spectrometer. In the R&D works at the present RIKEN facility, an overall efficiency of 5% for a 100 A MeV ^{8}Li ion beam from the present projectile fragment separator RIPS was achieved and the dependence of the efficiency on the ion beam intensity was investigated.

(2) Laser spectroscopy of trapped radioactive beryllium isotope ions

WADA, Michiharu, NAKAMURA, Takashi, TAKAMINE, Aiko, ISHIDA, Yoshihisa, OKADA, Kunihiro, LIOUBIMOV Vladimir, KANAI, Yasuyuki, YOSHIDA, Atsushi, KUBO, Toshiyuki, YAMAZAKI, Yasunori, WOLLNIK, Hermann, SCHUESSLER, Hans, NODA, Koji, OHTANI, Shunsuke, KATAYAMA Ichiro

As a first application of the prototype SLOWRI setup, we are applying hyperfine structure spectroscopy to the beryllium isotopes to determine in particular the anomalous radius of the valence neutron of the neutron halo nucleus ^{11}Be, and to determine the charge radii of these beryllium isotopes through laser-laser double resonance spectroscopy of laser-cooled ions. Laser cooling is an essential prerequisite for these planned experiments. However, the exact resonance frequencies of the cooling transitions for radioactive beryllium isotopes are not

known. In such light elements, the isotope shifts in the atomic transitions are larger than several 10 GHz and their dominant parts are due to complicated multi-electron correlations. Some theoretical works on the isotope shifts of the beryllium ion exist, however the values contradict each other at the level of accuracy needed.

The laser spectroscopy experiments for beryllium isotopes were performed at the prototype SLOWRI setup of the existing accelerator facility. The resonant frequencies of 2s $^2S_{1/2}$ - 2p $^2P_{3/2}$ transition of ^{7}Be+, ^{9}Be+ and ^{10}Be+ ions were determined to be 957,347.37(11) GHz, 957,396.515(14) GHz and 957,414.839(35) GHz, respectively. Then we determined the transition frequency of infinitely heavy 957,569.55(28) GHz and the differential mass polarization parameter 1,884.5(46) THz, for the first time.

Hyperfine structure spectroscopy of Be isotopes using the laser-microwave double resonance method to determine the Bohr-Weisskpf effect is also in progress.

(3) Development of a multi-reflection TOF mass spectrograph

WADA, Michiharu, ISHIDA, Yoshihisa, NAKAMURA, Takashi, TAKAMINE, Aiko, OKADA, Kunihiro, YAMAZAKI, Yasunori, WOLLNIK, Hermann,

The atomic mass is one of the most important quantity of a nucleus and has been studied in various methods since the early days of physics. Among many methods we chose a multi-reflection time-of-flight (MR-TOF) mass spectrometer. Slow RI beams extracted from the RF ion-guide are bunch injected into the spectrometer with a repetition rate of ∼500 Hz. The spectrometer consists of two electrostatic mirrors between which the ions travel back and forth repeatedly. These mirrors are designed such that energy-isochrononicity in the flight time is guaranteed during the multiple reflections while the flight time varies with the masses of ions. A mass-resolving power of $>$ 200,000 has been obtained with ∼500 reflections in a 30 cm length spectrometer. This mass-resolving power should allow us to determine ion masses with an accuracy of 10^{-7}. This accuracy is lower than that obtained in a Penning trap mass spectrometer, however, it is sufficient to study many r-process nuclides, for instance. The advantages of the MR-TOF spectrometer are: 1) short measurement periods, typically 2 ms, which allows all neutron rich nuclei to be investigated, 2) the device is compact and its operation is simple, especially, it is independent from the all upstream devices, accelerators and fragment separators, 3) ions of more than isobars can be measured simultaneously, so that mass reference can easily be established in the mass spectra. In total, the number of measurable nuclides within a limited beam time would be larger than that can be achieved by other methods. It should be noted here also that this method can be used even during a low-duty parasite beam time.

(4) Development of collinear fast beam apparatus for nuclear charge radii measurements

WADA, Michiharu, LIOUBIMOV Vladimir, SCHUESSLER, Hans, IIMURA, Hideki, ISHIDA, Yoshihisa, NAKAMURA, Takashi, TAKAMINE, Aiko, OKADA, Kunihiro, YAMAZAKI, Yasunori, WOLLNIK, Hermann,

The root-mean-square charge radii of unstable nuclei have been determined exclusively by isotope shift measurements of the optical transitions of singly-charged ions or neutral atoms by laser spectroscopy. Many isotopes of alkaline, alkaline-earth, noble-gases and several other elements have been measured by collinear laser spectroscopy since these ions have all good optical transitions and are available at conventional ISOL facilities. However, isotopes of other elements especially refractory and short-lived ones have not been investigated so far.

In SLOWRI, isotopes of all atomic elements will be provided as well collimated mono-energetic beams. This should expand the range of applicable nuclides of laser spectroscopy. In the first years of the RIBF project, Ni and its neighboring elements, such as Ni, Co, Fe, Cr, Cu, Ga, Ge are planned to be investigated. They all have possible optical transitions in the ground states of neutral atoms with presently available laser systems. Some of them have so called recycle transitions which enhance the detection probabilities noticeably. Also the multistep resonance ionization (RIS) method can be applied to the isotopes of Ni as well as those of some other elements. The required minimum intensity for this method can be as low as 10 atoms per second.

We have builded an off-line mass separator and a collinear fast beam apparatus with a large solid-angle fluorescence detector. A 617 nm transition of the metastable Ar+ ion at 20 keV was measured with both collinear and anti-collinear geometry that allowed us to determine the absolute resonant frequency of the transition at rest with more than 10^{-8} accuracy. Such high accuracy measurements for Ti and Ni isotopes are in progress.

Head
Hiroyoshi SAKURAI

Members
Michiharu Wada

R&D team for multiparticle spectrometer

1. Abstract

Main task of R&D team for multiparticle spectrometer is to make R&D on broad range multiparticle spectrometer SAMURAI (Superconducting Analyser for Multiparticles from RadioIsotope beams), which is planned to built at BIBF for nuclear structure experiments using RI beams at RIBF. Design of the large superconducting magnet is being designed helped by various companies. Various detectors necessary for large magnetic spectrometer are being developed and tested.

2. Major Research Subjects

(1) Design of large superconducting magnet system
(2) R&D on High-accuracy/high-rate position detectors
(3) R&D on High-accuracy velocity measuring detectors
(4) R&D on High-accuracy total energy detectors

3. Summary of Research Activity

(1) Design of Large Superconducting magnetic spectrometer
(Kobayashi, Yoneda, Otsu, Kubo, Sekiguchi, Nakamura, Chiga, Iwasa, Murakami)

Basic design of large superconducting dipole magnet, which is central part of the SAMURAI system, is being made in collaboration with outside companies.

(2) R&D of Various detectors for large superconducting magnetic spectrometer
(Kobayashi, Otsu, Sato)

As necessary detectors for large superconducting magnetic spectrometer, we have developed various dectors, such as high-accuracy/high-rate position detectors, high-precision velocity detectors, high-precision total-energy detectors. Their performances have been checked using heavy-ion beams at HIMAC accelerator facility.

Head
Hiroyoshi SAKURAI

Senior Visiting Scientist
Toshio Kobayashi (Grad. Sch. Sci. Fac. Sci., Tohoku Univ.)

Polarized RI Beam Team

1. Abstract

The team conducts the research and development on production of spin-polarized/alignment RI beams, and apply it to the research on nuclear physics and material science. The microscopic investigation of physical and chemical processes is performed by nuclear techniques which take advantage of the intrinsic nuclear properties and phenomena (spins, electromagnetic moments, decay modes etc.). In particular, the precession/resonance of a polarized/aligned nuclear spin under an external field is observed through change in the angular distribution of radiation, for the study of nuclear structures via nuclear moments. The same method, as well as the Moessbauer technique, are used for the investigation of condensed matter such as ferromagnets, fullerenes, systems with dilute magnetic impurities etc. by capitalizing radioactive nuclei as microscopic probes into them. All these research activities are to be extended to wide variety of unstable nuclei which the forth-coming facility, RI Beam Factory (RIBF), will provide. A method to produce beams of highly polarized radioactive nuclei, taking full advantage of RIBF, is being developed.

2. Major Research Subjects

(1) Production of spin-polarized RI beam with fragmentation reaction
(2) Production of spin-alignment RI beam
(3) Development of highly polarized slow RI beams
(4) Development of radioactive nuclear probes for condensed matter studies

3. Summary of Research Activity

(1) Production of fragment-induced spin polarization

In the production of RI beams with the projectile fragmentation reaction, spin-polarized RI beam can be produced in the projectile-fragmentation reaction by selecting the appropriate scattering angle and outgoing momentum. With the obtained spin-polarized nuclei, nuclear magnetic moments and electric quadrupole moments have been determined by means of the b-NMR method through the change in the angular distribution of the emitted b rays. The nuclear structure has been investigated for the nuclei far from the stability line based on this method. The sub-themes are the following.

(1) Production of the spin-polarized neutron-rich Al isotopes from ^{40}Ar-primary beams and measurements of the nuclear electro-magnetic moments. (Kameda, Ueno, Yoshimi, Sugimoto, Nagatomo, Shimada, Kobayashi)

(2) Production of the spin-polarized $^{33\text{-}34}$Al ($N > 20$) beams from ^{36}S-primary beams and measurements of the nuclear electric-quadrupole moments (Nagatomo, Ueno, Yoshimi, Kameda, Sugimoto, Shimada)

(3) Production of spin-polarized neutron-rich Si isotopes from ^{48}Ca-primary beams and measurements of the nuclear electro-magnetic moments. (Yoshimi, Ueno, Kameda, Sugimoto, Nagatomo, Shimada)

(2) Production of spin-aligned RI beams

(1) Production of spin-aligned nuclei is essentially important for the study on the nuclear structure through the measurement of excited-state nuclear moments, which is also useful to material sciences. Various techniques of the production method for obtaining spin-aligned RI beams have been developed. Sub-themes are the following.

(2) Production of spin-aligned ^{32m}Al beams in the projectile fragmentation and the measurement of the excited-state nuclear moment. (Kameda, Ueno, Yoshimi, Sugimoto, Nagatomo, Shimada)

Production of spin-aligned ^{134m}Ce beams as a probe of material science (Ueno, Kameda, Yoshimi, Shimada)

(3) Development of a new method for the production of spin-aligned RI beams via the two-step fragmentation reactions. (Ueno, Yoshimi, Kameda, Sugimoto, Nagatomo, Shimada)

(4) Studies on the properties of Transient Field at the high-velocity region. (Ueno, Yoshimi, Kameda, Shimada)

(5) Application of the Recoil-into-vacuum method to RI-beam experiments (Sugimoto, Yoshimi, Ueno)

(3) Production of highly spin-polarized low-energy RI beams

New methods and devices have been developed for producing highly spin-polarized RI beams in low beam-energy region to overcome difficulties expected in the above method 1. The high spin polarization and the low beam energy are important not only for nuclear-moment measurements but also for spin-related subjects in nuclear physics, fundamental physics, and material sciences. Sub-themes are the following.

(1) Development of a new atomic-beam resonance method to combine with fragmentation-based RI beams (Sugimoto, Yoshimi, Ueno)

(2) Production of low-energy spin-polarized ^{17}N beams via the transfer reactions based on the inverse kinematics and its application (Shimada, Sugimoto, Kameda, Yoshimi, Ueno)

(4) Development of RI probes and application for the condensed matter sciences

Utilizing RI beams as a probe, online Mössbauer spectroscopy and online perturbed angular correlation experiments have been carried out through the g-ray measurements. The microscopic structures, dynamics in ferromagnets, and properties of semiconductors have been investigated from the deduced internal local fields and the spin relaxation of the probe in materials. The methods and apparatus have been developed. Also, basic studies on the probe nuclei have been carried out. Sub-themes are the following.

(1) Production of high quality ^{57}Mn beams for the online Mössbauer spectroscopy (Kobayashi, Ueno, Yoshimi, Kameda)

(2) Development of the on-line perturbed angular-correlation method with ^{19}O beams as a new probe (Kobayashi, Ueno, Yoshimi, Kameda, Shimada)

Team Leader
Hiroyoshi SAKURAI

Members
Yoshio KOBAYASHI
Hideki UENO
Akihisa YOSHIMI

Rare RI-ring Team

1. Abstract

We are developing the isochronous storage ring to measure the mass for rare radioactive isotopes (Rare RI ring). It is assumed that uranium is synthesized by neutron capture process after the supernovae explosion (r-process). To prove r-process, mass measurements for the rare RI is indispensable. It is possible to inject the rare RI one by one to the ring (individual injection) since cyclotrons in RIBF provide continuous beams. To perform the individual injection, we need a long injection line. The isochronous storage ring and the individual injection are very unique system.

2. Major Research Subjects

(1) Developments of isochronous storage ring to measure mass of rare RI
(2) Developments of detectors for mass measurements

3. Summary of Research Activity

(1) Developments of isochronous storage ring to measure mass of rare RI

We are improving conceptual designs for an isochronous storage ring, kicker magnets, and the injection line to the storage ring. The storage ring consists of six sector magnets. The edge angles of each sector magnets compensate the first order isochronism. For the kicker magnets, we fixed rough specifications. For the injection line, we performed the first order ion-optical calculations. Furthermore, we performed magnetic field measurements of a present sector magnet in BigRIPS by using NMR with high accuracy on the last April.

(2) Developments of detectors for mass measurements

The group in Saitama University performed the experiment to measure the time resolution of thin plastic-scintillators in HIMAC. The results show, for heavy ion beams with 200 A MeV, reasonably good timing resolution can be achieved even in the thin scintillator with 10 micron thickness. The group in University of Tsukuba measured a response time of Hybrid Photo Detector (HPD), which can replace with traditional Photo Multi Tube (PMT). The results show that the response time of HPD is faster than that of PMT by about 10 ns.

Team Leader
Hiroyoshi SAKURAI

Research Associate
Yoshitaka YAMAGUCHI

Visiting Scientists
Akira OZAWA (Inst. Phys., Univ. of Tsukuba)
Yusuke YASUDA (National Inst. of Advanced Industrial Sci. and Tech.)

SCRIT Team

1. Abstract

We aim at the investigation of internal nuclear structure of short-lived radioactive nulei (RI) by means of electron scattering. Electron scattering for RI's has never been performed duo to inability to make target of these nuclei. An electron-RI collider system, which requires a huge accelerator complex, has so far been unique solition to overcom the difficulty. We are developing a novel internal target system named SCRIT (Self-Confining RI Ion Target) in an electron storage ring to make the experiment easier with much compact experimental system.

2. Major Research Subjects

Developement of the SCRIT technology and electron scattering for unstable nuclei

3. Summary of Research Activity

Development of a novel internal target of unstable nuclei (SCRIT) in an electron storage ring for electron scattering experiment

(Wakasugi, Suda, Ito, Emoto, Nakamura, Kurita, Tamae, Noda, Shirai, Yano)

We are now developing a novel internal target system, which is to be used in an electron storage ring. This is named SCRIT (Self-Confining Radioactive Ion Target). This technology can localize specific ions on the electron beam axis using so-called "ion-trapping" phenomenon and form a fixed target of unstable nuclei. This will realize electron-scattering experiments for short-lived nuclei that have never been succeeded in. The R&D study of the SCRIT is now under way at the KSR in Kyoto University. We confirmed that ^{133}Cs ions, which were injected from outside, were trapped in the SCRIT. The SCRIT technology will open a new application of electron rings.

Team Leader
Hiroyoshi SAKURAI

Members
Takashi EMOTO
Sachiko ITO
Masanori WAKASUGI

GARIS Team

1. Abstract

Development and maintenance of devices related to study of the superheavy elements.

2. Major Research Subjects

(1) Maintenance and development of a recoil separator.
(2) Development of rapid chemistry devices.

3. Summary of Research Activity

(1) Maintenance and development of recoil separator

A gas-filled recoil separator has been used as a main experimental device for the study of superheavy elements. We will develop and maintain the related devices. We will also offer user-support if a researcher wishes to use the devices for his/her own research program.

(2) Development of devices for fast chemistry

We do research and development of devices for fast chemistry of superheavy elements. We also offer user-support for potential users.

Team Leader
Kosuke MORITA

Members
Hiromitsu HABA
Kouji MORIMOTO

Special Postdoctoral Researcher
Daiya KAJI

Contract Technical Scientist
Akira YONEDA

Research Associate
Hidetoshi KIKUNAGA

Junior Research Associate
Takahiro AKIYAMA (Grad. Sch. of Sci. & Eng., Saitama Univ.)

BigRIPS Team

1. Abstract

This team is in charge of development, design and construction of BigRIPS separator and its related equipments, which will be employed for not only the production of RI beams but also the experimental studies using RI beams in the RI beam factory (RIBF) project.

2. Major Research Subjects

Development and construction of BigRIPS, RI-beam transport lines, and their related equipments

3. Summary of Research Activity

This team is in charge of development, design and construction of BigRIPS separator and its related equipments, which will be employed for not only the production of RI beams but also the experimental studies using RI beams in the RI beam factory (RIBF) project.

The research subjects may be summarized as follows:
Development, design and construction of BigRIPS separator and its related equipments such as ZeroDegree spectrometer.

(1) General studies on RI-beam production using in-flight scheme.

(2) Studies on ion-optics of in-flight separators, including particle identification of (3) RI beams and simulation of RI-beam production.

(4) Development of beam-line detectors and their data acquisition system.

(5) Experimental studies on production reactions and unstable nuclei.

(6) Development of superconducting magnets and their helium cryogenic systems.

(7) Development of a high-power production target system.

(8) Development of a high-power beam dump system.

(9) Development of a remote maintenance and remote handling systems.

(10) Operation, maintenance and improvement of BigRIPS separator system and its related equipments such as ZeroDegree spectrometer.

Team Leader
Hiroyoshi SAKURAI

Members
Toshiyuki KUBO
Masao OHTAKE
Yoshiyuki YANAGISAWA
Atsushi YOSHIDA
Kouichi YOSHIDA

Contract Researchers
Kensuke KUSAKA
Tetsuya OHNISHI

Research Associates
Naoki FUKUDA
Tomohito HASEYAMA

Part-time Staff
Hidekazu KUMAGAI

Senior Visiting Scientist
Susumu SHIMOURA (CNS, Grad. Sch. Sci., Univ. of Tokyo)

Computing and Network Team

1. Abstract

Development, management and operation of the computing and network environment, mail server and data acquisition system and control of the information security of the Nishina Center for Accelerator-Based Science.

2. Major Research Subjects

(1) Development, management and operation of the computing
(2) Development, management and operation of the mail server
(3) Development, management and operation of the data acquisition system
(4) Development, management and operation of the network environment
(5) Control of the information security

3. Summary of Research Activity

Development, management and operation of the computing and network environment, mail server and data acquisition system and control of the information security of the Nishina Center for Accelerator-Based Science.

For more information, please refer to the document in this report entitled "Network and Computing Environment for RIKEN Nishina Center" written by T. Ichihara, Y. Watanabe, K. Yoshida and A. Yoshida as page 199 and also the URL *http://ribf.riken.jp/comp/index-j.html*.

Team Leader
Takashi ICHIHARA

Member
Yasushi WATANABE

Detector Team

1. Abstract

This team is to organize various detector developments performed at in-house laboratories and groups, in order to improve mutual share of knowledge and experience.

2. Major Research Subjects

(1) Development of delay-line PPAC
(2) Development of transmitter/receiver for fast signal transmission through optical fibers

3. Summary of Research Activity

This team is now focusing on developments of delay-line PPAC and a pair of fast transmitter and receiver coupled with optical fibers for fast signal transmission. These two developments are essential for particle identification at BigRIPS.

(1) Delay-line PPAC

At BigRIPS, a purity of radioactive isotope beams (RIBs) is as low as 10% or less at medium and heavy mass region. Thus, development of detectors for high-rate use is one of goals in this team. With this respect, we have developed a position-sensitive Parallel Plate Avalanche Counter (PPAC). Delay-line read-out technique appropriate for high-rate use is employed for position determination. This PPAC has two stripped-electrodes for both horizontal and vertical positions, and this configuration leads to high performance in terms of efficiency as well as position resolution. More than ten PPACs are being installed at BigRIPS.

(2) Fast transmitter and receiver for optical fiber

In general co-axial metal wires are used for fast signal transmission. Instead, we have developed a special circuit of transmitter and receiver for optical fiber.

At a new facility of RIBF, circuits for detectors are located at several focal planes of the BigRIPS, and distances between focal planes and counting room are as long as 100 m. To introduce optical fibers in signal transmission, we focus on a common ground at each focal plane, and easily isolate the ground levels. A problem in use of optical fiber was no fast transmitter/receiver with a low cost, which are not available in market. We have developed a pair of fast transmitter and receiver for optical fibers with a semiconductor laser and photo diode. This circuit has a fast time response of more than 1 GHz. Attenuation of signal amplitudes is negligibly small even at a long distance transmission of more than 100 m. Many sets of transmitter/receiver for detectors at BigRIPS have been already manufactured, and optical fibers will be used for standard transmission of signals.

Head
Hiroyoshi SAKURAI

Contract Researcher
Akira YONEDA

Part time staff I
Hidekazu KUMAGAI

Senior Visiting Scientist
Hirohiko SHIMIZU (Inst. of Materials Structure Sci., KEK)

User Support Office

1. Abstract

The RIKEN RI Beam Factory is the world preeminent facility providing the greatest opportunities for scientific researches. It is our important mission to serve for a broad range of application of a large variety of researchers so that we bring out the best performance of the RI Beam Factory. We manage to facilitate the use of RI Beam Factory to the researchers both inside and outside of RIKEN, to support experiments using the accelerator complex, to exploit industrial application researches, and to promote the RI Beam Factory to interested researchers

2. Major Research Subjects

(1) Facilitation of the use of the RI Beam Factory
(2) Support of experiments in the RI Beam Factory
(3) Promotion of the RI Beam Factory to interested researchers

3. Summary of Research Activity

The RIKEN RI Beam Factory is the world preeminent facility providing the greatest opportunities for scientific researches. It is our important mission to serve for a broad range of application of a large variety of researchers so that we bring out the best performance of the RI Beam Factory. We manage to facilitate the use of RI Beam Factory to the researchers both inside and outside of RIKEN, to support experiments using the accelerator complex, to exploit industrial application researches, and to promote the RI Beam Factory to interested researchers

Team Leader
Toshimi SUDA

Members
Mieko KOGURE
Toshiko NAKAMURA

Technical Staff I
Narumasa MIYAUCHI

Assistant
Tomoko IWANAMI
Yuri TSUBURAI

Experimental Support Team

1. Abstract

We are supporting users of accelerators in the Nishina Center.

2. Major Research Subjects

No research.

3. Summary of Research Activity

Supporting activities are carried out for any experiments using accelerators of RILAC, AVF cyclotron, RRC and/or RIBF accelerators.

Team Leader
Masayuki KASE

Members
Nobuhisa FUKUNISHI
Naohito INABE
Osamu KAMIGAITO
Takahide NAKAGAWA
Hiroki OKUNO
Naruhiko SAKAMOTO
Masanori WAKASUGI
Tamaki WATANABE

Industrial Coorperation Team

1. Abstract

The scope of the industrial cooperation team includes industrial application of RIBF facility and research and development for industrial application of accelerator associated technologies.

2. Major Research Subjects

(1) Development of techniques for radioisotope production
(2) Application of advanced data acquisition and signal processing technologies

3. Summary of Research Activity

(1) Development of techniques for radioisotope production

At RIBF, various specific radioisotopes for research have been produced with the cyclotrons and the ion beams generated thereby and used for various joint research projects. As we plan to distribute commercially a few radioisotopes to nonaffiliated users, the production techniques are being developed for stable supply and quality level.

(2) Research and development of m-sequence modulation technique

"M-sequence modulation (Takeichi et al., 2007)" enables efficient acquisition and extraction of a continuous brain-activation signal. The stimulus is modulated by a pattern defined by an m-sequence. The measured brain-activation signal is then decoded by computing a cross-correlation function with the m-sequence and applying independent component analysis. We are currently working on investigations of further developments and applications to medical and health sciences, information communication, and other basic and industrial research fields.

Team Leader
Tadashi KAMBARA

Members
Tomoko ABE
Shuichi ENOMOTO
Hiroshige TAKEICHI

Temporary Staff
Ichiro SAKAMOTO

Part time staff
Taro YOSHIMI

Arbeit
Aya ISHIZUKA

Visiting Scientists
Makiko KAGA (National Inst. of Mental Health)
Atsuko GUNJI (National Inst. of Mental Health)
Michiteru KITAZAKI (Res. Center for Future Vehicle. Toyohashi Univ. of Tech.)

Student Trainees
Yasuhisa FUJIKI (Fac. of Eng., Toyohashi Univ. of Tech.)
Shinichiro HARIYAMA (Dept. of Knowledge-based Information Eng., Toyohashi Univ. of Tech.)
Shinichi ONIMARU (Dept. of Knowledge-based Information Eng., Toyohashi Univ. of Tech.)

Radiation Lab.

1. Abstract

Nucleons, such as protons and neutrons, are a bound state of constituent quarks glued together with gluons. The detail structure of nucleons, however, is not well understood yet. Especially the mechanism to build up the spin of proton, which is 1/2, is a major problem in physics of the strong force. The research goal of Radiation Laboratory is to solve this fundamental question using the first polarized-proton collider, realized at RHIC, Brookhaven National Laboratory (BNL) in USA. RHIC stands for Relativistic Heavy Ion Collider, aiming also to create Quark Gluon Plasma, the state of Universe just after the Big Bang. RIKEN-BNL Research Center (RBRC) directed by N. Samios carries our core team at BNL for those exciting researches. We are also doing pioneering researches at the domestic accelerators at RIKEN and High Energy Accelerator Research Organization (KEK). We have recently discovered mass modification of vector meson using the accelerator at KEK. We are also performing technical developments such as novel ion sources, super conducting detectors, fine pitch pixel detectors and neutron optical devices.

2. Major Research Subjects

(1) Spin physics with relativistic polarized-proton collisions at RHIC
(2) Study of nuclear matter at high temperature and/or at high density
(3) Technical developments on radiation detectors and accelerators

3. Summary of Research Activity

(1) Experimental study of spin structure of proton using RHIC polarized proton collider

[See: RIKEN-BNL Research Center Experimental Group (Heavy Ion Basic Science - Study of Spin Physics Using RHIC)]

(2) Experimental study of quark-gluon plasma RHIC heavy ion collider

[See: RIKEN-BNL Research Center Experimental Group (Heavy Ion Basic Science - Study of Spin Physics Using RHIC)]

(3) Study of nuclear medium effect on vector mesons at KEK-PS

The experiment KEK-PS E325 was performed from 1997 to 2002. We measure invariant mass spectra of e^+e^- and K^+K^- channels using 12-GeV proton + nucleus reactions, and investigate the spectral modification of vector mesons (φ, ρ and ω) which is theoretically expected due to the chiral symmetry restoration. Through the analyses until this year, we have confirmed that those three mesons are modified in nuclear matter. Especially the spectral modification of the φ meson is observed for the first time and is very important. We have press-released the results just after the acceptance of the paper by Physical Review Letters. The paper was also cited in Physical Review Focus.

(4) Study of Accelerator and Ion source

To achieve highly polarized beams in RHIC it is necessary to understand the AGS (RHIC injector synchrotron) spin dynamics. The normal-conducting partial-snake magnet, which we have developed for AGS years ago, now playing a more important role with the other super-conducting snake magnet, newly fabricated and installed in AGS. Several combinations of field strengths of these two magnets have been tried to achieve more sophisticated operation. We are also studying betatron tunes for the two snake configuration and we have currently achieved the AGS polarization of 65%. For future high-brightness heavy-ion accelerators, we are studying high current beam production using a new strategy called direct plasma injection scheme. Our world intensity record of Carbon beam production was followed by a record Aluminum beam which showed more than 70 mA. We have also proven the feasibility of high intensity beam production from cryo-cooled gas target.

(5) Detector development for PHENIX experiment

To improve the physics capability of the PHENIX detector system at RHIC, we are developing the silicon vertex detector (VTX). The VTX consists of two layers of silicon pixel detectors developed under the collaboration with CERN, and other two layer of silicon strip detector with BNL. RIKEN Radiation Laboratory is responsible for the ladder fabrication of the pixel detector and the sensor fabrication of strip detector. The firstly assembled prototype ladders were tested with cosmic rays and successfully operated through the PHENIX-equivalent data acquisition system. For the final product we are developing high-density ultra-thin flexible print board, and preparing for the mass production assembling with 10 μm accuracy.

(6) Research and development of superconductor radiation detectors

Superconductor radiation detectors are able to measure the energies of photons with a much better resolution than any type of conventional detectors. They are capable of detecting photons over a wide energy range and also

charged particles. We have been developing superconducting tunnel junctions (STJs) as high-resolution radiation detectors. This year, an anodization method was introduced in fabricating STJs with a large area ($500\,\mu$m $\times$ $500\,\mu$m) in order to reduce leakage current. We got eight STJs with reasonable uniformity. Using these new STJs, we have started a new experiment to measure neutron beta decays at Japan Atomic Energy Agency. New idea to prevent phonon events in STJ was tried in collaboration with Saitama University. We made new STJs which have polyimide buffer layer and found that such layers are effective to reduced phonon events.

(7) Neutron optics

Cold or thermal neutron beam is a high-sensitivity probe to study the structure of light elements such as hydrogen in any kind of material, including bio-molecules. However, its realistic applications are still limited since the numbers of available neutron sources are small and their intensities are low. This project aims to enhance the efficiency in using those precious neutron beams by improving the neutron beam optics, in order to maximize scientific outputs within a short period of time. This year an ellipsoidal neutron mirror and a new neutron detector with a good spatial resolution are developed for mfSANS (Mini Focusing Small Angle Neutron Scattering). We have tested the prototype of this system at LINAC in Hokkaido University. We successfully measured the neutron diffractions down to the momentum transfer region of $Q < 2 \times 10^{-3}A^{-1}$. We also developed "one-dimensional multi-channel neutron bender" as a neutron focusing device, whose first test was successfully performed at Tokyo University. To transfer these new technologies to public use, we have founded "Riken Venture Company", Japan Neutron Optics Inc. which has already started to distribute its products to other laboratories and universities.

(8) Theoretical study of hadron physics

We performed an analysis of fragmentation functions of mesons and baryons, which is the first global analysis of fragmentation functions fitted to the electron-proton data at HERA as well as the electron-positron data at LEP. The results are important for the measurement of gluon polarization in single pion productions at RHIC. The calculations of NLO QCD corrections are on-going for di-hadron productions in polarized hadronic processes, which provide us with an alternative way of accessing the gluon polarization.

The double transverse-spin asymmetries in transversely polarized Drell-Yan process are calculated at the small transverse momentum of dilepton ("peak region"). The soft gluon effects, relevant in the peak region are resummed to all orders of perturbation. We found that the asymmetries are flat and larger at the peak region than the asymmetries in the integrated cross section. We derived an asymptotic formula of the asymmetries in this region which enable us to extract the transversity easily from the experimental data of this process.

The QED structure functions of electron are calculated up to 5th order of the coupling constant. The obtained analytic formula is useful when we estimate the initial state radiation precisely in electron-positron, or electron-proton collisions.

NLO QCD corrections to Higgs boson production through vector boson fusion processes at LHC are calculated. The corrections turned out to be about 10% of LO result, improving the scale uncertainty significantly. Numerical studies with various experimental cuts are also performed.

Head
Hideto EN'YO

Members
Yasuyuki AKIBA
Yuji GOTO
Itaru NAKAGAWA
Yoshie OTAKE
Hiromi SATO
Atsushi TAKETANI
Yasushi WATANABE

Special Postdoctoral Researchers
Junkichi ASAI
Yoshinori FUKAO
Kenji MISHIMA
Megumi NARUKI

Contract Researchers
Katsuya HIROTA
Ryo ICHIMIYA

Kazuaki IKEDA
Soichiro KAMETANI
Hiroyuki KAWAMURA
Takahiro MORISHIMA
Ryotaro MUTO
Hiromi OKADA
Yoshiyuki ONUKI
Vladimir Rykov
Marco Stratmann
Tsuguchika TABARU
Satoshi YOKKAICHI

Contract Technical Scientists
Maki KUROSAWA

Part-time Staff (Research support)
Hiroyuki KANO

Senior Visiting Scientists
Ken-ichi IMAI (Grad. Sch. of Sci., Kyoto Univ.)
Toshiaki SHIBATA (Grad. Sch. of Sci. and Eng., Tokyo Inst. of Tech. Sch. of Sci.)
Hirohiko SHIMIZU (Inst. of Materials Structure Sci., KEK)
Koichi YAZAKI (Tokyo Woman's Christian Univ.)

Visiting Scientists
Tomohiro ADACHI (DAI-ICHI KIDEN CO.,LTD)
Christine A. AIDALA (Univ. Massachusetts, Amherst, USA)
Hiroshi AKOH (National Inst. of Advanced Industrial Sci. and Tech.)
Masahiro AOYAGI (National Inst. of Advanced Industrial Sci. and Tech.)
Masayuki ASAKAWA (Grad. Sch. of Sci., Osaka Univ.)
Alexander Bazilevsky (BNL, USA)
Wolfgang BENTZ (Tokai Univ.)
Mickey Chiu (Univ. of Illinois at Urbana, USA)
Seishi DAIRAKU (Grad. Sch. of Sci., Kyoto Univ.)
Sanatan Digal (Grad. Sch. of Sci., Univ. of Tokyo)
Frank ELLINGHAUS (Univ. of Colorado, USA)
Waled EMAM (Univ. of California at Riverside, USA)
Hirotsugu FUJII (Grad. Sch./College of Arts and Sciences, Univ. of Tokyo)
Haruhiko FUNAHASHI (Grad. Sch. of Sci., Kyoto Univ.)
Xiaohong GUO (Inst. Modern Phys. Chinese Acad. Sci., China)
Tetsuo HATSUDA (Grad. Sch. of Sci., Univ. of Tokyo)
Toshiyuki HATTORI (Res. Lab. for Nuclear Reactors, Tokyo Inst. of Tech. Sch. of Sci.)
Noriyosu HAYASHIZAKI (Res. Lab. for Nuclear Reactors, Tokyo Inst. of Tech. Sch. of Sci.)
Masanori HIRAI (Grad. Sch. of Sci. and Eng., Tokyo Inst. of Tech. Sch. of Sci.)
Kensuke HONMA (Grad. Sch. of Sci., Hiroshima Univ.)
Takuma HORAGUCHI (Grad. Sch. of Sci., Hiroshima Univ.)
Alekseev IGOR (ITEP, Russia)
Katsuya ISHIGURO (Grad. Sch. of Natural Sci. & Tech., Kanazawa Univ.)
Noriyoshi ISHII (Grad. Sch. of Sci. and Eng., Tokyo Inst. of Tech. Sch. of Sci.)
Barbara Jager (Univ. Karlsruhe, Inst. Theoretical Phys., Germany)
Robert Jameson (Goethe Universitat Frankfurt, Germany)
Osamu JINNOUCHI (Inst. of Particle and Nucl. Studies, KEK)
Masashi KANETA (Grad. Sch. of Sci., Tohoku Univ.)
Hirotsugu KASHIWAGI (Takasaki Advanced Radiation Res. Inst., JAEA)
Yuji KAWABATA (Kyoto Univ. Res. Reactor Inst.)
Takeo KAWASAKI (Grad. Sch. of Sci. and Tech., Niigata Univ.)
Akio KIYOMICHI (J-PARC, JAEA)
Jiro KODAIRA (Grad. Sch. of Sci., Hiroshima Univ.)
Yuji KOIKE (Grad. Sch. of Sci. & Tech., Niigata Univ.)
Sergei KONDRASHEV (ITEP, Russia)
Dmitiri KOTCHETKOV (Univ. New Mexico, USA)

Shunzo KUMANO (Inst. of Particle and Nuclear Studies, KEK)
Teiji KUNIHIRO (Yukawa Inst. for Theoretical Phys., Kyoto Univ.)
Masahiko KURAKADO (Academic Frontier Promotion Center, Osaka Electro-Communication Univ.)
Ming XIONG LIU (Los Alamos Nat. Lab., USA)
Keisuke MAEHATA (Fac. of Eng., Kyushu Univ.)
Yajun MAO (Peking Univ., China)
Yasuo MIAKE (Grad. Sch. of Pure and Applied Sci., Univ. of Tsukuba)
Shoichi MIDORIKAWA (Fac. of Software and Information Tech., Aomori Univ.)
Osamu MORIMATSU (Inst. of Particle and Nuclear Studies, KEK)
Hiroaki MYOREN (Grad. Sch. of Sci. & Eng., Saitama Univ.)
Sachio NAITO (Inst. of Materials Structure Sci., KEK)
Hiroshi NAKAGAWA (National Inst. of Advanced Industrial Sci. and Tech.)
Yoshifumi NAKAMURA (DESY, Germany)
Atsushi NAKAMURA (Information Media Center, Hiroshima Univ.)
Masashi OHNO (Sch. of Eng., Univ. of Tokyo)
Munehisa OHTANI (Inst. fuer Theoretische Physik, Universitact Regensburg, Germany)
Masahiro OKAMURA (BNL, USA)
Petra RIEDLER (CERN, Switzerland)
Koichi SAITO (Tokyo Univ. of Sci.)
Takuya SAITO (RCNP, Osaka Univ.)
Naohito SAITO (J-PARC, KEK)
Kenji SASAKI (Inst. of Particle and Nuclear Studies, KEK)
Shin-ya SAWADA (Inst. of Particle and Nuclear Studies, KEK)
Michiko SEKIMOTO (Inst. of Particle and Nuclear Studies, KEK)
Kenta SHIGAKI (Grad. Sch. of Sci., Hiroshima Univ.)
Shigetomo SHIKI (Academic Frontier Promotion Center, Osaka Electro-Communication Univ.)
Tatsushi SHIMA (RCNP, Osaka Univ.)
Takenao SHINOHARA (Advanced Sci. Res. Center, JAEA)
Kazutaka SUDO (Inst. of Particle and Nuclear Studies, KEK)
Toru SUGITATE (Grad. Sch. of Sci., Hiroshima Univ.)
Tsuneo SUZUKI (Grad. Sch. of Natural Sci. & Tech., Kanazawa Univ.)
Junichi SUZUKI (Advanced Sci. Res. Center, JAEA)
Dmitry SVIRIDA (ITEP, Russia)
Toru TAINO (Grad. Sch. of Sci. & Eng., Saitama Univ.)
Manobu TANAKA (Inst. of Particle and Nuclear Studies, KEK)
Kiyoshi TANIDA (Grad. Sch. of Sci., Kyoto Univ.)
Kazuo TANIGUCHI (Fac. of Eng., Osaka Electro-Communication Univ.)
Alexander TITOV (Flerov Lab. Nucl. Reactions, Joint Inst. Nucl. Res., Russia)
Manabu TOGAWA (Grad. Sch. of Sci., Kyoto Univ.)
Hisayuki TORII (Grad. Sch. of Sci., Hiroshima Univ.)
Xiaorong WANG (New Mexico State Univ., USA)
Satoru YAMADA (Advanced Sci. Res. Center, JAEA)
Yoshiaki YASUI (Tokyo Management College)
Imuran YOUNUS (Univ. of New Mexico, USA)

Students

Junior Research Associate
Kazuya AOKI (Grad. Sch. of Sci., Kyoto Univ.)
Kohei FUJIWARA (Grad. Sch. of Sciences & Tech., Niigata Univ.)
Tadaaki ISOBE (CNS, Grad. Sch. of Sci., Univ. of Tokyo)
Fukutaro KAJIHARA (CNS, Grad. Sch. of Sci., Univ. of Tokyo)
Kenichi NAKANO (Grad. Sch. of Sci. and Eng., Tokyo Inst. of Tech. Sch. of Sci.)
Yoshichika SEKI (Grad. Sch. of Sci., Kyoto Univ.)
Kohei SHOJI (Grad. Sch. of Sci., Kyoto Univ.)
Junpei TAKANO (Grad. Sch. of Sci. and Eng., Tokyo Inst. of Tech. Sch. of Sci.)
Yuji TSUCHIMOTO (Grad. Sch. of Sci., Hiroshima Univ.)

Part-time Staff (*Research support*)
Kohichi SAKASHITA (Tokyo Inst. of Tech. Sch. of Sci.)

Fuminori SAKUMA (Grad. Sch. of Sci., Kyoto Univ.)
Yoshihiro YAMAMOTO (The Univ. of Electro-Communications)

Part-time Staff (*Research assistant*)
Jun TAMURA (Grad. Sch. of Sci. and Eng., Tokyo Inst. of Tech. Sch. of Sci.)

Intern
Yuki MIYAMOTO (Tokyo Metropolitan College of aeronautical Eng.)
Joseph SEELE (Dept. Phys., Univ. of Colorado, USA)
Tsutomu WAKABAYASHI (Tokyo Metropolitan College of aeronautical Eng.)
Zhengyun You (Peking Univ., China)
Takeshi KANESUE (Fac. of Eng., Kyushu Univ.)

Student Trainees
Kazutaka AOKI (Grad. Sch. of Sci. & Eng., Saitama Univ.)
Hisato EGUCHI (Grad. Sch. of Sci. & Tech., Niigata Univ.)
Yusuke FUJISAWA (Grad. Sch. of Sci. & Eng., Saitama Univ.)
Masatoshi HAMADA (Fac. of Sci., Kyushu Univ.)
Masayasu HASEGAWA (Grad. Sch. of Natural Sci. & Tech., Kanazawa Univ.)
Hirokazu ISHII (Grad. Sch. of Sci. & Eng., Saitama Univ.)
Taku ITO (Grad. Sch. of Sci. and Eng., Tokyo Inst. of Tech. Sch. of Sci.)
Hiroki KANOH (Grad. Sch. of Sci. and Eng., Tokyo Inst. of Tech.)
Kenichi KARATSU (Grad. Sch. of Sci., Kyoto Univ.)
Motohiro KAWASHIMA (College of Sci., Rikkyo Univ.)
Kotaro KIJIMA (Grad. Sch. of Sci., Hiroshima Univ.)
Masahiro KONNO (Grad. Sch. of Pure and Applied Sciences, Univ. of Tsukuba)
Martin LEITGAB (Univ. Vienna, Austria)
Kouichi MATSUBARA (Grad. Sch. of Sci. & Eng., Saitama Univ.)
Kentaro MIKI (Grad. Sch. of Pure and Applied Sciences, Univ. of Tsukuba)
Koji MIWA (Grad. Sch. of Sci., Kyoto Univ.)
Shinji MOTOKI (Grad. Sch. of Biosphere Sci., Hiroshima Univ.)
Takahiro NAGAI (Sch. of High Energy Accelerator Sci., The Grad. Univ. for Advanced Studies)
Yoshihide NAKAMIYA (Grad. Sch. of Sci., Hiroshima Univ.)
Tomoaki NAKAMURA (Grad. Sch. of Sci., Hiroshima Univ.)
Misaki OUCHIDA (Grad. Sch. of Sci., Hiroshima Univ.)
Akikuni SATO (Grad. Sch. of Sci., Kyoto Univ.)
Toru SEKIDO (Grad. Sch. of Natural Sci. & Tech., Kanazawa Univ.)
Katsuyuki SENZAKA (Grad. Sch. of Sci., Kyoto Univ.)
Yosuke SERITA (Grad. Sch. of Sci. & Eng., Saitama Univ.)
Maya SHIMOMURA (National Inst. of Advanced Industrial Sci. and Tech.)
Jonathan Turner (Univ. of New Mexico, USA)
Satoru UEDA (Grad. Sch. of Pure and Applied Sciences, Univ. of Tsukuba)

Secretaries
Hitomi KANEHAMA
Noriko KIYAMA
Michiko MUROI

Advanced Meson Science Laboratory

1. Abstract

Particles like muon, pion, and kaon have finite life time. Implanting these particles into materials, varieties of objects are studied from new points of views. For instance, stopping positively charged muon in a material, we obtain information on the magnetic properties or the local field at the trapped site. Injecting negatively charged muon to mixture of deuterium and tritium, muon attracts surrounding atoms and is known to cause d-t fusions.

We are also proceeding studies with other meta-stable particles other than muons. Kaon is a meson which has strange quark as its composition, and introducing Kaons into nuclei, sizes of the nuclei are estimated to become smaller and the density larger. We are studying this subject by performing experiments. Also, producing Lambda particles from the Kaons and observing its decay, we obtain information on the weak interaction between two baryons which is usually hidden. We also study properties of nuclei in detail by making spectroscopy of pions bound to nuclei.

As is already clear, in our research we introduce different kind of impurites into objects, and study new states of matter, new phenomena, or the object properties.

2. Major Research Subjects

(1) Nuclear physics via muon catalyzed fusion and muonic atoms
(2) Condensed matter and material studies with muon
(3) Study of meson property inside nuclei
(4) Interaction between meson and nuclei

3. Summary of Research Activity

Meta-stable particles such as muon, pion and kaon have opened variety of scientific research areas. Especially, muon plays an important role. The research area ranges over particle physics to condensed matter studies and life science. Our core activities are based on the RIKEN-RAL Muon Facility located at the Rutherford Appleton Laboratory (UK), which provides the most intense pulsed muon beam. We have variety of important research activities such as muon-catalyzed fusion (μCF) and condensed matter physics by muon spin rotation/relaxation/resonance (μSR). On the other hand, pion and kaon shed a new insight to the nuclear physics. The recent discovery of deeply bound pionic state enables us to investigate the properties of mesons in nuclear matter. We aim to be a world-leading scientific research group using these light meta-stable particles.

(1) Condensed matter/materials studies with high energy accelerator producing particles and nuclei

There are three topics of material sciences studied by the muon-spin relaxation method at the RIKEN-RAL Muon facility in 2007.

1) From measurements of the muon-spin depolarization rate in magnetic fields, quantitative values of the transition rate of electrons between iron atoms in a ironmetal complexes have been firstly obtained.

2) In a Sm-based Ru-Fe skutterudite compound, a possibility of the appearance of an ordered state of a multipole moments has been pointed out.

3) A new condensed state of excited electronic states has been suggested in Tl-K quantum-spin systems from zero-field muon-spin relaxation method.

(2) Nuclear physics studies with muons, such as muon catalyzed fusion and muonic atoms

1) Muon catalyzed fusion (μCF)

We are studying the muon catalyzed fusion (μCF) processes in a wide range of hydrogen target conditions such as isotope mixtures and temperatures. This year, we studied the effect of ortho-para composition of D_2 molecules. The ddμ formation rate in pure gaseous deuterium target at 35 K was increased when we used ortho-rich D_2, while it was opposite with liquid target even at the same temperature. For the liquid D_2/T_2 mixture, we achieved the increase of dtμ formation by using ortho-D_2 for the first time.

2) Development towards muonic atom formation with unstable nuclei

Stopping negative muons in the solid hydrogen with implanted unstable atoms, muons transfer efficiently to the implanted nuclei from muonic hydrogen to form the muonic atoms. By observing muonic X-rays at muonic atom formations, fundamental experiments on the nuclear charge density distribution are in progress. The surface ionization ion source was installed in the experimental apparatus to produce alkaline ion beams, and carried out successfully the first experiment to measure an isotope energy shift of muonic X-rays originated from muonic ^{88}Sr and ^{86}Sr atoms.

3) Generation of ultra slow positive muon beam

We have constructed a new μSR spectrometer specialized for using low energy muon beam, whose kinetic

energy is variable from a few keV to a few tens of keV. This will extend the scope of μSR technique from a bulk material to surfaces and multi-layered materials. In order to demonstrate the new spectrometer's capability, we have carried out the first μSR experiment of a thin film of a perovskite-type manganese oxide, and successfully observed changes in spectra's shape which are associated to phase transitions.

(3) Study of deeply bound mesonic nuclei

1) Deeply bound kaonic nuclei

We have performed a high precision and small ambiguity spectroscopy on the mass of the strange tribaryon -S° (3115)-at the high energy accelerator research organization (KEK). We measured the momenta of protons emitted in the reaction between negatively charged K mesons and helium nuclei. Compared to the previous experiment, the mass resolution was improved by a factor of 2 and the statistical accuracy by a factor of about 10. We have newly installed detectors exclusively used for the measurement of the protons and realized small-ambiguity experiment. As a result, no structure was observed, in the spectrum, associated to the strange tribaryon with the natural width of 20 MeV/c^2, and the result was contradictory to the previous experiment. Statistical evaluation tells that the previous results are rejected by a confidence level of 99%. Theoretical studies are firmly predicting the existence of the strange tribaryon or states where K meson is deeply bound to helium nucleus. We need to continue further analysis of the experimental data investigating the possible existence of structures with larger widths. Especially, the experiment described below(3) is important in terms of the constraints set strongly to the existence of the deeply bound k states.

2) Deeply bound pionic and eta- nuclei

We made a spectroscopy experiment to measure deeply bound pionic states in several tin isotopes at the GSI, Germany, to investigate the pion-nucleus strong interaction. The results provided information on the iso-vector part of the strong interaction between pion and nucleus. More advanced discussion leads to the origin of the mass of matter, which is attributed to the quark condensation in the vacuum. Presently we are analyzing the data of eta-mesonic nuclei, and willing to extend our study to the heavier meson.

3) Precision X-ray measurement of kaonic atom

Simultaneously with the above experiment(1), we have performed an X-ray spectroscopy of atomic $3d \rightarrow 2p$ transition of negatively charged K mesons captured by helium atoms. Many kaonic atoms are known to be measured with various elements, however, there are very large deviations in the measured energy levels for the helium (and the oxygen) from the systematic expectations. The deviation may originate in technical issues in old experiments, and new and high precision data have been long awaited for. Also, the wave functions of the kaonic atoms are expected to reflect the information on the existence of the inner structure, namely strange tribaryon or deeply bound kaonic states. As a result of the experiment, we have succeeded in performing the spectroscopy and achieved $<$10 eV (σ) in the experimental resolution, which is by far improved from older experiments. The obtained results reject older data beyond any doubt, and the above deviation is dissolved. Presently, aiming at higher precision, we are proceeding the data analysis.

Head

Masahiko IWASAKI

Members

Katsuhiko ISHIDA
Kenta ITAHASHI
Yasuyuki MATSUDA
Teiichiro MATSUZAKI
Hiroaki ONISHI
Haruhiko OUTA
Isao WATANABE

Special Postdoctoral Researchers

Hidekatsu NEMURA
Shinji OKADA
Takatoshi SUZUKI
Dai TOMONO

Special Contract Researchers

Masami IIO
Takahisa KOIKE

Contract Researchers

Pavel BAKULE
Takayuki KAWAMATA
Seiko KAWAMURA
Takao SUZUKI

Visiting Scientists

Tadashi ADACHI (Grad. Sch. Eng., Tohoku Univ.)
Yoshitami AJIRO (Grad. Sch. Sci., Kyoto Univ.)
Jun AKIMITSU (Coll. Sci. Eng., Aoyama Gakuin Univ.)
Jūichirou ARAI (Fac. Sci., Tokyo Univ. Sci.)
Shingo ARAKI (Grad. Sch. Sci., Osaka Univ.)
Kunio AWAGA (Grad. Sch. Sci., Nagoya Univ.)
George BEER (Univ. of Victoria, Canada)
HyoungChan BHANG (Seoul National Univ., Korea)
N. Ludmila BOGDANOVA (ITEP, Russia)
Prasad Tara DAS (SUNY at Albany, USA)
Masaya ENOMOTO (Grad. Sch. Arts and Sci., Univ of Tokyo)
Mark FAYFMAN (Kurchatov Inst., Russia)
Yutaka FUJII (Fac. Eng., Fukui Univ.)
Masaki FUJITA (IMR, Tohoku Univ.)
Hideto FUKAZAWA (Grad. Sch. Sci. & Tech., Chiba Univ.)
Takayuki GOTO (Fac. Sci. & Tech., Sophia Univ.)
Makoto HAGIWARA (Fac. Eng. Design, Kyoto Inst. Technol.)
Ryugo HAYANO (Grad. Sch. Sci., Univ. of Tokyo)
Wataru HIGEMOTO (JAEA)
Masahiro HIRANO (JST)
Kazuto HIRATA (NIMS)
Emiko HIYAMA (Fac. Sci., Nara Women's Univ.)
Susumu IKEDA (KEK)
Yutaka IKEDO (Toyota Central R&D Labs.)
Fumihiro ISHIKAWA (Grad. Sch. Sci. & Tech., Niigata Univ.)
Shigeru ISHIMOTO (KEK)
Tomoichi ISHIWATARI (SMI, Austria)
Ryosuke KADONO (KEK)
Mineo KATO (JAEA)
Naritoshi KAWAMURA (KEK)
Jungho KIM (Seoul National Univ., Korea)
Yasushi KINO (Fac. Sci., Tohoku Univ.)
Akihiro KODA (KEK)
Yoh KOHORI (Fac. Sci., Chiba Univ.)
Yoji KOIKE (Grad. Sch. Eng., Tohoku Univ.)
Yoshitaka KUNO (Grad. Sch. Sci., Osaka Univ.)
Chow LEE (UCF, USA)
Shunsuke MAKIMURA (KEK)
Goro MARUTA (Grad. Sch. Sci., Hokkaido Univ.)
Satoru MATSUISHI (FCRC, Tokyo Tech.)
Yasuhiro MIYAKE (KEK)
Hitoshi MIYASAKA (Grad. Sch. Sci., Tohoku Univ.)
Soichiro MIZUSAKI (Coll. Sci. & Eng., Aoyama Gakuin Univ.)
Kazuhiko MUKAI (Toyota Central R&D Labs.)
Kazutaka NAKAHARA (KEK)
Takashi NAKAMURA (Grad. Sch. Sci. & Eng., Tokyo Tech.)
Takayoshi NAKAMURA (RIES, Hokkaido Univ.)
Satoshi NAKAMURA (Grad. Sch. Sci., Tohoku Univ.)
Takehito NAKANO (Grad. Sch. Sci., Osaka Univ.)
Nobuhiko NISHIDA (Fac. Sci., Tokyo Tech.)
Kusuo NISHIYAMA (KEK)
Hiroshi NOZAKI (Toyota Central R&D Labs.)
Yasuo NOZUE (Grad. Sch. Sci., Osaka Univ.)

Masaaki OHBA (Grad. Sch. Eng., Kyoto Univ.)
Susumu OHYA (Fac. Sci., Niigata Univ.)
Akira OSAWA (Fac. Sci. & Tech., Sophia Univ.)
Vassili PEREVOZCHIKO (VNIEF, Russia)
Leonid PONOMAREV (Kurchatov Inst., Russia)
Francis PRATT (RAL, UK)
Shin-ichi SAKAMOTO (JAEA)
Ryoichi SEKI (California State Univ., Northridge, USA)
Kouichiro SHIMOMURA (KEK)
Vyacheslas STORCHAK (Kurchatov Inst., Russia)
Patrick STRASSER (KEK)
Hiroyuki SUGAI (JAEA)
Jun SUGIYAMA (Toyota Central R&D Labs.)
Haruhiko SUZUKI (Grad. Sch. Nat. Sic. & Tech., Kanazawa Univ.)
Hiroyuki SUZUKI (NIMS)
Kazuyuki TAKAI (Grad. Sch. Sci. & Eng., Tokyo Tech.)
Keiji TAKEDA (ISSP, Univ. of Tokyo)
Hiroyuki TAKEYA (NIMS)
Manobu TANAKA (KEK)
Akihiro TANIGUCHI (KURRI, Kyoto Univ.)
Takashi TANIGUCHI (Coll. Sci. & Eng., Aoyama Gakuin Univ.)
Eiko TORIKAI (Grad. Sch. Medicine & Eng. Sci., Univ. of Yamanashi)
Akihisa TOYODA (KEK)
Kazuo UEDA (ISSP, Univ. of Tokyo)
Yun XUE (Grad. Sch. Nat. Sic. & Tech., Kanazawa Univ.)
Kazuyoshi YAMADA (IMR, Tohoku Univ.)
Arkady YUKHINCHUK (VNIIEF, Russia)
Johann ZMESKAL (SMI, Austria)

Research Consultants
Yoshinori AKAISHI
Masayasu KAMIMURA
Atsuko ITO

Students

Junior Research Associates
Kenichi HACHITANI (Grad. Sch. Sci. & Tech., Chiba Univ.)
Masaharu SATO (Grad. Sch. Sci. & Eng., Tokyo Tech.)

Student Trainees
Truong Cong DUAN (Grad. Sch. Sci., Osaka Univ.)
Hiroyuki FUJIOKA (Grad. Sch. Sci., Univ. of Tokyo)
Yoshiyuki FUKUDA (Grad. Sch. Sci. & Eng., Tokyo Tech.)
Toshio HANAKI (Grad. Sch. Fac. Sci. & Tech., Tokyo Univ. Sci.)
Yuzo HIRAYAMA (Grad. Sch. Sci. & Eng., Tokyo Tech.)
Takashi ITO (Grad. Sch. Sci. & Eng., Tokyo Tech.)
Satoshi ITOH (Grad. Sch. Sci., Univ. of Tokyo)
Keishi KANADA (Grad. Sch. Sci. & Tech., Sophia Univ.)
Wakako KANEKO (Grad. Sch. Eng., Kyoto Univ.)
Hirokazu KAWASHIMA (Grad. Sch. Sci. & Eng., Aoyama Gakuin Univ.)
Noriyuki KIDA (Grad. Sch. Arts and Sci., Univ. of Tokyo)
Mijung KIM (Seoul National Univ., Korea)
Yoshihiro KUBOTA (Grad. Sch. Sci., Tohoku Univ.)
Sougo KUROIWA (Grad. Sch. Sci. & Eng., Aoyama Gakuin Univ.)
Jun MATSUMOTO (Grad. Sch. Sci., Osaka Univ.)
Hayato MOCHIZUKI (Grad. Sch. Sci. & Tech., Niigata Univ.)
Yoshifumi NAGASAKI (Grad. Sch. Fac. Sci., Kanazawa Univ.)
Keisuke OMORI (Grad. Sch. Eng., Tohoku Univ.)
ROGER PINK (SUNY at Albany, USA)
Ayumi SAITO (Grad. Sch. Sci., Tokyo Metro Univ.)

Takehiro SAITO (Grad. Sch. Sci. & Tech., Sophia Univ.)
Katsunori TAKAHARA (Inter. Grad. Sch. of Sci. & Eng., Tokyo Tech.)
Yoichi TANABE (Grad. Sch. Eng., Tohoku Univ.)
Hideyuki TATSUNO (Grad. Sch. Sci., Univ. of Tokyo)
Yoshitake TODA (Inter. Grad. Sch. of Sci. & Eng., Tokyo Tech.)
Yoko TOMITA (Grad. Sch. Sci. & Eng., Aoyama Gakuin Univ.)
Fumiko YAMADA (Grad. Sch. Sci. & Eng., Tokyo Tech.)
Heejoong YIM (Seoul National Univ., Korea)

Secretaries
Yoko FUJITA
Mitsuko SUGIURA
Yuka TAKANO

Theoretical Physics Laboratory

1. Abstract

The aim of this laboratory is to reveal the laws of nature ranging from elementary particles to the universe. More precisely, the following three issues are pursued with their mutual relations emphasized:(1) Understanding the microscopic fundamental law of nature. In particular, trying to give a consistent definition of superstring and derive all the fundamental laws from one principle. (2) Understanding many-body systems. Both of the following two aspects are considered. One is the universal laws such as thermodynamics and the universality of spin systems, and the other is specific properties of individual systems such as hadrons, condensed matter, and the universe. (3) Computational science. Besides numerical analyses as an important tool for the above mentioned (1) and (2), aspects of fundamental mathematics are also pursued.

2. Major Research Subjects

(1) Constructive Definition of String Theory as Fundamental law of Physics
(2) Fundamental aspects of Quantum Field Theory and its applications
(3) High precision inspection of experimental and observational data

3. Summary of Research Activity

The ability to understand nature at its most profound level is a basic human desire. Science is founded on accumulated and tremendous efforts driven by that aspiration. The objective of our laboratory is to participate in the endeavor to better understand nature by adding our contributions to theoretical physics. The present seems to be a particularly exciting time for this as many developments appear to be about to converge and allow formation of the ultimate theory of everything.

We organize our research activities into three segments: the pursuit of the microscopic fundamental laws of physics, the study of many-body systems, and the science and technology of computation. These three aspects have an inseparable interrelation and are investigated in an integrated manner throughout the research conducted within this laboratory.

(1) Understanding the fundamental law of nature through string theory.

1) Non-perturbative effect for non-critical string

The analysis of the nonperturbative effect in the c=0 noncritical string theory defined by the one-matrix model is extended to the case of two-matrix models which provide nonperturbative definitions of c¡1 noncritical string theories. Then, universality of nonperturbative effects including their coefficients in a generic c<1 noncritical string theory is achieved in the sense that they are independent of details of potentials of the two-matrix models.

2) Matrix models and curved space-time

Incorporating curved space time into matrix models is pursued. In particular, a method in which larger additional degrees of freedom is introduced to represent space-time symmetry, is proposed.

3) Domain Wall in string theory

We investigate a global structure of the moduli space of the BPS domain wall system. I particular, we are interested in the case where the dimensions of the moduli space is greater than those expected from the index theorem. We also study the T-duality between the vortices and domain walls from a string theoretical point of view. We explicitly construct a vortex solution in the Higgs phase of supersymmetric gauge theory and find an exact correspondence between the solution and D-brane configuration in the domain wall side.

4) Non BPS branes and supergravity

We investigate the correspondences between a class of classical solutions of Type II supergravity (the three-parameter solution) and D-branes in the superstring theory. In addition to the mass, the RR-charge, the solution also carries the so-called dilaton charge, whose physical meaning was unclear. We find that the appearance of the dilaton charge is a consequence of deformations of the boundary condition from that of the boundary state for BPS D-branes. We also show that such deformed boundary states are realized as tachyonic and/or massive excitations of the open strings on D-brane systems.

5) D-branes and instantons

We have investigated instantons of four-dimensional SUSY gauge theory from the view point of superstring theory. A general prescription to construct the instanton solutions is known as the ADHM (Atiyah-Drinfeld-Hitchin-Manin) construction. In terms of superstring theory, instanton is understood as a bound state of D3-branes and D (-1)-branes. We consider a system of D3-branes and anti-D3-branes to construct the bound state via a tachyon condensation. As a result, we found that the tachyon profile contains all information on the instanton and the ADHM construction can be understood as an outcome of the gauge equivalence of this system in the low

energy limit. We also applied the same method to eight-dimensional gauge theory and showed that some solitonic solution of the eight-dimensional theory can be constructed by this method.

6) Application of string theory to cosmology

Cosmological scenarios alternative to inflation motivated by string theories are known. In cyclic scenario, or ekpyrotic scenario, the universe is considered as branes sitting in higher dimensional space time. The universe is assumed to start out from a static Minkowskian space-time and experience the big-bang as the collision of pair of branes (bounce). From the observational point of view, it is of importance to study the time evolution of cosmological fluctuation through the time of big bang. We studied the problem from the point of view of local causality through the bounce. Assuming the local causality condition, we derived the most general matching condition for the fluctuation between before and after the bounce. Especially, we found it is impossible to generate scale invariant spectrum without introducing non-local causality throughout the bounce. This work made clear the physical problem to obtain the scale invariant spectrum in the bouncing cosmology. We have also studied a toy model inspired by a low-energy effective action of non-commutative field theory and estimated the range of parameters to obtain scale invariant spectrum.

Another subject pursued was the possibility of obtaining inflation due to the modification of the dispersion relation. When non-equilibrium dynamics is taken into account, we observed that the inflation can be easily realized when the energy is a decreasing function of the momentum in high-energy regime. This result provides alternative way of realizing inflation in the framework of unified theory.

(2) Quantum field theory and physics of many body systems

1) Lattice formulation of supersymmetric gauge theory

We proposed a lattice formulation of low dimensional supersymmetric gauge theories, aiming at practical implementation for numerical simulations.

2) Lattice formulation of fermions coupled to gravity

We formulated lattice Dirac operator of the overlap-type that describes the propagation of a Dirac fermion in a gravitational field. We also analyzed global gauge anomalies associated with Majorana fermions in 8k and 8k+1 dimensions.

3) Mathematical aspects of 2-dimensional gauge theories and string.

We investigate a non-perturbative correction to the N=2 supersymmetric Yang-Mills theory from the discrete matrix model point of view. We utilize the D-brane picture in superstring theory and localization theorem in order to derive the discrete matrix model from 2-dimensional Yang-Mills theory on a compact 2-cycles in the ALE space. We also find the relationship to the Dijkgraaf-Vafa theory in the continuum limit.

4) Logarithmic Confromal Field Theory

The following topics are investigated: Free field representation for LCFT with boundary; The relation between Minimal String theory and LCFT; The relation between statistical models and LCFT.

5) Quantum field theory over the deformed commutation relation

A quantum theory of free scalar field based on the deformed Heisenberg algebra which is the correction of stringy physics is constructed.

6) Chern Simons Yang Mills Model

We have studied the Chern Simons Yang Mills Model. Non-commutative gauge theories on fuzzy spheres were obtained in such models. Fuzzy spheres look like dbrane configuration. k coincident fuzzy spheres generates the U(k) gauge group. In this direction, we are continuing effort to address some of the related issues.

(3) High precision calculation of field theory and computational science

1) High precision calculation of QED

We have announced the final result of our calculation of the electron anomalous magnetic moment. It contains up to the eighth-order of the perturbation theory of QED. The very reliable result was obtained by using high precision calculation on RIKEN's supercomputer system (RSCC). We also succeeded in automating the calculation of the tenth-order of the perturbation theory, particularly in constructing the ultra-violet subtraction terms. This is an important step to accelerate our calculation of the entire tenth-order contribution.

The dominant contribution from the tenth order to the muon anomalous magnetic moment was also announced by us. In contrast to the electron, some specific Feynman diagrams give rise to the large contributions to the muon anomaly. We explicitly evaluated about 2000 Feynman diagrams which are possible to give the leading and next-to-leading contributions.

2) Improved perturbation method and its applications

We apply improved perturbation method which is one of the variational schemes to Ising model in two-dimensions. It enables us to evaluate free energy and magnetization at strong coupling regions from weak coupling expansion even in the presence of the phase transition.

We determine approximated transition point in this scheme. In the presence of external magnetic field we can

see not only stable physical states but metastable one. This reserach motivated by availability of this method to IIB matrix model which is expected to show a phase transition from 10-dimensional universe to 4-dimensional universe.

Head
Hikaru KAWAI

Members
Hiroshi SUZUKI
Tsukasa TADA

Postdoctoral Researchers
Tsuguhiko ASAKAWA
Issaku KANAMORI
Tsunehide KUROKI
So MATSUURA
Kin-ya ODA
Kazutoshi OHTA
Yuuichirou SHIBUSA
Naoto YOKOI

Contract Researchers
Tatsumi AOYAMA
Hidenori FUKAYA
Ko FURUTA
Makiko MATSUKAWA

Visiting Scientists
Hajime AOKI (Fac. of Sci. and Eng., Saga Univ.,)
Jiro ARAFUNE (National Inst. for Academic Degrees and Univ. Evaluation)
Zyun F. EZAWA (Grad. Sch. of Sci., Tohoku Univ.)
Kazuo FUJIKAWA (College of Sci. and Tech., Nihon Univ.,)
Amihay HANANY (Massachusetts Inst. of Tech., USA)
Masashi HAYAKAWA (Grad. Sch. of Sci., Nagoya Univ.,)
Takeo INAMI (Fac. of Sci. and Eng., Chuo Univ.,)
Nobuyuki ISHIBASI (Grad. Sch. of Pure and Applied Sci., Univ. of Tsukuba,)
Satoshi ISO (High Energy Accelerator Res. Organization)
Hiroshi ITOYAMA (Grad. Sch. of Sci., Osaka City Univ.,)
Toichiro KINOSHITA (Cornell Univ., USA)
Yoshihisa KITAZAWA (High Energy Accelerator Res. Organization)
Ivan KOSTOV (Service de Physique Theoreique, CNRS, FRANCE)
Jnanadeva MAHARANA (Inst. of Phys., INDIA)
Jun NISHIMURA (High Energy Accelerator Res. Organization)
Fumihiko SUGINO (Okayama Inst. for Quantum Phys.)
Asato TSUCHIYA (Grad. Sch. of Sci., Osaka Univ.,)
Kensuke YOSHIDA (Univ. of Rome - La Sapienza, ITALY)
Alexei ZAMOLODCHIKOV (Universit'e Montpellier II, FRANCE)

Research Consultants
Keiji IGI
Hironari MIYAZAWA
Yoshio YAMAGUCHI

Junior Research Associate
Tomohisa TAKIMI (Kyoto Univ.)

Secretariy
Yumi KURAMITSU

Radiiation Biology Team

1. Abstract

Radiation biology team studies various biological effects of fast heavy ions. It also developes new technique to breed plants by heavy-ion irradiations. Fast heavy ions can produce localized dense ionizations in matters along their tracks, in contrast to photons (X rays and gamma rays) which produce randomly distributed isolated ionizations. These localized and dense ionization can cause double-strand breaks of DNA in cells which are not easily repaired and result in mutation more easily than single-strand breaks. A unique feature of our experimental facility at the RIKEN Ring Cyclotron (RRC) is that we can irradiate living bodies in atmosphere or in bottles since the delivered heavy-ion beams have energies high enough to penetrate deep in matter. This team utilize a dedicated beam line (E5B) of the RRC to irradiate cultivated cells, plants and animals with beams from carbon to iron. Its research subjects cover physiological study of DNA repair, genome analyses of mutation, and development of mutation breeding of plants by heavy-ion irradiation. Some new cultivars have already been brought to the market. It also studies the physical processes of radiation effects in solutions.

2. Major Research Subjects

(1) Study on the biological effects by heavy-ion irradiation
(2) Studies on ion-beam breeding and genome analysis
(3) New medical application of heavy-ion beams
(4) Formation of nano-particles in solutions by heavy-ion irradiations

3. Summary of Research Activity

We study biological effects of fast heavy ions from the RIKEN Ring Cyclotron using 135 MeV/N C, N, Ne ions, 95 MeV/N Ar ions and 90 MeV/N Fe ions. We also develop breeding technology of plants. Main subjects are:

(1) Study and application of heavy-ion induced plant mutation

In contrast to X rays and gamma rays, fast heavy ions are found to be useful for plant breeding since they only cause localized damage on DNA and can induce mutations more effectively with lower dosage. Our team utilizes beams of fast heavy ions from the RIKEN Ring Cyclotron to develop heavy-ion breeding techniques. Genome analyses are performed to reveal the relation between genotype and phenotype.

(2) Study of heavy ion-induced damage of DNA and its repair processes

We study the double-strand break of DNA induced by heavy-ion irradiation and its repair processes. DNA double strand break (DSB) is characteristic to heavy-ion irradiation and considered to be the characteristic lesion responsible for its biological effects. Cells have two pathways to repair DSB, NHEJ and HR, and it is unknown how the two pathways are involved in repairing the damage caused by heavy-ion irradiation. To elucidate it, we irradiate higher vertebrate cells lacking DNA repair proteins with C, Ar, or Fe ions and analyze them with colony formation assay and molecular biology methods.

Team Leader
Tadashi KAMBARA

Members
Tomoko ABE
Masako IZUMI
Yusuke KAZAMA
Hiroyuki SAITO
Teruyo TSUKADA

Technical Staff I
Yoriko HAYASHI

Part-time Staff I
Hideo TOKAIRIN

Part-time Staff II
Sumie OHBU

Visiting Scientists

Ryutaro AIDA (Natl. Inst. Floricult. Sci.)
Mari AMINO (Tokai Univ. Hospital)
Chang-Hyu BAE (Sunchon Natl. Univ., Korea)
Yasuhiro CHIMI (JAEA)
Hiroyuki DAIMON (Osaka Pref. Univ.)
Makoto FUJIWARA (Grad. Sch., Col. Arts Sci., Univ. of Tokyo)
Koji FURUKAWA (Mukoyama Orchids Co., Ltd.)
Yoshiya FURUSAWA (Natl. Inst. Radiol. Sci.)
Toshinari GODO (Botanic Gardens Toyama)
Misako HAMATANI (Hiroshima City Agric. Forest. Promot. Cen.)
Yasuhide HARA (Kanagawa Inst. Agric. Sci.)
Masanori HATASHITA (Wakasa Wan Energy Res. Cen.)
Atsushi HIGASHITANI (Grad. Sch. Life Sci., Tohoku Univ.)
Ryoichi HIRAYAMA (Natl. Inst. Radiol. Sci.)
Akiko HOKURA (Fac. Sci., Tokyo Univ. of Sci.)
Ichiro HONDA (Natl. Agric. Res. Cen.)
Mitsugu HORITA (Hokuren Agri. Res. Inst.)
Yuji ITO (Natl. Agric. Res. Cen., Hokkaido Region)
Akihiro IWASE (Grad. Sch. Engin., Osaka Pref. Univ.)
Hiroshi KAGAMI (Shizuoka Citrus Exp. Station)
Kensuke KAGEYAMA (Fac. Engin., Saitama Univ.)
Takeshi KANAYA (Suntory Flowers, Ltd.)
Si-Yong KANG (Dep. Rad. Plant Breed. Genet., KAERI, Korea)
Tomojirou KOIDE (Riken Vitamin Co., Ltd.)
Tsutomu KUBOYAMA (Ibaraki Univ.)
Norihiko MISHIMA (Fukuda Denshi Co., Ltd.)
Yutaka MIYAZAWA (Grad. Sch. Life Sci., Tohoku Univ.)
Kazumitsu MIYOSHI (Fac. Bioresour. Sci., Akita Pref. Univ.)
Toshikazu MORISHITA (Inst. Rad. Breeding, Natl. Inst. Agric. Res.)
Koji MURAI (Fukui Pref. Univ.)
Daisuke NAKADA (Ela Medical Japan Co. Ltd.)
Ishikawa NORITO (JAEA)
Mio OHNUMA (Inst. Mol. Cell. Biosci., Univ. Tokyo)
Norihiro OHTSUBO (Natl. Inst. Floricult. Sci.)
Fumihisa ONO (Grad. Sch. Natural Sci. & Tech., Okayama Univ.)
Tomo OOMIYA (Hokkaido Ornamental Plants Veg. Res. Cen.)
Kenji OSAWA (Nagano Agric. Res. Cen.)
Kouichi SAKAMOTO (YUKIGUNI AGURI Co.,Ltd.)
Tadashi SATO (Grad. Sch. Life Sci., Tohoku Univ.)
Hiroaki SERIZAWA (Nagano Veg. Ornamental Crops Exp. Station)
Takiko SHIMADA (Res. Inst. Agric. Resour., Ishikawa Agric. Coll.)
Fumio SUGAWARA (Tokyo Univ. of Sci.)
Keita SUGIYAMA (Nat. Inst. Veg. Tea Sci.)
Masao SUGIYAMA (Hokko Chem. Ind. Co., Ltd.)
Kazunori SUZUKI (Plant Biotech. Inst. Ibaraki Agric. Cen.)
Kenichi SUZUKI (Suntory Flowers, Ltd.)
Masao SUZUKI (Natl. Inst. Radiol. Sci.)
Hinako TAKEHISA (Grad. Sch. Life Sci., Tohoku Univ.)
Teruhiko TERAKAWA (Hokko Chem. Ind. Co., Ltd.)
Ken TOKUHARA (Dogashima Orchid Cen.)
Masanori TOMITA (CRIEPI)
Hisashi TSUJIMOTO (Fac. Agri., Tottori Univ.)
Kozo TSUKADA (Nippon Veterinary and Life Sci. Univ.)
Masao WATANABE (Fac. Agri., Tohoku Univ.)
Takuji YOSHIDA (Takii Seed Co., Ltd.)
Koichiro YOSHIOKA (Tokai Univ. Hospital)

Company-Sponsored Research Trainee

Ayako TABAYASHI (Mitsui Norin Co., Ltd.)

Research Fellows

Hideki ASAUMI (Ehime Agricultural Experiment Station)
Eikou OOYABU (Saga Pref. Agr. Res. Cen.)
Takenori SAITO (Shizuoka Tea Exp. Station)
Minoru SAITOH (Fukui Agr. Exp. Sta.)
Tsukasa SHIRAO (Kagoshima Biotechnology Inst.)
Kei-ichiro UENO (Kagoshima Biotechnology Inst.)

Students

Junior Research Associate
Hiroyuki ICHIDA (Grad. Sch. Sci. Tech., Chiba Univ.)

Student trainees
Naoki FUKUDA (Fac. Sci., Tokyo Univ. of Sci.)
Takayuki INOUE (Dept. Phys. Rikkyo Univ.)
Teruhiko KASHIWABARA (Fac. Sci., Tokyo Univ. of Sci.)
Nobuhiro MAEDA (Grad. Sch. Eng., Osaka Pref. Univ.)
Yoshitaka MATSUMOTO (Grad. Sch. Medicine & Sch., Chiba Univ.)
Kiyoshi NISHIHARA (Grad. Sch. Frontier Sci., Univ. of Tokyo)
Tatsuya ONO (Nagahama Inst. Bio-Sci. and Technol.)
Kazuhiro SASAKI (Grad. Sch. Life Sci., Tohoku Univ.)
Yuka TANAKA (Nagahama Inst. Bio-Sci. and Technol.)
Takashi YOKOYAMA (Dept. Phys. Rikkyo Univ.)

RI Applications Team

1. Abstract

RI Applications Team performs following researches at the heavy ion accelerators of RIBF: (1) With high-energy heavy ions from the RIKEN Ring Cyclotron, we produce multi-tracers which are mixtures of various radioactive nuclides, and use them in research fields like chemistry, biology, medicine, pharmaceutical and environmental sciences. (2) We study chemical properties of super-heavy elements (SHE's) with atomic numbers above 104, using a gas-jet transport system coupled to Gas-filled Recoil Ion Separator (GARIS) at RILAC. (3) We developes a new technology of trace-element analyses.

2. Major Research Subjects

(1) Developments and Application Studies on the Multitracer Technology
(2) Chemistry of super heavy elements
(3) The development of trace element analysis, using the accelerator techniques, and its application to geo and environmental sciences

3. Summary of Research Activity

RI applications team utilizes RIBF heavy-ion accelerators for following research subjects:

(1) Production and application of multi-tracers

With high-energy heavy ions from the RIKEN Ring Cyclotron, we produces multi-tracers which are mixtures of various radioactive nuclides, and use them in research fields like chemistry, biology, medicine, pharmaceutical, and environmental sciences.

(2) Chemistry of super-heavy elements

The electronic structure of superheavy elements (SHE's) with atomic numbers above 104 is strongly affected by the relativistic effects due to large nuclear charge. It is interesting to compare their chemical properties with those of the lighter elements in the same group on the periodic table. However, this frontier of chemistry is still unexplored since SHE's can be produced on one-atom-at-a-time scale at heavy-ion accelerators. We utilize Gas-filled Recoil Ion Separator (GARIS) at the RILAC to produce SHE atoms, and transport them by gas-jet system with high efficiency to a chemistry laboratory.

(3) Trace element analyses with accelerator technologies

In order to achieve ultra-high sensitivities down to 10^{-15}–10^{-17} in multiple trace-element analysis, we develop technique of accelerator mass spectroscopy (AMS) at the RILAC, with a combination of an ECR ion source and a linear accelerator. We also develop a compact mass spectrometer with a stand-alone ECR ion source. There techniques are applied in fields of cosmochemistry, geochemistry, biochemistry, pharmaceutical and environmental sciences, archeology, analysis of bio-trace element and materials science.

Team Leader
Tadashi KAMBARA

Members
Shuichi ENOMOTO
Hiromitsu HABA
Kazuya TAKAHASHI

Postdoctoral Researcher
Shinji SHIGYO

Research Associate
Yousuke KANAYAMA

Part-time Staff
Takashi NYU

Temporary Staff
Atsushi ISHIZAWA

Senior Visiting Scientists
Shuichi KIMURA (Showa Women's Univ.)

Visiting Scientists

Kazuhiko AKIYAMA (Tokyo Metropolitan Univ.)
Ryohei AMANO (Fac. Med., Kanazawa Univ.)
Wenjun DING (Colorado State Univ., USA)
Kazutoyo ENDO (Showa Pharm. Univ.)
Kaori ENOMOTO (Univ. Human Arts & Sci.)
Hiroshi HIDAKA (Fac. Sci., Hiroshima Univ.)
Seiichiro HIMENO (Fac. Pharm. Sci., Tokushima Bunri Univ.)
Takako IKEDA (Showa Women's Univ.)
Hiroko INAGE (Internat. Life Sci. Inst.)
Nobuyoshi ISHII (Natl. Inst. Radiol. Sci.)
Toshiaki ISHII (Natl. Inst. Radiol. Sci.)
Yuko ISHIKAWA (Kagawa Nutrition Univ.)
Shigenao KAWAI (Fac. Agri., Iwate Univ.)
Masuo KONDOH (Showa Pharm. Univ.)
Kenichiro MATSUMOTO (Natl. Inst. Health, USA)
Yoshitaka MINAI (Cen. Art. Sci., Musashi Univ.)
Takeshi MINAMI (Sch. Sci. Eng., Kinki Univ.)
Tomohiro NABEKURA (Fac. Pharm. Sci., Niigata Univ. Pharm. Appl. Life Sci.)
Yuichiro NAGAME (JAEA, Tokai)
Yukiko NAKANISHI (Grad. Sch. Hum. Life Sci., Showa Women's Univ.)
Van Chuyen NGUYEN (Jpn. Women's Univ.)
Yasumitsu OGURA (Grad. Sch. Pharm. Sci., Chiba Univ.)
Jun SAITO (Iwatsu Test Instrum. Corp.)
Tomofumi SAKURAGI (Natl. Inst. Radiol. Sci.)
Hiromu SAKURAI (Kyoto Pharm. Univ.)
Hiroshi SHIMIZU (Fac. Sci., Hiroshima Univ.)
Atsushi SHINOHARA (Grad. Sch. Sci., Osaka Univ.)
Hiroyuki SUZUKI (RI Res. Cen., Chiba Univ.)
Toshihiro SUZUKI (Meiji Pharm. Univ.)
Mikiko SUZUKI (Showa Women's Univ.)
Kazuo SUZUKI (Grad. Sch. Pharm. Sci., Chiba Univ.)
Keiko TAGAMI (Natl. Inst. Radiol. Sci.)
Masaaki TAKAHASHI (Grad. Sci. Agric. Biol. Sci., Osaka Pref. Univ.)
Yoshio TAKAHASHI (Grad. Sch. Sci., Hiroshima Univ.)
Miho TAKAHASHI (Tokyo Univ. Marine Sci. and Tech.)
Atsushi TAKEDA (Fac. Pharm. Sci., Univ. Shizuoka)
Haruna TAMANO (Fac. Pharm. Sci., Univ. Shizuoka)
Shinzo TANABE (Meiji Pharm. Univ.)
Tadayasu TOGAWA (Meiji Pharm. Univ.)
Takehiro TOMITANI (Chiba Univ.)
Atsushi TOYOSHIMA (JAEA)
Shigeo UCHIDA (Natl. Inst. Radiol. Sci.)
Kohshin WASHIYAMA (Fac. Med., Kanazawa Univ.)
Tokuko WATANABE (Aoyama Gakuin Women's Junior College)
Mineo YAMASAKI (Nara Med. Univ.)
Makoto YANAGA (Fac. Sci., Shizuoka Univ.)
Hiroyuki YASUI (Kyoto Pharm. Uni.)
Akihiko YOKOYAMA (Fac. Sci., Kanazawa Univ.)
Shigekazu YONEDA (Natl. Sci. Museu.)
Shozo YOSHIDA (Nara Med. Univ.)
Takashi YOSHIMURA (Grad. Sch. Sci., Osaka Univ.)

Visiting Technician

Ichiro SAKAMOTO

Research Consultants

Yasuyuki GONO
Kuniko MAEDA

Students

Part-time Staffs

Midori SASAKI (Tokyo Univ. Fish.)
Tatsuya URABE (Tokyo Univ. Fish.)

Student Trainees

Yusuke ADACHI (Kyoto Pharm. Univ.)
Tomoko ANDO (Showa Women's Univ.)
Ai HOSODA (Internat. Christian Univ.)
Terumi KATORI (Showa Women's Univ.)
Takehiko KURIBAYASHI (Grad. Sch. Sci., Osaka Univ.)
Yohei MITSUBORI (Fac. Sci. Tech., Tokyo Univ. of Sci.)
Kazuhiro OOE (Grad. Sch. Sci., Osaka Univ.)
Mizue OZAKI (Showa Women's Univ.)
Nobuko SAJI (Showa Women's Univ.)
Mayumi SHIBANUMA (Showa Women's Univ.)
Tomomasa TAKABE (Grad. Sch. Sci., Osaka Univ.)
Masaki TAKAHASHI (Meiji Pharm. Univ.)
Yuki TASHIRO (Grad. Sch. Sci., Osaka Univ.)

RIKEN-BNL Research Center
Experimental Group

1. Abstract

The RIKEN BNL Research Center (RBRC), Experiment Group studies the internal spin structure of the proton, using the first polarized proton collider at Brookhaven, RHIC. The group leads and participates in three general areas: developing the world's highest energy polarized proton beams, developing probes of the proton's spin content, and seeking a global understanding of all proton spin data. For the proton beam, the group has developed a new method to measuring the proton beam polarization at high energy which is non-destructive to the beam and robust. To study the proton structure, the group has identified very sensitive probes and is developing special apparatus and methods to select the interesting data as the collisions occur. Towards a global understanding of the internal structure of the proton, the group combines information from RHIC with earlier studies using electron and muon beams. In a new collaboration with the BELLE experiment at High Energy Accelerator Research Organization (KEK), we recently discovered that quark fragments can determine the spin direction of the mother quark.

2. Major Research Subjects

(1) Experimental Studies of the Spin Structure of the Nucleon
(2) Study of Quark-Gluon Plasma at RHIC
(3) Global QCD Analysis of the Spin Structure of the Nucleon

3. Summary of Research Activity

How is the spin of proton formed with 3 quarks and gluons? This is a very fundamental question in QCD, Quantum Chromo dynamics. The RHIC Spin Project has been established as an international collaboration between RIKEN and Brookhaven National Laboratory (BNL), to solve this problem by colliding two polarized protons for the first time in history. This also extended the physics capability of RHIC, Relativistic Heavy Ion Collider in BNL. At RHIC, Quark Gluon Plasma (QGP) is to be created by colliding two gold nuclei, through which we can study the state of the early Universe just after the Big Bang. In December 2001, polarized protons were successfully accelerated to 100 GeV, and collisions of transversely polarized protons were observed. Since then the spin experiment is on going.

The RIKEN-BNL Research Center was established in 1997 to support the RIKEN activities at RHIC in BNL, and also to promote theoretical studies related to RHIC, i.e. theories of strong interaction. The center's first director was T.D. Lee (Columbia University), and in October 2003, the former director of BNL, N.P. Samios, succeeded to the post of director. The center consists of a theory group lead by L. Mclerran (BNL) and an experimental group lead by H. En'yo, Chief scientist of RIKEN in Wako, who also is an associate director of RBRC.

(1) Experimental study of spin structure of proton using RHIC polarized proton collider

Although the RHIC operation in 2006 was threatened to be cancelled by the DOE budget problem in the beginning, we could start a polarized-proton collision run partially supported by a private donation. The PHENIX experiment collected data from March until June. The RHIC accelerator achieved $2 \times 10^{31}/\mathrm{cm}^2/\mathrm{s}$ of the average luminosity and 60% of the average beam polarization at the center-of-mass energy of 200 GeV. This polarized-proton was the second long run following the one in 2005. The present biggest goal is to elucidate a contribution of the gluon spin in the proton spin. From the 2005 data, we found the gluon polarization in the proton is smaller than we have expected. By accumulating data in this year and after, we will be able to obtain necessary statistics for determination of the gluon-spin contribution more precisely.

We are also investigating a contribution of the orbital-angular momentum of quarks and gluons in the proton which is especially important when the contribution of the gluon spin is small. In 2006, we collected the data with transversely-polarized proton collisions at 200 GeV to investigate the left-right asymmetry of the two-jet angular correlation. Theoretically this asymmetry has sensitivity for the orbital-angular momentum of quarks and gluons in the proton.

The 200 GeV experiment was performed for three months, and the PHENIX experiment recorded the data corresponding to 10 inverse picobarn of the integrated luminosity. After this, center-of-mass energy 62.4 GeV operation was performed with both transversely and longitudinally polarized proton collisions. Even though it was only a two-week operation, low-energy collisions can give us high-statistics data in the kinematic region where quarks or gluons have a large fraction of the proton momentum. At the end of the run, there was an accelerator development for collisions at the center-of-mass energy of 500 GeV in the future. Polarized proton beam was

accelerated up to the maximum energy of 250 GeV successfully without significant depolarization.

All the physics data in the 2006 run were transferred to RIKEN CC-J in almost real-time via the network between US and Japan. The physics analysis of the data is making steady progress. In the SPIN2006 international conference in October at Kyoto, various latest results were released by the PHENIX collaboration. From the 2006 data, preliminary results of neutral-pion double-helicity asymmetry at 62.4 GeV and 200 GeV were presented and discussed for the determination of the gluon-spin contribution to the proton spin. A preliminary result of cross section measurement of direct-photon production from the 2005 data was also presented. This is an important achievement for the double-helicity asymmetry measurement of direct-photon production in the near future, and for discussion of the capability of the perturbative QCD to apply for the RHIC data.

(2) Experimental study of Quark-Gluon Plasma using RHIC heavy-ion collider

The goal of high energy heavy ion physics at RHIC is study of QCD in extreme conditions i.e. at very high temperature and at very high energy density. Experimental results from RHIC have established that dense partonic matter is formed in Au+Au collisions at RHIC. The focus of the research program is now moving towards measurement of the properties of the matter. The main results of PHENIX that are published are as follows.

1) Measurement of single electrons from heavy flavor decays in p+p and Au+Au collisions. In p+p collisions, a FONLL pQCD calculation reproduces the data within theoretical uncertainties, indicating that heavy flavor production at RHIC energy is well understood within pQCD framework. In Au+Au collisions, strong suppression of electron spectrum at high transverse momentum (pT) as well as strong elliptic flow of single electrons is observed, indicating that heavy quarks strongly coupled with the dense matter produced in RHIC collisions. Comparison with the data and theoretical calculations suggests that the viscosity to entropy density ratio h/s is very small, close to the conjectured quantum lower bound.

2) Measurement of J/PSI in p+p and Au+Au collisions. The new data in p+p collisions has more than 10 times of statistics of previously published data. The first measurement in Au+Au shows strong suppression of J/PSI production in Au+Au relative to p+p. The magnitude of the suppression is similar to that was observed in Pb+Pb collisions at CERN SPS. The suppression is stronger in the forward rapidity than in central rapidity. These results are not explained by models invoking J/PSI destruction based on local energy density.

3) Modification of jet correlations. Azimuthal angle correlation of two high transverse momentum particles in p+p and peripheral Au+Au collisions exhibits clear back-to-back jet structure. The di-jet correlation is modified in central Au+Au collisions, suggesting that the parton fragmentation is strongly influenced by the dense matter. A systematic measurement of the jet correlation in Au+Au, Cu+Cu, and d+Au collisions are made.

(3) PHENIX detector upgrade

A silicon vertex tracker (VTX) is the first of major upgrade detectors for PHENIX. The detector will be jointly constructed with the US DOE. The VTX consisted of two inner layers of pixel detectors and two outer layers of strip detectors. The main points of progress in 2006 are as follows: 1) The US side of the project is included in FY07 president's budget. After a review by the US DOE, the US side of the project received approval. 2) First round prototypes of all components of the pixel detector have been complete. 3) A cosmic ray test of pixel system prototypes was performed. Clear tracks of cosmic rays are observed by three layers of pixel detectors. 4) Extensive radiation damage tests of the strip sensors were performed. Prototype sensors were placed in PHENIX IR to measure the radiation damage in the actual environment. 5) Mechanical and thermal engineering and design work of the VTX system has started.

We are participating another upgrade projects which include the muon arm upgrade, the construction of the reaction plane counter and the development of the nose cone calorimeter. Especially Perdekamp has gotten the NSF fund for the muon, and started prototype fabrications of resistive plate chambers and other necessary detectors.

Theory Group

1. Abstract

The RIKEN BNL Research Center was established in April 1997 at Brookhaven National Laboratory in New York, USA. The Center is dedicated to study of strong interactions, including hard QCD/spin physics, lattice QCD and RHIC physics through nurturing of a new generation of young physicist. The theory group consists of three sub groups: numerical lattice QCD, perturbative QCD and phenomenological QCD. The numerical lattice QCD group built a 600 GFlops QCDSP parallel supercomputer dedicated for the first-principle non-perturbative calculations of QCD. It pioneered the use of the domain-wall fermion method in QCD and we reported an important calculation of neutral Kaon CP-violations. As a new generation machine, QCDOC with 10 Tflops of computing power is completed in JFY2004. The perturbative QCD group has developed various new methods required for studying hadron structures, especially in spin physics research. The phenomenological QCD group has pioneered the researches of color superconductivity, isospin density, and small-x phenomena in extreme hadronic matters.

2. Major Research Subjects

(1) Perturbative QCD
(2) Lattice QCD numerical research
(3) Phenomenological QCD

3. Summary of Research Activity

The RIKEN-BNL Research Center was established in 1997 to support the RIKEN activities at RHIC in BNL, and also to promote theoretical studies related to RHIC, i.e. theories of strong interaction. The center's first director was T.D. Lee (Columbia University), and in October 2003, the former director of BNL, N.P. Samios, succeeded to the post of director. The center consists of a theory group lead by L. Mclerran (BNL) and an experimental group lead by H. En'yo, Chief scientist of RIKEN in Wako, who also is an associate director of RBRC.

Research in the RBRC theory group focuses on a wide variety of phenomena caused by the strong interaction, one of the four fundamental interactions in nature. The strong interaction is described theoretically by Quantum Chromodynamics (QCD), and the research projects in the RBRC theory group aim to elucidate various phenomena brought about by the strong interaction from the principles of QCD. Major subjects of our research include studies (a) based on lattice QCD, (b) on spin physics based on perturbative QCD, and (c) on QCD in extreme conditions such as high temperature, high density or high energy. RBRC offers RHIC Physics Fellowships, allowing joint appointments with universities. These Fellowships enable a talented researcher to maintain a tenure track position at his/her university as well as a Fellow position at RBRC for a certain period of time. This system was established in order to increase the research potential of RBRC and to disseminate its research activities and results. At present, RBRC has cooperative agreements with BNL, Columbia University, Massachusetts Institute of Technology, the State University of New York at Stony Brook, Texas A&M University, Purdue University, Iowa State University, Kanazawa University, and University of Tsukuba.

(1) Lattice QCD

QCDOC (QCD on chip), a second-generation lattice-QCD computer, was developed in the collaboration amongst this group, Columbia University and IBM. Three units of such a machine with 10 TFlops computing power are in operation since 2005; two in BNL (RBRC and DOE) and one in Edinburgh (UK-QCD), and formed a world-wide strong collaboration for the lattice QCD studies. Such computing power enables us to perform precise calculations with 3 quark flavors with proper handling on the chiral symmetry breaking. Several projects are on going; QCD thermodynamics in finite temperature/density systems as is produced in RHIC heavy-ion collisions, calculations of the nucleon axial charge and form factors which relates to the proton spin problem, and determination of meson's properties, mass, life, mixing parameters and form factors.

(2) Perturbative QCD and spin physics

The first few years running of RHIC spin experiment have motivated much theoretical developments in 2006. For example, in order to interpret the double spin asymmetry measurements for various processes at RHIC, the global analyses from several groups have been made last year, and they all found the large positive gluon polarization is disfavored from the RHIC results. Meanwhile, a remarkable progress has also been made in understanding the mechanisms for the nontrivial single transverse spin asymmetries (SSAs) observed by RHIC and other experiments. It was discovered that the two seeming quite different mechanisms for the SSAs are unified and describe the same physics in the overlap regions they both apply. The phenomenological application also

showed a successful description of the SSA data from fixed target experiments to RHIC collider experiments, and the detailed comparison between the theory and experiment have also raised a challenge for further developments.
(3) QCD under extreme conditions

To establish a microscopic picture of relativistic heavy ion collisions, QCD-based theoretical approaches are in progress. Especially the idea of "color glass condensation (CGC)" can be a key to understand the initial condition of heavy ion collision. We discussed a possible relation between CGC and the elliptic flow of particles which was discovered at RHIC. Other phenomenological approaches are in progress to understand the characteristics of strongly interacting quark gluon plasma (sQGP).

RIKEN BNL Research Center
Nicholas P. SAMIOS (Director)
Hideto EN'YO (Associate Director)

Experimental

Group Leader
Hideto EN'YO

Deputy Group Leader
Gerry M. BUNCE

Members
Yuji GOTO
Takashi ICHIHARA
Atsushi TAKETANI
Yasushi WATANABE
Yasuyuki AKIBA
Itaru NAKAGAWA
Abhay DESHPANDE[*2]
Douglas Edward FIELDS[*2]
Matthias GROSS PERDEKAMP[*2]
David KAWALL[*2]
Nobuyuki KAMIHARA[*4]
Kensuke OKADA[*2]
Wei XIE[*2]
Patricia LIEBING[*3]

Visiting Members
Naohito SAITO (KEK)
Zheng LEE (BNL)
Ralf-Christian SEIDL (DESY)
Kiyoshi TANIDA (Kyoto Univ.)
Akio OGAWA (BNL)

Theory

Group Leader
Larry McLERRAN

Deputy Group Leader
Anthony J. BALTZ

Members
Christopher DAWSON[*1]
Yasumichi AOKI[*2]
Thomas BLUM[*1]
Takeshi YAMAZAKI[*3]
Denes MOLNAR[*1]
Kirill TUCHIN[*1]
Urs WIEDEMANN[*1]

Fries RAINER[*1]
Tomomi ISHIKAWA[*3]
Feng YUAN[*3]
Agnes MOCSY[*3]
Marquet CYRILLE[*3]
Lichtl ADAM[*3]
Takumi DOI[*4]
Yoshitaka HATTA[*4]
Kenji FUKUSHIMA[*4]
Masakiyo KITAZAWA[*4]
Yoshimasa HIDAKA[*4]
Syoichi SASAKI[*1]
Peter PETRECZKY[*1]
Taku IZUBUCHI[*2]
Shinya AOKI[*2]

Visiting Members

Miklos GYULASSY (Columbia Univ., USA)
Robert L. JAFFE (Massachusetts Inst. Technol., USA)
Robert MAWHINNEY (Columbia Univ., USA)
Edward SHURYAK (State Univ. New York, Stony Brook, USA)
Shigemi OHTA (KEK)
Konstantinos ORGINOS (Massachusetts Instit. Technol., USA)
Kei IIDA (Kochi Univ.)
Tetsufumi HIRANO (Columbia Univ.)
Lin HUEY-WEN (Columbia Univ.)

Administration

Pamela ESPOSITO (Secretary)
Rae GREENBERG (Assistant)
Jane Lysik (Secretary)
Taeko ITO (Secretary)

Administrative Manager

Yoshio OKUIZUMI, Hiroshi MIYAMOTO

Deputy Administrative Manager

Ryosuke MARUYAMA

[*1] RIKEN BNL Fellow, [*2] RHIC Physics Fellow,
[*3] Research Associate, [*4] Special Postdoctoral Researcher

VI. LIST OF PUBLICATION AND PRESENTATION

Accelerator Development Gr.

Publications

[**Journal**]

(Original Papers) *Subject to Peer Review

Koseki T., Watanabe M., Watanabe S., Chiba Y., Goto A., Noda K., and Ohshiro Y.: "Broadband buncher cavity for beam transport line of HiECR Ion Source", Jpn. J. Appl. Phys. Pt.1 **45**, No. 5A, pp. 4227–4231 (2006). *

Ryuto H., Hasebe H., Fukunishi N., Yokouchi S., Goto A., Kase M., and Yano Y.: "Rotating charge strippers for acceleration of intense heavy-ion beams at RIKEN", Nuclear Instruments and Methods in Physics Research A **569**, No. 3, pp. 697–700 (2006). *

[**Book・Proc.**]

(Original Papers) *Subject to Peer Review

上垣外修一, 中川孝秀, 福西暢尚, 齋藤肇, 後藤彰: "理研リングサイクロトロンへの新入射器の検討", 第 3 回日本加速器学会年会・第 31 回リニアック技術研究会論文集, 仙台市, 2006–8, 東北大学, 加速器学会, 仙台, pp. 502–504 (2006).

Oral Presentations

(International Conference etc.)

Baba H., Shimoura S., Minemura T., Matsuyama Y., Saito A., Ryuto H., Aoi N., Gomi T., Higurashi Y., Ieki K., Imai N., Iwasa N., Iwasaki H., Kanno S., Kubono S., Kunibu M., Michimasa S., Motobayashi T., Nakamura T., Sakurai H., Serata M., Takeshita E., Takeuchi S., Ue K., Teranishi T., Yamada K., and Yanagisawa Y.: "Isoscalar monopole and dipole responses in unstable nucleus ^{14}O", Direct Reactions with Exotic Beams (DREB2005), (Michigan State University), East Lansing, June (2005).

Baba H., Shimoura S., Minemura T., Matsuyama Y., Saito A., Ryuto H., Aoi N., Gomi T., Higurashi Y., Ieki K., Imai N., Iwasa N., Iwasaki H., Kanno S., Kubono S., Kunibu M., Michimasa S., Motobayashi T., Nakamura T., Sakurai H., Serata M., Takeshita E., Takeuchi S., Teranishi T., Ue K., Yamada K., and Yanagisawa Y.: "Measurement of inelastic alpha scattering on ^{14}O", JINA Workshop on Nuclear Incompressibility and the Nuclear Equation of State, (JINA), Indiana, USA, July (2005).

Baba H., Shimoura S., Minemura T., Matsuyama Y., Saito A., Ryuto H., Aoi N., Gomi T., Higurashi Y., Ieki K., Imai N., Iwasa N., Iwasaki H., Kanno S., Kubono S., Kunibu M., Michimasa S., Motobayashi T., Nakamura T., Sakurai H., Serata M., Takeshita E., Takeuchi S., Teranishi T., Ue K., Yamada K., and Yanagisawa Y.: "Isoscalar monopole and dipole responces in ^{14}O", 2nd Joint Meeting of the Nuclear Physics Divisions of the APS and JPS (Hawaii 2005), Maui, USA, Sept. (2005).

Baba H., Shimoura S., Saito A., Minemura T., Matsuyama Y., Ryuto H., Aoi N., Gomi T., Higurashi Y., Ieki K., Imai N., Iwasa N., Iwasaki H., Kanno S., Kubono S., Kunibu M., Michimasa S., Motobayashi T., Nakamura T., Sakurai H., Serata M., Takeshita E., Takeuchi S., Teranishi T., Ue K., Yamada K., and Yanagisawa Y.: "Isoscalar compressional strengths in ^{14}O", 2nd International Conference on Collective Motion in Nuclei Under Extreme Conditions (COMEX2), (TU Darmstadt, GSI), Sankt Goar, Germany, June (2006).

Baba H., Shimoura S., Saito A., Minemura T., Matsuyama Y., Ryuto H., Aoi N., Gomi T., Higurashi Y., Ieki K., Imai N., Iwasa N., Iwasaki H., Kanno S., Kubono S., Kunibu M., Michimasa S., Motobayashi T., Nakamura T., Sakurai H., Serata M., Takeshita E., Takeuchi S., Teranishi T., Ue K., Yamada K., and Yanagisawa Y.: "Highly excited states of ^{14}O with the (α,α') reaction", 2nd German-Japanese Workshop on Nuclear Structure and Astrophysics, (RIKEN, CNS, DFG, GSI), Wako, Oct. (2006).

(Domestic Conference)

龍頭啓充, 長谷部裕雄, 福西暢尚, 後藤彰, 加瀬昌之, 矢野安重: "RIBF における U 加速のためのチャージストリッパーの開発状況", 第 3 回日本加速器学会年会・第 31 回リニアック技術研究会, 仙台, 8 月 (2006).

上垣外修一, 中川孝秀, 福西暢尚, 齋藤肇, 後藤彰: "理研リングサイクロトロンのための新入射器の検討", 第 3 回日本加速器学会年会・第 31 回リニアック技術研究会, 仙台, 8 月 (2006).

池沢英二, 加治大哉, 加瀬昌之, 上垣外修一, 中川孝秀, 坂本成彦, 奥野広樹, 稲辺尚人, 福西暢尚, 込山美咲, 木寺正憲, 日暮祥英, 龍頭啓充, 小原重夫, 藤巻正樹, 若杉昌徳, 長瀬誠, 影山正, 横内茂, 渡邉環, 米田晃, 後藤彰, 矢野安重: "超重元素探索実験のための理研重イオンリニアック運転", 第 3 回日本加速器学会年会・第 31 回リニアック技術研究会, 仙台, 8 月 (2006).

Accelerator Operation Gr.

Publications

[**Journal**]

(Original Papers) *Subject to Peer Review

Ryuto H., Abe T., Fukunishi N., Kase M., and Yano Y.: "Heavy-ion beam irradiation system for biological samples in RIKEN", Journal of Biomedical Nanotechnology **2**, No. 2, pp. 88–93 (2006).

Ryuto H., Hasebe H., Fukunishi N., Yokouchi S., Goto A., Kase M., and Yano Y.: "Rotating charge strippers for acceleration of intense heavy-ion beams at RIKEN", Nuclear Instruments and Methods in Physics Research A **569**, No. 3, pp. 697–700 (2006). *

Oral Presentations

(Domestic Conference)

龍頭啓充, 長谷部裕雄, 福西暢尚, 後藤彰, 加瀬昌之, 矢野安重: "RIBF における U 加速のためのチャージストリッパーの開発状況", 第 3 回日本加速器学会年会・第 31 回リニアック技術研究会, 仙台, 8 月 (2006).

池沢英二, 加治大哉, 加瀬昌之, 上垣外修一, 中川孝秀, 坂本成彦, 奥野広樹, 稲辺尚人, 福西暢尚, 込山美咲, 木寺正憲, 日暮祥英, 龍頭啓充, 小原重夫, 藤巻正樹, 若杉昌徳, 長瀬誠, 影山正, 横内茂, 渡邉環, 米田晃, 後藤彰, 矢野安重: "超重元素探索実験のための理研重イオンリニアック運転", 第 3 回日本加速器学会年会・第 31 回リニアック技術研究会, 仙台, 8 月 (2006).

坂本久雄, 堀米敦子, 向井弘樹, 日暮利江子, 藤田新, 上蓑義朋, 加瀬昌之: "理研 RIBF におけるウラン加速の安全管理", 第 3 回日本加速器学会年会・第 31 回リニアック技術研究会, 仙台, 8 月 (2006).

Accelerator Team

Publications

[**Journal**]

(Original Papers) *Subject to Peer Review

Bandyopadhyay A., Kamigaito O., Nayak S. K., Pandey H. K., Mondal M., and Chakrabarti A.: "Design of LINAC post-accelerator for VECC RIB facility using realistic field", Nuclear Instruments and Methods in Physics Research A **560**, 182–190 (2006). *

Kamigaito O.: "Circuit-model representation of external-Q calculation", Phys. Rev. Spec. Top.: Accel. Beams **9**, No. 6, pp. 062003-1–062003-7 (2006). *

Suda K., Okamura H., Uesaka T., Nishikawa J., Kumasaka H., Suzuki R., Sakai H., Tamii A., Ohnishi T., Sekiguchi K., Yako K., Sakoda S., Kato H., Hatano M., Maeda Y., Saito T., Ishida T., Sakamoto N., Sato Y., Hatanaka K., Wakasa T., and Kamiya J.: "Absolute Calibration of the Deuteron Beam Polarization at Intermediate Energies via the ^{12}C$(\vec{d},\alpha)^{10}$B$^*[2^+]$ Reaction", Nuclear Instruments and Methods in Physics Research A **572**, No. Issue 2, pp. 745–753 (2007). *

(Others)

藤澤高志, 上垣外修一: "導体及び導体薄膜の高周波損失について", HIMAC **116**, (2006).

[**Book・Proc.**]

(Original Papers) *Subject to Peer Review

上垣外修一, 中川孝秀, 福西暢尚, 齋藤肇, 後藤彰: "理研リングサイクロトロンへの新入射器の検討", 第 3 回日本加速器学会年会・第 31 回リニアック技術研究会論文集, 仙台市, 2006–8, 東北大学, 加速器学会, 仙台, pp. 502–504 (2006).

Oral Presentations

(International Conference etc.)

Yagi E., Hayashi T., Koike S., Yoshida T., Higami N., Hirabayashi K., Takebayashi A., and Ogiwara K.: "Lattice location of hydrogen in β -V_2H", International Symposium on Metal-Hydrogen Systems: Fundamentals and Applications (MH2006), Hawaii, USA, Oct. (2006).

(Domestic Conference)

上垣外修一, 中川孝秀, 福西暢尚, 齋藤肇, 後藤彰: "理研リングサイクロトロンのための新入射器の検討", 第 3 回日本加速器学会年会・第 31 回リニアック技術研究会, 仙台, 8 月 (2006).

池沢英二, 加治大哉, 加瀬昌之, 上垣外修一, 中川孝秀, 坂本成彦, 奥野広樹, 稲辺尚人, 福西暢尚, 込山美咲, 木寺正憲, 日暮祥英, 龍頭啓充, 小原重夫, 藤巻正樹, 若杉昌徳, 長瀬誠, 影山正, 横内茂, 渡邉環, 米田晃, 後藤彰, 矢野安重: "超重元素探索実験のための理研重イオンリニアック運転", 第 3 回日本加速器学会年会・第 31 回リニアック技術研究会, 仙台, 8 月 (2006).

八木栄一, 平林和紘, 村上洋一, 小池茂年, 樋上直太, 林達也, 武林昭子, 吉田徹, 飯田敬, 菅原孝昌, 宍戸統悦, 荻原清: "酸素を添加した Nb 中の水素の存在状態", 日本物理学会 2006 年秋季大会, (日本物理学会), 千葉, 9 月 (2006).

前田邦子, 浜中廣見, 荻原清, 長谷川賢一: "結晶分光 PIXE で化学状態の深さ分布を調べる", 第 23 回 PIXE シンポジウム, (PIXE 研究協会), 松島, 11 月 (2006).

Ion Source Team

Publications

[**Book・Proc.**]

(Original Papers) *Subject to Peer Review

上垣外修一, 中川孝秀, 福西暢尚, 齋藤肇, 後藤彰: "理研リングサイクロトロンへの新入射器の検討", 第 3 回日本加速器学会年会・第 31 回リニアック技術研究会論文集, 仙台市, 2006–8, 東北大学, 加速器学会, 仙台, pp. 502–504 (2006).

Oral Presentations

(Domestic Conference)

上垣外修一, 中川孝秀, 福西暢尚, 齋藤肇, 後藤彰: "理研リングサイクロトロンのための新入射器の検討", 第 3 回日本加速器学会年会・第 31 回リニアック技術研究会, 仙台, 8 月 (2006).

池沢英二, 加治大哉, 加瀬昌之, 上垣外修一, 中川孝秀, 坂本成彦, 奥野広樹, 稲辺尚人, 福西暢尚, 込山美咲, 木寺正憲, 日暮祥英, 龍頭啓充, 小原重夫, 藤巻正樹, 若杉昌徳, 長瀬誠, 影山正, 横内茂, 渡邉環, 米田晃, 後藤彰, 矢野安重: "超重元素探索実験のための理研重イオンリニアック運転", 第 3 回日本加速器学会年会・第 31 回リニアック技術研究会, 仙台, 8 月 (2006).

RILAC Team

Oral Presentations

(Domestic Conference)

池沢英二, 加治大哉, 加瀬昌之, 上垣外修一, 中川孝秀, 坂本成彦, 奥野広樹, 稲辺尚人, 福西暢尚, 込山美咲,

木寺正憲, 日暮祥英, 龍頭啓充, 小原重夫, 藤巻正樹, 若杉昌徳, 長瀬誠, 影山正, 横内茂, 渡邉環, 米田晃, 後藤彰, 矢野安重: “超重元素探索実験のための理研重イオンリニアック運転”, 第 3 回日本加速器学会年会・第 31 回リニアック技術研究会, 仙台, 8 月 (2006).

Cyclotron Team

Publications

[**Journal**]

(Original Papers) *Subject to Peer Review

Ryuto H., Hasebe H., Fukunishi N., Yokouchi S., Goto A., Kase M., and Yano Y.: “Rotating charge strippers for acceleration of intense heavy-ion beams at RIKEN”, Nuclear Instruments and Methods in Physics Research A **569**, No. 3, pp. 697–700 (2006). *

Oral Presentations

(Domestic Conference)

池沢英二, 加治大哉, 加瀬昌之, 上垣外修一, 中川孝秀, 坂本成彦, 奥野広樹, 稲辺尚人, 福西暢尚, 込山美咲, 木寺正憲, 日暮祥英, 龍頭啓充, 小原重夫, 藤巻正樹, 若杉昌徳, 長瀬誠, 影山正, 横内茂, 渡邉環, 米田晃, 後藤彰, 矢野安重: “超重元素探索実験のための理研重イオンリニアック運転”, 第 3 回日本加速器学会年会・第 31 回リニアック技術研究会, 仙台, 8 月 (2006).

藤縄雅: “理研 RI ビームファクトリーにおける電熱併給設備”, 日本大学生産工学部第 39 回学術講演会, (日本大学), 習志野, 12 月 (2006).

Beam Technology Team

Publications

[**Journal**]

(Original Papers) *Subject to Peer Review

Honda I., Kikuchi K., Matsuo S., Fukuda M., Saito H., Ryuto H., Fukunishi N., and Abe T.: “Heavy-ion-induced mutants in sweet pepper isolated by M1 plant selection”, Euphytica **152**, No. 1, pp. 61–66 (2006). *

Ryuto H., Abe T., Fukunishi N., Kase M., and Yano Y.: “Heavy-ion beam irradiation system for biological samples in RIKEN”, Journal of Biomedical Nanotechnology **2**, No. 2, pp. 88–93 (2006).

Ryuto H., Hasebe H., Fukunishi N., Yokouchi S., Goto A., Kase M., and Yano Y.: “Rotating charge strippers for acceleration of intense heavy-ion beams at RIKEN”, Nuclear Instruments and Methods in Physics Research A **569**, No. 3, pp. 697–700 (2006). *

(Review)

阿部知子, 林依子, 市田裕之, 龍頭啓充: “理研仁科加速器研究センターにおける重イオン加速器を用いた植物育種の実用化”, 加速器 **3**, No. 1, pp. 69–73 (2006).

[**Book・Proc.**]

(Original Papers) *Subject to Peer Review

上垣外修一, 中川孝秀, 福西暢尚, 齋藤肇, 後藤彰: “理研リングサイクロトロンへの新入射器の検討”, 第 3 回日本加速器学会年会・第 31 回リニアック技術研究会論文集, 仙台市, 2006–8, 東北大学, 加速器学会, 仙台, pp. 502–504 (2006).

(Review)

阿部知子, 龍頭啓充: “重イオンビームを用いた植物の品種改良法の実用化”, 第 30 回放射線科学研究会資料集, 大阪, 2006–7, 大阪ニュークリア, 大阪, pp. 17–22 (2006).

Oral Presentations

(International Conference etc.)

Saito H., Hayashi Y., Fukunishi N., Ryuto H., Suzuki K., Kanaya T., Sugiyama M., Terakawa T., Ohtsubo N., Aida R., and Abe T.: “Isolation of sterile mutants of floricultural plants using heavy-ion beam irradiation”, 27th International Horticultural Congress and Exhibition, (International Society for Horticultural Science), Seaul, Korea, Aug. (2006).

(Domestic Conference)

阿部知子, 龍頭啓充: “重イオンビームを用いた植物の品種改良法の実用化”, 第 30 回放射線科学研究会, (大阪ニュークリアサイエンス協会), 大阪, 7 月 (2006).

龍頭啓充, 長谷部裕雄, 福西暢尚, 後藤彰, 加瀬昌之, 矢野安重: “RIBF における U 加速のためのチャージストリッパーの開発状況”, 第 3 回日本加速器学会年会・第 31 回リニアック技術研究会, 仙台, 8 月 (2006).

上垣外修一, 中川孝秀, 福西暢尚, 齋藤肇, 後藤彰: “理研リングサイクロトロンのための新入射器の検討”, 第 3 回日本加速器学会年会・第 31 回リニアック技術研究会, 仙台, 8 月 (2006).

池沢英二, 加治大哉, 加瀬昌之, 上垣外修一, 中川孝秀, 坂本成彦, 奥野広樹, 稲辺尚人, 福西暢尚, 込山美咲, 木寺正憲, 日暮祥英, 龍頭啓充, 小原重夫, 藤巻正樹, 若杉昌徳, 長瀬誠, 影山正, 横内茂, 渡邉環, 米田晃, 後藤彰, 矢野安重: “超重元素探索実験のための理研重イオンリニアック運転”, 第 3 回日本加速器学会年会・第 31 回リニアック技術研究会, 仙台, 8 月 (2006).

竹久妃奈子, 阿部知子, 林依子, 神波千秋, 斉藤宏之, 市田裕之, 小沼亮子, 龍頭啓充, 福西暢尚, 宮沢豊, 東海林英夫, 保倉明子, 福田直樹, 中井泉, 佐藤雅志: “重イオンビーム照射による塩害水田耐性イネ突然変異系統の作出”, 日本育種学会第 110 回講演会, 松山, 9 月 (2006).

阿部知子, 林依子, 竹久妃奈子, 安田美智子, 市田裕之, 斉藤宏之, 柏原輝彦, 福田直樹, 小沼亮子, 保倉明子, 寺田靖子, 龍頭啓充, 福西暢尚, 宮沢豊, 仲下英雄, 工藤俊章, 中井泉, 佐藤雅志: “イネにおける加速器を用いた変異誘発法および変異体解析法の開発”, 日本育種学会第 110 回講演会, 松山, 9 月 (2006).

田平千香子, 漆川直希, 阿部知子, 阪本浩一, 斉藤宏之, 龍頭啓充, 福西暢尚, 村井耕二: “イオンビームによる一粒系コムギ突然変異体 fushi-darake の表現型および遺伝解析”, 日本育種学会第 110 回講演会, 松山, 9 月 (2006).

市田裕之, 松山知樹, 龍頭啓充, 福西暢尚, 阿部知子, 木庭

卓人: “根粒菌における突然変異誘発とその網羅的検出”, 植物微生物研究会 第16回研究交流会, 札幌, 9月 (2006).

市田裕之, 松山知樹, 龍頭啓充, 福西暢尚, 林依子, 阿部知子, 木庭卓人: “重イオンビームによって誘発されたDNA多型の解析”, 日本DNA多型学会第15回学術集会, (日本DNA多型学会), 福山, 11月 (2006).

Cryogenic Technology Team

Publications

[**Journal**]

(Original Papers) *Subject to Peer Review

Ryuto H., Hasebe H., Fukunishi N., Yokouchi S., Goto A., Kase M., and Yano Y.: “Rotating charge strippers for acceleration of intense heavy-ion beams at RIKEN”, Nuclear Instruments and Methods in Physics Research A **569**, No. 3, pp. 697–700 (2006). *

Oral Presentations

(Domestic Conference)

龍頭啓充, 長谷部裕雄, 福西暢尚, 後藤彰, 加瀬昌之, 矢野安重: “RIBFにおけるU加速のためのチャージストリッパーの開発状況”, 第3回日本加速器学会年会・第31回リニアック技術研究会, 仙台, 8月 (2006).

Heavy Ion Nuclear Physics Lab.

Publications

[**Journal**]

(Original Papers) *Subject to Peer Review

Suzuki K., Fujita M., Geissel H., Gilg H., Gillitzer A., Hayano R., Hirenzaki S., Itahashi K., Iwasaki M., Kienle P., Matos M., Munzenberg G., Ohtsubo T., Sato M., Shindo M., Suzuki T., Weick H., Winkler M., Yamazaki T., Sato M., and Yoneyama T.: “Deeply bound poonic 1s in Sn isotopes”, Nucl. Phys. A **721**, 831c–834c (2003). *

Adcox K., Bazilevsky A. V., Bunce G. M., Deshpande A., En'yo H., Fox B., Goto Y., Grosse Perdekamp M., Hayashi N., Ichihara T., Imai K., Ishihara M., Jacak B. V., Kobayashi H., Kurita K., Li Z., Mao Y., Murata J., Saito N., Sakuma T., Sato H., Shibata T., Sugioka M., Taketani A., Tojo J., Torii H., Watanabe Y., Yokkaichi S., and PHENIX C.: “PHENIX detector overview”, Nuclear Instruments and Methods in Physics Research A **499**, 469–479 (2003). *

Aizawa M., Kurita K., and PHENIX C.: “PHENIX central arm particle ID detectors”, Nuclear Instruments and Methods in Physics Research A **499**, 508–520 (2003). *

Akikawa H., En'yo H., Hayashi N., Ichihara T., Ishihara M., Kobayashi H., Kurita K., Li Z., Mao Y., Murata J., Saito N., Sato H., Shibata T., Sugioka M., Taketani A., Watanabe Y., Yokkaichi S., and PHENIX Collaboratio .: “PHENIX muon arms”, Nuclear Instruments and Methods in Physics Research A **499**, 537–548 (2003). *

Suzuki K., Fujita M., Geissel H., Gilg H., Gillitzer A., Hayano R., Hirenzaki S., Itahashi K., Iwasaki M., Kienle P., Matos M., Muenzenberg G., Otsubo T., Sato M., Shindo M., Suzuki T., Weick H., Winkler M., Yamazaki T., and Yoneyama T.: “Observattion of Pionic 1*s* States in Sn Nuclei and Its Implications on Chiral Symmetry Restoration”, Prog. Theor. Phys. Suppl., No. 149, pp. 32–41 (2003). *

Beer G. A., Bragadireanu A. M., Cargnelli M., Curceanu C., Egger J. -., Fuhrmann H., Giersch M., Guaraldo C., Iliescu M., Ishiwatari T., Itahashi K., Iwasaki M., Kienle P., Lauss B., Lucherini V., Ludhova L., Marton J., Mulhauser F., Ponta T., Schaller L. A., Sirghi D. L., Sirghi F., and Zmeskal J.: “Kaonic Hydrogen: *Status of the DEAR Experiment*”, Prog. Theor. Phys. Suppl., No. 149, pp. 240–246 (2003).

Petrascu M., Constantinescu A., Cruceru I., Giurgiu M., Isbasescu A., Petrascu H., Bordeanu C., Tanihata I., Motobayashi T., Kobayashi T., Morimoto K., Katori K., Ozawa A., Suda T., Yoshida K., Chiba M., Nishi Y., and Nishimura S.: “Pre-emission of correlated neutrons from ^{11}Li halo nuclei”, Nucl. Phys. A **734**, 327–330 (2004). *

Yamada K., Motobayashi T., and Tanihata I.: “RF deflector system for proton-rich RI beams in RIKEN”, Nucl. Phys. A **746**, 156c–160c (2004). *

Tanaka K., Fukuda M., Mihara M., Takechi M., Chinda T., Sumikama T., Kudo s., Matsuta K., Minamisono T., Ohtsubo T., Suzuki T., Momota S., Izumikawa T., Yamaguchi T., Oonish T., Ozawa A., Tanihata I., and Tao Z.: “Density Distribution of Proton Drip-Line Nucleus ^{17}Ne”, Nucl. Phys. A **746**, 532c–535c (2004). *

Suzuki T., Itahashi K., Iwasaki M., Matsuda Y., Okada S., Outa H., Sato M., Strasser P., Tomono D., and Yamazaki T.: “A search for deeply bound kaonic nuclear states”, Nucl. Phys. A **754**, 375c–382c (2005). *

Kimura K., Izumikawa T., Koyama R., Ohnishi T., Ohtsubo T., Ozawa A., Shinozaki W., Suzuki T., Takahashi M., Tanihata I., Yamaguchi T., and Yamaguchi Y.: “High-rate particle identification of high-energy heavy ions using a tilted electrode gas ionization chamber”, Nuclear Instruments and Methods in Physics Research A **538**, 608–614 (2005). *

Matsuo Y., Fukuyama Y., and Moriwaki Y.: “Temperature and pressure control of cold helium gas above liquid helium for laser spectroscopy of atoms and molecules at 3-30 K”, AIP Conf. Proc. **850**, 392–393 (2006). *

Funaki Y., Tohsaki A., Horiuchi H., Schuck P., and Ropke G.: “Inelastic form factors to alpha-particle

condensate states in ^{12}C and ^{16}O: what can we learn ?", Eur. Phys. J. A **28**, 259–263 (2006). ∗

Mazzocco M., Signorini C., Romoli M., De Francesco A., Dipietro M., Vardaci E., Yoshida K., Yoshida A., Bonetti R., De Rosa A., Glodariu T., Guglielmentti A., Inglima G., La Commara M., Martin B., Pierroutsakou D., Sandoli M., Soramel F., Stroe L., Kanungo R., Khai N., Motobayashi T., Nomura T., Ishikawa T., Ishiyama H., Jeong S., Miyatake H., Tanaka M., Sugai I., and Watanabe Y.: "Scattering of ^{11}Be halo nucleus from ^{209}Bi at the Coulomb barrier", Eur. Phys. J. A **28**, 295–299 (2006). ∗

Takeuchi S., Aoi N., Baba H., Fukui T., Hashimoto Y., Ieki K., Imai N., Iwasaki H., Kanno S., Kondo Y., Kubo T., Kurita K., Minemura T., Motobayashi T., Nakabayashi T., Nakamura T., Okumura T., Onishi T., Ota S., Sakurai H., Shimoura S., Sugo R., Suzuki D., Suzuki H., Suzuki M., Takeshita E., Tamaki M., Tanaka K., Togano Y., and Yamada K.: "Proton inelastic scattering on ^{32}Mg", J. Phys.: Conf. Series **49**, 153–154 (2006). ∗

Moriwaki Y., Matsuo Y., Fukuyama Y., and Morita N.: "Laser spectroscopic measurements of fine structure changing cross sections of alkali earth ions in collisions with molecular hydrogen (H_2, D_2)", J. Phys. B **39**, 4789–4797 (2006). ∗

Koseki T., Watanabe M., Watanabe S., Chiba Y., Goto A., Noda K., and Ohshiro Y.: "Broadband buncher cavity for beam transport line of HiECR Ion Source", Jpn. J. Appl. Phys. Pt.1 **45**, No. 5A, pp. 4227–4231 (2006). ∗

Ishiwatari T., Beer G. A., Bragadireanu A. M., Cargnelli M., Curceanu P. C., Egger J. P., Fuhrmann H., Guaraldo C., Iliescu M., Itahashi K., Iwasaki M., Kienle P., Lauss B., Lucherini V., Ludhova L., Marton J., Mulhauser F., Ponta T., Schaller L. A., Sirghi D. L., Strasser P., and Zmeslal J.: "New analysis method for CCD X-ray data", Nuclear Instruments and Methods in Physics Research A **556**, 509–515 (2006). ∗

Michimasa S., Shimoura S., Iwasaki H., Tamaki M., Ota S., Aoi N., Baba H., Iwasa N., Kanno S., Kubono S., Kurita K., Uesaka M., Minemura T., Motobayashi T., Notani M., Ong H., Saito A., Sakurai H., Takeshita E., Takeuchi S., Yanagisawa Y., and Yoshida A.: "Proton single-particle states in the neutron-rich ^{23}F nucleus", Phys. Lett. B **638**, 146–152 (2006). ∗

Dang N. D.: "Consistency of the particle-particle random-phase approximation and renormalization", Phys. Rev. C **74**, No. 2, pp. 024318-1–024318-7 (2006). ∗

Dang N. D. and Tanabe K.: "Self-consistent random-phase approximation at finite temperature within the Richardson model", Phys. Rev. C **74**, No. 3, pp. 034326-1–034326-15 (2006). ∗

Dang N. D. and Arima A.: "Comment on "Test of the modified BCS model at finite temperature"", Phys. Rev. C **74**, No. 5, pp. 509801-1–509801-2 (2006). ∗

Furukawa T., Matsuo Y., Hatakeyama A., Fukuyama Y., Kobayashi T., Izumi H., and Shimoda T.: "Measurement of a long electronic spin relaxation time of cesium atoms in superfluid helium", Phys. Rev. Lett. **96**, No. 9, pp. 095301-1–095301-4 (2006). ∗

Kobayashi T., Kato T., Matsuo Y., Nishimura M., Kawai J., and Hayashizaki Y.: "Ionization and Fragmentation of solid C_{60} by Femtosecond Laser Ablation", J. Chem. Phys. **126**, No. 6, pp. 061101-1–061101-3 (2007). ∗

Matsuo Y., Kobayashi T., Yonekura N., and Nakajima T.: "Photoionization characteristics of Sr into $5skl$ continua through the spin-resolved ion detection by laser-induced fluorescence", Jpn. J. Appl. Phys. Pt.1 **46**, 1181–1185 (2007). ∗

Dang N. D.: "Thermal pairing in Richardson model", Nucl. Phys. A **784**, No. 1-4, pp. 147–160 (2007). ∗

Suda K., Okamura H., Uesaka T., Nishikawa J., Kumasaka H., Suzuki R., Sakai H., Tamii A., Ohnishi T., Sekiguchi K., Yako K., Sakoda S., Kato H., Hatano M., Maeda Y., Saito T., Ishida T., Sakamoto N., Sato Y., Hatanaka K., Wakasa T., and Kamiya J.: "Absolute Calibration of the Deuteron Beam Polarization at Intermediate Energies via the $^{12}C(\vec{d},\alpha)^{10}B^*[2^+]$ Reaction", Nuclear Instruments and Methods in Physics Research A **572**, No. Issue 2, pp. 745–753 (2007). ∗

Oyamatsu K. and Iida K.: "Symmetry energy at subnuclear densities and nuclei in neutron star crusts", Phys. Rev. C **75**, 015801-1–015801-10 (2007). ∗

Mutou R., Chiba J., Enyo H., Fukao Y., Funahashi H., Hamagaki H., Ieiri M., Ishino M., Kanda H., kitaguchi m., Mihara S., Miwa K., Miyashita T., Murakami T., Nakura T., Naruki M., Ozawa K., Sakuma F., Sasaki O., Sekimoto M., Tabaru T., Tanaka K., Togawa M., Yamada S., Yokkaichi S., and Yoshimura Y.: "Evidence for in-medium modification of the ϕ meson at normal nuclear density", Phys. Rev. Lett. **98**, No. 4, pp. 042501-1–042501-4 (2007). ∗

(Others)

Funaki Y., Schuck P., Horiuchi H., Ropke G., Tohsaki A., and Yamada T.: "Alpha particle condensation in nuclear systems", AIP Conf. Proc. **853**, 140–145 (2006).

Funaki Y., Tohsaki A., Horiuchi H., Schuck P., and Ropke G.: "Alpha condensed state in ^{16}O", Mod. Phys. Lett. A **21**, No. 31/33, pp. 2331–2340 (2006).

Dang N. D.: "Giant resonances as fundamental modes of nuclear collective excitations", Frontiers of Basic Science: Towards New Physics, Earth and Space Science, Mathematics, Hanoi, Vietnam, 2005–9, Osaka University Press, Osaka, pp. 64–65 (2006).

Oral Presentations

(International Conference etc.)

Tanaka K., Fukuda M., Mihara M., Takechi M., Chinda T., Sumikama T., Kudo s., Matsuta K., Minamisono T., Ohtsubo T., Suzuki T., Momota S., Izumikawa T., Yamaguchi T., Oonish T., Ozawa A., Tanihata I., and Zheng T.: "Nucleon Density Distribution of Proton Drip-Line Nucleus ^{17}Ne", 4th International Conference on Exotic Nuclei and Atomic Masses (ENAM 04), (Oak Ridge National Laboratory), Pine Mountain, USA, Sept. (2004).

Yamada K., Motobayashi T., Aoi N., Baba H., Demichi K., Elekes Z., Gibelin J. D., Gomi T., Hasegawa H., Imai N., Iwasaki H., Kanno S., Kubo T., Kurita K., Matsuyama Y., Michimasa S., Minemura T., Notani M., Onishi T., Ong H., Ota S., Ozawa A., Saito A., Sakurai H., Shimoura S., Takeshita E., Takeuchi S., Tamaki M., Togano Y., Yanagisawa Y., Yoneda K., and Tanihata I.: "The first measurement of reduced transition probabilities for first 2^+ excited state in ^{46}Cr, ^{50}Fe, and ^{54}Ni", 4th International Conference on Exotic Nuclei and Atomic Masses (ENAM 04), (Oak Ridge National Laboratory), Pine Mountain, USA, Sept. (2004).

Baba H., Shimoura S., Minemura T., Matsuyama Y., Saito A., Ryuto H., Aoi N., Gomi T., Higurashi Y., Ieki K., Imai N., Iwasa N., Iwasaki H., Kanno S., Kubono S., Kunibu M., Michimasa S., Motobayashi T., Nakamura T., Sakurai H., Serata M., Takeshita E., Takeuchi S., Ue K., Teranishi T., Yamada K., and Yanagisawa Y.: "Isoscalar monopole and dipole responses in unstable nucleus ^{14}O", Direct Reactions with Exotic Beams (DREB2005), (Michigan State University), East Lansing, June (2005).

Baba H., Shimoura S., Minemura T., Matsuyama Y., Saito A., Ryuto H., Aoi N., Gomi T., Higurashi Y., Ieki K., Imai N., Iwasa N., Iwasaki H., Kanno S., Kubono S., Kunibu M., Michimasa S., Motobayashi T., Nakamura T., Sakurai H., Serata M., Takeshita E., Takeuchi S., Teranishi T., Ue K., Yamada K., and Yanagisawa Y.: "Measurement of inelastic alpha scattering on ^{14}O", JINA Workshop on Nuclear Incompressibility and the Nuclear Equation of State, (JINA), Indiana, USA, July (2005).

Togano Y., Gomi T., Motobayashi T., Ando Y., Aoi N., Baba H., Demichi K., Elekes Z., Fukuda N., Fulop Z., Hasegawa H., Higurashi Y., Ieki K., Imai N., Ishihara M., Ishikawa K., Iwasa N., Iwasaki H., Kanno S., Kondo Y., Kubo T., Kubono S., Kurita K., Matsuyama Y., Michimasa S., Minemura T., Miura M., Murakami H., Nakamura T., Notani M., Ota S., Saito A., Sakurai H., Serata M., Shimoura S., Sugimoto T., Takeshita E., Takeuchi S., Ue K., Yamada K., Yanagisawa Y., Yoneda K., Yoshida A., Futakami U., and Kunibu M.: "Coulomb dissociation of ^{27}P for Study of ^{26}Si(p,γ)^{27}P reaction", 2nd Joint Meeting of the Nuclear Physics Divisions of the APS and JPS (Hawaii 2005), Maui, USA, Sept. (2005).

Aoi N.: "Exploring the shell structure in very neutron rich pfg-shell nuclei through the γ-ray spectroscopy technique", 2nd Joint Meeting of the Nuclear Physics Divisions of the APS and JPS (Hawaii 2005), Maui, USA, Sept. (2005).

Baba H., Shimoura S., Minemura T., Matsuyama Y., Saito A., Ryuto H., Aoi N., Gomi T., Higurashi Y., Ieki K., Imai N., Iwasa N., Iwasaki H., Kanno S., Kubono S., Kunibu M., Michimasa S., Motobayashi T., Nakamura T., Sakurai H., Serata M., Takeshita E., Takeuchi S., Teranishi T., Ue K., Yamada K., and Yanagisawa Y.: "Isoscalar monopole and dipole responces in ^{14}O", 2nd Joint Meeting of the Nuclear Physics Divisions of the APS and JPS (Hawaii 2005), Maui, USA, Sept. (2005).

Michimasa S., Aoi N., Iwasa N., Iwasaki H., Kanno S., Kubono S., Kurita K., Minemura T., Motobayashi T., Notani M., Ong H., Ota S., Saito A., Shimoura S., Takeshita E., Tamaki M., Uesaka M., Yanagisawa Y., Yoshida A., Sakurai H., Takeuchi S., and Baba H.: "Measurement of proton transfer reaction for single-particle states in ^{23}F", 2nd Joint Meeting of the Nuclear Physics Divisions of the APS and JPS (Hawaii 2005), Maui, USA, Sept. (2005).

Yamada K., Iwasa N., Bishop S., Elekes Z., Gibelin J. D., Hosoi M., Ieki K., Ishikawa K., Iwasaki H., Kawai S., Kondo Y., Kubono S., Kurita K., Kurokawa M., Matsui N., Minemura T., Morikawa H., Nakamura T., Niikura M., Notani M., Ota S., Saito A., Sakurai H., Shimoura S., Sugawara K., Sugimoto T., Suzuki H., Suzuki T., Takeshita E., Takeuchi S., Tanihata I., Teranishi T., Togano Y., Yamaguchi K., Yanagisawa Y., and Motobayashi T.: "New Coulomb Excitation Measurement of ^{18}Ne", 2nd Joint Meeting of the Nuclear Physics Divisions of the APS and JPS (Hawaii 2005), Maui, USA, Sept. (2005).

Furukawa T., Matsuo Y., Hatakeyama A., Fukuyama Y., Kobayashi T., Izumi H., and Shimoda T.: "New laser spectroscopic method for the measurement of nuclear moments", 2nd Joint Meeting of the Nuclear Physics Divisions of the APS and JPS (Hawaii 2005), Maui, USA, Sept. (2005).

Motobayashi T.: "Perspective of nuclear physics and nuclear astrophysics studies with fast exotic beams", 2nd Joint Meeting of the Nuclear Physics Divisions of the APS and JPS (Hawaii 2005), Maui, USA, Sept. (2005).

Kanno S., Aoi N., Takeuchi S., Sakurai H., Glasmacher T., Mueller W. F., Bazin D., Bowen M. D., Campbell C. M., Cook J. M., Dinca D., Gade A., Iwasaki H., Kubo T., Kurita K., Motobayashi T., Nakamura T., Suzuki H., Terry J. R., Zwahlen H., and Yoneda K.: "Proton Inelastic scattering on ^{74}Ni", 2nd Joint Meeting of the Nuclear Physics Divisions of the APS

and JPS (Hawaii 2005), Maui, USA, Sept. (2005).

Furukawa T., Matsuo Y., Hatakeyama A., Ito T., Ota Y., Fukuyama Y., Kobayashi T., and Shimoda T.: "Laser-microwave double resonance method in superfluid helium for the measurement of nuclear moments", 11th International Workshop on Polarized Sources and Targets (PST05), (CNS and RIKEN), Tokyo, Nov. (2005).

Takeuchi S., Aoi N., Baba H., Fukui T., Hashimoto Y., Ieki K., Imai N., Iwasaki H., Kanno S., Kondo Y., Kurita K., Minemura T., Motobayashi T., Nakabayashi T., Nakamura T., Okumura T., Onishi T., Ota S., Sakurai H., Shimoura S., Sugo R., Suzuki D., Suzuki H., Suzuki M., Takeshita E., Tamaki M., Tanaka K., Togano Y., and Yamada K.: "Proton inelastic scattering of ^{32}Mg", International Symposium on Structure of Exotic Nuclei and Nuclear Forces (SENUF06), (University of Tokyo), Tokyo, Mar. (2006).

Takeuchi S.: "Development of hybrid array for γ-ray spectroscopy", International Workshop on "Nuclear Physics with RIBF", RIKEN, Mar. (2006).

Funaki Y., Yamada T., Horiuchi H., Tohsaki A., Schuck P., and Ropke G.: "Alpha condensed state in ^{16}O", RCNP Osaka Spring Workshop on Cluster Condensation and Nucleon Correlation in Nuclei, Ibaraki, Apr. (2006).

Dang N. D.: "Giant resonances under extreme conditions", International Conference on Current problems in nuclear physics and atomice energy (NPAE-Kyiv2006), (Kyiv institutre for nuclear research of National Academy of Sciences of Ukraine), Kyiv, Ukraine, May–June (2006).

Baba H., Shimoura S., Saito A., Minemura T., Matsuyama Y., Ryuto H., Aoi N., Gomi T., Higurashi Y., Ieki K., Imai N., Iwasa N., Iwasaki H., Kanno S., Kubono S., Kunibu M., Michimasa S., Motobayashi T., Nakamura T., Sakurai H., Serata M., Takeshita E., Takeuchi S., Teranishi T., Ue K., Yamada K., and Yanagisawa Y.: "Isoscalar compressional strengths in ^{14}O", 2nd International Conference on Collective Motion in Nuclei Under Extreme Conditions (COMEX2), (TU Darmstadt, GSI), Sankt Goar, Germany, June (2006).

Funaki Y., Yamada T., Tohsaki A., Horiuchi H., Schuck P., and Ropke G.: "Alpha cluster states in ^{12}C and ^{16}O", International Conference on Nuclear Structure '06 (NS06), (Oak Ridge National Laboratory), Oak Ridge, USA, July (2006).

Funaki Y., Yamada T., Tohsaki A., Horiuchi H., Schuck P., and Ropke G.: "Alpha condensed state in ^{16}O", International Workshop on Alpha Particle Condensation in Nuclear Systems, (University of Munich), Munich, Germany, Aug. (2006).

Michimasa S., Shimoura S., Iwasaki H., Tamaki M., Ota S., Aoi N., Baba H., Iwasa N., Kanno S., Kubono S., Kurita K., Minemura T., Motobayashi T., Notani M., Ong H., Saito A., Sakurai H., Takeshita E., Takeuchi S., Uesaka M., Yanagisawa Y., and Yoshida A.: "Proton shell structure in neutron-rich ^{23}F", International Conference on Nucleus Nucleus Collisions (NN2006), Rio de Janeiro, Brazil, Aug.–Sept. (2006).

Dang N. D.: "(invited lecture) "Superfluid-normal phase transition in finite systems and its effect on the damping of giant reasonances at finite temperature"", Predeal Summer School in Nuclear Physics "Collective Motion and Phase Transitions in Nuclear Systems", Predeal, Romania, Aug.–Sept. (2006).

Morita K., Morimoto K., Kaji D., Akiyama T., Goto S., Haba H., Ideguchi E., Katori K., Kikunaga H., Koura H., Kudo H., Ohnishi T., Ozawa A., Suda T., Sato N., Sueki K., Tokanai F., Xu H., Yamaguchi T., Yoneda A., Yoshida A., and YuLiang Z.: "Experiments on Synthesis of the Heaviest Elements at RIKEN (SHE and FFD)", Tours Symposium on Nuclear Physics VI (TOURS 2006), (Konan University), Tours, France, Sept. (2006).

Morita K., Morimoto K., Kaji D., Akiyama T., Goto S., Haba H., Ideguchi E., Katori K., Kikunaga H., Koura H., Kudo H., Ohnishi T., Ozawa A., Suda T., Sato N., Sueki K., Tokanai F., Xu H., Yamaguchi T., Yoneda A., Yoshida A., and YuLiang Z.: "Experiments on Synthesis of the Heaviest Elements at RIKEN Status and Perspectives", Workshop on the Atomic Properties of the Heaviest Elements: Towards the Island of Stability, (LMU-Muenchen), Germany, Chiemsee, Sept. (2006).

Funaki Y., Yamada T., Tohsaki A., Horiuchi H., Schuck P., and Ropke G.: "4 alpha condensed states in ^{16}O", 2nd German-Japanese Workshop on Nuclear Structure and Astrophysics, Wako, Oct. (2006).

Baba H., Shimoura S., Saito A., Minemura T., Matsuyama Y., Ryuto H., Aoi N., Gomi T., Higurashi Y., Ieki K., Imai N., Iwasa N., Iwasaki H., Kanno S., Kubono S., Kunibu M., Michimasa S., Motobayashi T., Nakamura T., Sakurai H., Serata M., Takeshita E., Takeuchi S., Teranishi T., Ue K., Yamada K., and Yanagisawa Y.: "Highly excited states of ^{14}O with the (α,α') reaction", 2nd German-Japanese Workshop on Nuclear Structure and Astrophysics, (RIKEN, CNS, DFG, GSI), Wako, Oct. (2006).

Suzuki Y., Horiuchi W., Sarhan B. A., and Kohama A.: "Structure of carbon isotopes studied with the analysis of reaction cross sections", 2nd German-Japanese Workshop on Nuclear Structure and Astrophysics, (DFG, GSI, University of Tokyo, and RIKEN), Wako, Oct. (2006).

Morita K., Morimoto K., Kaji D., Akiyama T., Goto S., Haba H., Ideguchi E., Katori K., Kikunaga H., Koura H., Kudo H., Ohnishi T., Ozawa A., Suda T., Sato N., Sueki K., Tokanai F., Xu H., Yamaguchi T.,

Yoneda A., Yoshida A., and YuLiang Z.: “Search for the Heaviest Elements at RIKEN”, 6th International Symposium on Advanced Science Research: Frontiers of Nuclear and Radiochemistry (ASR2006), (Advanced Science Research Center, Japan Atomic Energy Agency), Tokaimura, Oct. (2006).

(Domestic Conference)

米田健一郎: “Two neutron knockout reaction of proton rich nuclei ^{34}Ar, ^{30}S, and ^{26}Si”, 京都大学基礎物理学研究所研究会「弱結合系の束縛機構と新しいダイナミクス」, 京都, 12 月 (2005).

小濱洋央, 飯田圭, 親松和浩: ““黒い” 原子核描像に基づく核半径と反応断面積”, RIBF-Day1 実験を睨んだ反応断面積実験に向けたミニワークショップ, Wako, 1 月 (2006).

須田利美: “SCRIT 開発の現状”, RIBF-Day1 実験を睨んだ反応断面積実験に向けたミニワークショップ, 和光, 1 月 (2006).

青井考: “γ-spectroscopy experiment at BigRIPS”, RIBF に於ける γ 線核分光, 和光, 2–2 月 (2006).

加藤俊幸, 小林徹, 松尾由賀利, 西村美月, 小山理恵子, 松村米浩, 山本浩, 河合純, 林崎良英: “基板上試料におけるフェムト秒とナノ秒レーザーアブレーションの比較”, 第 53 回応用物理学関係連合講演会, 東京, 3 月 (2006).

竹下英里, 青井考, 大田晋輔, 武内聡, 鈴木宏, 馬場秀忠, Bishop S., 福井利晃, 井手口栄治, 家城和夫, 今井伸明, 岩崎弘典, 菅野祥子, 近藤洋介, 久保敏幸, 栗田和好, 日下健祐, 峯村俊行, 本林透, 中林彩, 中村隆司, 中尾太郎, 新倉潤, 奥村俊文, 王惠仁, 大西健夫, 櫻井博儀, 下浦享, 須合亮平, 鈴木大介, 鈴木賢, 玉城充, 田中鐘信, 栂野泰宏, 山田一成: “中性子過剰核 Cr 同位体の陽子非弾性散乱”, 日本物理学会第 61 回年次大会, 松山, 3 月 (2006).

道正新一郎, 下浦享, 岩崎弘典, 玉城充, 大田晋輔, 青井考, 馬場秀忠, 岩佐直仁, 菅野祥子, 久保野茂, 栗田和好, 峯村俊行, 本林透, 野谷将広, 王惠仁, 齋藤明登, 櫻井博儀, 竹下英里, 武内聡, 上坂明子, 柳澤善行, 吉田敦: “Single-particle states in ^{23}F by a proton transfer reaction”, 日本物理学会第 61 回年次大会, (日本物理学会), 松山, 3 月 (2006).

米田健一郎: “Two-neutron knockout reaction to $T_z = -2$ nuclei ^{24}Si, ^{28}S, and ^{32}Ar”, 日本物理学会第 61 回年次大会, 松山, 3 月 (2006).

赤石義紀, 山崎敏光: “ケイオン核—批判に答えて”, 日本物理学会第 61 回年次大会, 松山, 3 月 (2006).

炭竈聡之, 長友傑, 小倉昌子, 岩越丈尚, 中島良樹, 藤原裕樹, 松多健策, 南園忠則, 福田光順, 三原基嗣, 南園啓, 山口貴之: “質量数 A=8 体系 β 崩壊における中間子交換効果”, 日本物理学会第 61 回年次大会, 松山, 3 月 (2006).

古川武: “レーザー分光による超流動ヘリウム中での原子・原子核スピン物理の研究”, RIBF 核物理セミナー, 和光, 4 月 (2006).

青井考: “γ-spectroscopy on neutron rich nuclei”, RI ビーム科学シンポジウム, 新潟, 5 月 (2006).

武内聡, 青井考, 馬場秀忠, 福井利晃, 橋本佳子, 家城和夫, 今井伸明, 岩崎弘典, 菅野祥子, 近藤洋介, 栗田和好, 峯村俊行, 本林透, 中林彩, 中村隆司, 奥村俊文, 大西健夫, 大田晋輔, 櫻井博儀, 下浦享, 須合亮平, 鈴木大介, 鈴木宏, 鈴木賢, 竹下英里, 玉城充, 田中鐘信, 栂野泰宏, 山田一成: “^{32}Mg と ^{34}Si の γ 線核分光”, RIBF ミニワークショップ「Island of Inversion に関する実験・理論の現状と今後の展望–$7 < Z < 20$ 領域中性子過剰核の低励起状態に関する検討会–」, 和光, 5 月 (2006).

古川武, 松尾由賀利, 畠山温, 伊藤龍浩, 太田嘉穂, 藤掛浩太郎, 小林徹, 下田正: “超流動ヘリウム中に植え込まれた原子の超微細構造”, 原子・分子・光科学 (AMO) 第 3 回討論会, 東京, 6 月 (2006).

小濱洋央: “弾性散乱断面積と反応断面積”, RIBF ミニワークショップ「不安定核の弾性散乱」, (理研), 和光, 6 月 (2006).

船木靖郎, 山田泰一, Schuck P., 堀内昶, 東崎昭弘, Ropke G.: 理研 RIBF ミニワークショップ「陽子中性子の弱結合現象及び α 凝縮状態に関するミニワークショップ」, 和光, 7 月 (2006).

馬場秀忠: “DAQ system for RI-beam experiment at RARF and RIBF”, Annual RI Beam Factory (RIBF) Users Meeting 2006, 和光, 8 月 (2006).

松本琢磨: “^{6}He 核力クーロン力分解反応解析”, KEK 研究会「現代の原子核物理–多様化し進化する原子核の描像–」, つくば, 8 月 (2006).

船木靖郎, 山田泰一, Schuck P., 堀内昶, 東崎昭弘, Ropke G.: “Alpha condensed state in ^{16}O”, 日本物理学会 2006 年秋季大会, 奈良, 9 月 (2006).

飯田圭, 小濱洋央, 親松和浩: “反応断面積公式：不安定核への応用”, 日本物理学会 2006 年秋季大会, 奈良, 9 月 (2006).

田中鐘信, 山口貴之, 鈴木健, 小沢顕, 相場健, 青井考, 泉川卓司, 稲福清彦, 岩佐直仁, 上坂明子, 大坪隆, 小林圭, 小室麻里, 近藤洋介, 篠田遼子, 篠原摩有子, 鈴木宏, 武内聡, 竹下英里, 武智麻耶, 栂野泰宏, 中島真平, 中林彩, 馬場秀忠, 橋爪祐平, 福田光順, 松山貴史, 道正新一郎, 安野琢磨, 山田一成, 吉竹利織, 久保敏幸, 中村隆司, 櫻井博儀, 本林透: “中性子過剰核 ^{19,20,22}C の反応断面積測定”, 日本物理学会 2006 年秋季大会, 奈良, 9 月 (2006).

小濱洋央, 飯田圭, 親松和浩: “反応断面積と相互作用断面積：“黒い” 原子核描像に基づく解析”, 日本物理学会 2006 年秋季大会, 奈良, 9 月 (2006).

古川武, 松尾由賀利, 畠山温, 伊藤龍浩, 太田嘉穂, 藤掛浩太郎, 小林徹, 下田正: “超流動ヘリウム中のアルカリ金属原子のスピン偏極および磁気共鳴”, 日本物理学会 2006 年秋季大会, 奈良, 9 月 (2006).

野地俊平, 三木謙二郎, 矢向謙太郎, 川畑貴裕, 久保木浩功, 酒井英行, 関口仁子, 須田健嗣: “中性子偏極度計 SMART-NPOL の最適化解析”, 日本物理学会 2006 年秋季大会, 奈良, 9 月 (2006).

松本琢磨, 緒方一介, 江上智晃, 井芹康統, 八尋正信, 上村正康: “^{6}He 核力・クーロン分解反応の解析”, 日本物理学会 2006 年秋季大会, 奈良, 9–9 月 (2006).

青井考: “Status of γ-spectroscopy experiment and Day1 experiemnt at RIBF”, RIBF ミニワークショ

ップ「RIBF に於ける γ 分光実験 (II)」, 和光, 10 月 (2006).

古川武, 松尾由賀利, 畠山温, 伊藤龍浩, 太田嘉穂, 藤掛浩太郎, 小林徹, 下田正: "超流動ヘリウム中に植え込まれた原子の超微細構造", 第 3 回「停止・低速不安定核を用いた核分光研究」研究会, (京都大学原子炉実験所), 大阪府熊取, 11 月 (2006).

古川武, 松尾由賀利, 畠山温, 伊藤龍浩, 太田嘉穂, 藤掛浩太郎, 小林徹, 下田正: "超流動ヘリウム中におけるアルカリ金属原子の超微細構造", RIBF ミニワークショップ「レーザー光利用の次世代加速器実験：その発展と物理学への貢献」, 和光, 11 月 (2006).

田中鐘信, 山口貴之, 鈴木健, 小沢顕, 相場健, 青井考, 泉川卓司, 稲福清彦, 岩佐直仁, 上坂明子, 大坪隆, 小林圭, 小室麻里, 近藤洋介, 篠田遼子, 篠原摩有子, 鈴木宏, 武内聡, 竹下英里, 武智麻耶, 梅野泰宏, 中島真平, 中林彩, 馬場秀忠, 橋爪祐平, 福田光順, 松山貴史, 道正新一郎, 安野琢磨, 山田一成, 吉竹利織, 久保敏幸, 中村隆司, 櫻井博儀, 本林透: "^{22}C 及び炭素同位体の反応断面積実験", RIBF ミニワークショップ「反応断面積で探る核構造」, (RIKEN), 和光, 11 月 (2006).

飯田圭: "反応断面積の理論的解析", RIBF ミニワークショップ「反応断面積で探る核構造」, 和光, 11 月 (2006).

長友傑, 南園啓, 松多健策, Levy C. D., 三原基嗣, 炭竈聡之, 小沢顕, 田岸義宏, 小倉昌子, 松宮亮平, 福田光順, 山口充孝, Behr J. A., Jackson K. P., 藤原弘樹, 安野琢磨, 太田寛史, 橋爪祐平, 千葉明子, 南園忠則: "ベータ NMR 法を用いた質量数 20 体系の β 線角度分布の精密測定による第二種核子流の探索", 平成 18 年度京都大学原子炉実験所専門研究会「原子核プローブ生成とそれを用いた物性研究 (II)」, 大阪府熊取, 11–11 月 (2006).

船木靖郎, 山田泰一, 東崎昭弘, 堀内昶, Schuck P., Ropke G.: "有限核における α 粒子凝縮状態", 京都大学基礎物理学研究所 滞在型研究会「原子核クラスター物理の現状と展望」, (京都大学基礎物理学研究所), 京都, 12 月 (2006).

玉川徹, 岩本慎也, 早藤麻美, 福島かおり, 浜垣秀樹, 山口頼人, 牧島一夫, 宮坂浩正, 桜井郁也, 門叶冬樹, 犬塚将英: "理研における GEM 開発の現状と将来", 第 3 回マイクロパターンガス検出器（MPGD）研究会, (佐賀大学), 佐賀, 1 月 (2007).

松本琢磨, 江上智晃, 緒方一介, 井芹康統, 八尋正信, 上村正康: "不安定核分解反応による di-neutron 相関の研究", RCNP 研究会「核子多体系におけるクラスター現象」, (大阪大学核物理研究センター), 大阪, 2 月 (2007).

船木靖郎, 山田泰一, Schuck P., 堀内昶, 東崎昭弘, Ropke G.: "^{16}O における 4 α 凝縮状態", RCNP 研究会「核子多体系におけるクラスター現象」, (大阪大学核物理研究センター), 茨木, 2 月 (2007).

小林徹, 加藤俊幸, 松尾由賀利, 西村美月, 河合純, 林崎良英: "フェムト秒レーザーアブレーションによるフラーレンのイオン化および解離", 第 32 回フラーレン・ナノチューブ総合シンポジウム, (フラーレン・ナノチューブ学会), 名古屋, 2–2 月 (2007).

松尾由賀利, 小林徹, 中嶋隆: "超短レーザーパルス誘起スピン偏極の光学的検出理研", 第 54 回応用物理学関係連合講演会, 相模原, 3 月 (2007).

古川武, 松尾由賀利, 畠山温, 伊藤龍浩, 藤掛浩太郎, 小林徹, 下田正: "超流動ヘリウム中に植え込まれた原子の超微細構造", 日本物理学会 2007 年春季大会, 鹿児島, 3 月 (2007).

小濱洋央, 飯田圭, 親松和浩: "くろたま模型で眺めた相互作用断面積", 日本物理学会 2007 年春季大会, 八王子, 3 月 (2007).

伊藤龍浩, 古川武, 松尾由賀利, 畠山温, 小林徹, 藤掛浩太郎, 小田島仁司, 下田正: "超流動ヘリウム中における Al の偏極生成", 日本物理学会 2007 年春季大会, 鹿児島, 3 月 (2007).

Applied Nuclear Physics Lab.

Publications

[**Journal**]

(Original Papers) ∗Subject to Peer Review

Adcox K., Bazilevsky A. V., Bunce G. M., Deshpande A., En'yo H., Fox B., Goto Y., Grosse Perdekamp M., Hayashi N., Ichihara T., Imai K., Ishihara M., Jacak B. V., Kobayashi H., Kurita K., Li Z., Mao Y., Murata J., Saito N., Sakuma T., Sato H., Shibata T., Sugioka M., Taketani A., Tojo J., Torii H., Watanabe Y., Yokkaichi S., and PHENIX C.: "PHENIX detector overview", Nuclear Instruments and Methods in Physics Research A **499**, 469–479 (2003). ∗

Akikawa H., En'yo H., Hayashi N., Ichihara T., Ishihara M., Kobayashi H., Kurita K., Li Z., Mao Y., Murata J., Saito N., Sato H., Shibata T., Sugioka M., Taketani A., Watanabe Y., Yokkaichi S., and PHENIX Collaboratio .: "PHENIX muon arms", Nuclear Instruments and Methods in Physics Research A **499**, 537–548 (2003). ∗

Murata J., Horaguchi T., Kamihara N., Kobayashi H., Shibata T., and PHENIX C.: "Optical alignment system for the PHENIX muon tracking chambers", Nuclear Instruments and Methods in Physics Research A **500**, 309–317 (2003). ∗

Yoshimi A., Asahi K., Emori S., Tsukui M., and Oshima S.: "Nuclear Spin Maser Oscillation of ^{129}Xe by Means of Optical-Detection Feedback", Hyperfine Interact. **159**, No. 1/4, pp. 401–405 (2004). ∗

Ishikawa D., Inui M., Matsuda K., Tamura K., Baron A., Tsutsui S., Tanaka Y., and Ishikawa T.: "Collective dynamics in dense Hg vapour", J. Phys.: Condens. Matter **16**, L45–L50 (2004). ∗

Tanaka Y., Baron A., Kim Y., Thomas K. J., Hill J. P., Honda Z., Iga F., Tsutsui S., and Ishikawa D.: "Search for orbitons in $LaMnO_3$, $YTiO_3$ and $KCuF_3$ using high-resolution inelastic x-ray scattering", New J. Phys. (Web) (http://www.iop.org/EJ/journal/NJP **6**, 161-1–161-13 (2004). ∗

Baron A., Uchiyama H., Tanaka Y., Tsutsui S.,

Ishikawa D., Lee S., Heid R., Bohnen K., Tajima S., and Ishikawa T.: "Kohn Anomaly in MgB_2 by Inelastic X-Ray Scattering", Phys. Rev. Lett. **92**, 197004-1–197004-4 (2004). ∗

Uchiyama H., Baron A., Tsutsui S., Tanaka Y., Hu W., Yamamoto A., Tajima S., and Endoh Y.: "Softening of Cu-O Bond Stretching Phonons in Tetragonal $HgBa_2CuO_{4+\delta}$", Phys. Rev. Lett. **92**, 197005-1–197005-4 (2004). ∗

Uchiyama H., Baron A., Tsutsui S., Tanaka Y., Hu W., Yamamoto A., Tajima S., and Endoh Y.: "Phonon softening in $HgBa_2CuO_{4+\delta}$ observed by inelastic X-ray scattering", Phys. Stat. Sol.(c) **1**, No. 11, pp. 3130–3133 (2004). ∗

Asahi K., Kameda D., Ueno H., Yoshimi A., Uchida M., Miyoshi H., Shimada K., Nagae D., Kijima G., Haseyama T., Watanabe H., Takemura M., Arai T., Oshima S., and Umeya A.: "Study of electromagnetic moments in unstable nuclei with radioactive nuclear beams", J. Phys.: Con. Ser. **20**, 59–64 (2005). ∗

Kobayashi Y., Nonaka H., Miyazaki J., Kubo K., Ueno H., Yoshimi A., Miyoshi H., Kameda D., Shimada K., Nagae D., Asahi K., and Yamada Y.: "Reaction of ^{57}Mn implanted into solid oxygen", Hyperfine Interact. **166**, 357–361 (2006). ∗

Kubo K., Kobayashi Y., Nonaka H., Yamada Y., Sakai Y., Shoji H., and Matsue H.: "Neutron in-beam Mossbauer spectroscopic study of iron disulfide at room temperature", Hyperfine Interact. **166**, 425–428 (2006). ∗

Sugimoto T., Nakamura T., Fukuda N., Miura M., Kondo Y., Aoi N., Baba H., Bazin D., Gomi T., Hasegawa H., Hashimoto Y., Imai N., Kobayashi T., Kubo T., Motobayashi T., Ohara M., Saito A., Sakurai H., Shimoura S., Attukalathil V. M., Watanabe K., Watanabe Y., Yakushiji T., Yanagisawa Y., Yoneda K., and Ishihara M.: "Invariant-mass spectroscopy of the neutron-drip line nucleus ^{14}Be", J. Phys.: Con. Ser. **49**, 43–44 (2006). ∗

Asahi K., Uchida M., Shimada K., Nagae D., Kameda D., Ueno H., Yoshimi A., Takemura M., Arai T., Takase K., Inoue T., Kawamura H., Murata J., Watanabe H., Haseyama T., Kobayashi Y., Umeya A., and Ishihara M.: "Structure of unstable nuclei from nuclear moments and decays", J. Phys.: Con. Ser. **49**, 79–84 (2006). ∗

Kameda D., Ueno H., Asahi K., Takemura M., Yoshimi A., Haseyama T., Uchida M., Shimada K., Nagae D., Kijima G., Arai T., Takase K., Suda S., Inoue T., Murata J., Kawamura H., Kobayashi Y., Watanabe H., and Ishihara M.: "Nuclear moments of neutron-rich ^{32}Al", J. Phys.: Con. Ser. **49**, 138–139 (2006). ∗

Yagi E., Koike S., Sugawara T., Shisido T., Urai T., and Ogiwara K.: "Displaced-T site occupancy of hydrogen in Nb alloyed with a high concentration of Mo", J. Phys. Soc. Jpn. **75**, No. 3, pp. 034802-1–034802-7 (2006). ∗

Tsutsui S., Kobayashi Y., Okada T., Haba H., Onodera H., Yoda Y., Mizumaki M., Tanida H., Uruga T., Sekine C., Shirotani I., Kikuchi D., Sugawara H., and Sato H.: "A Possible Novel Magnetic Ordering in $SmRu_4P_{12}$", J. Phys. Soc. Jpn. **75**, 0937031–0937034 (2006). ∗

Cole A., Akimunne H., Austin S., Bazin D., van den Berg A., Berg G., Brown J., Daito I., Fujita Y., Fujiwara M., Gupta S., Hara K., Harakeh M., Janecke J., Kawabata T., Nakamura T., Robert D., Sherril B., Steiner M., Ueno H., and Zegers R.: "Measurement of the Gamow-Teller Strength Distribution in ^{58}Co via the ^{58}Ni(t, ^{3}He) reaction at 115 MeV/nucleon", nucl-ex **0603019**, 1–14 (2006). ∗

Sato W., Ueno H., Taniguchi A., Itsuki Y., Kasamatsu Y., Shinohara A., Asahi K., Asai K., and Ohkubo Y.: "Nuclear quadrupole relaxation of ^{140}Ce implanted in highly oriented pyrolytic graphite", Phys. Rev. B **74**, No. 21, pp. 214302-1–214302-7 (2006). ∗

Zegers R., Akimune H., Austin S., Bazin D., van den Berg A., Berg G., Brown J., Cole A., Daito I., Fujita Y., Fujiwara M., Gales S., Harakeh M., Hashimoto H., Hayami R., Hitt G., Howard M., Itoh M., Janecke J., Kawabata T., Kawase K., Kinoshita M., Nakamura T., Nakanishi K., Nakayama S., Okumura S., Richter W., Roberts D., Sherrill B., Shimbara Y., Steiner M., Uchida M., Ueno H., Yamagata T., and Yosoi M.: "The (t,3He) and (3He,t) reactions as probes of Gamow-Teller strength", Phys. Rev. C **74**, 024309-1–024309-15 (2006). ∗

Furukawa T., Matsuo Y., Hatakeyama A., Fukuyama Y., Kobayashi T., Izumi H., and Shimoda T.: "Measurement of a long electronic spin relaxation time of cesium atoms in superfluid helium", Phys. Rev. Lett. **96**, No. 9, pp. 095301-1–095301-4 (2006). ∗

Yoshida Y., Kobayashi Y., Hayakawa K., Yukihira K., Yoshida A., Ueno H., Shimura F., and Ambe F.: "In situ observation of substitutional and interstitial Fe atoms in Si after GeV-implantation: An in-beam Mössbauer study", Physica B **376/377**, 69–72 (2006). ∗

(Review)

吉見彰洋: "スピン偏極した不安定核ビームの新しい生成方法を目指した装置開発", CYRIC ニュース **40**, 4–7 (2006).

八木栄一: "核反応チャネリング法で見た金属・合金中の水素の存在状態", 固体物理 **41**, No. 11, pp. 728–736 (2006).

Oral Presentations

(International Conference etc.)

Yoshimi A., Asahi K., Ueno H., Kameda D., Takemura M., Uchida M., Shimada K., Nagae D., Arai T.,

Takase K., Inoue T., Kawamura H., Murata J., Kijima G., and Haseyama T.: "Electric quadrupole moments of neutron rich Al isotope", International Symposium on Exotic Nuclei (EXON 2006), (GSI, GANIL, RIKEN), Khanty-Mansiysk, Russia, July–July (2005).

Furukawa T., Matsuo Y., Hatakeyama A., Fukuyama Y., Kobayashi T., Izumi H., and Shimoda T.: "New laser spectroscopic method for the measurement of nuclear moments", 2nd Joint Meeting of the Nuclear Physics Divisions of the APS and JPS (Hawaii 2005), Maui, USA, Sept. (2005).

Furukawa T., Matsuo Y., Hatakeyama A., Ito T., Ota Y., Fukuyama Y., Kobayashi T., and Shimoda T.: "Laser-microwave double resonance method in superfluid helium for the measurement of nuclear moments", 11th International Workshop on Polarized Sources and Targets (PST05), (CNS and RIKEN), Tokyo, Nov. (2005).

Kameda D., Asahi K., Ueno H., Yoshimi A., Watanabe H., Haseyama T., Kobayashi Y., Uchida M., Shimada K., Nagae D., Kato G., Emori S., Kijima G., Takemura M., Arai T., Oshima S., Tsukui M., Yagi E., Kubo T., Yoshida A., and Ishihara M.: "Production of spin-polarized RI beams via projectile fragmentation and the application to nuclear moment measurements", 11th International Workshop on Polarized Sources and Targets (PST05), (RIKEN and The Center for Nuclear Study (CNS)), Tokyo, Nov. (2005).

Asahi K.: "Radioactive nuclear beams as microscopic probes in matter", University of California at Berkeley and Tokyo Institute of Technology Interdepartment Symposium on Nanoscience and Quantum Physics, Berkeley, USA, Jan. (2006).

Ueno H.: "Production of RI beams with RIPS in the RIBF configuration", Pre-Meeting "Council for China-Japan Research Collaboration on Nuclear Physics", Wako, Feb. (2006).

Sugimoto T., Nakamura T., Fukuda N., Miura M., Kondo Y., Aoi N., Baba H., Bazin D., Gomi T., Hasegawa H., Hashimoto Y., Imai N., Kobayashi T., Kubo T., Motobayashi T., Ohara M., Saito A., Sakurai H., Shimoura S., Attukalathil V. M., Watanabe K., Watanabe Y., Yakushiji T., Yanagisawa Y., Yoneda K., and Ishihara M.: "Invariant-mass spectroscopy of the neutron-drip line nucleus ^{14}Be", International Symposium on Structure of Exotic Nuclei and Nuclear Forces (SENUF06), (CNS and RIKEN), Tokyo, Mar. (2006).

Kameda D., Asahi K., Ueno H., Yoshimi A., Haseyama T., Watanabe H., Uchida M., Shimada K., Nagae D., Takemura M., Arai T., Kijima G., Takase K., Suda S., Inoue T., Kobayashi Y., Yagi E., Kubo T., Yoshida A., and Ishihara M.: "Nuclear moments of neutron-rich ^{32}Al($Z = 11, N = 19$)", International Symposium on Structure of Exotic Nuclei and Nuclear Forces (SENUF06), (The Center for Nuclear Study (CNS)), Tokyo, Mar. (2006).

Asahi K.: "Structure of unstable nuclei from nuclear moments and beta decays", International Symposium on Structure of Exotic Nuclei and Nuclear Forces (SENUF06), (CNS and RIKEN), Tokyo, Mar. (2006).

Yoshimi A., Asahi K., Uchida M., Inoue T., and Oshima S.: "Electric dipole moment induced from nucleus", International Workshop on "Nuclear Physics with RIBF", Wako, Mar. (2006).

Kameda D., Ueno H., Asahi K., Yoshimi A., Haseyama T., Watanabe H., Uchida M., Nagae D., Shimada K., Takemura M., Arai T., Takase K., Inoue T., Kato G., Kijima G., Emori S., Suda S., Tsukui M., Murata J., Kawamura H., Kobayashi Y., Yagi E., Kubo T., and Ishihara M.: "Nuclear moment measurements using spin-polarized RI beams via projectile fragmentation: Recent results and the prospect in RIBF", International Workshop on "Nuclear Physics with RIBF", Wako, Mar. (2006).

Ueno H.: "Present and future program driven by polarized-RI beams", International Workshop on "Nuclear Physics with RIBF", Wako, Mar. (2006).

Murata J.: "T-Violation Experiment using Electron Polarimeter", International Workshop on "Nuclear Physics with RIBF", Tokyo, Mar. (2006).

Ueno H.: "Nuclear moments of neutron-rich aluminum isotopes", 7th International Conference on Radioactive Nuclear Beams (RNB7), Cortina d'Ampezzo, Italy, July (2006).

Ueno H.: "Nuclear-moment research in RIKEN", 1st Annual RI Beam Factory (RIBF) Users Meeting 2006, Wako, Aug. (2006).

Ueno H.: "Study of unstable nuclei through the measurement of nuclear moments", 5th CNS International Summer School (CISS06), Wako, Aug. (2006).

Kameda D., Asahi K., Ueno H., Yoshimi A., Haseyama T., Watanabe H., Uchida M., Shimada K., Nagae D., Kijima G., Takemura M., Takase K., Arai T., Inoue T., Suda S., Murata J., Kawamura H., Kobayashi Y., and Ishihara M.: "Nuclear moments of neutron-rich ^{32}AL: Shell structure around the "Island of Inversion"", The XI International Conference on Nucleus Nucleus Collisions (NN2006), (University of Sao Paulo), Rio de Janeiro, Brazil, Aug.–Sept. (2006).

Ueno H.: "Measurement of nuclear moments at RIKEN", Tours Symposium on Nuclear Physics VI (TOURS 2006), Tours, France, Sept. (2006).

Nagatomo T., Minamisono K., Matsuta K., Levy C. D., Sumikama T., Ozawa A., Tagisi Y., Mihara M., Ogura M., Matsumiya R., Fukuda M., Yamaguchi M., Behr J. A., Jackson K. P., Fujiwara H., Ohta H., Yasuno T., Hashizume Y., and Minamisono T.: "Alignment Correlation Terms In β-Ray An-

gular Distributions From Spin Aligned ^{20}F And ^{20}Na", 17th International Spin Physics Symposium (SPIN2006), (Kyoto University), Kyoto, Oct. (2006).

Murata J., Asahi K., Kameda D., Kawamura H., Nagae D., Narota K., Shimada K., Toyoda T., Uchida M., Ueno H., and Yoshimi A.: "Beta Neutrino Correlation and T-Violation Experiment in Nuclear Beta Decay", 17th International Spin Physics Symposium (SPIN2006), (Department of Physics, Kyoto University), Kyoto, Oct. (2006).

Yoshimi A., Ueno H., Sugimoto T., Shimada K., Nagae D., Murata J., Kawamura H., Kameda D., and Asahi K.: "Development of Atomic Beam Resonance Method with RI beams", 17th International Spin Physics Symposium (SPIN2006), (Kyoto University), Kyoto, Oct. (2006).

Nagae D., Asahi K., Ueno H., Kameda D., Takemura M., Takase K., Yoshimi A., Sugimoto T., Nagatomo T., Kobayashi Y., Uchida M., Shimada K., Arai T., Inoue T., Kagami S., and Hatakeyama N.: "Experimental technique for nuclear moment measurements by the β-NMR method using spin polarized RI beams via projectile fragmentation reaction", 17th International Spin Physics Symposium (SPIN2006), (Kyoto University), Kyoto, Oct. (2006).

Kameda D., Asahi K., Ueno H., Yoshimi A., Haseyama T., Watanabe H., Uchida M., Nagae D., Shimada K., Takemura M., Arai T., Takase K., Inoue T., Suda S., Kobayashi Y., Murata J., Kawamura H., and Ishihara M.: "Nuclear moment measurements of neutron-rich Al isotopes using spin-polarized RI beams: Determination of the boundary of the "island of inversion"", 17th International Spin Physics Symposium (SPIN2006), (Kyoto University), Kyoto, Oct. (2006).

Ueno H.: "Nuclear-moment measurements at RIKEN and perspectives in RIBF", 17th International Spin Physics Symposium (SPIN2006), (Kyoto University), Kyoto, Oct. (2006).

Shimada K., Nagae D., Asahi K., Arai T., Takemura M., Inoue T., Takase K., Kagami S., Hatakeyama N., Kobayashi Y., Ueno H., Yoshimi A., Kameda D., Nagatomo T., Sugimoto T., Kubono S., Yamaguchi H., Wakabayashi Y., Amadio G., Hayakawa S., Murata J., and Kawamura H.: "Production of Polarized Radioactive Beams via The Inverse-kinematics Reactions and Their Applications", 17th International Spin Physics Symposium (SPIN2006), (Kyoto University), Kyoto, Oct. (2006).

Asahi K., Uchida M., Yoshimi A., Inoue T., and Oshima S.: "Search for an Atomic EDM with optical-coupling nuclear spin oscillator", 17th International Spin Physics Symposium (SPIN2006), (Kyoto University), Kyoto, Oct. (2006).

Yagi E., Hayashi T., Koike S., Yoshida T., Higami N., Hirabayashi K., Takebayashi A., and Ogiwara K.: "Lattice location of hydrogen in β -V_2H", International Symposium on Metal-Hydrogen Systems: Fundamentals and Applications (MH2006), Hawaii, USA, Oct. (2006).

(Domestic Conference)

上野秀樹: "停止・低速 RIB を用いた核モーメント測定", 第 2 回「停止・低速不安定核ビームを用いた核分光研究」研究会, (理研，KEK 他), 東海, 3 月 (2006).

亀田大輔: "中性子過剰 Al 同位体の核モーメントと周辺の殻構造", 理研シンポジウム「電磁モーメント，低エネルギー核分光から探る不安定核の構造—その現状と将来的課題—」, 和光, 3 月 (2006).

亀田大輔: "イントルーダー領域の中性子過剰核の電磁気モーメント測定", RIBF ミニワークショップ「Island of Inversion に関する実験・理論の現状と今後の展望–$7 < Z < 20$ 領域中性子過剰核の低励起状態に関する検討会–」, 和光, 5 月 (2006).

杉本崇: "中性子ドリップライン核 ^{14}Be の不変質量核分光", RIBF 核物理セミナー, 和光, 5 月 (2006).

古川武, 松尾由賀利, 畠山温, 伊藤龍浩, 太田嘉穂, 藤掛浩太郎, 小林徹, 下田正: "超流動ヘリウム中に植え込まれた原子の超微細構造", 原子・分子・光科学 (AMO) 第 3 回討論会, 東京, 6 月 (2006).

杉本崇: "Invariant-mass Spectroscopy of ^{14}Be", 第 5 回 CNS 国際サマースクール (CISS06), (東京大学原子核科学研究センター (CNS)), 和光, 8 月 (2006).

八木栄一, 平林和紘, 村上洋一, 小池茂年, 樋上直太, 林達也, 武林昭子, 吉田徹, 飯田敬, 菅原孝昌, 宍戸統悦, 荻原清: "酸素を添加した Nb 中の水素の存在状態", 日本物理学会 2006 年秋季大会, (日本物理学会), 千葉, 9 月 (2006).

古川武, 松尾由賀利, 畠山温, 伊藤龍浩, 太田嘉穂, 藤掛浩太郎, 小林徹, 下田正: "超流動ヘリウム中のアルカリ金属原子のスピン偏極および磁気共鳴", 日本物理学会 2006 年秋季大会, 奈良, 9 月 (2006).

古川武, 松尾由賀利, 畠山温, 伊藤龍浩, 太田嘉穂, 藤掛浩太郎, 小林徹, 下田正: "超流動ヘリウム中に植え込まれた原子の超微細構造", 第 3 回「停止・低速不安定核を用いた核分光研究」研究会, (京都大学原子炉実験所), 大阪府熊取, 11 月 (2006).

古川武, 松尾由賀利, 畠山温, 伊藤龍浩, 太田嘉穂, 藤掛浩太郎, 小林徹, 下田正: "超流動ヘリウム中におけるアルカリ金属原子の超微細構造", RIBF ミニワークショップ「レーザー光利用の次世代加速器実験：その発展と物理学への貢献」, 和光, 11 月 (2006).

吉見彰洋, 上野秀樹, 杉本崇, 旭耕一郎, 島田健司, 長江大輔, 亀田大輔, 村田次郎, 川村広和: "原子線法を用いた RI の核偏極生成のための開発研究", 平成 18 年度京都大学原子炉実験所専門研究会「原子核プローブ生成とそれを用いた物性研究 (II)」, 大阪府熊取, 11–11 月 (2006).

長友傑, 南園啓, 松多健策, Levy C. D., 三原基嗣, 炭竈聡之, 小沢顕, 田岸義宏, 小倉昌子, 松宮亮平, 福田光順, 山口充孝, Behr J. A., Jackson K. P., 藤原弘樹, 安野琢磨, 太田寛史, 橋爪祐平, 千葉明子, 南園忠則: "ベータ NMR 法を用いた質量数 20 体系の β 線角度分布の精密測定による第二種核子流の探索", 平成

18 年度京都大学原子炉実験所専門研究会「原子核プローブ生成とそれを用いた物性研究 (II)」, 大阪府熊取, 11–11 月 (2006).

吉見彰洋, 旭耕一郎, 内田誠, 井上壮志, 畠山直人: "低周波核スピンメーザーの開発と ^{129}Xe 原子 EDM 探索への応用", RIBF ミニワークショップ「レーザー光利用の次世代加速器実験：その発展と物理学への貢献」, 和光, 11–12 月 (2006).

杉本崇, 吉見彰洋, 上野秀樹, 村田次郎, 川村広和, 長江大輔, 島田健司, 旭耕一郎: "偏極不安定核生成のための原子線共鳴法の開発", 日本物理学会 2007 年春季大会, 八王子, 3 月 (2007).

古川武, 松尾由賀利, 畠山温, 伊藤龍浩, 藤掛浩太郎, 小林徹, 下田正: "超流動ヘリウム中に植え込まれた原子の超微細構造", 日本物理学会 2007 年春季大会, 鹿児島, 3 月 (2007).

伊藤龍浩, 古川武, 松尾由賀利, 畠山温, 小林徹, 藤掛浩太郎, 小田島仁司, 下田正: "超流動ヘリウム中における Al の偏極生成", 日本物理学会 2007 年春季大会, 鹿児島, 3 月 (2007).

Radioactive Isotope Physics Lab.

Publications

[**Journal**]

(Original Papers) ＊Subject to Peer Review

Takeuchi S., Aoi N., Baba H., Fukui T., Hashimoto Y., Ieki K., Imai N., Iwasaki H., Kanno S., Kondo Y., Kubo T., Kurita K., Minemura T., Motobayashi T., Nakabayashi T., Nakamura T., Okumura T., Onishi T., Ota S., Sakurai H., Shimoura S., Sugo R., Suzuki D., Suzuki H., Suzuki M., Takeshita E., Tamaki M., Tanaka K., Togano Y., and Yamada K.: "Proton inelastic scattering on ^{32}Mg", J. Phys.: Con. Ser. **49**, 153–154 (2006). ＊

Yoshida K., Yamagami M., and Matsuyanagi K.: "Pairing and continuum effects on low-frequency quadrupole vibrations in deformed Mg isotopes close to the neutron drip line", Nucl. Phys. A **779**, 99–115 (2006). ＊

Michimasa S., Shimoura S., Iwasaki H., Tamaki M., Ota S., Aoi N., Baba H., Iwasa N., Kanno S., Kubono S., Kurita K., Uesaka M., Minemura T., Motobayashi T., Notani M., Ong H., Saito A., Sakurai H., Takeshita E., Takeuchi S., Yanagisawa Y., and Yoshida A.: "Proton single-particle states in the neutron-rich ^{23}F nucleus", Phys. Lett. B **638**, 146–152 (2006). ＊

Majima T., Nakai Y., Mizuno T., Tsuchida H., and Itoh A.: "Fragmentation processes of C_{60} in multiple electron loss and capture collisions of 2-MeV Si^{2+}", Phys. Rev. A **74**, 033201-1–033201-7 (2006). ＊

Nakamura T., Wada M., Okada K., Ishida Y., Takamine A., Yamazaki Y., Kambara T., Kanai Y., Kojima T., Nakai Y., Oshima N., Yoshida A., Kubo T., Katayama I., Lioubimov V., Wollnik H., Varentsov V., and Schuessler H. A.: "Laser spectroscopy of ^{7,10}Be^{+} in an online ion trap", Phys. Rev. A **74**, 052503-1–052503-5 (2006). ＊

Hagino K., Lwin N. W., and Yamagami M.: "Deformation parameter for diffuse density", Phys. Rev. C **74**, 017310-1–017310-4 (2006). ＊

[**Book・Proc.**]

(Review)

佐藤勝彦, 望月優子: "元素の起源", シリーズ現代の天文学 I　人類の住む宇宙, 日本評論社, 東京, pp. 94–137 (2007).

(Others)

望月優子: "Investigating the origin of the elements with RI-Beam Factory", 密封・非密封事業所を対象とした平成 18 年度放射線業務従事者のための教育訓練講習会 II テキスト, 京都, 2006–10, 日本アイソトープ協会, 京都, pp. 17–27 (2006).

Oral Presentations

(International Conference etc.)

Baba H., Shimoura S., Minemura T., Matsuyama Y., Saito A., Ryuto H., Aoi N., Gomi T., Higurashi Y., Ieki K., Imai N., Iwasa N., Iwasaki H., Kanno S., Kubono S., Kunibu M., Michimasa S., Motobayashi T., Nakamura T., Sakurai H., Serata M., Takeshita E., Takeuchi S., Ue K., Teranishi T., Yamada K., and Yanagisawa Y.: "Isoscalar monopole and dipole responses in unstable nucleus ^{14}O", Direct Reactions with Exotic Beams (DREB2005), (Michigan State University), East Lansing, June (2005).

Togano Y., Gomi T., Motobayashi T., Ando Y., Aoi N., Baba H., Demichi K., Elekes Z., Fukuda N., Fulop Z., Hasegawa H., Higurashi Y., Ieki K., Imai N., Ishihara M., Ishikawa K., Iwasa N., Iwasaki H., Kanno S., Kondo Y., Kubo T., Kubono S., Kurita K., Matsuyama Y., Michimasa S., Minemura T., Miura M., Murakami H., Nakamura T., Notani M., Ota S., Saito A., Sakurai H., Serata M., Shimoura S., Sugimoto T., Takeshita E., Takeuchi S., Ue K., Yamada K., Yanagisawa Y., Yoneda K., Yoshida A., Futakami U., and Kunibu M.: "Coulomb dissociation of ^{27}P for Study of ^{26}Si(p,γ)^{27}P reaction", 2nd Joint Meeting of the Nuclear Physics Divisions of the APS and JPS (Hawaii 2005), Maui, USA, Sept. (2005).

Michimasa S., Aoi N., Iwasa N., Iwasaki H., Kanno S., Kubono S., Kurita K., Minemura T., Motobayashi T., Notani M., Ong H., Ota S., Saito A., Shimoura S., Takeshita E., Tamaki M., Uesaka M., Yanagisawa Y., Yoshida A., Sakurai H., Takeuchi S., and Baba H.: "Measurement of proton transfer reaction for single-particle states in ^{23}F", 2nd Joint Meeting of the Nuclear Physics Divisions of the APS and JPS (Hawaii 2005), Maui, USA, Sept. (2005).

Kanno S., Aoi N., Takeuchi S., Sakurai H., Glasmacher T., Mueller W. F., Bazin D., Bowen M. D., Campbell C. M., Cook J. M., Dinca D., Gade A., Iwasaki H., Kubo T., Kurita K., Motobayashi T., Nakamura T.,

Suzuki H., Terry J. R., Zwahlen H., and Yoneda K.: "Proton Inelastic scattering on ^{74}Ni", 2nd Joint Meeting of the Nuclear Physics Divisions of the APS and JPS (Hawaii 2005), Maui, USA, Sept. (2005).

Takeuchi S., Aoi N., Baba H., Fukui T., Hashimoto Y., Ieki K., Imai N., Iwasaki H., Kanno S., Kondo Y., Kurita K., Minemura T., Motobayashi T., Nakabayashi T., Nakamura T., Okumura T., Onishi T., Ota S., Sakurai H., Shimoura S., Sugo R., Suzuki D., Suzuki H., Suzuki M., Takeshita E., Tamaki M., Tanaka K., Togano Y., and Yamada K.: "Proton inelastic scattering of ^{32}Mg", International Symposium on Structure of Exotic Nuclei and Nuclear Forces (SENUF06), (University of Tokyo), Tokyo, Mar. (2006).

Yamagami M.: "New insight into collective excitations from the novel concept of single-particle motions in weakly-bound superfluid nuclei", International Workshop on "Nuclear Physics with RIBF", Wako, Mar. (2006).

Baba H., Shimoura S., Saito A., Minemura T., Matsuyama Y., Ryuto H., Aoi N., Gomi T., Higurashi Y., Ieki K., Imai N., Iwasa N., Iwasaki H., Kanno S., Kubono S., Kunibu M., Michimasa S., Motobayashi T., Nakamura T., Sakurai H., Serata M., Takeshita E., Takeuchi S., Teranishi T., Ue K., Yamada K., and Yanagisawa Y.: "Isoscalar compressional strengths in ^{14}O", 2nd International Conference on Collective Motion in Nuclei Under Extreme Conditions (COMEX2), (TU Darmstadt, GSI), Sankt Goar, Germany, June (2006).

Motizuki Y. and Madokoro H.: "The late-time supernova evolution induced by anisotropic neutrino radiation and the r-process environment (a poster paper)", International Symposium on Nuclear Astrophysics: Nuclei in the Cosmos 9, Geneva, Switzerland, June (2006).

Motizuki Y.: "Activities in Nuclear Astrophysics at Riken Nishina Center", Opening meeting of Japan-US Theory Institute for Physics with Exotic Nuclei, Wako, June (2006).

Azuma T., Nakano Y., Kondo C., Hatakeyama A., Komaki K., Nakai Y., Yamazaki Y., Takada E., and Murakami T.: "Autler-Townes doublet observed through doubly resonant coherent excitation", 22nd International Conference on Atomic Collisions in Solids (ICACS 2006), Berlin, Germany, July (2006).

Yamagami M.: "Pairing and continuum effects for low-frequency vibrational excitations", International Conference on Nuclei at the limits "Nuclear Structure '06", (Oak Ridge National Laboratory), Oak Ridge, USA, July (2006).

Azuma T., Nakano Y., Kondo C., Hatakeyama A., Komaki K., Nakai Y., Yamazaki Y., Takada E., and Murakami T.: "Crystal-dressed HCI observed through doubly-resonant coherent excitation", 13th International Conference on the Physics of Highly Charged Ions (HCI 2006), (Scool of Physics of University College Dublin and School of Physics l Science of Dublin City University), Belfast, UK, Aug.–Sept. (2006).

Michimasa S., Shimoura S., Iwasaki H., Tamaki M., Ota S., Aoi N., Baba H., Iwasa N., Kanno S., Kubono S., Kurita K., Minemura T., Motobayashi T., Notani M., Ong H., Saito A., Sakurai H., Takeshita E., Takeuchi S., Uesaka M., Yanagisawa Y., and Yoshida A.: "Proton shell structure in neutron-rich ^{23}F", International Conference on Nucleus Nucleus Collisions (NN2006), Rio de Janeiro, Brazil, Aug.–Sept. (2006).

Morita K., Morimoto K., Kaji D., Akiyama T., Goto S., Haba H., Ideguchi E., Katori K., Kikunaga H., Koura H., Kudo H., Ohnishi T., Ozawa A., Suda T., Sato N., Sueki K., Tokanai F., Xu H., Yamaguchi T., Yoneda A., Yoshida A., and YuLiang Z.: "Experiments on Synthesis of the Heaviest Elements at RIKEN (SHE and FFD)", Tours Symposium on Nuclear Physics VI (TOURS 2006), (Konan University), Tours, France, Sept. (2006).

Morita K., Morimoto K., Kaji D., Akiyama T., Goto S., Haba H., Ideguchi E., Katori K., Kikunaga H., Koura H., Kudo H., Ohnishi T., Ozawa A., Suda T., Sato N., Sueki K., Tokanai F., Xu H., Yamaguchi T., Yoneda A., Yoshida A., and YuLiang Z.: "Experiments on Synthesis of the Heaviest Elements at RIKEN Status and Perspectives", Workshop on the Atomic Properties of the Heaviest Elements: Towards the Island of Stability, (LMU-Muenchen), Germany, Chiemsee, Sept. (2006).

Baba H., Shimoura S., Saito A., Minemura T., Matsuyama Y., Ryuto H., Aoi N., Gomi T., Higurashi Y., Ieki K., Imai N., Iwasa N., Iwasaki H., Kanno S., Kubono S., Kunibu M., Michimasa S., Motobayashi T., Nakamura T., Sakurai H., Serata M., Takeshita E., Takeuchi S., Teranishi T., Ue K., Yamada K., and Yanagisawa Y.: "Highly excited states of ^{14}O with the (α,α') reaction", 2nd German-Japanese Workshop on Nuclear Structure and Astrophysics, (RIKEN, CNS, DFG, GSI), Wako, Oct. (2006).

Yamagami M.: "Pairing effects for collective excitations in weakly-bound nuclei", 2nd German-Japanese Workshop on Nuclear Structure and Astrophysics, Wako, Oct. (2006).

Motizuki Y. and Madokoro H.: "The late-time supernova evolution induced by anisotropic neutrino radiation and the r-process environment (I)", 2nd German-Japanese Workshop on Nuclear Structure and Astrophysics, Wako, Oct. (2006).

Madokoro H. and Motizuki Y.: "The late-time supernova evolution induced by anisotropic neutrino radiation and the r-process environment (II) -Effect of ν interactions", 2nd German-Japanese Workshop on Nuclear Structure and Astrophysics, Wako, Oct.

(2006).

Morita K., Morimoto K., Kaji D., Akiyama T., Goto S., Haba H., Ideguchi E., Katori K., Kikunaga H., Koura H., Kudo H., Ohnishi T., Ozawa A., Suda T., Sato N., Sueki K., Tokanai F., Xu H., Yamaguchi T., Yoneda A., Yoshida A., and YuLiang Z.: "Search for the Heaviest Elements at RIKEN", 6th International Symposium on Advanced Science Research: Frontiers of Nuclear and Radiochemistry (ASR2006), (Advanced Science Research Center, Japan Atomic Energy Agency), Tokaimura, Oct. (2006).

Motizuki Y., Makishima K., Takahashi K., Igarashi M., Bamba A., Nakai Y., Yano Y., Motoyama H., Kamiyama K., and Suzuki K.: "Antarctic ice as a probe of historical supernovae", The Extreme Universe in the Suzaku Era, Kyoto, Dec. (2006).

Motizuki Y. and Madokoro H.: "High entropy feasible for the r-process nucleosynthesis in 2-D hydrodynamical simulations of core-collapse supernovae(a poster paper)", International conference on Twenty Years after SN1987A, Waikoloa, USA, Feb. (2007).

(Domestic Conference)

山上雅之: "弱束縛系における一粒子波動関数の空間的構造変化：対相関と変形効果の競合", 日本物理学会第 60 回年次大会, (日本物理学会), 野田, 3 月 (2005).

山上雅之: "独立粒子描像の新展開", 小規模ワークショップ「RIBF に於ける γ 線核分光」, 和光, 2 月 (2006).

竹下英里, 青井考, 大田晋輔, 武内聡, 鈴木宏, 馬場秀忠, Bishop S., 福井利晃, 井手口栄治, 家城和夫, 今井伸明, 岩崎弘典, 菅野祥子, 近藤洋介, 久保敏幸, 栗田和好, 日下健祐, 峯村俊行, 本林透, 中林彩, 中村隆司, 中尾太郎, 新倉潤, 奥村俊文, 王惠仁, 大西健夫, 櫻井博儀, 下浦享, 須合亮平, 鈴木大介, 鈴木賢, 玉城充, 田中鐘信, 栂野泰宏, 山田一成: "中性子過剰核 Cr 同位体の陽子非弾性散乱", 日本物理学会第 61 回年次大会, 松山, 3 月 (2006).

道正新一郎, 下浦享, 岩崎弘典, 玉城充, 大田晋輔, 青井考, 馬場秀忠, 岩佐直仁, 菅野祥子, 久保野茂, 栗田和好, 峯村俊行, 本林透, 野谷将広, 王惠仁, 齋藤明登, 櫻井博儀, 竹下英里, 武内聡, 上坂明子, 柳澤善行, 吉田敦: "Single-particle states in ^{23}F by a proton transfer reaction", 日本物理学会第 61 回年次大会, (日本物理学会), 松山, 3 月 (2006).

山上雅之: "Di-neutron correlation in neutron-rich Mg isotopes", 日本物理学会第 61 回年次大会, (日本物理学会), 松山, 3 月 (2006).

炭竈聡之, 長友傑, 小倉昌子, 岩越丈尚, 中島良樹, 藤原裕樹, 松多健策, 南園忠則, 福田光順, 三原基嗣, 南園啓, 山口貴之: "質量数 A=8 体系 β 崩壊における中間子交換効果", 日本物理学会第 61 回年次大会, 松山, 3 月 (2006).

望月優子: "Investigating the origin of the elements with RI-Beam Factory", 教育セミナー (放射線業務従事者再教育), (東北原子力懇談会), 仙台, 4 月 (2006).

望月優子, 高橋和也, 馬場彩, 牧島一夫, 矢野安重, 五十嵐誠, 本山秀明, 神山孝吉, 鈴木啓助, 二河久子: "Solar cycles of 1000 years ago discovered from Antarctic ice core", 日本地球惑星科学連合 2006 年大会, 千葉, 5 月 (2006).

山上雅之: "不安定核における "自発的対称性の破れ" の発現機構", RIBF ミニワークショップ「Island of Inversion に関する実験・理論の現状と今後の展望–7 < Z < 20 領域中性子過剰核の低励起状態に関する検討会–」, (理研), 和光, 5 月 (2006).

武内聡, 青井考, 馬場秀忠, 福井利晃, 橋本佳子, 家城和夫, 今井伸明, 岩崎弘典, 菅野祥子, 近藤洋介, 栗田和好, 峯村俊行, 本林透, 中林彩, 中村隆司, 奥村俊文, 大西健夫, 大田晋輔, 櫻井博儀, 下浦享, 須合亮平, 鈴木大介, 鈴木宏, 鈴木賢, 竹下英里, 玉城充, 田中鐘信, 栂野泰宏, 山田一成: "^{32}Mg と ^{34}Si の γ 線核分光", RIBF ミニワークショップ「Island of Inversion に関する実験・理論の現状と今後の展望–7 < Z < 20 領域中性子過剰核の低励起状態に関する検討会–」, 和光, 5 月 (2006).

望月優子: "Investigating history of supernove and solar activities with Antarctice ice core (invited)", 星間物質ワークショップ 2006, (北海道大学), 札幌, 7–8 月 (2006).

金井保之, 中井陽一, 岩井良夫, 山崎泰規, 西尾和之, 益田秀樹: "金属キャピラリー通過後の多価イオンからの Auger 電子", 原子衝突研究協会第 31 回研究会, (原子衝突研究協会), 岡崎, 8 月 (2006).

中野祐司, 井上岳史, 近藤力, 東俊行, 畠山温, 中井陽一, 小牧研一郎, 山崎泰規, 高田栄一, 村上健: "結晶周期場により形成された重イオンのドレスト状態", 原子衝突研究協会第 31 回研究会, 岡崎, 8 月 (2006).

水野智也, 尾家隆司, 中井陽一, 土田秀次, 伊藤秋男: "MeV 重イオン衝突による二原子分子電離過程の配向依存性", 原子衝突研究協会第 31 回研究会, 岡崎市, 8 月 (2006).

近藤力, 中野祐司, 真杉三郎, 村中友子, 東俊行, 畠山温, 中井陽一, 小牧研一郎, 山崎泰規, 高田栄一, 村上健: "Resonant coherent excitation under a channeling condition in a thin crystal", 原子衝突研究協会第 31 回研究会, 岡崎, 8 月 (2006).

山上雅之: "重い不安定核における集団運動", KEK 研究会「現代の原子核物理–多様化し進化する原子核の描像–」, (高エネルギー加速器研究機構), つくば, 8 月 (2006).

東俊行, 中野祐司, 井上正人, 近藤力, 畠山温, 小牧研一郎, 中井陽一, 山崎泰規, 高田栄一, 村上健: "3 次元コヒーレント共鳴励起を利用した 2 重共鳴", 日本物理学会 2006 年秋季大会, 千葉, 9 月 (2006).

田中鐘信, 山口貴之, 鈴木健, 小沢顕, 相場健, 青井考, 泉川卓司, 稲福清彦, 岩佐直仁, 上坂明子, 大坪隆, 小林圭, 小室麻里, 近藤洋介, 篠田遼子, 篠原摩有子, 鈴木宏, 武内聡, 竹下英里, 武智麻耶, 栂野泰宏, 中島真平, 中林彩, 馬場秀忠, 橋爪祐平, 福田光順, 松山貴史, 道正新一郎, 安野琢磨, 山田一成, 吉竹利織, 久保敏幸, 中村隆司, 櫻井博儀, 本林透: "中性子過剰核 ^{19,20,22}C の反応断面積測定", 日本物理学会 2006 年秋季大会, 奈良, 9 月 (2006).

水野智也, 尾家隆司, 中井陽一, 土田秀次, 伊藤秋男: "高速重イオン荷電変換衝突に伴う CO 分子電離分解過

程の分子配向依存性", 日本物理学会 2006 年秋季大会, 千葉, 9 月 (2006).

中野祐司, 近藤力, 東俊行, 畠山温, 小牧研一郎, 中井陽一, 山崎泰規, 高田栄一, 村上健: "結晶周期場により形成される重イオンのドレスト状態の観測", 日本物理学会 2006 年秋季大会, 千葉, 9 月 (2006).

中井陽一, 中野祐司, 池田時浩, 金井保之, 神原正, 福西暢尚, 近藤力, 東俊行, 小牧研一郎, 山崎泰規: "チャネリング条件下におけるリチウム様 Fe イオンのコヒーレント共鳴励起:エネルギー付与との同時計測", 日本物理学会 2006 年秋季大会, 千葉, 9 月 (2006).

山上雅之, 清水良文: "不安定核における低エネルギー回転運動", 日本物理学会 2006 年秋季大会, 奈良, 9 月 (2006).

山上雅之: "Continuum effect for collective excitations in deformed weakly-bound nuclei", ミニワークショップ「原子核平均場模型の現代的展開」, (会津大学), 会津若松, 10 月 (2006).

山上雅之: "重い不安定核における新しい超流動性と集団運動", RIBF ミニワークショップ「RIBF に於ける γ 分光実験 (II)」, (理研), 和光, 10 月 (2006).

望月優子: "Investigating the origin of the elements with RI-Beam Factory", 放射線業務従事者のための教育訓練講習会, (日本アイソトープ協会), 京都, 10 月 (2006).

五十嵐誠: "ドームふじ浅層コアに記録されている超新星爆発の痕跡探査経過報告", 極域気水圏・生物合同シンポジウム 2006, (国立極地研究所), 東京, 11 月 (2006).

田中鐘信, 山口貴之, 鈴木健, 小沢顕, 相場健, 青井考, 泉川卓司, 稲福清彦, 岩佐直仁, 上坂明子, 大坪隆, 小林圭, 小室麻里, 近藤洋介, 篠田遼子, 篠原摩有子, 鈴木宏, 武内聡, 竹下英里, 武智麻耶, 梅野泰宏, 中島真平, 中林彩, 馬場秀忠, 橋爪祐平, 福田光順, 松山貴史, 道正新一郎, 安野琢磨, 山田一成, 吉竹利織, 久保敏幸, 中村隆司, 櫻井博儀, 本林透: "22C 及び炭素同位体の反応断面積実験", RIBF ミニワークショップ「反応断面積で探る核構造」, (RIKEN), 和光, 11 月 (2006).

長友傑, 南園啓, 松多健策, Levy C. D., 三原基嗣, 炭竈聡之, 小沢顕, 田岸義宏, 小倉昌子, 松宮亮平, 福田光順, 山口充孝, Behr J. A., Jackson K. P., 藤原弘樹, 安野琢磨, 太田寛史, 橋爪祐平, 千葉明子, 南園忠則: "ベータ NMR 法を用いた質量数 20 体系の β 線角度分布の精密測定による第二種核子流の探索", 平成 18 年度京都大学原子炉実験所専門研究会「原子核プローブ生成とそれを用いた物性研究 (II)」, 大阪府熊取, 11–11 月 (2006).

望月優子: "Investigating the origin of the elements with RI-Beam Factory", 埼玉大学原子核理論研究室セミナー, さいたま, 12 月 (2006).

望月優子: "The Universe, the Earth, and we, human beings", 埼玉大学理学部物理学科学術講演会, さいたま, 1 月 (2007).

望月優子, 間所秀樹: "The Late-time supernova evolution induced by anisotropic neutrino radiation and the r-process environment", 研究会「超新星を舞台とする高エネルギー物理現象」, (東京大学), 東京, 2 月 (2007).

間所秀樹, 望月優子: "非等方ニュートリノ輻射を伴う重力崩壊型超新星爆発の後期時間発展と r プロセスの環境", 日本天文学会 2007 年春季年会, 平塚, 3 月 (2007).

望月優子: "Investigating history of supernove with Antarctice ice core (invited)", CAWSES/IHY workshop, (日本学術会議国際対応分科会), 名古屋, 3 月 (2007).

望月優子, 間所秀樹: "High entropy feasible for the r-process nucleosynthesis in a 2-D hydrodynamical simulation of core-collapse supernovae", 国立天文台ワークショップ「R プロセス元素組成の統合的理解:量子ビームでさぐる宇宙進化の理解を目指して」, 三鷹, 3 月 (2007).

望月優子, 間所秀樹: "The Late-time supernova evolution induced by anisotropic neutrino radiation and the r-process environment", 日本物理学会 2007 年春季大会, 八王子, 3 月 (2007).

Superheavy Element Lab.

Publications

[**Journal**]

(Original Papers) *Subject to Peer Review

Mazzocco M., Signorini C., Romoli M., De Francesco A., Dipietro M., Vardaci E., Yoshida K., Yoshida A., Bonetti R., De Rosa A., Glodariu T., Guglielmentti A., Inglima G., La Commara M., Martin B., Pierroutsakou D., Sandoli M., Soramel F., Stroe L., Kanungo R., Khai N., Motobayashi T., Nomura T., Ishikawa T., Ishiyama H., Jeong S., Miyatake H., Tanaka M., Sugai I., and Watanabe Y.: "Scattering of ^{11}Be halo nucleus from ^{209}Bi at the Coulomb barrier", Eur. Phys. J. A **28**, 295–299 (2006). *

Asai M., Tsukada K., Ichikawa S., Sakama M., Haba H., Nishinaka I., Nagame Y., Goto S., Kojima Y., Oura Y., and Shibata M.: "Alpha decay of 238Cm and the new isotope 237Cm", Phys. Rev. C **73**, 067301-1–067301-4 (2006). *

Mutou R., Chiba J., Enyo H., Fukao Y., Funahashi H., Hamagaki H., Ieiri M., Ishino M., Kanda H., Kitaguchi M., Mihara S., Miwa K., Miyashita T., Murakami T., Nakura T., Naruki M., Ozawa K., Sakuma F., Sasaki O., Sekimoto M., Tabaru T., Tanaka K., Togawa M., Yamada S., Yokkaichi S., and Yoshimura Y.: "Evidence for in-medium modification of the ϕ meson at normal nuclear density", Phys. Rev. Lett. **98**, No. 4, pp. 042501-1–042501-4 (2007). *

Haba H., Tsukada K., Asai M., Toyoshima A., Ishii Y., Toume H., Sato T., Nishinaka I., Ichikawa T., Ichikawa S., Nagame Y., Sato W., Matsuo K., Kitamoto Y., Tashiro T., Shinohara A., Saito J., Ito M., Ikezawa T., Sakamaki M., Goto S., Kudo H., Kikunaga H., Arai M., Kamataki S., Yokoyama A., Akiyama K., Sueki K., Oura Y., Schaedel M., Bruechle W., and Kratz J. V.: "Extraction behavior of rutherfordium into tributylphosphate from hy-

drochloric acid", Radiochim. Acta **95**, 1–6 (2007). ∗

金山洋介, 羽場宏光, 榎本秀一, 天野良平: "コルヒチンによる ^{24}Na, ^{28}Mg, ^{43}K, ^{47}Ca, ^{48}V, ^{67}Cu 嗅覚輸送阻害効果の検討", 微量栄養素研究 **23**, 84–88 (2006). ∗

(Others)

Nagame Y., Akiyama K., Asai M., Goto S., Haba H., Hirata M., Ishii Y., Nishinaka I., Tome H., Toyoshima A., and Tsukada K.: "Chemical studies of the transactinide elements at JAEA", AIP Conf. Proc. **865**, 165–172 (2006).

Asai M., Tsukada K., Haba H., Toyoshima A., Ishii Y., Nagame Y., Nishinaka I., Ichikawa T., Kojima Y., and Sueki K.: "Alpha-gammma coincidence spectroscopy of 255No", JAEA-Review **2006**, No. 29, pp. 41–42 (2006).

Haba H., Tsukada K., Asai M., Toyoshima A., Ishii Y., Tome Y., Sato T., Nishinaka I., Ichikawa T., Ichikawa S., Nagame Y., Sato W., Matsuo K., Kitamoto Y., Tashiro T., Shinohara A., Saito J., Ito M., Ikezawa T., Sakamaki M., Goto S., Kudo H., Kikunaga H., Arai M., Kamataki S., Yokoyama A., Akiyama K., Sueki K., Oura Y., Schaedel M., Bruechle W., and Kratz J. V.: "Extraction behavior of Rf into tributylphosphate from hidrochloric acid", JAEA-Review **2006**, No. 29, pp. 57–58 (2006).

Ishii Y., Miyashita S., Mori T., Suganuma H., Tashiro T., Sakamaki M., Goto S., Tome Y., Toyoshima A., Haba H., Akiyama K., Asai M., Nishinaka I., Tsukada K., Oura Y., and Nagame Y.: "Cation-exchange behavior of Rf in HNO3/HF mixed solution system", JAEA-Review **2006**, No. 29, pp. 59–60 (2006).

Tsukada K., Toyoshima A., Haba H., Asai M., Akiyama K., Ishii Y., Tome Y., Nishinaka I., Sato T., Ichikawa S., Nagame Y., Yaita T., Goto S., Ikezawa T., Sato W., Matsuo K., Kitamoto Y., Tashiro T., Yokoyama A., Arai M., Sakama M., Oura Y., Sueki K., Shinohara A., and Kudo H.: "Chloride complex formation of Rf in HCl and $_3$OH mixed solution", JAEA-Review **2006**, No. 29, pp. 61–62 (2006).

[Book・Proc.]

(Others)

Nagame Y., Haba H., Tsukada K., Asai M., Toyoshima A., Akiyama T., Kaneko T., Hirai T., Goto S., Hirata M., Nishinaka I., and Ichikawa S.: "Few atom chemistry of the transactinide element rutherfordium (Rf)", Proceedings of the International Conference on Applications of High Precision Atomic and Nuclear Methods, 2-6 September 2002, Neptun, Romania, Neptun, Romania, 2002–9, IFIN-HH, Bucharest, pp. 334–343 (2005).

Nagame Y., Asai M., Haba H., Hirata M., Ishii Y., Nishinaka I., Toyoshima A., and Tsukada K.: "Aqueous Chemistry of the Transactinide Element, Rutherfordium (Rf)", Lecture Series on Computer and Computational Sciences Volume 7, Brill Academic Publishers, Leiden, pp. 927–930 (2006).

Oral Presentations

(International Conference etc.)

Tsukada K., Toyoshima A., Haba H., Asai M., Akiyama K., Ishii Y., Kaneko T. S., Nishinaka I., Nagame Y., Sueki K., Ito M., Saito J., Goto S., Kudo H., and Oura Y.: "Chloride complex formation of Rf in HCl and CH3OH mixed solution", Actinides 2005, (The University of Manchester), Manchester, UK, July (2005).

Kambara T., Kanai Y., Kojima T., Nakai Y., Yoneda A., and Yamazaki Y.: "Elastic waves from fast heavy-ion irradiation on solids", 18th International Acoustic Emission Symposium, Sagamihara, July (2006).

Kikunaga H., Haba H., Kaji D., Sato N., Akiyama T., Morimoto K., Yoneda A., Morita K., Takabe T., Ooe K., Shinohara A., Suzuki D., Nanri T., Yamazaki I., and Yokoyama A.: "Development of a gas-jet transport system coupled to GARIS for heavy element chemistry", 5th Workshop on Recoil Separator for Superheavy Element Chemistry (TASACA06), (GSI), Garching, Germany, Sept. (2006).

Morita K., Morimoto K., Kaji D., Akiyama T., Goto S., Haba H., Ideguchi E., Katori K., Kikunaga H., Koura H., Kudo H., Ohnishi T., Ozawa A., Suda T., Sato N., Sueki K., Tokanai F., Xu H., Yamaguchi T., Yoneda A., Yoshida A., and YuLiang Z.: "Experiments on Synthesis of the Heaviest Elements at RIKEN (SHE and FFD)", Tours Symposium on Nuclear Physics VI (TOURS 2006), (Konan University), Tours, France, Sept. (2006).

Haba H., Kaji D., Kikunaga H., Akiyama T., Sato N., Morimoto K., Yoneda A., Morita K., Takabe T., Tashiro Y., Kitamoto Y., Matsuo K., Saika D., Ooe K., Kuribayashi T., Yoshimura T., Shinohara A., and Toyoshima A.: "Superheavy Element Chemistry at RIKEN: Present Status and Perspectives", Tours Symposium on Nuclear Physics VI (TOURS 2006), (Konan University), Tours, France, Sept. (2006).

Morita K., Morimoto K., Kaji D., Akiyama T., Goto S., Haba H., Ideguchi E., Katori K., Kikunaga H., Koura H., Kudo H., Ohnishi T., Ozawa A., Suda T., Sato N., Sueki K., Tokanai F., Xu H., Yamaguchi T., Yoneda A., Yoshida A., and YuLiang Z.: "Experiments on Synthesis of the Heaviest Elements at RIKEN Status and Perspectives", Workshop on the Atomic Properties of the Heaviest Elements: Towards the Island of Stability, (LMU-Muenchen), Germany, Chiemsee, Sept. (2006).

Toyoshima A., Tsukada K., Asai M., Ishii Y., Nishinaka I., Sato T., Hirata M., Nagame Y., Haba H., Sato W., Tani Y., Hasegawa H., Matsuo K., Saika D., Kitamoto Y., Shinohara A., Goto S.,

Ito M., Saito J., Kudo H., Akiyama K., Sueki K., Yokoyama A., Oura Y., Schaedel M., Bruechle W., and Kratz J. V.: "Fluoride Complexation Study of Rutherfordium at JAEA", Workshop on the Atomic Properties of the Heaviest Elements: Towards the Island of Stability, (LMU Muenchen), Chiemsee, Germany, Sept. (2006).

Haba H., Kaji D., Kikunaga H., Akiyama T., Sato N., Morimoto K., Yoneda A., Morita K., Takabe T., Tashiro Y., Kitamoto Y., Matsuo K., Saika D., Ooe K., Kuribayashi T., Yoshimura T., Shinohara A., and Toyoshima A.: "Startup of Heavy Element Chemistry in RIKEN", Workshop on the Atomic Properties of the Heaviest Elements: Towards the Island of Stability, (LMU Muenchen), Chiemsee, Germany, Sept. (2006).

Ishii Y., Toume H., Toyoshima A., Asai M., Nishinaka I., Tsukada K., Nagame Y., Tashiro T., Shinohara A., Sakamaki M., Goto S., Kudo H., Akiyama K., Haba H., Oura Y., Miyashita S., Mori T., and Suganuma H.: "A cation-exchange study of fluoride complexation of rutherfordium (Rf) in HNO3/HF mixed solution system", 6th International Symposium on Advanced Science Research: Frontiers of Nuclear and Radiochemistry (ASR2006), (Advanced Science Research Center, Japan Atomic Energy Agency), Tokaimura, Oct. (2006).

Kasamatsu Y., Toyoshima A., Toume H., Tsukada K., Haba H., and Nagame Y.: "Adsorption of Nb, Ta and Pa on anion exchangers in HF/HNO3 media: Model experiments for the chemical study of Dubnium (Db)", 6th International Symposium on Advanced Science Research: Frontiers of Nuclear and Radiochemistry (ASR2006), (Advanced Science Research Center, Japan Atomic Energy Agency), Tokaimura, Oct. (2006).

Tsukada K., Toyoshima A., Haba H., Asai M., Akiyama K., Ishii Y., Tome H., Nishinaka I., Kaneko T. S., Ichikawa S., Nagame Y., Yaita T., Goto S., Ikezawa T., Sato W., Matsuo K., Kitamoto Y., Tashiro T., Yokoyama A., Arai M., Sakama M., Oura Y., Sueki K., Shinohara A., and Kudo H.: "Chloride complex formation of Rf in HCl and CH3OH mixed solution", 6th International Symposium on Advanced Science Research: Frontiers of Nuclear and Radiochemistry (ASR2006), (Advanced Science Research Center, Japan Atomic Energy Agency), Tokaimura, Oct. (2006).

Haba H., Kikunaga H., Kaji D., Sato N., Akiyama T., Morimoto K., Yoneda A., Morita K., Takabe T., Ooe K., Shinohara A., Suzuki D., Nanri T., Yamazaki I., and Yokoyama A.: "Development of a gas-jet transport system coupled to the RIKEN gas-filled recoil ion separator GARIS for superheavy element chemistry", 6th International Symposium on Advanced Science Research: Frontiers of Nuclear and Radiochemistry (ASR2006), (Advanced Science Research Center, Japan Atomic Energy Agency), Tokaimura, Oct. (2006).

Toyoshima A., Kasamatsu Y., Tsukada K., Haba H., Shinohara A., and Nagame Y.: "Development of an electrochemistry apparatus for an atom-at-a-time chemistry", 6th International Symposium on Advanced Science Research: Frontiers of Nuclear and Radiochemistry (ASR2006), (Advanced Science Research Center, Japan Atomic Energy Agency), Tokaimura, Oct. (2006).

Akiyama K., Haba H., Tsukada K., Asai M., Sueki K., Toyoshima A., Nagame Y., and Katada M.: "Metallofullerenes encaging californium", 6th International Symposium on Advanced Science Research: Frontiers of Nuclear and Radiochemistry (ASR2006), (Advanced Science Research Center, Japan Atomic Energy Agency), Tokaimura, Oct. (2006).

Kaji D., Haba H., Kikunaga H., Morimoto K., Yoneda A., Akiyama T., Ooe K., Nanri T., Sato N., Shinohara A., Suzuki D., Takabe T., Yamazaki I., Yokoyama A., and Morita K.: "Optimazation of a gas-filled recoil separator GARIS for the chemistry of superheavy elements", 6th International Symposium on Advanced Science Research: Frontiers of Nuclear and Radiochemistry (ASR2006), (Advanced Science Research Center, Japan Atomic Energy Agency), Tokaimura, Oct. (2006).

Morita K., Morimoto K., Kaji D., Akiyama T., Goto S., Haba H., Ideguchi E., Katori K., Kikunaga H., Koura H., Kudo H., Ohnishi T., Ozawa A., Suda T., Sato N., Sueki K., Tokanai F., Xu H., Yamaguchi T., Yoneda A., Yoshida A., and YuLiang Z.: "Search for the Heaviest Elements at RIKEN", 6th International Symposium on Advanced Science Research: Frontiers of Nuclear and Radiochemistry (ASR2006), (Advanced Science Research Center, Japan Atomic Energy Agency), Tokaimura, Oct. (2006).

Takabe T., Saika D., Matsuo K., Tashiro T., Ooe K., Kuribayashi T., Yoshimura T., Toyoshima A., Kikunaga H., Kaji D., Haba H., Kudo H., Mitsugashira T., and Shinohara A.: "Studies on the heavy element productions at RIKEN for chemical characterization of seaborgium", 6th International Symposium on Advanced Science Research: Frontiers of Nuclear and Radiochemistry (ASR2006), (Advanced Science Research Center, Japan Atomic Energy Agency), Tokaimura, Oct. (2006).

Toyoshima A., Kasamatsu Y., Tsukada K., Haba H., Asai M., Ishii Y., Toume H., Kaneko T. S., Nishinaka I., Nagame Y., Goto S., Ishiyama T., Sakamaki M., Kudo H., Akiyama K., Oura Y., Kikunaga H., Ooe K., Kuribayashi T., Shinohara A., and Yokoyama A.: "TOPO reversed-phase extraction behabior of rutherfordium in HCl solutions", 6th International Symposium on Advanced Science Research: Frontiers of Nuclear and Radiochemistry (ASR2006),

(Advanced Science Research Center, Japan Atomic Energy Agency), Tokaimura, Oct. (2006).

(Domestic Conference)

北本優介, 雑賀大輔, 松尾啓司, 高部智正, 田代祐基, 大江一弘, 栗林隆宏, 佐藤渉, 高橋成人, 吉村崇, 羽場宏光, 榎本秀一, 三頭聰明, 篠原厚: “金属-配位子間相互作用を利用した3価アクチノイドのキャピラリー電気泳動分離”, 日本化学会第 86 春季年会, (日本化学会), 船橋, 3 月 (2006).

石井康雄, 菅沼英夫, 羽場宏光, 秋山和彦, 當銘勇人, 豊嶋厚史, 浅井雅人, 塚田和明, 永目諭一郎: “超重元素ラザホージウムを模擬した同族元素 Zr，Hf の硝酸/フッ化水素酸系における陽イオン交換挙動”, 日本化学会第 86 春季年会, (日本化学会), 船橋, 3 月 (2006).

羽場宏光, 加治大哉, 高部智正, 秋山隆宏, 森本幸司, 森田浩介: “気体充填型反跳分離装置を前段分離装置として用いた新しい超重元素化学分析装置の開発”, 日本化学会第 86 春季年会, (日本化学会), 船橋, 3 月 (2006).

高部智正, 北本優介, 雑賀大輔, 松尾啓司, 田代祐基, 大江一弘, 栗林隆宏, 吉村崇, 羽場宏光, 加治大哉, 篠原厚: “理研 AVF サイクロトロンにおける重元素合成システムの整備と化学研究のためのノーベリウム同位体の製造”, 日本化学会第 86 春季年会, (日本化学会), 船橋, 3 月 (2006).

塚田和明, 豊嶋厚史, 羽場宏光, 浅井雅人, 秋山和彦, 石井康雄, 當銘勇人, 西中一朗, 佐藤哲也, 市川隆敏, 市川進一, 平田勝, 永目諭一郎, 矢板毅, 後藤真一, 坂牧雅巳, 池沢孝明, 佐藤渉, 松尾啓司, 北本優介, 田代祐基, 横山明彦, 新井理太, 鎌滝真次, 阪間稔, 大浦泰嗣, 末木啓介, 篠原厚, 工藤久昭: “超重元素ラザホージウムの塩化物錯体形成”, 日本化学会第 86 春季年会, (日本化学会), 船橋, 3 月 (2006).

加治大哉, 羽場宏光, 森本幸司, 秋山隆宏, 森田浩介, 佐藤望, 高部智正: “シーボギウム (Sg) の化学研究へ向けた 232Th+40Ar 反応による Sg 同位体の探索”, 日本化学会第 86 春季年会, (日本化学会), 船橋, 3 月 (2006).

豊嶋厚史, 羽場宏光, 塚田和明, 浅井雅人, 秋山和彦, 石井康雄, 當銘勇人, 西中一朗, 佐藤哲也, 市川隆敏, 永目諭一郎, 佐藤渉, 松尾啓司, 北本優介, 田代祐基, 篠原厚, 池沢孝明, 坂牧雅巳, 後藤真一, 工藤久昭, 新井理太, 鎌滝真次, 横山明彦, 大浦泰嗣, 末木啓介: “塩酸溶液系におけるラザホージウムの TBP 逆相抽出クロマトグラフィー”, 日本化学会第 86 春季年会, (日本化学会), 船橋, 3 月 (2006).

金山洋介, 羽場宏光, 榎本秀一, 天野良平: “^{24}Na, ^{28}Mg, ^{43}K, ^{47}Ca, ^{48}V, ^{67}Cu 鼻腔投与におけるコルヒチンの嗅覚輸送阻害効果の検討”, 第 23 回微量栄養素研究会シンポジウム, 京都, 6 月 (2006).

金山洋介, 榎本秀一, 羽場宏光, 天野良平: “Brain Delivery of Monovalent Metal Cations via Olfactory Pathway”, 第 16 回金属の関与する生体関連反応シンポジウム (SRM 2006)「生体超分子システムと金属」, (日本薬学会), 東京, 6 月 (2006).

池沢英二, 加治大哉, 加瀬昌之, 上垣外修一, 中川孝秀, 坂本成彦, 奥野広樹, 稲辺尚人, 福西暢尚, 込山美咲, 木寺正憲, 日暮祥英, 龍頭啓充, 小原重夫, 藤巻正樹, 若杉昌徳, 長瀬誠, 影山正, 横内茂, 渡邉環, 米田晃, 後藤彰, 矢野安重: “超重元素探索実験のための理研重イオンリニアック運転”, 第 3 回日本加速器学会年会・第 31 回リニアック技術研究会, 仙台, 8 月 (2006).

笠松良崇, 豊嶋厚史, 當銘勇人, 塚田和明, 羽場宏光, 永目諭一郎: “希フッ化水素酸系における Nb, Ta, Pa の陰イオン交換挙動”, 2006 日本放射化学会年会・第 50 回放射化学討論会, (日本放射化学会), 水戸，東海村, 10 月 (2006).

石井康雄, 當銘勇人, 豊嶋厚史, 浅井雅人, 西中一朗, 塚田和明, 永目諭一郎, 宮下直, 森友隆, 菅沼英夫, 田代祐基, 篠原厚, 坂牧雅巳, 後藤真一, 工藤久昭, 羽場宏光, 秋山和彦, 大浦泰嗣: “Rf の HNO3/HF における陽イオン交換挙動 (II)”, 2006 日本放射化学会年会・第 50 回放射化学討論会, (日本放射化学会), 水戸，東海村, 10 月 (2006).

羽場宏光, 加治大哉, 高部智正, 秋山隆宏, 森本幸司, 米田晃, 森田浩介: “理研気体充填型反跳分離装置 GARIS を前段分離装置として用いた新しい重元素化学分析装置の開発”, 2006 日本放射化学会年会・第 50 回放射化学討論会, (日本放射化学会), 水戸，東海村, 10 月 (2006).

豊嶋厚史, 笠松良崇, 塚田和明, 羽場宏光, 篠原厚, 永目諭一郎: “単一原子の電気化学的研究に向けた電解セルの開発”, 2006 日本放射化学会年会・第 50 回放射化学討論会, (日本放射化学会), 水戸，東海村, 10 月 (2006).

秋山和彦, 羽場宏光, 塚田和明, 浅井雅人, 豊嶋厚史, 矢板毅, 末木啓介, 永目諭一郎: “EXAFS を用いた Zr，Hf の塩酸系 TBP 抽出における錯体構造に関する研究”, 2006 日本放射化学会年会・第 50 回放射化学討論会, (日本放射化学会), 水戸，東海村, 10 月 (2006).

高部智正, 雑賀大輔, 松尾啓司, 田代祐基, 大江一弘, 栗林隆宏, 吉村崇, 豊嶋厚史, 菊永英寿, 加治大哉, 羽場宏光, 工藤久昭, 三頭聰明, 篠原厚: “理研におけるシーボーギウム化学研究に向けた重元素合成”, 2006 日本放射化学会年会・第 50 回放射化学討論会, (日本放射化学会), 水戸，東海村, 10 月 (2006).

菊永英寿, 羽場宏光, 加治大哉, 佐藤望, 森本幸司, 米田晃, 森田浩介, 高部智正, 大江一弘, 篠原厚, 鈴木大介, 南里朋洋, 山崎逸郎, 横山明彦: “238U(22Ne,5n) 反応によって製造された 255No の GARIS による分離分析：GARIS を前段分離装置として用いた超重元素化学研究に向けて”, 2006 日本放射化学会年会・第 50 回放射化学討論会, (日本放射化学会), 水戸，東海村, 10 月 (2006).

中嶋啓二, 笠松良崇, 佐藤渉, 菊永英寿, 高宮幸一, 三頭聰明, 中西孝, 大槻勤, 篠原厚: “^{229m}Th の可視・紫外・赤外領域における脱励起光測定”, 2006 日本放射化学会年会・第 50 回放射化学討論会, (日本放射化学会), 水戸，東海村, 10 月 (2006).

田代祐基, 雑賀大輔, 北本優介, 松尾啓司, 高部智正, 栗林隆宏, 大江一弘, 吉村崇, 佐藤渉, 高橋成人, 豊嶋厚史, 羽場宏光, 篠原厚: “複線式マイクロチップを用いた No2+迅速溶媒抽出”, 2006 日本放射化学会年会・第 50 回放射化学討論会, (日本放射化学会), 水戸，東海村, 10 月 (2006).

大江一弘, 栗林隆宏, 高部智正, 田代祐基, 北本優介, 雑賀

大輔, 松尾啓司, 高橋成人, 吉村崇, 高宮幸一, 柴田誠一, 羽場宏光, 榎本秀一, 篠原厚: “極低濃度タングステンの溶媒抽出挙動と電解酸化還元反応”, 2006 日本放射化学会年会・第 50 回放射化学討論会, (日本放射化学会), 水戸, 東海村, 10 月 (2006).

豊嶋厚史, 笠松良崇, 塚田和明, 羽場宏光, 浅井雅人, 石井康雄, 當銘勇人, 金子 (哲也) 佐藤, 西中一朗, 永目諭一郎, 後藤真一, 石山剛, 坂牧雅巳, 工藤久昭, 秋山和彦, 大浦泰嗣, 菊永英寿, 大江一弘, 栗林隆宏, 篠原厚, 末木啓介, 横山明彦: “塩酸溶液系におけるラザホージウムの TOPO 逆相抽出クロマトグラフ挙動”, 2006 日本放射化学会年会・第 50 回放射化学討論会, (日本放射化学会), 水戸, 東海村, 10 月 (2006).

羽場宏光: “理化学研究所における超重元素化学研究”, タンデム領域の重イオン科学研究会 (2006), (JAEA, KEK), 東海村, 12 月 (2006).

SCRIT Team

Oral Presentations

(Domestic Conference)

池沢英二, 加治大哉, 加瀬昌之, 上垣外修一, 中川孝秀, 坂本成彦, 奥野広樹, 稲辺尚人, 福西暢尚, 込山美咲, 木寺正憲, 日暮祥英, 龍頭啓充, 小原重夫, 藤巻正樹, 若杉昌徳, 長瀬誠, 影山正, 横内茂, 渡邉環, 米田晃, 後藤彰, 矢野安重: “超重元素探索実験のための理研重イオンリニアック運転”, 第 3 回日本加速器学会年会・第 31 回リニアック技術研究会, 仙台, 8 月 (2006).

Big RIPS Team

Publications

[**Journal**]

(Original Papers) *Subject to Peer Review

Mazzocco M., Signorini C., Romoli M., De Francesco A., Dipietro M., Vardaci E., Yoshida K., Yoshida A., Bonetti R., De Rosa A., Glodariu T., Guglielmentti A., Inglima G., La Commara M., Martin B., Pierroutsakou D., Sandoli M., Soramel F., Stroe L., Kanungo R., Khai N., Motobayashi T., Nomura T., Ishikawa T., Ishiyama H., Jeong S., Miyatake H., Tanaka M., Sugai I., and Watanabe Y.: “Scattering of ^{11}Be halo nucleus from ^{209}Bi at the Coulomb barrier”, Eur. Phys. J. A **28**, 295–299 (2006). *

Kameda D., Ueno H., Asahi K., Takemura M., Shirahama A., Haseyama T., Uchida M., Shimada K., Nagae D., Kijima G., Arai T., Takase K., Suda S., Inoue T., Murata J., Kawamura H., Kobayashi Y., Watanabe H., and Ishihara M.: “Nuclear moments of neutron-rich ^{32}Al”, J. Phys.: Con. Ser. **49**, 138–139 (2006). *

Nakamura T., Wada M., Okada K., Ishida Y., Takamine A., Yamazaki Y., Kambara T., Kanai Y., Kojima T., Nakai Y., Oshima N., Yoshida A., Kubo T., Katayama I., Lioubimov V., Wollnik H., Varentsov V., and Schuessler H. A.: “Laser spectroscopy of ^{7,10}Be^{+} in an online ion trap”, Phys. Rev. A **74**, 052503-1–052503-5 (2006). *

Suda K., Okamura H., Uesaka T., Nishikawa J., Kumasaka H., Suzuki R., Sakai H., Tamii A., Ohnishi T., Sekiguchi K., Yako K., Sakoda S., Kato H., Hatano M., Maeda Y., Saito T., Ishida T., Sakamoto N., Sato Y., Hatanaka K., Wakasa T., and Kamiya J.: “Absolute Calibration of the Deuteron Beam Polarization at Intermediate Energies via the ^{12}C$(\vec{d},\alpha)^{10}$B$^{*}[2^{+}]$ Reaction”, Nuclear Instruments and Methods in Physics Research A **572**, No. Issue 2, pp. 745–753 (2007). *

Oral Presentations

(International Conference etc.)

Kameda D., Asahi K., Ueno H., Shirahama A., Watanabe H., Haseyama T., Kobayashi Y., Uchida M., Shimada K., Nagae D., Kato G., Emori S., Kijima G., Takemura M., Arai T., Oshima S., Tsukui M., Yagi E., Kubo T., Yoshida A., and Ishihara M.: “Production of spin-polarized RI beams via projectile fragmentation and the application to nuclear moment measurements”, 11th International Workshop on Polarized Sources and Targets (PST05), (RIKEN and The Center for Nuclear Study (CNS)), Tokyo, Nov. (2005).

Kameda D., Asahi K., Ueno H., Shirahama A., Haseyama T., Watanabe H., Uchida M., Shimada K., Nagae D., Takemura M., Arai T., Kijima G., Takase K., Suda S., Inoue T., Kobayashi Y., Yagi E., Kubo T., Yoshida A., and Ishihara M.: “Nuclear moments of neutron-rich 32Al$(Z = 11, N = 19)$”, International Symposium on Structure of Exotic Nuclei and Nuclear Forces (SENUF06), (The Center for Nuclear Study (CNS)), Tokyo, Mar. (2006).

Kameda D., Ueno H., Asahi K., Shirahama A., Haseyama T., Watanabe H., Uchida M., Nagae D., Shimada K., Takemura M., Arai T., Takase K., Inoue T., Kato G., Kijima G., Emori S., Suda S., Tsukui M., Murata J., Kawamura H., Kobayashi Y., Yagi E., Kubo T., and Ishihara M.: “Nuclear moment measurements using spin-polarized RI beams via projectile fragmentation: Recent results and the prospect in RIBF”, International Workshop on “Nuclear Physics with RIBF”, Wako, Mar. (2006).

Morita K., Morimoto K., Kaji D., Akiyama T., Goto S., Haba H., Ideguchi E., Katori K., Kikunaga H., Koura H., Kudo H., Ohnishi T., Ozawa A., Suda T., Sato N., Sueki K., Tokanai F., Xu H., Yamaguchi T., Yoneda A., Yoshida A., and YuLiang Z.: “Experiments on Synthesis of the Heaviest Elements at RIKEN (SHE and FFD)”, Tours Symposium on Nuclear Physics VI (TOURS 2006), (Konan University), Tours, France, Sept. (2006).

Morita K., Morimoto K., Kaji D., Akiyama T., Goto S., Haba H., Ideguchi E., Katori K., Kikunaga H., Koura H., Kudo H., Ohnishi T., Ozawa A., Suda T., Sato N., Sueki K., Tokanai F., Xu H., Yamaguchi

T., Yoneda A., Yoshida A., and YuLiang Z.: "Experiments on Synthesis of the Heaviest Elements at RIKEN Status and Perspectives", Workshop on the Atomic Properties of the Heaviest Elements: Towards the Island of Stability, (LMU-Muenchen), Germany, Chiemsee, Sept. (2006).

Kameda D., Asahi K., Ueno H., Shirahama A., Haseyama T., Watanabe H., Uchida M., Nagae D., Shimada K., Takemura M., Arai T., Takase K., Inoue T., Suda S., Kobayashi Y., Murata J., Kawamura H., and Ishihara M.: "Nuclear moment measurements of neutron-rich Al isotopes using spin-polarized RI beams: Determination of the boundary of the "island of inversion"", 17th International Spin Physics Symposium (SPIN2006), (Kyoto University), Kyoto, Oct. (2006).

Morita K., Morimoto K., Kaji D., Akiyama T., Goto S., Haba H., Ideguchi E., Katori K., Kikunaga H., Koura H., Kudo H., Ohnishi T., Ozawa A., Suda T., Sato N., Sueki K., Tokanai F., Xu H., Yamaguchi T., Yoneda A., Yoshida A., and YuLiang Z.: "Search for the Heaviest Elements at RIKEN", 6th International Symposium on Advanced Science Research: Frontiers of Nuclear and Radiochemistry (ASR2006), (Advanced Science Research Center, Japan Atomic Energy Agency), Tokaimura, Oct. (2006).

Detector Team

Publications

[**Journal**]

(Original Papers) *Subject to Peer Review

Ariyoshi S., Otani C., Dobroiu A., Matsuo H., Sato H., Taino T., Kawase K., and Shimizu H.: "Superconducting Detector Array for Terahertz Imaging Applications", Jpn. J. Appl. Phys. Pt.2 **45**, No. 37, pp. L1004–L1006 (2006). *

Oral Presentations

(International Conference etc.)

Ariyoshi S., Otani C., Dobroiu A., Matsuo H., Sato H., Taino T., Kawase K., and Shimizu H.: "Terahertz Imaging with an STJ-based Linear Array Detector(Invited Oral)", Applied Superconductivity Conference 2006 (ASC 2006), Seattle, USA, Aug.–Sept. (2006).

Otani C., Ariyoshi S., Taino T., Dobroiu A., Shibuya T., Sato H., Shimizu H., and Kawase K.: "Development of Terahertz Imaging Detectors using Superconducting Tunnel Junctions", International Conference on Mesoscopic Superconductivity and Magnetism (MesoSuperMag 2006), (Argonne National Laboratory), Chicago, USA, Aug.–Sept. (2006).

Ariyoshi S., Otani C., Dobroiu A., Matsuo H., Sato H., Taino T., Kawase K., and Shimizu H.: "THz Imaging with a Linear Array Detector based on Superconducting Tunnel Junctions", 2006 Joint 31st International Conference on Infrared and Millimeter Waves and 14th International Conference on Terahertz Electronics (IRMMW-THz2006), (Shanghai Institute of Technical Physics (SITP)), Shanghai, China, Sept. (2006).

Otani C., Ariyoshi S., Taino T., Myoren H., Sato H., Shimizu H., Takada S., and Kawase K.: "Terahertz Detectors using Superconducting Tunnel Junctions (Invited)", 19th International Symposium on Superconductivity (ISS 2006), (International Superconductivity Technology Center (ISTEC)), Nagoya, Oct.–Nov. (2006).

Taino T., Ishii H., Yoshimura S., Otani C., Ariyoshi S., Myoren H., Kawase K., Shibuya T., Sato H., Shimizu H., and Takada S.: "Terahertz electromagnetic-waves detector using Nb-based superconducting tunnel junction on LiNb03 substrate absorber", 19th International Symposium on Superconductivity (ISS 2006), (ISTEC (International Superconductivity Technology Center)), Nagoya, Oct.–Nov. (2006).

Otani C., Ariyoshi S., Taino T., Sato H., Shimizu H., and Kawase K.: "Radiation Detectors using Superconducting Tunnel Junctions (invited lecture)", 14th International Symposium on Laser Spectroscopy (SOLS 2006), (KAERI), Daejeon, Korea, Nov. (2006).

Otani C., Ariyoshi S., Taino T., Dobroiu A., Sato H., Shimizu H., and Kawase K.: "Development of Terahertz Detectors using Superconducting Tunnel Junctions (invited)", 2nd CREST Nano-Virtual-Labs Joint Workshop on Superconductivity (NVLS2006), Kyoto, Dec. (2006).

Ariyoshi S., Otani C., Dobroiu A., Matsuo H., Taino T., Sato H., and Shimizu H.: "STJ-based direct detector array for terahertz imaging applications", 7th Workshop on Submillimeter-Wave Receiver Technologies in Eastern Asia/Workshop on the Development of Low-Noise Receiver Technology at Millimeter Waves and Terahertz Frequencies, (Nobeyama Radio Observatory), Sakai, Jan. (2007).

(Domestic Conference)

大谷知行, 有吉誠一郎, 佐藤広海, 川瀬晃道, 田井野徹, 清水裕彦: "超伝導トンネル (STJ) 素子によるテラヘルツ波アレイ検出器の開発とイメージング（招待講演）", 応用物理学会超伝導分科会第 33 回研究会「高感度分析・分光技術のための超伝導検出器」, (超伝導工学研究所), 東京, 6 月 (2006).

有吉誠一郎, 大谷知行, Dobroiu A., 松尾宏, 田井野徹, 佐藤広海, 清水裕彦: "スペース天文応用を目指したサブミリ波帯 STJ 検出器アレイの開発", 第 7 回宇宙科学シンポジウム, (宇宙航空研究開発機構宇宙科学研究本部), 相模原, 12 月 (2006).

有吉誠一郎, 大谷知行, Dobroiu A., 松尾宏, 佐藤広海, 田井野徹, 川瀬晃道, 清水裕彦: "超伝導検出器アレイを用いたテラヘルツイメージング", 電子情報通信学会電子デバイス研究会 2006 年度月間研究会（12 月）,

東京, 12 月 (2006).

Industrial Cooperation Team

Publications

[**Journal**]

(Original Papers) *Subject to Peer Review

Takeichi H., Koyama S., Matani A., and Cichocki A.: "Speech comprehension assessed by electroencephalography: a new method using m-sequence modulation", Neurosci. Res. **57**, No. 2, pp. 314–318 (2007). ∗

(Others)

竹市博臣, 小山幸子, 眞溪歩, Cichocki A.: "m 系列変調法による脳波計測：談話理解を例として", 物性研究 **87**, No. 4, pp. 608–610 (2007).

Oral Presentations

(International Conference etc.)

Takeichi H. and Koyama S.: "A study of scene perception and perceptual interaction by multiple bistability: shading-lighting", Cognitive Neuroscience Society 2006 Annual Meeting, San Francisco, USA, Apr. (2006).

Koyama S., Toyomaki A., Matsumoto H., Matsui M. F., Takeichi H., and Morotomi T.: "Auditory event-related brain potentials elicited by short gaps embedded in a continuous sound and by brief tones: a developmental study", Cognitive Neuroscience Society 2006 Annual Meeting, San Francisco, USA, Apr. (2006).

Takeichi H., Koyama S., Kimura M., Matsumoto H., Inoue Y., and Morotomi T.: "Visually evoked brain potentials associated with volumetric completion", 36th Annual Meeting of Society for Neuroscience (Neuroscience 2006), Atlanta, USA, Oct. (2006).

Takeichi H., Koyama S., Matsumoto H., Morotomi T., and Cichocki A.: "Assessment of Speech Comprehension: Applications of M-Sequence Modulation and Independent Component Analysis to Electroencephalography", 10th Tamagawa-Riken Dynamic Brain Forum (DBF2007), Hakuba, Mar. (2007).

(Domestic Conference)

竹市博臣, 小山幸子, 眞溪歩, Cichocki A.: "An independent component analysis of EEG response to spoken sentence modulated by m-sequence", 第 29 回日本神経科学大会（Neuroscience 2006）, 京都, 7 月 (2006).

竹市博臣, 小山幸子, 眞溪歩, Cichocki A.: "聴覚野におけるリアルタイム音声言語（談話）の処理の脳波を用いた検討", 脳と心のメカニズム第 7 回夏のワークショップ「感覚認知の計算理論とダイナミクス」, 札幌, 8 月 (2006).

竹市博臣, 小山幸子, 木村元洋, 松本秀彦, 井上康之, 北崎充晃, 諸冨隆: "視覚誘発電位を用いた三次元補完の検討", 日本心理学会第 70 回大会, 福岡, 11 月 (2006).

松本秀彦, 諸冨隆, 竹市博臣, 豊巻敦人, 小山幸子: "連続音中の短い無音部に対する中枢聴覚処理：ERP を用いた発達的変化の検討", 日本心理学会第 70 回大会, 福岡, 11 月 (2006).

松本秀彦, 諸冨隆, 竹市博臣, 豊巻敦人, 小山幸子: "音の持続呈示中の無音部に対する中枢聴覚処理の発達的特徴", 第 36 回日本臨床神経生理学会・学術大会, 横浜, 11–12 月 (2006).

竹市博臣, 小山幸子, 松本秀彦, 諸冨隆, Cichocki A.: "リアルタイム音声言語（談話）処理の脳波を用いた検討：再現性の確認", 脳と心のメカニズム第 7 回冬のワークショップ「Neuroeconomics」, 留寿都, 1 月 (2007).

竹市博臣, 竹内文也, 寺尾敦, 豊澤悠子, 小山幸子: "m 系列変調（劣化）音声に対する fMRI 応答", 脳機能解析学分野第 1 回シンポジウム, (北海道大学), 札幌, 1 月 (2007).

竹市博臣: "脳情報工学と情報脳科学", 電子情報通信学会 2007 年総合大会, 名古屋, 3 月 (2007).

Radiation Lab.

Publications

[**Journal**]

(Original Papers) *Subject to Peer Review

Adcox K., Bazilevsky A. V., Bunce G. M., Deshpande A., En'yo H., Fox B., Goto Y., Grosse Perdekamp M., Hayashi N., Ichihara T., Imai K., Ishihara M., Jacak B. V., Kobayashi H., Kurita K., Li Z., Mao Y., Murata J., Saito N., Sakuma T., Sato H., Shibata T., Sugioka M., Taketani A., Tojo J., Torii H., Watanabe Y., Yokkaichi S., and PHENIX C.: "PHENIX detector overview", Nuclear Instruments and Methods in Physics Research A **499**, 469–479 (2003). ∗

Aronson S. H., Ichihara T., Saito N., and PHENIX Collaboration .: "PHENIX Magnet System", Nuclear Instruments and Methods in Physics Research A **499**, 480–488 (2003). ∗

Aphecetche L., Bazilevsky A. V., Goto Y., Grosse Perdekamp M., and PHENIX Collaboration.: "PHENIX Calorimeter", Nuclear Instruments and Methods in Physics Research A **499**, 521–536 (2003). ∗

Akikawa H., En'yo H., Hayashi N., Ichihara T., Ishihara M., Kobayashi H., Kurita K., Li Z., Mao Y., Murata J., Saito N., Sato H., Shibata T., Sugioka M., Taketani A., Watanabe Y., and PHENIX Collaboration.: "PHENIX muon arms", Nuclear Instruments and Methods in Physics Research A **499**, 537–548 (2003). ∗

Adler S. S., Sato H., Taketani A., and PHENIX C.: "PHENIX on-line systems", Nuclear Instruments and Methods in Physics Research A **499**, 560–592 (2003). ∗

Adler S. S., Ichihara T., Jacak B. V., Watanabe Y., Yokkaichi S., and PHENIX C.: "PHENIX on-line and off-line computing", Nuclear Instruments and Methods in Physics Research A **499**, 593–602 (2003). ∗

Murata J., Horaguchi T., Kamihara N., Kobayashi H., Shibata T., and PHENIX C.: "Optical alignment system for the PHENIX muon tracking chambers", Nuclear Instruments and Methods in Physics Research A **500**, 309–317 (2003). ∗

Heuser J. M. and PHENIX Collaboration .: "Vertex detector upgrade plans for the PHENIX experiment at RHIC", Nuclear Instruments and Methods in Physics Research A **511**, 210–214 (2003). ∗

Kimura K., Izumikawa T., Koyama R., Ohnishi T., Ohtsubo T., Ozawa A., Shinozaki W., Suzuki T., Takahashi M., Tanihata I., Yamaguchi T., and Yamaguchi Y.: "High-rate particle identification of high-energy heavy ions using a tilted electrode gas ionization chamber", Nuclear Instruments and Methods in Physics Research A **538**, 608–614 (2005). ∗

Li Z., Enyo H., Eremin V., Goto Y., Li C. J., Taketani A., and Tojo J.: "Electron beam and laser testing on the novel stripixel detectors", Nuclear Instruments and Methods in Physics Research A **541**, No. 1/2, pp. 21–28 (2005). ∗

Suzuki T., Ishiguro K., Mori Y., and Sekido T.: "The Dual Meissner Effect and Magnetic Displacement Current", Phys. Rev. Lett. **94**, 132001-1–132001-4 (2005). ∗

Ishii N., Doi T., Iida H., Oka M., Okiharu F., Suganuma H., and Tsumura K.: "Anisotropic lattice QCD studies of penta-quarks and tetra-quarks", AIP Conf. Proc. **842**, 492–494 (2006). ∗

Kondrashev S., Kanesue T., Okamura M., and Sakakibara K.: "Features of ion generation using Nd-glass laser", J. Appl. Phys. **100**, No. 1, pp. 103301-1–103301-8 (2006). ∗

Takeuchi S., Aoi N., Baba H., Fukui T., Hashimoto Y., Ieki K., Imai N., Iwasaki H., Kanno S., Kondo Y., Kubo T., Kurita K., Minemura T., Motobayashi T., Nakabayashi T., Nakamura T., Okumura T., Onishi T., Ota S., Sakurai H., Shimoura S., Sugo R., Suzuki D., Suzuki H., Suzuki M., Takeshita E., Tamaki M., Tanaka K., Togano Y., and Yamada K.: "Proton inelastic scattering on ^{32}Mg", J. Phys.: Con. Ser. **49**, 153–154 (2006). ∗

Ariyoshi S., Otani C., Dobroiu A., Matsuo H., Sato H., Taino T., Kawase K., and Shimizu H.: "Superconducting Detector Array for Terahertz Imaging Applications", Jpn. J. Appl. Phys. Pt.2 **45**, No. 37, pp. L1004–L1006 (2006). ∗

Oda S., Hamagaki H., Ozawa K., Inuzuka M., Sakaguchi T., Isobe T., Gunji T., Morino Y., Saito S., Yamaguchi Y., Sawada S., and Yokkaichi S.: "Development of a time projection chamber using gas electron multipliers (GEM-TPC)", Nuclear Instruments and Methods in Physics Research A **566**, 312–320 (2006). ∗

Michimasa S., Shimoura S., Iwasaki H., Tamaki M., Ota S., Aoi N., Baba H., Iwasa N., Kanno S., Kubono S., Kurita K., Uesaka M., Minemura T., Motobayashi T., Notani M., Ong H., Saito A., Sakurai H., Takeshita E., Takeuchi S., Yanagisawa Y., and Yoshida A.: "Proton single-particle states in the neutron-rich ^{23}F nucleus", Phys. Lett. B **638**, 146–152 (2006). ∗

Tabaru T., Enyo H., Muto R., Naruki M., Yokkaichi S., Chiba J., Sekimoto M., Tanaka K., Sasaki O., Ieiri M., Funahashi H., Kitaguchi M., Kanda H., Mihara S., Miyashita T., Murakami T., Ozawa K., Hamagaki H., Sakuma F., Yamada S., Togawa M., Fukao Y., Ishino M., Miwa K., Nakura T., and Yoshimura Y.: "Nuclear mass number dependence of inclusive production of omega and phi mesons in 12-GeV p + A collisions", Phys. Rev. C **74**, 025201-1–025201-11 (2006). ∗

De Vita R., CLAS Collaboration ., and Nakagawa I.: "Search for the Θ^+ pentaquark in the reactions $\gamma p \to \overline{K}^0 K^+ n$ and $\gamma p \to \overline{K}^0 K^0 p$", Phys. Rev. D **74**, No. 3, pp. 032001-1–032001-16 (2006). ∗

Iida H., Doi T., Ishii N., Suganuma H., and Tsumura K.: "Charmonium properties in deconfinement phase in anisotropic lattice QCD", Phys. Rev. D **74**, 074502-1–074502-12 (2006). ∗

Naruki M., Fukao Y., Funahashi H., Ishino M., Kanda H., Kitaguchi M., Mihara S., Miwa K., Miyashita T., Murakami T., Nakura T., Sakuma F., Togawa M., Yamada S., Yoshimura Y., Enyo H., Muto R., Tabaru T., Yokkaichi S., Chiba J., Ieiri M., Sasaki O., Sekimoto M., Tanaka K. H., Hamagaki H., and Ozawa K.: "Experimental signature of medium modifications for ρ and ω mesons in 12 GeV p + A reactions", Phys. Rev. Lett. **96**, No. 9, pp. 092301-1–092301-4 (2006). ∗

McKinnon B., CLAS Collaboration ., and Nakagawa I.: "Search for Θ^+ pentaquark in the reaction $\gamma p \to pK^- K^+ n$", Phys. Rev. Lett. **96**, No. 21, pp. 212001-1–212001-6 (2006). ∗

Bai M., Roser T., Ahrens L., Alekseev I. G., Alessi J., Beebe-Wang J., Blaskiewicz M., Bravar A., Brennan J. M., Bruno D., Bunce G. M., Courant E., Drees A., Fischer W., Gardner C., Gill R., Glenn J., Haeberli W., Huang H., Jinnouchi O., Kewisch J., Luccio A., Luo Y., Nakagawa I., Okada H., Pilat F., MacKay W. W., Makdisi Y., Montag C., Ptitsyn V., Satogata T., Stephenson E., Svirida D., Tepikian S., Trbojevic D., Tsoupas N., Wise T., Zelenski A., Zeno K., and Zhang S. Y.: "Polarized Proton Collisions at 205 GeV at RHIC", Phys. Rev. Lett. **96**, 174801-1–174801-4 (2006). ∗

Mishima K., Sato H., Yamada S., Hirota K., Suzuki J., Oku T., Morishima T., Shimizu H., and Shinohara T.: "Development of measurement system of neutron β decay", Physica B **385/386**, No. 2, pp. 1219–1221 (2006). ∗

Taketani K., Funahasi H., Seki Y., Hino M., Kitaguchi M., Otake Y., and Shimizu H. M.: "Moire fringes of

cold neutron with large divergence angle", Physica B **385/386**, 1222–1224 (2006). ∗

Kawamura S., Kaneko J. H., Fujimoto H., Otake Y., Fujita F., Homma A., Sawamura T., Mikula P., and Furusaka M.: "Possibility of using a PMN-PT single crystal as neutron optical device", Physica B **385/386**, 1277–1279 (2006). ∗

Doi T., Blum T. C., Hayakawa M., Izubushi T., and Yamada N.: "The Isospin breaking effect on baryons with N(f) = 2 domain wall fermions", Proceedings of Science **LAT2006**, 174-1–174-7 (2006). ∗

Okamura M., Kashiwagi H., Sakakibara K., Takano J., Hattori T., Hayashizaki N., Jameson R., and Yamamoto K.: "High current carbon beam production with direct plasma injection scheme", Rev. Sci. Instrum. **77**, 03B303-1–03B303-3 (2006). ∗

Sakakibara K., Okamura M., Kondrashev S., Hattori T., Kashiwagi H., and Kanesue T.: "Analysis of Laser-Produced Heavy Ions for Direct Plasma Injection Scheme", Rev. Sci. Instrum. **77**, 03B304-1–03B304-3 (2006). ∗

Kashiwagi H., Fukuda M., Okamura M., Jameson R., Hattori T., Hayashizaki N., Sakakibara K., Takano J., Yamamoto K., Iwata Y., and Fujimoto T.: "Acceleration of high current fully stripped carbon ion beam by direct injection scheme", Rev. Sci. Instrum. **77**, 03B305-1–03B305-4 (2006). ∗

Muto R., Chiba J., Enyo H., Fukao Y., Funahashi H., Hamagaki H., Ieiri M., Ishino M., Kanda H., kitaguchi m., Mihara S., Miwa K., Miyashita T., Murakami T., Nakura T., Naruki M., Ozawa K., Sakuma F., Sasaki O., Sekimoto M., Tabaru T., Tanaka K., Togawa M., Yamada S., Yokkaichi S., and Yoshimura Y.: "Evidence for in-medium modification of the ϕ meson at normal nuclear density", Phys. Rev. Lett. **98**, No. 4, pp. 042501-1–042501-4 (2007). ∗

四日市悟, Chiba J., 延与秀人, 深尾祥紀, 舟橋春彦, 浜垣秀樹, Ieiri M., Ishino M., Kanda H., 北口雅暁, Mihara S., Miyashita T., 三輪浩司, 村上哲也, 武藤亮太郎, Nakura T., 成木恵, 小沢恭一郎, 佐久間史典, Sasaki O., 関本美知子, 田原司睦, Tanaka K., 外川学, Yamada S., Yoshimura Y.: "Experimental Study of in-medium meson modification at the KEK 12 GeV PS", 素粒子論研究 **114**, No. 2, pp. B7–B12 (2006).

[Book・Proc.]

(Original Papers) ∗Subject to Peer Review

Taketani K., Funahasi H., Seki Y., Hino M., Kitaguchi M., Maruyama R., Otake Y., and Shimiuzu H. M.: "Development of Mach-Zehnder Interferometer and "Coherent Beam Steering" Technique for Cold Neutrons", Foundations of Quantum Mechanics in the Light of New Technology (ISQM-Tokyo'05) Proceedings of 8th International Symposium, Hatoyama, 2005–8, World Scientific, Hatoyama, pp. 282–285 (2006). ∗

Oral Presentations

(International Conference etc.)

Ishii N., Doi T., Iida H., Oka M., Okiharu F., and Suganuma H.: "Penta-quark anti-decuplet in anisotropic lattice QCD", LATTICE 2004: 22nd International Symposium on Lattice Field Theory, (Fermi National Accelerator Laboratory), Batavia, USA, June (2004).

Doi T., Ishii N., Oka M., and Suganuma H.: "The lattice QCD simulation of the quark-gluon mixed condensate $g\langle\bar{q}\sigma_{\mu\nu}G_{\mu\nu}q\rangle$ at finite temperature and the phase transition of QCD", LATTICE 2004: 22nd International Symposium on Lattice Field Theory, Batavia, USA, June (2004).

Ishii N., Doi T., Iida H., Oka M., Okiharu F., and Suganuma H.: "Anisotropic lattice QCD studies of penta-quark anti-decuplet", International Workshop on PENTAQUARK04, (RCNP and JASRI), Harima Science Garden City, July (2004).

Doi T., Ishii N., Oka M., and Suganuma H.: "Thermal effects on quark-gluon mixed condensate $g\langle\bar{q}\sigma_{\mu\nu}G_{\mu\nu}q\rangle$ from lattice QCD", 2004 Gordon Research Conference on Photonuclear Reactions, Tilton, USA, Aug. (2004).

Yamada K., Motobayashi T., Aoi N., Baba H., Demichi K., Elekes Z., Gibelin J. D., Gomi T., Hasegawa H., Imai N., Iwasaki H., Kanno S., Kubo T., Kurita K., Matsuyama Y., Michimasa S., Minemura T., Notani M., Onishi T., Ong H., Ota S., Ozawa A., Saito A., Sakurai H., Shimoura S., Takeshita E., Takeuchi S., Tamaki M., Togano Y., Yanagisawa Y., Yoneda K., and Tanihata I.: "The first measurement of reduced transition probabilities for first 2^+ excited state in ^{46}Cr, ^{50}Fe, and ^{54}Ni", 4th International Conference on Exotic Nuclei and Atomic Masses (ENAM 04), (Oak Ridge National Laboratory), Pine Mountain, USA, Sept. (2004).

Ishii N., Doi T., Iida H., Oka M., Okiharu F., and Suganuma H.: "Penta-quark in anisotropic lattice QCD", 10th International Conference on the Structure of Baryons (Baryons 2004), Palaiseau, France, Oct. (2004).

Togawa M. and PHENIX C.: "Study of the gluon polarization in the proton with a silicon vertex upgrade at RHIC/PHENIX", 16th International Spin Physics Symposium (SPIN 2004), Trieste, Italy, Oct. (2004).

Watanabe Y.: "DAQ system for RI beam facilities: present and future", 5th Italy-Japan Symposium on Recent Achievements and Perspectives in Nuclear Physics, (Istituto Nazionale di Fisica Nucleare), Naples, Italy, Nov. (2004).

Okiharu F., Doi T., Ichie H., Iida H., Ishii N., Oka M., Suganuma H., and Takahashi T. T.: "Tetraquark and pentaquark systems in lattice QCD", Quark Nuclear Physics 2005: Nuclear and Hadronic Systems and Quark Degrees of Freedom, Pyoungchang, Ko-

rea, Feb. (2005).

Iida H., Doi T., Ishii N., and Suganuma H.: "J/Ψ at high temperatures in anisotropic lattice QCD", 23rd International Symposium on Lattice Field Theory (Lattice 2005), Dublin, Ireland, July (2005).

Doi T., Ishii N., Nemoto Y., Oka M., and Suganuma H.: "Anisotropic lattice QCD study of pentaquark baryons in spin 3/2 channel", 23rd International Symposium on Lattice Field Theory (Lattice 2005), Dublin, Ireland, July (2005).

Ishii N., Doi T., Nemoto Y., Oka M., and Suganuma H.: "Anisotropic lattice QCD studies of spin 3/2 penta-quark", 2nd Joint Meeting of the Nuclear Physics Divisions of the APS and JPS (Hawaii 2005), Maui, USA, Sept. (2005).

Togano Y., Gomi T., Motobayashi T., Ando Y., Aoi N., Baba H., Demichi K., Elekes Z., Fukuda N., Fulop Z., Hasegawa H., Higurashi Y., Ieki K., Imai N., Ishihara M., Ishikawa K., Iwasa N., Iwasaki H., Kanno S., Kondo Y., Kubo T., Kubono S., Kurita K., Matsuyama Y., Michimasa S., Minemura T., Miura M., Murakami H., Nakamura T., Notani M., Ota S., Saito A., Sakurai H., Serata M., Shimoura S., Sugimoto T., Takeshita E., Takeuchi S., Ue K., Yamada K., Yanagisawa Y., Yoneda K., Yoshida A., Futakami U., and Kunibu M.: "Coulomb dissociation of ^{27}P for Study of ^{26}Si(p,γ)^{27}P reaction", 2nd Joint Meeting of the Nuclear Physics Divisions of the APS and JPS (Hawaii 2005), Maui, USA, Sept. (2005).

Akiba Y.: "Hadronic Probes of dense matter at RHIC: From light to heavy flavors", 2nd Joint Meeting of the Nuclear Physics Divisions of the APS and JPS (Hawaii 2005), Maui, USA, Sept. (2005).

Doi T., Blum T. C., Hayakawa M., Izubushi T., and Yamada N.: "Isospin breaking of baryon masses from domain-wall lattice QCD", 2nd Joint Meeting of the Nuclear Physics Divisions of the APS and JPS (Hawaii 2005), Maui, USA, Sept. (2005).

Michimasa S., Aoi N., Iwasa N., Iwasaki H., Kanno S., Kubono S., Kurita K., Minemura T., Motobayashi T., Notani M., Ong H., Ota S., Saito A., Shimoura S., Takeshita E., Tamaki M., Uesaka M., Yanagisawa Y., Yoshida A., Sakurai H., Takeuchi S., and Baba H.: "Measurement of proton transfer reaction for single-particle states in ^{23}F", 2nd Joint Meeting of the Nuclear Physics Divisions of the APS and JPS (Hawaii 2005), Maui, USA, Sept. (2005).

Okada H.: "Measurement of the transverse-spin asymmetries in pp elastic scattering in the peak CNI region at RHIC", 2nd Joint Meeting of the Nuclear Physics Divisions of the APS and JPS (Hawaii 2005), Maui, USA, Sept. (2005).

Yamada K., Iwasa N., Bishop S., Elekes Z., Gibelin J. D., Hosoi M., Ieki K., Ishikawa K., Iwasaki H., Kawai S., Kondo Y., Kubono S., Kurita K., Kurokawa M., Matsui N., Minemura T., Morikawa H., Nakamura T., Niikura M., Notani M., Ota S., Saito A., Sakurai H., Shimoura S., Sugawara K., Sugimoto T., Suzuki H., Suzuki T., Takeshita E., Takeuchi S., Tanihata I., Teranishi T., Togano Y., Yamaguchi K., Yanagisawa Y., and Motobayashi T.: "New Coulomb Excitation Measurement of ^{18}Ne", 2nd Joint Meeting of the Nuclear Physics Divisions of the APS and JPS (Hawaii 2005), Maui, USA, Sept. (2005).

Ishii N., Doi T., Iida H., Nemoto Y., Oka M., Okiharu F., Suganuma H., and Tsumura K.: "Anisotropic lattice QCD studies of penta-quarks and tetra-quarks", Particles and Nuclei International Conference (PANIC05), Santa Fe, USA, Oct. (2005).

Takeuchi S., Aoi N., Baba H., Fukui T., Hashimoto Y., Ieki K., Imai N., Iwasaki H., Kanno S., Kondo Y., Kurita K., Minemura T., Motobayashi T., Nakabayashi T., Nakamura T., Okumura T., Onishi T., Ota S., Sakurai H., Shimoura S., Sugo R., Suzuki D., Suzuki H., Suzuki M., Takeshita E., Tamaki M., Tanaka K., Togano Y., and Yamada K.: "Proton inelastic scattering of ^{32}Mg", International Symposium on Structure of Exotic Nuclei and Nuclear Forces (SENUF06), (University of Tokyo), Tokyo, Mar. (2006).

Kondrashev S., Kashiwagi H., Kanesue T., Jameson R., Okamura M., Sakakibara K., and Tamura J.: "Acceleration of Intense Beams of Highly-Charged Ions using Direct Plasma Injection Scheme", 39th ICFA Advanced Beam Dynamics Workshop on High Intensity High Brightness Hadron Beams (ICFA HB2006), (KEK), Tsukuba, May–June (2006).

Huang H., Okamura M., and Takano J.: "Acceleration of Polarized protons in the AGS with Two Helical Partial Snakes", 10th biennial European Particle Accelerator Conference (EPAC'06), (EPAC), Edinburgh, UK, June (2006).

Kanesue T., Kondrashev S., Okamura M., and Sakakibara K.: "Ag Acceleration Using Direct Plasma Injection Method", 10th biennial European Particle Accelerator Conference (EPAC'06), (EPAC), Edinburgh, UK, June (2006).

Kondrashev S., Kanesue T., Okamura M., and Sakakibara K.: "Generation of Highly Charged Ions Using ND-glass Laser", 10th biennial European Particle Accelerator Conference (EPAC'06), (EPAC), Edinburgh, UK, June (2006).

Yokkaichi S.: "Medium modification of vector mesons in 12 GeV p+A reactions at KEK-PS", 9th International Workshop on Meson Production, Properties and Interaction (MESON2006), Cracow, Poland, June (2006).

Goto Y. and Forte S.: "Spin physics working group summary", 14th International Workshop on Deep Inelastic Scattering (DIS2006), (KEK (High Energy Accelerator Research Organization)), Tsukuba, July (2006).

Goto Y.: "Spin physics of the J-PARC dimuon experiment", Advanced Studies Institute: Symmetries and Spin (SPIN-Praha-2006), (Charles University in Prague, Faculty of Mathematics and Physics), Prague, Czech, July (2006).

Goto Y.: "Spin physics results at PHENIX", Advanced Studies Institute: Symmetries and Spin (SPIN-Praha-2006), (Charles University in Prague, Faculty of Mathematics and Physics), Prague, Czech, July (2006).

Ariyoshi S., Otani C., Dobroiu A., Matsuo H., Sato H., Taino T., Kawase K., and Shimizu H.: "Terahertz Imaging with an STJ-based Linear Array Detector(Invited Oral)", Applied Superconductivity Conference 2006 (ASC 2006), Seattle, USA, Aug.–Sept. (2006).

Otani C., Ariyoshi S., Taino T., Dobroiu A., Shibuya T., Sato H., Shimizu H., and Kawase K.: "Development of Terahertz Imaging Detectors using Superconducting Tunnel Junctions", International Conference on Mesoscopic Superconductivity and Magnetism (MesoSuperMag 2006), (Argonne National Laboratory), Chicago, USA, Aug.–Sept. (2006).

Michimasa S., Shimoura S., Iwasaki H., Tamaki M., Ota S., Aoi N., Baba H., Iwasa N., Kanno S., Kubono S., Kurita K., Minemura T., Motobayashi T., Notani M., Ong H., Saito A., Sakurai H., Takeshita E., Takeuchi S., Uesaka M., Yanagisawa Y., and Yoshida A.: "Proton shell structure in neutron-rich ^{23}F", International Conference on Nucleus Nucleus Collisions (NN2006), Rio de Janeiro, Brazil, Aug.–Sept. (2006).

Ariyoshi S., Otani C., Dobroiu A., Matsuo H., Sato H., Taino T., Kawase K., and Shimizu H.: "THz Imaging with a Linear Array Detector based on Superconducting Tunnel Junctions", 2006 Joint 31st International Conference on Infrared and Millimeter Waves and 14th International Conference on Terahertz Electronics (IRMMW-THz2006), (Shanghai Institute of Technical Physics (SITP)), Shanghai, China, Sept. (2006).

Seki Y., Funahasi H., Taketani K., Kitaguchi M., Hino M., Otake Y., and Shimiuzu H. M.: "Development of Neutron Interferometer with Wide-Gapped BSEs for Precision Measurements", 17th International Spin Physics Symposium (SPIN2006), (Department of Physics, Kyoto University), Kyoto, Oct. (2006).

Otani C., Ariyoshi S., Taino T., Myoren H., Sato H., Shimizu H., Takada S., and Kawase K.: "Terahertz Detectors using Superconducting Tunnel Junctions (Invited)", 19th International Symposium on Superconductivity (ISS 2006), (International Superconductivity Technology Center (ISTEC)), Nagoya, Oct.–Nov. (2006).

Taino T., Ishii H., Yoshimura S., Otani C., Ariyoshi S., Myoren H., Kawase K., Shibuya T., Sato H., Shimizu H., and Takada S.: "Terahertz electromagnetic-waves detector using Nb-based superconducting tunnel junction on LiNb03 substrate absorber", 19th International Symposium on Superconductivity (ISS 2006), (ISTEC (International Superconductivity Technology Center)), Nagoya, Oct.–Nov. (2006).

Otani C., Ariyoshi S., Taino T., Sato H., Shimizu H., and Kawase K.: "Radiation Detectors using Superconducting Tunnel Junctions (invited lecture)", 14th International Symposium on Laser Spectroscopy (SOLS 2006), (KAERI), Daejeon, Korea, Nov. (2006).

Enyo H.: "Experimental signatures for vector meson modification in nuclear medium", Yukawa International Seminar (YKIS) 2006 New Frontiers in QCD: Exotic Hadrons and Hadronic Matter, (Yukawa Institute for Theoretical Physics, Kyoto University), Kyoto, Nov.–Dec. (2006).

Otani C., Ariyoshi S., Taino T., Dobroiu A., Sato H., Shimizu H., and Kawase K.: "Development of Terahertz Detectors using Superconducting Tunnel Junctions (invited)", 2nd CREST Nano-Virtual-Labs Joint Workshop on Superconductivity (NVLS2006), Kyoto, Dec. (2006).

Sato H. and Mishima K.: "Low energy proton detector using STJ with large area", 2nd CREST Nano-Virtual-Labs Joint Workshop on Superconductivity (NVLS2006), (Nagoya University), Kyoto, Dec. (2006).

Ariyoshi S., Otani C., Dobroiu A., Matsuo H., Taino T., Sato H., and Shimizu H.: "STJ-based direct detector array for terahertz imaging applications", 7th Workshop on Submillimeter-Wave Receiver Technologies in Eastern Asia/Workshop on the Development of Low-Noise Receiver Technology at Millimeter Waves and Terahertz Frequencies, (Nobeyama Radio Observatory), Sakai, Jan. (2007).

(Domestic Conference)

竹下英里, 青井考, 大田晋輔, 武内聡, 鈴木宏, 馬場秀忠, Bishop S., 福井利晃, 井手口栄治, 家城和夫, 今井伸明, 岩崎弘典, 菅野祥子, 近藤洋介, 久保敏幸, 栗田和好, 日下健祐, 峯村俊行, 本林透, 中林彩, 中村隆司, 中尾太郎, 新倉潤, 奥村俊文, 王惠仁, 大西健夫, 櫻井博儀, 下浦享, 須合亮平, 鈴木大介, 鈴木賢, 玉城充, 田中鐘信, 栂野泰宏, 山田一成: "中性子過剰核 Cr 同位体の陽子非弾性散乱", 日本物理学会第 61 回年次大会, 松山, 3 月 (2006).

延與秀人: "ハドロン物理の新展開 – RHIC から J-Parc へ – (招待講演)", 日本物理学会第 61 回年次大会, 松山, 3 月 (2006).

道正新一郎, 下浦享, 岩崎弘典, 玉城充, 大田晋輔, 青井考, 馬場秀忠, 岩佐直仁, 菅野祥子, 久保野茂, 栗田和好, 峯村俊行, 本林透, 野谷将広, 王惠仁, 齋藤明登, 櫻井博儀, 竹下英里, 武内聡, 上坂明子, 柳澤善行, 吉田敦: "Single-particle states in ^{23}F by a proton transfer reaction", 日本物理学会第 61 回年次大会, (日本物

理学会), 松山, 3 月 (2006).

三島賢二, 佐藤広海, 大野雅史, 森嶋隆裕, 山田悟, 奥隆之, 鈴木淳市, 清水裕彦: “中性子ビームラインにおける原研 3 号炉での中性子ベータ崩壊実験 (NBD) について：超伝導検出器 (STJ) の運用”, 日本物理学会第 61 回年次大会, 松山, 3 月 (2006).

武内聡, 青井考, 馬場秀忠, 福井利晃, 橋本佳子, 家城和夫, 今井伸明, 岩崎弘典, 菅野祥子, 近藤洋介, 栗田和好, 峯村俊行, 本林透, 中林彩, 中村隆司, 奥村俊文, 大西健夫, 大田晋輔, 櫻井博儀, 下浦享, 須合亮平, 鈴木大介, 鈴木宏, 鈴木賢, 竹下英里, 玉城充, 田中鐘信, 栂野泰宏, 山田一成: “^{32}Mg と ^{34}Si の γ 線核分光”, RIBF ミニワークショップ「Island of Inversion に関する実験・理論の現状と今後の展望–$7 < Z < 20$ 領域中性子過剰核の低励起状態に関する検討会–」, 和光, 5 月 (2006).

大谷知行, 有吉誠一郎, 佐藤広海, 川瀬晃道, 田井野徹, 清水裕彦: “超伝導トンネル (STJ) 素子によるテラヘルツ波アレイ検出器の開発とイメージング（招待講演）”, 応用物理学会超伝導分科会第 33 回研究会「高感度分析・分光技術のための超伝導検出器」, (超伝導工学研究所), 東京, 6 月 (2006).

石井宏和, 吉村正太, 田井野徹, 明連広昭, 大谷知行, 渋谷孝幸, 有吉誠一郎, 佐藤広海, 延與秀人, 川瀬晃道, 高田進: “THz 波検出のための基板吸収型 STJ 検出器の高感度化”, 第 67 回応用物理学会学術講演会, 滋賀県草津, 8–9 月 (2006).

三島賢二, 佐藤広海, 山田悟, 森嶋隆裕, 奥隆之, 広田克也, 鈴木淳市, 清水裕彦: “超伝導検出器 (STJ) を用いた中性子 β 崩壊の測定”, 日本物理学会 2006 年秋季大会, 奈良, 9 月 (2006).

関義親, 舟橋春彦, 竹谷薫, 北口雅暁, 日野正裕, 大竹淑恵, 清水 (M) 裕彦: 日本中性子科学会第 6 回年会, 水戸, 12 月 (2006).

三島賢二, 佐藤広海, 山田悟, 森嶋隆裕, 広田克也, 鈴木淳市, 奥隆之, 篠原武尚, 清水裕彦: “超伝導トンネル接合素子を用いた中性子 β 崩壊測定実験”, 日本中性子科学会第 6 回年会, 水戸, 12 月 (2006).

有吉誠一郎, 大谷知行, Dobroiu A., 松尾宏, 田井野徹, 佐藤広海, 清水裕彦: “スペース天文応用を目指したサブミリ波帯 STJ 検出器アレイの開発”, 第 7 回宇宙科学シンポジウム, (宇宙航空研究開発機構宇宙科学研究本部), 相模原, 12 月 (2006).

有吉誠一郎, 大谷知行, Dobroiu A., 松尾宏, 佐藤広海, 田井野徹, 川瀬晃道, 清水裕彦: “超伝導検出器アレイを用いたテラヘルツイメージング”, 電子情報通信学会電子デバイス研究会 2006 年度月間研究会（12 月）, 東京, 12 月 (2006).

成木恵: “J-PARC E19 High-resolusion Search for Θ^+ Pentaquark in $\pi^- p \to K^- X$ Reaction”, 文部科学省科学研究費補助金特定領域研究「ストレンジネスで探るクォーク多体系」研究会 2006, (KEK), 熱海, 12 月 (2006).

成木恵: “Pentaquark Θ^+ Search in Hadronic Reaction”, RCNP 研究会「LEPS/SPring-8 新ビームライン」, 大阪, 1 月 (2007).

池田一昭, 広田克也, 佐藤広海, 大森整, 清水裕彦, 古坂道弘: “中性子ビーム用デバイスのための曲面スーパーミラーの開発”, 日本物理学会 2007 年春季大会, 鹿児島, 3 月 (2007).

三島賢二, 佐藤広海, 山田悟, 広田克也, 森嶋隆裕, 鈴木淳市, 奥隆之, 篠原武尚, 清水裕彦: “超伝導トンネル接合素子を用いた中性子ベータ崩壊からの低エネルギー陽子検出器の開発”, 日本物理学会 2007 年春季大会, 八王子, 3 月 (2007).

Advanced Meson Science Lab.

Publications

[**Journal**]

(Original Papers) ∗Subject to Peer Review

Miller J. P., Carey R. M., Logashenko V., Lynch K. R., Roberts B. L., Silenko A., Bennett G., Lazarus D. M., Leipuner L. B., Marciano W., Meng W., Morse W. M., Prigl R., Semertzidis Y. K., Balakin V., Bazhan A., Dunikov A., Khazin B., Khriplovich I. B., Sylvestrov G., Orlov Y., Jungmann K., Debevec P. T., Hertzog D. W., Onderwater C. J., Ozben C. S., Stephenson E., Auzinsh M., Cushman P., McNabb R., Shafer-Ray N., Yoshimura K., Aoki A., Kuno Y., Sato A., Iwasaki M., and Farley F. J.: “A New Experiment to Measure the Muon Electric Dipole Moment”, AIP Conf. Proc. **698**, 196–199 (2003).

Suzuki K., Fujita M., Geissel H., Gilg H., Gillitzer A., Hayano R., Hirenzaki S., Itahashi K., Iwasaki M., Kienle P., Matos M., Munzenberg G., Ohtsubo T., Sato M., Shindo M., Suzuki T., Weick H., Winkler M., Yamazaki T., Sato M., and Yoneyama T.: “Deeply bound poonic 1s in sn isotopes”, Nucl. Phys. A **721**, 831c–834c (2003). ∗

Suzuki K., Fujita M., Geissel H., Gilg H., Gillitzer A., Hayano R., Hirenzaki S., Itahashi K., Iwasaki M., Kienle P., Matos M., Muenzenberg G., Otsubo T., Sato M., Shindo M., Suzuki T., Weick H., Winkler M., Yamazaki T., and Yoneyama T.: “Observattion of Pionic 1*s* States in Sn Nuclei and Its Implications on Chiral Symmetry Restoration”, Prog. Theor. Phys. Suppl., No. 149, pp. 32–41 (2003). ∗

Itahashi K., Iwasaki M., and Suzuki T.: “Experimental Search for Kaonic Nuclear Bound States in the ^{4}He (stopped K^-,n) Reaction”, Prog. Theor. Phys. Suppl., No. 149, pp. 233–239 (2003).

Beer G. A., Bragadireanu A. M., Cargnelli M., Curceanu C., Egger J. -., Fuhrmann H., Giersch M., Guaraldo C., Iliescu M., Ishiwatari T., Itahashi K., Iwasaki M., Kienle P., Lauss B., Lucherini V., Ludhova L., Marton J., Mulhauser F., Ponta T., Schaller L. A., Sirghi D. L., Sirghi F., and Zmeskal J.: “Kaonic Hydrogen: *Status of the DEAR Experiment*”, Prog. Theor. Phys. Suppl., No. 149, pp. 240–246 (2003).

Curceanu C., Beer G. A., Bragadireanu A. M., Cargnelli M., Egger J. -., Fuhrmann H., Guaraldo C., Iliescu M., Ishiwatari T., Itahashi K., Iwasaki

M., Lauss B., Lucherini V., Ludhova L., Marton J., Mulhauser F., Ponta T., Schaller L. A., Seki R., Sirghi D., Sirghi F., Strasser P., and Zmeskal J.: "Last results from the DEAR experiment at DAΦNE", AIP Conf. Proc. **717**, 175–179 (2004).

Suzuki T., Itahashi K., Iwasaki M., Matsuda Y., Okada S., Outa H., Sato M., Strasser P., Tomono D., and Yamazaki T.: "A search for deeply bound kaonic nuclear states", Nucl. Phys. A **754**, 375c–382c (2005). ∗

Jönsson P. E., Takayama H., Aruga-Katori H., and Ito A.: "Dynamical breakdown of the Ising spin-glass order under a magnetic field", Phys. Rev. B **71**, 180412-1–180412-4 (2005). ∗

Jonsson P. E., Aruga-Katori H., Ito A., and Takayama H.: "Field effects in the Ising spin glass $Fe_{0.55}Mn_{0.45}TiO_3$—Absence of spin-glass transition in a magnetic field", Prog. Theor. Phys. Suppl., No. 157, pp. 38–41 (2005). ∗

Tomono D.: "Presicion measurement of the positive muon lifetime at the RIKEN-RAL muon facility", AIP Conf. Proc. **842**, 906–908 (2006). ∗

Tonishi J., Suzuki T., and Goto T.: "Anomalous Change of Hall Coefficient in Overdoped $La_{2-x}Sr_xCu_{1-y}Zn_yO_4$ around $x = 0.2$", AIP Conf. Proc. **850**, 407–408 (2006). ∗

Suzuki T., Ota T., Tonishi J., and Goto T.: "Increase of the sound velocity by magnetic fields in $La_{2-x}Sr_xCuO_4$ around $x = 0.220$", AIP Conf. Proc. **850**, 409–410 (2006). ∗

Inoue H., Tani S., Hosoya S., Suzuki T., Goto T., Tanaka H., Sasaki T., and Kobayashi N.: "^{2}D, $^{35/37}$Cl, $^{63/65}$Cu-NMR Study of the Quantum Spin System NH_4CuCl_3", AIP Conf. Proc. **850**, 1061–1062 (2006). ∗

Suzuki T., Saito T., Sasaki T., Osawa A., Goto T., Awaji S., Watanabe K., Kobayashi N., and Manaka H.: "Magnetic field effect on the magnetic torque and the magnetostriction in $(CH_3)_2CHNH_3CuCl_3$", J. Phys.: Con. Ser. **51**, 187–190 (2006). ∗

Fujiwara T., Inoue H., Osawa A., Tsunoda R., Goto T., Suzuki T., Shindo Y., Tanaka H., Sasaki T., Kobayashi N., Awaji S., and Watanabe K.: "Cu-NMR study on the disordered quantum spin magnet with the Bose-glass ground state", J. Phys.: Con. Ser. **51**, 199–202 (2006). ∗

Tonishi J., Ueda M., Suzuki T., Osawa A., Goto T., Adachi T., Koike Y., Fujita M., and Yamada K.: "Local structure in single crystals of La-based high T_c cuprates", J. Phys.: Con. Ser. **51**, 275–278 (2006). ∗

Suzuki T., Fujiwara T., Osawa A., Goto T., Yamada F., Tanaka H., and Watanabe I.: "Muon-Spin-Relaxation study on single crystals $Tl_{1-x}K_xCuCl_3$ with $x = 0.2$", J. Phys. Soc. Jpn. **75**, No. 2, pp. 025001-1–025001-2 (2006). ∗

Hachitani K., Amanuma H., Fukazawa H., Kohori Y., Koyama K., Kumagai K., Sekine C., and Shirotani I.: "Appearance of successive phase transition in $SmRu_4P_{12}$ under high magnetic fields probed by ^{31}P nuclear magnetic resonance", J. Phys. Soc. Jpn. **75**, No. 12, pp. 124712-1–124712-6 (2006). ∗

Hachitani K., Fukazawa H., Kohori Y., Watanabe I., Yoshimitsu Y., Kumagai K., Giri R., Sekine C., and Shirotani I.: "^{31}P-NMR and μSR studies of filled skutterudite compound $SmFe_4P_{12}$:evidence for heavy fermion behavior with ferromagnetic ground state", J. Phys. Soc. Jpn. **75**, No. 12, pp. 124717-1–124717-5 (2006). ∗

Attwood D., Bell P., Bull S., McMahon T., Wilson J., Fernow R., Gruber P., Jamdagni A., Long K., McKigney E., Savage P., Curtis-Rouse M., Edgecock T. R., Ellis M., Lidbury J., Murray W., Norton P., Peach K., Ishida K., Matsuda Y., Nagamine K., Nakamura S., Marshall G. M., Benveniste S., Cline D., Fukui Y., Lee K., Pischalnikov Y., Holmes S., and Bogacz A.: "The scattering of muons in low-Z materials", Nucl. Instrum. Methods Phys. Res. B **251**, 41–55 (2006). ∗

Matsuda Y., Bakule P., Iwasaki M., Matsuzaki T., Miyake Y., Ikedo Y., Strasser P., Simomura K., Makimura S., and Nagamine K.: "Generation of low-energy muons with laser resonant ionization", Nucl. Phys. B (Proc. Suppl.) **155**, 346–348 (2006). ∗

Ishiwatari T., Beer G. A., Bragadireanu A. M., Cargnelli M., Curceanu P. C., Egger J. P., Fuhrmann H., Guaraldo C., Iliescu M., Itahashi K., Iwasaki M., Kienle P., Lauss B., Lucherini V., Ludhova L., Marton J., Mulhauser F., Ponta T., Schaller L. A., Sirghi D. L., Strasser P., and Zmeslal J.: "New analysis method for CCD X-ray data", Nuclear Instruments and Methods in Physics Research A **556**, 509–515 (2006). ∗

Hachitani K., Fukazawa H., Kohori Y., Watanabe I., Sekine C., and Shirotani I.: "Evidence for magnetic ordering associated with metal-insulator transition in $SmRu_4P_{12}$ studied by muon spin relaxation", Phys. Rev. B **73**, 052408-1–052408-4 (2006). ∗

Saito T., Osawa A., Goto T., Suzuki T., and Watanabe I.: "Muon spin rotation and relaxation studies on the solid solution of the two spin-gap systems $(CH_3)_2CHNH_3$-$CuCl_3$ and $(CH_3)_2CHNH_3$-$CuBr_3$", Phys. Rev. B **74**, 134423-1–134423-5 (2006). ∗

Torikai E., Ito A., Watanabe I., and Nagamine K.: "μSR studies on the response of spin dynamics to applying or removing magnetic field — Typical Ising spin glass $Fe_{0.05}Mn_{0.05}TiO_3$", Physica B **374/375**, 95–98 (2006). ∗

Bakule P., Matsuda Y., Iwasaki M., Miyake Y., Nagamine K., Ikedo Y., Simomura K., and Strasser P.: "Pulsed source of ultra low-energy muons at RIKEN-RAL", Physica B **374/375**, 456–459 (2006). ∗

Miyake Y., Nishiyama K., Kawamura N., Makimura

S., Strasser P., Simomura K., Beveridge J. L., Kadono R., Fukuchi K., Sato N., Ueno K., Higemoto W., Ishida K., Matsuzaki T., Watanabe I., Matsuda Y., Iwasaki M., Nakamura S., Doornbos J., and Nagamine K.: "Status of J-PARC muon science facility at the year of 2005", Physica B **374/375**, 484–487 (2006). ∗

Jonsson P. E., Takayama H., Aruga-Katori H., and Ito A.: "Absence of phase transition in a magnetic field in the $Fe_{0.55}Mn_{0.45}TiO_3$ Ising spin glass", J. Magn. Magn. Mater. **310**, 1494–1499 (2007). ∗

Oral Presentations

(International Conference etc.)

Matsuda Y.: "Generation of ultra slow muon beam by laser resonant ionization of muonium atoms", 6th International Workshop on Neutrino Factories and Superbeams (NuFact 04), Osaka, July–Aug. (2004).

Iwasaki M.: "Kaonic deeply bound states, the first experimental results", International Conference on Exotic Atoms and Related Topics (EXA 05), (the Austrian Academy of Sciences), Vienna, Austria, Feb. (2005).

Suzuki T., Ota T., Tonishi J., and Goto T.: "Increase of the sound velocity by magnetic fields in $La_{2-x}Sr_xCuO_4$ around $x = 0.220$", 24th International Conference on Low Temperature Physics (LT24), (Department of Physics, University of Florida), Orlando, USA, Aug. (2005).

Iwasaki M.: "Strange trybaryon and present experimental program", 2nd Joint Meeting of the Nuclear Physics Divisions of the APS and JPS (Hawaii 2005), Maui, USA, Sept. (2005).

Akaishi Y.: "Kaonic nuclei in reply to recent criticisms (Theory)", International Workshop on Exotic hadronic atoms, deeply bound kaonic nuclear states and antihydrogen: present results, future challenges, (European Center for Theoretical Nuclear Physics and Related Areas), Trento, Italy, June (2006).

Iwasaki M.: "Kaonic-Helium 3d-2p *X*-ray experiment", International Workshop on Exotic hadronic atoms, deeply bound kaonic nuclear states and antihydrogen: present results, future challenges, (European Cneter for Theoretical Studies in Nuclear Physics and Related Areas), Trento, Italy, June (2006).

Kikkawa A., Katsumata K., Honda Z., Watanabe I., Suzuki T., and Matsuzaki T.: "Evolution of the spin-gap in a spin-ladder material detected by muSR technique", 1st International Symposium of Quantum Beam Science Directorate of JAEA (ICM2006 Satellite Conference), (JAEA), Tokai, Aug. (2006).

Ishida K.: "Muon catalyzed fusion", 8th International Workshop on Neutrino Factories nd Superbeams (NuFact 06), (University of California, Irvine), Irvine, USA, Aug. (2006).

Suzuki T., Watanabe I., Osawa A., Goto T., Yamada F., and Tanaka H.: "Muon-Spin-Relaxation study on randomness introduced $Tl_{1-x}K_xCuCl_3$ with $\boldsymbol{x} = 0.44$", An ICM2006 Satellite Conference: 1st International Symposium of Quantum Beam Science Directorate of JAEA, Advances in Neutron, Synchrotron Radiation, μSR and NMR Researches (QuBS2006), (Quantum Beam Science Directorate of JAEA), Tokai, Aug. (2006).

Jonsson P. E., Takayama H., Aruga-Katori H., and Ito A.: "Absence of phase transition in a magnetic field in the $Fe_{0.55}Mn_{0.45}TiO_3$ Ising spin glass", International Conference on Magnetism (ICM 2006), Kyoto, Aug. (2006).

Suzuki T., Saito T., Osawa A., Goto T., Sasaki T., Awaji S., Watanabe K., Kobayashi N., and Manaka H.: "Magnetic field effect on the magnetic torque and the magnetostriction in $(CH_3)_2CHNH_3CuCl_3$", Yamada Conference LX on Research in High Magnetic Fields (RHMF2006), (High Field Laboratory for Superconducting Materials Institute for Materials Research Tohoku University), Sendai, Aug. (2006).

Matsuda Y.: "Progress of laser ionization method for LEM", 1st Swiss Japan Workshop on the applications and on new developments in muon spectroscopy on novel materials, (High Energy Accelerator Research Organization), Tsukuba, Sept. (2006).

Bakule P.: "Laser ionization of muonium - pulsed ultra low energy muon source for material studies", International Conference on Laser Probing 2006 (LAP 2006), (Vienna University of Technology), Vienna, Austria, Sept. (2006).

Akaishi Y.: "Few-body antikaon nuclear bound states - theoretical view", 9th International Conference on Hypernuclear and Strange Particle Physics, Mainz, Germany, Oct. (2006).

Ishida K.: "RIKEN-RAL, now and in the future", Workshop on future developments of European muon sources, (NMI3), Abingdon, UK, Nov. (2006).

Koike T. and Harada T.: "DWIA calculation of ^{3}He (in-flight K^-,n) reaction", Yukawa International Seminar (YKIS) 2006 New Frontiers in QCD: Exotic Hadrons and Hadronic Matter, (Yukawa Institute for Theoretical Physics), Kyoto, Nov.–Dec. (2006).

Iwasaki M.: "Search for kaonic nuclear state by stopped K^- on helium target at kek", Yukawa International Seminar (YKIS) 2006 New Frontiers in QCD: Exotic Hadrons and Hadronic Matter, (Yukawa Institute for Theoretical Physics), Kyoto, Nov.–Dec. (2006).

(Domestic Conference)

蜂谷健一: "充填スクッテルダイト化合物 $SmRu_4P_{12}$ の μSR", 日本物理学会 2005 年秋季大会, 京都, 9 月 (2005).

川股隆行, 菅原直樹, Haidar S. M., 高橋伸雄, 宮島祐一, 野地尚, 小池洋二, 工藤一貴, 小林典男, 藤井裕, 菊池彦光, 千葉明朗, Petrakovskii G., Popov

M., Bezmaternikh L.: “$La_8Cu_7O_{19}$, Y_2BaNiO_5, CuB_2O_4 におけるスピン状態と熱伝導”, 科研費特定領域「異常量子物質の創製　新しい物理を生む新物質」成果報告会, 仙台, 1 月 (2006).

大平-河村聖子, 前川覚, 鍛治亮佑, 伊藤哲明: “量子スピンカゴメ格子磁性体 Cu-titmb の μSR 測定”, 日本物理学会第 61 回年次大会, 松山, 3 月 (2006).

赤石義紀, 山崎敏光: “ケイオン核－批判に答えて”, 日本物理学会第 61 回年次大会, 松山, 3 月 (2006).

鈴木栄男, 渡邊功雄, 藤原崇雄, 大沢明, 後藤貴行, 山田文子, 田中秀数: “量子スピン系 $Tl_{1-x}K_xCuCl_3$ ($\boldsymbol{x} = 0.2$) における μSR 測定”, 日本物理学会第 61 回年次大会, 愛媛大学, 3 月 (2006).

吉川明子, 勝又紘一, 本多善太郎, 渡邊功雄, 鈴木栄男, 松崎禎市郎: “スピンラダー物質 $Na_2Co_2(C_2O_4)_3(H_2O)_2$ の μSR 測定”, 日本物理学会 2006 年秋季大会, 千葉, 9 月 (2006).

大平-河村聖子, 齋藤麻優美, 宮坂等: “μSR 法でみた Mn^{III}_2-Ni^{II} 型単一次元鎖磁石のスピンダイナミクス”, 日本物理学会 2006 年秋季大会, 千葉, 9 月 (2006).

小池貴久, 原田融: “^{3}He 標的を用いた (in-flight K^-, n) 反応の DWIA 計算”, 日本物理学会 2006 年秋季大会, (日本物理学会), 奈良, 9 月 (2006).

岩崎雅彦: “KpX から K 核へ”, 日本物理学会 2006 年秋季大会, (日本物理学会), 奈良, 9 月 (2006).

松本琢磨, 緒方一介, 江上智晃, 井芹康統, 八尋正信, 上村正康: “6He 核力・クーロン分解反応の解析”, 日本物理学会 2006 年秋季大会, 奈良, 9 月 (2006).

石田勝彦: “理研 RAL ミュオン施設での研究の現状”, 仁科加速器研究センター原子核グループ月例コロキウム, 和光, 10 月 (2006).

蜂谷健一: “充填スクッテルダイト ^{31}P-NMR/μSR”, ボトムアップ若手の会第 1 回研究会：物理・化学・生物の融合を目指して, 和光, 11 月 (2006).

川股隆行, 宮島祐一, 高橋伸雄, 野地尚, 小池洋二, 工藤一貴, 小林典男: “5 本足スピン梯子格子系 $La_8Cu_7O_{19}$ とハルデンギャップ系 Y_2BaNiO_5 におけるスピンによる熱伝導”, ボトムアップ若手の会第 1 回研究会：物理・化学・生物の融合を目指して, 和光, 11 月 (2006).

川股隆行, 宮島祐一, 高橋伸雄, 野地尚, 小池洋二, 工藤一貴, 小林典男: “5 本足スピン梯子格子系 $La_8Cu_7O_{19}$ とハルデンギャップ系 Y_2BaNiO_5 におけるスピンによる熱伝導”, 東大物性研短期研究会「量子スピン系の物理」, 柏, 11 月 (2006).

松本琢磨, 江上智晃, 緒方一介, 井芹康統, 八尋正信, 上村正康: “不安定核分解反応による di-neutron 相関の研究”, RCNP 研究会「核子多体系におけるクラスター現象」, (大阪大学核物理研究センター), 大阪, 2 月 (2007).

小池貴久, 原田融: “^{3}He 標的を用いた (in-flight K^-,n) 反応の DWIA 計算 II”, 日本物理学会 2007 年春季大会, 八王子, 3 月 (2007).

Theoretical Physics Lab.

Publications

[**Journal**]

(Original Papers)　*Subject to Peer Review

Ishimoto Y.: “Two-point functions and logarithmic boundary operators in boundary logarithmic conformal field theories”, J. High Energy Phys. **8**, 039-1–039-22 (2004). *

Kinoshita T. and Nio M.: “Improved α^4 term of the muon anomalous magnetic moment”, Phys. Rev. D **70**, 113001-1–113001-27 (2004). *

Matsuo T. and Matsuura S.: “String Theoretical Interpretation for Finite N Yang-Mills Theory in Two Dimensions”, Mod. Phys. Lett. A **20**, No. 1, pp. 29–41 (2005). *

Kobayashi S., Asakawa T., and Matsuura S.: “Open string tachlon in supergravity solution”, Mod. Phys. Lett. A **20**, No. 15, pp. 1119–1134 (2005). *

Ishimoto Y. and Yamaguchi S.: “Minimal string theory is logarithmic”, Phys. Lett. B **607**, 172–179 (2005). *

Chu C., Furuta K., and Inami T.: “Locality, causality and noncommutative geometry”, Int. J. Mod. Phys. A **21**, No. 1, pp. 67–82 (2006). *

Asakawa T., Matsuura S., and Kobayashi S.: “Excited D-Branes and Supergravity Solutions”, Int. J. Mod. Phys. A **21**, No. 7, pp. 1503–1527 (2006). *

Aoyama T., Hayakawa M., Kinoshita T., and Nio M.: “Automated calculation scheme for α^n contributions of QED to lepton $g-2$: generating renormalized amplitudes for diagrams without lepton loops”, Nucl. Phys. B **740**, 138–180 (2006). *

Aoyama T. and Shibusa Y.: “Improved perturbation method and its application to the IIB matrix model”, Nucl. Phys. B **754**, 48–90 (2006). *

Aoyama T., Hayakawa M., Kinoshita T., and Nio M.: “Automated calculation scheme for α^n contributions of QED to lepton $g-2$”, Nucl. Phys. B (Proc. Suppl.) **157**, 106–110 (2006). *

Kinoshita T. and Nio M.: “Improved α^4 term of the electron anomalous magnetic moment”, Phys. Rev. D **73**, 013003-1–013003-28 (2006). *

Chu C., Furuta K., and Lin F.: “Nonlocal matching condition and scale-invariant spectrum in bouncing cosmology”, Phys. Rev. D **73**, 103505-1–103505-14 (2006). *

Eto M., Konishi K., Marmorini G., Nitta M., Ohashi K., Vinci W., and Yokoi N.: “Non-Abelian vortices of higher winding numbers”, Phys. Rev. D **74**, No. 6, pp. 065021-1–065021-19 (2006). *

Fukaya H., Hashimoto S., Ishikawa K., Kaneko T., Matsufuru H., Onogi T., and Yamada N.: “Lattice gauge action suppressing near-zero modes of H_W”, Phys. Rev. D **74**, 094505-1–094505-10 (2006). *

Aoyama T., Kuroki T., and Shibusa Y.: “Dynamical generation of non-Abelian gauge group via the

improved perturbation theory", Phys. Rev. D **74**, 106004-1–106004-14 (2006). ∗

Doi T., Blum T. C., Hayakawa M., Izubushi T., and Yamada N.: "The Isospin breaking effect on baryons with N(f) = 2 domain wall fermions", Proceedings of Science **LAT2006**, 174-1–174-7 (2006). ∗

Shibusa Y., Aoyama T., and Matsuo T.: "Improved Taylor Expansion Method in the Ising Model", Prog. Theor. Phys. **115**, No. 3, pp. 473–486 (2006). ∗

Hayakawa M. and Suzuki H.: "Gauge anomaly associated with the Majorana fermion in $8k + 1$ dimensions", Prog. Theor. Phys. **115**, No. 6, pp. 1129–1136 (2006). ∗

Hanada M., Kawai H., and Kimura Y.: "Curved superspaces and local supersymmetry in supermatrix model", Prog. Theor. Phys. **115**, 1003–1025 (2006). ∗

Hanada M., Kanai T., Kawai H., and Kubo F.: "Phase structure of the large-N reduced gauge theory and generalized Weingarten model", Prog. Theor. Phys. **115**, 1167–1177 (2006). ∗

Aoyama T., Kawai H., and Shibusa Y.: "Stability of 4-dimensional space-time from the IIB matrix model via the improved mean field approximation", Prog. Theor. Phys. **115**, 1179–1187 (2006). ∗

Hayakawa M., So H., and Suzuki H.: "Overlap lattice fermion in a gravitational field", Prog. Theor. Phys. **116**, No. 1, pp. 197–215 (2006). ∗

Aoyama T. and Kawai H.: "Higher order terms in the improved mean field approximation for the IIB matrix model and the emergence of four-dimensional space-time", Prog. Theor. Phys. **116**, No. 2, pp. 405–415 (2006). ∗

Fukaya H., Hayakawa M., Kanamori I., Suzuki H., and Takimi T.: "Note on massless bosonic states in two-dimensional field theories", Prog. Theor. Phys. **116**, No. 6, pp. 1117–1129 (2006). ∗

(Review)

鈴木博: "格子ゲージ理論におけるカイラル対称性の実現", 日本物理学会誌 **61**, No. 11, pp. 807–814 (2006).

[Book・Proc.]

(Others)

Ishimoto Y.: "Logarithmic correlation functions and moduli integrals in 2D minimal gravity", Proceedings of 4th International Symposium on Quantum Theory and Symmetries, Varna, Bulgaria, 2005–8, The Bulgarian Journal of Physics, Heron Press, Sofia, pp. 353–359 (2006).

Oral Presentations

(International Conference etc.)

Ishimoto Y.: "Logarithmic correlation functions in minimal string theory", International Workshop "Integrable Models and Applications", (European Collaboration Linking Integrability with other Disciplines 2002 - 2006), Sozopol, Bulgaria, Aug.–Sept. (2003).

Furuta K.: "Locality and evolution of cosmological perturbations", Summer School on Strings, (National Taiwan University), Taipei, Taiwan, July (2005).

Kuroki T. and Kawai H.: "Dijkgraaf-Vafa theory as large-N reduction", 4th International Symposium on Quantum Theory and Symmetries, (QTS), Varna, Bulgaria, Aug. (2005).

Furuta K.: "Locality and evolution of cosmological fluctuation", YITP workshop on String Theory and Quantum Field Theory, (Yukawa Institute for Theoretical Physics), Kyoto, Aug. (2005).

Doi T., Blum T. C., Hayakawa M., Izubushi T., and Yamada N.: "Isospin breaking of baryon masses from domain-wall lattice QCD", 2nd Joint Meeting of the Nuclear Physics Divisions of the APS and JPS (Hawaii 2005), Maui, USA, Sept. (2005).

Furuta K.: "Locality and evolution of cosmological fluctuation", 12th Vietnam School of Physics Workshop on Physics for Large and Small Scale, (Institute of physics and electronics), Hanoi, Vietnam, Jan. (2006).

Kanamori I., D'Adda A., Kawamoto N., Nagata K., and Saito J.: "Hermiticity and Majorana condition for two-dimensional super Yang-Mills on a lattice with Dirac-Kähler twist", Joint Meeting of Pacific Region Particle Physics Communities (DPF2006+JPS2006), (American Physical Society and Physical Society of Japan), Honolulu, USA, Oct.–Nov. (2006).

Eto M., Konishi K., Marmorini G., Nitta M., Ohashi K., Vinci W., and Yokoi N.: "Non-Abelian Duality from Vortex Moduli", Joint Meeting of Pacific Region Particle Physics Communities (DPF2006+JPS2006), (American Physical Society and Physical Society of Japan), Honolulu, USA, Oct.–Nov. (2006).

Fukaya H.: "Approaching the chiral limit in lattice QCD", 2006 International Workshop SCGT 06 "Origin of Mass and Strong Coupling Gauge Theories", (Nagoya University), Nagoya, Nov. (2006).

(Domestic Conference)

青山龍美, 早川雅司, 木下東一郎, 仁尾真紀子: "QED Tenth-order contributions to the lepton $g-2$", 日本物理学会第 61 回年次大会, 松山, 3 月 (2006).

澁佐雄一郎, 青山龍美, 黒木経秀: "改良された摂動論による行列模型におけるゲージ対称性の破れ", 日本物理学会第 61 回年次大会, 松山, 3 月 (2006).

澁佐雄一郎, 青山龍美, 松尾俊寛: "改良テーラー展開法における相転移", 日本物理学会第 61 回年次大会, 松山, 3 月 (2006).

尾田欣也: "Black hole production at collider", 京都大学基礎物理学研究所研究会「素粒子物理の進展」, 京都, 7–8 月 (2006).

仁尾真紀子: "量子電気理学の最前線", 2006 年度日本物理学会科学セミナー「朝永振一郎と 21 世紀の物理学：量子と時空の生み出す多様性」, 東京, 8 月 (2006).

花田政範, 古田黄, 川合光, 木村祐介: "Matrix model and field equations of massless fields in bosonic string theory", 理研シンポジウム「行列模型と弦理論」, 和光, 9 月 (2006).

小西憲一, Marmorini G., Vinci W., 横井直人: "Z_N vortices in $\mathcal{N} = 1^*$ SU(N) gauge theory", 2006 年度京都大学基礎物理学研究所研究会「弦理論と場の量子論における新たな進展」, 京都, 9 月 (2006).

尾田欣也: "Smoothing out negative tension brane", 2006 年度京都大学基礎物理学研究所研究会「弦理論と場の量子論における新たな進展」, 京都, 9 月 (2006).

金森逸作: "Hermiticity and Majorana condition for two-dimensional super Yang-Mills on a lattice with Dirac-Kaehler twist", 2006 年度基礎物理学研究所研究会「場の量子論の基礎的諸問題と応用」, (京都大学基礎物理学研究所), 京都, 12 月 (2006).

衛藤稔, Ferretti L., 小西憲一, Marmorini G., 新田宗土, 大橋圭介, Vinci W., 横井直人: "Non-abelian duality from vortex moduli", 2006 年度基礎物理学研究所研究会「場の量子論の基礎的諸問題と応用」, (京都大学基礎物理学研究所), 京都, 12 月 (2006).

深谷英則: "Topology in lattice QCD", 2006 年度基礎物理学研究所研究会「場の量子論の基礎的諸問題と応用」, (Yukawa Institute for Theoretical Physics, Kyoto University), Kyoto, 12 月 (2006).

Accelerator Applications Research Gr.

Publications

[**Journal**]

(Original Papers) *Subject to Peer Review

Nakamura T., Wada M., Okada K., Ishida Y., Takamine A., Yamazaki Y., Kambara T., Kanai Y., Kojima T., Nakai Y., Oshima N., Yoshida A., Kubo T., Katayama I., Lioubimov V., Wollnik H., Varentsov V., and Schuessler H. A.: "Laser spectroscopy of $^{7,10}Be^{+}$ in an online ion trap", Phys. Rev. A **74**, 052503-1–052503-5 (2006). *

(Review)

神原正: "重イオン照射による超音波の観測：イオンビーム地震学", 日本物理学会誌 **61**, No. 8, pp. 594–598 (2006).

Oral Presentations

(International Conference etc.)

Kambara T., Kanai Y., Kojima T., Nakai Y., Yoneda A., and Yamazaki Y.: "Elastic waves from fast heavy-ion irradiation on solids", 18th International Acoustic Emission Symposium, Sagamihara, July (2006).

Radiation Biology Team

Publications

[**Journal**]

(Original Papers) *Subject to Peer Review

Umebayashi Y., Honma M., Abe T., Ryuto H., Suzuki H., Shimazu T., Ishioka N., Iwaki M., and Yatagai F.: "Mutation induction after low-dose carbon-ion beam irradiation of frozen cultured cells", Biol. Sci. Space **19**, No. 4, pp. 237–241 (2005). *

Ikeda T., Kanai Y., Kojima T., Iwai Y., Kambara T., Yamazaki Y., Hoshino M., Nebiki T., and Narusawa T.: "Production of a microbeam of slow highly charged ions with a tapered glass capillary", Appl. Phys. Lett. **89**, 163502-1–163502-3 (2006). *

Takehisa H., Ueda T., Fukuta Y., Obara M., Abe T., Yano M., Yamaya T., Kameya T., Higashitani A., and Sato T.: "Epistatic interaction of QTLs controlling leaf bronzing in rice (Oryza sativa L.) groun in a saline paddy field", Breed. Sci. **56**, 287–293 (2006). *

Hokura A., Onuma R., Kitajima N., Terada Y., Saito H., Abe T., Yoshida S., and Nakai I.: "2-D X-ray fluorescence imaging of cadmium hyperaccumulating plants by using high-energy synchrotoron radiation X-ray microbeam", Chem. Lett. **35**, No. 11, pp. 1246–1247 (2006). *

Honda I., Kikuchi K., Matsuo S., Fukuda M., Saito H., Ryuto H., Fukunishi N., and Abe T.: "Heavy-ion-induced mutants in sweet pepper isolated by M1 plant selection", Euphytica **152**, No. 1, pp. 61–66 (2006). *

Kazama Y., Sugiyama R., Suto Y., Uchida W., and Kawano S.: "The clustering of four subfamilies of satellite DNA at individual chromosome ends in Silene latifolia", Genome **49**, 520–530 (2006). *

Ryuto H., Abe T., Fukunishi N., Kase M., and Yano Y.: "Heavy-ion beam irradiation system for biological samples in RIKEN", Journal of Biomedical Nanotechnology **2**, No. 2, pp. 88–93 (2006).

Miyazaki K., Suzuki K., Iwaki K., Kusumi T., Abe T., Yoshida S., and Fukui H.: "Flower pigment mutations induced by heavy ion beam irradiation in an interspecific hybrid of Torenia", Plant Biotechnol. **23**, No. 2, pp. 163–167 (2006). *

Nakano M., Nomizu T., Mizunashi K., Suzuki M., Mori S., Kuwayama S., Hayashi M., Umehara H., Oka E., Kobayashi H., Asano M., Sugawara S., Takagi H., Saito H., Nakata M., Godo T., Hara Y., and Amano J.: "Somaclonal variation in Tricyrtis hirta plants regenerated from 1-year-old embryogenic callus cultures", Sci. Hortic. **110**, 366–371 (2006). *

Ichida H., Matsuyama T., Abe T., and Koba T.: "DNA adenine methylation changes dramatically during establishment of symbiosis", The FEBS Journal **274**, 951–962 (2007). *

柏原輝彦, 保倉明子, 北島信行, 小沼亮子, 斉藤宏之, 阿部知子, 中井泉: "放射光蛍光 X 線分析を用いるヒ素高集積植物モエジマシダの根におけるヒ素の分布および化学形態分析", 分析化学 **55**, No. 10, pp. 743–748 (2006). *

(Review)

阿部知子, 林依子, 市田裕之, 龍頭啓充: "理研仁科加速

器研究センターにおける重イオン加速器を用いた植物育種の実用化", 加速器 **3**, No. 1, pp. 69–73 (2006).

[Book・Proc.]

(Original Papers) *Subject to Peer Review

Bae C., Lyu J., Abe T., Yano Y., Yoshida S., Lee Y., and Lee H.: "Effect of heavy-ion beam irradiation on in vitro cultured plant organisms", Proceedings of the 3rd Asian Particle Accelerator Conference (APAC 2004), Gyeongju, Korea, 2004–3, APAC 2004, Gyeongju, pp. 444–445 (2004). *

(Review)

Uchida W., Kazama Y., Matsunaga S., and Kawano S.: "A Wonder Plant-Microbe Interaction between White Campion and Anther Smut", Floriculture, Ornamental and Plant Biotechnology: Advances and Topical Issues (1st Edition), London, UK, 2006– Jaime A. Teixeira da Silva, Kagawa, pp. 236–242 (2006).

松山知樹, 市田裕之, 阿部知子, 浅見忠男, 中山秀人, 小池邦昭, 戎崎俊一: "ゲノムスキャニング多型解析によるシロイヌナズナ突然変異体の変異遺伝子迅速同定", DNA 多型, Vol.14, 日本 DNA 多型学会, 東京, pp. 144–146 (2006).

市田裕之, 米山勝美, 阿部知子, 松山知樹: "キャベツ萎黄病抵抗性 DNA マーカー周辺領域の解析", DNA 多型, Vol.14, 日本 DNA 多型学会, 東京, pp. 147–150 (2006).

阿部知子, 龍頭啓充: "重イオンビームを用いた植物の品種改良法の実用化", 第 30 回放射線科学研究会資料集, 大阪, 2006–7, 大阪ニュークリア, 大阪, pp. 17–22 (2006).

阿部知子: "各種園芸植物のイオンビームによる育種研究の成果", 第 8 回加速器利用技術セミナー「ビーム利用による農業・工業・医療の新時代」講演テキスト, 東海村, 2006–10, 放射線利用振興協会, 高崎, pp. 47–51 (2006).

(Others)

Onuma R., Hokura A., Kitajima N., Nakai I., Terada Y., Abe T., Saito H., and Yoshida S.: "Arsenic distribution and speciation in the arsenic hyperaccumulator fern by Micro-XRF imaging and Micro-XANES analysis", IPAP Conference series 7: Proceedings of 8th International Conference on X-ray Microscopy (XRM2005), Himeji, 2005–7, Institute of Pure and Applied Physics, Japan, Hyogo, pp. 326–327 (2006).

Oral Presentations

(International Conference etc.)

Yatagai F., Umebayashi Y., Honma M., Abe T., Suzuki H., Shimazu T., Ishioka N., and Iwaki M.: "A plan for ISS experiment to detect microgravity effects on mutation induction in relation to space radiation", 27th Annual Gravitational Physiology Meeting, (International Society for Gravitational Physiology), Osaka, Apr. (2006).

Yatagai F., Umebayashi Y., Honma M., Suzuki M., Abe T., Suzuki H., Shimazu T., Ishioka N., and Iwaki M.: "Sensitive Mutation-Detection in Human Cell for Space Environmental Radiation", 4th International Workshop on Space Radiation Research and 17th Annual NASA Space Radiation Health Investigators' Workshop, Moscow and St. Petersburg, Russia, June (2006).

Yatagai F., Umebayashi Y., Honma M., Abe T., Suzuki H., Shimazu T., Ishioka N., and Iwaki M.: "An application of LOH analysis for detecting the genetic influences of space environmental radiation", 36th COSPAR Scientific Assembly, Beijing, China, July (2006).

Yatagai F., Umebayashi Y., Honma M., Suzuki M., Abe T., Suzuki H., Shimazu T., Ishioka N., and Iwaki M.: "Influences of low-dose and low-dose-rate ionizing radiation on the mutation induction in human cell", COSPAR COLLOQUIUM on Mutagenic Consequences of the Space Environment, Xian, China, July (2006).

Lyu J., Abe T., Han H., Jung J., Lee H., Shin D., and Bae C.: "Identification of specific DNA bands in variegated orchid rhizomes induced by ion beam irradiation", 27th International Horticultural Congress and Exhibition, (International Society for Horticultural Science), Seoul, Korea, Aug. (2006).

Saito H., Hayashi Y., Fukunishi N., Ryuto H., Suzuki K., Kanaya T., Sugiyama M., Terakawa T., Ohtsubo N., Aida R., and Abe T.: "Isolation of sterile mutants of floricultural plants using heavy-ion beam irradiation", 27th International Horticultural Congress and Exhibition, (International Society for Horticultural Science), Seoul, Korea, Aug. (2006).

Kanai Y., Hoshino M., Ikeda T., Kambara T., Hellhammer R., Stolterfoht N., and Yamazaki Y.: "Two-dimensional images of slow neon ions guided by nanocapillaries in polymer foils", 16th International Workshop on Inelastic Ion-Surface Collisions (IISC-16), Hernstein, Austria, Sept. (2006).

(Domestic Conference)

竹久妃奈子, 上田忠正, 福田善通, 阿部知子, 矢野昌裕, 山谷知行, 佐藤雅志: "塩害水田におけるイネ葉身の Bronzing の発症を支配する 2QTL 間の相互作用", 日本育種学会第 109 回講演会, 東京, 3 月 (2006).

金子博, 松田靖, Poeaim A., 阿部知子, 村田達郎: "Zoysia minima におけるイオンビーム照射の影響", 日本育種学会第 109 回講演会, 東京, 3 月 (2006).

本多一郎, 菊地都, 松尾哲, 福田真知子, 林依子, 斉藤宏之, 阿部知子: "処理当代より見出したピーマン重イオン変異体の遺伝解析", 園芸学会平成 18 年度春季大会, 千葉, 3 月 (2006).

大沼みお, 横山敬士, 井上貴之, 市田裕之, 林依子, 阿部知子, 関根靖彦, 田中寛: "C イオンビーム照射による Cyanidioschyzon merolae の URA5.3 遺伝子変異株の取得", 第 3 回イオンビーム育種研究会大会, 千葉, 4 月 (2006).

大越一雄, 伊藤靖之, 関栄一, 渡邉学, 阿部知子: "重イオンビームを用いたベゴニア突然変異体の作出", 第 3

回イオンビーム育種研究会大会, 千葉, 4 月 (2006).

大坪憲弘, 間竜太郎, 阿部知子: “イオンビーム照射を利用した色変わり組換えトレニアの高品位化”, 第 3 回イオンビーム育種研究会大会, 千葉, 4 月 (2006).

市田裕之, 木庭卓人, 米山勝美, 松山知樹, 阿部知子: “DNA 二次元電気泳動による植物関連細菌ゲノムの網羅的変異解析法の開発”, 平成 18 年度日本植物病理学会大会, 札幌, 6 月 (2006).

阿部知子: “重イオンビームを用いた植物育種の実用化”, KEK セミナー, つくば, 6 月 (2006).

阿部知子, 龍頭啓充: “重イオンビームを用いた植物の品種改良法の実用化”, 第 30 回放射線科学研究会, (大阪ニュークリアサイエンス協会), 大阪, 7 月 (2006).

大坪憲弘, 間竜太郎, 阿部知子: “遺伝子組換え花きへの重イオンビーム照射による効率的な花色・花形変異の導入”, 第 24 回日本植物細胞分子生物学会大会・シンポジウム, つくば, 7 月 (2006).

竹久妃奈子, 阿部知子, 林依子, 神波千秋, 斉藤宏之, 市田裕之, 小沼亮子, 龍頭啓充, 福西暢尚, 宮沢豊, 東海林英夫, 保倉明子, 福田直樹, 中井泉, 佐藤雅志: “重イオンビーム照射による塩害水田耐性イネ突然変異系統の作出”, 日本育種学会第 110 回講演会, 松山, 9 月 (2006).

大坪憲弘, 山口博康, 間竜太郎, 阿部知子: “重イオンビーム照射を利用した色変わり組換えトレニアの効率的なバラエティ化”, 日本育種学会第 110 回講演会, 松山, 9 月 (2006).

齋藤利弥, 揚村京子, 波越啓太, 市田裕之, 林依子, 阿部知子, 西村実, 一谷勝之, 久保山勉: “イネ雑種弱勢原因遺伝子 Hwc2 の高密度連鎖解析と弱勢抑制変異体の染色体欠損領域について”, 日本育種学会第 110 回講演会, 松山, 9 月 (2006).

白尾吏, 上野敬一郎, 松山知樹, 市田裕之, 阿部知子: “イオンビーム育種により育成した秋輪ギク品種「新神」のレトロトランスポゾン配列を利用した品種同定”, 日本育種学会第 110 回講演会, 松山, 9 月 (2006).

阿部知子, 林依子, 竹久妃奈子, 安田美智子, 市田裕之, 斉藤宏之, 柏原輝彦, 福田直樹, 小沼亮子, 保倉明子, 寺田靖子, 龍頭啓充, 福西暢尚, 宮沢豊, 仲下英雄, 工藤俊章, 中井泉, 佐藤雅志: “イネにおける加速器を用いた変異誘発法および変異体解析法の開発”, 日本育種学会第 110 回講演会, 松山, 9 月 (2006).

西原潔, 風間裕介, 小泉綾子, 河野重行, 阿部知子: “重イオンビームを用いた雌雄異株植物ヒロハノマンテマの性転換変異体の作出”, 日本育種学会第 110 回講演会, (日本育種学会), 松山, 9 月 (2006).

田平千香子, 漆川直希, 阿部知子, 阪本浩一, 斉藤宏之, 龍頭啓充, 福西暢尚, 村井耕二: “イオンビームによる一粒系コムギ突然変異体 fushi-darake の表現型および遺伝解析”, 日本育種学会第 110 回講演会, 松山, 9 月 (2006).

高橋昌宏, 松田靖, 阿部知子, 村田達郎: “ニラ (Allium ramosum L.) におけるイオンビーム照射の影響”, 日本育種学会第 110 回講演会, 松山, 9 月 (2006).

市田裕之, 松山知樹, 龍頭啓充, 福西暢尚, 阿部知子, 木庭卓人: “根粒菌における突然変異誘発とその網羅的検出”, 植物微生物研究会 第 16 回研究交流会, 札幌, 9 月 (2006).

谷田貝文夫, 梅林志浩, 本間正充, 阿部知子, 鈴木ひろみ, 嶋津徹, 石岡憲昭, 岩木正哉: “ISS 利用実験計画：宇宙環境の変異誘発に及ぼす影響の推測”, 日本放射線影響学会第 49 回大会, (日本放射線影響学会), 札幌, 9 月 (2006).

小泉綾子, 西原潔, 天内康人, 石井公太郎, 風間裕介, 河野重行: “ヒロハノマンテマの無性花変異体と黒穂菌感染擬似雄蕊誘導体における B 機能遺伝子の発現”, 日本植物学会第 70 回大会, (日本植物学会), 熊本, 9 月 (2006).

風間裕介, 西原潔, 石井公太郎, 貴舩永津子, 西山りゑ, 河野重行: “ヒロハノマンテマの XY 性染色体上の対立遺伝子 SlAP3 と SlWUS の位置と構造比較”, 日本植物学会第 70 回大会, (日本植物学会), 熊本, 9 月 (2006).

西原潔, 風間裕介, 西山りゑ, 河野重行: “雌雄異株植物ヒロハノマンテマの XY 性染色体に連鎖する AP3 と他のホモログ”, 日本遺伝学会第 78 回大会, つくば, 9 月 (2006).

天内康人, 石井公太郎, 小泉綾子, 風間裕介, 河野重行: “雌雄異株植物ヒロハノマンテマの染色体末端サテライト DNA 構造の非一様性とその近傍を用いた FISH 解析”, 日本遺伝学会第 78 回大会, つくば, 9 月 (2006).

阿部知子: “各種園芸植物のイオンビームによる育種研究の成果”, 第 8 回加速器利用技術セミナー, (文部科学省), 東海村, 10 月 (2006).

阿部知子: “理化学研究所加速器を用いた植物の品種改良法の実用化”, 第 3 回大学発シーズ発表会, (木原記念横浜生命科学振興財団), 横浜, 11 月 (2006).

市田裕之, 松山知樹, 龍頭啓充, 福西暢尚, 林依子, 阿部知子, 木庭卓人: “重イオンビームによって誘発された DNA 多型の解析”, 日本 DNA 多型学会第 15 回学術集会, (日本 DNA 多型学会), 福山, 11 月 (2006).

西原潔, 石井公太郎, 小泉綾子, 風間裕介, 河野重行: “雌雄異株植物ヒロハノマンテマの XY 性染色体連鎖遺伝子と性染色体構造の比較”, 文部科学省科学研究費補助金特定領域研究「植物の生殖過程におけるゲノム障壁」第 1 回ワークショップ/国立遺伝学研究所研究集会/「高等植物の生殖形質におけるゲノム障壁制御遺伝子の分子遺伝学的解析」, 三島, 11 月 (2006).

風間裕介, 西原潔, 小泉綾子, 河野重行, 阿部知子: “高エネルギー重イオンビーム照射によるヒロハノマンテマ性転換変異体の作出”, 文部科学省科学研究費補助金特定領域研究「植物の生殖過程におけるゲノム障壁」第 1 回ワークショップ/国立遺伝学研究所研究集会/「高等植物の生殖形質におけるゲノム障壁制御遺伝子の分子遺伝学的解析」, 三島, 11 月 (2006).

小泉綾子, 天内康人, 石井公太郎, 西原潔, 風間裕介, 河野重行: “ヒロハノマンテマ無性花変異体 K034 の 2 つの表現型と Y 染色体欠損”, 文部科学省科学研究費補助金特定領域研究「植物の生殖過程におけるゲノム障壁」第 1 回ワークショップ/国立遺伝学研究所研究集会/「高等植物の生殖形質におけるゲノム障壁制御遺伝子の分子遺伝学的解析」, 三島, 11 月 (2006).

阿部知子: “シンクロトロン光の農業利用の可能性－植物における重金属観察および突然変異育種”, 平成 18 年度技術ワークショップ事業「シンクロトロン光利活

用勉強会」, (佐賀県立九州シンクロトロン光研究センター), 佐賀, 11 月 (2006).

阿部知子: “イオンビーム育種技術の開発”, 第 25 回法政大学イオンビーム工学研究所シンポジウム, (法政大学イオンビーム工学研究所), 小金井, 12 月 (2006).

遠藤隆, 那須田周平, 河原太八, 安井康夫, 笹隈哲夫, 笹沼恒男, 辻本壽, 田中裕之, 持田恵一, 川浦香奈子, 荻原保成: “NBRP「コムギ」複雑系ゲノム科学のモデル植物”, 第 28 回日本分子生物学会年会, 福岡, 12 月 (2006).

RI Applications Team

Publications

[Journal]

(Original Papers) *Subject to Peer Review

Tanaka M. and Takahashi K.: “Study on the salting-out effect using silica species by FAB-MS”, J. Solution Chem. **36**, 27–37 (2007). *

Haba H., Tsukada K., Asai M., Toyoshima A., Ishii Y., Toume H., Sato T., Nishinaka I., Ichikawa T., Ichikawa S., Nagame Y., Sato W., Matsuo K., Kitamoto Y., Tashiro T., Shinohara A., Saito J., Ito M., Ikezawa T., Sakamaki M., Goto S., Kudo H., Kikunaga H., Arai M., Kamataki S., Yokoyama A., Akiyama K., Sueki K., Oura Y., Schaedel M., Bruechle W., and Kratz J. V.: “Extraction behavior of rutherfordium into tributylphosphate from hydrochloric acid”, Radiochim. Acta **95**, 1–6 (2007). *

榎本香織, 金山洋介, 木村修一, 榎本秀一: “食肉成分が胃液分泌に及ぼす影響”, 微量栄養素研究 **23**, 74–76 (2006). *

金山洋介, 羽場宏光, 榎本秀一, 天野良平: “コルヒチンによる ^{24}Na, ^{28}Mg, ^{43}K, ^{47}Ca, ^{48}V, ^{67}Cu 嗅覚輸送阻害効果の検討”, 微量栄養素研究 **23**, 84–88 (2006). *

(Others)

Nagame Y., Akiyama K., Asai M., Goto S., Haba H., Hirata M., Ishii Y., Nishinaka I., Tome H., Toyoshima A., and Tsukada K.: “Chemical studies of the transactinide elements at JAEA”, AIP Conf. Proc. **865**, 165–172 (2006).

Haba H., Tsukada K., Asai M., Toyoshima A., Ishii Y., Tome Y., Sato T., Nishinaka I., Ichikawa T., Ichikawa S., Nagame Y., Sato W., Matsuo K., Kitamoto Y., Tashiro T., Shinohara A., Saito J., Ito M., Ikezawa T., Sakamaki M., Goto S., Kudo H., Kikunaga H., Arai M., Kamataki S., Yokoyama A., Akiyama K., Sueki K., Oura Y., Schaedel M., Bruechle W., and Kratz J. V.: “Extraction behavior of Rf into tributylphosphate from hidrochloric acid”, JAEA-Review **2006**, No. 29, pp. 57–58 (2006).

Tsukada K., Toyoshima A., Haba H., Asai M., Akiyama K., Ishii Y., Tome Y., Nishinaka I., Sato T., Ichikawa S., Nagame Y., Yaita T., Goto S., Ikezawa T., Sato W., Matsuo K., Kitamoto Y., Tashiro T., Yokoyama A., Arai M., Sakama M., Oura Y., Sueki K., Shinohara A., and Kudo H.: “Chloride complex formation of Rf in HCl and CH_3OH mixed solution”, JAEA-Review **2006**, No. 29, pp. 61–62 (2006).

[Book・Proc.]

(Others)

Nagame Y., Haba H., Tsukada K., Asai M., Toyoshima A., Akiyama T., Kaneko T., Hirai T., Goto S., Hirata M., Nishinaka I., and Ichikawa S.: “Few atom chemistry of the transactinide element rutherfordium (Rf)”, Proceedings of the International Conference on Applications of High Precision Atomic and Nuclear Methods, 2-6 September 2002, Neptun, Romania, Neptun, Romania, 2002–9, IFIN-HH, Bucharest, pp. 334–343 (2005).

Nagame Y., Asai M., Haba H., Hirata M., Ishii Y., Nishinaka I., Toyoshima A., and Tsukada K.: “Aqueous Chemistry of the Transactinide Element, Rutherfordium (Rf)”, Lecture Series on Computer and Computational Sciences Volume 7, Brill Academic Publishers, Leiden, pp. 927–930 (2006).

前田邦子: “機器分析の事典：波長分散型蛍光 X 線分析装置”, 機器分析の事典, 朝倉書店, 東京, pp. 37–40 (2005).

Oral Presentations

(International Conference etc.)

Kikunaga H., Haba H., Kaji D., Sato N., Akiyama T., Morimoto K., Yoneda A., Morita K., Takabe T., Ooe K., Shinohara A., Suzuki D., Nanri T., Yamazaki I., and Yokoyama A.: “Development of a gas-jet transport system coupled to GARIS for heavy element chemistry”, 5th Workshop on Recoil Separator for Superheavy Element Chemistry (TASACA06), (GSI), Garching, Germany, Sept. (2006).

Haba H., Kaji D., Kikunaga H., Akiyama T., Sato N., Morimoto K., Yoneda A., Morita K., Takabe T., Tashiro Y., Kitamoto Y., Matsuo K., Saika D., Ooe K., Kuribayashi T., Yoshimura T., Shinohara A., and Toyoshima A.: “Superheavy Element Chemistry at RIKEN: Present Status and Perspectives”, Tours Symposium on Nuclear Physics VI (TOURS 2006), (Konan University), Tours, France, Sept. (2006).

Toyoshima A., Tsukada K., Asai M., Ishii Y., Nishinaka I., Sato T., Hirata M., Nagame Y., Haba H., Sato W., Tani Y., Hasegawa H., Matsuo K., Saika D., Kitamoto Y., Shinohara A., Goto S., Ito M., Saito J., Kudo H., Akiyama K., Sueki K., Yokoyama A., Oura Y., Schaedel M., Bruechle W., and Kratz J. V.: “Fluoride Complexation Study of Rutherfordium at JAEA”, Workshop on the Atomic Properties of the Heaviest Elements: Towards the Island of Stability, (LMU Muenchen), Chiemsee, Germany, Sept. (2006).

Haba H., Kaji D., Kikunaga H., Akiyama T., Sato N., Morimoto K., Yoneda A., Morita K., Takabe

T., Tashiro Y., Kitamoto Y., Matsuo K., Saika D., Ooe K., Kuribayashi T., Yoshimura T., Shinohara A., and Toyoshima A.: "Startup of Heavy Element Chemistry in RIKEN", Workshop on the Atomic Properties of the Heaviest Elements: Towards the Island of Stability, (LMU Muenchen), Chiemsee, Germany, Sept. (2006).

Ishii Y., Toume H., Toyoshima A., Asai M., Nishinaka I., Tsukada K., Nagame Y., Tashiro T., Shinohara A., Sakamaki M., Goto S., Kudo H., Akiyama K., Haba H., Oura Y., Miyashita S., Mori T., and Suganuma H.: "A cation-exchange study of fluoride complexation of rutherfordium (Rf) in HNO3/HF mixed solution system", 6th International Symposium on Advanced Science Research: Frontiers of Nuclear and Radiochemistry (ASR2006), (Advanced Science Research Center, Japan Atomic Energy Agency), Tokaimura, Oct. (2006).

Tsukada K., Toyoshima A., Haba H., Asai M., Akiyama K., Ishii Y., Tome H., Nishinaka I., Kaneko T. S., Ichikawa S., Nagame Y., Yaita T., Goto S., Ikezawa T., Sato W., Matsuo K., Kitamoto Y., Tashiro T., Yokoyama A., Arai M., Sakama M., Oura Y., Sueki K., Shinohara A., and Kudo H.: "Chloride complex formation of Rf in HCl and CH3OH mixed solution", 6th International Symposium on Advanced Science Research: Frontiers of Nuclear and Radiochemistry (ASR2006), (Advanced Science Research Center, Japan Atomic Energy Agency), Tokaimura, Oct. (2006).

Haba H., Kikunaga H., Kaji D., Sato N., Akiyama T., Morimoto K., Yoneda A., Morita K., Takabe T., Ooe K., Shinohara A., Suzuki D., Nanri T., Yamazaki I., and Yokoyama A.: "Development of a gas-jet transport system coupled to the RIKEN gas-filled recoil ion separator GARIS for superheavy element chemistry", 6th International Symposium on Advanced Science Research: Frontiers of Nuclear and Radiochemistry (ASR2006), (Advanced Science Research Center, Japan Atomic Energy Agency), Tokaimura, Oct. (2006).

Toyoshima A., Kasamatsu Y., Tsukada K., Haba H., Shinohara A., and Nagame Y.: "Development of an electrochemistry apparatus for an atom-at-a-time chemistry", 6th International Symposium on Advanced Science Research: Frontiers of Nuclear and Radiochemistry (ASR2006), (Advanced Science Research Center, Japan Atomic Energy Agency), Tokaimura, Oct. (2006).

Kaji D., Haba H., Kikunaga H., Morimoto K., Yoneda A., Akiyama T., Ooe K., Nanri T., Sato N., Shinohara A., Suzuki D., Takabe T., Yamazaki I., Yokoyama A., and Morita K.: "Optimazation of a gas-filled recoil separator GARIS for the chemistry of superheavy elements", 6th International Symposium on Advanced Science Research: Frontiers of Nuclear and Radiochemistry (ASR2006), (Advanced Science Research Center, Japan Atomic Energy Agency), Tokaimura, Oct. (2006).

Takabe T., Saika D., Matsuo K., Tashiro T., Ooe K., Kuribayashi T., Yoshimura T., Toyoshima A., Kikunaga H., Kaji D., Haba H., Kudo H., Mitsugashira T., and Shinohara A.: "Studies on the heavy element productions at RIKEN for chemical characterization of seaborgium", 6th International Symposium on Advanced Science Research: Frontiers of Nuclear and Radiochemistry (ASR2006), (Advanced Science Research Center, Japan Atomic Energy Agency), Tokaimura, Oct. (2006).

Toyoshima A., Kasamatsu Y., Tsukada K., Haba H., Asai M., Ishii Y., Toume H., Kaneko T. S., Nishinaka I., Nagame Y., Goto S., Ishiyama T., Sakamaki M., Kudo H., Akiyama K., Oura Y., Kikunaga H., Ooe K., Kuribayashi T., Shinohara A., and Yokoyama A.: "TOPO reversed-phase extraction behabior of rutherfordium in HCl solutions", 6th International Symposium on Advanced Science Research: Frontiers of Nuclear and Radiochemistry (ASR2006), (Advanced Science Research Center, Japan Atomic Energy Agency), Tokaimura, Oct. (2006).

(Domestic Conference)

北本優介, 雑賀大輔, 松尾啓司, 高部智正, 田代祐基, 大江一弘, 栗林隆宏, 佐藤渉, 高橋成人, 吉村崇, 羽場宏光, 榎本秀一, 三頭聰明, 篠原厚: "金属-配位子間相互作用を利用した 3 価アクチノイドのキャピラリー電気泳動分離", 日本化学会第 86 春季年会, (日本化学会), 船橋, 3 月 (2006).

高部智正, 北本優介, 雑賀大輔, 松尾啓司, 田代祐基, 大江一弘, 栗林隆宏, 吉村崇, 羽場宏光, 加治大哉, 篠原厚: "理研 AVF サイクロトロンにおける重元素合成システムの整備と化学研究のためのノーベリウム同位体の製造", 日本化学会第 86 春季年会, (日本化学会), 船橋, 3 月 (2006).

塚田和明, 豊嶋厚史, 羽場宏光, 浅井雅人, 秋山和彦, 石井康雄, 當銘勇人, 西中一朗, 佐藤哲也, 市川隆敏, 市川進一, 平田勝, 永目諭一郎, 矢板毅, 後藤真一, 坂牧雅巳, 池沢孝明, 佐藤渉, 松尾啓司, 北本優介, 田代祐基, 横山明彦, 新井理太, 鎌滝真次, 阪間稔, 大浦泰嗣, 末木啓介, 篠原厚, 工藤久昭: "超重元素ラザホージウムの塩化物錯体形成", 日本化学会第 86 春季年会, (日本化学会), 船橋, 3 月 (2006).

豊嶋厚史, 羽場宏光, 塚田和明, 浅井雅人, 秋山和彦, 石井康雄, 當銘勇人, 西中一朗, 佐藤哲也, 市川隆敏, 永目諭一郎, 佐藤渉, 松尾啓司, 北本優介, 田代祐基, 篠原厚, 池沢孝明, 坂牧雅巳, 後藤真一, 工藤久昭, 新井理太, 鎌滝真次, 横山明彦, 大浦泰嗣, 末木啓介: "塩酸溶液系におけるラザホージウムの TBP 逆相抽出クロマトグラフィー", 日本化学会第 86 春季年会, (日本化学会), 船橋, 3 月 (2006).

金山洋介, 羽場宏光, 榎本秀一, 天野良平: "^{24}Na, ^{28}Mg, ^{43}K, ^{47}Ca, ^{48}V, ^{67}Cu 鼻腔投与におけるコルヒチンの嗅覚輸送阻害効果の検討", 第 23 回微量栄養素研究会シンポジウム, 京都, 6 月 (2006).

金山洋介, 榎本秀一, 羽場宏光, 天野良平: "Brain Deliv-

ery of Monovalent Metal Cations via Olfactory Pathway", 第 16 回金属の関与する生体関連反応シンポジウム (SRM 2006)「生体超分子システムと金属」, (日本薬学会), 東京, 6 月 (2006).

石井康雄, 當銘勇人, 豊嶋厚史, 浅井雅人, 西中一朗, 塚田和明, 永目諭一郎, 宮下直, 森友隆, 菅沼英夫, 田代祐基, 篠原厚, 坂牧雅巳, 後藤真一, 工藤久昭, 羽場宏光, 秋山和彦, 大浦泰嗣: "Rf の HNO3/HF における陽イオン交換挙動 (II)", 2006 日本放射化学会年会・第 50 回放射化学討論会, (日本放射化学会), 水戸, 東海村, 10 月 (2006).

豊嶋厚史, 笠松良崇, 塚田和明, 羽場宏光, 篠原厚, 永目諭一郎: "単一原子の電気化学的研究に向けた電解セルの開発", 2006 日本放射化学会年会・第 50 回放射化学討論会, (日本放射化学会), 水戸, 東海村, 10 月 (2006).

高部智正, 雑賀大輔, 松尾啓司, 田代祐基, 大江一弘, 栗林隆宏, 吉村崇, 豊嶋厚史, 菊永英寿, 加治大哉, 羽場宏光, 工藤久昭, 三頭聰明, 篠原厚: "理研におけるシーボーギウム化学研究に向けた重元素合成", 2006 日本放射化学会年会・第 50 回放射化学討論会, (日本放射化学会), 水戸, 東海村, 10 月 (2006).

菊永英寿, 羽場宏光, 加治大哉, 佐藤望, 森本幸司, 米田晃, 森田浩介, 高部智正, 大江一弘, 篠原厚, 鈴木大介, 南里朋洋, 山崎逸郎, 横山明彦: "238U(22Ne,5n) 反応によって製造された 255No の GARIS による分離分析：GARIS を前段分離装置として用いた超重元素化学研究に向けて", 2006 日本放射化学会年会・第 50 回放射化学討論会, (日本放射化学会), 水戸, 東海村, 10 月 (2006).

田代祐基, 雑賀大輔, 北本優介, 松尾啓司, 高部智正, 栗林隆宏, 大江一弘, 吉村崇, 佐藤渉, 高橋成人, 豊嶋厚史, 羽場宏光, 篠原厚: "複線式マイクロチップを用いた No2+迅速溶媒抽出", 2006 日本放射化学会年会・第 50 回放射化学討論会, (日本放射化学会), 水戸, 東海村, 10 月 (2006).

大江一弘, 栗林隆宏, 高部智正, 田代祐基, 北本優介, 雑賀大輔, 松尾啓司, 高橋成人, 吉村崇, 高宮幸一, 柴田誠一, 羽場宏光, 榎本秀一, 篠原厚: "極低濃度タングステンの溶媒抽出挙動と電解酸化還元反応", 2006 日本放射化学会年会・第 50 回放射化学討論会, (日本放射化学会), 水戸, 東海村, 10 月 (2006).

豊嶋厚史, 笠松良崇, 塚田和明, 羽場宏光, 浅井雅人, 石井康雄, 當銘勇人, 金子 (哲也) 佐藤, 西中一朗, 永目諭一郎, 後藤真一, 石山剛, 坂牧雅巳, 工藤久昭, 秋山和彦, 大浦泰嗣, 菊永英寿, 大江一弘, 栗林隆宏, 篠原厚, 末木啓介, 横山明彦: "塩酸溶液系におけるラザホージウムの TOPO 逆相抽出クロマトグラフ挙動", 2006 日本放射化学会年会・第 50 回放射化学討論会, (日本放射化学会), 水戸, 東海村, 10 月 (2006).

前田邦子, 浜中廣見, 荻原清, 長谷川賢一: "結晶分光 PIXE で化学状態の深さ分布を調べる", 第 23 回 PIXE シンポジウム, (PIXE 研究協会), 松島, 11 月 (2006).

川畑俊明, 鳥山保, 川崎克則, 長谷川賢一, 前田邦子, 小栗慶之: "固体高分子型燃料電池中の硫黄の分析用波長分散型粒子線誘起 X 線分析システムの構築", 第 23 回 PIXE シンポジウム, (PIXE 研究協会), 松島, 11 月 (2006).

Safety Management Gr.

Oral Presentations

(Domestic Conference)

坂本久雄, 堀米敦子, 向井弘樹, 日暮利江子, 藤田新, 上蓑義朋, 加瀬昌之: "理研 RIBF におけるウラン加速の安全管理", 第 3 回日本加速器学会年会・第 31 回リニアック技術研究会, 仙台, 8 月 (2006).

RIKEN BNL Research Center

Publications

[**Journal**]

(Original Papers) *Subject to Peer Review

Bazilevsky A. V. and PHENIX Collaboration .: "Event reconstruction in the PHENIX central arm spectrometers", Nuclear Instruments and Methods in Physics Research A **482**, 491–512 (2002). *

Adcox K., Bazilevsky A. V., Bunce G. M., Deshpande A., En'yo H., Fox B., Goto Y., Grosse Perdekamp M., Hayashi N., Ichihara T., Imai K., Ishihara M., Jacak B. V., Kobayashi H., Kurita K., Li Z., Mao Y., Murata J., Saito N., Sakuma T., Sato H., Shibata T., Sugioka M., Taketani A., Tojo J., Torii H., Watanabe Y., Yokkaichi S., and PHENIX C.: "PHENIX detector overview", Nuclear Instruments and Methods in Physics Research A **499**, 469–479 (2003). *

Aphecetche L., Bazilevsky A. V., Goto Y., Grosse Perdekamp M., and PHENIX Collaboration .: "PHENIX Calorimeter", Nuclear Instruments and Methods in Physics Research A **499**, 521–536 (2003). *

Akikawa H., En'yo H., Hayashi N., Ichihara T., Ishihara M., Kobayashi H., Kurita K., Li Z., Mao Y., Murata J., Saito N., Sato H., Shibata T., Sugioka M., Taketani A., Watanabe Y., Yokkaichi S., and PHENIX Collaboratio .: "PHENIX muon arms", Nuclear Instruments and Methods in Physics Research A **499**, 537–548 (2003). *

Allen M., Deshpande A., Fox B., and PHENIX C.: "PHENIX inner detectors", Nuclear Instruments and Methods in Physics Research A **499**, 549–559 (2003). *

Adler S. S., Ichihara T., Jacak B. V., Watanabe Y., Yokkaichi S., and PHENIX C.: "PHENIX on-line and off-line computing", Nuclear Instruments and Methods in Physics Research A **499**, 593–602 (2003). *

Murata J., Horaguchi T., Kamihara N., Kobayashi H., Shibata T., and PHENIX C.: "Optical alignment system for the PHENIX muon tracking chambers", Nuclear Instruments and Methods in Physics Research A **500**, 309–317 (2003). *

Okiharu F., Suganuma H., Takahashi T. T., and Doi

T.: "Multi-quarks and two-baryon interaction in lattice QCD", AIP Conf. Proc. **842**, 231–233 (2006). ∗

Doi T., Takahashi T. T., and Suganuma H.: "Meson-meson and meson-baryon interactions in lattice QCD", AIP Conf. Proc. **842**, 246–248 (2006). ∗

Takahashi T. T., Doi T., and Suganuma H.: "Nuclear force in lattice QCD", AIP Conf. Proc. **842**, 249–251 (2006). ∗

Ishii N., Doi T., Iida H., Oka M., Okiharu F., Suganuma H., and Tsumura K.: "Anisotropic lattice QCD studies of penta-quarks and tetra-quarks", AIP Conf. Proc. **842**, 492–494 (2006). ∗

Aoki S., Baer O., and Takeda S.: "Vector meson masses in 2+1 flavor Wilson Chiral Perturbation Theory", Phys. Rev. D **73**, No. 9, pp. 094501-1–094501-11 (2006). ∗

Aoki S., Baer O., Takeda S., and Ishikawa T.: "Pseudoscalar meson masses in Wilson chiral perturbation theory for 2+1 flavors", Phys. Rev. D **73**, No. 165, pp. 014511-1–014511-15 (2006). ∗

Aoki S. and Baer O.: "Automatic O(a) improvement for twisted-mass QCD in the presence of spontaneous symmetry breaking", Phys. Rev. D **74**, No. 3, pp. 034511-1–034511-17 (2006). ∗

Iida K. and Fukushima K.: "Instability of a gapless color superconductor with respect to inhomogeneous fluctuations", Phys. Rev. D **74**, 074020-1–074020-13 (2006). ∗

Iida H., Doi T., Ishii N., Suganuma H., and Tsumura K.: "Charmonium properties in deconfinement phase in anisotropic lattice QCD", Phys. Rev. D **74**, 074502-1–074502-12 (2006). ∗

Bai M., Roser T., Ahrens L., Alekseev I. G., Alessi J., Beebe-Wang J., Blaskiewicz M., Bravar A., Brennan J. M., Bruno D., Bunce G. M., Courant E., Drees A., Fischer W., Gardner C., Gill R., Glenn J., Haeberli W., Huang H., Jinnouchi O., Kewisch J., Luccio A., Luo Y., Nakagawa I., Okada H., Pilat F., MacKay W. W., Makdisi Y., Montag C., Ptitsyn V., Satogata T., Stephenson E., Svirida D., Tepikian S., Trbojevic D., Tsoupas N., Wise T., Zelenski A., Zeno K., and Zhang S. Y.: "Polarized Proton Collisions at 205 GeV at RHIC", Phys. Rev. Lett. **96**, 174801-1–174801-4 (2006). ∗

Aoki S. and Baer O.: "Automatic O(a) improvement for twisted-mass QCD", Proceedings of Science **LAT2006**, No. 165, (2006).

Doi T., Blum T. C., Hayakawa M., Izubushi T., and Yamada N.: "The Isospin breaking effect on baryons with N(f) = 2 domain wall fermions", Proceedings of Science **LAT2006**, 174-1–174-7 (2006). ∗

四日市悟, Chiba J., 延与秀人, 深尾祥紀, 舟橋春彦, 浜垣秀樹, Ieiri M., Ishino M., Kanda H., 北口雅暁, Mihara S., Miyashita T., 三輪浩司, 村上哲也, 武藤亮太郎, Nakura T., 成木恵, 小沢恭一郎, 佐久間史典, Sasaki O., 関本美知子, 田原司睦, Tanaka K., 外川学, Yamada S., Yoshimura Y.: "Experimental Study of in-medium meson modification at the KEK 12 GeV PS", 素粒子論研究 **114**, No. 2, pp. B7–B12 (2006).

Oral Presentations

(International Conference etc.)

Ishii N., Doi T., Iida H., Oka M., Okiharu F., and Suganuma H.: "Penta-quark anti-decuplet in anisotropic lattice QCD", LATTICE 2004: 22nd International Symposium on Lattice Field Theory, (Fermi National Accelerator Laboratory), Batavia, USA, June (2004).

Doi T., Ishii N., Oka M., and Suganuma H.: "The lattice QCD simulation of the quark-gluon mixed condensate $g\langle\bar{q}\sigma_{\mu\nu}G_{\mu\nu}q\rangle$ at finite temperature and the phase transition of QCD", LATTICE 2004: 22nd International Symposium on Lattice Field Theory, Batavia, USA, June (2004).

Ishii N., Doi T., Iida H., Oka M., Okiharu F., and Suganuma H.: "Anisotropic lattice QCD studies of penta-quark anti-decuplet", International Workshop on PENTAQUARK04, (RCNP and JASRI), Harima Science Garden City, July (2004).

Sugiyama J., Doi T., and Oka M.: "Pentaquark baryon from the QCD sum rule with the ideal mixing", International Workshop on PENTAQUARK04, (RCNP and JASRI), Harima Science Garden City, July (2004).

Doi T., Sugiyama J., and Oka M.: "Penta-quark baryon from the QCD sum rule", 2004 Gordon Research Conference on Photonuclear Reactions, Tilton, USA, Aug. (2004).

Doi T., Ishii N., Oka M., and Suganuma H.: "Thermal effects on quark-gluon mixed condensate $g\langle\bar{q}\sigma_{\mu\nu}G_{\mu\nu}q\rangle$ from lattice QCD", 2004 Gordon Research Conference on Photonuclear Reactions, Tilton, USA, Aug. (2004).

Ishii N., Doi T., Iida H., Oka M., Okiharu F., and Suganuma H.: "Penta-quark in anisotropic lattice QCD", 10th International Conference on the Structure of Baryons (Baryons 2004), Palaiseau, France, Oct. (2004).

Oka M., Sugiyama J., and Doi T.: "Pentaquark baryons in the QCD sum rule", 10th International Conference on the Structure of Baryons (Baryons 2004), Palaiseau, France, Oct. (2004).

Tabaru T.: "Heavy Quark and J/ψ Production at RHIC/PHENIX", 5th International Conference on Physics and Astrophysics of Quark Gluon Plasma (ICPAQGP 05), Salt Lake City, India, Feb. (2005).

Okiharu F., Doi T., Ichie H., Iida H., Ishii N., Oka M., Suganuma H., and Takahashi T. T.: "Tetraquark and pentaquark systems in lattice QCD", Quark Nuclear Physics 2005: Nuclear and Hadronic Systems and Quark Degrees of Freedom, Pyoungchang, Korea, Feb. (2005).

Iida H., Doi T., Ishii N., and Suganuma H.: "J/Ψ at high temperatures in anisotropic lattice QCD", 23rd

International Symposium on Lattice Field Theory (Lattice 2005), Dublin, Ireland, July (2005).

Doi T., Ishii N., Nemoto Y., Oka M., and Suganuma H.: "Anisotropic lattice QCD study of pentaquark baryons in spin 3/2 channel", 23rd International Symposium on Lattice Field Theory (Lattice 2005), Dublin, Ireland, July (2005).

Ishii N., Doi T., Nemoto Y., Oka M., and Suganuma H.: "Anisotropic lattice QCD studies of spin 3/2 penta-quark", 2nd Joint Meeting of the Nuclear Physics Divisions of the APS and JPS (Hawaii 2005), Maui, USA, Sept. (2005).

Fukushima K.: "Collective excitations in a superfluid of color-flavor locked quark matter", 2nd Joint Meeting of the Nuclear Physics Divisions of the APS and JPS (Hawaii 2005), Maui, USA, Sept. (2005).

Doi T., Blum T. C., Hayakawa M., Izubushi T., and Yamada N.: "Isospin breaking of baryon masses from domain-wall lattice QCD", 2nd Joint Meeting of the Nuclear Physics Divisions of the APS and JPS (Hawaii 2005), Maui, USA, Sept. (2005).

Okada K. and PHENIX C.: "Measurement of Direct Photons in sqrt(s)=200 GeV p+p collisions", 2nd Joint Meeting of the Nuclear Physics Divisions of the APS and JPS (Hawaii 2005), Maui, USA, Sept. (2005).

Sugiyama J., Doi T., and Oka M.: "QCD sum rule for spin-3/2 pentaquarks", 2nd Joint Meeting of the Nuclear Physics Divisions of the APS and JPS (Hawaii 2005), Maui, USA, Sept. (2005).

Ishii N., Doi T., Iida H., Nemoto Y., Oka M., Okiharu F., Suganuma H., and Tsumura K.: "Anisotropic lattice QCD studies of penta-quarks and tetra-quarks", Particles and Nuclei International Conference (PANIC05), Santa Fe, USA, Oct. (2005).

Doi T., Takahashi T. T., and Suganuma H.: "Meson-meson and meson-baryon interactions in lattice QCD", Particles and Nuclei International Conference (PANIC05), Santa Fe, USA, Oct. (2005).

Okiharu F., Suganuma H., Takahashi T. T., and Doi T.: "Multi-quarks and two-baryon interactions in lattice QCD", Particles and Nuclei International Conference (PANIC05), Santa Fe, USA, Oct. (2005).

Takahashi T. T., Doi T., and Suganuma H.: "Nuclear force in lattice QCD", Particles and Nuclei International Conference (PANIC05), Santa Fe, USA, Oct. (2005).

Aoki S.: "Lattice QCD simulations with light dynamical quarks", Quark Confinment and the Hadron Spectrum 7 (Acores-2006), (Universidade dos Azores), Ponta Delgada Azores, Portugal, Sept. (2006).

(Domestic Conference)

小濱洋央, 飯田圭, 親松和浩: ""黒い" 原子核描像に基づく核半径と反応断面積", RIBF-Day1 実験を睨んだ反応断面積実験に向けたミニワークショップ, Wako, 1 月 (2006).

岡田謙介, PHENIX C.: "Measurement of Direct Photon Production in p+p collisions at sqrt(s)= 200 GeV", 日本物理学会 2006 年秋季大会, 奈良, 9 月 (2006).

RIKEN Facility Office at RAL

Publications

[**Journal**]

(Original Papers) *Subject to Peer Review

Suzuki T., Itahashi K., Iwasaki M., Matsuda Y., Okada S., Outa H., Sato M., Strasser P., Tomono D., and Yamazaki T.: "A search for deeply bound kaonic nuclear states", Nucl. Phys. A **754**, 375c–382c (2005). *

Tonishi J., Suzuki T., and Goto T.: "Anomalous Change of Hall Coefficient in Overdoped $La_{2-x}Sr_xCu_{1-y}Zn_yO_4$ around $x = 0.2$", AIP Conf. Proc. **850**, 407–408 (2006). *

Suzuki T., Ota T., Tonishi J., and Goto T.: "Increase of the sound velocity by magnetic fields in $La_{2-x}Sr_xCuO_4$ around $x = 0.220$", AIP Conf. Proc. **850**, 409–410 (2006). *

Inoue H., Tani S., Hosoya S., Suzuki T., Goto T., Tanaka H., Sasaki T., and Kobayashi N.: "^{2}D, $^{35/37}$Cl, $^{63/65}$Cu-NMR Study of the Quantum Spin System NH_4CuCl_3", AIP Conf. Proc. **850**, 1061–1062 (2006). *

Suzuki T., Saito T., Sasaki T., Osawa A., Goto T., Awaji S., Watanabe K., Kobayashi N., and Manaka H.: "Magnetic field effect on the magnetic torque and the magnetostriction in $(CH_3)_2CHNH_3CuCl_3$", J. Phys.: Con. Ser. **51**, 187–190 (2006). *

Fujiwara T., Inoue H., Osawa A., Tsunoda R., Goto T., Suzuki T., Shindo Y., Tanaka H., Sasaki T., Kobayashi N., Awaji S., and Watanabe K.: "Cu-NMR study on the disordered quantum spin magnet with the Bose-glass ground state", J. Phys.: Con. Ser. **51**, 199–202 (2006). *

Tonishi J., Ueda M., Suzuki T., Osawa A., Goto T., Adachi T., Koike Y., Fujita M., and Yamada K.: "Local structure in single crystals of La-based high T_c cuprates", J. Phys.: Con. Ser. **51**, 275–278 (2006). *

Suzuki T., Fujiwara T., Osawa A., Goto T., Yamada F., Tanaka H., and Watanabe I.: "Muon-Spin-Relaxation study on single crystals $Tl_{1-x}K_xCuCl_3$ with $x = 0.2$", J. Phys. Soc. Jpn. **75**, No. 2, pp. 025001-1–025001-2 (2006). *

Hachitani K., Fukazawa H., Kohori Y., Watanabe I., Yoshimitsu Y., Kumagai K., Giri R., Sekine C., and Shirotani I.: "^{31}P-NMR and μSR studies of filled skutterudite compound $SmFe_4P_{12}$:evidence for heavy fermion behavior with ferromagnetic ground state", J. Phys. Soc. Jpn. **75**, No. 12, pp. 124717-1–124717-5 (2006). *

Attwood D., Bell P., Bull S., McMahon T., Wilson

J., Fernow R., Gruber P., Jamdagni A., Long K., McKigney E., Savage P., Curtis-Rouse M., Edgecock T. R., Ellis M., Lidbury J., Murray W., Norton P., Peach K., Ishida K., Matsuda Y., Nagamine K., Nakamura S., Marshall G. M., Benveniste S., Cline D., Fukui Y., Lee K., Pischalnikov Y., Holmes S., and Bogacz A.: "The scattering of muons in low-Z materials", Nucl. Instrum. Methods Phys. Res. B **251**, 41–55 (2006). ∗

Matsuda Y., Bakule P., Iwasaki M., Matsuzaki T., Miyake Y., Ikedo Y., Strasser P., Simomura K., Makimura S., and Nagamine K.: "Generation of low-energy muons with laser resonant ionization", Nucl. Phys. B (Proc. Suppl.) **155**, 346–348 (2006). ∗

Hachitani K., Fukazawa H., Kohori Y., Watanabe I., Sekine C., and Shirotani I.: "Evidence for magnetic ordering associated with metal-insulator transition in $SmRu_4P_{12}$ studied by muon spin relaxation", Phys. Rev. B **73**, 052408-1–052408-4 (2006). ∗

Saito T., Osawa A., Goto T., Suzuki T., and Watanabe I.: "Muon spin rotation and relaxation studies on the solid solution of the two spin-gap systems $(CH_3)_2CHNH_3$-$CuCl_3$ and $(CH_3)_2CHNH_3$-$CuBr_3$", Phys. Rev. B **74**, 134423-1–134423-5 (2006). ∗

Torikai E., Ito A., Watanabe I., and Nagamine K.: "μSR studies on the response of spin dynamics to applying or removing magnetic field — Typical Ising spin glass $Fe_{0.05}Mn_{0.05}TiO_3$", Physica B **374/375**, 95–98 (2006). ∗

Bakule P., Matsuda Y., Iwasaki M., Miyake Y., Nagamine K., Ikedo Y., Simomura K., and Strasser P.: "Pulsed source of ultra low-energy muons at RIKEN-RAL", Physica B **374/375**, 456–459 (2006). ∗

Miyake Y., Nishiyama K., Kawamura N., Makimura S., Strasser P., Simomura K., Beveridge J. L., Kadono R., Fukuchi K., Sato N., Ueno K., Higemoto W., Ishida K., Matsuzaki T., Watanabe I., Matsuda Y., Iwasaki M., Nakamura S., Doornbos J., and Nagamine K.: "Status of J-PARC muon science facility at the year of 2005", Physica B **374/375**, 484–487 (2006). ∗

Oral Presentations

(International Conference etc.)

Matsuda Y.: "Generation of ultra slow muon beam by laser resonant ionization of muonium atoms", 6th International Workshop on Neutrino Factories and Superbeams (NuFact 04), Osaka, July–Aug. (2004).

Suzuki T., Ota T., Tonishi J., and Goto T.: "Increase of the sound velocity by magnetic fields in $La_{2-x}Sr_xCuO_4$ around $x = 0.220$", 24th International Conference on Low Temperature Physics (LT24), (Department of Physics, University of Florida), Orlando, USA, Aug. (2005).

Kikkawa A., Katsumata K., Honda Z., Watanabe I., Suzuki T., and Matsuzaki T.: "Evolution of the spin-gap in a spin-ladder material detected by muSR technique", 1st International Symposium of Quantum Beam Science Directorate of JAEA (ICM2006 Satellite Conference), (JAEA), Tokai, Aug. (2006).

Ishida K.: "Muon catalyzed fusion", 8th International Workshop on Neutrino Factories nd Superbeams (NuFact 06), (University of California, Irvine), Irvine, USA, Aug. (2006).

Suzuki T., Watanabe I., Osawa A., Goto T., Yamada F., and Tanaka H.: "Muon-Spin-Relaxation study on randomness introduced $Tl_{1-x}K_xCuCl_3$ with $\boldsymbol{x}$ = 0.44", An ICM2006 Satellite Conference: 1st International Symposium of Quantum Beam Science Directorate of JAEA, Advances in Neutron, Synchrotron Radiation, μSR and NMR Researches (QuBS2006), (Quantum Beam Science Directorate of JAEA), Tokai, Aug. (2006).

Suzuki T., Saito T., Osawa A., Goto T., Sasaki T., Awaji S., Watanabe K., Kobayashi N., and Manaka H.: "Magnetic field effect on the magnetic torque and the magnetostriction in $(CH_3)_2CHNH_3CuCl_3$", Yamada Conference LX on Research in High Magnetic Fields (RHMF2006), (High Field Laboratory for Superconducting Materials Institute for Materials Research Tohoku University), Sendai, Aug. (2006).

Matsuda Y.: "Progress of laser ionization method for LEM", 1st Swiss Japan Workshop on the applications and on new developments in muon spectroscopy on novel materials, (High Energy Accelerator Research Organization), Tsukuba, Sept. (2006).

Bakule P.: "Laser ionization of muonium - pulsed ultra low energy muon source for material studies", International Conference on Laser Probing 2006 (LAP 2006), (Vienna University of Technology), Vienna, Austria, Sept. (2006).

Ishida K.: "RIKEN-RAL, now and in the future", Workshop on future developments of European muon sources, (NMI3), Abingdon, UK, Nov. (2006).

(Domestic Conference)

川股隆行, 菅原直樹, Haidar S. M., 高橋伸雄, 宮島祐一, 野地尚, 小池洋二, 工藤一貴, 小林典男, 藤井裕, 菊池彦光, 千葉明朗, Petrakovskii G., Popov M., Bezmaternikh L.: "$La_8Cu_7O_{19}$, Y_2BaNiO_5, CuB_2O_4 におけるスピン状態と熱伝導", 科研費特定領域「異常量子物質の創製　新しい物理を生む新物質」成果報告会, 仙台, 1 月 (2006).

大平-河村聖子, 前川覚, 鍛治亮佑, 伊藤哲明: "量子スピンカゴメ格子磁性体 Cu-titmb の μSR 測定", 日本物理学会第 61 回年次大会, 松山, 3 月 (2006).

鈴木栄男, 渡邊功雄, 藤原崇雄, 大沢明, 後藤貴行, 山田文子, 田中秀数: "量子スピン系 $Tl_{1-x}K_xCuCl_3$ ($\boldsymbol{x}$ = 0.2) における μSR 測定", 日本物理学会第 61 回年次大会, 愛媛大学, 3 月 (2006).

吉川明子, 勝又紘一, 本多善太郎, 渡邊功雄, 鈴木栄男, 松崎禎市郎: "スピンラダー物質 $Na_2Co_2(C_2O_4)_3(H_2O)_2$ の μSR 測定", 日本物理学会

2006 年秋季大会, 千葉, 9 月 (2006).

石田勝彦: “理研 RAL ミュオン施設での研究の現状”, 仁科加速器研究センター原子核グループ月例コロキウム, 和光, 10 月 (2006).

川股隆行, 宮島祐一, 高橋伸雄, 野地尚, 小池洋二, 工藤一貴, 小林典男: “5 本足スピン梯子格子系 $La_8Cu_7O_{19}$ とハルデンギャップ系 Y_2BaNiO_5 におけるスピンによる熱伝導”, ボトムアップ若手の会第 1 回研究会：物理・化学・生物の融合を目指して, 和光, 11 月 (2006).

川股隆行, 宮島祐一, 高橋伸雄, 野地尚, 小池洋二, 工藤一貴, 小林典男: “5 本足スピン梯子格子系 $La_8Cu_7O_{19}$ とハルデンギャップ系 Y_2BaNiO_5 におけるスピンによる熱伝導”, 東大物性研短期研究会「量子スピン系の物理」, 柏, 11 月 (2006).

VII. LIST OF PREPRINTS

(2006 Apr.–2007 Mar.)

RIKEN-AF-NP & RIKEN-NC-NP

471 M. Yamaguchi, Y. Tagishi, Y. Aoki, T. Iizuka, T. Nagatomo, T. Shinba, N. Yoshimaru, Y. Yamato, T. Katabuchi, and M. Tanifuji: "Analyzing power for 6Li(d, arufa)4He and 6Li(d, p)7Li reactions at a low incident energy"

472 S. Forte and Y. Goto: "SPIN PHYSICS"

473 T. Nakamura, M. Wada, K. Okada, A. Takamine, Y. Ishida, Y. Yamazaki, T. Kambara, Y. Kanai, T. M. Kojima, Y. Nakai, N. Oshima, A. Yoshida, T. Kubo, S. Ohyani, K. Noda, T. Katayama, V. Lioubinov, H. Wollnik, V. Varenysov, and A. Scuessler: "Laser spectroscopy of 7,10Be+ in an online ion trap"

1 W. Horiuchi, Y. Suzuki, B. Abu-Ibrahim, and A. Kohama: "Sysematic analysis of reaction cross sections of carbon isotopes"

2 K. Morita, K. Morimoto, D. Kaji, T. Akiyama, S. Goto, H. Haba, E. Ideguchi, K. Katori, H. Koura, H. Kudo, T. Onishi, A. Ozawa, T. Suda, K. Sueki, F. Tokanai, T. Yamaguchi, A. Yoneda, and A. Yoshida: "Experiments on Synthesis of an Isotope 277112 by 208Pb + 70Zn Reaction"

3 K. Morita, K. Morimoto, D. Kaji, T. Akiyama, S. Goto, H. Haba, E. Ideguchi, K. Katori, H. Koura, H. Kudo, T. Onishi, A. Ozawa, N. Sato, T. Suda, K. Sueki, F. Tokanai, T. Yamaguchi, A. Yoneda, and A. Yoshida: "Observation of Second Decay Chain from 273113"

4 Z. Elekes, Zs. Dombradi, N. Aoi, S. Bishop, Zs. Fulop, J. Gibelin, T. Gomi, Y. Hashimoto, N. Imai, N. Iwasa, H. Iwasaki, G. Kalinka, Y. Kondo, A. A. Korsheninnikov, K> Kurita, M. Kurokawa, N. Matsui, T. Motobayashi, T. Nakamura, T. Nakao, E. Yu, Nikolskii, T. K. Ohnishi, T. Okumura, S. Ota, A. Perera, A. Saito, H. Sakurai, Y. Satou, D. Sohler, T. Sumikama, D. Suzuki, M. Suzuki, H. Takeda, S. Takeuchi, Y. Togano, and Y. Yanagisawa: "Spectroscopic stucy of neutron shell closures via nucleon transfer in the near-dripline nucleus 23O"

5 J. Gibelin, D. Bernnel, T. Motobayashi, N. Aoi, H. Baba, Y. Blumenfeld, Zs. Dombradi, Z. Elekes, S. Fortier, N. Fracaria, N. Fukuda, T. Gomi, K. Ishikawa, Y. Kondo, T. Kubo, V. Lima, T. Nakamura, A. Saito, Y. Satou, E. Takeshita, S. Takeuchi, T. Teranishi, Y. Togano, A. M. Vinodkumar, Y. Yanagisawa, and K. Yoshida: "Measurement of the B(E2,0+1->2+1) in the N=16 nucleus 26Ne"

6 D. Kameda, H. Ueno, K. Asahi, M. Takemura, A. Yoshimi, T. Haseyama, M. Uchida, K. Shimada, D. Nagae, G. Kijima, T. Arai, K. Takase, S. Suda, T. Inoue, J. Murata, H. Kawamura, Y. Kobayashi, H. Watanabe, and M. Ishihara: "Measurement of the electric quadrupole moment of 23AL"

RIKEN-AF-AC

Not Applicable

VIII. LIST OF SYMPOSIA

(2006 Apr.–2007 Mar.)

1) Second expert meeting on critical issues on next-generation high-intensity fragment separators
10–13 May, Experimental Installations Operation Gr., RIKEN

2) Systematic Study of Island of Inversion Nuclei by AMD
22–23 May, User Liaison and Support Group, RIKEN

3) Experimental detail of p+6He(6Li)->n(p)+d+a (spectator) reaction
8 Jun., User Liaison and Support Group, RIKEN

4) RHIC Physics in the Context of the Standard Model
18–23 Jun., RIKEN BNL Research Center, USA

5) Folding model approach to nucleus-nucleus interactions and applications to nuclear reaction studies
23–24 Jun., User Liaison and Support Group, CNS, RIKEN

6) RIKEN Workshop on "Frontiers in the physics of quark-gluon plasma"
8–9 Jul., Enyo Radiation Lab., RIKEN

7) Simplified modeling of cluster-shell competition (SMSO) in C-isotopes
14–15 Jul., User Liaison and Support Group, RIKEN

8) QCD in Extreme Conditions
31 Jul.–2 Aug., RIKEN BNL Research Center, USA

9) Matrix models and string theory
23 Sep., Theoretical Physics Laboratory, RIKEN

10) International Workshop on RHIC Spin Physics
29–30 Sep., Enyo Radiation Lab., RIKEN

11) 2nd German-Japanese Workshop on Nuclear Structure and Astrophysics
4–7 Oct., Nuclear Physics Research Div., RIKEN

12) CNS-GRAPE collaboration for high-resolution gamma-ray spectroscopy at RIBF
16–17 Oct., User Liaison and Support Group, RIKEN

13) RIBF International Collaboration Workshop
6–9 Nov., Nuclear Physics Research Div., RIKEN

14) Present status and strategy at RIBF
17–18 Nov., User Liaison and Support Group, RIKEN

15) Hyperfine structure of alkali atoms in superfluid helium
30 Nov.–1 Dec., User Liaison and Support Group, RIKEN

16) In-beam gamma spectroscopy of the doubly magic nucleus 78Ni and its vicinity
6 Feb., User Liaison and Support Group, RIKEN

17) Large-Scale Self-Consistent Nuclear Mass Calculations
23–24 Feb., User Liaison and Support Group, RIKEN

18) Analysis of 8B elastic scattering experiments
2 Mar., User Liaison and Support Group, RIKEN

19) International Workshop: Joint JUSTIPEN-LACM Meeting
5–8 Mar., Nuclear Physics Research Div., Oak Ridge (USA)

20) Channelling of hydrogen by using nuclear reactions
15 Mar., User Liaison and Support Group, RIKEN

21) Domain Wall Fermions at en Years
15–17 Mar., RIKEN BNL Research Center, USA

22) Resent development and future prospect of the GEM based tracking detector
23 Mar., Advanced Meson Science Laboratory/Cosmic Radiation Laboratory, RIKEN

IX. LIST OF SEMINARS

(2006 Apr.–2007 Mar.)

Accelerator Division

1) Dr. Andrew M. Sessler (Lawrence Berkeley National Laboratory (USA)), 2 Oct.
"A Century of Particle Accelerators"

2) Dr. Takamichi Aoki (The University of Tokyo), 23 Mar.
"Design and Construction of a rebuncher for RIKEN RI Beam Factory"

3) Dr. Lukas Stingelin (Japan society for the Promotion of Science), 23 Mar.
"Study of new flattop resonator for RRC"

Nuclear Physics Research Division

1) Dr. Y. M. Zhao (Shanghai Jiao-Tong Univ. (China)), 7 Apr.
"Dimension of the single-j shell configurations and sum rules of angular momentum recoupling coefficients"

2) Dr. Shinya Wanajo (University of Tokyo), 13 Apr.
"The rp-process nucleosynthesis in core-collapse supernovae"

3) Dr. Masahiko Iwasaki (RIKEN Nishina Center), 18 Apr.
"Physics developed using K-meson: from KEK-PS to J-PARK"

4) Dr. Koji Niita (RIST), 19 Apr.
"PHITS – a Particle and Heavy Ion Transport code System - Models and Applications

5) Dr. Takatoshi Ichikawa (RIKEN Nishina Center), 25 Apr.
"Barrier for cold-fusion production of superheavy elements"

6) Dr. Takeshi Furukawa (RIKEN Nishina Center), 25 Apr.
"Spin physics of atoms and nuclei immersed in superfluid helium with laser spectroscopic method"

7) Dr. Yoichi Nakai (RIKEN Nishina Center), 9 May
"Fast ion – C60 collision and resonant coherent excitation of fast ion: examples of atomic physics experiments using accelerators"

8) Dr. Hidetoshi Kikunaga (RIKEN Nishina Center), 16 May
"Search for an isomer state of Th-229 with extremely low energy alpha-spectrometry"

9) Dr. Takashi Sugimoto (RIKEN Nishina Center), 16 May
"Invariant-mass spectroscopy of the neutron dripline nucleus 14B"

10) Dr. Claudia Hoehne (GSI, Germany), 17 May
"The high baryon density CBM experiment and other QCD related research activities at the future FAIR facility in Germany"

11) Dr. Yasuo Funaki (RIKEN Nishina Center), 23 May
"Alpha particle condensation in finite nuclei"

12) Dr. Yasuhisa Abe (RCNP, Osaka University), 27 May
"RIKEN Lecture Series on Nuclear Physics Course III "Nuclear dynamics – nuclear fusion and fission –" 1"

13) Dr. Akito Saito (University of Tokyo), 30 May
"Exotic cluster states in 12Be via α-inelastic scattering"

14) Dr. Makoto Ito (RIKEN Nishina Center), 30 May
"Unified studies on structures and reactions in light neutron-rich systems (Application to 10Be)"

15) Dr. Kazuo Horiuchi (Hirosaki University), 8 Jun.
"Ice core records of 10Be and solar activity in the past"

16) Dr. Hironari Miyazawa (University of Tokyo), 13 Jun.
"Nuclear Forces and Three-Body Forces"

17) Dr. Kenichi Matsuyanagi (Kyoto University), 14 Jun.
"RIKEN Lecture Series on Nuclear Physics Course II "Minimum of modern theory of nxuclear structure" 2"

18) Dr. Genji Hirata (Denken-Seiki Co., Ltd), 16 Jun.
"Foundation and practical technique of noise trouble measures"

19) Dr. Atsushi Kitagawa (N.I.R.S.), 20 Jun.
"Research for medical applications of the secondary beam at HIMAC"

20) Dr. Yoshiya Furusawa (N.I.R.S.), 20 Jun.
"Biological effect of 9C radio-active beam"

21) Dr. Satoru Terashima (RIKEN Nishina Center), 12 Jul.
"Deduced nuclear density distributions by using proton elastic scattering"

22) Dr. Takashi Nagatomo (RIKEN Nishina Center), 12 Jul.
"Search for the second class current by the precise measurement of the beta-ray angular distribution of the mirror pair 20F and 20Na"

23) Dr. Koji Kaya (RIKEN), 13 Jul.
"Nanometer Scale Chemistry: from Diatomic Molecule to Giant Cluster"

24) Prof. Alexander Titov (JINL, RUSSIA/RCNP, Osaka Univ.), 9 Aug.
"Θ formation in inclusive γ D $\rightarrow$ pK- X reaction"

25) Dr. Takashi Nakano (RCNP, Osaka University), 9 Aug.
"Status of the pentaquark search at LEPS"

26) Dr. Yasuo Yamamoto (Tsuru University), 21 Aug.
"How to make and use G-matrix interactions"

27) Associ. Prof. Badawy Abu-Ibrahim (Cairo Unv.), 5 Sep.
"Description of reaction cross sections in a parameter free eikonal model"

28) Dr. Hikaru Kawai (RIKEN Nishina Center), 12 Sep.
"String theory for amateurs: towards the theory of everything"

29) Dr. Katsuhiko Ishida (RIKEN Nishina Center), 17 Oct.
"Recent Progress at the RIKEN-RAL Muon Facility"

30) Dr. Matthias Schaedel (GSI, Germany), 20 Oct.
"Superheavy Element Chemistry at GSI – Past, Present and Future"

31) Prof. Guido Langouche (Institute for Radiation and Nuclear Physics, Katholieke Universiteit Leuven, Belgium), 26 Oct.
"Lattice site determination of Er in Si and GaN using electron emission channeling from radioactive isotopes produced at CERN ISOLDE"

32) Dr. Kazuhiro Oyamatsu (Aichi Shukutoku University), 31 Oct.
"Various phases of nuclear matter at around the normal nuclear density and nuclear pasta"

33) Dr. A. Nasirov (JINR, Russia), 2 Nov.
"Influence of the entrance channel dynamics on the evaporation residue formation in reaction of massive nuclei"

34) Dr. Tetsuo Hatsuda (Univesity of Tokyo), 2 Nov.
"Quantum Chromodynamics at Extreme Conditions"

35) Dr. Kenichi Matsuyanagi (Kyoto University), 24 Nov.
"RIKEN Lecture Series on Nuclear Physics Course II "Minimum of modern theory of nuclear structure" 3"

36) Prof. Toichiro Kinoshita (Lab. for Elementary Part. Phys., Cornell, USA), 28 Nov.
"Lepton g-2 and High Precision Test of QED – From 1947 to Present –"

37) Prof. Richard Boyd (National Astronomical Observatory of Japan), 12 Dec.
"Supernova Neutrinos, Neutrino Properties, and r-and n-Process Nucleosynthesis"

38) Dr. Heiko Scheit (RI Physics Lab., RIKEN), 26 Dec.
"The New Radioactive Nuclear Beam Facility REX-ISOLDE/MINIBALL: Sub-Barrier Coulomb Excitation of 30,32Mg and the "Island of Inversion""

39) Dr. Noriyoshi Ishii (Center for Computational Science, Tsukuba), 9 Jan.
"Nuclear Force from Lattice QCD"

40) Prof. Th. A. Rijken (Institute for Mathematics, Astrophysics and Particle Physics, University of Nijmegen, The Netherland), 9 Jan.
"Soft-core Baryon-baryon Interactions (ESC-model at Low and Intermediate Energies)"

41) Prof. Paul Mantica (NSCL, MSU, USA), 16 Jan.
"Beta-decay studies and low-energy nuclear structure near Ca-48"

42) Prof. Yoji Ohashi (Keio University), 23 Jan.
"BCS-BEC crossover in a superfluid Fermi gas"

43) Dr. Yasuyuki Akiba (RIKEN Nishina Center), 19 Mar.
"High Energy Heavy Ion Physics at RHIC"

Advanced Meson Science Laboratory

1) Dr. Kozi Nakai (KEK, JAPAN), 19 Apr.
"Development of SCITIC (Scintillation Track Im-

age Camera) and measurement of spin-orbit interaction in hyperon-nuclear scattering"

2) Dr. Daisuke Kamei (Applied Nuclear Physics Laboratory, RIKEN, JAPAN), 24 May
"Introduction of the beta-NMR method and the application to a study of nuclear structure for unstable nuclei"

3) Dr. Takashi Taniguchi (KEK, JAPAN), 31 May
"Development of front-end electronics for gas chambers with high speed bi-polar ASIC at KEK"

4) Dr. Hazuki Furukawa (Ochanomizu University, JAPAN), 8 Jun.
"Weakferromagnetic Superconductor ErNi2B2C and a possibility of the spontaneous vortex phase"

5) Dr. Noriyoshi Ishii (University of Tokyo, JAPAN), 14 Jun.
"5 quark picture of Lambda(1405) from anisotropic lattice QCD"

6) Dr. Norimichi Kojima (University of Tokyo), 19 Jun.
"Study on the ferromagnetism and the dynamical spin-crossover phenomenon coupled with spin and charge for iron mixed-valence complexes, A[FeII FeIII(dti)3](dto=C2O2S2)"

7) Dr. Hideto En'yo (Radiation Laboratory, RIKEN, JAPAN), 26 Jul.
"Mesons in Nucleus, seen in their e+e− decays"

8) Dr. Tatsuya Chujyo (University of Tsukuba, JAPAN), 13 Sep.
"The multigap resistive plate chamber (MRPC) as a new generation time-of-flight detector"

9) Dr. Kenichi Hachitani (Chiba University, JAPAN), 4 Oct.
"Possibility of Multipole Order in Filled Skutterudite SmRu4P12 $\sim\mu$SR and 31P-NMR study$\sim$"

10) Dr. Petros Aslanyan (JINR, RUSSIA), 6 Oct.
"The review of recent results for observation of Strangeness = +1, 0, −1, −2 exotic states with Lambda-hyperons and Ks0-mesons systems in p + propane collisionsat momentum 10 GeV/c"

11) Dr. Yasuyuki Ishii (Condensed Molecular Materials Laboratory, RIKEN, JAPAN), 30 Oct.
"High pressure experimental method for precise magnetic and transportproperty measurements of organic conductors"

12) Dr. Takahisa Koike (Advanced Meson Science Laboratory, RIKEN, JAPAN), 15 Nov.
"DWIA calculation of in-flight (K−,n) reaction spectra using helium 3 target"

13) Dr. Youichi Ikeda (Osaka University, JAPAN), 15 Nov.
"Study of strange dibaryon in the KNN-$\pi\Sigma$N coupled channel equation"

14) Dr. Takayuki Kawamata (Advanced Meson Science Laboratory, RIKEN, JAPAN), 23 Jan.
"Thermal conductivity and spin state in low-dimensional quantum spin systems"

15) Dr. Yoshio Yamaguchi (Theoretical Physics Laboratory, RIKEN, JAPAN), 8 Feb.
"Genesys of Meson Physics"

16) Dr. Hikomitsu Kikuchi (University of Fukui, JAPAN), 29 Mar.
"Observation of magnetization plateau in diamond chain compound"

Theoretical Physics Laboratory

1) Dr. Yasuhiro Abe (City College of New York (USA)), 19 May
"Construction of fuzzy S4 and its applications"

2) Dr. Yoshio Kikukawa (University of Tokyo (Japan)), 30 May
"Electroweak theory on the lattice with exact gauge invariance"

3) Dr. Asato Tsuchiya (Osaka University (Japan)), 9 Jun.
"Bubbling AdS, N = 4 SYM on RxS3 and theories with 16 supercharges"

4) Dr. Satoshi Iso (KEK (Japan)), 16 Jun.
"Hawking radiation and Anomalies"

5) Dr. Taku Izubuchi (Kanazawa University (Japan)), 7 Jul.
"Lattice QCD and QED"

6) Dr. Toshio Nakatsu (Osaka University (Japan)), 8 Jul.
"Amoebas and Instantons"

7) Dr. Yoshitake Hashimoto (Osaka City University (Japan)), 8 Jul.
"Introduction to tropical geometry"

8) Dr. Toshiaki Maeno (Kyoto University (Japan)), 8 Jul.

"Amoebas and their ultradiscretization"

9) Dr. Yutaka Sakamura (Osaka University (Japan)), 14 Jul.
"Scherk-Schwarz twist in 5D conformal supergravity"

10) Dr. Nobuhito Maru (University of Roma and INFN (Italy)), 21 Jul.
"Two-loop Calculation of Higgs Mass in Gauge-Higgs Unification"

11) Dr. Takao Suyama (Kyoto University (Japan)), 25 Jul.
"CFT for Closed String Tachyon Condensation"

12) Dr. Yutaka Hosotani (Osaka University (Japan)), 28 Jul.
"Dynamical Gauge-Higgs Unification and LHC Physics"

13) Dr. Amihay Hanany (MIT (USA)), 11 Aug.
"Tilings, Dimers, and Quiver Gauge Theories"

14) Dr. Giacomo Marmorini (Scuola Normale Superiore and INFN (Italy)), 25 Aug.
"Non-abelian vortices of higher winding number"

15) Dr. Akinori Kawachi (Tokyo Institute of Technology (Japan)), 1 Sep.
"Introduction to Quantum Computation"

16) Dr. Hirofumi Kubo (Kyushu University (Japan)), 6 Oct.
"Determining the power counting for nuclear EFT from Wilsonian Renormalizatin Group"

17) Dr. Shin Nakamura (Hanyang University (Korea)), 11 Oct.
"A Holographic Dual of RHIC Hydrodynamics"

18) Dr. Ho-Ung Yee (Korea Institute for Advanced Study (Korea)), 16 Oct.
"AdS/CFT with Tri-Sasakian Manifolds"

19) Dr. Nobuyasu Ito (University of Tokyo (Japan)), 20 Oct.
"Simulation study of transport phenomena"

20) Dr. Hoang Ngoc Long (Hanoi Institute of Physics (Vietnam)), 24 Nov.
"Neutrino mass and phenomenology of the economical 3-3-1 model"

21) Dr. Shoichi Ichinose (University of Shizuoka (Japan)), 27 Nov.
"Quantization of Fields in 5D Space-Time with Z_2 parity and Position/Momentum Propagator"

22) Dr. Kazuhiro Sakai (Keio University (Japan)), 1 Dec.
"Integrability in AdS/CFT Correspondence"

23) Dr. Yasuhiro Sekino (Okayama Institute for Quantum Physics (Japan)), 22 Dec.
"A Holographic Framework for Eternal Inflation"

24) Dr. Yutaka Okochi (California Institute of Technology (USA)), 19 Jan.
"Meta-stable vacua in supersymmetric gauge theories"

25) Dr. Yosuke Imamura (University of Tokyo (Japan)), 26 Jan.
"Anomalies in brane tilings"

26) Dr. Yoshiharu Kawamura (Shinshu University (Japan)), 27 Jan.
"Past and Future of Orbifold GUT – Towards Three Generation Model"

27) Dr. Yutaka Hosotani (Osaka University (Japan)), 27 Jan.
"Gauge Higgs Unification Models in Warped Space"

28) Dr. Tetsuya Shiromizu (Tokyo Institute of Technology (Japan)), 27 Jan.
"Possible Problems of Randall-Sundrum Gravity Theory"

29) Dr. Kei-Ichi Kondo (Chiba University (Japan)), 9 Feb.
"Mass gap and quark confinement from Yang-Mills theory to Faddeev model"

30) Dr. Toshihiro Matsuo (National Taiwan Normal University (Taiwan)), 16 Feb.
"Finite Temperature String in AdS3"

31) Dr. Poul H. Damgaard (Niels Bohr Institute (Denmark)), 23 Feb.
"Random Matrix Theory and low-energy constants of QCD"

32) Dr. Hidenori Sonoda (Kobe University (Japan)), 26 Feb.
"Application of the exact renormalization group to perturbation theory"

33) Dr. Kiyoshi Higashijima (Osaka University (Japan)), 2 Mar.
"Renormalizable Nonlinear Sigma Models in Three Dimensions"

Accelerator Applications Research Group

1) Dr. Reinhard Neumann (GSI (Germany)), 16 Mar.
"Materials research at GSI: Recent results on nanowires, ion irradiation at high pressure, and bio-experiments with heavy-ion microprobe"

JUSTIPEN Seminar

1) Prof. B. A. Brown (Michigan State Univ., USA), 17 Aug.
"New sd-shell Hamiltonians' "

2) Prof. C. Bertulani (Arizona Univ., USA), 1 Nov.
"New Directions in Nucl. Astrophysics"

3) Prof. Peter Moller (LANL), 11 Dec.
"New Calculations of Nucl. Structure Properties for Simulatin Data Bases with Focus on effects of triaxial Nuclear Shapes"

4) Dr. Yang Sun (Department of Physics and Joint Insitute for Nuclear Astrophycis, Univ. of Notre Dame, USA), 21 Dec.
"Projedcted Shell Model for Heavy Nuclei and Nucl. Astrophysics"

AUTHOR INDEX